U.S. DEPARTMENT OF COMMERCE
National Technical Information Service

N77-78644

Proceedings of the Conference on Waste Heat Management and Utilization Held at Miami Beach, Florida on May 9-11, 1976. Volume II

(U.S.) National Aeronautics and Space Administration, Washington, DC

Prepared for

Nuclear Regulatory Commission, Washington, DC

1976

NASA SCIENTIFIC
OPERATED BY INFORMATICS
BALTIMORE WASHINGTON INTERNATIONAL AIRPORT,

DOCUMENT REQUEST

DOCUMENT REQUESTED

A NASA ACCESSION NUMBER: N77 78644	OR B NACA/NASA REPORT NUMBER:
C (PLEASE DO NOT WRITE IN THIS SPACE)	
D COPY TYPE REQUESTED: case file	☐ MICROFICHE ☒ FULL SIZE

1

16

REQUESTER IDENTIFICATION

E REQUESTER'S FACILITY IDENT. NO.: 2523	F REQUESTER'S CONTRACT NO.:
G AUTHORIZED SIGNATURE AND DATE: Ellen Davis Nov 17, 1978	

NOTE: For prompt service, please follow instructions on back of last copy

1. SHIPPING COPY

OTHER BIBLIOGRAPHIC INFORMATION (ESSENTIAL IF ITEMS B ARE UNKNOWN

H DOCUMENT TITLE:	
I DATE OF REPORT:	J. AUTHOR(S):
K CORPORATE SOURCE:	L CORPORATE REPORT NO.:
	M CONTRACT NO.:

N. **MAILING LABEL** (must be imprinted on all copies include zip code)

Ellen Davis
NTIS

FF 492 DEC. 68

ANAGEMENT
AND
UTILIZATION

(NASA-TM-X-74100-Vol-2) PROCEEDINGS OF THE CONFERENCE ON WASTE HEAT MANAGEMENT AND UTILIZATION, VOLUME 2 (National Aeronautics and Space Administration) 861 p

N77-78644
THRU
N77-78680
Unclas
00/45 31217

Editors:
SAMUEL S. LEE
SUBRATA SENGUPTA

UNITED STATES ENVIRONMENTAL PROTECTIO

CITIZENSHIP
DUKE POWER
SERVICE

FPL
FLORIDA POWER & LIGHT COMPANY

VOL. 2

REPRODUCED BY
NATIONAL TECHNICAL
INFORMATION SERVICE
U. S. DEPARTMENT OF COMMERCE
SPRINGFIELD, VA. 22161

PROCEEDINGS OF THE CONFERENCE ON WASTE HEAT MANAGEMENT AND UTILIZATION

9 – 11 May, 1976
Miami Beach, Florida

Presented by:
Department of Mechanical Engineering,
University of Miami

Sponsored by:
National Aeronautics and Space Administration
United States Nuclear Regulatory Commission
United States Environmental Protection Agency
Duke Power Company
Florida Power and Light Company
School of Continuing Education, University of Miami

In Cooperation with:
American Society of Mechanical Engineers
Miami Section

Editors:
Samuel S. Lee, University of Miami
Subrata Sengupta, University of Miami

COLOR ILLUSTRATIONS REPRODUCED
IN BLACK AND WHITE

ACKNOWLEDGEMENTS

The Conference Committee gratefully acknowledges the support of the Keynote Speaker, Mr. Frank Staszesky. It also greatly appreciates the help of the Conference Banquet Speaker, Dr. Robert Uhrig.

Gratitude is also expressed to all the authors and speakers who made this conference a worthwhile endeavour in scientific communication.

The Session Chairmen and Co-Chairmen deserve special thanks for organizing and conducting the technical sessions.

The support of the numerous students and faculty of the University of Miami is gratefully acknowledged.

The invaluable help of the scientists and administrators of the sponsoring organizations was a key element in making this conference comprehensive. We express our sincerest gratitude to them.

Conference Committee
Miami, May, 1977

CONFERENCE COMMITTEE

Dr. Samuel S. Lee:
Conference Chairman
Chairman, Department of Mechanical Engineering,
University of Miami

Dr. Subrata Sengupta:
Conference Co-Chairman and Coordinator
Department of Mechanical Engineering,
University of Miami

Mr. Roy A. Bland:
Earth Resources Branch
National Aeronautics and Space Administration,
Kennedy Space Center

Mr. Frank Swanberg:
Health and Environmental Research Branch
United States Nuclear Regulatory Commission

Dr. Theodore G. Brna:
Emmission Effluent Technology Branch,
Utility and Industrial Power Division,
United States Environmental Protection Agency

Mr. Charles A. Dewey:
Civil-Environmental Division,
Duke Power Company

Mr. Charles Henderson:
Environmental Division,
Florida Power and Light Company

CONFERENCE SUPPORT

Arrangements:
Tony Pajares,
Lois Rosenzweig:
The School of Continuing Studies

Special Assistants:
Peter Kondis
Carol Glaze
Mary Rivera
Sally Pendleton

This publication is available at a cost of $55.00 from:
Mechanical Engineering Department
University of Miami
Coral Gables, Florida 33124

FOREWORD

In the United States, at present, approximately 350,000 MW of steam generating capacity is in the design or construction phase. This is about 80% of all the existing electrical powers generation capacity at the end of 1973. Compounding this trend is the possibility of 5 GW (5000 MW) energy parks which may become reality in the next decade. The possible environmental consequences need serious study. Considering, that for every unit of energy converted to electricity two units are rejected as waste heat, there is a need for utilization efforts.

While the present energy crisis has brought to focus the finite resources of our planet, it is essential to perpetuate the realization that our planet is a finite sink. It is, therefore, imperative to optimize the energy-environment-economy system in an integrated manner.

This conference was organized to provide a forum for inter-disciplinary exchange. The widely scattered biological, economic and engineering state-of-the-art knowledge could then be compiled into a single source, namely, the conference proceedings.

The conference gave equal emphasis to pollution abatement and utilization. Waste heat may come to be regarded as an important energy resource. This document, it is hoped, will serve the stated objectives.

Samuel S. Lee, Chairman
Subrata Sengupta, Co-Chairman

CONTENTS

WASTE HEAT MANAGEMENT AND UTILIZATION CONFERENCE

VOLUME I

Page No.

GENERAL SESSION (Session 1) 1-1

EPA VIEWS ON WASTE HEAT MANAGEMENT AND UTILIZATION 1-3
D. J. Graham, Environmental Protection Agency, Washington, D.C.

THE ROLE OF MODELING IN THE ASSESSMENT OF THERMAL POWER PLANT COOLING SYSTEM ON AQUATIC ENVIRONMENTS 1-13
R. A. Goldstein, J. Maulbetsch, R. Wyzga, Electric Power Research Institute, Palo Alto, California

PHYSICAL IMPACT OF WASTE HEAT DISPOSAL 1-15
S. S. Lee, S. Sengupta, University of Miami, Coral Gables, Florida

THE ANSWER IS BIOLOGICAL 1-17
D. Dunlop, Florida Power & Light, Miami, Florida

STANDARDS (Session 2A) 2A-1

AN APPROACH TO THERMAL WATER QUALITY STANDARDS 2A-3
C. Jeter, S. C. Department of Health & Environmental Control, Columbia, South Carolina

PROPOSED ANSI GUIDE FOR AQUATIC ECOLOGICAL SURVEYS AT THERMAL POWER PLANTS 2A-7
R. Hartman, Envirosphere Company, Norcross, Georgia

THERMAL GUIDELINES AS THEY APPLY TO THE STEAM ELECTRIC POWER GENERATING INDUSTRY 2A-12a
R. Schaffer, U. S. Environmental Protection Agency, Washington, D.C.

EVALUATING THE ADVERSE IMPACT OF COOLING WATER INTAKE STRUCTURES ON THE AQUATIC ENVIRONMENT 2A-25
S. Bugbee, U.S. Environmental Protection Agency, Washington, D.C.

Page No.

ECOLOGICAL EFFECTS I (Session 2B) 2B-37

TEMPERATURE INFLUENCES ON GROWTH OF AQUATIC ORGANISMS 2B-39
C. Coutant, Oak Ridge National Laboratory, Oak Ridge, Tennessee

COMPARISON OF ENVIRONMENTAL EFFECTS DUE TO OPERATION OF BRACKISH AND/OR SALT WATER NATURAL & MECHANICAL DRAFT COOLING TOWERS 2B-41
S. Laskowski, Picard, Low & Garrick, Inc., Washington, D.C.

A SYSTEMS APPROACH TO BIOLOGICAL AND THERMAL CONSIDERATIONS IN COOLING LAKE ANALYSES 2B-69
K. Robinson, R. W. Beck & Associates, Denver, Colorado

BIOLOGICAL EFFECTS OF THERMAL EFFLUENT FROM THE CUTLER POWER PLANT IN BISCAYNE BAY, FLORIDA 2B-91
H. J. Teas, R. C. Smith, University of Miami, Coral Gables, Florida

COOLING SYSTEM I (Session 2C) 2C-108

PROBLEMS OF DRY COOLING 2C-109
F. K. Moore, Cornell University, Ithaca, New York

WATER CONSERVATION AND WET-DRY COOLING TOWERS IN POWER PLANT SERVICE 2C-137
M. W. Larinoff, Hudson Products Corporation, Houston, Texas

MODIFICATIONS TO ONCE-THROUGH COOLING WATER DISCHARGE STRUCTURE TO ACHIEVE ENTRAINMENT MIXING AND LATERAL TRANSPORT OF THERMAL PLUMES 2C-139
D. E. Miller, Alabama Power Company, Birmingham, Alabama

DRY COOLING FOR POWER PLANTS: INCENTIVES, PROBLEMS AND RESEARCH/DEVELOPMENT ACTIVITIES 2C-170 a
B. M. Johnson, Battelle-Northwest Laboratories, Richland, Washington; J. S. Maulbetsch, Electric Power Research Institute, Palo Alto, California

COMPARISON OF ALTERNATIVE DIFFUSER DESIGNS FOR THE DISCHARGE OF HEATED WATER INTO SHALLOW RECEIVING WATER 2C-171
E. E. Adams, K. D. Stolzenbach, Massachussets Institute of Technology, Cambridge, Mass.

	Page No.
SOCIAL AND LEGAL ASPECTS (Session 3A)	3A-1
WASTE HEAT MANAGEMENT AND REGULATORY PROBLEMS W. L. Porter, Duke Power Company, Charlotte North Carolina	3A-3
SOCIAL ASPECTS OF REGULATING WASTE HEAT V. DePass, C. Newman, Consolidated Edison Company of New York, Inc., New York City, N.Y.	3A-15
SOCIAL ASPECTS OF THERMAL DISCHARGES FROM POWER PLANTS R. S. Thorsell, Edison Electric Institute, New York City, New York	3A-33
SCIENTISTS, ENGINEERS, AND LAWYERS: THE PHENOMENON OF INTERDISCIPLINARY UNDERSTANDING B. Shanoff, Environmental Protection Agency, Washington, D.C.	3A-35
ECOLOGICAL EFFECTS II (Session 3B)	3A-51
THE USE OF BIOLOGICAL/CHEMICAL INVESTIGATIONS FOR MANAGING THERMAL EFFLUENTS K. I. Kahl-Madsen, The Water Quality Institute, Denmark	3A-53
POWER GENERATION: EFFECTS ON THE AQUATIC ENVIRONMENT IN MASSACHUSETTS R. A. Isaac, Massachusetts Division of Water Pollution Control, Westborough, Massachusetts	3A-55
AVOIDANCE OF THERMAL EFFLUENT BY JUVENILE CHINOOK SALMON (ONCORHYNCHUS TSHAWYTSCHA) AND ITS IMPLICATIONS IN WASTE HEAT MANAGEMENT R. H. Gray, Battelle Pacific Northwest Laboratories, Richland, Washington	3A-73
THE BIOLOGICAL IMPACT OF THERMAL DISCHARGE EXCEEDING 95°F - A CASE STUDY OF ALLEN STEAM STATION, NORTH CAROLINA D. W. Anderson, A. Gnilka, Duke Power Company, Charlotte, North Carolina	3A-87
COOLING SYSTEMS II (Session 3C)	3C-113
COMPUTER ANALYSIS OF HEAT REJECTION SYSTEMS FOR COAL CONVERSION PROCESSES T. E. Eaton, C. E. Duncan, University of Kentucky, Lexington, Kentucky	3C-115

Page No.

STRATEGIES FOR WASTE HEAT MANAGEMENT OF ONCE-THROUGH COOLING SYSTEMS — 3C-119
B. Sill, Clemson University, Clemson, South Carolina

THERMAL IMPACT REDUCTION BY DILUTION, BIG BEND STATION, TAMPA, FLORIDA — 3C-143
W. J. Johnson, Tampa Electric Company, Tampa, Florida

WET/DRY COOLING FOR WATER CONSERVATION — 3C-163
G. A. Englesson, M. C. Hu, United Engineers, Philadelphia, Pennsylvania; W. C. Savage, U.S. ERDA, Washington, D.C.

OPTIMIZATION OF DRY COOLING SYSTEMS FOR 1000 MW FOSSIL FUEL POWER PLANTS — 3C-193
J. Fake, T. Rozenman, PFR Engineering Systems, Inc., Marina del Rey, California

NUMERICAL MODELING I (Session 4A) VOLUME II — 4A-1

NUMERICAL MODELS IN COOLING WATER CIRCULATION STUDIES: TECHNIQUES, PRINCIPLE ERRORS, PRACTICAL APPLICATIONS — 4A-3
G. S. Rodenhuis, Danish Hydraulic Institute, Horsholm, Denmark

PREDICTION OF TEMPERATURE RESULTING FROM ONCE-THROUGH COOLING OF A 5000 MWe POWER STATION ALONG AN ESTUARY — 4A-21
H. Ligteringen, Delft Hydraulics Laboratory, Delft, The Netherlands

A 3-DIMENSIONAL FREE SURFACE MODEL FOR THERMAL PREDICTIONS — 4A-23
S. Lee, S. Sengupta, C. Tsai, H. Miller, University of Miami, Coral Gables, Florida

A SYSTEMATIC APPLICATION OF TRANSIENT, MULTI-DIMENSIONAL MODELS FOR COMPLETE ANALYSIS OF THERMAL IMPACT IN REGIONS WITH SEVERE REVERSING FLOW CONDITIONS — 4A-43
A. H. Eraslan, Oak Ridge National Laboratory, Oak Ridge, Tennessee

REMOTE SENSING (Session 4B) — 4B-53

AERIAL REMOTE SENSING OF THERMAL PLUMES — 4B-55
R. A. Bland, NASA, Kennedy Space Center, Florida; H. Hiser, S. Lee, S. Sengupta, University of Miami, Coral Gables, Florida

Page No.

METEOROLOGICAL SATELLITES 4B-66a
M. Tepper, N. Durocher, NASA Headquarters, Washington, D.C.

THE LANDSAT PROGRAM 4B-67
H. Mannheimer, NASA Headquarters, Washington, D.C.

SEASAT SATELLITE 4B-77
W. McCandless, NASA Headquarters, Washington, D.C.

COST EFFECTIVE THERMAL MONITORING FOR STATE & LOCAL ACTIVITIES 4B-103
C. E. James, U.S. Environmental Protection Agency, Washington, D.C.

COOLING SYSTEMS III (Session 4C) 4C-106

THE THERMAL PERFORMANCE CHARACTERISTICS OF LARGE SPRAY COOLING PONDS 4C-107
R. D. Baird, D. M. Myers, Ford, Bacon & Davis Utah, Inc.; A. Shah, Spray Engineering Company, Salt Lake City, Utah

FIELD STUDY OF MECHANICAL DRAFT COOLING TOWER PLUME BEHAVIOR 4C-119
C. H. Goodman, E. Champion, Southern Company Services, Inc., Birmingham, Alabama; P.R. Slawson, Envirodyne Limited, Waterloo, Ontario, Canada

ATMOSPHERIC SPRAY - CANAL COOLING SYSTEMS FOR LARGE ELECTRIC POWER PLANTS 4C-121
R. W. Porter, S. Chaturvedi, Illinois Inst. of Technology, Chicago, Illinois

DRY/WET COOLING TOWERS WITH AMMONIA AS INTERMEDIATE HEAT EXCHANGE MEDIUM 4C-163
B. M. Johnson, R. T. Alleman, G. C. Smith, Battelle Pacific Northwest Laboratories, Richland, Washington

A COMPUTERIZED ENGINEERING MODEL FOR EVAPORATIVE WATER COOLING TOWERS 4C-180a
J. E. Park, Union Carbide Corporation, Oak Ridge, Tennessee

MANAGEMENT ASPECTS (Session 5A) 5A-1

HOW TO GET WASTE HEAT MANAGED 5A-1a
W. M. Rohrer, K. G. Kreider, University of Pittsburgh, Pittsburgh, Pennsylvania

Page No.

RESOURCE RECOVERY MODELS FOR REGIONAL PLANNING AND POLICY EVALUATION 5A-3
E. B. Berman, The Mitre Corporation, Bedford, Massachusetts

SELECTION OF ALTERNATIVE COASTAL LOCATIONS 5A-29
H. Schroder, Danish Hydraulic Institute, Horsholm, Denmark

USE OF ENVIRONMENTAL DATA FOR DETERMINING CONDENSER WATER SYSTEM ALTERNATIVES 5A-45
L. P. Beer, Roy F. Weston, Inc., West Chester, Pennsylvania

ECONOMIC ASPECTS (Session 5B) 5B-67

AN OPERATIONAL PROCEDURE FOR PREDICTING THE MOST ECONOMICAL USE OF CONDENSER COOLING MODES 5B-69
R. Waldrop, W. L. Harper, Tennessee Valley Authority, Norris, Tennessee

ECONOMICS OF BOILER BLOWDOWN WASTE HEAT RECOVERY 5B-81
M. R. Bary, Commonwealth Associates, Inc., Jackson, Michigan

MATHEMATICAL MODELING OF WASTE HEAT MANAGEMENT ALTERNATIVES FOR THE UNITED STATES 5B-83
H. J. Plass, University of Miami, Coral Gables, Florida

ENGINEERING TRADEOFFS GOVERNING WASTE HEAT MANAGEMENT AND UTILIZATION 5B-107
S. J. Daugard, T. R. Sundaram, Hydronautics, Inc., Laurel, Maryland

ENERGY RECOVERY THROUGH UTILIZATION OF THERMAL WASTES IN AN ENERGY-URBAN-AGROWASTE COMPLEX 5B-109
G. J. Trezek, L. F. Diaz, University of California at Berkeley, Berkeley, California

UTILIZATION (Session 5C) 5C-131

AN OVERVIEW OF WASTE HEAT MANAGEMENT IN TVA 5C-133
P. A. Krenkel, et al, Tennessee Valley Authority, Chattanooga, Tennessee

UTILIZATION OF POWER PLANT WASTE HEAT FOR HEATING 5C-157
R. W. Timmerman, Consultant, Boston, Mass.

Page No.

HEATING OF GREENHOUSES WITH TEPID WATER — 5C-177
A Fourcy, M. Dumont, A. Freychet, Instiut de Recherche Fondamentale, France

WASTE HEAT USE IN A CONTROLLED ENVIRONMENT GREENHOUSE — 5C-187
E. R. Burns, R. S. Pile, C. E. Madewell, Tennessee Valley Authority, Muscle Shoals, Alabama

UTILIZATION OF WASTE HEAT FROM POWER PLANTS BY SEQUENTIAL CULTURE OF WARM AND COLD WEATHER SPECIES — 5C-213
C. R. Guerra, B. L. Godfriaux, Public Service Electric and Gas Company, Newark, New Jersey

UTILIZATION II (Session 6A) — 6A-1

EXPERIENCE WITH A COMPUTER-BASED STUDY ON WASTE HEAT USAGE FOR INTEGRATED AGRICULTURAL PURPOSES IN MICHIGAN — 6A-3
I. P. Schisler, Michigan State University, East Lansing, Michigan

THE UTILIZATION OF WASTE HEAT FROM LARGE THERMAL POWER PLANTS — 6A-27
L. N. Reiss, Commonwealth Associates, Inc., Jackson, Michigan

USE OF WASTE HEAT FOR AQUACULTURE & AGRICULTURE IN CONJUNTION WITH A SURROGATE NUCLEAR ENERGY CENTER — 6A-29
R. K. Sharma, P. A. Merry, J. D. Buffington, S. W. Hong, and C. Luner, Argonne National Laboratory, Argonne, Illinois

INTEGRATED POWER, WATER AND WASTEWATER UTILITIES — 6A-31
J. P. Overman, C. W. Mallory, and H. M. Curran, Hittman Associates, Columbia, Maryland

NUMERICAL MODELING II (Session 6B) — 6B-32

COMPARISON OF PREOPERATIONAL HYDROTHERMAL PREDICTIONS AND OPERATIONAL FIELD MEASUREMENTS AT THREE NUCLEAR POWER PLANT SITES — 6B-33
G. S. Marmer, A. J. Policastro, Argonne National Laboratory, Argonne, Illinois

Page No.

THERMAL STRATIFICATION AND CIRCULATION OF WATER BODIES SUBJECTED TO THERMAL DISCHARGE 6B-37
A. N. Nahavandi, M. A. Borhani, New Jersey Institute of Technology, Newark, New Jersey

A 3-DIMENSIONAL RIGID-LID MODEL FOR THERMAL PREDICTIONS 6B-85
S. Sengupta, S. Lee, J. Venkata, C. Carter, University of Miami, Coral Gables, Florida

COOLING TOWER PLUMES (Session 6C) 6C-115

SENSITIVITY ANALYSIS AND COMPARISON OF SALT DEPOSITION MODELS FOR COOLING TOWERS 6C-117
T. Overcamp, G. W. Isreal, Clemson University, Clemson, South Carolina

VALIDATION OF SELECTED MATHEMATICAL MODELS FOR PLUME DISPERSION FROM NATURAL-DRAFT COOLING TOWERS 6C-135
A. J. Policastro, B. A. Devantier, Argonne National Laboratory, Argonne, Illinois, R. A. Carhart, University of Illinois, Urbana, Illinois

IMPORTANT CONSIDERATIONS IN A SIMPLE NUMERICAL PLUME MODEL 6C-137
L. D. Winiarski, Environmental Protection Agency, Corvallis, Oregon

UTILIZATION III (Session 7A) 7A-1

PROSPECTS FOR THE UTILIZATION OF WASTE HEAT IN LARGE SCALE DISTRICT HEATING SYSTEMS 7A-3
J. Karkheck, J. Powell, Brookhaven National Laboratory, Upton, New York

EXPLOITING NATURAL OYSTER POPULATIONS THROUGH WASTE HEAT UTILIZATION 7A-27
B. J. Neilson, Virginia Institute of Marine Science, Gloucester Point, Virginia

USING HEATED EFFLUENT FROM A 835 MWe NUCLEAR POWER REACTOR FOR SHELLFISH AQUACULTURE 7A-41
C. T. Hess, C. W. Smith, University of Maine, Orono, Maine

UTILIZATION AND DISSIPATION OF WASTE HEAT BY SOIL WARMING 7A-73
D. R. DeWalle, Pennsylvania State University, University Park, Pennsylvania

Page No.

POTENTIAL RESEARCH PROGRAMS IN WASTE ENERGY UTILIZATION 7A-87
C. C. Lee, Environmental Protection Agency, Cincinnati, Ohio

NUMERICAL MODELING III (Session 7B) 7B-110

MODELING OF A HEATED PLUME DISCHARGE FOR COMPLIANCE WITH WATER QUALITY STANDARDS 7B-111
F. G. Ziegler, Aware, Inc., Nashville, Tenn.

MODEL FOR SHORE-ATTACHED THERMAL PLUMES IN RIVERS 7B-113
P. P. Paily, NALCO Environmental Sciences, Northbrook, Illinois and W. W. Sayre, Institute of Hydraulic Research, University of Iowa, Iowa City, Iowa

SOME PRACTICAL ASPECTS OF THERMAL PLUME ANALYSIS 7B-135
L. L. Stookey, Manchester Laboratories, Inc. Manchester, Iowa

A LONGITUDINAL DISPERSION MODEL FOR SHALLOW COOLING PONDS 7B-143
M. Watanabe and G. H. Jirka, Massachusetts Institute of Technology, Cambridge, Mass.

COOLING SYSTEMS IV (Session 7C) 7C-145

COOLING WATER RESOURCES OF UPPER MISSISSIPPI RIVER FOR POWER GENERATION 7C-147
P. P. Paily, NALCO Envrionmental Sciences, Northbrook, Illinois, T. Y. Su, Sargent and Lundy Engineers, Chicao, Illinois, A. R. Giaquinta, J. F. Kennedy, Institute of Hydraulic Research, University of Iowa, Iowa City, Iowa

INLAND FLORIDA COOLING SYSTEMS 7C-179
A. F. Dinsmore, Brown & Root, Inc., Houston, Texas

INVESTIGATION OF THE FLUID MECHANICAL BEHAVIOR OF A THERMAL STORAGE RESERVOIR FOR DRY COOLED CENTRAL POWER STATIONS 7C-209
M. Golay & E. C. Guyer, Massachusetts Institute of Technology, Cambridge, Mass.

Page No.

DISPERSION OF HEAT AND HUMIDITY FROM ATMOSPHERIC SPRAY COOLING SYSTEMS 7C-243
R. W. Porter, R. H. Weinstein, S. Chaturvedi, R. Kulik, J. Paganessi, Illinois Institute of Technology, Chicago, Illinois

RECENT RESEARCH IN DRY AND WET/DRY TOWERS 7C-285
L. R. Glicksman, Massachusetts Institute of Technology, Cambridge, Massachusetts

UTILIZATION IV (Session 8A) VOLUME III 8A-1

AN OVERVIEW OF WASTE HEAT UTILIZATION RESEARCH AT THE OAK RIDGE NATIONAL LABORATORY 8A-3
M. Olszewski, S. Suffern, C. C. Coutant, K. K. Cox, Oak Ridge National Laboratory, Oak Ridge, Tennessee

DRIFT FROM THE CHALK POINT NATURAL DRAFT BRACKISH WATER COOLING TOWER: SOURCE DEFINITION, DOWNWIND MEASUREMENTS, TRANSPORT MODELING 8A-25
R. O. Webb, G. O. Schrecker, D. A. Guild, Environmental Systems Corporation, Knoxville, Tennessee

A SIMULATION OF WASTE HEAT UTILIZATION FOR GREENHOUSE CLIMATE CONTROL 8A-57
F. P. Incropera & M. C. Freemyers, Purdue University, West Lafayette, Indiana

THERMAL CONTROL OF A SHALLOW POND WITH WASTE HEAT FROM A CLOSED CYCLE COOLING SYSTEM 8A-97
F. Incropera J. Rog, Purdue University, West Lafayette, Indiana

THE AGROTHERM RESEARCH PROJECT 8A-131
H. Luckow, A. Reinken, Thyssen House, Dusseldorf, Germany

PHYSICAL MODELS (Session 8B) 8B-133

THE DISCHARGE OF A SUBMERGED BUOYANT JET INTO A STRATIFIED ENVIRONMENT 8B-135
S. Ostrach, Case Western Reserve University, Cleveland, Ohio

Page No.

HYDRAULIC INVESTIGATIONS OF THERMAL DIFFUSION DURING HEAT TREATMENT CYCLES: SANONOFRE NUCLEAR GENERATING STATION UNITS II AND III 8B-157
M. S. Isaacson, R. C. Y. Koh, E. J. List, California Institute of Technology, Pasadena, California

LABORATORY INVESTIGATION ON SOME FUNDAMENTAL ASPECTS OF THERMAL PLUME BEHAVIOR 8B-181
T. R. Sundaram, E. Sambuco, S. Kapur, A. Sinnarwalla, Hydronautics, Inc., Laurel, Maryland

CASE STUDIES I (Session 8C) 8C-183

SOME SOLUTIONS TO THERMAL PROBLEMS IN THE SOUTHEASTERN UNITED STATES 8C-185
C. H. Kaplan, U.S. Environmental Protection Agency, Atlanta, Georgia

WASTE HEAT IN THE CEGB 8C-197
P. F. Chester, Central Electricity Generating Board, Leatherhead, Surrey, England

THE EXCESSIVE BURDEN AND WASTE OF DUPLICATIVE REGULATION 8C-217
J. H. Hughes, Commonwealth Edison, Chicago, Illinois

NUMERICAL & REMOTE SENSING STUDIES OF LAKE BELEWS AN ARTIFICIAL COOLING LAKE 8C-229
B. McCabe, S. Sengupta, S. Lee, S. Mathavan, University of Miami, Coral Gables, Florida

UTILIZATION V (Session 9A) 9A-1

THE SHERCO GREENHOUSE: A DEMONSTRATION OF THE BENEFICIAL USE OF WASTE HEAT 9A-3
G. C. Ashley, J. S. Hietala, Northern States Power Company, Minneapolis, Minnesota

DECENTRALIZED ENERGY CONVERSION FOR WASTE HEAT UTILIZATION 9A-17
J. R. Schaefgen, U.S. Department of Commerce, National Bureau of Standards, Washington,D.C.

WASTE HEAT EMPLOYMENT FOR ACCELERATED REARING OF COHO SALMON 9A-19
E. Brannon, University of Washington, Seattle, Washington

Page No.

WASTE HEAT UTILIZATION FROM A UTILITY STANDPOINT: THE PROBLEM OF IMPLEMENTATION 9A-29
A. C. Gross, M. C. Cordaro, Long Island Lighting Company, Hicksville, New York

UTILIZATION OF WASTE HEAT FROM NUCLEAR POWER STATION FOR COMMUNITY SPACE CONDITIONING 9A-39
W. Steigelmann, Drexel University, Philadelphia, Pennsylvania

IMPACT ON WEATHER (Session 9B) 9B-41

ATMOSPHERIC EFFECTS OF WASTE HEAT DISSIPATED FROM LARGE POWER CENTERS 9B-43
C. M. Bhumralkar, J. A. Alich, Jr., Stanford Research Institute, Menlo Park, California

EVAPORATIVE COOLING POWER PLUMES: A REVIEW OF BEHAVIOR, PREDICTIONS, AND METEOROLOGICAL EFFECTS 9B-45
H. C. Benhardt, T.E. Eaton, University of Kentucky, Lexington, Kentucky

A NUMERICAL MODELING STUDY OF WASTE HEAT EFFECTS ON SEVERE WEATHER 9B-67
H. D. Orville, South Dakota, School of Mines and Technology, Rapid City, South Dakota

HEAT PLUMES OVER COOLING RESERVOIRS 9B-83
M. A. Estoque, H. P. Gerrish, University of Miami, Coral Gables, Florida

CASE STUDIES II (Session 9C) 9C-85

CASE STUDY - FLORIDA POWER AND LIGHT 9C-87
C. Henderson, Florida Power & Light Company, Miami, Florida

ASSESSING AND SOLVING ENRIONMENTAL PROBLEMS OF POWER PLANT COOLING: AN INTEGRATED APPROACH 9C-89
B. Chezar, R. H. Tourin, New York State Energy Research and Development Authority, New York, New York

THERMAL PLUME EVALUATION PROGRAM OF INDIAN POINT NUCLEAR POWER PLANT 9C-91
H. C. Moy, Consolidated Edison, New York, New York

Page No.

CASE STUDY: NEGOTIATION AND DEMONSTRATION DEVELOPMENT - 316A DEMONSTRATION TYPE II 9C-113
R. S. Schermerhorn, Impact - The Environmental Scientists & Engineers, Denver, Colorado

UTILIZATION VI (Session 10A) 10A-1

WASTE HEAT UTILIZATION FOR DEWATERING SEWAGE SLUDEGE 10A-3
R. E. Birner, A. Ernest, J. H. Schlinta, R. M. Manthe, Metropolitan Sewerage District of the County of Milwaukee, Milwaukee, Wisconsin

THERMODYNAMIC ANALYSIS OF RANKINE CYCLE ENERGY SYSTEMS UTILIZING WASTE HEAT 10A-25
C. D. Henry III, R. Fazzolare, University of Arizona, Tucson, Arizona

POWER PLANT WASTE HEAT - DISASTER OR BOON? 10A-33
K. S. Sunder Raj, Power Authority of the State of New York, New York, New York

WASTE HEAT UTILIZATION IN AQUACULTURE SOME FUTURISTIC AND PLAUSIBLE SCHEMES 10A-35
J. R. Wilcox, Florida Power & Light, Miami, Florida

IN-SITU DATA ACQUISITION (Session 10B) 10B-47

SUBMERGED MULTIPORT DIFFUSER THERMAL DISCHARGES FROM CONDEPTUAL DESIGN TO POSTOPERATIONAL SURVEY 10B-49
T. J. Tsai, B. E. Burris, Stone & Webster Engineering Corporation, Boston, Mass.

OBSERVATIONS OF THERMAL PLUMES FROM SUBMERGED DISCHARGES IN THE GREAT LAKES AND THEIR IMPLICATIONS FOR MODELING AND MONITORING 10B-71
J. D. Ditmars, R. A. Paddock, A. A. Frigo, Argonne National Laboratory, Argonne, Ill.

AN ANALYSIS OF THER THERMAL MONITORING DATA COLLECTED AT THE PEACH BOTTOM ATOMIC POWER STATION 10B-73
A. Witten, D. Gray, Oak Ridge National Laboratory, Oak Ridge Tennessee

MODELING THE INFLUENCE OF THERMAL EFFLUENTS ON ECOSYSTEM BEHAVIOR 10B-103
K. I. Dahl-Madsen, The Water Quality Institute, Denmark

Page No.

MONITORING (Session 10C) 10C-105

STATE OF THE ART OF THERMAL MONITORING PROGRAMS IN THE POWER INDUSTRY 10C-107
J. Z. Reynolds, Consumers Power Company, Jackson, Michigan

EVALUATION OF ENVIRONMENTAL IMPACT PREDICTIONS 10C-119
P. A. Cunningham, Oak Ridge National Laboratory, Oak Ridge, Tennessee

THE QUALITY AND COST OF INFERENCES CONCERNING THE EFFECTS OF NUCLEAR POWER PLANTS ON THE ENVIRONMENT 10C-139
D. A. McCaughran, University of Washington, Seattle, Washington

THE STATE-OF-THE-ART OF ENVIRONMENTAL AND THERMAL PERFORMANCE MONITORING TECHNIQUES FOR CLOSED-CYCLE COOLING SYSTEMS 10C-159
G. O. Schrecker, K. R. Wilber, R. O. Webb, Environmental Systems Corporation, Knoxville, Tennessee

OPEN SESSION I (Session 11A) 11A-1

EFFECTS AND CONSEQUENCES OF POWER PLANT INDUCED MORTALITY ON THE SAN FRANCISCO BAY-DELTA STRIPED BASS POPULATION 11A-3
M. W. Lorenzen, Tetra Tech, Inc., Lafayette, California

SURFACE HEAT TRANSFER FROM A GEOTHERMALLY-HEATED LAKE 11A-43
A. Miller, Jr., Brigham Young University, Provo, Utah; R. L. Street, Stanford University, Stanford, California

PATTERNS OF THERMAL PLUME CONFIGURATION: IMPLICATIONS FOR ENVIRONMENTAL IMPACT ASSESSMENT AND RESOURCE MANAGEMENT 11A-63
R. C. Baird, Geo-Marine, Inc, Richardson, Texas

A STRIPED BASS MODEL FOR POWER PLANT EVALUATION 11A-87
C. W. Chen, Tetra Tech, Inc., Lafayette, California

Page No.

OPEN SESSION II (Session 11B) 11B-111

PREDICTION OF COMBUSTION CHARACTERISITCS FOR REFUSE-DERIVED FUEL (RDF) 11B-113
R. J. Schoenberger, J. Gibs, Drexel University; K. Sonsteby, Pennsylvania Power & Light Company; A. M. Arndt, Lehigh County Authority; R. M. Gruninger, Malcolm Pirie, Inc., Philadelphia, Penn.

MINNESOTA AERIAL INFRARED PROGRAM 11B-115
S. Stewart, Minnesota

INTEGRATED STEAM SYSTEMS FOR ELECTRIC POWER GENERATION FROM WASTE HEAT 11B-117
J. P. Davis, Energy Systems Thermoelectron Corporation, Waltham, Mass.

EFFECTS ON ECOSYSTEMS 11B-131
M. T. Masnick, U.S. Nuclear Regulatory Commission, Washington, D.C.

A COMPARISON OF THE BIOLOGICAL EFFECT OF HEATED EFFLUENTS FROM TWO FOSSIL FUEL PLANTS IN THE FLORIDA SUBSTROPICS: ONE EAST COAST, ONE WEST COAST 11B-133
A. Thorhaug, University of Miami, Coral Gables, Florida

SESSION IV-A
NUMERICAL MODELING I

1-45-15

NUMERICAL MODELS IN COOLING WATER CIRCULATION STUDIES: TECHNIQUES, PRINCIPLE ERRORS, PRACTICAL APPLICATIONS

G. S. Rodenhuis
Danish Hydraulic Institute
DK-2970 Hørsholm, Denmark

ABSTRACT

Four principle models used in cooling water circulation studies are introduced. The coupling problems arising when information has to be transferred from one model to another are discussed and sources of possible errors identified. The errors introduced when the various equations involved are solved, are described together with possible techniques to avoid such errors. The paper demonstrates that no fail-safe methods are available and suggests that results are used only with full awareness of the possible errors.

INTRODUCTION

In a conference on waste heat management the objectives of the modeling work in connection with the design of a large thermal plant need no explanation. In this paper we shall look at the problems that arise and the possible errors that may occur when numerical models are used for predictions of the distribution of temperatures around the point of outfall and for the computation of the transport and dispersion of the waste heat in the receiving water body. Estimates of the possibility of recirculation and of the ecological impact are based on such models. The point that we wish to make is that results of such models should be used with a full awareness of problems and sources of possible errors.

Before going into these aspects of numerical modeling it may be relevant to set-off numerical modeling against physical modeling. Why is it that the modeling work is mainly done with the use of numerical models? The answer lies in the fact that dispersion of heat and transfer to the atmosphere are difficult to model and this is again related to modeling of the different scales of turbulence. Abraham - Ref.[1]- demonstrates in fact that turbulent stresses and transports can be modeled correctly, but only for conditions with a high Reynolds number and where

---

Figures referred in the text are given at the end of the paper.

Preceding page blank

a critical value for this number can be established as a solid experimental fact. Jet flow is a problem where this criterion applies.

For computations of the transport and dispersion of heat away from the outlet - the far-field - mathematical models have to be used. The fact that often irregular flow patterns and topographies have to be described means that mathematical models usually are numerical models rather than analytical. However, here the problem of correctly representing the physical processes is hardly smaller. This problem is principally related to lack of detail in the description in the models. The equations describing the instantaneous movements of particles in three dimensions are intractable. In order to have a"workable"model we have to use time and space averaged forms and this introduces dispersion terms. Fickian-type formulations appear to give a workable description. However, the wide variety of time and length scales involved makes a unified approach with universally applicable expressions for the dispersion coefficient in these formulations impossible. The correctness of the description of the physical processes in mathematical form is discussed extensively in the literature. Although we may here have a first source of errors, we do not intend to discuss these in this paper.

In order to arrive at "workable" models it is furthermore necessary to divide the region in which the processes of dilution, transport, dispersion and transfer to the atmosphere take place into a near-field around the discharge and a far-field, with different models for the processes in these fields. This introduces the problem of coupling these various models and here errors can be introduced. The models that we shall consider in this connection are a plume model for the near-field and hydrodynamic (HD) and transport-dispersion (TD) models for the far-field. The plume model we have in mind has the form of a Gaussian distribution of velocity and excess temperature around a centerline value. The hydrodynamic model in this connection is usually an expression of the vertically integrated equations of conservation of mass and momentum over one or two horizontal dimensions. Associated with this is a one or two dimensional TD-model. For later reference we give here the form for two-dimensions

$$\frac{\partial c}{\partial t} + u\frac{\partial c}{\partial x} + v\frac{\partial c}{\partial y} = \frac{1}{h}\,\frac{\partial}{\partial x}\,(hD_x\frac{\partial c}{\partial x}) + \frac{1}{h}\,\frac{\partial}{\partial y}\,(hD_y\frac{\partial c}{\partial y}) - \frac{\alpha c}{h} + \Sigma\,\frac{Q_L(c_L-c)}{h\;\Delta x\;\Delta y} \qquad (1.1)$$

where the rotation is

c - excess temperature
c_L - excess temperature discharged
u,v - horizontal velocity components, integrated over depth,

in resp. x- and y-directions
h - water depth
D_x, D_y - dispersion coefficients in resp. x- and y-directions
Q_L - discharge of outlet
α - first order decay factor for heat.

In order to assess ecological impact the three hydraulic models may be supplemented with an ecological mathematical model.

As will be discussed, coupling problems exist between all four models. Apart from errors arising from such problems the numerical solution of the actual equations may also introduce errors. These are usually related to a necessary discretisation of the domain of the models.

Before continuing with a discussion of possible errors it must be remarked that it lies in the nature of the problem that computed results even when including considerable errors usually look "reasonable". The TD-model seldom becomes unstable or otherwise indicates its incorrectness. It is difficult to judge from a plot of temperature contour lines whether the results are correct or incorrect.

COUPLING PROBLEMS

Coupling of Near-Field and Far-Field Models

At the outfall of a thermal power plant a certain mass of water with a certain amount of waste heat is discharged into the receiving water body with a certain amount of momentum. Using a plume model, the distribution of these quantities around the outfall can be modeled. The effect of introducing mass and momentum should be represented in the HD-model that is used to describe the far-field hydrodynamics and the excess temperature distribution around the outfall must be transferred to the TD-model. However, the resolution in HD and TD-models is usually quite different than that used in plume models. In fact most HD and TD-models have a discrete representation, whereas plume models usually have a continuous representation. In the process of transferring quantities computed in the plume model to the other models, errors are introduced.

Coupling Plume and HD-Model

Buoyancy and remaining jet momentum induce horisontal velocities in the receiving water body. If a high velocity surface jet is utilized the jet momentum can induce a current pattern which can be of considerable importance for the shape of the entire temperature field, especially in situations where the currents in the receiving water body are weak. One should consider here that the instantaneous shape of the jet usually is a meandering plume. Averaged over a certain time the jet appears as a much wider 'steady-state' plume. Clearly these effects are difficult to represent in, for example, a finite difference HD-model where the grid size must be in the order of hundreds of meters for reasons of computational economy.

Coupling HD and TD-model

The mass of the discharged water can be represented in the HD-model as lumped over a few meshes of the grid and this procedure needs not introduce errors. However, an error can be introduced by incorrect coupling of the equation of mass of the HD-model with the equations of the TD-model. The error can be easily avoided by following a correct modeling procedure. The point is, however, that when this error is made it is not easily detected. Another error, that of numerical dispersion, may mask it.

A HD-model is usually used to create the flow distribution in the receiving water body. Neglecting the contribution of the source in the mass-equation in this model will hardly be noticed in the velocity field obtained as the more important contribution of momentum is also - out of necessity - neglected. Observing little effect in the HD results may tempt one to neglect the source term in the mass equation when deriving the equations for the TD-model. We may illustrate this below.

In deriving the TD-equation (1.1) given in the previous section from the principle equation

$$\frac{\partial (hc)}{\partial t} + \mathrm{div}(h\bar{V}c) - \mathrm{div}(h\bar{\bar{D}}\,\mathrm{grad}\,c) + \alpha c = \Sigma Q_L c_L \qquad (2.1)$$

, the hydrodynamic mass equation

$$\frac{\partial h}{\partial t} + \mathrm{div}(h\bar{V}) = \Sigma Q_L \qquad (2.2)$$

, should be used. The source term resulting in eq. 1.1 has the form

$$\Sigma\ \frac{Q_L(c_L-c)}{h\ \Delta x\ \Delta y} \qquad (2.3)$$

However, if the contribution of the source is neglected in eq. 2.2 the source term will be

$$\Sigma\ \frac{Q_L\ c_L}{h\ \Delta x\ \Delta y} \qquad (2.4)$$

The notation here is that of the previous section with further

$\overline{V}$, the vector (u,v)

$\overline{\overline{D}}$, the matrix $\begin{bmatrix} D_x & 0 \\ 0 & D_y \end{bmatrix}$

The effect on the temperature distribution around the source is dramatic; the temperature will in fact rise with each following step in time in the computations. The effect is shown in Figs. 1.a, b and c, where results are presented obtained in connection with a site selection study made for a combined desalination and power plant on the east coast of Saudi Arabia. The discharge of this plant will be 176 m^3/s with an excess temperature of 7°C. Fig. 1.a shows the most correct solution in which the mass term is included in the equation and where no numerical dispersion is present. Fig. 1.b shows the same situation, now neglecting the mass term, but still without numerical dispersion: high temperature around the outlet causes the 1°C contour to stretch over a much larger area. Fig. 1.c shows the same situation now neglecting the mass term and with numerical dispersion. One observes that both errors almost cancel each other: the results resemble those of Fig. 1.a. So even with two considerable errors the results may still look reasonable! In Fig. 1.d results from a hydrodynamic model are shown for the strait between Saudi Arabia and the island of Bahrain. The velocity field for the TD-model is taken from this HD-model.

Coupling Plume and TD-model

The mass error and, as we shall see, also numerical dispersion can be avoided. Transferring the temperature distribution from the plume model to the TD-model presents a more principle problem. The usual approach is to assume that waste heat is distributed over a few grid spaces and uniformly mixed from bottom to surface. The integral value of excess temperature times volume, taken per unit time, is set equal to the waste heat discharged, but different volume, excess temperature products may be taken to correspond to the same amount of waste heat. It is difficult to make this distribution equivalent to that obtained in the plume model where the distribution is principly three-dimensional. Using a different number of grid spaces for the near field distribution gives different far-field contour lines. The difference is greatest close to the source and becomes less further away. However, with a very different near-field distribution the picture of the contour lines will be very different. An extreme example is given in Figs. 2.a and b. The results shown are obtained in connection with the site investigation for a 4000 MW nuclear plant in Denmark. Fig. 2.a shows the contour picture obtained with a near-field distribution over eight grid spacings, whereas in Fig. 2.b the distribution is over only one grid spacing. Of course the very high excess temperature in the last case will lead to a high rate of heat loss to the atmosphere and the contours cover a smaller area. Again numerical dispersion could mask the error caused by an incorrect near-field distribution.

The choice of near-field distribution in the TD-model must of course be guided by the results obtained in the plume model, but because of the different character of the two models the transfer will always be imperfect.

The problem outlined above is, however, not the only principle problem in coupling a plume model to a TD-model. The plume model assumes a certain temperature of the ambient water. Characteristics of the plume such as entrainement and buoyancy are dependent on this ambient temperature. One should realise in this connection that the 'far-field' is also present near the outlet. This is especially the case for a coastal outlet with an oscillating tidal current along the coast. In the case of a power plant with a large waste heat discharge the temperature in the area around the outlet will build up and the entraining water will already be heated. This leads us to a circular problem in modeling: in order to compute the near-field temperature distribution by means of a plume model the ambient temperature must be known, but in order to compute the ambient temperature one must compute the far-field distribution and this is in turn dependent on the near field distribution given by the plume. One is forced to some sort of iterative procedure if accurate answers are to be obtained.

After having looked at these problems of coupling we can conclude that our difficulties stem principally from handling the problem in separate models and from differences in resolution of these models. This approach is imposed by engineering necessity. The problem of difference in resolution may be reduced by using a model with varying resolution: detailed around the outlet, with a coarser grid away from the outlet. A Finite Element Model allows a net with small elements around the outlet gradually changing to larger elements further away. In a Finite Difference Model a change-of-scale can be used, using a local patch of high resolution in an otherwise coarse grid.

The circular problem of the value of the ambient temperature to be used in the plume computation is hard to overcome. One is in fact looking for a "complete" model, where the near-field and far-field temperatures are computed simultaneously. Attempts have been made to develop such a model using the Marker-in-Cell technique. The entire flow region in three dimensions is divided into a sufficient number of cells and the computation procedure is based on the approximate satisfaction of the integral form of the conservation equations for each cell at every time step; the approach is conceptually that of "box" modeling. The demand on computer storage and time is, however, excessive and for engineering applications not acceptable.

Coupling with Ecological Models

Temperature is an important forcing function in biological and chemical processes. Ecological models can be applied to compute the consequences of discharges of waste heat. However, such models usually deal with slowly varying processes with a time scale expressed in weeks and months. The information required has for example a form as "number of days per year for which a certain temperature level is exceeded". There is a clear conflict of time scales between the models for temperature distribution and the ecological models. The approach usually is to simulate in the temperature distribution models a short period that is statistically equivalent to the period required in the ecological model. This last period can be, for example, a year. This introduces a statistical interface between the temperature distribution models and the ecological model. Errors will be introduced, if the quality or quantity of the data on which the statistics are to be based, is insufficient.

There is also a conflict in the spatial scales between the HD- and TD-models and an ecological model. In a complex ecological model a large number of ordinary differential equations have to be solved for each mesh considered. If a grid of the same mesh size as used in the HD- and TD-models would be used in order to obtain detailed information on fluxes, the cost of computation would become prohibitive. An averaging of hydraulic conditions must be introduced with, as a consequence, a loss of accuracy.

For a more detailed discussion of the use of ecological models in power plant site studies we refer to the paper by K.I. Dahl Madsen - Ref.[2]- in this Conference.

NUMERICAL TECHNIQUES AND ERRORS

In this section we shall limit the discussion to errors in the TD-models and techniques to avoid these. Not that the other models have no errors, but particularly in the TD-model the errors are difficult to detect and the results may give a false impression of correctness. Moreover, the TD-model has a central rôle in waste heat studies.

When the continuous differential equation of transport and dispersion is represented on a discrete grid errors can be introduced. Well-known is the numerical dispersion that may be introduced. But although well-known it is difficult to avoid without introducing other errors. We may in short recall how this error is introduced. A simple finite difference approximation of the terms

$$\left[\frac{\partial c}{\partial t}\right]^{n+1}_{n,j} + \left[u\,\frac{\partial c}{\partial x}\right]^{n}_{n} - - - - \qquad (3.1)$$

to $$(c_j^{n+1} - c_j^{n})/\Delta t + u(c_j^{n} - c_{j-1}^{n})/\Delta x \qquad (3.2)$$

introduces the truncation error

$$u(\Delta x - u\Delta t)\,\frac{\partial^2 c}{\partial x^2} - - - - \qquad (3.3)$$

, which has the form of a dispersion term. The term depends on the choice of the grid and the magnitude of the advective velocity. Its value may be many times that of the physical dispersion and may completely invalidate the results.

In order to avoid this error one may resort to higher order difference approximations. However, then a residual numerical radiation and skewness appear. The various effects are illustrated in Fig. 3.

Numerical oscillations also may be introduced by use of an inappropriate scheme. For example, the transport equation

$$\frac{\partial c}{\partial t} + u\frac{\partial c}{\partial x} = 0 \qquad (3.4)$$

may be approximated by the centred, second order difference scheme

$$\tfrac{1}{2}\left(\frac{c_j^{n+1} - c_j^{n}}{\Delta t} + \frac{c_{j-1}^{n+1} - c_{j-1}^{n}}{\Delta t}\right) + \frac{u}{2}\left(\frac{c_j^{n+1} - c_{j-1}^{n+1}}{\Delta x} + \frac{c_j^{n} - c_{j-1}^{n}}{\Delta x}\right) = 0 \qquad (3.5)$$

However, when initially $c_j^{0} = 0$ for all j and u is constant, this provides

$$c_j^{1} = -\left(\frac{1 - u\frac{\Delta t}{\Delta x}}{1 + u\frac{\Delta t}{\Delta x}}\right)c_{j-1}^{1} \qquad (3.6)$$

$$= (-1)^j\left(\frac{1 - u\frac{\Delta t}{\Delta x}}{1 + u\frac{\Delta t}{\Delta x}}\right)^j c_0^{1} \qquad (3.7)$$

which oscillates for all Courant numbers $Cr = u\Delta t/\Delta x$, satisfying $|Cr|<1$.

Higher order approximations have the disadvantage that they extend over more and more grid points with increasing orders of approximation. This presents problems at the boundaries. Artificial assumptions for the approximation have to be made and errors are introduced.

One method to avoid all such types of errors is to apply a Lagrangian type of model. The advective term is then in fact cut out by moving in a local frame with the local velocity at each grid point. When this procedure is followed in a flow field varying in time and space, the grid will distort to unwieldy forms. Therefore the local frame is moved only for one time step and the information obtained is then transferred back to points in a fixed grid. One may also express it in a complimentary form: given a fixed grid at time $t_o + \Delta t$ where was the information now in grid point B at time t_o. The principle is illustrated in Fig. 4. Following this principle a practical model has been developed at the author's Institute.

The method requires a sophisticated interpolation technique to determine the values of concentration (or temperature) in the points at time t_o, relative to the given fixed grid. The interpolation used is based on a 12-point Everett interpolation. The "correctness" of this approach is best illustrated in a so-called rotation test in which a Gaussian distribution is rotated in a two-dimensional grid around a center point located outside the distribution. Results are presented in Fig. 5. It may be observed that the shape is fairly well preserved in this rather tough test.

This type of approach may also be used with a Finite Element Model. As the F.E.M. technique does not give solutions in discrete grid points, but as solution surfaces over elements, the interpolation is not required (- or is in fact already included in the F.E. M. technique). Clearly higher order elements are necessary to obtain results without erroneous dispersion. However, compared with finite difference schemes F.E.M. models are usually found to be considerably more expensive for time varying solutions.

The 12-point scheme introduced above also requires special formulations at the boundaries, but satisfactory approximations can be obtained. Simply using the correct zero concentration value for points beyond a land boundary gives good results. This is demonstrated in a so-called L-test in Fig. 6.a.

The propagation of a circular distribution around a sharp corner is depicted for a sequence of time steps. One observes that the circular form is preserved for the stretch before the corner. It is distorted beyond the corner, but this is physically realistic. The deformation is caused by the flow field around the corner. In order to illustrate how an incorrect scheme with considerable numerical dispersion may distort a circular distribution, corresponding results of such a scheme are shown in Fig. 6.b.

At open water boundaries also special attention is required. However, satisfactory results are usually obtained when such boundaries are recognized as being either inflow or outflow boundaries, with an assumption on the mixing conditions in the water body beyond the boundary.

A quite different method, that probably is the most accurate, is based on a spectral technique. The method is developed for an application in atmospheric pollution by Christensen and Pram - Ref. 4. The technique was applied to hydraulic problems in the author's institute. The method is very accurate, but computer costs are about four times as high as for the 12-point scheme. The method also has limitations with regard to resolution of realistic topographies. In short the technique is as follows: It is assumed that c can be approximated by a finite Fourier representation

$$f(x,t) = \sum_{k}^{K} A(k,t)\, e^{ikx}, \text{ with } i = \sqrt{-1} \qquad (3.8)$$

For a given continuous function f(x,t) one can always find A(k,t) such that f(x,t) = c(x,t) on grid points $x_j = j\Delta x$:

$$A(k,t) = \frac{1}{J} \sum_{j}^{J} c_j(t)\, e^{-ik\, j\Delta x} \qquad (3.9)$$

The simple equation

$$\frac{\partial c}{\partial t} + u\frac{\partial c}{\partial x} = 0 \qquad .10)$$

transforms to

$$\frac{\partial A(k,t)}{\partial t} + u\, i\, k\, A(k,t) = 0 \qquad (3.11)$$

From this equation A(k,t) can be computed at each new time $n\Delta t$ with A(k,t) given, c can be obtained from an inverse Fourier-transform. The point here is to note that the advection term in (3.11) is not approximated by a finite difference form so that numerical dispersion is avoided.

DISCUSSION

A discussion of modeling problems and errors may leave the reader with a rather gloomy impression of the whole modeling effort. And there is more, in addition to the problems discussed there are the difficulties encountered when dispersion coefficient and heat transfer coefficients have to be selected. Field investigations before the plant has been constructed can only give a very limited impression of the mixing characteristics of the receiving water body, as discharge volume, discharge momentum and buoyancy cannot be represented.

However, if the models are used with an awareness of the inaccuracies and if sensitivity tests are made for the important parameters, usefull predictions can be made. Such predictions would allow design considerations of outlet-intake construction cost against possible recirculation as discussed in the paper by Schrøder - Ref.[5] - in this Conference, and an evaluation of ecological consequences.

We may underline the above statement with a final result. The possibility of simulating the transport-dispersion process over an extended period of time in a realistic topography is illustrated in Fig. 7. The transport and dispersion of a conservative substance with an irregular release - 16 hrs out of 24 per day - is simulated. The area concerned is Køge Bay, south of Copenhagen. In a sequence of plots the development of the concentration field from an initial distribution to the situation after one week is shown. The results after one week are compared to measurements. One may observe that after having been through considerable changes, the characteristics of the field after seven days compare well with measurements.

ACKNOWLEDGEMENT

The present paper is based on research by the staff of the Computational Hydraulics Centre of the Danish Hydraulic Institute.

REFERENCES

1. Abraham, G. 'Methodologies for Temperature Impact Assessment'. European Course on Heat Disposal from Power Generation in the Water Environment. Delft Hydraulics Laboratory, Delft, the Netherlands, 1975.

2. Dahl Madsen, K.I., "Modeling the Influence of Thermal Effluents on Ecosystem Behaviour". This Conference.

3. Abbott, M.B., "Computational Hydraulics: A Short Pathology". Journal of Hydraulic Research 14 (1976) No. 4.

4. Christensen, O. and Prahm, L.P., "A Pseudospectral Model for Dispersion of Atmospheric Pollutants". Danish Meteorological Institute, Lyngbyvej 100, Copenhagen, Denmark. 1976.

5. Schrøder, H., "Selection of Alternative Coastal Locations". This Conference.

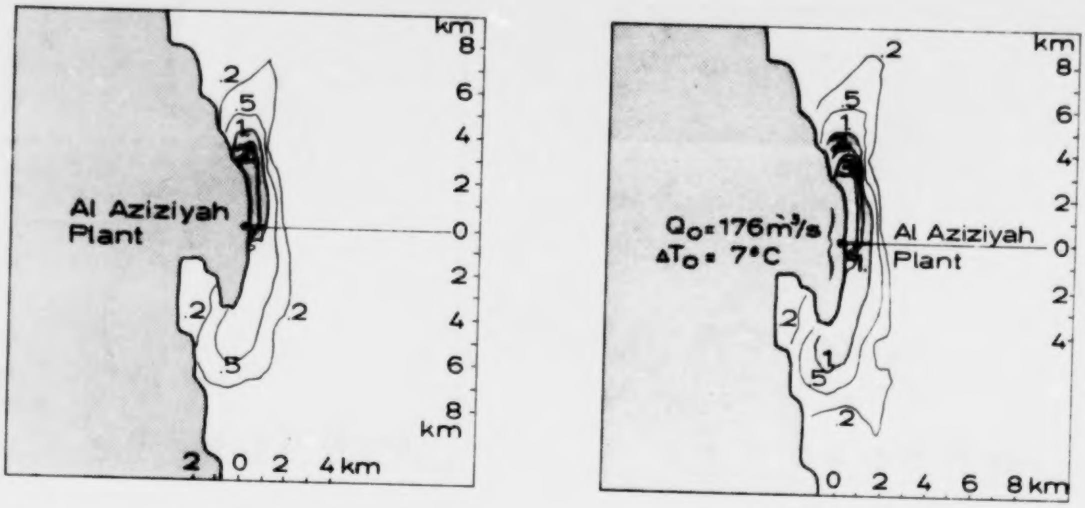
km
8
6
4
2
0
2
4
6
8
km
Al Aziziyah
Plant
.2
.5
1
.2
.2
.5
2 0 2 4km
km
8
6
4
2
0
2
4
Q_0=176m³/s
ΔT_0 = 7°C
Al Aziziyah
Plant
.2
.5
1
.2
1
.5
.2
0 2 4 6 8km

(a) most correct solution
- mass term included
- no numerical dispersion

(b) - mass term not included
- no numerical dispersion

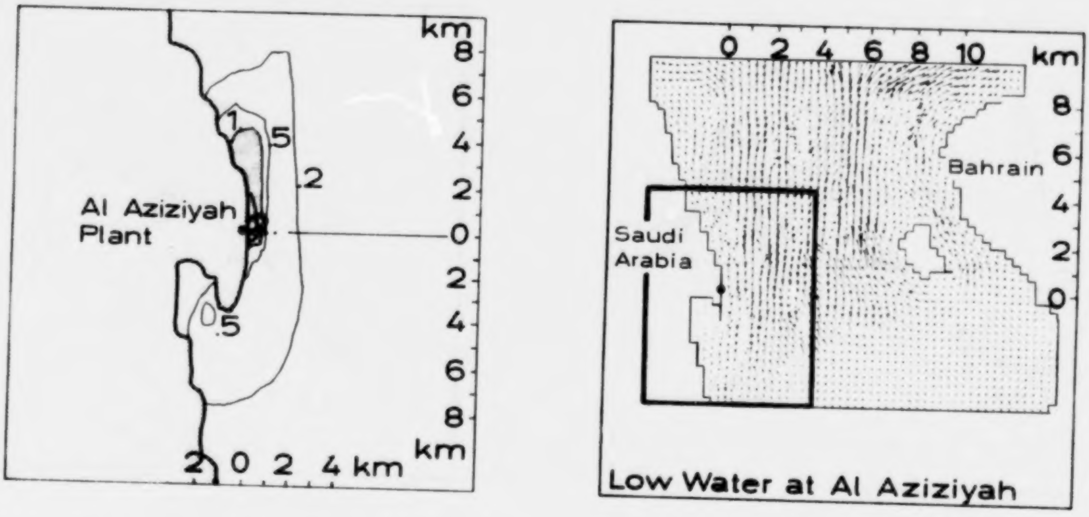
km
8
6
4
2
0
2
4
6
8
km
Al Aziziyah
Plant
1
.5
.2
0.5
2 0 2 4 km
0 2 4 6 8 10 km
8
6
4
2
0
Bahrain
Saudi
Arabia
Low Water at Al Aziziyah

(c) - mass term not included
- with numerical dispersion

(d) - flow pattern in the strait between Saudi Arabia and Bahrain

Fig. 1: Computed Temperature Contour Lines for the Al Aziziyah Desalination and Power Plant, with Different Types of Errors.

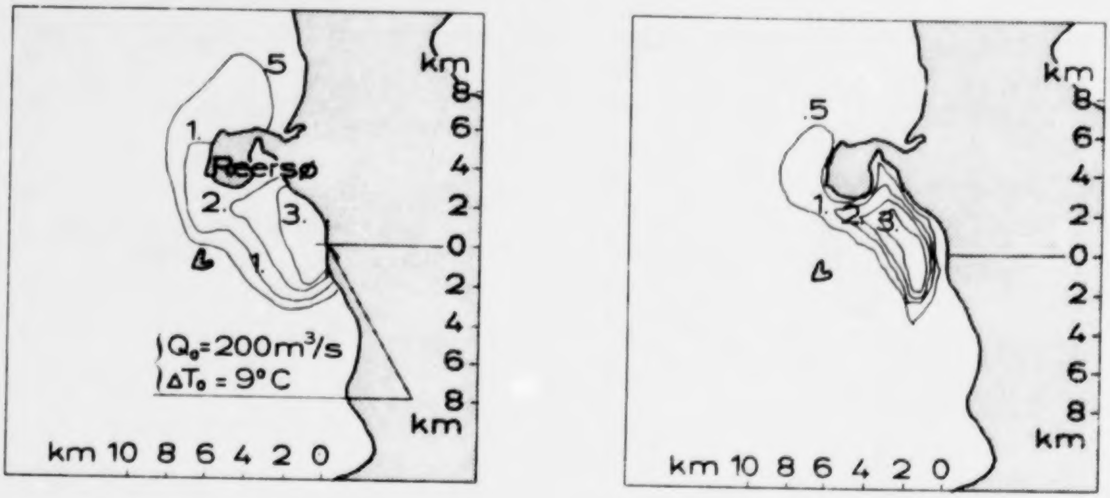
5
1.
Roersø
2.
3.
1.
km
8
6
4
2
0
2
4
6
8
km
Q_0=200m³/s
ΔT_0 = 9°C
km 10 8 6 4 2 0
.5
1. 2. 3.

(a) Near-field: Eight meshes (b) Near-field: One mesh

Fig. 2: Influence of near-field distribution on far-field contours.

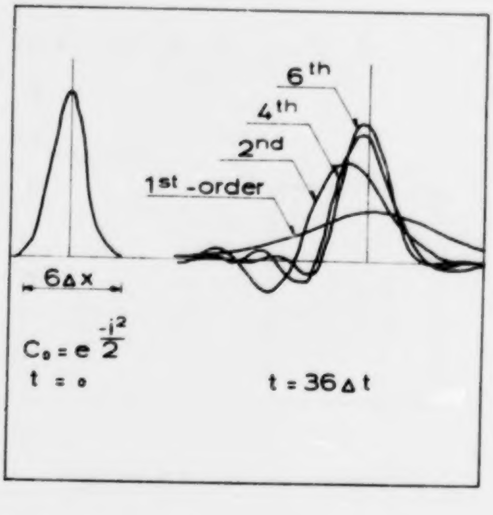

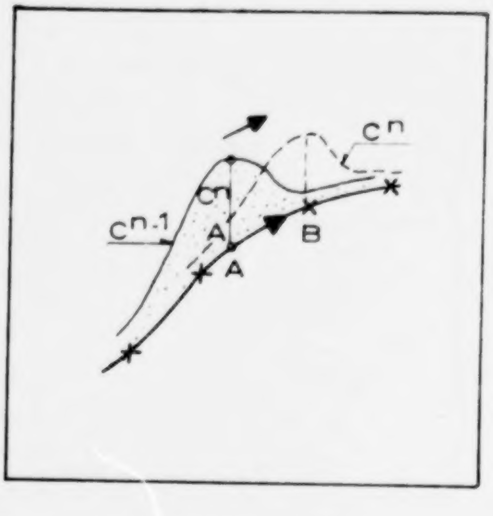
C^n
C^n
C^{n-1}
A
A
B

Fig. 3: Examples of Errors in Difference Approximations to Transport-Dispersion Equations.

Fig. 4: Principle of 12-Point Scheme.

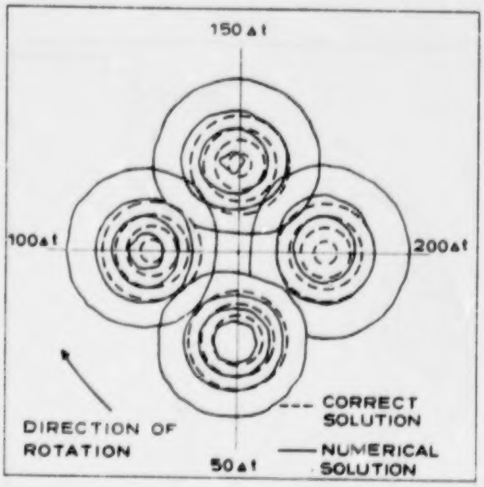

Fig. 5: Rotation Test,
12-Point Scheme.

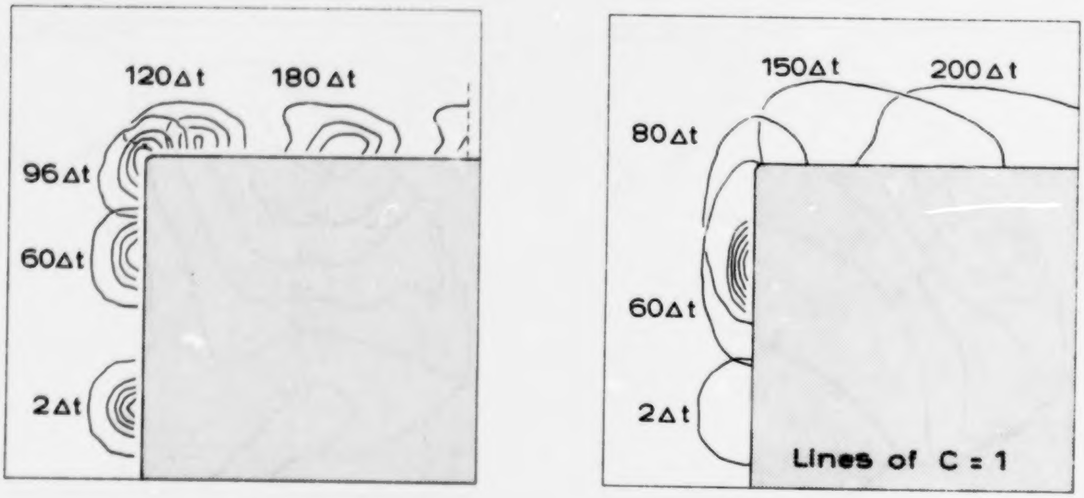

(a) 12-Point Scheme

(b) Scheme with Numerical dispersion

Fig. 6: L-Test of Different Difference Schemes.

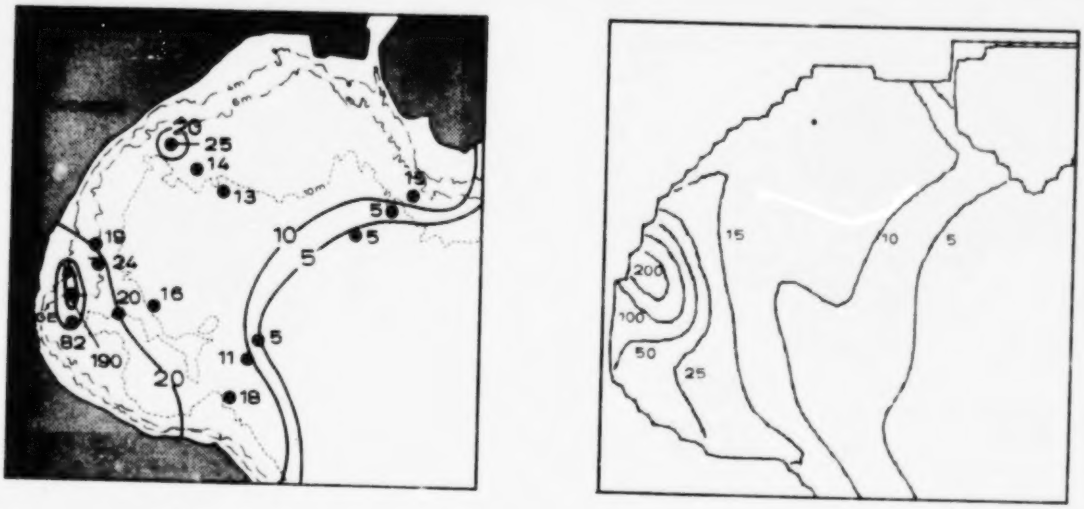
20
25
14
13
15
50
10
5
5
19
24
20
16
5
11
18
82
190
20
15
10
5
200
100
50
25

(a) - recorded 0 hrs

(b) - computed 23 hrs

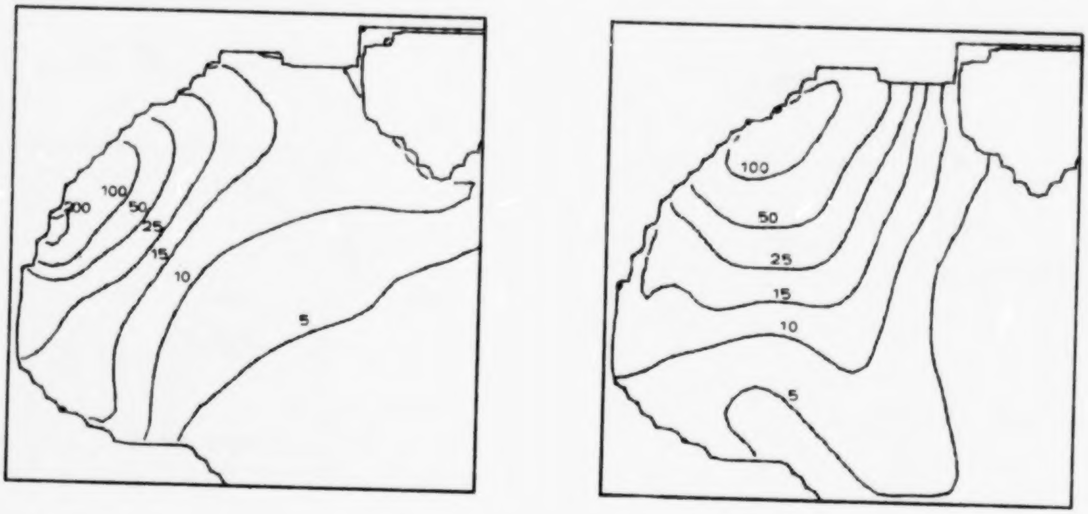
200
100
50
25
15
10
5
100
50
25
15
10
5

(c) - computed 71 hrs

(d) - computed 111 hrs

Fig. 7. a-d: Sequence of Recorded and Computed Concentration Contours for Køge Bay.
Source: 16 hrs on, 8 hrs off per 24 hrs, with 2 x 24 hrs off during weekend between 88 hrs and 144 hrs.
Load: 168 gram/sec.

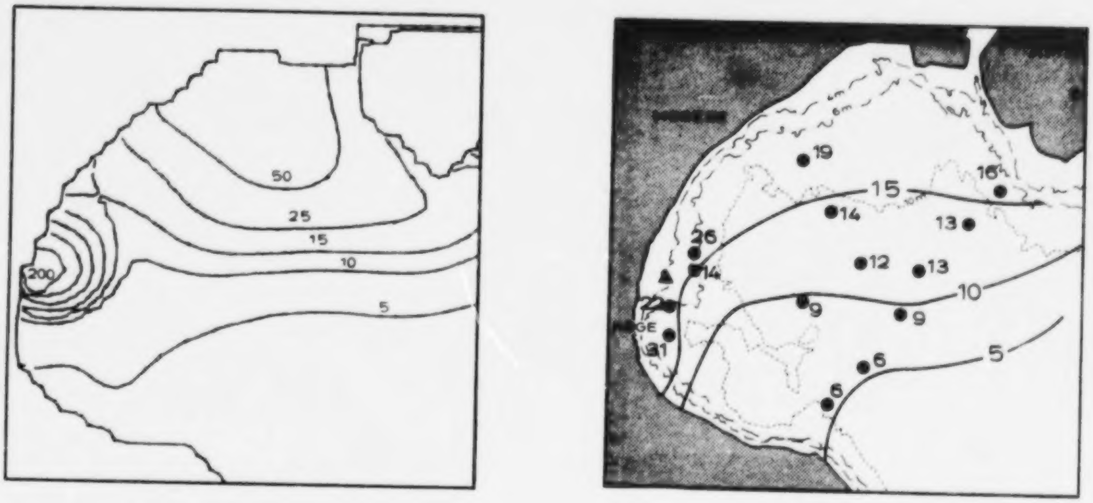
50
25
15
10
5
200
19
16
15
14
13
26
14
12
13
10
9
9
5
6
6
21

(e) - computed 168 hrs

(f) - recorded 168 hrs

Fig. 7. e-f: Sequence of Recorded and Computed Concentration Contours for Køge Bay, Continued.

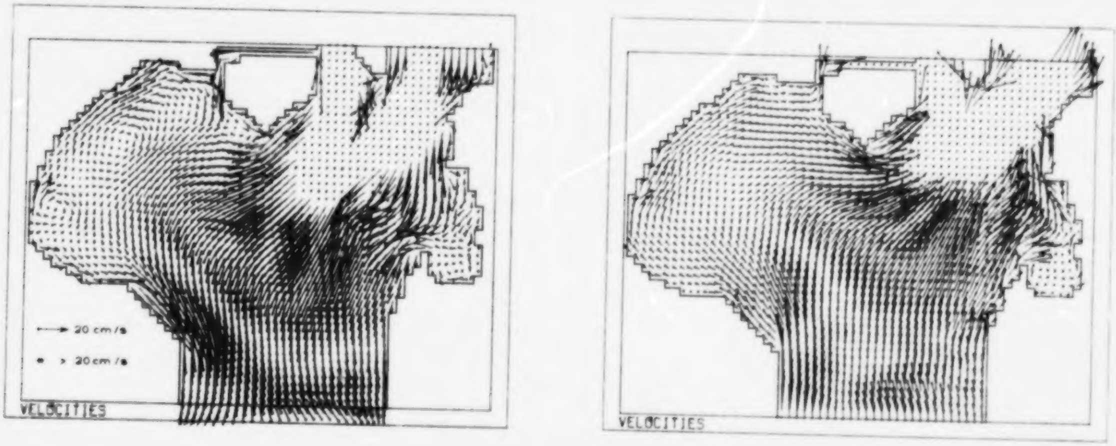
20 cm/s
> 20cm/s
VELOCITIES
VELOCITIES

(g) - typical flow pattern at 27 hrs, southgoing current in the Sound, westerly winds 10-15 m/s

(h) - typical flow pattern at 51 hrs, northgoing current in the Sound, southerly winds 8-10 m/s

Fig. 7. g-h: Typical Flow Patterns.

omIT

Waste heat management and utilization. Miami Beach, 9-11 May 1977

Abstract:

Prediction of temperatures resulting from once-through cooling of a 5000 MWe power station along an estuary.

The Borssele power-plant is located along the Western Scheldt estuary in the Netherlands. Its present capacity is 860 MWe.
In view of future demands for electrical energy, the possibilities have been investigated for a plant expansion to a capacity of 5000 MWe.
As the Western-Scheldt is a tidal estuary, during a certain part of each tidal period the cooling-water intake will be on the downstream side of the outlet. Consequently recirculation of heated effluent may occur, especially because of the relative short distance between the existing and the projected outlet and intake locations.
In view of these considerations the study concentrated upon the following questions:

- which design to select for the new intake and the new outlet to minimize recirculation, taking the existing cooling-water circuit into account
- predicting the temperatures in the existing and the new intake
- predicting the elevation in background temperatures of the ambient water.

Whereas the last question could be solved by mathematical computation, the first and the second questions necessitated the use of a hydraulic model. The effects of the design of intake and outlet and the irregularity of the near field geometry upon recirculation are not sufficiently incorporated in the existing mathematical prediction techniques.
The study was therefore divided into the following parts:

- a hydraulic model study to evaluate two basically different designs of both the new outlet and the intake and to optimize further the selected design
- a mathematical model study to determine the effect of return heat upon the intake temperatures and the environmental effects
- a field study to obtain data both to verify the hydraulic model and to be used as input for the mathematical model.

Preceding page blank

Two designs were tested in a non-distorted hydraulic model, having a scale of 1 in 75, representing a prototype area of 4 km along the shore on both sides of the plant site and 2 km perpendicular to the shore:

- a high initial mixing design, effectuated with a multiport diffuser system, in combination with open intake channels, and
- a low initial mixing design, achieved by means of a wide shallow outlet channel, in combination with a skimmer-wall intake.

As a result of this evaluation the multiport diffuser system was selected and further optimized in the model, which lead to considerable economization of the design.

The dispersive characteristics occuring in the estuary were obtained from instantaneous dye release measurements. The variation of concentration with time as observed in these experiments is assumed to be representative for all subsequent releases into which the continuous release of the heated effluent is divided. This assumption constitutes the basis of the superposition method. This method is applied in the two-dimensional mathematical model of the estuary. The computations resulted in time-dependent temperature elevations along the length of the estuary, indicating the extent of the volume of water affected by the effluent and the additional recirculation due to return heat, for various meteorological conditions.

The overall result of both hydraulic and mathematical analysis was the realization of a once-through cooling system combining minimum recirculation with an acceptable environmental impact.

2-45-20

THREE-DIMENSIONAL FREE SURFACE MODEL FOR THERMAL DISCHARGE

S.Lee, S. Sengupta, C. Tsai, H.Miller
Dept. of Mechanical Engineering
University of Miami
Coral Gables, Florida U.S.A.

(A) INTRODUCTION

As the result of economic and population growth, the demand for electrical power has been doubling every decade since World War II in the U.S. The rapid increase both in electricity production and in the unit size of thermal power plants has resulted in use of large quantities of water for cooling purposes. The most common system for heated effluents dsposal is the open cycle system where the condenser cooling water is discharged back into the natural waterway. Analysis of thermal discharge with a view to decreasing environmental effects and increasing the cooling efficiency has become an important part of power plant siting evaluations.

In the past years, numerical models have been developed by many researchers for predicting the velocity and temperature distribution in thermal plumes, such as Wada (1969), Koh and Fan (1971), Stolzenbach and Harleman (1972),Waldrop and Farmer (1974), Paul and Lick (1973) etc. A review of existing models is presented by Dunn and Policastro (1975). Most of the existing models cannot adequately account for time-dependent, three-dimensional flow fields, realistic bottom topography effects, and surface wave phenomenon. Since a buoyant plume is three-dimensional in character and is significantly effected by bottom topography, ambient currents and local meteorology, the need for "complete models" is acute.

A time-dependent, three-dimensional, free-surface, numerical model with both horizontal and vertical stretching has been developed for the thermal discharge study, and is presented in this paper. The effects of variable bottom topography, free surface elevations, surface heat transfer, currents, and meteorological conditions are considered in this model. The model can simulate the physical conditions needed to provide sufficient three-dimensional information for the studies of water quality to meet the appropriate standards. The model is not only a flexible and economical tool for the heated water disposal system design or improvement consideration, but also for monitoring thermal effects in the receiving domain.

Numerical integration of the governing equations (conservation of mass, conservation of momentum, and energy) is performed simultaneously by using finite difference approximations for the differential equation. Both surface and submerged types of discharge systems in a bay and coastal site have been modelled. The results from the computer model were compared satisfactorily both with airborne thermal scanner remote sensing data and in-situe ground truth measurements at Florida Power & Light Company's Cutler Ridge Plant and Hutchinson Island Nuclear Power Plant. Only the results for Hutchinson Island site will be presented here. The application of this model to a specific site, involves specification of initial conditions, boundary conditions, and information geometry of the discharge.

(B) FORMULATION AND BASIC EQUATIONS

Numerical modeling of heated water discharges involves the application of fundamental hydrodynamic and thermodynamic equations. Several assumptions have been made for this study, namely,

(1) The fluid flow is incompressible,
(2) The fluid flow is turbulent and that the molecular transport can be neglected in comparison with turbulent transport, approximated by eddy transport coefficients,
(3) Pressures are hydrostatic throughout the whole domain,
(4) The solid wall and bottom are adiabatic, and
(5) The density throughout the flow field is a function of temperature only.

A vertical coordinate transformation technique similar to Phillips (1957) is used to incorporate both free surface and variable bottom topography and the same number of grid points in vertical direction can be used in the model. The new sigma vertical coordinate system is obtained by letting

$$\sigma = \frac{\mathcal{Z}\ (x,y,z,t)}{H\ (x,y,t)} = \frac{z + \eta\ (x,y,t)}{h\ (x,y) + \eta\ (x,y,t)}$$

where $\mathcal{Z} = \mathcal{Z}\ (x,y,z,t)$ is the position of the fluid element relative to the free surface, $H = H\ (x,y,t)$ is the depth contour relative to the free surface, z represents the vertical position relative to the mean water level, η is the free surface elevation measured positively upward from mean water level, h represents the depth relative to the mean water level. The value of σ ranges from zero at free surface to unity at the bottom of the basin. This mathematical technique has been used for a variety of numerical models of geophysical fluid flow, e.g., Smagorinsky (1965), Arakawa (1972), for the atmosphere study and Freeman (1972), Sengupta and Lick (1974) for the study of lakes. Fig. 1 and Fig. 2 show the two coordinate systems before and after vertical coordinate transformation respectively.

It is desireable to obtain a more detailed description of the flow near the discharging area and meanwhile a large horizontal domain can be covered. If a constant grid size were used, then a large number of grid points and excessive computation time are needed for the model. In order to solve this problem, a horizontal stretching is used in both lateral and transverse directions to create a small grid size near the discharge area and larger grid size away from the discharge points. An arc-tangent equation was used by Waldrop and Farmer (1974) as the horizontal stretching. A hyperbolic sine stretching has been used in this study for both lateral and transverse directions, as shown below:

$$x = a + C_1 \sinh [C_2 (X - d)]$$

$$y = b + C_3 \sinh [C_4 (Y - e)]$$

where x, y are the real coordinate; X,Y are the stretched coordinate; a and b are the distance at which the minimum step size is desired; C_1, C_2, C_3, C_4, d,e, are the constants to be determined by the imposed conditions. By using this horizontal stretching, even increments of ΔX and ΔY can be used in the model for the variable physical grid sizes.

Applying the differential transformation relationships, the horizontal and vertical stretched governing equations in the $XY\sigma$ coordinate are:

Continuity Equation

$$\frac{\partial H}{\partial t} + X' \frac{\partial (Hu)}{\partial X} + Y' \frac{\partial (Hv)}{\partial Y} + H \frac{\partial \Omega}{\partial \sigma} = 0 \ldots\ldots\ldots\ldots (1)$$

Momentum Equation

u - momentum:

$$\frac{\partial (Hu)}{\partial t} + X' \frac{\partial (Huu)}{\partial X} + Y' \frac{\partial (Huv)}{\partial Y} + H \frac{\partial (u\Omega)}{\partial \sigma} =$$

$$H \left[- \frac{X'}{\rho} \left(\frac{\partial P}{\partial X} \right) + gX' \left(\sigma \frac{\partial H}{\partial X} - \frac{\partial \eta}{\partial X} \right) + f\, v \right]$$

$$+ K_H \left[(X')^2 \frac{\partial H}{\partial X} \frac{\partial u}{\partial X} + H (X')^2 \frac{\partial^2 u}{\partial X^2} + HX'' \frac{\partial u}{\partial X} \right]$$

$$+ K_H \left[(Y')^2 \frac{\partial H}{\partial Y} \frac{\partial u}{\partial Y} + H (Y')^2 \frac{\partial^2 u}{\partial Y^2} + HY'' \frac{\partial u}{\partial Y} \right]$$

$$+ \frac{1}{\rho} \left[\frac{\partial}{H \partial \sigma} \left(\rho K_V \frac{\partial u}{\partial \sigma} \right) \right] \ldots\ldots\ldots\ldots\ldots\ldots\ldots\ldots (2)$$

v - momentum:

$$\frac{\partial (Hv)}{\partial t} + X' \frac{\partial (Huv)}{\partial X} + Y' \frac{\partial (Hvv)}{\partial Y} + H \frac{\partial (v\Omega)}{\partial \sigma} =$$

$$H \left[- \frac{Y'}{\rho} \left(\frac{\partial P}{\partial Y} \right) + gY' \left(\sigma \frac{\partial H}{\partial Y} - \frac{\partial \eta}{\partial Y} \right) - f\, u \right]$$

$$+ K_H \left[(X')^2 \frac{\partial H}{\partial X} \frac{\partial v}{\partial X} + H (X')^2 \frac{\partial^2 v}{\partial X^2} + HX'' \frac{\partial v}{\partial X} \right]$$

$$+ K_H \left[(Y')^2 \frac{\partial H}{\partial Y} \frac{\partial v}{\partial Y} + H (Y')^2 \frac{\partial^2 v}{\partial Y^2} + HY'' \frac{\partial v}{\partial Y} \right]$$

$$+ \frac{1}{\rho} \left[\frac{\partial}{H \partial \sigma} \left(\rho K_V \frac{\partial v}{\partial \sigma} \right] \ldots\ldots\ldots\ldots\ldots\ldots\ldots\ldots (3)$$

Energy Equation

$$\frac{\partial (HT)}{\partial t} + X' \frac{\partial (HuT)}{\partial X} + Y' \frac{\partial (HuT)}{\partial Y} + H \frac{\partial (\Omega T)}{\partial \sigma}$$

$$= B_H \left[(X')^2 \frac{\partial H}{\partial X} \frac{\partial T}{\partial X} + H (X')^2 \frac{\partial^2 T}{\partial X^2} + HX'' \frac{\partial T}{\partial X} \right]$$

$$+ B_H \left[(Y')^2 \frac{\partial H}{\partial Y} \frac{\partial T}{\partial Y} + H (Y')^2 \frac{\partial^2 T}{\partial Y^2} + HY'' \frac{\partial T}{\partial Y} \right]$$

$$+ \frac{1}{\rho H} \left[\frac{\partial}{\partial \sigma} \left(\rho B_V \frac{\partial T}{\partial \sigma} \right) \right] \ldots\ldots\ldots\ldots\ldots\ldots\ldots\ldots (4)$$

Equation of State

$$\rho = F(T) = 1.000428 - 0.000019T - 0.000036T^2 \quad \text{..........(5)}$$

The relationship between real vertical velocity and vertical velocity in σ coordinate is derived as follows:

$$w = H\,\Omega + (\sigma - 1)\frac{d\eta}{dt} + \sigma\left(uX'\frac{\partial h}{\partial X} + v\,Y'\frac{\partial h}{\partial Y}\right) \quad \text{........(6)}$$

By integrating the continuity equation with respect to σ from surface to bottom we can get

$$\frac{\partial H}{\partial t} = -\int_0^1 \left[X'\frac{\partial(Hu)}{\partial X} + Y'\frac{\partial(Hv)}{\partial Y}\right] d\sigma - \left(w_b - u_b X'\frac{\partial h}{\partial X} - v_b Y'\frac{\partial h}{\partial Y}\right) \quad \text{..........(7)}$$

Substitute the above equation into continuity equation and integrate from surface to $\sigma = \sigma$, and the result can be obtained as

$$\Omega = \frac{1}{H}\int_0^\sigma \left[X'\frac{\partial(Hu)}{\partial X} + Y'\frac{\partial(Hv)}{\partial Y}\right] d\sigma + \frac{\sigma}{H}\int_0^1 \left[X'\frac{\partial(Hu)}{\partial X} + Y'\frac{\partial(Hv)}{\partial Y}\right] d\sigma + \frac{\sigma}{H}\left(w_b - u_b X'\frac{\partial h}{\partial X} - v_b Y'\frac{\partial h}{\partial Y}\right) \quad \text{............(8)}$$

where subscript b denotes at the bottom of basin and

$$X' = \frac{dX}{dx}\ ;\ Y' = \frac{dY}{dy}$$

$$X'' = \frac{d^2X}{dx^2}\ ;\ Y'' = \frac{d^2Y}{dy^2}$$

The hydrostatic relationship is used as the diagnostic equation for pressure

$$P(\sigma) = P(0) + gH\int_0^\sigma \rho(\sigma)\, d\sigma \quad \text{..........(9)}$$

where P (0) is the pressure at the free surface.

(C) INITIAL AND BOUNDARY CONDITIONS

In order to solve the set of governing equations, the initial and boundary conditions should be specified throughout the whole domain. This information may be obtained from remote sensing data, in-situ measurement and other sources. Boundary conditions are specified at the air-water interface, the bottom of basin, the lateral solid walls, discharge points, and open boundaries. At the air-water interface the wind stress and the heat transfer coefficient are specified. The condition of no slip at lateral solid wall and bottom of basin is used for the momentum equations.

At solid lateral walls and at the bottom of basin, adiabatic conditions are assumed. At points of thermal discharge, both velocity and temperature are specified. The domain is bound on three sides by open boundaries where conditions are most difficult to specify. At these boundaries, the outflow velocity gradient normal to boundary is considered zero and the inflow velocities are the known values. For the temperature, the second derivative is equated to zero for outflow, implying no diffusive heat transfer and convective heat transfer is dominated. For the inflow, the temperature is the same as ambient water temperature.

(D) METHOD OF SOLUTION

The set of governing equations are unsteady, non-linear and second order partial differential equations. With the widespread use of the high-speed digital computers, finite difference approximation methods for the partial differentiation are used for solving the numerical solution.

In the three-dimensional free surface model, central differencing is used for the space derivatives in the interior of the basin. Single-sided differencing is used for the space derivatives at the boundary. Forward differencing in time for the first time step and then the central differencing in time is used for predicting the new values of all the dependent variables. In order to insure the numerical stability, the convective terms, pressure term and Coriolis force term are calculated by using the values at present time, the viscous terms are calculated by using the values at previous time step $(t-\Delta t)$. All the dependent variables are computed at integral grid points of the basin.

A two-dimensional matrix (MAR) was created in the computation process for locating the position in the basin to insure the appropriate numerical scheme and boundary conditions are used in the computation. Different values of MAR were assigned to the different locations in the basin, such as MAR = 11 represents the points in the interior, and MAR = 0 represents points outside the domain.

The finite difference form of governing equations is solved simultaneously for each time step. Before the computation process, the initial conditions for all the dependent variables should be specified throughout the domain. The surface heights are computed from the vertically integrated continuity equation. The horizontal velocities are computed directly from the momentum equation. The vertical velocities are obtained from new horizontal velocities and surface heights into equation (6). The temperatures are calculated from the energy equation. The pressures are obtained from the hydrostatic relationship. This procedure is performed at each time step until the desired length of time has been achieved.

(E) APPLICATION

The three-dimensional free surface model has been applied to FPL's Hutchinson Island Nuclear Power Plant which is located about midway between the cities of Fort Pierce and Stuart on the eastern ocean coast of Florida. The objective of this study is to use this model to predict the velocity and temperature distribution caused by a submerged thermal discharge into the ocean under various environmental conditions. The 12 feet diameter submerged discharge pipeline is buried in the ocean bed and terminates at a point about 1200 feet offshore at a depth of 18 feet from mean water level. At its termination, a two port Y-type discharge is added with each arm being 7.5 feet in diameter. A short sloping concrete pan is located at the outlet to prevent scouring of the ocean floor. The submerged jet discharge exits horizontally with a relatively high velocity and rises to the surface owing to buoyancy effects and then spreads out by the action of turbulent mixing and ambient currents.

A numerical grid system of 20 x 20 in the horizontal plane and five grids in the vertical plane were chosen. The domain covered is 2000 meters parallel to the shore line and 2380 meters perpendicular to the shore (along the discharge pipe axis). Fig. 4 shows a vertical section along the discharge pipe axis, the vertical and horizontal stretching and its influence on the numerical grid system is apparent.

On June 2, 1976, the heated water had an exit velocity of 280 cm/sec (9.1 ft/sec) at each end of the Y-type discharging pipe. The ambient water temperature was about 25.5°C, discharge water temperature was 35°C, and air temperature was 29°C. The wind speed was 10 mph from the southeast. The ocean current was about 25 cm/sec predominantly northerly. The discharge conditions and the environmental conditions were incorporated into the model. It was found that the plume rapidly rises to the surface and spreads to the north owing to the current.

Fig. 5 shows the surface velocities predicted for environmental conditions of June 2, 1976. The imposed northerly current prevails away from the discharge and near the discharge points there is a source-like flow pattern because the plume rapidly rises to the surface and spreads. Fig. 6 shows the horizontal velocity on the plane 6.5 meters below the mean water level. The Y-type discharge pipe discharged horizontally with a relatively high velocity as can be seen at the discharge points, and then turned with the current. Fig. 7 shows the velocity distributions of the vertical section along the discharge pipe axis. The vortex just west of the discharge caused by the entrainment is clearly evident. Fig. 8 shows the velocity distributions of the vertical section I = 10 that is parallel to the shore line. The plume rises to the surface owing to the buoyancy and then is carried along with the current.

Fig. 9 shows the isotherms of a vertical section I = 9 that is perpendicular to the axis of the discharge pipe. The plume rises to the surface and then spreads out and is carried along with the current as is evident. Fig. 10 shows the surface isotherms from I.R. data in the morning at Hutchinson Island Power Plant on June 2, 1976. The submerged plume reises to the surface and spreads with the northerly current. The morning I.R. data base was used as the initial conditions for the model and the afternoon results were predicted by the model. The plume shifted eastwards during this period and the area of 26.5°C isotherm was reduced. The width of the thermal plume increased somewhat. Fig. 11 shows the comparison of surface isotherms obtained by the model prediction and I.R. measurement data. In general, the model prediction is observed to be in relatively good agreement with I.R. measurements.

(F) SUMMARY

The present study predicts the three-dimensional flow and temperature field in the receiving body of ocean water owing to the submerged discharge near the ocean floor. The effects of currents, wind, surface cooling, and bottom topography are combined in this complete field numerical model. The vertical and horizontal stretching provide more efficient use of this model and ease of boundary condition specification. The results from the model obtained indicate proper numerical behavior of the model. It can be concluded that the physical behavior of the plume is reproduced by the model with relatively good agreement. Further calibration efforts are still continuing. Some field experimental data will be obtained for using the final verification of the model.

(G) ACKNOWLEDGEMENTS

Authors of this paper would like to express their sincerest appreciation to Dr. M. Estoque for his many helpful suggestions and discussions in this work.

The research was sponsored by NASA under contract NAS10-8926.

REFERENCES

1. Lee and Sengupta, "Three-Dimensional Thermal Pollution Model", Detailed Technical Report to NASA, CR. No. 144858 Dept. of Mech. Engineering, Univ. of Miam, Dec.,1976.

2. Freeman, N.G., "A Modified Sigma Equations' Approach to the Numerical Modeling of Great Lakes Hydrodynamics", Journal of Geo. Research, Vol. 72, No. 6, Feb., 1972.

3. Waldrop, W.R., "Three-Dimensional Flow and Sediment Transport at River Mouths", Technical Report No. 150, Louisiana State University, Sept., 1973.

4. "Environmental Statement Related to the St. Lucie Plant Unit No. One", Florida Power and Light Company, June, 1973.

5. Parker and Krenkel, "Physical and Egnineering Aspects of Thermal Pollution", CRC Press, L970.

6. Phillips, N.A., "A Co-ordinate System Having Some Special Advantages for Numerical Forecasting", J. Meteorology, 14,1957.

7. Dunn, Policastro, & Paddock, "Evaluation of Mathematical Models for the Near and Complete Field", Argonne Nat. Laboratory, Report ANL/WR-75-3, August, 1975.

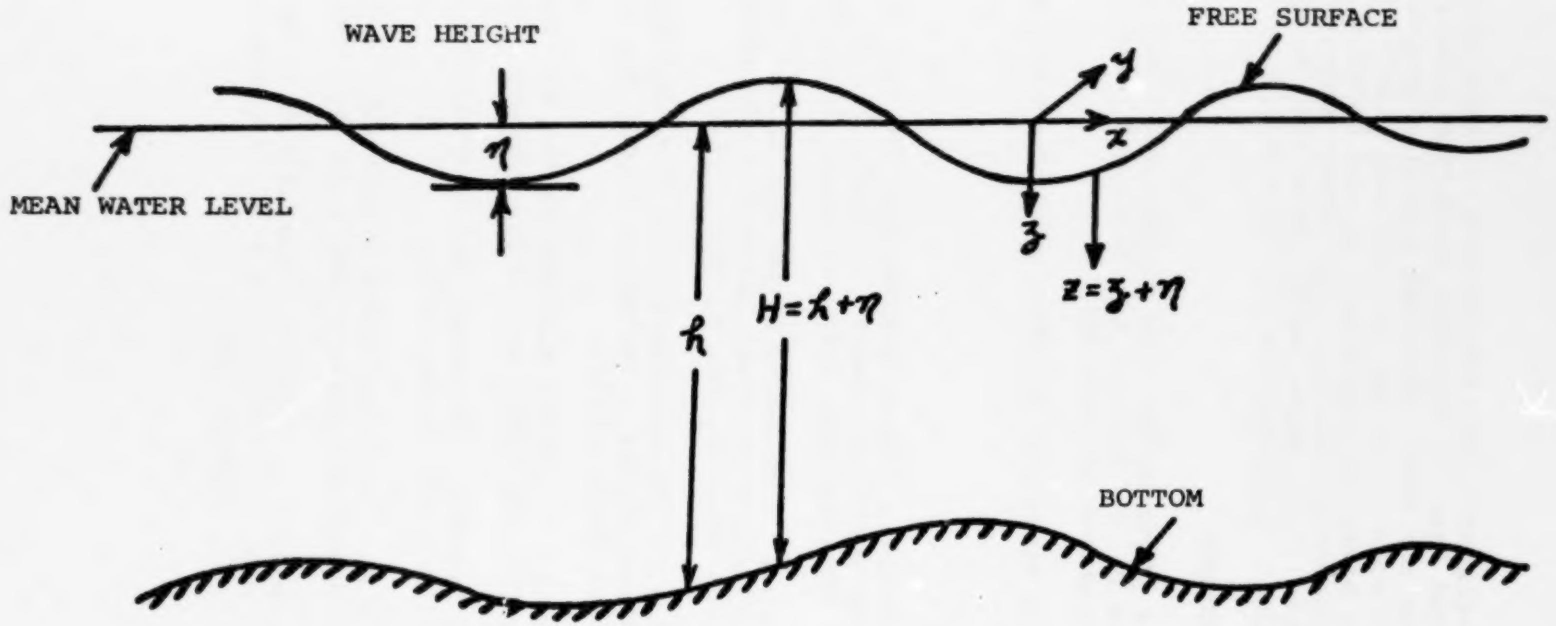
WAVE HEIGHT
FREE SURFACE
MEAN WATER LEVEL
η
y
x
ζ
$z=\zeta+\eta$
h
$H=h+\eta$
BOTTOM

FIG: (1) The xyz Coordinate System for the Free-Surface Model

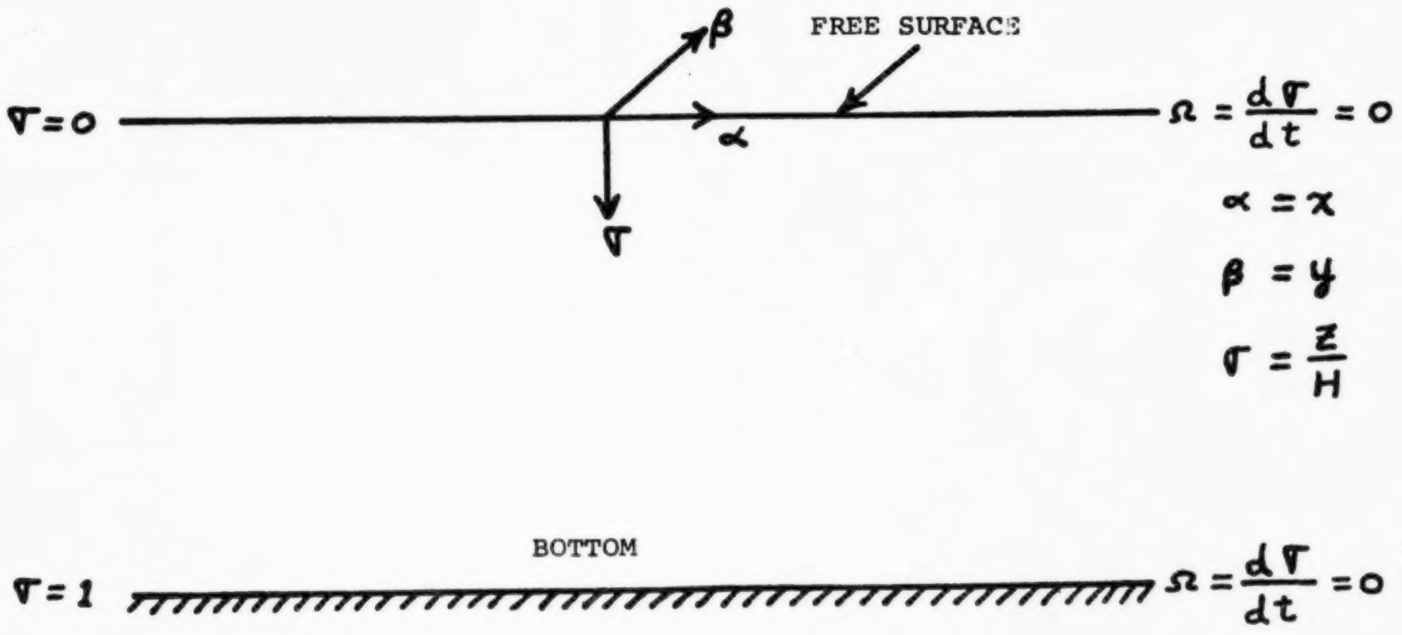
β
FREE SURFACE
σ=0
α
σ
Ω = dσ/dt = 0
α = x
β = y
σ = z/H
BOTTOM
σ=1
Ω = dσ/dt = 0

FIG: (2) The αβσ Coordinate System for the Free-Surface Model

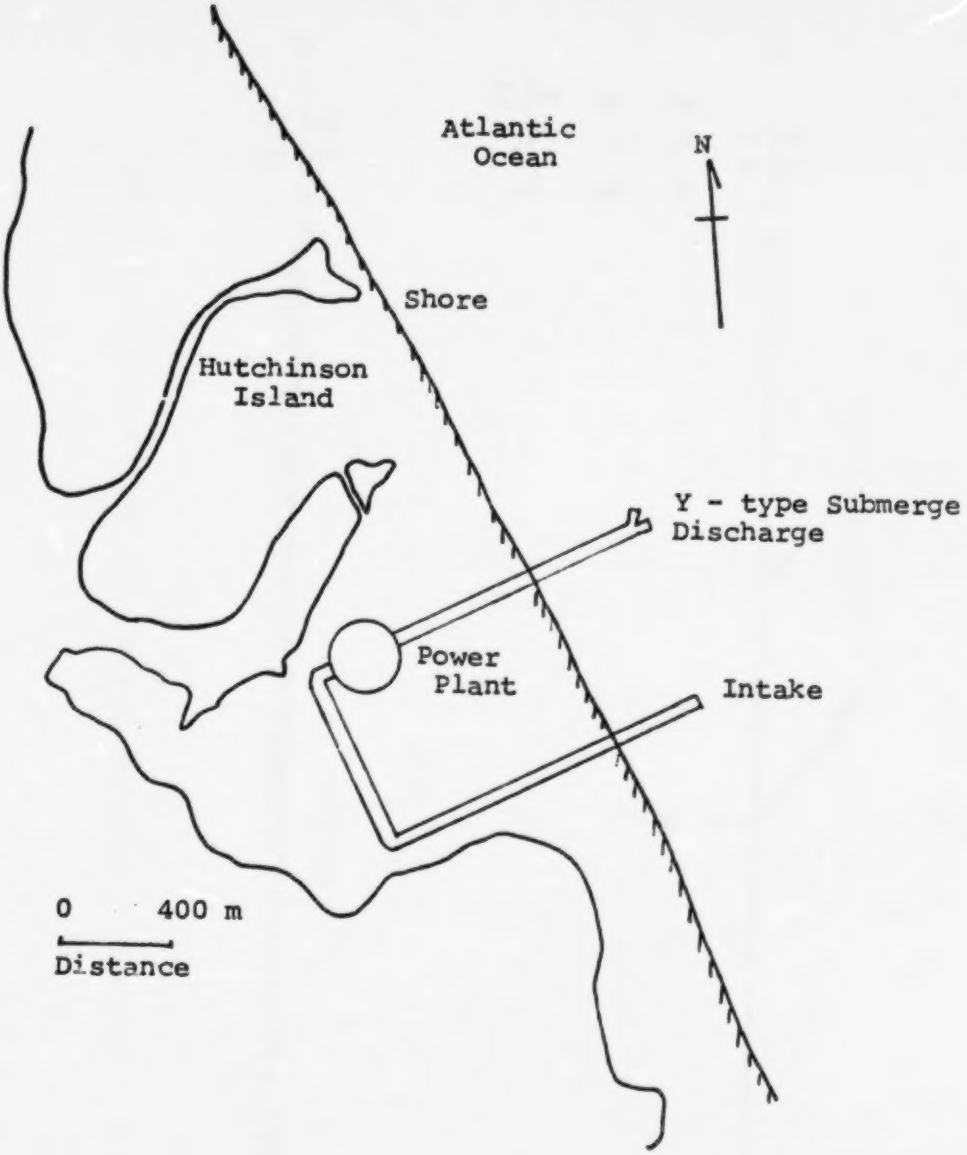
Atlantic Ocean
N
Shore
Hutchinson Island
Y - type Submerge Discharge
Power Plant
Intake
0 400 m
Distance

Fig. (3) Florida Power and Light Company's Hutchinson Island Site Power Plant

THERMAL POLLUTION LAB
UNIVERSITY OF MIAMI

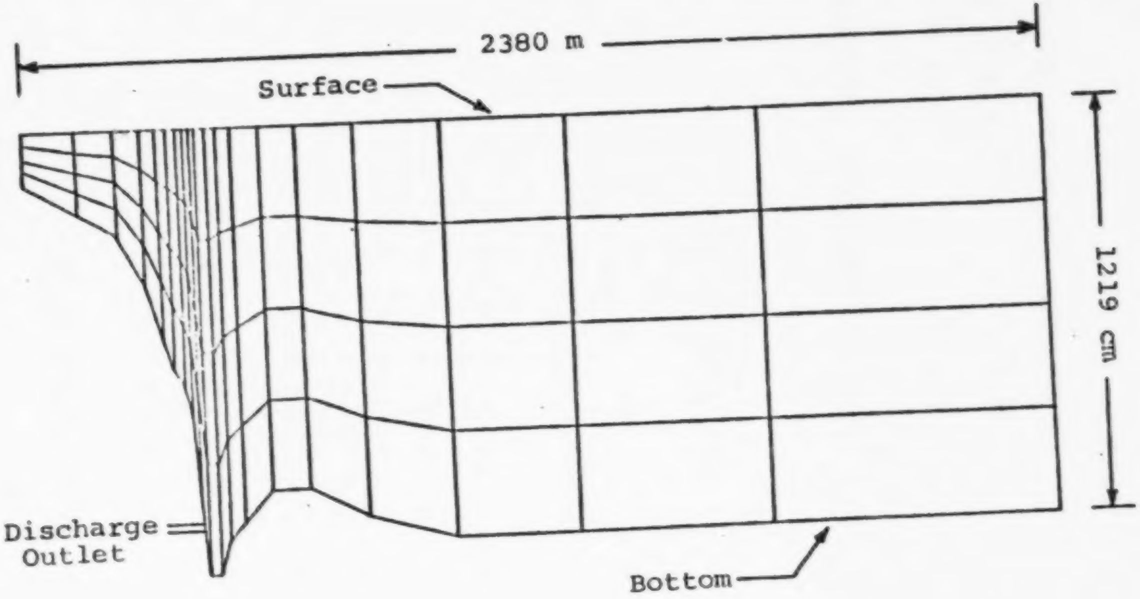
2380 m
Surface
1219 cm
Discharge
Outlet
Bottom

Fig.(4) · Distorted Vertical Section With Sigma Stretching For Free Surface Near Field Model Applied to Hutchinson Island Site

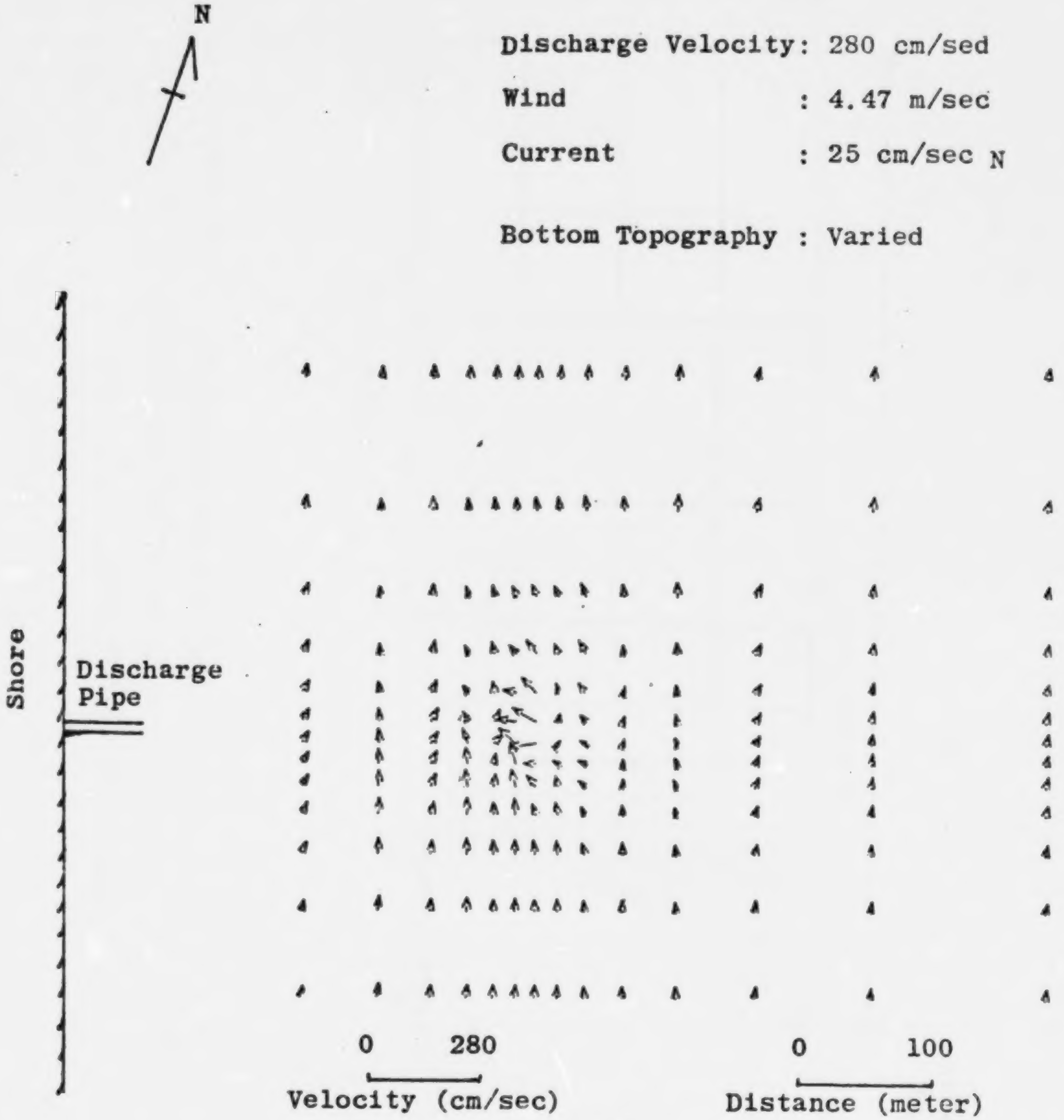

Discharge Velocity: 280 cm/sed

Wind : 4.47 m/sec

Current : 25 cm/sec N

Bottom Topography : Varied

Fig. (5) Surface velocity distribution with current, wind and bottom topography at Hutchinson Island Site (Free Surface Model)

Discharge Velocity: 280 cm/sec
Wind : 4.47 m/sec
Current : 25 cm/sec N.

Bottom Topography: Varied

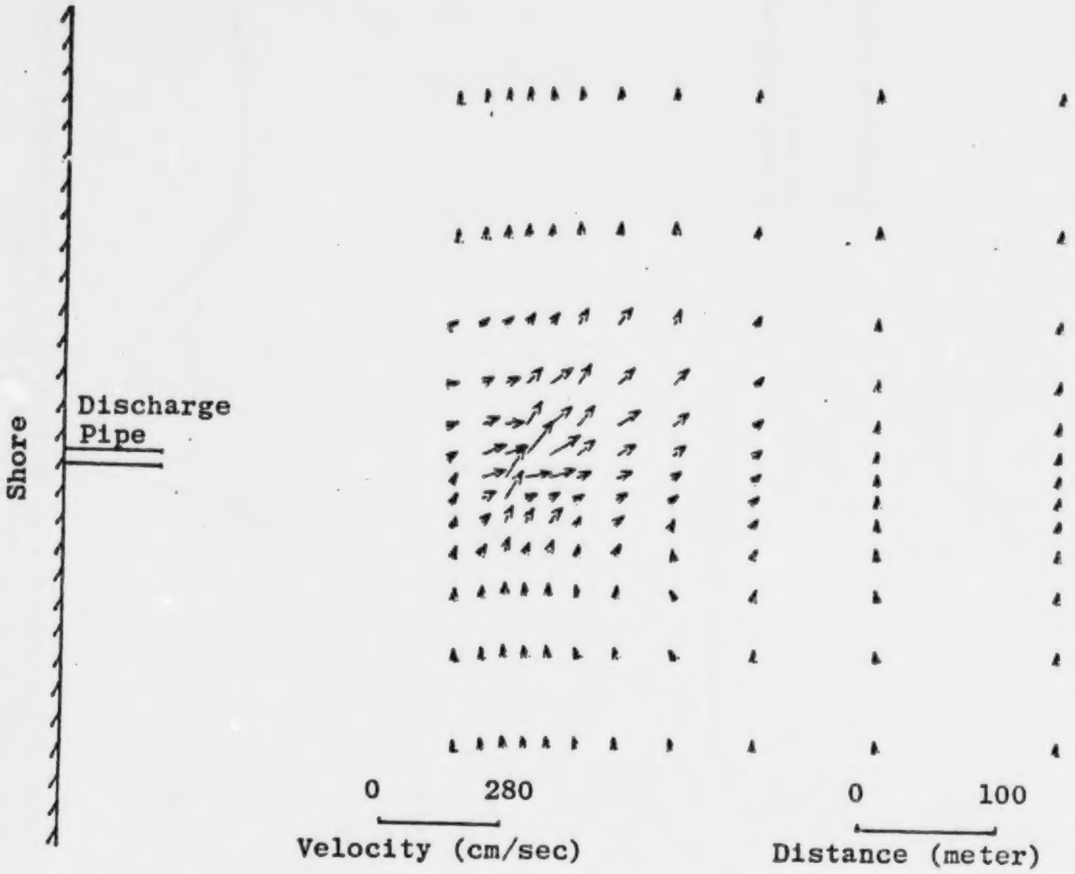

Fig. (6) Horizontal velocity distribution at the plant 6.5 meter below the free surface with current, wind and bottom topography at Hutchinson Island Site (Free Surface Model)

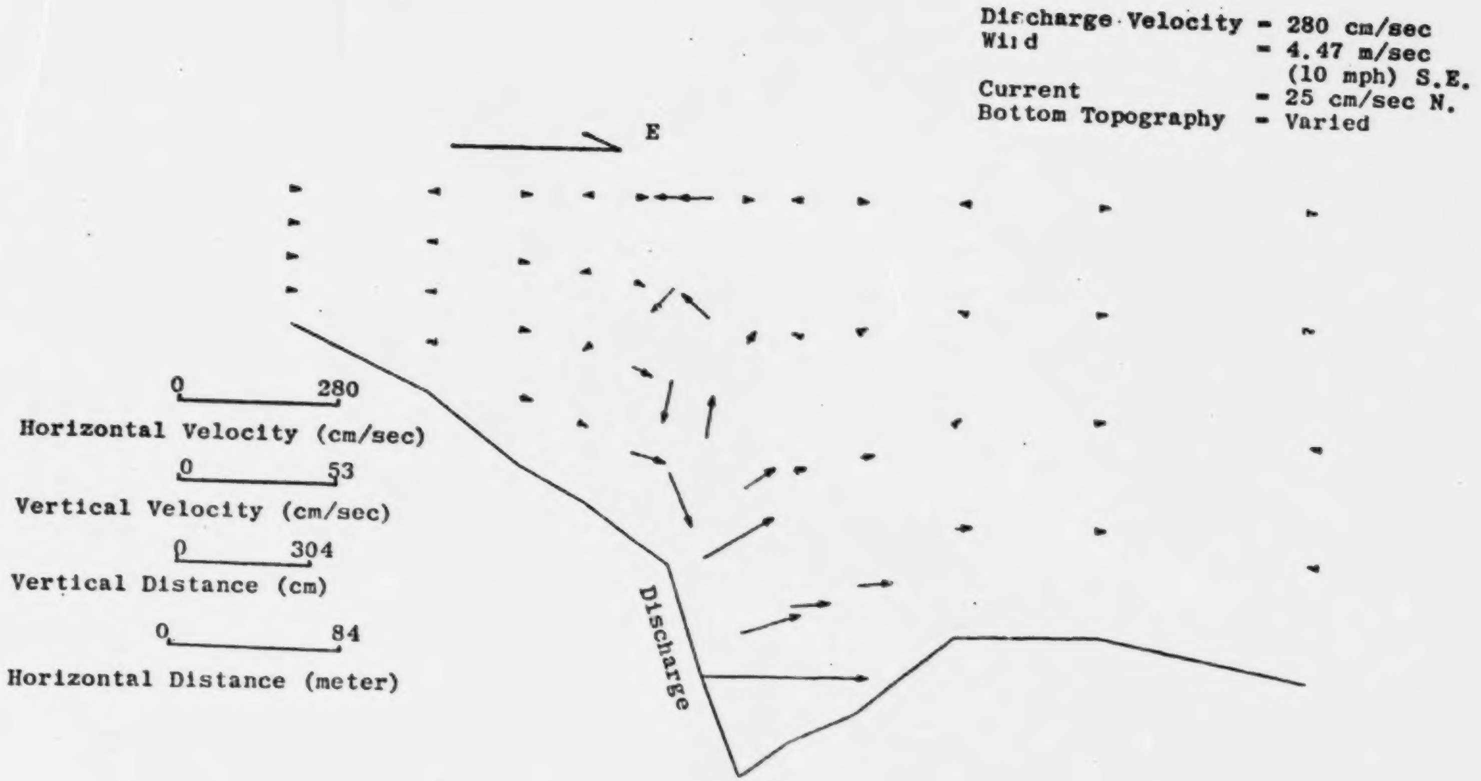

Fig. (7) Velocity distribution at section J-11 for Hutchinson Island Site with vertical scale exaggerated 5.25 times (Free Surface Model)

Discharge Velocity - 280 cm/sec
Wind - 4.47 m/sec (10 mph) SE
Current - 25 cm/sec N.
Bottom Topography - Varied

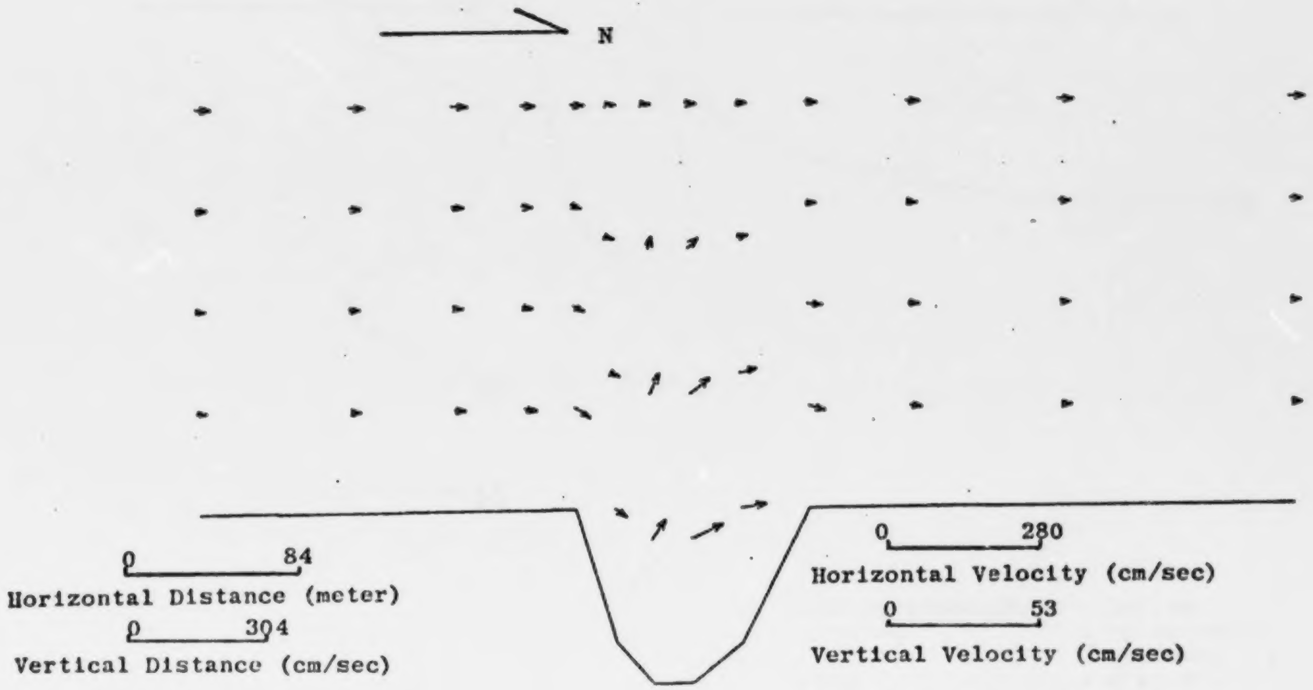
N
0 84
Horizontal Distance (meter)
0 304
Vertical Distance (cm/sec)
0 280
Horizontal Velocity (cm/sec)
0 53
Vertical Velocity (cm/sec)

Fig. (8) -- Velocity distribution at section I-10 for Hutchinson Island Site with vertical scale exaggerated 5.25 times (Free Surface Model)

Discharge Velocity : 280 cm/sec
Wind : 4.47 m/sec (10 mph) S.E.
Current : 25 cm/sec N.
Bottom Topography : Varied

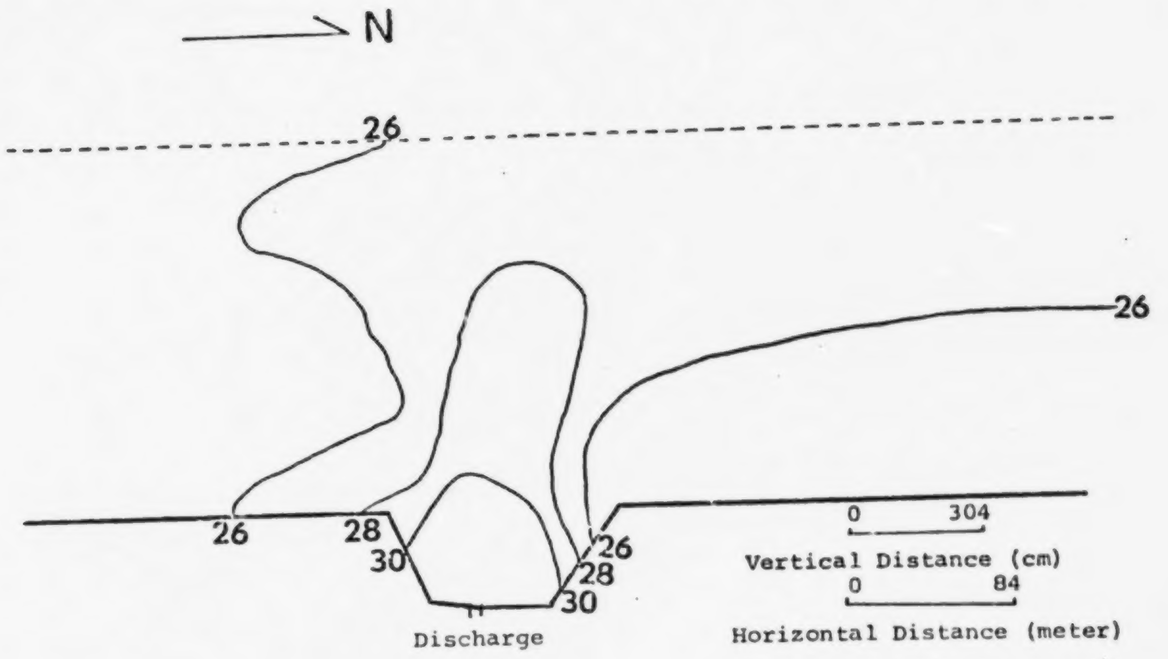
N
26
26
26
28
30
26
28
30
Discharge
0
304
Vertical Distance (cm)
0
84
Horizontal Distance (meter)

Fig. (9) Vertical isotherms at section I=9 for the Hutchinson Island Site (Free Surface Model)

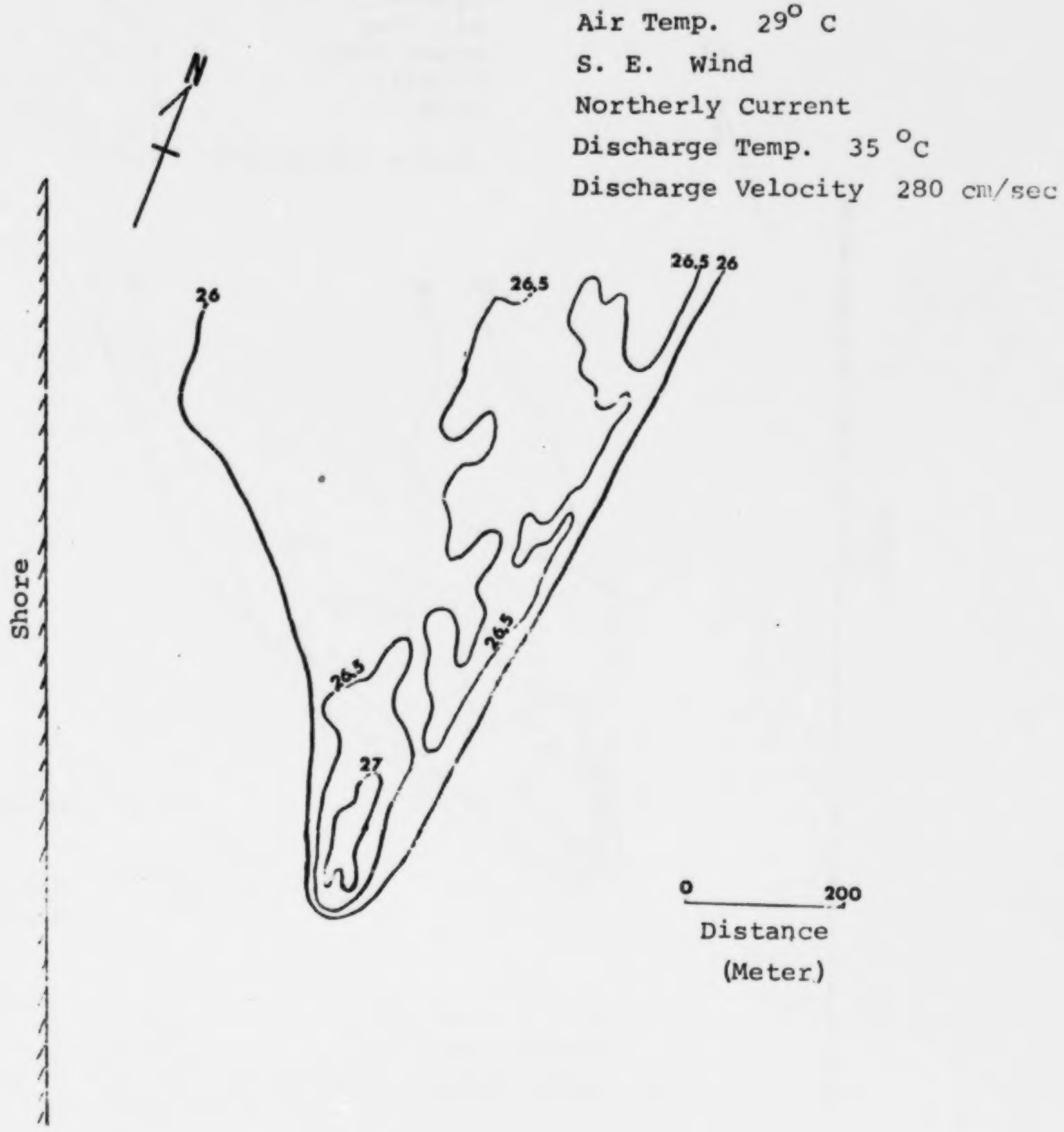
N
26
26.5
26.5
26
26.5
26.5
27
Shore
0
200
Distance
(Meter)

Air Temp. 29° C

S. E. Wind

Northerly Current

Discharge Temp. 35 °C

Discharge Velocity 280 cm/sec

Fig. (10) Surface Isotherms from I.R. Data at Hutchinson Island Power Plant, 2 June 1976, 1048-1059 EST

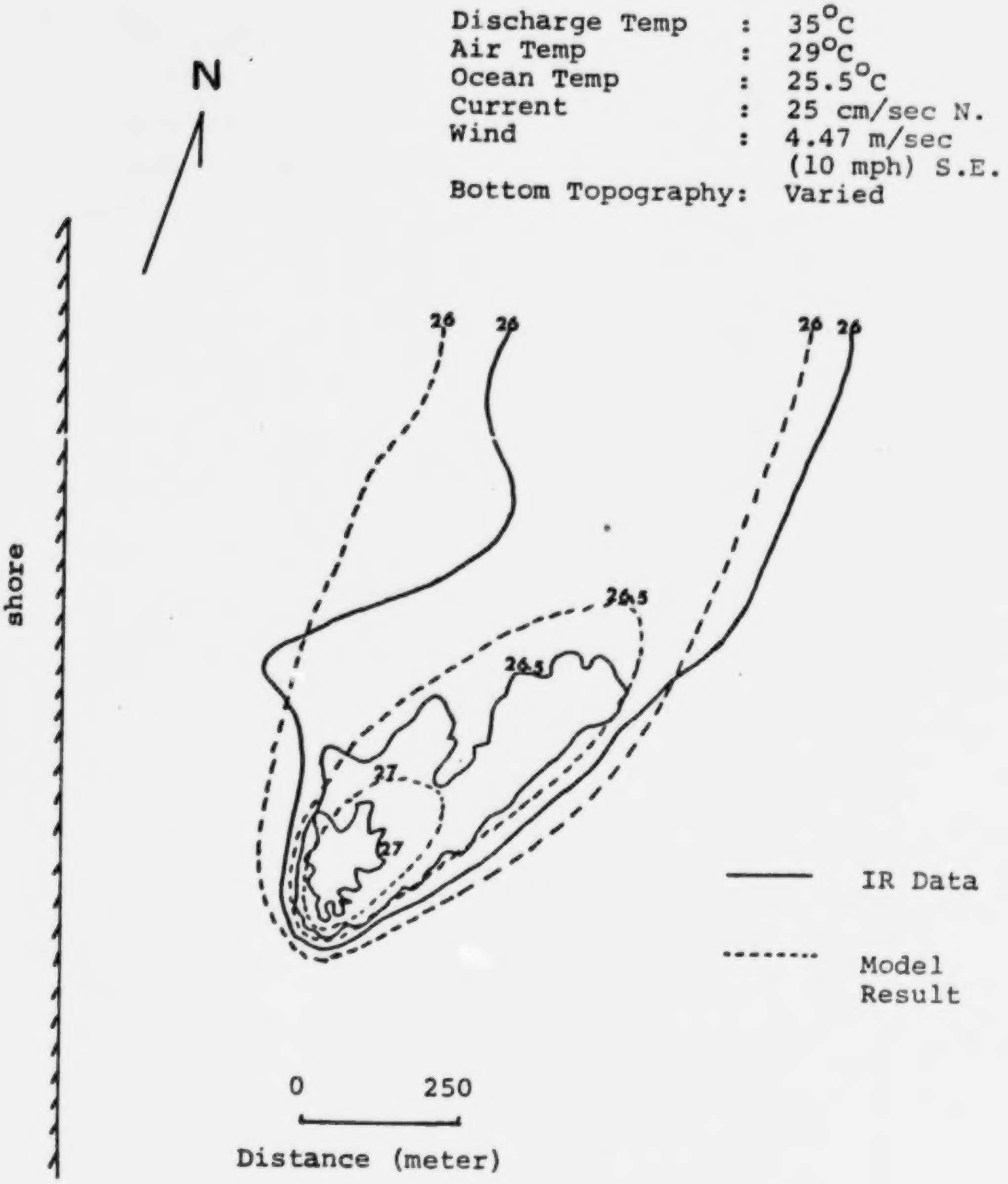

Discharge Temp : $35^{\circ}C$
Air Temp : $29^{\circ}C$
Ocean Temp : $25.5^{\circ}C$
Current : 25 cm/sec N.
Wind : 4.47 m/sec (10 mph) S.E.
Bottom Topography: Varied

Fig.(11) Comparison of model results and afternoon IR data at Hutchinson Island Site for June 2, 1976 (Free Surface Model)

omit

IV-A-43

SYSTEMATIC APPLICATION OF TRANSIENT, MULTI-DIMENSIONAL MODELS FOR COMPLETE ANALYSIS OF THERMAL IMPACT IN REGIONS WITH SEVERE REVERSING FLOW CONDITIONS

Reproduced from
best available copy.

Arsev H. Eraslan*
Oak Ridge National Laboratory
Oak Ridge, Tennessee 37830

and

Department of Engineering Science and Mechanics
The University of Tennessee
Knoxville, Tennessee 37916

ENERGY DIVISION

Research sponsored by U.S. Nuclear Regularoy Commission under Union Carbide Corporation's contract with the Energy Research and Development Administration

*Professor of Engineering Science & Mechanics, University of Tennessee, Consultant to Environmental Impact Section, Energy Division, Oak Ridge National Laboratory.

By acceptance of this article, the publisher or recipient acknowledges the U.S. Government's right to retain a nonexclusive, royalty free license in and to any copyright covering the article

IV-A-44

SYSTEMATIC APPLICATION OF TRANSIENT, MULTI-DIMENSIONAL MODELS FOR COMPLETE ANALYSIS OF THERMAL IMPACT IN REGIONS WITH SEVERE REVERSING FLOW CONDITIONS*

Arsev H. Eraslan*
Oak Ridge National Laboratory
Oak Ridge, Tennessee 37830
and
Department of Engineering Science and Mechanics
The University of Tennessee
Knoxville, Tennessee 37916

The assessment of the thermal impact of power plant operations in tidal estuaries and coastal regions and in certain controlled rivers and reservoirs with intermittent flow conditions requires the careful consideration of the effects of re-entrainment and re-circulation of the heated discharge water. The analysis of the thermal conditions cannot be based on standard near-field models (e.g., see Ref. 1) with modified, steady-state, parabolic jet solutions, since they cannot directly include the controlling re-entrainment and re-circulation effects. Under reversing flow conditions, the realistic assessment of the thermal impact requires complete thermal models which include both the near-field and the far-field effects in their general transient formulations.

In most cases it is usually more economical to employ different models, with different levels of complexity, in different regions, rather than implementing a single complex, three-dimensional, coupled hydrodynamic, thermal and water quality model for the entire region affected by the operation of the power plant. In particular, under tidal flow conditions, the computer run time required by a complex, three-dimensional model to simulate the quasi-steady state thermal conditions in a large flow region becomes prohibitive. Hence, although complex three-dimensional models may be essential to obtain accurate predictions under critical three-dimensional flow conditions, one- and two-dimensional models can generally be employed in the assessment of the thermal impact of large power plants in estuaries and coastal regions.

---

*Professor of Engineering Science & Mechanics, University of Tennessee, Consultant to Environmental Impact Section, Energy Division, Oak Ridge National Laboratory

Fast-transient (within tidal cycle), one-, two- and three-dimensional discrete-element far-field models [2-7] with computationally optimized codes have been developed for the assessment of thermal impact of large power plants in estuaries and coastal regions with geometrically complex shoreline and bathymetry conditions. These models have been recently extended to incorporate a systematic methodology for the matching of the near-field and far-field flow to include the important effects of re-entrainment and re-circulation. The zone-matching methodology, based on uniformly valid singular perturbation theory have been extensively used to simulate the re-entrainment and re-circulation problems associated with power plant discharges and intakes. A typical application of the zone-matching methodology is shown in Fig. 1 for a vertical submerged diffuser in moderate ambient cross-flow. The results of the study clearly indicate the formation of two vortices which substantially reduce the near-field dilution of the discharge due to the ambient far-field flow conditions.

The tidal-transient multi-dimensional thermal models were specifically developed for the simulation of the actual site-specific problems related to actual operational power plants. The one-dimensional model has been applied extensively to the simulation of the hydrodynamic, thermal and salinity conditions in the Hudson River to study the overall thermal impact of all operational power plants along the 152-mile estuary. The model predictions were continued for 183 days (April 1 - September 30) for both 1973 and 1974 with detailed site-specific conditions for freshwater flow rates, tidal conditions, atmospheric conditions and plant operational data. The results of the computer simulations agreed extremely well with the field-measured data for the complete duration of the study. (See Fig. 2).

The tidal-transient, two-dimensional, multi-layer, complete thermal models were also applied to study the temperature conditions in three large regions of the Hudson River. The computer simulations of the thermal conditions in regions containing Roseton and Danskammer, Indian Point and Lovett, and Bowline power plants agree reasonably well with the field-measured data accurate to hourly temporal resolutions within the tidal cycles. The agreement between computer simulations and the field-measured data for daily averaged temperatures was excellent for all regions. The detailed results of this extensive study are being prepared for presentation. Some of the preliminary two-dimensional results for the simulation of the temperature conditions in the region of Indian Point and Lovett power plants are shown in Fig. 4 during ebb tide in the river.

The fast-transient, two-dimensional complete thermal model was also applied to the simulation of the temperature conditions in the vicinity of the Peach Bottom Atomic Power Station in the Conowingo Reservoir. The reversing flow conditions in the region were determined based on the actual operational conditions of the upstream Holtwood Dam, the pump storage facility, and the downstream Conowingo Dam. In the applications, only the site-specific atmospheric conditions and plant operational data was input without any adjustment of the transport parameters of the model. The computer simulations and field-measured data agreed remarkably well as shown in Fig. 5.

In conclusion, the fast-transient, two-dimensional models which include the zone matching methodology for the interaction of the near-field and far-field effects can realistically incorporate the re-entrainment and re-circulation conditions. The results of applications of these models to various regions with severe reversing flow conditions concluded that the models can be employed to predict the thermal impact of power plant operations in controlled rivers, estuaries and coastal regions.

REFERENCES

Reproduced from best available copy.

1. Gerald H. Jirka, Gerrit Abraham, and Donald R. F. Harleman, "An Assessment of Techniques for Hydrothermal Prediction," MIT Report No. COO-2374-2, Ralph M. Parsons Laboratory for Water Resources and Hydrodynamics, Massachusetts Institute of Technology, Cambridge, Massachusetts, July (1975).

2. A. H. Eraslan, "Discrete-Element Computational Model for Predicting Hydrodynamic and Water Quality Conditions in Estuaries and Controlled Rivers," Trans. 11th Annual Meeting, Society of Engineering Science, Durham N. C. (1974).

3. A. H. Eraslan, "Transient, Two-Dimensional Discrete-Element, Far-Field Model for Thermal Impact Analysis of Power Plant Discharges in Coastal and Offshore Regions. Part I: General Description of the Mathematical Model and the Results of an Application," ORNL-4940, Oak Ridge National Laboratory (1974).

4. A. H. Eraslan, "A Transient, Two-Dimensional Discrete-Element Model for Far-Field Analysis of Thermal Discharges in Coastal Regions," Progress in Astronautics, Ed.: J. A. Schetz, Vol. 36, AIAA, MIT Press, Cambridge, Massachusetts (1974).

5. A. H. Eraslan, "A Tidal-Transient, Far-Field Model for Offshore Thermal Discharges," Trans. Am. Nucl. Soc., 18, 55 (1974).

6. A. H. Eraslan, "Mathematical Modeling of Thermal Discharges from Large Offshore Power Plants," (with J. M. Earton, R. D. Sharp, H. F. Baumann, and M. Siman-Tov), presented at the 11th Southeastern Seminar on Thermal Sciences, The University of Tennessee, Knoxville, Tennessee, April (1975).

7. A. H. Eraslan, "Discrete-Element Models for Thermal Impact Assessment of Large Power Plants in Estuaries and Coastal Regions," pre-

sented at the Twelfth Southeastern Seminar on Thermal Sciences, University of Virginia, Charlottesville, June (1976).

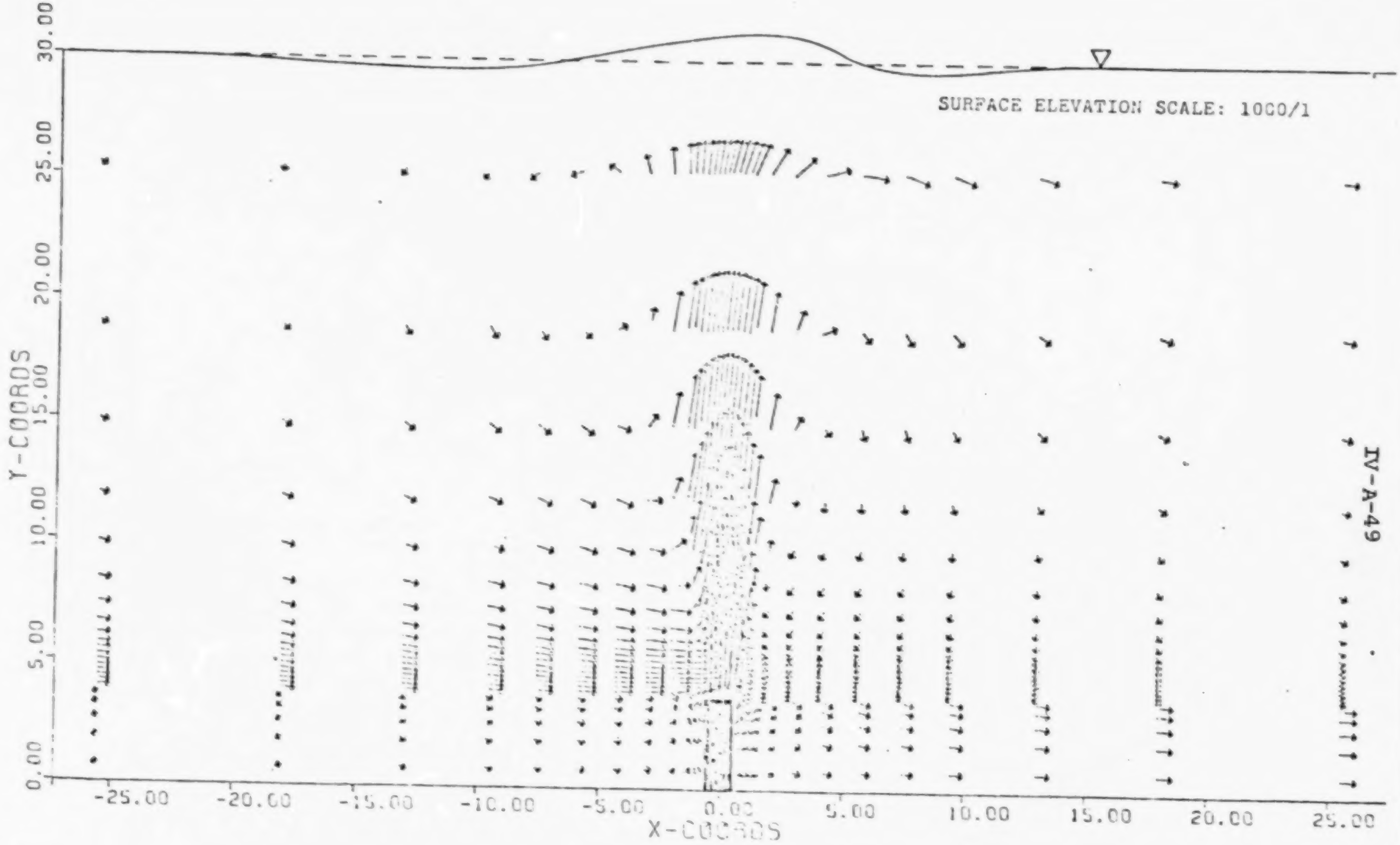

Fig. 1. Streak Lines for a Submerged Diffuser. Discharge Velocity 20.0 ft/sec. Cross-Flow Velocity 0.5 ft/sec.

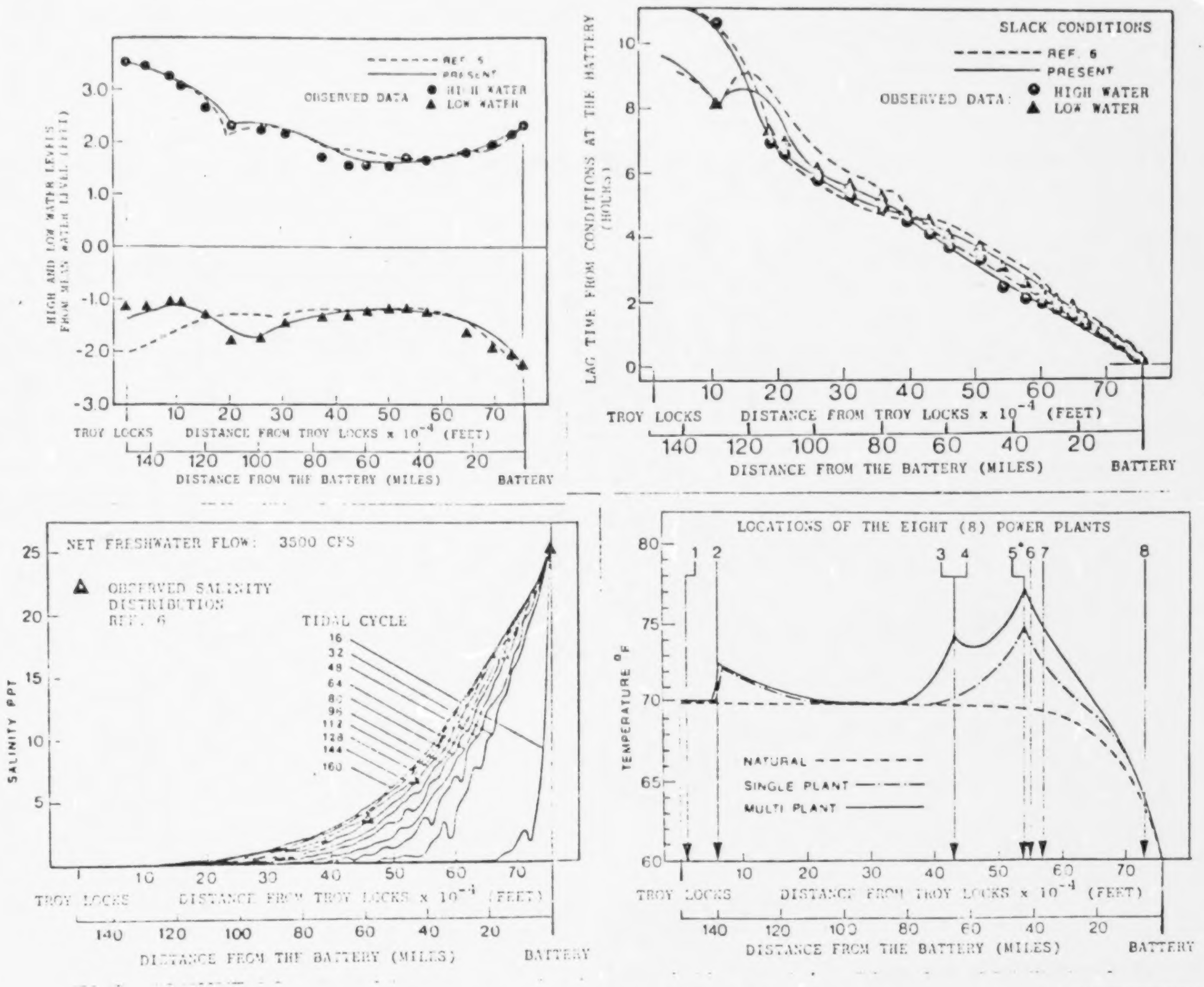

Fig. 2. Preliminary Results for the Simulation of Hydrodynamic, Salinity and Temperature Conditions along the Hudson River

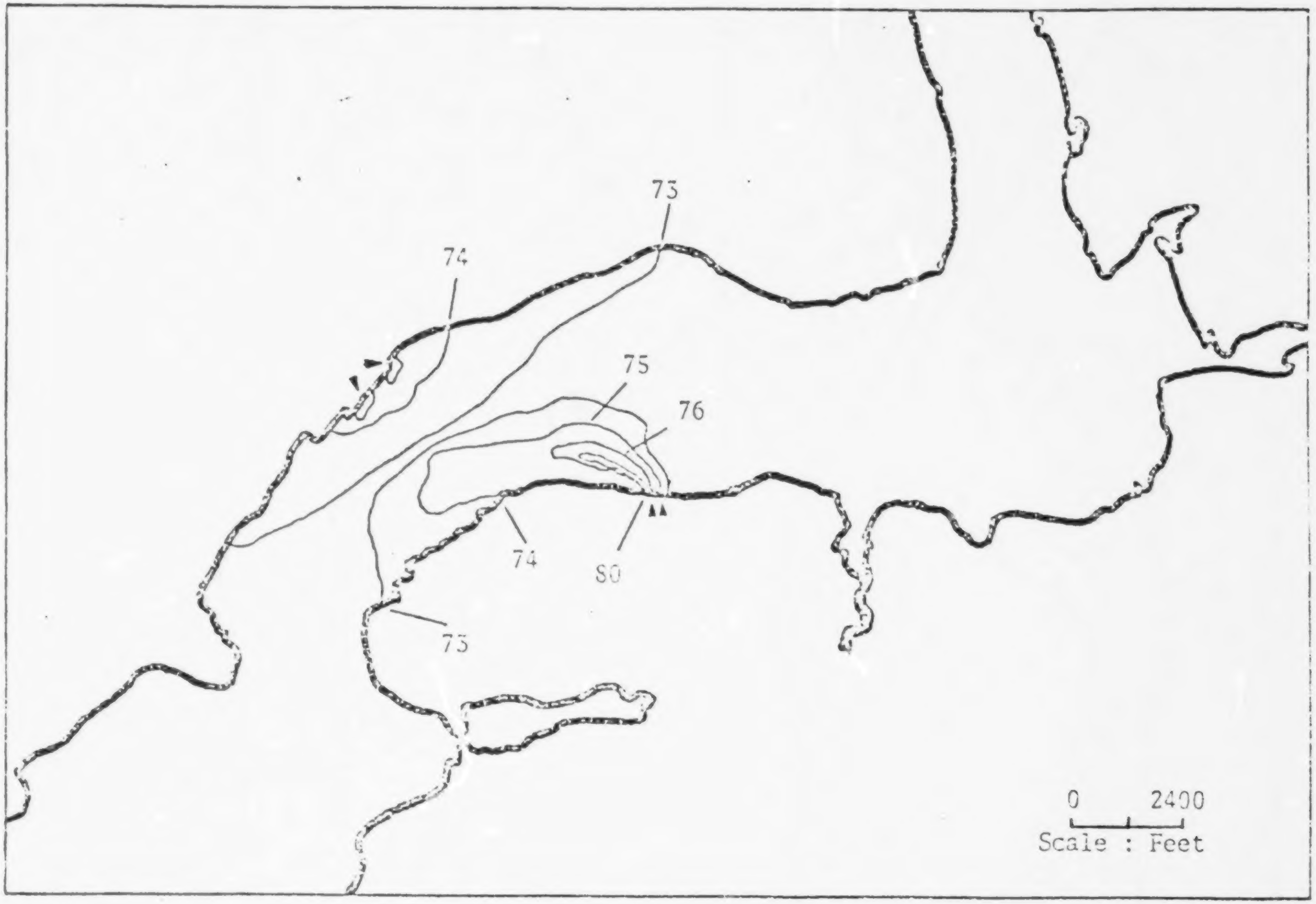
73
74
75
76
80
74
73
0
2400
Scale : Feet

Fig. 3. Preliminary Results of the Computer Simulations of the Temperature Conditions in the Vicinity of Indian Point in the Hudson River

Reproduced from best available copy.

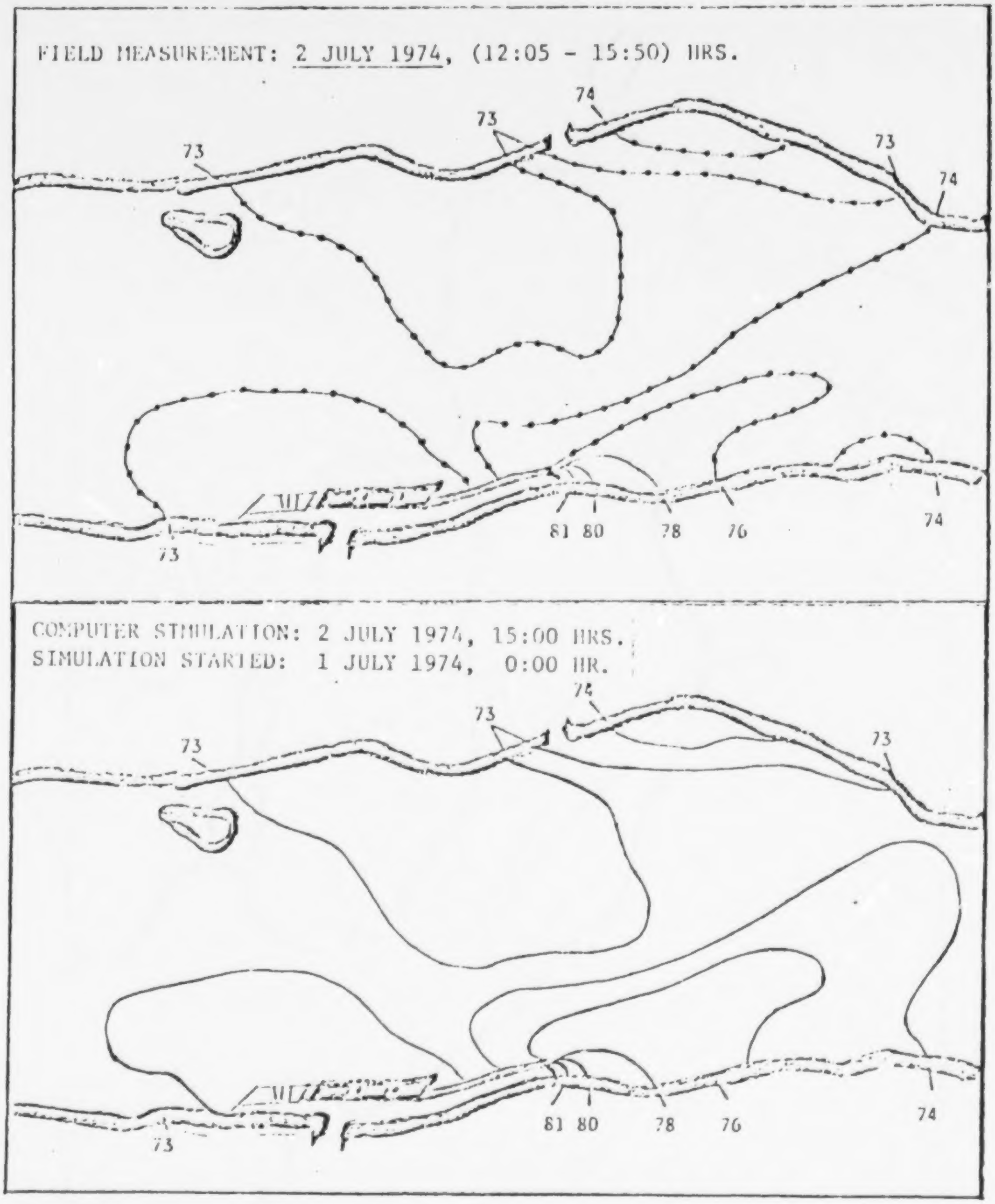
FIELD MEASUREMENT: 2 JULY 1974, (12:05 - 15:50) HRS.

COMPUTER SIMULATION: 2 JULY 1974, 15:00 HRS.
SIMULATION STARTED: 1 JULY 1974, 0:00 HR.

74
73
73
73
74
73
81
80
78
76
74
74
73
73
73
81
80
78
76
74
73

Fig. 4. Comparison of Computer Simulations and Field-Measured Data for the Thermal Discharge Conditions of Peach Bottom Atomic Power Station.

SESSION IV-B
REMOTE SENSING

3-45-9

AERIAL REMOTE SENSING OF THERMAL PLUMES

R. A. Bland
NASA Kennedy Space Center, Florida, U.S.A.

H. W. Hiser, S. S. Lee, and S. Sengupta
University of Miami
Coral Gables, Fla., U.S.A.

ABSTRACT

A twin Beechcraft airplane, operated by the NASA Kennedy Space Center, was used to provide thermal remote sensing data to assist in the development and initial application of a three-dimensional thermal plume mathematical model. The NASA aircraft was equipped with a Daedalus thermal scanner operating in the 8 - 14 μ region. Data from the scanner was recorded on analog magnetic tape which was converted to a color film product with specified temperature regimes identified by a unique color. A data collection mission usually consisted of two flights during the same day. Surface temperature contour maps were drawn from an early morning thermal scanner flight over a power plant discharge area; and this data, in conjunction with surface truth measurements, was used as the initial condition for a model test run. Approximately six hours later, another flight was made; and the resulting data was compared with the math model temperature contour predictions.

Thermal plume data from the two development sites in Florida selected for this model, Biscayne Bay and Hutchinson Island, is described in this paper. The rigid lid and free surface versions of this model are described in these conference proceedings under the numerical modeling section. Also, thermal plume data for the model's first application site, Lake Belews, North Carolina, is described. The thermal plume math model application at Lake Belews is also described in these conference proceedings under the case studies section.

1. INTRODUCTION AND BACKGROUND

Aerial remote sensing was used extensively to provide input data and verification of math model predictions during a three year effort to develop a universally applicable three-dimensional thermal plume math model. Remote sensing data was collected four times (on a seasonal basis) at three power plant discharge sites. These included two sites in Florida where versions of the model were developed. These were Biscayne Bay and Hutchinson Island, Florida. Biscayne Bay is a shallow estuary, and both the rigid lid and free surface models were developed at this site. The relatively small FPL power plant at Cutler Ridge provided classical thermal plume pictures in a very large receiving body of water. In contrast, the FPL St. Lucie Nuclear Power Plant discharges off shore Hutchinson Island some twelve hundred feet into the sea. Here, of course, only the free surface version of the model is

Preceding page blank

applicable. The third site, an initial application of the model, was at Lake Belews, North Carolina. This represented still a different geographical site. It is a small, deep cooling pond for the Duke Power Company Belews Power Station.

The math model development was greatly aided by this aerial remote sensing. Its primary value was the synoptic view provided of the thermal plumes. Various shapes of the plumes and naturally occurring temperature changes in the far field could readily be detected under diverse operation and environmental changes. In some data collection missions, two or even three successive days of data were collected. This enables one to run the model for twenty-four hours or longer and then compare the results with the infrared and ground truth data. Whenever possible, a ground truth boat was positioned under each flight line. The ground truth boat was used, not only to collect subsurface parameters, but also to correct the infrared data for changes brought about by atmospheric phenomena.

In these development and initial application activities for this state-of-the-art thermal plume math model, aircraft provided the basic remote sensing platform. Existing satellites, such as the NOAA-4 and DMSP satellites, played only a minor role as a thermal data source because of their resolution. However, the thermal sensors in the next generation of satellites will have much finer spatial resolution. Landsat "C," schedule to be launched by NASA the latter part of this year, or early 1978, will have a resolution of approximately 237 meters in its thermal band, [1]. Landsat "D," which is in the planning stages for the 1980's, probably will have a resolution of 90 to 120 meters in its thermal IR band [2]. Ultimately, satellites will be used, not only for global ocean surface temperature mapping, but also to provide the accurate, high resolution water temperature data needed for monitoring thermal plumes from power plant discharges.

2. THERMAL SCANNER SYSTEM

A variety of excellent airborne infrared systems are now available commercially. The Kennedy Space Center utilizes a Daedalus DS-1250 series line scanner. Remote sensing of 8-14 μm radiation is achieved by a Hg: Cd: Te detector. This detector has a 0.015-inch square sensitive area which is optimum for the resolution and temperature sensitivity required. This detector is mounted in an end-looking, metal-cased vacuum dewar which has sufficient liquid nitrogen coolant capacity for approximately six hours of operation before refilling. This system projects through the floor of the twin Beechcraft airplane, NASA-6, and has a scan angle of 120° centered about the vertical. The scanner contains a horizontally mounted telescope with its axis aligned along the direction of flight of the airplane. A mirror rotating at 3,600 RPM is mounted at 45° to the telescope and directs heat radiation from the earth into the system. A one-third rotation of the mirror covers a complete step perpendicular to the scanner axis. Optical resolution is approximately 1.7 milliradians, so the ground areas from which the detected signal is averaged becomes a function of height. The aircraft was normally flown at an altitude of 2,000 ft. which results in an accuracy of the infrared data being within the model's predicted accuracy of 0.5°C in the far field.

The video signal from the infrared detector is amplified and recorded on magnetic tape in the aircraft. An aircraft mounted drift sight and Doppler navigation system can monitor actual draft angle and spread. These data enable the operator to eliminate drift angle distortions and along track versus across track scale errors. An 18° F dynamic range between black bodies has been used primarily, but a 24° F and a 36° F range have been found more useful in some thermal plume imagery.

3. COLOR CODING OF ANALOG THERMAL SCANNER SIGNALS

Daedalus has developed a method, termed Digicolor, which converts the original analog signal information directly into color-coded strip map imagery. The basic Digicolor system limits the number of output colors to eight for any input condition. The sequential thermal relationship commencing at the "hottest" level for a given range is white, red, yellow, green, cyan, blue, magenta and black. White indicates temperatures in excess of the upper limit of the set of interest and black is the base level indicating temperatures below the lower limit of the set of interest. The six colors between white and black are the six calibrated levels of the set of interest. The reason for using only eight colors is to produce maximum color distribution between levels for ease of interpretation.

The six basic colors are directly related to a six-step digital level selector. The digital level selector is critically controlled to accept the incoming analog signal and divide any portion of the dynamic range selected into six linear increments. The first set is called the "master" and includes the entire peak-to-peak range between the two reference levels. The master set is carefully adjusted to sense the "hottest" and "coldest" peaks of the total signal since these are the two reference levels with which all additional slices will be compared.

The digital level selector employs a precision voltage divider network which assures precision subdivision. Once the master set is generated, numerous other subdivided sets may be generated accurately by switching to the desired range on the selector. Referring to the chart in Diagram 1, each color range contained in the master set may be subdivided into six more subsets. Note that level 6 (red) for the master set produces subset 6 which repeats the color range. Thus, when viewing the master set imagery, all of the data shown in red will be further divided into all six colors for set 6. Each film run representing a set is identified to avoid any confusion about set relationships.

Diagram 1 illustrates an example of how a magnetic tape signal from the Daedalus quantitative scanner of water thermal data would be converted into Digicolor. Note that the scanner's thermal reference sources (BB1 and BB2) were preset in flight to 66° F and 84° F, respectively. The two blackbody references are always tape recorded on the same track with the detector video to insure accurate voltage relationships irrespective of all amplifier gain adjustments. The calibrated range selected divides the detector video signal into 3° F increments for each master color range, i.e., the blue range of 69° F to 72° F. By analyzing the resulting Digicolor master film, an interpreter can, for example, rapidly determine the thermal distribution of a power plant thermal discharge. The master film has encompassed the entire dynamic range of information between the reference sources which in the example is 18° F. If additional thermal sensitivity is required, any (or all) of the six subsets may be reproduced by replaying the tape and switching to the subset(s) of interest. The subset colors are the same as the master colors, but they represent 1/6th the temperature range which in the example will now be 0.5° F per color. The chart shows that all of the information which produced red on the master film (81° F to 84° F) would be produced in the basic six colors if subset 6 were reproduced. The temperature distribution of subset 6 is illustrated in Diagram 2.

All other subsets can be reproduced in the same manner, or subsets may be "bridged." One example of bridging subsets would be to combine subsets 1 and 2 (66° to 72° F), which when printed out, would provide six colors, each representing 1° F increments. This could then be applied to subsets 3 and 4 (72° to 78° F), resulting in 1° F increments for that portion of the master range, etc. By combining subsets 1 through 4 inclusive, a 12° range is bridged, thus producing 2° F increments for each of the six colors. Variations of these examples may be employed as long as there is continuity between the subsets which are bridged.

4. SELECTED COLOR-CODED THERMAL PLUMES

Figures 1 and 2 are false color thermal infrared images of the discharge from the fossil-fueled Cutler Ridge power plant into Biscayne Bay at Miami. North is to the left in these illustrations. They were taken with the thermal scanner system aboard the aircraft.

Figure 1 was taken at approximately 0912 EDT on 15 April 1975. The sensor-indicated temperatures represented by colors are as follows: white >80° F, red 79-80, yellow 78-79, green 77-78, cyan 76-77, blue 75-76, magenta 74-75, and black <74° F. These temperatures are not corrected for attenuation by water vapor between the surface and the aircraft flight level which was 2000 ft. Boat measurements of surface water temperatures indicated that a +4° F (2.3°C) correction should be added to the remote sensed temperatures. The Cutler Ridge plant had a discharge volume of 43,200 m^3/hr at a temperature of 35.9° C (96.6°F). The surface wind was from the southwest at about 9.76 m/sec (19 knots). The bay is shallow in the area where the plume is discharged, slightly more than one meter in depth.

Figure 2 was taken at approximately 1345 EDT on 4 September 1975 from a 2000 ft. altitude. The colors depict the following uncorrected temperatures: white >90° F, red 88.5-90, yellow 87-88.5, green 85.5-87, cyan 84-85.5, blue 82.5-84, magenta 81-82.5, black <81° F. Boat measurements indicated that a +7° F (3.8° C) correction should be added to the remote sensed temperatures.

The plant discharge volume was 34,560 m^3/hr at a temperature of 40.6° C (105° F). The surface wind was from the southeast at 3.44 m/sec (6.5 knots). The differences in the shapes of the plumes in Figs. 1 and 2 are largely due to different tide conditions. In Figure 1, there was a flow or incoming tide counter to the plume; while in Fig. 2, the tide was ebbing and aided in stretching the plume.

Figures 3 and 4 are thermal infrared images of the mixing pond and main lake, respectively, at the Lake Belews, N.C., fossil-fuel plant of the Duke Power Company. These thermal scans were made between 0900 and 0955 EDT on 19 May 1976 with the aircraft flying at 2000 ft. above the surface. In these figures the uncorrected temperatures are: > white 86° F, red 83-86, yellow 80-83, green 77-80, cyan 74-77, blue 71-74, magenta 68-71 and black <68° F. On the right side of Fig. 3, the plant discharge into the mixing pond exceeded 86° F. The discharge from the mixing pond into the main lake at the top center of Fig. 4 was 83-86° F.

Lake Belews is a man-made lake with an area of 3,863 acres. It was created by building a dam on Belews Creek in 1970. There are two power units each with a capacity of 1143 megawatts. Cool water at an average rate of 238,000 m^3/hr is taken from the main lake. At full load, the temperature of the water is raised by 10° C (18° F), and the hot water is discharged into the mixing pond. The hot discharge is cooled slightly in the mixing pond because of the initial mixing with cooler water. The mixing pond is connected to the main lake through a narrow canal. The maximum depth of the mixing pond is 13.72 meters (45 ft). The maximum depth of the main lake is 38.2 meters (125.3 ft).

Figures 5 and 6 show the plume from the Hutchinson Island nuclear plant extending northward along the Atlantic coast during the time it was scanned, 1048-1059 EDT, on 2 June 1976. North is toward the bottom of the page in these two illustrations, and Fig. 6 is a continuation of Fig. 5. The aircraft flight altitude was 2000 ft., and the color-coded uncorrected temperatures are as follows: >White 88° F, red 85-88, yellow 82-85, green 79-82, cyan 76-79, blue 73-76, magenta 70-73, and black < 70° F. In this image all temperatures were greater than73° F. Boat measurements indicated that a +4° F (2.1° C) correction should be added to the remote sensed water surface temperatures.

The Florida Power and Light Company's Hutchinson Island Nuclear Power Plant is located about midway between the cities of Fort Pierce and Stuart on the Atlantic coast of Florida. The rating of the plant is to be 850 megawatts electrical. The 3.66 meters diameter submerged discharge pipeline is buried in the ocean bed and terminates at a point about 366 meters offshore and 5.48 meters below mean water level. At its termination, a two port Y-type discharge is added with each arm being 2.29 meters in diameter. A short sloping concrete pan is located at the outlet to prevent scouring of the ocean floor. On 2 June 1976, at 50 percent rated load, the heated discharge had a flow rate of about 363,000 GPM (82,437 m^3/hr) with an exit velocity of 280 cm/sec at each end of the Y-type discharging pipe. The discharge water temperature was 35° C (95° F). The ambient water temperature was about 25.5° C (78° F) and air temperature was 29° C (84° F). The wind speed was 10 mph (4.5 m/sec) and air temperature was 29° C (84° F). The wind speed was 10 mph (4.5 m/sec) from the southeast. The ocean current was about 25 cm/sec predominantly toward the north.

5. CORRECTION OF AIRCRAFT INFRARED MEASUREMENTS

Aerial measurements of surface thermal plumes which are made in the 8 to 14 micron region of the spectrum are subject to errors. The primary source of error is atmospheric water vapor absorption. Non-blackness of the water body can be another source of error. There is a strong ozone absorption band between 9 and 10 microns, but the maximum ozone concentration is at high altitudes so that it can be ignored for low altitude aircraft measurements. There is also some absorption by CO_2, mainly in the 13 to 14 micron region.

A literature search was made into the methods and models used by other researchers to correct aerial infrared data [3], [4], [5], [6], [7]. It was concluded that these models fail to give true absolute temperatures in the low latitudes and south and central Florida where there is a large concentration of moisture at low altitudes. Consequently, we chose to use the numerous ground truth water temperature measurements made with a Barnes PRT 5 instrument and various thermistors to directly correct the aircraft infrared data rather than apply a theoretical method. At least one data collecting boat was scheduled to be on several NASA-6 flight lines to determine if the delta temperature correction changed during the data collection mission.

Most corrections for the aircraft thermal IR data were of the order of plus 2 to 3 degrees C. The uncorrected infrared isotherms give excellent relative thermal patterns, and after ground truth corrections are applied, they provide high quality quantitative results for modelling applications.

6. REFERENCES

1. Landsat Data Users Handbook, Document No. 76SDS4258, NASA Goddard Space Flight Center, Greenbelt, Maryland, September 2, 1976.

2. Committee on Remote Sensing Programs for Earth Resource Surveys, Resource and Environmental Surveys from Space with the Thematic Mapper in the 1980's, Commission on Natural Resources, National Research Council, National Academy of Sciences, Washington, D.C., 1976.

3. Veziroglu, T.N., S.S. Lee, H. W. Hiser, N. L. Weinberg, J. G. Hirschberg and S. Sengupta, Application of Remote Sensing for Prediction and Detection of Thermal Pollution, Technical Report, NASA CR-139182, Clean Energy Research Institute, School of Engineering and Environmental Design, Univ. of Miami, Coral Gables, Florida, October 1974.

4. Lee, S. S., T. N. Veziroglu, S. Sengupta, and N. L. Weinberg, "Remote Sensing Applied to Thermal Pollution," Remote Sensing Applied to Energy-Related Problems Symposium Proceedings, Clean Energy Research Institute, School of Engineering and Environmental Design, Univ. of Miami, Coral Gables, Florida, December 1974.

5. Hiser, H. W., S. S. Lee, T. N. Veziroglu, and S. Sengupta, "Application of Remote Sensing to Thermal Pollution Analysis" Proceedings of the Fourth Annual Remote Sensing of Earth Resources Conference, University of Tennessee Space Institute, Tullahoma, Tenn, March 1975.

6. Veziroglu, T. N., S. S. Lee, H. W. Hiser, N. L. Weinberg, J. G. Hirschberg, and S. Sengupta, Application of Remote Sensing for Prediction and Detection of Thermal Pollution, NASA Contract NAS10-8740, John F. Kennedy Space Center, Florida, December 1975.

7. Byrne, J. D., Thermal Infrared Studies in the Biscayne Bay Area, NASA Contract NAS10-8926, John F. Kennedy Space Center, Florida, Master's Thesis, University of Miami, Dept. of Mechanical Engineering, Coral Gables, Fla., June 1976.

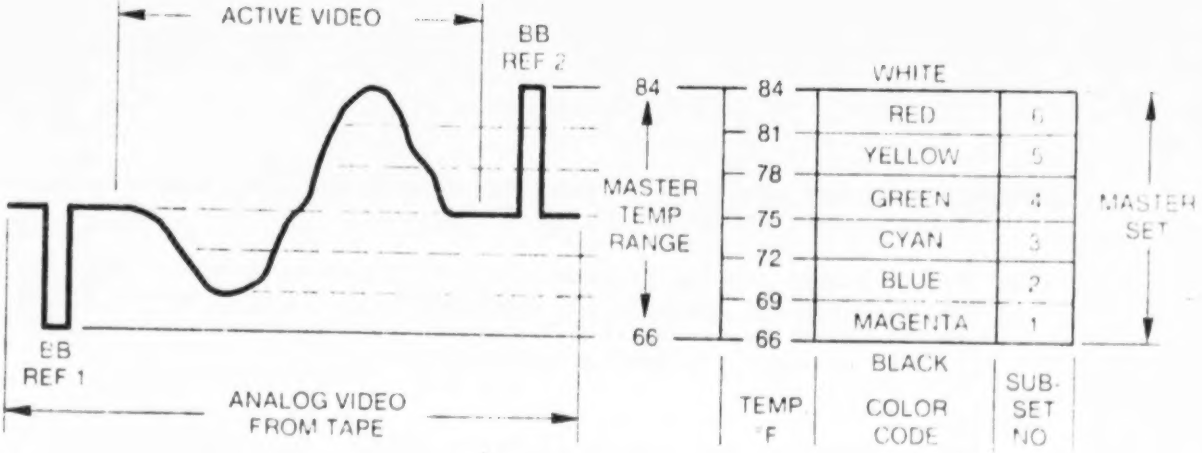
ACTIVE VIDEO
BB
REF 2
BB
REF 1
ANALOG VIDEO
FROM TAPE
84
MASTER
TEMP
RANGE
66
84
81
78
75
72
69
66
WHITE
RED
YELLOW
GREEN
CYAN
BLUE
MAGENTA
BLACK
6
5
4
3
2
1
MASTER
SET
TEMP
°F
COLOR
CODE
SUB-
SET
NO

Diagram 1.

Conversion from Magnetic Tape Data to Color Film

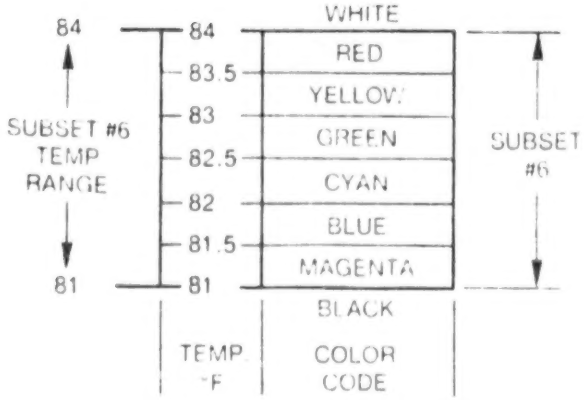
84
SUBSET #6
TEMP
RANGE
81
84
83.5
83
82.5
82
81.5
81
WHITE
RED
YELLOW
GREEN
CYAN
BLUE
MAGENTA
BLACK
SUBSET
#6
TEMP
°F
COLOR
CODE

Diagram 2

AERIAL REMOTE SENSING OF THERMAL PLUMES

LIST OF FIGURES

Figure 1 Biscayne Bay (Flow Tide) 0912 EDT, April 15, 1975 (74° - 80° F, 23.3° - 26.7° C, span on plume).

Figure 2 Biscayne Bay (Ebb Tide) 1345 EDT, September 4, 1975 (81° - 90° F, 27.2° - 32.2° C, span on plume).

Figure 3 Lake Belews Mixing Pond (Plant Discharge is at Right End) 0900 EDT, May 19, 1976 (68° - 86° F, 20.0° - 30.0° C, temperature span).

Figure 4 South End of Lake Belews Main Lake (Top center, discharge into lake from mixing pond) 0905-0955 EDT, May 19, 1976 (68° - 86° F, 20.0° - 30.0° C, temperature span).

Figure 5 Off Shore Hutchinson Island (North is toward bottom of page) 1048-1059 EDT, June 2, 1976 (70° - 88° F, 21.1° - 31.1° C, span on plume).

Figure 6 Off Shore Hutchinson Island (Cont. of Fig. 5) 1048-1059 EDT, June 2, 1976.

IV - B - 64

Figure 1

Figure 2

Figure 3

Figure 4

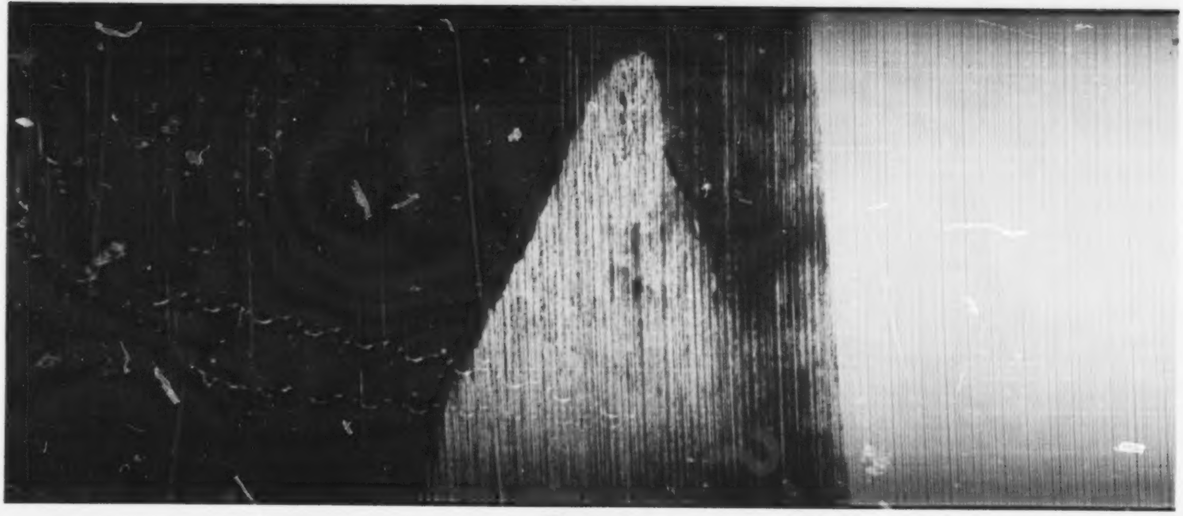

Figure 5

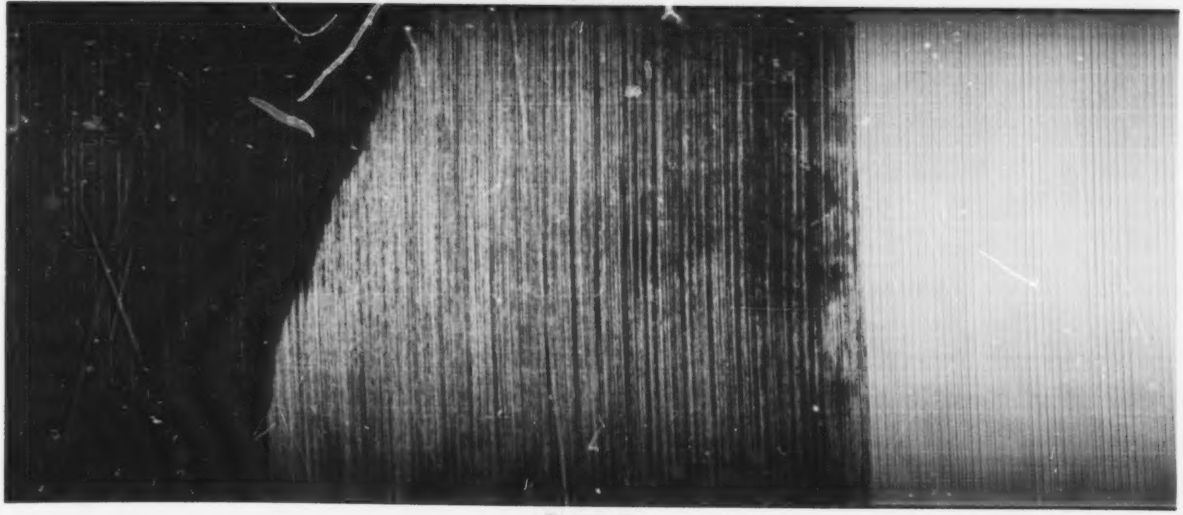

Figure 6

METEOROLOGICAL SATELLITES

M. Tepper, N. Durocher
NASA Headquarters
Washington, D. C.

IV-B-67 4-45-10

THE LANDSAT PROGRAM

H. Mannheimer
NASA Headquarters
Washington, DC, U.S.A.

ABSTRACT

This paper gives a description and present status of NASA's Landsat program, including the orbital coverage, payload, data processing, and data products. Data uses are discussed in general terms. Also discussed are NASA's plans for the Landsat-C and Landsat-D missions and the improved capabilities represented by these missions.

INTRODUCTION

The potential for global land survey utilizing spaceborne sensors began in the form of hand-held cameras operated by Gemini and Apollo astronauts. Observations were expanded into the infrared region of the electromagnetic spectrum in the later Apollo and Skylab flights. Meanwhile, the Tiros satellite became the first successful unmanned earth observatory equipped with small visible light TV cameras. In July 1972, however, a new era in spaceborne earth observation technology began with the launch of the first Earth Resources Technology Satellite, ERTS-1. The spacecraft was later more descriptively renamed Landsat-1. Landsat-1 was followed two and one-half years later by the launch of Landsat-2 in January 1975. A Landsat-C launch is planned for late 1977 or early 1978, and Landsat-D is scheduled to be launched in 1981.

MISSION DESCRIPTION

Landsat-1 and -2 were launched from the Western Test Range utilizing the two-stage Delta launch vehicle augmented by nine solid rockets. Landsat-C will be similarly launched. The spacecraft is placed in a circular, near-polar orbit with a 99° inclination which is sun-synchronous--that is, the orbital plane precession rate is equal to the earth's rotation rate about the sun, thus allowing the spacecraft to view a given point on the earth at the same local time for each orbit. This will permit essentially the same surface sun angle conditions to exist for a given time of the year for all imagery taken and simplify the data extraction. Orbital altitude is 495 nautical miles (917 kilometers). The orbit is nearly repetitive each day, and the exact ground track is repeated every 18 days or 251 orbits. On succeeding days, the ground track moves in a westerly direction and is separated by 159 kilometers from the preceding day's track. With both Landsat-1 and -2 in orbit, significant improvement in the study of dynamic observed phenomena is possible due to the resulting increased frequency of observation of a given area by the two-satellite system. Landsat-D's orbital altitude will be lowered to 438 nautical miles (705 kilometers) in order to achieve higher spatial resolution and to permit more economic Space Shuttle retrieval and replacement.

LANDSAT PAYLOADS

The Landsat-1 and -2 payloads, essentially identical, include a four-band Multispectral Scanner (MSS), a Return Beam Vidicon (RBV) camera system, and a Data Collection System (DCS) used to relay to a ground receiver measurements taken by remote, unmanned data collection platforms.

The MSS, the primary Landsat earth observation sensor, is an electronic imaging device, utilizing an oscillating flat mirror which reflects incoming earth-reflected electromagnetic energy onto the faces of twenty-four detectors through connecting glass fibers and appropriate color filters. Table 1 summarizes the MSS characteristics.

The instantaneous field of view of each detector subtends an earth-area square of 79 meters on a side from the nominal orbital altitude. Field stops are formed for each line imaged during a scan and, for each spectral band, by the square input end of an optical fiber. Six of these fibers in each of four bands are arranged in a 4 by 6 matrix in the focused area of the telescope.

Light impinging on each glass fiber is conducted to an individual detector through an optical filter, unique to the spectral band served. An image of a line across the swath is swept across the fiber each time the mirror scans, causing a video signal to be produced at the scanner electronics output for each of 24 channels. These signals are then sampled, digitized, and formatted into a serial digital data stream by a multiplexer. The sampling interval is 9.95 μsec, corresponding to a cross track motion of the instantaneous field of view of 56 meters.

The along-track scan is produced by the orbital motion of the spacecraft. The nominal orbital velocity causes an along-track motion of the subsatellite point of 6.47 km/sec neglecting spacecraft perturbation and earth rotation effects. By oscillating the mirror at a rate of 13.62 Hz, the subsatellite point will have moved 474 meters along track during the 73.42 millisecond active scan and retrace cycle. The width of the along-track field of view of six detectors is also 474 meters. Thus, complete coverage of the total 185 kilometer wide swath is obtained. The line scanned by the first detector in one cycle of the active mirror scan lies adjacent to the line scanned by the sixth detector of the previous mirror scan. Figures 1 and 2 show this scanning arrangement and composite scan pattern.

The four bands use the earth reflected energy to distinguish earth characteristics such as vegetation, water, crops, crop stress, geological phenomena, etc. Spectral information, or signatures, reflected in the four bands of the MSS cause variations in the output signals of the detectors proportional to variations in the received spectral energy. These analog signals are converted into a digital data stream for storage on one of two tape recorders onboard the satellite for subsequent transmission when over a ground station or are directly transmitted in real time to a ground receiving station. Each MSS image transmitted and processed by a ground station covers an area 100 by 100 nautical miles square (185 kilometers) with a spatial resolution of 79 meters. In the four and one-half years of Landsat-1 operation, approximately 250,000 MSS images have been processed, representing a repetitive observation area of approximately two billion, five hundred million square miles. Landsat-2's processed imagery represents a repetitive observation area of a little less than half of that of Landsat-1. As a note of interest, the Landsat-1 MSS mirror has thus far completed more than 130 million oscillations.

The second instrument system onboard Landsat, the RBV system, consists of three Return Beam Vidicon television-type cameras. The RBV's view the same 100 nautical mile square ground scene as does the MSS and collect reflected energy from the earth in three spectral bands from 0.475 to 0.83 micrometers. When the cameras are shuttered to collect data, the resulting image received is stored on the photosensitive face of each RBV tube, which are then scanned to produce video outputs. The cameras are scanned in sequence, requiring about 3.5 seconds to read out each of the three images. To produce overlapping images of the ground along the direction of satellite motion, the cameras are shuttered every twenty-five seconds.

The Landsat Data Collection System (DCS) obtains data from remote, automatic data collection platforms, which are equipped by specific investigators, and relays the data to ground stations whenever the Landsat spacecraft can mutually view any platform and any one of the ground stations. Each DCS platform collects data from as many as eight sensors, supplied by the cognizant investigator, sampling such local environmental conditions as temperature, stream flow, snow depth, or soil moisture. Data from any platform is available to investigators within 24 hours from the time the sensor measurements are relayed by the spacecraft. As a point of interest, the Landsat-1 and -2 DCS have conducted over 1,200,000 platform interrogations.

As previously mentioned, the payloads for Landsat-1 and -2 are identical. Landsat-C's payload will, however, include upgrading of the MSS and the RBV's in order to increase the usefulness and quality of the data collected. A fifth channel, sensing the 10.5 to 12.5 micrometer spectral band in the thermal infrared region, will be added to the MSS. This fifth band will provide a temperature resolution of 1.5° K at a spatial resolution of 240 meters and aid in the detection and analysis of dynamic changes that are characterized by temperature differences. The RBV system is being modified to a two-camera panchromatic system operating in the same 0.53 to 0.75 micrometer visible regions. Optics improvements in these two RBV cameras will result in a 40 meter RBV spatial resolution capability. A single RBV image will now be reduced to a 50 nmi scene; and, to insure total coverage of an MSS scene, each camera is now shuttered so that four RBV images are equivalent to one 100 nmi by 100 nmi MSS scene.

LANDSAT DATA PROCESSING AND DISSEMINATION

Landsat data is received at three U.S. ground stations and recorded on magnetic tapes. These magnetic tapes are shipped to a Data Processing Facility at Goddard Space Flight Center where required geometric and radiometric corrections are made to the data. The data is then archived and sent to the Federal Data Centers for distribution to the many users and use investigators. This processed imagery data is made available to users in the form of computer compatible magnetic tapes, 70 mm negatives, and black and white and color composite prints.

Interest in Landsat data is world-wide. Italy, Canada, and Brazil have constructed their own receiving and processing stations. These countries have direct access to the Landsat satellite and its imagery when it passes over their receiving stations and pay NASA an annual fee for this satellite service. About a half-dozen other countries have signed MOU's (Memorandum of Understanding) or are in the preliminary discussion stage preparatory to the installation of their own receiving and processing stations.

An upgraded data processing facility is being developed to support the Landsat program and will utilize an all-digital processing technique instead of the present hybrid system. This facility will also make it possible to process Landsat data on a routine basis in one to two days instead of the present five to seven days. This facility will be partially operational in September 1977 and fully operational by March 1978. This new capability will improve the timeliness of Landsat data and significantly improve useful data applications because the all-digital processing will significantly improve the geometric accuracy of the data and permit more sophisticated data extraction techniques.

SPACECRAFT STATUS AND PLANS

Landsat-1, designed for a one-year lifetime, passed its fourth anniversary in orbit this past July. To be sure, it has problems: both tape recorders are out of operation and the attitude control gas is almost gone. Nevertheless, it continues to return excellent data to the six direct readout stations located in the U.S. and abroad.

Landsat-2 continues to operate well after two years in orbit, but with only one tape recorder fully operable. To relieve the load on the remaining operable tape recorder, a portable ground station has been deployed in Pakistan for direct ground acquisition of MSS imagery in support of the LACIE program. A special LACIE recording capability has also been implemented at the Italian station to reduce the remaining tape recorder utilization.

The Landsat-C development is on schedule for a September 1977 launch readiness. The new five-band MSS and improved resolution RBV have been completed, shipped to the prime contractor, and integrated with the spacecraft. It is our plan to complete the spacecraft and all necessary functional and environmental tasks to insure a September 1977 launch readiness. However, we are considering an option to postpone the launch for a period, up to six months, to minimize the potential data gap in multispectral imagery before Landsat-D can be launched. The decision to delay the launch of Landsat-C is dependent on the continued satisfactory operation of Landsat-2, and the decision will probably not be made before this summer.

The procurement of a new-generation, significantly more powerful sensor, called the Thematic Mapper (TM), has been initiated; and a contractor to develop the instrument has been selected. Present plans call for delivery of a flight-worthy instrument by the middle of CY 1980. This will make the delivery of this new and powerful instrument compatible with the planned launch of Landsat-D in the first quarter of CY 1981.

Landsat-D, included in the FY 1978 budget submission as a New Start, will be the test bed for the Thematic Mapper. This instrument will provide significant improvements in the ability to detect and identify smaller areas because of its higher spatial resolution (30 meters) and be capable of discriminating significantly more shades of gray per picture element (256 or 64 radiometric resolution elements) than the Landsat-C MSS. Additionally, the TM will utilize additional, optimized spectral bands to provide increased refinement in the ability to classify vegetation, crops, crop status, and other natural resources and geological features. The performance characteristics of this instrument are given in Table 2.

Full utilization of the TM's resolution capability demands a more precise attitude control system than Landsat-C; additionally, the increased spatial and radiometric resolution require significant improvement in the spacecraft's data handling and communication system. To accommodate these new requirements, NASA has chosen the new multimission spacecraft as the spacecraft bus to support the TM.

Use of this spacecraft's modular concept will also permit Shuttle retrieval and the resultant repair or replacement of failed spacecraft elements when the Space Shuttle becomes operational. The transmission of the additional instrument data will be facilitated by utilization of the Tracking and Data Relay Satellite System (TDRSS) relay capability to a single U.S. ground receiving station. In this way, no onboard recording capability is required. As a backup to the single Landsat-D high gain TDRSS antenna, a direct readout capability to ground stations at X-band will also be provided. This will also allow the continued direct reception of imagery data by foreign ground stations.

We had originally planned to include an MSS in the instrument complement for Landsat-D, but the addition of this instrument was not authorized. Incorporation of the MSS would have provided data continuity to the domestic and foreign users who did not demand or require the improved TM data. NASA is presently surveying the user community to determine the degree of user demand in the continuity of MSS data and to solicit financial support to help defray the cost associated with the inclusion of the MSS on Landsat-D. If sufficient financial support is found, NASA will reconsider its decision not to fly the MSS. It should also be noted that the MSS would serve as a backup instrument to the new TM and, consequently, would reduce the Landsat-D mission risks.

TABLE 1

MULTISPECTRAL SCANNER CHARACTERISTICS

Band	Spectral Range (micrometers)	Radiometric Performance SNR (min.)	Radiometric Performance NETD (max.)	Spatial Resolution (meters)
1	0.50 - 0.60	71		79
2	0.60 - 0.70	57		79
3	0.70 - 0.80	38		79
4	0.80 - 1.10	77		79
5*	10.40 - 12.50		1.5°K	237

Digitization - 6 bits

Data Rate - 15 Mbits/sec

*Landsat-C only

TABLE 2

THEMATIC MAPPER CHARACTERISTICS

Band	Spectral Range (micrometers)	Radiometric Performance SNR (min.)	NETD (max.)	Spatial Resolution (meters)
1	0.45 - 0.52	85		30
2	0.52 - 0.60	170		30
3	0.63 - 0.69	143		30
4	0.76 - 0.90	249		30
5	1.55 - 1.75	75		30
6	10.40 - 12.50		$0.5^{\circ}K$	120

Digitization - 8 bits

Data Rate - 83 Mbits/sec

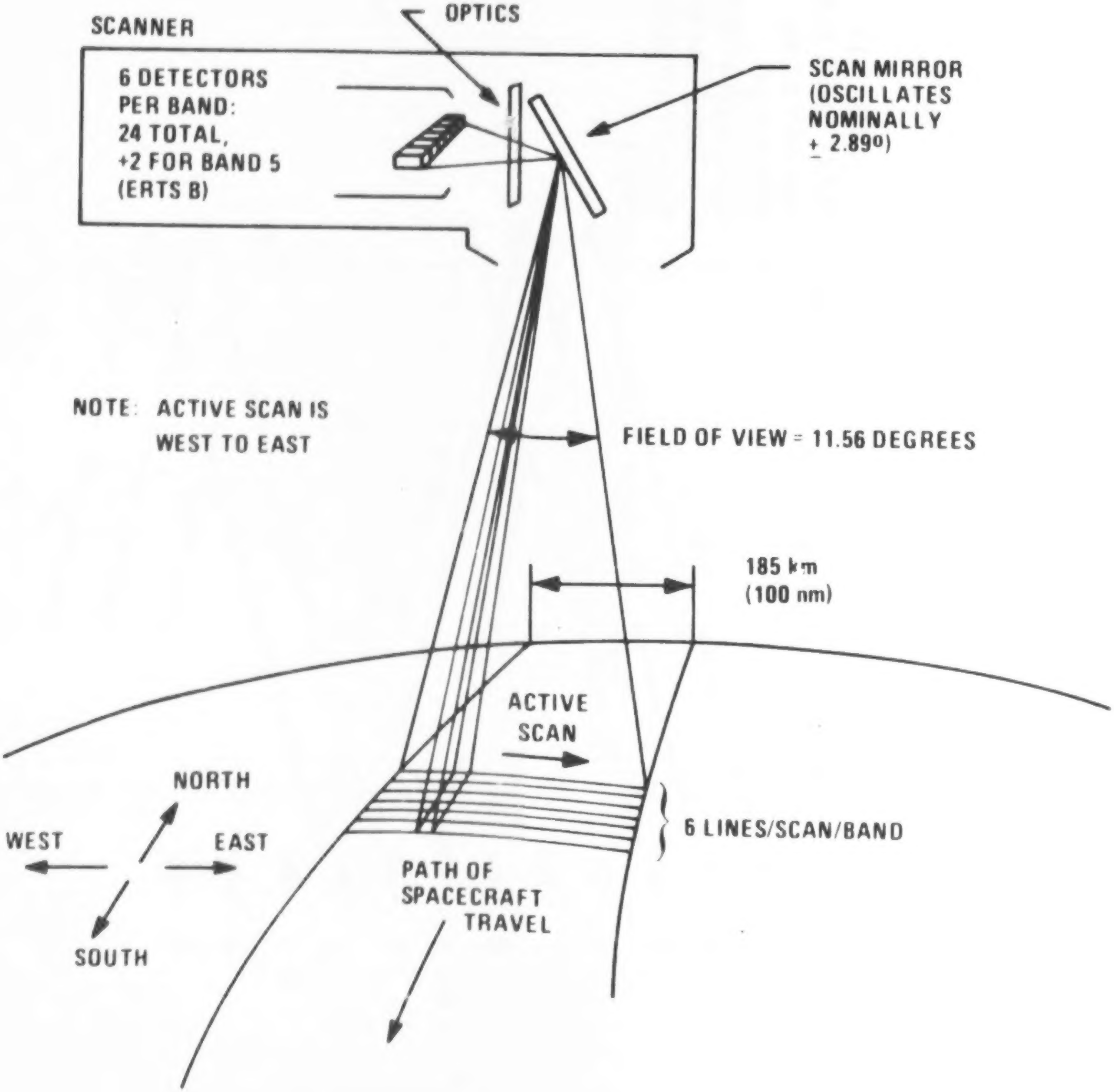
SCANNER
OPTICS
6 DETECTORS PER BAND: 24 TOTAL, +2 FOR BAND 5 (ERTS B)
SCAN MIRROR (OSCILLATES NOMINALLY ± 2.89°)
NOTE: ACTIVE SCAN IS WEST TO EAST
FIELD OF VIEW = 11.56 DEGREES
185 km (100 nm)
ACTIVE SCAN
NORTH
WEST
EAST
SOUTH
6 LINES/SCAN/BAND
PATH OF SPACECRAFT TRAVEL

Figure 1. MSS Scanning Arrangement

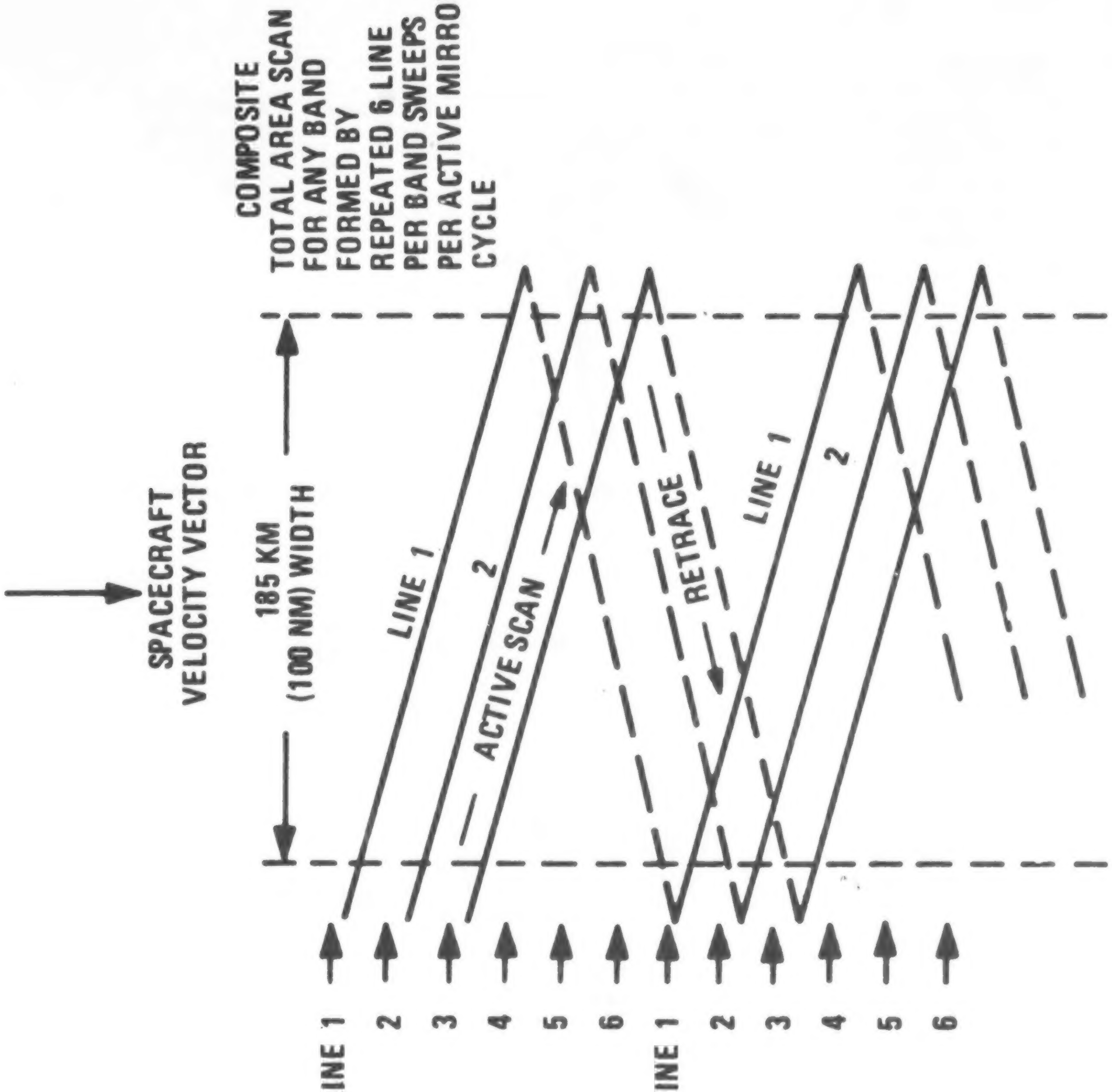
SPACECRAFT VELOCITY VECTOR
185 KM (100 NM) WIDTH
COMPOSITE TOTAL AREA SCAN FOR ANY BAND FORMED BY REPEATED 6 LINE PER BAND SWEEPS PER ACTIVE MIRROR CYCLE
LINE 1
2
ACTIVE SCAN
RETRACE
LINE 1
2
LINE 1
2
3
4
5
6
LINE 1
2
3
4
5
6
nTH MIRROR SCAN
n + 1ST MIRROR SCAN

Figure 2. Ground Scan Pattern for a Single MSS Detector

5-45-25

IV-B-77

SEASAT-A

REMOTE SENSING ENTERS THE MARINE ENVIRONMENT

S.W. McCandless, Jr.
Manager, (SEASAT Programs)
Office of Applications
NASA Headquarters
Washington, D. C.

ABSTRACT

In recent years the potential for remote sensing of physical phenomena has been advanced by research and by developments in the fields of meteorology and earth observations; with the exception of cloud cover photographs and infrared derived temperature determinations, little use has been made of such techniques for oceanological purposes. On the other hand, recognizing the dynamic nature of oceanological phenomena and the difficulty and expense of obtaining in situ measurements (particularly the needed globally consistent, geographically and temporally dense, data) a need exists to consider the potential for application of such tehniques to ocean-oriented phenomena. Now, the Seasat-A space program has been initiated as a "proof-of-concept" mission to evaluate the effectiveness of remotely sensing oceanological and meteorological phenomena from a satelliteborne platform in space, through utilization of remote sensors developed on previous space and aircraft programs. The users initiated Seasat-A nd continue to serve as the architects of the program. Requirements for a system, derived from the expressed needs of potential users of such data, are discussed, together with the current capabilities and limitations of spaceborne sensors to obtain such data. The goals of the Seasat-A spacecraft and its associated data system are described, as well as the approach planned to verify the measurements being taken and to confirm the benefits and effectiveness of the system in meeting the needs of the ocean-using community.

THE PAST

"In 1872 HMS Challenger left Portsmouth on a voyage that was to take her around the world, eight times across the Equator, into the Antarctic ice over 68,000 nautical miles at sea. She was a three-masted corvette with auxiliary steam, and, as well as a crew of 243 she carried a team of scientists led by Professor Wyville Thomson.

The voyage of the Challenger was a pioneer expedition of immense importance. It was sponsored by the British Government and organized by the Royal Society in collaboration with the University of Edinburgh, where the science of Oceanography was born. The ambitious aim of the voyage was to chart the depths, movement and content of the seas, to scour the oceans for marine life, for clues to climatic phenomena, and for minerals." (Ref. 1)

One hundred and five years later Seasat-A will be launched into earth orbit from Vandenberg Air Force Base, California. In less than five hours Seasat-A will have travelled a distance equivalent to that travelled by the Challenger and have embarked on a voyage of perhaps even greater importance.

The voyage of Challenger was initiated by the ocean-using community, both government and commercial, and the ocean scientists. The **Seasat** Program, which is under the sponsorship of the Office of Applications, Special Programs Division, National Aeronautics and Space Administration, in collaboration with the Jet Propulsion Laboratory of the California Institute of Technology, has its origins with these same users, and thus, blends the requirements of government and commercial sea users with those of the scientific community.

TODAY'S NEEDS

From a symposium in Williamstown, Mass., in 1969(2), the goals and objectives for observation, measurement, and interpretation of physical ocean phenomena have evolved, aided by continuing interaction between Ocean Users and System Designers. In 1972 NASA's Oceans Applications Programs objectives were published; they included specific recommendations from a group of governmental, institutional, and private ocean users working with the program. Since then, regular meetings of a Users Working Group have assisted NASA during all program phases beginning with the refinement of program requirements during the program definition phase, to take advantage of advancements in the field of remote sensing, and to resolve any apparent conflicts between requirements and capabilities, and to develop their own supporting programs. Currently, a formally organized Oceanology Advisory Subcommittee under the auspices of NASA's Applications Advisory Committee, derived from the Users Working Group, conducts regular quarterly meetings to continue these interactions. These continuing interactions have been essential in converting user requirements into a total system with the sole goal of providing continuous useful data to the Ocean using community in a timely manner.

The list of active users is large. From the federal government it includes the following:

- Department of Commerce (National Oceanic and Atmospheric Administration, Maritime Administration, National Marine Fisheries)
- Department of Defense (Defense Mapping Agency, Army Corps of Engineers, Navy Weather Service Command, Office of Naval Research, Naval Surface Weapons Center, Naval Research Laboratory, Naval Oceanographic Office)
- Department of Interior (Geological Survey)
- Department of Transportation (Coast Guard)
- Energy Research and Development Administration
- National Science Foundation
- National Academy of Sciences
- National Academy of Engineering

Institutional users who are active participants follows:

- Smithsonian Astrophysical Observatory; Environmental Center for Atmospheric Research
- Woods Hole Oceanographic Institution
- Scripps Institute of Oceanography
- City University of New York
- Battelle Memorial Institute

From the private sector, the user community includes representatives of the:

- shipping industry
- oil industry
- fishing industry
- and coastal industries

The private sector will most likely be the future prime economic and social beneficiary.

The ocean community, like many others - and probably more than most - suffers from a lack of data. Most current observations, obtained from shipboard personnel, suffer a degree of inconsistency in quality as well as in temporal correlation. Other more consistent observations, (the NOAA buoys are an example) are from a limited number of locations and leave vast areas of the globe with little or no coverage. On the other hand, satellite-derived cloud cover and infrared temperature data, while providing synoptic coverage (valuable in its own right), in general lacks correlation with wind and wave information and cannot penetrate cloud cover to measure ocean surface conditions. Thus, the effectivity of a monitoring and now-casting system for the oceans is very limited. For example, forecast of wave heights depends upon time and space forecasts of surface winds, themselves subject to considerable uncertainty. Similarly, locations of ocean currents are only approximately known and the ability of shipping and fishing interests to exploit ocean currents and upwellings is lacking. Long-range weather forecasting for both continental and ocean areas is dependent upon a space- and time-dense initialization of wind, temperature, and pressure data. It is estimated(3) that observations of ocean conditions in about the same frequency and spatial density as available now for the continents will be required for improved weather forecasting.

The measurement needs as expressed by the wide range of users are summarized in Table 1.(4) Essential ingredients in any future operational ocean dynamics monitoring system are the attainment of global, all-weather, coverage; near-realtime data processing, evaluation, and distribution of data; and user feedback of operational utility to ensure continued system responsiveness to needs. Current systems such as Seasat-A are not capable of meeting these requirements. For comparison purposes, Seasat-A capabilities are shown in Table 2. A more complete description of the Seasat-A system is included later in this paper.

In Table 3, the principal groups of users of data are correlated with estimated needs for data. An almost unanimous need for data on wind fields and wave height and direction is apparent.

Table 1

MEASUREMENT NEEDS

MEASUREMENT			RANGE	PRECISION/ ACCURACY	RESOLUTION	SPATIAL GRID	TEMPORAL GRID
TOPOGRAPHY	GEOID		5 cm TO 200 m	< ±10 cm	<10 km		WEEKLY TO MONTHLY
	CURRENTS, SURGES, ETC.		10 cm TO 10 m 5 TO 500 cm/sec	< ±10 cm +5 cm/SEC	10 TO 1000 m	<10 km	TWICE A DAY TO WEEKLY
SURFACE WINDS	AMPLITUDE	OPEN OCEAN	3 TO 50 m/s	+1 TO 2 m/s OR ±10%	10 TO 50 km	50 TO 100 km	2 TO 8/DAY
		CLOSED SEA			5 TO 25 km	25 km	
		COASTAL			1 TO 5 km	5 km	HOURLY
	DIRECTION		0 TO 360 DEG	±10 TO 20 DEG			
GRAVITY WAVES	HEIGHT		0.5 TO 20 m	+0.5 m OR +10 TO 25%	< 20 km	< 50 km	2 TO 8/DAY
	LENGTH		6 TO 1000 m	+10 TO 25%	3 TO 50 m		2 TO 4/DAY
	DIRECTION			+10 TO 30 DEG			
SURFACE TEMPERATURE	OPEN OCEAN		-2 TO 35°C	0.1 TO 2° RELATIVE 0.5 TO 2° ABSOLUTE	25 TO 100 km	100 km	DAILY TO WEEKLY WITH SPECTRUM OF TIMES OF DAY AND TIMES OF YR
	CLOSED SEA				5 TO 25 km	25 km	
	COASTAL				0.1 TO 5 km	5 km	
SEA ICE	EXTENT AND AGE			1 TO 5 km	1 TO 5 km	1 TO 5 km	WEEKLY
	LEADS		>50 m	25 m	25 m	25 m	2 TO 4/DAY
	ICEBERGS		>10 m	1 TO 50 m	1 TO 50 m		
OCEAN FEATURES	OPEN OCEAN			50 TO 500 m			TWICE DAILY TO DAILY
	COASTAL			10 TO 100 m			
SALINITY			0 TO 30 ppt	±0.1 TO 1 ppt	1 TO 10 km	100 km	WEEKLY
SURFACE PRESSURE			930 TO 1030 mb	±2 TO 4 mb	1 TO 10 km	1 TO 10 km	HOURLY

TABLE 2

GEOPHYSICAL OCEANOGRAPHIC MEASUREMENT CAPABILITIES FOR SEASAT-A

MEASUREMENT			RANGE	PRECISION/ACCURACY	RESOLUTION, km	SPACIAL GRID, km	TEMPORAL GRID
TOPOGRAPHY	GEOID	ALTIMETER	5 cm - 200 m	<± 20 cm	1.6 - 12	~10	LESS THAN 6 MONTHS
	CURRENTS, SURGES, ETC		10 cm - 10 m				
SURFACE WINDS	AMPLITUDE	MICROWAVE RADIOMETER	7 - 50 m/s	± 2 m/s OR ±10%	50	50	36 h TO 95% COVERAGE
		SCATTER-OMETER	3 - 25 m/s	± 2 m/s OR 10%	50	100	36 h TO 95% COVERAGE
	DIRECTION		0 - 360°	± 20°			
GRAVITY WAVES	HEIGHT	ALTIMETER	0.5 - 25 m	±0.5 TO 1.0 m OR ±10%	1.6 - 12	NADIR ONLY	1/14d NEAR CONTINENTAL U.S.
	LENGTH	IMAGING RADAR	50 - 1000 m	±10%	50 m		
	DIRECTION		0 - 360°	±15°			
SURFACE TEMPERATURE	RELATIVE	V&IR RADIOMETER	-2 - 35°C CLEAR WEATHER	1.5°	~5	~5	36 h
	ABSOLUTE			2°			
	RELATIVE	MICROWAVE RADIOMETER	-2 - 35°C ALL WEATHER	1°	100	100	36 h
	ABSOLUTE			1.5°			
SEA ICE	EXTENT	V&IR RADIOMETER		~5 km	~5	~5	36 h
		MICROWAVE RADIOMETER		10-15 km	10-15	10-15	36 h
		IMAGING RADAR		±25 m	25 m		1/14d NEAR CONTINENTAL U.S.
	LEADS		> 50 m	±25 m	25 m		
	ICEBERGS		> 25 m	±25 m	25 m		
OCEAN FEATURES	SHORES, CLOUDS, ISLANDS	V&IR RADIOMETER		~5 km	~5	~5	36 h
	SHOALS, CURRENTS	IMAGING RADAR		±25 m	25 m	25 m	1/14d NEAR CONTINENTAL U.S.
ATMOSPHERIC CORRECTIONS	WATER VAPOR & LIQUID	MICROWAVE RADIOMETER		±25 m	50	50	36 h

TABLE 3

OCEAN DATA APPLICATIONS

BENEFICIARIES \ PHENOMENA	WINDS	WAVES	TEMPS	CURRENTS	SEA ICE (LEADS/BERGS)	PRESSURE	SALINITY	UP-WELLINGS	POLLUTION	GEOID
1. TRANSPORTATION/ROUTING										
MARINE TRANSPORTATION	X	X		X	X					
NAVAL SHIPS	X	X		X	X	X				
2. OCEAN EXPLOITATION/USE										
FISHERIES	X	X	X	X			X	X	X	
OFFSHORE RIGS	X	X					X			
OCEAN MINING	X	X		X		X	X	X	X	
3. GENERAL SERVICES										
WEATHER FORECASTING	X	X	X			X				
COAST GUARD SERVICES	X	X	X	X	X				X	
LAW ENFORCEMENT	X	X	X	X					X	
GEOLOGICAL SURVEYS										X
ENVIRONMENTAL PREDICTION	X	X	X	X				X	X	
4. RESEARCH AND SCIENCE	X	X	X	X	X	X	X	X		X

THE FUTURE

As more complete and more accurate synoptic data of ocean surface conditions become available, additional uses for data can be anticipated. In general, these requirements can be expected to develop in the direction of improved information transfer and assimilation,more precise data, and complete global coverage on a daily scale. Also, it can be anticipated that information requirements will develop relative to conditions both above and below the surface of the sea - particularly the air sea interface and the atmosphere above the sea; and the dynamic upper levels of the ocean important to physical oceanography and biology.

Specific requirements can be foreseen as a result of increased marine activity in the Arctic Zone - particularly tied to the development of oil resources on the Alaskan North Slope and transportation of the products to the conterminous 48 states. The Arctic ice cover recedes from shore for only a very limited period of the year, and its subsequent approach and recedance are currently unpredictable for more than short time spans. Thus, the hazards of sea transportation to the North Slope could be greatly lessened by an understanding of development of ice leads and the forces influencing the dynamics of the Arctic ice cover. The difficulties experienced during summer 1975 at Point Barrow clearly point up the need for improvements in forecasting such phenomena.

Another example is the U.S. adoption of a 200-mile coastal fishing limit, which will increase monitoring, surveillance, and enforcement missions of the U.S. Coast Guard by an order of magnitude. At the same time many other countries (Mexico and Australia for example) are adopting similar limits with even less preparedness. As a result, the needs for a data system - to collect, assess, and alert - can be expected to proliferate.

Not least in importance is the strong potential for improvements in weather forecasting - both for ocean surfaces and adjacent continental masses (like our own Pacific Northwest) - that may ultimately result from increased knowledge of ocean surface conditions, heat transport, and ocean currents. Once we have the capability to collect such data and merge it with other sources of weather data to produce forecasts, the firmer the needs will become evident to achieve true long range predictions and better understanding of climatic processes.

EMERGENCE OF SEASAT

A means for synoptically monitoring wave heights and directional spectra, surface winds, temperature, ice, icebergs, storm surges, and other influences (or hazards) of the oceans is needed. Although remote sensing of such phenomena has not been widely accepted by the oceanic community, it appears that remote sensing may be the only approach that will yield consistent, spatially dense data. With the advancement in use of satelliteborne sensors by the Skylab, LandSat and MetSat programs, remote sensing of oceanic phenomena appears feasible. Certainly global coverage of internally consistent data is a basic attribute of satellite sensing. Thus, in response to user expressed interest and needs, a proof-of-concept satellite mission called Seasat-A intended to evaluate the feasibility of remote sensing techniques for oceanic phenomena, was initiated. The only issue to be resolved was the availability of instruments that could sense physical phenomena which, in turn, can be correlated with oceanic phenomena of interest.(5)

An array of suitable spaceborne sensors had been developed during earlier space programs, i.e., GEOS, Skylab and NIMBUS(6). As specific requirements were solicited within the using community, candidate instruments from this array were evaluated jointly by the users and NASA for application to the ocean dynamics mission - Seasat-A. A set of three active radars and two passive radiometers has been ultimately selected. The characteristics of these sensors are summarized in Fig. 1. The sensors include a pulse-compressed radar altimeter, a microwave radar scatterometer, a synthetic aperture imaging radar, a scanning multifrequency microwave radiometer, and a visible/infrared scanning radiometer.

The Seasat radar altimeter serves two functions(8): it monitors average wave height to within 0.5 to 1 meter along its narrow (2 to 12 km) swath by measuring the broadening of its returned echo caused by increased surface wave actions; it measures to a precision of 10 cm the relative shape of the ocean geoid due to gravity variations and ocean tides, surges, and currents. As surface winds increase, so does surface roughness or chop. The radar scatterometer measures the signal of its returned echoes. Signal strength increases with the increase in wind-driven waves, which can be converted directly into wind speed and direction. **The scatterometer measures wind speeds from 3 to 25 m/sec within 2 m/sec and direction within** 20 deg over two 500-km swaths on either side of the spacecraft ground track. The five-frequency microwave radiometer serves four functions: (1) it measures surface temperature by measuring the microwave brightness of the surface to within 1 deg C; (2) it measures foam brightness, which can in turn be converted into a measurement of high (up to 50 m/sec) wind speed; (3) it maps ice coverage; and (4) it provides atmospheric correction data to the active radars by measuring liquid and gaseous water content in the upper atmosphere. The surface

SENSOR	COMPRESSED PULSE ALTIMETER	MICROWAVE SCATTEROMETER	SYNTHETIC APERTURE IMAGING RADAR	MICROWAVE RADIOMETER	VISIBLE AND INFRARED RADIOMETER
SENSING OBJECTIVE	GLOBAL OCEAN TOPOGRAPHY GLOBAL WAVE HEIGHT	GLOBAL WIND SPEED AND DIRECTION	WAVELENGTH SPECTRA LOCAL HIGH-RESOLUTION IMAGES	GLOBAL ALL-WEATHER TEMPERATURE GLOBAL WIND AMPLITUDE GLOBAL ATMOSPHERIC PATH CORRECTIONS	GLOBAL CLEAR-WEATHER TEMPERATURE GLOBAL FEATURE IDENTIFICATION CLOUD COVERAGE
FREQ/ WAVE LENGTH	13.9 GHz	14.6 GHz		6.6, 10.69, 18, 22.235, 37 GHz 1.275 GHz	0.52 TO 0.73 μm 10.5 TO 12.5 μm
ANTENNA/ OPTICS	1 m PARABOLA	5 TO 2.7 m STICK ARRAYS	11 X 2.2 m PHASED ARRAY	0.8-M OFFSET PARABOLA	12.7 cm OPTICS
POWER	125 W AVE	165 W AVE	200 TO 250 W AVE	50 W	10 W
DATA RATE	8 kb/s	2 kb/s	15 TO 24 Mb/s	4 kb/s	12 kb/s
HERITAGE	SKYLAB/ GEOS-C	SKYLAB	APOLLO 17	NIMBUS G	ITOS

swath of the microwave radiometer is 920 km. The visible and infrared radiometer will provide clear weather surface temperature data, cloud coverage patterns, and corroborative images of ocean and coastal features with a resolution of 5 km over a swath of 1500 km. These four sensors, known as the global sensors, will monitor the oceans and adjacent coastal waters globally. Their data will be recorded on magentic tape recorders on board Seasat. The data will be played back while the satellite is over one of the ground stations supporting Seasat.

The fifth sensor, the synthetic aperture radar, will provide all-weather imagery of ocean waves, ice fields, icebergs, ice leads, and coastal conditions and dynamic processes to a resolution of 25 m over a 100-km swath. Because of the very high data bandwidth of the radar imagery, this sensor, with its own separate data system, will be operated only in realtime while within line-of-sight of specific tracking stations equipped to receive and record its data. Seasat's sensor coverage is depicted in Fig. 2. Virtual global coverage is achieved every 36 hours.

SEASAT-A MISSION

The Seasat-A program objectives stem from a balanced program providing proof-of-concept, which is research based as well as providing basic oceanographic and meteorological data that are operation and application oriented. Its combination of active radar and passive microwave and infrared instruments gives it the capability of observing the ocean on a day/night, nearly all-weather basis. Thus, quantitative measurements of the ocean surface can be obtained not only in clear weather, but also in regions covered by persistent cloud cover or during severe storms.

The specific Seasat-A objectives(7) are:

a. To Demonstrate the Capability For

  - Global monitoring of wave height and directional spectra, surface winds, ocean temperature, and current patterns
  - Measuring precise sea-surface topography
  - Detecting currents, tides, storm and surges.
  - Charting ice fields and navigable leads through ice
  - Mapping the global ocean geoid

b. To Provide For User Applications Such Data As

- Predictions of wave height, directional spectra and wind fields for ship routing, ship design, storm-damage avoidance, coastal disaster warning, coastal protection and development, and deep water port development
- Maps of current patterns and temperatures for ship routing, fishing, pollution dispersion, and iceberg hazard avoidance
- Charts of icefields and leads for navigation and weather prediction
- Charts of the ocean geoid fine structure

c. **To** Determine The Key Features Desired in Future Operational Systems For

- Global sampling
- Near-realtime data processing and dissemination
- User feedback for operational programming

d. To Demonstrate the Economic And Social Benefits of User Agency Products

The Seasat spacecraft bus, the Agena, first flown on military space missions in 1959 and subsequently on over 300 missions, has been configured to support the oceanographic mission requirements. The overall configuration of Seasat-A is shown in Fig. 3. The Seasat spacecraft comprises a standard satellite bus and a customized sensor module that supports and accommodates Seasat sensors and their antennas.

The single Seasat-A satellite is to be launched in the second quarter of Calendar Year 1978 from the Western Test Range into a near-polar (108-degree) circular orbit. The satellite will cruise at an altitude of 790 km, circling the earth every 101 minutes. Sensors with 1000 km cross-track coverage will provide global repeat coverage every 36 hours, using both day and night passes to complete the fill-in. This orbit will precess through a pattern that will begin to repeat ground tracks after about 4-1/2 months. During this time a first measurement precise determination of the ocean geoid with a 18 km a grid density will have been completed. Seasat's ground track for one day is shown in Fig. 4; its coverage extends over virtually all the unfrozen oceans, including the Alaskan North Slope to the Antartica, under all lighting conditions.

FIGURE 2

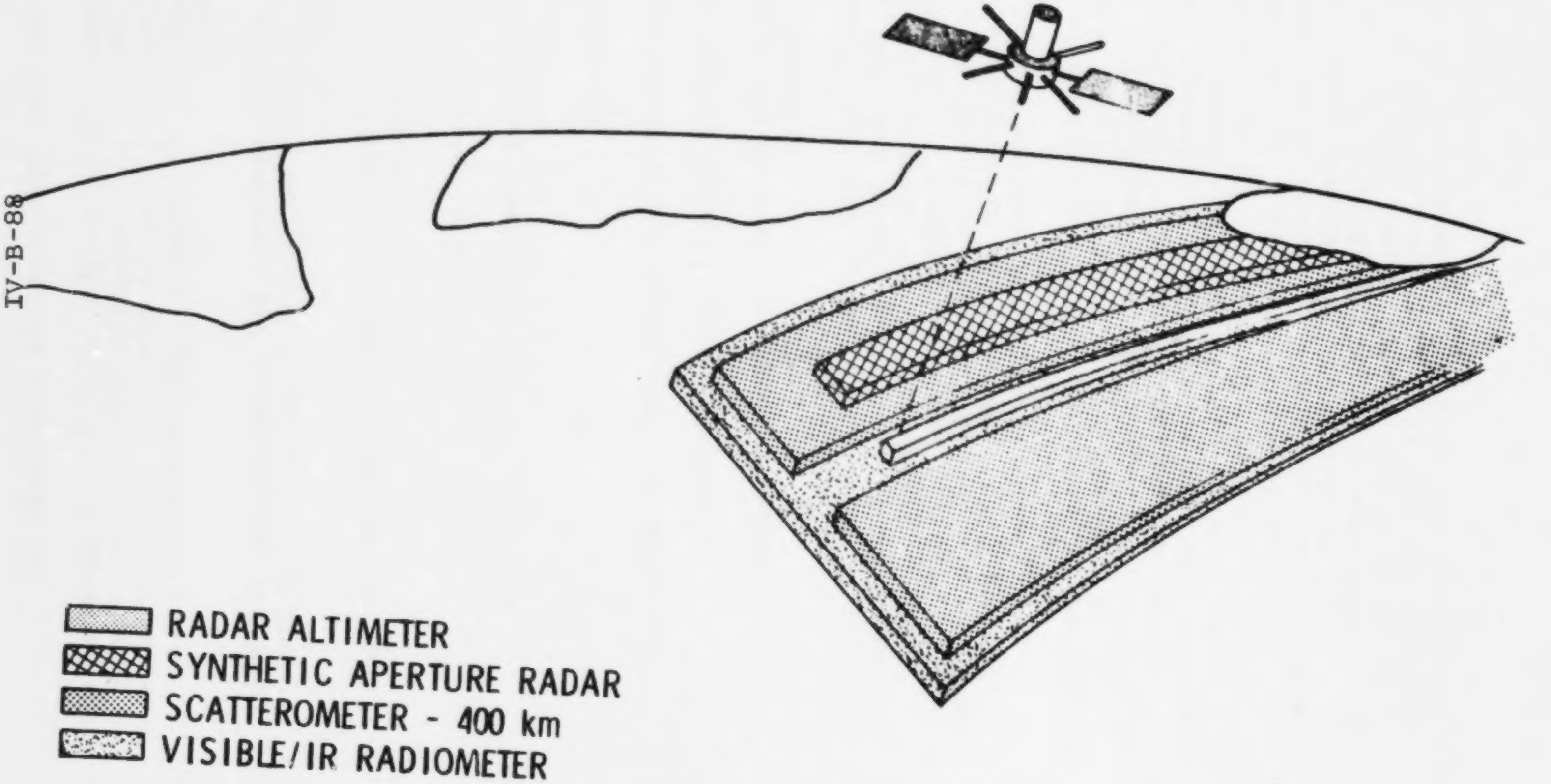
RADAR ALTIMETER
SYNTHETIC APERTURE RADAR
SCATTEROMETER - 400 km
VISIBLE/IR RADIOMETER

FIGURE 3

SEASAT-A MISSION

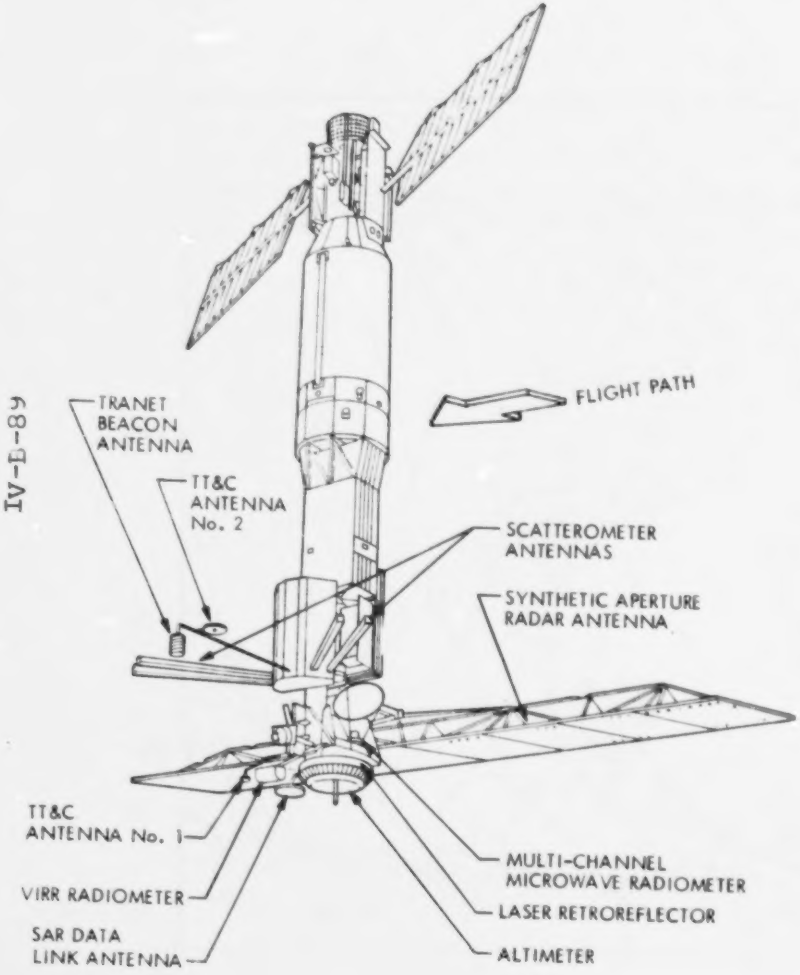
TRANET
BEACON
ANTENNA
TT&C
ANTENNA
No. 2
FLIGHT PATH
SCATTEROMETER
ANTENNAS
SYNTHETIC APERTURE
RADAR ANTENNA
TT&C
ANTENNA No. 1
VIRR RADIOMETER
SAR DATA
LINK ANTENNA
MULTI-CHANNEL
MICROWAVE RADIOMETER
LASER RETROREFLECTOR
ALTIMETER

- **MANAGEMENT**
  - OVERALL - NASA - OFFICE OF APPLICATIONS
  - SATELLITE SYSTEM - JPL
  - SATELLITE BUS/SENSOR MODULE SYSTEM INTEGRATION - LMSC
  - SENSORS
    - SCANNING MULTIFREQUENCY MICROWAVE RADIOMETER - JPL
    - RADAR SCATTEROMETER - GENERAL ELECTRIC
    - SYNTHETIC APERTURE RADAR - JPL
    - RADAR ALTIMETER - APL
    - VISUAL INFRARED RADIOMETER - NOAA
- **MISSION OBJECTIVES**
  - MEASURE GLOBAL OCEAN DYNAMICS AND PHYSICAL CHARACTERISTICS
  - DETERMINE KEY FEATURES OF AN OPERATIONAL SYSTEM
  - IMPROVE BODY OF SCIENTIFIC OCEAN DATA/KNOWLEDGE
  - DEMONSTRATE UTILITY OF DATA TO USER COMMUNITY
- **MISSION ORBIT**
  - ALTITUDE (CIRC) 800 Km
  - INCLINATION 108°
  - WEIGHT ON ORBIT 1820 Kg
- **LAUNCH DATA**
  - DATE MAY 1978
  - SITE VAFB SLC 3W
  - VEHICLE ATLAS F/AGENA
- **COST DATA**
  - SPACECRAFT $66.5M
  - LAUNCH SUPPORT $11.0M

NASA HQ ES77 2143 (1)
3 25 77

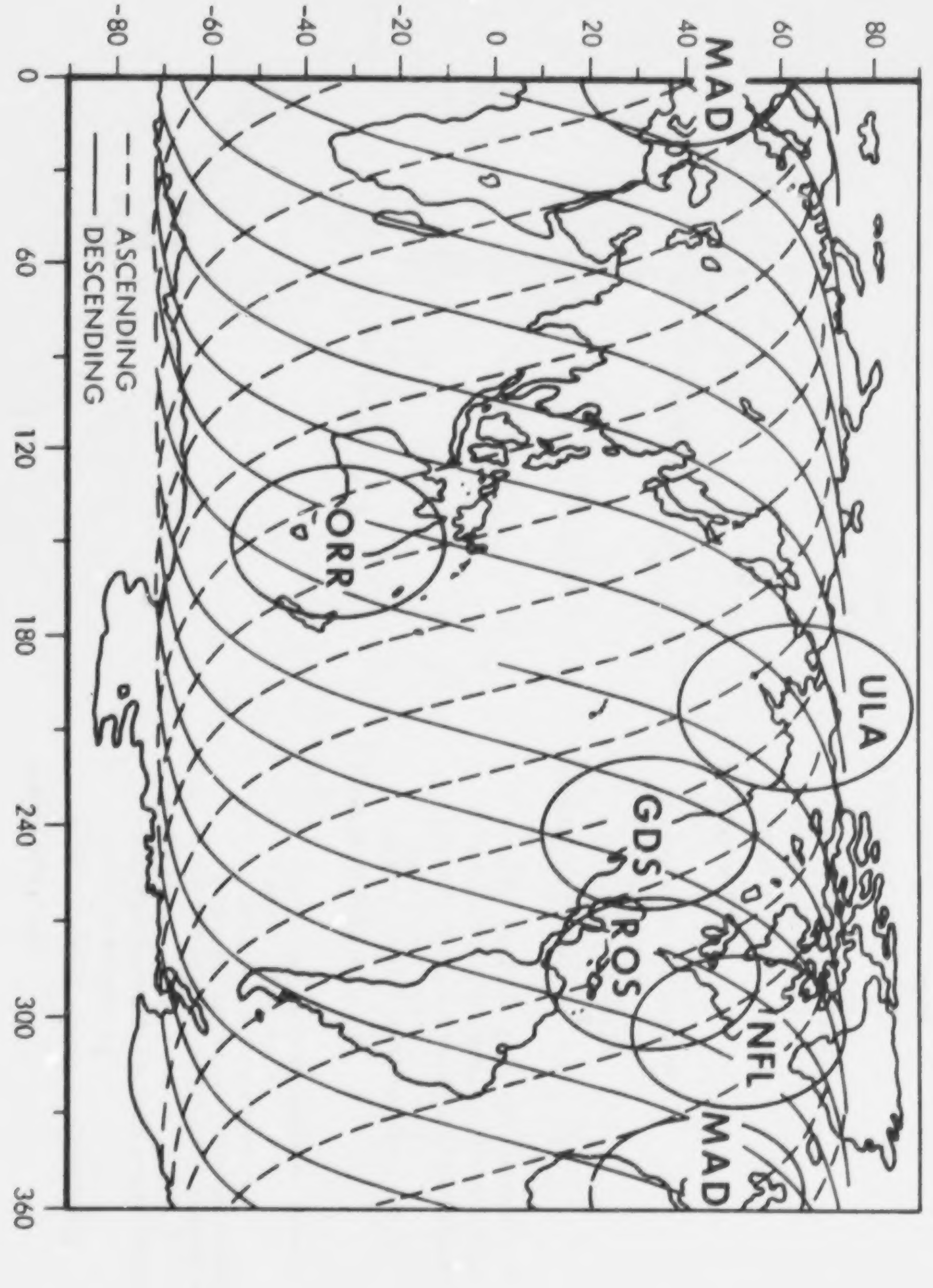
MAD
ULA
GDS
ROS
NFL
ORR
MAD
ASCENDING
DESCENDING
80
60
40
20
0
-20
-40
-60
-80
0
60
120
180
240
300
360

Fig. 4 SEASAT-A Trajectory and Ground Station Coverage

An ocean surface truth program has been initiated that will provide the user with insitu measurements of the sea-to-air interface that Seasat will monitor remotely from space. This program, already underway, will run through the proof-of-concept phase. It will provide the users with testdata from which algorithms for sensor data conversion can be formulated and with calibration and verification of the actual sensor performance from orbit. The ocean surface truth program is being operated concurrently with and will take full advantage of parallel ocean data tests being conducted by other government and academic agencies. The program will utilize data buoys, surface ships, and aircraft. NASA is currently designing several industrial Evaluation Experiments in cooperation with selected segments of the commercial ocean community. These experiments are intended to begin the transfer of ocean remote sensing technology to commercial users as well as to obtain experimental data to help validate previous economic benefit estimates. Further, these experiments will provide data to aid in the definition of those characteristics necessary for future Seasat systems which are of economic importance to commercial users.

The National Oceanic and Atmospheric Administration (NOAA), in cooperation with NASA expects to fund a number of scientific investigations within the non-Federal Ocean Research Community during 1978 and 1979. Cooperating also with NOAA is the Office of Naval Research (ONR), the National Science Foundation (NSF), the U.S. Coast Guard and the U.S. Geological Survey. This Solicitation of Investigations will provide support to the ocean science community for research activities utilizing Seasat-A data. Concurrently, it is expected that these investigations will augment the process of validating the scientific contribution expectations developed for Seasat-A.

USERS AND SEASAT DATA

Specific data acquisition, processing, and distribution plans. systems are currently being established by user organizations and NASA. Consistent with initial program formulation in 1973, NASA will establish proof-of-concept engineering and geophysical validation of Seasat data and users will provide the resources required for processing, analysis, dissemination and application of data peculiar to their special interests. Figure 5 provides a generalized view of this division of responsibilities.(9)

The data products of the Seasat sensors must serve a variety of users in a variety of forms. Weather data are highly perishable; to be of practical value, operationally, they must be processed (e.g., formatted, merged, blended, and analyzed) and applied in near realtime. Data older than 8 hours are of little interest except for climate studies or model development. At the opposite end of the spectrum is the geodesist, whose data are nearly time invariant. The geodesist's approach to analysis is often to fit and refit data for a bootstrap approach, finally achieving a best fit model of the ocean geoid. Some of the users will have sizable ground data systems available to assist them in processing and analysis; others will have only in expensive terminals with limited processing capability. Some users care only for specific outputs such as wind and wave data for use in ship routing; others, such as university researchers, want as much of the data as available for application to development of advanced prediction models. Thus, Seasat's end-to-end data system, consisting of NASA and user facilities equipment and communication networks, must be flexible and dynamic enough to meet the demands of this broad spectrum of currently identified and future user applications.

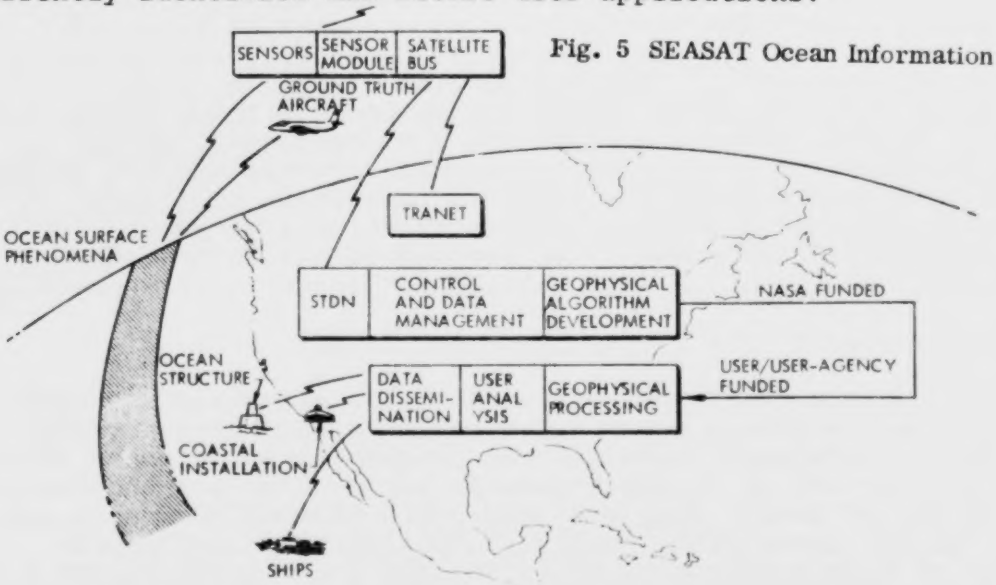
SENSORS
SENSOR MODULE
SATELLITE BUS
GROUND TRUTH AIRCRAFT
TRANET
OCEAN SURFACE PHENOMENA
STDN
CONTROL AND DATA MANAGEMENT
GEOPHYSICAL ALGORITHM DEVELOPMENT
NASA FUNDED
OCEAN STRUCTURE
DATA DISSEMI-NATION
USER ANAL YSIS
GEOPHYSICAL PROCESSING
USER/USER-AGENCY FUNDED
COASTAL INSTALLATION
SHIPS

Fig. 5 SEASAT Ocean Information System

As indicated, this system comprises all elements from remote sensing of the ocean phenomena through collection and storage. Elements of this end-to-end system include location and sensor Calibration, onboard the satellite or on the ground, transmission to the earth for storage, conversion to geophysical meaning, merging of the various sensor data, blending with supporting external data, delivery to the ultimate users for data analysis, interpretation, and utilization; this process is shown in a simplified format in Fig. 6. Some elements of the present data system described below provide an example of data flow to one of the many Seasat users, the Navy Fleet Numerical Weather Central.

a. The Satellite Data Subsystem comprises those elements onboard the spacecraft for collection, storage, and transmission to earth of the sensor data and for command, control, and tracking of the satellite. To facilitate access to the data and to reduce costs to small users, the Satellite Data Subsystem is designed to a block telemetry format. This format separates data from each sensor into individual time-tagged data blocks. In future Seasat systems it is expected that these data blocks will also be ground located and combined with other pertinent onboard engineering data.

b. The Ground Tracking and Data Acquisition Subsystem tracks the satellite, transits stored commands for sequencing satellite events and receives sensor and status data from the satellite for retransmission to other using subsystems.

c. The Mission Operations and Control Subsystem receives the tracking and global sensor data from the tracking stations, monitors satellite and sensor health, reduces tracking data to provide satellite ephemeris, merges satellite attitude data with ephemerides to facilitate sensor footprints, and delivers data to the Seasat project and other users. This subsystem also generates timed commands for transmission to the satellite.

d. The Project Data Processing Subsystem has the primary objective of providing data processing support to the proof-of-concept mission for sensor system engineering and geophysical validation. In this regard it will support user-directed experiment teams to quantize system performance characteristics with emphasis on geophysical validation. In this way we hope to encourage and provide technology to users to promote direct independent distributed theme oriented data utility by users.

e. One of these direct, independent, theme-peculiar User Data Systems is exemplified by the Navy Fleet Numerical Weather Center at Monterey, California. Global sensor

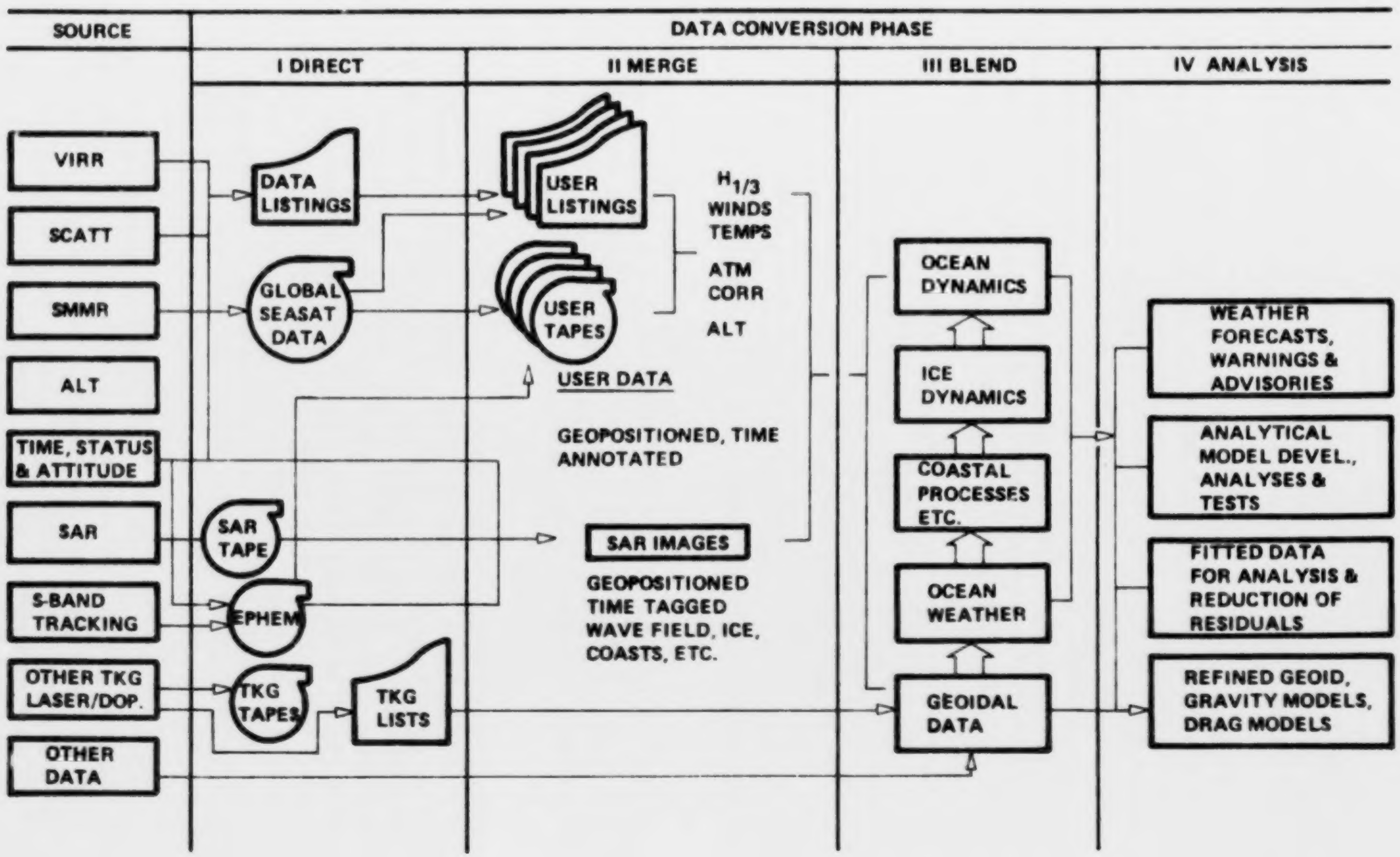
SOURCE
DATA CONVERSION PHASE
I DIRECT
II MERGE
III BLEND
IV ANALYSIS
VIRR
SCATT
SMMR
ALT
TIME, STATUS & ATTITUDE
SAR
S-BAND TRACKING
OTHER TKG LASER/DOP.
OTHER DATA
DATA LISTINGS
GLOBAL SEASAT DATA
SAR TAPE
EPHEM
TKG TAPES
TKG LISTS
USER LISTINGS
USER TAPES
$H_{1/3}$
WINDS
TEMPS
ATM CORR
ALT
USER DATA
GEOPOSITIONED, TIME ANNOTATED
SAR IMAGES
GEOPOSITIONED TIME TAGGED WAVE FIELD, ICE, COASTS, ETC.
OCEAN DYNAMICS
ICE DYNAMICS
COASTAL PROCESSES ETC.
OCEAN WEATHER
GEOIDAL DATA
WEATHER FORECASTS, WARNINGS & ADVISORIES
ANALYTICAL MODEL DEVEL., ANALYSES & TESTS
FITTED DATA FOR ANALYSIS & REDUCTION OF RESIDUALS
REFINED GEOID, GRAVITY MODELS, DRAG MODELS

Fig. 6 Data Flow

and status data as received at Fairbanks are retransmitted in near realtime to Monterey, where they are processed and redistributed to the operational ocean-using community, civilian and military, as weather maps and advisories, with less than 8 hours turnaround time.

f. The Synthetic Aperture Radar (SAR) Data Processing Subsystem supports the unique requirements of the imaging radar experiment. Wideband SAR data is recorded digitally at specially equipped stations. The tapes are delivered to the SAR data-processing system, where selected data are processed to image tapes which are in turn processed into images by the Earth Resources Observation System (EROS) Data Center and provided, along with ephemeris, attitude, and status data, to the SAR experiment team and to all other users on a cost reimbursable basis.

POTENTIAL BENEFITS

Studies have been conducted for NASA by ECON, Inc., of Princeton, N. J.(10) to make preliminary estimates of the potential economic benefits. Arctic operations, marine transportation, and offshore oil and natural gas exploration and operations show great potential. Ocean fishing operations also appear as a potentially large beneficiary, although this is strongly dependent upon the oceans' ability to replenish the source of supply. The study assumed a multi satellite operational system beginning in 1985.

From the outset no attempt was made to estimate the effects of improved ocean data upon land operations, even though there cannot fail to be improvements in weather forecasting; instead, the study was directed to consider only ocean-based beneficiaries and is highly conservative. Table 4 shows these applications deemed of sufficient potential to be included in the study. Case studies were performed to examine operating parameters, constraints, and structure of each selected maritime operation. Incremental parameter changes resulting from application of improved knowledge of weather or ocean conditions were evaluated in terms of resultant economic benefits. Considerable care was exercised in the conduct of each case study to permit generalization to the operation as a whole - both in scale, time, and geographical location. The most likely benefits resulting from **Seasat** were estimated by initially establishing that portion which was likely to be directly attributable to use of Seasat data. In some cases, due to uncertainty in rate of development of an industry or sector, it became necessary to establish upper and lower and most likely bounds on likely ranges of benefits. An example of case study results is shown in Table 5 for the North American Arctic Transit Case. Additional information on the methodology of the economic benefit studies is available in Ref. 10.

Summarized in Table 6 is the most likely range of benefits for the cases studied. Ocean mining benefits were omitted because insufficient data was available from which to derive adequate estimates of benefit. The largest single beneficiary is the marine transportation industry followed closely by off-shore oil and natural gas exploration and Arctic operations.

Table 4

SOURCE OF ECONOMIC BENEFITS

INDUSTRY OR SECTOR	MOST SIGNIFICANT CONTRIBUTOR
o OFF SHORE OIL AND NATURAL GAS	o IMPROVED WEATHER AND OCEAN CONDITION FORECASTS (PLATFORM INSTALLATION, PIPELAYING, AND TRENCHING)
o ARCTIC OPERATIONS	o RESOURCE TRANSPORTATION (IMPROVED ICE COVERAGE INFORMATION AND IMPROVED OCEAN CONDITION FORECASTS)
o OCEAN FISHING	o FORECASTING OF FISH POPULATION AND MIGRATION (OCEAN CURRENTS AND TEMPERATURES)
o MARINE TRANSPORTATION	o REDUCTION IN TRANSIT TIME, REDUCTION IN DAMAGE OR CASUALTY LOSSES AND REDUCTION OF INSURANCE RATES (IMPROVED WEATHER AND OCEAN CONDITION FORECASTS)

Table 5

NORTH AMERICAN ARCTIC TRANSIT CASE STUDY RESULTS

CASE STUDY RESULTS

- WESTERN ARCTIC 1992-2000
    - TRANSPORT 1.5 - 6.3 BILLION BARRELS OF OIL
    - NUMBER OF VOYAGES - 7900
    - QUANTITY OF OIL PER TANKER - 1.6 MILLION BARRELS
    - ANNUAL BENEFIT - $26 MILLION TO $494 MILLION*
- EASTERN ARCTIC 1990-2000
    - TRANSPORT OIL, LNG, HYDROCARBONS
    - PRODUCTION CONSISTENT WITH ALBERTA COMMISSION FINDINGS
    - NUMBER OF VOYAGES - ABOUT 13,000
    - AVERAGE ANNUAL BENEFIT - $152 MILLION*
    - BEAUFORT SEA BENEFIT - $70 MILLION ANNUALLY BECAUSE OF ECOLOGY*

*ANNUAL BENEFIT FROM ALL SOURCES OF IMPROVED WEATHER AND OCEAN CONDITION FORECASTS AND ICE RECONNAISSANCE

Table 6

SUMMARY OF MOST LIKELY RANGE OF BENEFITS EXCLUSIVE TO SEASAT

- PLANNING HORIZON TO YEAR 2000
- 10 PERCENT DISCOUNT RATE

INDUSTRY OR SECTOR	INTEGRATED BENEFIT ($1975 MILLIONS)
o OFFSHORE OIL AND NATURAL GAS	214 to 344
o OCEAN MINING	NOT ESTIMATED
o COASTAL ZONES	3 TO 81
o ARCTIC OPERATIONS	96 to 288
o MARINE TRANSPORTATION	583
o OCEAN FISHING	42 TO 380
o PORTS AND HARBORS	0.5
o UNCLASSIFIED MILITARY APPLICATIONS	28
TOTAL	966 TO 1704

CONCLUSIONS

Global, synoptic oceanic data, available relatively soon after collection, are needed to satisfy both current and future anticipated needs of the ocean using community. The Seasat-A spacecraft, using a carefully selected set of remote sensors, beginning with launch in the second quarter 1978, will perform a proof-of-concept mission to evaluate the potential for space-based sensor systems to collect oceanic data of significant value to users - particularly data on ocean weather and surface conditions. A sincere attempt has been made on this program to encourage both ultimate and intermediate users of oceanic data to become involved with definition of requirements. selection of sensors, and evaluation of future potential benefits. Plans are being made within NASA and NOAA Headquarters, in conjunction with OMB and members of Congressional staffs, to follow Seasat-A with additional developmental space flights leading perhaps to a future operational system.

The individual user might easily conclude that his ability to affect the outcome of a project, such as Seasat-A is slight. The very remoteness, impersonality, and technological complexity of space programs almost mandate such a conclusion. However, such is not the case with the Seasat project. For example, if improved data on predicted ocean weather and oceanic surface conditions are needed, make your wishes known. From your individual needs, future requirements will be developed. Your personal observations are needed on types of data desired, data distribution and access methods and time span, display techniques desired, and formats of data. Also, it will be necessary, in the course of the Seasat-A operation to correlate the remote observations with in-situ measurements. Shipboard observations of wind, sea state, and water temperature and underflights of Seasat-A will be necessary to provide calibration and/or correlation with Seasat-A'derived information - particularly from remote locations, during severe extremes of oceanic conditions.

A test program for economic verification is being planned. Many industry users have already come forward with requests to support these tests . A coordinated , NOAA, NASA, NSF, NAVY, DOI, and Coast Guard solicitation for scientific investigations is being developed.

Because of the diversity of possibilities in terms of potential participation in Seasat, a single contact is provided who can help you make the interfaces peculiar to your specific interests and needs. Inquiries should be directed to:

Dr. Alden A. Loomis
Co-Chairman of the Ocean Dynamics Advisory Subcommittee
Jet Propulsion Laboratory (183-501)
4800 Oak Grove Drive
Pasadena, CA 91103
Telephone 213-354-6629

Seasat was conceived by the users and implemented to meet their needs. The potential user community is expanding daily. Only through continued interaction will we have the vision to continue the promise of Seasat.

REFERENCES:

1. "The Voyage of the Challenger" Eric Linklater, Doubleday, Inc., 1974

2. The Terrestrial Environment: Solid Earth and Ocean Physics Application of Space and Astronomic Techniques, Report of a Study at Williamstown, Mass., to NASA, sponsored by NASA ERC, MIT Measurement Systems Laboratory, Cambridge, Mass., August 1969

3. John R. Apel, "SEASAT: A Spacecraft Views the Marine Environment with Microwave Sensors," statement presented before the Subcommittee on Space Science and Applications Committee on Science and Astronautics House of Representatives, 1974

4. Nagler, R. G., and McCandless, S. W., Jr., "Operational Oceanographic Satellites - Potentials for Oceanography, Climatology, Coastal Processes, and Ice," September 1975

5. Gray, Robert M., McCandless, S. W. Remote Sensing of Oceanological Phenomena through use of SEASAT-A.

6. Rose, Jr. R., and McCandless, S. Walter, "System Definition of SEASAT-A, An Ocean Observation Satellite," paper at AIAA 13th Aerospace Sciences Meeting, Pasadena, Calif., January 20 - 22, 1975

7. McCandless, S. W. Jr., "SEASAT-A - A Product of User Interest," December 1975

8. McCandless, S. W. Jr., and Eaton, W. T., "SEASAT-A - Accepting the Challenge of Challenger," April, 1976

9. Hooke, Adrian, "SEASAT-A End-to-End Data System," December, 1975

10. SEASAT Economic Assessment, Vol. I, Summary and Conclusions, Final Report of a Study to NASA, sponsored by Office of Applications, Contract No. NASW 2558, 31 August, 1975.

IV-B-103 OMIT

# COST EFFECTIVE THERMAL MONITORING
for
STATE AND LOCAL ACTIVITIES

Author: C.E. "Gene" James
Office of Monitoring & Technical Support
U. S. Environmental Protection Agency
Washington, D.C. 20460

The author briefly discusses various techniques for monitoring heat plumes and heat sources, using light aircraft equipped with various sensors in a POD attachment.

Compact thermal scanners are described as the most effective overhead monitoring techniques for identifying, tracking and plotting thermal differentials introduced by power plants and other industrial activities. Other techniques are also discussed. The capabilities of color and color infrared are placed in perspective regarding their use in monitoring the environmental impact of thermal pollution. These capabilities are reviewed in relation to their potential use in the Enviro-Pod system.

The Enviro-Pod is a recently developed light weight, low cost accessory that is designed for use on the Cessna 172 aircraft. Both still and motion pictures are used to illustrate this new capability which is being evaluated by the EPA Office of Research and Development.

The Enviro-Pod was designed for EPA by the USAF Avionics Laboratory, of the Air Force Systems Command. The objective of this development is to provide the environmentalist in the field with a cost effective and responsive method of conducting overhead monitoring (remote sensing) missions.

One of the requirements has been to provide a system that will make the data available for analysis with a minimum delay. Another facet of the POD concept is in conducting monitoring and enforcement actions, here it has the advantage of simplifying the "chain of evidence" as required for legal use.

The POD design uses interchangable and interconnecting modules. This modular design permits the POD to be separated into units small enough to be treated as luggage when traveling by commercial air. This capability was considered important where an environmentalist has to travel to distant locations. Once he arrives in the vicinity of areas where surveillance is planned the POD can be attached to a Cessna 172 aircraft which is available for rent at most airports in the United States.

Preceding page blank

Other than physical attachment the POD is entirely self contained. Only the control panel cable extends into the passenger compartment where it is available for inflight operation by the environmental observer.

The POD is 48" in length, 18" wide and has a depth of 15 inches. It attaches under the fuselage between the main wheels of the aircraft. The design provides ports for both vertical and forward oblique sensors. The sensors for instance can be operated either independently or simultaneously. Low light level television sensors with in flight recording and transmissions are being developed. Several thermal scanners and "flirs" are being investigated for general operational capabilities. Concepts for air and water sampling are also under consideration.

It is anticipated that this capability will allow overhead monitoring missions to be conducted at a frequency that will provide a basis for the data collected to be accepted with a degree of confidence that seldom exists in current operations.

Moreover, the present "state-of-the-art" in remote sensing requires that most overhead monitoring missions be supported with in-situ samples (ground truth) to collaborate and validate the remote sensing records. Here another potential advantage of the Enviro-Pod system is evident in that it can reduce the coordination and communications problems arising between the ground crews and flight crews involved in monitoring areas of environmental concern.

The introduction of light civilian type aircraft substantially reduces the cost of renting and operating overhead monitoring systems. In essence the capbility to monitor potential thermal problems has now been reduced in cost and complexitity to a point where field personnel who have first hand acquaintance with the problem now have the tools needed to seek acceptable solutions to environmental problems.

SESSION IV-C
COOLING SYSTEMS III

6-45-11

THE THERMAL PERFORMANCE CHARACTERISTICS OF LARGE SPRAY COOLING PONDS

R. D. Baird & D. M. Myers
Ford, Bacon & Davis Utah Inc.
Salt Lake City, Utah

A. Shah
Spray Engineering Company
Burlington, Massachusetts

ABSTRACT

In recent years, there has been a renewed interest in determining the performance characteristics of large spray cooling ponds, since the verification of the adequacy of pond design is difficult because of the limited amounts of performance data for large ponds. The results of previous well instrumented tests on a large pond at a nuclear power installation have been published and analyzed over the limited ranges of data for critical parameters. The findings of these tests are briefly discussed.

Testing has recently been performed on a large conventional spray cooling pond presently operating in southern Florida. This spray pond is similar in design to ponds used in nuclear power plants, and its performance characteristics are representative of those ponds. The paper describes the facility and testing procedures, and reports the results of preliminary testing. The new data reported broadens the data base that can be used by engineers to design large fixed piping spray pond systems.

INTRODUCTION

Spray cooling ponds have been used for many years as an efficient and economical means of dissipating waste heat. Past experience has shown that an 8 to 11° C (15 to 20° F) approach to wet bulb temperature for large ponds can be achieved with a straightforward system design which compares quite favorably to alternative waste heat rejection systems when operating costs and maintenance are considered. In applications where a closer approach is required, design modifications result in acceptible system performance, albeit at greater capital and operating costs.

Preceding page blank

In recent years, spray cooling ponds have been used in the nuclear power industry in safety related cooling water systems (Ultimate Heat Sinks) because of their reliability and adequate performance. However, considerable difficulties have plagued the design effort for spray cooling ponds for two reasons. First, the performance of spray cooling ponds is complex and strongly influenced by numerous variables whose effect on performance can only be described over the full range of variables by computer analyses. Secondly, a limited data base for the performance of large spray ponds makes very difficult the verification of design adequacy, through any means but actual pond performance testing.

It is precisely this lack of adequate performance data for large ponds which promted the investigation reported herein. Tests have been performed on a large spray cooling pond, and the data taken compares well with results of tests performed earlier at Rancho Seco.[1] The objectives of this paper are to briefly discuss factors significant in spray pond operation, to describe the facility tested and the test procedures used, to report test results, to compare the results to those of earlier tests, and to evaluate the needs for further testing.

GENERAL CONSIDERATIONS

There are many design parameters for spray cooling ponds which have significant effects on pond performance. Most important among these are the following; meteorology (including, but not limited to wet bulb temperature and wind velocity), hot water temperature, pond geometry (size, spray unit spacing, and nozzle elevation) and nozzle operating pressure.

Meteorology

Two uncontrollable variables which are dominant in determining spray cooling pond performance are the wet bulb temperature and the wind velocity.

Wet Bulb Temperature

The wet bulb temperature represents the minimum temperature to which a droplet could be cooled if it were allowed to come to equilibrium with its surroundings. However, in a spray cooling pond, the droplet flight time is such that equilibrium is not achieved and the actual temperature of the droplet as it enters the pond is significantly greater than local wet bulb temperature. A frequent practice is to relate the cooling achieved to the ambient wet bulb temperature as an expression of the pond performance.

Wind Velocity

Ambient wind speeds and directions markedly influence pond performance. At zero wind speed, the draft induced by the increased specific volume in and above the spray region over the ambient specific volume results in a supply of fresh air to interior zones of the spray region. As the winds increase, the plume is shifted downwind and the supply of fresh air to upwind portions of the spray region is enhanced. In general, the greater the wind speed, the greater is the availability of fresh air to all zones of the spray region, and the greater is the pond heat dissipation capability.

The wind direction has an important influence on pond performance if the spray region presentation changes with wind direction. For example, if a pond is designed so that the spray region is 91 m. (300 ft) long by 40 m. (130 ft) deep, pond performance will change with wind direction. The cooling will be greatest when the wind is perpendicular to the pond major axis and reduced when the wind is parallel to the major axis. In any case, however, the degree of cooling achieved will not be less than that for low wind speeds.

Hot Water Temperature

The slope of the water vapor pressure versus temperature curve increases monotonically with increasing temperature. Therefore, the potential for evaporation, with a given difference between hot water and wet bulb temperatures, is markedly greater when the hot water temperature is higher. Since the cooling resulting from spray cooling systems is dominated by that resulting from evaporation, performance in spray cooling ponds is more effective at higher hot water temperatures. Also, the higher hot water temperature and evaporation rate lead to increased induced air flow under low wind conditions.

Pond Geometry

Geometry factors which influence pond performance include pond size, spray unit spacing and nozzle elevation.

Pond Size

As the size of the spray region increases, the ratio of spray region perimeter to spray region area decreases. Since availability of fresh air is determined largely by the perimeter, the cooling which can be achieved per unit of sprayed mass decreases as the pond size increases. The practical effect of increased pond size is that droplets from the spray units located in the interior zones of the spray region are exposed to a degraded environment (with increased moisture content). The cooling of the droplets in interior zones is less than the cooling of droplets from spray units in exterior zones of the spray region where the moisture content of the air is nearer the ambient moisture content. The overall effect is that the average cooling achieved per unit mass sprayed decreases with pond size, even though the total cooling increases.

Spray Unit Spacing

As the spray unit spacing is increased, the availability of fresh air to each spray unit is increased such that each spray unit behaves more nearly like an isolated spray unit with an unlimited availability of fresh air. Thus, pond performance improves with increased spray unit spacing.

Nozzle Elevation

Increasing the nozzle elevation above the water level increases the droplet flight time and therefore increases the cooling of the droplets, though this effect is less significant than the previously mentioned geometric factors.

Nozzle Pressure

The pressure at which the nozzle operates influences droplet cooling because of two effects; the shift of droplet size distribution and a change of droplet flight time.

Droplet Size Distribution

As the nozzle pressure is increased, the droplet size distribution is generally shifted to smaller sizes. The energy in a droplet is proportional to its volume. However, heat transfer is governed by droplet surface area and since the ratio of area to volume increases as the droplet decreases in size, the cooling potential is greater for smaller droplets.

Droplet Flight Time

As the nozzle pressure is increased, the droplet exit velocities increase resulting in longer flight times and, as previously discussed, produces greater droplet cooling.

TESTING PROGRAM FOR THIS INVESTIGATION

This section will discuss the facility at which these tests were performed, the variables which were monitored, the testing procedure and results.

Test Facility

The facility at which these tests were performed is located in southern Florida where wet bulb temperatures are generally high. However, during the time when the testing was performed, unusually cool temperatures existed so performance data at higher wet bulb temperatures were not obtained.

The spray region is 101 m. (330 ft) long by 49 m. (160 ft) wide with the pond major axis oriented perpendicular to prevailing winds. The spray units consisted of 4 nozzles on 1.5 m. (5 ft) spray arms and a fifth nozzle on the junction box, except for spray units on the two exterior rows, which lacked the fifth nozzle. The spray units were spaced 4.0 m. (13 ft) apart on the rows which were separated by 7.6 m. (25 ft).

The spray flow rate varied from 2,780 l/sec (44,000 gpm) to 3,030 l/sec (48,000 gpm) at pressures of 69,000 Pa (10.0 psi) and 82,000 Pa (11.9 psi), respectively. The heat load was approximately 73.3 x 10^6 watts (250 x 10^6 BTU/hr).

The pond is oriented so that prevailing winds are perpendicular to the pond major axis.

Variables Monitored

In order to establish the performance characteristics of the spray cooling pond the following ambient variables were monitored; wind speed, wind direction, wet bulb temperature, and dry bulb temperature. In addition, the hot water temperature, the cooled water temperature, and the pond water temperature were recorded at appropriate times.

Testing Procedures

In the present tests, batch samples of cooled water were collected just as the droplets were about to enter the pond water, at several points within the spray region. The batches were collected in covered insulated containers which were located appropriately before the cover was removed for the collection time. The ambient conditions of wind speed and direction and dry bulb and wet bulb temperatures were recorded during the collection time and the batch temperatures, hot water temperature and pond water temperatures were measured and recorded immediately after each batch was collected. The hot water temperature changed slowly enough that no significant error was induced by not measuring this temperature simultaneously with batch collection.

During much of the testing, rather high winds dominated, which improved droplet cooling. Although it had been an objective to examine the degradation of pond performance as a function of depth into the spray region parallel to both the major and minor axes, these higher winds made edge effects much more significant, i.e., cooling around the perimeter perpendicular to the wind direction was markedly enhanced by the winds. Therefore, the degradation of cooling performance was examined only through the center of the spray region parallel to the pond minor axis.

The degradation data obtained are presented graphically in Figure 1. The edge effects are clearly visible from curves A and B. Intuition suggests that as the edge of the spray region is approached from interior zones, the rate of change of cooling achieved decreases due to a reduced rate of moisture addition to ambient air.

As winds increase, improved performance is observed deeper into the spray region from the upwind edge, and then cooling falls off rapidly. As the wind speed decreases to low values and the induced draft becomes the dominant air flow mechanism, the cooling at the downwind edge of the spray region increases relative to the cooling in the interior zones. This effect is shown in curves B and E of Figure 1.

As a matter of interest, several temperatures have been shown in Figure 2. An approach of approximately 10° C (18° F) was achieved, with a cooling range of about 7° C (13° F).

RESULTS OF PREVIOUS TESTING

Numerous spray pond tests have been performed to determine design performance. However, most of those tests were not instrumented well enough to provide data that can be used to gain significant insight into the effect of various parameters on performance. The only well instrumented testing that has been performed is that at the Rancho Seco Nuclear Power Plant of Sacramento Municipal Utility District in California. The results of that testing were presented in a report by the University of California, Berkeley, California. [1]

The tests done at Rancho Seco were instrumented comprehensively but were limited to a maximum hot water temperature of about 38° C (100° F). The results of the Rancho Seco tests [1] are presented in Figure 1 showing spray efficiency as a function of position in the spray region. The dependence of spray efficiency on wet bulb temperature is not indicated explicitly in the results, but the results do indicate the magnitude of efficiencies that can be expected at various depths into the spray region.

Although the spacing of the spray units was the same in both designs, the Florida pond had nearly twice the sprayed area, and almost twice the depth of spray region in the direction of the wind. The increased depth of spray region in the direction of the wind provides a better base for degradation data. Spray efficiency in the Florida testing was measured at six locations through the spray volume to quantify degradation, while the Rancho Seco tests apparently included three measurement points to describe degradation.

The results of the Florida testing indicate that a large spray pond may be expected to have spray efficiencies varying between 60% and 35% depending on position in the spray region and on the wet bulb temperatures and wind conditions.

CONCLUSIONS

The Florida tests significantly expanded the data base by providing data at higher nozzle pressure and for a higher water loading than those characterizing Rancho Seco. Even though these tests did not significantly expand the range of performance data with respect to hot water and wet bulb temperatures, the results of these tests reinforce the validity of the Rancho Seco tests. However, further testing needs to be performed with hot water temperatures in the range of 49° C (120° F) to 54° C (130° F) and with wet bulb temperatures in the range of 21° C (70° F) to 27° C (80° F) in order to provide actual operating data in design ranges similar to those encountered in conventional and nuclear Ultimate Heat Sink applications.

Since numerous mathematical models have been developed to predict spray pond performance outside the ranges where data exist, additional testing should be performed in order to demonstrate the credibility of these models.

REFERENCES

1. Schrock, Virgil E. and Trezek, George J., Rancho Seco Nuclear Service Spray Ponds Performance Evaluation, University of California, July 1, 1973.

TABLE 1. COMPARISON OF VARIABLES CHARACTERIZING TEST FACILITIES

		Florida	Rancho Seco
Spray Flow Rate	(l/sec)	2,780	1,010
	(gpm)	44,000	16,000
Sprayed Area	(m^2)	4,910	2,920
	(ft^2)	52,800	31,400
Nozzle Pressure	(Pa)	69,000	48,300
	(psi)	10	7
Nozzle Elevation	(m)	2.1	1.5
	(ft)	7	5
Nozzles per Spray Unit		5*	4

*See sub-section "Test Facility"

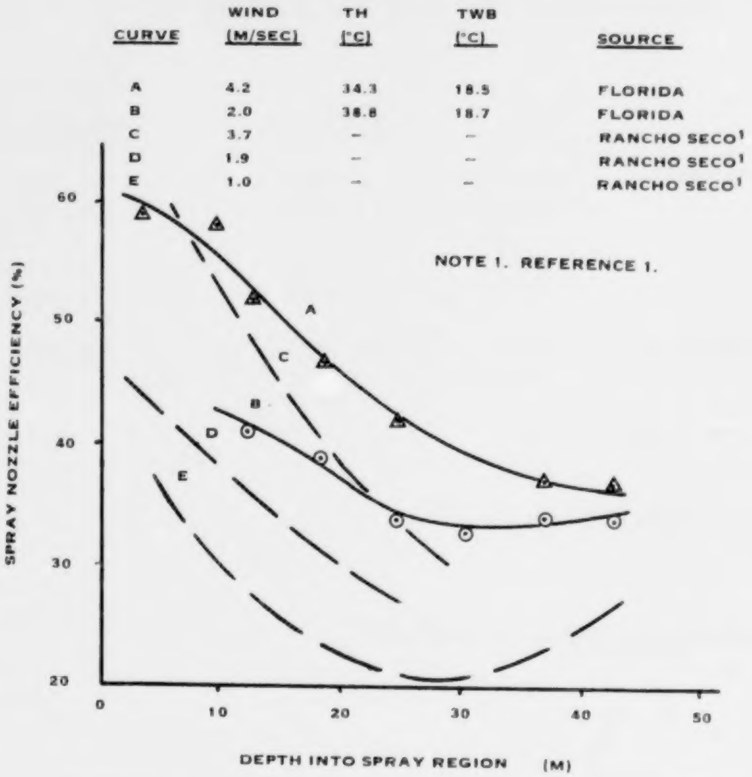

CURVE	WIND (M/SEC)	TH (°C)	TWB (°C)	SOURCE
A	4.2	34.3	18.5	FLORIDA
B	2.0	38.8	18.7	FLORIDA
C	3.7	–	–	RANCHO SECO[1]
D	1.9	–	–	RANCHO SECO[1]
E	1.0	–	–	RANCHO SECO[1]

NOTE 1. REFERENCE 1.

FIGURE 1. DEGRADATION OF PERFORMANCE WITH DEPTH INTO SPRAY REGION

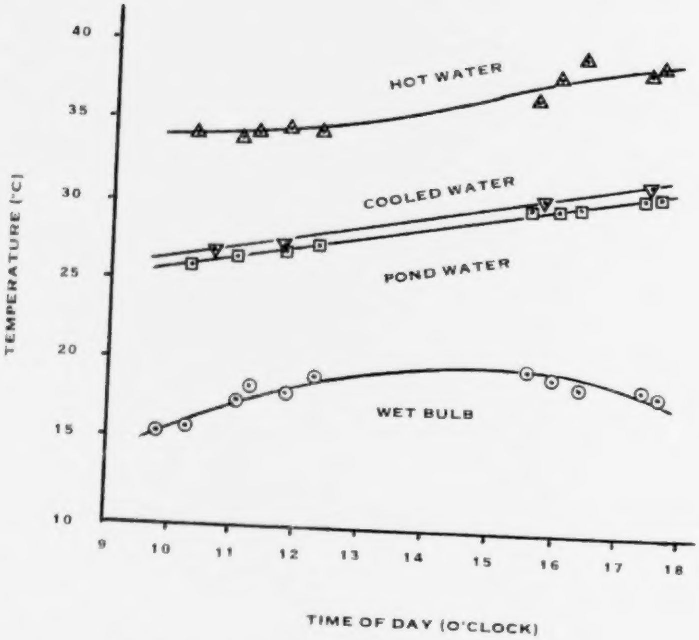

FIGURE 2. TEMPERATURES AS A FUNCTION OF TIME OF DAY

OMIT

FIELD STUDY OF MECHANICAL DRAFT COOLING TOWER PLUME BEHAVIOR

E. R. Champion*, C. H. Goodman*, P. R. Slawson**

At present, there is a need for a better understanding of the behavior of plumes from both natural and mechanical draft cooling towers. One would like to predict the extent of the visible condensed plumes under a variety of atmospheric conditions as well as excess moisture content above ambients in the vicinity of the cooling towers. This information coupled with a knowledge of local climatic conditions may enable one to more readily assess the environmental impact of these plumes.

There have been several large field programs carried out which should lead to a better understanding of natural draft cooling tower plume behavior. However, there is a considerable lack of data on mechanical draft cooling tower plume behavior. There are several analytical models that have been developed to predict plume rise and growth and also estimate the addition of moisture to the local environment. However, problems arise which must be taken into account in order to accurately model mechanical draft cooling tower plumes. These problems include specifications of source conditions to account for multiple sources, recirculation, and complexities arising from terrain, building, and cooling tower wake effects. Some amount of empiricism can

* Research Department, Southern Co. Services, Inc., Birmingham, Alabama

** Envirodyne Limited, Waterloo, Ontario, Canada

Preceding page blank

be included in the plume models to account for such things as tower wake effects if one has enough observational data upon which a reliable empiricism may be based. This requires full scale observational data complimented by physical modeling.

This paper discusses the field program methodology used to study the behavior of mechanical draft cooling tower plumes. The study was planned and implemented by Envirodyne Limited and the Research Department of Southern Company Services, Inc. The towers studied are part of an 880 MW_e coal fired steam electric generating unit. The studies were performed during February, 1975 and January-February, 1976. Analysis of the data will be the subject of later reports.

Factors to be discussed in detail include a description of the procedures and instrumentation needed for measuring (1) the cooling tower source parameters, (2) atmospheric variables and (3) photographing the visible plume in order to obtain the time mean behavior of the plume. Data reduction techniques will also be discussed.

7-45.41

ATMOSPHERIC SPRAY-CANAL COOLING SYSTEMS FOR LARGE ELECTRIC POWER PLANTS

R.W. Porter and S.K. Chaturvedi
Illinois Institute of Technology
Chicago, Illinois U.S.A.

ABSTRACT

Spray cooling systems are alternatives to cooling ponds and evaporative cooling towers for power plant condensers and nuclear ultimate heat sinks. Mathematical modeling is reviewed and simplified solutions are presented for thermal performance as a heat exchanger. The Number of Transfer Units (NTU) and a dimensionless air-vapor interference allowance were determined experimentally for "Ceramic" and "Richards" spray modules at Commonwealth Edison Company's Quad-Cities and Dresden Nuclear Stations in Illinois wherein spray canals are used for condenser cooling. The simplified NTU analysis provides an adequate basis for correlation of performance in terms of spray drop-wise parameters. The critical factor appears to be the interference allowance as governed by air-vapor flow and atmospheric dispersion.

INTRODUCTION

Summary

It is essential that reliable prediction techniques be available to insure proper cooling capacity for condenser heat rejection to the atmosphere from large electric power plants. Under design will result in decrease in thermal efficiency and, in the extreme, de-rating of generating capacity. Over design adversely affects energy costs and may even lead to exclusion from further consideration of an otherwise favorable system. The problem is acute for new larger plants of immense capital investment but which best utilize national energy resources, especially those of nuclear power and coal.

Cooling systems are also essential for various plant auxilaries and the so-called ultimate heat sinks (UHS) of nuclear-reactor safety logistics. In this case, dissipation of heat according to a prescribed history over an extended period is critical, and a validated design technique is mandatory.

Open spray cooling systems are an alternative to cooling ponds and evaporative cooling towers for supplemental or closed-cycle applications. Factors of land availability, cost and environmental impact must be considered on an individual basis. The spray canal wherein floating spray modules are placed mainly in series in an open channel has evolved for the condenser application. The channel typically contains 10^6 gpm (4 x 10^6 liters/min) of water with each module delivering about 10^4 gpm (4 x 10^4 l/m) of about 1-cm diameter drops, power by a nominally 75-hp (56-Kw) motorized pump. The spray pattern is about 5 m high and extends over from 200-600 m^2 of canal surface depending on the particular design. Both manifolded multiple cone-impact and single circular-slot nozzle designs have been utilized. The large drop size and relatively massive spray are compatible with the desire for large flow rates and small drift loss with the prevailing wind substantially in cross flow to the canal. Conversely, the finer in-place manifolded spray matrix has evolved for the spray-pond application to the UHS. In this case order-mm-diameter drops are generated in smaller sprays. The drop-wise parameters of the spray may be combined into a dimensionless group, Number of Transfer Units (NTU), which may be used to predict spray cooling range in terms of initial liquid temperature T and local wet-bulb temperature (WBT). The latter may be related to ambient WBT and T through a dimensionless interference allowance f which includes localized heating and humidification effects as well as larger-scale convective diffusion in the atmospheric boundary layer with an imbeded spray matrix.

The present paper summarizes the results to date of the IIT Waste Energy Management Project in the area of field experiments for determination of NTU and interference-allowance f carried out at Commonwealth Edison Company's Dresden and Quad-Cities Nuclear Stations which employ spray canals. A complete tabulation of the experimental results is contained in [1]. While experimental data are presented for local air-vapor interference which results in greater-than-ambient local wet-bulb temperature, comprehensive modeling of this aspect is reported in [2]. Dispersion of the buoyant discharge downwind is to appear separately. A complete evaluation of equations for direct-contact evaporative cooling for open sprays including solar and atmospheric radiation and non-unit psychrometric ratio which are neglected in the Merkel's equation most often applied is contained in [3]. The present data were correlated with the more detailed theory for selected cases in [1]. However, the simplified analysis [4] summarized here is adequate so long as the correct local interference allowance is used.

The field experiments reported earlier [3] for Dresden Station (Morris, Illinois) involved measuring canal temperatures upstream and downstream of a run of up to 40 4-spray Ceramic Cooling Tower Company (CCT) modules [5,6] arranged 2 units (modules) wide across the canal (Figure 1). Module parameters are summarized in Table 1. Correlation allowed for time of flow and average meteorological conditions. These data were used to imply canal-averaged NTU based on a previously assumed dimensionless interference allowance f to account for local elevation of wet-bulb temperature. A spray collection device was subsequently used to determine local NTU in various portions of the upwind and downwind sprays. The module NTU measurements were also accomplished at the 4-units-wide spray canal at Quad-Cities Nuclear Station (Cordova, Illinois) wherein are employed 176 CCT modules (Figure 2) and 152 single-spray Richards of Rockford (RR) modules [5,7] (Figure 3). However, at Quad-Cities additional measurements were made of actual local wet-bulb temperature and wind speeds as a function of the row position proceeding downwind. Thus, both local NTU and local dimensionless interference allowance were determined. The NTU data are correlated best with wind speed although wind angle, bank height and a natural convection parameter were also considered. By turning off one spray module at a time, it was possible to imply the difference between total and self interference; that is, of the entire system and of the individual module, respectively. Self interference is quite appreciable, and the first upwind row does not see the ambient WBT nor does absorbing self interference in NTU adequately scale the increment thereof for a single spray. Accounting for interference, NTU from canal (Dresden) and module (Dresden and Quad-Cities) experiments are in essential agreement. It now appears that NTU is the more easily established quantity and does not vary greatly over various operating conditions for a particular module(usually less than ±15%). On the other hand, dimensionless interference allowance requires more comprehensive modeling [2].

Review of Literature

Heat and mass transfer of liquid-water spray cooling in air and water vapor mixtures may be classified according to: 1. fundamental aspects, 2. droplet phenomena, 3. air-vapor flow, 4. unit and system performance. It is possible to go directly from Item 1 to 4 if the unknown parameters are determined experimentally. This approach is used in the present study although the other categories are briefly summarized.

Fundamental aspects of simultaneous heat and mass transfer are reviewed in detail in [8,9] as well as in many other standard texts. Both heat and mass transfer are governed by convective diffusion equations but the diffusivities a and D, respectively, differ in general. The interface between liquid and gas phases is bounded by saturated liquid and saturated vapor in air. The most general approach utilizes separate correlation for the sensible heat transfer coefficient H, and the mass transfer coefficient K. The total energy transport is due to the former involving temperature difference, and the latter which is due to vapor mass fraction difference. For air and water vapor, typically 85% of the energy transport is due to evaporation carrying enthalpy with it.

In practice, simultaneous correlations for heat and mass transfer are seldom available for geometries and dimensionless group ranges of interest. However, consideration of a wide range of theory and experiments has led to the "analogy of heat and mass transfer" wherein H and K are related by the psychrometric ratio P. For temperatures of interest, 0-50 C, and atmospheric pressure, Threlkeld reviewed the available data and concluded [9]

$$P = H/(c_s K) \approx (a/D)^{2/3} \qquad (1\text{-}1)$$

where c_s is humid heat, the specific heat of air and vapor at constant pressure per unit mass of (dry) air. Because $a/D \approx 1$ for air and water vapor, $P \approx 1$ which leads to considerable simplification and the well-known Merkel equation for direct-contact evaporative cooling. In this case, the net driving potential for energy transport is Carrier's sigma function or total heat, a specific enthalpy referenced to the saturated liquid state which depends only on WBT.

Droplet phenomena refers to the "near field" about individual droplets. The break-up of liquid jets into droplets depends on the balance between surface tension, internal circulation and aerodynamic forces including turbulent fluctuations [10]. The atmospheric free-fall velocity from a typical 5-m spray height is about 10 m/s which corresponds to a terminal velocity for about 7-mm diameter drops [11]. Larger drops than this are subject to very near the parabolic trajectory of free flight.

In principle, it is possible to solve simultaneously the fluid mechanics both within and outside a droplet if approximations are made in terms of spherical shape, high Reynolds number and uniform drop environment [12,13]. However, the departure of liquid drops from solid spheres in terms of heat and mass transfer is generally recognized, the classical correlations for steady state being due to Ranz and Marshall [14]. Recent studies by Yao and Schrock [15] are devoted toward correcting these correlations for freely falling drops. Given the drop-size distribution such as determined experimentally by optical techniques [16],it is nevertheless feasible to compute theoretical temperature-time histories and integrate these into bulk flow averages [17]. Hollands and Goel [18] relate NTU to such distributed effects through the definition of a mean particle (drop) size.

The problem of air-vapor flow through sprays was analyzed by Porter and Coworkers[3-5] through the experimentally determined dimensionless interference allowance which scales wet-bulb temperature increment with the difference between water temperature and ambient WBT. In [3] it is related to the effective L/G (liquid to gas) ratio of the flows. However, because air-vapor flow is not subject to well-defined channeling as in a cooling tower, the L/G parameter can not be realistically predicted. An alternate approach, due to Elgawhary and Rowe [19], defines an air cell which follows the droplets and receives the heat and mass transfer. The radius of the air cell is determined experimentally. Other similar models are reviewed by Ryan and Myers [20].

The most valid approach from a physical point of view is due to Chen and Trezek [21]. A quasi one-dimensional momentum balance on the spray is used to compute exit vertical and horizontal velocity in a step by step procedure going downwind. The forces are computed from theoretical drop drag forces integrated over an experimental drop-size distribution. In between sprays, an assumed ambient flow over the sprays is mixed with the horizontal exit flow using Schlicting's planar turbulent jet mixing solution [22]. However, Chen and Trezek must increase mixing by a factor of 135 to agree with their experiments using five sprays aligned with the prevailing wind. A major part of the discrepancy may be due to planar jet mixing not being the controlling phenomena, and three-dimensional end effects.

Unit and system performance relates to the cooling achieved by an individual spray or spray module (i.e., a unit) and an assembly of units (the system). Ryan and Meyer [20] summarize the various techniques in general. The discussion here will be limited to essentially NTU (Number of Transfer Unit) methods wherein the drop-wise parameters are combined into a dimensionless group (NTU or equivalent). Quantity NTU may be predicted from droplet theory or implied from measured cooling ranges of experiments. Other methods include detailed analysis of drop time-temperature histories without reduction to NTU or are fully empirical.

The NTU method for open sprays appears to originate with Kelley [7,23]. An average "enthalpy" difference was used in the NTU equation, and a step-by-step marching procedure was employed for canal performance. Hoffman [24] reported system performance data for several spray canals in terms of observed cooling range. Porter and Chen [5] reduced this data to NTU correcting for local WBT elevation using the nondimensional interference allowance f as determined from measurements at Dresden station downwind of sprays. Superposition was used to account for multiple upwind rows, and local "self" interference was neglected.

Porter [4] also developed a simplified analytical solution by assuming total heat is linear with adiabatic-saturation temperature and correlated the Hoffman data [24]. Later this method and a linearized corrected one including psychrometic ratio, radiation, etc., were applied to new experimental data directly taken by Porter and Coworkers at Dresden Station [3]. The corrections were found to be small. More important, values of NTU were found to be substantially lower than previously reported. This data is substantiated here as compared with the recent measurements on individual modules at both Dresden and Quad-Cities Stations.

Chen and Trezek [21] developed an NTU method for spray ponds but define NTU as "SER" (Spray Energy Release). The main feature of the SER method ,already discussed, is that the energy release of the spray is used to compute that gained by the air and vapor. Soo has shown the equivalence of the several approaches to the NTU method [25] and as an application considers the optimized performance of a spray-module system in terms of drop size and spray height as they affect pumping power for cooling duty. He concludes [26] optimum drop size is about 5-mm diameter and spray height about 4 m based on approximations and criteria employed.

Arndt and Barry [27] have developed a computer program that treats each spray element as a point source. Heat and humidity release is analyzed using NTU [24], and dispersion rates from air-pollution studies are used to determine local wet-bulb temperature by superposition and iteration. The recent approach of the present investigators [2] includes wind attenuation and atmospheric dispersion coupled with variable heat and humidity release in a unified fluid-dynamic analysis. Effects of parameters on systems performance are also discussed.

THEORETICAL ANALYSIS

Unit Performance

The statements of conservation of energy and mass for a steady monodisperse(single drop size) liquid-spray flow with an exposed surface-area element dA, as in control Volume I of Figure 4 are

$$d\,(\dot{m}_s i_L(T'))-i_g(T')\,d\dot{m}_s = H\,dA(T_{DB}-T') \qquad (2\text{-}1)$$

$$d\dot{m}_s = K'\,dA\left[\omega/(1+\omega)-\omega_S(T')/(1+\omega_S(T'))\right] = K'/(1+\bar{\omega})\cdot dA(\omega-\omega_S(T')) \qquad (2\text{-}2)$$

where $\dot{m}_s$ is spray mass flow rate, i water specific enthalpy, H sensible heat transfer coefficient, T temperature, K mass transfer coefficient based on (water) vapor mass fraction, a fundamental driving potential for mass transfer [28], ω is specific humidity (mass of vapor per mass of dry air), and s denotes spray, L liquid water, g saturated water vapor, DB dry-bulb temperature (DBT), S saturated air-vapor mixture, prime the local spray temperature, and the bar an average condition. By definition, H and K are based on contact area A. Effects of the drop-size distribution are discussed at the end of the present section. Radiation is included in the corrected analysis of [1,3] but is neglected here.

Assuming $i_L = i_f$ where f denotes saturated liquid and $di_f = c_w dT'$ where c_w is specific heat of liquid water, assumptions which are virtually exact for present purposes, the above combines to

$$\dot{m}_s c_w dT' = -K\, dA \left(Pc_s(T' - T_{DB}) + i_{fg}(T')(\omega_S(T') - \omega)\right) \quad (2\text{-}3)$$

where $P = H/(c_p K') = H/(c_s K)$ is the psychrometric ratio, i_{fg} is water latent heat, c_p is specific heat, $c_s = (1+\bar{\omega})c_p$ is the humid heat and $K = K'/(1+\bar{\omega})$. Note that the factor $1+\bar{\omega}$ has been absorbed, and no appreciable error has been introduced by using humidity as the driving potential.

It is convenient to recast Eq.(2-3) in terms the air-vapor wet-bulb temperature(WBT) T_{WB} which is the equilibrium liquid water temperature T', when Eq.(2-3) is identically zero. Substituting this expression to eliminate T_{DB} and ω, the result is

$$\dot{m}_s c_w dT' = -K\, dA \Big[h(T') - h(T_{WB}) - c_{pa}(1 - Pc_s/c_{pa})(T' - T_{WB}) - \omega(i_{fg}(T') - i_{fg}(T_{WB}))\Big] \quad (2\text{-}4)$$

where h is Carrier's sigma function(total heat) which is defined as [29]

$$h(T_{AS}) \equiv \hat{i}(T_{DB}, \;) - \omega i_f(T_{AS}) \approx c_{pa} T_{AS} + \omega_S(T_{AS}) i_{fg}(T_{AS}) \quad (2\text{-}5)$$

Quantity T_{AS} denotes adiabatic-saturation temperature (AST), $\hat{i}$ is enthalpy of air and vapor per unit mass of dry air and c_{pa} is specific heat of dry air. Quantity h is tabulated in [29]. The AST is a thermodynamic property while the WBT is a transport property which is the same for the spray and a wetted-wick psychrometer presuming equal psychrometric ratios P. The relationship between AST and WBT is given in [1,3,9]. For air and water vapor where $P \approx 1$, the difference between them is of order 0.1 C and is of secondary importance [1,3].

Assuming $Pc_s/c_{pa} = 1$ and neglecting the variation in latent heat, assumptions relaxed in [1,3] and also shown to be of secondary importance

$$c_w \int_{T_s}^{T} \frac{dT'}{h(T')-h(T_{WB})} = NTU \qquad (2\text{-}6)$$

where the Number of Transfer Units $NTU \equiv \overline{KA/\dot{m}_s}$, T is the canal temperature at the spray nozzle intake and T_s is the final sprayed water temperature. Eq.(2-6) is Merkel's equation of direct-contact evaporative cooling. In a cooling tower, a similar energy balance on the air and vapor yields $dh(T_{WB})/dT = -c_w L/G$ where L/G is the liquid-to-gas mass ratio [30]. In the present case L/G is not well defined and so an average local T_{WB} is used instead. The relation of T_{WB} to the ambient $T_{WB\infty}$ is through the "interference allowance" discussed later.

In the present simplified analysis, Eq.(2-6) is integrated by assuming $b = dh(T)/dT = b(T_f) \equiv b_f$, a constant, where T_f is a "film temperature" used for property evaluation. Quantity b is tabulated in Table II using h(T) data of [29]. For a temperature interval bounded by $T_{WB\infty}$ and T_H, a hot water temperature, it is suggested to use $T_f = (T_H + T_{WB\infty})/2$. Because the quantity b is slowly varying, no appreciable error is introduced in typical cases as shown in [1,3]. Thus, the dimensionless module cooling range is

$$(T-T_s)/(T-T_{WB}) = 1-\exp(-ntu\; b_f/c_w) \qquad (2\text{-}7)$$

where a new symbol ntu is used for NTU in order to distinguish the specific theory utilized when Eq.(2-7) is used to imply NTU from experimentally observed temperatures. For example, in [1,3] it is shown that experimentally implied NTU do differ slightly when non-unit psychrometric ratio, radiation and nonlinear total heat are incorporated in more general theory. The designation NTU is used in a broad sense to indicate $\overline{KA/\dot{m}_s}$.

In [4,5], NTU is defined in terms of an average-drop trajectory analysis where it is shown NTU = $(\overline{K_d A_d/m_d})t$ where m is mass, t time of flight and d denotes drop. The droplet approach has also been used by Chen and Trezek [21] and Soo [25,26]. It is apparent that NTU for the overall spray interface and the mean drop trajectory are equivalent and equal when they lead to the same equation (2-7).

As discussed at the onset, the basic equations (2-1) and (2-2) apply to a monodisperse system. Drop-size distribution will result in variable exchange with the environment causing a drop-size dependent distribution of temperature and evaporation as modified by heat and mass interchange due to drop break up and coalescence. Quantity NTU may be regarded as that of an equivalent monodisperse system of appropriate mean drop size if certain conditions are met, namely combined heat and mass transfer with a Merkel-type equation, uncoupled drop motion, and negligible drop internal thermal resistance [18]. In particular, the last condition may not be entirely realistic [15]. Thus, for sprays of appreciable drop size distribution, the apparent NTU may depend to some extent on prevailing conditions. The most direct measurement of NTU involves sampling the spray temperature of individual modules and determining the local average WBT. Eq.(2-7) then yields NTU or more precisely ntu, to identify the theory used. Results are discussed in the next major section.

The evaporation can be computed by integrating Eq.(2-2) or by using an average Bowen ratio of sensible to evaporative heat transfer $\bar{B} = (Pc_s/i_{fg})(\bar{T}-T_{DB})/(\omega_S(\bar{T})-\omega)$ where $\bar{T}$ is an average liquid water temperature and $Pc_s/i_{fg} \approx 0.00038\ C^{-1}$. In this case the fraction of spray flow rate evaporated is directly related to the spray cooling.

$$\alpha = (c_w/i_{fg})(T-T_s)/(1+\bar{B}) \qquad (2\text{-}8)$$

where $c_w/i_{fg} \approx 0.0017\ C^{-1}$. Evaporation of sprayed water is small(typically 1 or 2%), and from the thermal point of view results are weakly dependent on $\bar{B}$. Thus, spray performance depends mainly on the wet-bulb temperature rather than both the dry-bulb temperature and the humidity. The upper limit on evaporative make-up water required can be computed assuming $\bar{B} = 0$.

Air-Vapor Circulation Interference

The air-vapor mixture is heated and humidified as it comes in contact with the spray. As noted earlier, for flow within a cooling tower this is accounted for by an energy balance $dh(T_{WB})/dT = -c_w L/G$. Integrating using $b_f = dh/dT'_{WB}$ limits of T_{WB_∞}, T_{WB} and T_s^w, T for L and G in counter flow, and (2-7)

$$T_{WB_i} = T_{WB_\alpha} + f_i(T - T_{WB_\alpha}) \qquad (2\text{-}9)$$

where for each row i of modules across the canal

$$f_i = (c_w/b_f)(L/G)_i(1 - \exp(-ntu\ b_f/c_w)) \qquad (2\text{-}10)$$

It should be noted that the standard counter-flow configuration assumed is arbitrary. Further, values of L/G are virtually impossible to predict or measure for open sprays especially when imbeded in a spray system. Thus, Eq.(2-10) is not actually utilized by the present investigators except to demonstrate the basic nondimensional scaling in Eq.(2-9). A fluid dynamic theory for f based on analyzing wind attenuation and atmospheric diffusion is contained in [2].

The f quantity is bounded $0 \leq f \leq 1$ considering the possible interval between the ambient state and equilibrium with the canal. Like NTU, it contains parameters which may be predicted from more detailed theory, but which also may be implied experimentally in connection with Eq.(2-9) as discussed later.

Spray-Canal Peformance

As discussed in [3-5] typical spray canals are very well mixed,and so the temperature T is considered constant in a canal section. Across each pass of modules, n, the canal will be cooled according to the fraction of the canal water sprayed. For each row i of m rows across the canal, simple mixing considerations for Control Volume II(Figure 4) yield

$$dT_i/dn = -mr(T - T_{si}) \qquad (2\text{-}11)$$

where r is the ratio of module flow rate to initial canal flow rate and where the small loss of evaporative flow is neglected in the mass balance as justified in [1,3]. The module cooling range $T-T_{si}$ is given by Eq.(2-7). Using Eqs.(2-7) and (2-9) in (2-11) and averaging across the canal to obtain the average dT/dn and integrating from the canal-intake hot water temperature (HWT) T_H to the canal-discharge cold water temperature (CWT) T_C

$$(T_C-T_{WB_\infty})/(T_H-T_{WB_\infty}) = \exp\left[-Nr(1-\bar{f})\left(1-\exp(-ntu\, b_f/c_w)\right)\right] \qquad (2\text{-}12)$$

where $N = nm$, the number of modules, and where $\bar{f}$ is the arithmetic average value for m rows across the canal.

While evaporation is small, it is important for make up including blow down and for environmental considerations. The rate of evaporation as a fraction of initial canal flow, e, is by definition given by $de/dn = mr\alpha$. This may be integrated from $e(0) = 0$ by using (2-8) and (2-11). The resulting exponential relation may be approximated

$$e = \left[c_w/\left(i_{fg}(1+\bar{B})\right)\right](T_H-T_C) \qquad (2\text{-}13)$$

and which also follows directly from the definition of Bowen's ratio. As an example, a 14-C cooling range leads to 2.4% evaporation of canal flow in the worst case of $\bar{B} = 0$.

The above approach assumes a steady state in terms of a uniform T_{WB}, ntu and f (meteorological dependent) as well as r and T_H (canal-intake dependent). By using time-averaged-over-flow meteorological data, a "slug of fluid" can be followed through the canal by knowing the time of discharge into the system and the time of flow. Conversely, by measuring the temperatures, ntu can be implied. However, the circulation allowance $\bar{f}$ must be defined.

FIELD EXPERIMENTS

Instrumentation and Techniques

As summarized in Table III, both local module experiments and overall canal experiments were performed. In the former case, local WBT and wind speed and/or spray temperature were sensed. In the latter case, only canal temperatures at the ends of the run of modules were obtained.

Determination of ambient conditions was similar in both cases.

Canal and spray water temperatures were detected by Atkins thermistor sounding probes and bridges. In Exp. 1, canal water temperatures were monitored at a mid-channel location at the canal-segment intake and discharge ends. In module-NTU measurements (Exps. 2-5), canal water temperature was monitored locally at the test module or immediately upstream. A water collection device was designed and constructed to collect spray water after flight and measure a radially integrated spray temperature. The collector was a 3-ft diameter funnel and floated about 6 inches out of the water when operating. A thermistor was positioned at the throat in a shielded perforated case in about 4 inches of water. Measurements were made approximately every 90° about the spray pattern proceeding from upwind rows. When the collector was properly positioned via cables from shore, the thermistor bridge was switched from the canal temperature sensor to the spray-collector temperature sensor and held for several minutes to get a gust-averaged value. Canal water temperature was monitored below the surface. As noted previously, experience has shown very little variation in canal temperature at a section.

Wet-bulb and dry-bulb temperatures were obtained from Atkins psychrometer modules and thermistor bridges. Wind run was determined from contact anemometers calibrated in the IIT 4 x 6 foot environmental wind tunnel to ±0.1 m/s. Wind direction was obtained with a bivane with a potentiometer element. Ambient meteorological conditions were measured sufficiently upwind to avoid interference and at a 2-m elevation over grade. Local conditions were measured directly over the module motor 2m over the water level. Bridges and recorders were calibrated in the field using a calibrated decade-resistance substitution device. Recorded temperature data were accurate within ±0.1C.

In canal-NTU tests, all meteorological data were subsequently averaged over the time of flow of each slug corresponding to a hot-water temperature (HWT) reading. The cold-water temperature (CWT) was read from the continuous data allowing for time of flow. Canal flow was determined using a Weathermeasure helical propeller contact flow meter and a Heath digital electronic depth sounder (±0.3m). The canal bottom and banks were defined in contour and velocity-sounded at 3 equally spaced points each in width and depth. Velocity was first averaged in width and then the vertical profile was integrated graphically allowing for a thin viscous sublayer at the bottom. Resultant canal flow rates agreed with manufacturer's lift-pump specifications to ±5%.

In the module-NTU tests, spray temperature and local wet-bulb temperature were sampled sufficiently long to allow averaging over gusts. Typically, several (3-4) cycles were obtained over a few minutes duration. Canal temperature and ambient conditions were then referred to the test interval. In obtaining average wind speed, wind run was summed over the period. In most cases, it was not possible simultaneously to measure local wet-bulb temperature and spray temperature. This was due to the time-consuming procedure of moving the psychrometer from module to module in the various rows. In the Richards modules, the mooring cables were in the way of the collector which further slowed the process. Where simultaneous wet-bulb temperature was not available to correlate with spray temperature, the nearest-time data for dimensionless interference allowance was applied to the prevailing ambient wet-bulb and canal temperatures. This allowance corresponded to measurements under very similar conditions.

Time averaged parameters are listed in Table III. The natural-convection buoyancy parameter is the maximum possible fractional density increment of the air-vapor mixture as it is heated and humidified by spray at an average temperature $\bar{T}$. Thus

$$|\Delta\rho|/\rho = T_{DB_{\alpha}}^{-1}(\bar{T}-T_{DB_{\alpha}}) + (\omega_S(\bar{T})-\omega_{\alpha}) \qquad (3\text{-}1)$$

where the first coefficient is approximately $-\rho^{-1}\partial\rho/\partial T$, $T_{DB\alpha}$ is ambient absolute temperature and the second coefficient is $-\rho^{-1}\partial\rho/\partial\omega \approx 11/18$. Also listed are film temperature which gives the approximate temperature level of the overall system, wind speed (WS) wind direction (WD) in terms of angle of incidence to the canal, and bank height. A complete tabulation of individual temperature and other data is contained in [1]. The complete data for Exp. 1 is also tabulated in [3].

Local-Interference Data

The experiments wherein local WBT and wind-speed data were obtained are Exps. (3a)-(5b) of Table III. All data were obtained at the Quad-Cities Station 4-row canal. The location of the measurements for the Ceramic modules is noted by the solid squares in Figure 2. In the Richards case, measurements were on center of the circles (sprays) of Figure 3. The basic approach was to alternately take measurements with the module tested both on (spray on) and off (spray off) while the other modules were running. The difference in readings is attributed to "self interference". Some data were also taken with a single module or single row of modules (denoted S). The psychrometer and anemometer were not submerged in the spray itself.

As discussed previously, the appropriate nondimensional WBT interference allowance is defined

$$f \equiv (T_{WB}-T_{WB_\infty})/(T-T_{WB_\infty}) \qquad (3-2)$$

Similar, a dimensionless wind-speed (WS) interference factor is

$$g \equiv (WS_\infty-WS)/WS_\infty \qquad (3-3)$$

and both quantities are bounded between 0 and 1.

Data for Ceramic modules were obtained on 2 occasions at the same location (Exps. 3b and 5a). The reduced data are listed in Tables IV and V. The test conditions (Table III) compare although buoyancy was a little stronger in Exp. 5a and the WS a little higher in Exp. 3b. The important thing to note in Tables IV and V is that the difference between (self) spray off and (self) spray on is appreciable and can not be neglected. As discussed earlier, the difference is attributed to self interference of the particular module tested. While the average values of $\bar{f}$ for (self) spray off are 0.20 and 0.29 for the two cases and this compares well with the previous recommended allowance of 0.22 [3],[4], the total interferences are much greater at 0.37 and 0.46, respectively. Self interference had been neglected from the point of view that NTU based on approach WBT was sufficient to describe performance of a single module. However, it is now clear that observed large self interference will not scale properly without account of $T-T_{WB_\infty}$ as incorporated in f.

The data for f (WBT) are plotted in Figure 5 for the case of (self) spray-on for both experiments as a function of row position. It should be noted that this f is the total operational interference allowance. The case of Exp. 3b is interesting in that the last two downwind rows exhibit some recovery back towards ambient WBT. Such phenomenon was also observed by Chen and Trezek [21] and was attributed to backside natural convection. However, in the present case, Exp. 3b has the lower buoyancy parameter and the greater wind speed which is not consistent with the argument. Instead it is possible that the difference is within experimental error.

The maximum error of the interference allowance based on accuracy of measured local wet-bulb temperature is estimated at ±15%, about the average scatter in the data. This percentage is based on f equal to a ratio of temperature differences, each temperature measured accurate to 0.1 C. The numerator is about 1-3 C (±7-20%) and the denominator 10-40 C (±0-2%) which adds to 7-22%. The bars with data points in Figure 5 represent the range of observed data. Also noted is a bar for ±15% error in the vicinity of the back-row decrease which could explain the behavior.

The nondimensional wind-speed interference factor g is plotted in Figure 6. In this case, there is substantially greater difference in the two experiments. The difference on the downwind side seems to be due to large fluctuations probably associated with large-scale atmospheric turbulence and unsteadiness after passing through and over the sprays. Whether this might affect performance to a like variation could be asked. However, the velocity of the spray ranges to order 10 m/s as discussed previously and so wind-speed changes of order 1 m/s or less should be of second-order importance. It indeed appears that the large local WS variations do not greatly affect f or, as shown later, NTU.

Data for the Richards modules (Figure 3) are shown in Table VI. Again, the difference between (self) spray off and (self) spray on is appreciable although the spray-off interference is somewhat less than that previously recommended [3,4]. Nevertheless, the total interference (spray on) is about 50% greater. Also shown in the table are data for essentially a single module (S') wherein 11 neighboring modules were nonoperational as illustrated by nearly zero influence of other modules with spray off. The data show that Richards-module self interference dominates over that of other surrounding modules. This may not be surprising in view of the spaces between Richards spray pattern (Figure 3). The f and g data are plotted versus row position in Figure 7 and 8, respectively, for the case of spray on.

NTU (ntu) Data

In this section, the experimental data are presented as reduced to NTU using the simplified analysis ($NTU \equiv ntu$). Data are reduced based on:

a) Canal measurements using assumed interference allowance (Exp. 1).
b) Module measurements using assumed interference allowance (Exp. 2).
c) Module measurements using measured interference allowance (Exp. 3-5).

Exp. 1-2 were performed at Dresden Station while the remainder were for Quad-Cities Station.

The NTU based on observed canal cooling performance of Ceramic modules at Dresden Station are plotted versus ambient wind speed in Figure 9. It is recalled that the canal segment has 2 rows across the canal and 20 passes along the canal for a total of 40 maximum operating modules. Quantity NTU were implied from canal temperatures at either end of the segment and therefore may be interpreted as "canal (averaged) NTU". An assumed average interference allowance of $\bar{f} = 0.10$ was used [3-4]. This allowance was predicated on $f = 0$ for the upwind row and $f = 0.20$ for the downwind row based a 40-ft (12.2-m) row spacing [5]. As discussed in the previous section, measured local WBT indicate somewhat higher interference in the first two rows of the 4-row Quad-Cities system. Data do not correlate very well with any single parameter. The lower-wind-speed data tend to indicate greater NTU with larger buoyancy parameter at the same 2.1-m bank height. However, the data for the greatest buoyancy parameter (0.09) may not have the greatest NTU because of the large bank height in this case. Insufficient data is available for independent correlation with all the parameters. As discussed later, the overall variation in NTU is not very great anyway.

For the purpose of an error analysis of the accuracy of ntu, for small ntu and $b_f/c_w \approx 1$, $\exp(-ntu\ b_f/c_w) \approx 1 - ntu\ b_f/c_w$. It can be shown from Eqs. (2-7) and (2-12) and the above that ntu for either a module or canal is approximately proportional to the ratio of cooling range to difference between canal temperature and WBT. Under typical conditions for either the present short canal or modules more generally, the numerator of the ratio is accurate to 0.2 C of 1-3 C (7-20%) while the denominator is accurate to 0.2 C of about 10-30 C (1-2%) which combines to an error from 8-22%. Thus, the average experimental accuracy for ntu is estimated within about ±15%. An error bar of ±15% is also shown in Figure 9, and the data show scatter not much greater than that.

The data of Figure 9 are substantially lower than that of [4] based on temperature data reported by Hoffman [24]. Present ntu range from 0.12 to 0.23 over 2.5-6.5 m/s. While previous ntu data ranged from 0.27 to 0.57 over 1-6.5 m/s [4]. However, the data base of Hoffman [24] was not fully documented, and module-NTU data discussed below tend to support the lower values found here.

Module NTU (ntu) also were determined at Dresden Station (Exp. 2). In this case, the spray was collected directly, and Eq.(2-7) yielded the value of NTU. The geometry is shown in Figure 1 and the NTU data in Table VII. As noted, Row I is always upwind as are "clock positions" 6 and 9. The experiment was performed in the center of a run of 8 continuous passes (16 modules). Data are selectively reduced for f = 0, 0.1 and 0.20. The first-row f was previously taken as 0, the second-row f as 0.20, and the average f as 0.10 [3-5]. As mentioned earlier, NTU is not expected to be greatly sensitive to f for a 2-row canal. We do not regard the reported distribution of NTU within the spray as being particularly significant in view of the use of a single WBT for a given spray. More significant is the spray-averaged NTU for each of the two rows. The module averaged NTU (ntu) were based on

$$\exp(-\text{ntu}\ b_f/c_w) = \sum_i \exp(-\text{ntu}_i\ b_f/c_w) \qquad (3\text{-}4)$$

which is equivalent to averaging the spray temperature except variation of WBT is accounted for.

The upwind row definitely tends to a greater NTU when the same f is employed. However, if sufficiently high f is used for the second row compared with the first, the two

NTU can be brought into agreement. Of the data shown, ntu = 0.116 with f = 0 for Row I is closest to ntu = 0.091 with f = 0.20 for Row II. These are the "previously recommended" local f values [5]. It is concluded that NTU is about the same for both rows but, of course, the local WBT is greater for Row II. As discussed in the previous section, there is considerable wind attenuation in spray systems as reflected in the g factor. However, NTU is apparently dominated by drop-wise factors due to the high trajectory velocity. Accordingly, wind attenuation would be expected to affect WBT (through f) more than affect NTU. Using f = 0.1, the pass-averaged ntu = 0.105 at 4.6 m/s (Exp. 2) is compatible with the lower range of canal-averaged ntu (Exp. 1) as shown in Figure 9.

Module NTU were also obtained for Ceramic modules at Quad-Cities Station (Exps. 3a and 5b) as illustrated in Figure 2. Data are listed in Tables VIII and IX. The experimental f is based on having the individual module "spray on" which includes self interference. As in the case of Dresden Station, the present data (Tables VIII and IX) show a trend toward greater NTU on the windward side of an individual spray although the use of a single WBT for an individual spray probably precludes qunatitative resolution of NTU within a spray. The spray-averaged data are plotted in Figure 10. The vertical bars denote ranges of observed data while the symbols are at the average values.

In the case of Exp. 5b (Table IX), it was noted during the experiment that the cone-impact supports of the spray nozzles were producing somewhat abnormal spray patterns over 0.5m of the perimeter at the usually selected 3-6-9-12 O'clock positions. Therefore, alternate positions shifted 45^o (1:30-4:30-7:30-10:30) were selected. The abnormal pattern may be due to algae growth, but did not appreciably alter the overall pattern. It is interesting to note that the phenomenon was not observed in the earlier experiment (Table VIII) and that data appear consistant considering the difference in wind speed and experimental accuracy. It is uncertain whether the true integrated module NTU would be greater (due to WBT venting) or less (due to drop coalescence) than that of the normal spray pattern. All that can be said is that the abnormality is localized and because the physical extent is only a total of about 2m of the 40m perimeter, the integrated NTU is likely not altered more than about 5%.

As noted in the tables, some experimental f values used in data reduction were actually obtained from data taken at a different time. However, the local WBT used in reducing NTU was based on the actual prevailing ambient WBT and canal temperature. Some cases where both instantaneous and other f values were used are shown in Table IX. The NTU agree with the ±15% error estimate which supports the approach. Also noted in Table VIII are some single row ("S") data taken by turning off the 3 other rows for 3 passes (150 m), and data were taken in the center of the run. The average module NTU is 0.144 for the single row which compares with the pass-averaged value of 0.136 for 4 rows well within ±15%.

Once again, the evidence points toward NTU being primarily dominated by drop-wise phenomena and independent of conditions when local WBT is employed. The above module NTU data are plotted versus wind speed in Figure 11. In one case (Exp. 5b), data are plotted using both ambient and local wind speed, the effect being inconclusive. While there is a trend toward greater module NTU at greater wind speed, as was the case for canal NTU in Figure 9 , the effect is not large. Indeed , based on local WBT

$$\text{ntu (Ceramic)} = 0.15 \pm 15\% \qquad (3\text{-}5)$$

$$1 \leq WS \leq 6 \text{ m/s}$$

fits 67% of the 33 data of both Figure 9 and Figure 11. All but one of the data (97%) are bounded by ntu = 0.15 ±33% over the WS interval 1-6 m/s.

Data were also taken for the Richards of Rockford modules at Quad-Cities (Exp. 4a) with the geometry of Figure 3. Data are listed in Table X and were based on simultaneous local WBT measurements. Unfortunately, mooring cables prevented convenient traversing of the Richards spray. Time was available only for a few samples as noted. Fortunately, these included a single module case (3 passes otherwise turned off, an interval of 120 m) and a Row IV (most downwind) case which probably bound the possible range of NTU for prevailing conditons. Using the experimental f, ntu module-averaged are 0.058 and 0.066 respectively which together average to 0.062 ±6%, well within the ±15% estimated error. We conclude, based on local WBT

$$\text{ntu (Richards)} \approx 0.06 \qquad \text{WS} \approx 2 \text{ m/s} \tag{3-6}$$

but must caution against any confidence in using such a value owing to the extremely limited data base. Further, caution must be made against a comparison of Eq. (3-5) and Eq. (3-6), without further considerations. The flow rates of the two modules differ for Ceramic and Richards (10,000 gpm and 12,000 gpm-nominal, repectively) as likely do cost and possibly numerous other factors such as pump power, maintenance, reliability, etc.

SUMMARY OF CONCLUSIONS

Equations for unit (spray or spray module) and systems (spray canal) cooling were derived from fundamental consideration of heat and mass transfer wherein the principal unknown drop parameters are combined into NTU. A dimensionless interference allowance f was introduced to incorporate local heating and humidification effects.

While the present data base is limited, it appears as though NTU for a particular spray module is relatively constant and independent of conditions so long as a local wet-bulb temperature is employed in the equations, such as that 2m over the water surface at the center of the module in plan. The dimensionless interference allowance relates the local increment of wet-bulb temperature above ambient to the local liquid water and ambient wet-bulb temperatures. The present experimental values as a function of position windward through the spray field may be useful for estimating performance under similar conditions and for developing fluid dynamic models of the effect.

REFERENCES

1. Yang, U.M. and Porter, R.W., "Thermal Performance of Spray Cooling Systems-Theoretical and Experimental Aspects", IIT Waste Energy Management Report TR-76-1, December 1976.

2. Chaturvedi, S. and Porter, R.W., "Air-Vapor Dynamics in Large-Scale Atmospheric Spray Cooling Systems", IIT Waste Energy Management Report TR-77-1, March 1977.

RWP

3. Porter, R.W., Yang, U.M. and Yanik, A., "Thermal Performance of Spray Cooling Systems", Proceedings of American Power Conference, Vol. 38, 1976, p. 1458-1472.

4. Porter, R.W., "Analytical Solution for Spray-Canal Heat and Mass Transfer", Joint ASME Paper 74-HT-58, AIAA Paper 74-764, July 1974.

5. Porter, R.W. and Chen, K.H., "Heat and Mass Transfer of Spray Canals", Journal of Heat Transfer,Vol. 96,3 August 1974,p. 286.

6. Frohwerk, P.A., "Spray Modules Cool Plant Discharge Water", Power, Vol. 115, September 1971, p. 52-53.

7. Kelley, R.B., "Large Scale Water Cooling Via Floating Spray Devices", Energy Production and Thermal Effects Ann Arbor Science Publishers, January 1974, p. 92.

8. Sherwood, T.K., Pigford, R.L., and Wilke, C.R., Mass Transfer,McGraw-Hill, NY, 1975, p. 26.

9. Thelkeld, J.L., Thermal Environmental Engineering, Prentice Hall, Englewood Cliffs, Part III, 1970.

10. Levich, V.G., Physicochemical Hydrodynamics, Prentice Hall, Englewood Cliffs, 1962.

11. Gunn,R. and Kinzer, G.D., "The Terminal Velocity of Fall for Water Droplets in Stagnant Air", Journal of Meteorology, Vol. 6, August 1949 , p. 243-248.

12. Chao, B.T., "Transient Heat and Mass Transfer to a Translating Droplet", Journal of Heat Transfer, Vol. 91, No. 2, May 1969, p. 273.

13. Mori, Y. et al., "Unsteady Heat and Mass Transfer from Spheres", International Journal of Heat and Mass Transfer, Vol. 12, 1969, p. 571.

14. Ranz, W.E. and Marshall, W.R. Jr. , "Evaporation From Drops", Chemical Engineering Progress, Vol. 48, 1952, p. 141-146, 173-180.

15. Yao, S.C. and Schrock, V.E., "Heat and Mass Transfer from Freely Falling Drops", Journal of Heat Transfer, Vol. 98, February 1976, p. 120-126.

16. Hebden, W.E. and Shah, A.M., "Effects of Nozzle Performance on Spray Ponds", Proceedings of American Power Conference, Vol. 38, 1976, p. 1449-1457.

17. Chen, K., Heat and Mass Transfer from Power Plant Spray Cooling Ponds", Ph.D Dissertation, University of California, Berkeley, May 1975.

18. Hollands, K.G.T. and Goel, K.C., "Mean Diameters in Parallel-Flow and Conter-Flow Aerosol Systems", Journal of Heat Transfer, Vol. 98, May 1976, p. 297-302.

19. Elgawhary, A.M. and Rowe, A.M., "Spray Pond Mathematical Model for Cooling Fresh Water and Brine", Environmental and Geophysical Heat Transfer, ASME HT-Vol. 4, 1971.

20. Ryan, P.J. and Myers, D.M., "Spray Cooling: A Review of Thermal Performance Models", Proceedings of American Power Conference, Vol. 38, 1976, p. 1473-1481.

21. Chen, K.H. and Trezek, G.J., "Spray Energy Release (SER) Approach to Analyzing Spray System Performance", Proceedings of American Power Conference, Vol 38, 1976, p. 1435-1448.

22. Schlichting, H., Boundary Layer Theory, 6th Edition, McGraw-Hill, New York, 1968.

23. Kelley, R.B., "Large-Scale Spray Cooling", Industrial Water Engineering, Vol. 8 August-September 1971, p. 18-20.

24. Hoffman, D.P., "Spray Cooling for Power Plants", Proceedings of American Power Conference, Vol. 35, 1973, p. 702.

25. Soo, S.L., "System Considerations in Spray Cooling and Evaporation", Proceedings of American Power Conference, Vol. 38, 1976, p. 1482-1486.

26. Soo, S.L., "Power Spray Cooling-Unit and System Performance", ASME Paper 75-WA/Pwr-8, December 1975.

27. Arndt, C.R. and Barry, R.E., "Simulation of Spray Canal Cooling for Power Plants-Performance and Environmental Effects", ASME Paper 76-WA/HT-28, December 1976.

28. Bird, R., Stewart, W.E. and Lightfoot, E.N., Transport Phenomena, Wiley, NY, 1960, p. 495.

29. Berry, C.H., "Mixtures of Gases and Vapors", Mechanical Engineer's Handbook, Edited by T. Baumeister, McGraw-Hill, NY, 1958, p. 4-82.

30. Frass, A.P. and Ozisik, M.M., Heat Exchanger Design, Wiley, NY, 1965, Chapter 15.

TABLE I. SPRAY MODULE PARAMETERS

	Ceramic Cooling Tower(CCT) Co.	Richards of Rockford(RR)
Flow Rate (ℓ/min)	3.8×10^4	4.5×10^4
Sprays/Module	4	1
Pump Motor Power (Kw)	51	56
Spray Diameter (m)	12.2	16.0
Spray Height (m)	5.5	5.2

TABLE II. TABULATION OF $b(T)/c_w = h'(T)/c_w$.

T(C)	0	10	20	30	40
0	0.395	0.545	0.785	1.185	1.845
1	0.410	0.563	0.816	1.239	1.930
2	0.415	0.584	0.850	1.293	2.030
3	0.425	0.606	0.888	1.347	2.125
4	0.430	0.627	0.924	1.407	2.238
5	0.445	0.650	0.960	1.470	2.345
6	0.485	0.677	1.001	1.537	2.465
7	0.500	0.700	1.045	1.609	2.590
8	0.510	0.726	1.090	1.660	2.720
9	0.530	0.754	1.135	1.755	2.870

TABLE III. SUMMARY OF FIELD EXPERIMENTS ("D" DENOTES DRESDEN STATION AND "Q" QUAD-CITIES STATION).

Exp.	Date	Station and Module	Object	T_f (C)	WS (m/s)	WD (°)	$\frac{\|\Delta\rho\|}{\rho}$	z_B (m)
1	3-17-75	D,CCT	(canal ntu)	11	3.0	84-89	.09	2.4
	3-18-75	"	"	18	5.0-6.4	51-74	.03	2.3
	8-20-75	"	"	32	2.5-3.0	7-90	.06	2.1
	8-21-75	"	"	32	2.6-3.5	71-86	.05	2.1
2	6-16-76	"	(module ntu)	24	4.6	10	.065	2.4
3a	6-30-76	Q,CCT	(module ntu)	23	4.6	19	.043	2.0
3b	7-1-76	"	f	24	2	52	.035	2.0
4a	7-27-76	Q,RR	(module ntu& f)	29	2.2	97	.045	1.2
4b	7-29-76	"	f	29	2.1	118	.078	2.7
5a	9-28-76	Q,CCT	f	20	1.3	30	.043	2.0
	9-29-76	"	"	20	1.8	61	.041	2.0
5b	9-29-76	"	(module ntu& f)	20	2.4	81	.038	2.0

TABLE IV. INTERFERENCE ALLOWANCE OF EXP. 3b, CERAMIC MODULES (ROW I IS UPWIND).

Row_i	f_i		g_i	
	Spray Off	Spray On	Spray Off	Spray On
I	0.20	0.20	0.27	0.39
"	0.06	0.23	0.13	0.40
I(avg.)	0.13	0.21	0.20	0.40
II	0.28	0.49	0.35	0.50
"	0.27	0.47	0.29	0.54
II(avg.)	0.27	0.48	0.32	0.52
III	0.25	0.38	0.28	0.37
"	0.31	0.46	0.32	0.50
III(avg.)	0.28	0.42	0.30	0.44
IV	0.15	0.40	0.46	0.08
"	0.11	0.38	0.25	0.40
IV(avg.)	0.13	0.39	0.36	0.24
Overall Avg.	0.20	0.37	0.30	0.40

TABLE V. INTERFERENCE ALLOWANCE OF EXP. 5a, CERAMIC MODULES (ROW I IS UPWIND)

	f_i		g_i	
Row_i	Spray Off	Spray On	Spray Off	Spray On
9-28-76				
I	0.164	0.096	0.03	0.21
"	0.029	0.317	0.28	0.18
I (avg.)	0.097	0.207	0.15	0.20
II	0.270	0.454	0.09	0.05
"	0.323	0.338	-	0.02
II (avg.)	0.297	0.396	0.09	0.03
9-29-76				
I	0.191	0.228	0.34	0.04
"	0.168	0.374	0.30	0.09
I (avg.)	0.180	0.301	0.32	0.07
II	0.284	0.409	0.07	0.08
"	0.200	0.307	0.21	0.30
II (avg.)	0.242	0.358	0.14	0.19
III	0.278	0.425	0.32	0.30
"	0.310	0.437	0.37	-
III (avg.)	0.294	0.431	0.35	0.30
IV	0.429	0.563	0.26	0.47
"	0.429	0.486	0.45	0.32
IV (avg.)	0.429	0.524	0.36	0.40
Overall Avg.	0.29	0.46	0.29	0.24

TABLE VI. INTERFERENCE ALLOWANCE OF EXP. 4a AND 4b, RICHARDS MODULES (ROW I IS UPWIND, "S" IS FOR SINGLE MODULE)

Row$_i$	f_i		g_i	
	Spray Off	Spray On	Spray Off	Spray On
Exp. 4a				
IV	-	0.390	-	0.38
"	-	0.391	-	0.45
"	-	0.384	-	0.36
"	-	0.341	-	0.32
IV(avg.)	-	0.376	-	0.38
S	-	0.158	-	0.42
"	-	0.161	-	0.42
"	-	0.149	-	0.38
S(avg.)	-	0.156	-	0.41
Exp. 4b				
I	0.056	0.031	0.22	0.33
II	0.111	0.218	0.05	0.26
"	0.186	0.420	0.05	-
II(avg.)	0.149	0.319	0.05	0.26
III	0.172	0.315	-	-
"	0.243	0.303	-	-
III(avg.)	0.208	0.309	-	-
IV	0.174	0.323	-	-
Overall Avg.	0.15	0.25	-	-
S	0.007	0.314	-	-
"	0.014	0.234	-	-
S(avg.)	0.011	0.274	-	-

TABLE VII. MODULE NTU(ntu) OF EXP. 2 BASED ON RECOMMENDED INTERFERENCE f [3,4], CERAMIC MODULES, DRESDEN STATION ("CLOCK POSITION" 6 AND 9 ARE ALWAYS UPWIND).

	ntu(based on:)		
Row i	$f = 0$	$\bar{f} = 0.1$	$f = 0.2$
I- 6	0.086	0.096	
I- 3	0.086	0.096	
I-12	0.138	0.154	
I- 9	0.157	0.176	
I(avg.)	0.116	0.130	
II- 6		0.072	0.082
II- 3		0.117	0.133
II- 3		0.080	0.089
II-12		0.080	0.089
II- 9		0.054	0.061
II(avg.)		0.080	0.091
Overall		0.105	

TABLE VIII. MODULE NTU (ntu) OF EXP. 3a, CERAMIC MODULES, BASED ON EXPERIMENTAL f WITH SPRAY ON FROM EXP. 3b.

Row i	ntu
I - 6	0.132
3	0.097
12	0.124
9	0.156
I(avg.)	0.127
II- 6	0.136
3	0.217
12	0.169
9	0.260
II(avg.)	0.196
III-6	0.146
3	0.147
12	0.145
9	0.141
III(avg.)	0.145
IV- 6	0.162
3	0.112
12	0.149
9	0.240
IV(avg.)	0.166
Overall(avg.)	0.158

TABLE IX MODULE NTU(ntu) OF EXP. 5b, CERAMIC MODULES, BASED ON EXPERIMENTAL f WITH SPRAY ON.

Row i	ntu (based on:) f(5a)	f(5b)
I- 7:30	0.132	-
4:30	0.139	-
1:30	0.145	-
10:30	0.095	-
I(avg.)	0.128	-
II- 4:30	0.178	-
7:30	0.229	-
10:30	0.105	-
1:30	0.120	-
II(avg.)	0.158	-
III- 4:30	0.133	-
7:30	0.152	-
10:30	0.099	-
1:30	0.117	-
III(avg.)	0.125	-
IV- 4:30	0.139	0.126
7:30	0.140	-
10:30	0.141	-
1:30	0.120	0.126
IV(avg.)	0.135	-
Overall (avg.)	0.136	-
S- 4:30	-	0.170
1:30	-	0.118
S(avg.)	-	0.144

TABLE X. MODULE NTU(ntu) OF EXP. 4a, RICHARDS MODULES EXPERIMENTAL f.

Row i	f Experimental	ntu (Exp. f)
IV- 9	0.390	0.074
6	0.391	0.068
12	0.384	0.084
3	0.340	0.039
IV(avg.)	0.376	0.066
S- 3	0.158	0.046
6	0.161	0.074
12	0.149	0.053
S(avg.)	0.156	0.058

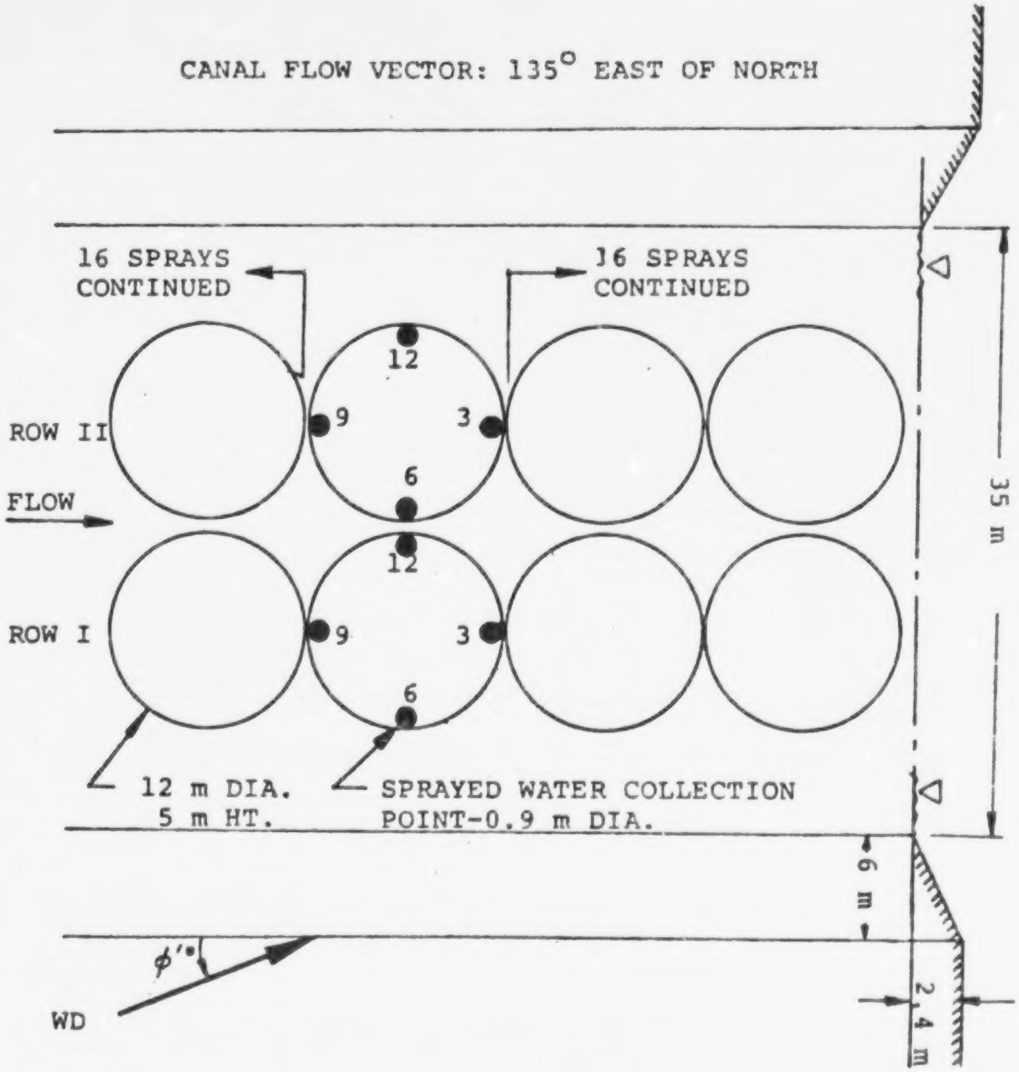
CANAL FLOW VECTOR: 135° EAST OF NORTH
16 SPRAYS CONTINUED
16 SPRAYS CONTINUED
ROW II
FLOW
ROW I
12
9
3
6
12
9
3
6
12 m DIA.
5 m HT.
SPRAYED WATER COLLECTION POINT-0.9 m DIA.
35 m
6 m
2.4 m
φ'°
WD

Figure 1 . Geometry of Ceramic Modules at Dresden Station (Experiment 2).

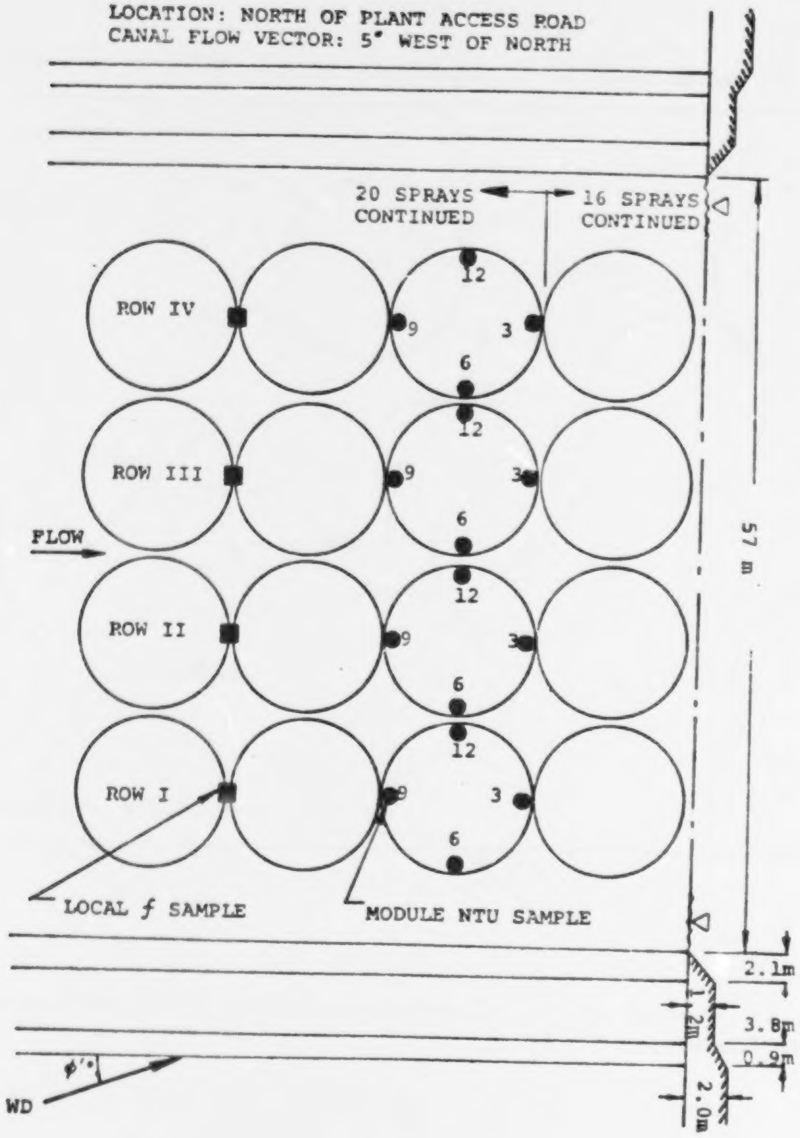
LOCATION: NORTH OF PLANT ACCESS ROAD
CANAL FLOW VECTOR: 5° WEST OF NORTH
20 SPRAYS CONTINUED
16 SPRAYS CONTINUED
ROW IV
ROW III
ROW II
ROW I
12
9
3
6
FLOW
57 m
LOCAL ƒ SAMPLE
MODULE NTU SAMPLE
2.1m
1.2m
3.8m
0.9m
2.0m
φ°
WD

Figure 2. Geometry of Ceramic Modules at Quad-Cities Station (Experiment 3).

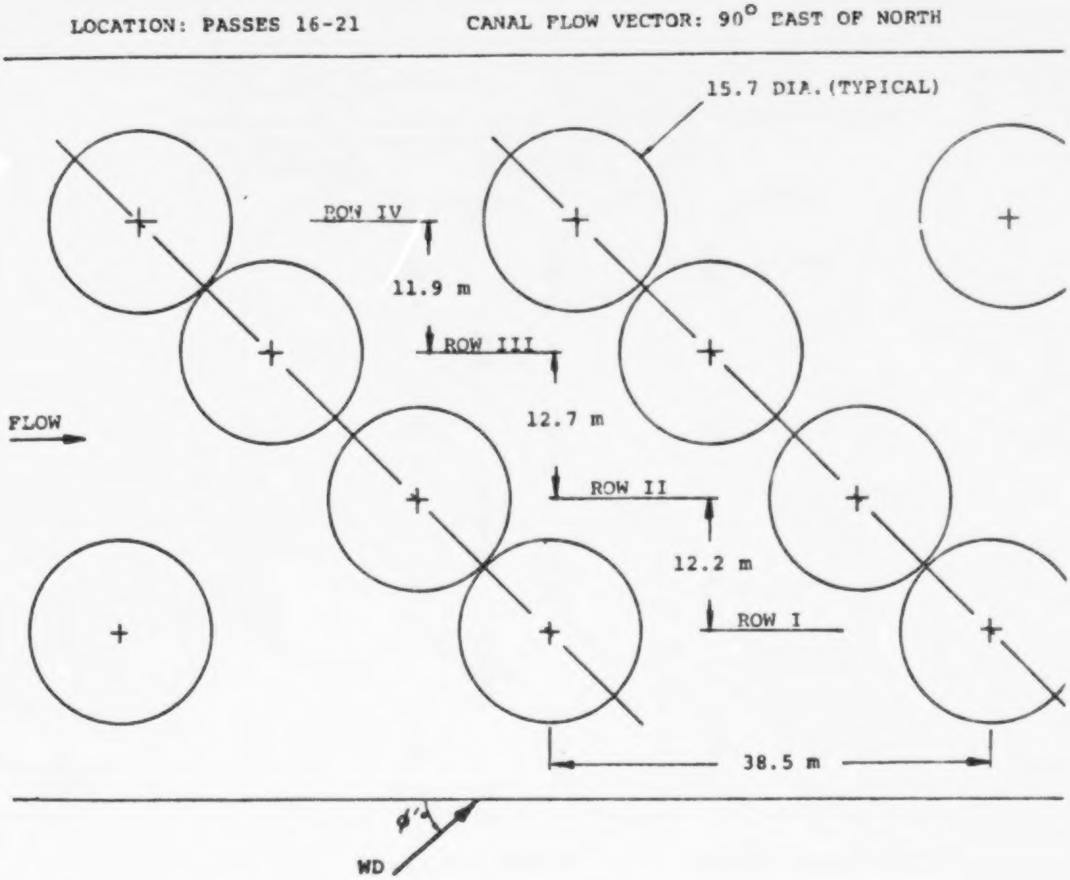
LOCATION: PASSES 16-21
CANAL FLOW VECTOR: 90° EAST OF NORTH
15.7 DIA. (TYPICAL)
ROW IV
11.9 m
ROW III
12.7 m
FLOW
ROW II
12.2 m
ROW I
38.5 m
ϕ'
WD

Figure 3. Geometry of Richards Modules at Quad-Cities Station (Experiment 4).

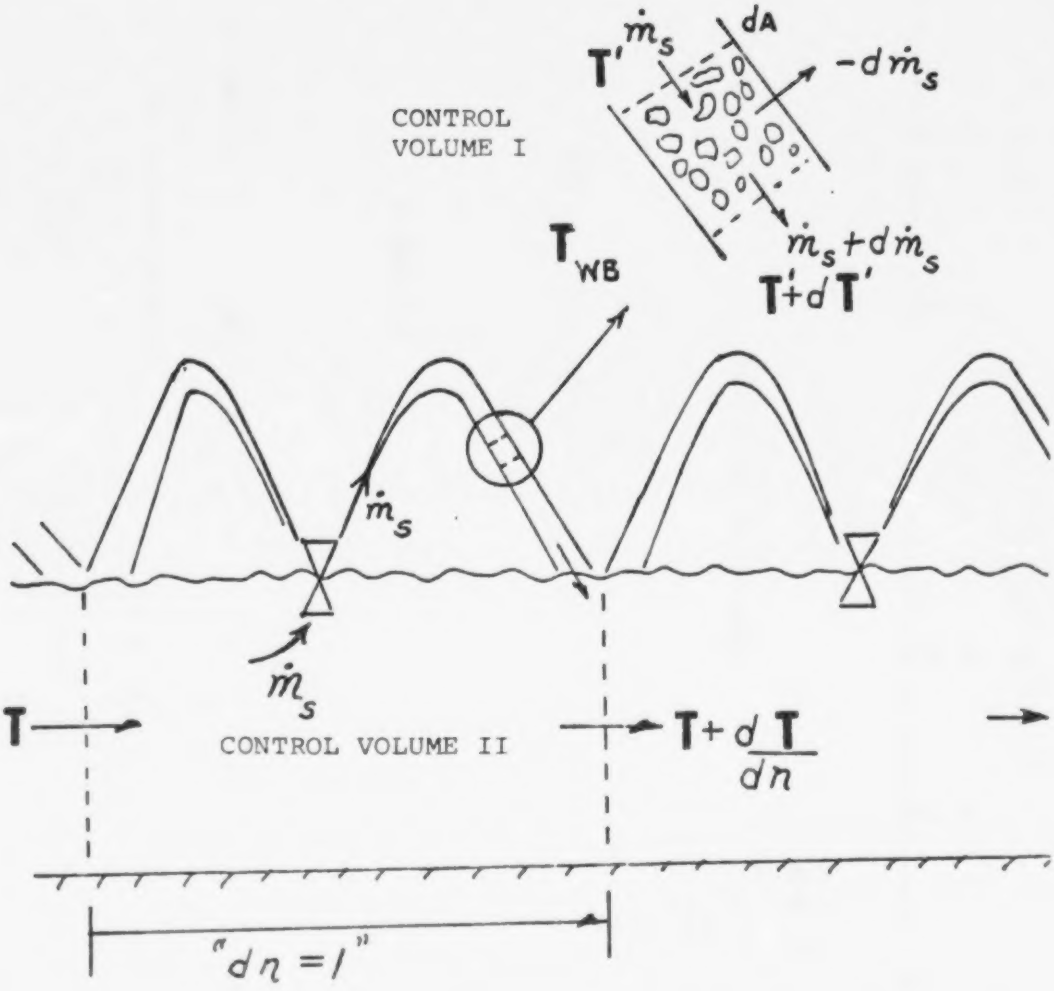
CONTROL
VOLUME I
T'
$\dot{m}_s$
dA
$-d\dot{m}_s$
$\dot{m}_s + d\dot{m}_s$
$T' + dT'$
T_{WB}
$\dot{m}_s$
$\dot{m}_s$
T
CONTROL VOLUME II
$T + \frac{dT}{dn}$
"$dn = 1$"

Figure 4. Control Volumes for Spray (I) and Canal (II).

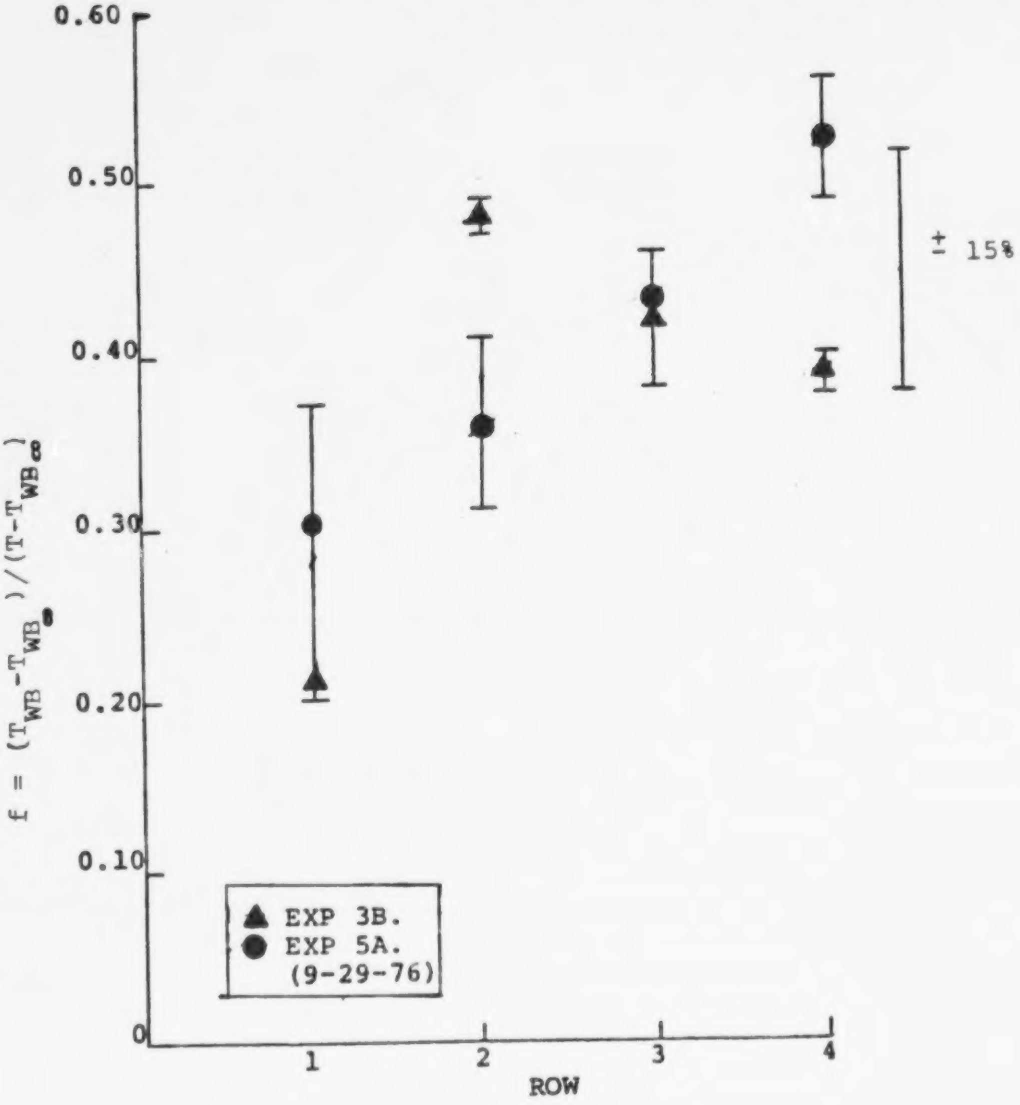

Figure 5. Local WBT Interference Allowance (Spray On) for Ceramic Modules at Quad-Cities Station.

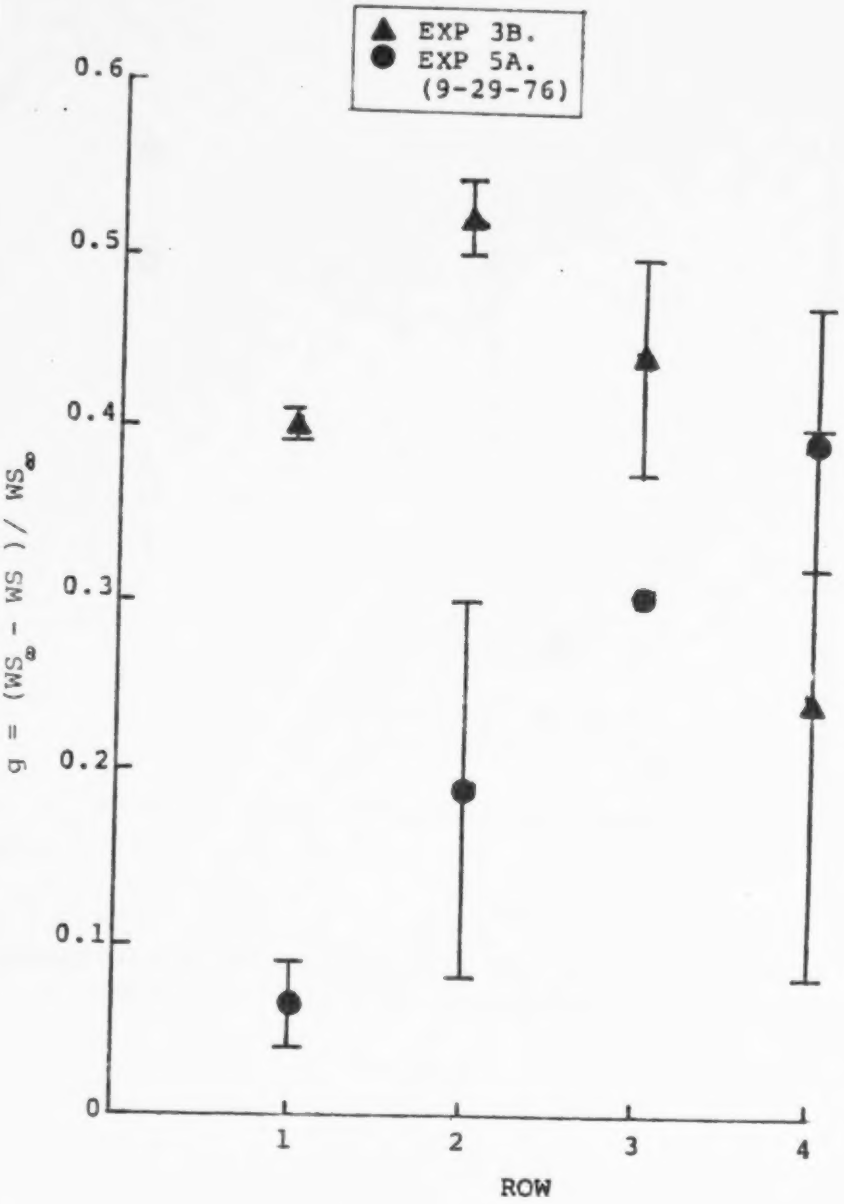

Figure 6. Local Wind Speed Increment Ratio versus Row Position for Ceramic Module.

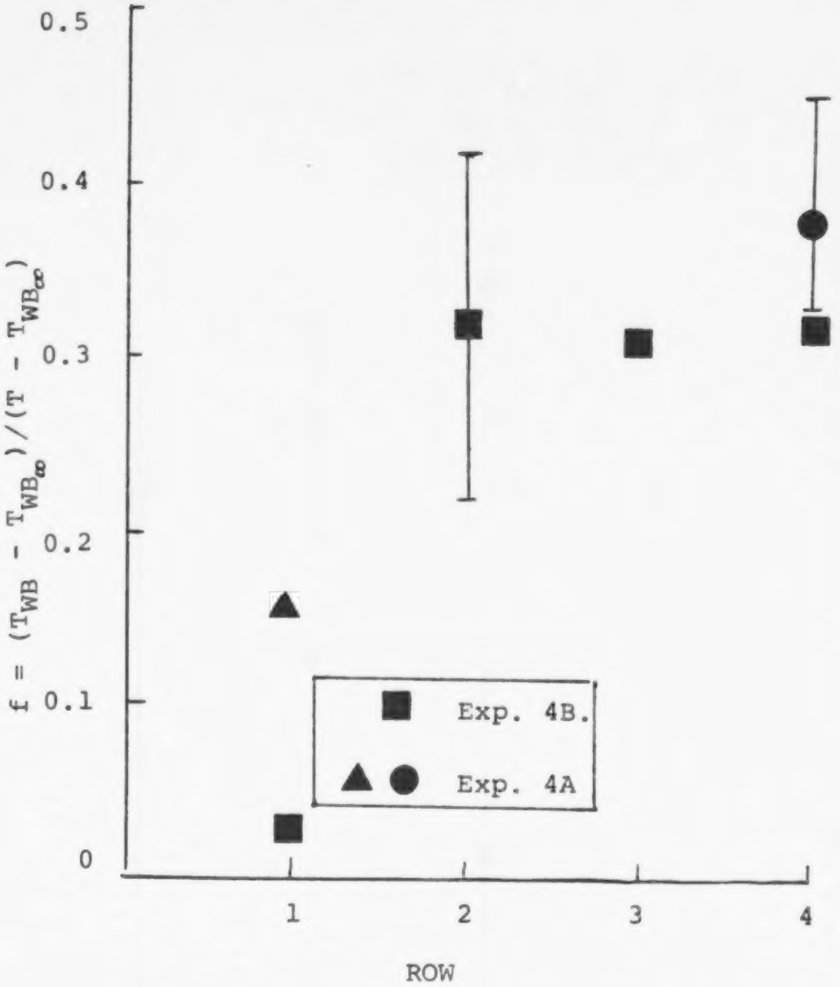

Figure 7. Local WBT Interference Allowance(Spray On) for Richards Modules at Quad-Cities Station.

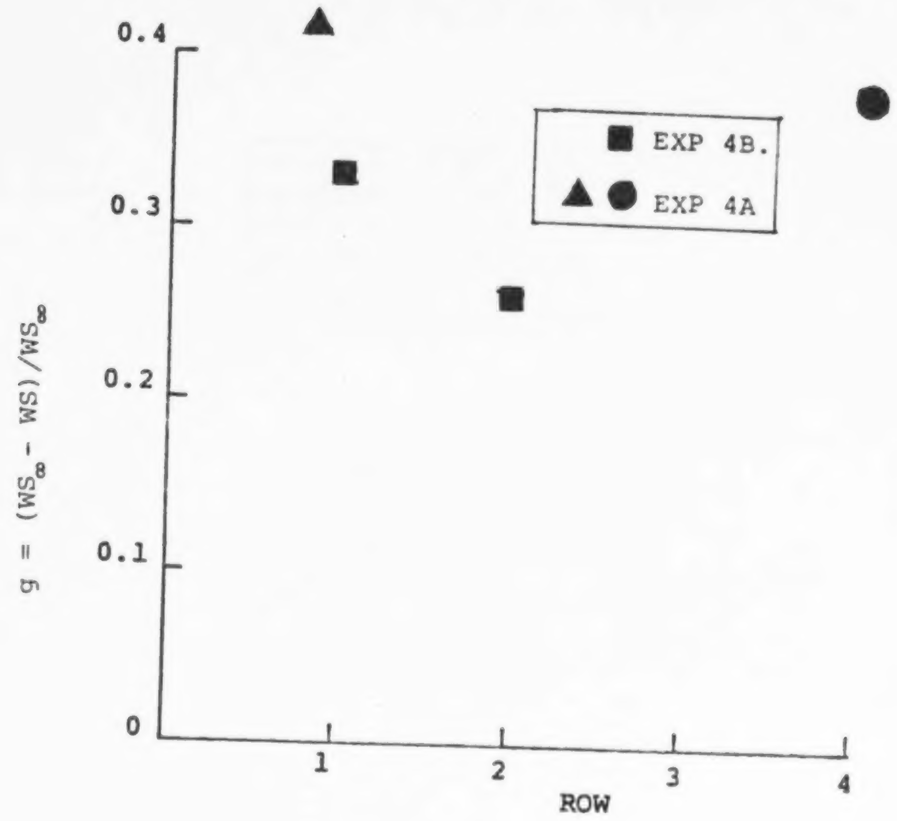

Figure 8. Local Wind Speed Increment Ratio (Spray On) versus Row Position for Richards Module at Quad-Cities Station.

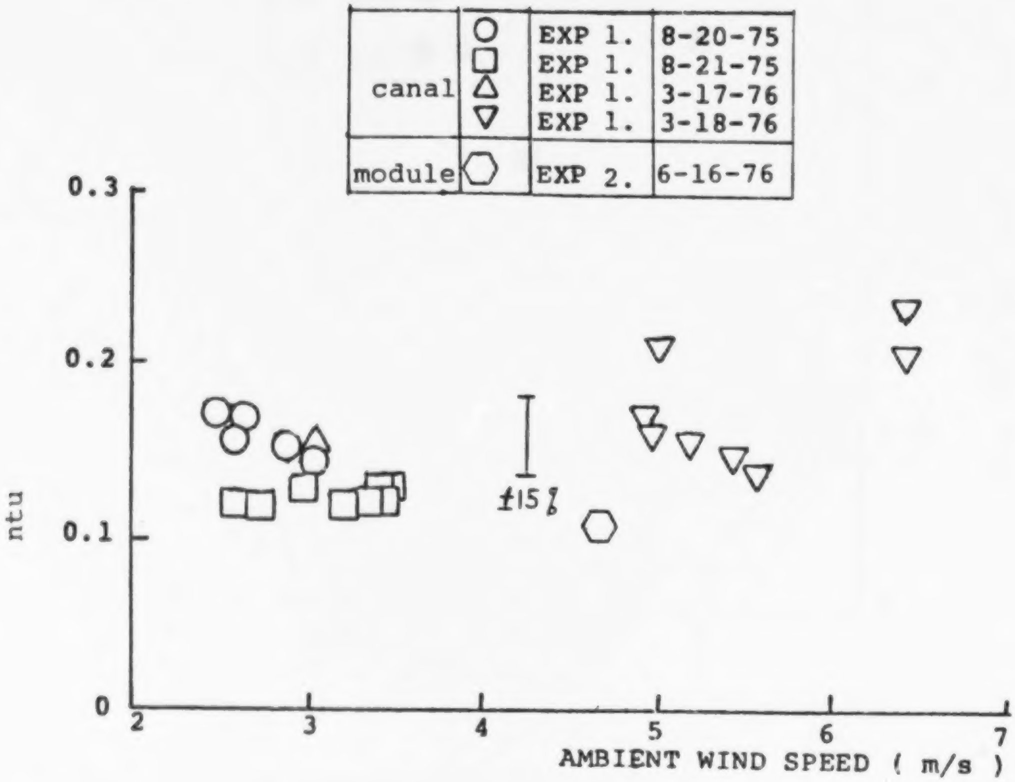

Figure 9. Canal and Module ntu Based on Interference Allowance of 0.1 for 2-Row Ceramic Modules at Dresden Station .

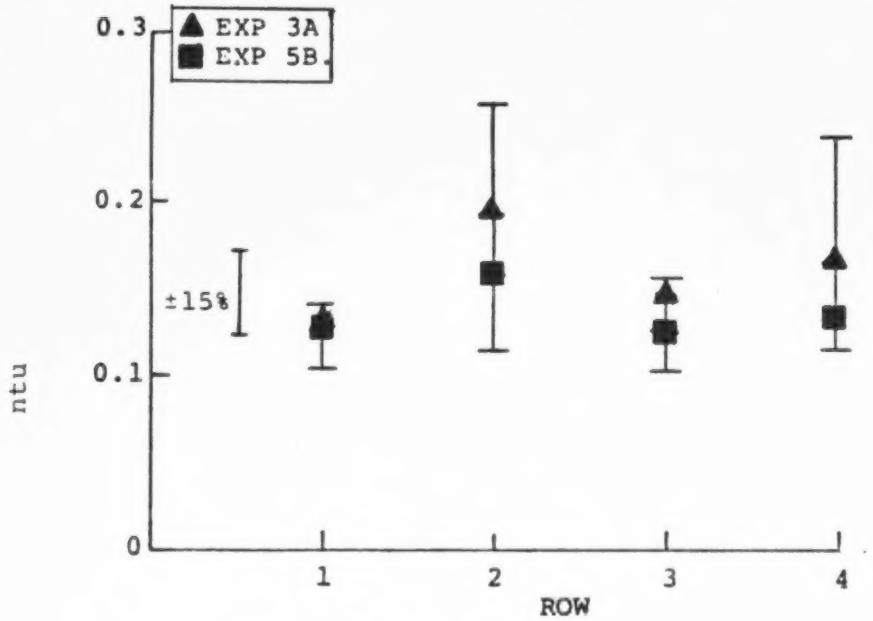

Figure 10. Module ntu Based on Exp.f, Ceramic Modules at Quad-Cities Station.

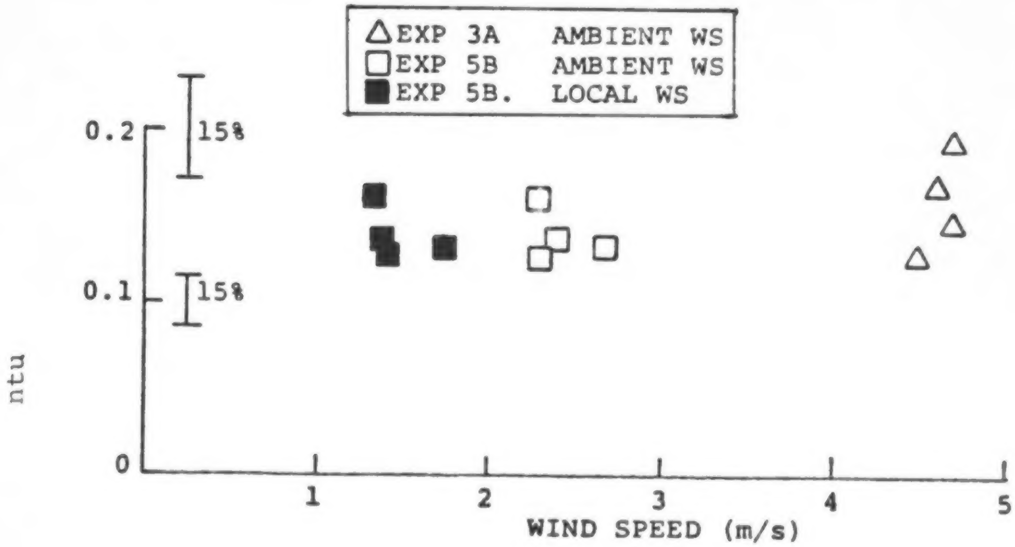

Figure 11. Module ntu Based on Experimental f, Ceramic Modules, Quad-Cities Station.

41

8-45-16

DRY/WET COOLING TOWERS WITH AMMONIA AS INTERMEDIATE HEAT EXCHANGE MEDIUM

R. T. Allemann, B. M. Johnson, and G. C. Smith
Battelle-Northwest
Richland, Washington U.S.A.

ABSTRACT

Engineering conceptual studies were made of several dry cooling towers for a 500 MW_e power plant. The most economical method used ammonia as a heat exchange medium. The ammonia condenses the turbine steam in a condenser-reboiler while being evaporated itself. The ammonia vapor is condensed and then recycled from a dry cooling tower. The lowest cost approach utilized a water deluge on the tower during the hottest ambient conditions to effect water savings of 80% over an all evaporative system. The total capital, and capitalized operating cost saving for the deluged/ammonia cooling system over a conventional wet/dry tower is potentially 15 to 30% for a typically $30 million tower.

INTRODUCTION

Under the auspices of the Division of Nuclear Research of the United States Engergy Research and Development Administration (ERDA) studies have been performed of dry cooling of power generation plants, its feasibility, cost, and growth potential. As part of these studies cost projections were made for several "advanced concepts," i.e. ideas for dry cooling which are not state-of-the-art (currently marketed), nor evolutionary developments from the state-of-the-art. The cost studies showed that unless dry-cooling systems could be greatly improved, they would be more expensive than evaporative cooling and would never capture a significant share of steam power plant cooling as long as water was available for consumptive use.[1] However, the studies showed that significant reductions in dry cooling cost could be afforded by using some sort of wet cooling augmentation during the hottest weather periods.

In the course of evaluating various systems for power plant cooling two major points became recognized:

1. Wet cooling would probably be used to supplement dry cooling even at the sites with high water cost.
2. Potentially, an intermediate heat transfer fluid (specifically ammonia) could be used in a power plant cooling system at less cost for dry or wet/dry tower cooling than other systems evaluated.

Preceding page blank

Water Augmentation

Let's discuss more fully the first point, that of using water to augment a dry cooling tower. The cost of dry cooling is in large measure assessed because of the loss of efficiency of the steam power plant when the condenser operates at higher back pressure on hot days. Fig. 1 shows a typical example of this effect. The dry bulb temperature is shown versus the cumulative number of hours at a given temperature or above. The dashed lines show the normalized power output under the temperature conditions for various size dry towers. Hence on hot days, either a larger dry tower must be built or less efficiency must be accepted for the power plant. If a larger tower is built, the cost of electricity produced is more even though it allows higher-than-rated plant output on the cold days.

If the dry cooled plant falls below its rated output during the extremely hot periods then the load must be made up by other base plants, auxiliary plants, or by designing a larger plant (i.e. shifting the design point) in the first place. The cost attributable to dry cooling can vary significantly depending on which of these methods of "capability penalty" (capacity and energy charges) is used. There is some variation in treatment among various dry cooling cost assessments in the literature. However, by any method, the cost for straight dry cooling is high, particularly for a summer peaking demand typical of nearly all utility systems in the United States.

The hot period penalty could be greatly reduced if some means were found to augment the cooling during that time. For example, a separate wet tower could be used, or as we are suggesting here the dry surface could be flooded with water, "deluged," in order to provide more heat transfer by virtue of the driving temperature differences of water evaporation tending toward the wet bulb rather than the dry bulb temperature. A power demand curve for this situation is shown in Fig. 2. Note that the sharp rise in the effective temperature of the heat sink is cut off and that the dry tower is large enough to handle the load for most of the cooling year. This approach is, of course, not a new idea. People pour water on their car radiators to gain extra cooling and separate wet sections or separate wet towers are currently manufactured as state-of-the-art. The deluging idea is suggested for use because it should cost less than the other methods.

Simply spraying the surfaces runs the risk of corroding or fouling the surfaces due to deposition of salts from the evaporated water. With the deluge approach, the surfaces are protected by the "delugeate." Some small-scale experience with this concept exists. Plate-fin tube surfaces have been tested in Hungary for an extended period through many cycles of wet and dry operation, and are to be used in a demonstration plant at Ivanivo, near Moscow in the Soviet Union. Fig. 3 shows a schematic view of the cross section of plate-fin tubes being deluged. The air is cross flow to the delugeate. Analytical evaluation and laboratory experiments show that heat transfer increases by a factor of two to five when deluge is used.

The surface and arrangement just described can be used under license. It will be further evaluated in laboratory experiments in this country before a decision is made to use it in a large-scale demonstration. Other surfaces will also be tested in direct-augmentation arrangements.

Ammonia System

The second major point recognized was that use of an intermediate fluid could reduce the cost of dry cooling systems. The application of an intermediate fluid which undergoes a change of phase evolved from consideration of a binary cycle. In a binary cycle, work is extracted from the lower temperature portion of the Rankine cycle using a second fluid which is vaporized by condensing steam at a relatively high temperature (hence relatively high pressure) and is allowed to expand through a turbine to a low temperature and pressure, at which point it is condensed. The incentive for the use of the second fluid was that one could greatly reduce the equipment size of the low pressure turbine and thus save money by choosing a fluid which had a low specific volume and other favorable properties over the operating range. A study by the Franklin Institute[2] showed that the binary cycle would reduce plant cost under certain assumed conditions. However, for dry-cooled plants under the most likely set of conditions, the study concluded that one was further ahead to simply let the ammonia serve as a heat exchange fluid rather than a second "working fluid."

We continued such studies at PNL to critically compare the use of ammonia with other new concepts, such as the use of plastic tubes for the heat exchange surface. These studies led to the recommendation that the use of ammonia as an intermediate heat transfer medium together with the use of the deluge concept provides the best possibilities for markedly reducing the cost of dry (dry/wet) cooling systems.

System Description

The ammonia heat transport system for power plant heat rejection is functionally similar in many respects to the "direct" system in which the exhaust steam from the last stage of the turbine is ducted directly to an air-cooled condenser. The principal difference is the existence of a steam condenser/ammonia reboiler in which ammonia is "substituted" for steam as the medium for transporting heat from the turbine to the tower (heat sink). In all respects the ammonia system, with vapor moving from the reboiler to the air-cooled condenser and liquid returning to the reboiler, will function and respond to load changes in the same manner as the direct system.

Fig. 4 is the process flow sketch. Exhaust steam from the last stage of the turbine is condensed in the condenser/reboiler located directly below the turbine. Instead of water circulating through the tubes, liquid ammonia is boiled as it is pumped through the tubes underpressure, set by the operating temperature in the condenser. The flow rate of ammonia is set to yield a vapor quality emerging from the tube varying from 50% to

90%. This two-phase mixture is passed through a vapor-liquid separator from which the vapor is sent to the air-cooled condenser, while the liquid is combined with the ammonia condensate from the dry tower and recycled back through the condenser/reboiler.

The vapor from the vapor-liquid separator flows to the dry tower under the driving force of the pressure difference between these two components created by the temperature difference and the associated vapor pressure of the ammonia.

The vapor is condensed in the air-cooled (dry) tower. The ammonia vapor is condensed in a single pass cocurrent downflow arrangement, emerging at the bottom header as a saturated liquid at essentially the same pressure as at the inlet header. The liquid flows to a liquid receiver and then out through a vapor trap by gravity to a transfer line and thence back to the condenser/reboiler. Isolation valves at the inlet and outlet manifolds of a tower section will provide a means of removing sections of the tower from service as may be required for maintenance or reduced cooling capability.

Fig. 5 shows the temperature relationship of the ammonia system as compared to that of a conventional dry tower cooling system. The main difference is the relatively constant temperature difference in the condenser/reboiler between the condensing steam and the boiling ammonia and the increased mean temperature difference in the ammonia tower. This saves tower cost. The condenser/reboiler cost is not increased greatly despite the lower average temperature difference because of the high boiling-heat-transfer coefficient of ammonia. The vapor flows through the supply piping at near-saturation conditions. However, there is a pressure drop in the piping system from frictional effects. In this thermodynamic regime of ammonia vapor, this pressure drop is accompanied by a drop in temperature. At the tower, the vapor is condensed inside the metal finned tubes at constant temperature. The condensed ammonia is then collected and returned to the condenser/reboiler. The basic terminology is the same as for the state-of-the-art system except that the parameter, $RANGE_{Water}$, is eliminated and replaced by the vapor supply piping temperature drop, TTD2. Because of the economic trade-offs, the $RANGE_{Air}$ is somewhat larger for the ammonia system than for state-of-the-art systems.

The effect of deluge or water augmentation on these diagrams is to make the air range from the wet bulb temperature to the saturation temperature (hence less airflow is needed) and larger heat transfer driving temperature differences will exist. The deluge water would be at an intermediate temperature below the ammonia condensing temperature. Another possibility is to augment condensation of the ammonia with a separate loop wet tower rather than to deluge. The deluge has the mass transfer driving force of high temperature water throughout whereas the augmenting wet tower would have a range of water temperature. We are looking closely at this idea.

Choice of Heat Transfer Fluid

Early studies considered a variety of fluids, particularly refrigerants, which could be used in the phase-change mode to transport heat from the turbine to the air-cooled heat rejection system. Selection of the best fluid was based on a number of factors including the size of the ducts required to transport the fluid. A large heat of vaporization (h_{fg}) and a low specific volume of vapor (V_g) contribute to a large heat flux and small transport lines. However, the allowable vapor velocity ($U_{allowable}$) in the transfer line is also related to the specific volume (V_g) by the relationship

$$\frac{U^2_{allowable}}{V_g} = \text{constant}, \qquad \text{or} \qquad U_{allowable} \sim \sqrt{V_g} \qquad .$$

Hence a "figure of merit" from the standpoint of duct size is $h_{fg}/\sqrt{V_g}$.

TABLE I shows the properties and figure of merit of several heat transfer fluids considered.

The advantage of ammonia in this respect is clear. Consideration must also be given to the operating pressure and the impact on equipment cost. The temperature on which the above table is based (150°F) is somewhat higher than will probably be experienced. 135°F (equivalent to about 5 in. Hg back pressure) is more representative, at which temperature the ammonia pressure is approximately 350 psi.

The freezing point of anhydrous ammonia is -108°F. Thus no concern for freezing need be considred in design, which eliminates the need of louvers and quick-drain provisions in the cooling tower.

The relatively high operating pressure required with the use of ammonia necessitates the use of heavier, more expensive piping, but it has the ameliorating feature that a relatively large pressure drop can occur between the plant and the dry tower with little change in temperature because of the steep slope of the vapor pressure temperature curve. Thus vapor is easily transported to the tower with little degradation of the available ITD (initial temperature difference) at the tower. If a "direct" steam system were used, the pressure drop between the turbine and condenser would have to be kept very low since low pressure steam at the same temperature is much more sensitive to pressure drop in the steam ducts than ammonia.

The significant advantages of the ammonia system include the following:

a. Isothermal condensation in the dry tower and consequently a larger temperature driving force for heat transfer than an indirect system. Hence less surface area is required.

b. Much lower volumetric flow rate and specific volume of the vapor result in smaller transfer lines between the plant and the tower, and in the tower.

c. No problems with freezing in the dry tower and consequently no requirement for louvers, drain valves or other low temperature safety systems.

d. No pumping required to move vapor to the tower and very little pumping required to move liquid back to the plant because of its low viscosity.

Available Technology for Ammonia Use

The use of ammonia is very general in the chemical process industry and agriculture. Consequently, criteria for design of production processes, the practices for handling large quantities, the codes and standards for storage and use, and for maintenance and safety are very extensive.

Considerable information is available on the questions of materials selection and corrosion performance. A PNL report[3] concludes:

"Candidate materials for use in the cooling cycle of a power plant ammonia heat rejection system are aluminum, carbon steel and stainless steel. Other materials are rejected as candidates on the basis of incompatibility with ammonia (e.g., copper-base alloys).

"Corrosion of aluminum alloys 1100 and 3003 is negligible in anhydrous ammonia and these would be satisfactory for service in both the condenser/reboiler and the air-cooled ammonia condenser. However, aluminum is susceptible to impingement attack by saturated, high-velocity steam. Thus if aluminum is used in the condenser/reboiler, the first several rows of tubes must be either constructed of stainless steel or protected with stainless steel sleeves.

"Carbon steel is a satisfactory construction material for relatively pure ammonia. High strength carbon steel is susceptible to stress-corrosion cracking in air-contaminated ammonia. Susceptibility increases with the yield strength of the steel. Cracking is caused by levels of oxygen and nitrogen as low as 1 to 2 ppm. Water added to a concentration of 0.1% to 0.2% is effective in inhibiting stress-corrosion cracking of susceptible steels in air-contaminated ammonia. Water added to liquid ammonia is effective in inhibiting stress-corrosion cracking of steel in contact with the vapor phase. Stainless steels of all types are resistant to corrosion in liquid and gaseous ammonia.

Small "leakages of ammonia through the condenser/reboiler should not have an adverse effect on condensate chemistry. In fossil-fuel plants and pressurized-water reactors, leaks of ammonia into the condensate can be easily detected and will not cause accelerated corrosion of materials in the condensate/feedwater cycle. In boiling-water reactors, ammonia is rapidly decomposed radiolytically; the only problem caused by an ammonia leak would be an increased volume of condensable gases (H_2 and N_2) in the condenser."

General Design Criteria

Aside from the applicable codes for pressure systems operating in the range of 350 to 400 psi and the selection of construction materials which avoids the use of any copper-containing alloys in contact with ammonia, the design criteria associated with the anticipated application of ammonia will have few restrictions.

Double tube sheets and/or welding of tubing to tube sheets and headers in the condenser/reboiler and in the dry tower will probably be a requirement, both because of the pressure and because of the ammonia characteristics (reactions with copper, toxicity). However, the construction practice is well established and should not introduce a large premium on construction costs. Inspection of a small representative sample of welded joints (perhaps 5%) rather than complete radiographic inspection is believed to be sufficient.

Heat transfer coefficients can be predicted to essentially the same degree of reliability as in a water system. However, no tube-side fouling resistance factor is required in the design of an ammonia system because of the purity of the fluid and the small likelihood for the continuing introductionof noncondensibles once they are initially removed from the system following startup (due to the high operating pressure).

Safety and Maintenance Experience

Ammonia plant safety has been the subject of considerable attention in the chemical process industry and a number of professional society symposia. American Standard Safety Requirements for the storage and handling of anhydrous ammonia have been established by the American Standards Association under the sponsorship of the Compressed Gas Association.

The construction of ammonia plants has become somewhat routine; we understand for example, that a major chemical company which normally carries out all its own plant design and construction, contracts out all ammonia plant construction on a turn-key basis to one of several firms who construct such plants. During several visits to industrial operations which included ammonia manufacturing plants, the comment was heard repeatedly that the operation and maintenance of the ammonia unit is routine and its portion of plant maintenance cost is very low. Repairs of leaking valves and other similar packing can generally be done without deactivating the component.

It is not possible to accurately project the maintenance and operations (M&O) performance of an ammonia heat rejection system from the M&O performance of an ammonia manufacturing plant. Since the ammonia tends not to foul or corrode the condenser and the condenser is the major source of present downtime in fossil and nuclear fueled power plants, there is a rationale for projecting a greater reliability for the ammonia system than for the conventional. The impact of plant availability on power cost is very significant; but the anticipated availability of commercial ammonia dry cooled systems can only be developed after demonstration experience has been obtained.

Economic Evaluation

An economic study was made to see if there is incentive to solve the technical aspects or demonstrate the technical feasibility of an ammonia cooling system, i.e. even if a wet/dry ammonia system can be made to work will it be economical enough to use? A computer optimization study on dry towers alone[4] suggested that the ammonia intermediate cooling system was a lower cost method of dry cooling than other methods (under the typical conditions of fuel pricing, penalties and demand chosen). For the wet/dry system, since no optimization was available, the method of comparison was to write design criteria for several different concepts (named in TABLE II) for the same site and for the same annual water use (about 20% of a fully evaporative system).[5] This study was based on the San Juan site in New Mexico, with fixed demand. Using these criteria, a design and cost estimate was performed by an independent architect engineering firm to obtain the estimated capital cost of a 500 MW_e plant cooling system.

TABLE II shows the capital cost estimates with escalation and contingency. The capital costs include the steam condenser, piping, fill and drain system, water quality control, cover gas, cooling towers, buildings, electrical, overhead and profit, and management.

TABLE III gives the operating costs of the cooling system. Credit is taken for the fuel savings when the system can be run more efficiently at less than the design back pressure. To make a comparison for the cost of the cooling system, the operating costs were capitalized on the basis of a fixed charge rate of 18% and added to the basic capital cost (neglecting escalation and contingency) and are shown in TABLE IV. This comparison shows that there is potential for producing a lower cost we/dry cooling system than current state-of-the-art systems. The one with the greatest potential cost savings is the metal-finned-tube tower with deluge using ammonia as an intermediate heat transfer fluid. The six million dollars difference between the baseline (integrated dry/wet) system and the ammonia cooling system represents a savings of approximately 18%.

Summary

Studies have been carried out on the feasibility and economic incentive to develop an advanced concept of wet/dry cooling for power plants. This advanced concept uses ammonia as an intermediate heat transport medium between the turbine exhaust steam and the cooling tower air, and uses water for augmentation by directly deluging the heat transfer surface in the tower during periods of high ambient temperature. For the selected coal-fired-plant-study-site, total capitalized (including operations costs) savings could be 12 dollars per installed kW. With this type of incentive, further technological development of the ammonia concept is warranted.

References

1. B. M. Johnson, J. S. Maulbetsch, "Dry Cooling for Power Plants: Incentives, Problems, and Research and Development Activities," paper for Conference on Waste Heat Management and Utilization (Miami Beach, May 9-11, 1977).

2. R. G. Seth and W. Steigelman, Binary-Cycle Power Plants Using Dry Cooling Systems, Part I: Technical and Economic Evaluation, F-C 3023, The Franklin Institute Research Labs, Philadelphia, PA 19103, January 1972.

3. D. R. Pratt, "Compatibility of Ammonia with Candidate Dry Cooling System Materials," BNWL 1992, April 1976.

4. B. C. Fryer, Daniel J. Braun, David J. Braun, L. E. Wiles and D. W. Faletti, "An Engineering and Cost Comparison of Three Different All-Dry Cooling Systems, BNWL-2121, Battelle Pacific Northwest Laboratories, Richland, WA, September 1976.

5. F. R. Zaloudek, R. T. Allemann, D. W. Faletti, B. M. Johnson, H. L. Parry, G. C. Smith, R. D. Tokarz and R. A. Walter, "A Study of the Comparative Costs of Five Wet/Dry Cooling Tower Concepts," BNWL-2122, Battelle Pacific Northwest Laboratories, Richland, WA, September 1976.

TABLE I

	Physical Properties of Selected Refrigerants at 150°F				
ASHRAE Refrigerant Number	Chemical Name/ Formula	Saturation Pressure PSIG	Specific Vol. of Vapor V_g ft^3/lb	h_{fg}-Heat of Vaporization Btu/lb	$h_{fg}/\sqrt{V_g}$
R-717	Ammonia	420	0.675	416	506
R-22	$CHClF_2$	382	0.124	56.6	160
R-600a	Isobutane	128	0.619	119	151
R-114	$CClF_2$ $CClF_2$	94.9	0.293	45.9	85
R-718	Water (vapor)	-11.0	97.1	1010	102
R-718	Water (liq.)	0	0.0163	25(i.e. a temp. range of 25°F)	196

TABLE II

RESULTS OF CAPITAL COST ESTIMATES OF ALTERNATIVE HEAT REJECTION CONCEPTS FOR SAN JUAN UNIT 3 ($ THOUSANDS, 1976)

	Estimated Capital Cost	Escalation	Contingency	Total
Integrated Dry/Wet (Baseline)	$22,789	$5,638	$ 8,573	$37,000
Separate Dry/Wet	29,276	7,243	10,981	47,500
Metal Fin-Tube/Deluge	28,882	7,145	10,773	46,800
Plastic Tube/Deluge	24,311	6,014	9,075	39,400
Deluge/Ammonia Heat Transport	23,128	5,721	8,651	37,500

TABLE III

ESTIMATED ANNUAL OPERATING COSTS ($/YEAR)

	Circulation Pump Cost	Induced Draft Fan Cost	Reduced Back Pressure Savings	Water Treatment Cost	Deluge Pump Cost	Total Cost
Integrated Dry/Wet	628,000	1,228,000	-56,000	330,000	-0-	2,130,000
Separate Dry/Wet	967,000	1,312,000	-56,000	356,000	-0-	2,579,000
Deluge/Finned Tube	783,000	1,017,000	-230,000	130,000	13,000	1,712,000
Plastic Tube	650,000	598,000	-235,000	131,000	8,000	1,152,000
Ammonia	34,000	1,047,000	-220,000	75,000	25,000	962,000

TABLE IV

SUMMARY OF COMPARATIVE CAPITAL COSTS

	Basic Capital Cost	Capitalized Operating Cost	Comparable Capital Cost
Integrated dry/wet	$22,789,000	$11,836,000	$34,625,000
Separate dry/wet	29,276,000	14,330,000	43,606,000
Metal fin-tube/deluge	28,882,000	9,512,000	38,394,000
Plastic tube/deluge	24,344,000	6,400,000	30,744,000
Metal fin-tube/deluge/ammonia	23,152,000	5,342,000	28,494,000

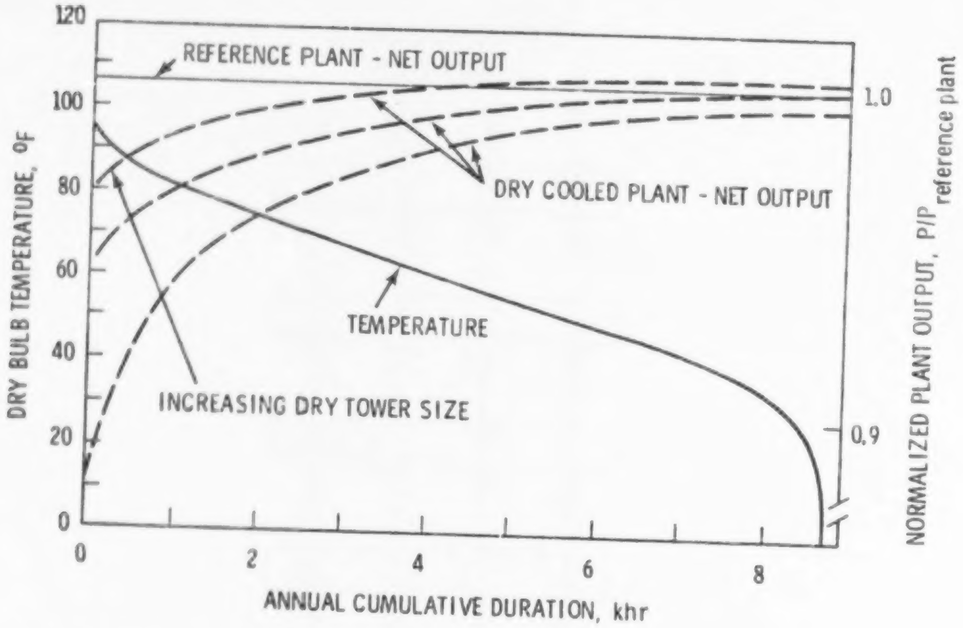

Figure 1. Relative Performance of a Dry Cooled Plant with Fixed Steam Source

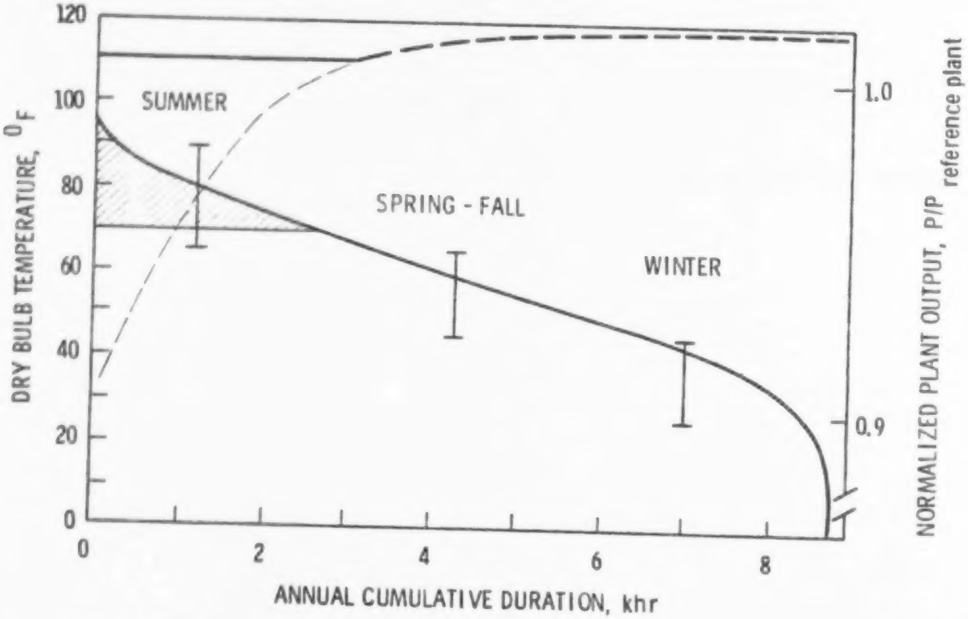

Figure 2. Wet Augmentation of Dry Cooling

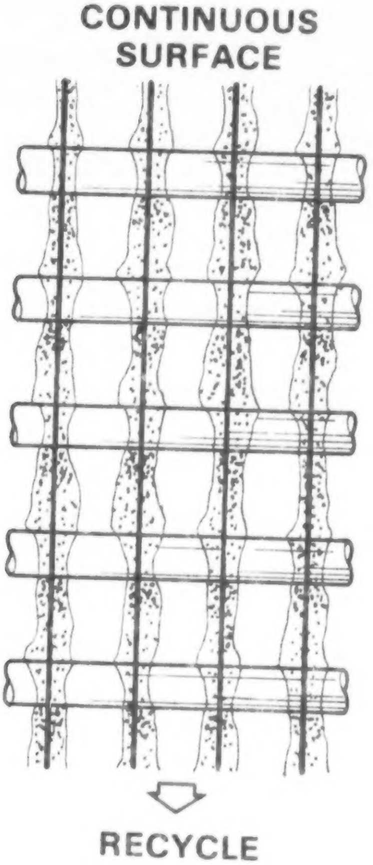
CONTINUOUS SURFACE
RECYCLE

Figure 3. Deluge on Plate Fin

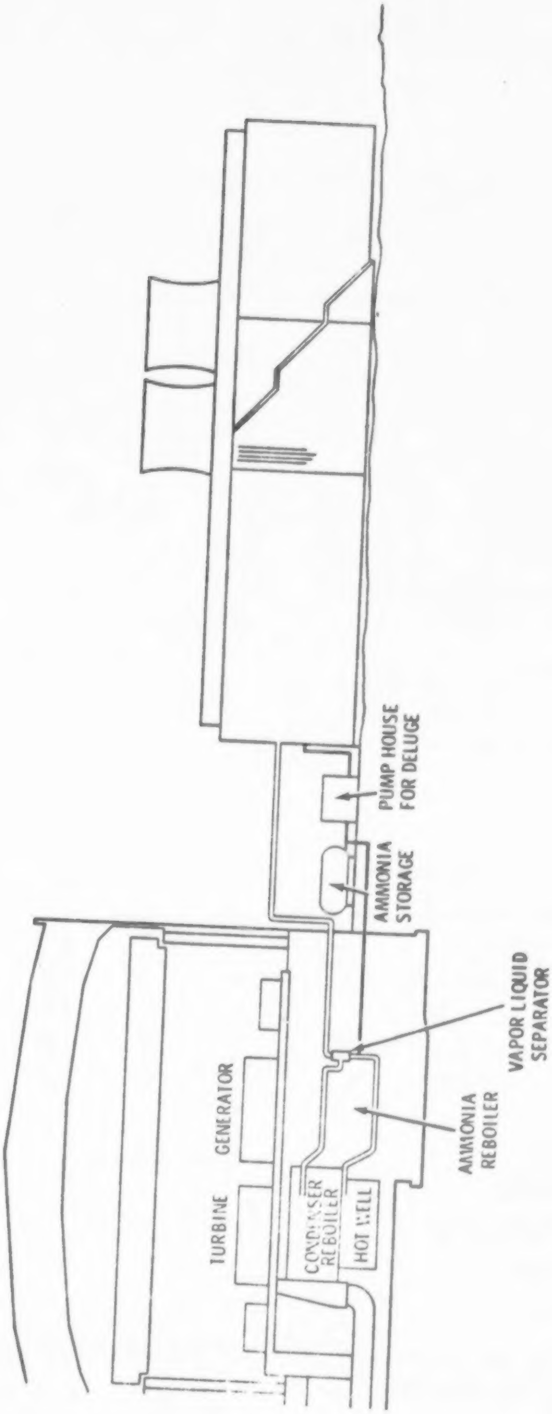
TURBINE
GENERATOR
CONDENSER REBOILER
HOT WELL
AMMONIA REBOILER
VAPOR LIQUID SEPARATOR
AMMONIA STORAGE
PUMP HOUSE FOR DELUGE

Figure 4. Layout of Steam Plant with Ammonia

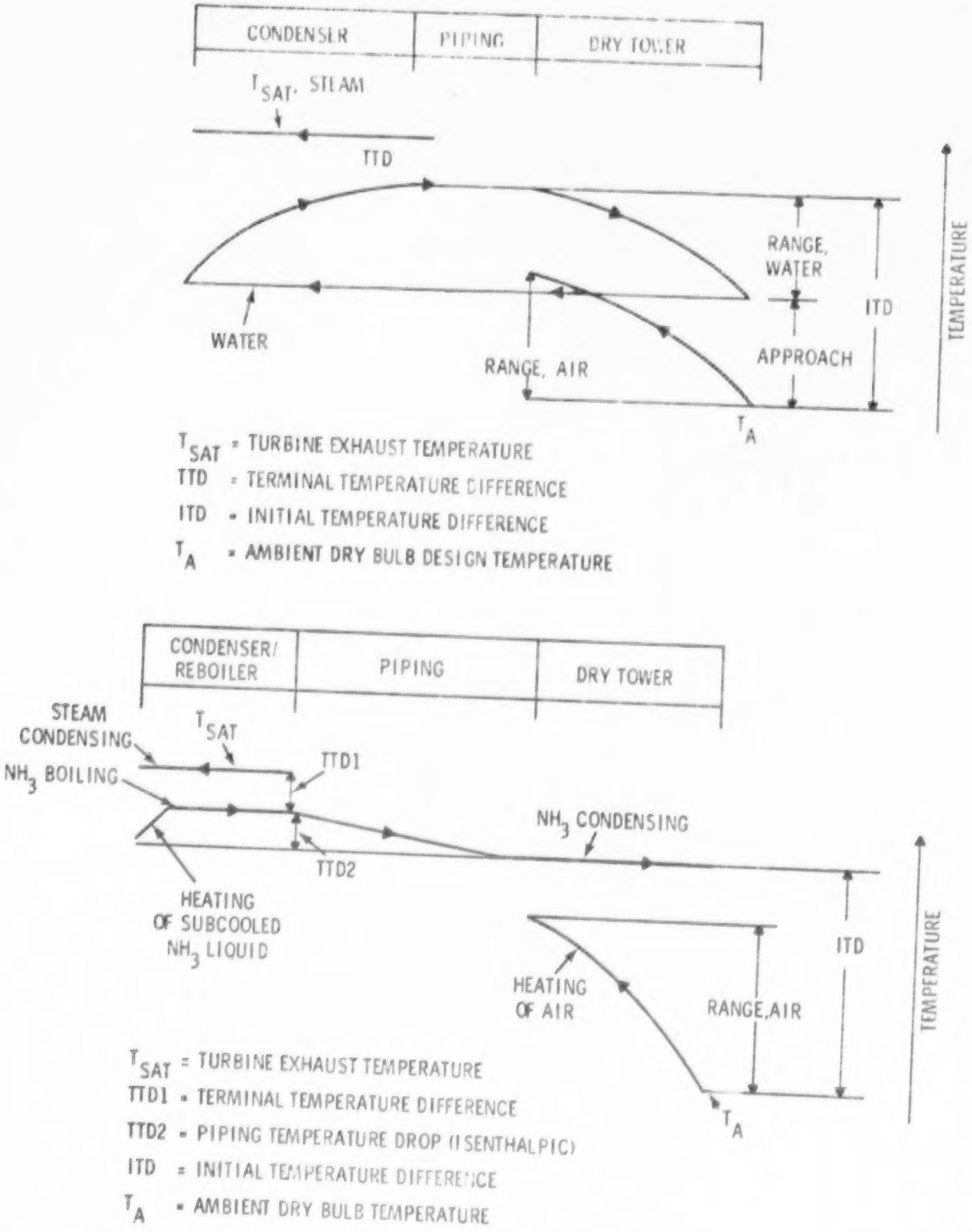
CONDENSER
PIPING
DRY TOWER
T_{SAT}, STEAM
TTD
RANGE, WATER
ITD
TEMPERATURE
WATER
RANGE, AIR
APPROACH
T_A
T_{SAT} = TURBINE EXHAUST TEMPERATURE
TTD = TERMINAL TEMPERATURE DIFFERENCE
ITD = INITIAL TEMPERATURE DIFFERENCE
T_A = AMBIENT DRY BULB DESIGN TEMPERATURE
CONDENSER/ REBOILER
PIPING
DRY TOWER
STEAM CONDENSING
T_{SAT}
TTD1
NH_3 BOILING
NH_3 CONDENSING
TTD2
HEATING OF SUBCOOLED NH_3 LIQUID
ITD
TEMPERATURE
HEATING OF AIR
RANGE,AIR
T_A
T_{SAT} = TURBINE EXHAUST TEMPERATURE
TTD1 = TERMINAL TEMPERATURE DIFFERENCE
TTD2 = PIPING TEMPERATURE DROP (ISENTHALPIC)
ITD = INITIAL TEMPERATURE DIFFERENCE
T_A = AMBIENT DRY BULB TEMPERATURE

Figure 5. Comparison of Temperature Relationship for Conventional and Ammonia Coolant Dry Cooling Systems

3 OF 9

N77

78644

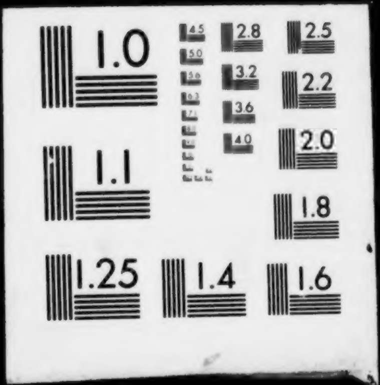
1.0
4.5
5.0
5.6
6.3
7.1
2.8
3.2
3.6
4.0
2.5
2.2
2.0
1.1
1.8
1.25
1.4
1.6

IV-C-179

9-45-20

K/CSD/INF-77/1

Contract No. W-7405 eng 26

COMPUTER SCIENCES DIVISION

A COMPUTERIZED ENGINEERING MODEL FOR EVAPORATIVE WATER COOLING TOWERS

J. E. Park
J. M. Vance*
K. E. Cross
N. H. Van Wie

Paper to be presented
at the

Conference on Waste Heat Management and Utilization

Miami Beach, Florida

May 9-11, 1977

UNION CARBIDE CORPORATION, NUCLEAR DIVISION
operating the
Oak Ridge Gaseous Diffusion Plant . Oak Ridge National Laboratory
Oak Ridge Y-12 Plant . Paducah Gaseous Diffusion Plant
for the
ENERGY RESEARCH AND DEVELOPMENT ADMINISTRATION

---

*Gaseous Diffusion Development Division

By acceptance of this article, the publisher or recipient acknowledges the U.S. Government's right to retain a nonexclusive, royalty-free license in and to any copyright covering the article.

IV-C-180a

A COMPUTERIZED ENGINEERING MODEL FOR EVAPORATIVE WATER COOLING TOWERS

J. E. Park,* J. M. Vance,
K. E. Cross and N. H. Van Wie
Union Carbide Corporation, Nuclear Division
Oak Ridge, Tennessee, U.S.A.

ABSTRACT

The evaporative cooling tower is often used to reject waste heat from industrial processes, especially power plants and chemical facilities. In this paper, we present a consistent physical model for crossflow and counterflow cooling towers which imposes rigorous heat and mass balances on each increment of the tower under study. Individual towers are characterized by specification of a mass evaporation rate equation.

The solution algorithm allows reduction of test data, interpolation of the reduced data, and comparison of test results to design data. These capabilities can be used to evaluate acceptance tests for new towers, to monitor changes in tower performance as an aid in planning maintenance, and to predict tower performance under changed operating conditions.

INTRODUCTION

The rejection of waste heat is a necessary element in the operation of chemical plants, power plants, and gaseous diffusion plants. These particular processes are of interest because of the enormous quantities of heat involved. For instance, a nuclear-powered electrical generating facility of 1000-megawatts [Mw(e)] capacity will reject about 10^8 Btu/min to the ambient. If the temperature rise in the condenser is limited to 20° F, 0.6×10^6 gpm of water must be circulated.

Frequently, this water is cooled and reused in order to reduce water treatment costs and to avoid possible environmental damage. Usually, this recirculated water is cooled using cooling towers in which the bulk of the water is cooled by evaporating a portion into the surrounding atmosphere.

The costs of new cooling towers are substantial. Figures of up to $20/kw of electrical generating capacity are typical, making the cooling tower system for a 1000-Mw(e) nuclear plant worth as much as $20 million. Therefore, the cost and performance of cooling towers and associated peripheral equipment must be included in the trade-offs required in designing the integrated *optimum* process plant.

---

*Will present paper.

A mathematical model of the cooling tower, manipulated by computer, can provide cooling tower cost and performance data. Inputs and computed results can link this model to the adjoining elements in the system. Also, systematic analysis of data produced by tests of existing cooling towers can be used to identify deterioration and to predict tower performance as operating conditions change. An increase of a few degrees in the temperature of the supply water to the condensers of a power plant can increase the annual energy costs substantially. If such a temperature rise can be attributed to a decrease in tower performance, repairs to offset deterioration and restore cooling capacity may be justified easily, allowing repairs to be planned and funds to be budgeted in an orderly fashion.

COOLING TOWER CODE UTILIZATION - TYPICAL PROBLEMS

The problems usually encountered in analysis of cooling towers for large process plants fall into three general classes which are discussed in some detail in this section.

Analysis of Test Data

Typically a cooling tower yields a set of data at each operating condition tested. Measurements include wet-bulb temperature and barometric pressures of the ambient air, volume flow rate for the fan(s), temperatures of water entering and leaving the tower and flow rate of water onto the tower. A cooling tower is similar to other heat transfer equipment with respect to possessing a performance coefficient which is most often expressed as a function of mass flow rates. The problem is to determine the performance coefficient grouping, $K'aV/C_pL$, and the associated mass flow ratio,

$$\theta \equiv \frac{\text{Water Flow Rate Onto Tower}}{\text{Mass Flow of Dry Air Through Tower}} \equiv \frac{L}{G} \quad . \tag{1}$$

Data taken at several operating conditions can be reduced with the code and the performance line constructed as indicated in Figure 1.

Comparison of Test Results to Design Point

Design conditions for a tower are quite often represented by a single point on a plot, such as Figure 1. Given the performance line (from recent tests, as above) and the manufacturer's design point, the objective is to calculate quantitative measures of the distance between that line and point. To put the problem in perspective, suppose that the point were the manufacturer's guaranteed performance on a new tower and the line were the result of a preacceptance test on that tower. For the hypothetical case shown, the distance between the two could represent serious economic loss to the purchaser. Adjustment of the purchase price can be more rationally negotiated if the distance between line and point can be quantified. The vertical distance (constant θ) between the point and the line can be quantified as an increase in cold or supply water temperature if the tower is operated at the mass flow ratio, atmospheric conditions and water temperature difference being specified in the design. Another distance of interest is along the constant approach line and quantifies the reduction in water flow rate required to meet the water inlet conditions. A plant operator can convert either of these quantities to an economic loss or gain, as the case may be.

The Tower as Part of a Heat Rejection System

A cooling tower frequently is required to accept a given rate of hot water from a process plant and cool that water to a specified temperature so that it can be returned (after replacing evaporative losses) to the plant for reuse. In such a case, the following parameters will be known: water flow rate, fan volume flow rate, performance line for the tower, wet-bulb temperature and barometric pressure of the ambient air, temperature of makeup water available, temperature difference between water at plant intake and plant discharge, and return water temperature desired. The tower may be capable of exceeding the requirements or its capacity may be inadequate. If excess capacity is available, a portion of the hot water from the plant bypasses the tower and is mixed with the cooled portion of the flow to provide the desired return temperature. The objective of the calculation is to determine the amount of water bypassed, as well as mass flow of air required and rate of water loss due to evaporation. If the tower performance does not meet the plant cooling requirements, the objective is to determine what conditions can be met. As in the previous case, air mass flow rates and evaporative losses are interesting by-products of the calculation.

The potential user of the model presented in this paper should be aware of the limitations of the model. The model is keyed to analysis of existing towers, or to forecast requirements of cooling tower cells of established performance. It is not intended to be able to synthesize a tower design from elemental fill data. Scaling of tower size should be done by adding or subtracting integer numbers of identical tower cells. Although it might be possible to scale height or plan area for identical fill geometry, no experience can be reported here for such calculations. It should also be noted that this model is not intended for use with natural draft towers and that all fans on the forced draft installations being studied must be running.

DERIVATION OF MODEL EQUATIONS

The description of the cooling tower is split into overall (macroscopic) balances of mass and energy and detailed (microscopic) balances of small elements. The microscopic equations which are derived below merely express the mass and energy balances on air and water across the increment and the rate-of-transfer of mass between the water and air. Heat transfer, in all cases, has been assumed to be adequate to maintain the air at the local saturation temperature.

Consider a small increment of tower volume (Figure 2a). Water enters the top and falls through the increment. The water may be thought to be falling as a sheet or film, or as drops of various sizes. In any case, a portion of the water evaporates. Air enters the volume increment from below and exits at the top, carrying the vaporized portion of the water and some droplets with it. The heat required to vaporize the water lost to the air stream is drawn from the unvaporized water, cooling it. This process is repeated through a number of increments, so that the water arriving at the bottom of the tower is cooled appreciably at the expense of some evaporative loss.

The heat lost by the water is equated to that gained by the air, giving

$$C_p(m_1t_1 - m_2t_2) = G(h_1 - h_2) + 32(m_1 - m_2) \quad .^* \tag{1}$$

m_1 and m_2 are the liquid flow rates entering and leaving the volume, G is mass flow rate of dry air and h_1 and h_2 are enthalpies for saturated air, per unit mass of dry air.

The mass lost by the water is added to the air stream and is expressed as a change in specific humidity (H) of the saturated air:

$$m_1 - m_2 = G(H_1 - H_2) \quad . \tag{3}$$

Equations 1 and 3 express universal physical laws; they apply regardless of the amount of water evaporated. The amount of mass evaporated is expressed in terms of a mass transfer coefficient and driving potential:

$$m_1 - m_2 = \left(\frac{m_1 + m_2}{2}\right) \frac{K'a}{L} \delta V(H'' - H) \quad . \tag{4}$$

H is the specific humidity of the air locally in the volume and H" is the specific humidity of air evaluated at the local water temperature.

Equation 4 is strictly an empirical rate equation. Most often the product K'a would be taken as constant for a tower operating at a particular L/G (water flow to air flow) ratio.

The local mass flow rate $(m_1 + m_2)/2$ is a qualitative measure of variation in shear forces on the drop which should affect the mass transfer rate. Since the coefficient K'a will normally be extracted from experimental data taken over a limited range of air and water flows, this empirical coefficient should not be extrapolated over great variations.

---

[*] The enthalpy of liquid water, $h_L(t)$, is normally calculated using a constant specific heat (with a value of unity) and a zero value at 32°F,

$$h_L(t) = (1)(t - 32) \tag{2}$$

The volume increment is just the total volume of fill divided by the number of increments,

$$\delta V = V/N \quad . \tag{5}$$

The rate equation (4) then takes a familiar form:

$$m_1 - m_2 = \frac{C_p}{N} \left(\frac{m_1 + m_2}{2}\right)\left(\frac{K'aV}{C_p L}\right)(H'' - H) \quad . \tag{4a}$$

These equations (1), (3), and (4a) describe the conservation of mass, energy and the evaporation rate across a small increment of fill as shown in Figure 2a. If the air flow rate G in Eq. (1) is replaced by C, the air flow rate per vertical increment,

$$C = G/N \quad ,$$

and the locations of the variables on the increments are shifted (Figure 2b), the same balance equations are used for an increment of fill in a crossflow tower.

The selection of the humidity potential H" - H as a driving force for mass transfer rather than the air enthalpy potential h" - h as a driving force for heat transfer was, to some extent, arbitrary. Aside from personal taste, one advantage and one disadvantage accrue from this choice of rate mechanisms. As an advantage, the Lewis relation (ratio of overall mass transfer to overall heat transfer equals unity) is not required to hold. This compares to the classic model of Baker and Shryock [1] in which the Lewis relation was required to allow an essential algebraic manipulation. As a disadvantage, a difficulty is encountered in integrating Eq. (4a). While the enthalpy of air is nearly constant at fixed dry bulb temperature regardless of the wet bulb temperature, the humidity for fixed dry bulb temperature increases markedly as the wet bulb temperature is increased. Thus, the present model depends on the humidity of the inlet air (i.e, both wet and dry bulb) while the results from the enthalpy-driven models depend only on the wet bulb temperature. Development of an appropriate inlet humidity specification is presently under way.

Solution of Microscopic Balance Equations

The microscopic balance equations (1,3,4a) describe the changes in temperature, enthalpy, humidity and mass flow across an increment of cooling tower volume. The linking of these equations into a model for a crossflow and counterflow tower configuration is described in this section.

A schematic of the increment structure for a crossflow tower is shown in Figure 3. A sweep of the increments starts at the top left, where a hot water temperature and air inlet temperature are known (or assumed). Solving Eqs. (1,3,4a) for the first increment advances the air temperature one increment to the left and the water temperature one increment downward.

By repeating this process for each increment in turn, the water temperature distribution at the bottom and the air temperature distribution into the center of the tower are calculated. The water temperature off the tower is a mass-weighted average of the temperature from each bottom increment. The air temperature is taken as saturated at the average enthalpy.

To solve the equations for one increment, an iterative approach is used. Outlet conditions are assumed, the driving potential is estimated at the center of the increment, and the estimates are corrected. This process is repeated until the correction is arbitrarily small. Details are presented in [2]. Applying the driving potential at the center of the increment is the key to the second-order accuracy of the calculation.

The counterflow tower is modeled as a single vertical column of increments. The scheme is to start at the top and solve each increment iteratively, working to the bottom of the tower. As with the crossflow tower, the driving potential is evaluated at the center of the increment to give second-order accuracy.

Solution of the Macroscopic System

The macroscopic equations are derived from each specific application of the model. For example, reduction of a set of test results to a mass transfer coefficient requires the matching of measured temperatures to values calculated using an assumed mass transfer value. In this problem, the macroscopic equations are of the form,

"Temperature of Cold Water = Measured Value."

With the measured parameters specified in that way, the value of the mass transfer coefficient can be systematically (and automatically) varied to match the data with the calculated values. Another useful form of the macroscopic equations balances a process heat rejection load with the heat rejected by a connected tower.

In both cases (and others), the macroscopic equations are used to set up a multivariable Newton's method, generating corrections for assumed values of the variables linking the macroscopic equations to the tower models. Details are available in [2].

DISCUSSION OF SOME SAMPLE CALCULATIONS

In this section, the results of several typical calculations are examined.

Several sets of test data and a design point for the same tower are given in Table 1. Performance coefficients generated using the model are also tabulated. The data have been reduced using both the crossflow and counterflow algorithms. The values from the crossflow model are higher than the corresponding points from the counterflow routine. This is expected; to do the same cooling job, the lower thermal efficiency of the crossflow layout would require more active volume (V greater), more effective mass transfer (K larger), or more fill (area or a greater). The performance coefficients for the crossflow analysis are shown on Figure 4.

The operating profile of air and water temperatures and local evaporation rates is shown in Figure 5 for a counterflow tower operating at the design point listed in Table 1. At the top of the tower, the evaporation rate is highest, but drops rapidly as the water falls through the tower and cools. The water is cooled more rapidly (in terms of temperature reduction per increment) in the upper sections of the tower. The air and water temperature curves approach a limiting value (the wet bulb temperature of the inlet air) near the bottom of the tower.

Figure 6 illustrates the convergence of the solution for the incremental (difference) equations to the limiting case of an infinite number of increments. A single set of data has been reduced using the counterflow routine with 6, 10, 20, and 80 increments in the integration routine. When the performance coefficient, $K'aV/L$, is plotted against the number of increments N, the *kneed* curve results which shows a rapid change followed at large N by asymptotic approach to a constant value. If $K'aV/L$ is plotted against $1/N^2$, the data are covered by a straight line. This linearity indicates that the algorithm is *second-order accurate*; that is, the solution to the discrete balance equations approaches the differential limit (infinite number of increments) as the square of the number of increments. From Figure 6, one can see that the solution of $1/N^2 = 0$ ($N^2 \rightarrow \infty$) is virtually indistinguishable from the solution for $N = 80$. From an economic viewpoint, the $N = 20$ solution varies about 0.05% from the $N = 80$ solution while the computing time varies by about a factor of 4:

$$T_{80}/T_{20} \approx \frac{80}{20} = 4 \quad .$$

On this basis, it is recommended that 20-25 increments be used with the present algorithm for analyzing counterflow cooling towers. For the crossflow algorithm, analysis shows that

$$T_{80}/T_{20} \approx \left(\frac{80}{20}\right)^2 = 16 \quad .$$

Figure 7 is a summary of the calculated results for a particular crossflow cooling tower operated at a particular set of conditions. Detailed profiles of water temperature, air temperature and local evaporation rate for this tower are shown in Figures 8 through 10.

Figure 8 shows the local water temperatures calculated across several horizontal sections in the tower. As expected, the largest portion of the temperature drop occurs in the upper sections of the tower. The top 5% of the fill, for example, accounts for about 12% of the cooling. The bottom 40% of the fill accounts for about 20% of the cooling. This is due to the higher evaporation rates from the hotter water to the larger driving force at the upper left corner of the tower. Below the uppermost sections, the temperature drop across each section is roughly constant from left to right (the temperature curves appear to be roughly parallel). A similar pattern appears in Figure 10 for the local evaporation rate.

In Figure 9, the local saturation temperature for the air is plotted. The air entering nearest the top is exposed to the hottest water and thus gains the most heat. Air in lower horizontal sections is exposed to cooler water and thus gains less energy.

In Figure 10, the local evaporation rates are plotted. The evaporation rates are highest in the upper left corner of the tower where the hottest water meets the coldest air. In the lower portion of the tower, the rates are roughly constant across any horizontal section. This is related to the nearly uniform changes in water temperature seen in Figure 8. The shape of the curve labeled *15* (15% of the fill height below the top of the fill) requires some discussion. The heat transferred from water to air in any section is divided between sensible heat transfer (convection) and latent heat transfer (evaporation). As hotter water is encountered by hotter air, the balance between sensible heat transfer and latent heat transfer shifts. Transfer coefficients change only slightly, but the humidity difference driving the mass transfer (evaporation) increases more than the temperature difference driving the sensible heat transfer. Thus, more heat is transferred by evaporating the water. Since the latent heat of water drops as the temperature increases, the amount of water evaporated to absorb the heat increases. As the air proceeds further to the right in the tower, both driving forces decrease and the total evaporation decreases.

To summarize, the basic physical laws of mass and energy conservation are satisfied to the accuracy of the iteration convergence. The algorithms used for the counterflow and crossflow models are *second-order* accurate and a choice of 20-25 integration increments gives adequate accuracy without inordinate use of expensive computing time. Finally, detailed plots of air temperature, water temperature, and local evaporation rate calculated throughout typical crossflow and counterflow towers are in agreement with physical intuition. The foregoing should aid in establishing confidence in the validity of the physical model and the computer program which evaluates the model.

CONCLUSIONS

In this report, the main features of the mathematical model of the physical transport processes occurring in an induced draft evaporative cooling tower are summarized. Studies of sample problems are presented.

The overall conservation laws for mass and energy are satisfied rigorously, regardless of the number of increments used for integration; this approach allows careful checks on the computer program. The evaporative mass loss is calculated using a modification of the usual rate equation based on the specific humidity difference between water and air as a driving force. Heat transfer rates, if calculated, would be just sufficient to keep the air saturated with moisture. The usual additional assumption that the Lewis relation is unity [1] is not made and, in fact, is redundant. Mass and energy losses by the water are included in the balance equations. Evaporation losses have been calculated (or estimated) in some earlier work [1,3] using the approximate numerical integration of approximate differential equations. The exact (numerical) solution of the incremental balance equations is preferable.

The numerical procedure for solving the model equations is outlined. Computational results indicate that the algorithm is second order in accuracy, allowing as few as 20 increments to be used to integrate the balance equations.

Successful use of these models to optimize the thermal control system for proposed new gaseous diffusion plants by adding or subtracting tower cells of known size and performance has not been detailed here. The success of those applications indicates that the present model has utility in designing optimum heat rejection systems for power stations or chemical process facilities.

REFERENCES

1. Baker, Donald R. and Howard A. Shryock, "A Comprehensive Approach to the Analysis of Cooling Tower Performance," Journal of Heat Transfer, August, 1961, pp. 339-350.

2. Cross, K. E., J. E. Park, J. M. Vance and N. H. Van Wie, Theory and Application of Engineering Models for Cross-Flow and Counterflow Induced Draft Cooling Towers, Union Carbide Corporation, Nuclear Division, Oak Ridge, Tennessee, Report K/CSD-1, May 1976 (available from the National Technical Information Service, U. S. Department of Commerce, 5285 Port Royal Road, Springfield, Virginia 22161, Price: Printed Copy $5.00; Microfiche $2.25).

3. Yadigaroghi, G. and E. J. Pastor, "An Investigation of the Accuracy of the Merkel Equation for Evaporative Cooling Tower Calculations," ASME Paper 74-HT-59, July, 1974.

Table 1

Typical Test Results for a Cooling Tower
With Performance Coefficient Calculated Using
Both Crossflow (XF) and Counterflow (CF) Algorithms

	1	2	3	4	Design
Water Flow, 10^6 gal/day	4.22	7.93	6.62	8.89	10.29
Air Flow, 10^6 cfm	0.85	0.85	0.85	0.85	0.5
Water On, °F	125.0	129.8	126.5	135.7	132.3
Water Off, °F	73.3	84.5	80.5	89.9	90.0
Air Wet Bulb, °F	61.8	65.5	62.4	71.1	80.0
Barometer, psia	14.64	14.67	14.62	14.63	14.696
L/G	0.423	0.843	0.687	0.980	1.172
K'aV/L, CF	2.011	1.341	1.440	1.203	1.869
K'aV/L, XF	2.476	1.712	1.789	1.554	2.933

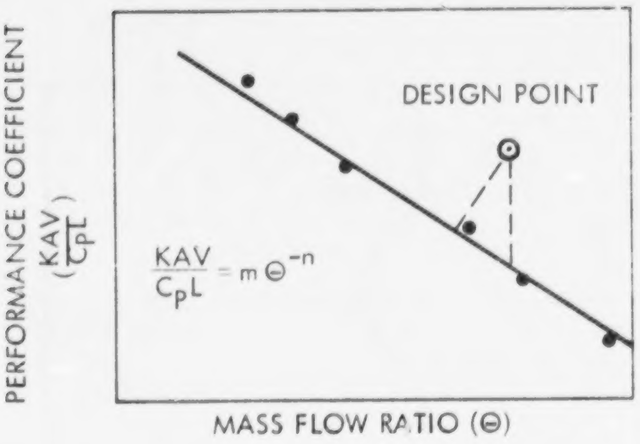

Figure 1. COMPARISON OF DESIGN POINT TO TEST DATA.

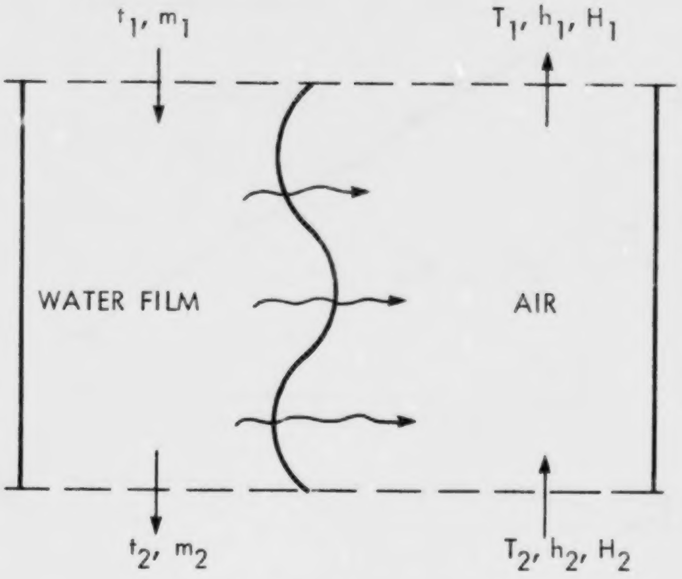
t_1, m_1
T_1, h_1, H_1
WATER FILM
AIR
t_2, m_2
T_2, h_2, H_2

Figure 2a. INCREMENT OF THE FILL VOLUME OF A COUNTERFLOW COOLING TOWER.

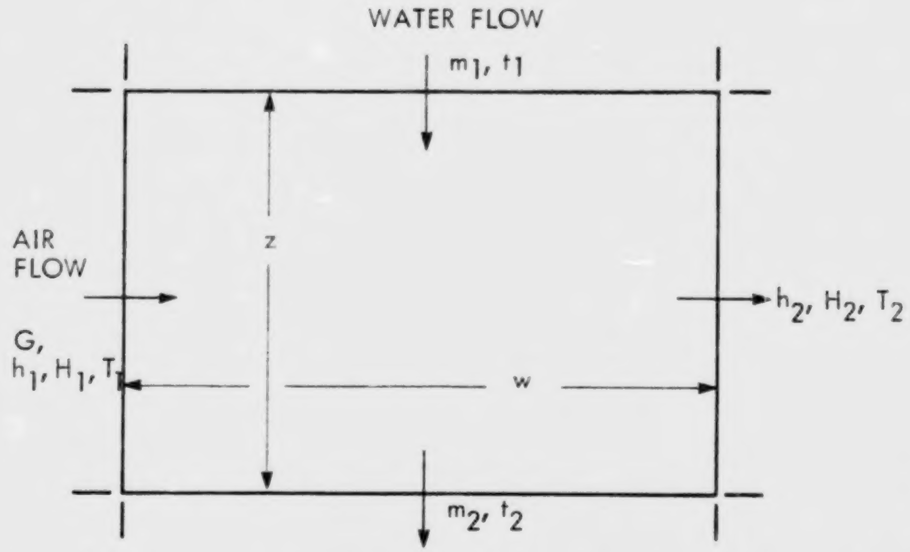
WATER FLOW
m_1, t_1
AIR FLOW
z
h_2, H_2, T_2
G,
h_1, H_1, T_1
w
m_2, t_2

Figure 2b. INCREMENTAL VOLUME OF FILL IN CROSS-FLOW COOLING TOWER.

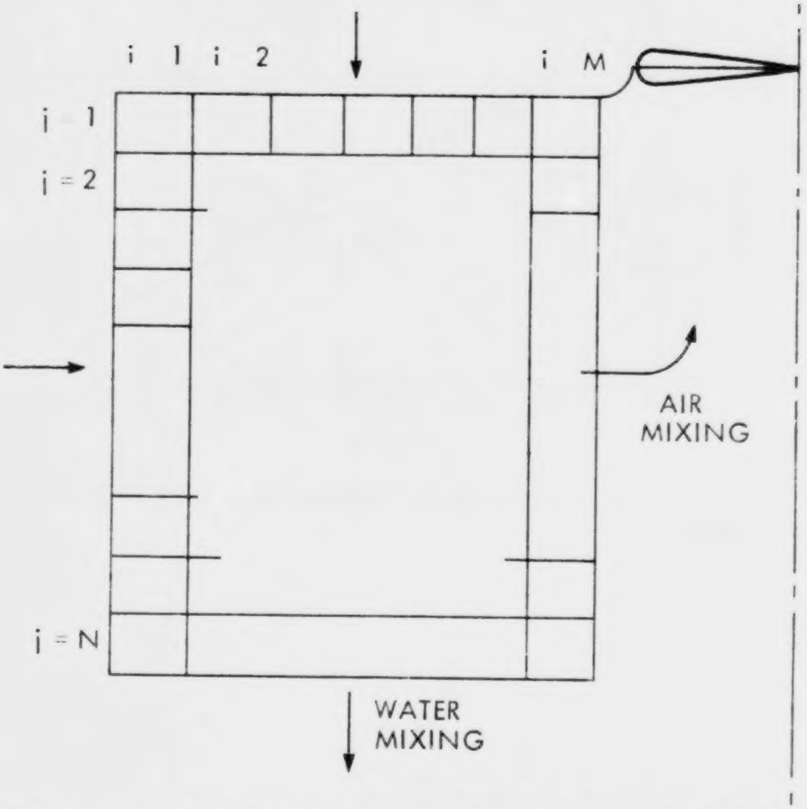
i = 1
i = 2
i = M
j = 1
j = 2
j = N
AIR
MIXING
WATER
MIXING

Figure 3. DIVISION OF CROSS-FLOW TOWER INTO INCREMENTAL VOLUMES SHOWING SUBSCRIPTING CONVENTION.

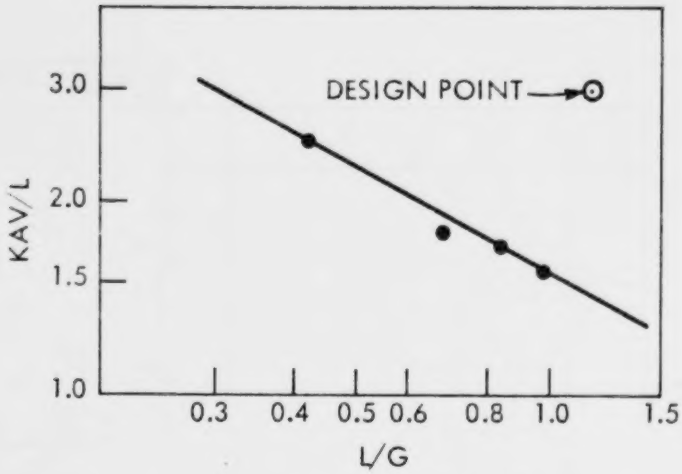

Figure 4. TEST RESULTS FOR CROSS-FLOW COOLING TOWER.

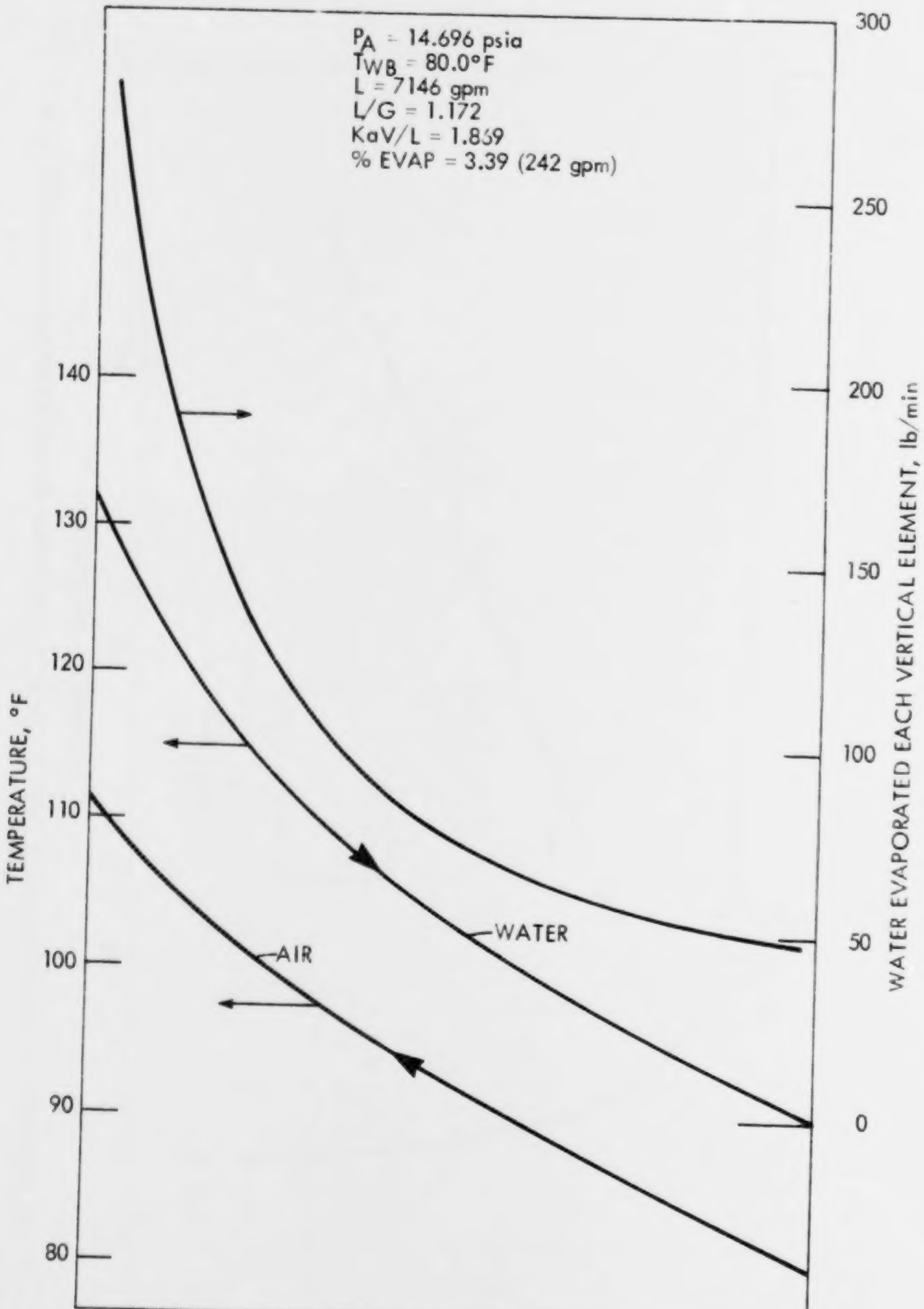

Figure 5. COUNTERFLOW TOWER PROFILES

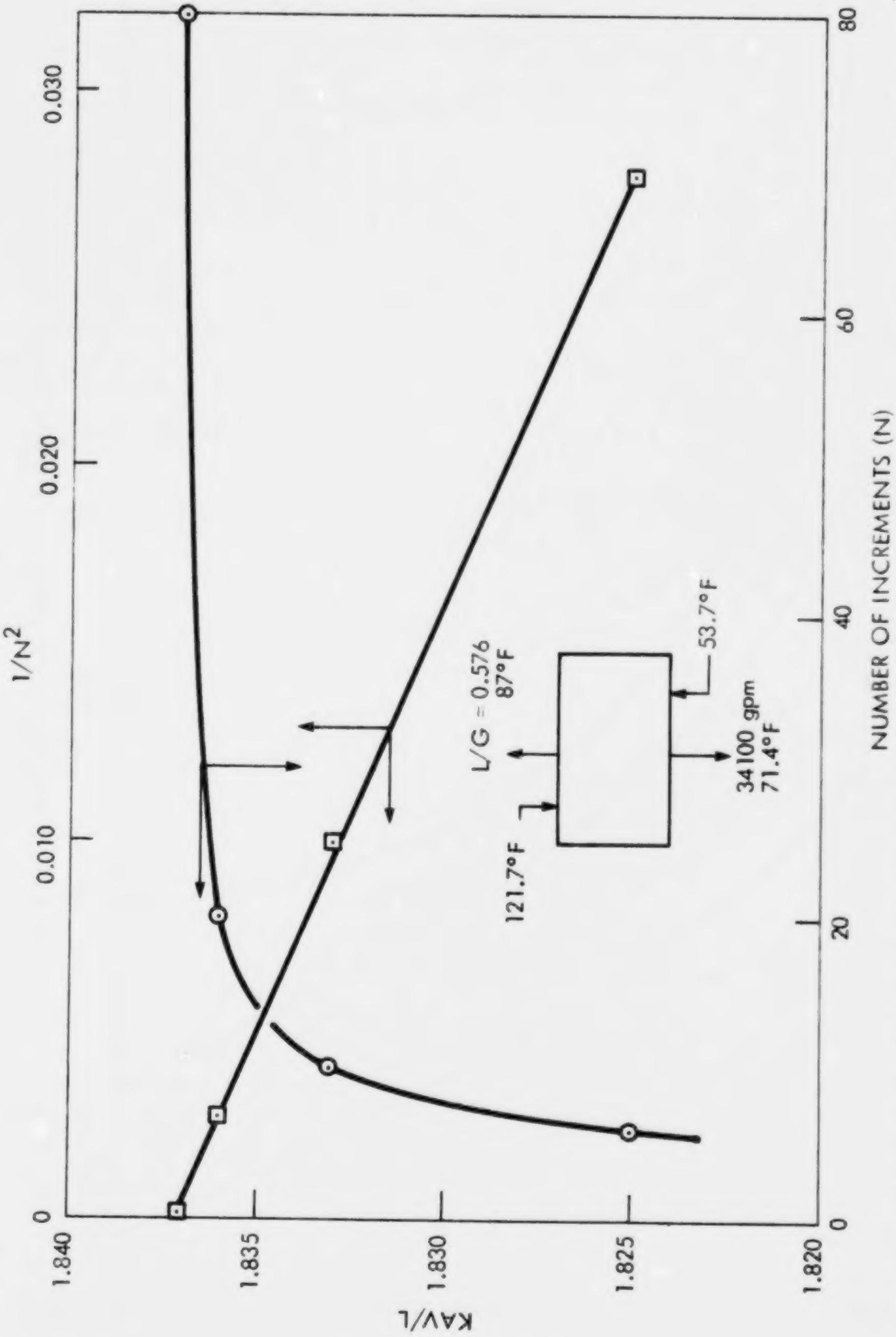

Figure 6. SENSITIVITY OF PERFORMANCE COEFFICIENT TO NUMBER OF INCREMENTS-COUNTERFLOW TOWER.

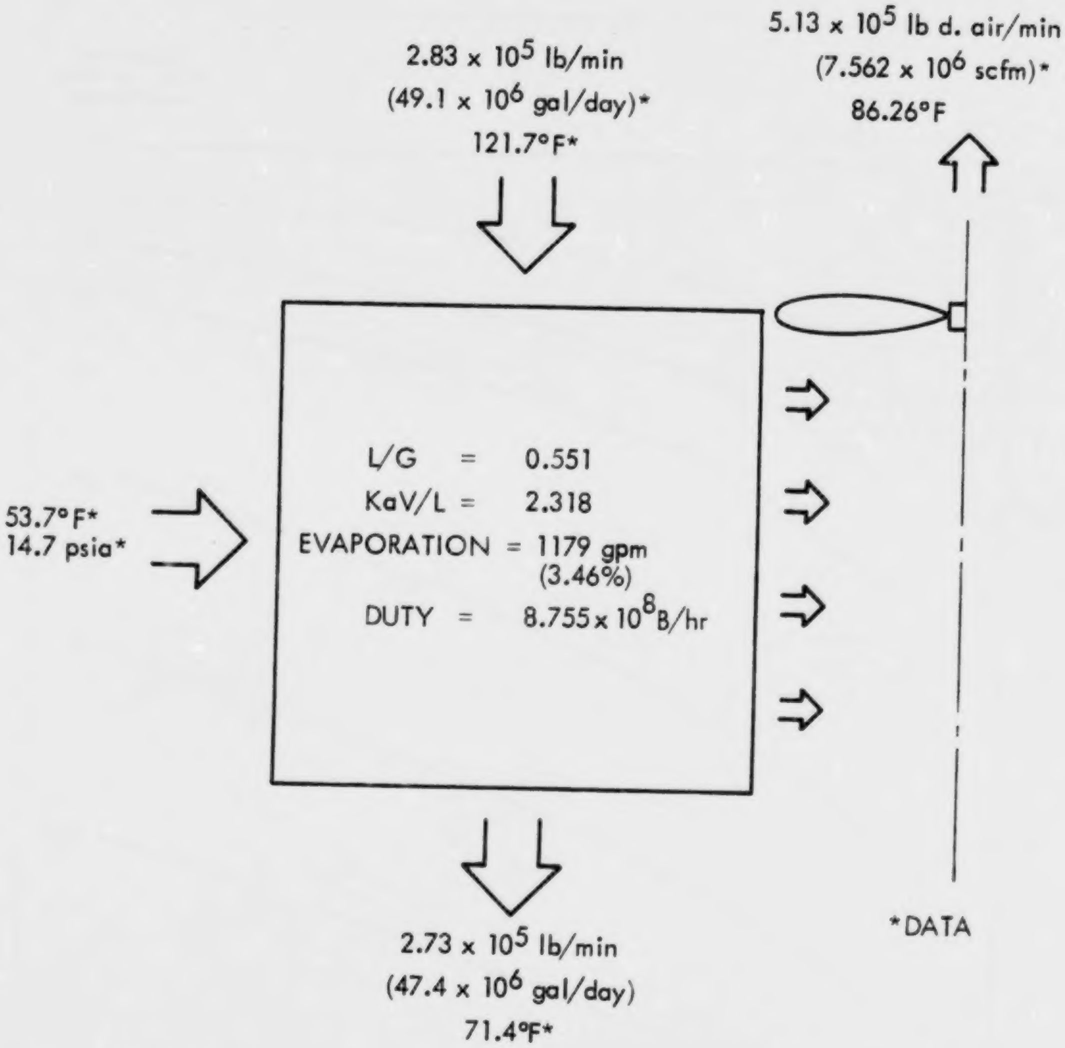

5.13 x 10^5 lb d. air/min
(7.562 x 10^6 scfm)*
86.26°F
2.83 x 10^5 lb/min
(49.1 x 10^6 gal/day)*
121.7°F*
53.7°F*
14.7 psia*
L/G = 0.551
KaV/L = 2.318
EVAPORATION = 1179 gpm
(3.46%)
DUTY = 8.755 x 10^8B/hr
2.73 x 10^5 lb/min
(47.4 x 10^6 gal/day)
71.4°F*
*DATA

Figure 7. DATA AND CALCULATED INFORMATION FOR A TYPICAL CROSS-FLOW COOLING TOWER.

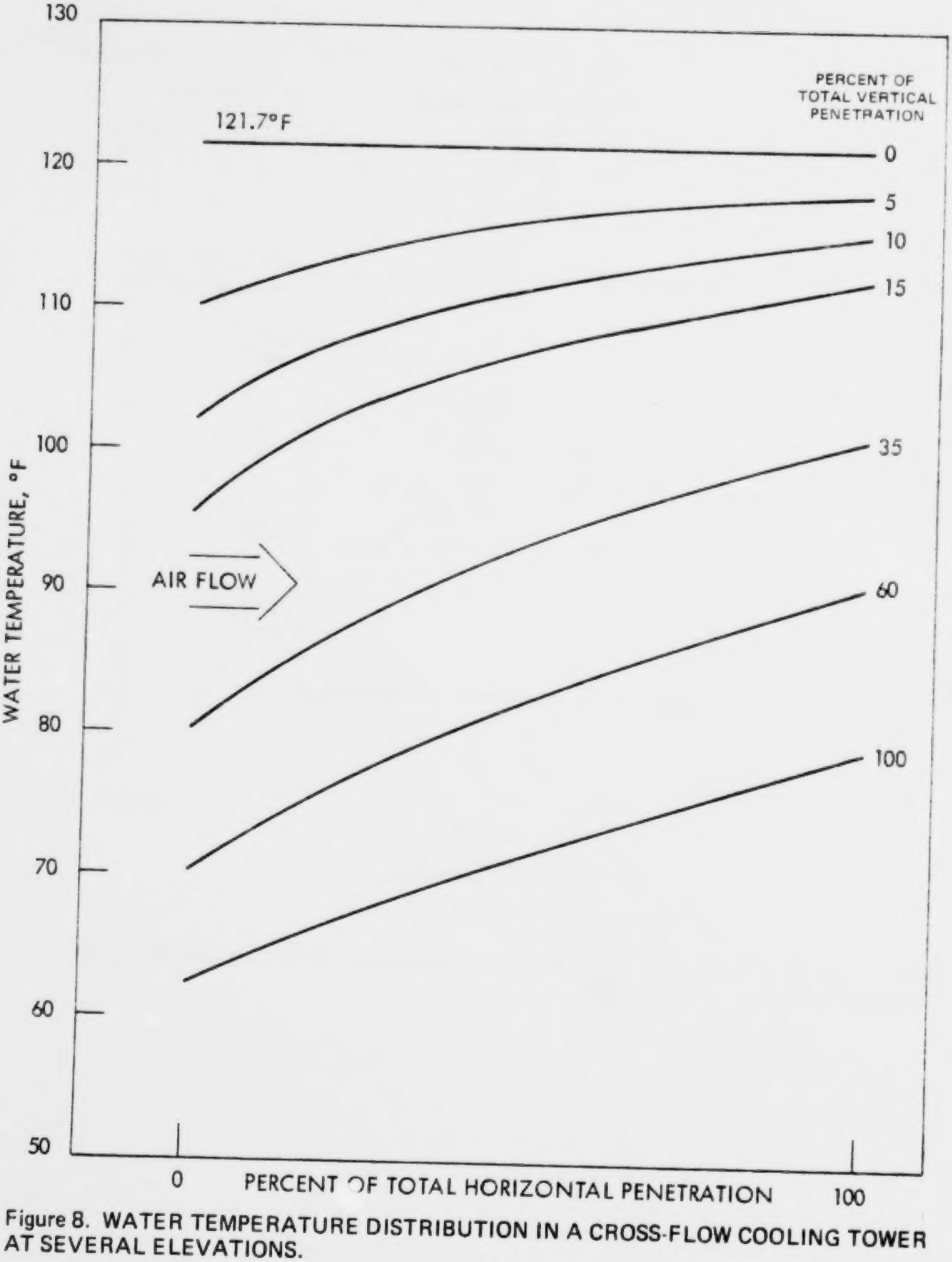

Figure 8. WATER TEMPERATURE DISTRIBUTION IN A CROSS-FLOW COOLING TOWER AT SEVERAL ELEVATIONS.

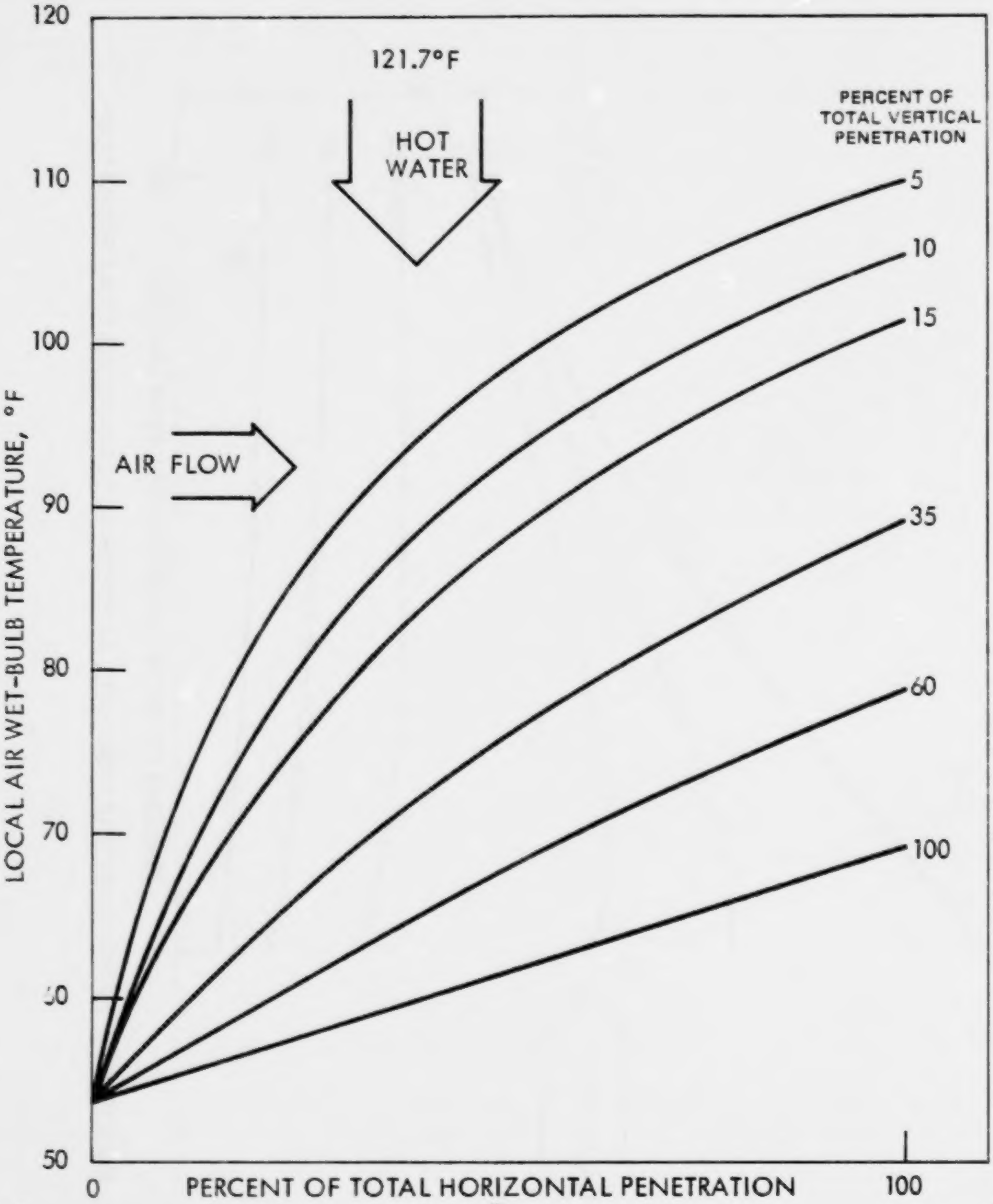

Figure 9. AIR WET-BULB TEMPERATURE DISTRIBUTION IN A CROSS-FLOW COOLING TOWER AT SEVERAL ELEVATIONS.

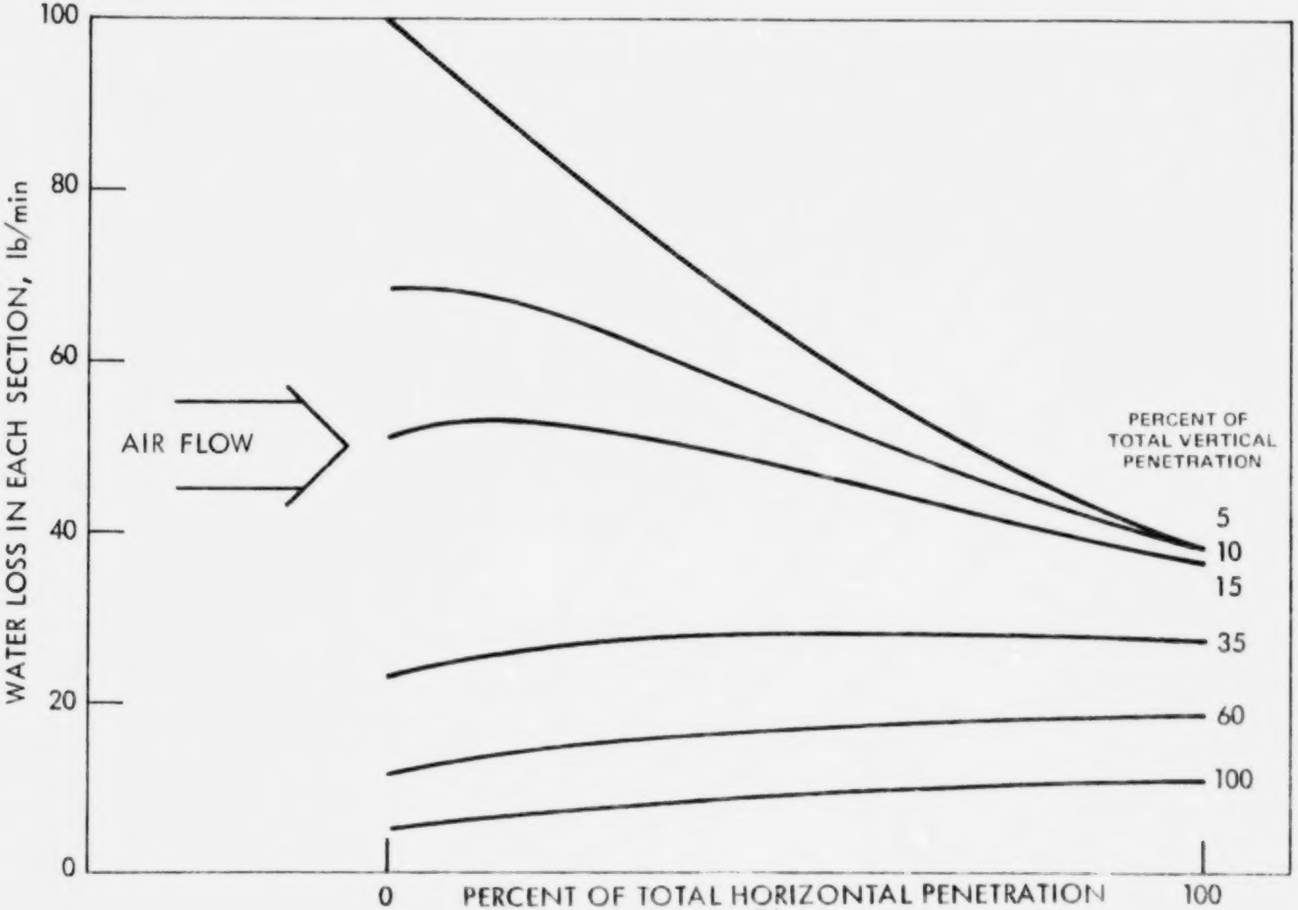

Figure 10. PROFILES OF WATER EVAPORATION RATE AT SEVERAL ELEVATIONS IN A CROSS-FLOW TOWER.

SESSION V-A
MANAGEMENT ASPECTS

OMIT

ABSTRACT
OF
HOW TO GET WASTE HEAT MANAGED

K.G. Kreider[1] and W.M. Rohrer, Jr.[2]

Many of the problems of waste heat management are not primarily technical ones, but rather are related to managerial practices and attitudes, and to a general insufficiency of technical resources in small and medium sized industrial units. The solutions to the prevelant problem of unrecovered waste heat lie in the education of management and in making technical resources more available to them.

The Waste Heat Management Guidebook, NBS Handbook number 121 is technically sound but written at a level that makes it useful for industrial managers, regardless of their individual backgrounds. It covers such topics as sources and uses of waste heat, determination of heat recovery equipment specifications, economics of waste heat recovery, a number of case histories, commercial options in heat recovery equipment and instrumentation for quantifying waste heat.

The U.S. Department of Commerce has recently developed the Energy Information Workbook which is a guide for management in conducting a complete energy audit and in setting up an energy information system as part of the management information system. The workbook shows how to start with a knowledge of purchased energy flows at the property line and end up with the in-plant energy distribution and heat balances of the intensive energy consuming systems. This sort of knowledge is critical in making decisions about waste heat management.

The Energy Analysis and Diagnostic Center at the University of Pittsburgh has been active for a number of years in education and research in energy conservation. Students and staff have been interacting with industrial managers and engineers, probing the questions of how to provide the needed information for small and medium businesses which will induce them to venture into waste heat management and to carry it on successfully. As yet the questions are largely unanswered, but the experience of participating in more than fifty active projects has lead to some conclusions and these will be discussed.

---

[1] Industry Program, Office of Energy Conservation, Institute for Applied Technology, National Bureau Standard.

[2] Energy Analysis and Diagnostic Center, Mechanical Engineering Department, University of Pittsburgh.

10-45-26

RESOURCE RECOVERY MODELS FOR REGIONAL PLANNING AND POLICY EVALUATION

Edward B. Berman
The MITRE Corporation
Bedford, Massachusetts U.S.A.

ABSTRACT

MITRE has designed and developed several models for regional resource recovery planning. These models have been applied in several planning and policy evaluation programs, and, from this work, insights have been gained into the economics of regionalization in resource recovery planning. The models and application programs are described, and the insights are discussed.

INTRODUCTION

In this paper, we shall describe models for regional resource recovery planning, and their application programs. From this work, we have gained many insights into the economics of regionalization; but given the early stage of our work, and the crude state of our data, these insights are not answers, but rather questions to be asked, and suggestions for further investigation.

BACKGROUND

In resource recovery, there is an economic push towards regional solutions -- to take advantage of the substantial economies of scale in processing. But regionalization in turn generates two problems:

- a complexity in system design (see Figure 1)
- a difficulty in achieving a consensus among the large number of autonomous decision-makers in a large region.

The planning model is intended to help with both problems:

- by sorting out the many locational, process selection, and transportation link selection issues, and identifying a minimum-cost solution; and

Preceding page blank

ECONOMIC ELEMENTS OF
A REGIONAL RESOURCE RECOVERY SYSTEM

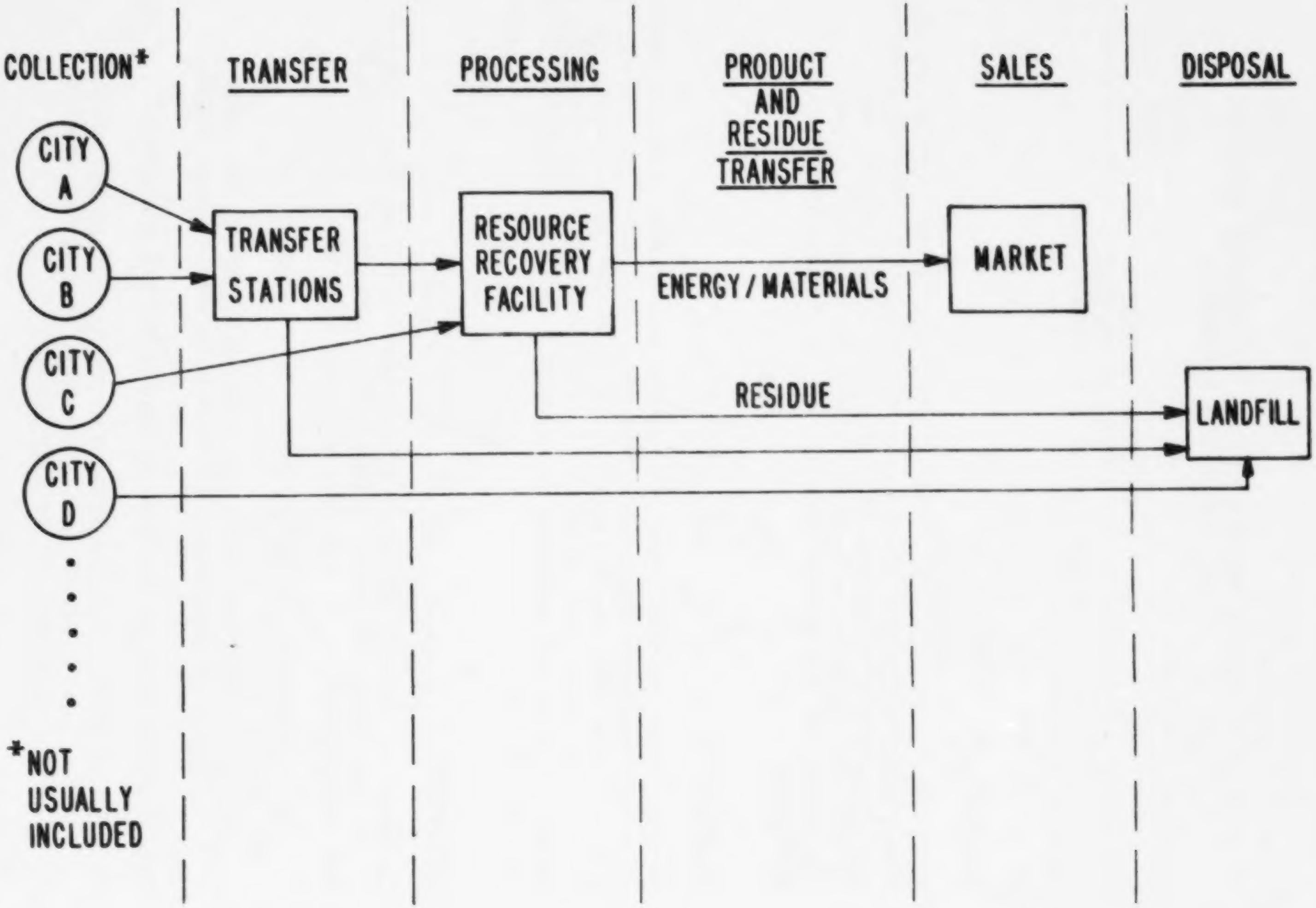
COLLECTION*
TRANSFER
PROCESSING
PRODUCT AND RESIDUE TRANSFER
SALES
DISPOSAL
CITY A
CITY B
CITY C
CITY D
TRANSFER STATIONS
RESOURCE RECOVERY FACILITY
ENERGY/MATERIALS
MARKET
RESIDUE
LANDFILL
*NOT USUALLY INCLUDED

Figure 1

EBB

- by assisting the consensus by illuminating at least what cost differences are associated with political issues, and thereby assisting in their solution.

Figure 2 illustrates the basic tradeoff on centralization for a hypothetical region. The processing cost per ton declines continually as we move to the right in that figure, towards fewer, and larger, plants. This is the effect of the economies of scale. On the other hand, the haulage cost per ton, required to gather the waste into the processing centers, increases as we move to the right, towards more centralized solutions. In determining the proper degree of centralization we seek to minimize the sum of processing plus haul cost. Figure 2 illustrates the cost comparison for the four, two, and one plant cases, with the two-plant case showing the lowest total cost for processing and haul. Note that the solution must be discrete -- we cannot have one and one-half plants in our region.

Figure 3 illustrates some of the non-economic effects of regionalization. The processing plus haul costs curve would indicate a preferred plant size, and hence degree of centralization, at the lowest point of that curve. Other elements, which are difficult to quantify, such as political difficulty, implementation time, and possible vulnerability (to strike, unexpected breakdown, etc.) will tend to increase with larger region size. The vulnerability might be ameliorated by a modular plant design, but the other elements are intrinsic to the political process of consensus. In a state in which a state-wide authority over solid waste tonnage has been established, most of these political costs are absent, but in most states these costs exist, and should be considered. Their presence should tend toward the selection of smaller region sizes. The models and model applications we shall describe below ignore these latter costs, and hence tend to generate larger region sizes than would be appropriate for most states.

THE MODELS

We shall describe two models:

- WRAP (Waste Resources Allocation Program)
- RAMP (Recovery and Market Planning).

WRAP was designed and developed by MITRE with EPA support. WRAP is fully operational, fully documented, and available to the public through EPA.

RAMP is in an experimental stage. It is essentially hand-operated and undocumented. We have been using it at MITRE, and expect to develop it for public use in the near future. The application programs described below have been run on RAMP.

EBB

CENTRALIZATION TRADE-OFF: ECONOMIES OF SCALE vs. HAULAGE

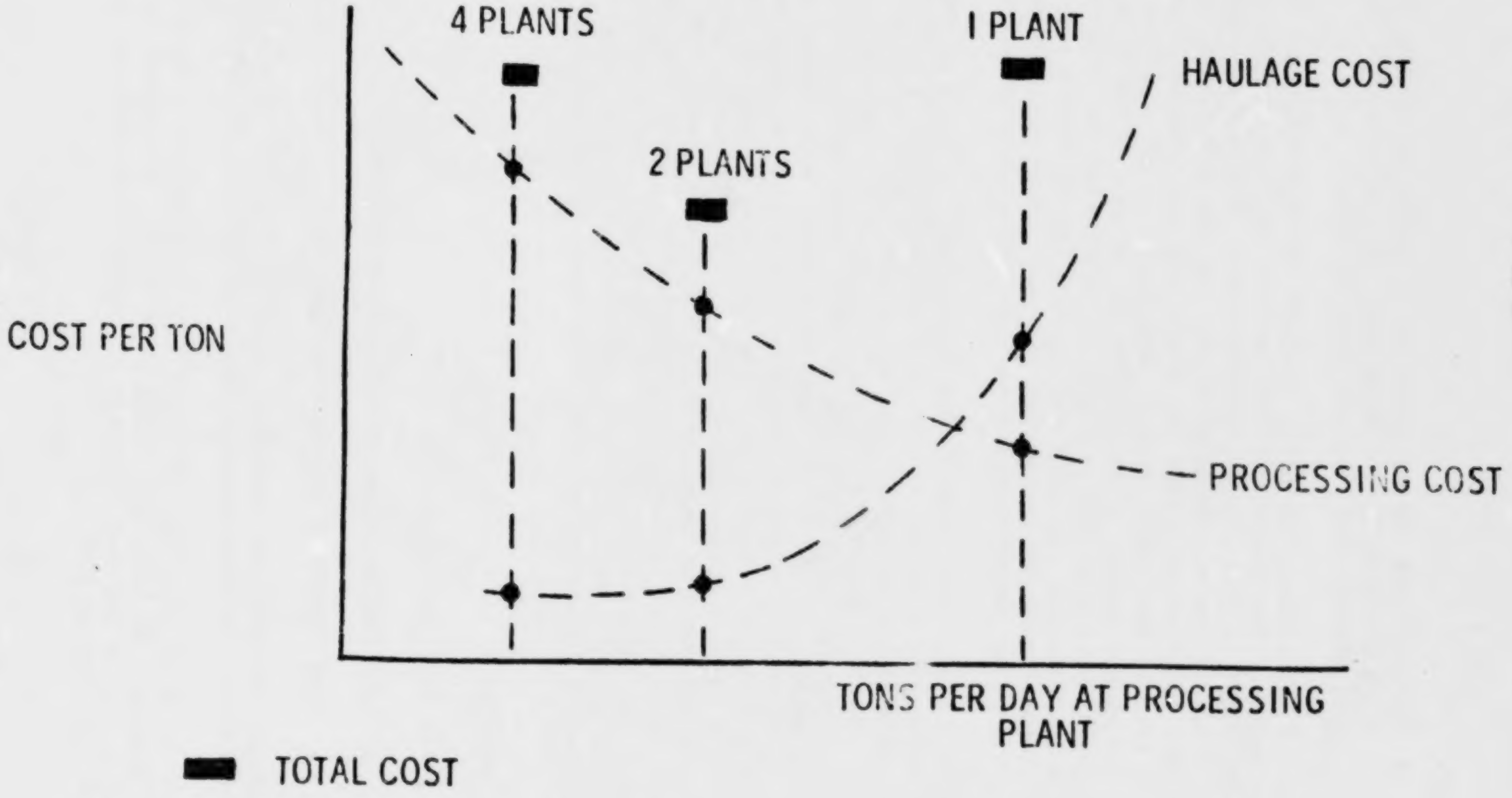

Figure 2

OVERALL DECISION CRITERION

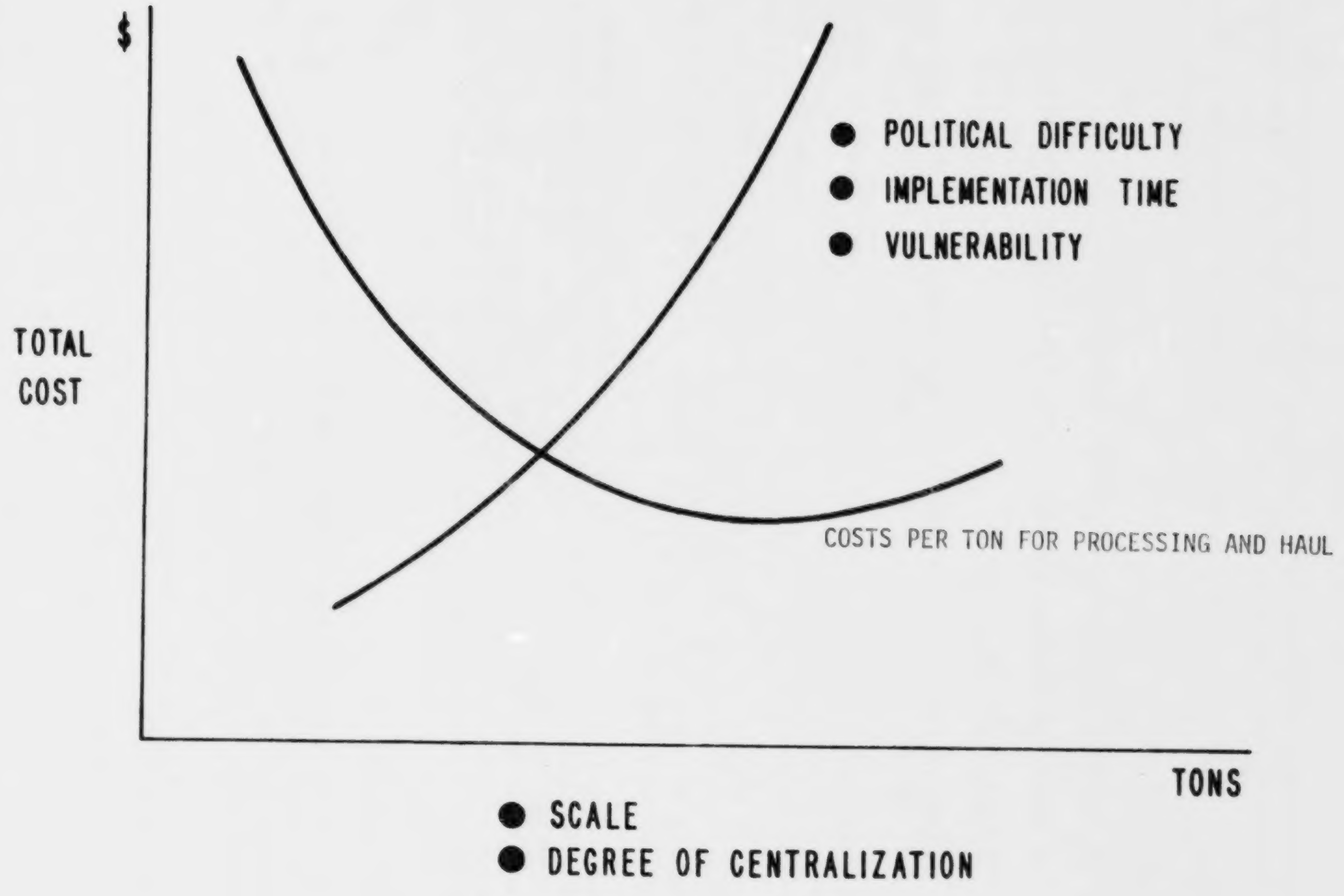

Figure 3

EBB

Figure 4 shows WRAP providing guidance to the decision-maker (the fellow on the right) on site selection, process selection, and other matters.

Figure 5 shows an overview of WRAP. The model will generate a regional plan which is the lowest cost plan which meets all requirements. In the process, it will:

- select sites, from among those offered
- select a process for each site, from among those offered
- size each site, and
- determine all links and flows from sources of waste generation to processing sites, and among processing sites.

The model uses a fixed-charge linear programming algorithm as the optimizer, which permits it to represent economies of scale (total cost curves which increase at a decreasing rate of increase) through linear segmentation, as in Figure 6. Ordinary linear programming encompasses cost functions defined as slopes only. With the use of the fixed charge algorithm (the fixed charges are the vertical intercepts of the cost functions) it becomes possible to represent the typical economy of scale cost function to any level of accuracy desired.

Figure 7 illustrates the levels of processing and allowed linkages in WRAP. Note that there are two levels of transfer station and two levels of secondary processing permitted. The former permits the model to select truck transfer linked to rail transfer. The latter permits more flexible structuring of process alternatives. There can be only one level of primary processing since, by definition, that implies an input of raw refuse and an output of something else.

RAMP Capabilities

RAMP offers a capability to study the saturation of markets and to optimize in the face of it, as illustrated by Figure 8. Note that in WRAP, all markets must be fixed price and unlimited in size. In RAMP, markets may be declining in price, and limited in size.

MODEL APPLICATIONS

The Planning Application

A model application for regional resource recovery planning should do two things: (1) it should help sort out the many variables and identify a minimum cost solution, and (2) it should help illuminate issues through

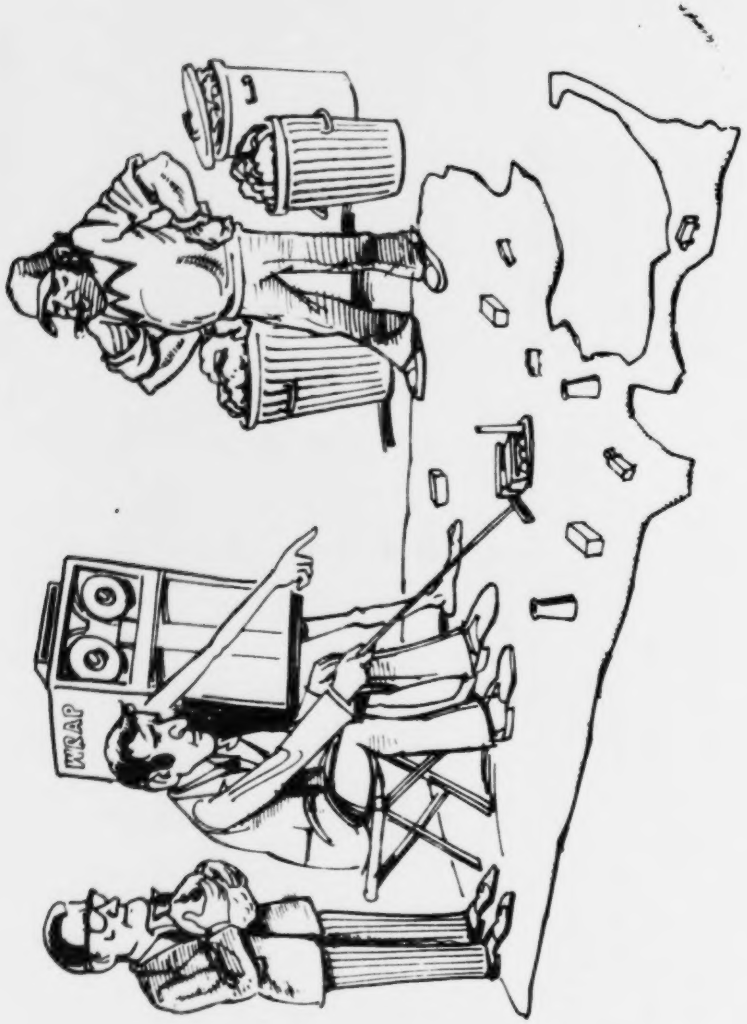

Figure 4

EBB

MODEL OVERVIEW

INPUTS:

ZONES

WASTE AT
EACH CENTROID
LOCATION

PROCESSING SITES

LOCATION
POSSIBLE PROCESSES
COSTS: FIXED + VARIABLE
FLOW COEFFICIENTS
MAX. TONNAGE

DISPOSAL SITES

LOCATION
COSTS: FIXED + VARIABLE
LAND AVAILABLE

LINKS

COSTS: VARIABLE

MODEL:

OPTIMIZER
FIXED CHARGE LINEAR PROGRAMMING MODEL

OUTPUTS:

COMPREHENSIVE REGIONAL SOLID WASTE
MANAGEMENT PLAN

- LOWEST COST
- MEET ALL REQUIREMENTS

BY

SITE SELECTION
TECHNOLOGY SELECTION
SIZING
LINKS AND FLOWS

Figure 5

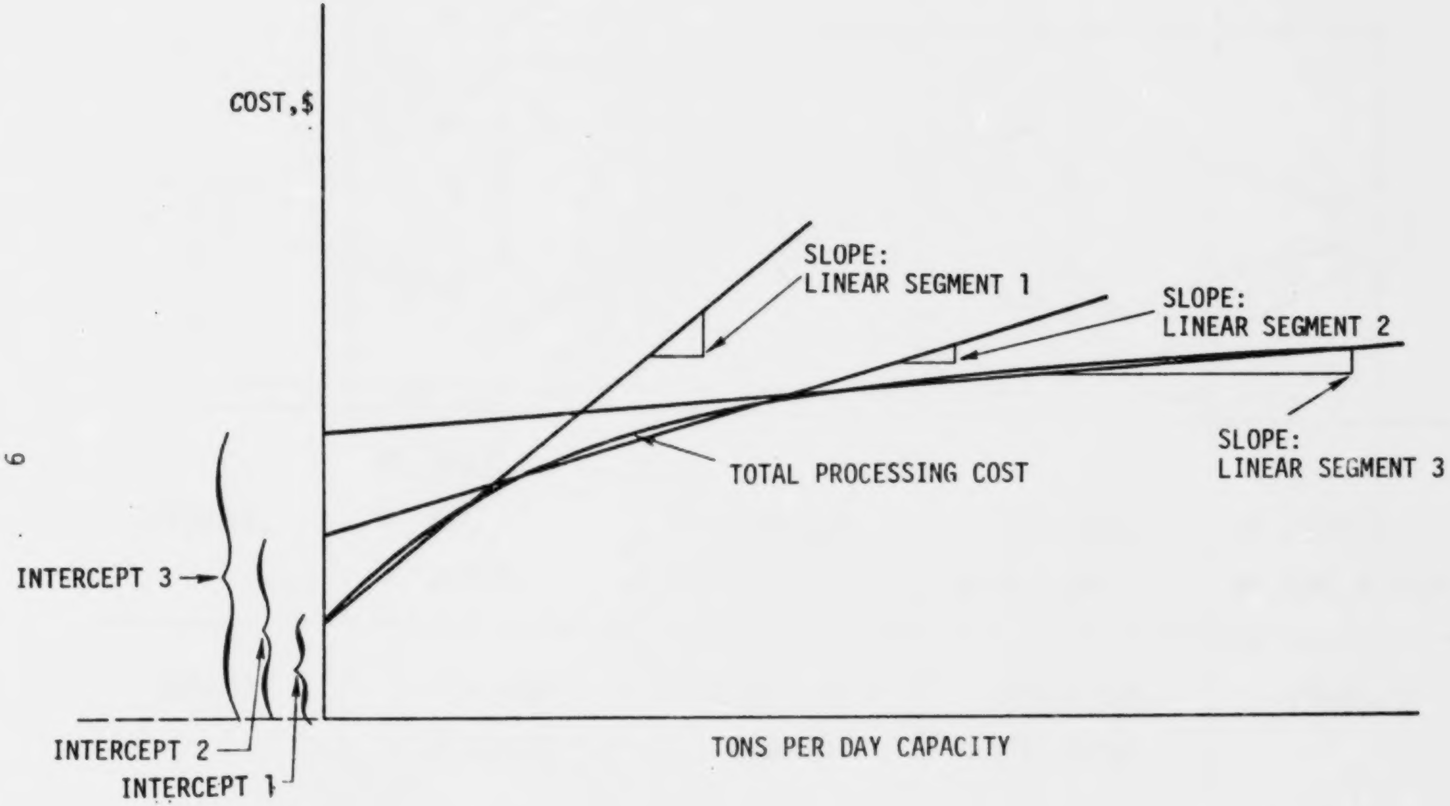
COST,$
SLOPE:
LINEAR SEGMENT 1
SLOPE:
LINEAR SEGMENT 2
SLOPE:
LINEAR SEGMENT 3
TOTAL PROCESSING COST
INTERCEPT 3
INTERCEPT 2
INTERCEPT 1
TONS PER DAY CAPACITY

Figure . Piecewise Linear Approximation of a Concave Function
(Representing Economies of Scale)

Figure 6

LEVELS OF PROCESSING PERMITTED

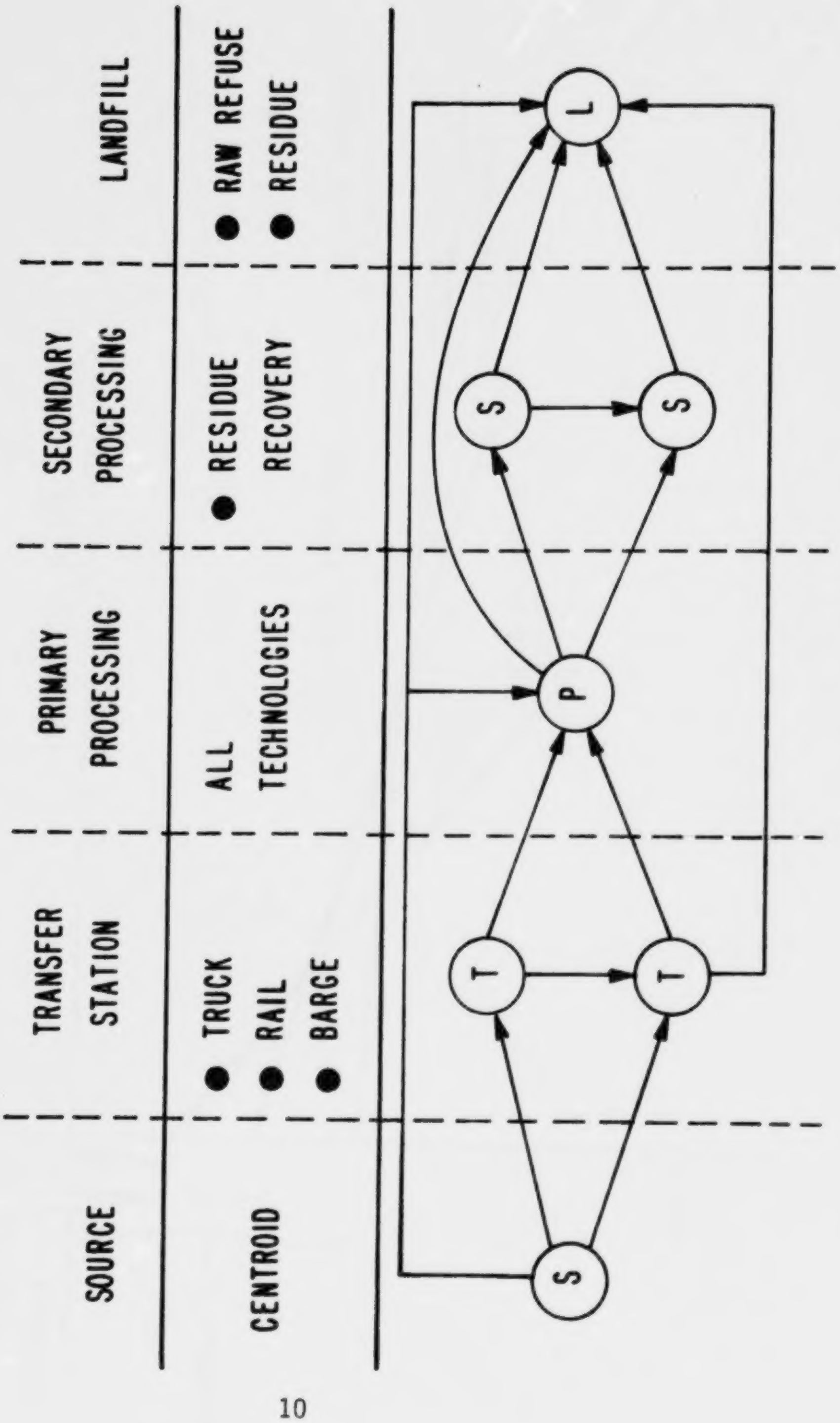
SOURCE
CENTROID
TRANSFER STATION
● TRUCK
● RAIL
● BARGE
PRIMARY PROCESSING
ALL TECHNOLOGIES
SECONDARY PROCESSING
● RESIDUE RECOVERY
LANDFILL
● RAW REFUSE
● RESIDUE
S
T
T
P
S
S
L

Figure 7

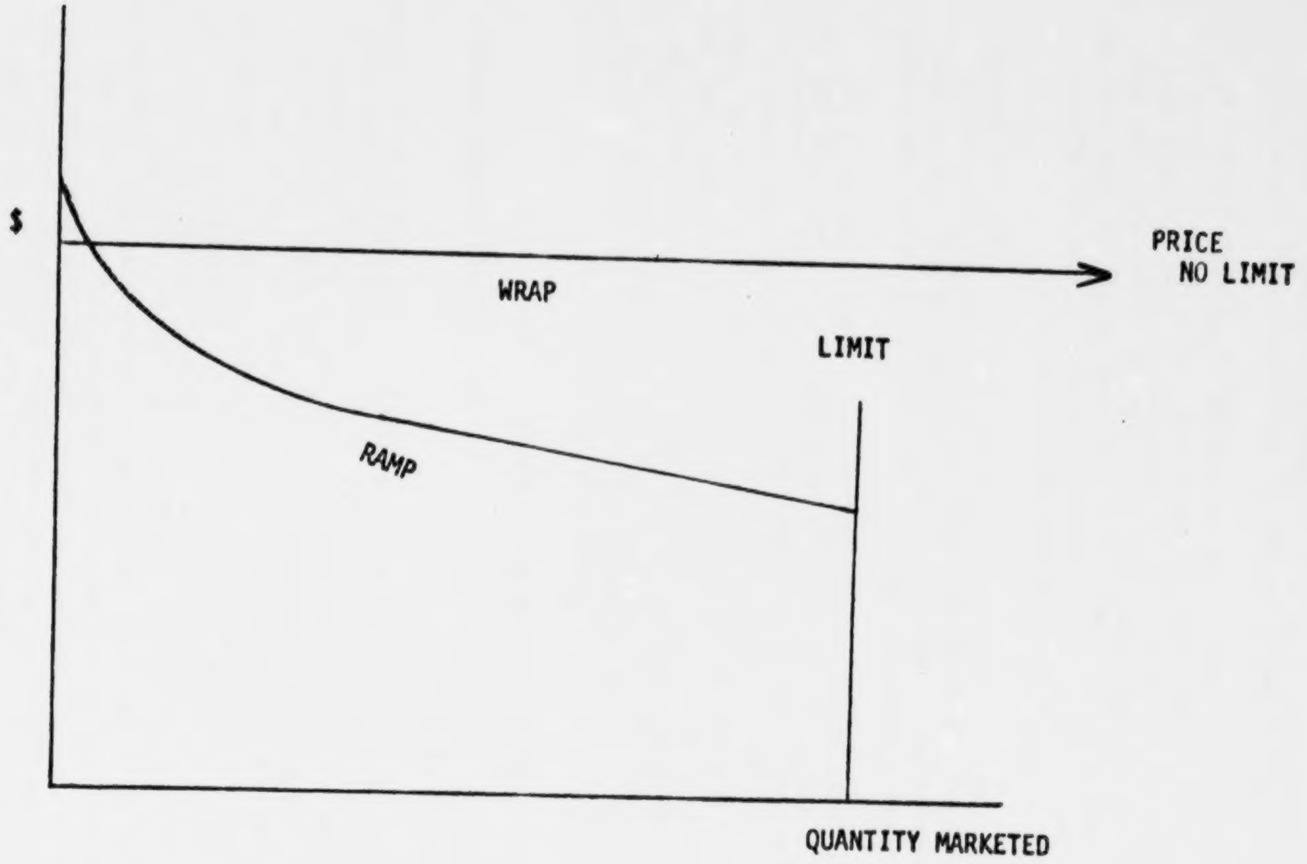

MARKETING IN WRAP AND RAMP

Figure 8

answering what-if questions. Figure 9 illustrates a number of what-if questions that have been answered in earlier applications of the model.

In illuminating issues, an application consisting of several "cases" is defined, and the model is run once for each case. Each case defines a particular situation of interest. It is important to note the fact that the model defines the minimum cost structure and the system cost for each case, so that in comparing the costs of two or more cases, we know that we are dealing with a meaningful cost difference -- none of the difference can be ascribed to a "poor" solution for one of the cases.

The model run for each case finds a solution which will handle all wastes, meet all environmental standards and meet the defined state of political acceptability represented by the case. Thus the incremental cost of moving from case to case represents the cost of easing a political constraint.

Figure 10 illustrates a hypothetical application. The economically preferred solution is shown on the left, representing the minimum cost way of handling the wastes and meeting environmental and other real constraints, such as tonnage and traffic limits. Each step to the right represents easing a political constraint, by abandoning a controversial site, or abandoning a controversial process, or opting for a politically easier regional structure, etc. The model defines the incremental cost of each such step, and in so doing, clarifies the importance of the political issue for all sides of the argument. It is hoped that this clarification of the incremental cost involved in an issue would help resolve it.

The Eastern Massachusetts Planning Application

Figure 11 illustrates the system costs per ton in a recent Eastern Massachusetts application of RAMP.

Since fixed-charge linear programming is a difficult kind of model to handle, it was not until run C that the base case, or economically preferred solution, was obtained. In run D, the ECOFUEL II process, with questionable markets for its products, was dropped. In run D, the model selected an incineration/steam/electric power option at one site, in lieu of the ECOFUEL II process at two sites which had been selected in run C. The system cost increased as illustrated in Figure 11. In run E, the Haverhill site, which has been subject to major planning as a primary processing site, and which turned up in runs A through D with only a transfer station, was forced into the solution for 2,880 tons per day of primary processing, representing the 53 communities included in the plan. The model elected to use that site for 11,000 tons per day of processing, using the Incineration/steam/electric power process. (The ECOFUEL II process was again introduced into this and succeeding runs, but with a limited market; it was not selected in runs E or F.) Since the City of Haverhill had in fact approved only 3,000 tons per day, an upper bound at that limit was entered into run F, and the model

ILLUMINATION OF ISSUES

WHAT-IF QUESTIONS:

WHAT-IF THE REGION SIZE IS --- ?
ST. LOUIS : STATE - BY - STATE
MASS : LARGE vs SMALL REGION

WHAT-IF A KEY PROCESS NOT AVAILABLE ?
FOR POLITICAL REASONS --- LANDFILL
FOR TECHNICAL REASONS --- GAS PYROLYSIS

WHAT-IF A KEY SITE NOT AVAILABLE ?
IT IS WORTH ________ TO FIGHT FOR THE SITE

WHAT-IF A KEY MARKET NOT AVAILABLE ?

WHAT-IF THERE ARE ESTIMATION ERRORS ?
TONNAGE ---MARKET PRICES---PROCESS COSTS ?

RESULT:-----COST------ STRUCTURE

Figure 9

THE PLAN SET

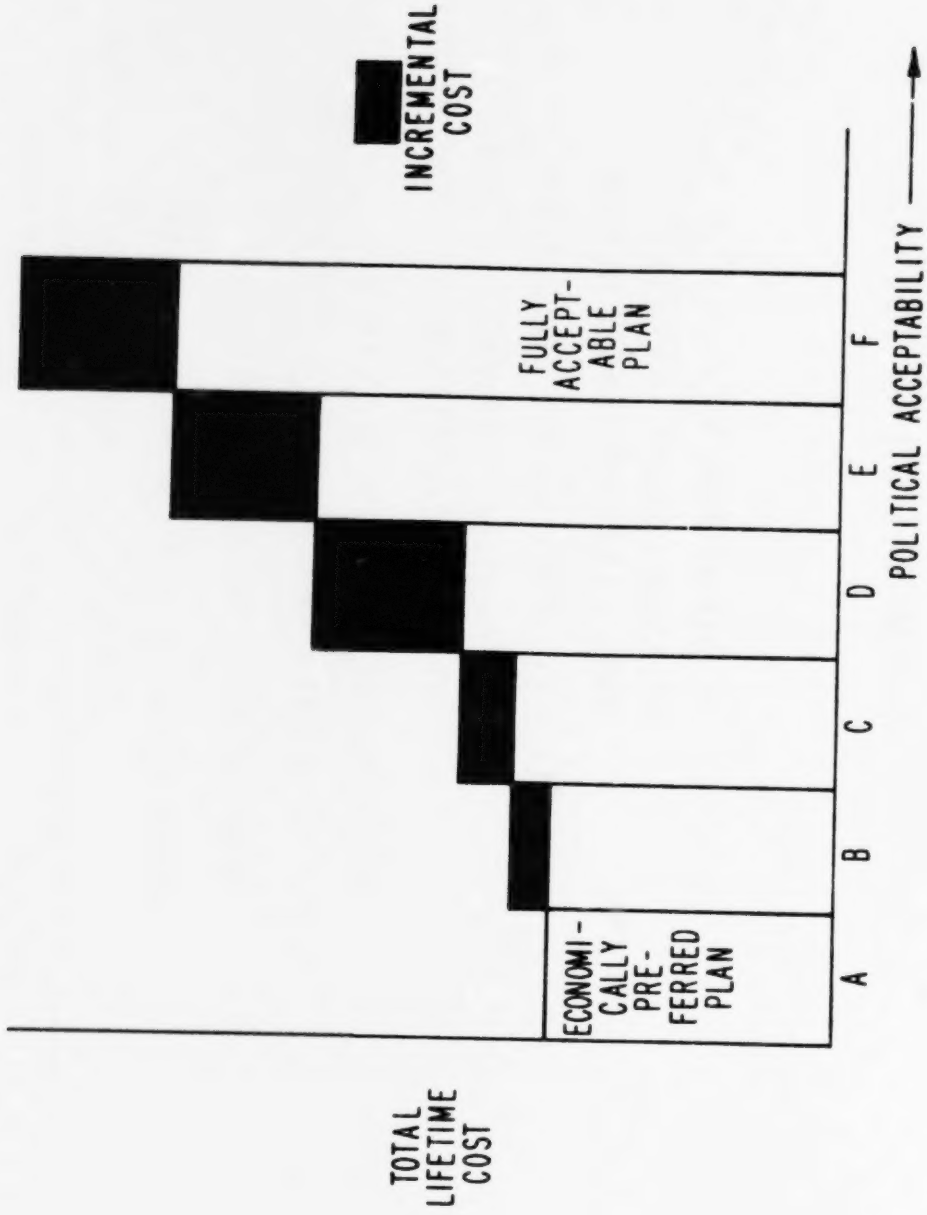

Figure 10

EBB

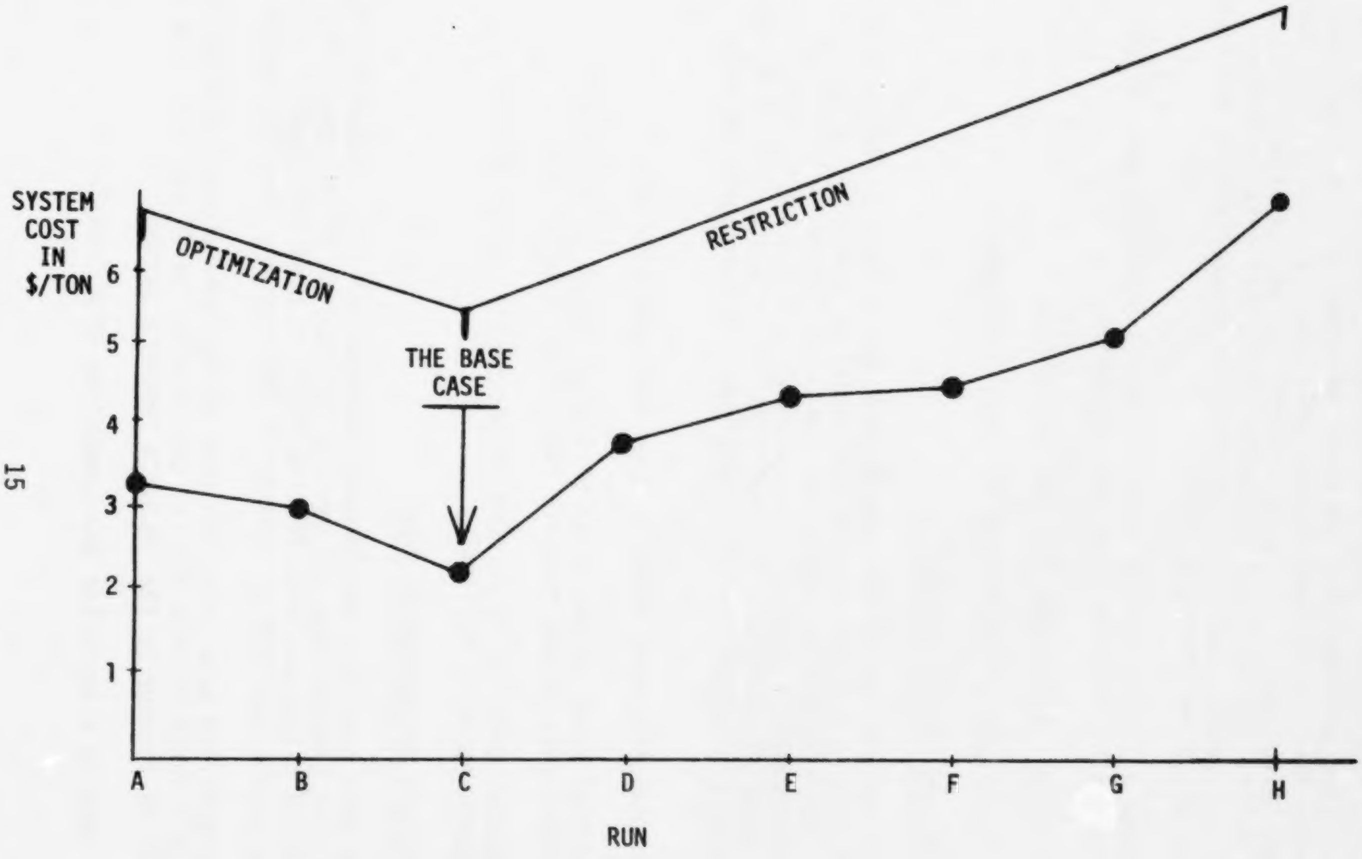

COST SUMMARY: EASTERN MASS. REGION RUNS

Figure 11

rerun. The model chose to allocate 3,000 tons per day to Haverhill (the upper limit rather than the lower limit) and selected a site on Route 128 near the Waltham/Weston line for 8,000 tons per day. In run G, we forced 379 tons per day, representing long-term contracts, into an existing ECO-FUEL II site at East Bridgewater. The model selected to divert just that amount of tonnage from the Waltham/Weston site, leaving roughly 7,600 tons per day at that latter site. In run H, a 3,000 ton per day limit was placed on all sites, and the model picked an additional site in Boston. Note that the incremental cost of this constraint (essentially a political constraint) was $1.80 per ton system-wide.

All runs included a lock-in of 712 tons per day at RESCO, Saugus, Massachusetts, representing existing long-term contracts.

Figure 12 and Table I illustrate the run G solution.

Table II displays summary information for runs C through H.

USING THE MODEL FOR POLICY EVALUATION

The RAMP model was run, using the same Eastern Massachusetts region previously studied, plus a new three-state region called INOKY (Indiana, Ohio, Kentucky), to evaluate policy issues for the U. S. Congress, Office of Technology Assessment, as part of an assessment on resource recovery, recycling, and reuse of materials from municipal solid waste. The runs described below will be documented in a supplement to the report on that assessment.

The effects of two different kinds of subsidies were studied:

1. a subsidy equal to the value of ferrous scrap in the market (assumed paid to the resource recovery processor) and
2. a capital grant of 75 percent of the capital costs of new resource recovery facilities.

Summary of Eastern Massachusetts Runs

In Run 1, the base case, the Non-Recovery Alternative (i.e., landfill) was offered at a cost ranging from $20 per ton (Boston) to $7 per ton. This represented MITRE's best estimate for the costs of haul and landfill processing. The result was 100% of tonnage in the resource recovery system.

In Run 2, the modified base case, the cost of the Non-Recovery Alternative was lowered to a range of from $12 per ton (Boston) to $2 per ton. The result was 95.1% of tonnage in the resource recovery system.

This run was used as a basis for the comparison with runs 3-6.

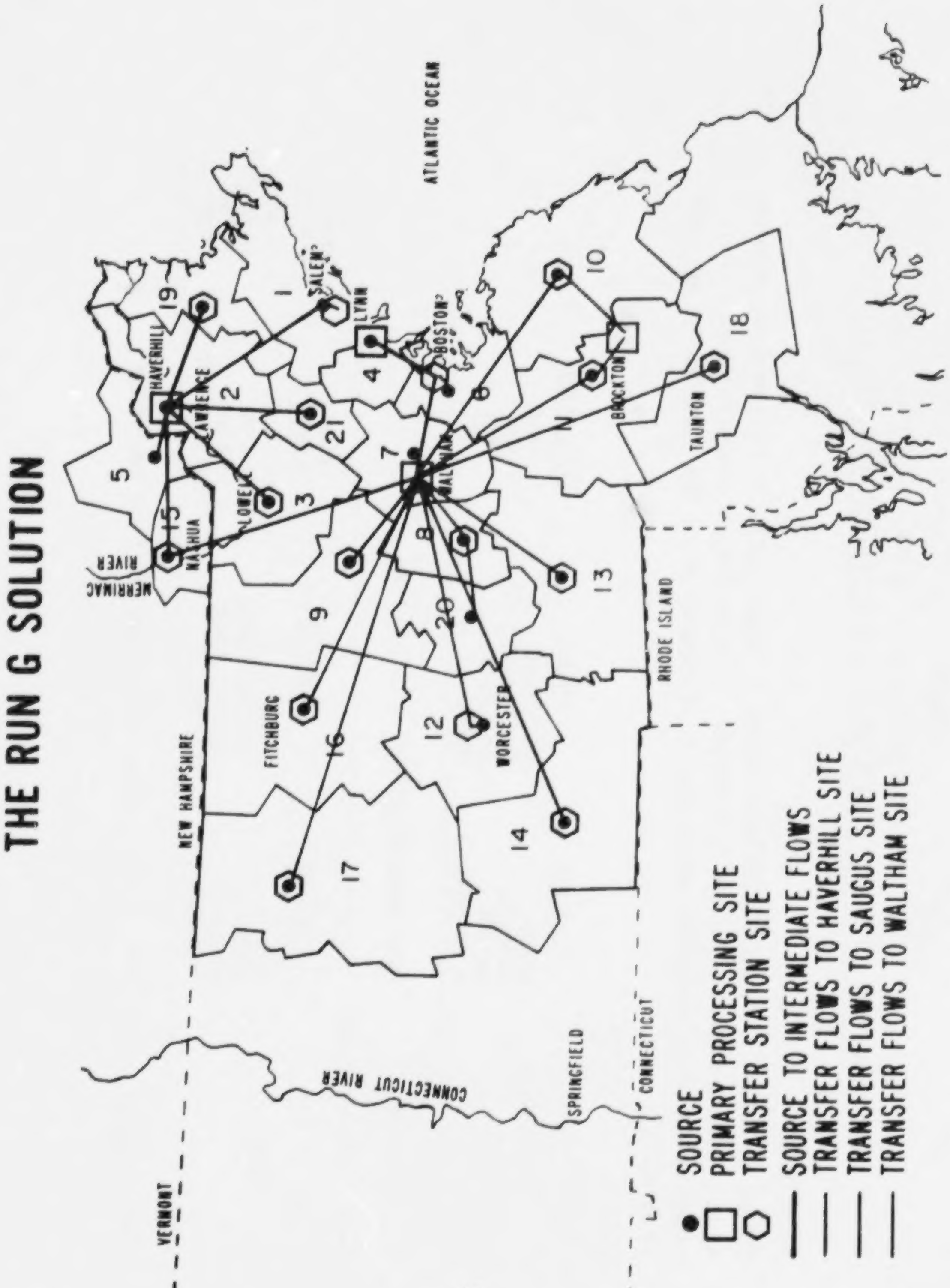
THE RUN G SOLUTION
ATLANTIC OCEAN
NEW HAMPSHIRE
VERMONT
CONNECTICUT
RHODE ISLAND
MERRIMAC RIVER
CONNECTICUT RIVER
SPRINGFIELD
FITCHBURG
WORCESTER
NASHUA
LOWELL
LAWRENCE
HAVERHILL
SALEM
LYNN
BOSTON
WALTHAM
BROCKTON
TAUNTON
1
2
3
4
5
6
7
8
9
10
11
12
13
14
15
16
17
18
19
20
21
SOURCE
PRIMARY PROCESSING SITE
TRANSFER STATION SITE
SOURCE TO INTERMEDIATE FLOWS
TRANSFER FLOWS TO HAVERHILL SITE
TRANSFER FLOWS TO SAUGUS SITE
TRANSFER FLOWS TO WALTHAM SITE

Figure 12

Table I

RUN NARRATIVE: RUN G

LOCK IN E. BRIDGEWATER COMMUNITIES

ASSUMPTIONS:

ECOFUEL II PROCESS AT E. BRIDGEWATER ONLY; ECOFUEL II MARKET LIMITED AT $1.40/MBTU AND UNLIMITED AT 40¢/ MBTU; 53 COMMUNITIES LOCKED IN AT HAVERHILL AT 2,880 TPD; 10 COMMUNITIES LOCKED IN AT SAUGUS AT 712 TPD; 5 COMMUNITIES LOCKED IN AT E. BRIDGEWATER AT 379 TPD; 3,000 TON PER DAY LIMIT AT HAVERHILL

SOLUTION:

	LOCATION	PROCESS	LEVEL (TPD)
PROCESSING:	SAUGUS	INCIN/STEAM	1200
	HAVERHILL	INCIN/ELECT	3000
	WALTHAM	INCIN/ELECT	7613
	E. BRIDGEWATER	ECOFUEL II	379

TRANSFER: TRUCK TRANSFER STATIONS AT 21 LOCATIONS

	LOCATION	COMMODITY	ANNUAL QUANTITY	ANNUAL VALUE $M
MARKETS:	LYNN	STEAM	2.05 B LBS	4.65
	HAVERHILL	ELECTRIC POWER	0.52 BKWH	10.40
	WALTHAM	ELECTRIC POWER	1.33 BKWH	26.60
	FITCHBURG	ECOFUEL II	9.22×10^{11} BTU	1.29

SYSTEM SUMMARY ANNUAL COST: $19.9M / ANNUAL TONS: 3.8M / COST PER TON: $5.24

Table II

SUMMARY OF EASTERN MASSACHUSETTS REGION RUNS

[10 SAUGUS COMMUNITIES LOCKED IN AT 712 TPD IN ALL RUNS]

RUNS A-C: BASE CASE (RUN C WAS FIRST OPTIMIZING RUN)		
SPECIAL ASSUMPTIONS:	UNLIMITED ECOFUEL II MARKET	RESULTS: (RUN C) SAUGUS (INCIN/STEAM) AT 1200 TPD LOWELL (ECOFUEL II) AT 5421 TPD BOSTON (ECOFUEL II) AT 5571 TPD
	SYSTEM COST: $2.25 PER TON	
RUN D: ELIMINATE ECOFUEL II FROM ALL SITES		
SPECIAL ASSUMPTIONS:	NONE	RESULTS: SAUGUS (INCIN/STEAM) AT 6081 TPD LOWELL (INCIN/ELECT) AT 6110 TPD
	SYSTEM COST: $3.94 PER TON	
RUN E: LOCK IN HAVERHILL COMMUNITIES		
SPECIAL ASSUMPTIONS:	53 HAVERHILL COMMUNITIES LOCKED IN AT 2,880 TPD ECOFUEL II AT E. BRIDGEWATER ONLY LIMITED ECOFUEL II MARKET	RESULTS: SAUGUS (INCIN/STEAM) AT 1,200 TPD HAVERHILL (INCIN/ELECT) AT 10,992 TPD
	SYSTEM COST: $4.50 PER TON	
RUN F: TONNAGE LIMIT AT HAVERHILL		
SPECIAL ASSUMPTIONS:	53 HAVERHILL COMMUNITIES LOCKED IN AT 2,880 TPD TONNAGE LIMIT AT HAVERHILL AT 3,000 TPD ECOFUEL II AT E. BRIDGEWATER ONLY LIMITED ECOFUEL II MARKET	RESULTS: SAUGUS (INCIN/STEAM) AT 1,200 TPD HAVERHILL (INCIN/ELECT) AT 3,000 TPD WALTHAM (INCIN/ELECT) AT 7,992 TPD
	SYSTEM COST: $4.62 PER TON	
RUN G: LOCK IN E. BRIDGEWATER COMMUNITIES		
SPECIAL ASSUMPTIONS:	53 HAVERHILL COMMUNITIES LOCKED IN AT 2,880 TPD TONNAGE LIMIT AT HAVERHILL AT 3,000 TPD 5 E. BRIDGEWATER COMMUNITIES LOCKED IN AT 379 TPD ECOFUEL II AT E. BRIDGEWATER ONLY LIMITED ECOFUEL II MARKET	RESULTS: SAUGUS (INCIN/STEAM) AT 1,200 TPD HAVERHILL (INCIN/ELECT) AT 3,000 TPD WALTHAM (INCIN/ELECT) AT 7,613 TPD E. BRIDGEWATER (ECOFUEL II) AT 379 TPD
	SYSTEM COST: $5.24 PER TON	
RUN H: 3000 TPD LIMIT AT ALL SITES		
SPECIAL ASSUMPTIONS:	53 HAVERHILL COMMUNITIES LOCKED IN AT 2,880 TPD 5 E. BRIDGEWATER COMMUNITIES LOCKED IN AT 379 TPD ECOFUEL II AT E. BRIDGEWATER ONLY LIMITED ECOFUEL II MARKET TONNAGE LIMIT AT ALL SITES AT 3,000 TPD	RESULTS: SAUGUS (INCIN/STEAM) AT 2,768 TPD HAVERHILL (INCIN/ELECT) AT 3,000 TPD WALTHAM (INCIN/ELECT) AT 3,000 TPD E. BRIDGEWATER (ECOFUEL II) AT 423 TPD BOSTON (INCIN/ELECT) AT 3,000 TPD
	SYSTEM COST: $7.03 PER TON	

In run 3, the equivalent of the market value of ferrous scrap was assumed to have been paid as a subsidy directly to the resource recovery processor. The result was 96.1% of tonnage in the resource recovery system.

In Run 4, capital costs of new resource recovery systems were assumed to be subsidized to the extent of seventy-five percent of system capital costs. The result was 98.3% of tonnage in the resource recovery system.

In Run 5, a smaller region size was simulated by applying a 2,000 ton per day limit at all sites. The result was 36.1% of tonnage in the resource recovery system.

In Run 6, a smaller region size with a better shredded fuel market was simulated. The 2,000 TPD limit at all sites was repeated, but with the addition of an improved market for shredded fuel, and with the offering of a shredded fuel process (ECOFUEL II) at more locations. The result was 52.5% of tonnage in the resource recovery system.

Table III presents a statistical summary of the six policy evaluation runs in Eastern Massachusetts.

Summary of INOKY Runs

The general structure of the series of seven INOKY runs is shown in Figure 13. In all runs the same alternatives were offered for processing technologies and locations, and for transportation linkages. Runs 1 to 3 differed from 4 to 7 in the lower non-recovery alternative (NRA) costs for the latter.

Run 1 is the base case for all runs, from which the effects of a ferrous scrap subsidy (run 2) and a capital subsidy (run 3) were studied. The subsidies were defined as in the Eastern Massachusetts runs. The percentages of INOKY tonnage in resource recovery were 92.0 in run 1, 97.4 in run 2, and 95.0 in run 3.

Since runs 1, 2, and 3 had all generated strong resource recovery solutions, the NRA was made more attractive in run 4 (decreased by $2 per ton in all zones) to evaluate how robust the resource recovery solution was. Run 4 generated a solution with 81.6 percent of all tonnage in resource recovery.

Run 5 introduced a 2,000 ton-per-day limit at all sites to simulate the inability to form regions of the size generated in runs 1 through 4, for any of a number of reasons ranging from the difficulty in achieving political consensus in a large region to the non-availability of technical planning support. Run 5, using the favorable landfill prices of run 4, generated a 69.3 percent resource recovery solution. Run 5 then was used as a base case to evaluate again the effects of a ferrous scrap subsidy (run 6) and a capital subsidy (run 7). In run 6, 84.2 percent of the tonnage went into resource recovery, and in run 7 76.8 percent of the tonnage was so allocated.

Table III

Policy Evaluation Runs in Eastern Massachusetts

STATISTICAL SUMMARY OF RUNS (Annual Flows and Costs)
Total for Region: 3,803,700 tons

	RUN					
	1	2	3	4	5	6
System Cost (million dollars)	12.0	11.4	7.4	-5.7	23.2	16.2
System Cost Per Ton (dollars)	3.15	3.01	1.96	-1.49	6.09	4.26
Tons in Resource Recovery (thousand tons)	3804	3619	3656	3739	1372	1996
Percent in Resource Recovery	100.0	95.1	96.1	98.3	36.1	52.5
Unincinerated Ferrous (thousand tons)	8.3	8.3	13.5	8.3	26.2	113.6
Incinerated Ferrous (thousand tons)	258.0	245.0	242.4	253.5	69.9	26.2
Electric Power (million KWH)	18154	1751	1729	1818	349	0
ECOFUEL II (BTU x 10^{10})	96	96	157	96	303	1314
Steam (billion lbs)	2.05	2.05	2.05	2.05	2.05	2.05
Cost of Subsidy Per Year (million dollars)	NA	NA	4.1*	17.3	NA	NA
One-Time Cost of Subsidy (million dollars)	NA	NA	NA	176.8	NA	NA
Cost of Subsidy Per Incremental Ton in Resource Recovery (dollars)	NA	NA	112*	144	NA	NA
Cost of Subsidy Per Incremental Ton of Ferrous (dollars)	NA	NA	1595*	2059	NA	NA
Cost of Subsidy Per Ton of Ferrous Converted to Unincinerated Form (dollars)	NA	NA	1525*	∞	NA	NA

*Only the portion of the ferrous market subsidy cost which flows to the resource recovery system is considered.

STRUCTURE OF INOKY RUNS

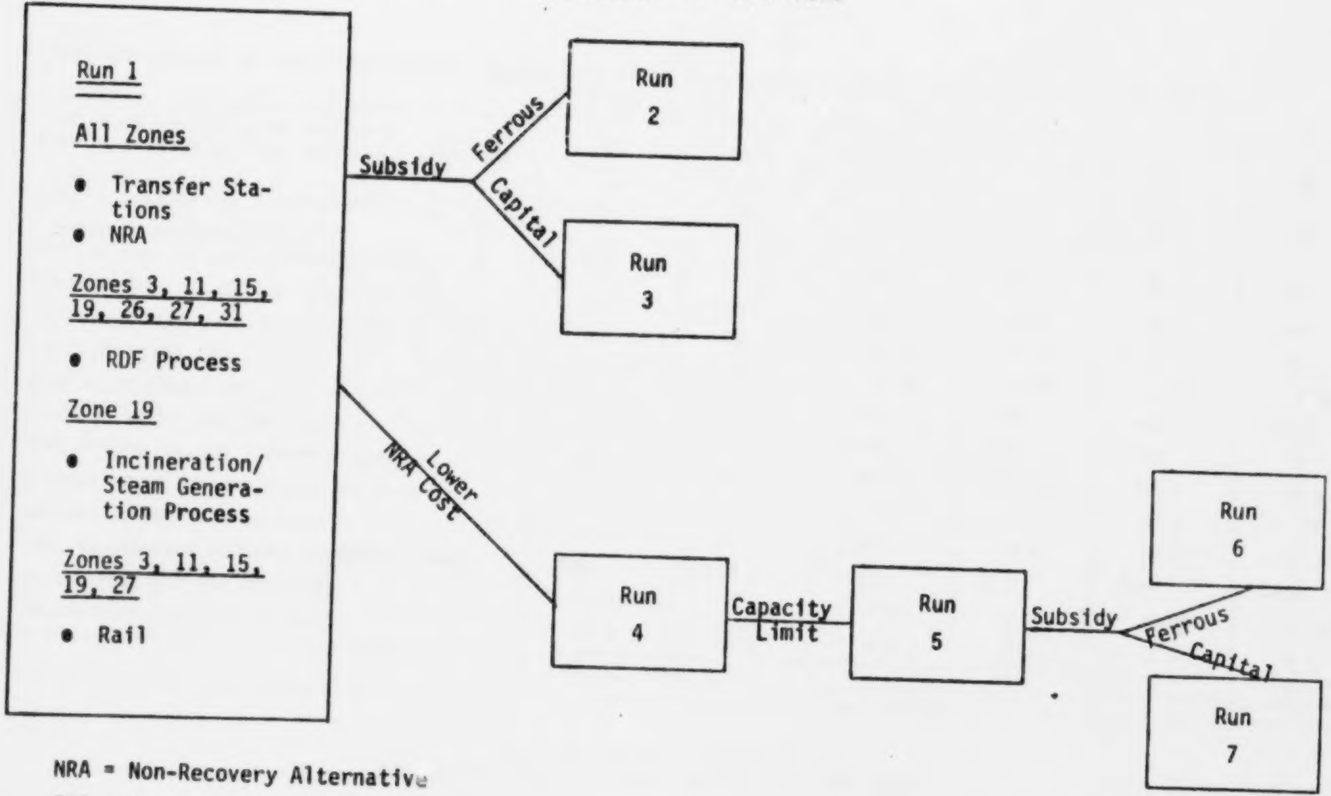
Run 1
All Zones
• Transfer Stations
• NRA
Zones 3, 11, 15, 19, 26, 27, 31
• RDF Process
Zone 19
• Incineration/Steam Generation Process
Zones 3, 11, 15, 19, 27
• Rail
Subsidy
Ferrous
Capital
Run 2
Run 3
Lower NRA Cost
Run 4
Capacity Limit
Run 5
Subsidy
Ferrous
Capital
Run 6
Run 7

NRA = Non-Recovery Alternative

RDF = Refuse-Derived Fuel

Figure 13

Table IV presents a statistical summary of the INOKY runs; Table V presents the structures of solutions of those runs, and Figure 14 displays the structure of the base case (run 1).

Analysis of Policy Runs

In should be noted that the resource recovery system appears viable in both the Eastern Massachusetts and INOKY regions without subsidy, if the economies of scale, which appear to be available from centralized processing, are not barred by political considerations or by an insufficiency of planning capability.

Subsidy or resource recovery in both regions would be expensive, partly because so much of it would be "windfall" (that is, would lower the cost of resource recovery which would take place anyways). Subsidy in both regions would also ineffective for the reason that there is little room for improvement.

CONCLUSION

We are convinced as a result of these runs that the selection of the correct region size is an important adjunct of regional resource recovery planning, and can influence the viability of resource recovery considerably.

Table IV

POLICY EVALUATION RUNS IN INOKY
STATISTICAL SUMMARY OF RUNS (ANNUAL FLOWS AND COSTS)
TOTAL FOR REGION: 4,709,400 TONS PER YEAR

	Runs						
	1	2	3	4	5	6	7
System Cost	-$9,636,363	-$17,917,332	-$17,391,648	-$10,960,652	-$7,226,758	-$13,923,315	-$15,959,875
System Cost Per Ton	-$2.05	-$3.80	-$3.69	-$2.33	-$1.53	-$2.96	-$3.39
Tons in Resource Recovery	4,331,200	4,585,800	4,473,600	3,841,000	3,263,100	3,965,300	3,615,400
Percent in Resource Recovery	92.0	97.4	95.0	81.6	69.3	84.2	76.8
Unincinerated Ferrous (Thousand Tons)	290.0	307.9	298.4	255.7	215.3	264.4	238.3
Incinerated Ferrous (Thousand Tons)	13.1	13.1	14.7	13.1	13.1	13.1	14.7
Aluminum (Thousand Tons)	20.7	22.0	21.3	18.3	15.4	18.9	17.0
Glass (Thousand Tons)	487.7	517.6	501.7	430.0	362.0	444.6	400.7
Electric Power	00.0	00.0	00.0	00.0	00.0	00.0	00.0
Steam (Million Pounds)	1,029	1,029	1,155	1,029	1,029	1,029	1,155
Refuse-Derived Fuel (BTU x 10^9)	29,002.4	30,786.0	29,840.3	25,573.1	21,527.1	26,441.8	23,831.4
Cost of Subsidy Per Year (Million Dollars)	NA	8.556	8.376	NA	NA	7.371	9.753
One-Time Cost of Subsidy (Million Dollars)	NA	NA	85.4	NA	NA	NA	99.4
Cost of Subsidy Per Incremental Ton in Resource Recovery (Dollars)	NA	33.58	58.74	NA	NA	10.50	27.70
Cost of Subsidy Per Incremental Ton of Ferrous (Dollars)	NA	479.7	839.1	NA	NA	150.0	395.7

Table V

SOLUTION STRUCTURES OF POLICY EVALUATION RUNS IN INOKY

	Run 1 (Base Case)	Run 2 (Ferrous Subsidy)	Run 3 (Capital Subsidy)	Run 4 (Decreased NRA)	Run 5 (Decreased NRA, Capacity Limit)	Run 6 (Ferrous Subsidy Decreased NRA Capacity Limit)	Run 7 (Capital Subsidy, Decreased NRA, Capacity Limit)
Processing **501 (Anderson)** Annual Tonnage Daily Tonnage Process	(Truck Transfer Station)		420,700 1,348 RDF-Seg. 2	(Truck Transfer Station)	280,100 898 RDF-Seg. 2	Same as Run 3	Same as Run 5
503 (Indianapolis) Annual Tonnage Daily Tonnage Process	1,346,200 4,315 RDF-Seg. 3	Same as Base Case	925,500 2,966 RDF-Seg. 2	1,310,400 4,199 RDF-Seg. 3	624,000 2,000 RDF-Seg. 2	A: 406,300 1,302 RDF-Seg. 2 B: 624,000 2,000 RDF-Seg. 2	A: 624,000 2,000 RDF-Seg. 2 B: 163,500 524 RDF-Seg. 1
511 (Cincinnati) Annual Tonnage Daily Tonnage Process	1,311,600 4,204 RDF-Seg. 3	1,331,000 4,266 RDF-Seg. 3	Same as Run 2	1,237,300 3,966 RDF-Seg. 3	A: 613,300 1,966 RDF-Seg. 2 B: 624,000 2,000 RDF-Seg. 2	A: 624,000 2,000 RDF-Seg. 2 B: 624,000 2,000 RDF-Seg. 2	Same as Run 5
515 (Louisville) Annual Tonnage Daily Tonnage Process	1,094,100 3,507 RDF-Seg. 3	1,260,400 4,040 RDF-Seg. 3	1,120,300 3,591 RDF-Seg. 3	795,700 2,550 RDF-Seg. 2	624,000 2,000 RDF-Seg. 2	Same as Run 5	A: 624,000 2,000 RDF-Seg. 2 B: 91,600 294 RDF-Seg. 1
519 (Lexington) Annual Tonnage Daily Tonnage Process	187,800 602 Inc./Steam-Seg. 1	Same as Base Case	210,700 675 Inc./Steam-Seg. 1	Same as Base Case	Same as Base Case	Same as Base Case	Same as Run 3
526 (Owensboro) Annual Tonnage Daily Tonnage Process	(Truck Transfer Station Process 901 in all runs)						
527 (Evansville) Annual Tonnage Daily Tonnage Process	391,300 1,254 RDF-Seg. 2	460,400 1,476 RDF-Seg. 2	Same as Base Case	309,900 993 RDF-Seg. 2	Same as Run 4	454,400 1,456 RDF-Seg. 2	Same as Run 4
531 (Bowling Green) Annual Tonnage Daily Tonnage Process	(Truck Transfer Station)		74,100 238 RDF-Seg. 1	(Truck Transfer Station)			Same as Run 3
NRA Annual Tonnage Daily Tonnage	378,4001 1,213	123,600 396	235,800 756	868,300 2,783	1,446,300 4,636	744,200 2,385	1,094,200 3,507

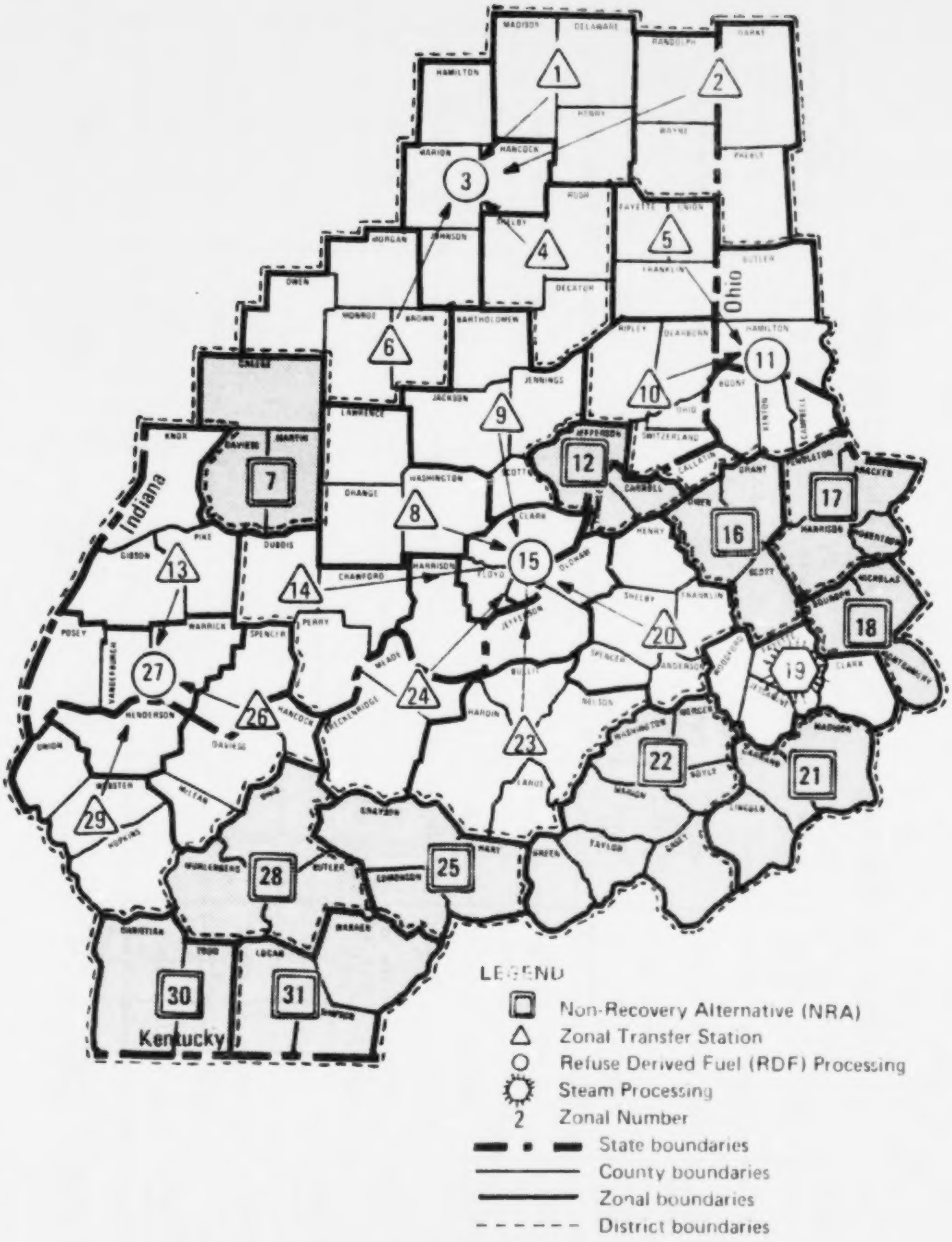
Indiana
Ohio
Kentucky
1
2
3
4
5
6
7
8
9
10
11
12
13
14
15
16
17
18
19
20
21
22
23
24
25
26
27
28
29
30
31
MADISON
DELAWARE
RANDOLPH
DARKE
HAMILTON
HENRY
WAYNE
PREBLE
MARION
HANCOCK
RUSH
FAYETTE
UNION
SHELBY
MORGAN
JOHNSON
BUTLER
FRANKLIN
DECATUR
OWEN
MONROE
BROWN
BARTHOLOMEW
RIPLEY
DEARBORN
GREENE
JENNINGS
BOONE
LAWRENCE
JACKSON
OHIO
SWITZERLAND
KNOX
DAVIESS
MARTIN
JEFFERSON
KENTON
CAMPBELL
GALLATIN
GRANT
PENDLETON
BRACKEN
ORANGE
WASHINGTON
SCOTT
CARROLL
HARRISON
CLARK
PIKE
GIBSON
DUBOIS
CRAWFORD
FLOYD
OLDHAM
SHELBY
FRANKLIN
NICHOLAS
BOURBON
POSEY
WARRICK
SPENCER
PERRY
MEADE
ANDERSON
WOODFORD
FAYETTE
JESSAMINE
CLARK
MONTGOMERY
VANDERBURGH
HENDERSON
HANCOCK
BRECKINRIDGE
BULLITT
NELSON
MERCER
MADISON
HARDIN
DAVIESS
UNION
WEBSTER
MCLEAN
LARUE
BOYLE
MARION
LINCOLN
HOPKINS
GRAYSON
HART
GREEN
TAYLOR
CASEY
MUHLENBERG
BUTLER
EDMONSON
CHRISTIAN
TODD
LOGAN
WARREN
SIMPSON
LEGEND
Non-Recovery Alternative (NRA)
Zonal Transfer Station
Refuse Derived Fuel (RDF) Processing
Steam Processing
2 Zonal Number
State boundaries
County boundaries
Zonal boundaries
District boundaries

Structure of the Base Case (Run 1)

Figure 14

11-45-15

V-A-29

SELECTION OF ALTERNATIVE COASTAL LOCATIONS

Hans Schrøder
Danish Hydraulic Institute
DK 2970 Hørsholm, Denmark

ABSTRACT

Factors of importance in power plant site selection for once - through cooling water systems situated on sea coasts are reviewed. Principles of recirculation management are indicated and briefly discussed in view of the implications of this approach on the environmental aspects of the problem. The need to recognize that the waste heat problem is not solved by prescribing zero recirculation is stressed.

INTRODUCTION

Selection of coastal sites for large power plants must consider the recirculation aspects as well as the possibility of environmental side effects.

All heat rejected from power plants is ultimately dissipated to the atmosphere which is achieved by raising the water temperatures above their natural ambient level over a substantial area. Hence, for a given site and heat load the excess temperature distribution can only to a limited extent be managed by engineering design.

Recirculation resulting from the rise of ambient temperature in the vicinity of the intake can be made subject to a rational management. Investments in marine installations should be adjusted, not necessarily to minimize recirculation, but to minimize the total cost of power loss due to recirculation and costs of marine installations.

An approach based on recirculation management principles does not appear to be in conflict with considerations with respect to the question of thermal impact on the acquatic environment at a given site.

MANAGEMENT PRINCIPLES

In general terms the objective of waste heat management is to minimize the sum of construction and plant operation costs and possible damages to the equatic invironment. Consequently a possible objective function is:

$$F = R + D + C \qquad (1)$$

where R is the cost of a decreased plant efficiency due to recirculation, D is the cost of damages imposed on the environment, and C is the cost of construction of the marine installations of the cooling water system.

The term D is controversial and quantification in terms of money is elusive, if at all possible. Nevertheless this aspect of the waste heat problem plays a major role in plant site selection considerations. For power plants located at rivers this is understandable since waste heat disposal can cause temperature barriers, whereas it is less obvious for coastal locations where the influence of the waste heat disposal is of a local character.

Another characteristic feature of the term D is that there are strict limits as to the extent by which the environmental impact can be managed by the lay-out of the cooling water system for a given plant site and a given rate of heat rejection.

The term R which represents the power loss due to recirculation can be influenced to a great extent by a proper determination of the positioning of intake and outfall.

Recirculation Optimization

It appears worthwhile to consider the objective function

$$F = R + C \qquad (2)$$

to investigate the consequences of this approach, and to raise the question of a possible conflict between a recirculation optimization and a total optimization (equation (1)).

This approach is clearly applicable to cooling ponds where environmental damages to the equatic environment need not be considered. With the numerical modeling techniques available today the elements necessary to perform a recirculation optimization are available.

Differentiation of the reduced objective function leads to the simple result that a total cost minimum is found when the marginal costs of decreasing the intake temperature equals the marginal cost of efficiency loss due to recirculation:

$$\frac{dR}{d\Delta Ti} = \frac{dC}{d\Delta Ti} \qquad (3)$$

where ΔTi is the water temperature above its natural equilibrium at the intake.

It should be noted that apart from the hydraulic complexity of the problem, a rigorous analysis is difficult to perform since the cost of efficiency loss can be evaluated in numerous ways. Furthermore, the effect of a certain degree of recirculation can to some extent be catered for in the design of the steam condensers. Regardless of the difficulties inherent in the problem it seems appropriate to perform an analysis of this type rather than to rely on arbitrary criteria with respect to the acceptable level of recirculation.

Note that the term recirculation designates indirect recirculation (intake located in the far-field). Direct passage of heated water from outfall to intake is assumed to be nonexistent.

PLANT SITE SELECTION

In principle, all terms in the objective function should be evaluated to provide a proper basis for a decision with respect to selection of potential sites. This in turn would require a full investigation of hydraulic and biological aspects at each site. However, a general knowledge with respect to flow patterns of the site is often sufficient as a basis for preliminary excess temperature field computations and subsequent evaluation of biological effects. In this way the various sites can be given priority, and a few be selected for detailed hydraulic and biological studies.

In the following, the main features of a site selection are discussed, and a sample computation of the optimum recirculation is given.

Total Energy Budget

The ultimate sink of waste heat is the atmosphere. Under equilibrium conditions, or as an average over a sufficiently long period of time, the total rate of heat dissipation over the influenced water surface area therefore must equal the rate of heat supply.

For simplicity the rate of additional heat loss which takes place to the atmosphere when the temperature is raised ΔT above its natural equilibrium is assumed to be given by:

$$H = f\ \Delta T\ \mathrm{Watt/m^2} \qquad (4)$$

Conservation of energy requires that the surface rate of heat loss integrated over the entire excess temperature field equals the rate of heat supply:

$$Q \Delta T_o \rho\ C_p = f \int_A \Delta T dA \qquad (5)$$

where Q is the cooling water discharge, ΔT_o is the temperature increase over the condensers, ρ is the density of water and Cp is the specific heat.

Evidently, the magnitude of the integral in equation (5) is fixed for a given heat supply and completely independent of the currents , the mixing processes of the receiving water body and the mode of discharge. Furthermore, the integral is independent of the vertical distribution of the excess temperature. These factors only affect the shape of the temperature field. Thus, in discharge areas with a considerable tidal activity the excess temperature distribution will tend to attain a more uniform distribution that in areas where the natural energy available for the spreading is lower. The result will be that the excess temperatures in receiving waters with a high level of mixing in the vicinity of the outfall will be relatively low, whereas the excess temperatures further away will be relatively high. Thus, the area encircled by lines through equal low excess temperatures will increase with increasing tidal and mixing intensity of the receiving water.

It is worthwhile to note that the shape of the excess temperature field is determined to a very high extent by the ability of the tidal currents to yield an initial spreading of the source. This appears to be a factor of considerable importance as compared to the effect which can be obtained by a submerged diffuser.

If a high velocity surface jet is utilized the jet momentum can induce a current pattern which can be of considerable importance for the shape of the entire temperature field in situations where the tidal currents are weak.

Contrary to the distribution of the surface excess temperatures, the total amount of heat stored in the water depends on the transport and mixing characteristics of the receiving water as well as the mode of discharge. The heat storage is reduced by floating the heated water onto the receiving water. In this way the surface heat loss may not be significantly altered but the heat storage can be reduced considerably and temperature changes at the bottom of the receiving water avoided.

The Relevance of Initial Dilution

A considerable attention has previously been given to the question of the so-called near field, i.e. the zone in the vicinity of the outfall where outfall conditions significantly affect the temperature field. This is especially relevant for small discharges as far as evaluation of the risk of direct recirculation is concerned. However, for cooling water discharges from large power plants heat stored in the discharge area can easily attain a significant level whereby the entraining water is already heated.

The statement above especially applies to a situation in which the heated water is discharged through a diffuser in a receiving water characterized by an oscillating tidal flow. In this case discharge may take place over a diffuser length of a few hundred meters while the tidal current provides a spreading of the source equal to the tidal excursion which may be several kilometers. Furthermore, since the diffuser jets entrain water which is already heated the dilution obtained could be illusory.

If, on the other hand, the heated water is discharged as a horizontal surface jet with an initial velocity comparable to the tidal velocity the momentum of the jet will induce a circulation pattern which may have a considerable effect on the temperature distribution. The temperature field is then stretched in the direction of the jet and thus distorted as compared to the diffuser situation. However, regardless of the mode of discharge the surface heat loss integrated over the whole warm water surface remains the same.

Thermal regulations which prescribe maximum surface temperature differentials can on the grounds above be said to have little meaning for large cooling water discharges. In this connection it should be emphasized that this aspect is only to a limited extent manageable by the design of the intake and outfall structures.

In order to make reliable predictions of the temperature field in the vicinity of the outfall the practising engineer is faced with the problem of predicting the effect of the interaction between the near- and the far-field. A computation based on the assumption that water unaffected by the discharge is available for dilution will inevitably lead to erroneous results.

The Effect of Tidal Currents and Mass Injection

An idealized example in which heat is injected to a semi-infinite region of open and shallow water is considered. It is furthermore assumed that the excess temperature is uniformly distributed over the depth d. The effect of a tidal current becomes apparent when the water is considered to remain at rest and the heat source to move sinusoidally over the tidal excursion, J.M. Williams [1] . The heat can in this situation be assumed to take place over a line source with a distribution and a resulting excess temperature field shown in principle in Fig. 1.

An approximate solution with respect to the temperature distribution in the center line of the oscillating temperature field can be obtained by considering the one-dimensional conservation of heat equation:

$$\frac{d^2\Delta T}{dx^2} - \frac{Q}{edD}\frac{d\Delta T}{dx} - \frac{f}{dD\rho Cp}\Delta T = 0 \qquad (6)$$

where the symbols not previously defined are:

x is the coordinate in the direction perpendicular to the coast, D is the dispersion coefficient in the direction perpendicular to the coast and e is an equivalent tidal excursion.

Equation (6) ignores the effect of heat dispersion in the direction of the current, and will for this reason give conservative estimates of the excess temperatures. This will particularly be the case for the lowest excess temperatures. However, the longitudinal dispersion effect can to some extent be catered for by using a tidal excursion which is somewhat greater than the true excursion.

The soulution to equation (6) is:

$$\Delta T = \Delta Tm \exp (\alpha x) \qquad (7)$$

where

$$\alpha = \frac{1}{2} \frac{Q}{edD} \left[1 - \sqrt{1+4 \frac{fe^2 dD}{\rho C_p Q^2}} \right] \qquad (8)$$

and ΔTm is the maximum temperature along the coast subject to the condition that the total rate of heat dissipation is equal to the rate of supply:

$$\Delta Tm = \frac{Q\rho Cp\alpha}{ef} \Delta To \qquad (9)$$

where ΔTo is the excess temperature at the point of discharge and Q is the cooling water flow.

For large cooling water discharges Q and a small tidal excursion equation (8) can be approximated by:

$$\alpha = \frac{fe}{\rho C_p Q} \qquad (10)$$

in which case equation (7) is modified to:

$$\Delta T = \Delta To \exp (- \frac{fe}{\rho C_p Q} x) \qquad (11)$$

For conditions normally encountered, the approximation used to derive equation (11) becomes good when the discharge exceeds 50-100 m^3/s corresponding to 1000-2000 MW nuclear power plants. Thus, for plants of this size the injection of mass becomes the dominating heat transport mechanism in the oscillating flow situation considered above. Note that equation (11) represents the solution to equation (6) when omitting the diffusive term.

Clearly, the idealized example above contains too many approximations to provide a proper basis for a determination of the positioning of intake and outfall. On the other hand, a useful insight with respect to orders of magnitude and parameter sensitivity can be gained with a very limited effort.

Another idealized example which is useful to consider refers to the situation in which heat is injected over a vertical line source in an infinite region of shallow water with horizontal and isotropic diffusion. The conservation of heat equation is in this case:

$$\frac{d^2 \Delta T}{dr^2} + \left(1 - \frac{Q}{2\pi dD}\right) \frac{1}{r} \frac{d\Delta T}{dr} - \frac{f}{\rho C_p dD} \Delta T = 0 \qquad (12)$$

where r is the radial coordinate with origin at the source.

The solution to this general equation contains the modified Bessel function of second kind and of order $-\frac{1}{4}\frac{Q}{\pi dD}$.

For the special case when Q equals $2\pi dD$ the solution becomes:

$$\Delta T = \Delta T_o \exp\left(-\sqrt{\frac{f}{\rho C p d D}}\, r\right) \qquad (13)$$

For very large flows the solution is approximated by:

$$\Delta T = \Delta T_o \exp\left(-\frac{\pi f}{\rho C_p Q} r^2\right) \qquad (14)$$

Note that the temperature at the source in this case, where no tidal activity is assumed to be present, becomes equal to the temperature of the source itself for relatively low discharges. For conditions normally encountered this is the case for discharges in the order of 20 m^3/s and above.

The Effect of a Residual Drift

The idealized examples above will rarely apply without modifications to real situations. For a more refined analysis, two-dimensional time-dependent numerical models based on flow patterns generated by hydrodynamic models should be applied. Techniques applied in numerical modeling of this type is described in a paper presented by G.S. Rodenhuis at this Conference [2].

One of the reasons for the need for numerical modeling is the inability of analytical methods to incorporate the effect of irregular flow patterns, irregular topographies and the combined effect of the mass injection effect and the important effect of a residual current.

Clearly, the presence of a residual drift current is of decisive importance for the shape of the temperature field, and hence for biological assessments and positioning of intake and outfall. A residual drift current of, say, 3 cm/s would be about one magnitude greater than the advection velocity caused by the mass injection considered in the oscillating flow example above. This will clearly have the effect of transforming the temperature field into a relatively narrow plume along the coast in the direction of the drift current. Furthermore, since unaffected water is continuously fed into the plume, a considerable decrease of maximum excess temperatures and a corresponding increase of temperatures further downstream will take place.

The recognition of the effect of a drift current should be duely reflected in the planning of field measurements and the subsequent data processing.

In areas where the wind is a dominating factor in the generation of the flow pattern which therefore is of a stochastic nature, a deterministic model approach is less suitable. As a compromise, deterministic numerical models can be run over a period long enough to contain the characteristic statistical features of the natural conditions in order to produce results which can be interpreted accordingly. Another possibility is to perform a number of model runs using parameter-sets which combine into a known frequency of occurrence.

Finally, pure stochastic models can be employed. This approach is rarely used in this context, even though it would appear probable that this would be appropriate both for purposes of recirculation management and for assessments of biological effects. The advantages with respect to elucidation of both aspects appear to be self-evident, although it is unconceivable to apply a stochastic model without resort to some type of deterministic approach.

RECIRCULATION MANAGEMENT - AN EXAMPLE.

According to equation (7) the optimum recirculation is found by equating the marginal costs of power loss and construction costs:

$$\frac{dR}{d\Delta T_i} = \frac{dC}{d\Delta T_i}$$

Cost of Power Loss Due to Recirculation

Harlemann [3] indicates the following relation for the change in basic plant efficiency for a typical boiling water or pressurized water reactor plant:

$$\frac{\Delta E}{E} = \frac{T_d - T_1}{T_2 - T_d} \qquad (16)$$

where $T_d - T_1$ is the deviation in (^oF) from the design steam condensing temperature, T_2 is the maximum operating temperature of the plant, and T_d is the design steam condensing temperature. Equation (16), which qualitatively is correct [3] , shows that there is a nearly linear relationship between power loss and deviations from the design temperature. Consequently, the present value of power loss due to the presence of temperatures increased ΔT_i over the natural equilibrium at the intake can be written as:

$$R = \Delta E \ f \ \Delta T_i \ PVF \qquad (17)$$

where ΔE is the power loss per degree increase in intake water temperature, f is the cost of 1MW year, PVF is the present value factor.

These factors are tentatively evaluated as follows:

$\Delta E = 0.0035 \, E \text{ MW } {}^oC^{-1}$

$f = 20 \text{ \$ } (MWh)^{-1} = 175{,}000 \text{ \$ } (MW\ year)^{-1}$

PVF = 14 for a 5% discount rate and a period of 25 years.

For a 2000 MW power plant the marginal present value of power loss is estimated at 17 million dollars per degree centigrade.

Construction Costs.

In the example considered above it is assumed that the plant's required 100 m^3/s of cooling water is conveyed through large submerged conduits from an intake structure several hundred meters from the shore, see Fig. 1. The outfall is assumed to be located at the shore. For simplicity it is furthermore assumed that the construction and pumping costs can be expressed as:

$$C = Px \qquad (18)$$

P is the cost per unit lenght and x is the distance between intake and outfall.

The time averaged excess temperature distribution in the outfall-intake line is assumed approximated by an exponential decay, equation (7). The marginal cost of construction and pumping can then be computed as:

$$\frac{dC}{d\Delta T_i} = \frac{P}{\alpha \Delta T_i} \qquad (19)$$

Substitution of equation (17) and (18) in (3) leads to the optimal excess temperature at the intake:

$$\Delta T_i \text{optim} = \frac{P}{\Delta E \ f \ PVF \ \alpha} \qquad (20)$$

from which the optimal distance between outfall and intake is readily computed using equation (7).

The cost of the marine installations (including pumping) of the type considered is estimated at 80,000 US $ per meter.

The exponent α in equation (7) is assumed to be increased by the action of a residual tidal drift current as compared to the value one would obtain in the case of a purely oscillating flow. The magnitude of the exponent is estimated at 0.003 m^{-1}.

With the above cited figures the optimum recirculation becomes

$$\Delta T_i \text{optim} = \frac{80\ 10^3}{17\ 10^6\ 3\ 10^{-3}} \simeq 1.6\ {}^oC.$$

Because of the exponential decay of the excess temperature with distance from the outfall and because of the considerable construction costs involved, deviations from the optimum temperature will inevitably lead to a considerable increase in the total cost.

The choice of magnitude of the various parameters involved in the analysis above can of course be discussed and a sensitivity test would in an actual case be required. Furthermore, the effect of increased ambient temperatures in the far-field can to some extent be catered for in the design of the steam condensers. However, in any case, the analysis stresses the importance of a reliable prediction of the excess temperature distribution.

As a practical comment to the example considered it should be noted that it would appear to be advantageous to discharge in the off-shore position using a high velocity jet, and to take water in close to the shore. Furthermore, a position of the intake upstream relative to the outfall conduits should be considered. Thus, in order to perform a complete analysis, two dimensions for determination of the optimum intake position would need be considered.

RECIRCULATION AND BIOLOGICAL EFFECTS

The question whether or not decisions based on recirculation management principles could be in conflict with biological demands is difficult to assess. Apart from the very limited effect of the efficiency decrease due to recirculation, the same quantity of heat is rejected to the environment. The fact that recirculation is present only means that the excess temperature field is "concentrated" to a higher extent in the area between outfall and intake than would be the case if no recirculation was present at all.

Additionally, it appears that a recirculation management analysis would always tend to yield solutions which are preferable from a biological point of view as well since sites and intake-outfall lay-out solutions causing relatively small areas to be subject to high excess temperatures would be preferred for both reasons.

There may,however,be coastal sites which for biological reasons should not be used. It should be noted that as far as decimation of marine organism due to entrainment in the cooling water system is concerned, this aspect is independent of the question of the distribution of an excess temperature field. This and other biological aspects can be assessed using a numerical modeling technique described in the paper presented by B. Møller and K.I. Dahl-Madsen at this Conference [4].

DISCUSSION

The aim of the considerations presented in this paper has been to elucidate some of the important elements in the analysis of the waste heat management problem. Therefore, the methods indicated above do by no means represent a state-of-the-art of modeling techniques but should be regarded as tools which can be used for purposes of quick approximations, sensitivity analyses and systems analysis.

The main object of this paper is that it addresses the genuine need to recognize that the waste heat problem is not simply solved by prescribing maximum surface temperature differentials in the receiving water and requiring zero recirculation.

REFERENCES

1. Williams, J.M.: "A Numerical Model of the Temperature Distribution in the Vicinity of Sizewell Power Station Outfall". Rapp. P.-v. Réun. Cons. Int. Explor Mer, 167: 171-176. Dec. 1974.
2. Rodenhuis, G.S.: "Numerical Models in Cooling Water Circulation Studies: Techniques, Principle Errors, Practical Applications". This Conference.
3. Harlemann, D.R.F.: "Energy Conversion and Waste Heat in the Environment". In European Course on Heat Disposal From Power Generation in the Water Environment. Delft Hydraulics Laboratory in Cooperation with

Massachusetts Institute of Technology. Delft, June 1975.

4. Møller B. and Dahl-Madsen, K.I.: "Modeling the Influence of Thermal Effluents on Ecosystem Behaviour". This Conference.

5. Thomann, R.V.: "Systems Analysis and Water Quality Management". McGraw-Hill 1972.

IDEALIZED TEMPERATURE DISTRIBUTIONS AT THE SLACK TIDES OF AN OSCILLATING TIDAL FLOW FIELD

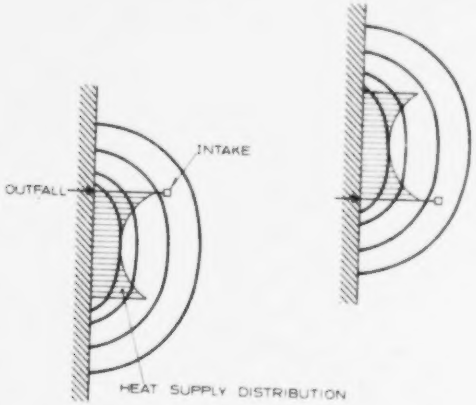
INTAKE
OUTFALL
HEAT SUPPLY DISTRIBUTION

ILLUSTRATIONS OF THE RECIRCULATION MANAGEMENT EXAMPLE

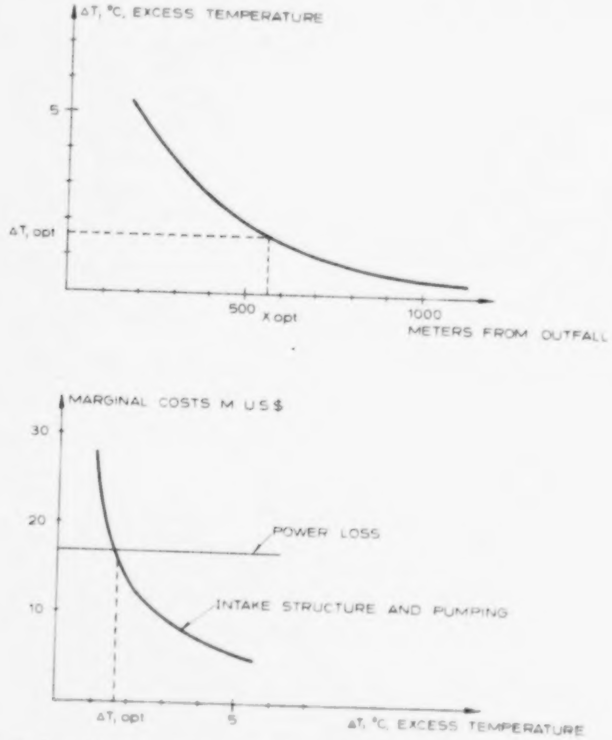

Fig 1 Idealized temperature distribution and marginal cost analysis.

V-A-45

12-45-21

USE OF ENVIRONMENTAL DATA FOR DETERMINING CONDENSER WATER SYSTEM ALTERNATIVES

L.P. Beer
Roy F. Weston, Inc.
West Chester, Pennsylvania U.S.A.

ABSTRACT

Environmental data can and should be used for determining condenser water system alternatives to effect the protection of the use of the receiving water body. A well-designed thermal effects study program will include physical, chemical, and biological data. The type and amount of data must be considered in the experimental design of the study plan so that the data will be useful in providing engineering design criteria to minimize environmental degradation. These data will be used for such condenser water system alternatives as once-through cooling with no special intake or discharge structures, modifications to intake and discharge design, use of extended discharge canals, diffuser pipes, cooling canals (both with and without spray modules), cooling ponds, and mechanical and natural draft cooling towers.

INTRODUCTION

Environmental data can be used for the design of condenser water system alternatives to effect the protection of the use of the receiving water body. A well-designed thermal effects study program would include physical, chemical and/or biological data collection. The type and amount of data to be collected must be considered when developing the experimental design of the study plan so that the data will be useful to provide engineering design criteria to minimize environmental degradation. It is essential that data be collected in a well-integrated and organized manner so that manipulation of these data will result in conclusions that are useful in deciding on alternative designs. Collection of data "just for the sake of collection" has no value except to confuse the issue and actually hamper the development of the resulting conclusions and recommendations.

This paper will address the collection of physical, chemical and biological data as part of an experimental design to evaluate alternative condenser water systems including once-through cooling, modified intake and discharge structures, intake and discharge canals, cooling canals, cooling ponds, cooling canals and ponds with spray modules, and both mechanical and natural draft cooling towers. This paper is the result of study programs conducted by the author at the site of power stations on the Ohio, Illinois, Mississippi and St. Johns rivers, as well as smaller rivers, Lake Michigan and the Florida coast.

Preceding page blank

Physical Data

The collection of physical data will include temperature, current movement, bathymetry, sediment transport, meteorological measurements, thermal transfer, a combination of field and analytical techniques for ambient and plume observations, and predictive modeling procedures. Thermal plume and ambient observations probably represent the most difficult aspects of a physical data collection program associated with a power station. This is particularly true in the case of estuaries and other tidally-influenced systems. In the case where the aquatic system is tidally-influenced and, therefore, ambient thermal conditions vary during a tidal cycle, it is essential to conduct the field measurement program within a very short period of time (approximately one to two hours) during each of the four tidal cycles. In the case of a tidally-influenced system, plume observations and ambient conditions have to be evaluated within the period not to exceed one to two hours, otherwise the plume and ambient conditions represent a combination of two or more tidal cycles and, therefore, two or more thermal conditions. In the case of a lake-river discharge, it is essential to conduct a field survey when the power plant has been discharging condenser waters at a constant rate for at least 12 to 24 hours prior to the time of measurement, and the system has reached equilibrium. Typical plume isothermal sections are shown in Figures 1 and 2.

Computer and physical models can be used to predict plume dispersion as well as ambient thermal conditions in aquatic environments. Comparison of plume and ambient predictions with actual field conditions is needed to verify or modify model assumptions. Figures 3, 4 and 5 are examples of graphical representations of plume predictions using computer modeling techniques.

If, for example, physical measurements are needed to help design spray modules for use in an intake or discharge canal, then such data as thermal profiles, current velocities (both horizontally and vertically), thermal transfer (solar radiation, etc.), and meteorological (wind speed and direction, lapse rates, etc.) will be required. Tank studies to determine spray modules efficiency both with and without induced air movement by use of fans, will be required under controlled conditions. Temperature measurement in the water entering the center of the spray module as well as in the spray periphery of discharge from the module, determinations of amounts of water being withdrawn from the tank, effects of interference between and among spray modules, as well as drift conditions will need to be evaluated. Use of computer modeling techniques will be required to determine suitable spacing and configuration of spray modules to minimize "shading" effects and drift loss.

Chemical Data

Chemical data for input to the engineering design of condenser water systems principally relate to dissolved oxygen (DO) and nutrients. Although DO is typically considered a physical measurement, for purposes of this discussion, it is considered part of chemical data analysis. Dissolved oxygen measurements, on the intake and discharge canals and in the area of the discharge plume are needed in cases where the same water bodies have DO levels approaching upper lethal limits for most fishes. In the case of lakes, such as Lake Michigan, measurements of oxygen and nitrogen to determine supersaturation values that might affect and cause "gas bubble disease" may be needed. Nutrient information is required in order to evaluate synergistic effects of nutrients presence and elevated water temperatures in order to decide upon points of withdrawal and discharge of intake and discharge systems. Based on dissolved oxygen, nutrients, and in some instances nitrogen data, the intake and the discharge structures can be designed to make adequate use of the existing environment: for example, withdrawal of near-shore waters in areas that are thermally mixed with placement of the discharge into the hypolimnion of deeper waters where, in general, low dissolved oxygen levels are prevalent.

Biological Data

Biological information includes benthic invertebrates, zooplankton and phytoplankton, periphyton, icthyoplankton, and fish. Of particular interest and need are the types and numbers of organisms as well as their location and habitat preference. Data such as pollution/thermal tolerance and migrational behavior are needed. The use of tag and recapture methods as well as selective fish sampling methods (including electro-shocking) is also useful. Statistical techniques and initial experimental biological design projects can be used to determine the numbers of samples required as well as the frequency of sampling. For example, it is desirable to run a short-term benthic invertebrate sampling program in areas where biological productivity is pronounced. Evaluations of "representativeness" on samples collected using various types of dredges including Ponar, Ekman, Peterson and others can be determined by comparing the composition of biological samples from replicate samples using these techniques.

CONDENSER WATER SYSTEM ALTERNATIVES

Examples of the use of physical, chemical and biological environmental data in the design of condenser water system alternatives to effect the efficient utilization of water bodies and the protection of the receiving water body or its enhancement are indicated in Table 1.

CONCLUSIONS

Physical, chemical and biological data from studies in the vicinity of power stations can be of considerable value when designing alternate condenser water systems to effect the most efficient use of the receiving water body and prevent degradation of waters. The state-of-the-art of collecting environmental data, experimental design of study programs, and design of condenser water system alternatives is advanced to the point that a minimal amount of environmental data can be developed, analyzed and interpreted for the sole purpose of providing design criteria for thermal discharges to protect the aquatic environment.

Table 1

Type of Structure/ Design	Figure No./ Schematic	Data Required Physical	 Chemical	 Biological
Inlet pipe structure	Figures 6,7	current velocity, dissolved oxygen, water temperature	nutrients	fish and zooplankton presence, thermal tolerance, temperature and swim speed relationship.
Intake structures: traveling screens, skimmer walls, trash racks.	Figure 8	current velocity		swim speed preference of fishes, fish eating habits (bottom feeders, plankton feeders, carnivores, etc.).
Condenser tubes (velocity & pressure) chlorination versus mechanical cleansers		current velocity, pressure	chlorine	zooplankton, ichthyoplankton, temperature and pressure tolerance, size and types of organism as affecting by mechanical, chemical and thermal damage to eggs, larvae fry, zooplankton.
Discharge pipe structure	Figures 1-5, 9, 10.	current, velocity, water temperature, dissolved oxygen, turbidity, modeling (computer & physical)	nutrient analysis	fish, migratory habits, habitat preference, thermal and dissolved oxygen preferences, feeding habits, swim speed preference.

Table 1
(continued)

Type of Structure/ Design	Figure No./ Schematic	Data Required		
		Physical	Chemical	Biological
Discharge water structures: cooling towers, submerged or surface jet spray canals, diffuser pipe, cooling pond or once-through system	Figures 11, 12, 13, 14, 15	dissolved oxygen, temperature turbidity, meteorological conditions, current velocity and direction, thermal transfer	dissolved oxygen, nutrient levels, total organic carbon, trace metals	zooplankton, phytoplankton, periphyton, ichthyoplankton
Pond for biological replacement 1/	Figure 15	water temperature, current velocity, turbidity, dissolved oxygen	nutrient data, trace metals.	entrainment, impingement data, zooplankton, ichthyoplankton, habitat preference, temperature tolerance, physical/chemical/biological relationships
Mariculture/aquaculture facilities; marinas & other recreational structures; artificial heating of homes; agricultural designs. 2/		complete	complete	complete

1/ A holding pond can be used to raise organisms which would then be discharged into the discharge canal or directly into the receiving water body to replace entrained organisms that were killed during the passage through the condenser water system; still in experimental stage of development and evaluation.

2/ The beneficial uses of heated waters can be categorized into the following major divisions: mariculture and aquaculture, heated waters to keep marinas and other recreational structures free from ice, artificial heating of homes, agricultural uses; in addition, use of waste steam for beneficial industrial purposes is feasible.

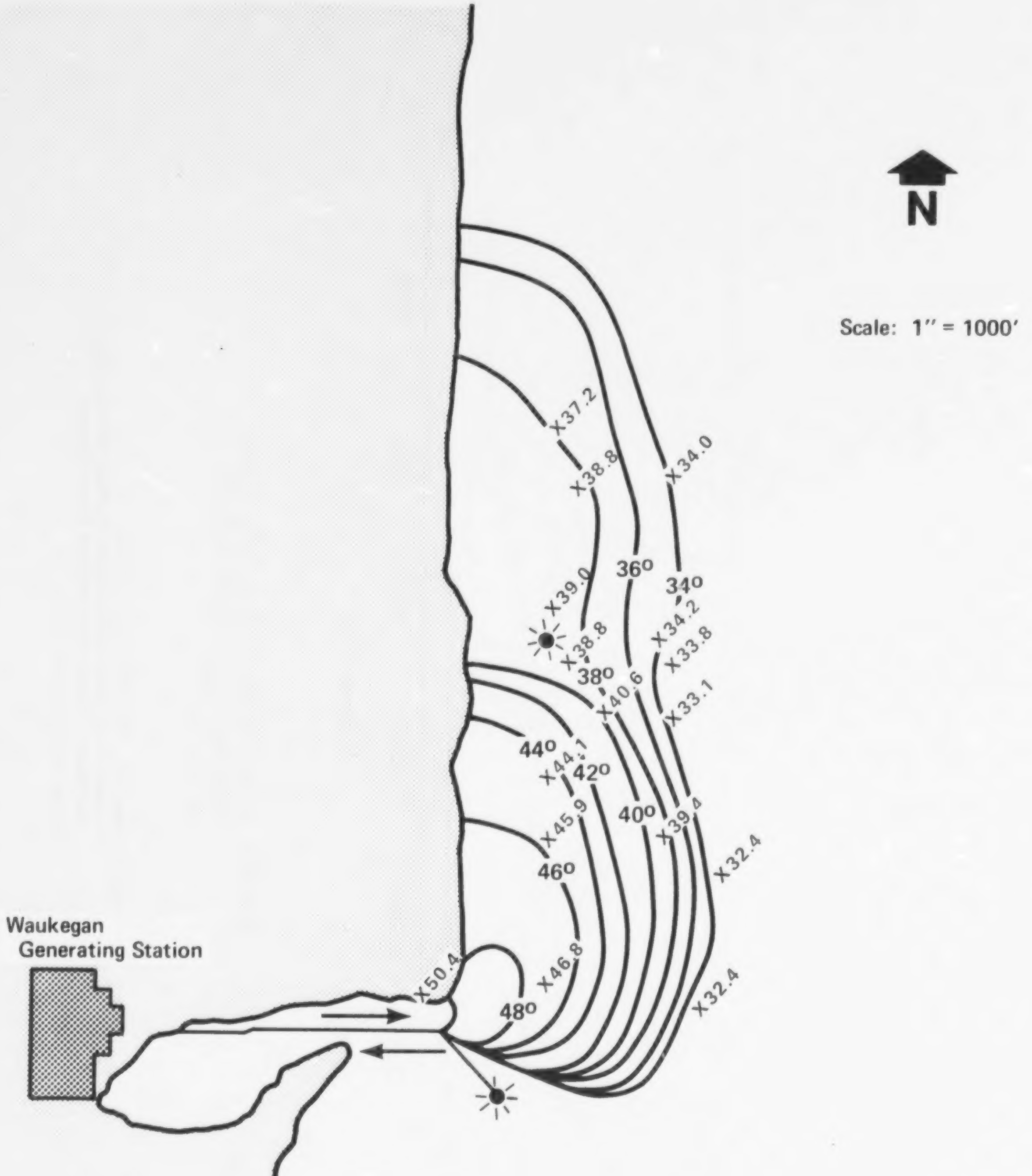
N
Scale: 1" = 1000'
X37.2
X34.0
X38.8
36°
34°
X39.0
X34.2
X38.8
X33.8
38°
X40.6
X33.1
44°
X44.1
42°
40°
X45.9
X39.4
X32.4
46°
Waukegan
Generating Station
X50.4
X46.8
48°
X32.4

Figure 1. Surface Water Temperatures on Feb. 21, 1970

Reference: Pipes, W.O., D.W. Pritchard and L.P. Beer.
"Condenser Water Discharge Plumes from Waukegan Generating Station under Winter Condition." Commonwealth Edison Company
Chicago, Illinois (January, 1973)

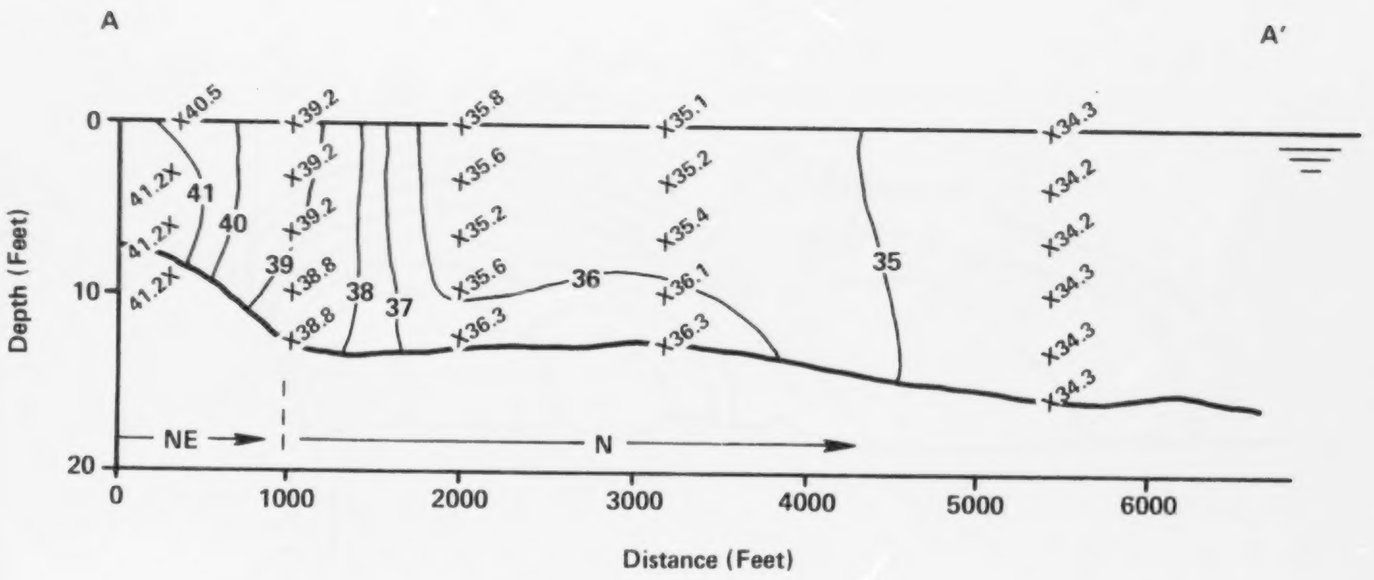

Figure 2: Vertical Section Showing Temperatures along Centerline of Discharge Plume on Feb. 16, 1971

Reference: Pipes, W.O., D.W. Pritchard and L.P. Beer.
"Condenser Water Discharge Plumes from Waukegan Generating Station under Winter Condition." Commonwealth Edison Company
Chicago, Illinois (January, 1973)

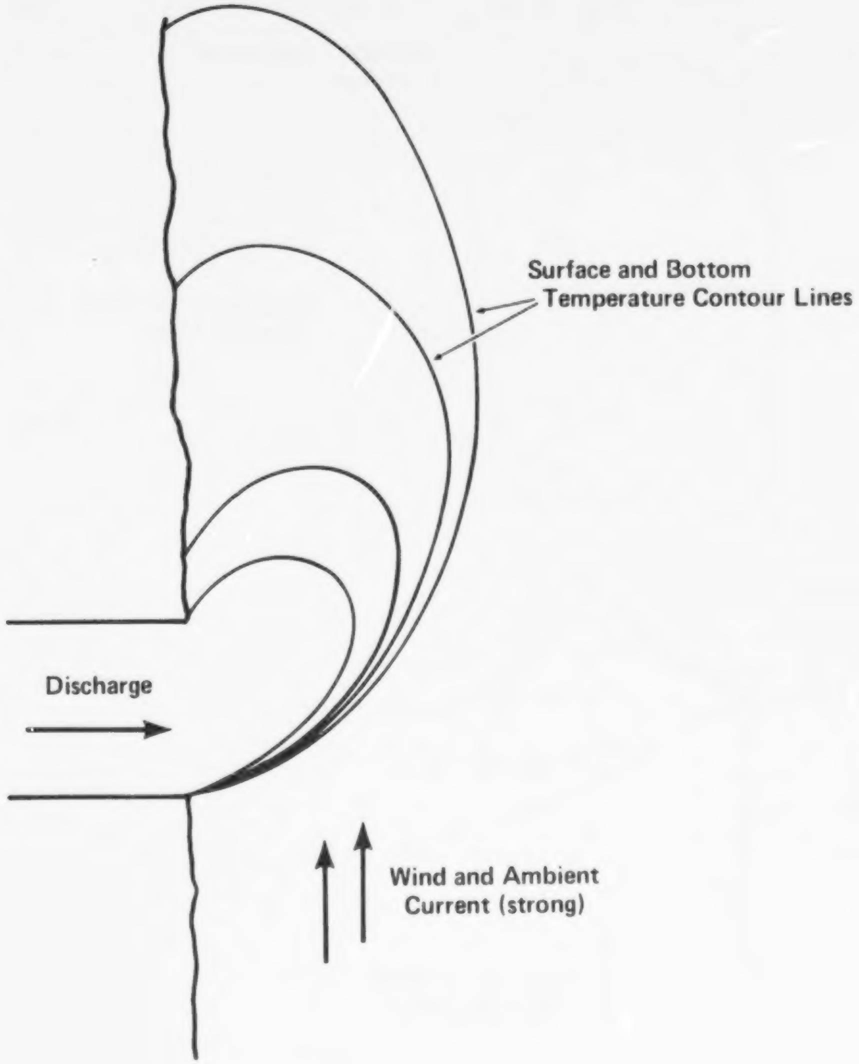
Surface and Bottom
Temperature Contour Lines
Discharge
Wind and Ambient
Current (strong)

Figure 3. Hypothetical Case 1. Winter Discharge Plume for Shoreline Discharge

Reference: Pipes, W.O., D.W. Pritchard and L.P. Beer.
"Condenser Water Discharge Plumes from Waukegan Generating Station under Winter Condition." Commonwealth Edison Company
Chicago, Illinois (January, 1973)

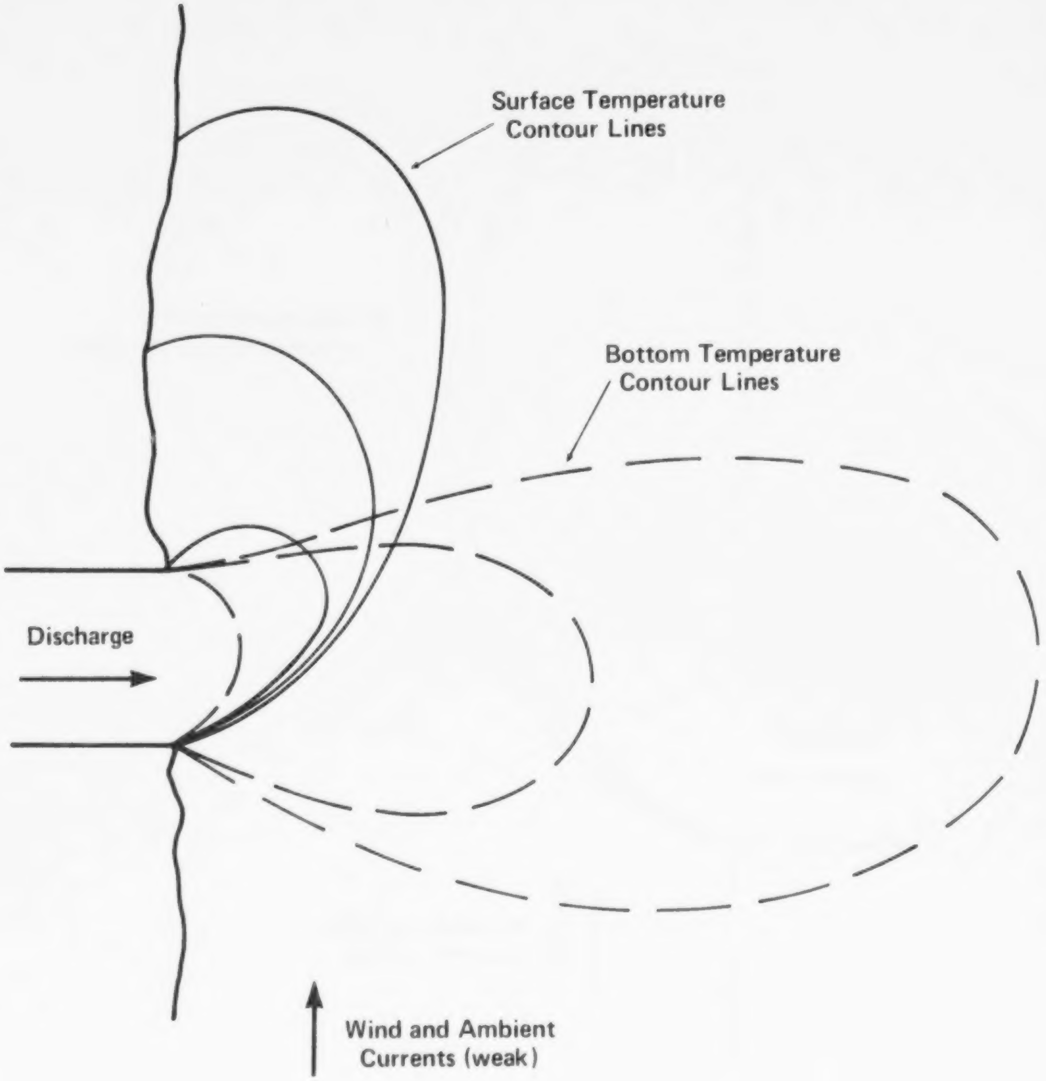
Surface Temperature Contour Lines
Bottom Temperature Contour Lines
Discharge
Wind and Ambient Currents (weak)

Figure 4. Hypothetical Case 2. Winter Discharge Plume for Shoreline Discharge

Reference: Pipes, W.O., D.W. Pritchard and L.P. Beer. "Condenser Water Discharge Plumes from Waukegan Generating Station under Winter Condition." Commonwealth Edison Company Chicago, Illinois (January, 1973)

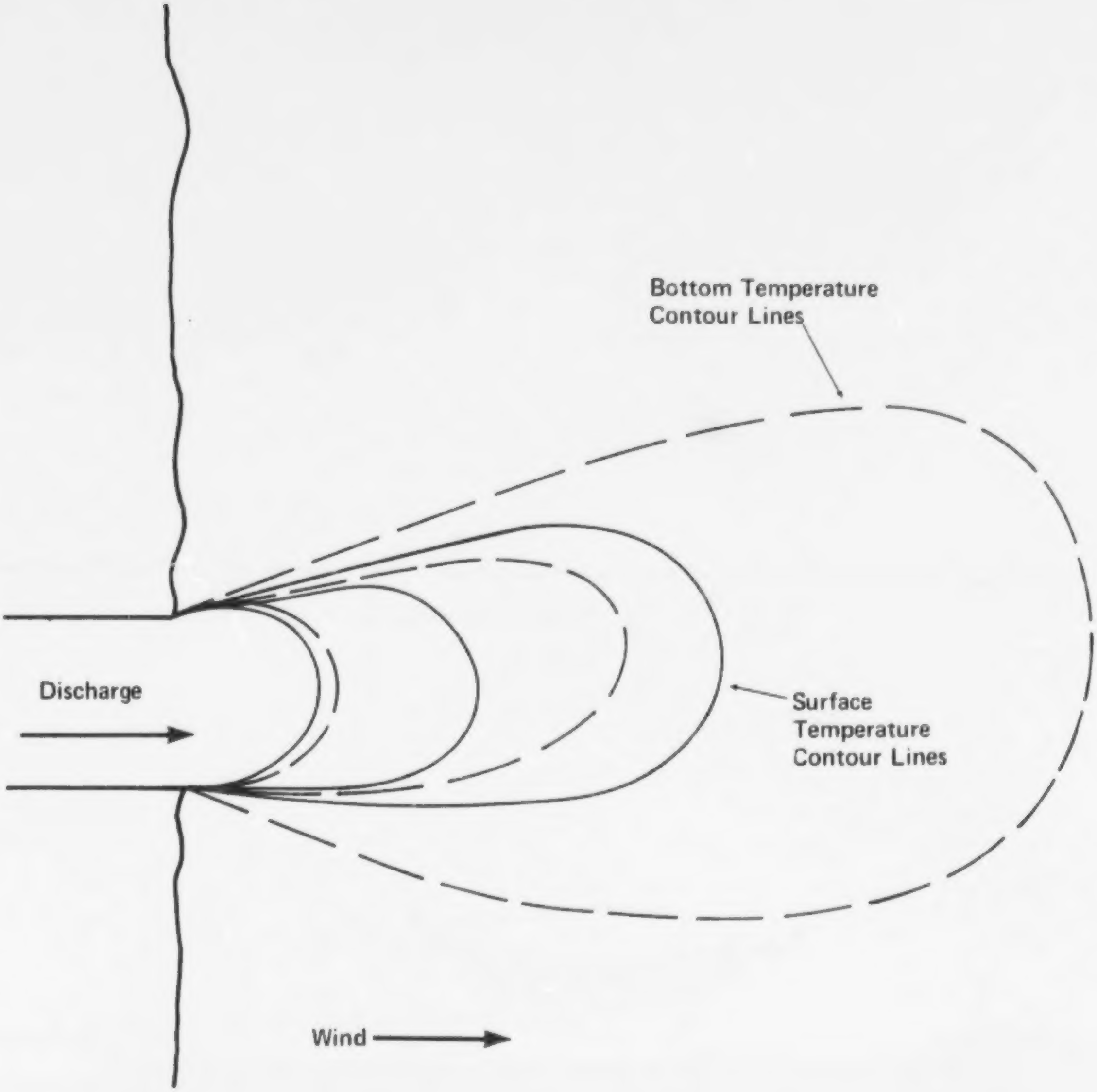
Bottom Temperature Contour Lines
Discharge
Surface Temperature Contour Lines
Wind

Figure 5. Hypothetical Case 3. Winter Discharge Plume for Shoreline Discharge

Reference: Pipes, W.O., D.W. Pritchard and L.P. Beer.
"Condenser Water Discharge Plumes from Waukegan Generating Station under Winter Condition." Commonwealth Edison Company
Chicago, Illinois (January, 1973)

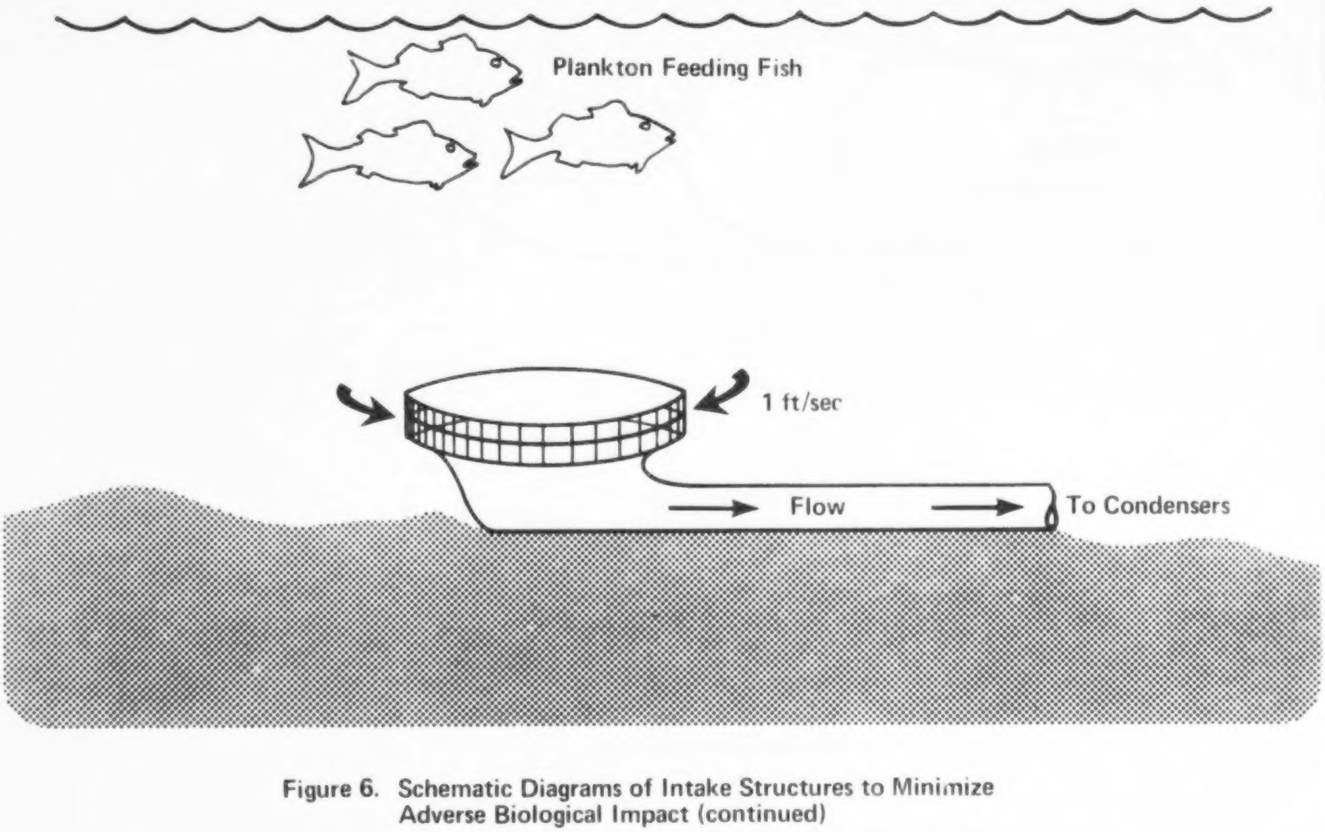
Plankton Feeding Fish
1 ft/sec
Flow
To Condensers

Figure 6. Schematic Diagrams of Intake Structures to Minimize Adverse Biological Impact (continued)

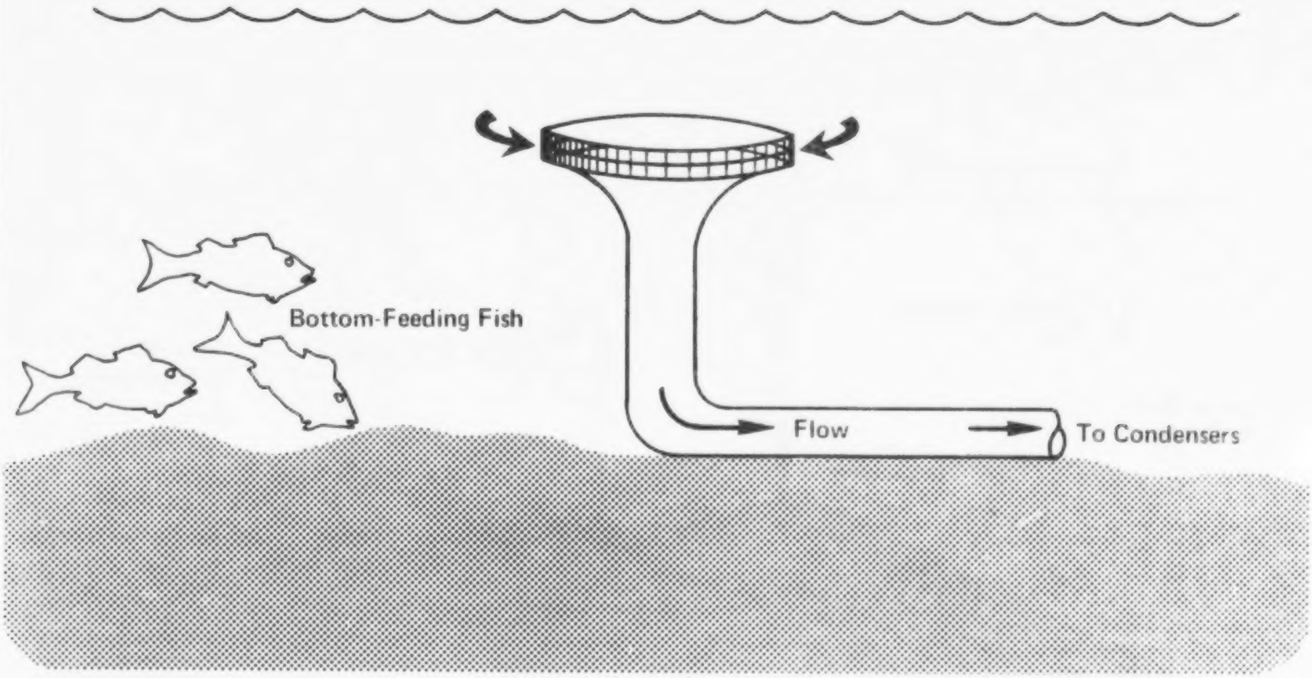
Bottom-Feeding Fish
Flow
To Condensers

Figure 7. Schematic Diagrams of Intake Structures to Minimize Adverse Biological Impact (continued)

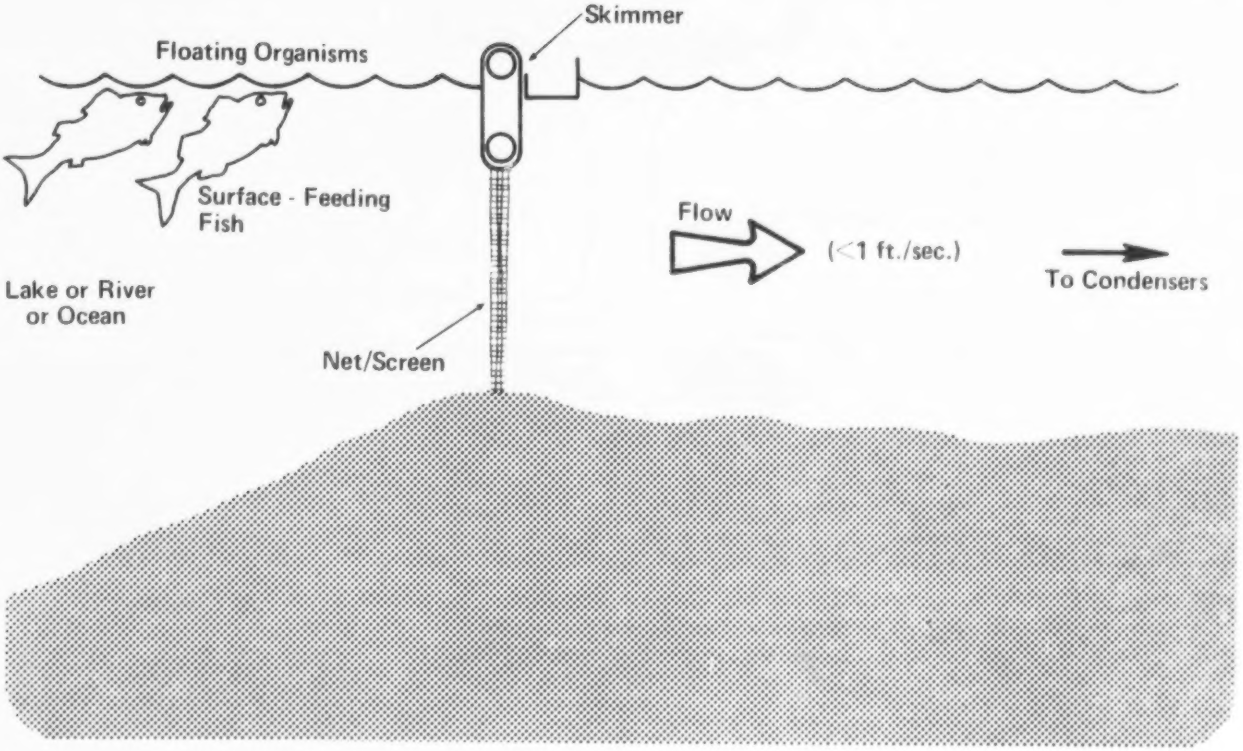
Skimmer
Floating Organisms
Surface - Feeding Fish
Flow
(<1 ft./sec.)
To Condensers
Lake or River or Ocean
Net/Screen

Figure 8. Schematic Diagrams of Intake Structures to Minimize Adverse Biological Impact

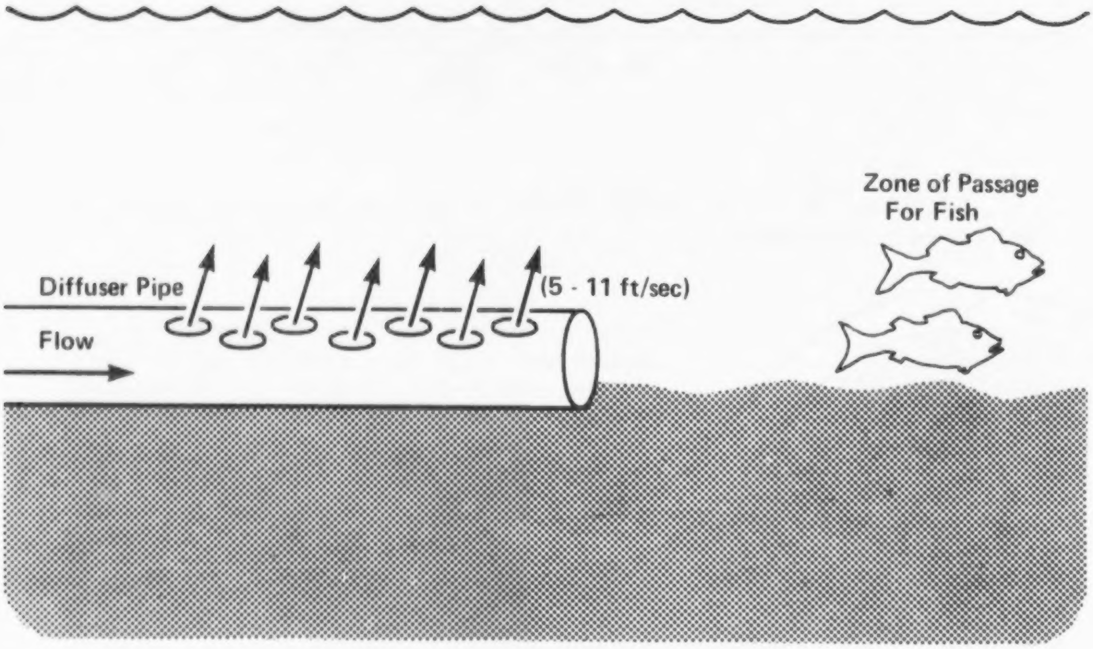
Zone of Passage
For Fish
Diffuser Pipe
(5 - 11 ft/sec)
Flow

Figure 9. Schematic Diagrams of Discharge Structures to Minimize Adverse Biological Impact

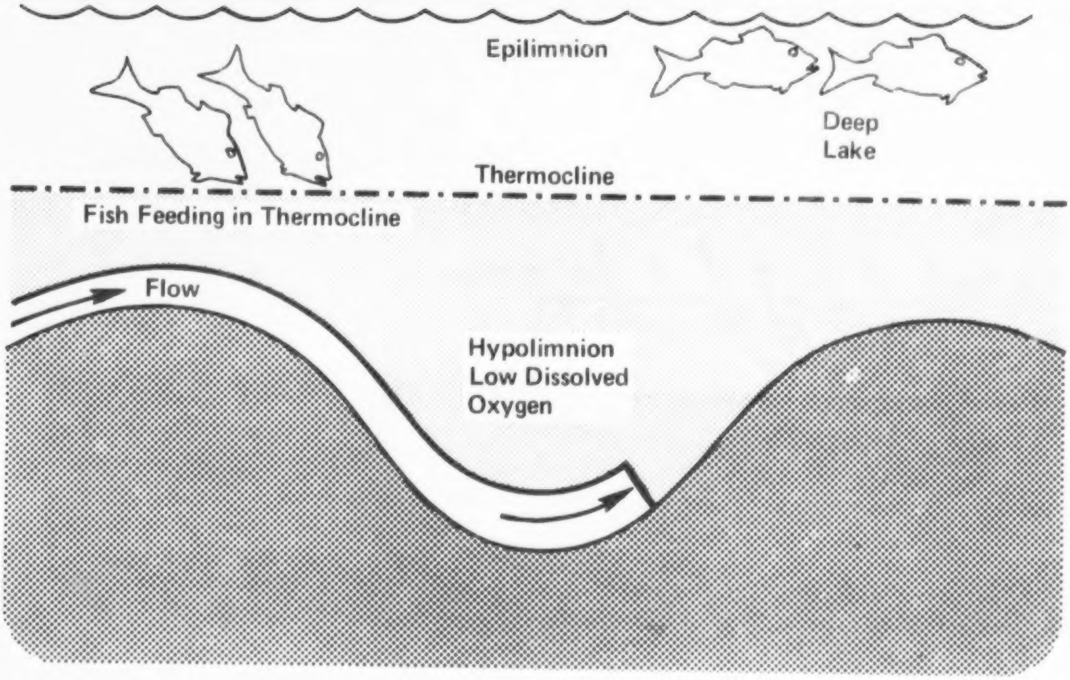
Epilimnion
Deep
Lake
Thermocline
Fish Feeding in Thermocline
Flow
Hypolimnion
Low Dissolved
Oxygen

Figure 10. Schematic Diagrams of Discharge Structures to Minimize Adverse Biological Impact (continued)

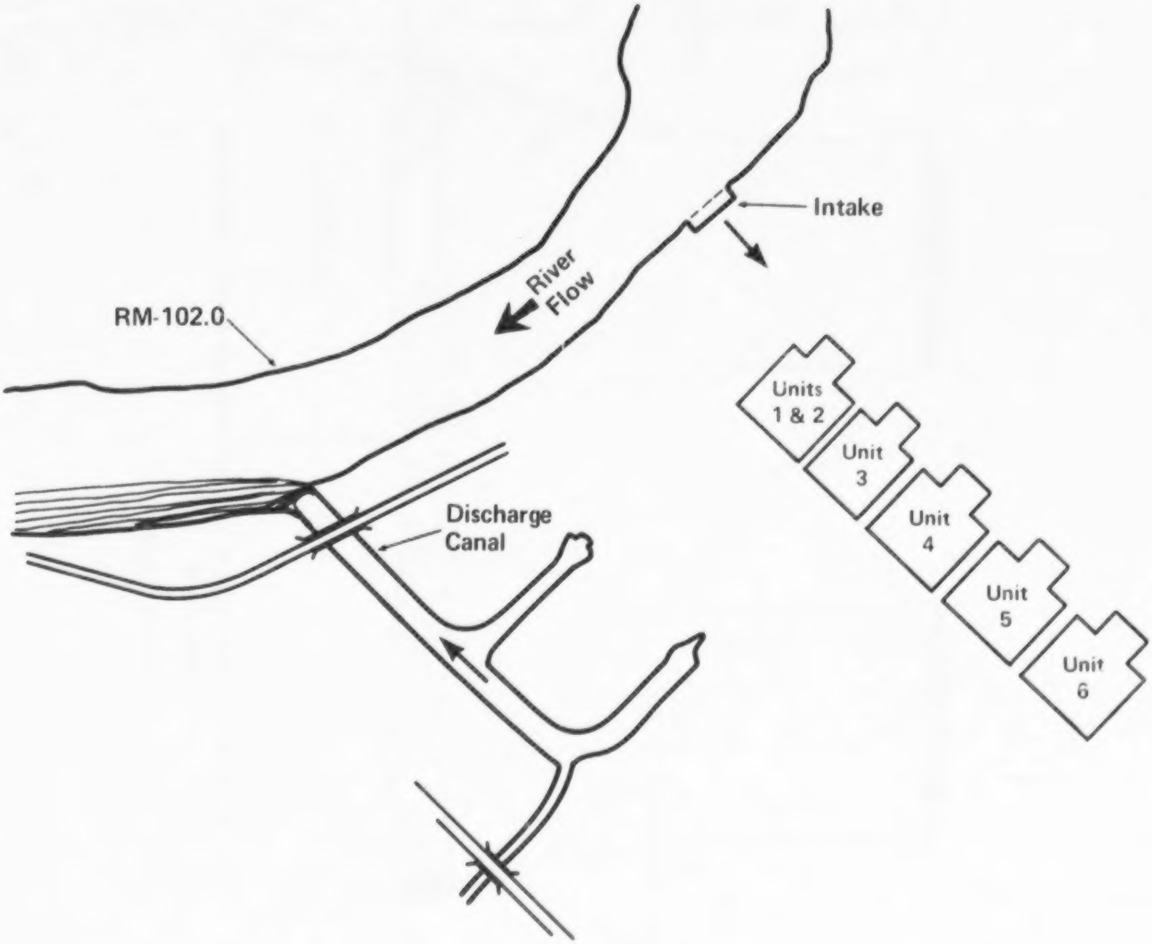
Intake
River Flow
RM-102.0
Units 1 & 2
Unit 3
Unit 4
Unit 5
Unit 6
Discharge Canal

Figure 11. Discharge Structures/Condenser Water Alternatives

Plan View Once-Through System

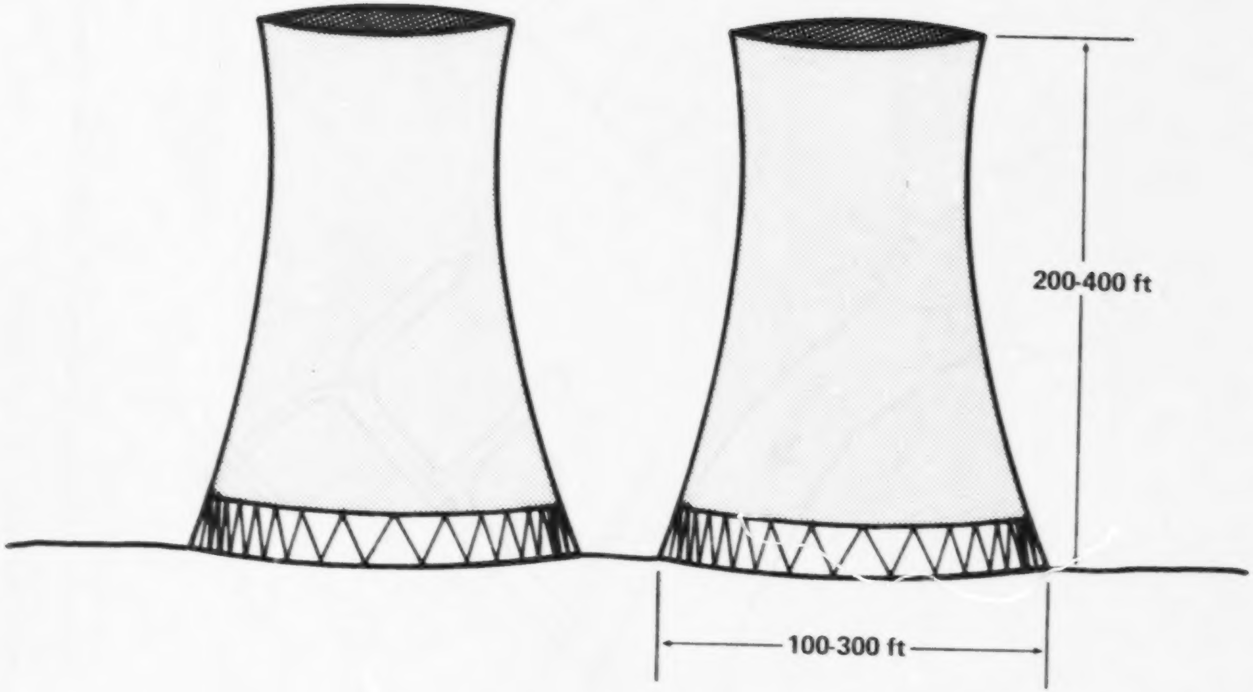
200-400 ft
100-300 ft

Figure 12. Discharge Structures/Condenser Water Alternatives (continued)

Cooling Towers

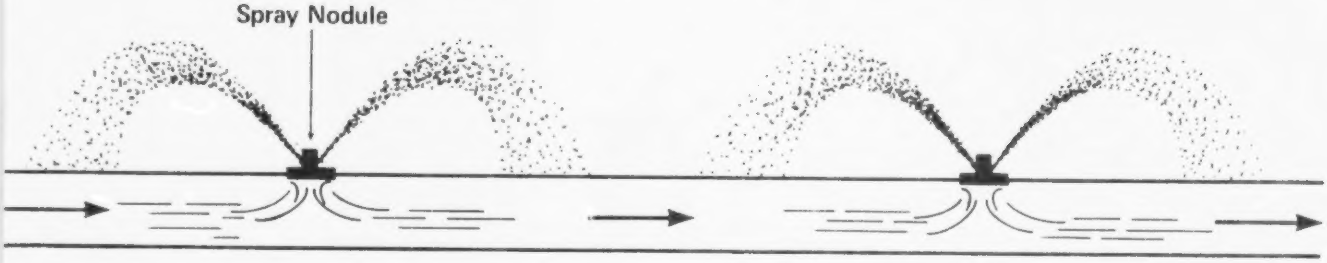
Spray Nodule

Figure 13. Discharge Structures/Condenser Water Alternatives (continued)

Spray Canals

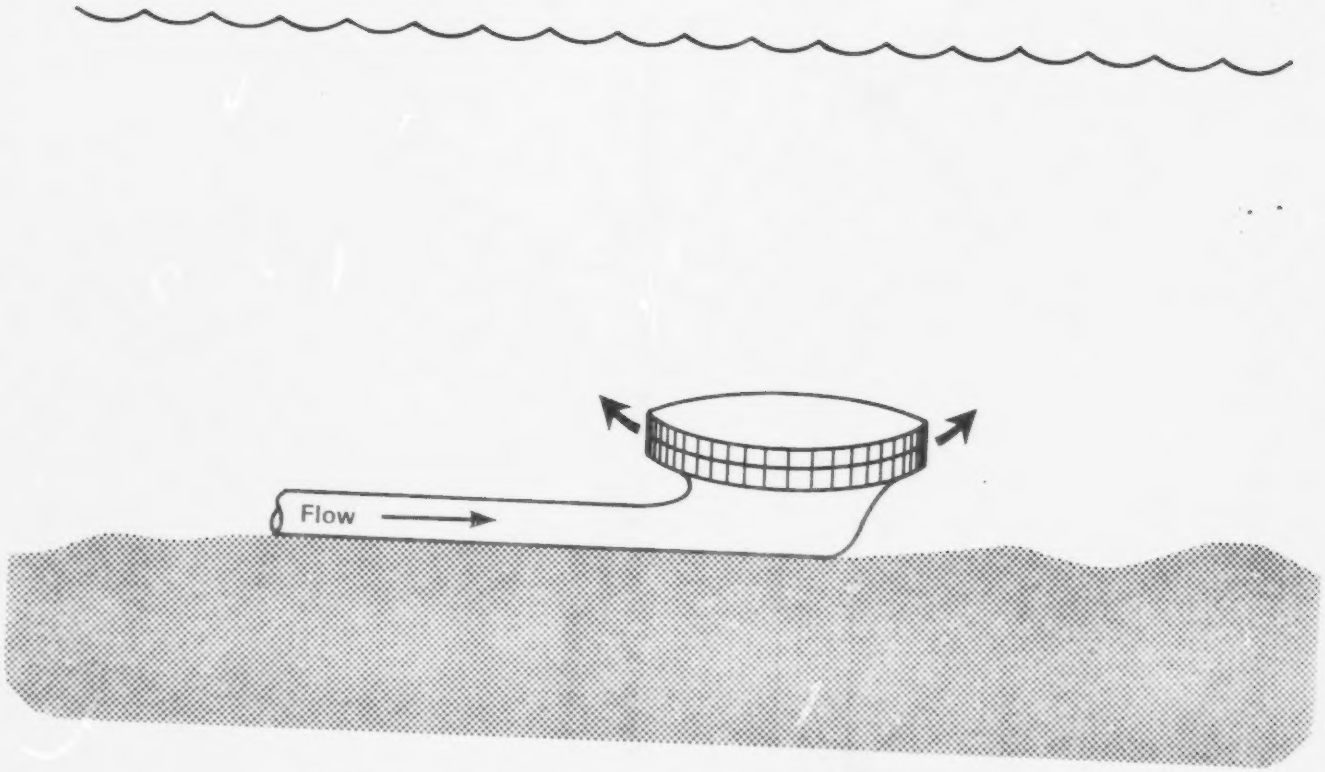

Figure 14. Discharge Structures/Condenser Water Alternatives (continued)

Submerged Discharge

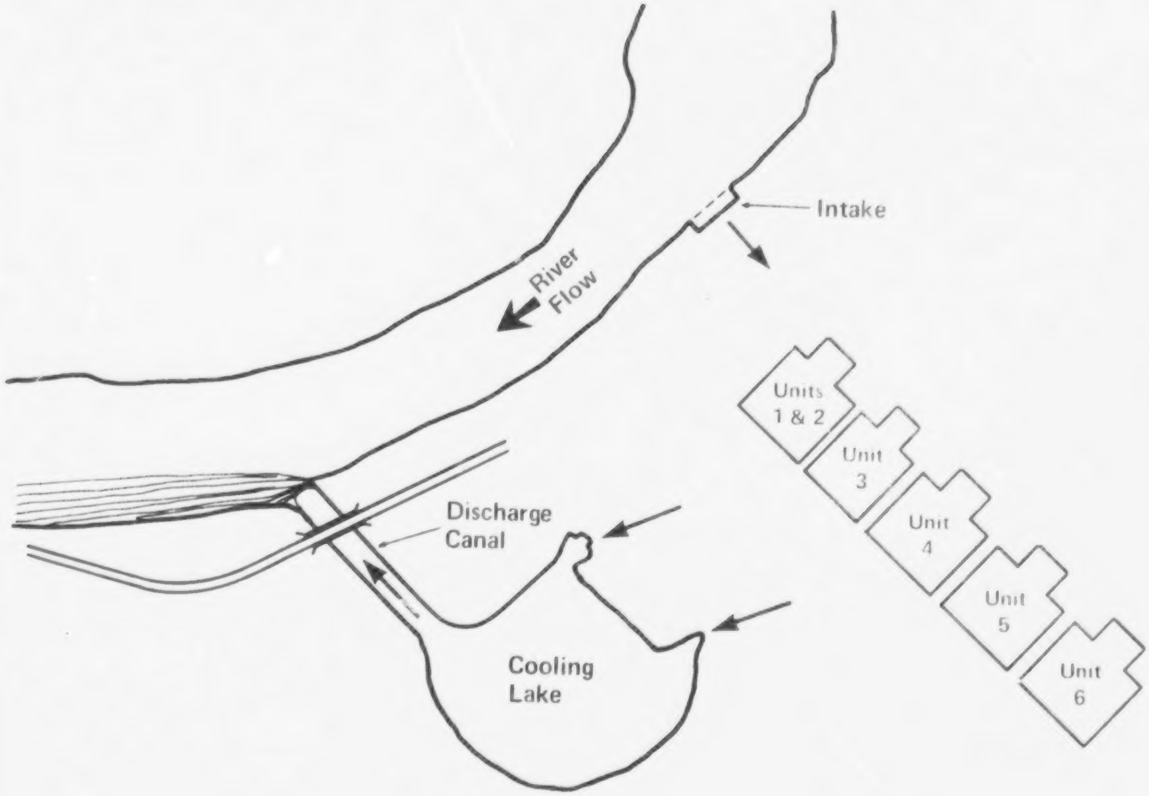
Intake
River
Flow
Units
1 & 2
Unit
3
Unit
4
Unit
5
Unit
6
Discharge
Canal
Cooling
Lake

Figure 15. Discharge Structures/Condenser Water Alternatives (Continued)

Plan View D - Cooling Lake

SESSION V-B
ECONOMIC ASPECTS

Preceding page blank

13-45-11

AN OPERATIONAL PROCEDURE FOR PREDICTING THE MOST ECONOMICAL USE OF CONDENSER COOLING MODES

W. L. Harper and W. R. Waldrop
Water Systems Development Branch, Tennessee Valley Authority
Norris, Tennessee USA

ABSTRACT

A technique is presented for estimating the most economical use of the cooling towers at the Tennessee Valley Authority (TVA) Browns Ferry Nuclear Plant while complying with the applicable thermal water quality standards of the State of Alabama. This plant is designed to operate in either of three condenser cooling modes: Open Cycle in which the condenser cooling water is discharged directly into the river through submerged diffusers; Helper Mode in which the cooling water is routed through the cooling towers prior to being discharged into the river through the diffusers; and Closed Cycle in which the cooling tower effluent is returned to the intake for reuse as condenser cooling water. The energy required for pumping and the loss of plant operating efficiency is minimized by computing the least amount of cooling tower operation required for each hour to comply with the Alabama thermal standards for the Tennessee River.

The procedure requires projections for the heat transfer rate from the condenser to the cooling water, the rate of cooling from the cooling towers, and the dispersion of heated effluent in the river. Plant performance curves and projected generating levels are used to estimate the condenser heat disposal rate. Cooling tower performance estimates, projected meteorology, and incoming water temperatures are used for estimating cooling tower effluent temperatures. Projected operation of upstream and downstream hydroelectric plants is used to compute river flows in the vicinity of the diffuser. These flows, along with upstream ambient river temperature, the temperature of the effluent, and results of laboratory and theoretical investigations of diffuser-induced mixing are used to compute the downstream temperature in the river. This program is used daily by the personnel of the Browns Ferry Nuclear Plant to predict the most efficient cooling mode for each hour throughout the following 24 hour period.

INTRODUCTION

TVA's Browns Ferry Nuclear Plant, situated on Wheeler Reservoir of the Tennessee River in north Alabama (Figure 1), was designed to generate 3456 MW. This plant was originally designed to operate in Open Mode for condenser cooling. In this mode, the plant pumps 4410 cubic feet per second (cfs) of water from the river and through the steam condenser

Preceding page blank

where the cooling water is heated approximately 25°F before being discharged through submerged multiport diffusers in the river.

The river flow past the submerged diffuser is primarily determined by the discharges from Wheeler Dam 19 miles downstream and Guntersville Dam 55 miles upstream of the nuclear plant. The mean annual flow rate of the river is 45,000 cfs. Since discharges from these dams are normally used for hydroelectric generation at periods of peak power demand, the flow in Wheeler Reservoir is often unsteady. As a result, flows near the plant site usually change drastically throughout the day and may, for an hour or so, reverse due to a "sloshing" effect of the reservoir. During such periods of low flow, there is an insufficient supply of cool river water available for mixing with the diffuser discharge; consequently, compliance with the thermal water quality standards is not possible when operating in the Open Mode of condenser cooling during low flows. These water quality standards permit a maximum plant-induced mixed temperature rise of 5°F and a maximum downstream temperature of 86°F. TVA maintains three permanent water temperature monitors downstream of the mixing zone of the diffusers to demonstrate compliance with these standards.

After delineation of the possible environmental consequences of this method for disposing of the excess heat from the condensers, and later the enactment of the thermal water quality standards, the nuclear plant was retrofitted with six mechanical draft cooling towers, two per unit. This provides the plant operators with the option of cooling the condenser cooling water when the thermal discharge of the Open Mode can contribute to a violation of the thermal standards. The effluent from the cooling towers can either be routed to the diffusers for discharge into the river (Helper Mode), or routed to the plant intake channel for reuse as condenser cooling water (Closed Mode). These three possible modes of operation of the Browns Ferry Nuclear Plant cooling system are illustrated in Figure 2.

This paper describes a computer model for analyzing the heat rejection rate of the plant and the pertinent meteorological and river conditions for the purpose of advising the plant operators of the most economical method of routing the condenser cooling water while assuring compliance with the thermal water quality standards.

FACTORS INFLUENCING CHOICE OF COOLING MODES

The possible environmental consequences of thermal discharges are well documented and the thermal water quality standards were promulgated to prevent adverse effects upon the aquatic ecosystem. The environmental advantages between the Open and Helper Modes are variable; the discharge rates are comparable, 4410 cfs for Open Mode versus 3675 cfs for Helper Mode. However, the discharge temperature for the Helper Mode, which depends upon meteorology, is normally cooler than that of Open Mode.

The discharge rate for Closed Mode is only about 110 cfs; therefore, the discharge during Closed Mode has a negligible effect on the downstream temperature of the river.

The environmental effects of plant intakes are also of concern. Fish may be trapped within intake structures or canals and become impinged against the intake screens. Fish too small to be impinged on the intake structures may be entrained into the cooling system of the plant. Although impingement and entrainment of fish must be evaluated for each plant, the number of fish affected is usually proportional to the flow rate of condenser cooling water pumped from the river. Therefore, the environmental effects at the plant intake are approximately the same for Helper Mode and Open Mode operation. The Closed Mode of operation is superior with respect to intake environmental effects since only a small quantity of water (approximately 220 cfs) is pumped from the river for "makeup."

The cooling tower lift pumps, fans and peripheral equipment require approximately 56 MW for normal operation. This is power which would be included in the net output of the plant in Open Mode, but which must now be obtained from other sources. In Closed Mode, there is an additional loss of net power generated due to the decreased efficiency which results from increased cooling water temperature. The precise loss in efficiency varies as a function of meteorology, but a conservative estimate of this loss, based on a Carnot cycle, is one percent of total generation or 35 MW. This results in a total loss of 91 MW in Closed Mode.

The cost of the power required to recover these losses varies with the source from which the power is obtained. The additional expense of Helper and Closed Mode operation will range from $560 per hour to $3,640 per hour or more, depending upon the source of the replacement power. This does not include depreciation of the cooling tower pumps, fans, etc. It is obvious, therefore, that unnecessary cooling tower operation can result in considerable cost to TVA and its consumers.

The relative environmental and economic advantages and disadvantages of each mode of cooling system operation are summarized in Table 1.

PROGRAM PARAMETERS AND COMPUTATIONS

The mixed temperature in the river downstream of the plant depends upon the performance of several subsystems of the plant cooling system. These will be discussed individually.

Temperature Increase Across Condensers

The condenser rise was determined by calibration tests which equated heat rejection (BTU/sec) with plant generation levels (MW). For a known condenser flow rate, the increase in temperature was easily computed.

Cooling Tower Performance

The cooling tower effluent temperature is primarily a function of the wet bulb temperature of the air and the temperature of the hot water from the condenser. The wet bulb temperature is computed from the dry bulb temperature and the dew point. An example of the tower performance curves is presented in Figure 3.

Multiport Diffuser Mixing

The mixed temperature of the river downstream of the plant depends upon the flow rate and temperature of both the thermal discharge and the river. The discharge conditions depend upon the mode of cooling and the condenser and, if applicable, cooling tower performance.

River flows over the diffuser are computed with a one-dimensional, unsteady finite-difference flow model. Hourly releases from Guntersville and Wheeler Dams are input as boundary conditions. A water temperature monitor [Ref. 1] upstream of the plant provides an ambient river temperature at initiation of a computer run. Subsequent river temperatures are computed by superimposing a statistical diurnal and annual cycle.

The mixing induced by the high velocity (approximately 10 ft/sec) jets of the submerged multiport diffuser is highly dependent upon the flow rate in the river. Model studies of this diffuser [Ref. 2] and theoretical techniques for this general class of diffuser [Ref. 3] were used to generate diffuser mixing curves such as those presented in Figure 4.

OPERATION OF THE COMPUTER MODEL

The computer program is used daily by personnel of the TVA Load Control Center in Chattanooga, Tennessee, to predict the optimum mode of cooling for the following 24 hours at the Browns Ferry Nuclear Plant. As input, the program uses ambient river temperature and projected hourly values of (a) Browns Ferry Nuclear Plant generation (MW); (b) flow releases from Guntersville Dam; (c) flow releases from Wheeler Dam; and (d) air temperature and dew point. The program uses these inputs to compute the mixed temperature in the river downstream of the diffusers for each of the following 24 hours. For each hour, computations are first performed for the most economical mode (Open Cycle), but if the thermal water quality standards cannot be satisfied, the program automatically cycles to Helper Mode and finally to Closed Mode if necessary. A flow chart for this computer program is presented in Figure 5.

Predicted mixed downstream river temperature, plant-induced heating and recommended cooling modes for each of the next 24 hours are transmitted to the operators at the Browns Ferry Nuclear Plant. Within practical limits, the nuclear plant operators follow these recommendations. If it is necessary to deviate significantly from any of the projections, the program is rerun to determine if changes in the recommended mode of cooling are required.

Table 2 presents typical results of a computation during a period of low river flows. Releases from Guntersville Dam varied between 0 and 45,000 cfs and releases from Wheeler Dam varied between 0 and 58,000 cfs. The resulting flows near the Browns Ferry Nuclear Plant were quite unsteady, as shown in Table 2. The net generation of the plant was a constant 2900 MW throughout this period. Predicted mixed temperatures (T_M) and plant-induced temperature rises (ΔT_M) in the river immediately downstream of the diffuser correspond to the mode of cooling recommended for that particular hour.

The column showing the approximate cumulative cost incurred by cooling tower operation during this period is not included in routine computations. These costs are based upon purchasing this power from outside utilities at an estimated rate of $40 per MW-hr. At those rates, the total cost of operating the towers for the minimum time suggested was $23,000. Without a sophisticated computation scheme of this type, it is likely that the cooling system of this nuclear plant would be operated in the Closed Mode throughout most of this 24-hour period. The cost of Closed Mode cooling for 24 hours at the maximum estimated rate is $87,000. However by using this predictive technique, TVA could effect a savings of as much as $64,000 while placing no undue thermal stress upon the aquatic ecosystem of the Tennessee River.

CONCLUSIONS

The condenser cooling system of the TVA Browns Ferry Nuclear Plant is designed to operate in three modes: Open, Helper and Closed. Open Mode discharges the cooling water directly to the river; Helper Mode routes the cooling water through cooling towers prior to discharge; and Closed Mode recycles the cooling tower effluent to the intake for reuse in condenser cooling.

Much of the time the plant can operate in the Open Mode without violating the thermal water quality standards and overstressing the aquatic ecosystem. However, because the river flows near the plant are often unsteady as a result of releases from upstream and downstream hydroelectric plants, the Helper and Closed Modes must be used periodically. The power required to operate these towers, and, for the case of Closed Mode, the loss in plant efficiency resulting from warmer temperatures of condenser cooling water, dictate that the cooling towers should be operated no more than necessary to protect the environment.

The factors influencing the choice of cooling mode are complex and include computations of heat rejection rate of the condenser, cooling tower performance, river flow and temperature, and submerged diffuser mixing. A computer program has been developed which analyzes hourly projections of plant generations, river flows, ambient river temperatures, and meteorology for the following 24 hours, and predicts the most efficient mode of cooling which will assure compliance with the thermal water quality standards for each hour. This program is run daily at TVA's Load Control Center in Chattanooga and results are transmitted to the Browns Ferry Nuclear Plant. An example of a typical 24-hour operation demonstrated that using the cooling towers only when necessary could save as much as $64,000 per day when compared with Closed Mode cooling for the same period. This was accomplished without violating the thermal water quality standards.

TABLE 1: RELATIVE ENVIRONMENTAL AND ECONOMIC IMPACT OF THE THREE COOLING MODES

Cooling Mode	Power Loss Due to Cooling Tower Operation	Cost to Replace Lost Power		Relative Aquatic Environmental Impact	
		Within TVA @$10/MW-hr	Outside TVA @$40/MW-hr	Intake	Discharge
Open	0	0	0	xx	xx
Helper	56 MW	$560/hr	$2240/hr	xx	x
Closed	91 MW	$910/hr	$3640/hr	--	--

TABLE 2: PREDICTED RESULTS FOR TYPICAL 24-HOUR OPERATION OF THE BROWNS FERRY COOLING SYSTEM

Hour	River Flows (cfs)	T_m (°F)	ΔT_m (°F)	Cooling Mode	Cumulative Estimated Cost (Dollars)
1200	33,650	38.8	2.6	Open	0
1300	28,899	39.3	3.0	Open	0
1400	19,543	40.8	4.5	Open	0
1500	17,221	39.8	3.4	Helper	0
1600	15,147	40.5	4.1	Helper	$ 2,240
1700	25,034	40.0	3.5	Open	4,480
1800	29,313	39.5	3.0	Open	4,480
1900	35,668	39.0	2.5	Open	4,480
2000	30,422	39.4	2.9	Open	4,480
2100	30,028	39.4	3.0	Open	4,480
2200	26,825	39.7	3.3	Open	4,480
2300	24,204	40.0	3.7	Open	4,480
2400	17,315	39.1	2.9	Helper	6,720
0100	12,361	40.2	4.0	Helper	8,960
0200	10,121	36.3	0.2	Closed	12,600
0300	8,571	36.4	0.4	Closed	16,240
0400	12,591	40.0	4.2	Helper	18,480
0500	18,098	38.7	2.9	Helper	20,720
0600	18,384	38.9	3.1	Helper	22,960
0700	34,005	38.5	2.7	Open	22,960
0800	41,125	38.1	2.2	Open	22,960
0900	43,226	38.0	2.0	Open	22,960
1000	39,272	38.3	2.2	Open	22,960
1100	39,981	38.4	2.2	Open	22,960
1200	40,728	38.4	2.2	Open	22,960

REFERENCES

1. Driver, E. E. and W. R. Waldrop, "The Tennessee Valley Authority's Program for Monitoring Water Temperature in the Vicinity of Thermal Power Plants," Proceedings of the XVIth Congress of IAHR, Vol. 3, pp 556-563, Sao Paulo, Brazil, July 1975.

2. Harleman, D.R.F., L. C. Hall, and T. G. Curtis, "Thermal Diffusion of Condenser Cooling Water During Steady and Unsteady Flows with Application to the TVA Browns Ferry Nuclear Plant," MIT, Report No. 111. Cambridge, MA. September 1968.

3. Jirka, G. and D.R.F. Harleman, "The Mechanics of Submerged Multiport Diffusers for Buoyant Discharges in Shallow Water," MIT. Report No. 169, Cambridge, MA. March 1973.

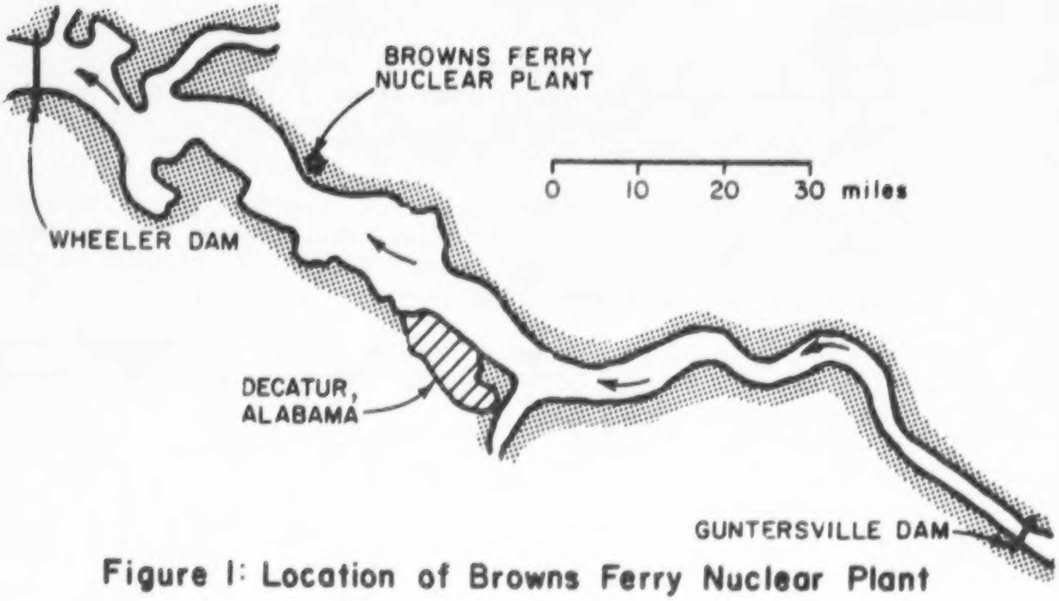
BROWNS FERRY
NUCLEAR PLANT
0
10
20
30 miles
WHEELER DAM
DECATUR,
ALABAMA
GUNTERSVILLE DAM

Figure 1: Location of Browns Ferry Nuclear Plant

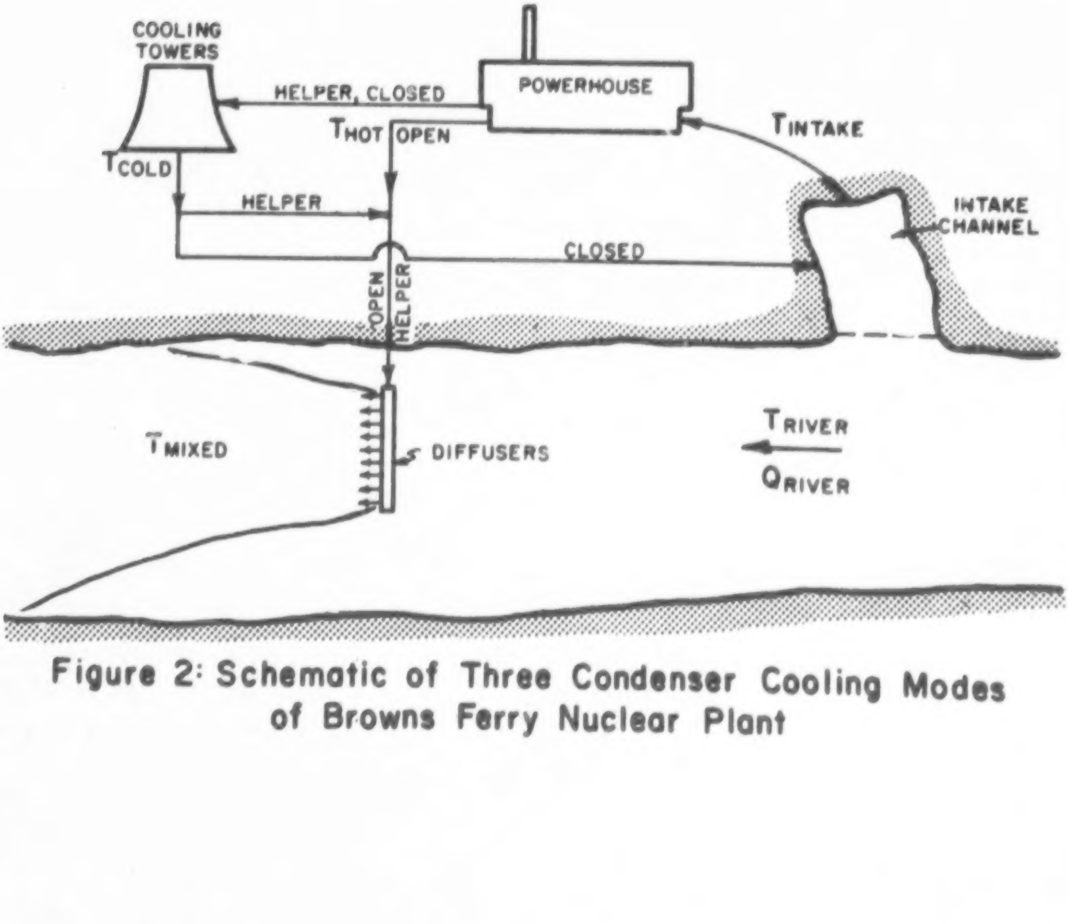
COOLING
TOWERS
HELPER, CLOSED
POWERHOUSE
T_{HOT} OPEN
T_{INTAKE}
T_{COLD}
HELPER
INTAKE
CHANNEL
CLOSED
OPEN
HELPER
T_{MIXED}
DIFFUSERS
T_{RIVER}
Q_{RIVER}

Figure 2: Schematic of Three Condenser Cooling Modes of Browns Ferry Nuclear Plant

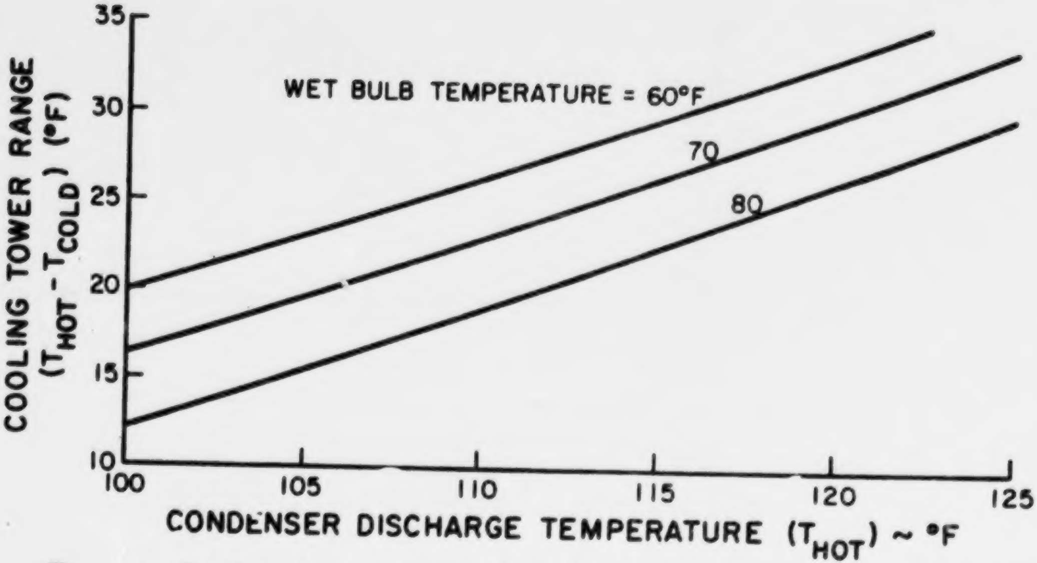

Figure 3: Cooling Tower Performance at Design Flow Rate

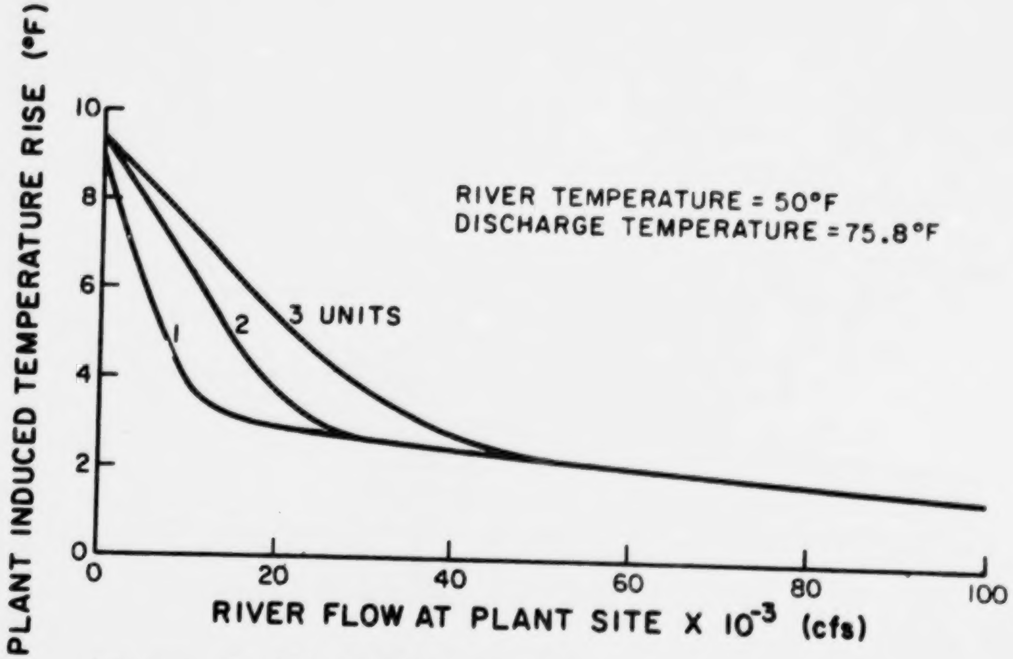

Figure 4: Mixed Temperature Increase Downstream of Diffuser

11

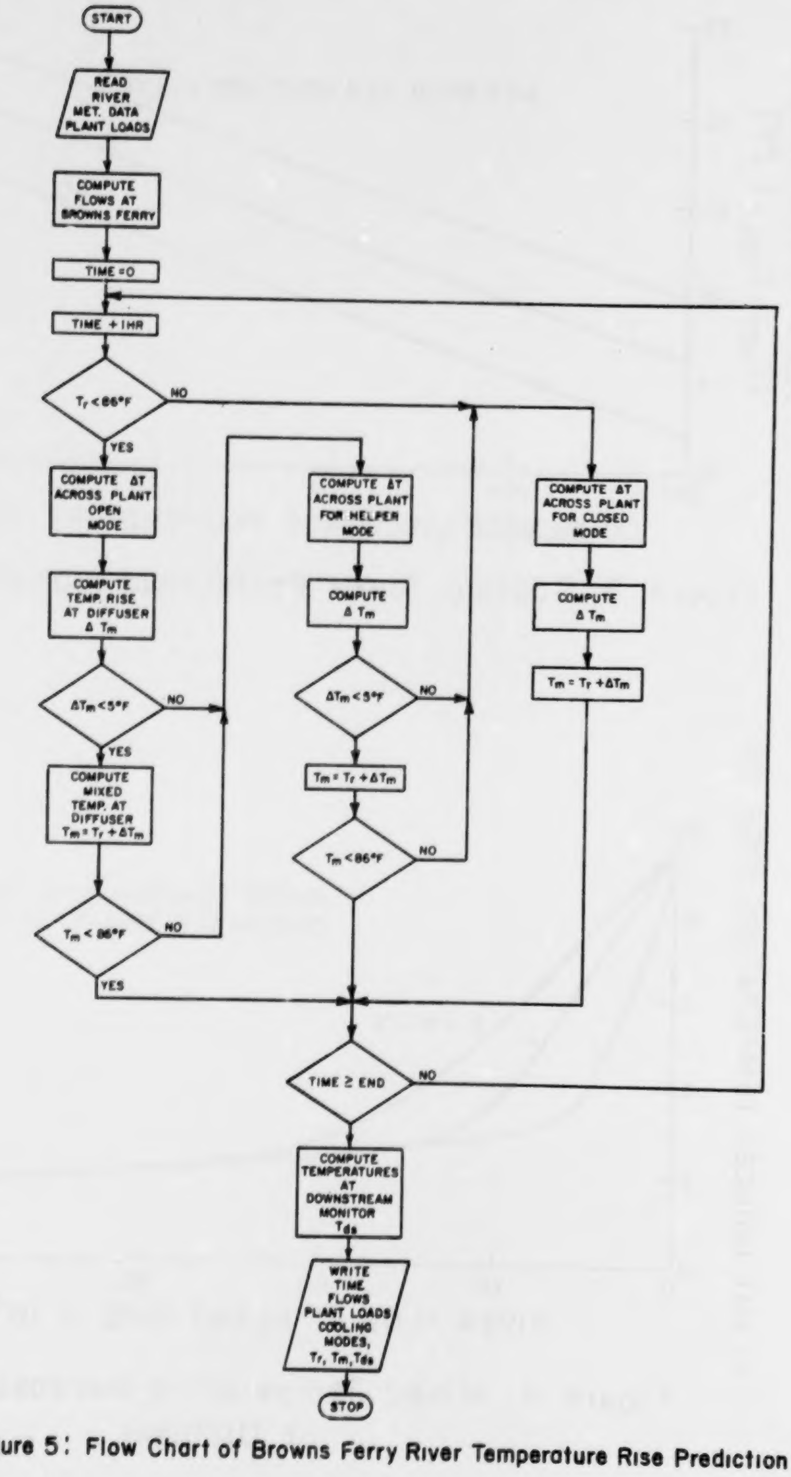
START
READ
RIVER
MET. DATA
PLANT LOADS
COMPUTE
FLOWS AT
BROWNS FERRY
TIME = 0
TIME + 1HR
$T_r < 86°F$
NO
YES
COMPUTE ΔT
ACROSS PLANT
OPEN
MODE
COMPUTE
TEMP. RISE
AT DIFFUSER
ΔT_m
$\Delta T_m < 5°F$
NO
YES
COMPUTE
MIXED
TEMP. AT
DIFFUSER
$T_m = T_r + \Delta T_m$
$T_m < 86°F$
NO
YES
COMPUTE ΔT
ACROSS PLANT
FOR HELPER
MODE
COMPUTE
ΔT_m
$\Delta T_m < 5°F$
NO
$T_m = T_r + \Delta T_m$
$T_m < 86°F$
NO
COMPUTE ΔT
ACROSS PLANT
FOR CLOSED
MODE
COMPUTE
ΔT_m
$T_m = T_r + \Delta T_m$
TIME ≥ END
NO
COMPUTE
TEMPERATURES
AT
DOWNSTREAM
MONITOR
T_{ds}
WRITE
TIME
FLOWS
PLANT LOADS
COOLING
MODES,
T_r, T_m, T_{ds}
STOP

Figure 5: Flow Chart of Browns Ferry River Temperature Rise Prediction Program

omit

TITLE: ECONOMICS OF BOILER BLOWDOWN
HEAT RECOVERY - by M. R. Bary

ABSTRACT: This paper deals with suitability of waste heat recovery from boiler blowdowns of existing power plants. Code requirements of many states are prohibiting utilities to dump the blowdown into water bodies, and asking them to install blow-off tanks.

From actual study of some existing power plants it has been determined that in some cases it is more economical to recover the waste heat in the blowdown and in some other cases it is not economically justified. The paper will discuss the factors that influence the choice of a heat recovery system from the economic standpoint. It also provides general guidelines for proper selection of such recovery systems and describes typical system components.

14-45-23

MATHEMATICAL MODELING OF WASTE HEAT MANAGEMENT ALTERNATIVES FOR THE UNITED STATES

H. J. Plass, Jr.
Dept. of Mechanical Engineering
University of Miami
Coral Gables, Florida U.S.A.

ABSTRACT

Waste heat resulting from electric power generation can produce serious local environmental problems in water bodies which receive the heat. It is possible through added devices or system modifications to divert some of this waste heat to the atmosphere or to useful purposes for the consumer. This paper examines two alternatives to once-through cooling, where all the waste heat is received by a local natural water body. These are (A) dry cooling towers, and (B) the Modular Integrated Utility System (MIUS). In the first case the waste heat is rejected immediately to the atmosphere, and in the second a substantial fraction of the waste heat is utilized in the local community for hot water, space heat, sewage treatment, etc. prior to its release to the atmosphere. Results are obtained using an equilibrium model for the U.S. energy-environment economic system developed previously by the author.

Preceding page blank

1. INTRODUCTION

The conversion of thermal energy from the combustion of fuel, or from the nuclear fission process, to electrical energy yields approximately two times as much rejected low grade thermal energy, or waste heat, as electrical energy produced. Since the efficiency of electric power production is increased by reducing the temperature of the exhaust steam as much as possible, large amounts of cooling water from rivers, lakes, or the sea must be used as the temporary receiver of this heat, which eventually is transferred to the atmosphere and then into space. During power plant operation the rate of addition of heat to the water body exceeds the rate of transfer of heat to the atmosphere and therefore the water body becomes warmer than it would normally be under natural conditions. This alteration in temperature causes changes in the local ecology of the water body. Some of these changes are undesirable, and could be considered as environmental damage. The effects of rejected heat on the ecology of the water which receives it are well summarized in Refs. [1], [2], and [3].

To reduce or prevent the environmental damage associated with heated water, alternative schemes have been used or proposed. Among these are wet cooling towers, cooling ponds, dry cooling towers, and various ways in which some of the rejected heat can be utilized prior to its ultimate transfer to the atmosphere. References [1] and [3] contain brief descriptions of such systems. One possible system which utilizes much of the waste heat in the Modular Integrated Utility System (MIUS), discussed in Reference [4]. The waste heat from the electric power plant is utilized for residential and commercial space and water heating, as for sewage treatment. Two obvious benefits of a MIUS are the reduction of environmental damage to the natural water body, and the reduction in fuel energy required for space and water heating. These benefits are not without their costs, however. Construction and operation of a MIUS requires capital, labor and energy, which must be considered in the overall assessment of its effectiveness.

This paper considers two alternative systems for the management of waste heat from electric power plants in the U.S. and compares their behavior with that of a reference system in which it is assumed that all cooling for power plants is of the once-through type. The two alternatives considered are: (A) dry cooling towers for all plants, and (B) the use of MIUS's on all plants. The first alternative has been chosen as the ultimate in prevention of undesirable environmental effects from waste heat. Heat transfer to the atmosphere is direct without loss of water through evaporation, and without associated undesirable atmospheric moisture. The second alternative is chosen for its added benefit of energy conservation.

The analysis for the two alternative systems are made using a simple model of the U.S. energy-economic-environment system developed by the author, Ref. [5]. The reference case (in which once-through cooling of power plants is assumed) is developed from economic data in Ref. [7], using environmental costs and control costs given in Refs. [4] and [8]. The model, shown in Fig. 1, assumes quantitative relationships between the energy flows (F's) the goods flows (GU's) the service flows (SU's), the labor (L's) and the environmental services (WU's). Envrionmental damage is accounted for in unwanted goods (GUc*), unwanted service (SU_c*), and decrease in labor productivity in a polluted surroundings. Control costs are accounted for by the monetary value of the environmental services (WU's). All quantitative relationships are determined from system coefficients which relate various outputs to various inputs. Simple analyses, presented in this paper, yield the modified coefficients for the alternative systems considered. Information other than environmental damage and environmental service costs can be obtained from the computed results. These include fuel energy used in each sector, labor used in each sector, distribution of goods and services, and the material well-being of the consumer. The effectiveness of the considered alternative depends on all of these results.

2. DISCUSSION OF THE MODEL

The model as shown in Fig. 1 in a closed-system equilibrium model. Exports and imports are not included, and each sector is assumed to operate in a steady-state equilibrium for which the output value added by the sector is equal to the values contributed by the inputs. Each alternative which is considered is an instantaneous alternative; no changes over time are considered for the total labor and the total energy resource reserves available. Technology changes required for the particular alternative, and rearrangements of the capital necessary for their accomplishment are assumed to be instantaneous. This approach enables one to answer the question: "What would have occurred if we had done these things instead of what we did do?"

2.1 Notation for the Model

The symbols appearing in Fig. 1, and in the equations describing the system operation are defined below, together with the units for each quantity.

E = extraction of energy resources

PG = production of goods

PS = production of services

W = waste removal and control

F_E = fuel to extract fuel (QBtu/yr)[a]

F_{PG} = fuel to production of goods sector (QBtu/yr)

F_W = fuel to pollution control secotr (QBtu/yr)

F_{PS} = fuel to service sector (QBtu/yr)

F_C = fuel to cosumer (QBtu/yr)

L_E = labor for extraction of fuel (B pers-hr/yr)[b]

L_W = labor for pollution control (B pers-hr/yr)

L_{PG} = labor for goods production (B pers-hr/yr)

L_{PS} = labor for service production (B pers-hr/yr)

GU_E = goods units[c] required by extraction (B units/yr)[b]

GU_W = goods units required by pollution control (B units/yr)

GU_{PS} = goods units required by the service sector (B units/yr)

GU_C = goods units purchased by the consumer (B units/yr)

GU_C^* ="unwanted" goods purchased by consumer to combat effects of pollution (B units/yr)

SU_{PG} = service units[d] required by goods production sector (B units/yr)

SU_C = service units purchased by the consumer (B units/yr)

SU_C^* = "unwanted" service units purchased by the consumer to combat pollution (B units/yr)

WU_E = pollution control units[c] required by the extraction sector (B units/yr)

WU_{PG} = pollution control units required by the goods production sector (B units/yr)

WU_{PS} = pollution control units required by the service production sector (B units/yr)

ℓ = hourly wage (\$/per-hr)

p_F = fuel price (\$/MBtu)[f]

p_G = goods price (\$/unit)

p_S = service price (\$/unit)

[a] QBtu = 10^{15} Btu

[b] B pers-hr = 10^9 pers-hr;
B units = 10^9 units

[c] Goods units = part of L_{PG} required for goods used

[d] Service units = part of L_{PS} requir[illegible] for services used

[e] Pollution control units = part of L_W required for the particular control effort considered

[f] MBtu = 10^6 Btu

2.2 Basic Equations for the Model

The quantities defined above are assumed to be related as follows:

Fuels used:

The fuels used by each sector are proportional to their outputs. The fuel used by the consumer depends on the consumption rate for goods. That is:

$$F_{PG} = B_{PG} \left(GU_E + GU_{PS} + GU_W + GU_C + GU_C^* \right) \tag{1}$$

$$F_W = B_W \left(WU_E + WU_{PG} + WU_{PS} \right) \tag{2}$$

$$F_{PS} = B_{PS} \left(SU_{PG} + SU_C + SU_C^* \right) \tag{3}$$

$$F_C = B_C \left(GU_C + GU_C^* \right) \tag{4}$$

In the above, B_{PG}, B_W, B_{PS}, and B_C are constants determined from economic and technical data. See Ref. [7].

The goods (units) and service (units) required by E, PG, PS, and W are proportional to the labor effort expended, and are diminished by a productivity reduction factor dependent upon the level of pollution in the environment. That is:

$$GU_E = \gamma_E L_E (1-\gamma w^2) \tag{5}$$

$$GU_W = \gamma_W L_W (1-\gamma w^2) \tag{6}$$

$$GU_{PS} = \gamma_{PS} L_{PS} (1-\gamma w^2) \tag{7}$$

$$SU_{PG} = \sigma_{PG} L_{PG} (1-\gamma w^2) \tag{8}$$

In the above, γ is constant determined by loss of performance data given in Ref. [2], and w is the fraction of the total possible effluent from all sources. The other coefficients are determined from economic data.

Outputs:

The output of each sector is assumed to be proportional to the labor invested, diminished by the environmental loss-of-productivity factor just mentioned.

$$F_{PG} + F_W + F_{PS} + F_C = (\beta_E - f_E)\, L_E\, (1-\gamma w^2) \qquad (9)$$

$$GU_E + GU_W + GU_{PS} + GU_C + GU_C^* = L_{PG}\, (1-\gamma w^2) \qquad (10)$$

$$SU_{PG} + SU_C + SU_C^* = L_{PS}\, (1-\gamma w^2) \qquad (11)$$

$$WU_E + WU_{PG} + WU_{PS} = L_W\, (1-\gamma w^2) \qquad (12)$$

In the above, β_E and f_E, are constants determined by the fractions of the various energy resources used and the difficulty of extracting each.

Full employment:

The total labor available is assumed constant. Only the distribution changes. That is:

$$L_E + L_W + L_{PG} + L_{PS} = L_T \qquad (13)$$

Economic equilibrium:

The value of the inputs to each sector is assumed to be equal to the value added by the sector. That is:

$$\frac{p_F}{\ell}(F_{PG} + F_W + F_{PS} + F_C) = L_E + \frac{p_W}{\ell} WU_E + \frac{p_G}{\ell} GU_E \qquad (14)$$

$$\frac{p_G}{\ell}(GU_E + GU_W + GU_{PS} + GU_C + GU_C^*) =$$

$$L_{PG} + \frac{p_W}{\ell} WU_{PG} + \frac{p_S}{\ell} SU_{PG} + \frac{p_F}{\ell} PG \qquad (15)$$

$$\frac{p_W}{\ell}(WU_{PG} + WU_{PS}) = L_W + \frac{p_F}{\ell} F_W + \frac{p_G}{\ell} GU_W \qquad (16)$$

$$\frac{p_S}{\ell}\left(SU_{PG} + SU_C + SU_C^*\right) = L_{PS} + \frac{p_F}{\ell}F_{PS} + \frac{p_G}{\ell}GU_{PS} + \frac{p_W}{\ell}WU_{PS}$$

In the above, ℓ = hourly wage.

Consumer choice:

The amounts of goods, and services, purchased by the consumer are dependent on the consumer income, the prices of fuel, goods, and services, and the perceived benefit or utility from each unit purchased. The following utility function is assumed:

$$R = A\left[1 - \exp\left(-\frac{GU_C}{G_M}\right)\right] + B\left[1 - \exp\left(-\frac{SU_C}{S_M}\right)\right] \qquad (18)$$

The quantity R is assumed to be a maximum subject to the income constraint:

$$\left(\frac{p_G}{\ell} + B_C \frac{p_F}{}\right)\left(GU_C + GU_C^*\right) + \frac{p_S}{\ell}\left(SU_C + SU_C^*\right) = L_T \qquad (19)$$

Environmental effects other than loss of producitvity:

The amounts of environmental improvement services to each sector as given by:

$$WU_E = h(1-w)^2 L_E \qquad (20)$$

$$WU_{PG} = h(1-w)^2 L_{PG} \qquad (21)$$

$$WU_{PS} = h(1-w)^2 L_{PS} \qquad (22)$$

In the above, h is a constant depending on the kinds and amounts of fuels used. The consumer must also purchase certain "unwanted" goods and services to combat undersirable effects of pollution, namely:

$$GU_C^* = kw^2(GU_C) \qquad (23)$$

$$SU_C^* = kw^2(SU_C) \qquad (24)$$

In the above, k is a constant determined by the kinds, and amounts of fuels used.

3. NUMERICAL VALUES OF COEFFICIENTS

The procedure for determing the numerical values of the coefficients for the reference system, in which once-through cooling is assumed for all electric power plants, is outlined in Ref. [5]. In that reference four assumed mixes of fuel are considered. Here we donsider only one mix, namely that labeled as Case I in Ref. [5]. Values for the reference case (and the two alternatives) are tabulated in Table 1.

The corresponding coefficients for (A) the dry cooling towers alternative and for (B) the MIUS alternative are obtained by accounting for changes in environmental damage, environmental treatment costs, fuel used, equipment used, and labor required when one of the alternatives is substituted for the reference system. In all cases the levels of activity for the 1975 projection given in Ref. [7] are assumed.

3.1 Alternative (A) - Dry Cooling Towers

The use of dry cooling towers eliminate the environmental damage resulting from heated water. This affects the total amounts of unwanted goods and services GU_c^* and SU_c^*, and consequently affects the coefficient k. For heated water, the consumer-perceived environmental damage is approximately the cost to the consumer of having to pay for extra transportation to obtain the water recreation or esthetic benefit provided only by unheated water. According to Ref. [2], p. 162, 1300 acres of water are required to dissipate 75% of the rejected heat for once-through cooling of a 1000Mw plant under usual operating conditions. Assuming 21 QBtu/yr of fuel energy for the U.S. electrical generation sector in 1975, Ref. [7], and assuming a 33 1/3% thermal efficiency, the amount of waste heat which must be rejected to water is 14 QBtu/yr and the amount of electrical energy produced is 7 QBtu/yr. This is equivalent to an average electrical power output of 2.34×10^5 Mw. The amount of water affected by once-through cooling is therefore 3.04×10^5 acres. If this is assumed to be allocated to rivers having an average width of 1000 feet, the total river length affected is 1.32×10^7 feet. Assuming the total population is distributed in N cities of 100,000 population, we obtain N = 2130 such cities, with a prorated share of river affected equal to 6200 feet. This is approximately one mile of river for each 100,000 population. Assume that 1/4 of the population must drive an extra distance of 2 miles per water recreation trip, and that 25 such trips are made each year.

At 15¢ per mile this yields an environmental cost to the consumer of 0.375 B$/yr. as a result of heated water. This is allocated to GU_c^* and SU_c^* in the same proportions as GU_c^* and SU_c^* occur in the results of the reference case. See Ref.[5]. We get ΔGU_c^* and ΔSU_c^* for heated water to be 0.078 and 0.297 B$/yr respectively. Thus, one could expect approximately a 10% reduction in GU_c^* and SU_c^* for the alternative (A), dry cooling towers. Thus, k for dry cooling towers = 0.9 x k for the reference system.

According to Ref. [8] dry cooling towers require from $20 to $30 per kilowatt for capital equipment, and results in a 1% to 3% increase for the cost of electricity. The capital cost increase is approximately 10% of the plant cost, and increases the goods flow GUw to the environmental service sector. Assuming that 14% of the service in the PS sector is for electrical energy distribution service ($ value of electricity sold rel. to toal service $), it is possible to estimate the increment to GUw thus:

$$\Delta GUw = 2\% \times 10\% \times 14\% \times GU_{PS} \times 1/3 = 0.11 \text{ B units/yr}$$

Here GU_{PS} was assumed to equal 26 B units/yr. See Ref. [5].

The last factor (1/3) is a result of assuming that the electrical energy sold to consumers in their homes is approximately 1/3 of the total. The increase in ΣWU, the environmental service is 2% x electricity cost to all users converted to units of environmental service. This yields ΔWU = 0.16 B units/yr, or about 8% of the total ΣWU provided in the reference case. Thus, h with dry cooling towers = 1.08 in the reference case.

The values of the coefficients β_w and γ_w are also changed by the introduction of cooling towers. The values for these coefficients are obtained by requiring economic equilibrium for the W sector of Fig. 1 with the previously obtained values of ΔGUw and $\Delta(\Sigma WU)$ added to the reference values obtained from Ref. [5]. The corresponding increase in labor is assumed to be found from

$$\frac{\Delta Lw}{(Lw)\text{ ref.}} = \frac{1}{3}\,\frac{(\Delta GU_w)}{(GU_w)_{ref}}$$

where the factor 1/3 expresses approximately the relation between added capital and added labor for a capital intensive industry (Barry Commoner, Ref. [9]). Balancing the dollar flow results in $\Delta F_w = 0.22$ QBtu/yr for the case, w = 0, maximum environmental controls. Therefore:

$$B_w = \frac{(Fw)\ ref + \Delta Fw}{(\Sigma WU)\ ref + \Delta(\Sigma WU)} = 0.5566\ \frac{MBtu}{W\text{-}unit}$$

$$\gamma_w = \frac{(GUw)\ ref + \Delta GUw}{(Lw)\ ref + \Delta Lw} = 0.4419\ \frac{goods\ unit}{pers - hr}$$

Using the previous arguments concerning k and h, we get

$$k = 0.9\ (k)_{ref} = 0.0374$$
$$h = 1.08\ (h)_{ref} = 0.0130$$

All other system coefficients are assumed unchanged. All system parameters for the dry cooling tower case are tabulated in Table 1.

3.2 Alternative (B) - MIUS

A description of the MIUS system is given in Ref. [4]. It is a system which recycles waste heat, liquid and solid wastes. The waste heat is utilized to provide hot water and space heating to the residential and commercial buildings in the community which also receives the electric power generated. Waste water from these customers is treated and re-used as make-up water for power plant cooling and for the operation of cooling towers. Solid wastes are incinerated to provide added heat to the power plant.

According to the authors of Ref. [4], slightly more than 1/4 of the rejected heat from the power plant cannot be utilized and must be handled by cooling towers. A conservative estimate, for the purposes of the analysis in this paper, is that 2/3 of the power plant waste heat is utilized for space and water heating. It is assumed that the total fuel energy required for residential and commercial use is reduced by an amount equal to the waste heat energy utilized. Also according to Ref. [4], a MIUS having an electric power output of 2500Kw will serve 720 units in the residential sector, plus the required commercial enterprises which accompany this community. For a 2500Kw plant the waste heat generation rate, assuming a thermal efficiency of 33 1/3%, is 1667 Kw, of which 2/3 is utilized. Thus, the utilized waste heat rate is 1111Kw or 3.79×10^6 Btu/hr. Assuming that the utilized heat is shared equally by residential and commercial users, each residential unit utilizes 2630 Btu/hr. Although it is not likely that all households in the U.S. could participate in MIUS's, it is assumed for purposes of simple analysis that such is possible.

Therefore, for the entire U.S, with approximately 65.4 million units, the annual utilized waste heat energy in the residential sector is 1.51 QBtu/yr. An equal amount is assumed to be utilized in the service sector.

Consider first the revisions for MIUS in the environmental services sector W. Let w = 0, which means that all wastes are treated. For MIUS less effort, fuel and capital are required to completely treat all effluents of the system because only 1/3 of the heated water from power plants must be handled by cooling towers. In the previous analysis for cooling towers it was shown that h, the system parameter which relates the needed environmental service WU to the labor effort invested, had to be increased by 8% over the reference case in which once-through cooling is assumed. For MIUS, we wimply reduce the 8% to 1/3 of 8% or 2.6%. Therefore, $h_{MIUS} = 1.026\ h_{ref}$. For dry cooling towers it was shown that the increment in environmental service units was 0.16 B units/yr. For MIUS we assume that this increase is 1/3 as great, or 0.053 B units/yr. Therefore, $(\Sigma WU)_{MIUS} = 2.105$ B units/hr.

The increment in goods units to W, ΔGU_w, relative to the reference system, is taken to be 1/3 of the ΔGU_w for dry cooling towers. Thus, ΔGU_w for MIUS is approximately 0.04 B units/yr, and $(GUw)_{MIUS} = 0.87$ B units/yr for w = 0, whereas in the reference case (GU_w) ref. = 0.84 B units/yr. Assuming that the percent increase in fuel for W is equal to the percent increase in GU , we get $(F_W)_{MIUS} = 1.056$ QBtu/yr. The relative increment in labor is smaller than that for fuel and capital since we are dealing with a capital intensive and energy intensive device. We take $(L_W)_{MIUS} = \Sigma WU = 2.105$ B pers-hr/yr. From these values, we can obtain $(B_W)_{MIUS}$ and $(\gamma_W)_{MIUS}$ as follows:

$$(B_W)_{MIUS} = \frac{F_W}{\Sigma WU} = 0.5017 \text{ M Btu/unit}$$

$$(\gamma_W)_{MIUS} = \frac{GU_W}{L_W} = 0.4152 \text{ goods unit/pers-hr}$$

Next, consider the consumption sector C. The total fuel for C in the MIUS alternative is (F_C) ref - ΔF = 22.28 - 1.51 = 21.27 QBtu/yr. Assuming the same prices as in the reference case, (See Table 2) and assuming that dollars saved on fuel are spent for the added service which MIUS provides, it can be shown that $(SUc)_{MIUS} = 75.42$ B serv. units/yr. The value of $(GU_C)_{MIUS}$ is assumed equal to that for the reference case, for the purposes of computing the system parameter B_C. We get

$$(Bc)_{MIUS} = \frac{F_c}{GU_c} = 1.0757 \text{ MBtu/goods unit}$$

Consider next the service (PS) sector. The fuel saved for PS is assumed to be equal to that saved for C. Thus, $(F_{ps})_{MIUS}$ = 22.80 - 1.51 = 21.29 QBtu/yr. Assuming ΔSu produced is equal numerically to the labor L_{ps}, and that the only increment is service units for MIUS is that mentioned above, we get $(\Delta SUc)_{MIUS}$ = 0.20 B serv.units/yr. Therefore, $(SUc)_{MIUS}$ = 75.40 B serv.units/yr. Assuming that $(GU_{ps})_{MIUS}$ and $(SU_{pg})_{MIUS}$ are equal to the corresponding values for the reference system, a dollar balance for PS yeilds (L_{ps}) = 114.52 B pers-hr/yr. This is not equal to $(\Sigma SU)_{MIUS}$, as required by the model. Therefore, we average L_{ps} and ΣSU to compute the system parameters γ_{ps} and B_{ps} for MIUS. We get

$$(\gamma_{ps})_{MIUS} = \frac{(GU_{ps})_{MIUS}}{\frac{1}{2}(L_{ps} + \Sigma SU)_{MIUS}} = 0.2388 \ \frac{\text{goods unit}}{\text{pers-hr}}$$

$$(B_{ps})_{MIUS} = \frac{(F_{ps})_{MIUS}}{\frac{1}{2}(L_{ps} + \Sigma SU)_{MIUS}} = 0.1870 \ \frac{\text{MBtu}}{\text{serv.unit}}$$

One final comment should be made about the values of the system parameters γ, h, and k obtained above. These are determined by the amount of effluent contributed to the environment by the total system. They were computed for w = 0 relative to the reference case for w = 0. Now to accomplish w = 0 for MIUS requires less effort since for MIUS the total fuel consumed is less and therefore the total effort to clean up the energy-related effluents is less. Since effort to clean up pollution is assumed in the model to be proportional to the square of the effluent removed, it seems appropriate to reduce all parameters computed above by the ratio $(F_{MIUS}/F_{ref})^2$ = 0.9239. Thus, we get corrected values for γ,h, and k as follows

$(\gamma)_{MIUS} = 0.03696$

$(h)_{MIUS} = 0.01138$

$(k)_{MIUS} = (0.9239) \left[(k) \text{ dry towers}\right] = 0.03459$

The entire set of system parameters for MIUS is presented in Table 1.

4. COMPUTED RESULTS AND CONCLUSIONS

The set of equations (1) through (24) are solved using the pattern of solution presented in Ref. [5] for (A) the dry cooling towers and for (B) the MIUS. Results are listed in Tables 3 and 4 respectively. An added variable is labeled E.S.C./Income(%). E.S.C. = the "Environmental Social Cost", E.S.C. = $p_G (GU_c^*) + p_S (SU_c^*) + p_W (\Sigma WU) + \gamma w^2$ (Income). The first two terms are the direct cost to the consumer for "unwanted" goods and services required because the environment is bad. The third term is the cost of improving the environment through environmental services, and the last term is the cost in lost production due to reduced worker performance in a polluted environment. Since income is the product of the hourly wage l and the total work force L_T, it is possible to use the price ratios $p_{F/\ell}$, $p_{G/\ell}$, $p_{S/\ell}$ and $p_{W/\ell}$ found by solving the system equations of Ref. [5], one gets

$$\frac{\text{E.S.C.}}{\text{Income}}(\%) = \frac{\frac{p_G}{\ell}(GU_c^*) + \frac{p_S}{\ell}(SU_c^*) + \frac{p_W}{\ell}(\Sigma WU) + \gamma w^2 L_T}{L_T} \times 100$$

Examination of the results for the environmental social cost as a percent of income indicate that a minimum for each system occurs near w = 0.2. It is seen that the alternative (A) Dry Cooling Towers requires approximately a 9% greater share of income for optimum environmental control than for once-through cooling, whereas the alternative (B) MIUS requires a 6% smaller share of income for optimum environmental control.

Comparisons of the results for GU_c and SU for the three systems indicate that for the alternative (A) Dry Cooling Towers, the values of both GU_c and SU_c are only slightly less than those for once-through cooling, which means that the added effort for environmental control is not felt by the consumer as lost purchasing power. It is felt primarily as the worth while expense of a less disturbing environment. Note that the argument which is sometimes presented is not true, namely that if it were not for the expense of pollution control, a larger proportion of the consumer's income would be available for desireable goods and service. This "extra" income goes instead for defenses against pollution damage. Dry cooling towers provide almost a zero net benefit. They could possibly be perceived as a system with positive net benefit if the utility function for the consumer were modified to include the environmental quality. The advantages of the MIUS are more evident. The value of GU_c for MIUS is slightly greater than GU_c for once-through cooling, whereas SU_c for MIUS is less. This is an indication that the prices for goods and services in MIUS tend to shift the consumer's demand toward goods. Many consumers would perceive this is a net benefit. The most obvious benefit of MIUS is its energy saving feature. Note that the total fuel energy F for MIUS is 6% less than that for once-through cooling for essentially the same state of well-being for the consumer. Less fuel used means less extraction labor and therefore greater employment in the production sector. MIUS provides the same environmental protection as dry cooling towers at less cost to society for controls, and with less demand for energy resources.

REFERENCES

[1] John M. Fowler, "Energy and the Environment", McGraw - Hill Book Co. (1975), Chapter 8.

[2] Gerald Garvey, "Energy,Ecology, Economy", W.W. Norton & Co. (1972), Chapter 8.

[3] Richard Wilson and William Jones, "Energy, Ecology and the Environment", Academic Press (1974), Chapter 4.

[4] W.R. Mixon and J.O. Kobb, "Modular Integrated Utility Systems (MIUS)", Proceedings of Energy Conservation: A National Forum, University of Miami (1975), p. 431.

[5] H.J. Plass, Jr., "A Detailed Analysis of the Environmental Effects of Energy Utilization in the U.S. Economy", Proceedings of the University of Missouri-Rolla Energy Conference (1976).

[6] Science and Public Policy Program, University of Oklahoma Report, "Energy Alternatives: A Comparative Analysis," U.S. Government Printing Office (1975).

[7] Ford Foundation Energy Policy Project, "A Time to Choose", Ballinger Publishing Co. (1974).

[8] Council on Economic Priorities, "The Price of Power" (1972).

[9] Barry Commoner, "Energy, the Environment and the Economy", an address before The Energy Problem Continues,Kellog Center for Continuing Education, Michigan State University (1975).

TABLE 1

SYSTEM COEFFICIENTS

SYSTEM COEFFICIENTS		REF. SYST.	DRY COOLING TOWERS	MIUS
B_{PG}	(MBtu/goods unit)	0.5044	0.5044	0.5044
B_{PS}	(MBtu/serv.unit)	0.2018	0.2018	0.1870
B_C	(MBtu/goods unit)	1.1521	1.1521	1.0759
B_W	(MBtu/W-unit)	0.4945	0.5566	0.5017
γ_E	(goods unit/pers-hr)	0.4092	0.4092	0.4092
γ_W	(goods unit/pers-hr)	0.4092	0.4419	0.4152
γ_{PS}	(goods unit/pers-hr)	0.2336	0.2336	0.2388
σ_{PG}	(serv.unit/pers-hr)	0.7523	0.7523	0.7523
γ	(dimensionless)	0.0400	0.0400	0.03696
β_E	(MBtu/pers-hr)	9.9795	9.9795	9.9795
f_E	(MBtu/pers-hr)	0.7621	0.7621	0.7621
A	(dimensionless)	0.4698	0.4698	0.4698
B	(dimensionless)	1.1122	1.1122	1.1122
G_M	(B goods units)	20.26	20.26	20.26
S_M	(B serv.units)	76.98	76.98	76.98
h	(W-units/pers-hr)	0.0120	0.0130	0.01138
k	(dimensionless)	0.0416	0.0374	0.03459
L_T	(B pers-hr)	173.0	173.0	173.0

TABLE 2
SYSTEM VARIABLES vs. w. REFERENCE CASE (1975)

VARIABLE		w=0	w=0.2	w=0.4	w=0.6	w=0.8
p_F/ℓ	(pers-hr/MBtu)	0.216	0.214	0.214	0.214	0.216
p_G/ℓ	(pers-hr/goods unit)	2.350	2.333	2.329	2.336	2.356
p_S/ℓ	(pers-hr/serv.unit)	1.617	1.606	1.602	1.608	1.621
p_W/ℓ	(pers-hr/W-unit)	2.068	2.062	2.065	2.076	2.097
L_E	(B pers-hr)	7.801	7.801	7.800	7.800	7.800
L_W	(B pers-hr)	2.051	1.321	0.749	0.336	0.085
L_{PG}	(B pers-hr)	50.189	50.227	50.256	50.277	50.289
L_{PS}	(B pers-hr)	112.959	113.652	114.195	114.586	114.825
GU_E	(B units/yr)	3.192	3.187	3.172	3.146	3.110
GU_W	(B units/yr)	0.839	0.540	0.304	0.136	0.034
GU_{PS}	(B units/yr)	26.387	26.507	26.505	26.382	26.137
GU_C	(B units/yr)	19.770	19.880	19.821	19.596	19.210
GU_C^*	(B units/yr)	0.000	0.033	0.132	0.293	0.511
WU_E	(B units/yr)	0.094	0.060	0.034	0.015	0.004
WU_{PG}	(B units/yr)	0.602	0.386	0.217	0.097	0.024
WU_{PS}	(B units/yr)	1.356	0.873	0.493	0.220	0.055
SU_{PG}	(B units/yr)	37.757	37.725	37.566	37.279	36.864
SU	(B units/yr)	75.202	75.620	75.396	74.541	73.076
SU_C^*	(B units/yr)	0.000	0.126	0.502	1.116	1.946
F_{PG}	(OBtu/yr)	25.315	25.294	25.187	24.994	24.717
F_W	(WBtu/yr)	1.014	0.652	0.368	0.164	0.041
F_{PS}	(QBtu/yr)	22.799	22.898	22.897	22.791	22.579
F_C	(QBtu/yr)	22.777	22.942	22.988	22.915	22.721

TABLE 2 (cont'd.)

VARIABLES	w=0	w=0.2	w=0.4	w=0.6	w=0.8
F_E (QBtu/yr)	5.946	5.935	5.906	5.859	5.791
F (Qbtu/yr)	77.847	77.721	77.346	76.723	75.849
E.S.C./Income, (%)	2.45	1.90	2.18	3.28	5.18

TABLE 3

SYSTEM VARIABLE vs. w. DRY COOLING TOWERS

VARIABLE		w=0	w=0.2	w=0.4	w=0.6	w=0.8
P_F/ℓ	(pers-hr/ MBtu)	0.216	0.214	0.214	0.214	0.216
P_G/ℓ	(pers-hr/goods unit)	2.358	2.338	2.331	2.337	2.356
P_S/ℓ	(pers-hr/serv. unit)	1.623	1.609	1.604	1.608	1.621
P_W/ℓ	(pers-hr/W-unit)	2.162	2.154	2.156	2.167	2.188
L_E	(B pers-hr)	7.814	7.809	7.805	7.803	7.801
L_W	(B pers-hr)	2.220	1.430	0.811	0.364	0.092
L_{PG}	(B pers-hr)	50.223	50.249	50.268	50.282	50.292
L_{PS}	(B pers-hr)	112.743	113.512	114.116	114.551	114.815
GU_E	(B units/yr)	3.197	3.190	3.174	3.147	3.110
GU_W	(B units/yr)	0.981	0.631	0.356	0.159	0.040
GU_{PS}	(B units/yr)	26.340	26.474	26.487	26.374	26.134
GU_C	(B units/yr)	19.707	19.843	19.811	19.615	19.259
GU_C^*	(B units/yr)	0.000	0.030	0.119	0.264	0.461
WU_E	(B units/yr)	0.102	0.065	0.037	0.016	0.004
WU_{PG}	(B units/yr)	0.653	0.418	0.235	0.105	0.026
WU_{PS}	(B units/yr)	1.466	0.944	0.534	0.238	0.060
SU_{PG}	(B units/yr)	37.782	37.742	37.575	37.283	36.866
SU_C	(B units/yr)	74.961	75.476	75.360	74.614	73.257
SU_C^*	(B units/yr)	0.000	0.113	0.451	1.005	1.754
F_{PG}	(QBtu/yr)	25.332	25.305	25.193	24.997	24.718
F_W	(QBtu/yr)	1.236	0.795	0.449	0.200	0.050

TABLE 3 (cont'd.)

VARIABLE	w=0	w=0.2	w=0.4	w=0.6	w=0.8
F_{PS} (QBtu/yr)	22.752	22.870	22.881	22.784	22.577
F_C (QBtu/yr)	22.705	22.896	22.961	22.902	22.719
F_E (QBtu/yr)	5.955	5.942	5.910	5.861	5.793
F (QBtu/yr)	77.980	77.806	77.396	76.745	75.857
E.S.C./Income, (%)	2.77	2.09	2.23	3.19	4.95

TABLE 4

SYSTEM VARIABLES vs. w. MIUSs FOR ALL ELECTRIC POWER

VARIABLE		w=0	w=0.2	w=0.4	w=0.6	w=0.8
$P_{F/\ell}$	(pers-hr/ MBtu)	0.216	0.214	0.214	0.214	0.216
$P_{G/\ell}$	(pers-hr/goods unit)	2.356	2.340	2.335	2.342	2.360
$P_{S/\ell}$	(pers-hr/serv. unit)	1.627	1.615	1.612	1.617	1.629
$P_{W/\ell}$	(pers-hr/W-unit)	2.087	2.081	2.083	2.093	2.113
L_E	(B pers-hr)	7.488	7.485	7.483	7.481	7.481
L_W	(B pers-hr)	1.947	1.253	0.710	0.319	0.081
L_{PG}	(B pers-hr)	50.685	50.720	50.750	50.771	50.786
L_{PS}	(B pers-hr)	112.881	113.543	114.057	114.430	114.653
GU_E	(B units/yr)	3.086	3.081	3.066	3.043	3.011
GU_W	(B units/yr)	0.802	0.516	0.291	0.130	0.032
GU_{PS}	(B units/yr)	26.956	27.076	27.076	26.962	26.732
GU_C	(B units/yr)	19.840	19.947	19.907	19.715	19.381
GU^*_C	(B units/yr)	0.000	0.028	0.110	0.246	0.429
WU_E	(B units/yr)	0.085	0.055	0.031	0.014	0.003
WU_{PG}	(B units/yr)	0.577	0.369	0.208	0.092	0.023
WU_{PS}	(B units/yr)	1.285	0.827	0.467	0.208	0.052
SU_{PG}	(B units/yr)	38.130	38.100	37.953	37.687	37.303
SU_C	(B units/yr)	74.751	75.171	75.014	74.295	73.022
SU^*_C	(B units/yr)	0.000	0.106	0.415	0.925	1.617
F_{PG}	(QBtu/yr)	25.565	25.545	25.447	25.268	25.011
F_W	(QBtu/yr)	0.977	0.628	0.354	0.158	0.039

TABLE 4 (cont'd.)

VARIABLE	w=0	w=0.2	w=0.4	w=0.6	w=0.8
F_{PS} (QBtu/yr)	21.109	21.201	21.203	21.114	20.933
F_C (QBtu/yr)	20.852	20.881	20.968	21.112	21.314
F_E (QBtu/yr)	5.706	5.696	5.669	5.625	5.566
F (QBtu/yr)	74.722	74.581	74.230	73.663	72.887
E.S.C./Income, (%)	2.35	1.79	1.98	2.91	4.57

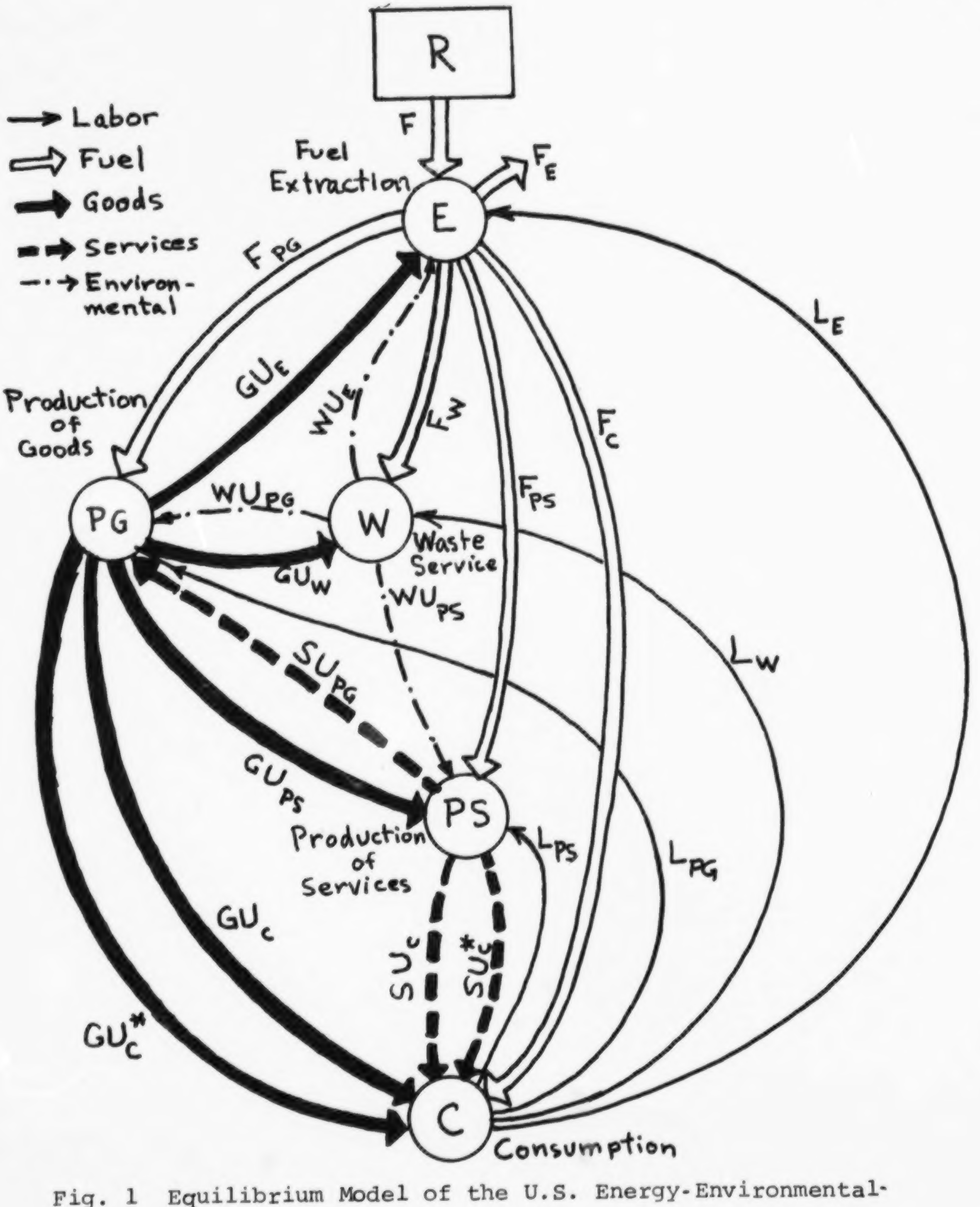
R
F
Labor
Fuel
Goods
Services
Environmental
Fuel Extraction
E
F_E
F_{PG}
L_E
GU_E
WU_E
F_W
F_C
Production of Goods
PG
WU_{PG}
W
Waste Service
F_{PS}
GU_W
WU_{PS}
SU_{PG}
L_W
GU_{PS}
PS
Production of Services
L_{PS}
L_{PG}
GU_C
SU_C
SU_C^*
GU_C^*
C
Consumption

Fig. 1 Equilibrium Model of the U.S. Energy-Environmental-Economic System

omit

V-B-107

Abstract Submitted to the Conference on Waste Heat Management and
Utilization, Miami Beach, Florida, May 9-11, 1977

ENGINEERING TRADEOFFS GOVERNING WASTE HEAT MANAGEMENT AND UTILIZATION

by

S. J. Daugard and T. R. Sundaram

ABSTRACT

For several years proponents of "waste" heat utilization have developed and demonstrated many idealized applications. Inevitably, it has been suggested that since these conservation schemes have been demonstrated under experimental conditions, full-scale technological development is feasible. However, these proof-of-concept technological demonstrations do not mean that "waste" heat utilization concepts can necessarily achieve successful or widespread application. In fact, even if major system-development efforts were to begin today, practical large-scale "waste" heat utilization systems are still several years off.

The present paper discusses engineering, economic and social tradeoffs that must be considered as a necessary prerequisite to the full-scale practical development of "waste" heat utilization systems. The paper makes a distinction between "waste" heat and "low temperature" heat and analyzes the practical and engineering tradeoffs associated with the utilization of each. The engineering tradeoffs are evaluated following a systematic approach, with the power plant being considered as the "heat source", and the "waste" heat utilization system as a "sink". The interactions of heat demands of the sink on the heat-supplying capability of the source and the delivery of the heat between the source and sink are among the many engineering tradeoffs considered.

"Waste" heat utilization can have tremendous short- and long-term impacts on all sectors of the economy. However, the impacts cannot, and should not, be viewed in terms of projections based on

Preceding page blank

present-day engineering, economic and social considerations; rather, they have to be viewed in terms of the fundamental changes that are necessary over the next several decades in the nature of generation and utilization of energy in this country if we are to achieve energy independence. Thus, waste-heat utilization has to be viewed in terms of other low-temperature, energy-conversion systems which are presently under active development, such as the Ocean Thermal Energy Conversion (OTEC) and Solar Pond systems. Much of the technology that is being developed for these low-temperature, solar-energy systems (such as low-temperature, low-pressure turbines, generation of alternative fuels, in-situ production of various manufactured products, agricultural drying and industrial-process-heat applications) may be directly applicable to waste-heat utilization systems. These aspects are also discussed in the present paper.

Given sufficient time, most of the major obstacles confronting "waste" heat utilization can be overcome through research and development efforts. However, successful application of "waste" heat utilization will never be achievable unless regional and national guidance is provided. Energy conservation is a national concern and without such guidance, local efforts at "waste" heat utilization are likely to fail. The paper points out several major management obstacles that confront the successful employment of large-scale "waste" heat utilization systems.

V-B-109

15-45-21

ENERGY RECOVERY THROUGH UTILIZATION OF THERMAL WASTES IN AN ENERGY-URBAN-AGRO-WASTE COMPLEX

L.F. Diaz and G.J. Trezek
University of California
Berkeley, California U.S.A.

ABSTRACT

A quantitative description of the inter-relationships between energy production and conservation, agriculture and waste treatment are given. This area of study, more conveniently referred to as the energy-urban-agro-waste complex is an emerging technology which is stimulated by the realization that there are finite limits to material, energy and land resources.

Solid, liquid and thermal waste contain sizeable amounts of energy which, if properly harvested, can provide new sources of energy as well as alleviating certain disposal problems. The genesis of the modeling stems from the needs of the community or population center, which requires energy and food, and gives off solid and liquid wastes.

The analysis procedure provides the capability of analyzing the fact that wastes generated by one system could become part of the feedstock for other systems. The details of the material and energy balance are given for two possible configurations of the energy-urban-agro-waste complex. In one configuration, the heat rejected from a power plant is utilized by an evaporative pad greenhouse agricultural system as well as for thermal maintenance of sludge digesters. The products from waste processing are returned back to the power plant as an energy source.

Other by-products such as CO_2 from digestion are utilized for agro enhancement. Agricultural wastes are also recycled as an energy source. The other configuration, which was investigated involves the use of waste heat in the production of algae for animal feed as well as deriving other products from the cellulosic content of the waste stream.

INTRODUCTION

The needs of a community to provide important services in light of dwindling supplies of energy, raw materials and land have motivated the study of the elemental relationships within an energy-urban-agro-waste complex. The underlying approach used in this study consists of simulating the integration of a community with its electric generating stations, its liquid and solid waste treatment plants, and its food production facilities such that the outputs from a given plant are in a form that can be readily used by the community or by other plants. Traditionally, the various demands of the community have been serviced by separate and often competing facilities. For example, energy is typically supplied by a power plant which utilizes virgin natural resources and discharges its waste heat in a manner which burdens the environment. Similarly, waste treatment systems have often relied on land disposal which requires certain energy inputs and produces no net useable products even though the entering material stream has a certain hierarchy of values. Agricultural systems required to meet the food requirements of humans and animals are often separated from the community and require their own energy inputs.

A characterization of the energy and food requirement, in terms of protein, as well as liquid and solid waste generation levels and the potential energy content recoverable from these wastes are shown in Table I as a function of residential population. An analysis of the information contained in Table I indicates that a population size of 500,000 will require energy and waste treatment facilities of a typically produced capacity consistent with good economies of scale. For example, the size of the power plant required is on the order of 1000 MW, while 1125 TPD and 50 MGD solid and liquid waste treatment facilities would be needed. Further, the potential energy which could be extracted from the solid and liquid wastes in the form of refuse derived fuel (RDF) and methane would account for about 8.1% of the energy requirements of the power plant. Protein requirements on the order of 38.5 TPD would also be required.

Depending upon the nature, needs, and geographical location of the community or population center, a variety of configurations of an energy-agro-waste complex are possible. Two basic systems of a general nature were selected for modeling. Each system shown schematically in Figure 1 and 2 contains a conventional power plant, sewage treatment facility and a refuse processing facility capable of recycling solid waste into materials and energy. The heat rejected from the power plant is subjected to various dispersal systems such as wet and dry cooling towers and spray and cooling ponds as well as useful aspect system involving biological process such as agriculture, anaerobic digestion, algae production, and aquaculture. The latter were selected not only because they offer flexibility in system planning but more importantly, because of their compatibility with the temperature of condenser cooling water typically discharged from power plants.

SYSTEM COMPONENT MODELS

A description of the models used to characterize the elements of the energy-agro-waste complex follow:

Power Plant Model

This model, developed by Olszewski [1], utilizes a value for the condenser effectiveness to obtain the turbine exhaust pressure. Pressure and heat rate are then used to calculate the power production, from which a generator efficiency is obtained followed by the gross power plant output. With regard to the heat rejection system, this model requires only the total condenser flow rate and the temperature of the incoming cooling water.

Wet Cooling Tower Model

The design of this model was such that the same cooling characteristics would be obtained irrespective of flow rate. The underlying assumption was that a cooling tower can be designed and built to achieve a certain degree of heat rejection from a predetermined quantity of cooling water for a given set of climatic conditions. The design approach for the cooling tower was 14°F; and the design wet bulb temperature, 76°F.

Cooling Pond Models

The thermal performance and mass transfer, evaporation and drift, are computed with this model after specification of the pond size, circulating water flow rate, and ambient conditions of temperature, humidity, wind speed, and solar day and radiation. In the case of the spray pond, the overall pond spray nozzle efficiency must also be specified along with a relation for the drift characteristics as a function of wind speed. The energy balance relation consists of solar, convective, radiative, evaporative, and spray energy transfers and energy storage due to pond heat capacity. This relation together with the mass balance yields values of the pond temperature and inventory. The model can be used in either mode and also in an intermittent sense when the spray is turned on or off to accommodate the specification of maximum and minimum pond temperatures. The details of these models appear elsewhere [2,3,4,5] and are verified by experimental results.

Anaerobic Digester Model

In the thermal model for the anaerobic digester, the feed (at a known average temperature) is circulated through a heat exchanger, where it is heated by a portion of the hot effluent from the power plant. The temperature increase of the digester feed is calculated, using the heat exchanger effectiveness. Subsequently, the average gas production is calculated in terms of ft^3/lb. VS added based on the feed temperature and on data obtained in the previous digestion studies [6,7,8]. The number of digesters, their volumes, and feed flow rates must be known. Knowing these, the amount of condenser effluent diverted to the digesters may be varied, such as to maintain the digester contents at temperatures close to optimum.

Evaporative Pad Greenhouse

Agricultural production of food is considered in terms of the use of a modified-evaporative pad greenhouse as conceived by Beall and Samuels [9,10]. In essence, their system consists of a standard commercial greenhouse (with a double roof) equipped with fans and aspen fiber pads. Warm condenser cooling water is allowed to flow through the pad. The condenser water is cooled as it passes through the pad, thereby controlling the temperature within the house. In this manner, the greenhouse is used as a heat rejection system during both summer and winter operations. In the summer, the fans draw ambient air through the pads into the house. The air flows through the growing section and is finally forced back to the outside. In this mode the greenhouse functions in a manner similar to that of a wet cooling tower. In the winter, the louvers for allowing ambient air to enter and leave the house are closed. The house then acts as a closed system, and air is circulated through the space between the ceiling and the roof (attic). During winter operation, water condenses in the attic. The condensed water is collected and recirculated, thereby minimizing make-up water requirements.

A thermal model considers the details of the heat and mass transfer within the pad as well as the house [11,12]. By inputting the meteorological conditions, air and water pad flow rates and pad water inlet temperature, the ambient conditions within the house can be predicted as a function of time. This greenhouse model has been verified with actual operating data [11,12]. The house configuration used here consisted of a floor area of 50 x 100 ft, heights of 8 ft and 14 ft in the growing section and overall respectively, and a pad volume of 66 ft^3.

Waste Treatment Systems

The models for material and energy recovery were developed from fundamental investigations conducted at both the 5 TPH refuse processing facility located at the University and also at large scale commercial installations. The details of how the solid waste stream can be processed into heavy and light fractions resulting from shredding and air classification have been previously presented [13,14]. Basically, ferrous, aluminum and glass can be recovered from the heavy fraction while mixed paper waste, fibre, or refuse derived fuel in a fluff or densified form (RDF or dRDF) can be obtained from the light fraction. Certain materials such as putrecibles and other light fraction rejects of an organic nature can be used as feed stock for methane gas production via anaerobic digestion. The condition used for the treatment of liquid wastes via algae production are consistent with those given by Oswald [15], that is, average temperatures on the order of 68°F are needed. An optimum temperature of 85°F was selected for aquaculture systems.

NATURE OF SYSTEMS ANALYZED

The pathways for the flow of energy and materials within each of the two systems selected for analysis are diagrammed in Figures 1 and 2. Basic elements such as the power plant, refuse processing facility, and sewage treatment plant are common to both systems. The basic difference between the systems is in the manner in which the thermal effluents are handled; namely, in system 1, the primary mode of power plant reject heat dispersal is through some conventional cooling and the evaporative pad greenhouse while in system 2, ponds for aquaculture and algae, production are substituted for the agricultural complex. Specifically, the following pathways are delineated: a) the major avenues of energy flow which include, i) electrical energy production, ii) energy contained in thermal effluents which enters the so-called useful aspect systems, and iii) energy contained in the waste stream which is eventually utilized for primary electrical energy production; b) treatment of waste disposal encompassing the refuse processing and wastewater treatment facilities and agricultural wastes; c) materials recovery from the solid and liquid waste streams; d) food production; and e) other secondary flows such as the use of CO_2 produced in the digester gas for agricultural enhancement in the greenhouse, production of soil conditioners from digested sludges, etc.

In this particular study, emphasis was placed on the detailed consideration of the thermal dissipation and utilization aspects. The refuse processing facility and the wastewater treatment system were considered as being passive; that is, their quantative interaction in the previously described flow pathways is governed by the population size described in Table I. Calculations are performed on the basis of a diurnal cycle for both summer and winter operating conditions predicated on the requirement that the power plant is always able to meet the 1000 to 1100 MW requirement. After climatic conditions are selected, changes in water flow rate allocation to various elements within the system will ultimately be registered as affecting the power plant condenser temperature. The selection of the climatic conditions used in this study were influenced by the results of a previous feasibility study [16] which showed that agro systems of the type considered here were better suited to certain climatic, hence geographical, conditions than others. Consequently, the climatic conditions of Phoenix, Arizona, which also corresponds to a population size on the order of 500,000, were used in study of the two systems.

SIMULATION RESULTS

Systems 1 and 2 were studied under various conditions which are given in Tables II and III respectively.

System 1

System 1 was subjected to four cases which illustrated the effect of a) changing the condenser flow rate (cases I and II) and b) changing the flow rates to various sub-systems for constant condenser flow rate (cases III and IV). At the high condenser flow rate, the power production was essentially unaffected during summer and winter operation while at the lower flow rate a slight drop, from 1108 MW to 1089 MW, occurred as a result of seasonal operation. As shown in Figs. 3 and 4, the condenser cooling water temperature difference increased from 17.5°F to 26.5°F with decreased condenser flow.

Ten digesters having a 30 ft height, 100 ft diameter, 737 GPM sludge flow rate, and a 9000 GPM heating water flow rate were used in the models. Sludge was considered to enter at a constant temperature of 55° in the winter and 65°F in the summer. Using an exchanger effectiveness of 0.9, digester temperatures of 96°F and 73°F could be maintained a high condenser flow rate during summer and winter operation respectively. The relative gas production at these temperatures were 0.55 x 10^7 and 0.30 x 10^7 ft^3/day. Reducing the condenser flow rate caused the average digester temperature to increase to 104°F and 81°F for summer and winter operation respectively with corresponding gas productions of 0.46 x 10^7 and 0.40 x 10^7 ft^3/day. The temperature difference of the circulating flow through the digesters is shown in Figs. 3 and 4 on a diurnal basis for summer and winter operation respectively. It should be noted that only about 1% of the total condenser flow rate would be required to maintain the digesters at or near optimum temperature levels.

Reducing the flow rate to the evaporative pad greenhouses from 450,000 GPM to 300,000 GPM caused the number of houses in the complex to be reduced from 3,750 to 2,500 consistent with a 90 GPM individual house flow rate. When the total condenser flow rate is decreased, the temperature of the water entering a greenhouse pad increases by about 8°F for both summer and winter operation under the conditions stated above. The temperature of the heated condenser effluent entering and exiting the pads is plotted in Fig. 3. As it is shown in Fig. 3, during the summer the inlet temperature fluctuated between 95°F and 101°F while the outlet temperature varied between 65°F and 77°F. The inlet and outlet temperatures for winter operation are plotted in Fig. 4. The results show that the temperature of the condenser water entering the pads fluctuated between 72°F and 78°F. The temperature of the water exiting the pad decreased from 2 to 4 degrees. The temperature to note that during the winter, some ambient air must be allowed in the house in order to reduce the relative humidity. The corresponding mass evaporation rate changed from an average of about 1250 lb/hr to 1600 lb/hr in the summer and from about 50 lb/hr to 100 lb/hr during the winter.

For cases I and II the pond thermal performance did not change considerably as it is shown in Figs. 3 and 4. During summer operation, the average temperature discharged from the pond was about 75.4°F and 73.7°F for the high and low condenser flow rates while the temperature remained nearly constant at 51°F during winter operation. Evaporation and drift losses were on the order of 0.54 x 10^7 lb/hr and 0.36 x 10^7 lb/hr for summer and winter conditions respectively and did not change appreciably under the range of flow rate variation considered here.

In cases III and IV the flow rates to the various sub-systems were changed for a constant condenser flow rate of 900,000 GPM. The average power output remains essentially constant. Since the digester flow rate remained at 9000 GPM, the digester temperatures were similar to those previously given; specifically, temperatures of 97.6°F and 74.8°F were obtained in case III and 95.3°F and 71.1°F in case IV for summer and winter conditions respectively.

Evaluation of the greenhouses indicates that the average temperature drop from 102°F to 100°F occurs when the total flow to the complex was reduced during summer conditions. During winter operation, the temperature of the incoming water to the pad in case III was about 4°F higher than that in case IV; consequently, the average temperature leaving the pad was 74.4°F and 70.7°F for the two cases respectively.

The spray pond behaved similar to that previously described. Pond temperature around 78°F occurred for cases III and IV during summer and about 71.5°F for both cases during winter. Water loss proportional to those previously given occurred.

System 2

A description of the combination of conditions investigated for system 2 are given in Table III. In this system configuration all the ponds are operated as cooling ponds. Since one set of ponds was used for aquaculture and the other for algae production, it was important to ascertain the conditions of temperature stability for both summer and winter operation which can be achieved by seasonally varying the flow rates to each subsystem.

When the system is operated under the conditions of case V, the average power production is about 1100 MW and the average sludge temperatures in the digesters are about 101°F and 78°F for summer and winter operation respectively as demonstrated in Figs. 5 and 6. Average summer and winter temperatures of 83°F and 67°F occurred in the algae pond at the 100,000 GPM flow rate; diurnal temperature changes for both summer and winter are plotted in Figs. 5 and 6. The elevated summer temperature produced evaporation rates of about 0.83×10^6 to 0.18×10^7 lb/hr. As shown in Figs. 5 and 6, the average temperature of the aquaculture ponds for summer and winter was about 85°F and 68°F.

After these results were obtained, the remaining two cases were concerned with varying the subsystem flow rates in order to achieve constant seasonal temperature. Under these conditions, a wet cooling tower large enough to accommodate peak flow rates would be necessary. Reducing the flow rate to the aquaculture pond to 20,000 GPM only reduced the summer pond temperature to about 78°F; approximately 10°F higher than optimum. At the 100,000 GPM flow rate, thermal conditions near optimum are maintained during winter. In general, flow rates to the aquaculture pond on the order of 150,000 to 200,000 would be sufficient to keep the pond at near optimum temperature levels during summer whereas flow rates of about 600,000 GPM would be required for winter operation.

It should be noted that because of the fact that certain subsystems did not experience large temperature changes, diurnal temperature variations were given for cases I and V only. A more detailed description of the results obtained for all the cases studied can be found in Reference 17.

CONCLUDING REMARKS

Although this study is only an initial step, the results indicate that a combination of ponds, evaporative pad greenhouses, digesters and cooling towers can provide sufficient cooling for a 1000 MW power plant without large losses in power production. However, safety reasons and land requirements make it necessary to keep a cooling tower in the system. The data show that anaerobic digesters are not effective as heat rejection systems, since it would require only about 1% of the total cooling water flow from a complex to maintain the digesters at an optimum temperature level.

These results also indicate that the energy rejected in the cooling water of an electric generating station can be used to maintain optimal thermal environments for various biological processes such as algae production, agriculture, aquaculture, and anaerobic digestion. The feasibility of maintaining these processes in their thermal "optimal" zone is demonstrated. Further, the effect of fluctuations in ambient conditions can be reduced simply by varying the amount of cooling water diverted to each sub-system.

By using the global approach, the efficiency of energy and material utilization can be maximized while reducing detrimental ecological effects. Complete utilization of the models requires the consideration of the dynamics of all system elements along with economic considerations.

REFERENCES

1. Olszewski, M., "Optimal Design of Nuclear Steam Power Plants Using Dynamic Programming", M.S. Thesis, Rutgers University, 1972.
2. Schrock, V.E. and G.J. Trezek, "Rancho Seco Nuclear Service Spray Ponds Performance Evaluation", Report No. WHM-4, College of Engineering, University of California, Berkeley, July, 1973.
3. Schrock, V.E., G.J. Trezek, and L.R. Keilman, "Performance of a Spray Pond for Nuclear Power Plant Ultimate Heat Sink", ASME, 75-WA/HT-41, 1975.
4. Chen, K.H. and G.J. Trezek, "Spray Energy Release (SER) Approach to Analyzing Spray System Performance", Proceedings of the American Power Conference, April, 1975.
5. Chen, K.H. and G.J. Trezek, "Thermal Performance Models and Drift Loss Predictions for a Spray Cooling System", In Press, Journal of Heat Transfer.
6. Golueke, C.G., "Temperature Effects on Anaerobic Digestion of Raw Sewage Sludge", Sewage Works Journal, 30, Oct. 1958, pp. 1225-1232.
7. Diaz, L.F., Kurz, F., and G.J. Trezek, "Methane Gas Production as Part of a Refuse Recycling System", Compost Science, Vol. 15, No. 3, 1974, pp. 7-13.
8. Diaz, L.F. and G.J. Trezek, "Bio-gasification of a Selected Fraction of Municipal Solid Wastes", In Press, Compost Science.
9. Beall, S.E. and G. Samuels, "How to Make a Profit on Waste Heat", Nuclear Technology, Vol. 12, pp. 12-17, Sept., 1971.
10. Beall, S.E., "Uses of Waste Heat", ASME Paper No. 70-WA/Ener-6. Presented at the 1970 Winter Annual Meeting, Nov. 29-Dec. 3, 1970.
11. Olszewski, M., "Agricultural Greenhouse Uses of Power Plant Reject Heat", Ph.D. Thesis, University of California, Berkeley, 1975.
12. Olszewski, M. and G.J. Trezek, "Performance Evaluation of an Evaporative Pad Greenhouse System for Utilization of Power Plant Reject Heat", J. of Environmental Quality, Vol. 5, No. 3, July-Sept., 1976, pp.
13. Savage, G., Diaz, L.F., and G.J. Trezek, "The Cal Recovery System: A Resource Recovery System for Dealing with the Problems of Solid Waste Management", Compost Science, Vol. 16, No. 5, 1975, pp. 18-21.
14. Trezek, G.J. and C.G. Golueke, "Availability of Cellulosic Wastes for Chemical or Bio-Chemical Processing", AIChE Symposium Series 158,

Bio-Chemical Engineering-Energy, Renewable Resources and New Foods, Vol. 72, 1976, pp. 52-57.

15. Oswald, W.J., "Ecological Management of Thermal Discharges", J. of Environmental Quality, Vol. 2, No. 2, April-June 1973, pp. 203-207.

16. Trezek, G.J. and M. Olszewski, "Feasibility of Using an Evaporative Pad Greenhouse Agricultural Complex for Reject Heat Dispersal", In Proceedings of 9th Inter-Society Energy Conversion Conference, San Francisco, California, 1974.

17. Diaz, L.F., "Energy Recovery through Bio-Gasification of Municipal Solid Wastes and Utilization of Thermal Wastes from an Energy-Urban-Agro-Waste Complex", Ph.D. Thesis, University of California, Berkeley, 1976.

LIST OF TABLES

Table I Energy and Protein Requirements and Liquid and Solid Waste Generation for Various Populations

Table II Cases Analyzed for System 1

Table III Cases Analyzed for System 2

TABLE I

ENERGY AND PROTEIN REQUIREMENTS AND LIQUID AND SOLID WASTE GENERATION FOR VARIOUS POPULATIONS

Population	Total(1)	Organic Fraction(2)	Sewage(3)	Sludge(4)		Average(5) Daily Electrical Energy Requirements	Fossil(6) Fuel Requirements For Power Plant	Waste Heat From Power Plant	Energy(7) Recoverable From Solid Wastes	Protein(8) Requirement
	TPD	TPD	MGD	TPD Dry	TPD Wet	$\frac{BTU}{day}\times 10^9$	$\frac{BTU}{day}\times 10^9$	$\frac{BTU}{day}\times 10^9$	$\frac{BTU}{day}\times 10^9$	Tons/day
50,000	112.5	22.5	5	5.9	146.3	3.51	10.63	7.12	0.863	3.85
100,000	225.0	45.0	10	11.7	292.5	7.01	21.25	14.24	1.727	7.70
150,000	337.5	67.5	15	17.6	438.8	10.52	31.88	21.36	2.591	11.55
200,000	450,0	90.0	20	23.4	585.0	14.03	42.50	28.47	3.455	15.4
250,000	562.5	112.5	25	29.3	731.3	17.53	53.13	35.60	4.319	19.25
300,000	675.0	135.0	30	35.1	877.5	21.04	67.75	42.71	5.183	23.1
400,000	900.0	180.0	40	46.8	1,170.0	28.05	85.00	56.95	6.91	30.8
500,000	1,125.0	225.0	50	58.5	1,462.5	35.07	106.26	71.19	8.638	38.5
600,000	1,350.0	270.0	60	70.2	1,755.0	42.08	127.51	85.43	10.366	46.20
800,000	1,800.0	360.0	80	93.6	2,340.0	56.10	170.01	113.91	13.821	61.6
1,000,000	2,250.0	450.0	100	117.0	2,925.0	70.13	212.52	142.39	17.277	77.0

(1) 4.5 lbs/capita-day

(2) Segregated at processing plant

(3) 100 gal./capita-day

(4) 2340 lbs. of dry solids/10^6 gals (primary and activated)

(5) Based on 70,130 BTU/day

(6) Assuming a thermal efficiency of 33%

(7) RDF at 6700 BTU/lb and CH_4 at 1000 BTU/ft^3

(8) Based on recommended daily allowance of 0.154 lb/capita

Case No.	I	II	III	IV
Condenser Flow Rate (GPM)	900,000	600,000	900,000	900,000
Wet Cooling Tower Flow Rate (GPM)	450,000	300,000	600,000	300,000
Digesters Flow Rate (GPM)	9,000	9,000	9,000	9,000
Greenhouses Flow Rate (GPM)	337,500	225,000	225,000	180,000
No. of Greenhouses	3,750	2,500	2,500	2,000
Spray Pond Flow Rate (GPM)	450,000	300,000	300,000	600,000
Pond Area (Acres)	1,020	1,020	1,020	1,020

TABLE II

Cases Analyzed for System 1

Case No.						
Season	Summer	Winter	Summer	Winter	Summer	Winter
Condenser Flow Rate (GPM)	900,000	900,000	900,000	900,000	900,000	900,000
Wet Cooling Tower Flow Rate (GPM)	600,000	600,000	650,000	400,000	730,000	200,000
Spray Pond Flow Rate (used as cooling pond) (GPM)	200,000	200,000	200,000	400,000	150,000	600,000
Spray Pond Area (Acres)	150	150	150	150	150	150
Digesters Flow Rate (GPM)	8,000	8,000	8,000	8,000	8,000	8,000
Cooling Pond Flow Rate (GPM)	100,000	100,000	50,000	100,000	20,000	100,000
Cooling Pond Area (Acres)	150	150	150	150	150	150

TABLE III Cases Analyzed for System 2

LIST OF FIGURES

Figure 1 - Schematic Diagram of System 1

Figure 2 - Schematic Diagram of System 2

Figure 3 - Circulating Water Temperatures in the Subsystems of System 1 under the Conditions of Case I - Summer Operation

Figure 4 - Circulating Water Temperatures in the Subsystems of System 1 under the Conditions of Case I - Winter Operation

Figure 5 - Circulating Water Temperatures in the Subsystems of System 2 under the Conditions of Case V - Summer Operation

Figure 6 - Circulating Water Temperatures in the Subsystems of System 2 under the Conditions of Case V - Winter Operation

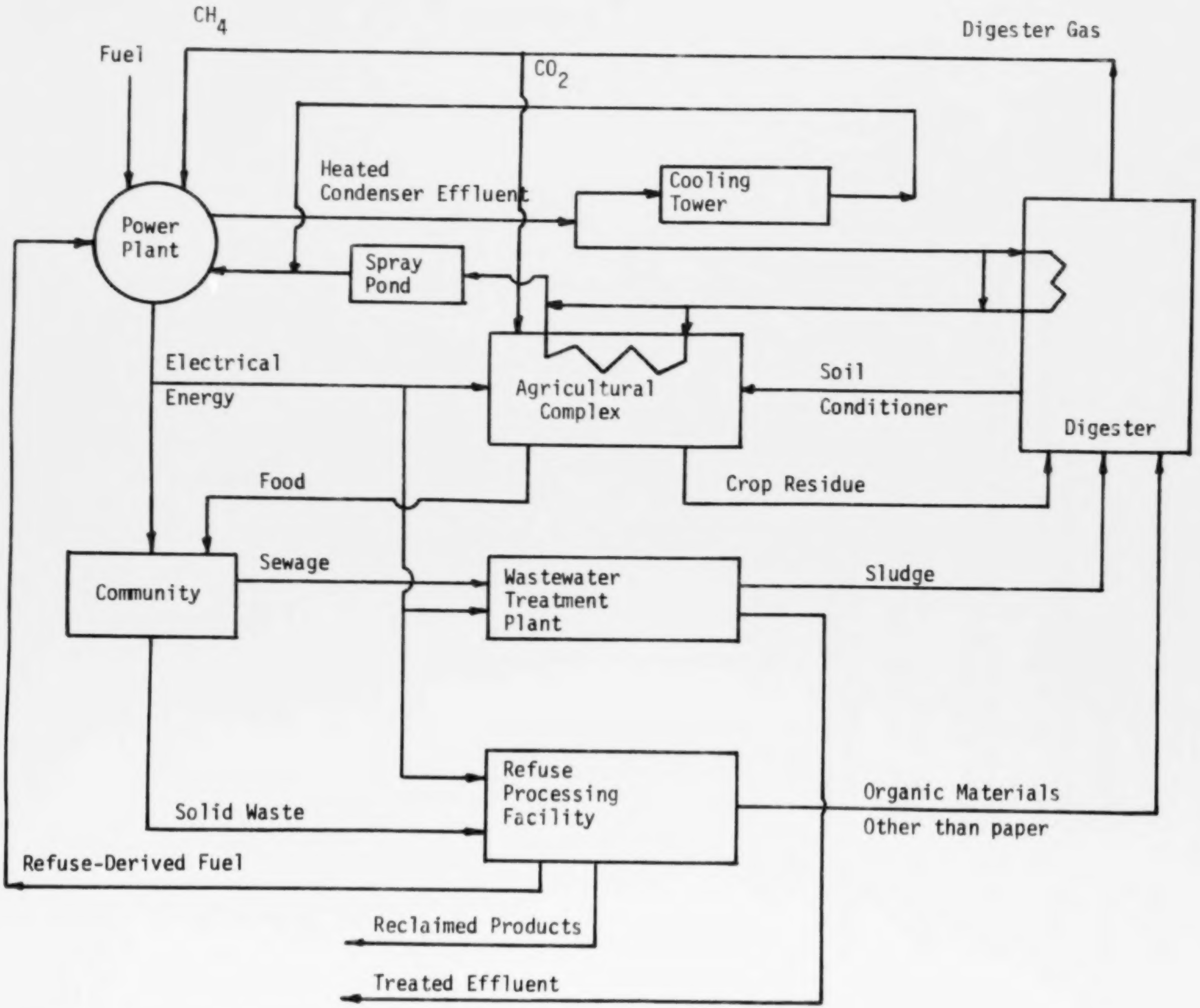
CH$_4$
Fuel
Digester Gas
CO$_2$
Heated
Condenser Effluent
Cooling Tower
Power Plant
Spray Pond
Electrical
Energy
Agricultural Complex
Soil
Conditioner
Digester
Food
Crop Residue
Community
Sewage
Wastewater Treatment Plant
Sludge
Refuse Processing Facility
Solid Waste
Organic Materials
Other than paper
Refuse-Derived Fuel
Reclaimed Products
Treated Effluent

Fig. 1 Schematic Diagram of System 1

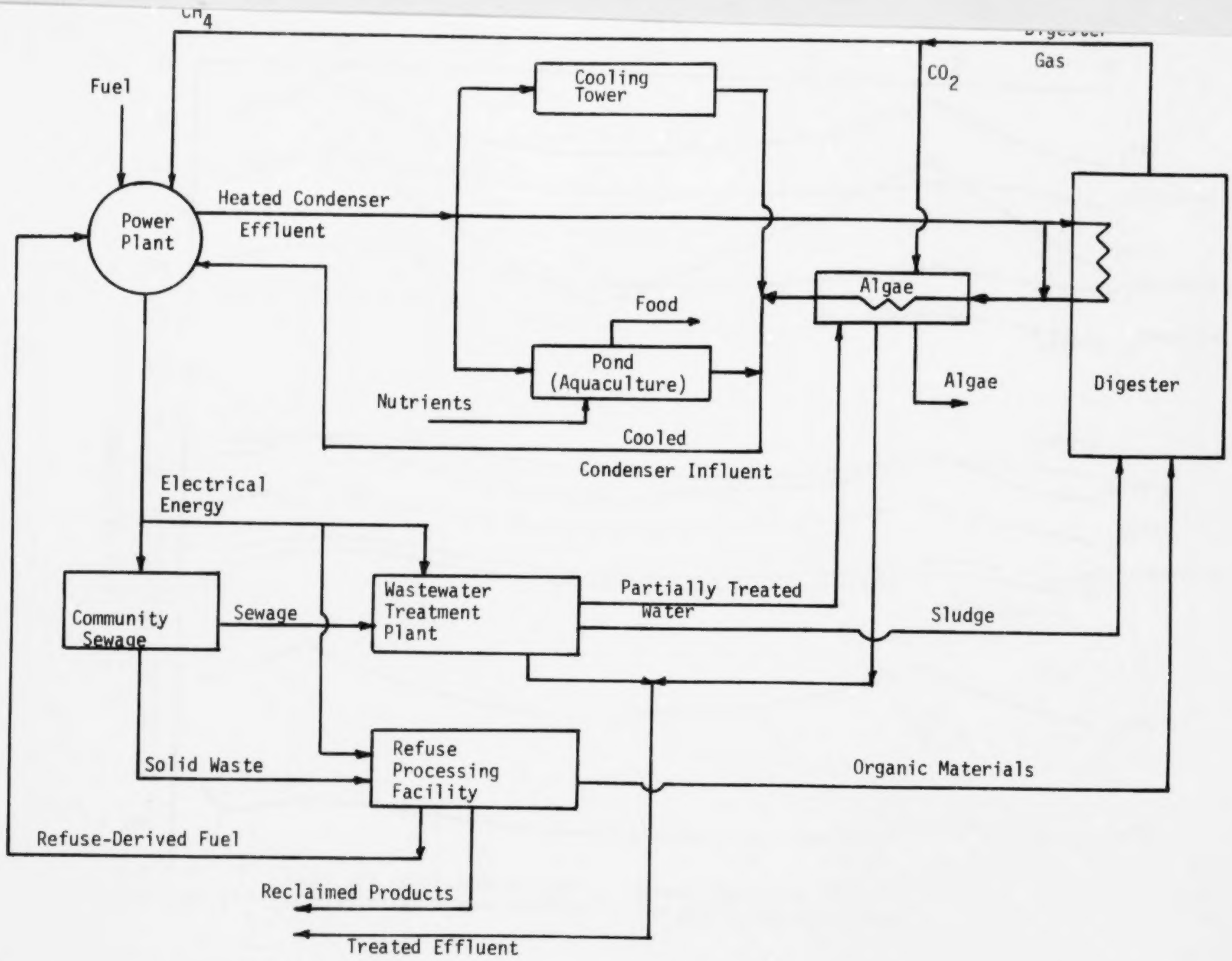
CH4
Gas
Fuel
Cooling Tower
CO2
Power Plant
Heated Condenser Effluent
Algae
Food
Pond (Aquaculture)
Algae
Digester
Nutrients
Cooled Condenser Influent
Electrical Energy
Community Sewage
Sewage
Wastewater Treatment Plant
Partially Treated Water
Sludge
Solid Waste
Refuse Processing Facility
Organic Materials
Refuse-Derived Fuel
Reclaimed Products
Treated Effluent

Fig. 2 Schematic Diagram of System 2

Fig. 3 Circulating Water Temperatures in the Subsystems of System 1 under the Conditions of Case I - Summer Operation

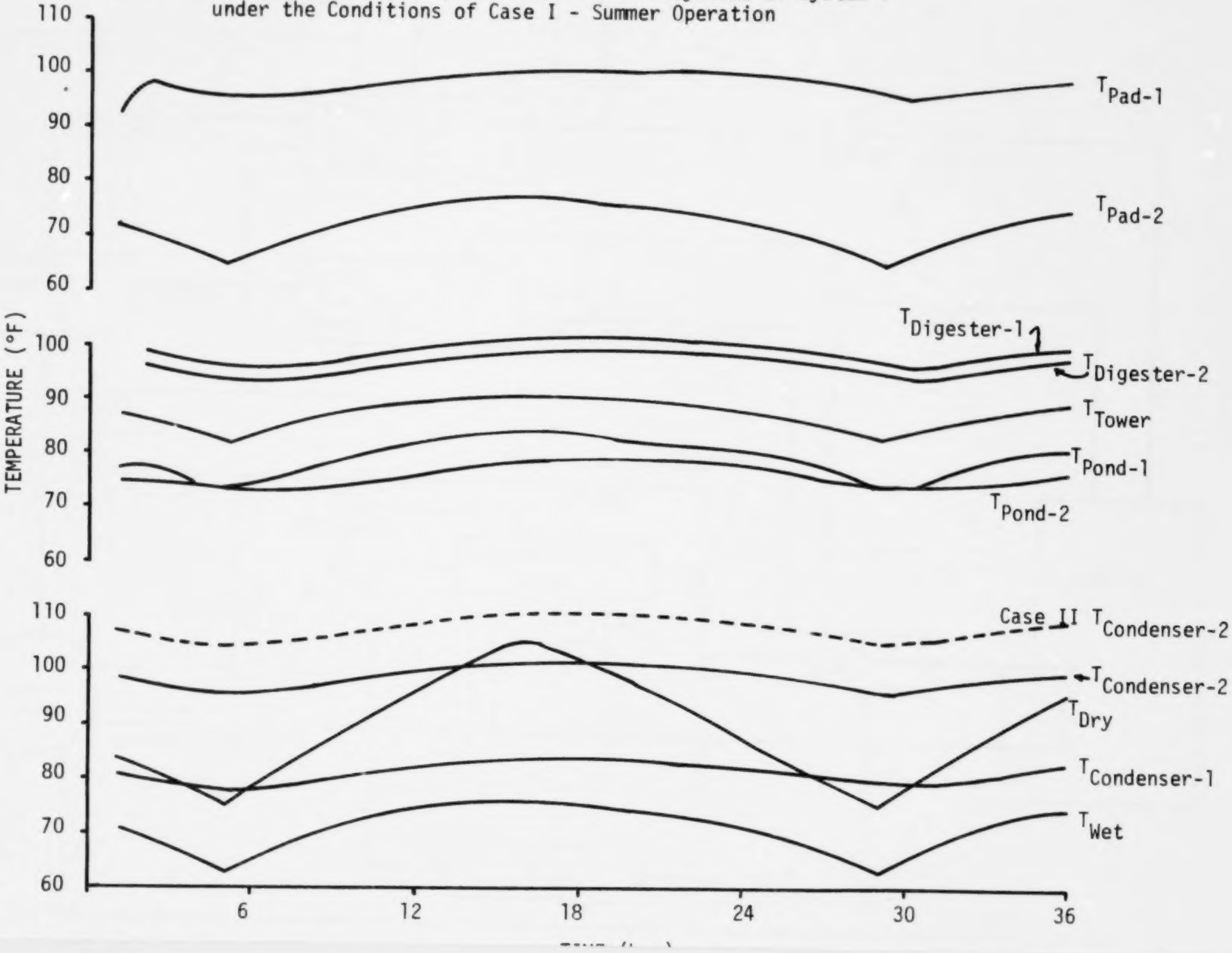

Fig. 4 Circulating Water Temperatures in the Subsystems of System 1 under the Conditions of Case I - Winter Operation

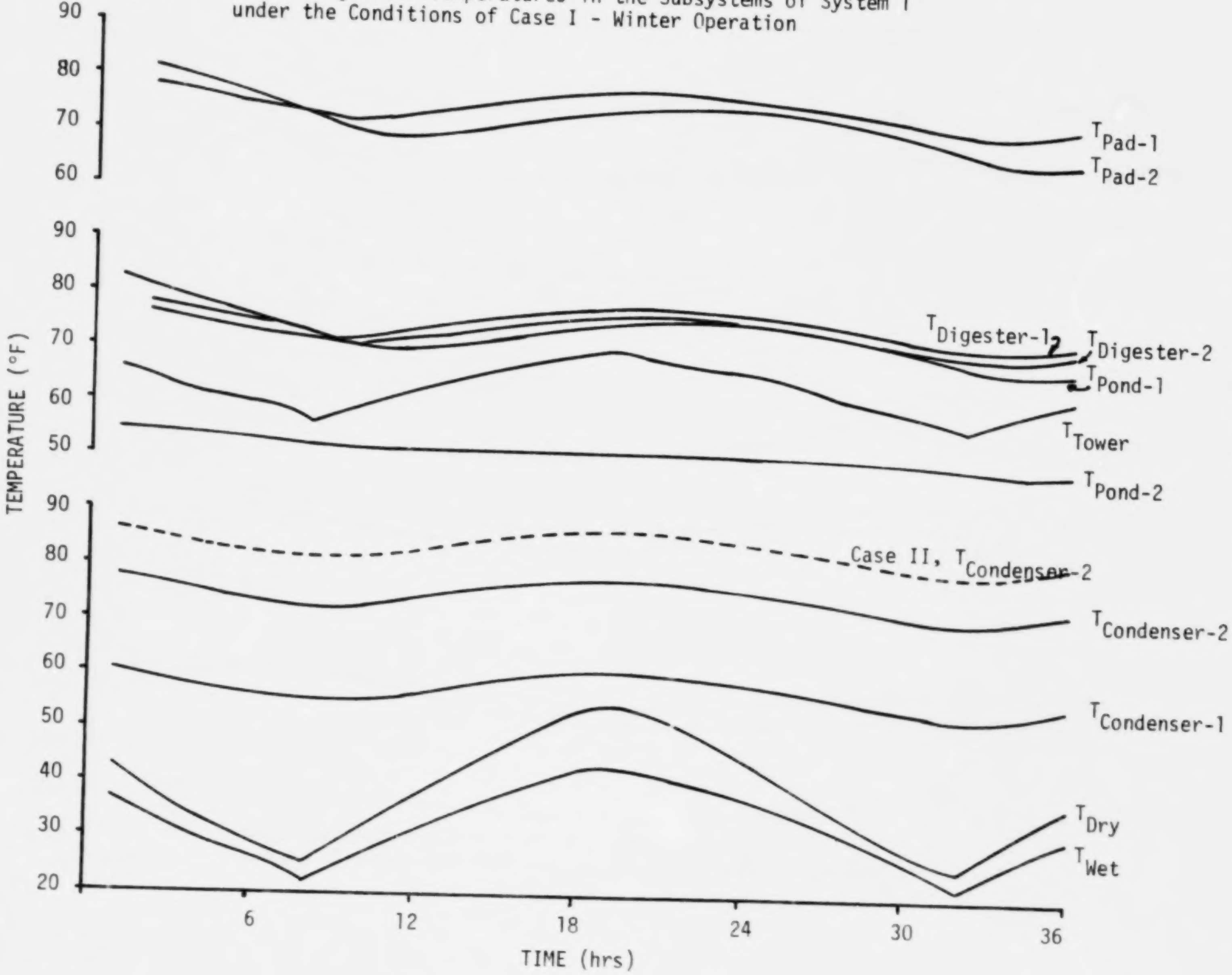

Fig. 5 Circulating Water Temperatures in the Subsystems of System 2 under the Conditions of Case V - Summer Operation

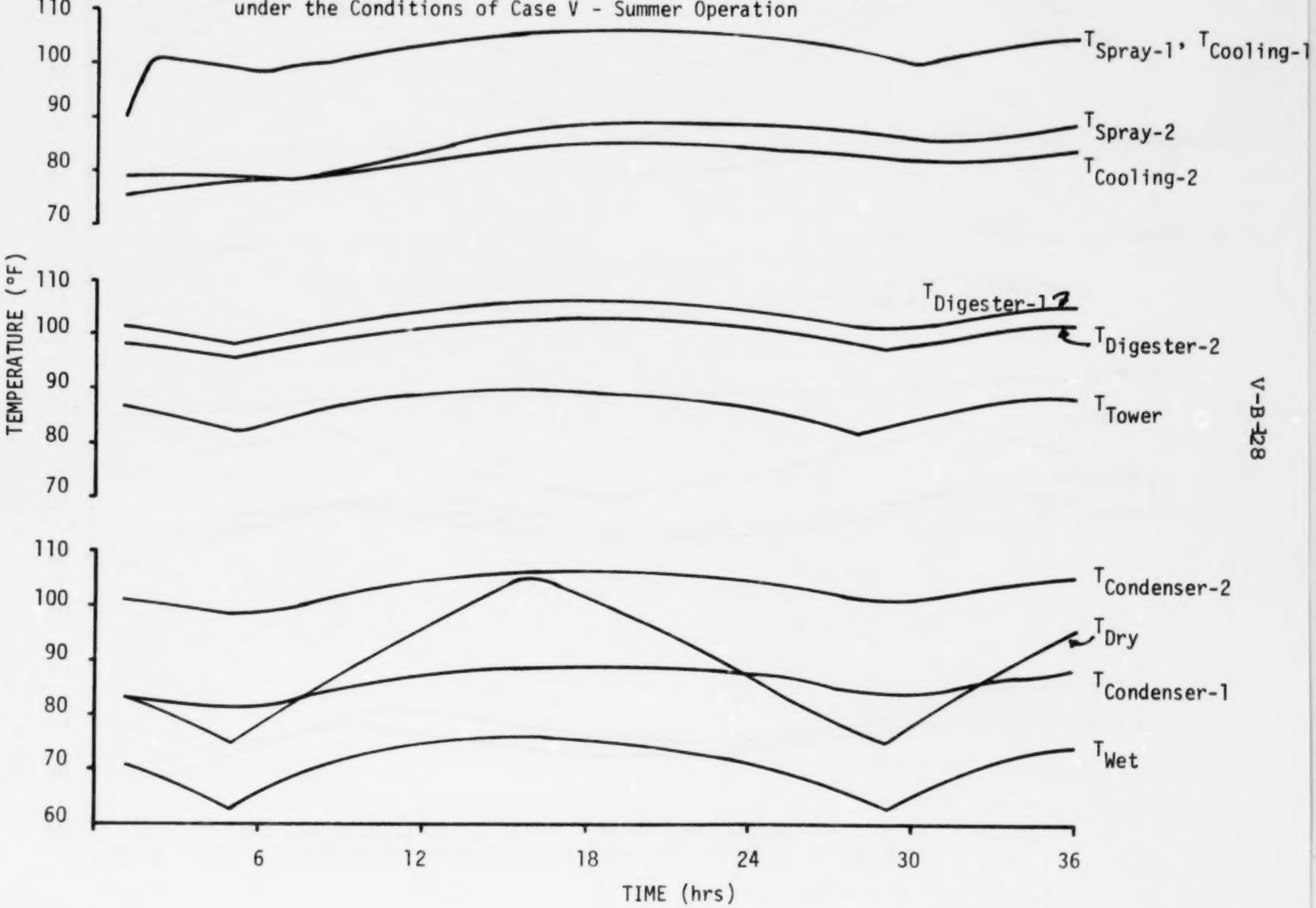

Fig. 6 Circulating Water Temperatures in the Subsystems of System 2 under the Conditions of Case V - Winter Operation

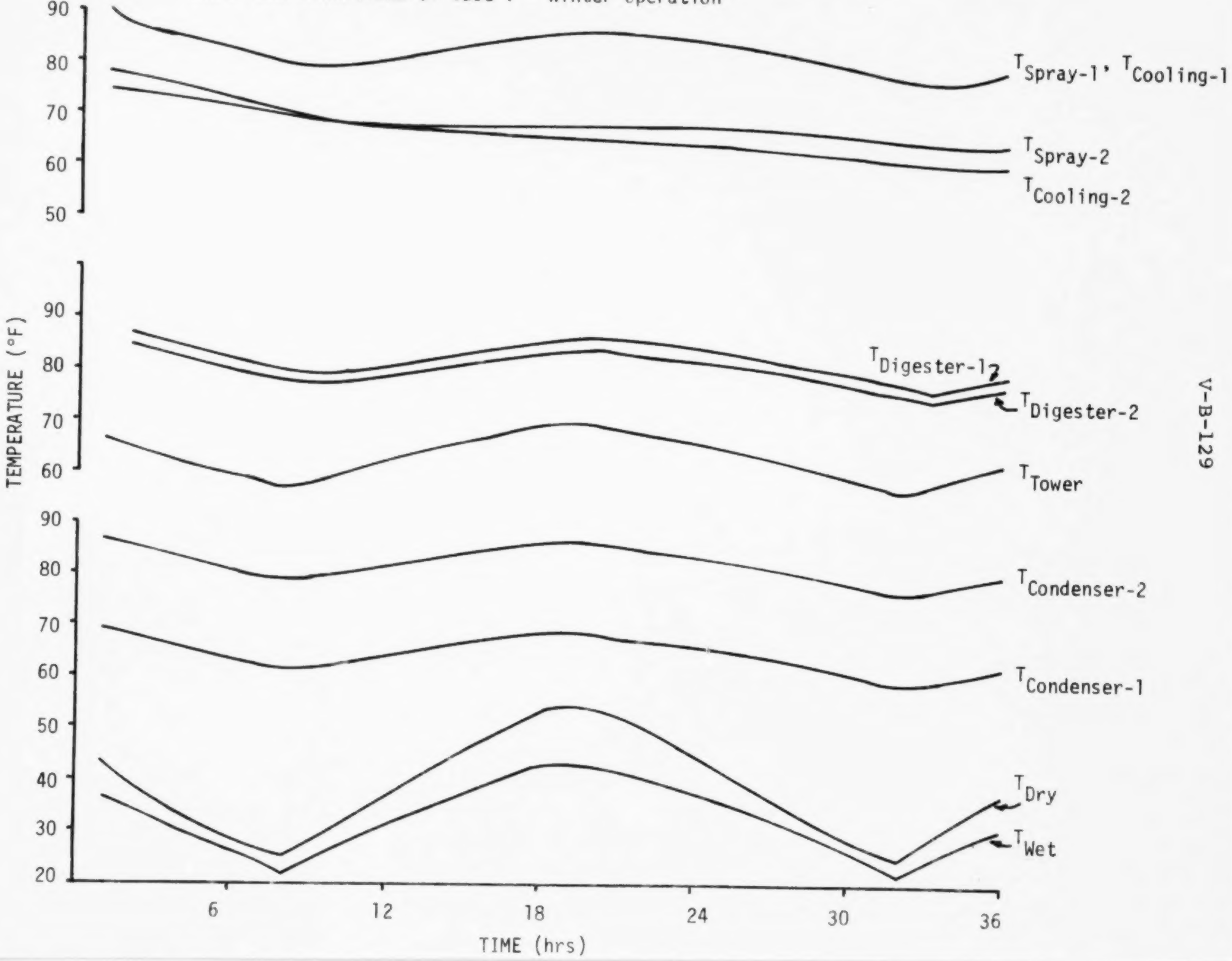

SESSION V-C
UTILIZATION I

Preceding page blank

OMIT

V-C-133

An Overview of Waste Heat Management In TVA

P. A. Krenkel[a], B. J. Bond[b], C. F. Bowman[c], R. H. Brooks[d],
G. E. Hall[e], C. J. Powell[f], A. O. Smith[g], W. R. Waldrop[h]

Chattanooga, Tennessee 37401
March 1977

Abstract

The Tennessee Valley Authority has responded to the problem of waste heat by investigating its various facets. Computer models predict behavior of thermal plumes. Effects on aquatic biota are being studied. The problem of managing waste heat is being attacked through research in three areas: (1) improvement in efficiency of power generation to reduce waste heat; (2) use of waste heat for beneficial purposes; and (3) management of waste heat to reduce its impact on the environment.

THIS ARTICLE IS A GOVERNMENT PUBLICATION AND NOT SUBJECT TO COPYRIGHT.

a. Director, Division of Environmental Planning
b. Assistant Director, Division of Agricultural Development
c. Senior Mechanical Engineer, Division of Engineering Design
d. Assistant Chief, Water Quality and Ecology Branch, Division of Environmental Planning
e. Chief, Fisheries and Water Fowl Resources Branch, Division of Forestry, Fisheries and Wildlife Development
f. Research Coordinator, Power Research Staff, Office of Power
g. Fisheries Biologist, Division of Forestry, Fisheries, and Wildlife Development
h. Research Engineer, Division of Water Management

Preceding page blank

INTRODUCTION

Although emerging technology holds promise for greater efficiency in converting heat to electrical energy, present steam-electric generating plants are, at best, capable of converting only 40 percent of heat to electricity. TVA and most producers of electricity now use large volumes of water to dissipate the unused or "waste" heat. TVA is, where necessary, endeavoring to find methods to minimize or eliminate the heat in condenser cooling water that may impact aquatic environments. Furthermore, with a growing demand for energy, TVA is focusing attention on using waste heat for beneficial purposes rather than simply dissipating it.

16-45-25

THERMAL DISCHARGES

Behavior Of Thermal Discharges

Before judgments can be made about the impacts of thermal discharges, data must be available on how thermal plumes behave in the aquatic environment. TVA's Division of Water Management is developing computer models for analyzing the effects of thermal discharges from steam plants on temperatures and velocities in a receiving body of water. These models numerically simulate boundary conditions in the particular body of water being modeled. The numerical models are of two broad classes. One class, a 2-dimensional, unsteady model encompasses an entire reservoir or a long reach of a river and predicts effects over a period of several months or for as long as a year. The second class of model is a 3-dimensional, unsteady model that offers relatively fine resolution within about 10 km of the plant for periods of several hours or days. Figures 1 and 2 are examples of results produced by these two models.

Effects Of Thermal Discharge

Since 1973 TVA has been actively investigating the effects of thermal discharges on the aquatic communities in bodies of water receiving heated water from its steam plants. Section 316(a) of the Federal Water Pollution Control Act Amendments of 1972 allows dischargers of waste heat to demonstrate that impacts from specific plants do not harm aquatic environments receiving the thermal effluents. TVA established a program in accordance with Section 316(a) to assess the impact of thermal effluent from eight of TVA's fossil-fueled steam plants. Most of these eight plants are on multipurpose, flow-through reservoirs; the aquatic habitats near the plants are neither entirely lacustrine nor riverine but involve environments that at times resemble one or the other. The TVA 316 studies were divided into two approaches: the nonfisheries aspect and the fisheries aspect. In addition, a special project has been implemented to assess long-term, sublethal thermal effects.

Nonfisheries

In evaluating the impact of thermal discharge from fossil-fueled power plants, TVA's biologists have found that the effects of these discharges are generally inconsistent with regard to temperature difference, ambient temperatures, power production, etc. No definitive correlations of cause and effect have been determined from the data for any nonfisheries community. The impacts seem to be intermittent types of responses (i.e., one study period may exhibit an effect in a community and the next nine study periods may not). The inconsistency of these responses suggests that the nonfisheries communities are not altered on a long-term basis by the thermal discharge.

Phytoplankton--This community consists of microscopic unicellular and multicellular nonvascular plants passively supported in the water column. The thermal effect studies for this community have shown that, in general, there are no significant differences between control and experimental stations. When an effect is observed, it usually occurs as an alteration in cell densities. At one plant during 16 study periods, no significant differences in population between control and experimental stations were determined for 14 study periods. In one of the remaining two periods, the cell densities decreased 52 percent downstream. In the other period the densities increased 1,048 percent.

Periphyton--Periphyton are microscopic plants and animals that attach to, but do not penetrate into, a submerged substrate. The most frequent responses of the sessile algal community (phytoperiphyton), when changes were found, were reductions or increases in the biomass of the community. Thermophilic "nuisance" algae such as blue-green algae dominated the community in less than five percent of the cases studied.

Aquatic Macrophytes--Aquatic macrophytes are the rooted and floating vascular plants. No significant response by aquatic vascular plants to thermal discharges was identified.

Zooplankton--Zooplankton are microscopic animals suspended in the water column that are capable of swimming short distances or avoiding weak currents. Reductions in total numbers and in total biomass and shifts in dominant taxa were documented occasionally at some of the study sites. However, these effects were encountered infrequently and would not be interpreted to pose a problem to the environment when considered along with other data.

Additional studies were conducted in 1974 and 1975 to determine the percentage of the zooplankton killed by passage through the condenser cooling system. Although all samples have not yet been processed, these studies indicate the percentages of mortality to be low except at plants where chloride is used as a biocide or where there is a great rise in temperature as water passes through the cooling system. Effects at these plants are similar to those reported in the literature.

Benthos--Benthos is a generic term for all organisms that are attached to, resting on, or living in the bottom sediments of a body of water. This assemblage is comprised of such organisms as aquatic insects, aquatic worms, freshwater mussels, clams and snails. In cases in which an effect was observed in this community, it was manifested by a decrease in diversity. Modified drift studies showed that suspension in the thermal plume did not significantly alter body functions of mayfly and damselfly larvae.

Fisheries

Fisheries studies were conducted in the vicinity of these eight TVA plants during 1974-1975. Results indicate that some species avoid plant discharge areas during warmest periods of the summer and that others are attracted to discharge areas during winter. There is no change in the distribution of species, however. In addition, there are typically no changes in growth, condition, parasite loads, gonadal maturation, and spawning times in fish exposed to thermal discharges. No barriers to spawning migration have been found at TVA plants, nor has there been any documented fish kill resulting from cold shock because of power plant shutdown. Analyses of historical data (in some cases including preoperational data) have revealed no changes in reservoir fish populations that could be attributed to heated effluents.

Assessment of Long-Term Thermal Effects

TVA, in cooperation with the Environmental Protection Agency, is also studying the long-term sublethal effects of thermal discharges on selected species of fish and associated aquatic flora and fauna.

A thermal research facility was completed in 1974 at Browns Ferry Nuclear Plant on Wheeler Reservoir in Alabama. Water is pumped through a series of 12 channels 114m x 4.3m x 2m (figure 3), each with identical substrate of natural reservoir sediments and limestone rocks (figure 4). Water temperature, dissolved oxygen, pH, and flow rate for each channel are monitored continuously. Water that is 2, 4, and 6°C above ambient river temperature will flow through three sets of three channels and river water at ambient temperature will flow through one set of three channels (which will serve as experimental controls).

Preliminary experiments have been conducted since 1974 under ambient river temperatures to produce baseline data on rates of natural colonization of periphyton, macroinvertebrates and plankton in the channels. Assessments were made on growth, survival, and reproduction of seven species of fish with emphasis on smallmouth bass, bluegill, sauger, and walleye. Experiments at elevated temperatures will begin in Spring, 1977.

USE AND MANAGEMENT

TVA is actively engaged in research in each of three approaches to the problem of using or managing waste heat. The first approach is to use more of the heat in the production of electricity (i.e., increase the efficiency of power generation). The second approach is to use the rejected heat for some beneficial purpose other than the production of electricity. The remaining option is to manage the waste heat so that it will have minimum adverse impact on the environment.

Improved Power Plant Efficiency

A highly desirable solution to the problem of waste heat would be to utilize more of the heat to generate electrical power and thereby reduce the discharge of waste heat. TVA, either directly or through participation with other organizations, is involved in research into technologies such as high-temperature gas turbines, fuel cells, and magnetohydrodynamic generators, which hold promise for improving power plant efficiencies as much as 50 percent. For many years to come, however, 50 to 60 percent of the heat produced by fuels will be wasted and will require disposal or will be available for beneficial use.

Beneficial Use Of Waste Heat

Another desirable approach to dealing with waste heat is to find a beneficial use for it. In 1969 TVA began its first research project in beneficial uses of waste heat--the intensive culture of catfish in the thermal discharge from condenser cooling at Gallatin Steam Plant. In 1971 the Board of Directors of TVA approved a broad program for evaluating beneficial uses of waste heat. TVA's policy is to concentrate on the use of true waste heat--heated water as it leaves the power plant with no alterations to the overall thermal cycle. Several studies are in progress at TVA.

Raceway Catfish Production

TVA's first study of beneficial use of waste heat was a cooperative effort with a private corporation and involved the production of catfish in the heated-water discharges from Gallatin Steam Plant. The objectives of the study were to (1) determine the effects of stocking density and water flow on growth, feed conversion, and mortality of catfish; (2) develop effective control of disease in densely stocked catfish; (3) develop treatment for waste produced by a catfish culture; (4) test aeration and oxygenation systems; and (5) evaluate the environmental impact and economic feasibility of the system.

The project was judged technically feasible and was concluded in 1974. Economic feasibility is yet undetermined. Results, however, indicate a significant potential for commercial success of high-density culture of catfish at power plants.

TVA is involved in a multiagency proposal for research in aquaculture that could lead to the design and construction of a larger scale demonstration of catfish production at a TVA power plant. The Gallatin project forms a basis for this expanded effort.

Greenhouse Heating and Cooling

Heat energy in water that has been used for cooling condensers can be used to heat or cool greenhouses. A prototype greenhouse, which uses simulated waste heat, has been in operation at Muscle Shoals, Alabama, for several years and has provided engineering, horticultural, and economic data. A waste heat research facility at TVA's Browns Ferry Nuclear Plant, scheduled for completion in late 1977, will be used for further evaluation of the technology developed with the prototype greenhouse. Figure 5 shows the design of the planned experimental greenhouse at Browns Ferry. Research continues at the prototype facility to document horticultural, engineering, and economic data for different crops and to make comparisons with data from conventional greenhouses.

Biological Recycling of Livestock Wastes

Research is in progress at the National Fertilizer Development Center, Muscle Shoals, Alabama, to evaluate the use of waste heat in managing livestock manure and producing useful byproducts. Recycling systems will also help a livestock enterprise to function with minimum environmental impact. This project will principally investigate the feasibility of using heated water to grow aquatic plants to remove nutrients from animal wastes. Another part of the system is being operated to determine the usefulness of the aquatic plants as a primary source of food for such aquatic animals as fish, freshwater mussels, and other aquatic animals that may then be harvested and used as a high-protein supplement for livestock rations and possibly even for human consumption (figure 6). The aquatic animals being produced in the recycling system are sent to Auburn University for evaluation as a high-protein supplement for livestock rations.

Soil Heating

Field test plots are being used to evaluate the use of waste heat from power plants for producing agricultural and horticultural crops. Results to date indicate that heating of soil can double the yields of some vegetable crops. Figure 7 shows an example of the difference between plants grown in heated soil compared to plants grown in unheated soil. Research at Muscle Shoals involves the use of a soil heating system to determine responses of crops to varying water temperatures and methods of heat application to simulate the diverse systems of power plants expected for the TVA system of the future. A prototype greenhouse was erected in 1976 over soil warmed by heated water (figure 8). Additional research is planned that will identify the optimum water temperature for maximum plant growth during spring and fall. Investigations are also planned to determine the maximum water temperatures that can be tolerated in midsummer without a reduction in plant growth.

Temperature Control for Livestock Facilities

Previous research indicates that livestock convert feed to body weight more efficiently when the temperature of the environment is controlled. With swine, maximum efficiency of feed conversion takes place at a constant temperature of about 60°F, and comparable results are expected with other livestock. Waste heat research in temperature control, already completed in the greenhouse experiments, will be useful in developing an environmental control system for confined livestock. The system has the potential for reducing the total amount of grain needed to bring livestock to a marketable size. The literature is being reviewed during 1977. If the review shows justification for design and construction of a pilot-scale, temperature-controlled facility for livestock production, using waste heat, it will be planned for 1978.

Because the economics of waste heat utilization are, at present, dwarfed by the economics of power production, care must be taken to ensure that appropriate consideration is given to both objectives. For example, at TVA's Hartsville Nuclear Plant, special connections will be provided on both the hot water and cold water conduits of the heat rejection system so that waste heat may be provided at optimum temperature and cost. Waste heat utilization processes must not, however, interfere with efficient and environmentally acceptable dissipation of waste heat and must not create conditions that would adversely affect the economic generation of power.

Heat Rejection Technologies

The remaining option for the control of waste heat is to manage the thermal discharge so that costs and environmental impacts are minimized. TVA conducts research to advance the state of the art in heat rejection technology and to determine the environmental impacts of these technologies.

Because the selection and sizing of a heat rejection system has a great impact on the economics of generation of electrical power, it is important to choose the optimum combination of design parameters. Computer optimization programs have facilitated this search for optimum combinations and have pointed out combinations involving a broad spectrum of heat dissipation devices.

Within TVA there are several research projects in progress to evaluate various heat rejection technologies.

TVA Spray Project

TVA is considering a project to determine its ability to design spray systems for either ultimate heat sink or condenser cooling. The project would use a full-scale test facility with an ultimate heat sink to provide data necessary for a comprehensive analysis of spray phenomena.

Wet/Dry Cooling Tower Project

TVA and EPA will jointly investigate new wet/dry cooling tower technology. The wet/dry cooling tower (figure 9) is an attractive alternative to all wet or all dry cooling towers because the wet/dry tower can operate for thermal performance, water conservation, and plume abatement. The project requires a full-scale wet/dry tower with necessary instrumentation and experienced personnel. Data will be gathered on thermal performance, water consumption, and plume abatement. These data will be used to accurately predict the performance of wet/dry cooling towers.

Prediction of Scale Formation

Recirculating evaporative cooling systems will be studied to enable TVA to predict the maximum concentrations of scale-producing material that can be present in cooling water without producing scale in cooling towers. The preliminary goal will be to identify the relationships that control CO_2 transfer from the cooling tower. A pilot cooling tower will be used in this study. Data from utilities in the United States that use wet cooling towers will also be studied to determine factors that cause scaling. Results of the project will be used to predict the maximum concentration of scale-producing material that can be sustained in TVA's systems that use cooling towers. The pilot tower will be used at various locations to verify results.

CONCLUSION

Fossil-fueled and nuclear generating plants will be found with the problem of waste heat for some time to come. Methods of dealing with the problem must include considerations of the possible environmental impacts of thermal discharges and, where possible, considerations of useful applications of this waste heat in an energy-hungry society. Close cooperation between all applicable sciences will be important to the continuing development of new uses and controls for waste heat.

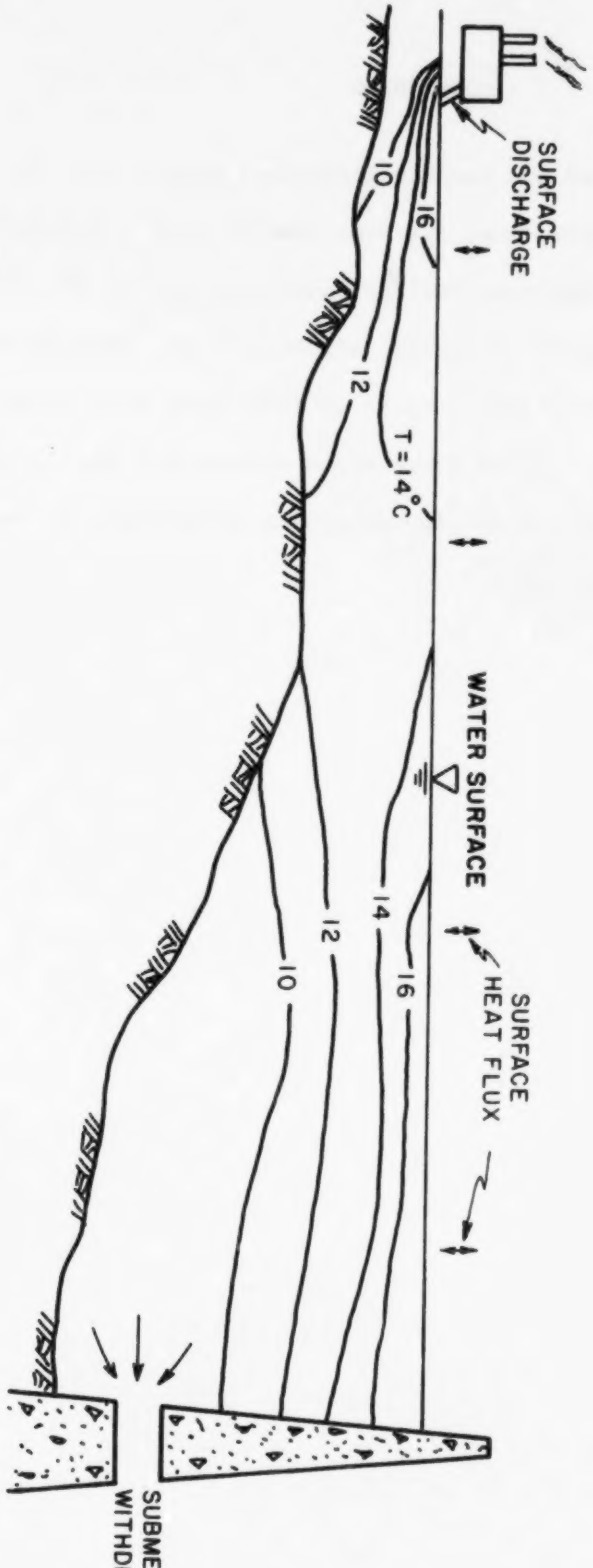
SURFACE DISCHARGE
10
16
12
T=14°C
WATER SURFACE
14
12
10
16
SURFACE HEAT FLUX
SUBMERGED WITHDRAWAL

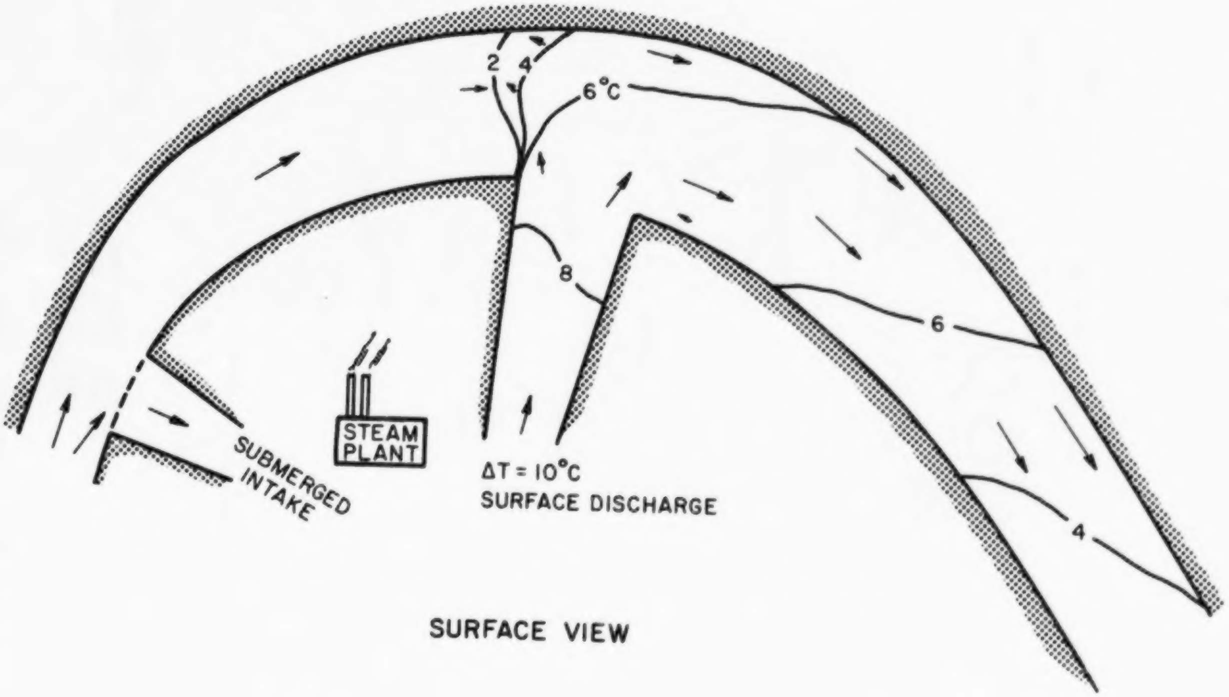
2
4
6°C
8
6
4
STEAM PLANT
SUBMERGED INTAKE
ΔT = 10°C
SURFACE DISCHARGE

SURFACE VIEW

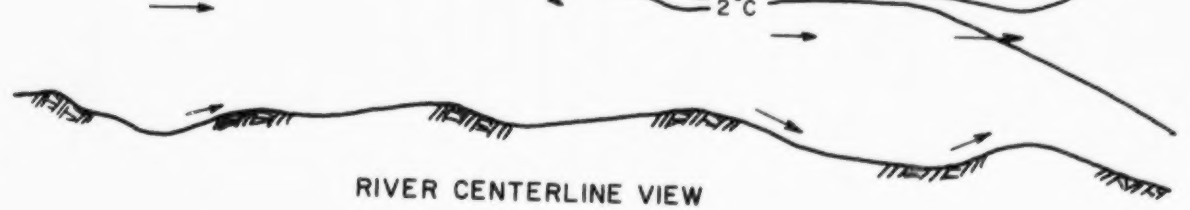
WATER SURFACE
6
4
2°C

RIVER CENTERLINE VIEW

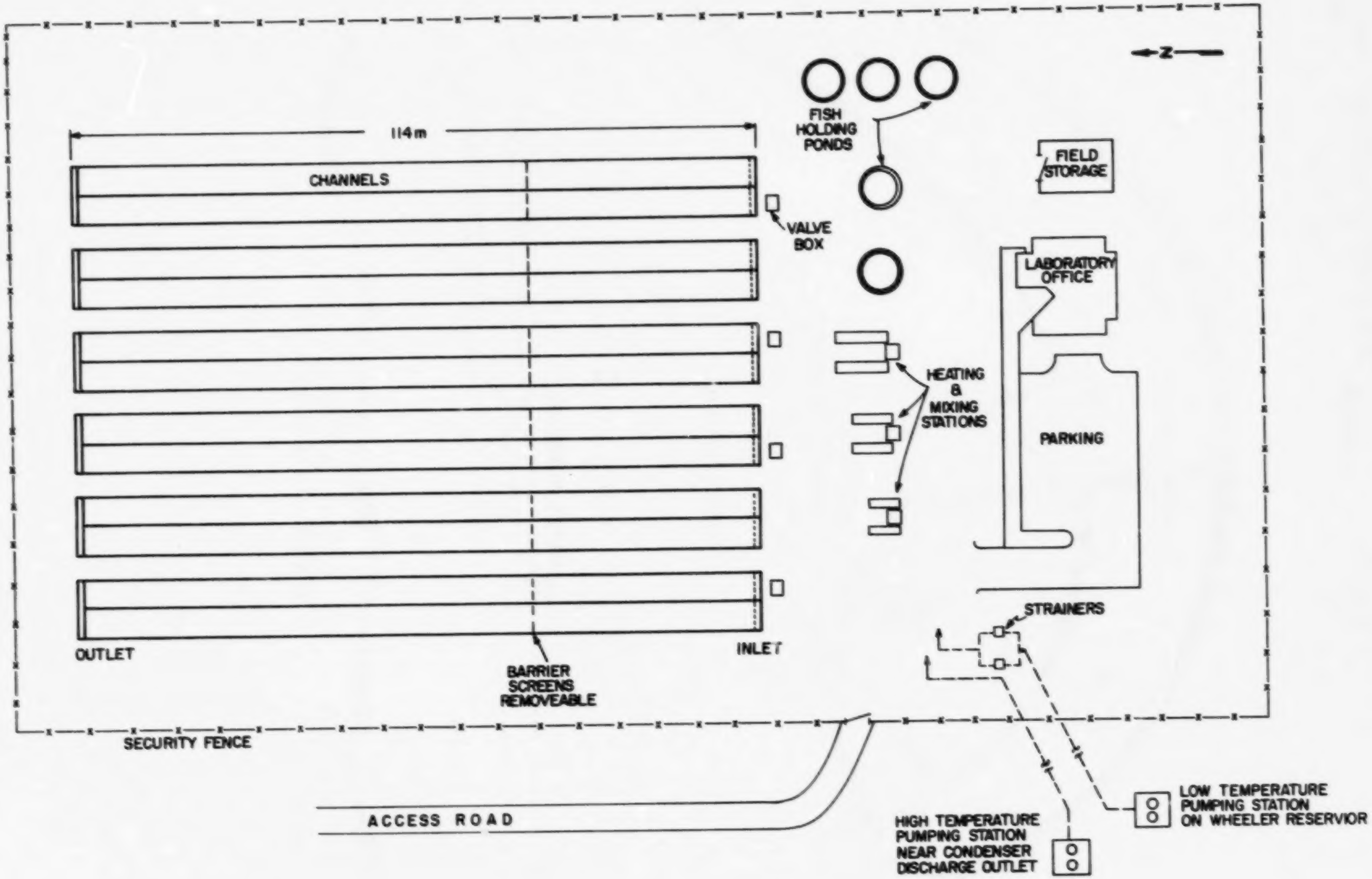
N
FISH HOLDING PONDS
FIELD STORAGE
114m
CHANNELS
VALVE BOX
LABORATORY OFFICE
HEATING & MIXING STATIONS
PARKING
STRAINERS
OUTLET
INLET
BARRIER SCREENS REMOVEABLE
SECURITY FENCE
ACCESS ROAD
LOW TEMPERATURE PUMPING STATION ON WHEELER RESERVIOR
HIGH TEMPERATURE PUMPING STATION NEAR CONDENSER DISCHARGE OUTLET

PLANVIEW OF EXPERIMENTAL CHANNELS AND AUXILIARY FACILITIES

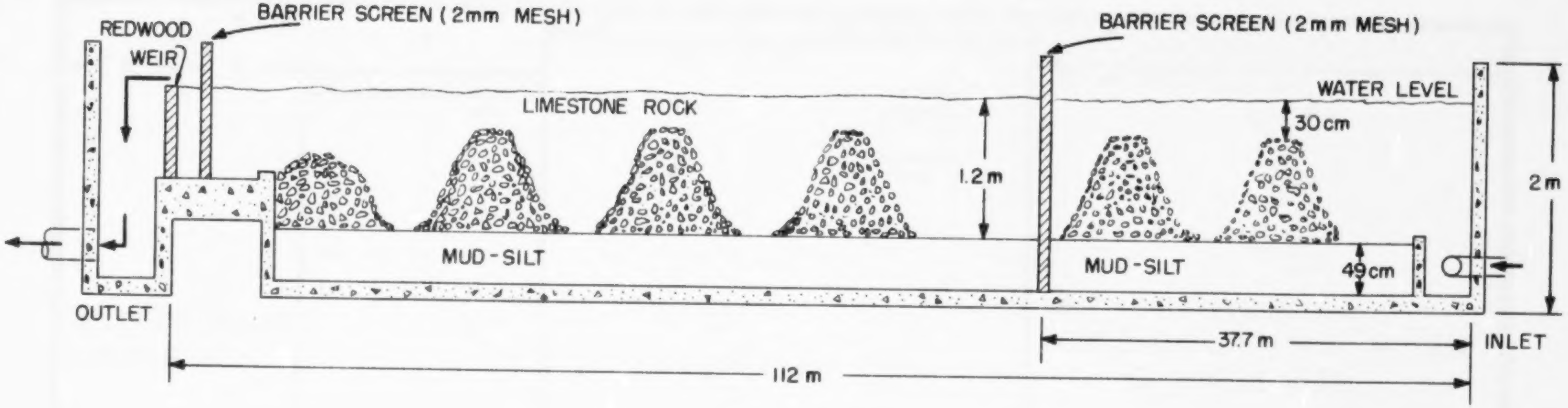
REDWOOD
WEIR
BARRIER SCREEN (2mm MESH)
BARRIER SCREEN (2mm MESH)
WATER LEVEL
LIMESTONE ROCK
30cm
1.2m
2m
MUD-SILT
MUD-SILT
49cm
OUTLET
INLET
37.7m
112m

PROFILE OF BROWNS FERRY EXPERIMENTAL CHANNEL

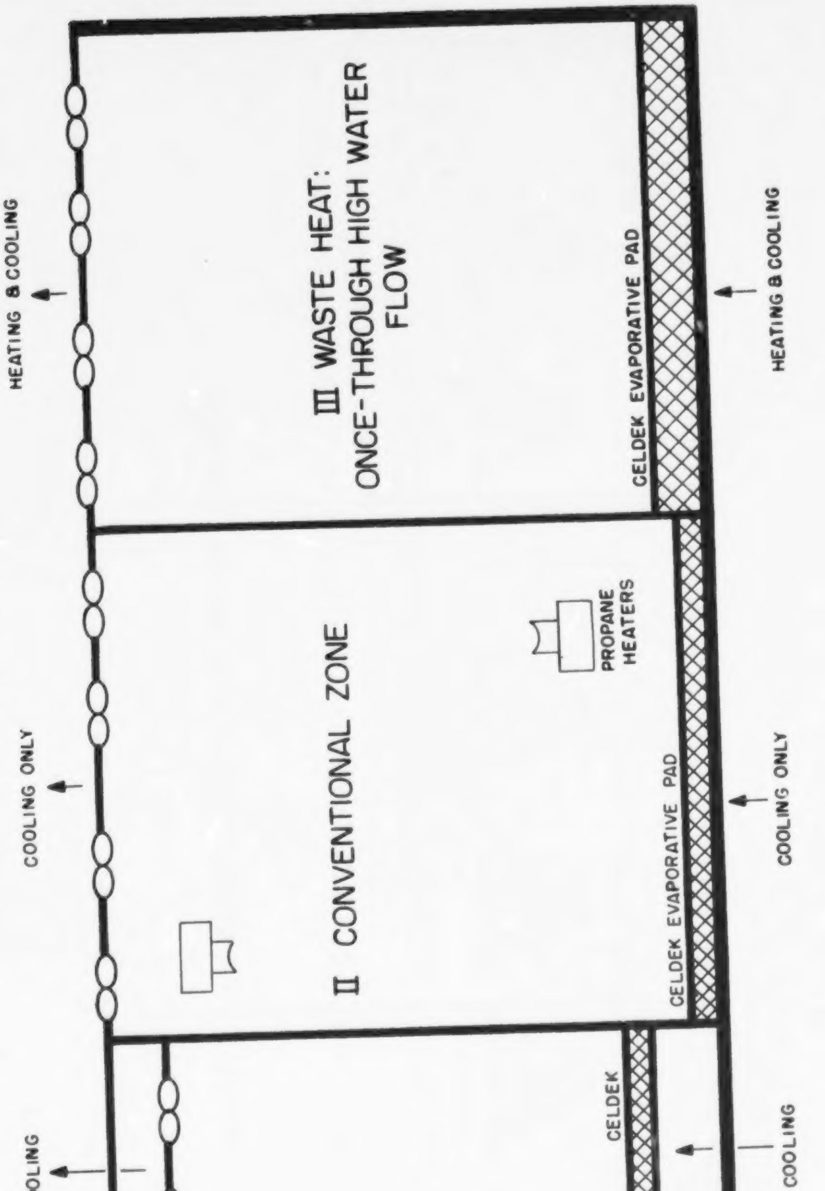
III WASTE HEAT: ONCE-THROUGH HIGH WATER FLOW
HEATING & COOLING
CELDEK EVAPORATIVE PAD
HEATING & COOLING
II CONVENTIONAL ZONE
PROPANE HEATERS
COOLING ONLY
CELDEK EVAPORATIVE PAD
COOLING ONLY
I WASTE HEAT: RECIRCULATION
COOLING
HEATING
CELDEK EVP PAD
COOLING
CELDEK
COOLING
OR
HEATING
COOLING

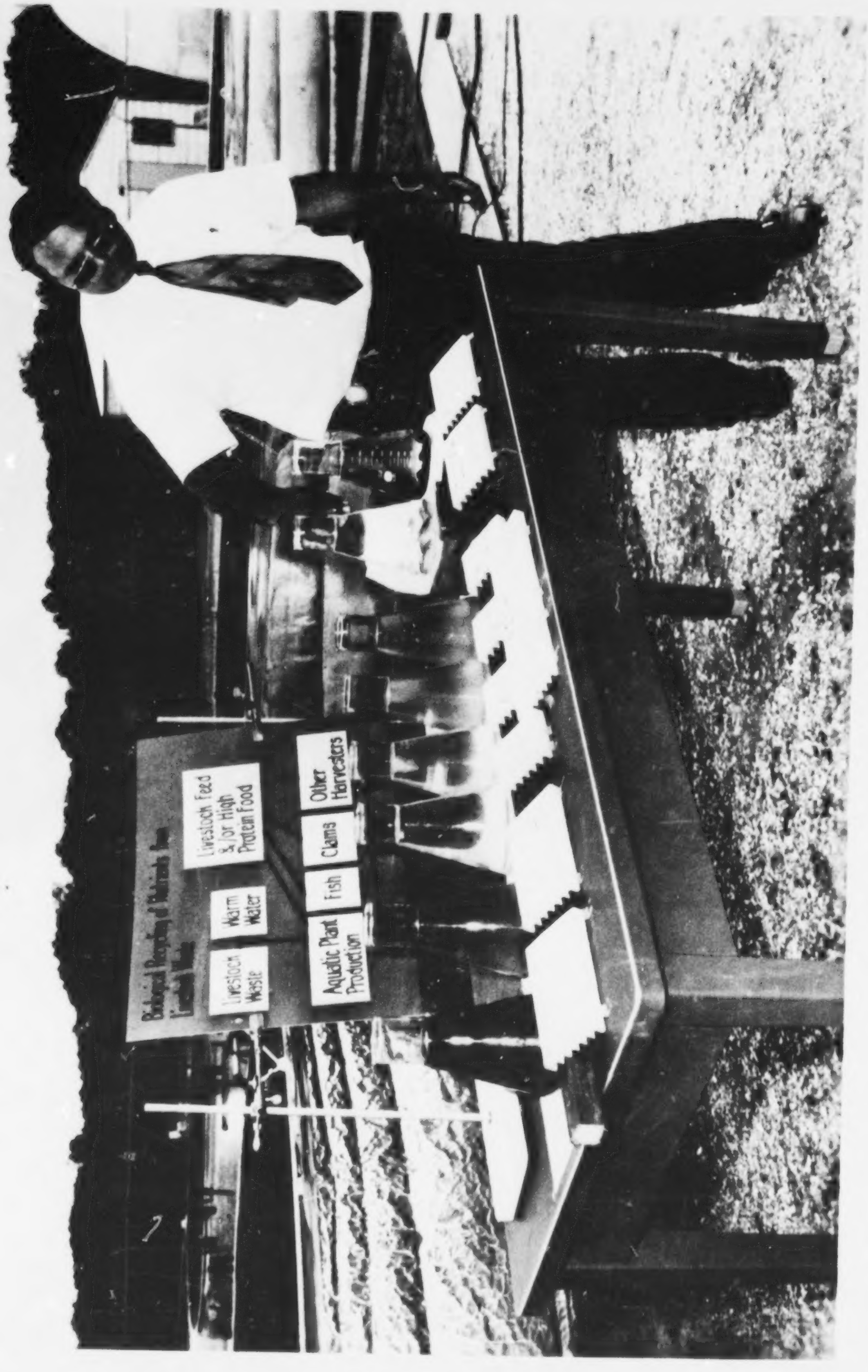
Biological Recycling of Nutrients From
Livestock Waste
Livestock Waste
Warm Water
Livestock Feed &/or High Protein Food
Aquatic Plant Production
Fish
Clams
Other Harvesters

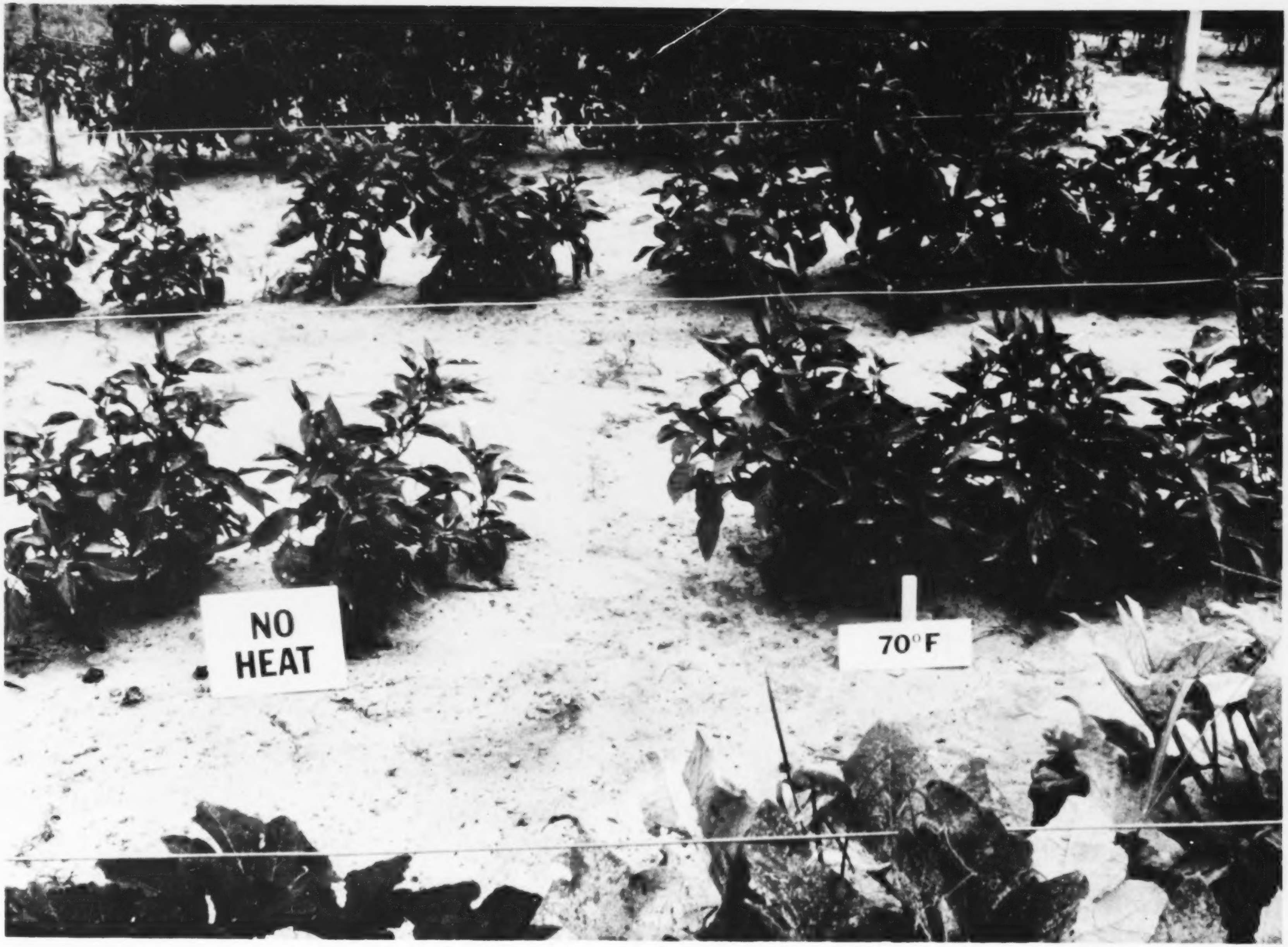
NO HEAT
70°F

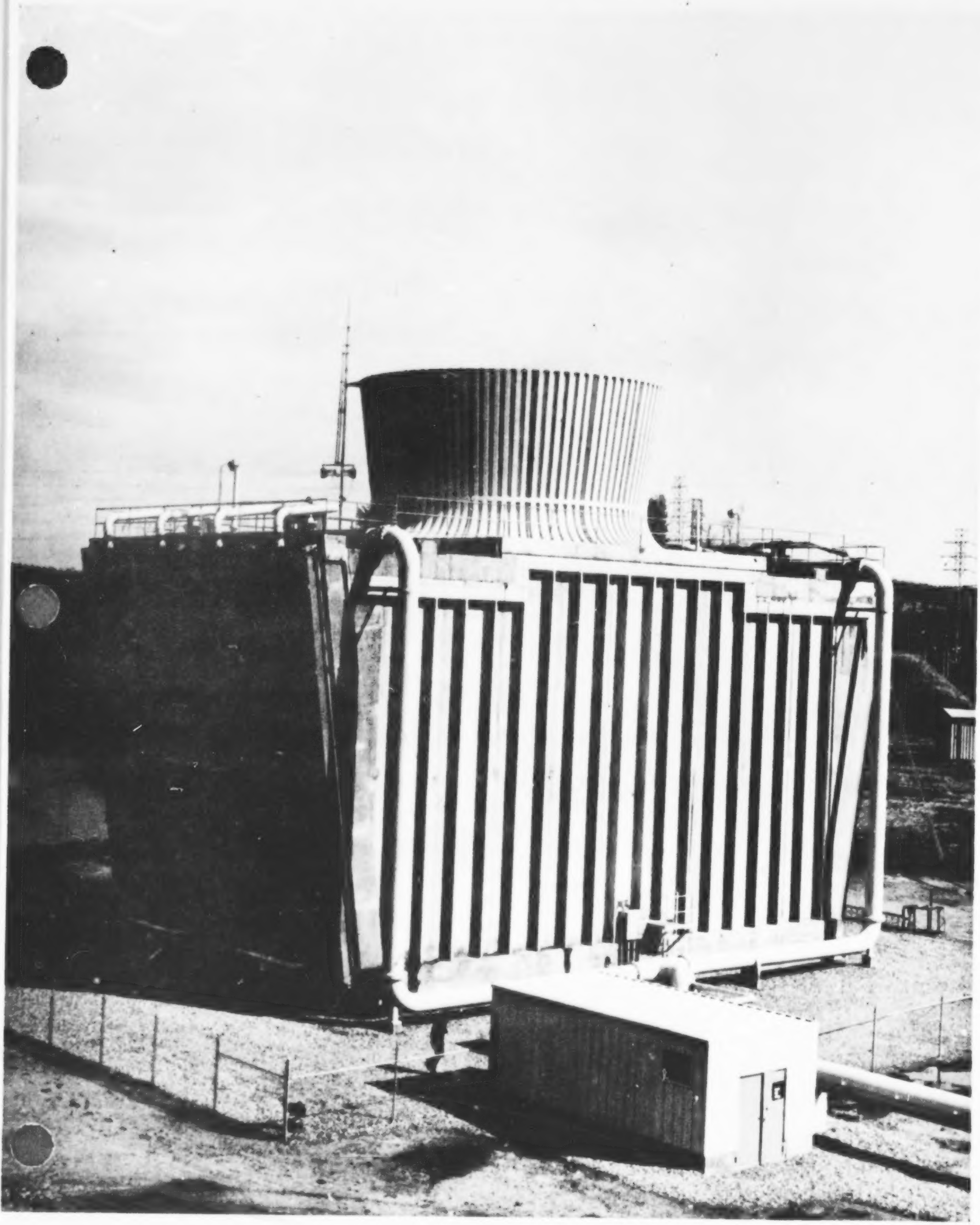

17-45-19

UTILIZATION OF POWER PLANT WASTE HEAT FOR HEATING

R. W. Timmerman
Consulting Mechanical Engineer
Boston, Massachusetts U.S.A.

ABSTRACT

This paper describes progress to date in development of a new system for the utilization of power plant waste heat for heating buildings, which makes power plant waste heat competitive with heavy oil, and possibly cheaper than light oil under present day New England conditions. This system consits of modifications to the power plant condenser to produce water at temperatures between 105F and 120F, a novel once-thru piping scheme, and a multistage heat pump and control system. The heated water is carried underground in ordinary reinforced concrete pressure pipe. The paper presents results of preliminary economic studies which show that waste heat appears to be an economically viable source of heating energy at the present stage of technology. The paper concludes with a discussion of further research needs.

INTRODUCTION

In recent years there has been some interest in the utilization of power plant waste heat. In addition to uses such as heating greenhouses, and aquaculture, use of waste heat for heating buildings has been investigated. [1,2]

My own interest dates from the early 1970's, but I did not begin the work on which this paper is based until early in 1975. This paper is in the nature of a progress report of work to date, and as such does not represent finished work. Please note also that much of the technology described in this report is covered by U.S. Patents Pending.

Two schemes for the use of power plant waste heat for heating buildings have evolved: High temperature schemes employing extraction steam, and low temperature schemes which use waste heat directly as it comes from the condensers. The various cogeneration schemes are a subset of the high temperature schemes. This paper presents a third alternative, which is a medium temperature scheme, operating at supply temperatures on the order of 105 to 120F.

The remainder of the paper is divided into 3 parts: definition of the problem, the solution proposed, and the results of the economic study.

DEFINITION OF THE PROBLEM

Simply stated, the problem of waste heat utilization is to find economical uses for power plant waste heat. In the case of heating systems, it is possible to develop a set of engineering guidelines, which serve to further define the problem, and also point in the direction of a possible solution.

Engineering Guidelines

1. The scheme should require no major power plant modifications, nor major design changes in new plants. This makes it possible to use the waste heat output of existing plants, and keeps the capital costs down. It also reduces the amount of new technology that must be sold to the generally conservative utility industry.

2. The cost of interference with normal power plant economic dispatch is to be borne by the heating customers. For example, if the plant must run to meet the heating load, at a time when it is not economical for power generation, the cost of operation will be borne by the heating customers. Likewise, the cost of any degradation of the heat rate is for the account of the heating customers.

3. Total cost of heat delivered in a form the customer can use should be competitive with oil or gas, also in that form. This generally means charging boiler efficiency against oil or gas.

4. Likewise, the economics should be based on real world conditions. The carrying charges should include realistic taxes and interest rates. The load factor should be a realistically achievable value, without resort to unrealistically high summer loads.

5. Sufficient standby capacity should be provided to cover normal operating contingencies, such as power plant outages. Murphy's Law applies to power plants, so it is not realistic to assume that all maintenance can and will be done in the off season.

6. The heat must be delivered in a form that can be used by at least the majority of existing building heating systems.

These guidelines seem to be a bit strict, but I believe that they are necessary. Waste heat systems are capital intensive, and unless they are government subsidized, the capital will have to come from the normal capital markets. The only way of convincing investors to put up the money is to convince them that they stand a reasonable chance of getting their money back, with interest.

Implications of Engineering Guidelines

Although most of the implications of these guidelines are fairly straightforward, there are some that are rather subtle, but with far-reaching implications.

One inexpensive way to meet the standby requirement is to use a grid connected system, supplied by several heating sources. This offers the same benefit to heating systems that power grids have, namely reduction in the amount of standby capacity. However, in order to feed several sources into a grid, they all must be compatible. If the heating medium is hot water, all sources must discharge at about the same temperature. Generally it is less expensive to produce a stream of fluid at temperature T directly, than it is to produce it by mixing two streams, one at T minus ten degrees, and the other at T plus ten degrees, due to the irreversible nature of the mixing process. In addition, suddenly introducing a stream of fluid that differs sufficiently from the average to change the average temperature will probably create some problems for the terminal apparatus.

Neither schemes based on extraction steam, nor schemes based on condenser water can meet this criterion. Both turbine extraction pressures and circulating water outlet temperatures vary with load on the machine. This is a more severe problem for systems using extraction steam, because the extraction steam pressure is not only the determinant of energy level in the steam, but is also the driving force producing flow in the piping system. Therefore, if the pressures at the various plants deviated very far from the equilibrium value, the flow pattern would not be what was desired. Systems using circulating water would only be troubled by problems of temperature incompatibility, which are more manageable. The need to meet electric loads in a manner that would not cause great temperature and pressure incompatibility problems for the heating system is an extremely difficult and expensive dispatching problem.

The requirement that deviations from normal dispatch be borne by the heating system discourages systems that require certain plants to be run to meet heating load, regardless of power load. Likewise, systems that provide power as a by-product of heating are at an economic disadvantage, because the power generated is not firm power, but varies with heating load. Since standby facilities are needed to meet the power load when there is no heating load, the power produced as by-product is priced as by-product power, instead of firm power. This reduces the credit for power production.

DESCRIPTION OF THE UTILIZATION SYSTEM

My scheme is an attempt to avoid these problems and still meet the economic requirements. I propose to use a grid-connected system to insure reliability. The heat source will be condenser circulating water at a controlled temperature of 100F to 120F. Use of a controlled outlet temperature at this level has two benefits: The water temperature is closer to the required utlization temperature, and all plants are made compatible with each other. The cost of the heat will be determined by the difference in heat rate of the various power plants under normal conditions and the heat rate while delivering water at the controlled outlet temperature. This particular choice of outlet temperature comes about from trying for the highest possible outlet temperature that existing turbines are capable of. This avoids the problem of selling power companies on new technology, and avoids building special purpose plants which have poor performance when heating is not required. The back pressure of existing turbines is limited to 5 inches of mercury, which works out to 133.75F, which in turn makes possible a maximum outlet temperature in the 100 to 120F range.

Conduit Design

A great simplification of the conduit design is possible in the 100 to 120 F temperature range. Most underground heat conduits have a well deserved bad reputation for high installed costs, and for high maintenance costs. However, ordinary reinforced concrete pipe is permitted by the piping code for temperatures under 150F. Heat loss of large diameter pipes is on the order of one or two degrees in ten miles, with ordinary sand used as insulation. Sand has a number of advantages over other insulation materials: It is readily available at low cost, installation is simple and fast, it drains water easily, and it is not damaged by water. The last benefit is rather important, because underground conduits will flood, and therefore should be designed so as not to be damaged by flooding.

Ordinary bell and spigot pipe joints have sufficient flexibility to accommodate thermal expansion. Guides are not needed, because the sand insulation has sufficient bearing capacity to support and guide the pope. This obviates the need for manholes to contain the exapnsion joints and guides, reducing both the construction cost of the manholes, and the maintenance cost of the expansion joints. As with any bell and spigot joint system, anchors are needed at changes of direction. However, by elimination the expansion joints, the anchors can be simpler, cheaper and farther apart.

Supply and Return Piping Configuration

Two configurations of supply and return piping are possible: conventional two pipe design and a once-thru system. The conventional two pipe system employs supply and return lines, with fluid flowing in a circuit. This is the conventional approach, and is most economical for short and intermediate range transmission.

In addition, it is possible to dispense with the return line if both the plant and the utilization point are located on a common body of water. In this case the water is taken in at the power plant, heated in the power plant, and transmitted to the point of use. It is cooled at the point of use, and discharged back to the body of water.

The once thru system has an inherently low utilization efficiency, since the plant takes in water at temperatures in the 32 to 40F range in the winter, and discharges at temperatures in the 100 to 120F range. Utilization apparatus will probably not be able to cool the water down past, say 80F. This results in utilization efficiencies on the order of 50%.

For a given power plant output, a one pipe system will have roughly half the water flow of a two pipe system, since the utilization apparatus operates through about the same temperature difference in both cases. The once thru system will use only half the plant output, but to do this will move only half the water, thru half the distance, resulting in a saving in both capital cost and pumping power cost. As a result, the best application of a once thru system is for long distance transmission of heat from a plant with a cheap heat source, such as coal or nuclear.

Conversion Systems at the Point of Use

There are three obstacles to the direct use of waste heat in building heating systems: low supply temperatures, high temperature drop, and possible corrosion problems.

The supply temperature in the 120F range is slightly lower than commonly used supply temperatures in building heating systems. Furthermore, a fairly high temperature drop between supply and return is essential to the economics of the system, by keeping transmission and distribution pipe sizes within reason, and by keeping the utilization efficiency up on once thru systems. High temperature drop implies a low outlet temperature, probably in the 70 to 90F range. This results in a much lower average temperature than most building heating systems are designed for. While it should be possible to design a heating system for a new building for these conditions, it probably is not practical to retrofit an existing heating system for these temperature levels.

A third problem is possible corrosion. Many of the systems along the coast will employ salt water. Even if salt water is not used directly in a two pipe, closed loop system, there is still the possibility of salt entering the system as plants are switched in and out of the system. In order to protect the building heating system from corrosion due to salt water, it becomes necessary to install some sort of heat exchanger to isolate the waste heat system from the building heating system.

Instead of a passive heat exchanger, it is possible to use a heat pump. This will isolate not only the salt water, but the low temperature levels as well. A heat pump will make it possible to operate the building heating system at some higher temperature level than the waste heat system, thereby reducing the retrofit problems.

ENGINEERING DETAILS

While the system has been outlined in broad detail, there are two crucial parts of the system which I would like to discuss in greater detail. These are the power plant modifications necessary to produce 120F water, and the terminal apparatus.

Power Plant Modifications

One of the goals of a good waste heat system is minimum interference with normal power plant operation and design, and especially, minimum interference with normal economic dispatch. Since the heating and power loads vary independently of each other, it follows that some means must be provided to decouple the two.

The grid connected system permits plants to be added or subtracted from the heating system as needed to meet the heating load. It is also feasible to introduce some storage into the system to meet short term peak loads. In order to be able to switch a plant in and out of the heating system at will, it is necessary that the plant modifications for producing 120F water do not interfere with normal plant operations. In particular, the modifications must not affect the heat rate of the plant when it is not delivering heat to the system.

Conventional power plant condensers are designed for water temperature rises on the order of 20 to 40F. With wintertime water temperatures in the 35 to 40F range, the outlet temperatures will fall in a range between 55F and 80F, which is well below the desired 100 to 120F range. If the plant is part of a two pipe system, the temperature rise needed will be on the order of 40 to 60F, which is at the high end of the normal operating range. Therefore, some means must be provided to produce the desired temperature rise, while keeping the condensing temperature as close as possible to the outlet water temperature, and not restricting the output of the turbine.

The approach temperature is the difference between the condensing temperature and the circulating water outlet temperature. A circulating water outlet temperature on the order to 120F is desired, without exceeding the maximum condensing temperature of 133.75F (5 inches of mercury back pressure). This allows for an approach of 13.75F, instead of the normal design approach of 20 to 30F. Refer to Figure 1, which shows the temperature conditions inside a condenser.

In the following discussion, the notation below will be used:

T_{cond}	Condensing Temperature
T_{cwin}	Circulating Water Inlet Temperature
T_{cwout}	Circulating Water Outlet Temperature
R	$T_{cwout}-T_{cwin}$
E	Condenser Effectiveness
U	Overall Heat Transfer Coefficient
A	Surface Area of Condenser
C	Hourly Heat Capacity of Cooling Water (Cooling water mass flow times specific heat)

By definition,

$$E = \frac{T_{cwout}-T_{cwin}}{T_{cond}-T_{cwin}} = \frac{R}{T_{cond}-T_{cwin}} \qquad (1)$$

This can be rearranged to read:

$$T_{cond}-T_{cwout} = \frac{(1-E)}{E} R \qquad (2)$$

Waste heat applications usually require R on the order of 2 to 4 times design, with an approach ($T_{cond}-T_{cwout}$) on the order of half design. Examination of equation 2 shows that E must be increased by a considerable amount in order to produce the desired approach.

For a condenser:

$$E = 1- \exp(-UA/C) \qquad (3)$$

With existing condensers, A is fixed. With the condenser for a power plant being designed, A can be varied, but economic limitations will place an upper limit on A. Examination of equation (3) shows that as C decreases, E increases. This is partially offset by the reduction in U which takes place when the velocity thru the tubes is reduced, which in turn is a direct consequence of reducing C. If a condenser originally designed for single pass design is converted to multipass design, the mass flow thru the condenser can be reduced, without reducing the velocity, thereby keeping U at or near the design values. At the same time, the reduction in C will permit an increase in E, the effectiveness.

Although research in this area is still underway, preliminary results are that a single pass condenser designed for 25F water temperature rise and 32F approach can be used successfully to produce water at 112F when converted to multipass.

Another reason for keeping the water velocity in the tubes at or near design values is to reduce corrosion problems in the tubes. It is well known that certain minimum water velocities are needed to preclude condenser tube fouling.

Under certain conditions, it may be possible to operate a multipass condenser with multiple pressure zones. When this can be done it reduces the heat rate penalty which is incurred when discharging heat at 120F. The heat rate is improved because the average back pressure is reduced in multipass operation over single pass operation.

While space does not permit a discussion of the technique for switching from single space to multipass, I would like to point out that a technique has been developed which permits switching to take place without interrupting normal circulating water flow. This should permit such conversions to occur with the power plant on line.

Heat Pump

The need for the heat pump has already been discussed. While previous work in waste heat utilization has used single stage heat pumps [1,2], there are some inherent limitations of single stage heat pumps that render them not particularly well suited for waste heat utilization.

Figure 2 is a T-S diagram of a conventional Carnot cycle heat pump. The heating and cooling which the heat source and heat sink undergo are shown by the dotted lines. The Carnot cycle requires constant temperature heat addition and rejection. In this case, heat addition and rejection do not take place at constant temperature. Consequently, there is a loss in efficiency, due to the irreversible nature of heat transfer thru a finite temperature difference. While the Brayton cycle would be a much better match to the conditions, the heat transfer between the gas used as a Brayton cycle working fluid and the liquid used to carry waste heat is inherently poor, negating much of the advantage.

Another approach is to use a series of Carnot cycles to approximate the actual cooling and heating curves. This is illustrated in Fig. 3. A comparison has been made between a single stage heat pump and a 3 stage heat pump, both with the same heat exchanger terminal differences and the same compressor efficiency. Both heat pumps take in water at 120F, discharge it at 90F, while heating water from 130F to 160F. Under the conditions used in the study, the single stage heat pump had a COP of 5.32, while the 3 stage machine had a COP of 6.95. The 3 stage machine will require 78% of the power input of the single stage machine.

The second problem is the difficulty in economically matching the output of the heat pump with the load. The output of a convector is governed by equation 4: [3]

$$H = c(T_s - T_a)^n$$

H	Heating output
c	Rating constant, determined by test
T_s	Average supply temperature
T_a	Air temperature
n	1.3 for cast iron radiators 1.4 for baseboard radiation 1.5 for convectors

For example, if a system of baseboard radiation was designed for 160F supply temperature, and 130F return temperature (average temperature 145F), with air temperature at 65F, reducing the output to half would require an inlet temperature of 121F and a return temperature of 106F, assuming constant mass flow thru the baseboard unit.

An all air system can be operated with either constant air volume, and variable supply temperature, or constant supply temperature and variable air volume. The later approach has become increasingly popular in recent years. It is not the approach of choice for waste heat utilization.

The least expensive way to operate a waste heat utilization system is to control the temperature of a heated space by varying the supply temperature of the fluid heating the space. This reduces the heat pump temperature lift at low loads. Lower temperature lift translates into higher COP, and less power consumption. This is illustrated by Figure 4, which shows the frequency of occurance of outside air temperatures for Boston, and also the hot water supply temperatures required to meet the heating loads created by these outside temperatures.

Heat pumps designed for waste heat applications will deliver only a fraction of the heating output when used for air conditioning. This is because the compressor suction pressure in cooling applications is only a fraction of the suction pressure in heating applications. The low suction pressure reduces the inlet density, reducint the compressor capacity. I estimate that the cooling capacity of a heat pump designed for waste heat utilization is only 20% of the heating capacity.

ECONOMICS

In order to accurately assess the economics of the system, I have made what I believe are rather conservative assumptions. I assumed that the waste heat transmission and distribution system would be owned and operated by an electric power company, which would have a fixed charge rate of 20%. I assumed that the terminal equipment would be owned and operated by the customer, with the same fixed charge rate. Electric power costs of 5¢ per kwhr and oil costs for steam power plants of $2.00 per million btu were used.

Transmission and distribution piping costs were computed from various pipeline costs reported in Engineering News-Record, and are based on construction in moderately congested areas (not heavily congested downtown areas).

Owning and operating costs of the heat pump were based on the following:

- Fixed charge rate of 20%
- Cost of heat pump @ $225/ton of capacity (15000 btu/hr heating)
- Credit for cooling capacity of 20% of heating capacity
- Carrying charges applied to cost of heat pump, less 20% cooling credit, less cost of a heating boiler of the same capacity.
- Yearly average COP of 14
- Electric power cost of 5¢/kwhr
- Diesel fuel at $3.00/million btu

For comparison purposes, heating costs using fossil fuel were computed on the following basis:

- Boiler efficiency 80%
- #2 Fuel oil at 47¢/gallon ($3.40/million btu.)
- #6 Fuel oil at $2.00/million btu
- No carrying costs for the heating boiler are included, since the carrying costs for the heat pump are computed on a differential basis with a conventional heating boiler.

Two cases were considered. The first is a residential district, which is principally 5 storey brick row houses. In this case, electricly driven heat pumps would be used. The second case is a large institution, using Diesel engine driven heat pumps with recovery of the exhaust heat, and heat from the water jacket. Both cases are described in Table 1, and the economics are compared in Table 2.

Both of these cases are based on a one pipe system transmitting heat from a fossil fueled power plant. Two more cases investigated differences in cost of a two pipe system, and differences in cost of heat from a nuclear powerplant. Bost of these studies were concerned with costs up to the distribution system only.

Case 3 is a comparison of the cost of heat delivered to the distribution system from a two pipe transmission system supplied by a fossil plant. The conclusions of the analysis are that a two pipe system is slightly less expensive than a single pipe system for the distribution of the heat from oil fired plants due to the higher utilization efficiency. Case 3 is presented in Table 3.

Case 4 is an investigation of the cost of heat from a plant burning cheap fuel, located some distance from a center of utilization. These costs are typical of the economics of waste heat from nuclear plants. Cost of waste heat from base load coal fired plants will be only slightly higher. Case 4 is presented in Table 4.

In order to establish a point of reference for these fuel costs, it is necessary to compute the cost of heating by oil. With the base figures given above, the cost of heating by #2 fuel oil is $4.25/million btu, and the cost of heating by #6 oil is $2.50/million btu.

We can draw some conclusions from these results:

1. Waste heat from fossil fueled power plants is cheaper than #2 fuel oil, up to 10 miles from the plant, under present New England Conditions.
2. Waste heat is about 15% more expensive than a large user than #6 fuel oil, under the same conditions as 1 above.
3. Waste heat from a nuclear plant is cheaper than waste heat from a fossil fuel plant, up to at least 30 miles from the plant.

RESEARCH NEEDS

This paper represents work in progress, and does not represent final conclusions. A considerable amount of further work needs be done before the economic feasibility of power plant waste heat for heating is established. I have mapped out a research program to further investigate the technical and economic feasibility of waste heat utilization. In the order in which they should be done, these steps are:

1. Investigate the suitability of actual power plants as heat sources.
2. Design, build and test a prototype heat pump. Compute cost to manufacture and sell.
3. Design, install, and test a prototype underground heat pipeline. Estimate cost to install in large quantities.

4. Select an area for a demonstration project. Layout the system, and estimate the cost. Model several years operation of the system, and determine savings over oil.

5. From 4, determine economic feasibility. Redesign if necessary and possible.

6. Build and test an actual demonstration project.

The intriguing thing about use of power plant waste heat for heating is that it offers the potential of economically saving large quantities of energy with relatively low development costs.

REFERENCES

1. Aamot, Haldor W. C., Management of Power Plant Waste Heat in Cold Regions, NTIS REPORT AD/A-003 217 December 1974

2. Ileri, A., Reistad, G. M., and Schmisseur, W. E. Urban Utilization of Waste Energy From Therman-Electric Power Plants, ASME paper 75-Pwr-12

3. ASHRAE Guide, 1967, pp 348-349

TABLE 1
DESIGN BASIS OF COST STUDY

ITEM	CASE 1	CASE 2
Transmission System	10 Miles: Plant to Distribution 3 Miles: Distribution to body of water	10 Miles: Plant to Distribution 3 Miles: Distribution to body of water
Distribution System	Small lines serving each building	Few large lines to central heat pumps
Heat Pump Drive	Electric	Diesel
Type of buildings served	5 storey brick row house	Large instutional
Utilization Efficiency	37.5%	50%

TABLE 2
COST COMPARISON OF CASES 1 AND 2

ITEM	CASE 1	CASE 2
Cost of heat at plant	$0.85/million btu	$0.64/million btu
Transmission and pumping	$0.75/million btu	$0.75/million btu
Distribution	$0.31/million btu	$0.16/million btu
Heat pump carrying cost	$0.40/million btu	$0.50/million btu
Heat pump operating cost	$1.05/million btu	$0.80/million btu
Total cost	$3.36/million btu	$2.85/million btu
Cost of heating with #2 oil	$4.25/million btu	
Cost of heating with #6 oil		$2.50/million btu

TABLE 3
CASE 3 COST COMPARISON

ITEM	1 PIPE	2 PIPE
Line length supply and return	13 miles	20 miles
Transmission cost	$0.75/million btu	$1.15/million btu
Efficiency of use	37.5%	100%
Cost of heat at 37.5% efficiency	$0.85/million btu	
Cost of heat at 100% efficiency		$0.32/million btu
Total Cost	$1.60/million btu	$1.47/million btu

TABLE 4
CALCULATION OF COST OF NUCLEAR HEAT

Design Basis

Hours of operation	4800 hrs/yr
Plant size	1100 Mw
Heat produced per kwhr generated	8500 btu/kwhr
Fuel cost	\$0.30/million btu
Utilization efficiency	37.5%

Pipe Data

Size	96 inch
Pressure drop/100 ft.	0.228 feet of water @ 240,000 gpm
Pipe cost, installed	\$300.00/foot

Calculations

Heat moved: 4800 hrs/yr X 8500 btu/kwhr X 1,100,000 kwhr/hr X .375 = 16.83 X 10^{12} btu/yr

Pumping Power:

$$\frac{\text{840,000 gpm X 8.31 lbs/gallon X 0.228 ft./100 ft. X 52.8 100 ft./mile X .746}}{\text{33000 ft. - lbs/hp X 0.80 (Pump effic.) X 0.90 (Motor effic)}}$$

= 754 kw/mile

Total yearly pumping cost	\$181,000/mile - year

Carrying cost per mile: 300 dollars/ft. X 5280 ft./mile X 0.20 fixed charge rate = \$181,000
(Per year)

Total cost per million btu/mile: (\$350,000 + \$181,000)/16.83 X 10^6 = \$0.0316

Cost of moving 30 miles	\$1.00/million btu
Cost of heat at plant @ \$0.30/million btu	\$0.10/million btu
Total cost for heat and 30 mile transmission	\$1.10/million btu

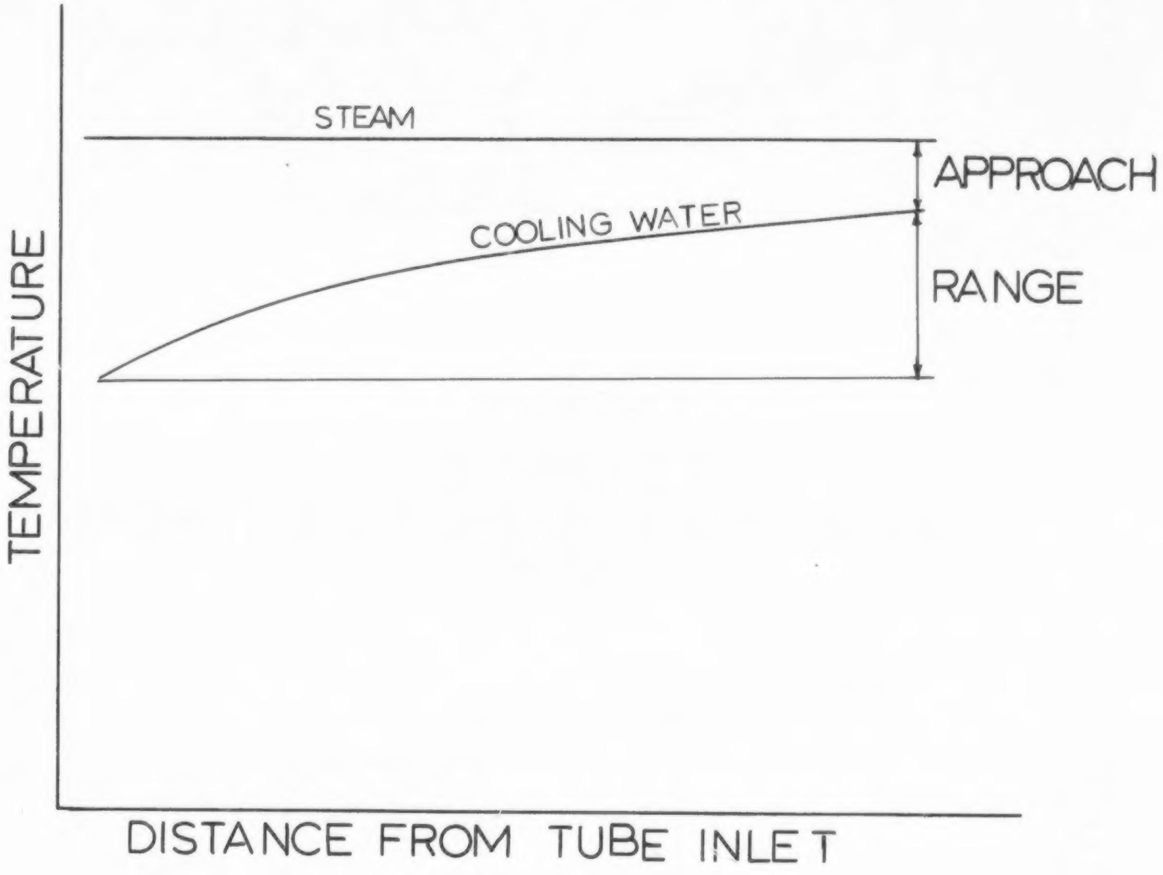

FIGURE 1

TEMPERATURE PROFILE IN A CONDENSER

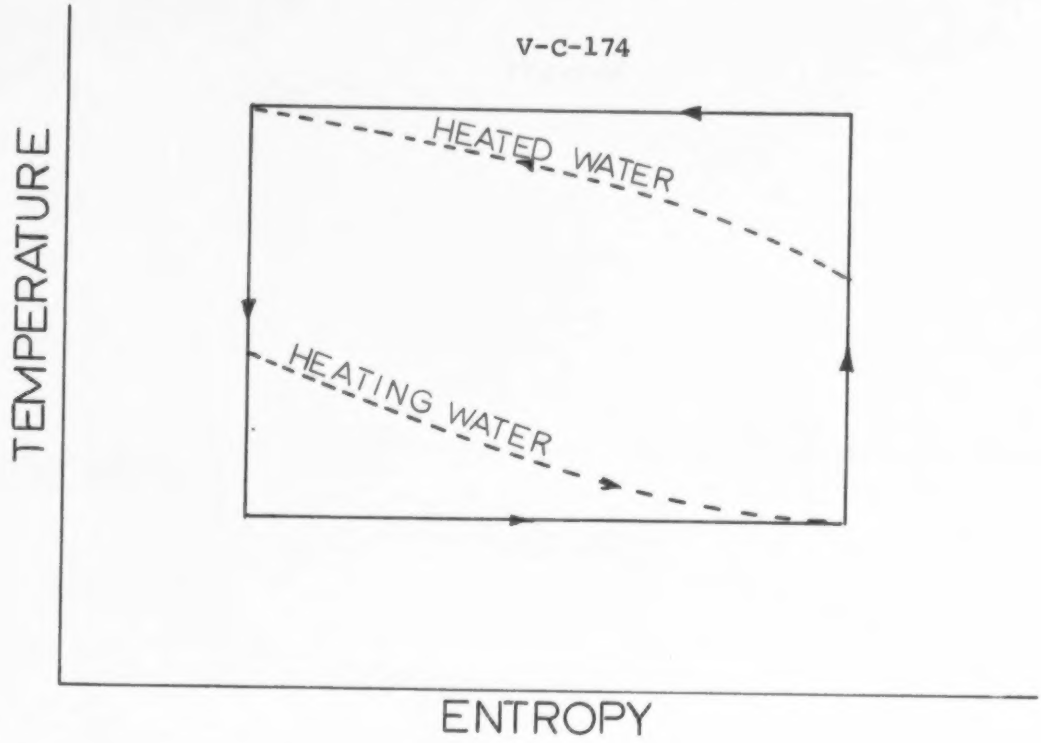
TEMPERATURE
HEATED WATER
HEATING WATER
ENTROPY

FIGURE 2

T-S DIAGRAM FOR CARNOT CYCLE HEAT PUMP

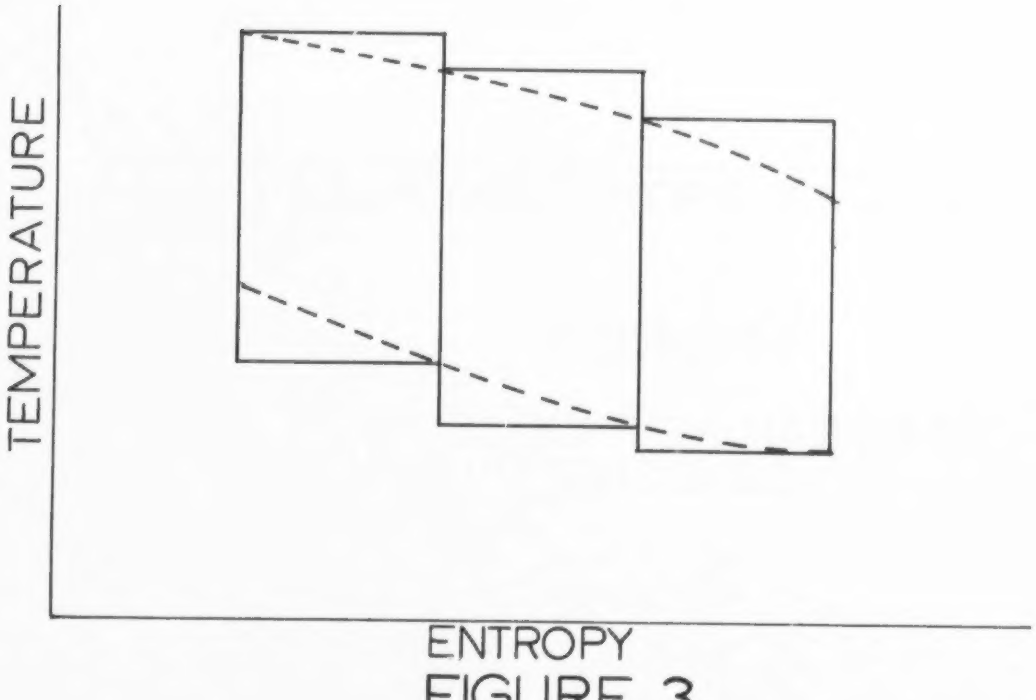
TEMPERATURE
ENTROPY

FIGURE 3

T-S DIAGRAM FOR MULTISTAGE HEAT PUMP

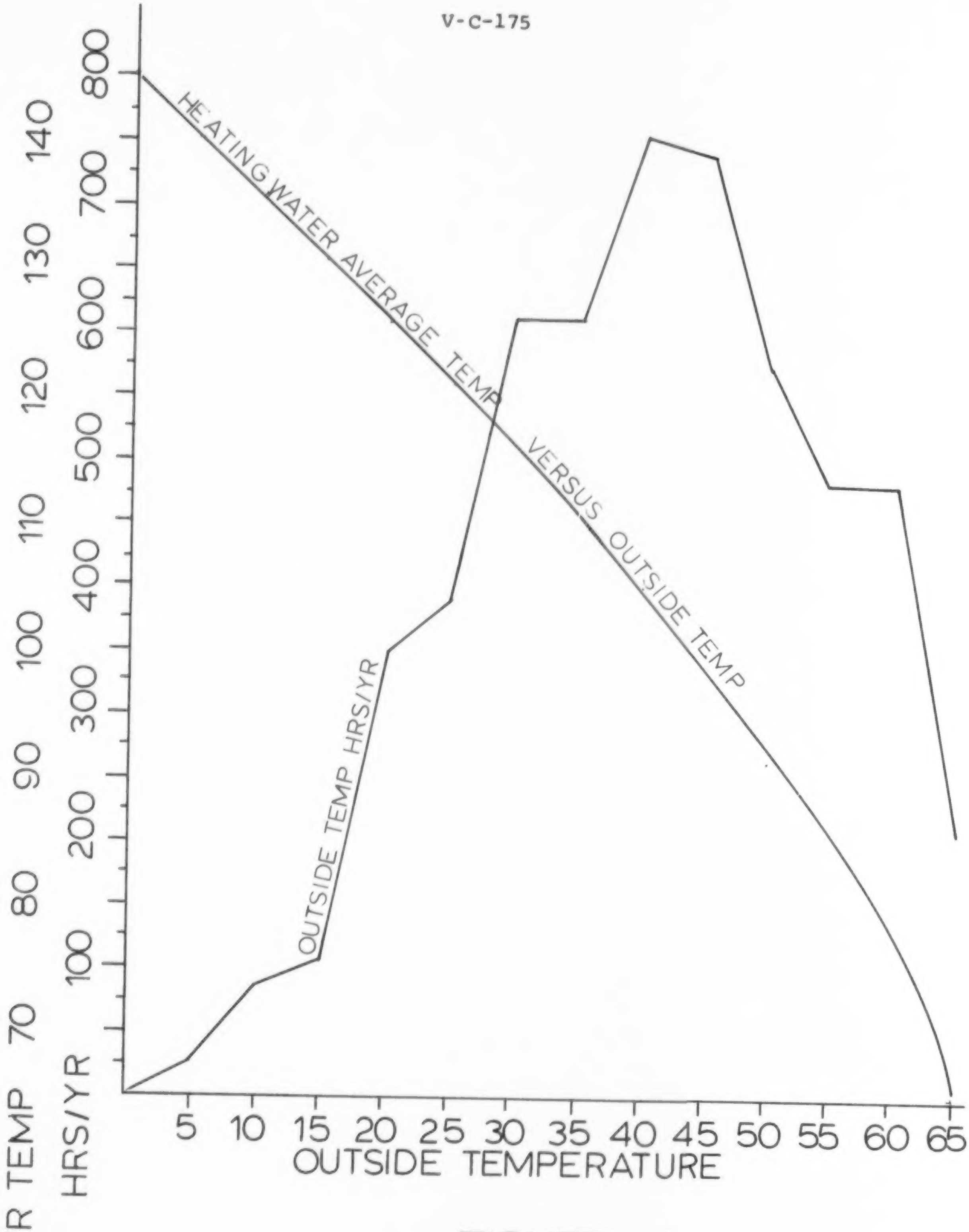
HEATING WATER AVERAGE TEMP VERSUS OUTSIDE TEMP
OUTSIDE TEMP HRS/YR
WATER TEMP
HRS/YR
70
80
90
100
110
120
130
140
100
200
300
400
500
600
700
800
5
10
15
20
25
30
35
40
45
50
55
60
65
OUTSIDE TEMPERATURE

FIGURE 4

18-45-9

V-C-177

HEATING OF GREENHOUSES WITH TEPID WATER

A. Fourcy(1), M. Dumont(2), A. Freychet(1)
C.E.A.-Centre d'Etudes Nucléaires
DRF-G.-Laboratoire de Biologie Végétale
Grenoble - France

ABSTRACT

Heating greenhouses with low grade calories needs large exchanging surfaces between the warming fluid and the surrounding of the crops. Such exchanging surfaces in the atmosphere are not compatible with the light requirements. Underground heating is not efficient to maintain adequat aerial temperature. In this paper, we present an original device of heating by plastic exchanger on the soil as it has been applied with success to several horticultural crops at the Nuclear Center of Grenoble. Tepid water at a range of temperature from 12 to 40°C is distributed at low pressure in flat flexible polyvinyl chloride or polyethylene sleeves lying between the plant rows. For high density crops as chrysanthemum or salads, each plant is growing in an eyelethole fitted up for this purpose. The plastic sleeve is then looking like a flat pillow.

This economical device has a favorable effect on both growing and yield. The air temperature is not needed so high and the root activity is enhanced by the soil warming under the plastic covering. Soil evaporation is limited and weeds are controlled. Neither the soil structure is damaged, nor pests are increasing in a significant way compared with a conventional greenhouse, after three years of operation. Besides, excess heat coming from sun radiations during summer is absorbed by circulating water and stored in a reservoir for night compensation.

The following crops had been tested : lettuce, strawberry, tomato, cucumber, aubergine,Jamaïca pepper, cuttings of ornamental plants, Tokyo chrysanthemum and rose tree. Other crops are feasible. The method is now developping near thermal power plants where low grade calories are largely available. In France, about 9 ha of greenhouses using this technique are under work.

INTRODUCTION

Covered crops protected against low temperature or excessive evapotranspiration are developping rapidly. This trend is correlated to growing use of plastics in Agriculture. During last years, increasing price of energy was accompanied by considerable amounts of low grade calories, the effect of

(1)- DRF-Biologie Végétale
(2)- DTCE-Service des Transferts Thermiques

Preceding page blank

which in the environment is indesirable.

The purpose of our research is to develop a heating system able to use tepid water in greenhouses in place of hot water or warm air. Plants need no more than 25°C in their surroundings. The problem is to transfer calories from the heating fluid to the crop environment with large exchanging surfaces without reducing the light level.

To convince producers of the feasibility of heating greenhouses with tepid water, we have carried out an experimentation in Grenoble and will give some results about american *Chrysanthemum.*

1. DISTRIBUTION OF LOW GRADE CALORIES TO COVERED CROPS.

1.1. Available devices and discussion

Several ideas have been exposed or experimented for distribution of low grade calories, for instance pipes in the soil or water film dropping down on the top of the greenhouse. The first device used for open field warming of the soil is not effective enough to maintain the required temperature in the greenhouse atmosphere, the exchange between pipe, soil and air being slow.

The second one presents difficulties of technology and maintenance. It needs many cleaning of the wet surface on the greenhouse.

A basic principle was to have tepid water running through the crop rows in open ditches. This device, good for thermal exchanges is not always feasible, due to the lack of surface and a 100% humidity indoors.

1.2. Description of the plastic exchanges on the soil

The best place to regulate plant temperature is the soil surface : distribution of calories up for leaves and down for roots, eventually, absorption of excess heat from incident radiations, control of soil evaporation and no effect on lighting by lack of aerial facilities. To allow soil preparation, movable plastic sleeves are displayed on the soil just before setting young plants. Tepid water at a range of temperature from 12°C to 40°C is distributed at low pressure in this sort of pillows made from polyvinyl or polyethylene : the flat shape is maintained by eyelets, the hole of which being available to grow high density crops through them.

Fig. 1. Shape of two types of flexible plastic sleeves.

Fig. 2. General aspect of the equipped greenhouse.

This system has been previously described in a paper presented at OSLO, 1974 [1] and is asked for patent in U.S.A. under the n° 539.106.

1.3. Advantage of the system

The first aim of this original device is to valorize tepid water. But other advantages appears. One of them is the thermal "inertia" of the greenhouse as a consequence of the large amount of water circulating (12 l. per meter of sleeve) or stocked in a reservoir of about 1 m^3 for 16 m^2 under crop. In case of a lack in the tepid water supply, time is available to prevent damages. The plastic covering controls soil evaporation and weed development. It maintains a good equilibrium between root and leave activity. It is clearly demonstrated that a lower temperature above the crop is balanced by warming effect coming from the bottom.

In the french climate where the heating capacity of the system must be 160 Kcal/h/m^2, good results are obtained by covering 50 to 80% of the soil surface and using water at 30-35°C in winter. We have noted 9°C in the greenhouse atmosphere for an outdoors temperature of -11°C.

Fig. 3. Outdoors and indoors temperatures in Celsius degrees from December 27, 1976 to January 2, 1977 at Grenoble, France.

2. DESCRIPTION OF AN EXPERIMENTAL CROP USING TEPID WATER : GROWING AMERICAN CHRYSANTHEMUM.

2.1. Some aspects of this crop

Though many horticultural plants take advantage of our device, chrysanthemum is particularly demonstrating since this high density crop (64 plants per square meter) covers 3/4 of the total surface in cultivation and grows in strictly definite conditions. The flower is appreciated in all season for its beauty and its long live after picking up. The knowledge of the standard cultivation in conventional greenhouse has permitted to clearly point out the value of heating with tepid water.

We have chosen the most popular american varieties cultivated in France. See TABLE 1.

TABLE 1. Chrysanthemum varieties and number of cuttings for the 170 m^2 experience in greenhouse with heating by low grade calories.

2.2. Main facts concerning the crop

Fertilization :		
- Potassium sulphate	4 Kg/a)	Oct. 10, 1976
- Superphosphate	2 Kg/a)	" " "
Plantation of rooted cuttings		Nov. 05, 1976
Fertilization		
- Potassium nitrate	2 Kg/a)	Nov. 22, 1976
- Ammonitrate	0,6 Kg/a)	

Pesticides treatments

- Benlate	60 g/100 l.	Nov. 05, 1976
- TMTD	325 g/100 l.	" " "
- Pentac WP Quino	125 g/100 l.	Feb. 02, 1977

Dwarfing treatment with Alar 85 at 25 cm^3 of concentrated solution per liter

only for :

- CRACKERJACK	Dec. 06, 1976 Dec. 30, 1976 Janv. 31, 1977
- NICOLETTE	Dec. 06, 1976
- STARSTREAM	Dec. 06, 1976

Lighting : 2 hours in the middle of the night
from Nov. 11, 1976 to Dec. 12, 1976

First flower Feb. 15, 1977
2 weeks before scheduled with conventional greenhouse.

2.3. Favorable effect of heating at the soil surface level.

The measured temperatures as they appear on the Fig. 3 and 4 were below the recommanded ones in night time. Fig. 4 shows a higher temperature between plants than above them.

Fig. 4. Compared temperatures above plants (h = 1.5 m) and between plants.

The usual test of air temperature above the growing crop is no longer significant. In conventional greenhouse heated by the ambient air, variety such as "Tampa","Deep Tuneful" and "B.Y. Tuneful" would have no growing under 16°C. In our case, despite of a lower temperature in the air, we had a better precocity which is a good economical factor for the producer.

CONCLUSION

Heating greenhouse with tepid water near thermal power plant is no longer a problem. In France, 9 hectares of greenhouses are already under work for several types of market gardenning or flower production : lettuce, strawberry, tomato, cucumber, aubergine, Jamaïca pepper, cuttings of ornamental plants, chrysanthemum and rose tree. Other crops are feasible depending on the producer willing.

Bibliography

[1] - BALLIGAND P., GRAUBY A., FOURCY A., BOUVIER de CACHARD M., DUMONT M. Use of thermal wastes for Agriculture, Pisciculture and domeshome heating. OSLO, 26-30 Août 1974. IAEA SM 187/33.

TABLE 1

Chrysanthemum varieties and number of cuttings for the 170 m^2 experience in greenhouse with heating by low grade calories.

Variety	Number of cuttings
Galaxy	250
Yellow Galaxy	250
Crakerjack	500
Starstream	1 000
Deep tuneful	250
B.Y. tuneful	250
Dark illini Springtime	500
Golden Tokyo	500
Super White H 9	250
Super White low T°	250
Pink Winner	500
Tokyo	500
Nicolette	250
Tanja	250
	5 500

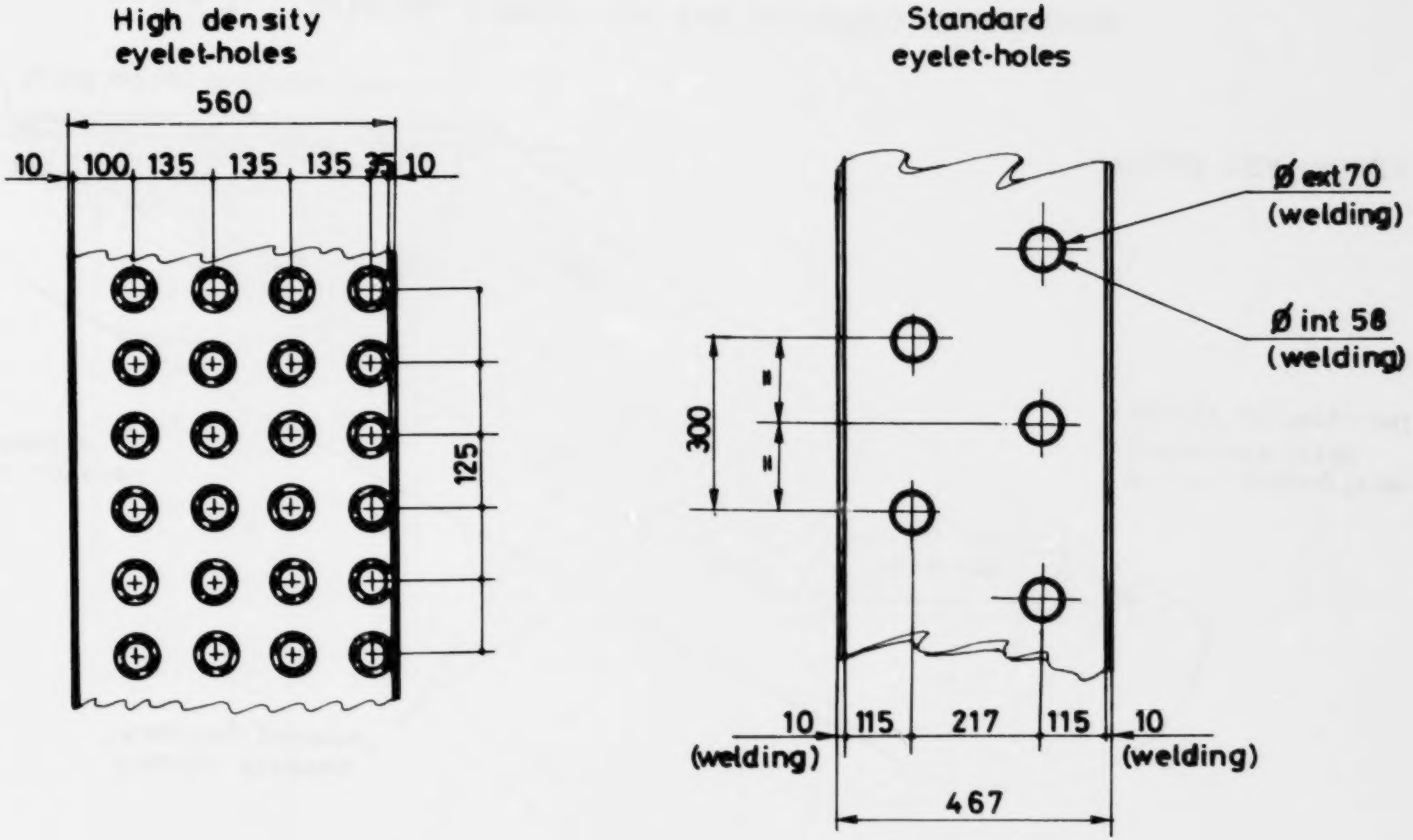
High density
eyelet-holes
560
10
100
135
135
135
35
10
125
Standard
eyelet-holes
Ø ext 70
(welding)
Ø int 58
(welding)
300
=
=
10
(welding)
115
217
115
10
(welding)
467

-Patent CEA. FRANCE-

Measurements in millimeters-

Fig.1 SHAPE OF FLAT FLEXIBLE PLASTIC SLEEVES -

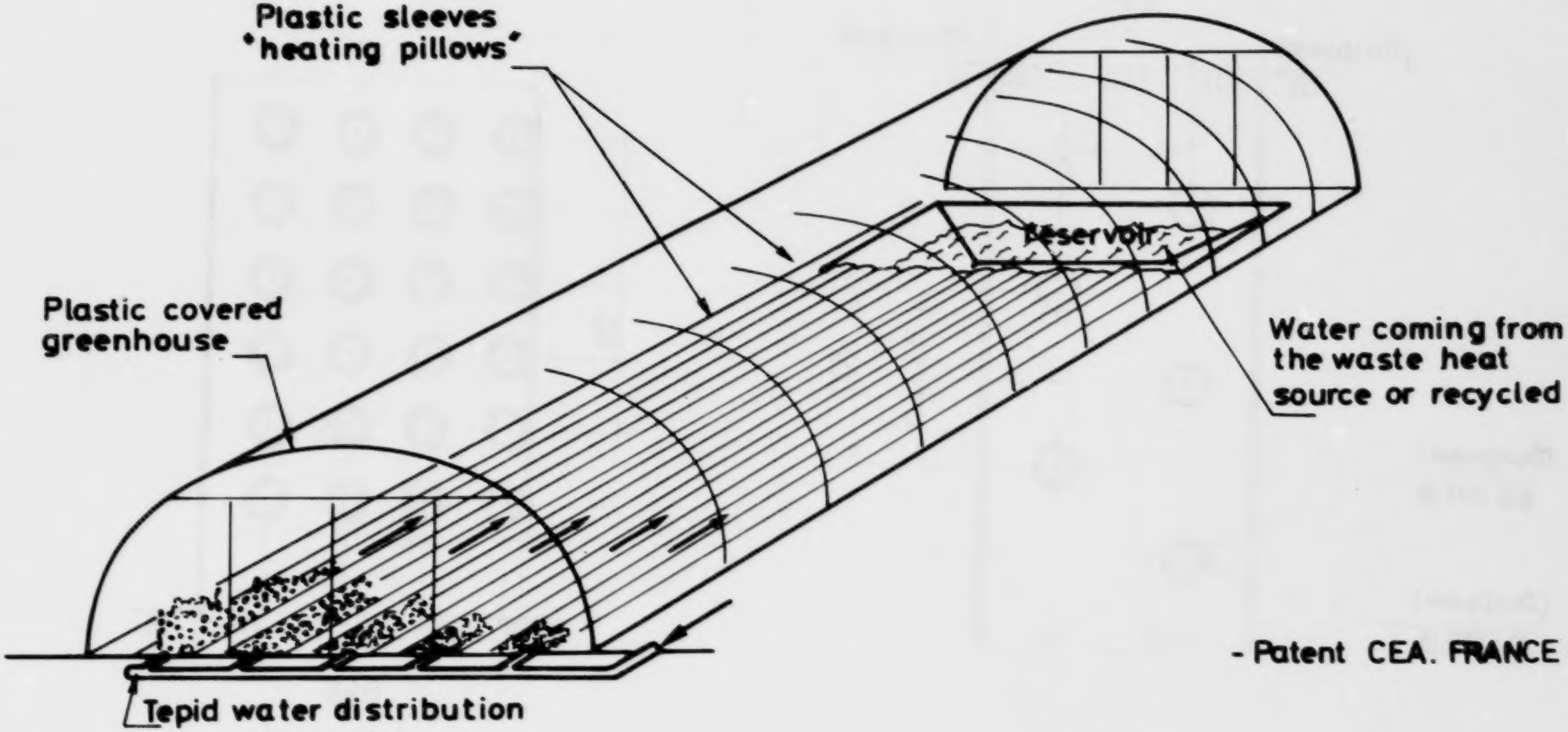
Plastic sleeves
'heating pillows'
Plastic covered
greenhouse
Reservoir
Water coming from
the waste heat
source or recycled
Tepid water distribution

- Patent CEA. FRANCE -

Fig. 2 GENERAL ASPECT OF THE EQUIPPED GREENHOUSE_

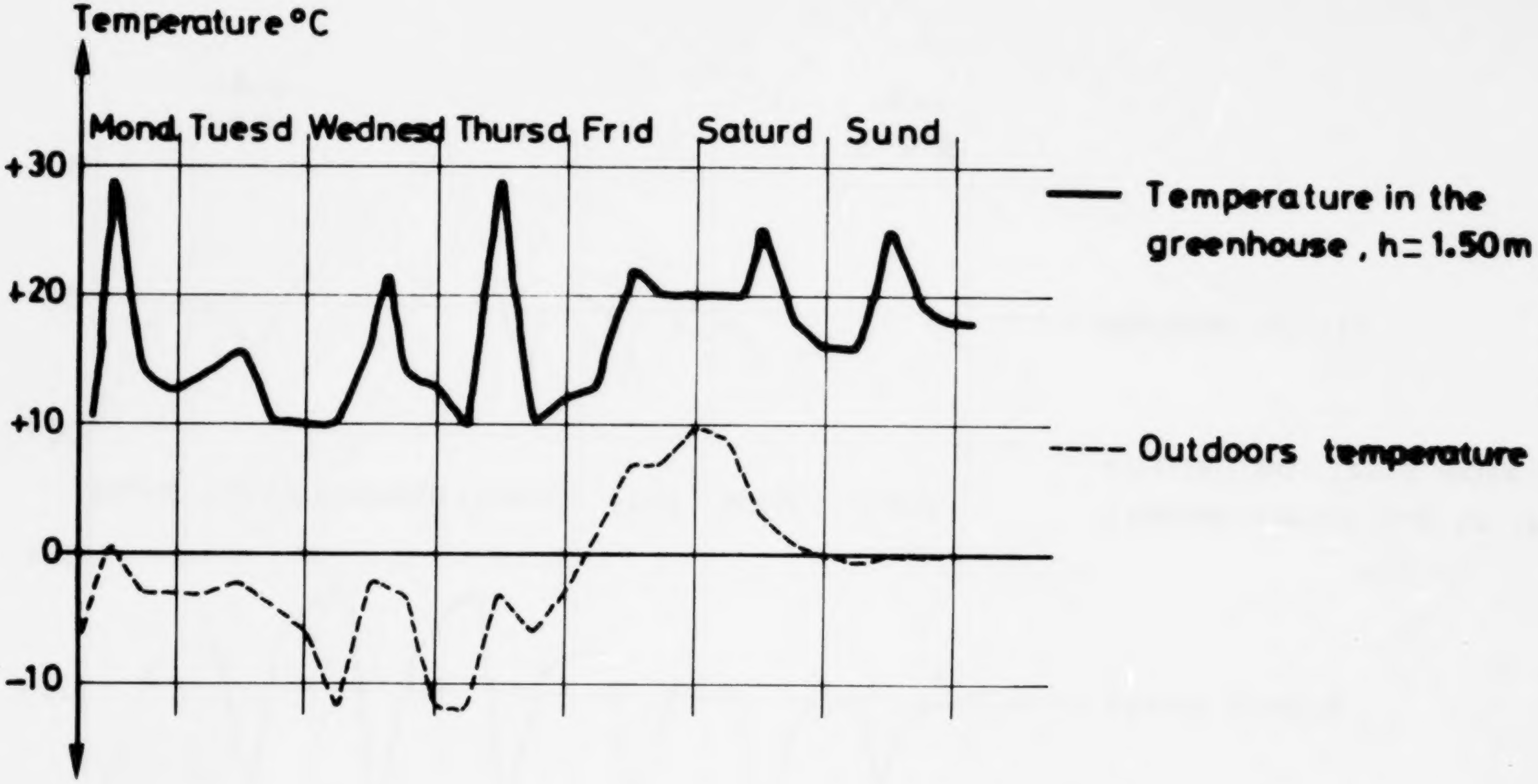

Fig. 3 INDOORS AND OUTDOORS TEMPERATURES FROM DECEMBER 27, 1976 TO JANUARY 2, 1977 AT GRENOBLE, FRANCE.

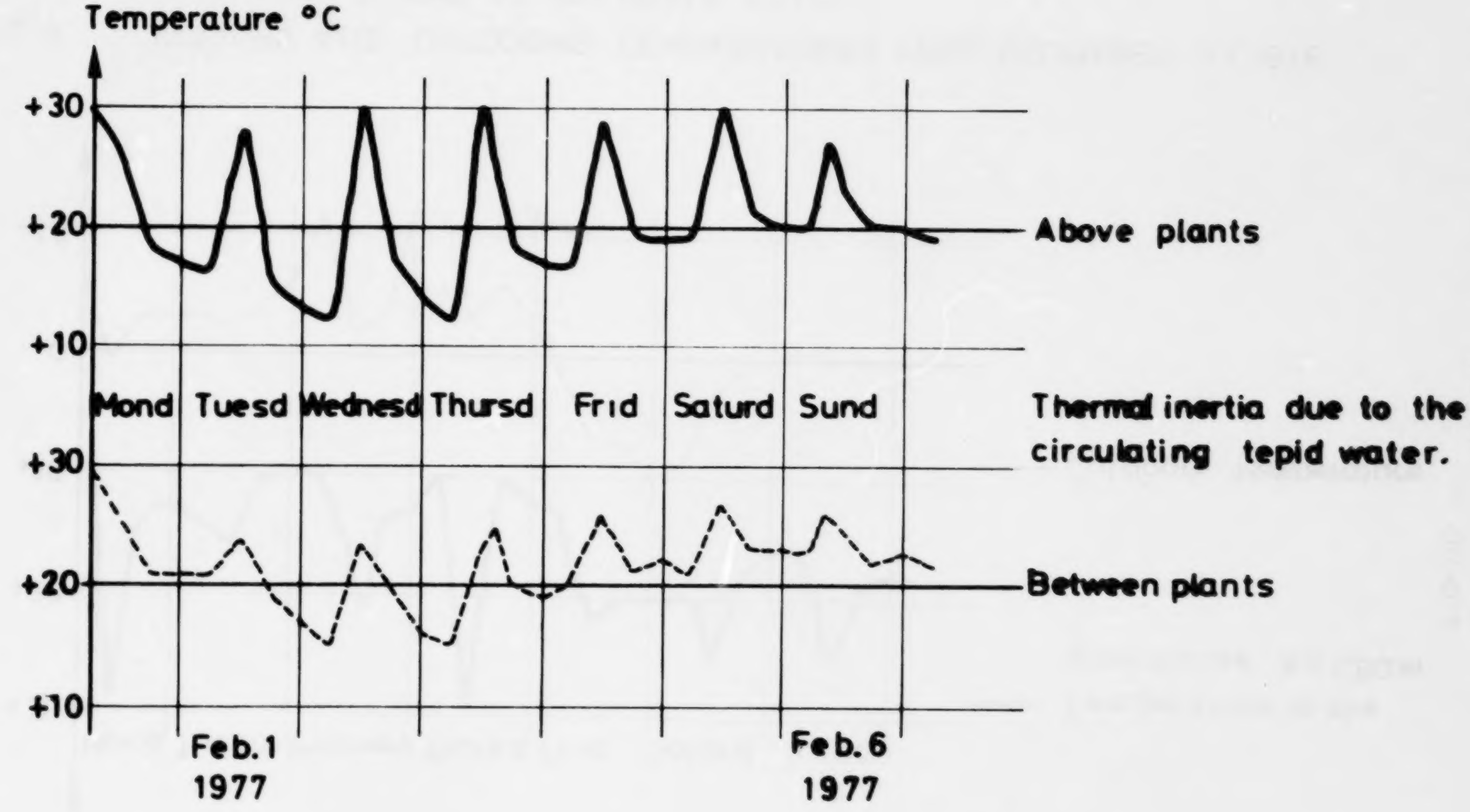

Fig. 4 COMPARED TEMPERATURES ABOVE PLANTS (h=1.50m) AND BETWEEN PLANTS_

19-45-26

WASTE HEAT USE IN A CONTROLLED ENVIRONMENT GREENHOUSE

E. R. Burns, R. S. Pile, and C. E. Madewell
Tennessee Valley Authority
Muscle Shoals, Alabama U.S.A.

ABSTRACT

The Tennessee Valley Authority has operated a pilot-scale waste heat greenhouse at Muscle Shoals, Alabama, since 1973. A conventional 7.3 x 30.5 meter glass-glazed structure has been modified to accommodate an environmental control system designed to use low-temperature warm water. The system uses a direct-contact heat exchanger surface for both heating and cooling.

The environmental control system has been evaluated over a wide range of ambient conditions, water temperatures, and water and air flow rates to establish operating parameters and capabilities associated with the waste heat system. Primary horticultural emphasis has been on the selection of adapted vegetable cultivars and on developing cropping management practices compatible with the waste heat environment.

An estimated cost comparison between the waste heat system and a conventional system indicated higher initial capital investment requirements but an overall cost advantage for the waste heat system.

INTRODUCTION

The primary objectives of the TVA waste heat utilization program are to identify potential uses of the energy contained in power plant discharge water and to develop and demonstrate technology to use this energy in efficient agricultural and aquacultural systems. The low temperature of the water as it exits power plant condensers limits its usefulness in traditional heating systems.

Approximately 50 percent of the total energy input in a coal-fired electric generating plant i[illegible] lost to the condenser cooling water as waste heat and 10 percent [illegible] lost from the stack. The remaining 40 percent of the energy input is the generated electricity. The overall efficiency of nuclear plants is less, about 35 percent for a light water reactor. Approximately 65 percent of the energy input is discharged in the condenser cooling water.

The temperature of water and quantities discharged vary with design and site characteristics. For example, the temperature of the discharge from a low temperature rise condenser is only 6° to 11° C (ΔT) above the intake water. For a once-through system with a ΔT of 8° C, about 0.038 m^3/s water is required for each megawatt (MW) of generating capacity.

For a once-through, high-temperature rise condenser, the ΔT is from 14° to 17° C and requires about 0.022 $m^3/s \cdot MW$. Condensers for systems including cooling towers have ΔT's in the order of 18° to 21° C. For a cooling tower system with a ΔT of 21° C, about 0.021 $m^3/s \cdot MW$ is required. In the TVA area, river temperatures vary from about 5° C during winter months to 29° C during the summer. Thus, condenser discharge temperatures from a once-through system with a low ΔT would vary from 10° C in cold weather to 38° C during the summer; whereas, the high ΔT condenser discharge would vary from about 18° to 46° C. Normally, both the entry and exit temperatures of water from a cooling tower system are more uniform and more desirable for beneficial uses.

Waste heat utilization technology in economical production systems must be developed and demonstrated before significant use of waste heat resources can be realized. Guidelines need to be established for interfacing these systems with power plants. A number of projects are underway by TVA to develop technologies to utilize waste heat. This report focuses on a system developed to control greenhouse environments. System components were tested, crop production was evaluated, and a cost comparison of the waste heat system with a conventional system was made.

DESCRIPTION OF FACILITY

The interior of a 7.3- x 30.5-meter aluminum-framed, glass-glazed greenhouse was modified to accommodate a waste heat environmental control system for pilot studies. Modifications of the greenhouse (figure 1) included installation of the following: (1) a bank of evaporative pads and associated water distribution system, (2) a fin-tube heat exchanger, (3) a fiberglass attic forming a recirculation plenum, (4) motorized shutters to allow recirculation or once-through air flow, (5) attic vent fans, (6) a temperature control and instrumentation system, and (7) a water boiler to provide simulated power plant cooling water.

Due to the low wintertime temperatures of cooling water from open mode power plants and low efficiencies of conventional heat exchangers with this temperature water, a direct-contact evaporative pad system was developed and evaluated as the primary heat exchanger.

Two evaporative pad materials, aspen pads and CELdek[1] have been evaluated as direct-contact heat exchangers. An aspen pad bank 7.3 m wide by 2.4 m high and approximately 5 cm thick was initially used as the heat exchange surface. Results of experiments reported by Furlong [1] indicated superior performance of CELdek over aspen pads in a bimodal heating and cooling application. In June the aspen pads were replaced with the CELdek pad 7.3 m wide, 1.2 m deep, and 30.5 cm thick.

---

1. A cellulose paper impregnated with antirot salts, rigidifying saturants, and wetting agents formed in a cross-fluted arrangement with 403 m^2 of surface area per m^3. Manufactured by the Munters Corporation, Fort Myers, Florida.

The water for heating or cooling was distributed to the pad through a perforated 5 cm diameter PVC pipe discharging upward into an impingement cover made with half of a 15 cm diameter PVC pipe. After passing through the pad, the water was collected in a sump for recirculation through the water boiler or direct return to the pad system. Heating was accomplished by recirculating saturated or nearly saturated air through the evaporative pad over which warm water was flowing. The evaporative pad was also used for cooling, using either warm water at low flow rates or nonheated recirculated water.

A 6.1- by 2.1-m copper-tubed, aluminum-finned dry heat exchanger with an extended surface area of 409 m^2 and an overall heat transmission coefficient of 12.37 $W/m^2 \cdot °C$ at design conditions was located downstream of the evaporative pad. The fin-tube heater could be used to supply some dry heat to lower the relative humidity in the growing area. The evaporative pad and fin-tube could be operated either in parallel or in series.

A 180-kW electric water boiler was used to simulate power plant cooling water for the system. Water temperature was set at the expected average monthly temperature for the Browns Ferry Nuclear Plant and varied from about 21° C in January to 43° C in August.

Growing area temperature was controlled by the amount of air recirculated through the house. The possible air flow modes were (1) once-through, (2) 25-percent, (3) 50-percent, (4) 75-percent, and (5) 100-percent recirculation. Two fan speeds were also available. Control was achieved by individually opening or closing each of four banks of louvers on the inlet, outlet, and recirculation flow paths. The louvers were opened with relay-actuated motors and closed with springs. Five thermistors in the greenhouse supplied temperature signals for the control system.

Two 1.1-kW, 2-speed exhaust fans were used for air movement within the greenhouse. Rated air flow rates for the fans were 8.5 m^3/s with fans at low speed and 17.0 m^3/s at high speeds. The fans were located in a recessed area at the rear of the structure to exhaust air when cooling or direct flows upward into the attic plenum to be recirculated when heating. Two thermostat-controlled attic vent fans were used to prevent excessive temperatures in the attic during periods of high solar radiation and no air recirculation.

Instrumentation for the greenhouse consisted of detectors for water flows, water and air temperatures, and humidity, plus appropriate readout and recording equipment. Orifices were used to measure total, pad, and fin-tube water flows. Circular 24-hour charts were used for recording various flows. A visual indication of makeup flow was obtained from a small rotameter with a range of 1.9 to 22.7 l/min.

Visual indicators on the control panel indicated fan speed and louver position, which were also recorded on a strip chart. The TVA weather station at Muscle Shoals provided hourly summaries of wind speed and direction, dry bulb and dew point temperatures, barometric pressure, and solar and total radiant flux.

ENVIRONMENTAL CONTROL SYSTEM EVALUATIONS

Environmental control system components were evaluated in terms of their capabilities and operating parameters during both heating and cooling modes of operation. Results of engineering tests with the CELdek pad system are summarized in this paper. More complete descriptions of specific tests and results are included in progress reports on the waste heat greenhouse project [2, 3].

Air Flow Rates

Air flow rates within the greenhouse were measured with an Alnor velometer, Type 3002, No. 14335, at the exit of the evaporative pad material. The pad exit area of 8.6 m^2 was divided into 18 sections of equal area, and air flow rates were measured at each section for all possible combinations of fan speeds and shutter positions. The average air flow rates measured are shown in figure 2. With the air flow system operating with no recirculation, the measured air flow rate was 85 percent of the rated fan capacity at high speed and 98 percent with fans on low speed. Volume air change rate was 1.7 times per minute with full fan speed and full ventilation and 1.0 time per minute with slow fan speed and full ventilation.

Heating System Performance

The primary function of the environmental control system during the heating mode was to maintain the growing area temperature within the acceptable range for crop production with water temperatures corresponding to the predicted monthly average open mode condenser cooling water temperatures at the Browns Ferry Nuclear Plant.

Operating parameters were varied in both attended and unattended experiments. Seasonal condenser cooling water temperatures are essentially fixed for a given power plant, but simulated discharge temperatures in these tests were varied to better characterize system performance. During unattended tests, conditions were preset and data were recorded continuously.

During attended experiments, the greenhouse was allowed to stabilize under a given set of conditons. This usually required from 15 minutes to 1 hour.

The CELdek heating system was evaluated at water flow rates of 12.4 and 18.6 l/min per meter of pad width with water temperatures ranging from about 20° to 32° C. An attempt was made to conduct these tests under similar ambient conditions, and all heating data discussed were collected at night to eliminate the effect of solar radiation. Ambient temperature averaged -1° C and varied from +4° to -6° C. The capacity of the water boiler limited the warm water temperatures and flow rates evaluated.

The lowest water flow supplied enough heat to maintain an acceptable growing area temperature (14° C) using 20° C water and full air recirculation. Less air recirculation was required to maintain acceptable growing area temperatures using higher water temperatures and flow rates.

The lowest ambient temperature encountered during attended tests was -6° C. The pad water flow rate was 18 l/min·m. Greenhouse night temperatures were maintained at 16.7° and 18.9° C with respective water temperatures of 19.4° and 22.2° C.

The amount of energy transferred in the CELdek heating system was difficult to quantify. Both heat and mass transfer occurred from the warm water to the air, and temperature stratification occurring downstream of the evaporative pad made reliable air temperature measurement difficult. An effort was made to quantify the change in energy of the greenhouse air at various pad water temperatures as it passed through the evaporative pad system. The pad flow rate was maintained at 18.6 l/min·m, and the results are shown in figure 3. Energy transferred ranged from 105 kW with 20.0° C water to 172 kW with 29.7° C water. These results were obtained with ambient temperatures of -5.6° to +3.9° C with fans operating on high speed resulting in 100-percent air recirculation.

The effect of mass transfer is included in the upper line shown in figure 3. A significant relationship between the total amount of energy transferred to the air and the water temperature was found. The relative humidity within the greenhouse remained at saturation during all tests with 100-percent recirculation and with no solar radiation or fin-tube flow. Under these conditions, air heating is accomplished along the saturation line. Using a psychromatic chart, effects of heat and mass transfer were separated and the sensible heat transfer for the water flow rate of 18.6 l/min·m at various water temperatures was plotted (lower line in figure 3). After separating the effects of mass transfer, the heat transferred in the pad system exhibited less dependence on water temperature, and the correlation between the heat energy transferred and the water temperature used was not significant. However, mass transfer does have an effect on the greenhouse environment due to the energy released as condensation occurs throughout the greenhouse as saturated air is cooled.

The effect of air flow rates on greenhouse heating at various water flow rates and temperatures was determined. At pad water flow rates of 18.6 l/min·m or greater, water temperature $\geq$21° C, and with the air recirculation system on automatic operation, acceptable temperatures were maintained with fans either on slow speed or full speed. However, temperatures were more uniform with fans on full speed during periods of high heat loss and low water temperatures, indicating that the higher air flow rates would be desirable during these periods.

Experiments were conducted to determine the performance of the fin-tube heater using the lower temperature water and three water flow rates (30.3, 36.3, and 68.1 l/min). The tests were made at night with fans operating at slow speed. A sufficient pad water flow rate was maintained to ensure that the air leaving the evaporative pad and entering the fin-tube heater was saturated.

During nighttime operation, with 100-percent air recirculation and without the fin-tube heater in operation, the greenhouse air was saturated throughout the growing area; and during periods of low ambient conditions, the growing area was noticeably foggy. The lowest fin-tube water flow rate (30.3 l/min) and the lowest water temperature (21.7° C) evaluated provided sufficient dry heat to alleviate the foggy conditions.

A hand-held motorized psychrometer was used to measure relative humidity downstream of the fin-tube heater for the 36.3 and 68.1 l/min flow rates. Average nighttime relative humidity was reduced from saturation to 97 percent and 92 percent, respectively, using 21.7° and 27.2° C water at 36.3 l/min and 93 percent and 90 percent at 68.1 l/min.

Greenhouse temperatures and relative humidities during a typical 4-day heating period in December 1975 are shown in figure 4. Both low and high solar radiation were experienced during periods of low ambient temperatures. Temperatures and relative humidities shown are representative of greenhouse conditions during the heating mode. The evaporative pad flow rate was 170 l/min, fin-tube heater flow rate was 56 l/min, and the water temperature fluctuated from 21° to 24° C.

Cooling Evaluations - Warm Water

The cooling performance of the evaporative system was evaluated using warm water at the predicted summer temperatures for the Browns Ferry power plant discharge water. Cooling effectiveness was measured during August 1976 on clear days with the exhaust fans operating on high speed and with no air recirculation within the greenhouse. Pad flow rates of 6.2, 12.4, and 18.6 l/min·m were characterized with water temperatures ranging from ambient wet bulb temperatures to approximately 35° C. For each run set conditions were established, and the greenhouse operated for 30 minutes before temperature and relative humidity measurements were taken. Four portable Taylor hygrometers and a portable motorized psychrometer were used to measure air temperatures and relative humidities.

Water temperatures evaluated were again limited by the output of the boiler providing the warm water. Ambient temperature, solar radiation, and wet bulb depression were different for each run; but an attempt was made to conduct the experiment on days with similar ambient conditions, and trends shown should be valid.

Ambient conditions, greenhouse temperatures, and cooling efficiencies achieved are shown in table 1. The cooling effect, measured as the decrease in air temperature divided by the ambient wet bulb depression, is expressed in percent. As could be expected, the cooling effect decreased as water temperature and flow rate increased. The poorest cooling performance measured, 58 percent, occurred at a water flow rate of 12.4 l/min·m with 32.3° C water; but the entering air immediately downstream of the pads was cooled to an average temperature of 23.3° C, while the average greenhouse temperature was 25.3° C, an acceptable temperature for plant growth. For all flow rates and water temperatures evaluated, the water exiting the pad was cooled to near the ambient wet bulb temperature.

Cooling Evaluations - Recirculated Water

If cooling the power plant discharge water during the summer months were not one of the objectives of the greenhouse, more efficient greenhouse cooling could be obtained by recirculating water over the evaporative pads in a closed system. The cooling process then becomes one of adiabatic saturation; that is, the temperature of the recirculated water approaches the wet bulb temperature of the incoming air, and the water is not cooled further. Evaporation occurs as unsaturated air is pulled across the pad. Energy from the incoming air supplies the latent heat of vaporization for the water that is evaporated, and the dry bulb temperature is lowered corresponding to the amount of heat expended in this evaporation.

Cooling efficiencies were determined for various water flow rates over a range of ambient conditions. In all cases, water flow rate was set and the greenhouse operated for several days. Data were collected on clear days when the ambient conditions dictated high fan speed and once-through air flow. The greenhouse control day temperature set point was 26.7° C for all experiments in an attempt to maintain optimum growing temperatures for cucumbers.

Data were analyzed and efficiencies determined during periods when the solar load was greater than 473 W/m^2, and the incoming wet bulb depression varied from 2.2° to 8.9° C. The cooling efficiencies measured at flow rates of 12.4, 18.6, 22.4, 26.1, and 29.8 l/min·m and corresponding ambient wet bulb depressions are shown in table 2. All wet and dry bulb temperatures used in calculating efficiencies were averages for one hour. Numbers in parentheses indicate the number of measurements obtained at the indicated ambient wet bulb depression and flow rates.

Regression analyses indicated a significant relationship between the cooling effect and the ambient wet bulb depression, both for each flow rate and for all flow rates combined. Regression equations for the different flow rates were not significantly different.

The average cooling efficiency for all conditions tested was 86.1 percent, which was adequate to maintain acceptable greenhouse temperatures. The lowest water flow rate evaluated, 12.4 l/min·m, was sufficient to keep the pad surface visibly wetted.

Following manufacturer recommendations, the cooling efficiency should have been approximately 91 percent at a water flow rate of 18.6 l/min·m with the high fan speed air velocity of 1.7 m/s through the evaporative pad material.

The effect of fan speed on the amount of cooling in the pad system and on the increase in air temperature through the greenhouse was also determined. Greenhouse temperatures were measured with recirculated pad water flow rates of 12.4, 18.6, and 24.8 l/min·m with the two different fan speeds available. Ambient conditions were similar for each run. The average cooling efficiency in the evaporative pad for all water flow rates was 74.0 percent with slow fan speed and 81.7 percent with full fan speed. As the air passed through the greenhouse, an average temperature increase of 4.2° C was measured for the slow fan speed and 3.3° C for full fan speed. The lower cooling efficiency and the greater increase in temperature through the greenhouse associated with the slow fan speed resulted in an average exit temperature 0.2° C higher than ambient conditions. With maximum fan speed, the exiting greenhouse air temperature was an average of 2.3° C lower than ambient temperature.

Figure 5 depicts greenhouse temperatures and relative humidities during a typical 6-day cooling period in July 1975 and illustrates typical conditions at various locations within the greenhouse during cooling with recirculated water and high solar loads. Data were collected immediately downstream of the evaporative pad ("N") and at the exit of the growing area ("S"). The fin-tube heater was not used during this period, and air flow rates were dictated by the control system.

HORTICULTURAL EVALUATIONS

Experiments were designed to study growth responses, measure yields, and identify and solve problems associated with production of tomatoes and cucumbers in the humid waste heat greenhouse environment.

Procedure

The experimental growing area consisted of six troughs constructed on a 1/2-percent slope from 1.9-cm plywood and lined with 6-mil polyethylene. Three troughs on the west side of the greenhouse were 0.6 by 18.3 m, and those on the east side 0.6 by 21.3 m. Aisles between troughs were 0.5 m wide except for the center aisle, which was 1.2 m to accommodate personnel, equipment, and visitors. Bottoms of the troughs were lined with 5 cm of pea gravel, and a slotted 3.8-cm diameter PVC pipe was placed in the center of the troughs lengthwise to ensure proper drainage of excess water and nutrient solution. Twenty cm of washed river sand was placed on top of the pea gravel for the growing medium. Nutrient solution was distributed via twin-wall irrigation tubing. The sand culture system and nutrient solutions used were based on systems described by Jensen [4, 5, 6], which have been used successfully in Arizona and other areas.

Cucumber Trials--Two cucumber crops were grown from February 3, 1975, to August 21, 1975. The Femfrance cultivar was selected. Two-week-old seedlings for the spring crop were transplanted into the sand beds on February 2, 1975, at a density of 0.67 m^2/plant, equal to about 14,800 plants/ha. This crop was terminated April 28, 1975. The summer crop was transplanted June 10, 1975, and terminated August 21. Cucumbers were pruned and trained according to the procedure reported by Bauerle [7].

Cucumber production was measured in five sections of the greenhouse to determine the degree of uniformity of production throughout the growing area. The control system was preset to maintain temperatures between 18° and 21° C at night and 27° to 30° C during the day using water at the predicted monthly discharge temperatures from Browns Ferry Nuclear Plant for heating. Tap water was used for cooling during the summer crop. Temperature and realtive humidity measurements were made at 0.5, 1.4, and 2.3 m elevations in the five sections.

Tomato Trials--Following the 1975 summer cucumber experiments, tomato trials were initiated. After cucumber plants were removed, sand beds were fumigated with Vapam at the rate of one liter/9.3 m^2. The environmental control system was preset to maintain the following established temperature conditions for optimum tomato production:

Light Conditions	Temperature (°C)
Bright days	24-26
Medium bright days	22-23
Dull days	20-22
Nights following bright or dull days	15-17
Nights following prolonged periods of dull days	14-16

The Tropic cultivar, which had performed best in previous tests in the waste heat environment [2], was selected for the fall 1975 crop. Four-week-old plants were transplanted into the growing area on September 8. Plants were set 61 cm apart in two rows 30 cm apart in each trough. This spacing gave approximately 0.36 m^2 of growing area per plant, equivalent to 27,400 plants per hectare.

Nutrient solution was applied once per day for the first week after transplanting and twice per day the next three days. The control system was then set to automatically irrigate with nutrient solution for five minutes three times per day, at 8 a.m., 12 noon, and 4 p.m. Chapin twin-wall irrigation tubing was used to distribute the nutrient solution. Tomato plants were tied, pruned, and pollinated according to recommended procedures [8].

Beginning the second week after transplanting, chlorthalonil (Bravo, Termil) was used at 7- to 14-day intervals to control diseases. Cultural practices to aid in disease control consisted of removing lower tomato leaves from the plants as the clusters matured to allow better air drainage throughout the greenhouse. Insecticides were applied as insect problems developed. The insecticide used was determined by the specific insect problem.

Insect	Insecticides Used
Spider mites	dimethoate (Cygon, Defend)
Aphids	malathion, diazinon, or Cygon
Whiteflies	Cygon, methomyl (Lannate, Nudrin), Vapona

The fin-tube heater was used when prolonged periods of cold, cloudy weather occurred to reduce relative humidity for effective pollination and to assist in disease control programs.

Temperature and relative humidity were recorded automatically at various locations in the greenhouse. Harvest operations were begun November 10 and continued until December 22.

Studies with tomatoes were continued in the spring of 1976 to evaluate tomato cultivars, planting densities, and cropping systems in an attempt to identify a system of tomato production compatible with the waste heat environment. These studies were conducted without using the fin-tube heater to determine if tomatoes could be produced in a humid waste heat greenhouse without the use of humidity reduction equipment.

Disease control was attempted by staying on a rigid fungicide spray schedule. Preventive applications of Bravo and benomyl (Benlate) were made at weekly intervals. Plants were monitored for disease symptoms during each pollination and pruning operation. As the incidence of disease increased, additional fungicide applications were made and plant foliage removed to improve air circulation. Insecticides listed previously were applied as needed to control insects.

The Tropic and Floradel tomato varieties were evaluated at two planting densities. Plants were set in rows 30 cm apart in troughs and spaced 46 or 61 cm apart within rows to give 0.36 and 0.26 m^2 per plant, respectively. This is equivalent to plant populations of 27,400 and 38,300 plants per hectare. Each plot was 1.5 m long and contained five and seven plants, respectively, for the two planting densities. Treatments were arranged in a randomized complete block design and replicated six times.

Another study was conducted to determine if removing the top portion of the tomato plants after the third cluster set fruit would allow high density planting and multiple cropping to increase annual production per square meter of greenhouse space. In this study, Tropic and Floradel were grown at 30.5- (0.18 m^2/plant) and 45.7-cm (0.26 m^2/plant) spacings within rows. Also included in the study were two semideterminate varieties--Homestead 24 and Bonnies NWR--at the 45.7-cm spacing. Two crops with these treatments were grown during the period January 23 to August 10, 1976. Yields were compared with those obtained from a conventional planting of Floradel and Tropic at the 45.7-cm spacing. These treatments were arranged in a randomized complete block design and replicated three times.

Five-week-old plants for these studies were transplanted on January 23, 1976. The plants for the second crop in the topping experiments were transplanted May 10. Tomato harvest was begun on April 7 and completed in all except the topping experiments July 23. The harvest period for the first crop in the topping experiments extended from April 7 to May 4. The second crop was harvested from July 12 to August 10.

Results and Discussion

Cucumber Trials--Some variation occurred in production of cucumbers in the test sections of the greenhouse with yields from the spring crop ranging from 6.5 to 7.4 kg/plant. Yields from the summer crop ranged from 5.3 kg to 6.2 kg/plant. Average yield from the two crops was 6.9 and 6.3 kg/plant, respectively. At the planting density of 14,800 plants/ha, these yields are equivalent to 102.1 and 93.2 tonnes per hectare.

The environmental control system using simulated power plant discharge water during the winter and spring and tap water in the summer kept the average greenhouse temperatures within the acceptable range for cucumber production. Horizontal temperature variations of 1.7° to 3.3° C occurred in the five sections monitored, and vertical differences from 1.1° to 2.8° C occurred in each section.

Daytime humidity measurements varied considerably among sections at all three elevations (68 to 98 percent), especially during periods of low sunshine as frequently occurred during this crop. However, from these limited data and observations during production, no correlation could be made between humidity levels in various sections with plant diseases and crop yields. These observations on European cucumbers confirm earlier results, showing them to be well adapted to the waste heat greenhouse environment.

Tomato Trials--During the fall and winter of 1975, the environmental control system utilizing simulated condenser cooling water maintained greenhouse temperatures within the optimum range for greenhouse tomato production throughout the growing period from mid-September to late December. The coldest ambient temperature (-10° C) during this crop occurred on December 19. Greenhouse temperatures at the monitoring stations ranged from 17° to 20° C. These temperature levels were achieved using warm water at 25° C at a flow rate of 170 l/min over the pad and 57 l/min through the fin-tube heat exchanger.

There was little variation in yield of tomatoes in different sections in the greenhouse. On the west side, yields ranged from 2.8 to 3.0 kg/plant and on the east side 2.8 to 3.1 kg/plant. The average yield per plant over the entire greenhouse was about 3.0 kg/plant.

A high incidence of plant disease occurred during the fall crop. Botrytis (Botrytis cinerea) outbreaks coincided with prolonged periods of low solar radiation. Weekly applications of Bravo-6F fungicide, removal of lower tomato leaves to improve air circulation, and the use of the fin-tube heater to lower humidity succeeded in bringing the disease under control.

The system continued to maintain optimum temperature levels for tomatoes during the winter, spring, and summer of 1976. Yield and size of tomatoes from the experiment evaluating planting density and cultivars are shown in table 3. There was no statistical difference in the yield of Floradel and Tropic cultivars among planting densities. There was a significant difference between the two densities. The low plant population averaged almost 8.6 kg of marketable fruit per plant as compared with 6.7 kg at the higher density. However, yield per unit area of greenhouse space was greater at the higher density planting, almost 257 t/ha as compared with 236 t/ha at the lower density. There was no significant reduction in size of marketable fruit by increasing the planting density. The Tropic cultivar produced larger No. 1 fruit than Floradel, averaging almost 226 g as compared with 183 g.

There were no production problems identified that were related to the high planting density. At both densities, vegetation lapped in the narrow aisles by the time of the first harvest. This complicated operations such as pollinating, pruning, spraying, and harvesting. Wider row spacings would have made these tasks easier and also would probably have improved air circulation. These preliminary results indicate that high density planting of tomatoes in the waste heat environment may be possible to increase annual production, but sufficient space is needed between rows to accommodate personnel for routine chores.

Results of the topping experiment are shown in table 4. Tropic and Floradel produced higher yields than the semideterminate varieties (Bonnies NWR and Homestead 24). Most plants of the semideterminate varieties had self-topped at the time Tropic and Floradel were topped, and many plants had four to five clusters. Floradel and Tropic plants topped after the third cluster produced fewer tomatoes per plant, but more tomatoes per hectare when grown at the high density planting (54,800 plants/hectare), indicating that high density planting of topped plants may be practical. However, the two crops of topped plants did not produce as many tomatoes as a single crop of the same varieties grown from January 22 to July 16, 1976, in an adjacent growing area.

Normally, yield and quality are better from the lower clusters of greenhouse-grown tomatoes. The effect of topping generally causes an increase in size of fruit. However, in this study, fruit-set on upper clusters was very good and quality was excellent; therefore, the advantages from topping were not as evident. Less labor for pruning, tying, and spraying was required by the topped plants. This offset the extra transplanting labor and expense of growing and setting new plants. The primary advantage of the topped plants was that disease control was less difficult. The shorter plants were easier to cover with fungicide sprays and allowed better air circulation. The main disadvantage of a topping system is the long period of vegetative growth required for each crop for such a short harvest period. Such a system might have potential in a waste heat environment if plantings in a commercial facility could be staggered so that a constant supply of fruit could be made available to a market or timed so the harvest periods would coincide with high demand periods.

Experiments conducted in the waste heat greenhouse during the spring of 1976 showed that under the conditions experienced, good yields of tomatoes may be produced in the humid waste heat environment without using a fin-tube heater or other equipment to reduce the relative humidity, provided special attention is given to disease prevention and control. Preventive fungicide applications were made on a weekly basis, and plants were closely monitored for symptoms of disease outbreak. During prolonged periods of low solar radiation, botrytis outbreaks occurred even though weekly spray applications of Bravo were being made. The most severe outbreak during the spring crop occurred during early May. The disease caused a yield reduction because a number of young fruit aborted. The disease outbreak was arrested by increasing the frequency of fungicide application to once every five days for three applications and using a combination of Bravo and Benlate. In addition, lower leaves and excess plant foliage were removed to improve air circulation.

Although good yields were achieved without humidity reduction equipment, additional studies are being conducted to determine if disease control can be achieved under more adverse ambient conditions.

COST ADVANTAGE OF THE WASTE HEAT SYSTEM

A 1974 survey of the vegetable greenhouse industry in the seven Valley States [9] indicated that the industry was growing. At that time, there were 561 growers operating 1,492 houses. Since 1974, the rate of expansion of the greenhouse industry has decreased. One of the major problems facing the future development of the Valley greenhouse industry is high heating cost. The waste heat greenhouse system appears to offer an opportunity to help reduce cost. A comparison between the initial capital cost requirements for components of a waste heat system and a conventional system is shown in table 5. The comparison was made assuming that the power plant discharge water is made available at the greenhouse site.

For a 223 m^2 greenhouse, the initial capital investment would be about \$6,388 higher for the waste heat system. Much of this extra cost is associated with the recirculation attic, exhaust fans, and shutter system. Changes to reduce cost, such as eliminating the attic and recirculating air through an adjacent parallel greenhouse, are planned for a commercial-scale greenhouse to be constructed at the Browns Ferry Nuclear Plant.

Table 6 indicates the annual cost advantage for the waste heat greenhouse system. The importance of the cost of fuel for the conventional house is evident. Assuming that marketable crop yields and quality are not significantly different between the two systems, there is an annual cost advantage of $980. In addition, traditional fossil fuels are conserved. Projecting these savings to a hectare-size house shows an estimated waste heat system annual cost advantage of about $44,000 and conservation of over 823 m^3 of fuel even after adjustment is made for the extra electricity used by the waste heat system.

CONCLUSIONS

Results from these studies show that the environmental control system using simulated power plant discharge water can maintain adequate greenhouse temperatures for tomato and cucumber production. Components of the environmental control system, including CELdek as a direct contact heat exchange surface, performed adequately.

The high relative humidities associated with the system required special attention to plant disease. Effective disease control required a rigid fungicide spray program, good sanitation, and cultural practices to improve air circulation. Good production of tomatoes was achieved without the use of the fin-tube heater to reduce relative humidity levels during the spring of 1976. However, additional studies are needed over a wide range of ambient weather conditions before a conclusion is made regarding the necessity of the dry heat exchanger.

The cost comparison between the environmental control system of the waste heat greenhouse and a conventional system showed that although the initial capital investment requirements for the waste heat system were higher there was an overall annual cost advantage. Future advantages are anticipated to be even greater as fuel costs continue to rise.

REFERENCES

1. Furlong, W. K. *Physical Characterization of CELdek Material in a Simulated Greenhouse Environment*. Oak Ridge National Laboratory, Oak Ridge, Tennessee, ORNL-TM-4815, October 1975.

2. Madewell, C. E., et al. *Using Power Plant Discharge Water in Greenhouse Vegetable Production*. TVA progress report, Bulletin Z-56, January 1975.

3. Burns, Earl R., Robert S. Pile Carl E. Madewell, John B. Martin, and Johnny Carter. *Using Power Plant Discharge Water in Controlled Environment Greenhouses*. TVA progress report II, Bulletin Z-71, December 1976.

4. Jensen, M. H. "The Use of Waste Heat in Agriculture," *Waste Heat Utilization Proceedings of the National Conference*, October 27-29, 1971, Gatlinburg, Tennessee. Distributed by the National Technical Information Service, USDC, Springfield, Virginia, CONF-711031, May 1972.

5. Jensen, M. H. "Arizona Research in Controlled Environment Agriculture," *Tennessee Valley Greenhouse Vegetable Workshop* proceedings, Muscle Shoals: Tennessee Valley Authority, Bulletin Y-94, June 1975.

6. Jensen, M. H., and H. M. Eisa. *Controlled-Environment Vegetable Production: Results of Trials at Puerto Penasco, Mexico, 1968-1970*. Environmental Research Laboratory, University of Arizona, Tucson, Arizona, 1972.

7. Bauerle, William L. "Cultural Requirements for Lettuce and Cucumbers," *Tennessee Valley Greenhouse Vegetable Workshop* proceedings, Muscle Shoals: Tennessee Valley Authority, Bulletin Y-94, June 1975.

8. Brooks, William M. *Growing Greenhouse Tomatoes in Ohio*. Ohio State University, Cooperative Extension Service, Bulletin SB-19, November 1973.

9. Davis, A. C., and J. B. Martin, Jr. "Greenhouse Research and Education Situation in Tennessee Valley States," *Tennessee Valley Greenhouse Vegetable Workshop* proceedings, Muscle Shoals: Tennessee Valley Authority, Bulletin Y-94, June 1975.

TABLE 1

AMBIENT CONDITIONS, GREENHOUSE TEMPERATURES, AND COOLING EFFICIENCIES DURING SUMMER COOLING TESTS WITH WARMED WATER USING FULL FAN SPEED AND ONCE-THROUGH COOLING TVA WASTE HEAT GREENHOUSE, MUSCLE SHOALS, ALABAMA, 1976

Run	Pad Flow (1/min·m)	Water Temp. (°C)		Ambient		Greenhouse Temperatures (°C)[a]				Cooling Efficiency[b] (%)
		In	Out	Temp. (°C)	Wet Bulb Depression (°C)	N db	N wb	S db	S wb	
1	6.2	23.1	22.0	29.7	8.1	22.1	21.6	26.1	23.3	95
2	12.4	23.1	22.0	29.3	7.7	22.9	22.0	26.1	22.9	83
3	18.6	23.1	22.2	29.7	7.8	23.4	22.5	26.9	23.5	81
4	6.2	30.0	22.8	31.7	9.7	24.0	23.2	28.3	24.7	79
5	12.4	25.6	18.9	26.6	8.3	20.7	19.8	25.1	21.9	71
6	18.6	25.6	20.0	30.6	11.4	21.9	20.8	25.5	22.1	76
7	6.2	32.8	19.4	27.5	9.2	21.3	20.4	25.3	21.7	67
8	12.4	30.3	21.4	30.6	10.6	23.4	22.7	27.6	23.7	67
9	18.6	30.3	21.1	29.4	10.6	22.6	21.6	26.5	23.1	65
10	6.2	35.0	19.9	30.0	11.7	22.8	21.4	27.4	23.6	62
11	12.4	32.2	20.6	28.9	9.9	23.3	22.4	27.3	25.6	57

a. "N" or "S" denotes north or south end of greenhouse, "db" is dry bulb temperature, and "wb" is wet bulb temperature.

b. Cooling efficiency is normally used to express cooling effectiveness under adiabatic saturation conditions but is used here to indicate relative cooling effects.

TABLE 2

COOLING EFFICIENCIES MEASURED AT VARIOUS FLOW RATES AND WET BULB DEPRESSIONS TVA WASTE HEAT GREENHOUSE MUSCLE SHOALS, ALABAMA, 1976

Ambient Wet Bulb Depression (°C)	Cooling Efficiency (%)				
	Q = 12.4[a]	Q = 18.6	Q = 22.4	Q = 26.1	Q = 29.8
8.9	-	-	-	-	91.0 (2)
8.3	100.0 (1)[b]	-	-	-	88.2 (4)
7.8	-	-	-	-	82.0 (1)
7.2	90.5 (2)	-	-	-	88.3 (3)
6.7	-	83.0 (1)	-	91.5 (2)	86.3 (3)
6.1	-	91.0 (1)	-	84.0 (2)	91.0 (2)
5.6	90.0 (2)	85.0 (2)	82.0 (2)	90.0 (4)	85.0 (3)
5.0	81.3 (3)	83.5 (2)	89.0 (3)	79.7 (3)	78.0 (2)
4.4	88.0 (1)	87.5 (2)	92.5 (4)	72.0 (2)	84.5 (2)
3.9	89.5 (2)	85.5 (2)	-	81.5 (2)	71.0 (1)
3.3	92.0 (1)	83.0 (1)	-	100.0 (1)	83.5 (2)
2.8	-	80.0 (1)	-	-	-
2.2	-	75.0 (1)	-	88.0 (1)	88.0 (1)
Average Efficiencies	88.7 (12)	84.2 (13)	89.0 (9)	85.0 (17)	85.7 (26)

a. Flow rates are in l/min·m.
b. Numbers in parentheses are the number of observations at the conditions indicated.

TABLE 3

MARKETABLE YIELD AND SIZE OF TROPIC AND FLORADEL TOMATOES AT TWO PLANTING DENSITIES IN THE TVA WASTE HEAT GREENHOUSE AT MUSCLE SHOALS, ALABAMA

JANUARY 22 - JULY 16, 1976

		Yield of Marketable Tomatoes[b]		Average Tomato Size (g)		
Variety	Planting Density[a]	Per Plant (kg)	Per Hectare (Tonnes)	No. 1	No. 2	Culls
Tropic	27,400	8.67 a	238 a	230 a	252	105
Floradel	27,400	8.53 a	234 a	181 b	266	88
Tropic	38,300	6.72 b	257 b	221 a	266	130
Floradel	38,300	6.72 b	257 b	184 b	249	82

a. 27,400 plants/ha = 0.36 m^2 per plant (45.7 cm in rows).
38,300 plants/ha = 0.26 m^2 per plant (61.0 cm in rows).

b. Average of six replications. Means followed by the same letter are no different at the 5% level of probability.

TABLE 4

YIELD OF TOMATOES TOPPED AFTER THE THIRD CLUSTER IN THE TVA WASTE HEAT GREENHOUSE AT MUSCLE SHOALS, ALABAMA JANUARY 22 - AUGUST 10, 1976[a]

		Yield of Marketable Tomatoes[b]					
		kg/plant			t/ha		
Cultivar	Density (plants/ha)	Crop 1	Crop 2	Total	Crop 1	Crop 2	Total
Floradel	54,800	2.3 b	2.3 b	4.6 b	113 a	127 a	240 a
Tropic	54,800	2.1 b	2.2 b	4.3 b	118 a	119 a	237 a
Floradel	38,300	2.6 a	2.6 a	5.3 a	102 a	101 b	204 b
Tropic	38,300	2.9 a	2.5 ab	5.4 a	111 a	94 bc	205 b
BNWR	38,300	2.4 ab	2.1 bc	4.5 bc	92 b	79 c	172 c
HS-24	38,300	1.6 b	1.8 c	3.4 c	51 c	68 c	119 d
Tropic (not topped)	38,300			6.7			257
Floradel (not topped)	38,300			6.7			257

a. Untopped plants grown from January 22-July 16 in an adjacent experimental area replicated six times.

b. Average of three replications. Means followed by the same letter are no different at the 5% level of probability. Yields from the untopped Tropic and Floradel plants were not statistically compared with other yields.

TABLE 5

INITIAL CAPITAL INVESTMENT COSTS COMPARISON OF COMPONENTS THAT ARE DIFFERENT FOR THE MUSCLE SHOALS WASTE HEAT GREENHOUSE SYSTEM (223 m^2) AND A CONVENTIONAL GREENHOUSE SYSTEM, 1975

Item[a]	Waste Heat	Conventional
CELdek system	$ 1,573	$ 975
Conventional heating system	--	1,353
Fin-tube heater and piping	650	--
Fiberglass attic and recirculation chamber	3,250	--
Exhaust fans and shutters	3,627	1,779
Extra space required	1,200	--
Extra doors	195	--
Total	$10,495	$4,107

[a] Installation cost was assumed to be about 30 percent of materials cost.

TABLE 6

ESTIMATED ANNUAL COST COMPARISONS OF ITEMS THAT ARE DIFFERENT IN THE MUSCLE SHOALS WASTE HEAT SYSTEM (223 m^2) AND A CONVENTIONAL SYSTEM OF SIMILAR SIZE, 1975

	Cost per Year		
Item	Waste Heat System	Conventional System	Waste Heat Compared With Conventional
	$		
Initial capital (amortized at 9% for estimated life of item[a])	1,418	618	+800
Operating Costs:			
Fuel (LP gas at $100/$m^3$)	--	2,000	-2,000
Electricity (2.5¢/kWh)	466	316	+150
Maintenance (1 or 5%)[b]	220	150	+ 70
Total Cost	2,104	3,084	-980

a. Ten years was used for estimated life of CELdek, pumps, and motors, except for shutter motors where 5 years was used. Fifteen years was used for fiberglass. Other major structure items were assumed to last 20 years. The salvage values were assumed to be zero.

b. One percent of item cost including installation was used for maintenance on structural items, and 5 percent was used for pumps, motors, etc.

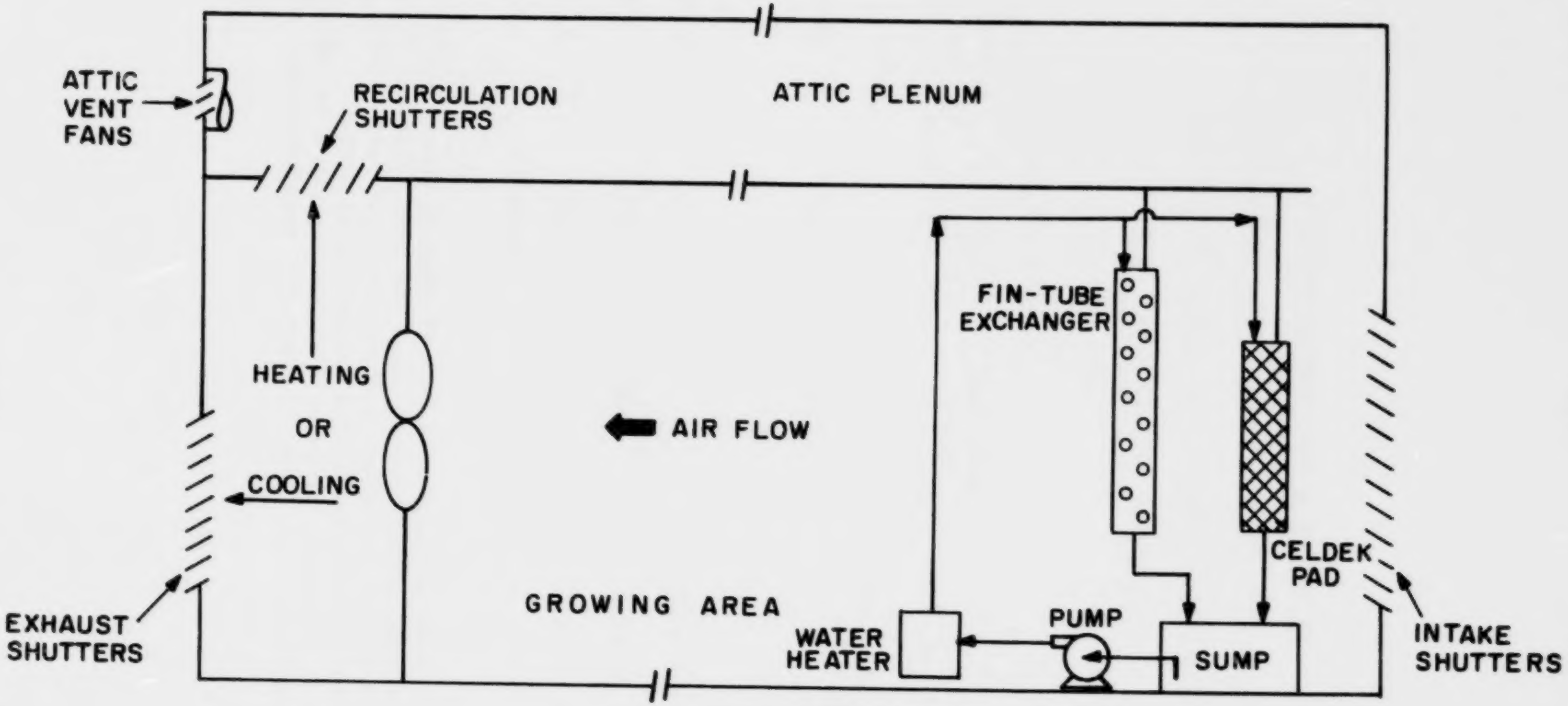
ATTIC VENT FANS
RECIRCULATION SHUTTERS
ATTIC PLENUM
FIN-TUBE EXCHANGER
HEATING
OR
COOLING
AIR FLOW
CELDEK PAD
EXHAUST SHUTTERS
GROWING AREA
WATER HEATER
PUMP
SUMP
INTAKE SHUTTERS

Figure 1. Schematic Drawing of Waste Heat Research Greenhouse, Muscle Shoals, Alabama.

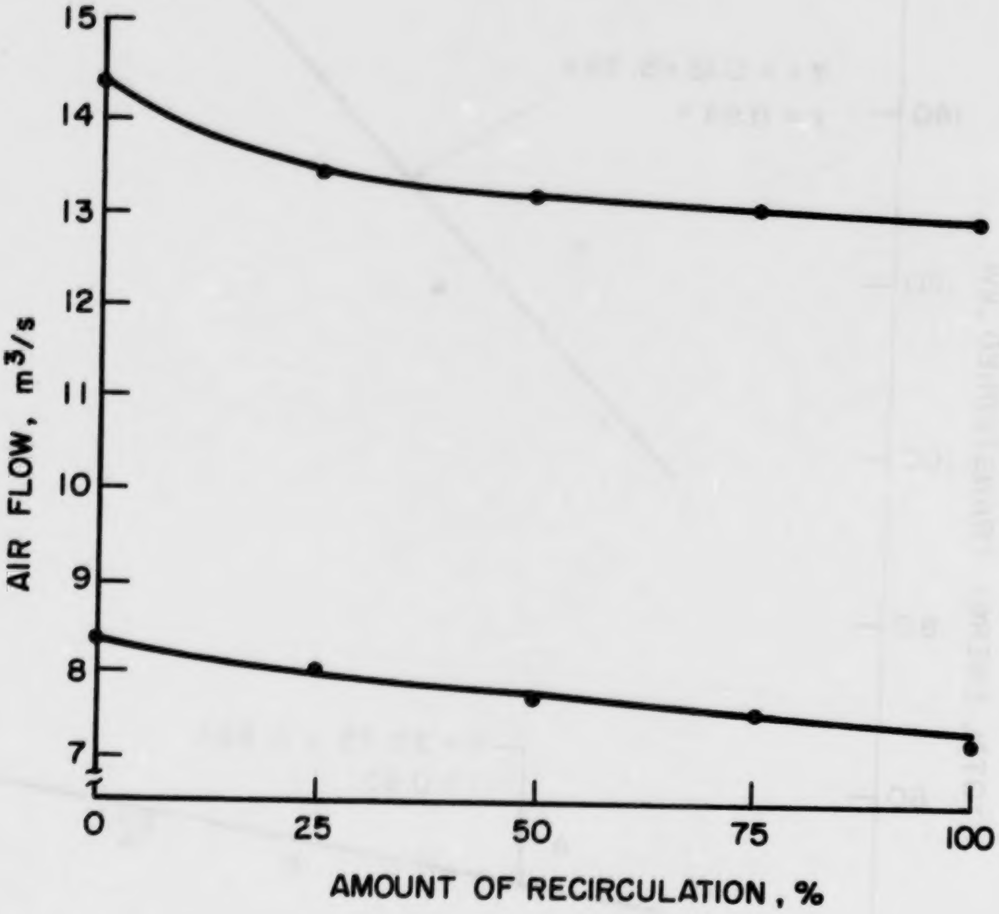

Figure 2. Greenhouse Air Flow Rates as Affected by Amount of Air Recirculation, Waste Heat Greenhouse, Muscle Shoals, Alabama.

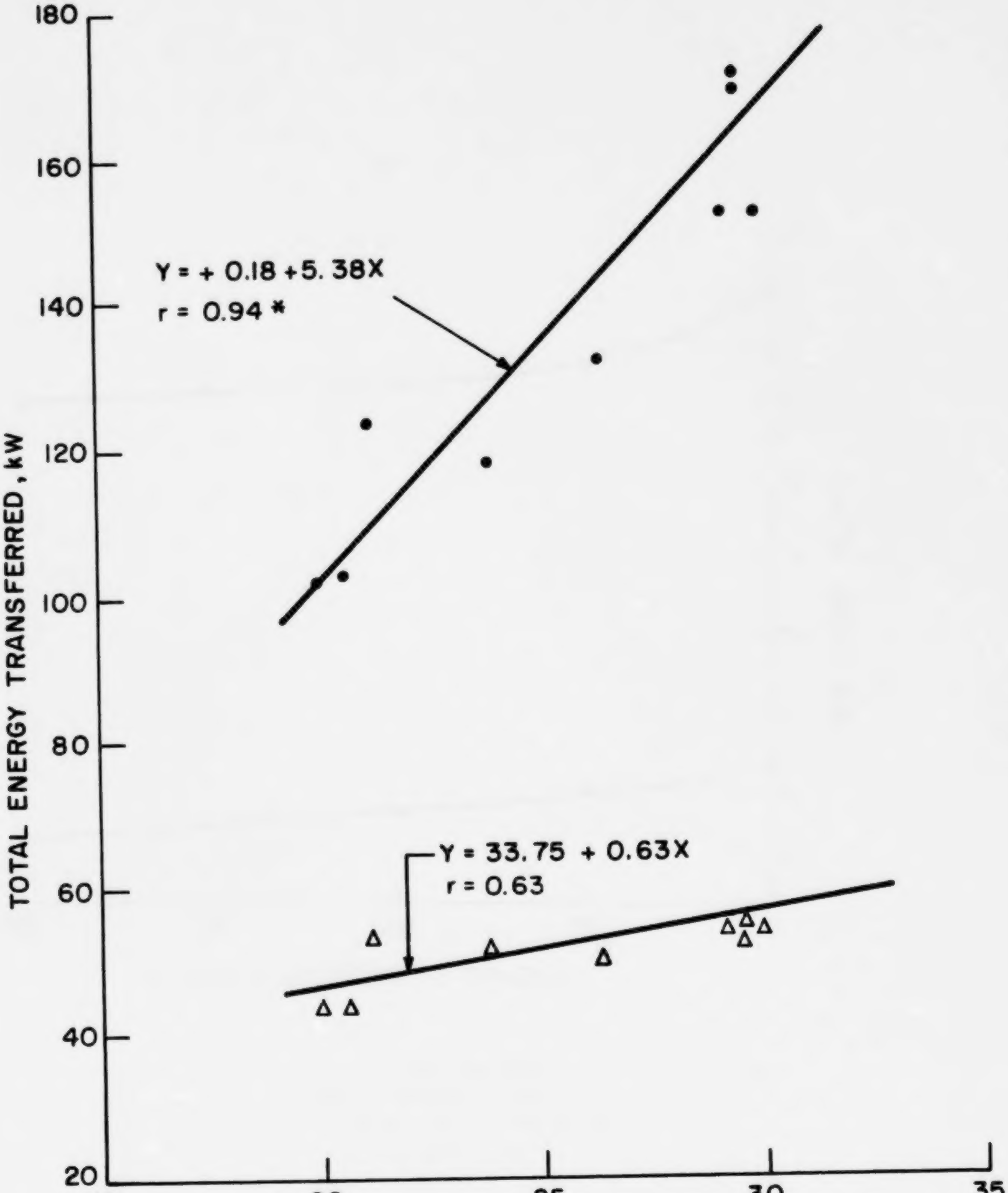

Figure 3. Energy Exchange in the Evaporative Pad with Various Water Temperatures, Waste Heat Greenhouse, Muscle Shoals, Alabama.

*Denotes Significance at 5-Percent Level of Probability.

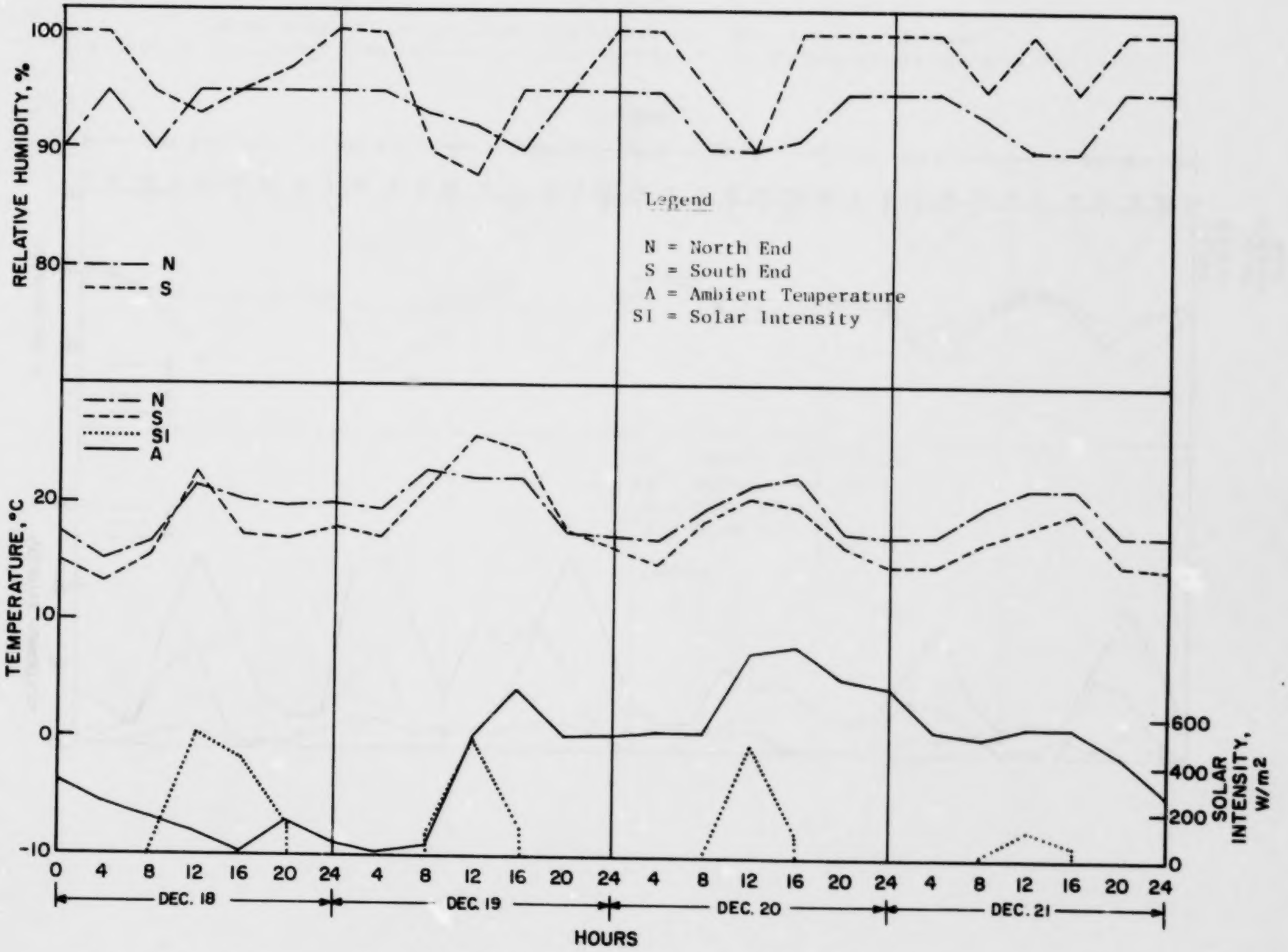

Figure 4. Greenhouse Temperatures, Relative Humidity, and Ambient Conditions During a Typical 4-Day Heating Period, Waste Heat Greenhouse, Muscle Shoals, Alabama.

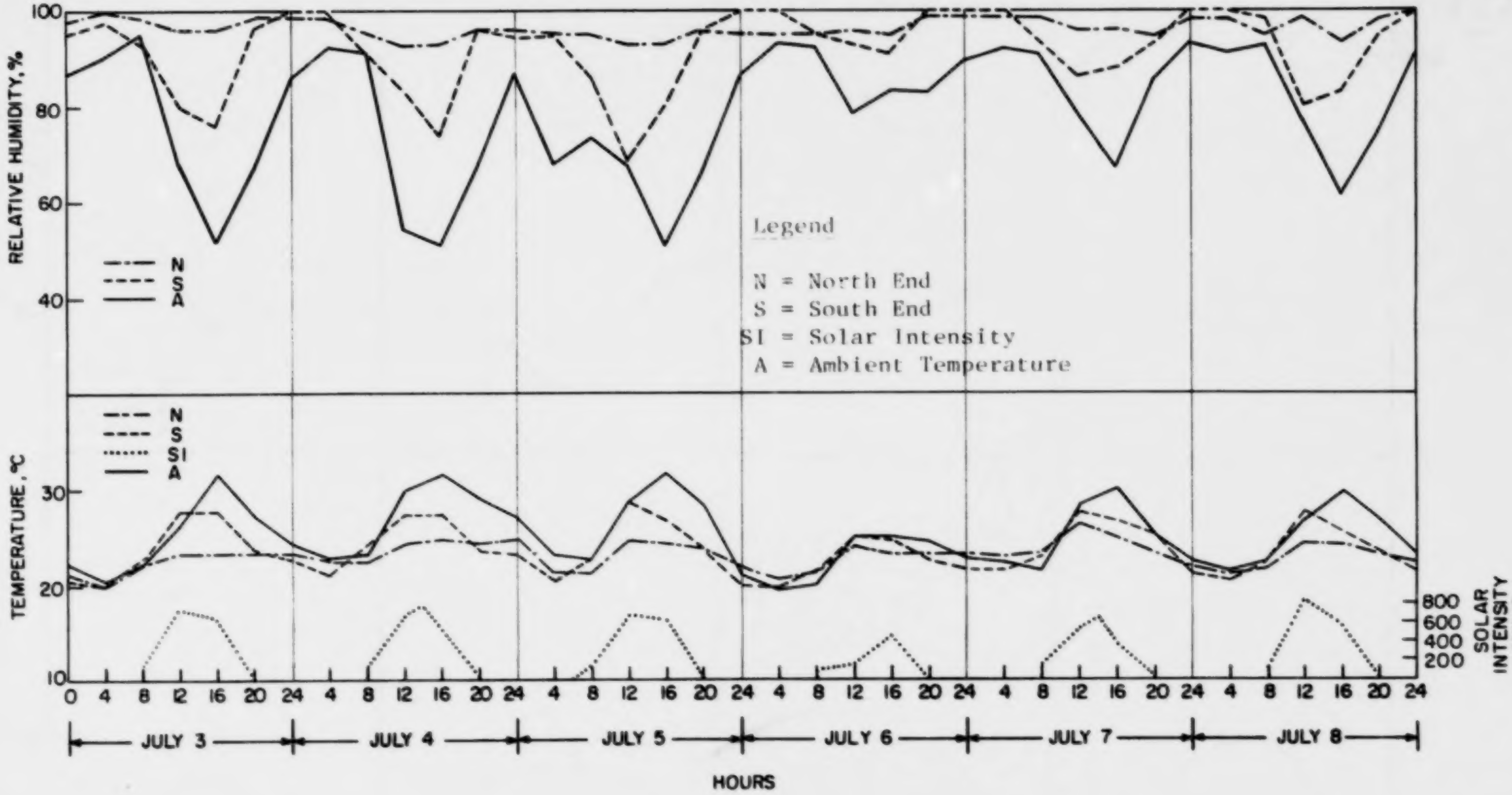

Figure 5. Greenhouse Temperatures, Relative Humidity, and Ambient Conditions During a Typical 6-Day Cooling Period, Waste Heat Greenhouse, Muscle Shoals, Alabama.

2045-20

V-C-213

UTILIZATION OF WASTE HEAT FROM POWER PLANTS BY SEQUENTIAL CULTURE OF WARM AND COLD WEATHER SPECIES

C. R. Guerra, B. L. Godfriaux and C. J. Sheahan
Public Service Electric and Gas Company
Newark, New Jersey U.S.A.

ABSTRACT

Aquaculture operations utilizing thermal discharges from power plants may significantly contribute to energy conservation and food production in the future. Commercialization of this technology will however, require the development of aquaculture schemes which do not interfere with the principal functions of the power plant but still operate reliably and economically under varying environmental conditions.

For the past three years, field experiments at a power generating station along the Delaware River have successfully demonstrated the concept of sequential (diseasonal) aquaculture. This process involves growing warm weather species during the warm months of the year and cold weather species during the cold season. The research, under the sponsorship of NSF/RANN, has recently been expanded to a proof-of-concept scale. The principal project objectives include the evaluation of the commercial feasibility of the concept, in particular, the overall process reliability, reproducibility of results and aquaculture product acceptability.

A pilot aquaculture facility is being used to rear freshwater shrimp, Macrobrachium rosenbergii, and rainbow trout, Salmo gairdneri, utilizing the thermal discharges from the Mercer Generating Station (Trenton, New Jersey). Delaware River water on passing through condensers of two 300 MW turbines gains thermal energy (up to 6°C) and provides two thermal regimes, of semi-annual frequency, in the plant effluents: one suited for shrimp and the other for trout. This diseasonal aquaculture scheme causes minimal interference with power plant operation and no modifications of the condenser operation or thermal discharge pattern.

Adult shrimp are conditioned for spawning and the hatched larvae reared indoors during winter and early spring. Juvenile shrimp are transferred to raceways and ponds by May. Marketable adult shrimp (greater than 11 cm) are harvested in the fall. Rainbow trout fingerlings are stocked in November, grown outdoors during the colder months and harvested by May (28 cm size).

The research is being carried out at the power plant facilities equipped to rear all stages of the shrimp life cycle and with flow capabilities to maintain up to 36,000 kg of trout. Supporting research is being conducted at Trenton State College and Rutgers University laboratories. Long Island Oyster Farms and the NJ Department of Agriculture are also participating in the project.

Experiments are being conducted to increase the shrimp stacking density by increasing the effective surface area of tanks, ponds and raceway, using various designs of submerged substrates. The trout experiments are designed to test increasing trout stacking densities in the untreated thermal effluent. Methods for waste heat dissipation are also being studied to better control the temperature regimes for shrimp and for trout. Tests for product quality control and market acceptance have been satisfactory.

A summary of the results to date and a description of the plans for the proof-of-concept evaluation are the subject of this report.

INTRODUCTION

For every unit of coal or oil burned in an electric generating plant, about one-third of the energy is converted to electricity. The other two-thirds of this energy is released to the environment as waste heat in the plant condenser cooling water and in stack gases.

Aquaculture research to determine whether the giant Malaysian freshwater shrimp species, Macrobrachium rosenbergii, and rainbow trout, Salmo gairdneri, could be successfully reared in the Mercer Generating Station heated discharge water during the warmer and colder months, respectively, was begun in August 1973.

Public Service Electric and Gas Company (PSE&G) provided the aquaculture site and the initial capital to build the original pilot aquaculture facility and initiate the research. Starting in July 1974, the National Science Foundation, Research Applied to National Needs Program (NSF/RANN) awarded PSE&G two grants to cover most of the pilot research expenses to November 1976. In November 1976, NSF/RANN provided a proof-of-concept grant to enlarge the present aquaculture facilities and to continue the research program.

The pilot aquaculture research project was conducted by PSE&G jointly with Trenton State College; Rutgers, The State University and Long Island Oyster Farms, Inc. Trenton State College operated the aquaculture facility at the Mercer Generating Station and conducted all testing at the site. Rutgers University ran the laboratory experiments to determine the physiological limits of various environmental parameters and nutritional requirements of the two species chosen for culture in the Mercer discharge water. Long Island Oyster Farms provided aquaculture expertise and a number of juvenile and adult shrimp required by the project.

The proof-of-concept project will involve the same organizations mentioned above. In addition, Buchart-Horn Inc. will perform the design and engineering of the aquaculture facilities, and the NJ Department of Agriculture will supply a farm cooperator to rear rainbow trout fingerlings for stocking the grow-out facilities at the power plant.

The aquaculture facilities are located at PSE&G's Mercer Generating Station four miles south of Trenton, New Jersey, on the Delaware River (Fig. 1). The station, which is coal-fired, generates some 600 MW of power and discharges approximately 450,000 gpm of heated discharge water at a maximum of 6°C above the ambient Delaware River water temperature. The thermal discharges derive from two condensers coupled to a twin set of 300 MW steam driven turbines. The power generating units are of base load (continuous) operation. Chlorine is used for condenser biofouling control. Godfriaux et al. (1975) has described the pilot aquaculture facilities.

SUMMARY OF PILOT STUDY RESULTS

The main purpose of the pilot study was to evaluate the biological feasibility of sequentially rearing the freshwater shrimp *Macrobrachium rosenbergii* (de Man) and rainbow trout *Salmo gairdneri* (Richardson) in the thermal effluent of a fossil fueled generating station using river water. Secondary objectives were to make preliminary evaluations of the engineering and economic feasibility of rearing the above mentioned species in thermal effluents and to make some preliminary assessments of product quality.

1. Biological Feasibility

Large, natural, seasonal temperature fluctuation of surface water (6°C to 30°C) between the warmer and colder months of the year occur in many areas of the nation. Power plant discharges add an approximately constant thermal increment

(6°C to 15°C) with the resulting aquatic environment being thermally distinct and suited for culture of a cold and warm weather species on a semiannual basis. This new aquaculture concept is called "diseasonal aquaculture" and has been found to be operationally feasible for rainbow trout and freshwater shrimp at Mercer Station.

Both species responded well to the thermal effluent environment. Growth and food conversion rates were equal to the better growth and food conversion rates cited in the literature for both species. There were no serious disease outbreaks for either species. The use of vertical draped netting in a pond and raceway, to increase submerged surface area, increased shrimp production threefold relative to the production from existing operations elsewhere. Temperature limits in the thermal effluent acceptable for *Macrobrachium rosenbergii* and rainbow trout culture were 15°C to 37.5°C and 0.4°C to 26.5°C, respectively. There was a temperature-dissolved oxygen interaction at the upper thermal limit for both species, which tended to depress the temperature limits.

Some difficulties were encountered in rearing the larval stages of *Macrobrachium rosenbergii*. Success was dependent on having available suitable quantities of brine shrimp (*Artemia*) larvae for the feeding of *Macrobrachium rosenbergii* larvae. Non-*Artemia* larvae diets did not allow *Macrobrachium* larvae to complete their growth through their larval stages. Only two mishaps occurred which caused significant mortalities. Rainbow trout were found to be very sensitive to the chlorine residual in the station effluent during periods of generating station chlorination, and the shrimp suffered when there was a combination of momentary high temperature water (35°C) and low dissolved oxygen in the raceway water.

2. Engineering Feasibility

The basic attitude taken during the experimentation was that aquaculture operations must adapt to the operating characteristics of an electric generating station. Any substantial modifications of an existing electric generating station could probably never be paid for by the additional profits derived from the aquaculture operations.

Experience has indicated that three generating units would be preferable at an electric generating station, if a continuous supply of heated effluent is desired. This feature becomes more important the higher a particular generating unit raises the water temperature above ambient.

Certain operating problems were countered with simple, inexpensive solutions. The sensitivity that rainbow trout showed to chlorine residuals during station chlorination of its cooling waters, was solved by automatically shutting down the aquaculture facility intake pumps and aerating the rearing raceways and ponds. When the temperature of the station thermal effluent was approaching upper thermal limits of trout or shrimp, water was sprayed into the ponds or raceway to lower the water temperature a few degrees.

An inexpensive telephone alarm system was installed to alert project personnel when water temperature, dissolved oxygen or pressure were recorded outside permissible values. These were the only engineering problems encountered in the study.

3. Economic Feasibility

Intensive, waste heat aquaculture which employs the use of high water flow rates appears to be an attractive investment (9 to 55% return on investment). Although both shrimp and rainbow trout are biologically feasible for culture in the Mercer Generating Station thermal effluent, recent projections indicate rainbow trout would provide between 77 percent and 95 percent of the total yearly revenues with present technology.

Since only about four hectares of land are available for a commercial aquaculture facility at the Mercer Generating Station, and the production of both shrimp and trout is almost tripled per unit area of raceway when raceway depth is increased (from 0.9 m to 2.4 m), the most efficient production unit appears to be the deeper raceway. The deeper raceway requires increased water flow rates or a supplemental water aeration/oxygen injection system to maintain desired levels of dissolved oxygen and minimize the build-up of metabolic wastes.

4. Product Quality

Heavy metal and arsenic analyses were conducted at various times for *Macrobrachium rosenbergii* reared at the Mercer Aquaculture Facility and overseas locations. There was little difference between these shrimp sources. Mercer rainbow trout were also examined for heavy metals and arsenic, and both Mercer shrimp and rainbow trout were analyzed for polychlorinated biphenyls (PCBs). All results were within permissible levels.

Restaurant evaluation of the shrimp were favorable with respect to flavor, color and texture. The Department of Food Science, Rutgers University did note on one occasion, a slight "earthy" flavor in a taste test on Mercer reared rainbow trout. However, in most taste trials, the trout was found to be quite tasty. Small volumes of trout were sold at a local fish market and the shrimp served at a local restaurant.

PROOF-OF-CONCEPT AQUACULTURE RESEARCH PLANS

1. Layout of Facility

The general layout of the proof-of-concept aquaculture facilities is shown in Figure 2. It includes two laboratory nurseries and grow out facilities.

The two laboratories are Lord and Burnham "Gro-Mar" greenhouse units 6.7 m X 14.6 m. Laboratory I (Fig. 3) is used as a hatchery for *Macrobrachium rosenbergii*. It has special tanks for brood stock, for culturing the early and late larval stages of shrimp and for hatching of brine shrimp eggs. It also serves as a holding area for post-larvae and early juvenile shrimp until they are placed in the covered, outdoor, heated, nursery raceways.

There are six early larval rearing tanks. Each tank measures 56 cm in diameter and is basically cone shaped. The tanks are made of a fiberglass reinforced polyester resin with an FDA approved gelcoat on the interior surface. Also located in Laboratory I are twenty-one late larval brood stock and post-larval rearing tanks which are low cost, concrete, cemetery vaults (2.2 m X 0.8 m X 0.7 m). They were painted on the inside with an FDA approved epoxy paint to achieve water-tightness.

Laboratory II serves as the rainbow trout hatchery and fry rearing building (Fig. 4). It contains two, eight tray, salmonid battery incubation units; eight 3 m X 0.9 m X 0.6 m trout fry/fingerling rearing troughs and five 2 m square rearing tanks with round corners. The heat exchanger which will be described in a later section is also located here.

Figure 2 shows five main grow-out raceways. One is an existing 50 m X 2.4 m X 0.9 m V-shaped, liner raceway. The other four raceways will be of concrete. Two will be 3.6 m wide and the other two 2.4 m wide. One two-unit raceway set will be 2.4 m deep and the other two-unit set will be 0.9 m deep. All four raceways will be 30 m in length.

The facilities include six 12.2 m X 1.8 m X 0.9 m nursery raceways (Fig. 2). These raceways will be covered with a low cost plastic sheet structure to reduce water heat loss during the colder months of shrimp juvenile rearing. The plastic walls will be rolled down during hot weather (trout fingerling rearing).

Two other elements of the pilot facility will be retained. One is Pond I which is a 27.5 m X 7.6 m X 0.9 m PVC liner lined pond. The other is Pond II (15 m X 15 m X 1.8 m) which is similarly liner lined and will be modified into a temperature equalization pond. Both ponds are shown in Figure 2.

Other features of the facilities include a PVC liner lined dual lagoon type waste treatment system consisting of aeration and settling lagoons (6.1 m X 6.1 m X 2.4 m each) and a food storage/workshop building.

2. Pumps and Piping System

There are three sources of water for use in the proof-of-concept aquaculture facility: generating station heated effluent, Delaware River ambient water and well water. TABLE I lists the maximum flow of each water source available to each aquaculture facility process unit, and Figure 5 shows a schematic of the process water flow to the various units within the aquaculture facility.

Well water is supplied to each process unit, except Laboratory I, and is individually valved for control. Tempered water from the temperature moderation pond (which mixes ambient river and station discharge canal water) is also supplied to each process unit. The six nursery raceways are supplied ambient river water and waste, heat exchanger water from Laboratory I, in addition to tempered water and well water for a wider range of water temperature control. The temperature moderation pond is supplied with water from all three sources for blending purposes. Raceway cleanings are taken by underflow piping or pumped directly to the waste treatment facility for settling and aeration prior to discharge to the power station discharge canal.

There are four station discharge canal water intake pumps: two rated for 3,000 liter/minute and two 5,700 liter/minute. There are two 1,900 liter/minute ambient river water intake pumps and two new 7,600 liter/minute temperature moderation pond pumps for tempered water distribution to the process units. There are also two 1,900 liter/minute well pumps. In the event of a temperature moderation pond breakdown of the pumps or pond itself, discharge canal and river ambient water can bypass the temperature moderation pond and go directly to the process units. The piping system incorporates no lead base materials and to avoid problems with pluggage of the pump inlet strainer, back flushing by gravity is used.

3. Air Supply System

The air supply for all aquaculture facilities is taken from the 21 kgs/cm^2 power plant air system. Air filters were installed upstream of the air pressure regulator to prevent oil traces from the plant centifugal air compressors from entering the culture tanks and ponds. The station air pressure was reduced to 0.4 kgs/cm^2 for its use within the aquaculture facility. To prevent water build up and possible upstream freezing of the air line or oil carry over, the air filters are bled off on a continuous basis. A portable air compressor will be rented if required to maintain dissolved oxygen levels in the main rearing units during the months of March through May when the trout biomass will be at its highest.

4. Heat Exchanger System

The heat exchanger is used to heat the Mercer discharge canal water being supplied to Laboratory I where the shrimp are kept during the colder months of the year. The heat exchanger system is part of a closed loop heating system. The system is located in Laboratory II and supplies heated station discharge water to Laboratory I. A 3 hp, 2,550 rpm centrifugal pump feeds city water to two RUDD, industrial type, gas-fired heaters. The heaters are rated at a total output of 1 X 10^9 joules/hr and input of 1.3 X 10^9 joules/hr. The hot water heaters are capable of raising 115 liters/minute of water 22°C above ambient on a continuous basis. The heaters are thermostatically controlled to shut off at a predetermined temperature.

The heated water output from the RUDD heaters is supplied to a single plate type heat exchanger. The heat exchanger is rated at 0.95 X 10^9 joules/hr at about 115 liters/minute. The heat exchanger plates are made of titanium. A plate type heat exchanger was selected due to the limited space available as well as for ease of cleaning. A back flush system is incorporated on the heat exchanger which utilizes 6 kgs/cm^2 city water. With this method the flow is reversed on the canal water side of the exchanger, and this removes any debris build up. The exchanger has operated according to design since installation. Internal inspections have found the exchanger clean.

5. Water Monitoring and Alarm System

An alarm system is used to provide notifications to the aquaculture project manager, the generating station control operator (in the power plant control room), and outside aquaculture personnel in the event of any abnormal environmental conditions in the project. The various parameters being monitored (water temperature, water pressure, dissolved oxygen and air pressure) are sensed by appropriate primary elements which activate electrical switching devices. The electrical output of these devices is sent to a common control relay. This relay is used to initiate an electronic telephone dialer system. The telephone dialer uses a pre-recorded magnetic tape cartridge that contains telephone numbers and a message. It is used to call and inform outside people that an alarm condition exists. The dialer system is a modification of a commercially available system made by Dytron, Inc. for fire and security uses in residential and industrial applications.

6. Aquaculture Waste Water Treatment

As stipulated in the EPA Draft Development Document for Proposed Effluent Limitations Guidelines and New Source Performance Standards for the Fish Hatcheries and Farms - by Schneider (1974), process water flow may be discharged directly back into the water source. However, water used for raceway cleaning should be settled (sediment removed) before effluent is returned to receiving waters.

7. Chlorine Control System

The Fisher-Porter chlorine control equipment has been modified to include an electrical interlock with the heated discharge water intake pumps. The operation of the interlock system depends on the opening of the chlorine dilution water valve. Upon activation of the control relay for the dilution water valve, an auxiliary relay causes the heated discharge water pump contactor to open thereby stopping the pumps. An additional feature of this system is the ability to operate only one pump at a time or to override the system completely in the manual mode.

8. Water Chemistry and Bacteriology

Bacterial counts in the Delaware River and Mercer discharge canal are highest during the summer and early fall. This also coincides with periods of greater total chlorine occurring in the Delaware River. Total chlorine concentrations of up to 0.1 ppm were recorded before passage through the Mercer

Generating Station. This is believed to be the result of discharges of local sewage treatment plants further up river which encourage bacterial blooms due to the high temperatures of the Delaware River. The sewage treatment plants try to suppress these bacterial blooms by increasing the amount of chlorine added to the sewage discharges.

9. Sequence of Culture Operations - Shrimp and Trout

Figure 6 shows the sequence of shrimp and trout culture operations through the year. In Laboratory I, shrimp (*Macrobrachium rosenbergii*) brood stock are spawned in late December early January, and the resulting fertilized eggs are hatched by the beginning of February. The shrimp larval cycle is completed some time in early March, in Laboratory I, and then the post-larvae are transferred to the covered nursery raceways where they are grown to 3-5 cm juveniles by mid-May. At this time, the juvenile shrimp are transferred to the outdoor pond or raceways where they are kept until they reach a length of 12-15 cm (September-October) when they are harvested.

In December, rainbow trout eyed eggs are placed in battery incubation trays in Laboratory II. Egg hatching is completed by the end of December. The yolk-sac fry are then placed in rearing troughs also located in Laboratory II and are grown to a length of 9 cm by mid-May when the trout fingerlings are transferred to the outdoor nursery raceways. The fingerlings are held in the nursery raceways until mid-November when they should be approximately 20 cm long. They are then transferred to the outdoor production raceways and harvested at approximately 30 cm in length at the beginning of May.

10. Production Capabilities for Shrimp and Trout

TABLE II summarizes the projected production capacity of the proof-of-concept facilities. The production capacities for rainbow trout could be greatly increased in the two 2.4 m deep raceways by increasing the trout stocking densities higher than indicated in TABLE II. These rearing units will then be available for the rearing of alternate species.

CONCLUSIONS

Our experience thus far has indicated that sequential rearing of the freshwater shrimp, *Macrobrachium rosenbergii*, and rainbow trout, *Salmo gairdneri*, is a promising aquaculture alternative to use the heated effluent from the Mercer Generating Station. Chlorination of the cooling water in the plant steam condensers has caused some problems in rearing a chlorine sensitive species such as rainbow trout, but this problem has been avoided by shutting down the aquaculture intake pumps during the chlorination periods.

Increasing the trout stocking densities results in dissolved oxygen becoming the limiting factor during the water intake shutdowns. This situation is expected to be resolved by water aeration, recirculation and oxygenation as required. Shrimp production is dependent on high culture densities which we hope to achieve by submerged substrates and separated habitats in deeper raceways.

ACKNOWLEDGMENTS

This research is being funded by NSF/RANN Grants AEN 74-14079 ENV 76-19854 A01 and GI-43925, and PSE&G Authorizations RD-378 and RD-443. Other contributions to the project have been made by Long Island Oyster Farms, Trenton State College, Rutgers University and the New Jersey Department of Agriculture.

Many persons from outside the project have provided valuable suggestions and help to this work. We would like to acknowledge in particular the help provided by: Dr. E. H. Bryan (Program Manager, Environmental Systems and Resources, NSF/RANN), and Mr. J. Steinsieck (Superintendent, Mercer Station, PSE&G). We would also like to thank personnel in both Production and Engineering Departments of PSE&G for their assistance and cooperation in this project.

REFERENCES

1. Godfriaux, B. L., H. J. Valkenburg, A. Van Riper and C. R. Guerra 1975: Power plant heated water use in aquaculture: pp. 233-250. In Proceedings of the Third Annual Pollution Control Conference of the Water and Wastewater Equipment Manufacturers Association (Ed. V. W. Langworthy). 915 pp.

2. Schneider, R. F. 1974: Development Document for Proposed Effluent Limitations Guidelines and New Source Performance Standards for the Fish Hatcheries and Farms (Draft). Environmental Protection Agency, Office of Enforcement, National Field Investigations Center, Denver, Colorado. 237 pp.

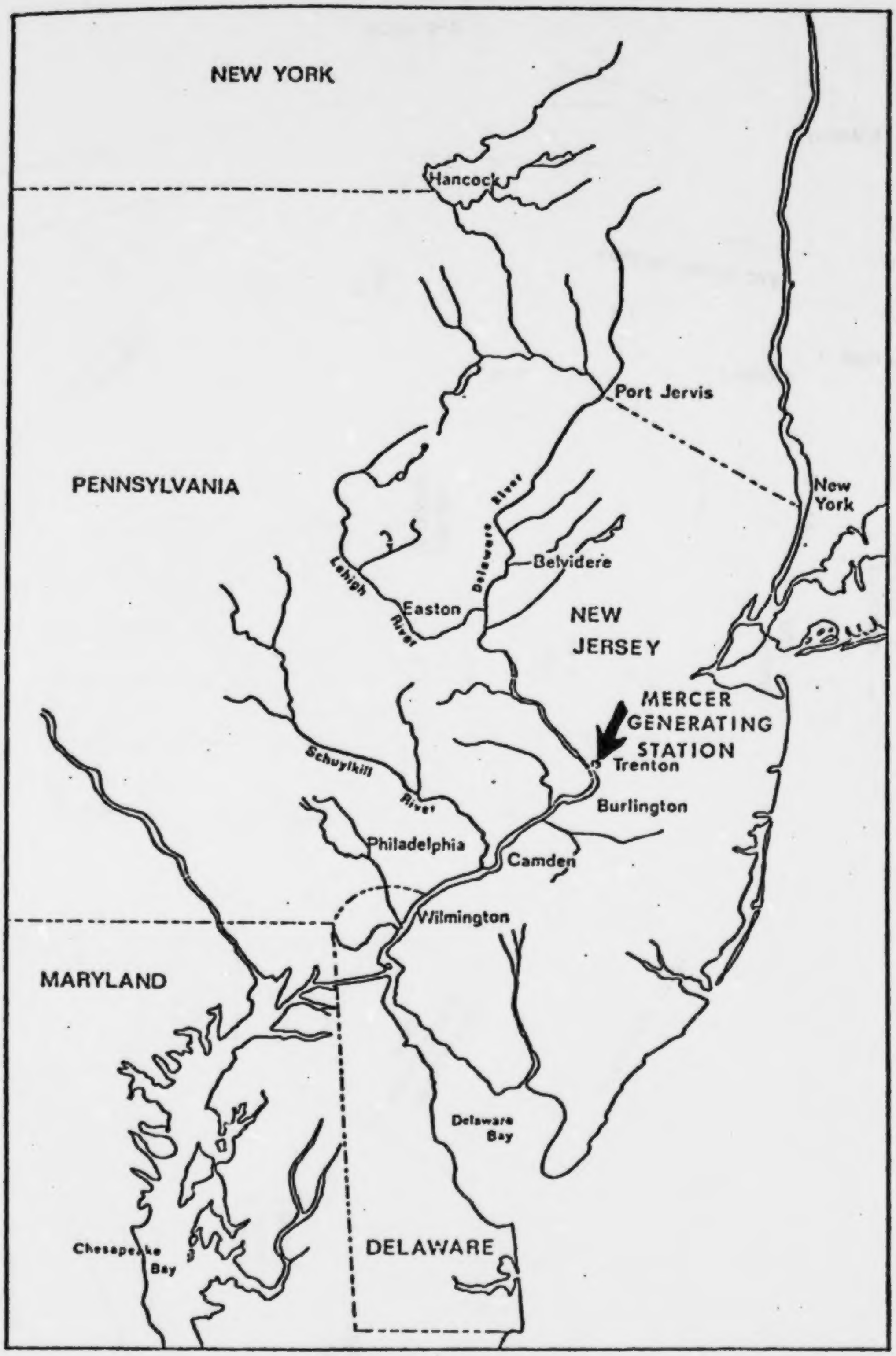
NEW YORK
Hancock
Port Jervis
PENNSYLVANIA
New York
Delaware River
Belvidere
Lehigh River
Easton
NEW JERSEY
MERCER GENERATING STATION
Trenton
Schuylkill River
Burlington
Philadelphia
Camden
Wilmington
MARYLAND
Delaware Bay
Chesapeake Bay
DELAWARE

Figure 1. Map of the Delaware River Drainage Basin Showing the Location of the Mercer Generating Station

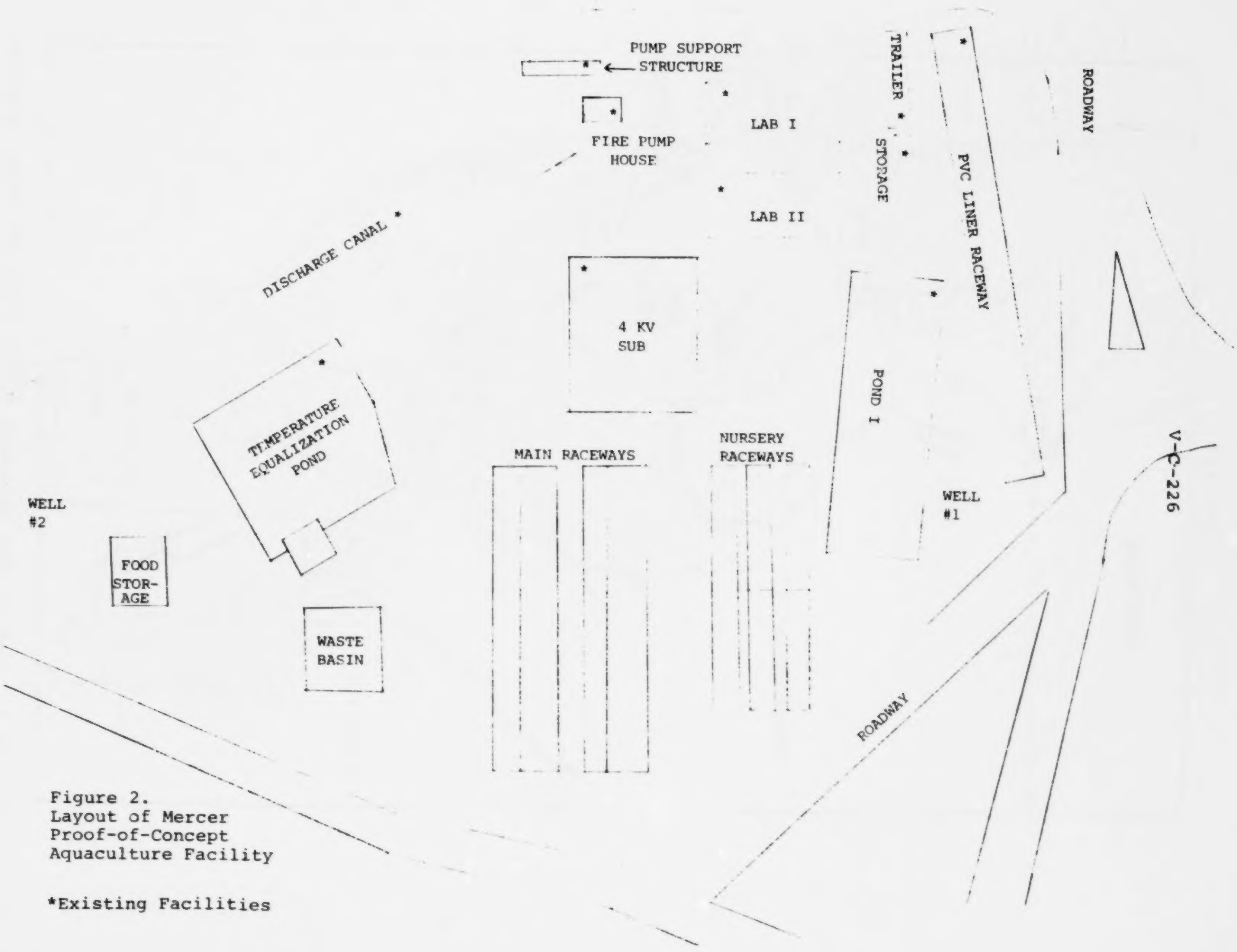
PUMP SUPPORT STRUCTURE
FIRE PUMP HOUSE
LAB I
LAB II
TRAILER
STORAGE
PVC LINER RACEWAY
ROADWAY
DISCHARGE CANAL
4 KV SUB
POND I
WELL #1
NURSERY RACEWAYS
MAIN RACEWAYS
TEMPERATURE EQUALIZATION POND
WELL #2
FOOD STORAGE
WASTE BASIN
ROADWAY

Figure 2.
Layout of Mercer
Proof-of-Concept
Aquaculture Facility

*Existing Facilities

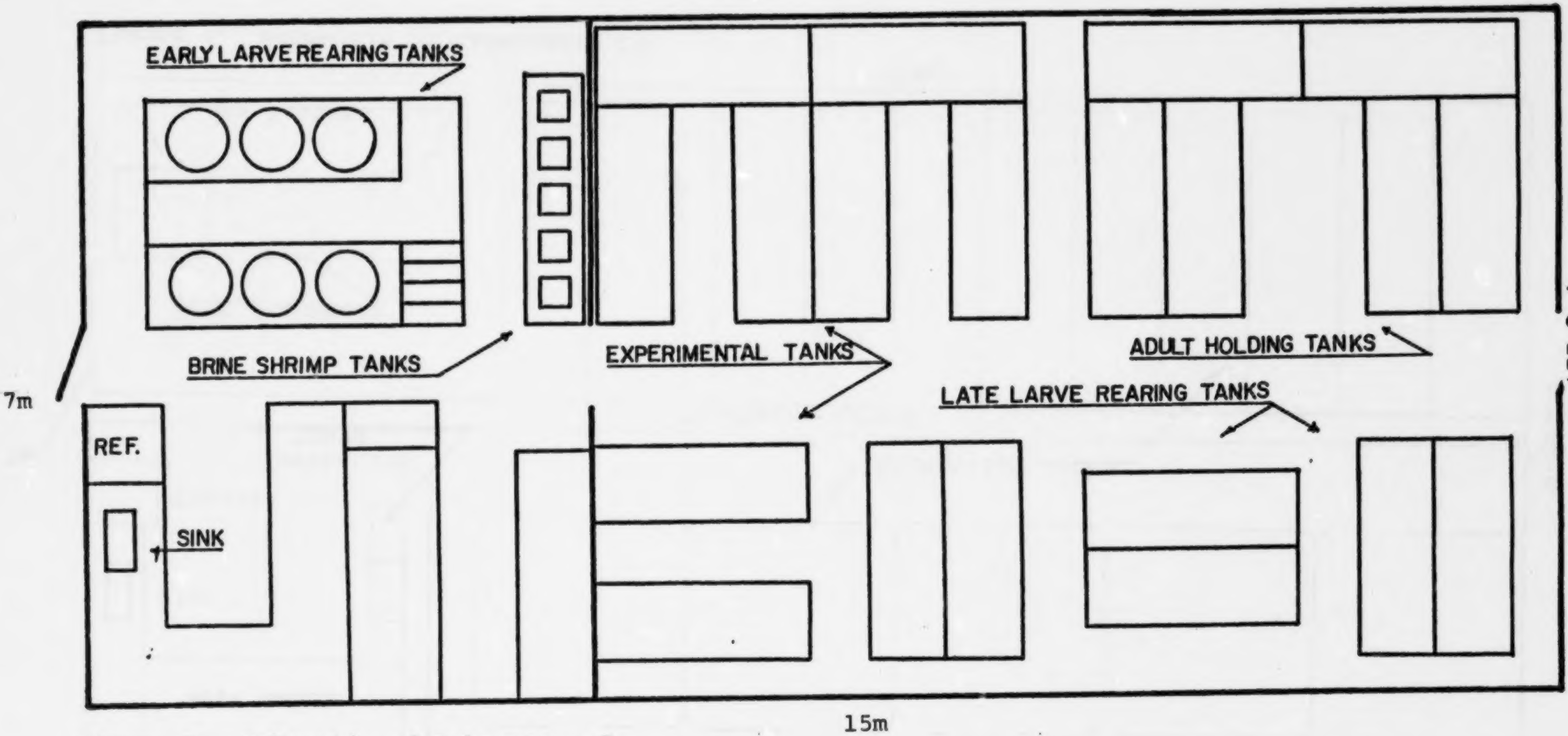
EARLY LARVE REARING TANKS
BRINE SHRIMP TANKS
EXPERIMENTAL TANKS
ADULT HOLDING TANKS
LATE LARVE REARING TANKS
REF.
SINK
7m
15m

Figure 3. Schematic of Laboratory I

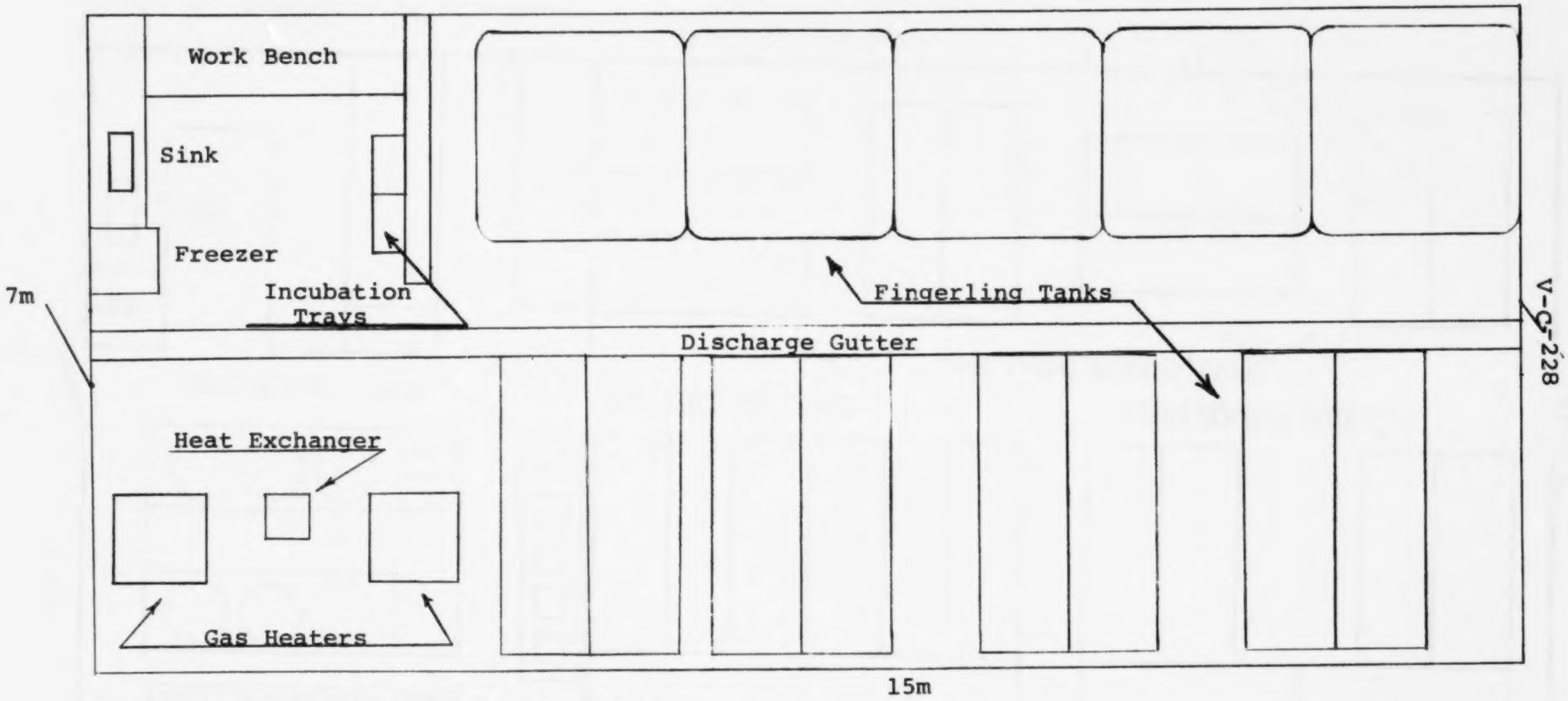
Work Bench
Sink
Freezer
Incubation Trays
Fingerling Tanks
7m
V-C-228
Discharge Gutter
Heat Exchanger
Gas Heaters
15m

Figure 4. Schematic of Laboratory II

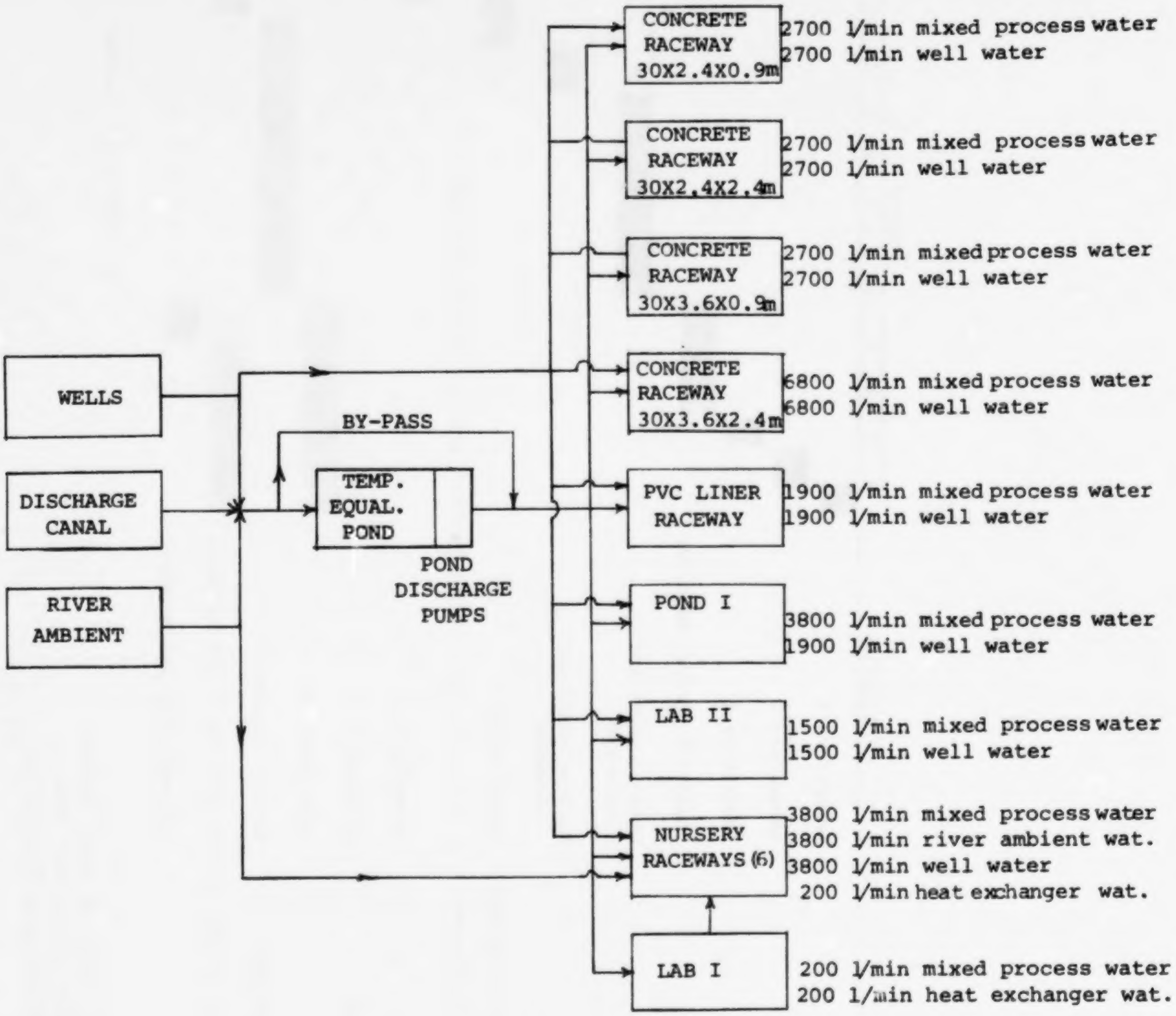
CONCRETE RACEWAY 30X2.4X0.9m
2700 l/min mixed process water
2700 l/min well water
CONCRETE RACEWAY 30X2.4X2.4m
2700 l/min mixed process water
2700 l/min well water
CONCRETE RACEWAY 30X3.6X0.9m
2700 l/min mixed process water
2700 l/min well water
CONCRETE RACEWAY 30X3.6X2.4m
6800 l/min mixed process water
6800 l/min well water
WELLS
BY-PASS
DISCHARGE CANAL
TEMP. EQUAL. POND
PVC LINER RACEWAY
1900 l/min mixed process water
1900 l/min well water
POND DISCHARGE PUMPS
RIVER AMBIENT
POND I
3800 l/min mixed process water
1900 l/min well water
LAB II
1500 l/min mixed process water
1500 l/min well water
NURSERY RACEWAYS (6)
3800 l/min mixed process water
3800 l/min river ambient wat.
3800 l/min well water
200 l/min heat exchanger wat.
LAB I
200 l/min mixed process water
200 l/min heat exchanger wat.

Figure 5. Simplified Flow Schematic of the Mercer Aquaculture Facility

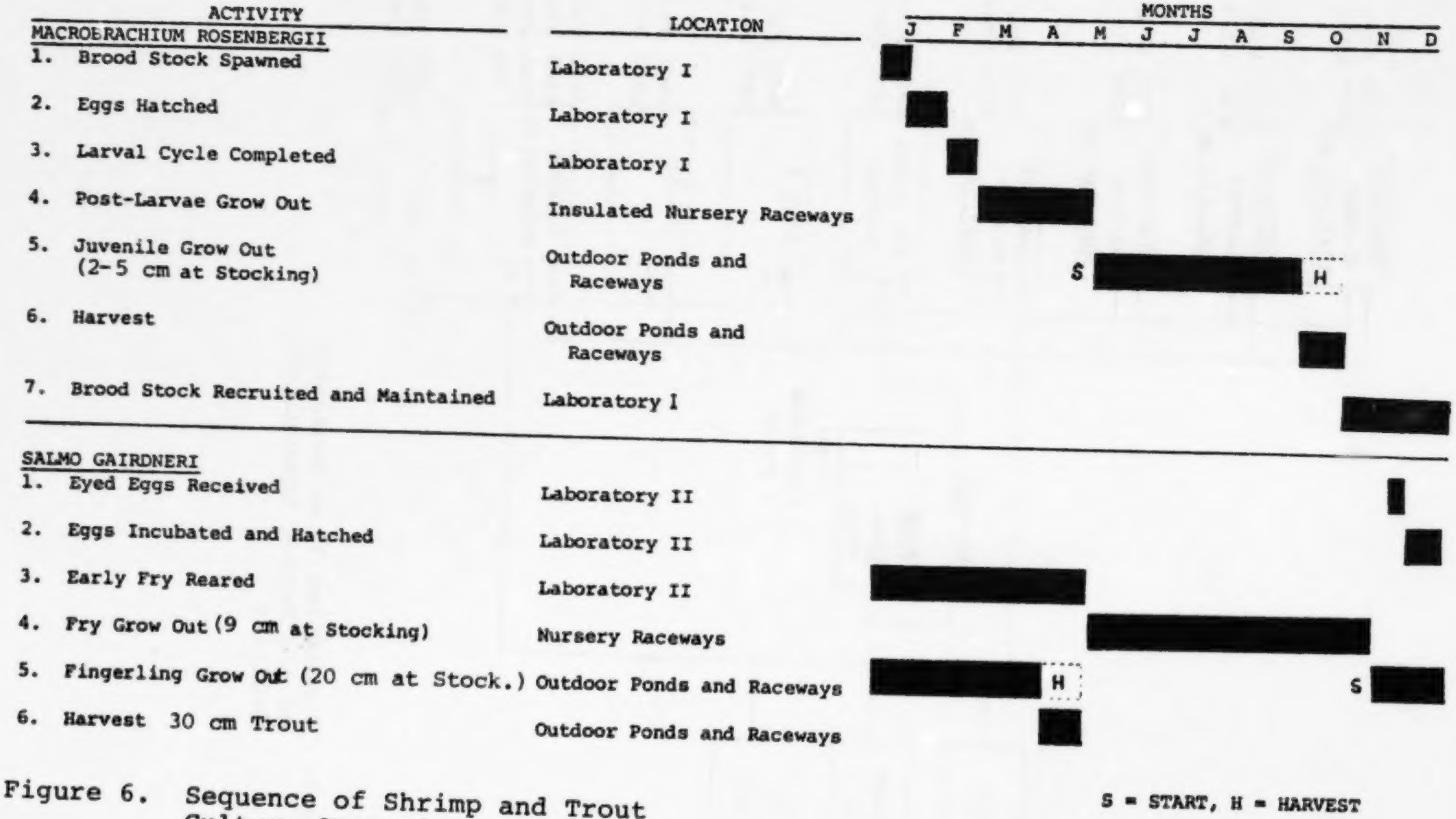

Figure 6. Sequence of Shrimp and Trout Culture Operations at the Mercer Aquaculture Facility

TABLE I. PROCESS WATER FLOW ALTERNATIVES (LITERS/MIN.)

Process Unit	Mixed Process[1] Water (Max. Inflow)	Ambient River Water (Cap. 3800 1/m)	Well Water (Cap. 3800 1/m)	Heat Exchanger Water (Cap. 200 1/m)	Station Heated Effluent (Cap. 17,400 1/m)
Laboratory I	200	-	-	200	-
Laboratory II	1,500	-	1,500	-	-
Existing Raceway(50m X 2.4m X 0.9m)	1,900	-	1,900	-	-
Pond I	3,800	-	1,900	-	-
Temperature Equalization Pond(Pond II)	25,000[2]	3,800	3,800	-	17,400
Concrete Raceway(30m X 2.4m X 0.9m)	2,700	-	2,700	-	-
Concrete Raceway(30m X 2.4m X 2.4m)	6,800	-	3,800	-	-
Concrete Raceway(30m X 3.6m X 0.9m)	2,700	-	2,700	-	-
Concrete Raceway(30m X 3.6m X 2.4m)	6,800	-	3,800	-	-
6-Nursery Raceways(12.2m X 1.8m X 0.9m)	3,800	3,800	3,800	(200)[3]	-

1. Obtained by blending of plant discharge water, ambient river water and well water as needed.

2. Equalization pond throughput capacity is presently only 15,000 1/m.

3. This heated water is derived from the Laboratory I discharge.

TABLE II. SUMMARY OF FACILITIES FOR TROUT AND PRAWN PRODUCTION

Grow-Out Facilities	No.	Dimensions (m)	Area (m^2)	Volume (m^3)	Trout No. Stocked	Trout Harvest (kg)	Shrimp No. Stocked	Shrimp Harvest (kg)
Main Raceway	1	30m X 2.4m X 0.9m	73	66	13,200[1]	4,545[7]	8,800[6]	191[8]
Main Raceway	1	30m X 3.6m X 0.9m	110	99	13,200[1]	4,545[7]	13,400[6]	282[8]
Main Raceway	1	30m X 2.4m X 2.4m	73	176	26,200[1]	9,090[7]	22,600[6]	475[8]
Main Raceway	1	30m X 3.6m X 2.4m	110	264	26,200[1]	9,090[7]	35,400[6]	745[8]
Pond I	1	27m X 7.6m X 0.9m	209	188	13,200[1]	4,545[7]	27,000[6]	567[8]
PVC Liner Raceway	1	50m X 2.4m X 0.9m	120	108	13,200[1]	4,545[7]	-	-
				TOTALS	92,400	36,360	107,200	2,260
Nursery Facilities								
Hatchery Building (Lab I)	1	6.7m X 14.6m	98	-	-	-	300,000[4]	-
Hatchery Building (Lab II)	1	6.7m X 14.6m	98	-	125,000[2]	-	-	-
Nursery Raceways	6	12.2m X 1.8m X 0.9m	131	118	100,000[3]	-	175,000[5]	-

Notes

1 - 20cm fingerlings (10.7 animals/kg)
2 - eyed-larvae to yolk-sac fry
3 - 9cm fingerlings
4 - fertilized eggs to newly metamorphosed post larvae
5 - 1cm PL shrimp stocked at 214 animals/m^2; draped netting added to increase total surface area
6 - 5cm to 6cm shrimp juveniles at 22 animals/m^2; draped netting (approximately 0.3m apart) added to increase total surface area
7 - 30cm trout - 380 g average individual weight @ 1.3kg trout/liter/min. to 2.4kg/liter/min.
8 - 14cm shrimp - 30 g average individual weight @ 16 animals/m^2 of total surface area

SESSION VI-A
UTILIZATION II

21-45-23

VI-A-3

EXPERIENCES WITH A COMPUTER-BASED STUDY ON WASTE HEAT USAGE FOR INTEGRATED AGRICULTURAL PURPOSES IN MICHIGAN

I. P. Schisler, R. L. Meekhof, L. J. Connor, F. W. Bakker-Arkema,
G. E. Merva, M. G. Roth, V. M. Schultink, B. A. Stout,
R. L. Tummala, J. C. VanKuiken, and L. P. Walker
Michigan State University
East Lansing, Michigan U.S.A.

ABSTRACT

A computer based study to assess the feasibility of agricultural utilization of reject heat from a nominal 1000 MWe power plant began in September 1973 by an interdepartmental team at MSU. This paper reviews and interprets the results of this systems study. Components used include numerical models representing three agricultural subsystems: pond heating for catfish culture, field warming for vegetable production, and greenhouse heating for ornamental flowers as well as models for the power plant thermal discharge and a cooling reservoir for the dissipation of heat not usable by the agricultural subsystems. The components of the system were integrated by optimizing a net present value criterion. Ownership-management options for operating the agricultural subsystems are suggested. This paper presents impressions on the usefulness of the factors included in the methodology used. Future research needs for this methodology are outlined.

INTRODUCTION

Over the last decade there have been numerous conferences to assess the potential for and problems with utilizing reject heat in beneficial ways. The early conferences usually had two separate components: (1) a collection of technical papers with each paper on a specific aspect of waste heat utilization, and (2) a concluding statement or set of recommendations reiterating the diverse factors that need to be considered in a unified assessment. When discussions were held at Michigan State University (MSU) in September 1973 to institute a feasibility study on waste heat utilization in Michigan, the consensus of opinion was that (1) adequate technical data for Michigan conditions could be developed from the results of field experiments conducted elsewhere, and (2) that a computer based approach could be used to get a low cost, rapid, overall assessment. The key feature of the proposed study was the interaction over the duration of the study by the small but multidisciplinary group. The group would be forced--by the necessity of developing mathematical models and analysis techniques--to isolate the dominant factors in previous research.

Preceding page blank

The tentative organization of the study was defined in the following way. The candidate agricultural uses of waste heat were selected from systems studied by others [1,2] with guidance from Dr. Larry Boersma [3] including preprint material from his research then in progress [4]. Adequate data seemed to be available to model pond warming for freshwater fish culture, greenhouse heating, soilwarming for vegetable production, and several uses. Because the initial goal in the computer study was to develop an analysis "tool", the study was limited to these three agricultural uses. The work by Boersma's group [4,p.243] showed that important parameters in several components of a combined waste heat system could be defined, but they did not have time available to develop an integrated system. A combined system is one consisting of several components that are independent. An integrated system is one where the size of the components, or their arrangement, or their operation is chosen to optimize a criterion. Previously Price [5,6] had integrated the sizes of three components (fish pond, greenhouse, and recreational lake) in a system using the criterion of maximum overall size of the component uses. It was optimized by a sensitivity study involving heat dissipation models and actual weather data. It was suspected that the cost of transporting the enormous quantity of low temperature water to the components of the agricultural system might be an important parameter [7,8]. Also a detailed economic analysis of the cost and revenue in the agricultural components would certainly be important to agribusiness [9]. Finally, a net present value criterion was taken as the criterion that would be used to integrate the three agricultural subsystems.

The eleven university personnel involved with the project for varying periods of time presented their preliminary conclusions based on this criterion in December 1975 [10]. During the first part of 1976, two of the personnel continued to made refinements on the study [11].

Examples could be given of papers in ther literature where waste heat computer models were used for the following goals: (1) development of mathematical models that accurately represent the collected experimental data for specific agricultural uses, (2) development of detailed design specifications for a specific subsystem, (3) approximate evaluation of an informative criterion, and (4) computational procedures to optimize some criterion. The essence of the MSU study involves the last two items. Informative information includes: cooling system net present value, enterprise shadow prices, agribusiness net present value, and environmental concerns.

Separable programming and a net present value criterion were a useful way to study the agricultural utilization of reject heat.

NET PRESENT VALUE

Net present value (NPV) is used by the electric utility industry to compare alternative conventional cooling systems. It is used to justify decisions on the cooling system to their investors and to state regulatory agencies.

The net present value method accounts for the time value of money in combining the investment in initial capital and annual costs. The NPV was used as the criterion that was optimized to define the size and temperatures of the agricultural subsystems. For the agricultural subsystems the net present value is of the form:

$$Z^{**} = \sum_{j=1}^{S} A_j \left[\sum_{i=1}^{n} \left(\frac{R - C}{(1 + r)^i} \right)_{ji} - K_j \right] \qquad (1)$$

where

Z^{**} = Net present value of the integrated subsystems, positive terms j for properly chosen subsystems,
S = Number of subsystems, agricultural plus reservoir,
A = Area or size of subsystem j, acres
R = Annual gross revenue for subsystem j,
C = Annual cost for subsystem j,
r = Discount rate or opportunity cost for capital,
K = Initial capital outlay for subsystem j,
n = Life of project or planning horizon, years,
i = Index for time,
j = Index for subsystem.

While this objective function is usable for determining the optimal subsystem sizes, it does not allow comparisons with conventional cooling methods because it does not account for the cost in transporting the warm water to the subsystems. The NPV for the water transport system is of the form:

$$Z^{*} = - \sum_{i=1}^{n} \frac{P^{*}_{i}}{(1 + r)^i} - K^{*} \qquad (2)$$

where the additional variables are

Z^{*} = Net present value of water transport system, or of conventional cooling system, always negative.
K^{*} = Capital outlay for water transport system,
P^{*}_{i} = Makeup power and other annual costs for water transport.

The same form for Z^{*} is used to compute the net present value of conventional cooling, with different suitable values for P^{*} and K^{*} of course. For the integrated agricultural system, $Z = Z^{*} + Z^{**}$.

The optimal integrated system contained 100 acres of tomato fields, 160 acres of catfish ponds, a 350 acre cooling lake, and no greenhouses. Bakker et al. [10] concluded that the NPV for this integrated agricultural system makes it competitive with conventional cooling methods. The slightly revised NPV comparisons from Meekhof [11] are shown in table 1. The NPV for the integrated agricultural system is less negative than the corresponding value for conventional cooling. Although the NPV is positive for each agricultural system, the value for the cooling reservoir has a slightly greater magnitude and is negative. When the NPV for the water transport shown in table 6 is included the total NPV is about as negative as that for a conventional cooling tower.

SHADOW PRICES

One of the programming techniques used to optimize the integrated system was linear programming (LP). The LP output gives shadow price information useful to agribusiness in decision making.

Shadow prices for activities (subsystems) indicates the effect on NPV of expanding the size of an enterprise. Shadow prices for constraints indicate the effect on the NPV for all subsystems of removing marketing and other constraints. Positive values are an indication of what entrepeneurs would pay for one additional unit. Table 3 [from 11] gives sample shadow prices for the optimal system. The negative value for waste heat in September indicates that adding a subsystem operating in that month would be desirable. The magnitudes of the other shadow prices show that the fish enterprise resource is the major limiting factor. An explicit constraint in the LP program limited the catfish enterprise to less than 160 acres.

Several resources are limited in the waste heat system and are represented by explicit and implicit constraints in the LP problem. Available markets limit the sizes of the tomato and catfish enterprises. The total quantity of waste heat is limited by the size of the electric power plant, assumed to be 1000 MWe. Because the reject heat is used to keep the subsystem temperatures above specified levels, the heat dissipation considerations discussed later imply (1) the maximum size of each subsystem is limited, and (2) a reservoir is required for both supplemental cooling after water is cooled below the specified temperature level and as a place to dump reject heat directly from the power plant when no subsystem can use it. Reservoir size required for this cooling is shown by month in table 2.

The LP output gives cost of forcing in activities. This serves to rank the relative profitability of enterprises and gives the order they would come into the system if more waste heat were available. More waste heat would become available if the sizes of subsystems currently included in the system were reduced. Table 4 [from 11] shows the greenhouse enterprise is less desirable than other possible enterprises including more units of soilwarming and fish culture operated at "non-optimal" temperatures. Greenhouses are undesirable because the capital and annual costs given in table 5 are higher than that for other systems, while their rate of heat dissipation occupies a middle position.

INSTITUTIONAL ARRANGEMENTS

Institutional aspects involve the contractural arrangements for the personnel to manage the waste heat system and for the capital to construct and operate the system. Possible options are listed in table 10. Costs incurred by a body seeking fee simple acquisition include payment of interest and principal on bonds raised to finance purchase of the land, administrative costs, cost of compensating the affected communities for property taxes foregone where land is purchased by a tax exempt body and leased back for agriculture-aquaculture. Should the utility company decide not to fully control the total integrated system and not raise the capital for one or all the separate subsystems, it can enter a contractual agreement with private entrepreneurs to supply waste heat water.

The options are limited by two positions held by the electric utility industry [12]: (1) reliability in the operation of the heat dissipation system is essential because the cost of plant shutdown or operation at reduced capacity is significant, and (2) direct utility management of the agricultural system is neither a goal nor outcome regardless of the financial incentives. This viewpoint limits the options to either purchase and leaseback or contractual firm. In purchase and leaseback the utility provides the capital and leases the facility to a single management firm which maintains and operates all subsystems over the lifetime of the power plant. In the contractual agreement a cooperative group of firms agree to construct and operate the agricultural system with the utility assuming the cost for the water transport system.

Table 6 [from 11] shows the net present value (NPV) comparisons for these three options. In purchase and leaseback free, agribusiness gets all the revenue and pays managerial and operating capital costs while the utility bears the capital cost for the subsystems and water transport system. In purchase and leaseback rent, agribusiness pays the managerial costs and costs for operating capital while the utility uses the remaining revenue to defray costs for capital for the subsystems and water transport system. In the contractual firms option, agribusiness bears all initial capital costs for the subsystems and the utility agrees to supply free waste heat and pays the firsm for their dissipation of the waste heat. A payment is necessary because the difference between the utility operation of only the water transport system and the utility operation of the total system is negative; hence, a payment would be set by bargaining between the utility and the firm. The details on the methods used to calculate the values in table 6 are given in Meekhof [11]; they involve an economic breakdown of the terms in equation (1).

POLICY CONSIDERATIONS

The MSU study was limited to heat dissipation, economic, and institutional arrangements. However, other factors affect the desirability of adoption of agricultural usage of waste heat. Some of these are contained in a study on energy parks in Michigan. Others are shown in studies by others on once through cooling to the Great Lakes.

Economic Expansion

Beneficial agricultural uses of waste heat were included as one collocated industry in an energy park study funded by the Federal Energy Administration [13]. Unlike concurrent energy park studies where the park would be located on federal land, the Michigan study assumed the hypothetical park could obtain privately held land near Harbor Beach in Michigan's thumb for the 9510 acre 23125 MWe complex (13 nuclear and 8 fossil fuel units).

This peripheral involvement in the energy park study occurred relatively early in the MSU study. The components suggested and their sizes are shown in tables 7 and 8. The sizes were determined by marketing constraints. The initial capital and annual costs were estimated from costs for enterprises not using waste heat. The heat dissipated was estimated from the optimal temperatures for the subsystems. Three interesting points emerged from the study. First, over seventy-five percent of the waste heat could not be used beneficially either at high temperatures for industrial and urban uses or at low temperatures for agricultural uses. Second, the measures for the benefits are related to economic expansion either as jobs created or as production from energy dependent industry. And third, it was postulated that some environmental groups would say "... (the park) should be accomplished only if the economic and social benefits overwhelm the economic, social,and environmental costs. The arguments must be unquestionably convincing and the documentation must be of unquestionable integrity".

This last point has implications even for the agricultural system, alone. The primary impact in the local economic environment of the agricultural system would be caused by the manner in which the land is acquired. The conversion of of 960 acres of land to purposes other than it has been traditionally used will affect the distribution of wealth and income in the community, the revenue base of the local governmental unit, existing input suppliers growth or decay, the long range planning incentives of the remaining agricultural land holders, and the existing marketing channels for agricultural and aquacultural commodities.

Once Through Cooling

The comparisons in table 1 assume the alternative conventional cooling is limited to cooling towers. If once through cooling were possible several of the results would be changed. The least negative conventional cooling system would be once through cooling. Because the reservoir would be eliminated, the NPV for the integrated agricultural system would improve. However, the discharge water temperature might vary by about fifteen degrees Fahrenheit [14,Fig.5] which would made it more difficult to design the agricultural subsystem to maintain an optimal temperature.

Environmental groups prevented the operation of the 700 MWe Palisades Nuclear Plant in 1971 until a commitment was made to install a mechanical draft cooling tower by 1974 [14]. The setting of agreed on environmental standards is a complex issue. Current concern includes [15,14]:

1. a lack of quantitative estimate of potential effects,
2. an increase of attached filamentous algae along the shoreline,
3. and the need to assure protection and propagation of a balanced indigeneous population of fish and ther aquatic species.

Legislationand court action over the last several years on these issues from a national perspective is outlined in a recent Congressional Research Service review [17]. A lower standard for thermal discharge but not discharge from the agricultural system is permitted if the native ecosystem survives intact [16]. Research to quantify the effects on once through cooling are in progress. An Argonne study found no adverse effects on the migratory behavior of fish tagged at the Point Beach Plant [18]. A continuing MSU Institute of Water Research study has found effects imparted to fish, if any, at the Monroe Plant on Lake Erie were soon dispersed into the lake population and became unidentifiable [19].

CONCLUSIONS FOR THE INTEGRATED SYSTEM

The mathematical variables used contained useful information, although their numerical values are only approximate. Thus, the net present value criterion is a useful way to structure a study of waste heat.

The comparative NPV's do not either clearly prove or disprove the concept of waste heat utilization. Because the net present value for the integrated agricultural system is not more negative than conventional cooling methods, beneficial use of waste heat is not clearly disproved.

Feasible institutional arrangements can be made, but the negative NPV implies the electric utility must indirectly pay the agricultural complex to dissipate heat.

Because water transport NPV dominates the analysis, the primary technical problem is the system for water transport. The water from the power plant to the 160 acres of fish ponds is carried by a concrete pipe 600 feet long and 10 feet in diameter.

NPV is not a totally acceptable criterion. The NPV certainly represents waste heat dependent economic expansion in a new industry (catfish culture in a cold climate), or in retaining an existing industry (heated greenhouses in the presence of rising natural gas prices and supplies), but in soilwarming can be positive even when no waste heat is utilized.

A small demonstration project would serve to replace the secondary and synthetic data used with more accurate primary data. It would also improve liaison with agribusiness.

SIMULATION DEVELOPMENT

The MSU study manipulated mathematical models rather than executing field experiments. An effort was made to structure the simulation and optimization in a manner familiar to the electric utility industry. Desalination of sea water by nuclear power plants [20] seemed to be a problem analogous to the MSU study on waste heat utilization. This view was expressed by the MSU group several years ago [21]. The analogy proved to be poor. It is worthwhile to outline this formulation of the waste heat problem. Although the computer code developed for it was not effective for optimization, the code is quite useful as a matrix generator for a linear (separable) programming formulation of the problem.

Initial Formulation

As an optimization problem the goal is to maximize the net present value. To accomplish this the four type of variables in the NPV equation (1) are manipulated: R, K, C, and A. The revenue (R) is the price of the product time the quantity produced. The production in each subsystem depends on its temperature: thus, models are needed to predict temperature for a specified quantity of reject heat and to predict biological growth rate at a given temperature. At the time it seemed reasonable to assume that the agricultural waste heat complex would contain as many as eight subsystems: soilwarming, fish culture, greenhouses, waste treatment, algae culture, irrigation, recreational lake, and animal shelters. Thus, the problem was one of allocating the heat between the competing subsystems. It also seemed reasonable to assume the initial capital (K) and combined annual pumping and operating costs (C) could be found after the system was optimized. Also the water transport NPV (Z*) was not assignable to any particular subsystem even based on the quantity of water used.

To develop the methodology or "tool", soilwarming and fish culture were chosen as good candidate subsystems. To satisfy the 1983 zero discharge requirements a cooling reservoir (lake) was included. Thus given a power plant with a known quantity of reject heat at a known temperature, the problem was (1) to allocate the heat to two competing agricultural subsystems on a monthly basis, and (2) to determine the size of each agricultural subsystem. Temperatures for optimal growth were avaiable in the literature. Applying this methodology to all eight candidate subsystems, the optimization would give (1) the best size for each subsystem (including some of size zero), and (2) would determine whether a particular subsystem should be operated at a "non-optimal" temperature in some months in order to make the best total system. Thus, the best uses would be selected and the problem of designing for utilization versus dissipation posed by Shapiro [23] would be solved.

Next an optimization technique was selected. The mathematical optimization technique would need to handle constraints because the sume of the reject heat allocated to the subsystems was limited by the reject heat available from the power plant. Because the equation to be developed for the heat transfer and biological growth had not been decided on a general mathematical programming procedure was selected. The "complex" method [22] met both these requirements. The method handles constrained, multi-variable problems and only requires computation of functional values, not gradients.

Subsystems

The major research effort in small scale waste heat field studies is defining the effect of temperature on growth, while a major economic concern is to have marketable products from the heated enterprises. The same concerns were present during the development of mathematical models for the revenue (R) in equation (1). The variable R is the first of four types of variables to optimize in equation (1). Selecting enterprises for the subsystems was not difficult: for candidate "crops" lists of optimal temperature for growth were developed and lists of comparative economic advantages of production were developed. The crops were the best from the combined list. Catfish was chosen for the fish enterprise because a detailed economic analysis was available [24]. Tomatoes and several other field crop varieties were selected for the soil warming enterprise and the economics developed at MSU. Ornamental flowers were selected for the greenhouse enterprise and the economics also modelled at MSU.

The price assumptions were: per pound channel catfish $0.30, per bushel tomatoes $5.50, ornamental flower rotation and price; 6-inch Chrysanthemums $2.60, 6-inch Poinsettias $3.25, 6-inch Lilies $2.60, 4-inch Geraniums $0.65.

The heat dissipation was modelled by algebraic energy balance equations. The optimization method assigned a quantity of heat to be dissipated to these equations and the corresponding subsystem temperature computed. For the fish pond and cooling reservoir, the three equations (10,15,17) in Edinger et al. [25] were solved simultaneously to yield the thermal exchange coefficient and equilibrium temperature. Values for Meyer's evaporation term were C_1=11 and f =0.00682 + 0.000682 W, where W is windspeed in mph. For the soilwarming system, the climatic data based Kendrick-and-Havens heating pipe model developed by Dewalle [26] was used. The heat required to maintain greenhouses at specified levels of temperature was computed with the model by Walker [27] with the ventilation rates adjusted for those used in waste heat greenhouses [28].

Having established the temperatures, the quantity of crops from the subsystems could be predicted. The growth of catfish used a model of the form:

$$\frac{dW}{dt} = \mu W \qquad (3)$$

where W is the weight of harvested fish and μ is a parameter modelled by a Lagrangian interpolation polynomial using data from Andrews [29].

The growth of field crops used a model from Paltridge and Denhold [30] of the form:

$$\frac{dG}{dt} = \alpha G H(s-t) - \beta G \qquad (4)$$

$$\frac{dW}{dt} = \beta G H(t-s) \qquad (5)$$

where G is vegetative material, W is harvested material (tomatoes), H is a step function, s is a switch time, and β is related to soil temperature. Both equations (3) and (4) are reasonable approximations to experimental data. Conventional production values were used for the greenhouse enterprise. The revenue (R) from each subsystem is simply the quantity of harvested material times its price.

Initial Optimization

The difficulties with the assumptions in the initial formulation became obvious when optimization was tried. These were related to: (1) the definition of a harvestable crop, (2) design of the water transport and (3) institutional limitations on the number of subsystems.

The formulated optimization problem allocates heat to the subsystems on a monthly basis. Only monthly climatic data was readily available. However, the harvestable material is only defined in a particular month for tomatoes and in a particular size interval for fish. This problem was handled by (1) optimizing on a yearly rather than a monthly basis and (2) using a sensitivity study to define input conditions for fish size at harvest. The monthly heat allocation pattern was represented as the sum of certain Walsh functions. Each function is a pattern with either unity or zero in a given month; i. e., to allocate the same unknown heat dissipation to the fish pond in the three months January, February and December the function has the form (1,1,0,0,0,0,0,0,0,0,0,1). The optimization routine found the best amplitudes for these functions. A total of five functions was adequate for the allocation to two systems over twelve months; thus, the number of optimization variables was reduced from 24 to 5. The use of Walsh functions would provide a reasonable approximation to a specific optimal temperature pattern obtained analytically by others for lobster culture [31].

Associated with each monthly heat dissipation is a water flow rate to each subsystem. When these monthly flow rates were used to determine a water transport system, a more serious problem arose. The flow rates are shown in table 9 for three Walsh functions for fish ponds and two for soilwarming.

The water transport system determines the next three optimized variables in the NPV equation: C, K, and Z*. The annual costs (C) are determined by the flow rate and the friction head loss in an established, well-known manner. The flow rates are given and the headloss is computed by assuming the pipe diameter and (1) assigning a roughness length, (2) using a Moody diagram to compute the dimensionless friction factor, and (3) using the Darcy-Weisbach equation to compute the head loss. This procedure was repeated trying different diameters until a satisfactory engineering design was obtained. The wide variation in flow rates shown in table 9 made this design not totally satisfactory. A computer program for the calculations involved was found too late in the project to be used [32]. Although more designs could have been tried using the program, the problem of the variations would have made it difficult to choose correct pipe diameters and pump sizes.

In the initial formulation it was assumed that the water transport design would not be a problem. In reality the flow rates shown in table 9 vary by a factor of 2 for soilwarming and by a factor of 5 to 15 for fish pond depending on whether the system operates in winter or not. Thus, the water transport costs need to be related to the optimized heat dissipation patterns in order to properly optimize equation (1). The best way to optimize might be to use LP to select from a set of discrete designs.

The value of the NPV given in equation (1) depends on the sizes specified for the subsystems (A) which is the last optimized variable. Heat dissipation considerations only place an upper bound on each subsystem size. The determination of the mix of sizes that optimize the NPV is determined largely by institutional factors. The terms in the NPV equation are basically a subsystem size times revenue generated (or indirectly heat dissipated). Some subsystems generate large revenues but dissipate heat poorly, others generate small revenues but dissipate heat effectively. Thus while revenue and heat dissipation considerations could indicate the best mix is all greenhouses or all fish culture doing so would possibly mean excessively large amounts of land and/or capital, or large seasonal excess capacity in operating capital, labor, or managerial skill. Also it could create an inability of the marketing structure in the region to handle all the agricultural and aquacultural commodies.

Thus, optimizing the NPV equation is not a problem of finding the best heat dissipation pattern and compatible size mix, but one of finding sizes that are feasible for the institutional arrangement. Table 10 is a list of possible institutional arrangements. As indicated previously the best options are: purchase and leaseback and contractual rent.

SIMULATION STUDY

The results presented in this paper were obtained using the following procedure. The problem of selecting optimal uses was considered more as a sensitivity problem than as an optimization problem. An LP program was used for the major analysis with technical coefficients set from the "complex" program used as a matrix generator. The constraint section of the "complex" program was used to set pairs of subsystem size and temperature levels. The constraints on heat and flow rates were checked with the subsystem models. Associated with the temperature levels are crop growth rates and hence revenue. Enterprise costs were calculated in detail at a few sizes and separable programming was used to interpolate between these values.

Separable Programming

Several related procedures are called separable programming. The MSU study used the procedure introduced by Charnes and Lemke [33]. The separable technique was used to (1) handle the nonlinearity in the cost coefficients and (2) to determine whether subsystems should be operated at non-optimal temperature. Other aspects of the LP technique were (3) selecting a reservoir size from the twelve monthly values, and (4) combining capital and net revenue internally to obtain the net present value.

The form of the tableau is illustrated in table 11 for a simple set of conditions. The system represents three components: a fish enterprise operated at the optimal temperature, a fish enterprise operates at a non-optimal temperature, and a cooling lake. The year has two time periods: summer and winter. The fish enterprises only operate in summer. The variables in the tableau are:

d = Discount factor obtained by summing the opportunity cost over the planning horizon, with (R-C) outside the summation,
H = Heat dissipated for a size S in the agricultural subsyste, million BTU per hour,
Q = The quantity of reject heat, million BTU per hour,
N = The positive net revenue (R-C) from equation (1)
K = Initial capital from equation (1),
S = Size of the subsystem that detailed costs were compiled, it can be zero,
S* = Size at a level 2 design temperature,
h = Heat dissipated by the reservoir per acre, million BTU per hour per acre.

The way the four computational features are achieved can be understood by studying the tableau.

Several aspects of the tableau and programming method are of interest. The heat dissipation rates, H, are non-negative; that is, heat is transferred from the subsystems to the environment,not vice versa. Hence the maximum size of each subsystem is limited by heat dissipation considerations since the quantity of heat rejected from the power plant is limited. More importantly the agricultural subsystems only contribute to the net present value if they also dissipate heat.

The size of the agricultural subsystem is limited to be between sizes S_1 and S_2 by the separable constraint; thus, S_1 should be set to zero if the subsystem if not necessarily in the integrated system. Unlike the "complex" program where the subsystem costs could not be related to the water transport costs and design, different discrete water transport designs can be specified as level 1 and level 2 subsystems in the LP program. The "complex" program has some features that can be used to set technical coefficients: given a quantity of heat to be dissipated it will check the implicit constraints on power plant temperature and on designed pumping rates and obtain a feasible subsystem operating temperature for heat transfer considerations.

Program Notes

The mathematical methods developed by the MSU group and those developed by the Price group at Cornell[34] have helped to isolate the key variables in the waste heat problem.

Several aspect and potentials of the LP programming method beyond the goals of the MSU study should be noted.

The technique used for internal discounting has been used in another context to weight monetary and pollution costs [35]. This could be used in waste heat by replacing the variable S with a measure of production of catfish wastes and a weight analogous to the discount put in the objective function in order to find a least cost, least pollution integrated system.

The pumping costs imply that the benefits from the agricultural system is derived at the cost of using limited energy resources to pump the water. This trade-off has been discussed in a nice mathematical way in the context of altering the thermal plume by pumping by others [37]. In the LP analysis the variable S could be replaced by a measure of energy usage and the weighted NPV obtained.

Finally, linear (separable) programming is also a method familiar to the electric utility industry in the context of designing a dry cooling tower [38] and better for the waste heat problem than [20,21].

REFERENCES

1. Mathur, S. P. and R. Stewart (1970) Conference on Beneficial Uses of Thermal Discharges, New York State Department of Environmental Conservation, Albany New York, September 17-18.
2. Yarosh, M. (1971) Proceedings of the National Conference on Waste Heat Utilization, NTIS CONF-711031, Gatlinburg Tennessee, October 27-29, 337pp.
3. Boersma, L. L. (1973) Utilization of Power Plant Waste Heat, Michigan State University, Institute of Water Research Seminar, December 17-18.
4. Boersma, L. L., L. R. Davis, G. M. Reistad, J. C. Ringle and W. E. Schmisseur (1974) A Systems Analysis of the Economic Utilization of Warm Water Discharge from Power Generating Stations, Oregon State U., Engineering Experiment Station Report No. 48, 257 pp.
5. Price, D. R. (1971) Utilization of Thermal Discharge from Power Plant Condensers, Ph. D. Thesis Purdue U., Dissertation Abstract 32-B, 4558, No. 72-8011.
6. Price, D. R. and R. M. Peart (1973) Simulation Model to Study the Utilization of Waste Heat Using a Multiple Reservoir and Greenhouse Complex, J. Environmental Quality, 2 216-224.
7. Ackermann, W. C. (1971) Research Needs on Waste Heat Transfer from Large Sources into the Environment, Zion Illinois Conf., NTIS PB-219056, 41pp.
8. Hill, C. T. (1972) Thermal Pollution and its Control, Environmental Affairs J., 2 406-420.
9. Johns, R. W., R. J. Folwell, R. T. Dailey and M. E. Wirth (1971) Agricultural Alternatives for Utilizing Off-Peak Electrical Energy and Cooling Water, Department of Agricultural Economics, Washington State University, 123pp.
10. Bakker-Arkema, F. W., L. J. Connor, R. L. Meekhof, G. E. Merva, M. G. Roth, I. P. Schisler, V. M. Schultink, B. A. Stout, R. L. Tummala, J. C. VanKuiken and L. P. Walker (1975) Waste Heat Utilization from Power Plants in Agriculture, ASAE papers Number 75-3526 to 75-3532, Available from ASAE, St. Joseph, Michigan USA.
11. Meekhof, R. L. (1977) The Economic Feasibility of Utilizing Waste Heat from Electrical Power Plants in Integrated Agricultural and Aquacultural Systems Under Michigan Conditions, Ph. D. Thesis Department of Agricultural Economics, Michigan State University, 204pp.
12. Rochow, J. J. and R. L. Hall (1975) Waste Heat Utilization from Power Plants in Agriculture: Industrial Viewpoint, ASAE paper No. 75-3527
13. Schisler, I. P., R. L. Meekhof, V. M. Schultink, L. P. Walker (1975) Agricultural-Aquacultural Systems, in A Program to Study the Feasibility of Energy Park Sites in Michigan, FEA Contract No. CO-05-50316-00, Environmental Research Institute of Michigan.

14. Reynolds, J. Z. (1974) Control of Thermal Discharge to the Great Lakes, A.I.Ch.E. Symposium Series No. 136, 258-265.
15. Fetterolf, C. (1970) Are We in Hot Water with Thermal Discharge?, Michigan Water Pollution Control Association Papers, 45 33-40.
16. Rasmussen, F. (1973) The Federal Water Pollution Control Act Amendments of 1972, Wisconsin Law Review, 892-907.
17. Donnelly, W. H. (1973) Factors Affecting Federal Research for Thermal Effects, pp 4-24, in Energy Production and Thermal Effects, Ann Arbor Science Publishers.
18. Romberg, G. P., S. A. Spigarelli, W. Prepejchal and M. M. Thommes (1974) Migratory Behavior of Fish Tagged at a Nuclear Power Plant Discharge into Lake Michigan, Proceedings Conference on Great Lakes Research, 17 68-77.
19. Lavis, D. S. and R. A. Cole (1976) Distribution of Fish Population near a Thermal Discharge into Western Lake Erie, MSU Institute of Water Research Report 32.9, 51pp NTIS PB251208.
20. Fan, L. T., C. L. Hwang, N. C. Pereira, L. E. Erickson and C. Y. Cheng (1972) Systems Analysis of Dual-Purpose Nuclear Power and Desalting Plants 1 Optimization, Desalination 11 217.
21. Schisler, I. P. (1974) Simulation Studies to Select Optimal Agricultural/Aquacultural Uses of Waste Heat, pp 53-55 in Future Developments in Waste Heat Utilization, Oregon State U., Engineering Experiment Station Circular No. 49, 110pp.
22. Richardson, J. A. and J. L. Kuester (1973) Algorithm 454: The Complex Method for Constrained Optimization, Comm ACM 16 487-489.
23. Shapiro, H. N. (1974) Agricultural Uses of Waste Heat: A Discussion of Constraints, pp 96-97 in OSU EES Circular 49.
24. Foster, T. H. and J. E. Waldrop (1972) Cost Size Relationships in the Production of Pond Raised Catfish for Food, Mississippi State U. AES Bulletin No. 792, 69pp.
25. Edinger, J. E., D. W. Duttweile and J. C. Geyer (1968) the Response of Water Temperature to Meteorological Conditions, Water Resources Research, 14 1237-1244.
26. DeWalle, D. R. (1974) Model for Estimation of Surface Temperature of Heated Soil from Climatic Data, pp 182-195 in An Agro-Power-Waste Water Complex for Land Disposal of Waste Heat and Waste Water, Pennsylvania State U., Institute Land Water Resources No. 86.
27. Walker, J. N. (1965) Predicting Temperature in Ventilated Greenhouses, ASAE Transactions, 445-448.
28. Ashley, G. C., R. V. Stansfield, A. M. Flikke and L. L. Boyd (1974) Design and Operating Experience with a Research Greenhouse Heated and Cooled with Warm Water, pp 76-81 in Oregon State University Circular 49.
29. Andrews, J. W.,L. H. Knight and T. Murai (1972) Temperature Requirements for High Density Rearing of Channel Catfish from Fingerling to Market Size, Progressive Fish Culturist, 34 240-241.

30. Paltridge, G. W. and J. V. Denholm (1974) Plant Yield and the Switch from Vegatative to Reproductive Growth, J. Theoretical Biology, 44 23-34.
31. Botsford, L. W., H. E. Rauch and R. A. Shleser (1974) Optimal Temperature Control of a Lobster Plant, IEEE Transactions Automatic Control, 19 541-543.
32. Carnahan, B. and J. O. Wilkes (1972) Simulation of a General Piping and Pumping Network, pp 71-116 in Computer Programs for Chemical Engineering Education: Design, CACHE.
33. Charnes, A. and C. E. Lemke (1954) Minimization of Nonlinear Separable Functionals, Naval Research Logistics Quarterly, 1 301-312.
34. Price, D. R., D. A. Haith, and B. A. Bucholz (1975) System Studies of Agricultural Uses of Power Plant Condenser Effluent, ASAE Paper No. 75-3543.
35. Candler, W. and M. Boehlje (1971) Use of Linear Programming in Capital Budgeting with Multiple Goals, American J. Agricultural Economics, 53 325-330.
36. Candler, W. (1973) Linear Programming in Capital Budgeting with Multiple Goals, pp 416-428 in Multiple Criteria Decision Making, University of South Carolina Press.
37. Sill, B. L. and A. Gnilica (1976) Optimal Discharge of Power Plant Cooling Water, Progress in Astronautics and Aeronautics, 36 281-293.
38. Ecker, J. G. and R. D. Wiebking (1975) Application of Geometric Programming to Energy Related Design Problems, pp 153-175 in Energy: Mathematics & Models, SIAM.

ACKNOWLEDGEMENTS

This research was supported by Consumers Power Co. (Jackson, Mi.), the Michigan Agricultural Experiment Station, and Detroit Edison (Detroit, Mi.). The results presented are a product of the eleven member MSU research team, especially material adapted from the doctoral thesis by Ron Meekhof. Advise was provided by J. J. Rochow, R. L. Hall, J. H. Kline, and R. E. Albrecht from the sponsoring electric utilities. Views expressed are those of the main author.

TABLE 1
COMPARISON OF COOLING METHODS NET PRESENT VALUE (Z) (IN THOUSANDS OF DOLLARS)

Discount Rate and Planning Horizon	Agricultural Method at Optimum	Wet Mechanical Draft	Wet Natural Draft
10% at 30 years	-43395	-56912	-64344
12% at 30 years	-38783	-52123	-59255
15% at 30 years	-33708	-46923	-53730
10% at 25 years	-42255	-55690	-63046
12% at 25 years	-38092	-51382	-58423
15% at 25 years	-33465	-46568	-53352

TABLE 2
MONTHLY RESERVOIR REQUIRED FOR SUPPLEMENTAL COOLING (ACRES)

Month	Area	Month	Area
January	151	July	350
February	143	August	357
March	195	September	357
April	200	October	242
May	313	November	218
June	329	December	154

TABLE 3
SHADOW PRICES FOR OPTIMAL SYSTEM
(IN THOUSAND OF DOLLARS PER ACRE)

	10% at 25 years	15% at 25 years	10% at 30 years	15% at 30 years
Fish Pond Activity	96.6	69.2	100.	69.9
Soilwarming Activity	1616.	937.	1713.	952.
Fish Pond Resource	39.3	27.3	40.9	27.7
Soilwarming Resource	17.1	11.1	18.6	11.3
(IN THOUSAND OF DOLLARS PER MILLION BTU)				
September Waste Heat Resource	-0.975	-0.766	-1.01	-0.774

TABLE 4
COMPETITIVE POSITION OF NON-BASIS ACTIVITIES
(IN THOUSANDS OF DOLLARS PER ACRE)

Order	Activity	Cost
5	Tomatoes, 75 Acres at 10 % Below Optimal	282.
6	Tomatoes, 75 Acres at Optimal Temperature	295.
9	Fish Ponds, 160 Acres at 10% Above Optimal	482.
14	Greenhouse, 1.25 Acres at Optimal Temperature	622.

TABLE 5
ECONOMIC COEFFICIENTS IN NPV EQUATION FOR OPTIMAL SYSTEM
(IN THOUSANDS OF DOLLARS PER ACRE)

Subsystem	Initial Capital, K	Annual Costs, C	Annual Revenue, R
Fish Pond	11.9	11.4	16.5
Soilwarming	7.75	2.09	4.18
Greenhouse	260.	239.	
Reservoir	10.5	1.61	ZERO

TABLE 6
MANAGEMENT COMPARISONS
NET PRESENT VALUE
(IN THOUSANDS OF DOLLARS)

Rate and Horizon	Total Utility Operation	Purchase Leaseback Free	Purchase Leaseback Rent	Utility Water Transport
10% at 30 years	-43395	-60542	-53146	-39967
12% at 30 years	-38783	-53372	-47052	-34905
15 % at 30 years	-33708	-45623	-40471	-29424
10% at 25 years	-42255	-60738	-53616	-40676
12% at 25 years	-38092	-52293	-46139	-34123
15% at 25 years	-33465	-45090	-40018	-29034

TABLE 7
COLLOCATED INDUSTRY AND AGRICULTURE
HYPOTHETICAL ENERGY PARK AT HARBOR BEACH

Industry	Capacity
Paper Mill	2,000 tons per day
Chemical Complex	$240 million annual sales
Petroleum	250,000 bbls per day
Coal Gasification Plant	250 million cfd of gas (300 Btu/cu ft)
Mini Steel Mill	150,000 tons per year
Biocomplex	**Capacity**
Irrigation	3200 acres outside park
Catfish Culture	500 acres in 20 acre ponds
Greenhouse	300 acres (vegetables and flowers)
Grain Drying, Low Temperature	20 million bushels per year
Waste Treatment	85 acres of algae ponds
Park City	
District Heating	135,000 people in 10 square miles.

TABLE 8
PARK REQUIREMENTS
HYPOTHETICAL ENERGY PARK AT HARBOR BEACH

Measure	POWER PLANT	INDUSTRIAL PARK	BIO-COMPLEX	PARK CITY	TOTAL
Land (acres)	9510	3000	960	6400	19870
Capital (million dollars, 1975)	10490	1000	59	. .	11549
Operating Labor (man equivalent)	1600	6400	300	. .	8300
Water Usage (million gpd)	170	52	27	. .	249
Heat Dissipated (million BTU/hr)	117800	14000	19200	2850	153850

Source: [13] volume 1, tables 1 and 24.

TABLE 9
MONTHLY FLOW RATES FOR OPTIMAL SYSTEM
(IN THOUSANDS OF GALLONS PER MINUTE)

Month	Fish Pond	Soilwarming	Cooling Reservoir
January	463.6	...	86.4
February	342.1	...	207.9
March	130.0	...	420.0
April	128.9	...	421.1
May	29.9	10.9	509.2
June	31.1	6.2	512.7
July	32.6	6.3	511.1
August	33.2	...	516.8
September	33.9	...	516.1
October	271.6	...	278.4
November	170.9	...	379.1
December	527.8	...	22.2

TABLE 10
SITE ACQUISITION AND MANAGEMENT OPTIONS

- Fee Simple Acquisition
  - Purchase and Manage
  - Purchase and Leaseback
  - Purchase and Resale on Condition

- Less than Fee Simple Acquisition
  - Purchase Easements

- Contractural Agreements - For Rent Property Interest
  - Waste Heat Water Cooperative
  - Contractual Arrangement

- Public Authority

TABLE 11
SCHEMATIC REPRESENTATION OF THE SIMPLEX TABLEAU

	Slack Winter Reject Heat	Slack Summer Reject Heat	Area Fish Level 1	Area Fish Level 2	Capital Both Fish and Lake	Net Revenue Fish Discounted	Cooling Lake Costs Discounted	Lake Heat Dissipated Winter	Lake Heat Dissipated Summer	Cooling Lake Size Annual	Fish Size 1 Level 1	Fish Size 2 Level 1	Fish Size 1 Level 2	Fish Size 2 Level 2		Constraint
Objective Function	0	0	0	0	-1	d	-d	0	0	0	0	0	0	0	.=.	Z**
Winter Reject Heat	0	0	0	0	0	0	0	1	0	0	0	0	0	0	.=.	Q
Summer Reject Heat	0	0	0	0	0	0	0	0	1	0	H_1	H_2	H_1^*	H_2^*	.=.	Q
Winter Lake Heat	1	0	0	0	0	0	0	1	0	$-h_1$	0	0	0	0	.=.	0
Summer Lake Heat	0	1	0	0	0	0	0	0	1	$-h_2$	0	0	0	0	.=.	0
Capital Transfer	0	0	0	0	-1	0	0	0	0	k_2	K_1	K_2	K_1^*	K_2^*	.=.	0
Revenue Transfer	0	0	0	0	0	-1	0	0	0	0	N_1	N_2	N_1^*	N_2^*	.=.	0
Lake Cost Transfer	0	0	0	0	0	0	-1	0	0	C	0	0	0	0	.=.	0
Level 1 Separable	0	0	0	0	0	0	0	0	0	0	1	1	0	0	.=.	1
Size Transfer	0	0	-1	0	0	0	0	0	0	0	S_1	S_2	0	0	.=.	0
Level 2 Separable	0	0	0	0	0	0	0	0	0	0	0	0	1	1	.=.	1
Size Transfer	0	0	0	-1	0	0	0	0	0	0	0	0	S_1^*	S_2^*	.=.	0
Separable Mix	0	0	0	0	0	0	0	0	0	0	1	1	1	1	.=.	2

OMIT

The Utilization of Waste Heat From Large Thermal Power Plants

L. N. Reiss,
Commonwealth Associates Inc.

The utilization of waste heat from large thermal power plants must be considered in the selection of plant sites to develope total energy systems. Established uses and current research projects are discussed including aquaculture, agriculture and district heating. Several potential uses are examined.

Preceding page blank

omit

VI-A-29

ABSTRACT

USE OF WASTE HEAT FOR AQUACULTURE AND AGRICULTURE IN CONJUNCTION WITH A SURROGATE NUCLEAR ENERGY CENTER

R. K. Sharma, P. A. Merry, J. D. Buffington, S. W. Hong, C. Luner

Argonne National Laboratory

A clustering trend is evident in the siting of nuclear power plants, with a number of sites having two to four units. Recent studies have been made of possible sites and the feasibility and practicability of clustering units at nuclear energy centers (NEC). One such study was the U. S. Nuclear Regulatory Commission's "Nuclear Energy Center Site Survey - 1975" performed in part by Argonne National Laboratory. A suitable surrogate site was chosen in the upper St. Lawrence region of New York and the probable impacts associated with construction and operation assessed.

Siting and development of an NEC poses many problems associated with land and water use. However, some of these problems might be somewhat mitigated if, in addition to the production of electricity, the land and water were used for ventures such as aquaculture or agriculture. Not only would land be available, but there would be a constant and reliable source of heated water. For instance, for a 20-unit center (1200 MWe/unit) using once-through cooling, water would be discharged at a rate of approximately 37,000 cfs at a ΔT of about 20°F. With an evaporative "closed-cycle" cooling system operating at a concentration factor of six, blowdown would be about 120 cfs, the temperature being dependent on local meteorological conditions. With either type of cooling system, vagaries of operation would be dampened by the number of units. At the New York "surrogate" NEC, fish farming and truck farming might be profitably undertaken. Since

Preceding page blank

cooling water would have to be pumped over 25 miles from the St. Lawrence River, use of the water for aquaculture or agriculture could help offset the capital and operating expense of pumping the water. Most of the waste heat at the NEC would be disposed of through the latent heat of evaporation in the cooling towers (1.6×10^{11} Btu/hr, water evaporating at 580 cfs). With a fish farm or greenhouse system combined with the cooling tower system, more heat could be disposed of as sensible heat, thereby reducing evaporative losses and conserving water. A side benefit might be the reduction of meteorological impacts, such as snow enhancement, associated with the wet-evaporative cooling system.

The feasibility of aquaculture and agriculture in conjunction with nuclear energy centers will be discussed from such perspectives as land and water use, biology, water quality, nutrition, economics, marketing, and regulation.

Omit

VI-A-31

INTEGRATED POWER, WATER, AND WASTEWATER UTILITIES

Charles W. Mallory
Henry M. Curran, Ph.D.
Jack P. Overman

Abstract

Integrated power, water, and wastewater utilities have the potential for more efficient utilization of land and water resources, producing a net reduction in undesirable process effluents, and achieving at reduced cost many of the environmental quality goals sought by our nation. In particular the use of waste heat for the beneficiation of wastewater treatment is sufficiently promising to merit further investigation. An integrated facility was studied which supplies 1000 Mw of electric power, provides secondary treatment for 50 MGD of wastewater, and produces 47.5 MGD of high quality potable water utilizing low quality steam and waste heat. A research and development program was defined for further design and performance information necessary for full scale integrated facilities. Additionally, another concept was marginally explored for utilizing waste heat in advanced wastewater treatment by using secondary treated wastewater for power plant cooling and evaporation to concentrate pollutants and reduce the amount of wastewater requiring advanced wastewater treatment.

HITTMAN ASSOCIATES, INC.
9190 RED BRANCH ROAD
COLUMBIA, MARYLAND 21045

SESSION VI-B

NUMERICAL MODELING II

omIT

VI-B-33

ABSTRACT

COMPARISON OF PREOPERATIONAL HYDROTHERMAL PREDICTIONS AND OPERATIONAL FIELD MEASUREMENTS AT THREE NUCLEAR POWER PLANT SITES

G. J. Marmer and A. J. Policastro

Division of Environmental Impact Studies
Argonne National Laboratory

This paper evaluates the performance of the preoperational hydrothermal modeling and field data acquisition carried out at three nuclear power plant sites where once-through cooling is employed. The purpose of our study was to assess the quality of operational field data on plume dispersion acquired by the utilities to satisfy environmental technical specifications and water quality standards. This work, in part, involved the assessment of the preoperational thermal plume modeling carried out by the utilities for the plants. The three sites chosen for our study were: the Kewaunee (surface discharge) and Zion (submerged discharge) plants located on Lake Michigan and the Quad Cities plant (submerged discharge) located on the Mississippi River. Each plant had detailed preoperational plume predictions available (for Kewaunee, Zion -- an analytical model; for Quad Cities -- a physical hydraulic model) as well as a large quantity of plume data taken after the plant was operational.

At Kewaunee, the Pritchard model was employed to predict plume characteristics under various outfall and ambient conditions before plant operation. Operational measurements revealed that the model underpredicted plume dispersion in the near field and grossly overpredicted dispersion in the far field. Plume lengths were within a factor of 3 of predictions, plume widths within a factor

of 2 and plume areas within a factor of 10. The utility tuned the Pritchard model to the Kewaunee data and was subsequently able to fit the data to within a factor of 2 in centerline length and width, and a factor of 5 in area. Field measurements were generally satisfactory except that plumes were difficult to measure under stratified conditions. Unfortunately, no plume measurements were made in the winter when the plumes were expected to be largest.

At Zion, the Pritchard model was employed to predict plume characteristics before plant operation. This model gave satisfactory forecasts in only 20% of the cases and these were when the model assumptions were most nearly satisfied (no stratification, no reentrainment, one-unit operation). Otherwise, surface area predictions were often optimistic by an order of magnitude. A modified version of the model was developed by Pritchard to handle these effects, but in this form, the model is not predictive. Some input quantities needed by the model require examination of the plume data themselves or else require some model-data fitting. Field measurements were very good and the use of dye under stratified ambient conditions was extremely helpful in delineating the extent of the plume.

For the Quad Cities plant, a physical model was used to design the discharge configuration. These studies employed an undistorted model in the near field to simulate jet diffusion and buoyant spreading and a distorted model in the far field to determine how the discharge of the heated effluent should be distributed across the river. Tests were conducted for the minimum river flow, the average river flow, and for two intermediate flows. Twenty-six field surveys were made over a two-year period to validate the laboratory model; the data obtained were quite good. Unfortunately, the actual river flows were above average for most of the surveys which prevented direct comparisons of model predictions with the field data. The difficulty in matching prototype ambient conditions with model conditions underscores a major problem in validating physical hydraulic model predictions. However, in all field surveys, the temperature standards were always satisfied.

Work done under the auspices of the Nuclear Regulatory Commission.

22-45-48

VI-B-37

THERMAL STRATIFICATION AND CIRCULATION OF WATER BODIES SUBJECTED TO THERMAL DISCHARGE

A. N. Nahavandi and M. A. Borhani
New Jersey Institute of Technology
Newark, New Jersey U.S.A.

ABSTRACT

A three-dimensional analytical model for large water bodies is presented. Time histories and spatial distribution of pressure, velocity and temperature in water bodies, subjected to thermal discharge, are determined employing a digital computer. The dynamic response is obtained for a rectangular water body by applying a finite difference method to the mass, momentum, and energy balance equations. The distinctive feature of this analysis, as compared to previous studies, is the calculation of pressure and water level from equations of motion without simplifying assumptions such as hydrostatic pressure approximation and rigid-lid concept. The mathematical formulation is verified by applying this analysis to cases where the final steady state flow patterns have been determined analytically or experimentally by others. The problem of thermal discharge entering a river is then analyzed. The time histories of the velocity and temperature distribution are obtained. These results provide the values of temperature rise and the rate of temperature rise needed for the assessment of thermal pollution in water bodies.

INTRODUCTION

Thermal power and industrial processing plants use large quantities of cooling water from natural or artificial water bodies and return the water to the source at higher temperatures. When the thermal discharge from a plant, into a water body, raises the water temperature by such an extent as to damage aquatic life or other legitimate uses of the water source, some degree of thermal pollution exists.

To assess the extent of a thermal pollution, utilities, ecologists, federal and state agencies as well as the public are interested in determining the space and time distribution of temperature within a water body, when it is subjected to a prescribed thermal load.

The theoretical analysis of the dynamic behavior of a large water body, subjected to thermal discharge, is based on the solution of space- and time-dependent conservation and state equations. Conservation of mass, momentum, and energy for the water flow in the impoundment together with the equation of state, provide a sufficient number of partial differential equations and algebraic relations in space and time for the solution of the problem. Although, these equations have been known for over a century, due to their highly nonlinear nature, a direct closed form analytical solution is considered practically impossible for most general cases involving realistic geometries and boundary conditions. The available mathematical solutions of problems involving thermal discharge are severely limited by the many simplifying assumptions made in order to achieve a solution. In fact, analytical solutions to the problems of thermal discharge are obtained only for problems involving simple geometry and boundary conditions. Solutions to more realistic geometries and boundary conditions can be sought only by the development of computer modeling in three-dimensions under transient conditions.

Current three-dimensional computer simulation of thermal discharge into water bodies are based on a number of simplifying assumptions discussed hereunder:

1. Compliance with the Conservation of Mass and Momentum

Generally, the three components of water velocity are found from the longitudinal, lateral, and vertical momentum equations. These three components of velocity should satisfy the conservation of mass equation. A major difficulty arises when simultaneous compliance with the principles of conservation of mass and momentum cannot be ensured. Under the Boussinesq approximation, the conservation of mass reduces to zero divergence for the water velocity (with no mass storage term) i.e. the sum of all inflows to and outflows from any fluid control volume in the flow field must vanish. Since the new velocity components, calculated by the integrations of the momentum equations do not necessarily satisfy the continuity equation, the mass balance would be disturbed, thereby yielding a small surplus or deficit inflow at certain control volumes. To resolve this dilemma, Brady and Geyer [1] hypothesize that the surplus or deficit inflows redistribute in all directions by equal magnitude. Obviously, the disadvantage of this velocity adjustment technique is that the adjusted velocities no longer satisfy the momentum equations. Considering a water body, such as a river, flowing longitudinally with a laterally uniform velocity distribution, and applying the appropriate boundary conditions on the lateral velocities at the thermal discharge location, they found that the out-of-balance surplus inflow to each adjacent cell is exceptionally large. When their model attempts to distribute this surplus inflow among the surrounding fluid cells, the resulting vertical velocity adjustment becomes excessively large which aborts the run. Brady and Geyer, referred to this problem as the "vertical overresponsiveness of the model" and devised schemes to suppress the associated undesirable vertical fluctuations by either: 1) temporarily suppressing vertical redistribution such that each fluid layer achieves its own mass balance independently; or 2) temporarily enforcing a rigid lid at the fluid free surface such that a zero vertical velocity is maintained at the most upper layer of the model at every fluid cell. The rigid lid assumption is used by many authors to simplify the solution to the stratification and circulation in water bodies [2, 3, 4]. Obviously, this situation calls for an improved approach for a simultaneous compliance with the conservation equations of mass and momentum.

2. Surface Flow Distribution

The treatment of the slope variation at the water free surface constitutes another major difficulty. The upwelling (or downwelling) flow at the surface creates positive (or negative) surge waves [5, 6]. The mathematical modeling of these phenomena under unsteady flow conditions is complicated. To resolve this difficulty Waldrop and Farmer [7] first assumed that the vertical component of velocity near the surface will be redirected in the horizontal direction (in x and y directions) and the surface will move. Later Waldrop and Farmer [8] in a major effort to resolve the surface flow distribution problem introduced a mass balance at the free surface and extended their horizontal momentum equations to elements near the water surface. This situation calls for further studies of the behavior of the free surface under unsteady flow conditions.

3. Pressure Distribution

The velocity components in the flow field are extremely sensitive to values of nodal pressures. Slight changes in the pressure distribution would affect the circulation in the water body considerably. The calculation of the correct pressure distribution is, therefore, of paramount importance. Most authors [9, 10, 11, 12, 13, 14, 15] assume that the total dynamic pressure at each point in the flow is equal to hydrostatic pressure obtained under static conditions. This assumption, referred to as hydrostatic approximation, leads to inaccuracies in regions of severe upwelling and downwelling which will adversely affect the correctness of circulation velocities. Thus, a better technique for the computation of the pressure field is called for.

4. Numerical Stability

Calculations of space and time increments for obtaining a stable numerical solution of partial differential equations of mass, momentum and energy conservation is a difficult task. Most authors resort to overly simplified criteria for the establishment of the upper bound of the integration time step for an assumed set of space increments. Brady and Geyer [1] state that the maximum integration step appears to be limited by relationships between the velocities and the smallest cell dimensions in each direction. Waldrop and Farmer [7], and Harlow and Welch [16] resort to a stability limit calculated on the basis of one-dimensional, unsteady incompressible flow equations with a free surface. This limit imposes an upper bound on their integration time step equal to the ratio of the smallest cell size and the surface wave speed. More accurate means for the prediction of the space and time increments are needed.

Most authors believe that much work is still required to refine various features of the present unsteady three-dimensional computer models before the present models can be applied to situations involving significant stratification effects, or fluctuations in flow in water bodies.

The main objectives of the present study are as follows:

1) To develop an improved three-dimensional analytical model for the mathematical description of a large rectangular water body subjected to a thermal discharge.

2) To develop a numerical integration technique for solving the above mathematical model on a digital computer.

3) To develop a digital computer program for predicting the thermal stratification and circulation phenomena in a given rectangular water body subjected to thermal discharge and to determine the time histories and spatial distribution of pressure, velocity and temperature fields within the water body.

The major contribution and distinctive features of the present study, as compared with the previous works in this general area, can be summarized as follows:

A) Compliance with the conservation of mass and momentum is obtained by the introduction of two flow regions in the entire flow field: a) the water-level region containing a portion of water near the free surface in which the water level rises or falls, as the case may be,during the dynamic solution; and b) the sub-water-level region located under the water level region which remains totally filled with fluid at all times during the transient. As will be seen later, the superimposition of a three-dimensional grid on these two regions facilitates the simultaneous compliance with the principles of conservation of mass and momentum for the entire flow field without any mass imbalance.

B) A different set of differential equations for the conservation of mass, momentum and energy is applied to the cells located in the water-level and sub-water-level flow regions. This is necessary because the cells in the sub-water-level region have a variable height while the cells in the sub-water-level region have a constant height.

C) The pressure distribution is obtained by combining the momentum and continuity equations. This feature eliminates the need for the hydrostatic pressure approximation.

D) A detailed numerical stability analysis is performed which provides accurate criteria for the selection of the space and time increments.

MATHEMATICAL FORMULATION

Simplifying Assumptions

The mathematical formulation in this study is based on the following assumptions:

1) The equations of motion, energy and continuity are applied in their time-smoothed form to turbulent incompressible three-dimensional flow with Cartesian coordinates, as shown in Figure 1, with z positive upward.

2) It is assumed that Boussinesq's approximation applies. In other words, densities are treated as constants except in terms involving gravity. This allows natural circulation to take place. Furthermore, density in the body force term is considered to be a function of temperature only.

3) The effects of turbulence are modeled by using eddy transport coefficients. Horizontal and vertical momentum eddy viscosities and thermal eddy diffusivities are considered as constants throughout the body of water though different magnitudes for horizontal and vertical directions.

4) It is assumed that there are no internal heat sources and the heat exchange between the water body and the atmosphere takes place near the water free surface.

5) Loss of mass due to evporation at the surface and conductive heat transfer through the impoundment solid boundaries are generally small and are neglected.

6) The Coriolis forces acting on the water body is considered to be negligible.

The boundary conditions of the problem involve: 1) the geometry of the impoundment including the thermal discharge inlet, as well as the river inflows and outflows configurations; 2) the mass flow rates of the inflows across the boundaries; and 3) the level, pressure and temperature along the inlet boundaries. It is assumed that all of the above parameters are known.

The initial conditions of the problem includes the pressure, velocity, level and temperature distributions of the impoundment at time t = 0. These variables are computed by the present program by first performing a dynamic analysis under no thermal discharge conditions and then using the calculated pressure, velocity, level and temperature distributions, as initial conditions, in a dynamic analysis involving a thermal discharge.

Governing Equations

The mathematical formulation of the sub-water-level flow region consists of the following fundamental equations [17].

Momentum equations:

$$\frac{\partial u}{\partial t} + u\frac{\partial u}{\partial x} + v\frac{\partial u}{\partial y} + w\frac{\partial u}{\partial z} = -\frac{1}{\rho_0}\frac{\partial p}{\partial x} + \nu_h\left(\frac{\partial^2 u}{\partial x^2} + \frac{\partial^2 u}{\partial y^2}\right) + \nu_v\frac{\partial^2 u}{\partial z^2} \qquad (1)$$

$$\frac{\partial v}{\partial t} + u\frac{\partial v}{\partial x} + v\frac{\partial v}{\partial y} + w\frac{\partial v}{\partial z} = -\frac{1}{\rho_0}\frac{\partial p}{\partial y} + \nu_h\left(\frac{\partial^2 v}{\partial x^2} + \frac{\partial^2 v}{\partial y^2}\right) + \nu_v\frac{\partial^2 v}{\partial z^2} \qquad (2)$$

$$\frac{\partial w}{\partial t} + u\frac{\partial w}{\partial x} + v\frac{\partial w}{\partial x} + w\frac{\partial w}{\partial z} = -\frac{1}{\rho_0}\frac{\partial p}{\partial z} + \nu_h\left(\frac{\partial^2 w}{\partial x^2} + \frac{\partial^2 w}{\partial y^2}\right) + \nu_v\frac{\partial^2 w}{\partial z^2} - g\frac{\rho}{\rho_0} \qquad (3)$$

Continuity equation:

$$\frac{\partial u}{\partial x} + \frac{\partial v}{\partial y} + \frac{\partial w}{\partial z} = 0 \qquad (4)$$

Energy equation:

$$\frac{\partial T}{\partial t} + u\frac{\partial T}{\partial x} + v\frac{\partial T}{\partial y} + w\frac{\partial T}{\partial z} = D_h\left(\frac{\partial^2 T}{\partial x^2} + \frac{\partial^2 T}{\partial y^2}\right) + D_v\frac{\partial^2 T}{\partial z^2} \qquad (5)$$

Equation of state:

$$\rho = \rho\ (T) \qquad (6)$$

In this study, the thermal discharge parameters are used as reference values for the non-dimensionalization of the governing equations. Let U_0, ρ_0, T_0 and d_0 be the velocity, density, temperature and half width of thermal discharge flow respectively. The dimensionless quantities are defined by

$$x^* = \frac{x}{d_0} \qquad y^* = \frac{y}{d_0} \qquad z^* = \frac{z}{d_0} \qquad (7)$$

$$u^* = \frac{u}{U_0} \qquad v^* = \frac{v}{U_0} \qquad w^* = \frac{w}{U_0} \qquad (8)$$

$$t^* = \frac{tU_0}{d_0} \qquad T^* = \frac{T}{T_0} \qquad p^* = \frac{p}{\rho_0 g d_0} \qquad (9)$$

$$\rho^* = \frac{\rho}{\rho_0} \qquad (10)$$

Employing the above dimensionless variables in the continuity, momentum and energy equations, one obtains the time derivatives for velocity components u, v, w and temperature T in parabolic differential form as follows:

$$\frac{\partial u^*}{\partial t^*} = - u^* \frac{\partial u^*}{\partial x^*} - v^* \frac{\partial u^*}{\partial y^*} - w^* \frac{\partial u^*}{\partial z^*} - \frac{1}{F_0^{\,2}} \frac{\partial p^*}{\partial x^*}$$

$$+ \frac{\nu_h}{\nu_0} \frac{1}{R_0} \left(\frac{\partial^2 u^*}{\partial x^{*2}} + \frac{\partial^2 u^*}{\partial y^{*2}}\right) + \frac{\nu_v}{\nu_0} \frac{1}{R_0} \frac{\partial^2 u^*}{\partial z^{*2}} \tag{11}$$

$$\frac{\partial v^*}{\partial t^*} = - u^* \frac{\partial v^*}{\partial x^*} - v^* \frac{\partial v^*}{\partial y^*} - w^* \frac{\partial v^*}{\partial z^*} - \frac{1}{F_0^{\,2}} \frac{\partial p^*}{\partial y^*}$$

$$+ \frac{\nu_h}{\nu_0} \frac{1}{R_0} \left(\frac{\partial^2 v^*}{\partial x^{*2}} + \frac{\partial^2 v^*}{\partial y^{*2}}\right) + \frac{\nu_v}{\nu_0} \frac{1}{R_0} \frac{\partial^2 v^*}{\partial z^{*2}} \tag{12}$$

$$\frac{\partial w^*}{\partial t^*} = u^* \frac{\partial w^*}{\partial x^*} - v^* \frac{\partial w^*}{\partial y^*} - w^* \frac{\partial w^*}{\partial z^*} - \frac{1}{F_0^{\,2}} \frac{\partial p^*}{\partial z^*} - \frac{\rho^*}{F_0^{\,2}}$$

$$+ \frac{\nu_h}{\nu_0} \frac{1}{R_0} \left(\frac{\partial^2 w^*}{\partial x^{*2}} + \frac{\partial^2 w^*}{\partial y^{*2}}\right) + \frac{\nu_v}{\nu_o} \frac{1}{R_0} \frac{\partial^2 w^*}{\partial z^{*2}} \tag{13}$$

$$\frac{\partial T^*}{\partial t^*} = - u^* \frac{\partial T^*}{\partial x^*} - v^* \frac{\partial T^*}{\partial y^*} - w^* \frac{\partial T^*}{\partial z^*}$$

$$+ \frac{D_h}{\nu_0} \frac{1}{R_0} \left(\frac{\partial^2 T^*}{\partial x^{*2}} + \frac{\partial^2 T^*}{\partial y^{*2}}\right) + \frac{D_v}{\nu_0} \frac{\partial^2 T^*}{\partial z^{*2}} \tag{14}$$

with continuity and state equations given by

$$\frac{\partial u^*}{\partial x^*} + \frac{\partial v^*}{\partial y^*} + \frac{\partial w^*}{\partial z^*} = 0 \tag{15}$$

$$\rho^* = \rho^* (T^*) \tag{16}$$

In the above equations, the following dimensionless numbers are used

1) Froude number $F_0 = U_0/(gd_0)^{1/2}$ (17)

2) Reynolds number $R_0 = U_0 d_0/\nu_0$ (18)

Equations (11) to (16) are a set of six equations that will be used for the determination of six unknowns, u*, v*, w*, p*, ρ* and T* as functions of time and space.

The final equations, including the pressure equation, are obtained from the above equations as follows. First, the continuity equation is differentiated with respect to time to give

$$\frac{\partial}{\partial t^*} \left(\frac{\partial u^*}{\partial x^*} + \frac{\partial v^*}{\partial y^*} + \frac{w^*}{\partial z^*} \right) = 0 \tag{19}$$

The order of differentiation in equation (19) is then interchanged

$$\frac{\partial}{\partial x^*} \left(\frac{\partial u^*}{\partial t^*} \right) + \frac{\partial}{\partial y^*} \left(\frac{\partial v^*}{\partial t^*} \right) + \frac{\partial}{\partial z^*} \left(\frac{\partial w^*}{\partial t^*} \right) = 0 \tag{20}$$

To facilitate spatial differentiations indicated by eq. (20), eq. (11) through (13) are first rewritten in the following form

$$\frac{\partial u^*}{\partial t^*} = Q_y^* - \frac{1}{F_0^2} \frac{\partial p^*}{\partial x^*} \tag{21}$$

$$\frac{\partial v^*}{\partial t^*} = Q_y^* - \frac{1}{F_0^2} \frac{\partial p^*}{\partial y^*} \tag{22}$$

$$\frac{\partial w^*}{\partial t^*} = Q_z^* - \frac{1}{F_0^2} \frac{\partial p^*}{\partial z^*} \tag{23}$$

where

$$\begin{aligned} Q_x^* &= - u^* \frac{\partial u^*}{\partial x^*} - v^* \frac{\partial u^*}{\partial y^*} - w^* \frac{\partial u^*}{\partial z^*} \\ &\quad + \frac{\nu_h}{\nu_0} \frac{1}{R_0} \left(\frac{\partial^2 u^*}{\partial x^{*2}} + \frac{\partial^2 u^*}{\partial y^{*2}} \right) + \frac{\nu_v}{\nu_0} \frac{1}{R_0} \frac{\partial^2 u^*}{\partial z^{*2}} \end{aligned} \tag{24}$$

$$\begin{aligned} Q_y^* &= - u^* \frac{\partial v^*}{\partial x^*} - v^* \frac{\partial v^*}{\partial y^*} - w^* \frac{\partial v^*}{\partial z^*} \\ &\quad + \frac{\nu_h}{\nu_0} \frac{1}{R_0} \left(\frac{\partial^2 v^*}{\partial x^{*2}} + \frac{\partial^2 v^*}{\partial y^{*2}} \right) + \frac{\nu_v}{\nu_0} \frac{1}{R_0} \frac{\partial^2 v^*}{\partial z^{*2}} \end{aligned} \tag{25}$$

$$\begin{aligned} Q_z^* &= - u^* \frac{\partial w^*}{\partial x^*} - v^* \frac{\partial w^*}{\partial y^*} - w^* \frac{\partial w^*}{\partial z^*} \\ &\quad + \frac{\nu_h}{\nu_0} \frac{1}{R_0} \left(\frac{\partial^2 w^*}{\partial x^{*2}} + \frac{\partial^2 w^*}{\partial y^{*2}} \right) + \frac{\nu_v}{\nu_0} \frac{1}{R_0} \frac{\partial^2 w^*}{\partial z^{*2}} - \frac{\rho^*}{F_0^2} \end{aligned} \tag{26}$$

with

$$\frac{\partial w^*}{\partial z^*} = - \left(\frac{\partial u^*}{\partial x^*} + \frac{\partial v^*}{\partial z^*}\right) \tag{27}$$

substituting eqs. (21) through (23) into (20) yields

$$\nabla^2 p^* = F_0^2 \left(\frac{\partial Q_x^*}{\partial x^*} + \frac{\partial Q_y^*}{\partial y^*} + \frac{\partial Q_z^*}{\partial z^*}\right) \tag{28}$$

This elliptic differential equation will provide a means for the calculation of the pressure distribution in the water body. Eqs. (27), (24), (25), (26), (28), (21), (22), (14) and (16) constitute our final equations which will be solved for updated values of w^*, Q_x^*, Q_y^*, Q_z^*, p^*, u^*, v^*, T^*, and ρ^* respectively. It should be noted that:
The vertical momentum equation (23) is used indirectly in this computation through its usage in the derivation of the pressure equation (28). Since the water level variation provides a vertical freedom for the water body, it is imperative to calculate the vertical velocity component w^* from the continuity equation and not by the application of the momentum equation in the vertical direction equation (23). However, the momentum balance in the vertical direction is fully satisfied since eq. (23) is explicitly used in the derivation of the pressure equation (28). In fact, eq. (23) may be easily derived from the final equation stated above.

The mathematical formulation for the water-level flow region is derived by the application of the fundamental equations of mass, momentum and energy as follows. The water level in cells located at the air-water interface varies with time and space. For this reason, the continuity equation, as given by eq. (27), is not valid for these cells. Application of a mass balance to such a cell with all sides fixed in space except the top which moves with the water level, yields

$$\begin{aligned}\frac{\partial}{\partial t} (\rho \Delta x \Delta y\ H) = {} & (\rho u \Delta y\ H)_x - (\rho u \Delta y\ H)_{x+\Delta x} \\ & + (\rho v \Delta x\ H)_y - (\rho v \Delta x\ H)_{y+\Delta y} \\ & + (\rho w \Delta x \Delta y)_z - (\rho w \Delta x \Delta y)_{z+H}\end{aligned} \tag{29}$$

The last term represents the mass flux leaving the water level surface. Since the evaporation losses are considered insignificant, this term is equal to zero. Dividing both sides of the above equation by $\rho\Delta x\Delta y$, considering ρ to be constant and equat to ρ_0 consistent with Boussinesq approximation used earlier, letting Δx, Δy approach zero and using dimensionless variables yields

$$\frac{\partial H^*}{\partial t^*} = - \frac{\partial}{\partial x^*}(u^* H^*) - \frac{\partial}{\partial y^*} (v^* H^*) + w^* \tag{30}$$

where

$$H^* = \frac{H}{d_0} \tag{31}$$

Similarly, application of the energy and momentum balance to the water-level region gives:

$$\frac{\partial T^*}{\partial t^*} = - u^* \frac{\partial T^*}{\partial x^*} - v^* \frac{\partial T^*}{\partial y^*} + \frac{D_h}{\nu_0} \frac{1}{R_0 H^*} [\frac{\partial}{\partial x^*} (H^* \frac{\partial T^*}{\partial x^*}) + \frac{\partial}{\partial y^*} (H^* \frac{\partial T^*}{\partial y^*})] - \frac{D_v}{\nu_0} \frac{1}{R_0 H^*} \frac{\partial T^*}{\partial z^*} - \frac{S_0}{H^*} (T^* - E^*) \tag{32}$$

$$\frac{\partial u^*}{\partial t^*} = - u^* \frac{\partial u^*}{\partial x^*} - v \frac{\partial u^*}{\partial y^*} - \frac{1}{F_0^2 H^*} \frac{\partial H^* p^*}{\partial x^*} + \frac{\nu_h}{\nu_0} \frac{1}{R_0 H^*} [\frac{\partial}{\partial x^*} (H^* \frac{\partial u^*}{\partial x^*}) + \frac{\partial}{\partial y^*} (H^* \frac{\partial u^*}{\partial y^*})] - \frac{\nu_v}{\nu_0} \frac{1}{R_0 H^*} \frac{\partial u^*}{\partial z^*} + \frac{1}{2} \frac{C_{fx} \rho_a^* W_x^{*2}}{H^*} \tag{33}$$

$$\frac{\partial v^*}{\partial t^*} = - u^* \frac{\partial v^*}{\partial x^*} - v^* \frac{\partial v^*}{\partial y^*} - \frac{1}{F_0^2 H^*} \frac{\partial H^* p^*}{\partial y^*} + \frac{\nu_h}{\nu_0} \frac{1}{R_0 H^*} [\frac{\partial}{\partial x^*} (H^* \frac{\partial v^*}{\partial x^*}) + \frac{\partial}{\partial y^*} (H^* \frac{\partial v^*}{\partial y^*})] - \frac{\nu_v}{\nu_0} \frac{1}{R_0 H^*} \frac{\partial v^*}{\partial z^*} + \frac{1}{2} \frac{C_{fy} \rho_a^* W_y^{*2}}{H^*} \tag{34}$$

Where S_0, the Stanton number, is defined by

$$S_0 = \frac{K}{\rho_0 C_p U_0} \tag{35}$$

and

$$\rho_a{}^* = \frac{\rho_a}{\rho_0} \tag{36}$$

$$W_x^* = \frac{W_x}{U_0} \qquad W_y^* = \frac{W_y}{U_0} \tag{37}$$

The pressure at the air-water interface is always atmospheric and can be considered equal to zero no matter what the water level may be at any instant of time. For this reason, the pressure at the center of the water level can be considered to be hydrostatic, i.e. for the water level element

$$p^* = \rho^* H^* \tag{38}$$

This equation may also be derived by applying a momentum balance, in the vertical direction, in the water-level flow region and noting that the water vertical velocity in this region is relatively small and therefore negligible. The pressure distribution given by eq. (38) is substituted into the horizontal momentum equations.

It is important to realize the difference between the flow patterns in the flow field and the water level elements. In the flow field elements, an increase in the fluid boundary velocity, will induce horizontal velocity components. However, the time constant associated with the momentum equations will not permit these equations to respond instantaneously to the boundary velocity disturbance at the river or thermal discharge inlets. Because of the flow incompressibility and since the fluid vertical inertia is considerably smaller than the horizontal inertias, the mass imbalance will result in a positive vertical fluid motion designated as "upwelling". This vertical motion will continue upward until it reaches the water level element where by virtue of eq. (30) will cause the water level to rise. This rise is large for elements close to the boundary disturbance and small for elements farther away. This spatial change affects the horizontal momentum equation (33) and (34) and induce a horizontal flow in the water level elements which in turn tends to reduce the water level through eq. (30). A reverse situation takes place when the boundary velocity is decreased. The mass imbalance will result in a negative fluid motion, designated as "downwelling". This will cause the lowering of the water level with an attendant horizontal flow into the element to increase the water level.

Boundary Conditions

The water body boundary surfaces may be classified as follows:

Type (1): The surface boundary located at the water level free surface.

Type (2): The lateral solid-fluid boundary located at the interface between the impoundment wall and the water body.

Type (3): The bottom boundary located at the bottom of the impoundment.

Type (4): The fluid-fluid boundary located at the interface between the water body in the region of interest and surrounding waters.

For the surface boundary, the pressure is considered atmospheric at the air-water interface and is set equal to zero. For the lateral solid-fluid and bottom boundaries, application of the momentum equation in the direction normal to the boundaries gives the following equation respectively

$$\frac{\partial p^*}{\partial y^*} = F_0^2 \frac{\nu_h}{\nu_0} \frac{1}{R_0} \frac{\partial^2 v^*}{\partial y^{*2}} \tag{39}$$

$$\frac{\partial p^*}{\partial z^*} = -\rho^* + F_0^2 \frac{\nu_v}{\nu_0} \frac{1}{R_0} \frac{\partial^2 w^*}{\partial z^{*2}} \tag{40}$$

For the fluid-fluid boundaries, the pressure distribution at the inflow interfaces is considered to be static. The pressure distribution at any outflow interface node is set equal to that of the adjacent node in the flow field. The surrounding waters entering a water body is characterized by a uniform channel flow. The pressure variation at any cross-section of a uniform channel flow may be proved to be hydrostatic by applying the Bernoulli's equation. This equation is applied to two streamlines, one at the top of the channel and the other at an arbitrary depth. Since, in steady, frictionless, one-dimensional, uniform channel flow the constant in the Bernoulli equation is the same for all streamlines, it can be easily shown that the pressure distribution across the channel, as well as the interface between the channel and the impoundment is hydrostatic.

For the surface boundary, the wind effect produces shear at the water surface which is equal to the shear stress in the fluid near the surface as indicated in eqs. (33) and (34) based on the assumption that the wind velocity components are steady and moderate with zero vertical components and the skin coefficients may be taken from experimental measurements [18, 13]. For the lateral solid-fluid and bottom boundaries, the velocity components normal to the boundaries is always zero. The tangential velocity components is calculated by the application of no-slip condition. With this condition, both tangential velocity components at the solid boundary are set equal to zero. The no-slip boundary condition is ideal for very fine grid spacing. However, computational economy requires a coarse grid spacing for most dynamic three-dimensional hydrothermal analyses. Since, a coarse grid does not afford sufficient resolution at the boundary, a limited amount of numerical error will be induced in the solution. For the fluid-fluid boundaries, the velocity distribution at the inflow interfaces is set equal to the channel inflow velocity distribution which is considered to be a known function of time. The velocity distribution at any outflow interface node is set equal to that of the adjacent node in the flow field.

For the surface boundary, the rate of heat dispersion through the water (involving both conduction and turbulent thermal diffusion) is equal to the heat transfer from water to air as indicated in eqs. (32) and (35) based on values of the heat exchange coefficient K and equilibrium water temperature E, both estimated in terms of meteorological conditions [19].

For the lateral solid-fluid and bottom boundaries the heat transfer is considered to be negligible leading to zero temperature gradient at the boundary. The temperature distribution at the fluid-fluid boundaries is treated similar to the velocity distribution. The temperature at the inflow interface is set equal to the channel inflow temperature which is considered to be a known function of time. The temperature at any outflow interface node is set equal to that of the adjacent nodes in the flow field.

The water level at the fluid-fluid boundaries is treated similar to the temperature distribution. The water level at the inflow interface is set equal to the channel inflow water level which is considered to be known. The water level at outflow interface nodes are set equal to that of the adjacent nodes in the flow field. For the lateral solid-fluid, the water level is calculated from vertical velocity components at surface boundary nodes.

In the development of pressure equation, values of $\partial Q_x^*/\partial x^*$ $\partial Q_y^*/\partial y^*$, and $\partial Q_z^*/\partial z^*$ should be evaluated in the flow field. It was shown earlier that variables Q_x^*, Q_y^*, and Q_z^* are related to the velocity field by eqs. (24), (25), and (26). It should be realized that the only spatial derivatives of Q_x^* needed in the present analysis is $\partial Q_x^*/\partial x^*$. Calculation of $\partial Q_x^*/\partial x^*$ in the fluid cell next to the boundary requires the calculation of Q_x^* at the boundaries normal to the x axis. Similarly, calculation of $\partial Q_y^*/\partial y^*$ and $\partial Q_z^*/\partial z^*$ require the calculation of Q_y^* and Q_z^* at the boundaries normal to the y and z axis respectively. For the surface boundary, only Q_z^* is needed. As stated earlier, since the vertical velocity component in the water level element is small, eq. (26) gives

$$(Q_z^*)_{z^* = z_s^*} = -\frac{\rho^*}{F_0^2} \tag{41}$$

For the lateral solid-fluid boundaries, only the component of Q^* normal to the solid boundary is required. Since the velocity component normal to the solid boundary is zero, eq. (25) will,therefore, give

$$(Q_y^*)_{y^* = 0} = (Q_y^*)_{y^* = y^*_{max}} = \frac{\nu_h}{\nu_0} \frac{1}{R_0} \frac{\partial^2 v^*}{\partial x^{2*}} \tag{42}$$

For the bottom boundary only Q_z^* is needed. Simplification of eq. (26) at the bottom boundary gives

$$(Q_z^*)_{z^* = 0} = -\frac{\rho^*}{F_0^2} + \frac{\nu_v}{\nu_0 R_0} \left(\frac{\partial^2 w^*}{\partial z^{*2}}\right) \tag{43}$$

For the fluid-fluid boundary, the surrounding waters entering the water body is characterized by a uniform channel flow, with a uniform velocity at any cross section and zero axial pressure gradient. As an example, application of the momentum equation along the channel flowing in the x-direction gives

$$(Q_x^*)_{x^*=0} = 0 \qquad (44)$$

NUMERICAL SOLUTION

The numerical scheme, used in this study, is mainly based on the application of spatial and temporal finite difference technique to the governing equation described in the previous section. This scheme is divided into the following steps [17]:

1) Initialization and setting of boundary conditions

2) Calculation of vertical velocity component

3) Calculation of pressure distribution

4) Calculation of the time derivatives for the horizontal velocity components and temperature

5) Calculation of the time derivative for the water level, horizontal velocity components and temperature in the water level elements

6) Time integration and updating of the horizontal velocity components and temperature

7) Time integration and updating of the water level, velocity components, and temperature in the water level elements

8) Calculation of density distribution

After the completion of the last step, the problem time is incremented, the computational procedure is repeated starting at the second step, and the integration cycle is continued until the final problem time is reached.

The initial conditions of the problem consist of the initial values of temperature, velocity components, and pressure at time $t = 0$. These quantities are most easily obtained by the application of the present dynamic analysis. To demonstrate this application, let us consider that it is desired to determine the dynamic response of a water body when it is subjected to a prescribed thermal discharge. The solution to the problem can be obtained in two steps. In the first step, the dynamic response is obtained by setting the thermal discharge temperature equal to the river inflow temperature. Maintaining the atmospheric and the inflow conditions unchanged, the water body will reach equilibrium conditions and the pressure, velocity and temperature distribution will be obtained. In the second step, these equilibrium conditions are entered as the initial conditions and the thermal discharge temperature is set equal to the prescribed value. Again, if the atmospheric and inflow conditions are held unchanged, the water body will reach new equilibrium conditions. An examination of this dynamic response will enable the program user to predict the effects of the thermal discharge on the state of the water body. The results of this study could then be used to determine if the state's allowable temperature standards have been violated. These standards generally vary from state to state. Many states impose a maximum allowable water temperature, a temperature rise, and a rate of temperature rise on the use of water bodies.

From the temporal viewpoint, the boundary conditions stated earlier are of two types -- time-independent and time-dependent. The setting of the time-independent boundary conditions are undertaken prior to the beginning of the dynamic solution. The time-dependent boundary conditions are satisfied during the execution of the integration cycle. For example, the time-dependent boundary conditions on vertical velocity and pressure are satisfied during the execution of steps 2 and 3 stated above, respectively.

Numerical Stability and Convergence

The numerical procedure, presented in the previous section, involves spatial integration for the calculation of the vertical velocity components and pressure, as well as time integrations for the calculation of the horizontal velocity components and temperature. These spatial and time integration procedures are plagued by numerical stability problems caused by round-off errors in the numerical solution and convergence problems caused by the truncation error due to the finite magnitude of the space and time increments. A summary of the results for the selection of space and time increments are presented hereunder [17]:

$$(\Delta x_i + \Delta x_{i-1}) \leqslant \frac{4D_h}{|u|} \tag{45}$$

$$(\Delta y_j + \Delta y_{j-1}) \leqslant \frac{4D_h}{|v|} \tag{46}$$

$$(\Delta z_k + \Delta z_{k-1}) \leqslant \frac{4D_v}{|w|} \tag{47}$$

$$\Delta t \leqslant 1/(8D_h/(\Delta x_i + \Delta x_{i-1})^2 + 8D_h/(\Delta y_j + \Delta y_{j-1})^2 + 8D_v/(\Delta z_k + \Delta z_{k-1})^2) \tag{48}$$

$$\Delta t \leqslant 1/(2|u|/(\Delta x_i + \Delta x_{i-1}) + 2|v|/(\Delta y_j + \Delta y_{j-1})) \tag{49}$$

$|u|$, $|v|$, and $|w|$ are the estimated maximum absolute values of the velocity components which could occur during the transient. It is true that these values are not known a priori, but an estimate of the maximum values can generally be made.

PRESENTATION OF RESULTS

The mathematical formulation and the computer program, developed in this study, is verified by applying the dynamic analysis to a number of cases where the final steady-state solution is either known experimentally or the flow pattern has been determined by other investigators. These verification studies are considered in the next section.

Verification Studies

The following problems were selected for verification purposes:

1) Experimental studies on the laminar flow development in a square duct [20]

2) Natural circulation in a pond partially heated from the bottom or the side

The first study consists of a duct with a square cross section with a spatially and temporally uniform input velocity at the duct entrance. Since the geometric dimensions of the laboratory model used in the experimental studies were small and our interest here is in water bodies of appreciable size, the similarity between the present and the experimental study is based on two dimensionless parameters: 1) the quotient of aspect ratio x/D to Reynolds number; and 2) the ratio of the fluid velocity to the average inlet velocity. The geometric and hydraulic input data for this case is given in Table I and Fig. 2a. The computational grid used in this dynamic analysis consists of 13 x 5 x 5 mesh points with non-uniform spacing in the longitudinal direction and uniform spacing in the square cross section as shown in Table II. The initial values of the velocity components in the flow field were selected uniform in the longitudinal direction equal to the inlet velocity with zero transversal and vertical velocities. The dynamic solution was continued until the flow pattern in the duct reached steady state. Typical time histories for a number of upstream and downstream points along the duct axial central plane are obtained and used to plot the final steady state centerline and vertical velocity profiles in the square duct. These velocity profiles, in non-dimensional form, are compared in Figs. 2b and 2c with the experimental results of Goldstein and Kreid [20] who measured the laminar flow development in a square duct using laser-doppler flowmeter. This comparison shows that the results of this study are in good agreement with the experimental data. This confirms that the present formulation can predict the three dimensional flow behavior of water bodies.

The second study consists of natural circulation in a pond heated from the bottom or the side with uniform initial temperature, zero initial velocities and zero inlet and outlet mass flux. The geometric and hydraulic input data for this case is given in Table III. The computational grid used in the dynamic analysis consists of 10 x 6 x 6 mesh points with uniform spacing in the longitudinal and transversal directions and non-uniform spacing in the vertical direction. Two cases were examined. In these cases, a step temperature is applied to a portion of side wall or the bottom surface of the pond. The dynamic response of the pond is obtained for each case and the natural circulation flows developed are compared with expected flow patterns. Typical natural circulation flow patterns for partially heated side wall and bottom surface are shown in Figs. 3, 4, 5, and 6 at times t = 40 and t = 25 seconds respectively into the transient. An examination of these flow patterns demonstrates that for the case of partially heated side wall one natural circulation vortex in transversal direction and two symmetric natural circulation vortices in the longitudinal direction are developed which loose their strength as the distance from the heated wall increases (see Figs. 3,4). For the case of partially heated bottom surface, two symmetric natural vortices in vertical-longitudinal and vertical-diagonal planes are developed which loose their strength with increasing distance from the heated surface (see Figs. 5,6). In both cases, described above, the natural circulation vortices formed and the resultant mixing are caused by density differences in the water body. These results establish that the present formulation can predict the three dimensional flow and thermal aspects of water bodies.

Circulation and Stratification in Water Bodies

The present mathematical formulation is applied to the study of circulation and stratification of large water bodies. The water body is considered to be flowing initially at a uniform velocity and temperature and suddenly exposed to a 90° angle jet with higher velocity but the same temperature. This problem is referred to as three-dimensional non-buoyant jet in a cross current. When the dynamic problem reaches steady state, the water jet temperature is suddenly raised to simulate a thermal discharge. This problem is referred to as three-dimensional buoyant jet in a cross current. To facilitate the understanding of the results, the two problems indicated above (i.e. non buoyant and buoyant jets) are discussed separately but the time histories of the results are shown on the same plots for easy reference.

1) Three Dimensional Non-Buoyant Jet in a Cross Current

The problem of a three-dimensional non-buoyant jet in a cross current, as modeled in Fig. 1, was first analyzed. The geometric and hydraulic input data for the case studied are given in Table IV. The water body is assumed to be flowing initially at a uniform velocity of 0.40 ft/sec when suddenly exposed to a jet velocity of 2.00 ft/sec at a 90 degree angle. The surface wind velocity is considered to be zero. Furthermore, the temperature of the thermal discharge is equal to the water body temperature to simulate a non-buoyant jet. A three-dimensional grid was superimposed on the flow field as detailed in Table V. The boundaries of this grid coincide with the physical river boundaries. The nodal points, where the hydrothermal variables are defined, are located at point ijk of each grid and are shown in Fig. 7. The time histories of the dynamic variables are shown, for points A,B,C,D,E.F,G,and H marked in Fig. 7, as follows:

1) Velocity components and water level for two nodes A and B in front of the incoming jet at the free surface shown in Figs. 8 and 9

2) Velocity components for two nodes C and D in front of the incoming jet at 12.75 feet below the free surface shown in Figs. 10 and 11

3) Velocity components and water level for two nodes E and F located upstream and downstream respectively at the free surface shown in Figs. 12 and 13

4) Velocity components of two nodes G and H located upstream and downstream respectively at 12.75 feet below the free surface shown in Figs. 14 and 15

Examination of the above plots shows the following features:

Considering the flow at the water surface, the transversal velocities at points A and B, in front of the incoming jet, rise initially with a subsequent rise in the vertical velocity leading to a rise in water level in the neighborhood of the incoming jet which in turn affects the field flow conditions as time progresses. Since the total head associated with the jet and river flow entries are constant, on a short term basis an increase in the water level must be accomplished with a corresponding decrease in the field velocity. The disturbance caused by the incoming jet travel from the discharge point both upstream and downstream of the river. This demonstrates the propagation of the surface gravity waves (surge waves). As time progresses, these disturbances reach the river exit and are reflected back upstream. This demonstrates the reflection of the surface gravity waves from the river exit. However, on a long term basis, a further increase in the water level in the neighborhood of the incoming jet causes additional horizontal velocity components for further downstream points which will gradually affect the downstream flow. These flow patterns are observed both in axial and transversal direction as discussed hereunder:

a) The increase in the water level initially decelerates the axial flow on a short term basis. With a further increase in the water level, the axial flow at various points accelerate to their final steady state values which are larger for the downstream points and smaller for the upstream points from the incoming jet position as expected. These effects can be clearly observed in u/U_0 curves for points E, B and F in Figs. 12, 9 and 13 where the transient start with a small dip in the flow rate followed by a steep rise settling to its final steady state value.

b) Similarly, the transversal flow generated by the incoming jet, increases the water level, which in turn, decelerates the transversal flow. However, since, unlike the axial flow patterns, the boundary condition in the transversal direction (solid wall) does not accomodate flow, the transversal flow reaches its final steady state value without undergoing large swings observed in the axial flow curves. These effects can be clearly observed in v/U_0 curves for points A and B in Figs. 8 and 9 where the transversal flow after the initial rise undergoes a reduction in magnitude followed by a mild rise settling to its final steady state values.

At the end of transients discussed above, the increase in transversal flow caused by the incoming jet is accommodated by an increase in the axial flow. For this reason, the water level reaches a steady state value which in turn results in zero vertical velocity and constant axial and transversal flows, observed in Figs. 8 and 9, as the end of non-buoyant analysis is approached.

Examining the flow at 12.76 feet below the water surface, the axial flow exhibit a pattern similar to that of the water surface except that the results are further accentuated due to the bottom boundary condition. Figs. 11, 14 and 15 show that the flow transients u/U_0 start with a relatively large dip followed by relatively smaller rise as it approaches its final steady state value. The effect of the non-slip bottom boundary condition is to reduce the final steady state value to a quantity below that of the surface and to enlarge the initial dip. Furthermore, the shear initiated by the incoming jet creates transversal flow components v/U_0 at this level as observed in Figs. 10 and 11. The transversal flow reduces from the top to the bottom. At the end of transients discussed above, the increase in transversal flow caused by the incoming jet cannot be fully accommodated by an increase in the axial flow in cells near the solids boundaries. For this reason, a downward velocity component develops which induces a vertical downward velocity in the upper cells, observed in w/U_0 curve in Fig. 10. This downward flow extends in a few cells from the jet entrance and is changed to an upwards flow in cells in the center of the flow field.

2) Three Dimensional Buoyant Jet in a Cross Current

The problem of a three-dimensional buoyant jet in a cross current is next analyzed. The geometric and hydraulic input data for this case is exactly similar to the non-buoyant jet case detailed in Fig. 1 and Table IV. The water body is assumed to be initially under the steady state conditions reached in the non-buoyant case discussed earlier when the thermal discharge temperature is suddenly increased from 75°F to 90°F.

The dynamic buoyant jet problem is analyzed in a manner similar to the non-buoyant jet [illegible]. However, in view of the introduction of thermal effects, the water body becomes stratified as discussed hereunder. The time histories of the dynamic variables are shown, for points A,B,C,D,E,F,G, and H marked on Fig. 7, as a continuation of the non-buoyant time history plots in Figs. 8 to 15. Examination of these plots shows the following features:

The effect of the heated thermal discharge entering the flow field can be decomposed into two components: 1) unheated discharge entering the flow field studied in the non-buoyant case problem; and 2) thermal effect of the discharge considered in a heated wall studied earlier under the topic of ponds partially heated from the side. According to the above decomposition, the velocity time history plots on Figs. 8 to 15 for buoyant case should be the sum of the non-buoyant case and the corresponding heated wall problem.

Examining the flow at the water surface at points A and B, in front of the incoming jet, the transversal velocity for the buoyant case shows a small increase in the steady state as compared with the non-buoyant results due to the natural circulation caused by the heated wall. This additional transversal velocity induces an axial velocity transient similar in nature to the non-buoyant case. However, since the magnitude of the transversal velocity transient is small, the resultant axial velocity transient would also be small. This behavior can be clearly observed in u/U_0 and v/U_0 curves in Figs. 8 and 9 which also show the temperature transients T/T_0 for both points A and B. A similar pattern can also be observed at the surface points E and F in Figs. 12 and 13 as well as the points C, G, and H located at 12.75 feet below the water surface in Figs. 10, 14 and 15.

At the end of the transients, the coldest and the hottest regions are at the river and the thermal discharge entrances respectively. For this reason, the strongest natural circulation patterns would develop mainly between these coldest and hottest regions. A comparison of the surface velocity vectors at points A and E and the velocity vectors at 12.75 feet depth for buoyant and non-buoyant cases confirm the existance of this natural circulation pattern. The surface velocity field at the end of the transient is shown in Fig. 16. The slowing down of the entrance flow near the thermal discharge entrance and the turning of the thermal discharge and incoming flows as a result of their interaction can be clearly seen in this figure.

The thermal plume effect is shown in Figs. 17 to 22. Isotherms are plotted for the water surface as well as the vertical planes in the longitudinal and transversal direction at times 60 and 500 seconds after the initiation of the heated discharge. An examination of these plots indicates the following features:

1) The stratification pattern is three dimensional in nature and shows the expansion of the thermal plume in all directions. In view of the prevailing advective currents this expansion is much more intense toward the downstream as compared to the other directions (vertical and upstream) as expected.

2) The three distinctive regions which constitute the characteristic behavior of a stratified water body (epilimnion, thermocline and hypolimnion can be clearly observed in Fig. 22.

3) These results provide the water temperature rise and the rate of temperature rise needed for the assessment of the extent of thermal pollution in the water body.

As a further verification on the validity of the results a mass and energy balance was performed on the water body as shown in Table VI. This table shows that conservation equations are satisfied with a good accuracy. The small magnitude of the surface heat transfer verifies the often used assumption that, at high values of equilibrium temperature used herein, the contribution of heat exchange to the atmosphere is insignificant and may be neglected in simplified analyses for the purpose of near field studies.

NOMENCLATURE

c_p	Specific heat of water
c_{fx}	Skin coefficient along x-axis
c_{fy}	Skin coefficient along y-axis
d_o	Half width of thermal discharge
D_h	Horizontal eddy diffusivity of heat
D_v	Vertical eddy diffusivity of heat
E	Water equilibrium temperature
F_0	Froud number
g	Gravitional acceleration
H	Water level height in the water level element
K	Heat exchange coefficient for water-air interface
p	Pressure
R_0	Reynolds number
S_0	Stanton number
T_0	Thermal discharge temperature
T	Local water temperature
t	Time
U_0	Thermal discharge velocity
u	Horizontal velocity components in x-direction
v	Horizontal velocity components in y-direction
w	Vertical velocity components in z-direction
W_x	Wind velocity components in x-direction
W_y	Wind velocity components in y-direction
x,y,z	Cartesian coordinate system
Δx_i	Dimension of element i in x-direction
Δy_j	Dimension of element j in y-direction
Δz_k	Dimension of element k in z-direction

Greek Symbols

ρ	Local density of water
ρ_0	Thermal discharge density
ρ_a	Air density
ν_h	Horizontal eddy viscosity
ν_v	Vertical eddy viscosity
ν_0	Thermal discharge kinematic viscosity
∇^2	Laplacian operator $\frac{\partial^2}{\partial x^2} + \frac{\partial^2}{\partial y^2} + \frac{\partial^2}{\partial z^2}$

Superscripts

*	Refers to non-dimensional quantities

Subscripts

0	Refers to thermal discharge
s	Refers to values of variables at the free surface
i,j,k	Indices referring to the location of nodal points along x,y, and z axes respectively

REFERENCES

1. Brady, D.K. and Geyer, J.C., "Development of a General Computer Model for Simulating Thermal Discharge in Three Dimensions", Report No. 7, Cooling Water Studies for Edison's Electric Institute, New York, N.Y., 1972.
2. Liggett, J.A., "Unsteady Circulation in Shallow Homogeneous Lake", Proceedings of the ASCE, Journal of the Hydraulics Division, HY4, July 1969, pp. 1273-1288.
3. Liggett, J.A. and Hadjitheodorou, C., "Circulation in Shallow Homogeneous Lakes", Proceedings of ASCE, Journal of the Hydraulic Division, HY2, March 1969, pp. 609-620.
4. Sengupta, S., "A Three-Dimensional Numerical Model for Closed Basins", ASME Publication No. 76-WA/HT-21, 1976, pp. 1-16.
5. Streeter, V.L., Fluid Mechanics, McGraw-Hill Book Co., Inc., 1958.
6. Hirt, C.W. and Shannon, J.P., "Free-Surface Stress Conditions for Incompressible-Flow Calculations", Journal of Computational Physics, Vol. 2, 1968, pp. 403-411.
7. Waldrop, W.R. and Farmer, R.C., "Three-Dimensional Computation of Buoyant Plumes", Journal of Geophysical Research, Vol. 79, No. 9, March 1974 pp. 1269-1276.
8. Waldrop, W.R. and Farmer, R.C., "Thermal Plumes form Industrial Cooling Water", Proceedings of the 1974 Heat Transfer and Fluid Mechanics Institute, Stanford University Press, 1974.
9. Waldrop, W.R. and Farmer, R.C., "A Computer Simulation of Density Currents in a Flowing Stream", Symposium on Unsteady Flow in Open Channels, BHRA, April 1976.
10. Waldrop, W.R. and Farmer, R.C., "Thermal Effluent-River Interaction", Proceedings Comptes-Rendus, Vol. 3, 1975, Sao Paulo, Brazil, pp. 221-229.
11. Liggett, J.A., "Cell Method for Computing Lake Circulation", Proceedings of ASCE, Journal of the Hydraulics Division, HY3, March 1970, pp. 725-743.
12. Elwin, E.H. and Slotta, L.S., "Streamflow Effects in a Stratified Model Reservoir", ASCE National Water Resources Engineering Meeting, Memphis, Tenn. January 1970.
13. Leendertse, J.J., Alexander, R.C., and Shiao-Kung, L., "Three-Dimensional Model for Estuaries and Coastal Seas", Vol. 1, Principles of Computation, prepared for the Office of Water Resources Research, Department of the Interior R-1417-OWRR, December 1973, Rand, Santa Monica, California.
14. Marchuk, G.I., "About Formulation of Problems on the Dynamics of the

Ocean", International Symposium on Stratified Flows, Novosibirsk, 1972.

15. Harleman, Donald, R.F., "Thermal Stratification Due to Heated Discharges", International Symposium of Stratified Flows, Novosibirsk, 1972.
16. Harlow, F.H. and Welch, J.E., "Numerical Calculation of Time-Dependent Viscous Incompressible Flow of Fluid with Free Surface", Los Alamos Scientific Laboratory, Los Alamos, N.M., 1965.
17. Borhani, M.A., "Thermal Stratification and Circulation of Water Bodies Subjected to Thermal Discharges", Doctoral Dissertation, New Jersey Institute of Technology, 1977.
18. Liu, H. and Presez, H.J., "Wind-Induced Circulation in Shallow Water", Proceedings of ASCE, Journal of the Hydraulics Division, HY7, July 1971, pp. 923-935.
19. Edinger, J.E., Brady, D.K., and Geyer, J.C., "Heat Exchange and Transport in the Environment", Report No. 14, Cooling Water Discharges, Edison Electric Institute, New York, 1974.
20. Goldstein, R.J. and Kried, O.K., "Measurement of Laminar Flow Development in a Square Duct Using a Laser-Doppler Flowmeter", Journal of Applied Mechanics, ASME Vol. 34, 1976, pp. 813-818.

TABLE I - THE GEOMETRIC AND HYDRAULIC INPUT DATA FOR LAMINAR FLOW IN A SQUARE DUCT

Specifications	Dimensions	
	British Unit	SI Unit
Water Body Length	280 ft	85.34 m
Water Body Width	72 ft	21.946 m
Water Body Depth	72 ft	21.946 m
Inlet Water Velocity	1 ft/sec	0.3048 m/sec
Water Temperature	75 °F	23.89 °C
Reynolds Number, R_0	20.83	20.83
Hydraulic Diameter of Square Duct, D	72 ft	21.946 m

TABLE II - GRID DIMENSIONS FOR THE LAMINAR FLOW IN A SQUARE DUCT

Element No.	x		y		z	
	ft	m	ft	m	ft	m
1	10	3.048	18	5.486	18	5.486
2	10	3.048	18	5.486	18	5.486
3	10	3.048	18	5.486	18	5.486
4	10	3.048	18	5.486	18	5.486
5	20	6.096	18	5.486	18	5.486
6	30	9.144				
7	30	9.144				
8	30	9.144				
9	30	9.144				
10	30	9.144				
11	30	9.144				
12	30	9.144				
13	30	9.144				

TABLE III - GEOMETRIC AND HYDRAULIC INPUT DATA FOR PARTIALLY HEATED POND

Specifications	Dimensions			
	British Unit		SI Unit	
Water Body Length	540	ft	164.592	m
Water Body Width	250	ft	76.2	m
Water Body Depth	20.5	ft	6.248	m
Water Body Temperature	75	°F	23.89	°C
Water Body Equilibrium Temperature	74	°F	23.33	°C
Temperature of Heated Area	100	°F	37.77	°C
Reference Velocity, U_0	1	ft/sec	0.3048	m/sec
Reference Length, d_0	50	ft	15.24	m
Reference Temperature, T_0	100	°F	37.77	°C
Reference Time, t_0	50	sec	50	sec
Reference Density, ρ_0	61.9963	lbm ft^{-3}	960.590	kg m^{-3}
Reference Pressure, p_0	21.52	lbf in^{-2}	14639.4	kg m^{-2}
Reynolds Number, R_0	0.6061	x 10^7	0.6061 x	10^7
Heat Exchange Coeff., K	100	Btu/ft^{2}day°F	23.64	W/m^2°C

TABLE IV - GEOMETRIC AND HYDRAULIC INPUT DATA FOR THREE-DIMENSIONAL, NON-BUOYANT AND BUOYANT JETS IN A CROSS CURRENT

Specifications	Dimensions			
	British Unit		SI Unit	
Water Body Length	600	ft	182.88	m
Water Body Width	360	ft	109.73	m
Water Body Depth	16.5	ft	5.03	m
Jet Width, 2 d_0	100	ft	30.48	m
Jet Depth	5.75	ft	1.75	m
Jet Velocity, U_0	2	ft/sec	.61	m/sec
River Velocity	.4	ft/sec	.12	m/sec
Water Body Temperature	75	°F	23.89	°C
Water Body Equilibrium Temperature	74	°F	23.33	°C
Thermal Discharge Temperature, T_0	90	°F	32.22	°C
Reference Time, t_0	25	sec	25	sec
Reference Density, ρ_0	62.1156	lbm ft^{-3}	962.730	kg m^{-3}
Reference Pressure, p_0	21.56	lbf in^{-2}	14672.0	kg m^{-2}
Reynolds Number, R_0	0.1212	x 10^8	0.1212 x	10^8
Heat Exchange Coeff., K	100	Btu/ft^{2}day°F	23.64	W/m^2°C

TABLE V - GRID DIMENSIONS FOR THREE DIMENSIONAL NON-BUOYANT AND BUOYANT JETS IN A CROSS CURRENT

Element No.	x		y		z	
	ft	m	ft	m	ft	m
1	65	19.81	50	15.24	3.5	1.07
2	60	18.29	50	15.24	4.0	1.22
3	55	16.76	55	16.76	5.0	1.52
4	50	15.24	60	18.29	4.0	1.22
5	50	15.24	65	19.81	3.5	1.07
6	55	16.76	70	21.34		
7	60	16.76	70	21.34		
8	65	19.81				
9	70	21.34				
10	70	21.34				

TABLE VI - MASS AND ENERGY BALANCE

Mass or Energy Balance	Incoming Flow	Thermal Discharge	Outgoing Flow	Surface Flow	Percent Error
Mass Balance, in 10^6 lbm/sec	0.12252	0.08464	0.20748	0.0	0.15
Energy Balance, in 10^8 Btu/sec	0.09189	0.07454	0.16204	0.15096×10^{-4}	0.18

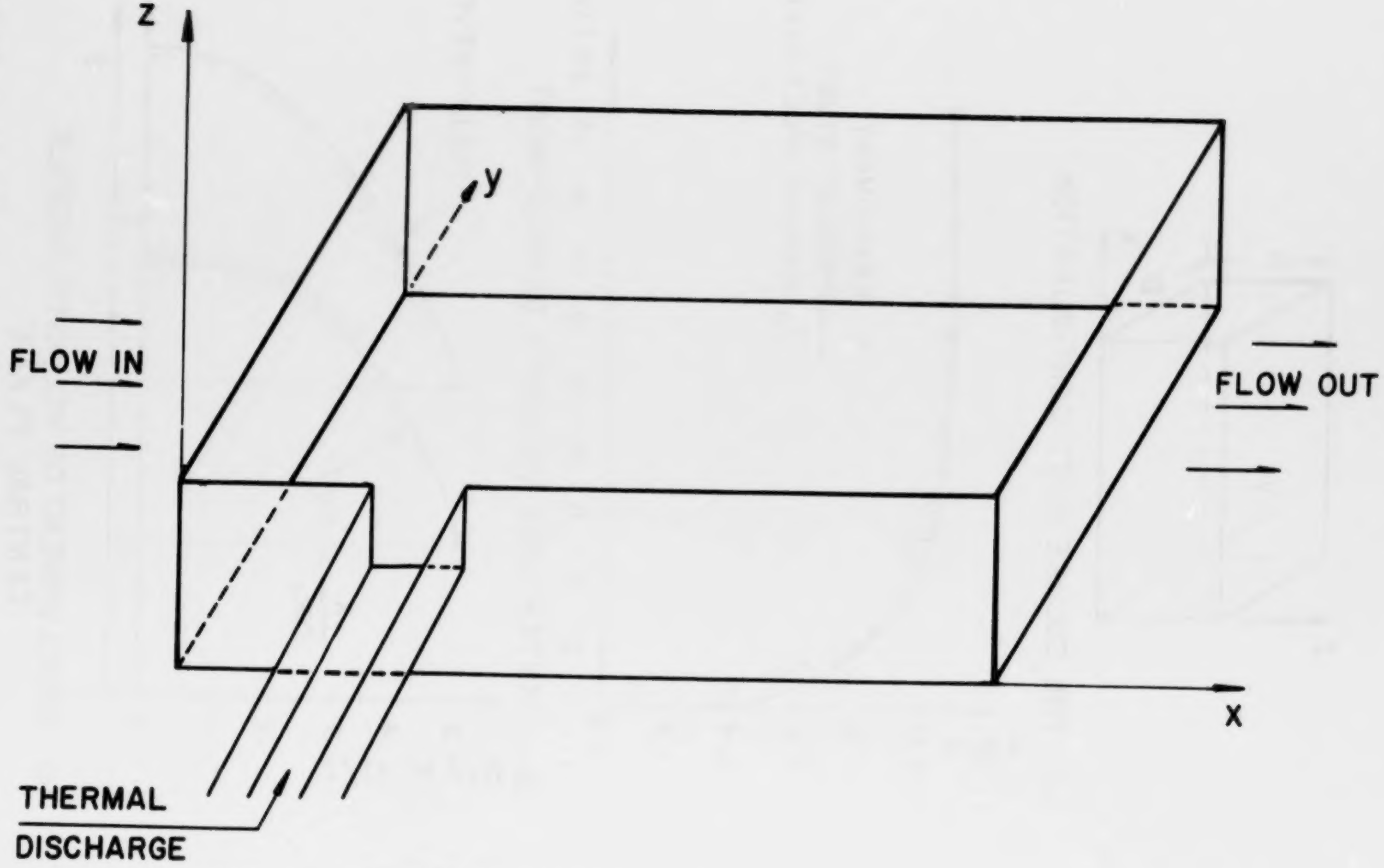
z
y
FLOW IN
FLOW OUT
x
THERMAL
DISCHARGE

FIG I. SCHEMATIC DIAGRAM OF THE WATER BODY

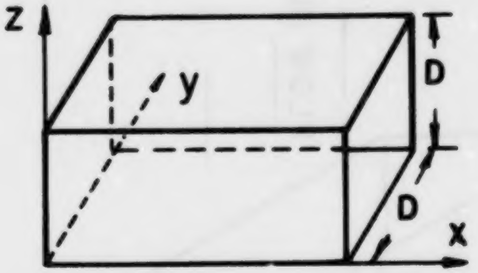

(a) THE SQUARE DUCT CONFIGURATION

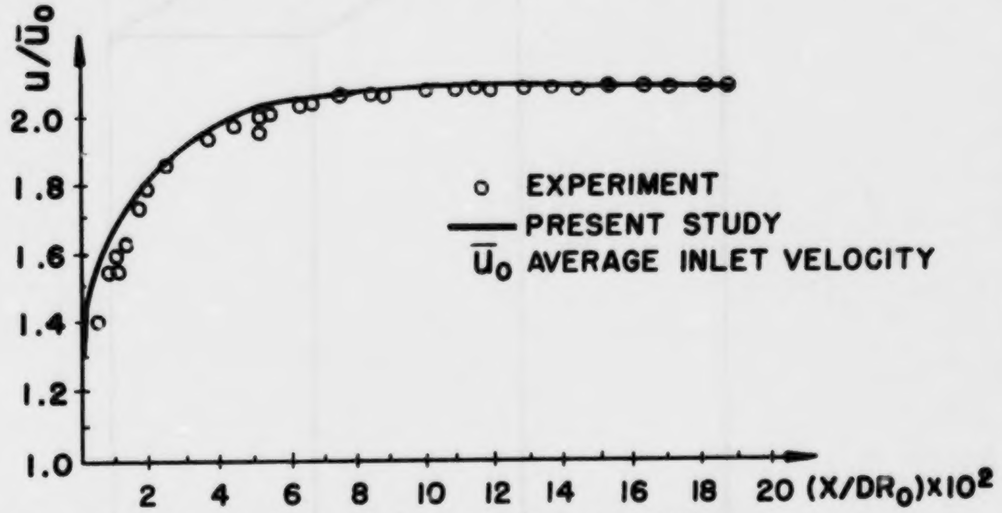

(b) CENTER-LINE VELOCITY DEVELOPMENT

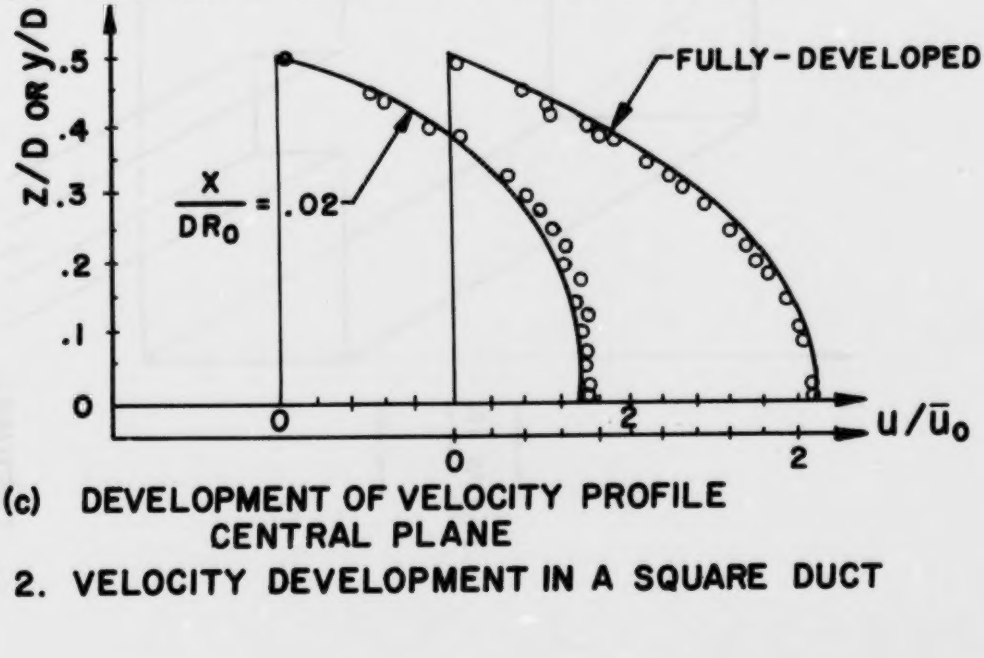

(c) DEVELOPMENT OF VELOCITY PROFILE CENTRAL PLANE

FIG 2. VELOCITY DEVELOPMENT IN A SQUARE DUCT

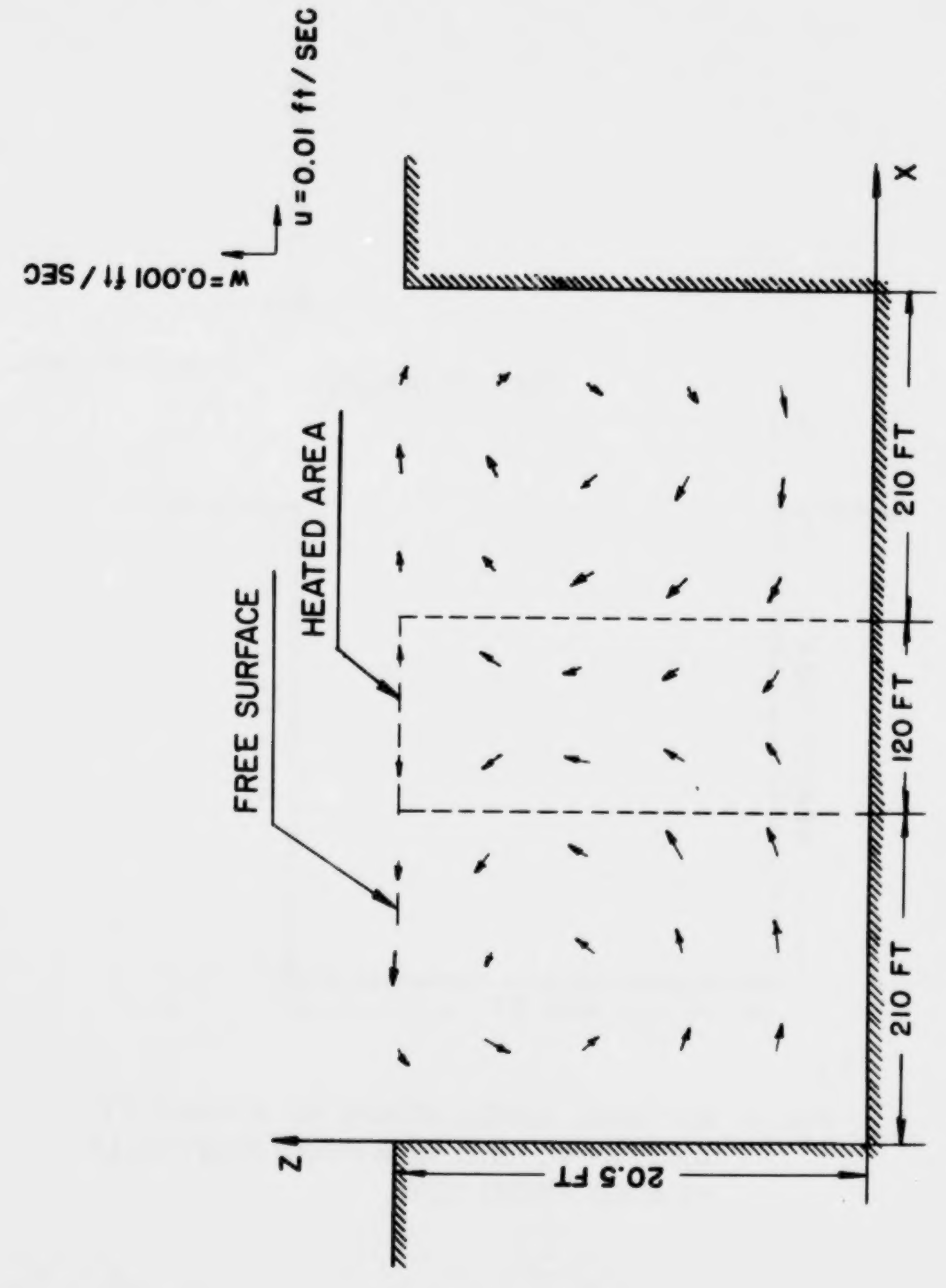
w=0.001 ft/SEC
u=0.01 ft/SEC
FREE SURFACE
HEATED AREA
Z
X
20.5 FT
210 FT
120 FT
210 FT

FIG 3. NATURAL CIRCULATION AT $y=100$ FT. AND $t=40$ SEC IN A POND PARTIALLY HEATED FROM SIDE.

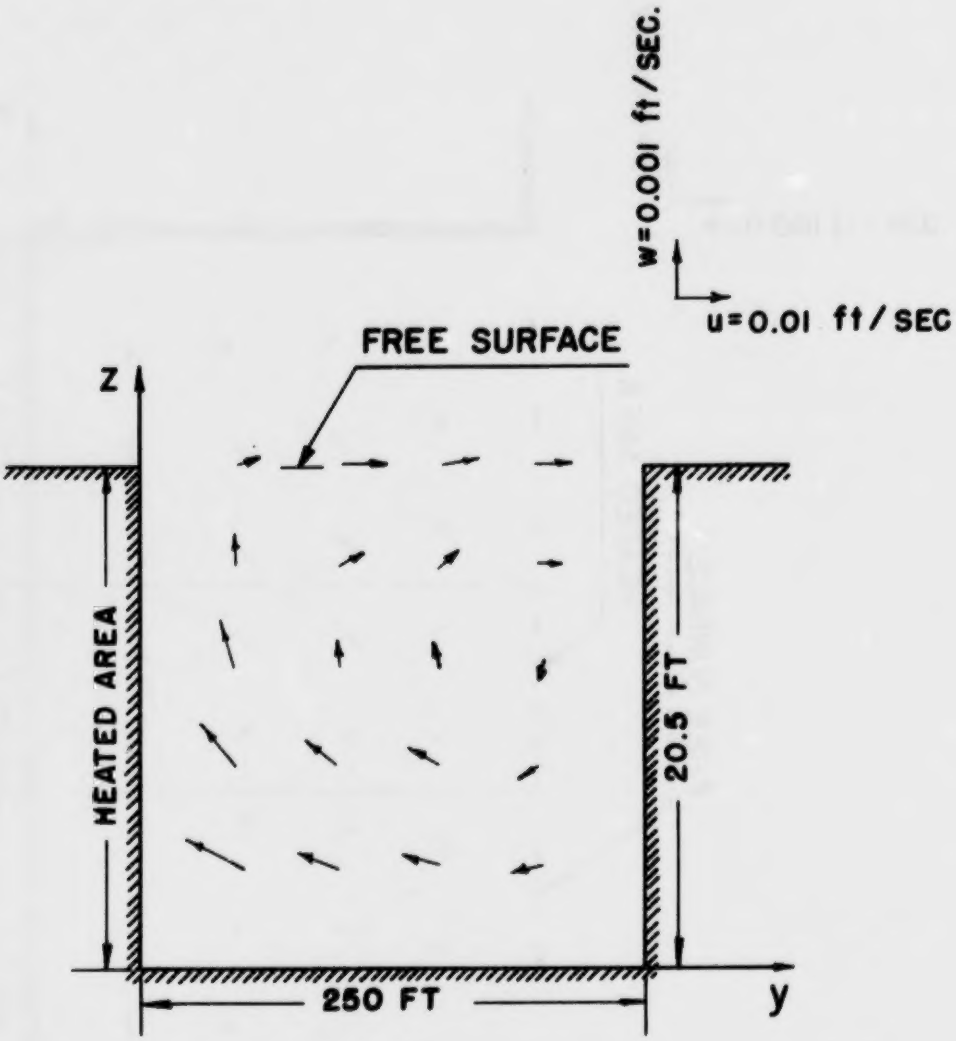
w=0.001 ft/SEC.
u=0.01 ft/SEC
FREE SURFACE
Z
HEATED AREA
20.5 FT
250 FT
y

FIG 4. NATURAL CIRCULATION AT X=240 FT. AND t=40 SEC. IN A POND PARTIALLY HEATED FROM SIDE.

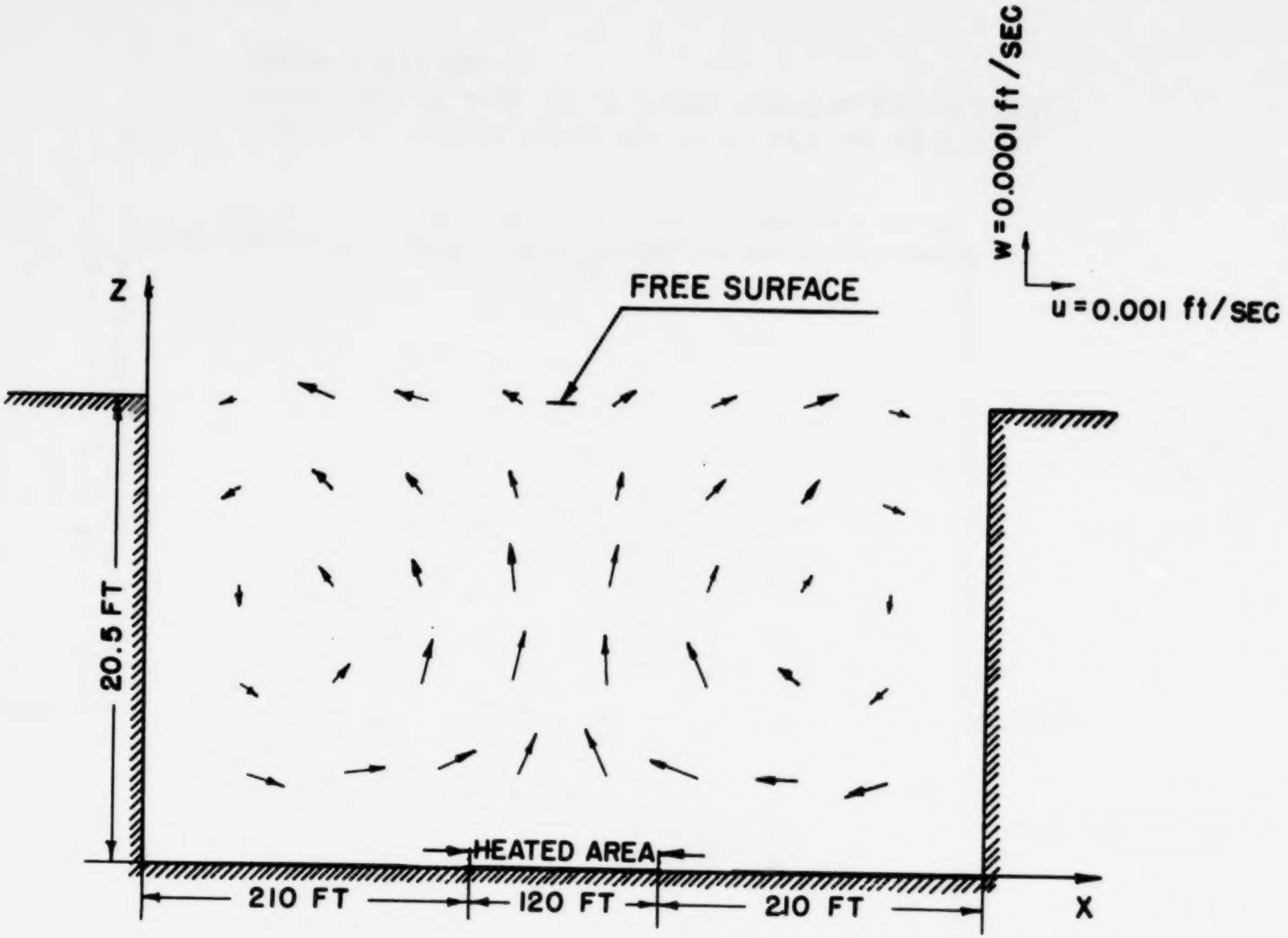
w=0.0001 ft/SEC
u=0.001 ft/SEC
Z
FREE SURFACE
20.5 FT
HEATED AREA
210 FT
120 FT
210 FT
X

FIG 5. NATURAL CIRCULATION AT y=100 FT. AND t= 25 SEC. IN A POND PARTIALLY HEATED FROM BOTTOM.

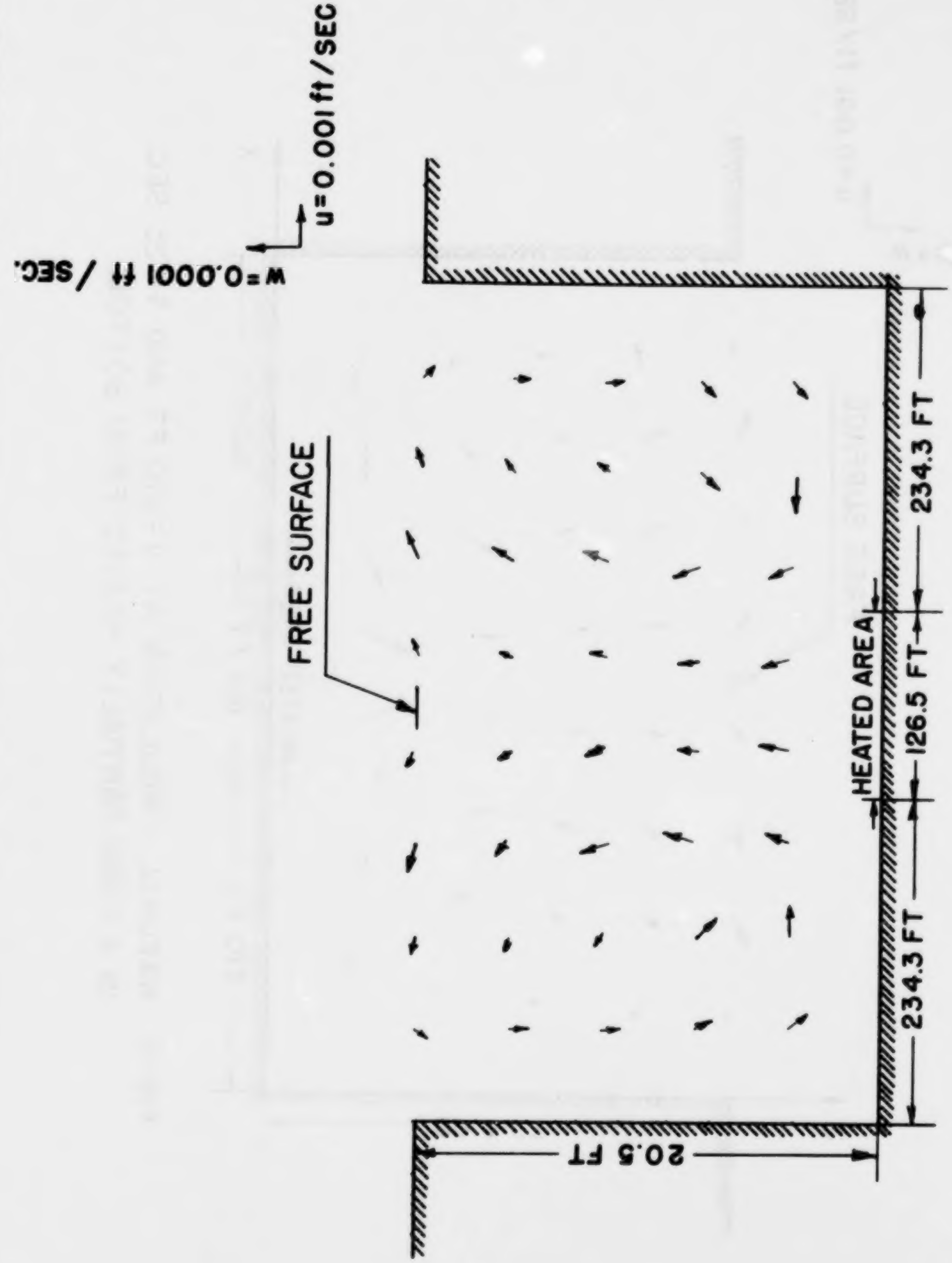
w=0.0001 ft / SEC.
u=0.001 ft/SEC
FREE SURFACE
HEATED AREA
234.3 FT
126.5 FT
234.3 FT
20.5 FT

FIG 6. NATURAL CIRCULATION AT t = 25 SEC IN VERTICAL DIAGONAL PLANE IN A POND PARTIALLY HEATED FROM BOTTOM

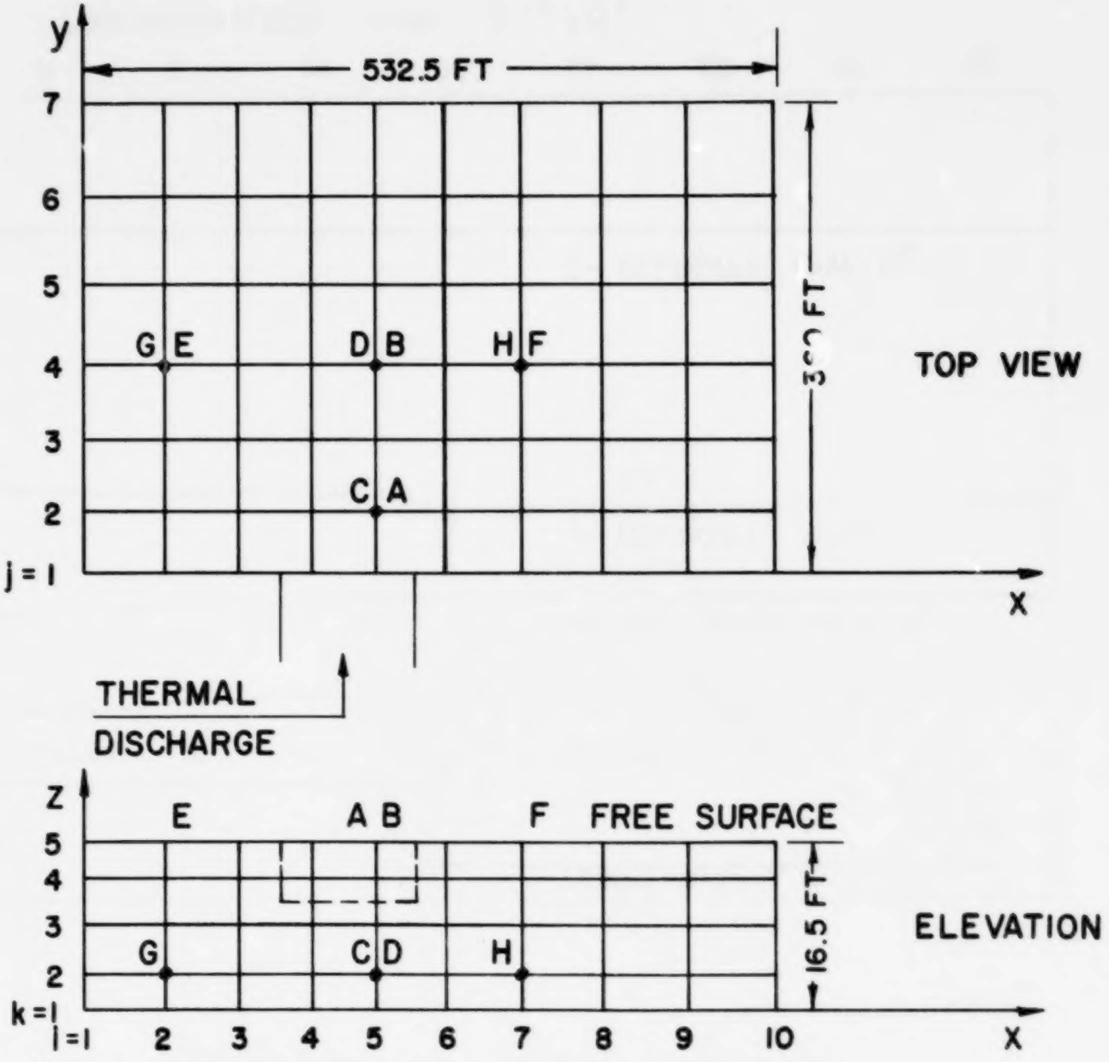
y
532.5 FT
7
6
5
4
3
2
j = 1
G E
D B
H F
C A
300 FT
TOP VIEW
X
THERMAL
DISCHARGE
Z
E
A B
F
FREE SURFACE
5
4
3
2
k = 1
G
C D
H
16.5 FT
ELEVATION
i = 1
2
3
4
5
6
7
8
9
10
X

FIG 7. GRID WORK WITH VARIABLE MESH SIZE SUPERIMPOSED ON THE WATER BODY

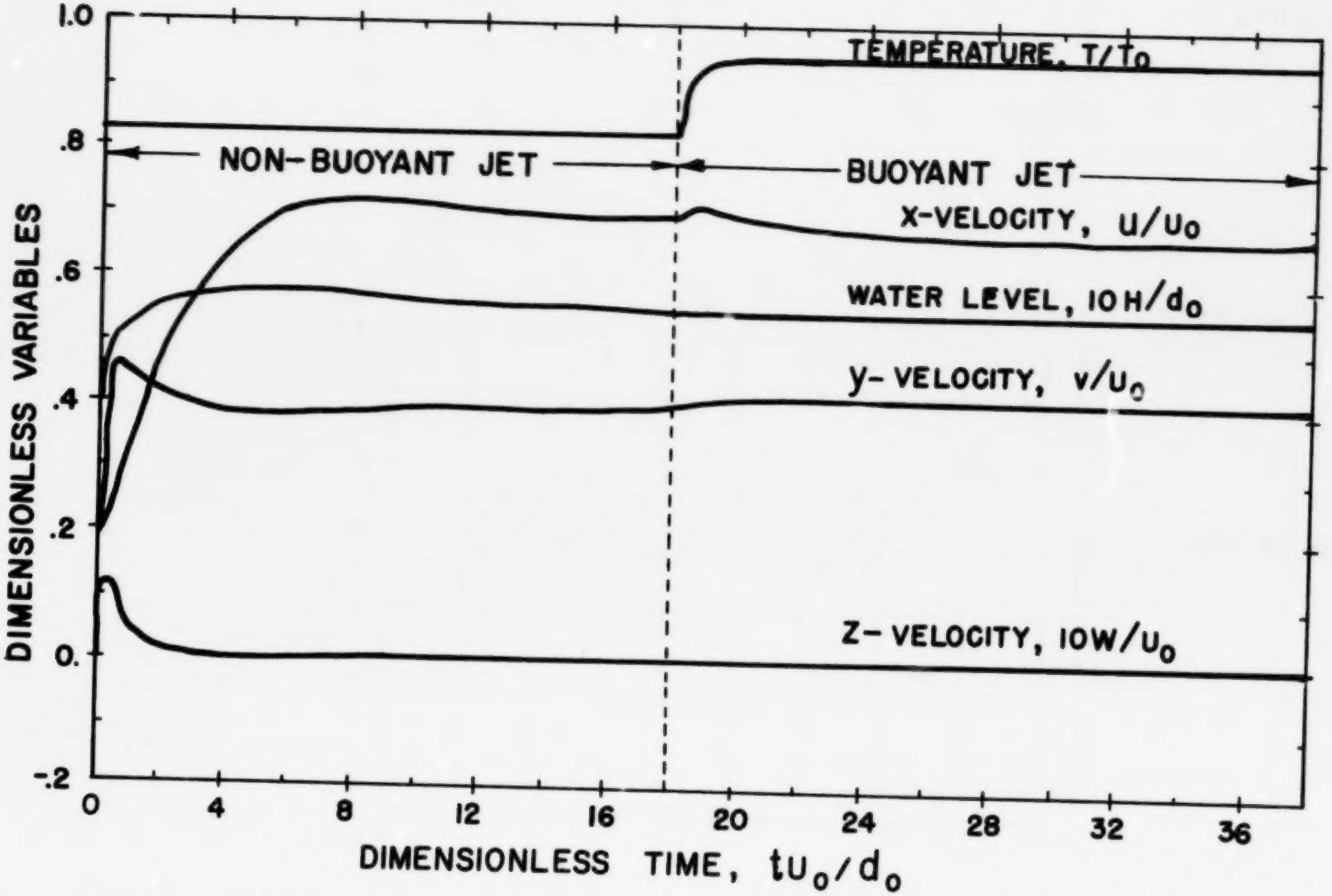

FIG 8. TIME HISTORIES OF VARIABLES AT POINT "A" IN THE WATER BODY SUBJECTED TO NON-BUOYANT AND BUOYANT JETS

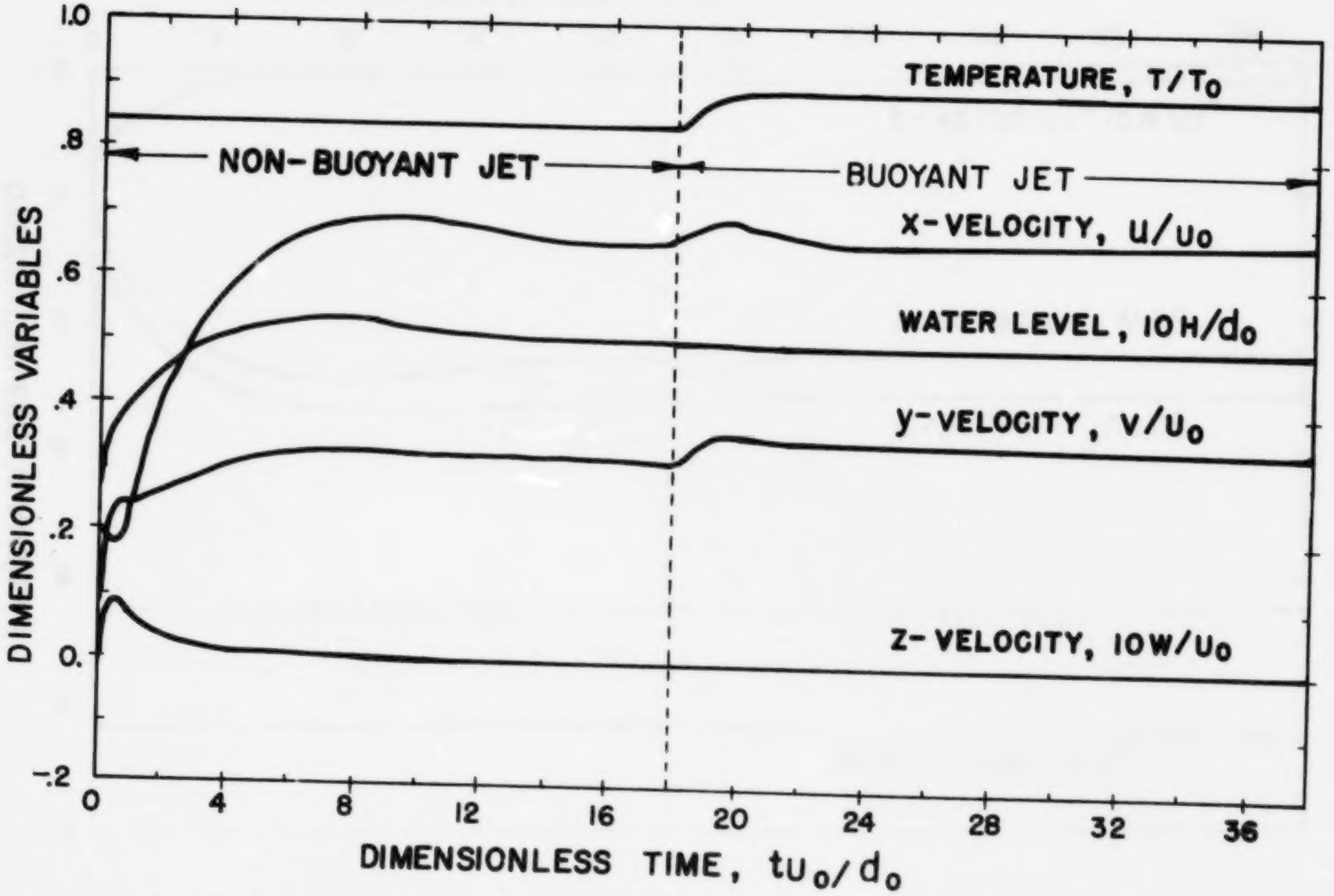

FIG 9. TIME HISTORIES OF VARIABLES AT POINT "B" IN THE WATER BODY SUBJECTED TO NON-BUOYANT AND BUOYANT JETS

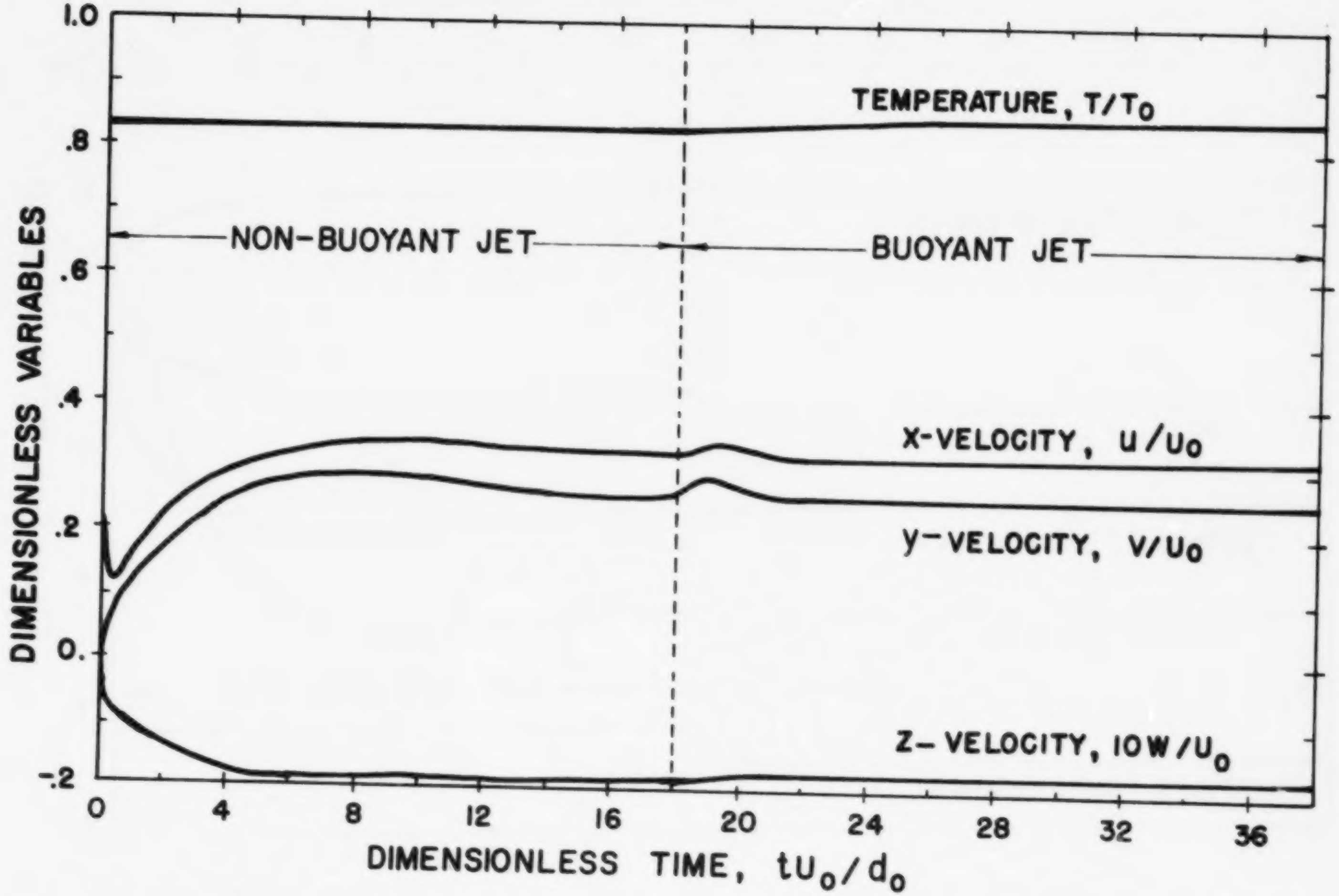

FIG 10. TIME HISTORIES OF VARIABLES AT POINT "C" IN THE WATER BODY SUBJECTED TO NON-BUOYANT AND BUOYANT JETS

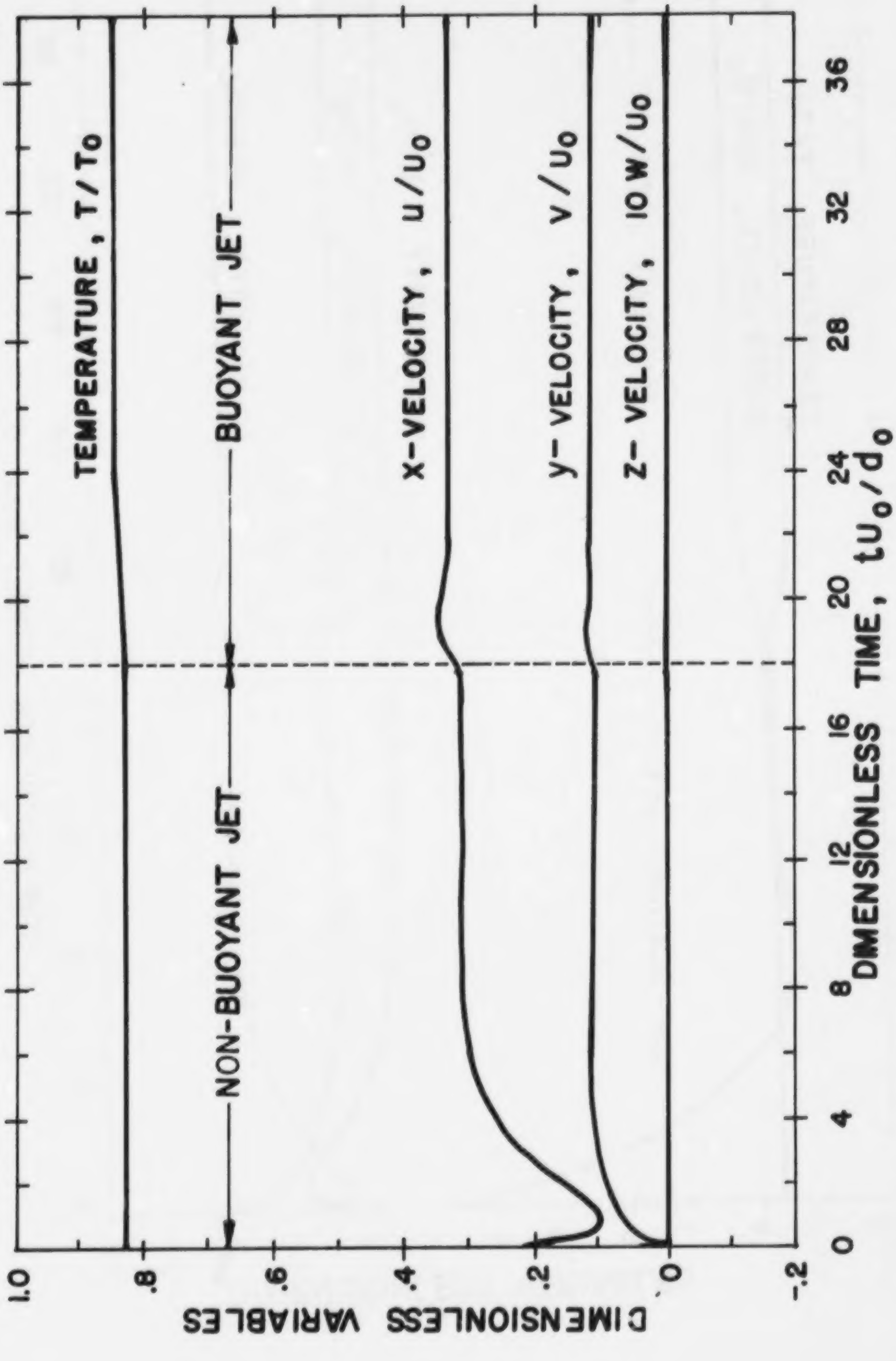

FIG 11. TIME HISTORIES OF VARIABLES AT POINT "D" IN THE WATER BODY SUBJECTED TO NON-BUOYANT AND BUOYANT JETS

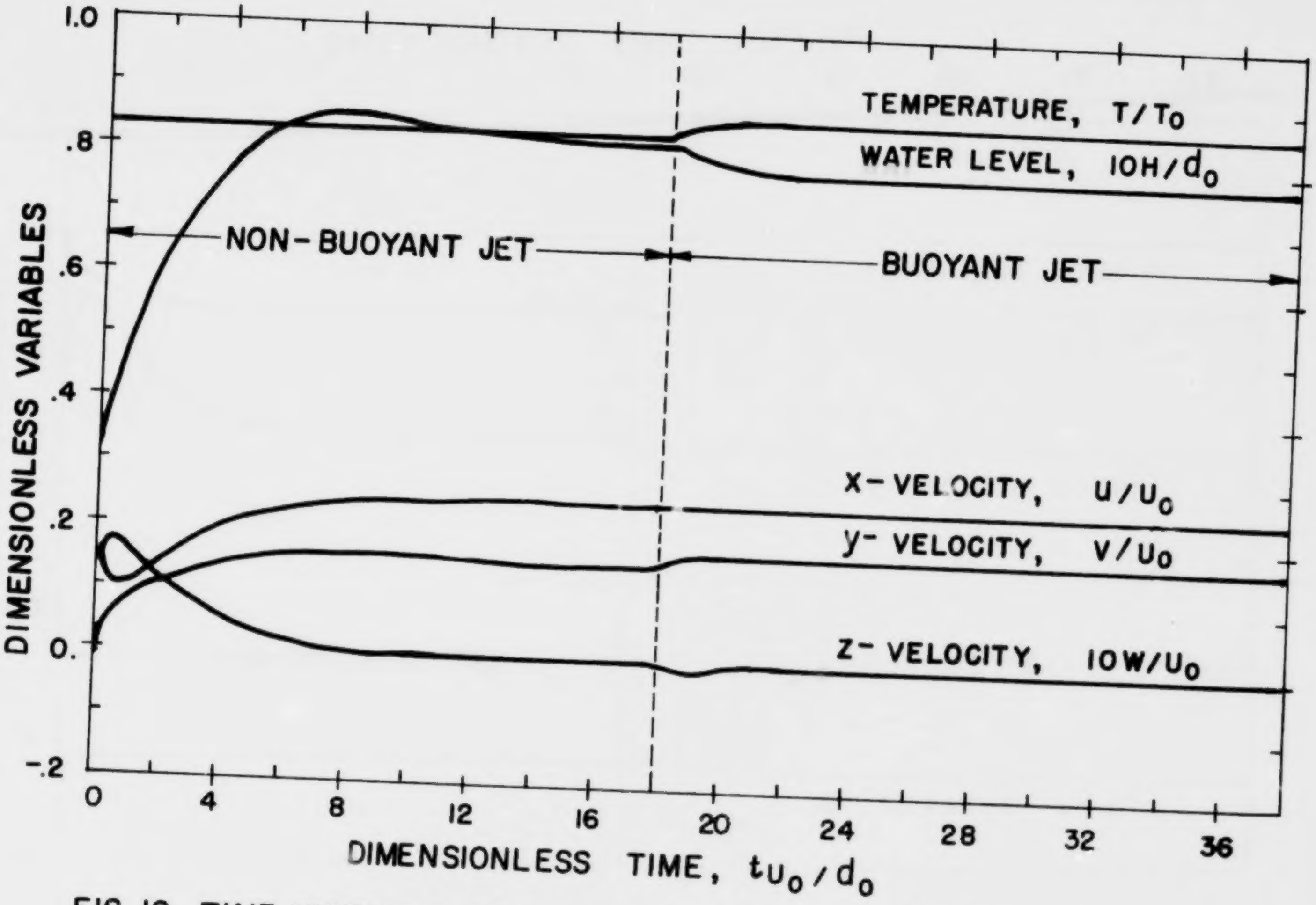

FIG 12. TIME HISTORIES OF VARIABLES AT POINT "E" IN THE WATER BODY SUBJECTED TO NON-BUOYANT AND BUOYANT JETS

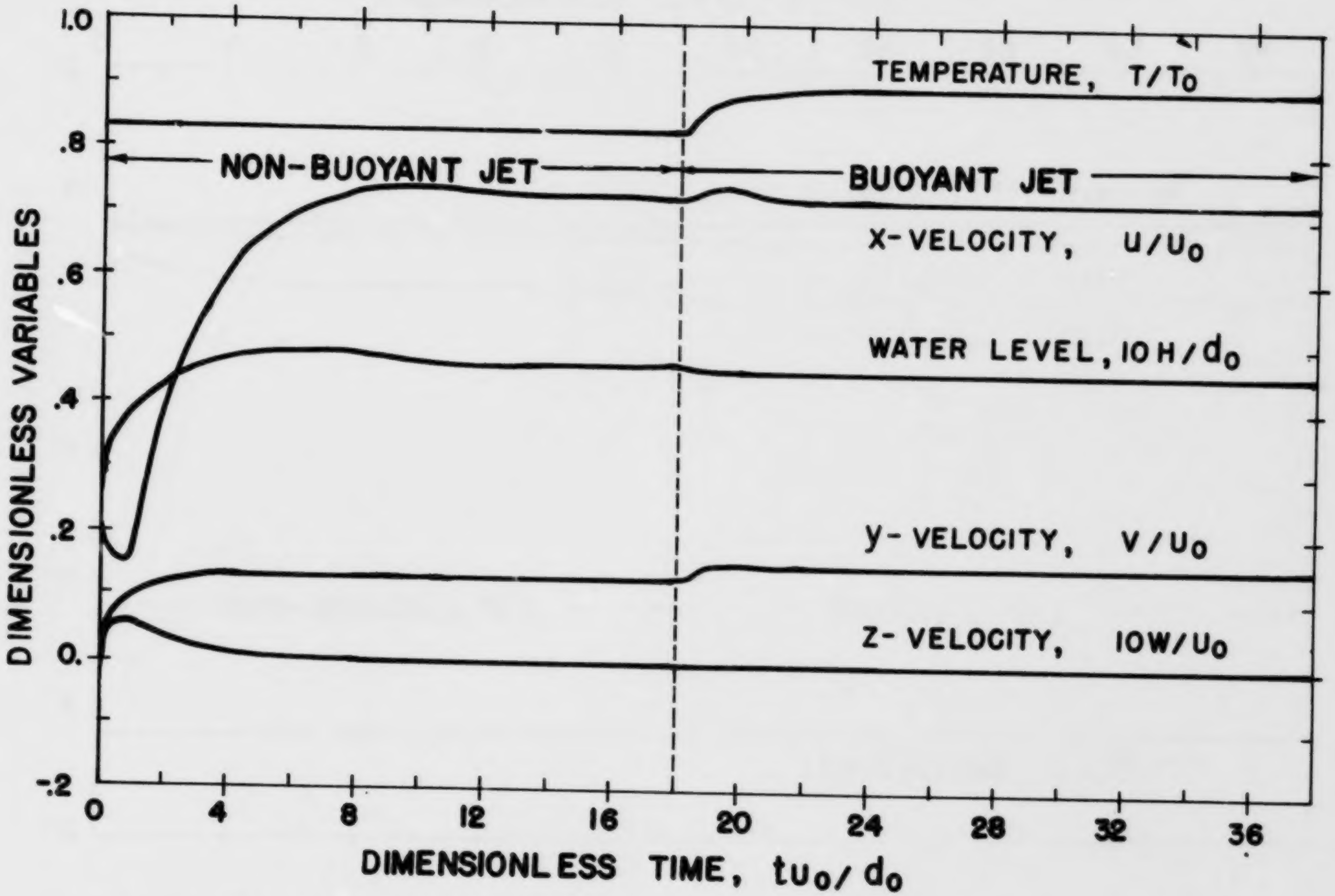

FIG 13. TIME HISTORIES OF VARIABLES AT POINT "F" IN THE WATER BODY SUBJECTED TO NON-BUOYANT AND BUOYANT JETS

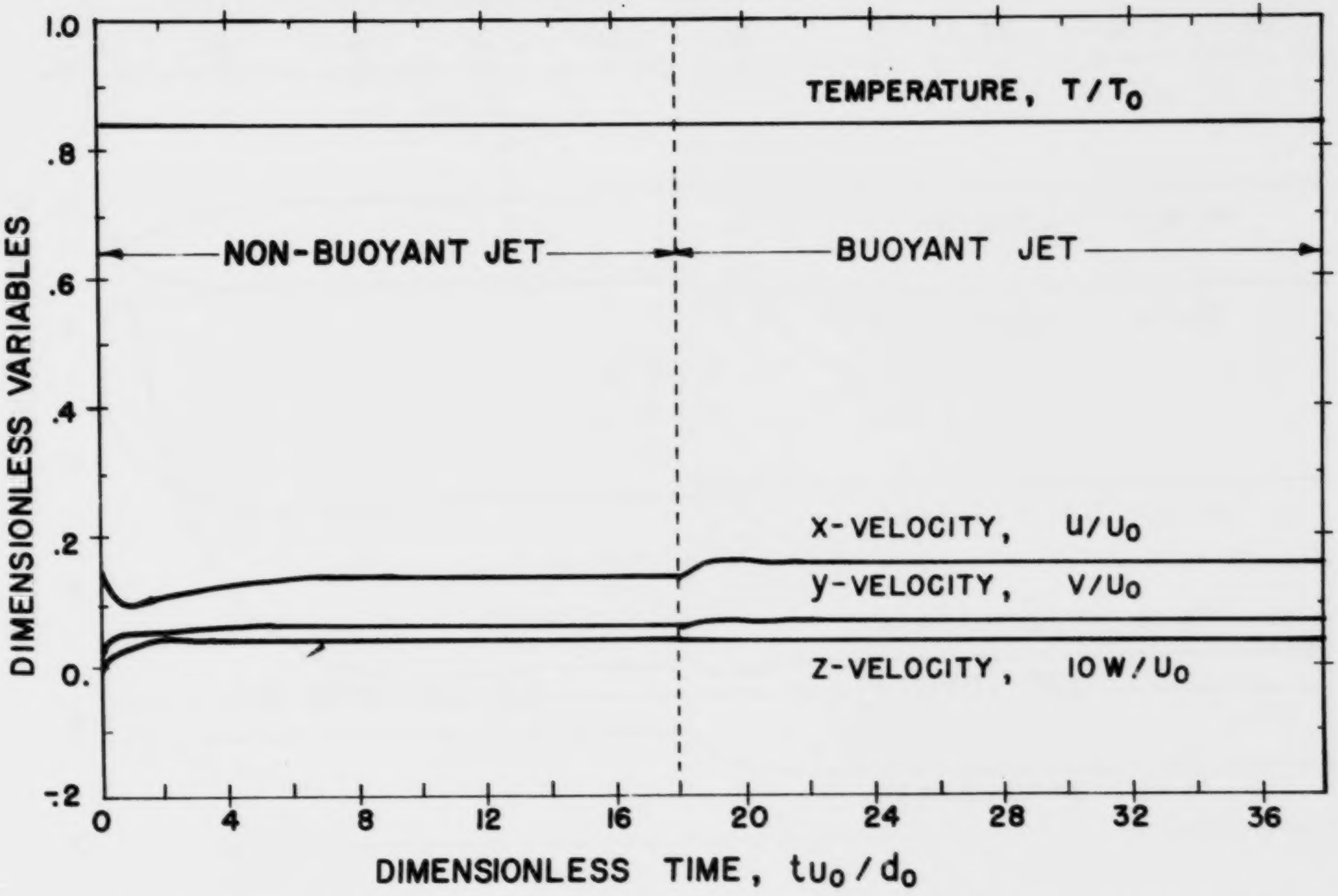

FIG 14. TIME HISTORIES OF VARIABLES AT POINT "G" IN THE WATER BODY SUBJECTED TO NON-BUOYANT AND BUOYANT JETS

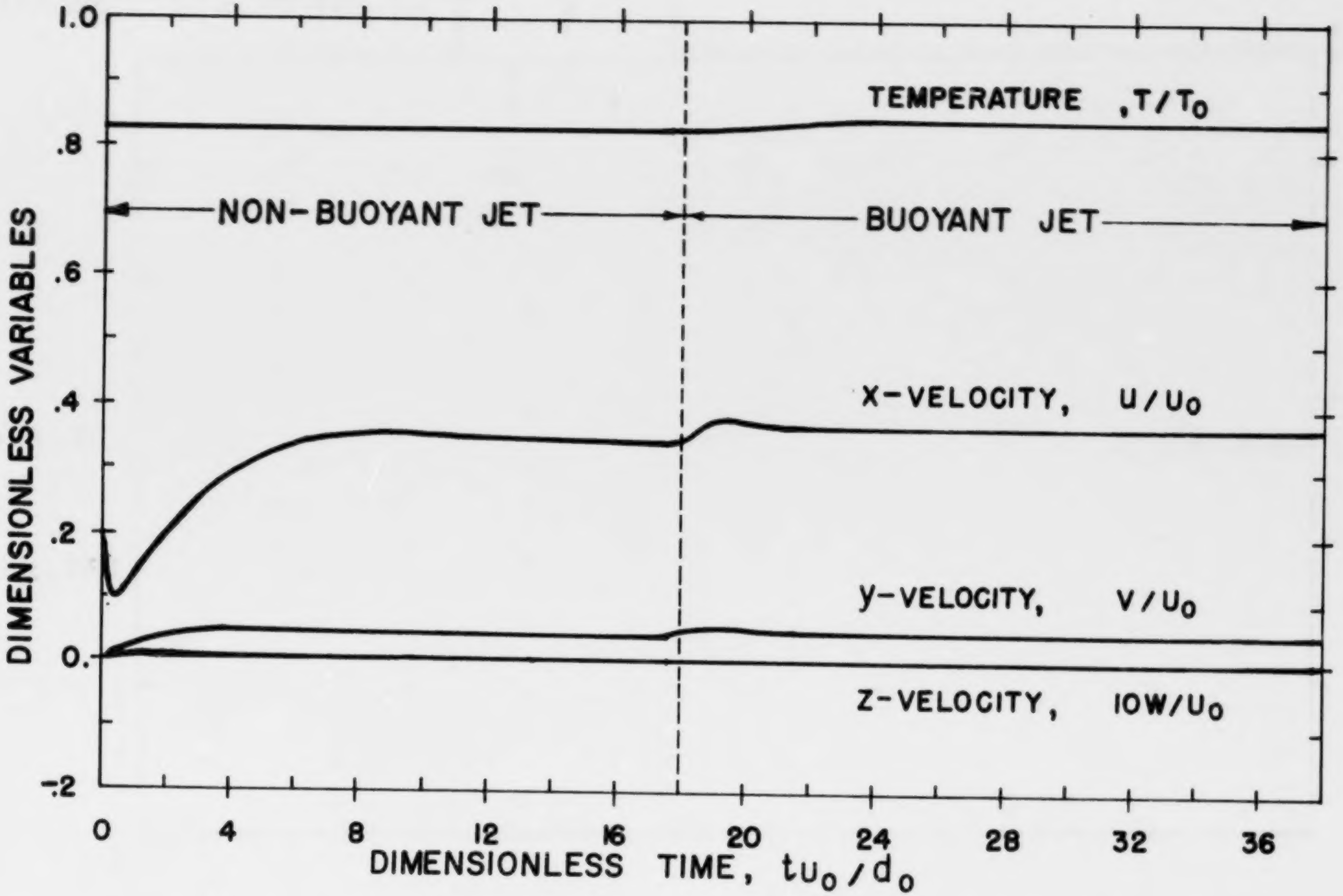

FIG 15. TIME HISTORIES OF VARIABLES AT POINT "H" IN THE WATER BODY SUBJECTED TO NON-BUOYANT AND BUOYANT JETS

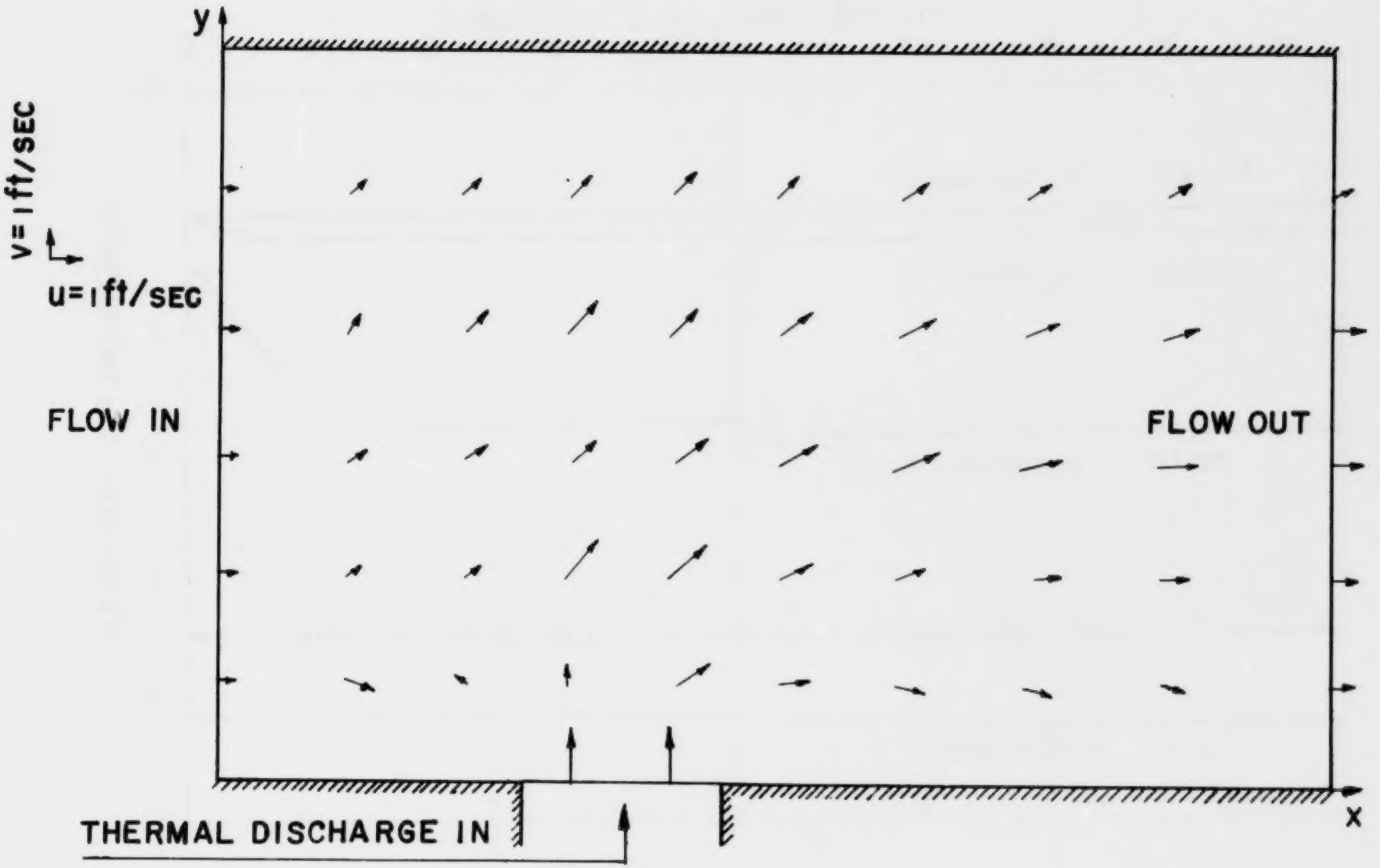
y
v=1ft/SEC
u=1ft/SEC
FLOW IN
FLOW OUT
x
THERMAL DISCHARGE IN

FIG 16. SURFACE VELOCITY FIELD AT t= 500 SEC. IN THE WATER SUBJECTED TO A BUOYANT JET

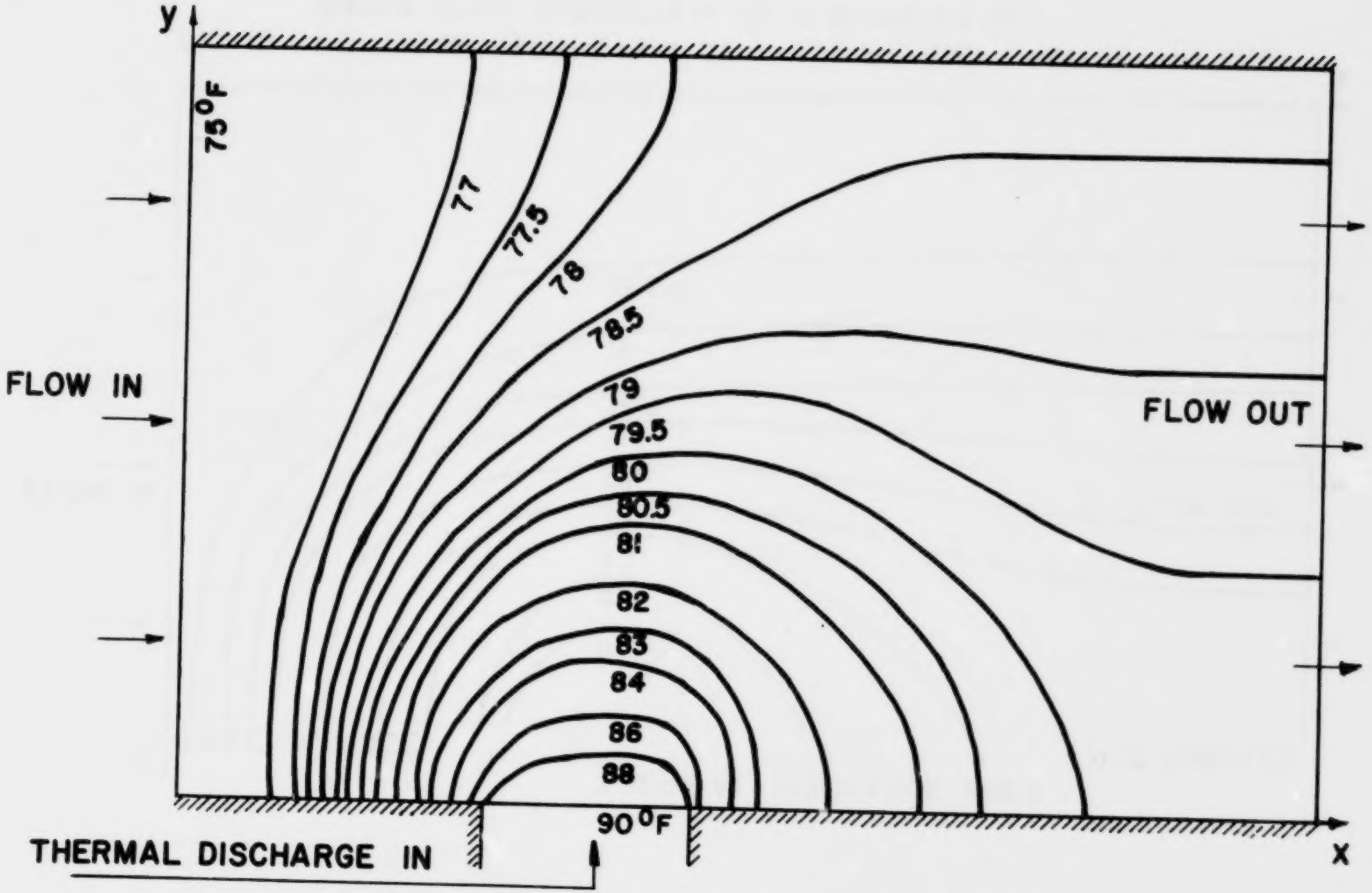

FIG 17. SURFACE ISOTHERMS AT $t = 60$ SEC. IN THE WATER BODY SUBJECTED TO A BUOYANT JET

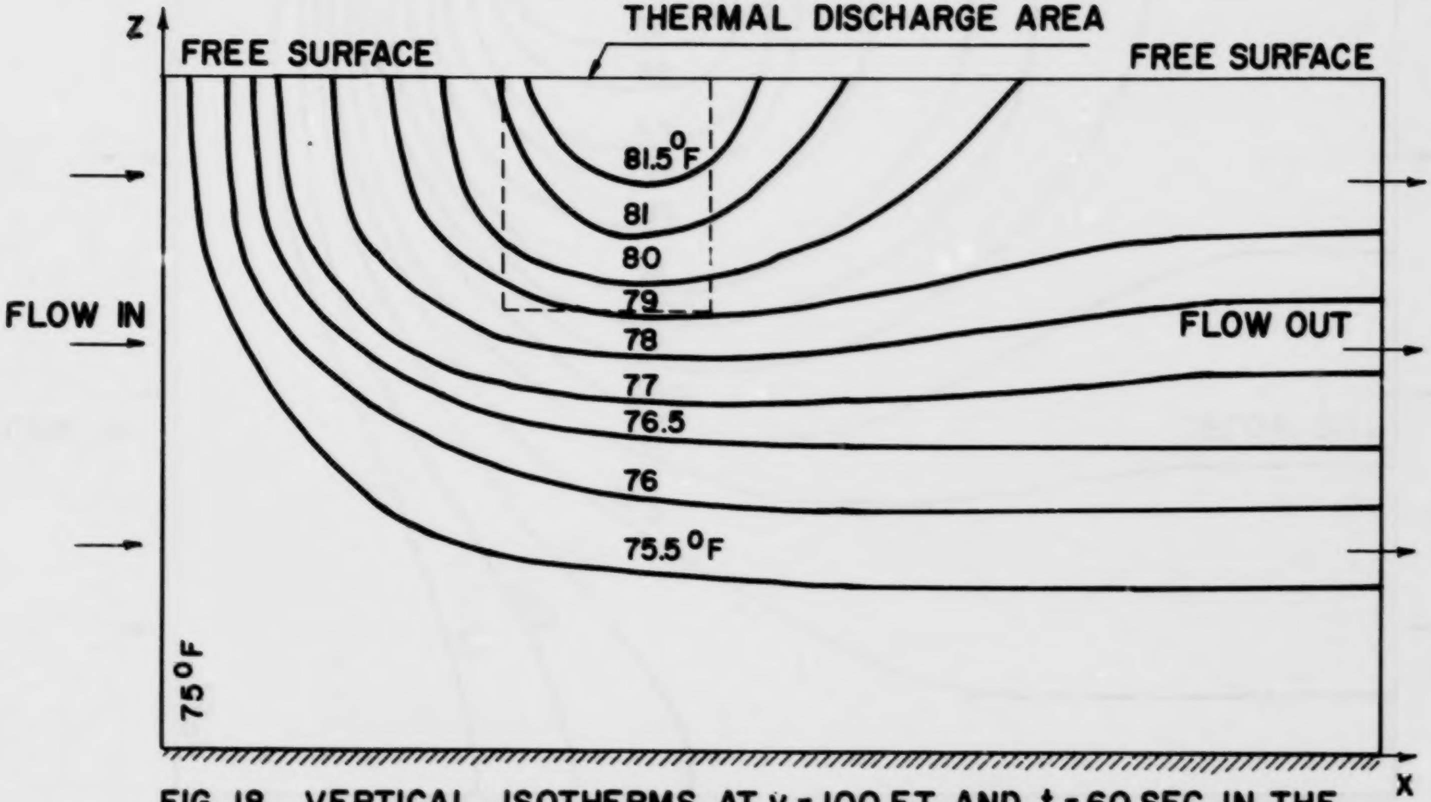

FIG 18. VERTICAL ISOTHERMS AT $y = 100$ FT. AND $t = 60$ SEC. IN THE WATER BODY SUBJECTED TO A BUOYANT JET

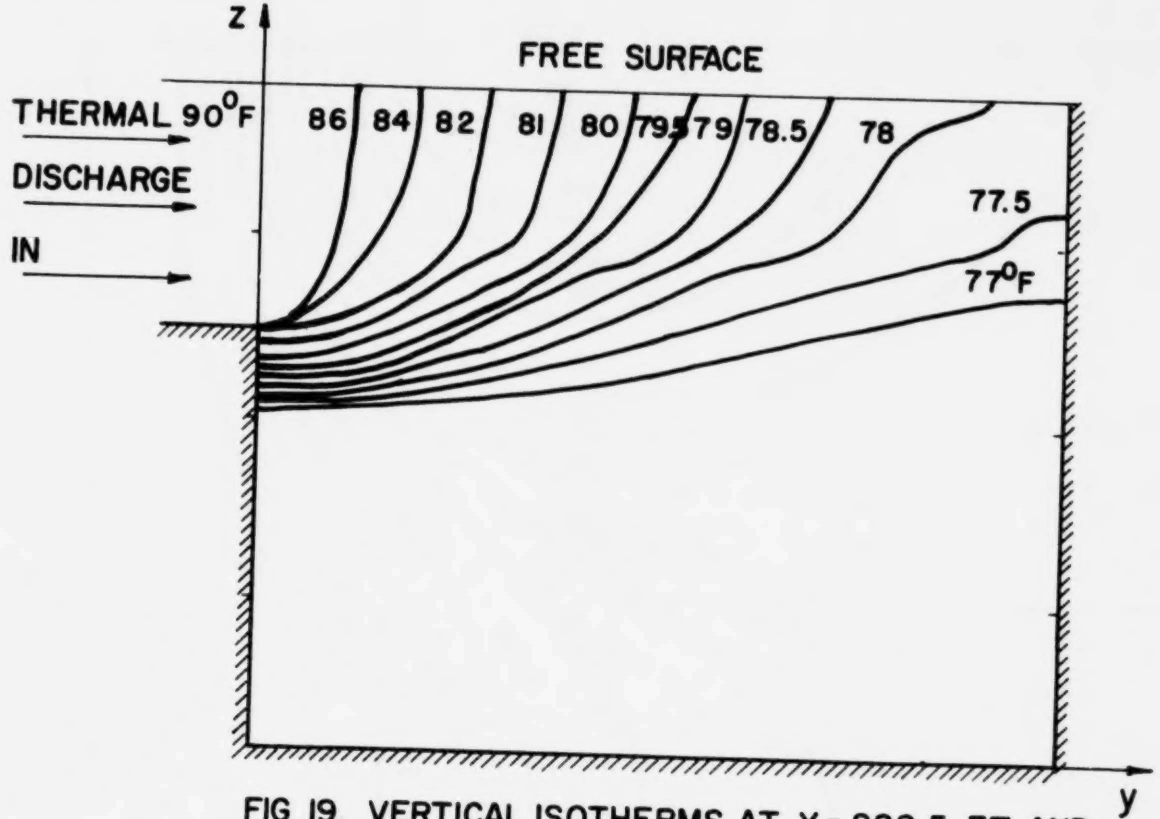

FIG 19. VERTICAL ISOTHERMS AT X = 222.5 FT. AND t = 60 SEC. IN THE WATR BODY SUBJECTED TO A BUOYANT JET

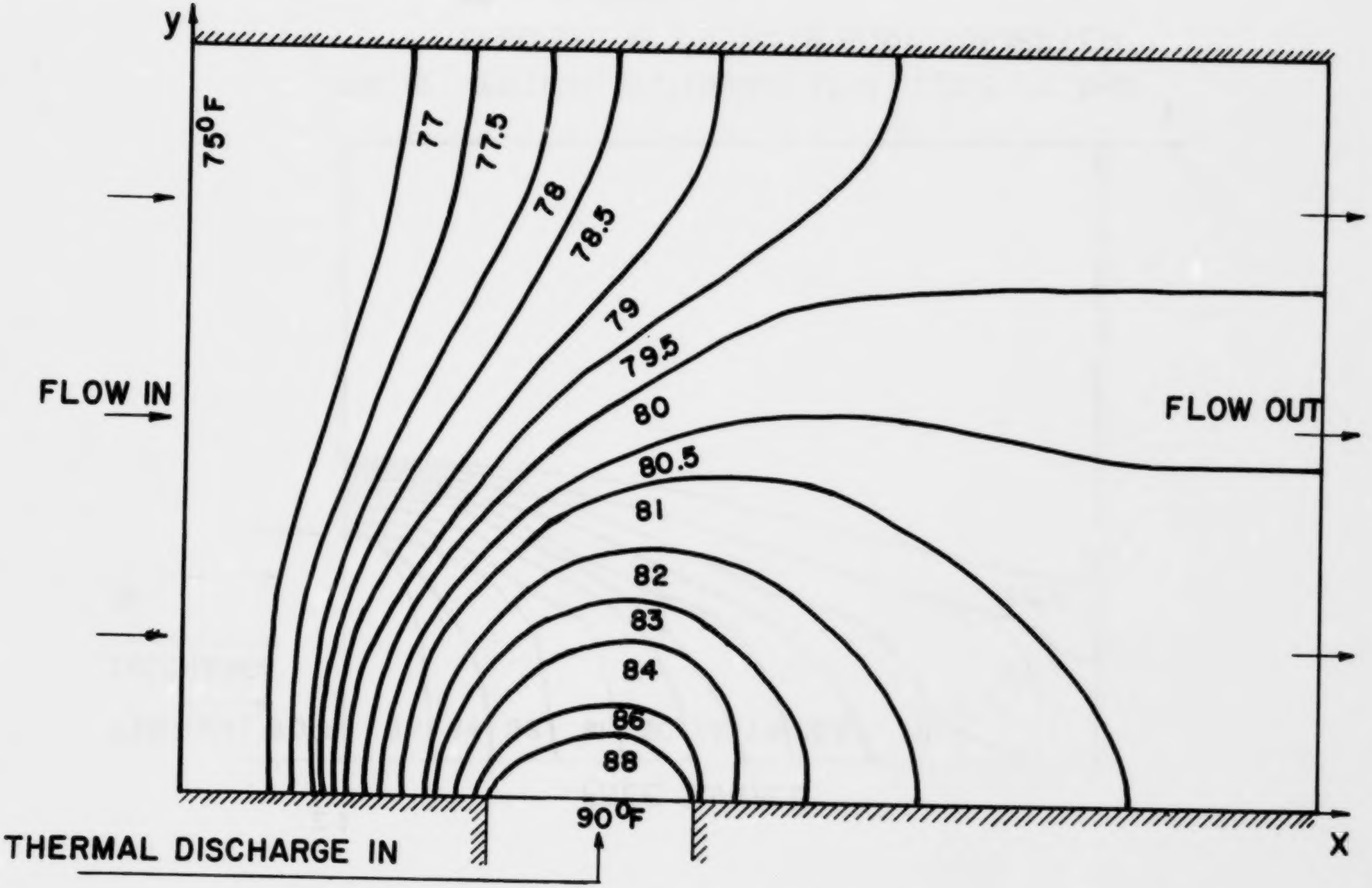

FIG 20. SURFACE ISOTHERMS AT $t = 500$ SEC. IN THE WATER BODY SUBJECTED TO A BUOYANT JET

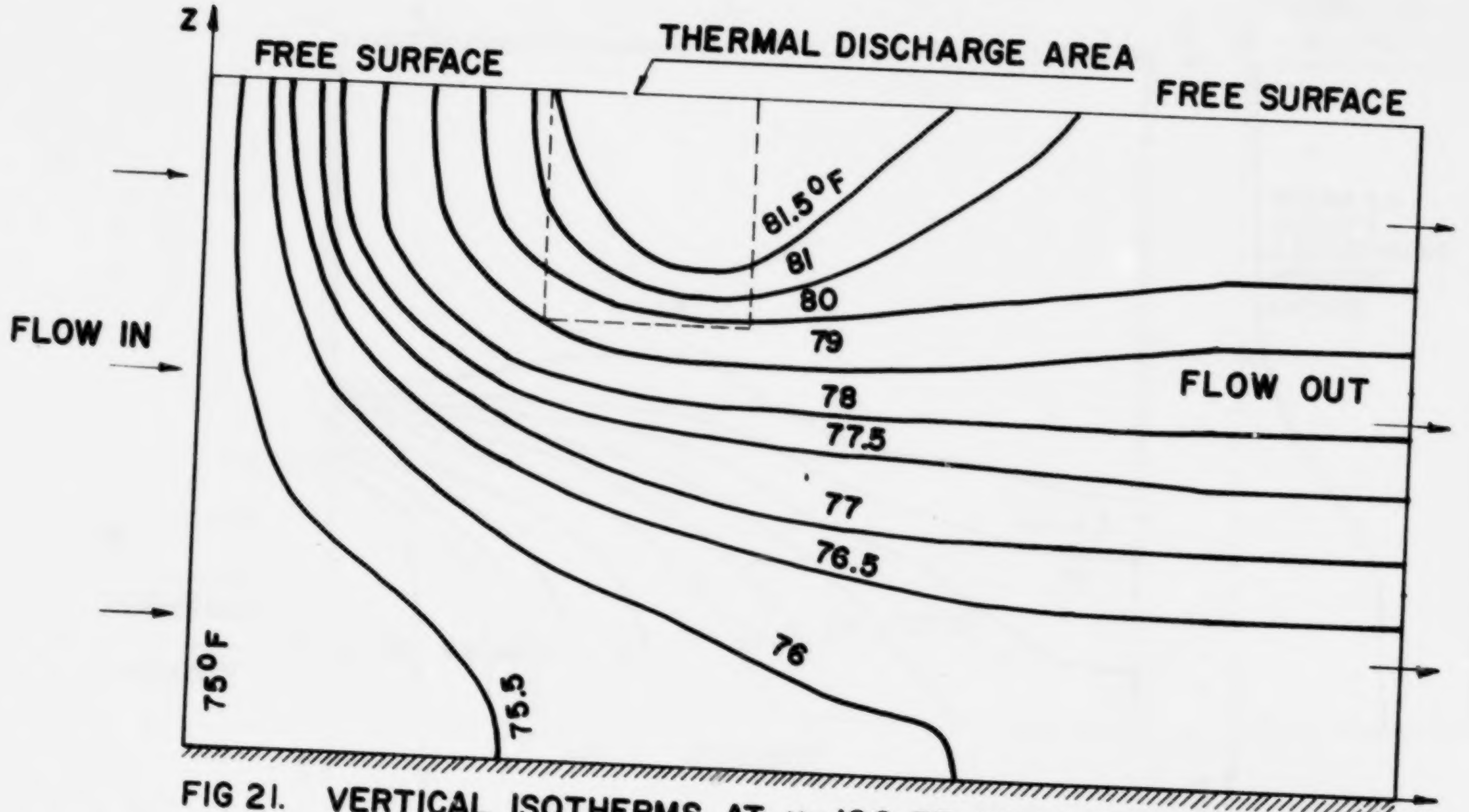

FIG 21. VERTICAL ISOTHERMS AT $y = 100$ FT. AND $t = 500$ SEC. IN THE WATER BODY SUBJECTED TO A BUOYANT JET

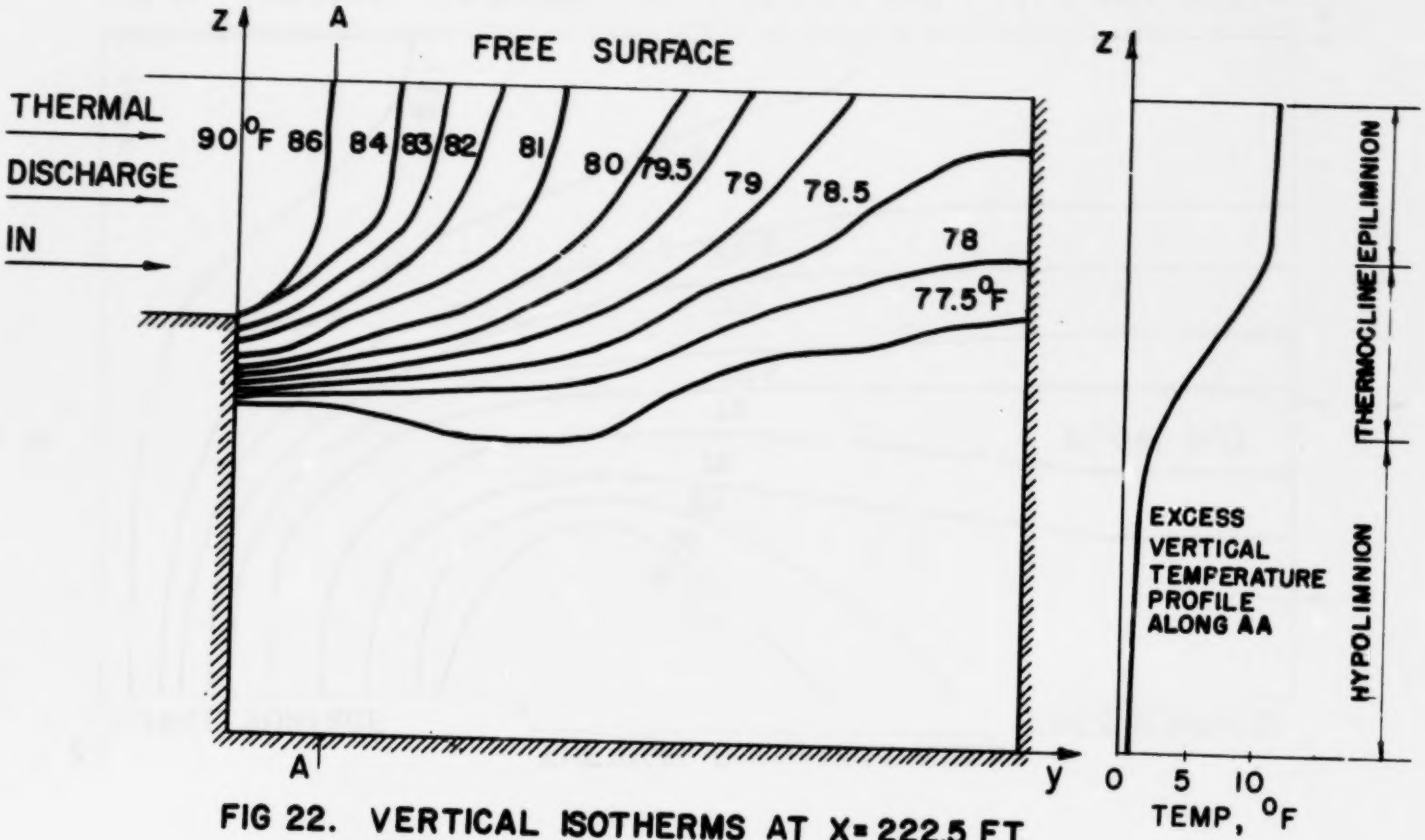

FIG 22. VERTICAL ISOTHERMS AT X = 222.5 FT. AND t = 500 SEC. IN THE WATER BODY SUBJECTED TO A BUOYANT JET

23-45-30

VI-B-85

A THREE-DIMENSIONAL RIGID-LID MODEL FOR THERMAL PREDICTIONS

S. Sengupta, S. Lee, J. Venkata, C. Carter
Dept. of Mechanical Engineering
University of Miami
Coral Gables, Florida U.S.A.

ABSTRACT

A three-dimensional methematical model to predict velocities and temperature anamolies is presented. The effects of bottom topography, wind, surface heat transfer and currents are included. A co-ordinate transformation which maps variable depth basin to a constant one is used. The rigid-lid assumption is invoked. A Poissons equation is derived as the predictive equation for surface pressure. Explicit schemes are used in time to integrate the primitive conservation equations and an iterative scheme is used to solve the Poisson's equation. The model was applied to Florida Power and Light (FPL) company's fossil fuel power plant at Cutler Ridge site for April 15,1975, outfall conditons. Infra red (IR) data in the morning (0912 EST) on April 15, 1975 was used as initial conditions for temperature. The model was run for 2 hours 38 minutes and compared with IR data at (1150 EST) on the same day. The predicted results compare favorably with IR data.

NOMENCLATURE

A_H	Horizontal kinematic eddy viscosity
A_v	Vertical kinematic eddy viscosity
A_{ref}	Reference kinematic eddy viscosity
B_H	Horizontal diffusivity
B_v	Vertical diffusivity
B_{ref}	Reference diffusivity
g	Accleration due to gravity
h	Depth at any location of the basin
H	Reference depth
I	Grid index in x-direction or α direction
J	Grid index in y-direction or β direction
K	Grid index in z-direction or γ direction
K_s	Surface heat transfer coefficient
L	Horizontal length scale
P	Pressure
P_s	Surface pressure
Pr	Turbulent Prandtl number $\frac{A_{ref}}{B_{ref}}$
Pe	Peclet Number
Re	Reynolds Number
T	Temperature
T_{ref}	Reference temperature
T_E	Equilibrium temperature
t	Time
Δt	Time step used
TTOT	Total time
u	Velocity in x-direction

v	Velocity in y-direction
w	Velocity in z-direction
x	Horizontal co-ordinate
y	Horizontal co-ordinate
z	Vertical co-ordinate
α	Horizontal co-ordinate in the stretched system
α_L	$= \alpha$ at $I = IN$
β	Horizontal co-ordinate in the stretched system
β_L	$= \beta$ at $J = JN$
γ	Vertical co-ordinate in the stretched system
μ	Absolute viscosity
ρ	Density
$(\bar{\ })$	Dimensional quantity
$(\sim)$	Dimensional mean quantity
$(\ )_{ref}$	Reference quantity

INTRODUCTION

A major source of thermal pollution in rivers, lakes and estuaries is the surface discharge of heated water from condensers of fossil and nuclear power plants. In order to design intake and outfall structures to avoid recirculation, sufficient knowledge of flow and temperature distribution in the receiving water near the discharge is necessary. Most of the previous work for the near field problem is of integral type. Some of the important work in integral models are that of Carter and Reiger (1974), Hoopes, Zeller and Rohlich (1971), Stolzenbach and Harleman (1973), Hirst (1972) and Stefan and Vaidyaraman (1971). Dunn, Policastro and Paddock (1975) discuss most of the integral models and their drawbacks. They also discuss numerical models, their advantages and disadvantages. Some of the numerical models for heated discharges are those of Brady and Geyer (1972), and Waldrop and Farmer (1974). All the above mentioned models both integral as well as numerical suffer some common disadvantages. These models also do not have adequate verification. The handbook prepared by Shirazi and Davis (1974) for surface ischarges using formulations by Prych (1972) is the most readily usable predictive tool available at present. To date, there is no three-dimensional model which incorporates the effects of bottom topography, wind, surface heat transfer and current which has been extensively verified. These factors play an important role in the dispersion of heat. The present approach tries to incorporate all these relevant mechanisms using the divergence of Navier Stokes model developed by Sengupta and Lick (1974).

For calibration and model verification, FPL's power plant at Cutler Ridge site in Florida is considered. The objective of the present investigation was to predict velocity and temperature anamolies in the near field (i.e., the region which is most affected by the heated discharge). The region of interest is approximated to 525m along the axis of the jet and 425m across the axis of the jet. Figs. 1 and 2 show the basin and grid system.

BASIC EQUATIONS

The equations which describe the behaviour of fluid flow are those expressing the conservation of mass, momentum and energy. In order to keep the generalized nature of the model all significant terms in the conservation equations are retained. This includes the effects of buoyancy, inertia, coriolis, density and turbulent mixing. Wind shear, surface heat transfer and cross flow are also considered. The details of the derivation of the equations are presented in Sengupta and Lick (1974).

Assumptions and Approximations

The rigid-lid approximation is made. The rigid-lid approximation is that a rigid wall is placed on the top which allows horizontal velocities, but forces vertical velocities at the surface to zero. This approximation was used by Bryan (1969) Sengupta and Lick (1974) and several others.

This approximation is permissible as it eliminates surface gravity waves and are thereby associated instabilities. This approximation allows use of larger time steps thus saving computer time.

Since the velocities are small, the vertical momentum equation is replaced by the hydrostatic approximiation.

Turbulence is modelled using eddy transport coefficients. Constant, but different values are used for horizontal and vertical directions. The eddy transport coefficients are found by trial and error method till the correct values are obtained.

In order to overcome programming difficulties the equations are stretched vertically using the transformation,

$$\gamma = Z / h(x,y)$$

Now the equations will be transformed from (x,y,z) coordinate system to a more convenient coordinate system (x,y,γ) or for convenience (α,β,γ). The advantage of this transformation is that the same number of grid points can be used in the vertical direction at shallow as well as deeper parts. Now the equations after using the above transformation will take the form shown below:

continuity

$$\frac{\partial(hu)}{\partial\alpha} + \frac{\partial(hv)}{\partial\beta} + \frac{\partial\Omega}{\partial\gamma} = 0 \qquad (1)$$

momentum-u

$$\frac{\partial(hu)}{\partial t} + \frac{\partial(huu)}{\partial\alpha} + \frac{\partial(huv)}{\partial\beta} + h\,\frac{\partial(\Omega u)}{\partial\gamma} - \frac{h}{R_B}\,v = -h\,\frac{\partial Ps}{\partial\alpha}$$

$$- hB_x + \frac{1}{Re}\,\frac{\partial}{\partial\alpha}\left(h\frac{\partial u}{\partial\alpha}\right) + \frac{1}{Re}\,\frac{\partial}{\partial\beta}\left(h\frac{\partial u}{\partial\beta}\right) + \frac{1}{\varepsilon^2 Re}\,\frac{1}{h}\,\frac{\partial}{\partial\gamma}\left(A_v^*\,\frac{\partial u}{\partial\gamma}\right) \qquad (2)$$

momentum-v

$$\frac{\partial(hv)}{\partial t} + \frac{\partial(huv)}{\partial\alpha} + \frac{\partial(hvv)}{\partial\beta} + h\,\frac{\partial(\Omega v)}{\partial\gamma} + \frac{h}{R_B}\,u = -h\,\frac{\partial Ps}{\partial\beta}$$

$$-hB_y + \frac{1}{Re}\,\frac{\partial}{\partial\alpha}\,\frac{(h\partial v)}{\partial\alpha} + \frac{1}{Re}\,\frac{\partial}{\partial\beta}\,\frac{(h\partial v)}{\partial\beta} + \frac{1}{\varepsilon^2 Re}\,\frac{1}{h}\,\frac{\partial}{\partial\gamma}\left(A_v^*\,\frac{\partial v}{\partial\gamma}\right) \qquad (3)$$

hydrostatic equation

$$\frac{\partial p}{\partial\gamma} = Eu\,(1+\rho)\,h \qquad (4)$$

energy

$$\frac{\partial(hT)}{\partial t} + \frac{\partial(huT)}{\partial\alpha} + \frac{\partial(hvT)}{\partial\beta} + h\,\frac{\partial(\Omega T)}{\partial\gamma} = \frac{1}{Pe}\,\frac{\partial}{\partial\alpha}\,\frac{(h\partial T)}{\partial\alpha}$$

$$+ \frac{1}{Pe}\,\frac{\partial}{\partial\beta}\,\frac{(h\partial T)}{\partial\beta} + \frac{1}{Pe\,\varepsilon^2}\,\frac{1}{h}\,\frac{\partial}{\partial\gamma}\left(B_v^*\,\frac{\partial T}{\partial z}\right) \qquad (5)$$

Eq of state

$$\rho = f'(T) \qquad (6)$$

Poisson equation

$$\frac{\partial^2 Ps}{\partial\alpha^2} + \frac{\partial^2 Ps}{\partial\beta^2} = \frac{1}{h}\,\frac{\partial}{\partial\alpha}\,(-Ax_1 + Ax_2 + Cx - x_p) + \frac{1}{h}\,\frac{\partial}{\partial\beta}\,(-Ay_1 -$$

$$Ay_2 + Cy - Y_p) - \frac{1}{h}\left\{ \frac{\partial h}{\partial\alpha}\,\frac{\partial P_s}{\partial\alpha} + \frac{\partial h}{\partial\beta}\,\frac{\partial Ps}{\partial\beta} \right\} - \frac{\partial(\Omega)}{\partial t}\,(z = 0) \qquad (7)$$

where

$u = \tilde{u}/Uref; \quad v = \tilde{v}/U_{ref}; \quad w = \tilde{w}/U_{ref}; \quad t = \tilde{t}/t_{ref}$

$x = \tilde{x}/_{L}; \quad y = \tilde{y}/_{L}; \quad z = \tilde{z}/_{H}; \quad \epsilon = H/_{L}$

$P = \tilde{P}/_{\rho_{ref} U^{2}_{ref}}; \quad T = \frac{\tilde{T}-Tref}{T_{ref}}; \quad \rho = \frac{\tilde{\rho}-\rho_{ref}}{\rho_{ref}}$

$A^{*}_{H} = A_{H}/A_{ref}; \quad A^{*}_{V} = A_{V}/A_{ref}; \quad B^{*}_{H} = B_{H}/B_{ref}; \quad B^{*}_{V} = B_{V}/B_{ref}$

$t_{ref} = L/_{U_{ref}}$

$Re = \frac{U_{ref}L}{A_{ref}}; \quad R_{B} = \frac{U_{ref}}{fL}; \quad Pr = \frac{A_{ref}}{B_{ref}}$

$Pe = Re \, . \, Pr = \frac{U_{ref}L}{B_{ref}}; \quad Eu = \frac{qH}{U_{ref}{}^{2}}$

In all the above terms "ref" stands for reference quantities, H and L are vertical and horizontal length scales. The variables with wavy lines on top are dimensional quantities. If A_H = Aref and B_H = B ref then $A^{*}_{H} = B^{*}_{H} = 1$. If Pr = 1 then $A_{ref} = B_{ref}$

and

$$B_{x} = Eu\frac{\partial h}{\partial \alpha} \int_{o}^{\gamma} \rho \, d\gamma + Euh\frac{\partial}{\partial \alpha} \int_{o}^{\gamma} \rho \, d\gamma - Eu\gamma \frac{\partial h}{\partial \alpha} \rho$$

$$B_{y} = Eu\frac{\partial h}{\partial \beta} \int_{o}^{\gamma} \rho \, d\gamma + Eu\,h\frac{\partial}{\partial \beta} \int_{o}^{\gamma} \rho \, d\gamma - Eu\gamma \frac{\partial h}{\partial \beta} \rho$$

$$\tilde{w} = \gamma \left(\tilde{u} \frac{\widetilde{\partial h}}{\partial x} + \tilde{v} \frac{\widetilde{\partial h}}{\partial y} \right) + \tilde{h}\,\tilde{\Omega}$$

$$\Omega = \frac{\partial \gamma}{\partial \tilde{t}}$$

$$A_{x_1} = \int_{o}^{1} \left\{ \frac{\partial}{\partial \alpha} (huu) + \frac{\partial}{\partial \beta} (huv) + h\frac{\partial}{\partial \gamma} (\Omega u) \right\} d\gamma$$

$$A_{X_2} = \frac{h}{R_B} \int_0^1 v\,d\gamma$$

$$C_X = \frac{1}{Re} \int_0^1 \left\{ \frac{\partial}{\partial\alpha} \left(h \frac{\partial u}{\partial\alpha}\right) + \frac{\partial}{\partial\beta} \left(h \frac{\partial u}{\partial\beta}\right) + \frac{1}{\epsilon^2 h} \frac{\partial}{\partial\gamma} \left(A_V^* \frac{\partial u}{\partial_\gamma}\right) \right\} d\gamma$$

$$X_p = Eu \int_0^1 h \left\{ \frac{\partial h}{\partial X} \int_0^\gamma \rho\,d\gamma + h \frac{\partial}{\partial\alpha} \int_0^\gamma \rho\,d\gamma - \gamma \frac{\partial h}{\partial\alpha} \rho \right\} d\gamma$$

$$A_{Y_1} = \int_0^1 \left\{ \frac{\partial}{\partial\alpha} (huv) + \frac{\partial}{\partial\beta} (hvv) + h \frac{\partial(\Omega v)}{\partial\gamma} \right\} d\gamma$$

$$A_{Y_2} = \frac{h}{R_B} \int_0^1 u\,d\gamma$$

$$C_Y = \frac{1}{Re} \int_0^1 \left\{ \frac{\partial}{\partial\alpha} \left(h \frac{\partial v}{\partial\alpha}\right) + \frac{\partial}{\partial\beta} \left(h \frac{\partial v}{\partial\beta}\right) + \frac{1}{\epsilon^2 h} \frac{\partial}{\partial\gamma} \left(A_V^* \frac{\partial v}{\partial\gamma}\right) \right\} d\gamma$$

$$Y_p = Eu \int_0^1 h \left\{ \frac{\partial h}{\partial\beta} \int_0^\gamma \rho\,d\gamma + h \frac{\partial}{\partial\beta} \int_0^\gamma \rho\,d\gamma - \gamma \frac{\partial h}{\partial\beta} \rho \right\} d\gamma$$

The last term in equation (7) is the Hirt and Harlow (1967) correction term. This term is not set equal to zero even though the rigid-lid conditions imply W (Z = 0) = 0. This is in anticipation of the errors which will arise when the Poisson equation is solved by iterative technique. If these errors are not corrected, the continuity equation will not be satisfied leading to accumilation or loss of fluid from the system.

Equations 1 through 7 form the set of equations which are to be solved with appropriate boundary conditions.

Boundary Conditions

The boundary conditions used are shown in Fig. 3. The conditions on solid walls and bottom are no slip and no normal velocity for all time for the momentum equations, except $W \neq 0$ at side wall due to hydrostatic approximation. The temperature boundary condition at solid walls and bottom is handled by assuming the walls and bottom adiabatic. The boundary condition for velocity and temperature at open boundaries is $\frac{\partial f}{\partial n} = 0$, where $\frac{\partial f}{\partial n}$ is velocity or temperature gradient normal to the boundary. At the air-water interface the boundary condition on the momentum equations are obtained in the form of wind stress. The temperature boundary condition at the air water interface due to Edinger & Geyer (1971) is

$$\text{Heat flux} = \Delta Q = K_s \ (\tilde{T}_E - \tilde{T}_S)$$

where K_s is surface heat transfer coefficient and T_E and T_S are equilibrium and surface temperatures. The boundary conditions for the Poisson equation are Neuman type along solid boundary and along open boundaries the pressure is assumed constant.

The boundary conditions in summary for the stretched system of equations are:

Along the shore:

$$u = 0$$

$$v = 0$$

$$\Omega \neq 0$$

$$\frac{\partial T}{\partial Y} = \frac{\partial T}{\partial \beta} - \frac{\gamma}{h} \frac{\partial h}{\partial \beta} \frac{\partial T}{\partial \gamma} = 0$$

At the bottom of the basin ($\gamma=1$):

$$\Omega = 0$$

$$u = 0$$

$$v = 0$$

$$\frac{\partial T}{\partial \gamma} = 0$$

Along free boundaries:

At $(\alpha = 0, \beta, \gamma)$

$U_{I=1, K} = U_{I=2, K}$

$v = 0$

$w \neq 0$

$T_{I=1, K} = T_{I=2, K}$

P_s = constant

At $(\alpha = \alpha_L, \beta, K)$

$U_{I=IN, K} = U_{I=IN-1, K}$

$v = 0$

$w \neq 0$

$T_{I=IN, K} = T_{I=IN-1, K}$

P_s = constant

At $(\alpha, \beta = \beta_L, \gamma)$

$V_{JN, K} = V_{JN-1, K}$

$u = 0$

$w \neq 0$

P_s = constant

At inflow boundaries, the velocity of current is specified

At the air-water interface

$\Omega = 0$ (Rigid-lid)

$$\frac{\partial u}{\partial \gamma} = \left(\frac{hH}{U_{ref} A_V}\right) \tau_{sx}$$

$$\frac{\partial v}{\partial \gamma} = \left(\frac{hH}{U_{ref} A_V}\right) \tau_{\mathcal{Z}y}$$

$$\frac{\partial T}{\partial \gamma} = \left(\frac{hHK_s}{B_z}\right) (T_E - T_s)$$

ARRANGEMENT OF VARIABLES AND GRID SYSTEM

The grid system and arrangement of variables are shown in Fig. 4. u and v are located on integral nodes (I,J,K) on the horizontal (x,y) plane. P, T, W, ρ are located at half grid points ($I + \frac{1}{2}$, $J + \frac{1}{2}$, k). This arrangement is repeated in $\mathcal{Z}$ direction. This kind of arrangement allows better meshing of the variables without calculating all variables at all nodes of the staggered mesh system. Constant grid spacing is used in σ or $\mathcal{Z}$ direction. Constant grid spacing is also used in x and y (or α and β) directions.

METHOD OF SOLUTION

The method of solution is explicit using forward time central space (FTCS) schemes except in the diffusion term. The diffusion terms are differenced by the Dufort-Frankel scheme. The initial values of variables are specified and then the equations are integrated marching in time. The only iterative procedure involves the solution of the equation for surface pressure.

Since it is not possible to make a strict stability analysis for the system of equation under consideration, one-dimensional Burgers equation is used for stability analysis.

The stability citerion for the equations under consideration is therefore:

convective criterion

$$u \frac{\Delta \bar{t}}{\Delta \tilde{x}} + v \frac{\Delta \bar{t}}{\Delta \tilde{y}} + w \frac{\Delta \bar{t}}{\Delta \tilde{\mathcal{Z}}} \leq 1$$

diffusion

$$A_H \frac{\Delta \bar{t}}{(\Delta \tilde{x})^2} + A_H \frac{\Delta \bar{t}}{(\Delta \tilde{y})^2} + A_V \frac{\Delta \bar{t}}{(\Delta \tilde{\mathcal{Z}})^2} \leq \frac{1}{2}$$

$$B_H \frac{\Delta\bar{t}}{(\Delta\tilde{x})^2} + B_H \frac{\Delta\bar{t}}{(\Delta\tilde{y})^2} + B_V \frac{\Delta\bar{t}}{(\Delta\tilde{z})^2} \leq \tfrac{1}{2}$$

The equations are solved on a UNIVAC/1106 computer at the University of Miami.

RESULTS

The region of influence of the Cutler Ridge plume has been approximated to a rectangular domain as shown in Fig. 1. It extends 425 meters in lateral extent and 525 meters in longitudinal extent. The discharge is taken as 25 meters wide. The numerical grid system is shown in Fig. 2. It has 18 and 22 nodes across and along the axis of the jet respectively. There are 5 nodes in the vertical direction.

In order to understand the physical processes involved and to investigate the numerical behaviour of the model several simplified cases were executed before the final calibration and verification run for April 15,1975.

Case 1

This case was designed to study the effects of bottom topography. A section of bottom topography can be seen in Fig. 5. The topography is symmetrical about the discharge centerline. The canal is 6 meters deep gradually merging into the bay which is 1.2 meters deep. The steady state surface velocities are symmetrical as expected, since the effects of wind and current are neglected and the bottom topography is symmetrical about the centerline. These results are shown in Fig. 6. There is a reduction in velocities in the bottom layers owing to bottom shear. Fig. 5 shows centerline surface velocity with distance from discharge origin at different times. The steady state curve (155 min) shows that the velocity decays to about 75 meters and then gradually increases to a value slightly higher than the initial discharge velocity at a distance of 175 meters. The reason for this is that the depth is initially constant along the jet and the velocity decays as expected. However, after 75 meters the depth decreases linearly to 1.2 meters in the next 75 meters thus causing a constricting effect which increases the velocity offsetting the decrease caused by lateral mixing. Here again it can be seen that the time to reach steady state increases with distance from the jet origin.

Case 2

The effects of density variations is studied in this case. The basin was taken as constant depth 1.2 meters and effects of wind and current neglected. The discharge temperature is 35.9°C and the ambient temperature is 28.0°C. Fig. 7 shows the surface isotherms. The inertial core of the discharge can be seen as an elongated wedge of warm water at the mouth of the discharge. The isotherms are symmetrical as expected, since the effects of wind and current are neglected. The centerline temperature decay of the plume is shown in Fig. 8. The behaviour is very similar to the surface velocity decay. This is because the dispersal of heat and momentum essentially have the same mechanisms. The temperature decay near the origin is therefore followed by a region of rapid decay caused by entrainment. Finally as the difference in temperature is reduced the temperature asymptotically approaches the ambient value.

Case 3

This case includes the effects of strong wind along with density variations on a discharged plume into a constant depth basin. The wind was blowing at 6.71 m/sec (15 mph) 160°N. Fig. 9 shows surface velocities. The wind driven current is very dominant for most of the flow. The effect of wind slowly reduced in the bottom layers, finally being dominated by bottom shear near the floor of the basin. Fig. 10 shows the skewed plume. The plume is turned towards the west. The skewing increases with time until a steady state is reached.

Case 4

The data base for this case is obtained from the field experiments conducted at the Cutler Ridge site on April 15, 1975. The initial temperature conditions are taken from the morning IR data (0911-0912 EST) and ground truth data on April 15,1975. The computations were continued for 2 hrs. 38 min. Fig. 11 shows isotherms predicted by the model along with IR data (11:45-11:55 EST) on April 15,1975. As can be seen there is reasonably good agreement between IR data and model predicted results. Fig. 12 shows temperature decay along J at I=11 (close to centerline) predicted by the model along with IR data. There is a good agreement between IR data and model results. The isotherms along I and J sections are shown in Figs. 13 and 14 respectively.

TABLE 1

CASE NO.	DEPTH	DENSITY	WIND STRESS (WIND SPEED)	CURRENT	REMARKS
1	Variable	Constant	None	None	Steady State (TTOT = 155 min) Δt = 30 sec.
2	Constant (1.2 m)	Variable	None	None	TTOT = 1/2 hr. Δt = 15 sec.
3	Constant (1.2 m)	Variable	15 mph 6.71 m/sec	None	TTOT = 2 1/2 hrs. Δt = 15 sec
4	Constant (1.2 m)	Variable	15 mph 6.71 m/sec	3 cm/sec south	TTOT = 2 hrs. 38 min. Δt = 10 sec.

The following values are used in the above cases:

Discharge Vel : 20 cm/sec K_S = 100 BTU/$^{\circ}$F-Ft^{2}-day

Discharge Temp: 35.9°C

Initial Temp : 28.0°C

Air Temp : 29.5°C

Case 4 is ran with IR data initial conditions

Stratification near discharge with isothermal conditions away from the plume can be seen in Fig. 13.

SUMMARY

Simple cases have been investigated to obtain an understanding of the basic mechanisms of the behaviour of a buoyant surface jet. Effects of wind, topography and current have been documented. Comparison with data bases obtained for field measurements, (both in-situ and airborne IR) is good. The model can be used either for preparation of environmental impact satements or research in buoyant surface jets.

ACKNOWLEDGEMENTS

The authors wish to thank National Aeronautics and Space Administration, Kennedy Space Center, for the financial assistance provided under contract NASA10-8740. NASA-KSC personnel were also responsible for providing remote sensing support.

REFERENCES

1. Brady, D. and Geyer, J., "Development of General Computer Model for Simulating Thermal Discharges in Three-Dimensions", Report No. 7, Dept. of Geography and Environmental Eng., Johns Hopkins University, Baltimore, Md. (1972).

2. Bryan,K., "A Numerical Method for the Study of the World Oceans", Journal of Computational Physics, Vol. 4, 1969.

3. Carter, H.H. and Reiger, R., "The three-dimensional Heated Surface jet in a Cross Flow", Technical Report 88, Chesapeake Bay Institute, Johns Hopkins University, Baltimore, Md. (1974)

4. Dunn, W.E., Policastro, A.J., and Paddock, R.A., "Surface Thermal Plumes: Evaluation of Mathematical Models for the Near and Complete Field", Water Resources Research Program, Energy and Environmental Systems Division, Argonne National Laboratory, Argonne, Illinois (Part one and two) (1975).

5. Edinger, J.E. and Geyer, J.C., "Heat Exchange in the Environment", E.E.I. publication, No. 65-902, Edison Electric Institute, 1971.

6. Hirst, E., "Buoyant Jets with Three-Dimensional Trajectories", Journal of Hydraulics Division, ASCE, Vol. 98, Nov.,

1972, pp 1999-2014.

7. Hirt, C.W. and Harlow, F.W., "A General Corrective Procedure for the Numerical Solution of Initial Value Problems", Journal of Computational Physics, Vol. 2, 1967.

8. Hoopes, J.A., Zeller, R.W., and Rohlich, G.A., "Heated Surface Jets in a Steady Crosscurrent", Journal of Hydraulic Div., ASCE, Vol. 97, Sept. 1971, pp 1403-1426.

9. Prych, E., "A Warm Water Effluent Analyzed as A Buoyant Surface Jet", Swedish Meteorological and Hydrological Inst., Hydraulic Series No. 21 (1972).

10. Sengupta, S. and Lick, W.J., "A Numerical Model for Wind Driven Circulation and Temperature Fields in Lakes and Ponds, FTAS/TR-74-99, Case Western Reserve University, 1974.

11. Shirazi, M. and Davis, L., AWorkbook of Thermal Plume Prediction", Vol. 2, Surface Discharge Pacific Northwest Environmental Research Laboratory Report EPA-R2-72-0056, Corvallis, Oregon, (May,1974).

12. Stefan,H., and Vaidyaraman,P., "Jet-Type Model for the Three-Dimensional Thermal Plumes in a Crosscurrent and Under Wind", Water Resources Research, Vol. 2, No. 4 (Aug.,1972) pp 998-1014.

13. Stolzenbach, K., and Harleman,D., "Three-Dimensional Heated Surface Jets', Water Resources Research Vol. 9, No. 1 (Feb.,1973).

14. Waldrop, W.R. and Farmer, R.C., "Three-Dimensional Computation of Buoyant Plumes", Journal of Geophysical Research, Vol. 79, No. 9 (March,1974).

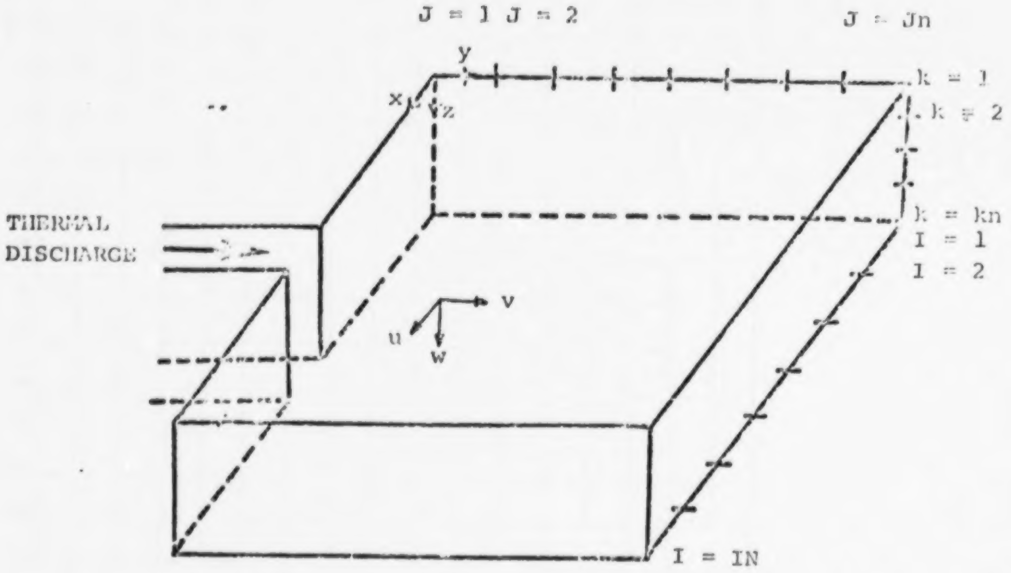
J = 1 J = 2
J = Jn
y
x
z
k = 1
k = 2
k = kn
I = 1
I = 2
I = IN
THERMAL
DISCHARGE
u
v
w

Fig. 1 Coordinate and Grid System

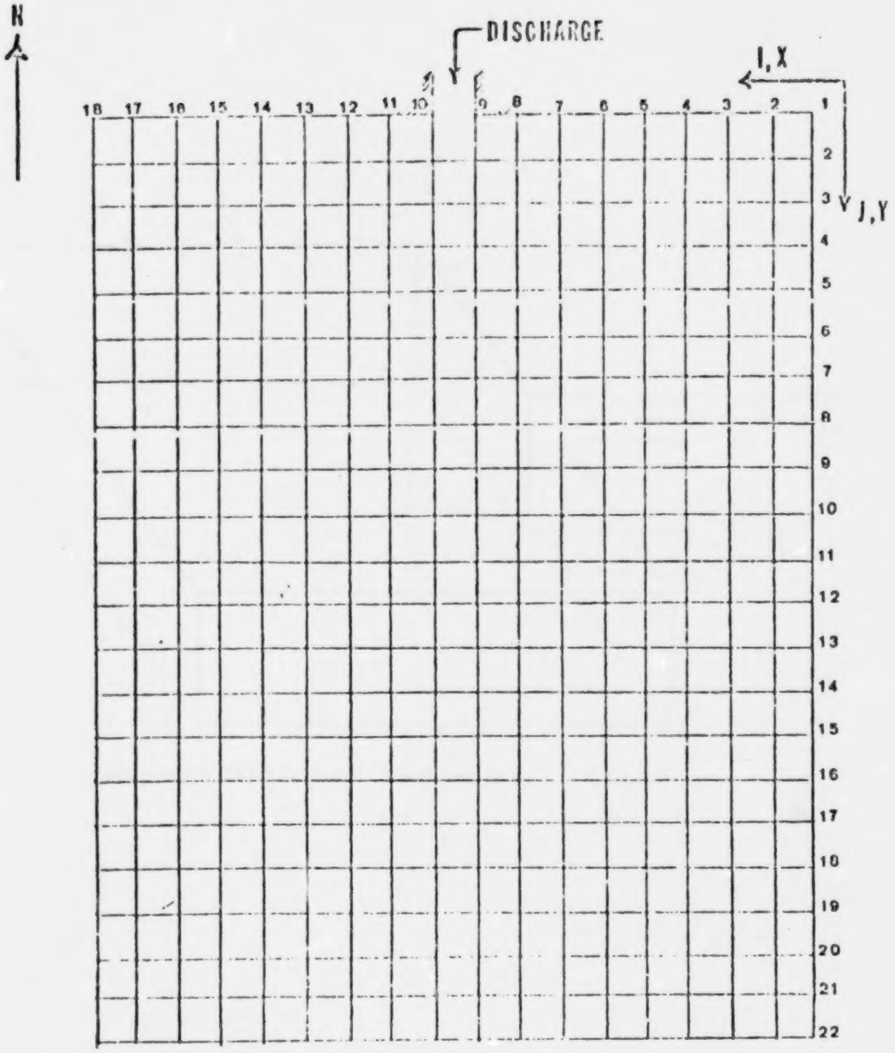
N
DISCHARGE
I,X
J,Y
18
17
16
15
14
13
12
11
10
9
8
7
6
5
4
3
2
1
2
3
4
5
6
7
8
9
10
11
12
13
14
15
16
17
18
19
20
21
22

Fig. 2 Grid System For Rigid-Lid Near Field Model of Cutler Ridge Site

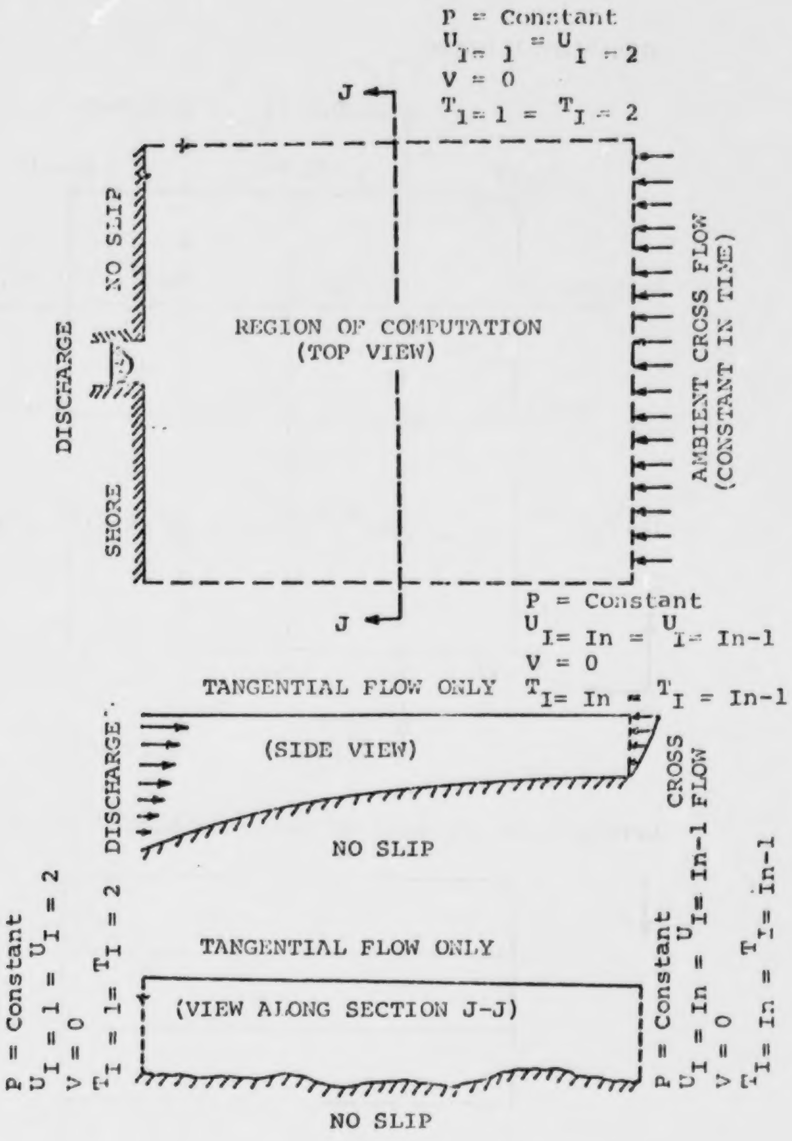
P = Constant
U I= 1 = U I = 2
V = 0
T I= 1 = T I = 2
J
J
NO SLIP
DISCHARGE
SHORE
REGION OF COMPUTATION
(TOP VIEW)
AMBIENT CROSS FLOW
(CONSTANT IN TIME)
P = Constant
U I= In = U I= In-1
V = 0
T I= In = T I = In-1
TANGENTIAL FLOW ONLY
DISCHARGE
(SIDE VIEW)
CROSS FLOW
NO SLIP
P = Constant
U I = 1 = U I = 2
V = 0
T I = 1= T I = 2
TANGENTIAL FLOW ONLY
(VIEW ALONG SECTION J-J)
P = Constant
U I = In = U I= In-1
V = 0
T I= In = T I= In-1
NO SLIP

Fig. 3. Boundary Conditions for the Region of Computation

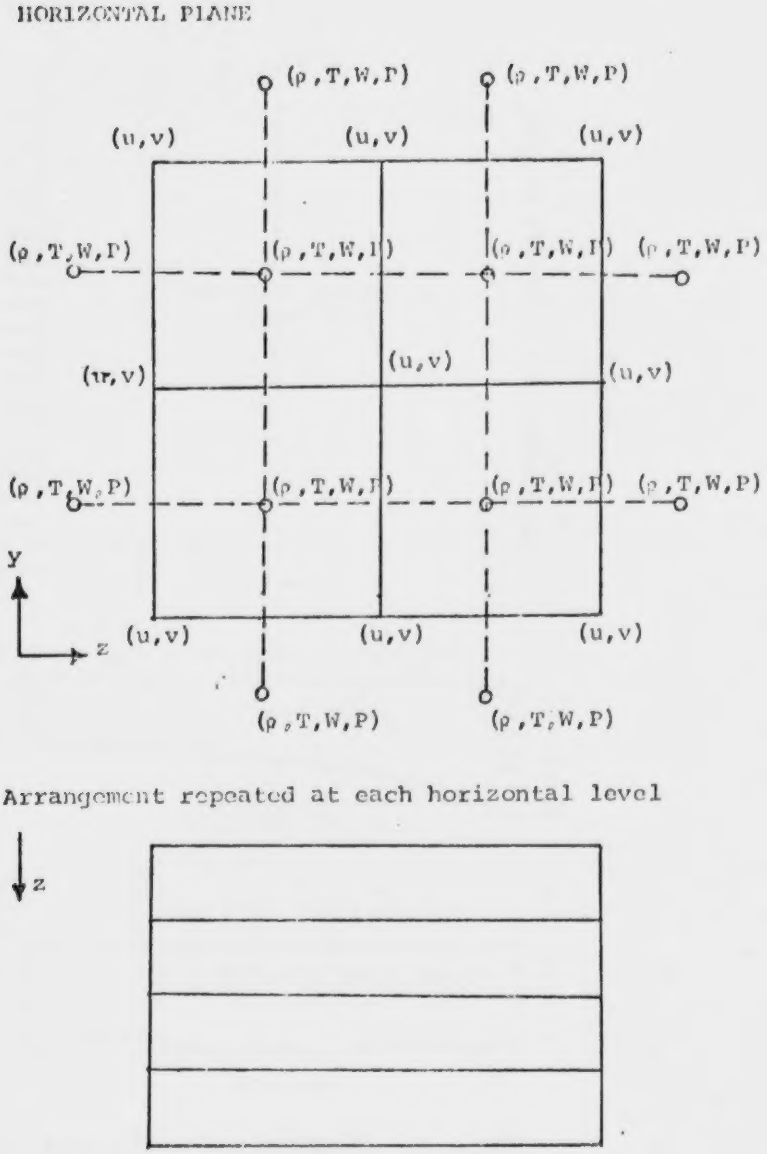
HORIZONTAL PLANE
(ρ,T,W,P)
(ρ,T,W,P)
(u,v)
(u,v)
(u,v)
(ρ,T,W,P)
(ρ,T,W,P)
(ρ,T,W,P)
(ρ,T,W,P)
(u,v)
(u,v)
(u,v)
(ρ,T,W,P)
(ρ,T,W,P)
(ρ,T,W,P)
(ρ,T,W,P)
Y
z
(u,v)
(u,v)
(u,v)
(ρ,T,W,P)
(ρ,T,W,P)
Arrangement repeated at each horizontal level
z

Fig. 4 Arrangement of Staggered Grid and Variables

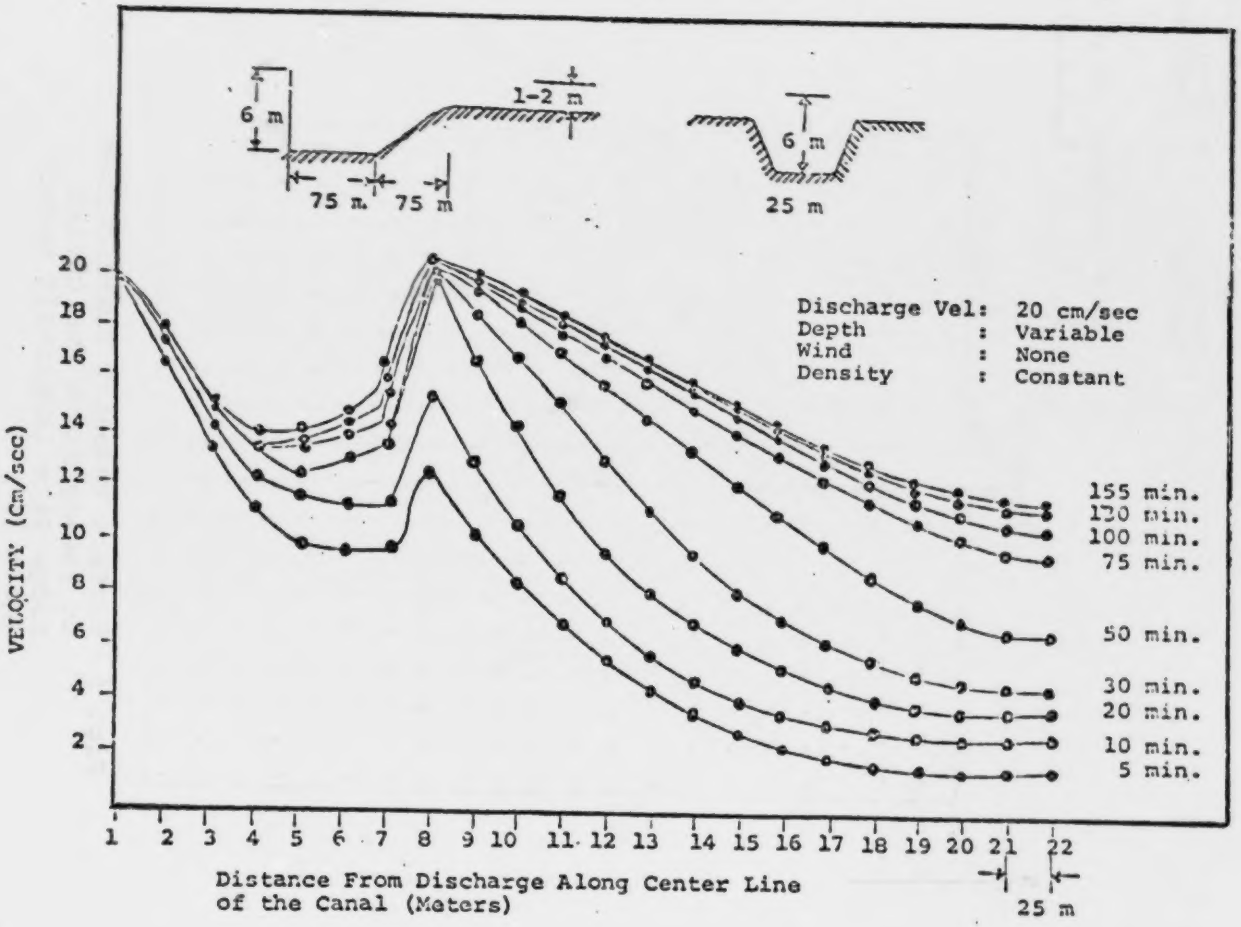

Fig. 5 Center Line Velocity Decay (Rigid-Lid Model) (Case 1)

Discharge Vel: 20 cm/sec
Depth : Variable
Wind : None
Density : Constant

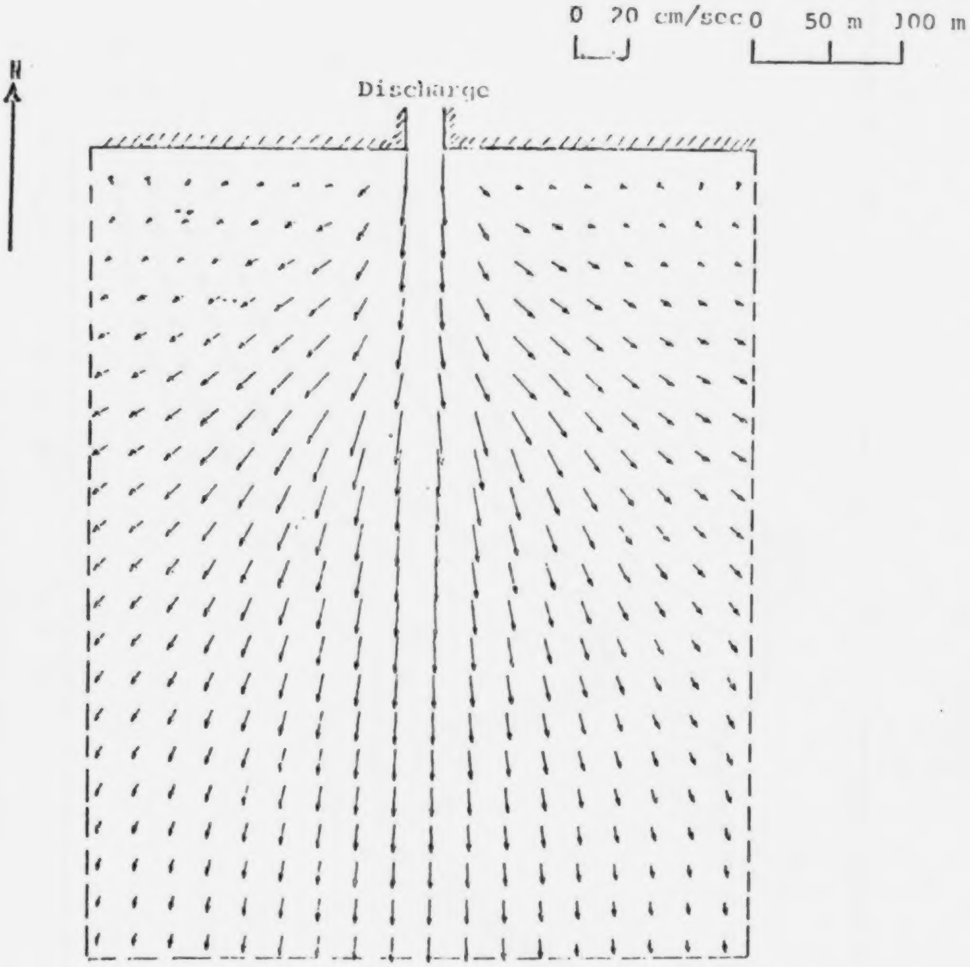

Fig. 6 **Surface Velocity Distribution at Steady State For Cutler Ridge Site (Rigid-lid Model) (Case 1)**

Discharge Velocity : 20 cm/sec
Discharge Temperature : 35.9°C
Depth : 1.2 m
Density : Variable
Wind : None
T_{air} : 29.5°C
$T_{initial}$: 28.0°C
t_{total} : 30 min.

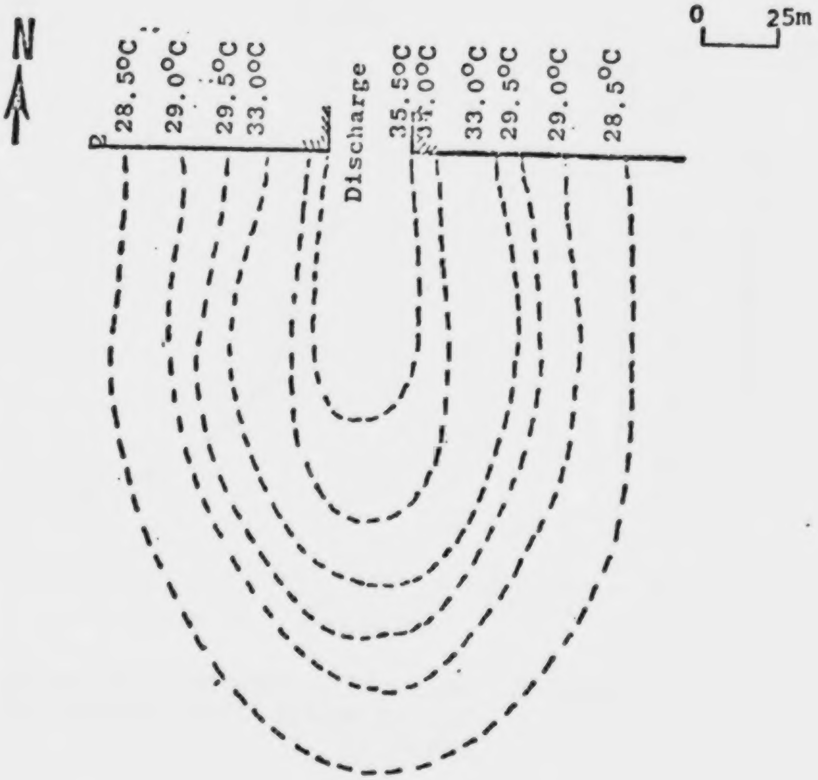
0
25m
N
28.5°C
29.0°C
29.5°C
33.0°C
Discharge
35.5°C
34.0°C
33.0°C
29.5°C
29.0°C
28.5°C

Fig. 7 Surface Isotherms for Cutler Ridge Site (Rigid-Lid) (Case 2)

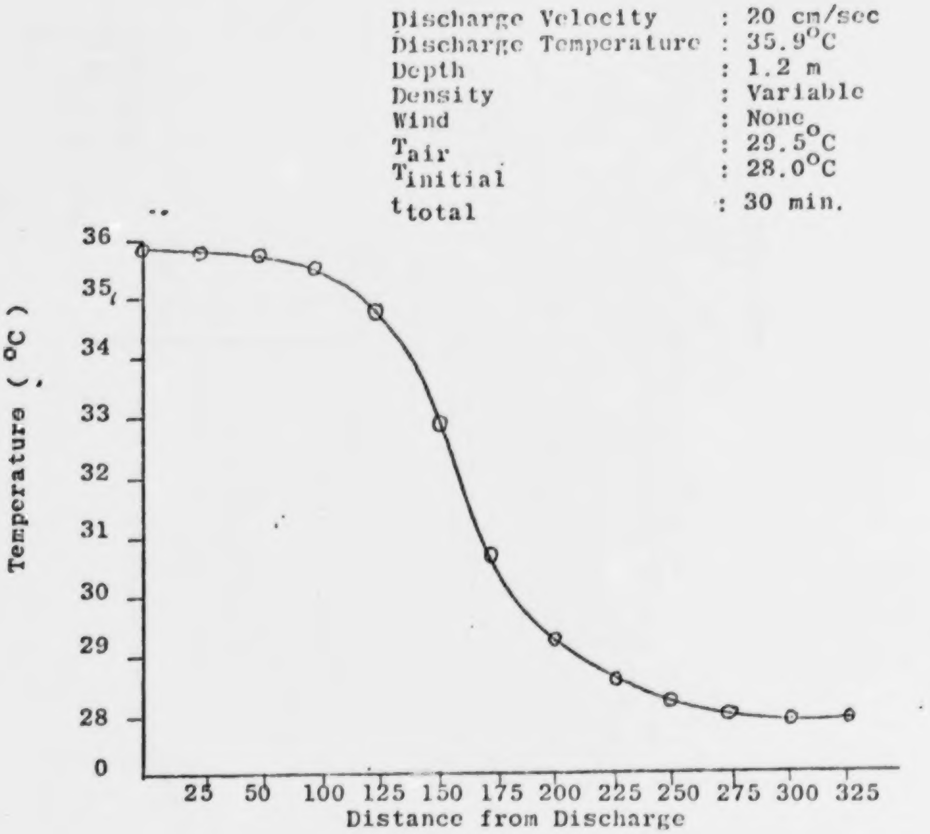

Fig. 8 Centerline Temperature Decay For Cutler Ridge Site (Rigid-Lid Model) (Case 2)

Discharge Vel: 20 cm/sec
Depth : 1.2 m
Density : Variable
Wind : 6.71 m/sec
(15 mph) 160°N

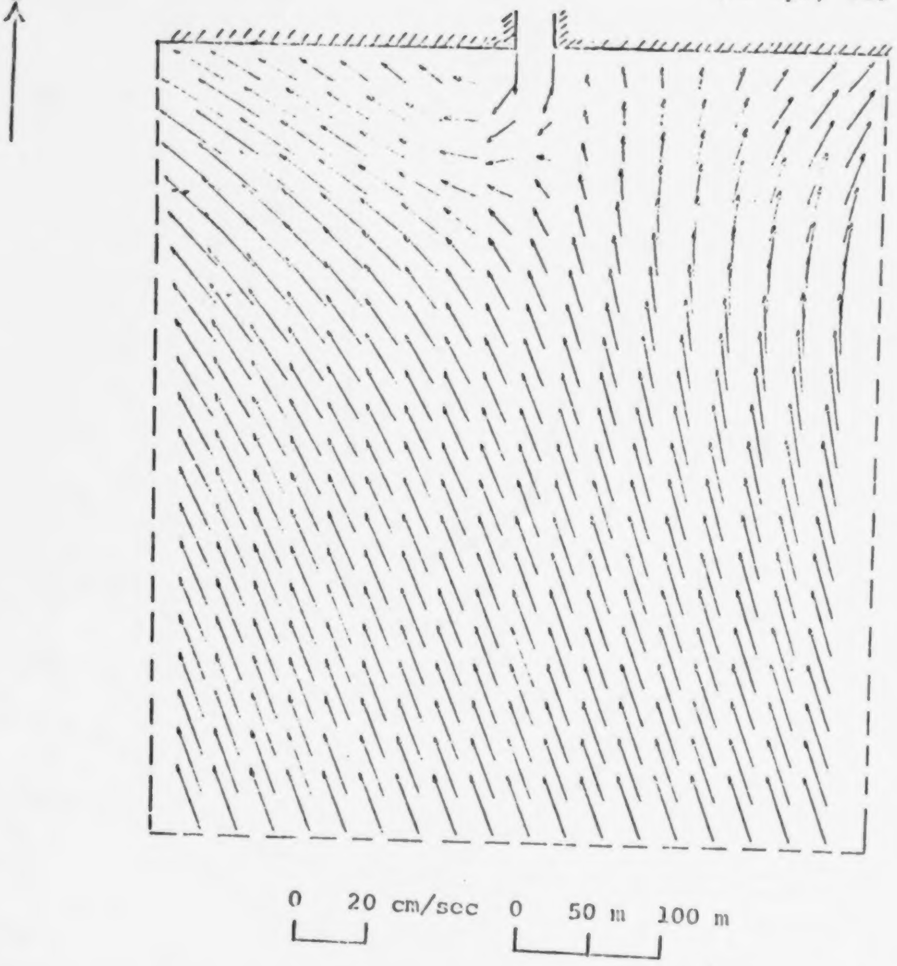

Fig. 9 Surface Velocity Distribution 2½ Hours After Discharge For Cutler Ridge Site (Rigid-Lid Model) (Case 3)

Discharge Velocity : 20 cm/sec
Discharge Temperature : 35.9°C
Depth : 1.2 m
Density : Variable
Wind : 6.71 m/sec
15 mph 160°N
T_{air} : 29.5°C
$T_{initial}$: 28.0°C
t_{total} : 2½ hrs.

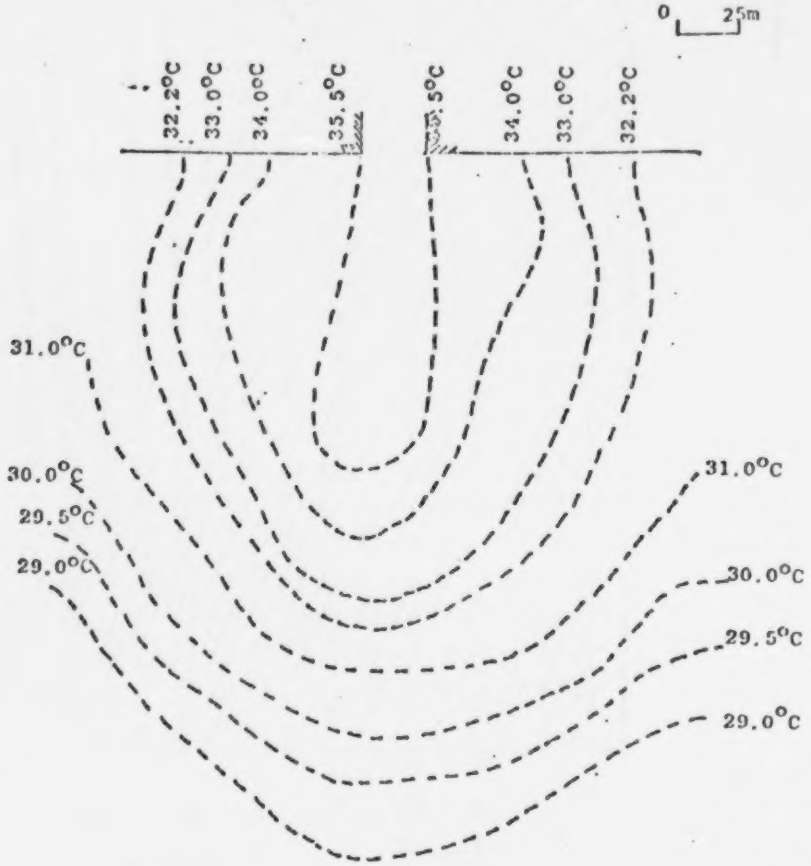

Fig. 10 Surface Isotherms for Cutler Ridge Site (Rigid-Lid) (Case 3)

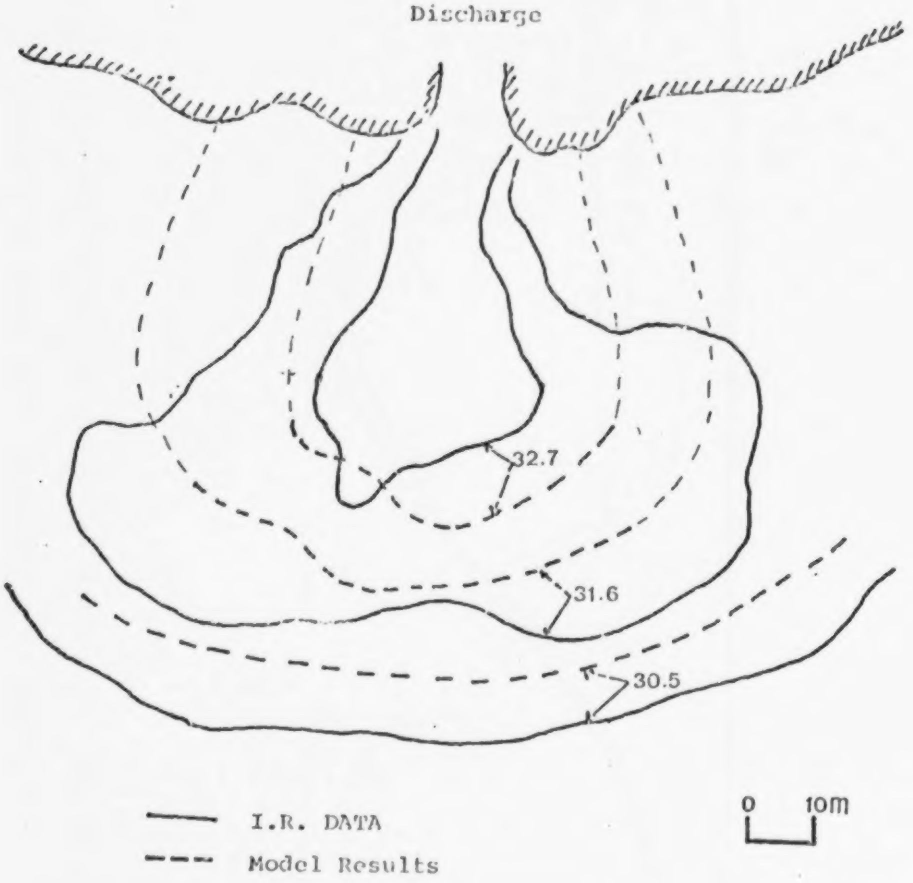
Discharge
32.7
31.6
30.5
0
10m
I.R. DATA
Model Results

Fig. 11 Comparison of Isotherms for April 15,1975 (11:55 am) (Case 4)

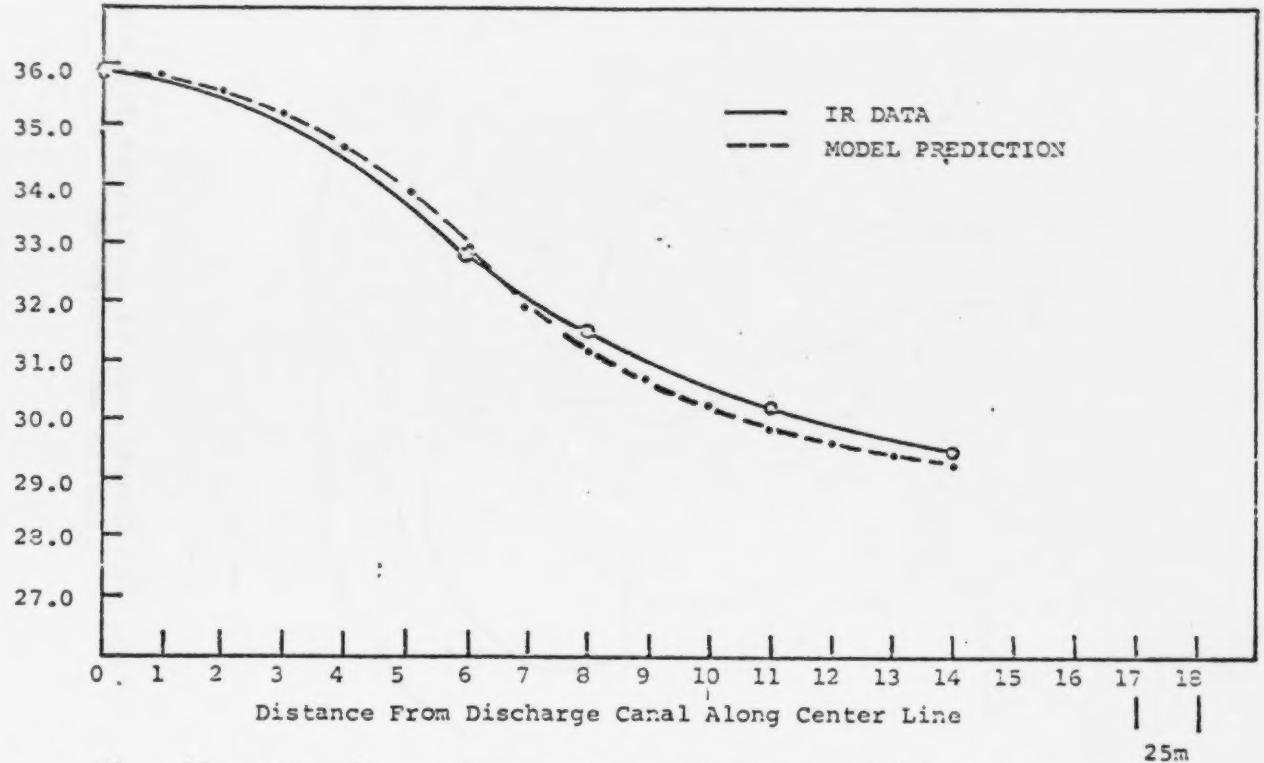

Fig. 12 Comparison of Temp Decay at I = 10 Along J (close to centerline) for April 15,1975 (11:55) (Case 4)

Date:	April 15, 1975
Discharge Vel:	20 cm/sec
Discharge T:	35.9°C
Density:	Variable
Wind:	6.71 m/sec
T air:	29.5°C
T initial:	28.0°C
Current:	3 cm/sec from South

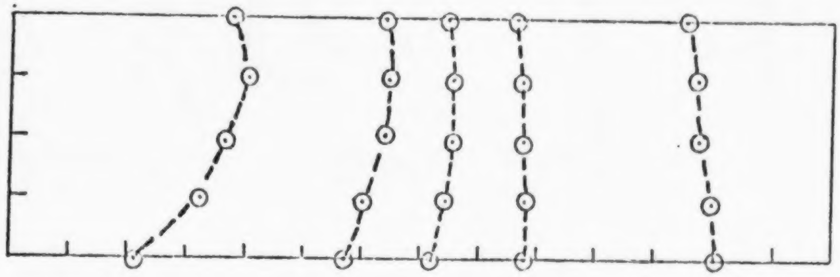

Fig. 13 Vertical Section Isotherms Along Canal Center Line for April 15,1975 at Cutler Ridge Site (Rigid-Lid) (Case 4)

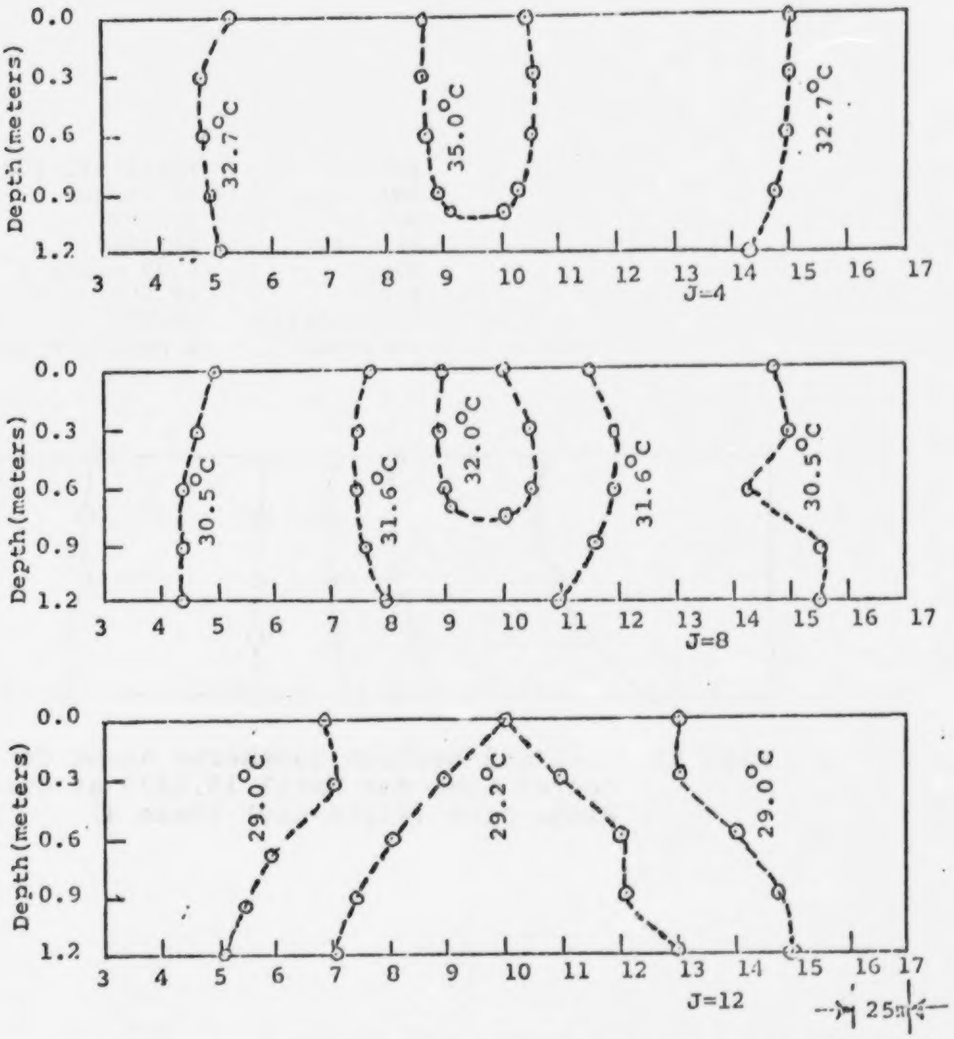

Fig. 14 Vertical Section Isotherms at Different J Sections for April 15,1975 at Cutler Ridge Site (Rigid-Lid) (Case 4)

SESSION VI-C
COOLING TOWER PLUMES

24 45-17

VI-C-117

SENSITIVITY ANALYSIS AND COMPARISON OF SALT DEPOSITION MODELS FOR COOLING TOWERS

T. J. Overcamp
Environmental Systems Engineering
Clemson University
Clemson, South Carolina, U.S.A.

ABSTRACT

This paper is directed toward those individuals in industry, consulting firms and regulatory agencies who must make estimates of the impact of salt deposition from evaporative cooling towers using salt water. These towers emit small droplets, called drift, which contain the dissolved salts in the cooling water. If the deposition of salt from these droplets is sufficiently high, damage to vegetation may occur. At the present there has been little information published on the sensitivity of deposition models to the input variables or comprehensive comparisions of various models. In this paper, two basic models for estimating deposition from natural draft cooling towers are compared. The first is a simple trajectory model that ignores turbulent dispersion and the second is a more complex model incorporating atmospheric turbulence and stability. The major conclusions of the paper are: the trajectory model gives comparable results compared to the more sophisticated model, and the deposition calculations are exceedingly sensitive to the initial droplet size distribution.

INTRODUCTION

In addition to the huge amounts of water vapor and tiny fog droplets which are nearly pure, condensed water, a cooling tower emits larger droplets, called drift, containing the dissolved salts and bacteria present in the cooling water. Initially, these droplets will rise in the plume's updraft, but due to their high settling velocity, they will fall free of the plume. Then in the drier ambient air, they will evaporate, settle downward and be dispersed by atmospheric turbulence. Eventually they will impact on the ground or on vegetation in the area downwind of the tower. If the cooling tower uses brackish or sea water, or if toxic biocides or corrosion inhibitors are added to the water, the deposition of these droplets may injure the vegetation around the tower. To avoid this potential damage, design specifications for modern salt water towers typically include the requirement that the drift emission rate be less than 0.002% of the total flow of the circulating water which corresponds to emissions on the order of tens of liters of drift water per minute.

To ascertain if these emissions can cause an appreciable impact on the surroundings, some investigators have developed mathematical models to

Preceding page blank

estimate the salt deposition, and others have embarked on field measurements of deposition and vegetation damage around large cooling towers such as the extensive study at Chalk Point, Maryland [1]. Only at the conclusion of such studies and careful analyses of the data can this question be answered and the results extrapolated to future sites.

The mathematical deposition models play an important role in both interpreting the ongoing field measurements and in assessing the impact of future towers. Since the development of the first model by Hosler, Pena and Pena [2], a succession of models have been presented including those by Roffman and Grimble [3], Laskowski [4], Hanna [5], and Israel and Overcamp [6]. They all share many similarities, but each new model takes some unique approaches to the problem and their estimates can be significantly different. Since there is no comprehensive set of deposition measurements at the present, none of the models can be verified. This leaves consultants, electric utilities, and regulatory agencies in a quandary about the appropriateness of these or any other models in the environmental assessment of a large cooling tower.

One approach to resolve some of these differences is to choose a model and adapt it to test the various assumptions proposed by other modelers. This has the advantage that all other details of the basic model are the same so that any differences in the predictions are the result of the assumption being tested. If the predictions differ significantly, field experiments can be designed to test this assumption.

This study is an attempt at such an inter-model comparison. The basic model chosen was an updated version of the Israel - Overcamp model [6] applied to natural draft towers. It was modified to allow computation of the deposition by either the ballistic or trajectory method introduced by Hosler _et al_. [2], or the Gaussian diffusion approach of others. Several different models for the rise of a droplet above the tower were included. There were run for various meteorological and cooling tower conditions including two different droplet distributions reported in the literature. The deposition predictions were compared and certain cases are presented in this paper. The major conclusions are: the trajectory model can give comparable results to the equivalent Gaussian diffusion-deposition model; the deposition in the first several kilometers is very sensitive to the emission droplet size distribution; and the deposition estimates are sensitive to the model chosen for the effective height of emission of the droplet.

DEPOSITION MODELS

Natural draft cooling towers emit a wide size range of droplets with a maximum diameter in the order of 1000μm and a mass median diameter less than 100μm [7]. The terminal velocities of these droplets range up to 4 m/s. When emitted they rise up in the moist plume, but they will eventually break away from its updraft, settle downward, evaporate and be dispersed by atmospheric turbulence.

Most deposition models share certain features. They all divide the droplet emission size distribution into discrete size intervals and usually treat the droplets in each interval independently. All models have some method of estimating the break-away point or effective height of emission of the droplets. The models use a variety of approaches for computing the evaporation, settling, and dispersion of the droplets ranging from simple ballistic or trajectory models [2] to those which simultaneously integrate three dimensional diffusion equations for evaporating droplets [3].

The basic model chosen is a modified version of that described by Israel and Overcamp [6]. For this study, it is put in a sector-averaged form such as would be used for climatological estimates of long-term salt deposition. The model has been adapted to use several sub-models for calculating the effective height of emission of the drops and to use either the trajectory or diffusion approaches to computing deposition.

Effective Height of Emission

Three possible mechanisms for droplets breaking away from the plume's updraft are gravitational settling, centrifugal forces due to the swirling motion in the counter-rotating vortices of a bent-over plume, and diffusive forces ejecting droplets from the plume. At this time, no satisfactory model exists for the diffusive mechanism [8]. Estimates can be made about the relative magnitudes of gravitational and centrifugal forces on the droplet. The gravitational acceleration is g, whereas the centrifugal is v^2/R in which v is a characteristic tangential velocity and R is the local radius of curvature. For an order of magnitude estimate, let v be the exit velocity and R_0 be the tower's exit radius. Then the ratio of centrifugal to gravitational forces on the droplet, S is*

$$S = \frac{v^2}{gR_0} \qquad (1)$$

For a hyperbolic tower, v is of the order of 5 m/s and R_0 is of the order of 30 m. Therefore, S is about 0.1 or less which implies that for the plume as a whole gravitational forces dominate. On the other hand, at high wind speeds, a small vortex pair has been observed to form at the lip of the tower as the plume is partially pulled into the tower's wake [9]. In this case centrifugal forces may dominate and eject drops from the vortices near the top of the tower.

If it is assumed that its gravitational settling is the primary mechanism for a droplet to breakaway from the plume, it is reasonable to further assume that this will occur when the droplet's settling velocity exceeds the local updraft velocity in the plume. Hosler _et al_. [2] used this approach with the assumption that the vertical velocity in the plume, w, varied linearly from its value at the tower exit, w_o, to zero at the ultimate rise of the plume. Israel and Overcamp [6] and also Hanna [5] used the "2/3 rise law" of a buoyant plume in a neutral atmosphere to derive an expression for the characteristic vertical velocity within the plume. Equating the local vertical velocity to the droplet's terminal velocity, v_D, the distance above the tower where the droplet breaks free from the plume is

---

* The S parameter or separation is commonly used in the analysis of the relative importance of centrifugal to gravitational forces in a cyclone separator used in the control of particulate emissions.

$$\Delta H_D = \frac{2}{3\beta^2} \frac{F_o}{u v_D^2} \tag{2}$$

in which u is the mean wind speed, β is the entrainment coefficient, and F_o is the initial buoyancy flux which is defined as:

$$F_o = g w_o R_o^2 \quad \frac{T_{pv} - T_{av}}{T_{pv}} \tag{3}$$

R_o is the exit radius of the tower, and T_{pv} and T_{av} are the virtual temperatures at the exit and in the ambient [10].

The value of the entrainment coefficient for the bent-over plume, β, has been reported to have a wide range of values in the literature. In a recent review on plume rise, Briggs [11] finds that 0.5 gives the best fit for the visible depth of the plume and $\beta = 0.6$ is best for the radius of the effective mass of the plume. In this study a value of 0.5 was chosen as opposed to the 0.7 used by Israel and Overcamp [6]. With a smaller value of β, the Equation 2 predicts a higher rise above the tower. In principle, for this application β should actually be chosen on the basis of either fitting measurements of vertical velocities to the plume rise law, or, if possible, by fitting actual measurements of the breakaway point of droplets to Equation 2.

Equation 2 assumes that the plume originates as a point source of buoyancy with no vertical velocity. Since a natural draft tower has an exit diameter on the order of 60m and an exit velocity of around 5 m/s, this assumption may be questionable. The basic entrainment equations for a bent-over plume can be integrated for a source with finite initial size and vertical velocity. Appendix A describes one such derivation and gives a set of equations that can be solved for the height above the tower, ΔH_D, where the plume's updraft velocity equals the droplet's settling velocity. Using either Equation 2 or the solution in Appendix A for ΔH_D, the effective height of emission for a droplet, H_D, is the sum of its rise above the tower, ΔH_D, and the height of the tower, H_s,

$$H_D = H_s + \Delta H_D \tag{4}$$

Since either atmospheric turbulence or stability will eventually limit the effective rise of plume, Equation 2 is not valid for small droplets with low settling velocities. An upper bound can be set as the ultimate rise of the plume. This model uses the dry plume rise equations of Briggs [12]. For a stably stratified atmosphere the rise of the plume is

$$\Delta H_e = 2.9 \left(\frac{F_o}{us}\right)^{1/3} \qquad (5)$$

in which s is $(g/T)/(\partial\theta/\partial z)$ and θ is the potential temperature. For unstable or neutral conditions the plume rise is

$$\Delta H_e = 1.6 \frac{F_o}{u}^{1/3} (3.5x^*)^{2/3} \qquad (6)$$

in which $x^* = 34\ F_o^{0.4}$ with x^* in meters and F_o in m^4/s^3. In a recent paper, Wigley [13] argues that for a stable atmosphere, the final plume rise be lowered by approximately (R_0/β) to account for the finite initial size of the plume. This is also suggested in Equation A5 for a plume in the neutral case, but has not been incorporated in this model.

An example will show the effect of these plume models in estimating H_D. For a cooling tower with a height of 125m, exit diameter of 60m, and initial buoyancy flux of 2000 m^4/s^3 and with a wind speed of 4 m/s and neutral stability, Figure 1 shows the effective height of emission, H_D, for the linear model similar to that used by Hosler et al. [2], the point source plume model of Equation 2, and the finite source plume model of Appendix A. For large droplets, the linear model predicts a higher rise than either the point or finite source models. The point source prediction is greater than for the finite source model, but the difference is significant for only the largest droplets.

Evaporation and Settling

In the model for this study, it is assumed that droplet begins evaporation when it breaks away from the moist plume. The evaporation equation used is similar to that given by Mason with the incorporation of the ventilation factor to account for the increased evaporation due to the droplet's motion [14,6]. The settling velocities use Stokes law or empirical equations fitted to the data of Gunn and Kinzer [15] on the terminal velocity of drops.

The two basic approaches to computing deposition are the ballistic or trajectory approach of Hosler et al. [2] that ignores atmospheric turbulence or a downward-sloping Gaussian plume that attempts to account for turbulence.

The trajectory method used in this study integrates the evaporation and droplet settling equations to determine the time for a droplet to fall a distance, H_D, its average settling velocity, $\bar{v}_d$, and the downwind distance where it strikes the ground, x_D, which is given by

$$x_D = \frac{H_D u}{\bar{v}_D} \qquad (7)$$

The model is applied by dividing the emission droplet distribution into discrete size intervals. The sector-averaged deposition for the droplet class bounded by D_i and D_{i+1} is

$$\omega_i = \frac{Q_{D_i}}{\frac{\pi}{16}\left(x_{D_{i+1}}^2 - x_{D_i}^2\right)} \qquad (8)$$

in which Q_{D_i}, the total emission of salt in the interval, is spread over a 22½° sector between the distances $X_{D_{i+1}}$ and X_{D_i}.

In diffusion-deposition methods, a downward-sloping Gaussian plume is used to simulate the effects of atmospheric turbulence. In this model, the general equation for deposition developed by Overcamp [16] is used to compute the deposition due to the droplets of a given size:

$$\omega_i(x) = \frac{v_D' \, Q_{D_i} \, (1+\alpha)}{\sqrt{2\pi} \; u \left(\frac{\pi x}{8}\right)} \exp\left[-(H_D - \bar{v}_D x)^2 / 2\sigma_z^2\right] \qquad (9)$$

in which α is the partial image coefficient, $\bar{v}_D$ is the average settling velocity and v_D' is the final or deposition velocity. A discussion of how these velocities are determined is given in Appendix B.

Unlike the trajectory method in which only one droplet class contributes to the deposition at any particular downwind distance, many droplet size classes can deposit at a location. The total deposition at any distance downwind is found by summing Equation 7 for all the droplet sizes.

MODEL COMPARISON

Prior to presenting model comparisons, it is important to recognize that it is unreasonable to expect that any deposition model can be verified to any greater degree than our present ability in predicting the SO_2 concentrations due to an elevated, buoyant release. For this gaseous case, it is often quoted that for any given situation, the Gaussian plume model "should be correct within a factor of 3" [17]. Therefore, it is unrealistic to anticipate that detailed verification of any salt deposition model could be made to within better than a factor of two or three or more without an exhaustive series of tests under repeatable meteorological conditions with simultaneous emission drop distribution measurements. Therefore, if two models give comparable results for the same input conditions, it may be futile to attempt to resolve any minor differences with field measurements. On the other hand, field experiments will be invaluable to determine if the predictions are correct as to the magnitude and location of the deposition.

In view of the above, a series of deposition calculations will be compared for the models discussed in the preceding section. For the calculation, the tower height is 125m and its exit diameter is 60m. The updraft velocity is 5 m/s and the buoyancy flux is 2000 m^4/m^3, and the atmospheric stability class for the diffusion model is Pasquill C. Except in one case, the relative humidity is 70%. The salt concentration of the droplets is assumed to be 35,000 ppm and to be sodium chloride. The total salt emission from the tower is 0.01 kg/s which roughly corresponds to a drift rate of 0.002% of the circulatory water flow. It should be noted that the measured drift rate at Chalk Point has been reported to be significantly lower [7].

The two different emission droplet distributions used are given in Table I. The first one, designated as the small distribution, was taken from an earlier paper [6]. It has droplet sizes ranging up to 450 μm in diameter. The second, designated as the large distribution, came from preliminary droplet measurements at Chalk Point, Maryland* and has been used in an early attempt at a model validation [18]. Its droplets range in size up to 800 μm. Later measurements at Chalk Point show that droplets over 1000 μm are emitted [7].

Figure 2 shows the salt deposition estimates using the sector-averaged, finite source plume, diffusion model for both the small and large droplet distributions. Although the total salt emissions are identical for both, the large droplet distribution case predicts a factor of 40 higher maximum deposition than does the small distribution. For the large case, there is a distinct maximum at 300m downwind of the tower. For the smaller case, there is a broad peak extending from 1 to 10 km downwind.

To help explain these differences, Figure 3 shows the contribution of the 16 individual droplet size intervals to the total deposition for the large distribution. The droplets larger than 450 μm account for all of the deposition in the first kilometer. The peak is a result of this small fraction of the salt that is in the large droplets falling on such a small area. The sharpness of the deposition peak for the droplet size classes with the largest droplets is probably an artifact of the model. This model assumes that all the droplest in a particular size interval are emitted from a single point located at a height H_D above the ground and directly over the center of the tower. The model could be modified to account for the finite size of the tower and distribution of the droplets across the tower as suggested by Hanna and Gifford [19]. Or a different approach could be to use a source function that distributed the emissions of a given size interval over a range of altitudes centered about the point H_D above the ground. Either of these methods would broaden the individual deposition peaks and slightly lower the maximum at the expense of substantially increased computation time and probability for error.

---

*These size distributions were calculated from data supplied by Environmental Systems Corporation, Knoxville, TN.

Figure 4 shows a comparison between the total deposition predicted by the trajectory and diffusion method with both using the same model for computing the effective height of emission. Since the trajectory model predicts that only one size droplet can fall at a particular point, it is easy to relate each "step" of prediction with one droplet size interval. Comparing Figures 3 and 4, it can be seen that the location and magnitude of the deposition due to the larger drops is similar for both models. As the droplets get smaller and their settling velocities decrease, atmospheric turbulence will begin to dominate. For the smallest droplets, it will be the principal mechanism in bringing droplets near the ground. Figure 3 shows this effect. The maxima of the smaller droplet interval deposition curves are 8 to 15 km from the tower, and they all are quite broad in contrast to the distinct, narrow curves for the larger droplets. On the other hand, the trajectory model predicts the small droplets will fall only very far from the tower. Figure 4 shows that the 125 μm size interval droplets deposit between 13 and 38 km from the tower. The smaller ones fall still further out. This shortcoming of the trajectory approach has been noted by Pena and Hosler [20] and is implied in Hanna's [5] suggestion to use a trajectory approach for droplets with initial diameters greater than 200 μm and the normal Gaussian model for the smaller ones.

Figure 5 shows a similar comparison for the small droplet class. Again the agreement is reasonable within the context of a factor of two or three. But because of the trajectory model's inability to treat small droplets properly, the similarity of predictions beyond 10 km for both Figures 4 and 5 may be partially coincidental because they depend on the relative magnitudes of salt in the smaller size intervals.

Figures 6 and 7 show the effect on total deposition of the linear, point and finite source models for estimating the effective height of emission. For both the large and small distributions there is little difference between the point source and the finite source models. But for the large droplet distribution, there is nearly an order of magnitude lower peak deposition for the linear plume model than the other plume models. The explanation can be readily seen in Figure 1. The linear model predicts a substantially higher effective height of emission than the models based on a plume model. For the small distribution there is little significant difference among the models because the predictions for the effective height of emission are approximately the same.

The last comparison of this study shows the effect of humidity on the deposition patterns. Figure 8 gives the deposition for the finite source plume model for 90% and 70% relative humidity. Somewhat surprisingly, there is little difference in deposition for the large distribution case. This is because the largest droplets with settling speeds of in the order of several meters per second only stay in the air for 1 to 3 minutes and do not evaporate very much irrespective of the humidity. For the small distribution case, its biggest droplets are in the air for a longer time and do evaporate. With low relative humidity, the droplet will evaporate faster, lower its settling velocity, and land farther out. This will lower the peak deposition.

CONCLUSIONS

This paper presents a comparison of various assumptions that have been proposed for salt deposition models for natural draft cooling towers. Deposition calculations are presented that show that the trajectory method can give very comparable results to the more sophisticated Gaussian diffusion model. These calculations are very sensitive to the emission drop size distribution spectrum and the model used for estimating the effective height of emission of the drift droplets.

For those who evaluate the environmental impact assessment for cooling towers using salt water, it is concluded that the droplet size distribution may be as important, or possibly more important, than the actual model used in the assessment especially if there is concern about the salt deposition within the first kilometer of the tower.

Finally, it is encouraged that other investigators will adopt this approach to the sensitivity of their model so that it can be determined whether the above conclusions can be applied to all models or if they are a peculiarity of the basic model chosen for this study.

APPENDIX A

The entrainment equations for a buoyant plume in a neutral atmosphere can be integrated with finite initial size and vertical velocity. The equations for conservation of mass, momentum and buoyancy in a neutral atmosphere are [11,21]

$$u \frac{dR^2}{dx} = 2\beta w R \qquad \text{(A1)}$$

$$u \frac{d}{dx}(R^2 w) = \frac{F}{u} \qquad \text{(A2)}$$

$$F = F_o \qquad \text{(A3)}$$

These equations can be integrated with the initial conditions $R = R_o$ and $w = w_o$ to give an equation for the vertical velocity as a function of downwind distance

$$w = \frac{R_o^2 w_o + F_o x / U^2}{\left[R_o^3 + \frac{3\beta R_o^2 w_o x}{u} + \frac{3\beta}{2}\frac{F x^2}{u^3}\right]^{2/3}} \qquad \text{(A4)}$$

Another equation can be found for the rise above the tower

$$z = \frac{1}{\beta} \left[R_o^3 + \frac{3\beta R_o^2 w_o x}{u} + \frac{3\beta F_o x^2}{2u^3} \right]^{1/3} - \frac{R_o}{\beta} \qquad \text{(A5)}$$

By setting w equal to the droplet settling velocity, v_D, Equations (A4) and (A5) can be solved to determine the height above the tower where the droplet breaks away from the plume, ΔH_D. This solution is analogous to Equation (2) for the point source plume.

APPENDIX B

Equation (9) has two droplet settling velocities: $\bar{v}_D$, the average settling velocity, and $\bar{v}_D'$, the final or deposition velocity. For these evaporating droplets, both velocities should be a function of distance. But for computational simplicity, one set of these velocities is chosen for each droplet size interval. The settling velocity and evaporation are integrated for a droplet emitted from height H_D. The integration continues until it strikes the ground, or if the droplet is small, until it is carried downwind a distance equal to x_{max}, the point of maximum ground level concentration of gaseous emissions from height H_D. The distance x_{max} is approximately given by

$$\sigma_z (x_{max}) = \frac{H_D}{\sqrt{2}} \, . \qquad \text{(B1)}$$

This latter condition recognizes that the maximum deposition of the droplets occurs no further away than does the maximum for gases. This prevents calculating very small values of average settling velocities for small droplets released from a great height as is the case with the trajectory model. It should give a good representation of the settling velocities near the maximum of its deposition curve.

REFERENCES

1. Pell, J., "The Chalk Point Cooling Tower Project," *Cooling Tower Environment - 1974*, ERDA Symposium Series, CONF-740302, available from the National Technical Information Service (NTIS), Springfield, Va., ($13.60), 1975, pp 88-127.

2. Hosler, C. L., J. Pena and R. Pena, "Determination of Salt Deposition Rates from Evaporative Cooling Towers," *J. Engineering for Power*, v. 96, 1974, pp 283-291.

3. Roffman, A., and R. E. Grimble, "Drift Deposition Rates from Wet Cooling Systems," *Cooling Tower Environment - 1974*, NTIS, 1975, pp 585-597.

4. Laskowski, S. M., "Mathematical Transport Model for Salt Distribution from a Saltwater Natural-Draft Cooling Tower," *Cooling Tower Environment - 1974*, NTIS, 1975, pp 598-613.

5. Hanna, S. R., "Fog and Drift Deposition from Evaporative Cooling Towers," *Nuclear Safety*, v. 15, 1974, pp 190-196.

6. Israel, G. W. and T. J. Overcamp, "Drift Deposition Model for Natural-Draft Cooling Towers," *Cooling Tower Environment - 1974*, NTIS, 1975, pp 614-628.

7. Webb, R. O., G. O. Schrecker and D. A. Guild, "Drift Data from a Large Natural Draft Brackish Water Cooling Tower and Brackish Water Particulate Scrubber," presented at The Cooling Tower Institute 1977 Annual Meeting, Houston, Texas, 20pp.

8. Slinn, W. G. N., "An Analytical Search for the Stochastic-Dominating Process on the Drift-Deposition Problem," *Cooling Tower Environment - 1974*, NTIS, 1975, pp 483-500.

9. Bøgh, P., "Experience with Combined Wind Tunnel-Plume Model Analysis of Cooling-Tower Environmental Impact, *Cooling Tower Environment - 1974*, NTIS, 1975 pp 265-290.

10. Briggs, G. A., "Comments on 'Bent-Over Vapor Plumes'," *J. Applied Meteorology*, v. 10, 1971, p 1040.

11. Briggs, G. A., "Plume Rise Predictions," *Lectures on Air Pollution and Environmental Impact Analysis*, American Meteorological Society, Boston, 1975, pp 72-74.

12. Briggs, G. A., "Some Recent Analyses of Plume Rise Observations," Proceedings of the Second International Clean Air Congress, Washington, D. C., 1970, pp 1029-1032, H. M. Englund and W. T. Berry (Eds.), Academic Press, N. Y., 1971.

13. Wigley, T. M. L., "Maximum Rise of Cooling Tower Plumes," J. Applied Meteorology, v. 15, 1976, pp 1112-1113.

14. Mason, B. J., The Physics of Clouds, Oxford University Press, 2nd Ed., 1971, pp 124-125.

15. Gunn, R. and G. D. Kinzer, "The Terminal Velocity of Fall for Water Droplets in Stagnant Air," J. Meteorology, v. 6, 1949, pp 243-248.

16. Overcamp, T. J., "A General Gaussian Diffusion-Deposition Model for Elevated Point Sources," J. Applied Meteorology, v. 15, 1976, pp 1167-1171.

17. Turner, D. B., "Workbook of Atmospheric Dispersion Estimates," U. S. Environmental Protection Agency, AP-26 (revised), 1970, 84pp.

18. Israel, G. W., T. J. Overcamp and W. J. B. Pringle, "A Method to Measure Drift Deposition from Saline Natural Draft Cooling Towers, submitted to Atmospheric Environment.

19. Hanna, S. R., and F. A. Gifford, "Meteorological Effects of Energy Dissipation at Large Power Parks," Bulletin of the American Meteorological Society, v. 56, 1975, pp 1069-1076.

20. Pena, J. A., and C. L. Hosler, "Influence of the Choice of the Plume Diffusion Formula on the Salt-Deposition-Rate Calculation," Cooling Tower Environment - 1974, NTIS, 1975, pp 563-584.

21. Csanady, G. T., "Bent-Over Vapor Plumes," J. of Applied Meteorology, v. 10, 1971, pp 36-42.

TABLE I

DROPLET SIZE DISTRIBUTIONS

Small			Large		
Droplet Interval µm	Characteristic Diameter µm	Mass %	Droplet Interval µm	Characteristic Diameter µm	Mass %
0-50	25	19.4	0-50	40	38.4
50-100	75	33.7	50-100	80	24.2
100-125	113	8.9	100-150	125	13.4
125-150	138	8.9	150-200	175	6.9
150-175	163	5.9	200-250	225	3.7
175-200	188	5.9	250-300	275	2.3
200-225	213	3.85	300-350	325	2.1
225-250	238	3.85	350-400	375	2.0
250-275	263	2.3	400-450	425	1.8
275-300	288	2.3	450-500	475	1.5
300-325	313	1.3	500-550	525	1.1
325-350	338	1.3	550-600	575	0.73
350-375	363	0.75	600-650	625	0.48
375-400	388	0.75	650-700	675	0.31
400-425	413	0.4	700-750	725	0.21
425-450	438	0.4	750-800	775	0.16

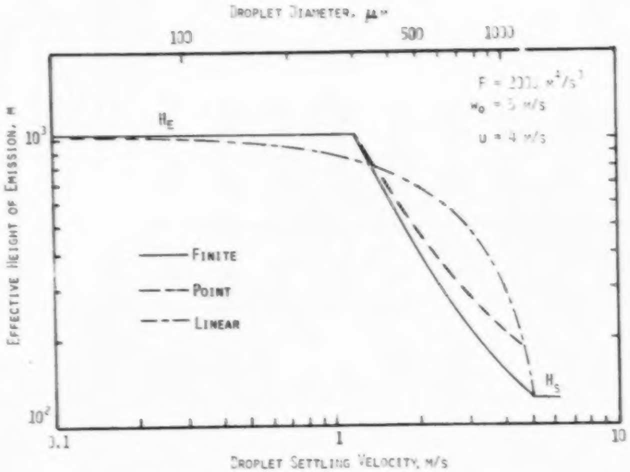

Figure 1. Effective Height of Emission versus Droplet Diameter and Settling Velocity

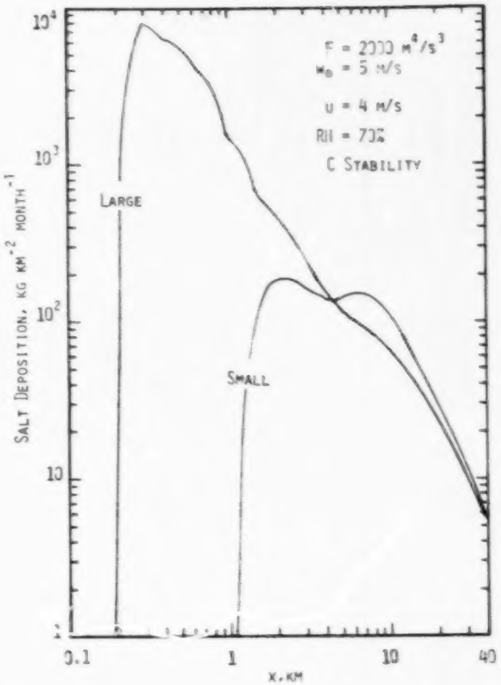

Figure 2. Salt Deposition for the Finite Source, Plume, Diffusion - Deposition Model

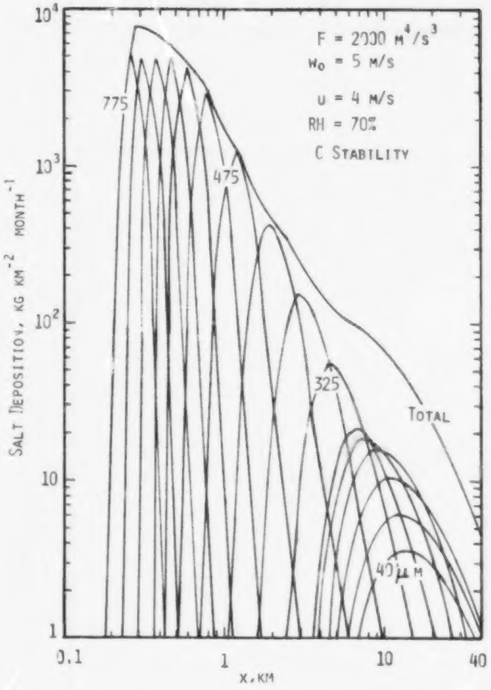

Figure 3. Salt Deposition for the Finite Source, Plume, Diffusion Deposition Model Showing the Contribution of the Individual Droplet Classes

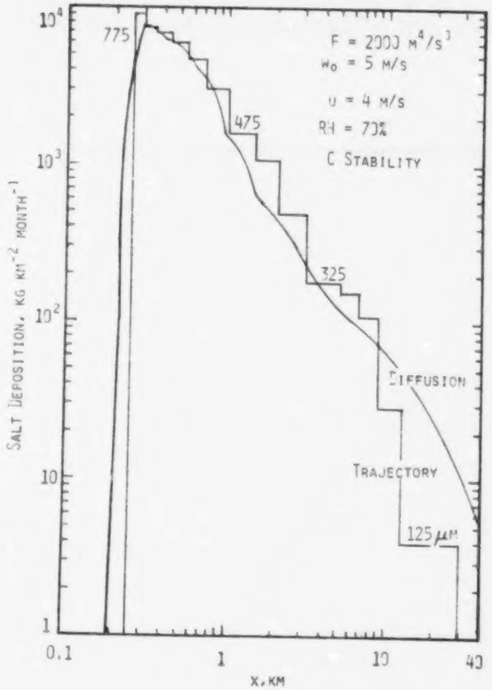

Figure 4. A Comparison Between the Trajectory and the Diffusion-Deposition Model for the Large Droplet Class

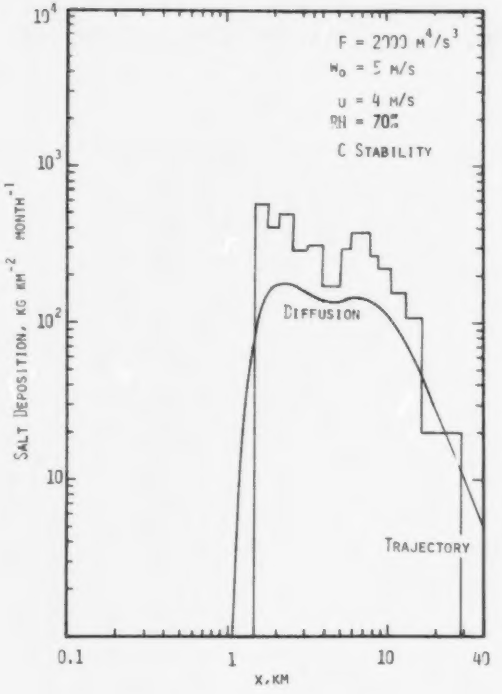

Figure 5. A Comparison Between the Trajectory and the Diffusion-Deposition Model for the Small Droplet Class

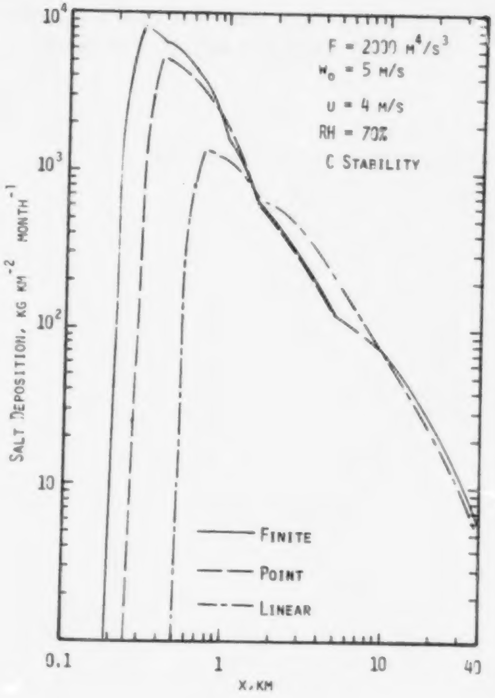

Figure 6. Salt Deposition for the Diffusion-Deposition Model Using the Finite, Point and Linear Plume Models for the Large Droplet Distribution

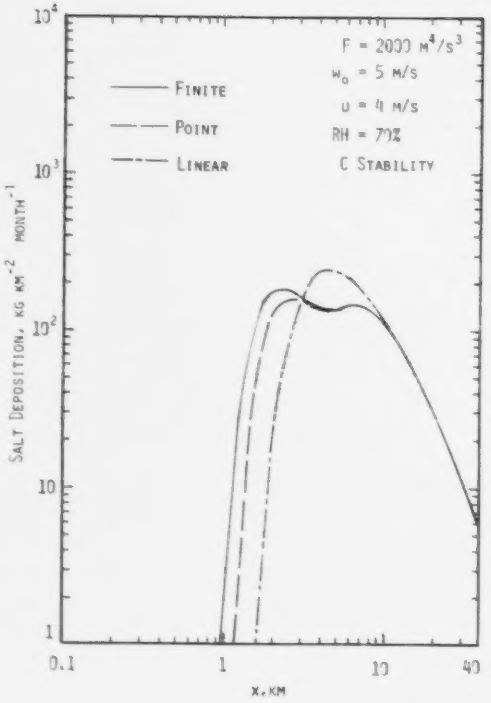

Figure 7. Salt Deposition for the Diffusion-Deposition Model Using the Finite, Point and Linear Plume Models for the Small Droplet Distribution

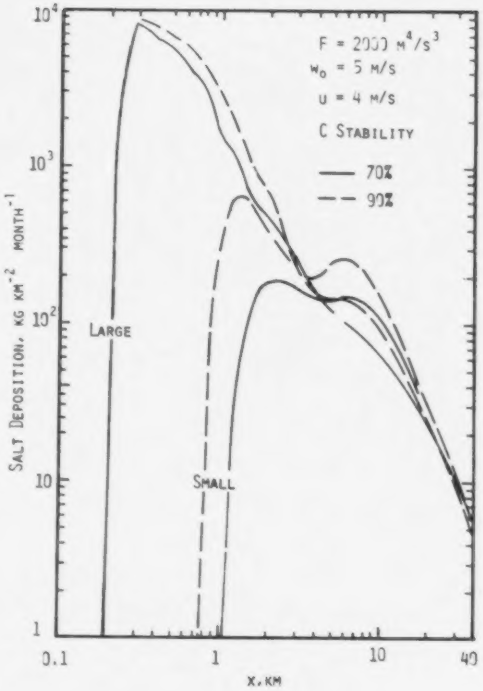

Figure 8. The Effect of Humidity on the Salt Deposition for the Finite Source Plume, Diffusion-Deposition Model

omit

VI-C-135

Validation of Selected Mathematical Models for Plume Dispersion from Natural-draft Cooling Towers

A. J. Policastro
Argonne National Laboratory

R. A. Carhart
University of Illinois/Chicago Circle

B. A. DeVantier
Argonne National Laboratory

Environmental impact statements for proposed nuclear power plants require the calculation of the dispersion of the waste heat generated. The trend towards the use of evaporative cooling towers makes the modeling of atmospheric dispersion from these towers an important consideration.

Our paper summarizes the results of our ongoing validation study of models for single and multiple natural draft cooling towers. Twelve models have been chosen based upon their current use in environmental impact assessment work. Model predictions of plume rise and visible plume profiles have been compared to field data taken at the Amos, Chalk Point, Lünen, Meppen, Neurath, and Paradise Plants. Complete model-data comparisons are presented. A critique is made of model assumptions with a review of the most successful simulations.

The Winiarski-Frick model appears to be the most accurate in comparison to single-tower data. Predictions of visible plume length are generally within a factor of 2. All models for multiple tower plume dispersion significantly overpredict plume rise and length.

Preceding page blank

25-45-13

VI-C-137

IMPORTANT CONSIDERATIONS IN A SIMPLE NUMERICAL PLUME MODEL

L.D. Winiarski
Corvallis Environmental Research Laboratory
Environmental Protection Agency
Corvallis, Oregon U.S.A.

ABSTRACT

A simple, inexpensive, numerical plume model based on conservation laws applied to average properties of a puff of plume material can be used to predict the trajectory, width and dilution of plumes, provided that appropriate consideration is given to the average effect of large scale vortex action on both the plume and the surroundings. Consideration of the mechanics of formation of the vortices, as well as momentum balances on a control volume consisting of the total bent over plume provides quantitative limits for these effects. The model predictions show good agreement with a variety of laboratory and field data.

INTRODUCTION

The prediction of the trajectory, dilution and spread of a buoyant plume or jet is an important problem in many diverse fields. The subject might be the discharge of a smoke stack or cooling tower into the atmosphere, the discharge of a submerged jet into a river or ocean or the injection of fuel into a combustion chamber.

IMPORTANT CONSIDERATIONS

It is possible (in principle at least), given enough computer time and core storage, to input this problem in a general purpose, three-dimensional, fluid dynamics computer code where the numerical grid extends to cover the region of the ambient fluid likely to be influenced by the plume. By using a large number of relatively closely spaced grid points one could minimize the uncertainty of some assumptions. Unfortunately this is too expensive.

Resolution and Diffusion

It is not practical to use a grid scale small enough to eliminate the uncertainty. The mathematical description is always uncertain because the distinction between flow defined by a definite velocity vector and flow implied by a diffusion representation is really a mathematical artifice related to the scale of the phenomenae involved relative to the resolution of the calculation system (e.g. the size of the numerical calculation system).

Preceding page blank

Vortex Motion

Transport by small vortex motion is often accounted for by a diffusion term. However, a significant feature of plume motion is vortex circulations which are of the same scale as the width of the plume. This motion is responsible for most of the entrainment into the plume, therefore it deserves special consideration. To attempt to model the vortex flow in detail would be prohibitively expensive. However, the overall effect of these flows must be included in simple models in a manner that is as consistent as possible with basic conservation principles.

Pressure forces

It is important that model take into account the fact that the plume disturbs the surroundings. The plume experiences a drag due to the fact that it must accelerate not only the mass that it absorbs into the plume but also a portion of the surroundings. The energy for these circulations that are set up in the surroundings must come from the plume. In a simple model it is necessary to make some assumptions as to the magnitude and distribution of the external forces acting on the plume. A check on the overall consistency of these assumptions can be made by considering the integral of these forces on a control volume encompassing the entire bent over plume. The summation of the net vertical component of external forces should equal the initial vertical flux of momentum. The total change of horizontal momentum flux of the initial mass flow should equal the summation of the net horizontal forces on the bent-over plume control volume. These ideas have been important in the development of a successful, inexpensive plume model.

CALCULATION PROCEDURE

Start by defining an initial mass or puff of material (M_o) with density (p_o) issuing out of a stack of radius (b_o) with an initial velocity (V_o) in a time instant (Δt).

$$M = p_o \pi b_o^2 V_o \Delta t$$

The initial length (H) of the element is:

$$H = V_o \Delta t$$

Calculate the amount of mass (ΔM) entrained into this puff in the time instant Δt. Calculate the horizontal (F_h) and vertical components (F_v) of the pressure force acting on the plume. The mass entrained and this pressure force are crucial items to plume prediction. The logic for their calculation will be explained later.

The new mass of the puff is simply the old mass plus the amount entrained during the time instant.

$$M^{t+\Delta t} = M^{t}+\Delta M$$

The change in horizontal momentum (Mu) of the plume equals the horizontal momentum added by the entrained mass plus the impulse added by the horizontal pressure

$$\Delta(Mu) = W\Delta M + F_h \Delta t$$

Note that the horizontal momentum added by the entrained mass comes about by virtue of the fact that this mass comes from the ambient fluid which has a horizontal wind velocity (W).

The new horizontal momentum of the parcel is simply the old horizontal momentum plus the change in horizontal momentum

$$(Mu)^{t+\Delta t} = (Mu)^{t} + \Delta Mu$$

The new horizontal velocity u, of the parcel is:

$$u^{t+\Delta t} = \frac{(Mu)^{t+\Delta t}}{M^{t+\Delta t}}$$

The vertical velocity can be solved in a similar manner. First, consider the case of a neutrally buoyant discharge. The change in vertical momomentum of the parcel is due to the vertical component of the pressure force provided the undisturbed ambient has no vertical velocity.

$$\Delta(Mv) = F_v \Delta T$$

The new vertical momentum of the parcel is

$$(Mv)^{t+\Delta t} = Mv^{t} + \Delta Mv$$

The new vertical velocity is

$$v'^{t+\Delta t} = \frac{(Mv)^{t+\Delta t}}{M^{t+\Delta t}}$$

The effect of buoyancy is actually a modification of the pressure field and hence F_v; however, it can be approximated by a modification of Archimedes principle to compute the acceleration (a) due to buoyant force (F_b).

$$a = \frac{F_b}{M_{total}} = \frac{\text{displaced fluid weight—parcel weight}}{\text{total mass moved}}$$

Expressed in terms of the density (ρ), the gravitational acceleration (g), and the volume (vol) of the parcel, this is:

$$a = \frac{(\rho_{amb}-\rho)\ (vol)\ g}{(\rho+\rho_{amb})\ (vol)}$$

The buoyancy correction to the vertical velocity then is

$$\Delta v = a\Delta t \approx \frac{(\rho_{amb}-\rho)\ g\ \Delta t}{2\rho}$$

$$v^{t+\Delta t} = v'^{t+\Delta t} + \Delta v$$

This approximation for the buoyancy computation which accounts for the displaced ambient mass or virtual mass is not well known; however, evidence for this has been documented 1 (Ref. 3).

The buoyancy calculation depends on updating the density of the parcel at each time step. This can be done from conservation considerations. In the simplest case, the temperature (t) is

$$T^{t+\Delta t} = \frac{M^t T + (\Delta M) T_{amb}}{M^{t+\Delta t}}$$

The specific concentration of other parameters (e.g. moisture) can be found in the same way.

Use ambient pressure (P) in an equation of state to find the density. For example, the equation for air is:

$$\rho^{t+\Delta t} = \frac{P}{RT^{t+\Delta t}}$$

Refinements to the temperature and density calculations can be made to account for the moisture effects.

The horizontal (X) and vertical (Y) displacements are simply:

$$X^{t+\Delta t} = X^{t} + \frac{u^{t}+u^{t+\Delta t}}{2} \Delta t$$

$$Y^{t+\Delta t} = Y^{t} + \frac{v^{t}+v^{t+\Delta t}}{2} \Delta t$$

The total velocity (V) is:

$$V = \sqrt{u^{2}+v^{2}}$$

The length (H) of the parcel along the trajectory changes slightly because the parcel ahead is moving at a velocity less than the parcel behind. This can lead to a change in length:

$$\Delta H = \frac{\partial V}{\partial s} H \Delta t = \frac{\partial V}{\partial t} \frac{\partial t}{\partial s} H \Delta t$$

$$H^{t+\Delta t} = \Delta H + H^{t} = \frac{H^{t}(V^{t}-V^{t-\Delta t})}{\sqrt{(\Delta x)^{2}+(\Delta y)^{2}}} \Delta t + H^{t}$$

An average radius for the puff can be found from:

$$\rho \pi b^{2} H = M$$

$$b = \sqrt{\frac{M}{\rho \pi H}}$$

Time can be updated and the process repeated:

$$t=t+\Delta t$$

Although this integration system is very simple, it is comparable to more elegant integration systems and has been used to illustrate a published inconsistency in the use of such a system (Ref. 2).

With the basic integration system this simple, attention can be focused on the entrainment and force computation. The problem is to compute these terms in the most physically consistent manner. This is not an easy task. Some insight can be obtained by close observation of an individual puff of material issuing from an orifice.

As the puff emerges from the orifice the ambient fluid is displaced and largely forced to move around to fill the void behind. Relative to the parcel the ambient fluid has an impinging velocity. As the ambient fluid slides around the parcel the shearing action sets up a toroidal vortex which entwines ambient fluid into its center. Initially, the vortex is approximately spherical but can become more like the familiar smoke ring.

Laboratory experiments have shown that the initial growth of the radius with respect to distance is about 1 to 4 (Ref. 4).

This is precisely the rate of growth that would be calculated by assuming that all of the material swept through by a spherical parcel is entrained in the parcel. This implies that the relative impingement velocity and the projected area are the significant controlling parameters. If the frequency of emitted puffs is increased, a continuous plume is developed. However, close inspection of the plume will still show the vestiges of the individual vortices on the edges of the plume. In this case, the vortices can only entrain ambient fluid on the outside edges. The slippage or difference between the plume parcel velocity and that component of the ambient velocity parallel to the plume results in a shearing action which keeps the rolling vortices in motion. The removal of some of the ambient by this shearing entrainment results in an apparent suction or aspiration of the ambient into the plume. This entrainment can be specified by the product of the lateral area of the plume segment, the previously mentioned slippage velocity, and an aspiration or entrainment coefficient (α).

$$\text{Aspiration} = \alpha\rho 2b\pi H|V-W\cos\Theta|$$

The order of magnitude of this entrainment coefficient is known from experiments of jet discharges in quiescent mediums to be about 0.1 (Ref. 5). In the case of a wind, the component of the wind velocity perpendicular to the plume induces circulation analogous to the circulation of an isolated parcel, except the motion is essentially two-dimensional instead of three-dimensional. That is, two counter rotating vortices are formed which can lead to a splitting (bifurcation) of the plume.

This motion is the two-dimensional analogue of the relative wind impinging on a single moving parcel; therefore, it is logical to assume that the maximum entrainment due to this motion could also be found by multiplying the impinging velocity component by normal area.

$$\text{Impingement} \approx \rho\, W \sin\Theta\ 2bH$$

These two entrainment calculations, illustrated in Figure 1, represent logical limits for each mechanism but they are not necessarily mutually exclusive.

The maximum horizontal momentum that the plume could extract from the wind both by mass that is acutally absorbed into the plume or pressure forces due to deflected mass, can be no greater than the combined momentum of these masses in the ambient.

With this as a postulate for the horizontal momentum, and an assumption for F_h one can estimate the amount of mass actually entrained.

$$\Delta M = (\text{Aspiration} + \text{Impingement} - \frac{F_h \Delta t}{W})$$

The problem then reduces to estimating F_h, a precise formulation for F_h is not known, however, a preliminary function for F_h is

$$F_h = (\text{Aspiration} + \text{Impingement})\ (W-u)$$

The model results using this estimate for F_h are shown next. Figure 2 is a comparison of model predictions with two data sets for the near field region of a non-buoyant jet. Figure 3 is a comparison of the model predictions with measurements taken in the cooling tower plume.

Figure 4 is a comparison of model-predicted trajectories to a regression fit of Fan's data. Figure 5 shows more completely the predicted average width of the plume and average plume temperature or dilution. More information on the model is available in Reference 6.

IMPROVEMENTS TO PLUME MODELS

This distinction between what should be treated as classical turbulent diffusion and what are deterministic motions should be made on the basis of the scale of motion involved, the formulation of the basic law and the degree of resolution implied in the solution procedure.

Advances in plume models will come about through a better understanding and more precise description of entrainment and interaction with the pressure field around the plume, which in this simple model is prescribed through the force and buoyancy calculation.

Conservation of mass, momentum and energy over a control volume encompassing the whole plume should be the goal. The degree to which this is achieved is a check on the consistency of the calculation procedure.

Detailed, three-dimensional, finite volume, numerical calculation with a grid spacing fine enough to predict the self generated circulations is presently too expensive for parametric studies of plume behavior. However, a few such calculations could lead to a better understanding of how the force, buoyancy, and entrainment might be specified more precisely in simple, less expensive, calculation systems.

CONCLUSIONS

A simple, physical calculation scheme based on average mass, and momentum can yield reasonable predictions of plume behavior.

In a steady wind, the high degree of entrainment that occurs relatively close to the orifice can be largely accounted for by deterministic, self induced entrainment mechanisms. Further downstream where the plume horizontal velocity approaches the wind velocity, the diffusion or spread of the plume is controlled by ambient turbulence. However, by then the properties of the plume have already been significantly diluted.

RECOMMENDATION

Plume modeling and measurement should make a distinction between entrainment that is due to self-generated vortices and an apparent entrainment or spreading that is a result of fluctuations in wind direction which can cause the plume to oscillate back and forth.

The prescription of the momentum and entrainment calculations should be made as consistent as possible with an overall mass momentum, and energy budget of the whole plume.

REFERENCES

1. Batchelor, G. K. An Introduction to Fluid Dynamics. Cambridge University Press, 1967, paperback reprint 1974.

2. Frick , W. F. and Winiarski, L. D. Comments on The Rise of Moist, Buoyant Plumes. J. of Applied Meteorology, Vol. 14 No. 3, April 1975. p. 421.

3. Hamilton, P. M. The Application of a Pulsed-Light Rangefinder (Lidar) to the Study of Chimney Plumes Phil. Frans. Roy. Soc. Lond. A 265, p. 153. 1969.

4. Turner, J. S. The Flow Into an Expanding Spherical Vortex Journal of Fluid Mechanics, Vol. 18, part 2, p. 195. 1964

5. Turner, J. S. Buoyancy Effects in Fluids Cambridge University Press, 1973.

6. Winiarski, L. D. and Frick, W. F. Cooling Tower Plume Model. EPA-600/3-76-100, Ecological Research Series, U.S. Environmental Protection Agency, Corvallis, Oregon 97330, 1976.

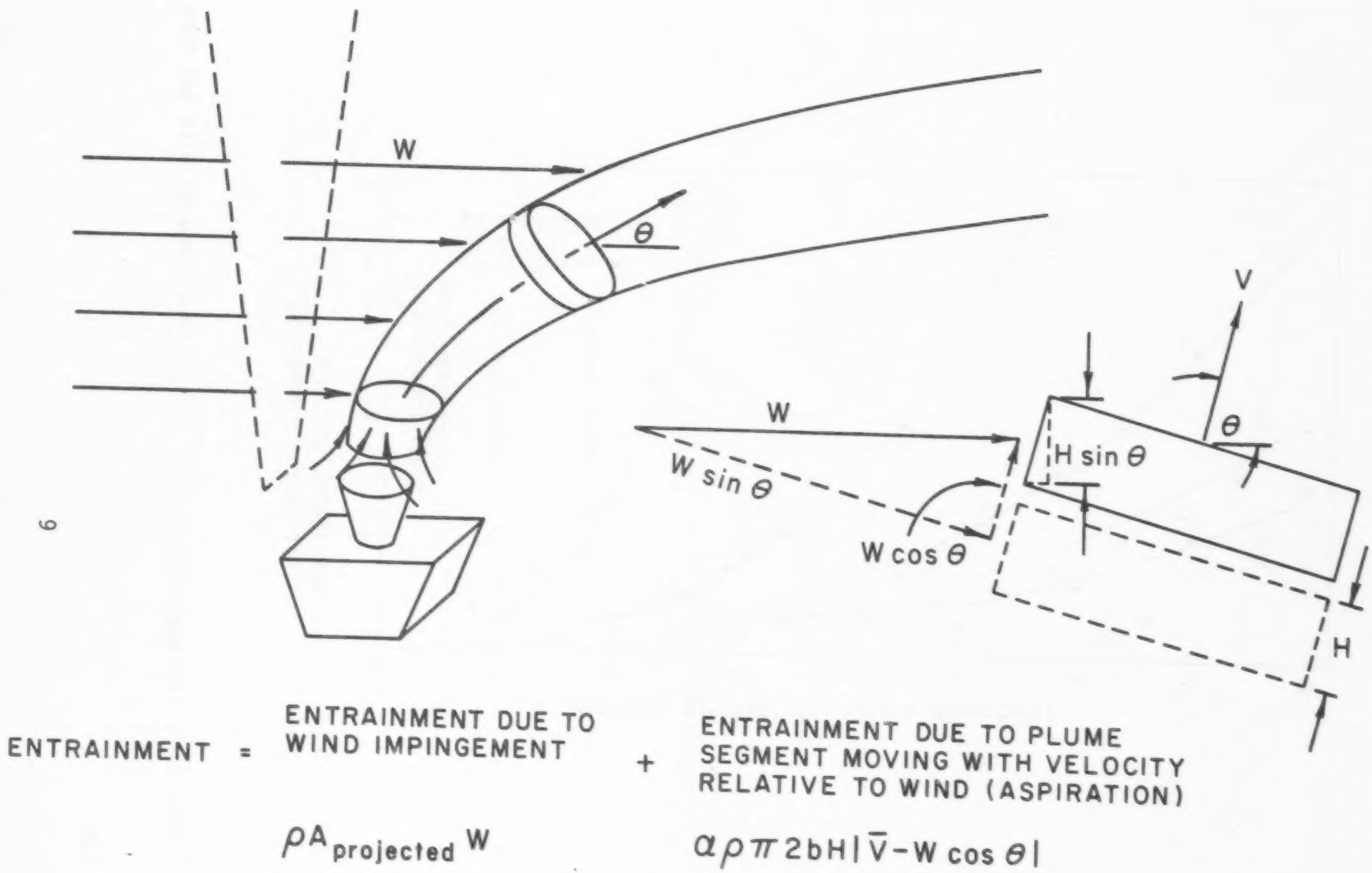

ENTRAINMENT = ENTRAINMENT DUE TO WIND IMPINGEMENT + ENTRAINMENT DUE TO PLUME SEGMENT MOVING WITH VELOCITY RELATIVE TO WIND (ASPIRATION)

$\rho A_{\text{projected}} W$ $\qquad$ $\alpha \rho \pi 2bH|\bar{V} - W\cos\theta|$

Figure 1. Entrainment mechanisms.

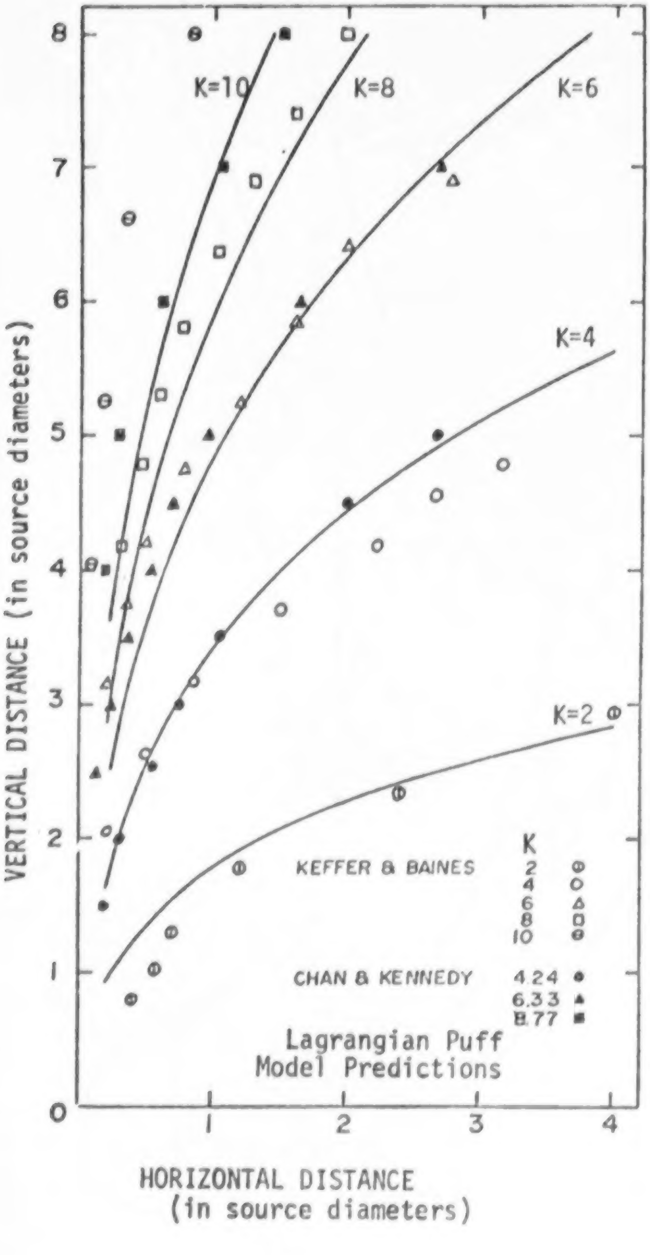

Figure 2. Lagrangian Puff Model predictions compared with jet data.

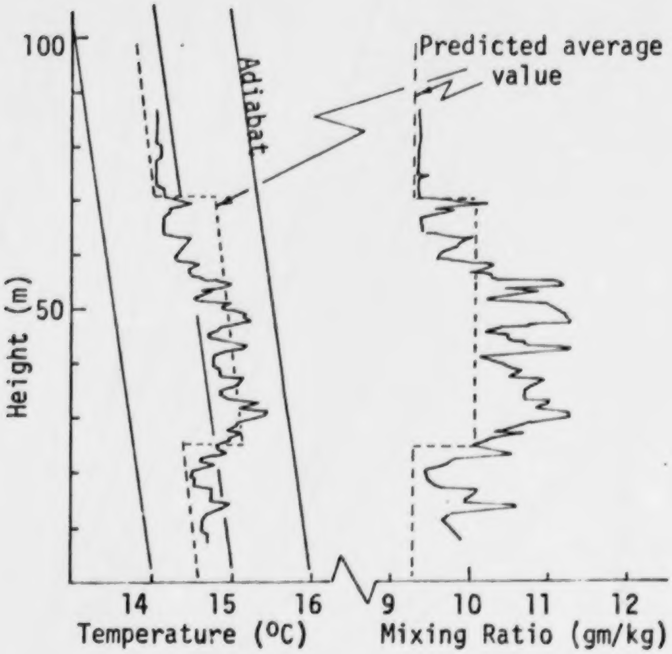

Figure 3. Single cell cooling tower plume profile. Average of Runs 1 and 2.

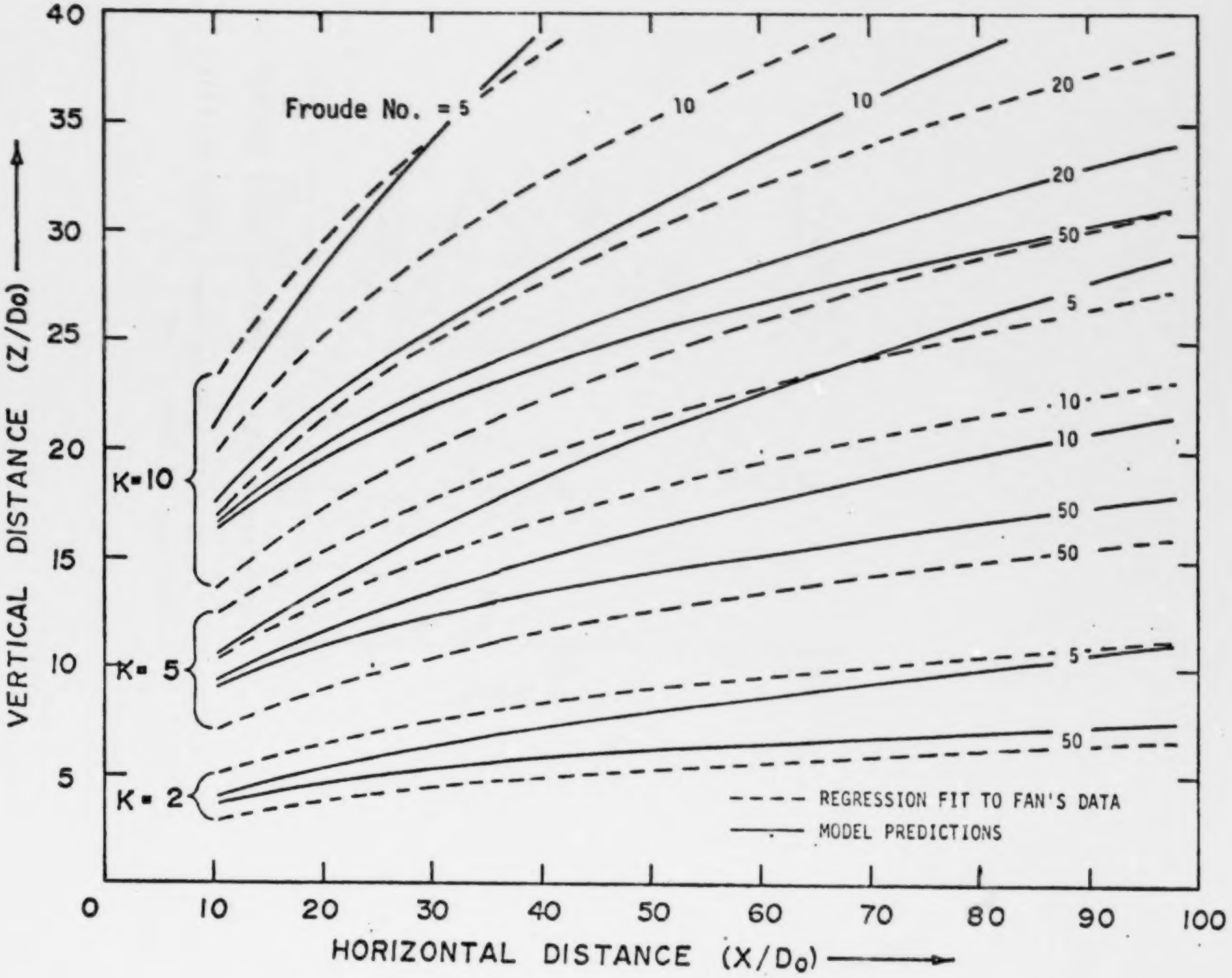

Figure 4. Comparison between model trajectory predictions and regression fit trajectories based on Fan.

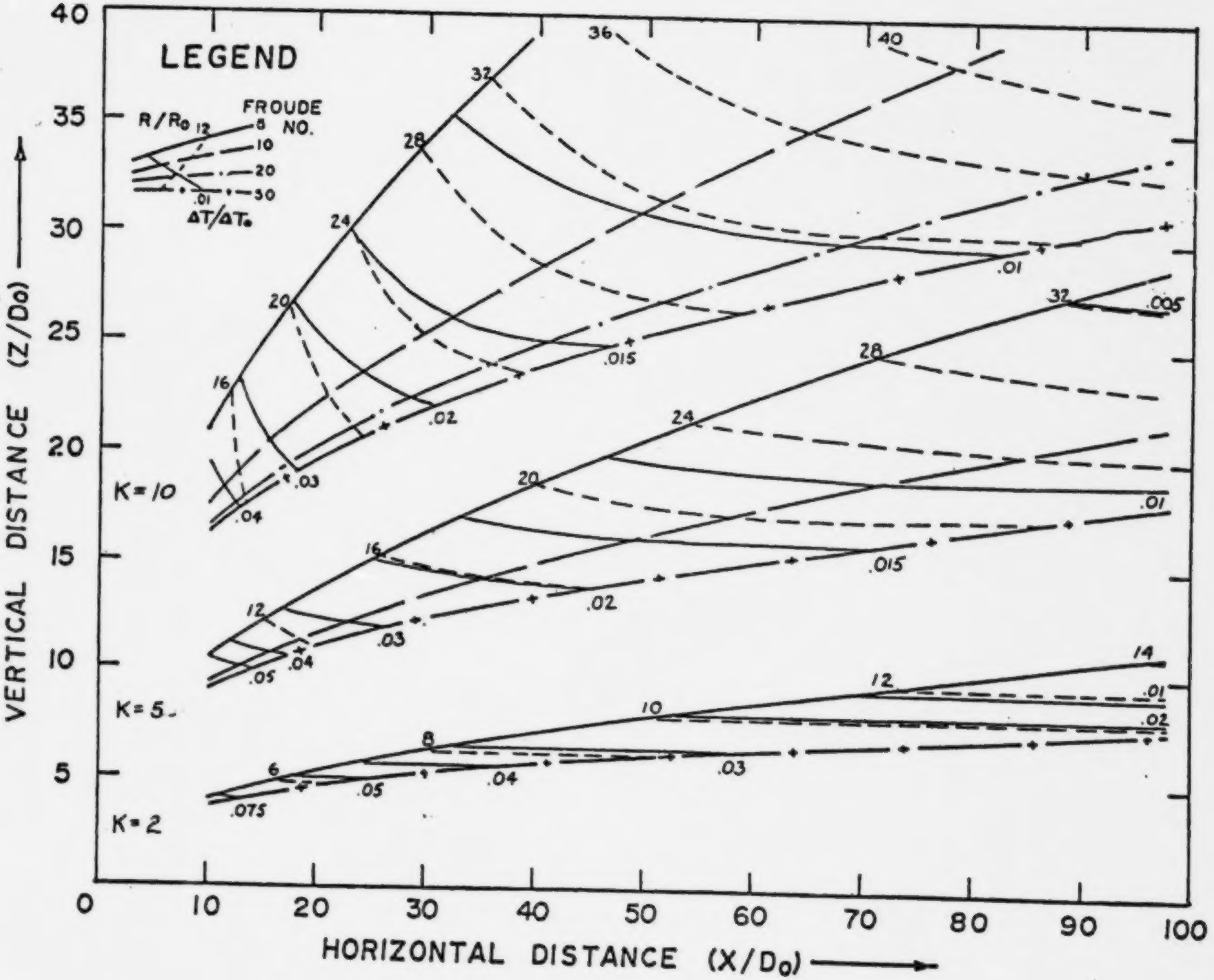

Figure 5. Model predictions of buoyant temperature plume in water.

omit

VI-C-151

Title: Natural Draft Cooling Tower Plume Behaviour at Paradise Steam Plant

by P.R. Slawson

Abstract:

A field study on the observation of natural draft cooling tower plume behaviour was carried out at the Tennessee Valley Authority's Paradise Steam Plant during the period January 31, to February 12, 1973. This study was the second phase of a study first initiated in September of 1972. The first phase results have been previously reported on. Details of the experimental technique and measurements of some of the observed time-mean condensed (visible) plumes are presented with corresponding ambient air and source parameters. The governing equations for a simple one-dimensional moist plume are integrated in closed form using some simplifying assumptions and numerically in their more general form to produce the basis for two vapour plume models. A comparison between some of the observed time-mean plumes and the closed form solution model predictions are presented. The visible plume centre-line trajectories and plume boundaries are reasonably well predicted using measured source and ambient air data within the limits of scatter of that data. Visible plume length predictions are very sensitive to errors in the magnitude of ambient air relative humidity, particularily when the relative humidity is high and ambient temperatures are low. Tower downwash effects which may greatly influence plume trajectory and growth are accounted for in a very simple way. The numerical integration model predicts the plume behaviour more accurately than the closed form integration model in the presence of strong vertical wind shear and or an elevated inversion.

Preceding page blank

Session VII-A

Utilization III

26-45-24

PROSPECTS FOR THE UTILIZATION OF WASTE HEAT IN LARGE SCALE DISTRICT HEATING SYSTEMS

J. Karkheck and J. Powell
Brookhaven National Laboratory
Upton, New York U.S.A.

ABSTRACT

District heating is one potential application for power plant reject heat. In addition to reduction in plant thermal pollution, it offers the potential to conserve over one billion barrels of oil per year. Detailed analyses of model district heating systems for nine U.S. urban areas, including projected heat costs, are presented. In addition, projections of nationwide levels of implementation of district heating systems are discussed. Results show that about half of the current population could be served through district heating at heat cost levels equal to the effective heat cost of imported oil.

INTRODUCTION

Steam-electric generating plants produce waste heat in amounts exceeding the total U.S. space and water heat net demand. The current annual rate of production of about 8×10^{15} BTU will roughly double by the end of the next decade, based on current growth projections of the electric industry.[1] In addition, the geographical distribution of such plants is favorable for transmission of hot water to all but a few urban areas. This hot water could then be used in district heating systems to meet the demands of the residential and commercial sectors for space and water heat. Utilization of this byproduct in this manner offers several incentives. It allows immediate cutback in fossil fuel consumption. It relieves the environment from bearing the burden of huge amounts of excess heat. It opens the supply of fossil fuels to more complex applications where these are used to greater advantage. It raises the energy conversion efficiency of electric plants considerably, and, as we have shown in this study, it can be quite economical.

We pursue these points in the following sections. In particular, in Section II we discuss technical and economic aspects of the adaptation of electric plants to a dual role as heat-electric energy sources. In Section III we discuss the analyses of nine diverse urban regions made for the purpose of estimating unit heat costs under actual conditions. In Section IV we present a generalization of these analyses to the national level where we investigate the maximum degree of implementation of district heating nationwide within the current economic limits imposed by the cost of imported crude. This price ceiling also limits the fossil fuel conservation potential of the district heating scheme. Section V contains concluding remarks.

II. DUAL HEAT-ELECTRIC GENERATION

For conventional fossil fuel fired steam-electric plants the average efficiency of conversion of fuel energy to electricity is 33%. Fifty-two percent of the fuel energy is discarded through the condenser as waste heat and 15% is lost up the stack or within the plant. In existing LWR nuclear power plants the waste heat is about 62% of the input energy, in plant losses amount to 5%, and electricity is produced at the same efficiency.[2] The waste heat from the steam condenser corresponds to the saturation temperature of steam at an absolute pressure of about 0.05 atm., which is normally the outlet pressure from the steam turbine. The waste heat temperature is thus about 100°F, so applications for this low quality heat are extremely limited in scope. Though the quantity of heat is large, the small temperature difference between exhaust conditions and atmospheric ambient or even winter conditions poses technical and economic obstacles for utilization of the heat. For example, use of this heat for space heating of residences and commercial buildings would require the use of very large distribution pipes and huge heat exchangers to effect the transport of sufficient amounts of heat. Additionally, water at 100°F is not suited for such uses as laundering, dishwashing, and personal hygiene. Thus consumers of this low grade heat would have to maintain conventional heating units to meet these demands.

A tradeoff can be instituted to increase the feasibility of this district heating concept. This tradeoff is used in the Soviet Union to very great extent and is gaining wide acceptance in Northern Europe. If the outlet steam pressure to the condenser is increased to 1 atm., the steam condenses at 212°F which is sufficiently hot for economical transport of hot water and for use in both space and water heating applications. The principal effects of this alteration is turbine operating conditions are reduction in electric production efficiency from the normal 33% to about 25%, and production of higher quality reject heat in even greater amounts. This last fact ensures that sufficient heat would be available in the winter.

The overall energy conversion efficiency of heat-electric plants operating at these backpressure conditions ranges from 85% for fossil fueled plants to 95% for LWR's. Roughly 10 units of useable heat are produced for each unit of electric that is lost.[3] On this basis, the lost electric revenue can be recovered by charging for heat at 10% of the electric rate. In today's terms this makes the heat resource worth 77¢ per million BTU.[4] As can be seen from Figure 1, the penalty for backpressuring is not strongly dependent on temperature within a range around 212°F, which we have demonstrated to be suitable for district heat use. On the other hand, the penalty for extracting steam is about twice that for backpressure to 212°F. Backpressuring is a more efficient process than steam extraction because it allows deposition of all heat of condensation at a lower yet useful temperature. The additional heat obtained by extracting steam is small compared to the heat of condensation and does not compensate for the additional loss of electricity. Thus, steam extracted heat is more than twice as expensive at the source. Moreover, direct transport of steam to the consumer, which is the practice in existing district heating systems in this country, is fraught with technical and economic drawbacks not encountered by hot water transport technology.

First, the volume density of heat in hot water at 212°F is greater--by more than a factor of ten--than that in steam at conditions such as those in Figure 1. This means that much greater volumes of steam must be transported to satisfy a given demand. If this transport is over distances of tens of miles, such as may be encountered in distributing over an entire city from a rural power plant site, the pumping energy expenditure for steam transport is ten or more times greater than for hot water at equal heat delivery rates. In addition, steam lines must be carefully graded and expansion joints and manholes provided at frequent intervals, the latter to draw off steam condensate which in turn makes the heat loss from a steam pipe much greater than from a hot water pipe. So it is clear at the outset that steam district heating is considerably less attractive than hot water district heating. The rapid growth of hot water district heating in Europe is sufficient testimony. From this analysis it is obvious that the extraction of useable reject heat from power plants is not the economic obstacle to the implementation of district heating technology in this country since the estimated value of reject heat is considerably less than the effective heat costs of natural gas and imported oil.

III. ANALYSES OF REGIONAL MODEL DISTRICT HEATING SYSTEMS

The feasibility of district heating is controlled by the cost of transporting the heat from the source to the consumer. In view of this, we have developed a methodology for projecting such costs and used actual urban conditions in constructing model district heating systems. We studied nine urban regions that collectively display a wide variation in the parameters that are the primary determinants of unit heat cost. These regions are New York City, Chicago, Philadelphia, Los Angeles, Baton Rouge, New Orleans, Jersey City, Newark, and Paterson. They show great variety in climate, size, population and population density, housing profile, working conditions, and labor costs.

The goal of our analysis is to project heat demand in each region, design appropriate hot water piping systems to distribute this heat, and compute unit heat costs based on district heating system capital and operations costs and yearly heat demand.

Per Capita Heat Demand

Space heat demand is conveniently expressed on a per capita basis assuming the values shown in Table I.[5] Entry A shows that there are 375 ft^2 of residential and 110 ft^2 of commercial floor space per person in this country at this time. These figures hold for the Northeast, North Central, South, and West decomposition of the country and are assumed to hold regionally as well. Entry B shows the geographical breakdown of net heat demand for various structures in terms of floor space. These net values correspond to losses through the surfaces of the structure and are the appropriate figures to use because our system suffers no conversion losses within a structure.

From this Table, it is seen that heat demand depends on the regional housing profile, that is, the proportion of the population residing in apartments, single and multi-family houses. This information is obtained from Census data, but for practical convenience we classed all individuals residing in structures of 5 or more dwelling units as apartment dwellers with an average per capita demand of 10 BTU/ft^2/degree-day, and all other individuals are classed as single family house dwellers at an average per capita demand of 15 BTU/ft^2/degree-day. While these assumptions appear to inflate the projected heat demand, detailed analysis shows that the discrepancies so introduced are small.

In addition, it is seen from entry B that the commercial floor space mix is needed. This is provided in entry C and from these we calculate an average demand of 9.1 BTU/ft^2/degree-day for all commercial structures. Using the per capita floor space allotments, we compute per capita net space heat demands of 5625, 3750, and 1000 BTU/person/degree-day for house residential, apartment residential, and commercial applications respectively.

The hot water supply system design capacity is based on the space heat demand for the coldest month in each region. Climatological data is based on the U.S. Weather Bureau degree-day compolation. We use "climate" to mean the maximum monthly mean degree deviation from the 65°F reference temperature, and "duration of heating season" to be the number of heating days under "climate" conditions to make up the total degree-day compilation. Multiplying the per capita space heat demand figures by "climate" and summing over the populace to be served by district heating yields the system power design capacity.

We propose that a 75°F drop in water temperature within each structure is feasible. This falls within the inlet design temperature of 210°F at the plant and exit temperature of 125°F at each structure and an allowance for conduction losses through the distribution pipes. This translates to an anticipated useful heat transport of 622.5 BTU per gallon of hot water.

In addition to the space heat load, there is a sizeable water heating load. Again, discounting conversion and radiation losses, we consume 6 x 10^{6}BTU and 1.75 x 10^{6}BTU per person through residential and commercial hot water consumption per year. We assume these to be uniform across the country throughout the year and average them over a 16 hour day to construct power demand. We find that this additional power can be supplied without changing the hardware design discussed above by just increasing pumping pressures by easily tolerable amounts. This attractive feature lends a great deal of flexibility to an installed piece of hardware not only in meeting peak power needs but also in supplying outlying areas encompassed in future expansion of the district heating system.

Populace Served

Simple arguments can be given to support the contention that the most densely populated sections of a region are most economically served by district heating. In this light we sought to determine those sections within each region which display the greatest population densities. This was done by analyzing Census Tract data to determine the population density of each tract, which thus yields a fine grained population density profile, and then by aggregating numerous tracts under certain criteria to ensure that the tracts selected are contiguous and that the sections so developed are large in area and encompass the greatest population densities. As an example of this procedure, we show the maps for Philadelphia in Figure 2. At this point we abandon the explicit detail of distributions of population and utilize only gross demographic information, of the type shown in Figure 2, in later calculations. That is, regional cost projections presented here are based on service only to these heavily utilized sections but this should not be construed as our assessment of the extent of applicability of district heating in each region. The results show that our tract selection criteria are too stringent, but no attempt was made in the regional studies to reanalyze toward maximal implementation.

The inaccuracy introduced by erasing the tract detail is studied by constructing distribution systems for the extreme cases of completely random distribution of housing and commercial structures and completely segregated zoning of house, apartment, and commercial structures. Results (Table II, col. A and D) show that such effects are small.

Pipe System

The hot water system consists of four levels of supply lines. Rural transmission lines run from power plants to city limits. City transmission lines are smaller trunk lines which feed into each section as shown in Figure 2. Distribution lines fan out from these through each street and connection is made to each structure from the distribution lines. Polymer lined polymer concrete (PLPC) pipe was chosen for transmission, distribution, and apartment and commercial connection service because of its extreme durability and strength. Chlorinated polyvinylchloride (CPVC) pipe is designated for house connection service also for its durability and ease of installation. Feed lines are insulated with 2 inches of rigid urethane foam to provide very good moisture resistance and highly cost effective suppression of conduction losses. Heat losses over each entire system range from equivalent temperature drops of 2°F in New York to 11°F in Baton Rouge. When pumping energy expenditure is taken into consideration, these values decrease to 1°F in New York and 10°F in Baton Rouge. This is so because the pumping energy is expended against friction.

Installed pipe costs are computed for five of the regions based on current installed costs of cold water lines in these regions. These latter are adapted to our purposed by disaggregating labor and materials costs and resumming the costs that accomodate the insulated PLPC pipe and labor and resurfacing costs scaled to the appropriate dimensions for burial of the larger insulated pipe. Since the hot water system is closed, we need to provide return lines which can be buried in the same trench. Figure 3 shows the installed cost curves for a unit length of complete pipe system. The variation between regions is due entirely to variations in working conditions and labor costs. The jump at 50 inches I.D. is due to pressure capacity differences. The smaller pipes are designed for 325 PSI capacity whereas the larger pipes, to be used exclusively for transmission, are designed for 400 PSI capacity. These values provide margins of at least 100% above system operating conditions.

Rural installed costs are constructed in a similar manner using oil pipeline installation costs as a guide. These would lie slightly below the New Orleans curve in Figure 3.

System cost is computed simply on the basis of total length of each diameter of pipe required. Transmission lengths are shown in Figure 2 for Philadelphia. The design envisaged here permits the heat source to be located at a single site roughly 25 Mi distant from the city limits. Pipe diameters are obtained from Figure 4 which shows capacity for different frictional pressure drops. Water capacity translates to heat capacity through the factor 622.5 BTU/gallon. We analyzed the sensitivity to increased transmission pressure drop for the two curves shown and found (Table II,col. B and C) this to be a small effect. Distribution pipe diameters are determined through estimating the number and average length of distribution mains and then correlating these with population served per main to determine power demand, hence diameter. Total distribution length is also obtained from this calculation. These results now yield the total system capital cost. Potential retrofit and connection charges are not included in the system capital cost. Maximum connection charges occur in New York where a house connection with 3/4 inch CPVC pipe costs $261, and an apartment or commercial connection with 4 inch PLPC pipe costs $953. These costs are highly competitive with oil and gas burner costs, but burners have a lifetime that is 25% that of the district heating system and require maintenance. Retrofit to structures that already have piping or air ducts would be minimal, amounting to a heat exchanger. Electrically heated buildings would require extensive retrofitting.

Finally, unit heat costs are computed on the basis of 10% amortization of capital, that is, a mortgage of 50 years, and operations costs consisting of pumping at a charge of $10 per million BTU for pumping energy. The sum of these is divided by the total heat demand for a year. Unit heat charges for several scenarios are shown in Table II. Again, random refers to the case of homogeneous distribution of residential and commercial structures throughout the sections served; and ordered means complete segregation of houses, apartments, and commercial structures. For comparison, imported crude combusted at 60% efficiency has an effective cost of $4.50 per million BTU. The cost of the heat at the plant is omitted here. The analysis given in Section II renders this to be 77¢ per million BTU, but an alternate analysis may be given based on the premise that any given electric utility which also sells heat will meet its electrical demand by operating additional plants and not by importing electricity as the first analysis assumes. Since most utilities peak in the summer, they have intermediate load plants which are not used extensively in the winter months. However, sale of both heat and electrical energy could lead to greater use of these intermediate load plants, and, in effect, greatly increase the energy baseload of the utility. In this case the cost of heat at the plant will be determined by the cost of extra fuel used by the utility. This mode of operation greatly favors coal and nuclear power plants since the value of heat from these is 34¢ and 15¢ per million BTU respectively, but $1 per million BTU from oil fired plants. Siting restrictions on the former plants will influence the cost of heat at the point of use in varying degrees depending on the size of the total district heating load. Figure 5 illustrates the effect that rural siting of power plants has on heat cost ($M=10^6$). It is assumed in each case that the power plants are located at a single site. Remote siting of plants may disfavor the application of district heating to the warmer areas of the country and to small cities. These considerations indicate that the market potential for district heating might temper future power plant siting policies.

Table III contains a summary of the chief characteristics of each region and its model district heating system. The Jersey City, Newark, and Paterson SMSA regions are interesting in themselves because each consists of many small cities, in fact all but the cities of Newark and Jersey City have populations less than 100,000, each of which alone would not be as amenable to district heating.

IV. PROJECTIONS OF NATIONWIDE IMPLEMENTATION OF DISTRICT HEATING

This study sought to define the limits for nationwide implementation of district heating at costs equal to those of currently used energy sources. National projections are based on average values for "climate" (28°F),"heating season duration" (152 days) and unit installed costs (those of Philadelphia). These averages are obtained from a sample of all cities with 100,000 or greater population. At present, these cities contain one-third of the urbanized population of 155 million and constitute a good sample of the regions that can be economically served by district heating.

From the average climate and heating season duration we can project average per capita net power demand and annual per capita heat load and it remains to design proper distribution systems. The parameters relevant to this task are per capita demand, housing profile, population density, size and shape of the region to be served. Since we did not study each city in detail, we instead examined the influence of size and simple shapes on heat cost. We found that a square region, 20 Mi^2 in area, produces average costs. From the detailed regional analyses we were able to establish a relation between housing profile and population density. Thus having fixed the per capita demand and geometry of the regions, national cost projections become a study of the relations between heat cost and population density. Figure 6 shows such a curve based on supply of space and water heat, and including costs for pumping but not heat at the source, to regions with random distribution of structures. Shown for comparison are the cost projections obtained from the detailed regional analyses for the same scenario (Table II, col. A). The close agreement is gratifying since it shows that the curve, which is based on national averages, can be understood to reflect actual regional values.

We projected levels of implementation under various constraints by coupling this cost profile to the population density studies of Haaland and Heath.[6] Table IV gives serviceable population levels at selected ceiling charges, i.e., the marginal cost for adding the last incremental district heating systems. The first three ceiling charges correspond to the effective heat costs of: (1) natural gas, (2) imported oil, and (3) electricity at the point of consumption, including conversion efficiencies.[7] Since virtually all citizens bear the cost of imported oil to some extent, district heating could probably be implemented at that level with all customers being charged a uniform price. For a nationwide nuclear electric utility this permits district heating service to more than half the 1970 population, i.e., to about 110 million. For an oil electric utility, at current oil prices, half the 1970 population could be served at the same $4.50 per million BTU level, including cost of heat at the plant.

Impact on Utilities and Fossil Fuel Consumption

The impact of district heating on utilities and conservation potential is demonstrated for three reference years[8] in Table V. The district heat load was assumed to be distributed among steam-electric plants by fuel type in proportion to the projected installed capacities. The extra fuel required by utilities is a reflection of the loss in electric production efficiency due to backpressure turbine operation and is independent of whether a heat-electric utility imports electricity or operates additional plants to compensate. The proliferation of nuclear power projected here might not come to pass, but coal fueled plants, a likely alternative, though more efficient than LWR's thus effecting slightly greater energy savings, produce a similar profile. It is important to note that district heating with power plant reject heat is a more efficient, direct, and economical means to replace natural oil and gas heating fuels with coal and nuclear fuel than coal gasification or nuclear powered electrification for up to about 50% of the population.

The population levels in Table V were chosen for illustrative purposes. Increases in total population might open new markets for district heating and allow expansion of established systems into suburban areas. Future economic conditions may also favor higher levels of implementation of district heating. Thus, the conservation potential could be greater than projected here. The gas that would be conserved could be redirected into applications that would further decrease oil consumption. The equivalent oil savings shown in the table reflects this possibility. Thus we project that had district heating service using power plant reject heat been used by 50% of the population in 1972, the savings in fossil fuel would have been equivalent to 1.1 billion barrels of oil per year. At 1975 prices, this would amount to a reduction in balance of payments of $13 billion. The capital investment to install district heating systems to this level of service is estimated at $180 billion, 1975 dollars. This projected oil savings is actually greater than the amount of oil used by the space heating sector in 1972, and the same holds true for the 1985 and 2000 projections. Thus, we anticipate that district heat service could eliminate the use of oil for space and water heating applications. The saturation effect in equivalent oil savings is due to reduction in per capita demand because of better insulation of buildings, projected to become a significant factor about the year 2000.

Comparison With Competing Technologies

Other technology options may effect a reduction in our dependence on imported oil. Coal gasification to produce synthetic oil and gas could feasibly make us energy self-sufficient, and electric heating powered by coal or nuclear plants could produce the same effect. Of course, neither of these technologies result in the utilization of power plant reject heat and the latter exacerbates the problem of waste heat disposal. District heating offers additional economic incentives as well.

Capital investment (1975 dollars) per kilowatt capacity (Figure 7) is more favorable for district heat service to about 70 million people than competitive technologies, and is competitive with electric heat up to 50% of the population. The values shown for the electric plant option are for 1000 MW base load plants with a 30 year planning lifetime. Here, in fact, the district heating option should be substantially more attractive than Figure 7 indicated, because its planning lifetime will be equal to its operating lifetime which should be considerably longer than the assumed 50 year amortization peroid. Consequently, the district heating scheme should have a substantial advantage over more conventional options which would require more frequent augmentation and would probably incur large escalations in capital cost when additions are made.

Energy cost to the consumer is least sensitive to basic fuel cost in the district heating option. Figure 8 shows the average charge for heat at point of consumption, including end use conversion losses but not end use equipment cost. Electricity cost reflects the greater insulation efficiency of buildings certified for electric heating, but takes no account of the cost for this construction. Here again district heat service to 50% of the population is competitive with other "new" technologies. An increase in the cost of fuel would be passed on to the consumer in all cases. The relative scale factors relating the proportional increases in fuel charge for the three heating options are 3 for electricity customers, 1.3 to 1.6 for synthetic fuel customers, and 0.35 to 0.40 for district heat customers.

V. CONCLUDING REMARKS

In view of the limitations of U.S. oil and gas resources and our increasing dependence on imports, it is necessary for the United States to take definite steps to reduce consumption, and the implementation of district heating would constitute a sizable step in this direction. District heating is also a practical means to utilize a large portion of that two-thirds of power plant energy input now rejected as heat. Development of this resource would broaden the energy baseload of electric utilities and provide additional income.

District heating fed by electric plant waste heat is tractable with today's electric generation technology. The prospects for district heating are even brighter when viewed in terms of advanced technology. Both the low fuel cost and the possibility of conjoining useful waste heat production with electric generation in a total energy operating mode serve to enhance the economics of district heating and broaden the base level energy demand. The need for electricity in our economy is certain and its role is expected to expand. Thus, we can rely on the production of useful waste heat in the long term. Hence, this district heating concept transcends the very basic questions about fuel resources and management.

REFERENCES

1. "Federal Power Commission Steam-Electric Plant Construction Cost and Annual Production Expenses, Twenty-Fourth Annual Supplement, 1971", Government Printing Office, Washington, D.C.

2. D. Rimberg, "Utilization of Waste Heat from Power Plants", Noyes Data Corporation, Park Ridge, New Jersey, 1974.

3. P. Margen, "The Use of Heat from Nuclear Stations for Residential Heating", ASME/ANS International Conference on Advanced Nuclear Energy Systems, Session VII, Paper A, Pittsburgh, 1976.

4. M. Beller, Ed. "Sourcebook for Energy Assessment", Report BNL 50483, Brookhaven National Laboratory, New York, 1975.

5. Data in Table I is adapted form "Project Independence Blueprint, Final Task Force Report, Conservation Vol. I: Residential and Commercial Energy Use Patterns, 1970-1990", Federal Energy Administration.

6. C. M. Haaland and M. T. Heath, Demography II (No. 2), 321, May, 1974.

7. M. Beller, Ibid.

8. M. Beller, Ibid.

TABLE I

FLOOR SPACE CHARACTERISTICS

	RESIDENTIAL	COMMERCIAL
TOTAL U.S.	75,600 X 10^6 ft.^{2}	21,610 X 10^6 ft.^{2}
PER CAPITA	375 ft.^{2}	110 ft.^{2}

A) Floor Space

	Single Family	Multi Family House	Low Rise Apartment	High Rise Apartment	Offices	Retail	Schools	Hospitals	Other Commercial
NORTHEAST	15	12.4	10.4	9.7	12.2	6.7	10.9	13.2	6.7
NORTH CENTRAL	14.5	13.4	10.5	9.6	12.5	6.8	10.9	13.3	6.8
SOUTH	13.5	12	8.5	7.5	14.8	6.3	11	12.8	6.3
WEST	14.4	12.9	8.5	7.3	12.1	6.2	10.8	12.5	6.2

B) Space Heat Demand, Btu/ft^2/degree-day

	Offices	Retail	Schools	Hospitals	Other
NORTHEAST	16.9	20.3	21.5	8	33.3
NORTH CENTRAL	14.1	20.4	23.6	7	34.9
SOUTH	15	18	25.6	6.9	34.6
WEST	17.3	19.4	21.9	5.4	36.1

C) Commercial Floorspace Inventory by Percent

TABLE II

PROJECTIONS OF UNIT HEAT CHARGES ($ PER 10^6BTU)

	A	B	C	D	E
New York	.96	----	1.14	.90	1.15
Chicago	.80	1.03	.93	.78	1.16
Philadelphia	.88	1.11	1.03	.80	1.05
Los Angeles	1.74	2.63	2.47	1.51	1.82
New Orleans	1.23	2.46	2.35	1.14	1.61
Baton Rouge	1.98	3.43	3.32	1.87	2.56
Jersey City	.88	1.26	1.05	.84	1.14
Newark	.93	1.14	1.05	.83	1.14
Paterson	.98	1.31	1.19	.95	1.33

A - Random Distribution, Space and Water Heat Service

B - Ordered Distribution, Space Heat Service, Low Pressure Drop Design

C - Ordered Distribution, Space Heat Service, High Pressure Drop Design

D - Ordered Distribution, Space and Water Heat Service

E - Same as D and Includes Rural Transmission Line

TABLE III

SUMMARY OF REGIONAL ANALYSES

	New York	Chicago	Philadelphia	Los Angeles	New Orleans	Baton Rouge	Jersey City SMSA	Newark SMSA (Part)	Paterson SMSA (Part)
POPULATION SERVED BY DISTRICT HEATING (1000's)	7500	1098	1543	933	185	74	503	481	173
PERCENT OF REGIONAL POPULATION SERVED	95	33	79	33	81	45	83	64	50
AVERAGE DENSITY OF POP. SERVED (PEOPLE/MI^2)	40400	35000	24000	13200	18100	8500	30400	25100	18100
HOUSING PROFILE (% APT. DWELLERS)	66	60	16	50	25	13	48	48	33
CLIMATE (^{o}F)	33	40	32	12	11	13	33	33	33
HEATING SEASON DURATION (DAYS)	150	158	152	168	107	120	150	150	150
DESIGN CAPACITY FOR SPACE HEAT LOAD (MW)	16200	2900	3800	774	148	74	1160	1100	420
ANNUAL HEAT LOAD (10^{12}BTU)	256	46	59	18	2.7	1.3	18	17	6.5
DISTRICT HEATING SYSTEM CAPITAL COST ($ x 10^6)	2528	457	574	296	41	32	184	177	78

TABLE IV

PROJECTIONS OF NATIONWIDE SERVICE LEVELS

NUMBER OF PEOPLE SERVED (MILLIONS, 1970 CENSUS)	CEILING CHARGE (DOLLARS/10^6BTU)	AVERAGE CHARGE (DOLLARS/10^6BTU)
38	2.10 [=Natural gas]	1.25
73	4.50 [=Imported oil]	2.15
102	9.00 [=Electricity]	3.50
110	11.50	4.50 [=Imported oil]

TABLE V

PROJECTIONS OF ANNUAL FUEL AND ENERGY SAVINGS

		1972	1985		2000	
DISTRICT HEAT SERVICE TO		50% OF THE POPULATION	50% OF THE 1972 POP.	50% OF THE 1985 POP.	50% OF THE 1972 POP.	50% OF THE 2000 POP.
DISTRICT HEAT DEMAND, QUADS (10^{15}BTU = 1mQ = 1 QUAD)		3.6	3.6	4.13	3.6	5.14
STEAM-ELECTRIC GENERATION FUEL MIX-PERCENT	OIL	18.8	8.3		3.3	
	COAL	51.5	44.0		30.0	
	GAS	25.9	9.4		3.2	
	NUCLEAR	3.8	38.3		63.5	
EXTRA FUEL REQUIRED BY POWER PLANTS IN DUAL MODE OPERATION [WITH DISTRICT HEATING], QUADS	OIL	.28	.13	.14	.05	.07
	COAL	.77	.66	.76	.45	.64
	GAS	.39	.14	.16	.05	.07
	NUCLEAR	.05	.49	.57	.82	1.16
ANNUAL SAVINGS FOR U.S. ENERGY SYSTEM [INCLUDING REDUCTION IN OIL AND GAS FOR HEATING]	NET	4.8mQ	4.9mQ	5.2mQ	4.9mQ	5.0mQ
	OIL	2.5mQ	2.6mQ	3.0mQ	2.7mQ	3.3mQ
	GAS	3.1mQ	3.4mQ	3.6mQ	3.5mQ	3.5mQ
	OIL EQUIV.	1.1 x 10^9bbl	1.2 x 10^9bbl	1.3 x 10^9bbl	1.2 x 10^9bbl	1.32 x 10^9bbl

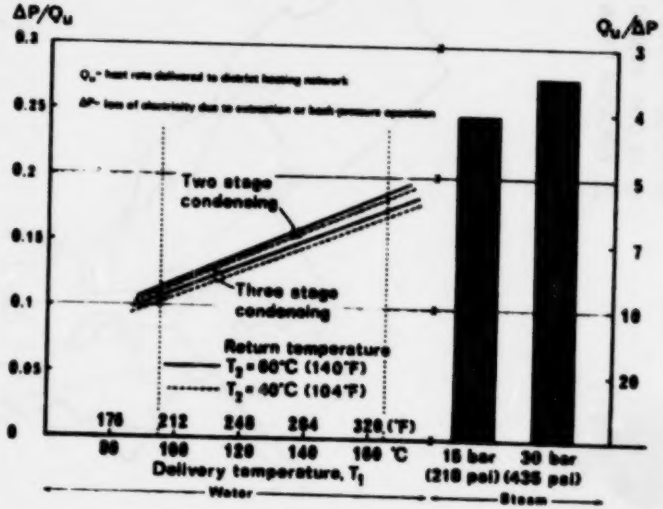

Fig. 1. Electricity Sacrifice (ΔP) to Produce Usable Heat (Qu) (Adapted from Ref. 3.)

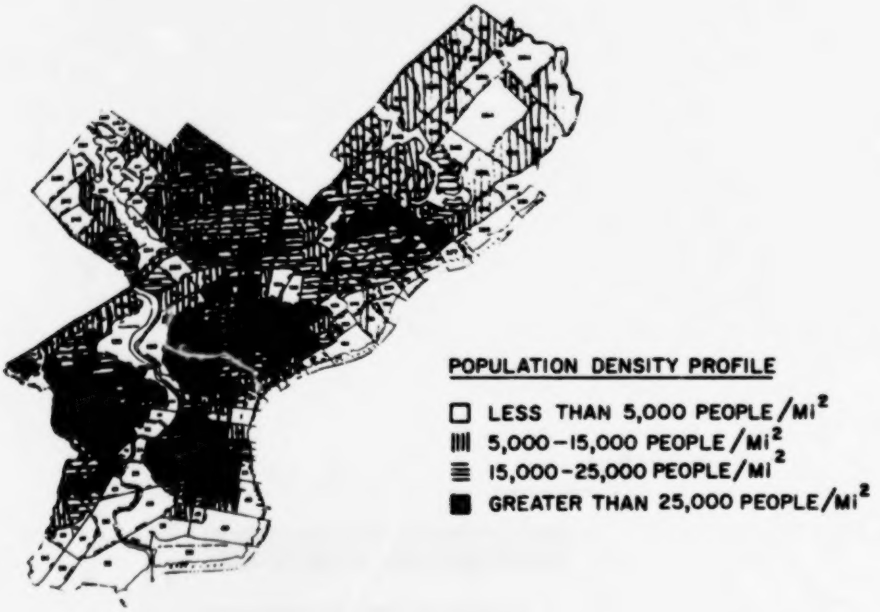
POPULATION DENSITY PROFILE
☐ LESS THAN 5,000 PEOPLE/MI^2
▥ 5,000–15,000 PEOPLE/MI^2
≣ 15,000–25,000 PEOPLE/MI^2
■ GREATER THAN 25,000 PEOPLE/MI^2

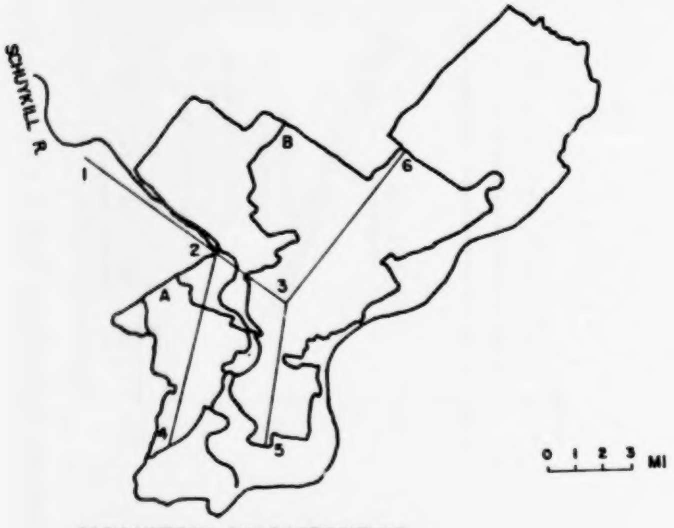
SCHUYLKILL R.
1
B
6
2
3
A
4
5
0 1 2 3 MI

PARAMETERS CHARACTERIZING DISTRICT HEATED SECTORS

TRANS. LINE	
SEGMENT	LENGTH
2-4	7.2 MI
2-3	3.2 MI
3-5	5.2 MI
3-6	6.8 MI

SECTION	AREA MI^2	POPULATION	POP. DENSITY PEOPLE/MI^2	HOUSING (APT)
A	13.9	343,000	24,600	16 %
B	50.2	1,200,000	24,000	16 %

Fig. 2. City of Philadelphia. Population and Housing Profile, and Model Transmission Line Design

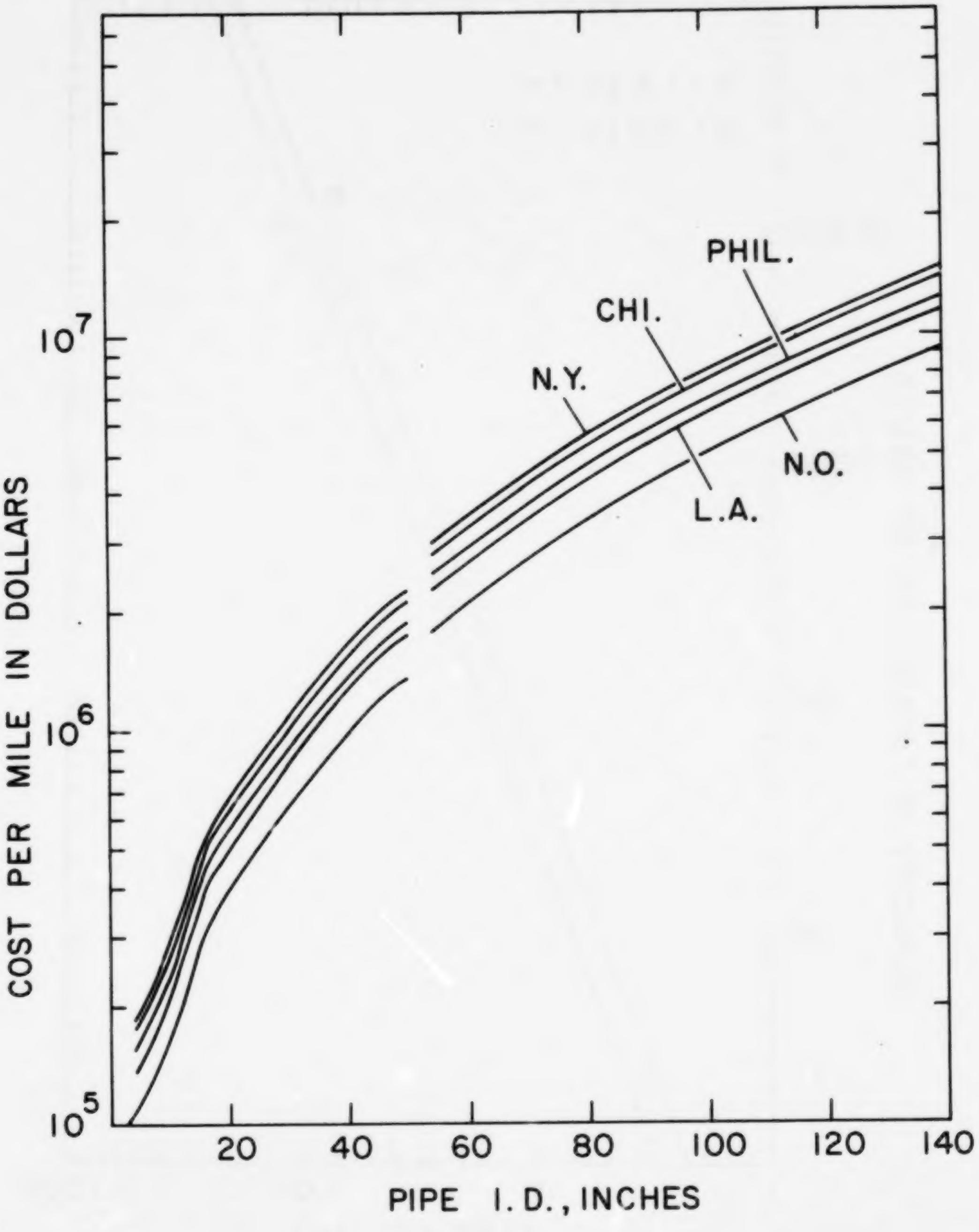

Fig. 3. INSTALLATION COSTS OF HOT WATER PIPE
(COMPLETE SYSTEM)

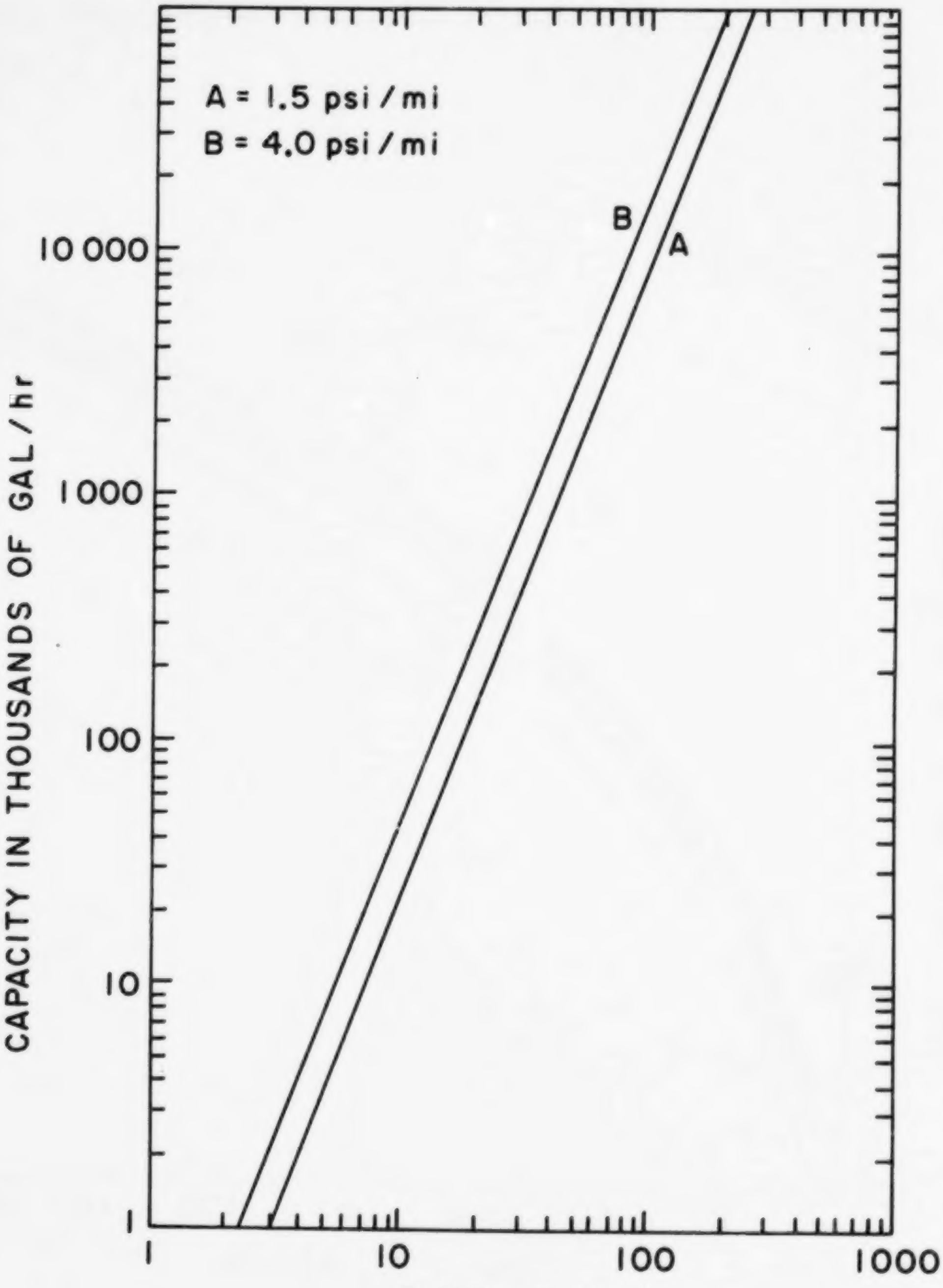

Fig. 4. PIPE DIAMETER VERSUS CAPACITY FOR PRESSURE DROP

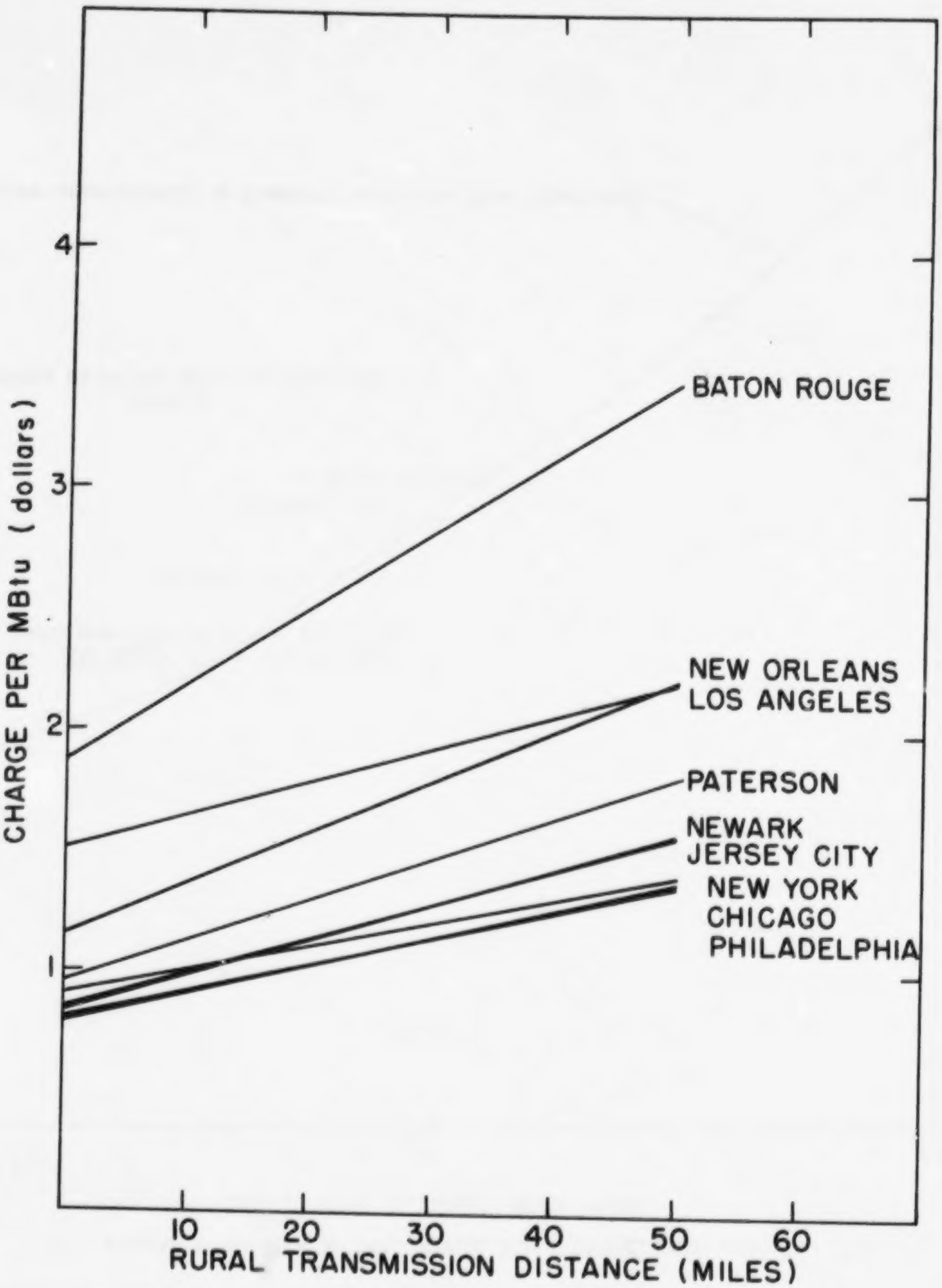

Fig. 5. TOTAL ENERGY CHARGE AT COMBINED SERVICE

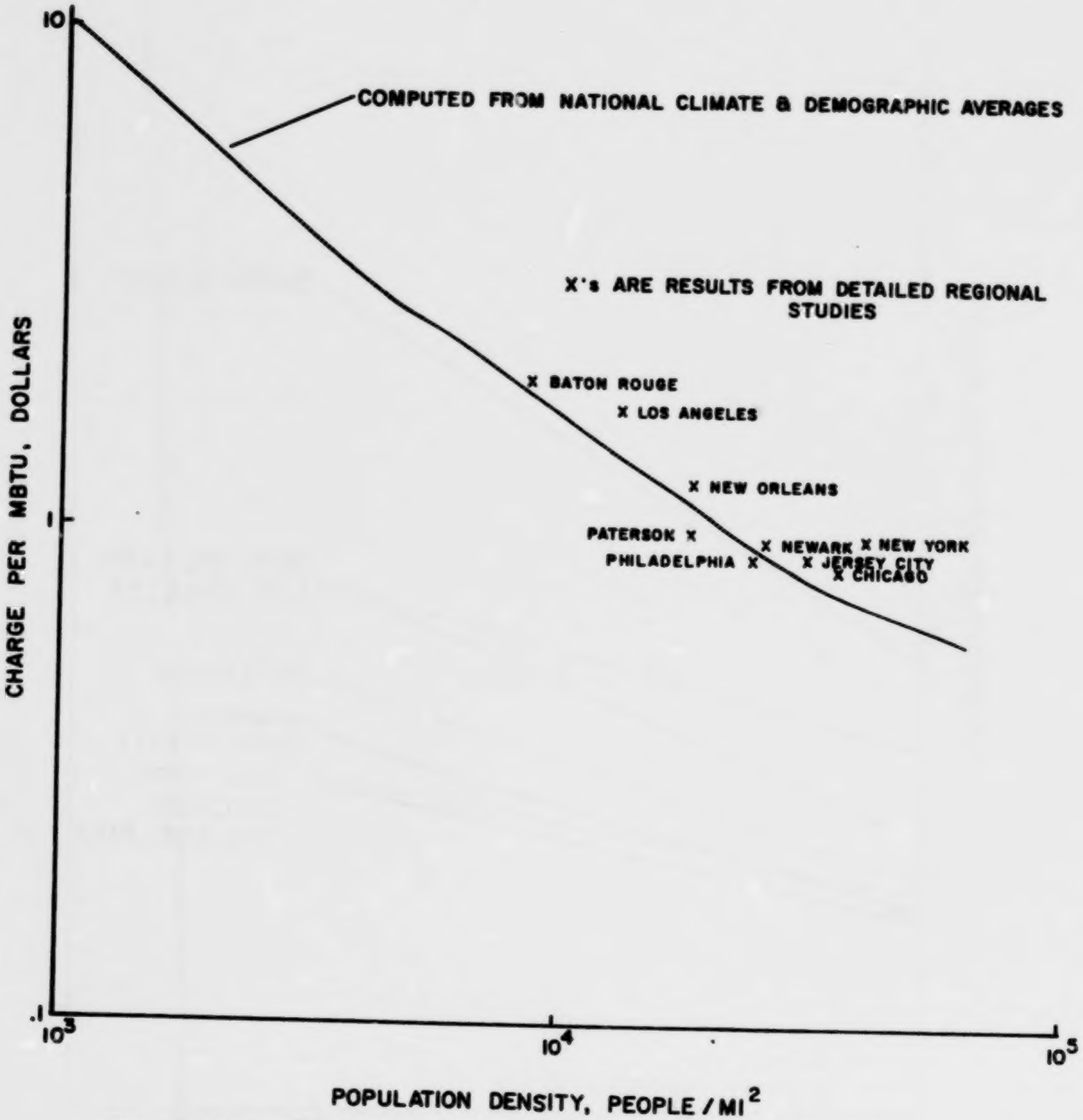

Fig. 6. UNIT HEAT CHARGE FOR SPACE AND WATER HEAT SUPPLY

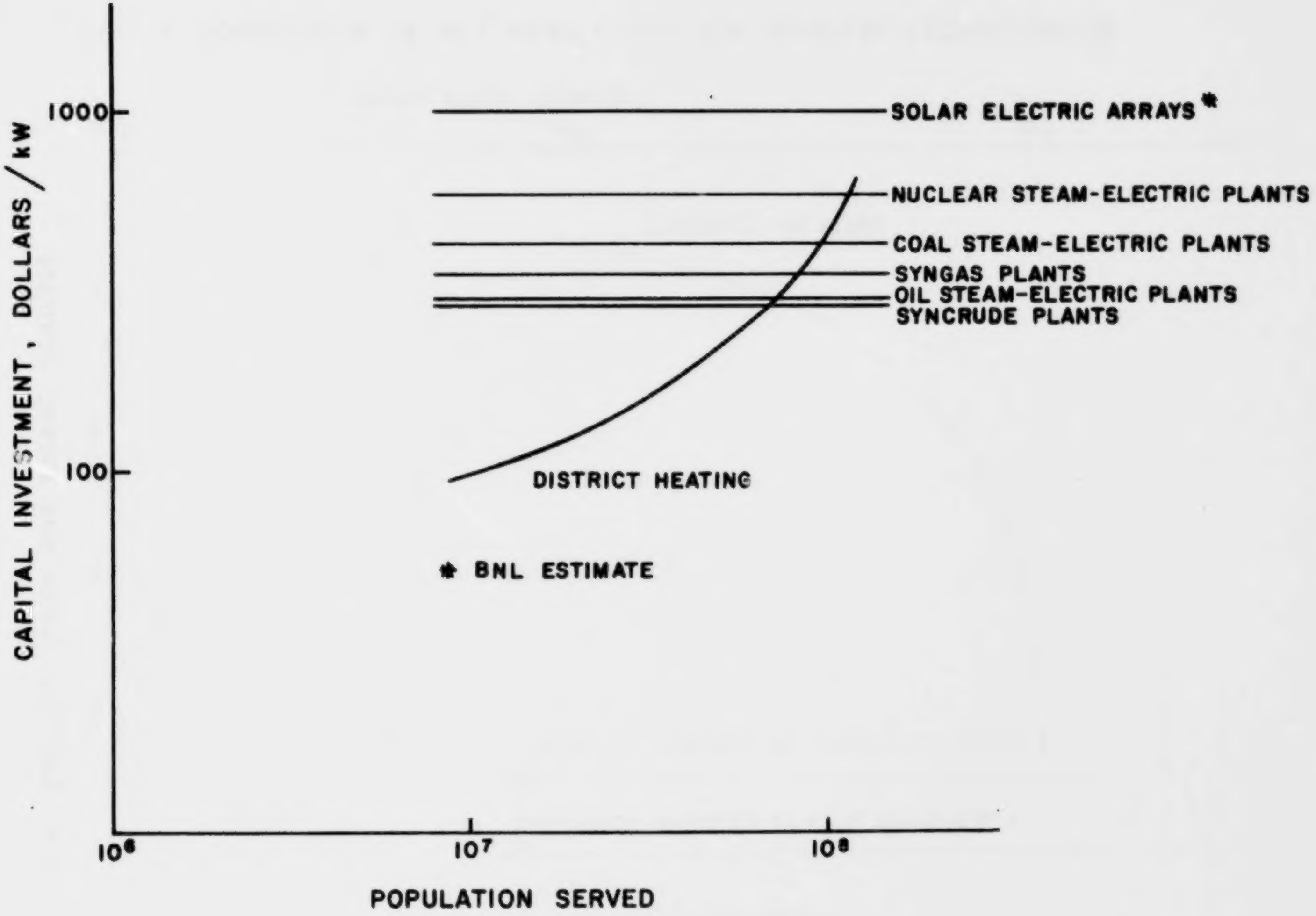

Fig. 7. COMPARISON OF CAPITAL INVESTMENT FOR SEVERAL TECHNOLOGIES

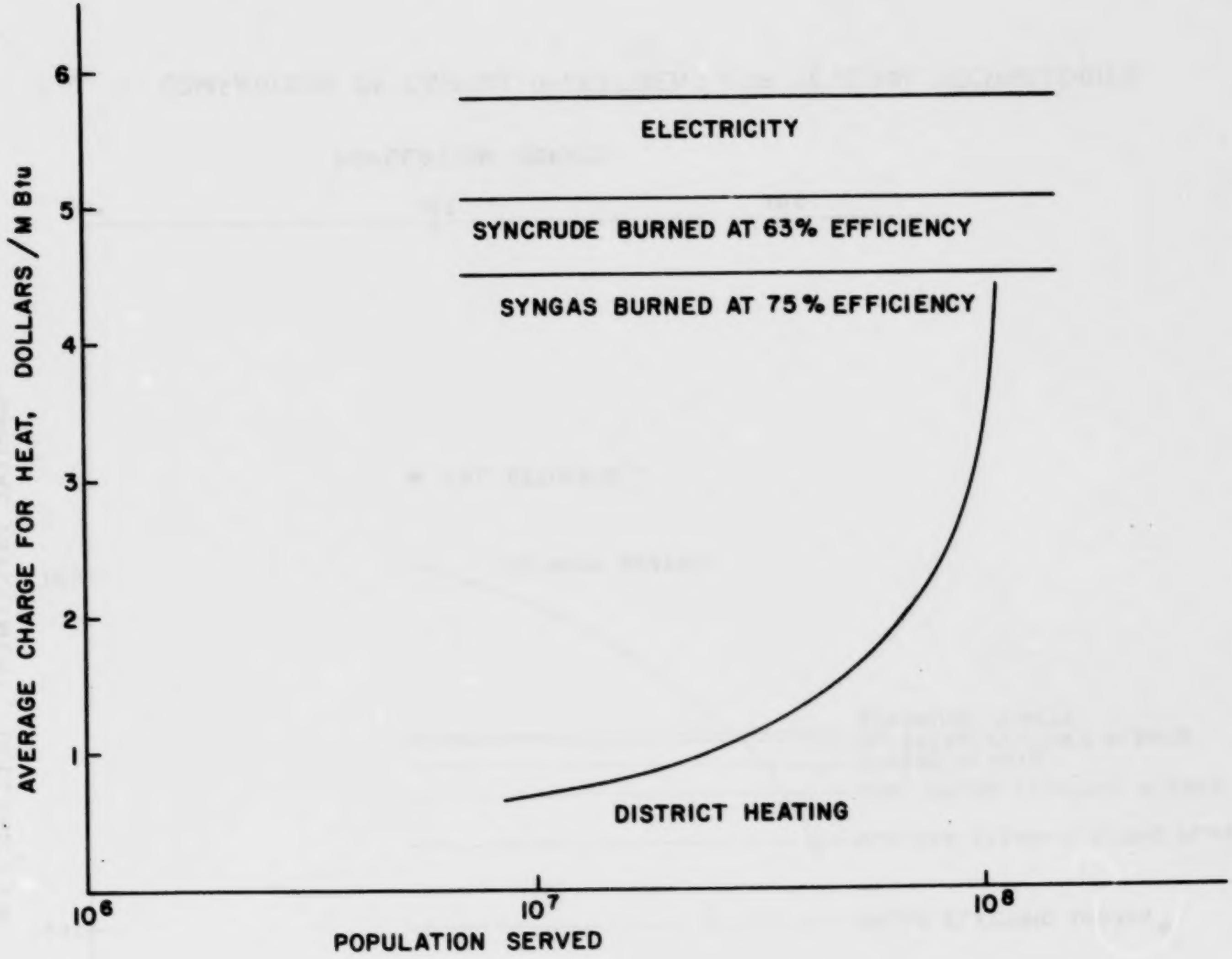

Fig. 8. COMPARISON OF NET HEAT COSTS FOR SEVERAL TECHNOLOGIES

27-45-14

EXPLOITING NATURAL OYSTER POPULATIONS THROUGH WASTE HEAT UTILIZATION

B. J. Neilson
Virginia Institute of Marine Science
Gloucester Point, Virginia U.S.A.

ABSTRACT

Oysters are filter-feeding organisms which can accumulate substances to concentrations far above those found in the surrounding water. Large acreages of estuary bottoms have been classified as restricted for shellfish culture due to the presence of pollutants in the water and therefore, the likelihood of high levels of pollutants in oysters grown in those environments. Depuration is a natural process whereby oysters and other shellfish cleanse themselves of accumulated contaminants when they are placed in a clean environment. Recent studies have shown that bacterial depuration of oysters is feasible for the waters of Chesapeake Bay. Depuration is not possible, though, when water temperatures are below 10°C. Furthermore, both the rate of depuration and the reliability of the process increase with higher temperatures for the 10° to 20° C range. Utilization of waste heat from power generating stations would allow depuration to continue during winter months and could improve the quality of the product during the spring and fall.

INTRODUCTION

Chesapeake Bay and its tributaries have been noted for an abundant and pleasing variety of seafood since the days of Christopher Newport. One important species is the Eastern Oyster, Crassostrea Virginica, which has been harvested by the Indians and the early settlers and others up to present times. It is a bottom dwelling organism that is unable to move after it has set or attached itself to a suitable hard surface. Consequently, these animals are highly susceptible to environmental changes, predators and pollution. Natural populations in the estuaries of the Chesapeake Bay system are limited by low salinities occurring in the upriver sections. Areas wherein the end of summer salinity is greater than 15 parts per thousand experience high mortalities due to both predators and disease [1]. As a result oysters exist in large numbers only in those reaches of the estuaries characterized by moderate to low salinity.

The oyster is a filter-feeding organism that strains food from the water it pumps. A portion of the solids is digested and eventually voided as feces; the remainder is released immediately at the oyster's mouth and is called psuedofeces. The amount of feces and psuedofeces produced will be a function of the turbidity of the water and the pumping rate of the oyster. Pumping rates can be very high (greater than thirty liters per hour) at some periods, but a more typical rate would be 5 to 10 liters per hour [2]. Material filtered from the water by the oyster may contain substances other than food particles. In particular, compounds associated with suspended sediments, e.g. bacteria, heavy metals, and pesticides, will tend to be accumulated, but dissolved compounds can be taken up too [3]. Because during a single day, an oyster will pump a volume of water much larger than its body volume, concentrations can be greatly magnified. This process of accumulating water constituents to concentrations much higher than those found in the surrounding water is often called bioconcentration. The levels found in the oysters will be dependent not only on the amount of the substance in the water and sediment, but also on the availability to the oyster [4]. The concentration factor will vary from one water constituent to another and will tend to increase as the pumping rate increases.

DEPURATION

Depuration, the natural process whereby oysters and other shellfish cleanse themselves of accumulated contaminants when placed in a clean environment, is essentially the reverse of bioconcentration. Just as the uptake of water constituents is dependent on the amount and availability of the compound and the biological activity of the oyster, so too does the depuration rate vary with each substance and the pumping rate of the oyster. Chemical compounds which are incorporated into the flesh of the oyster require long periods, say several months to a year or more, to be purged. Pathogens, however, are believed to reside in the intestines of the oyster and in the mantle fluid. Depuration of bacteria and viruses can be accomplished in a relatively short period of time. Many states have regulations which permit shellfish from polluted waters to be relaid in clean water. In Virginia, the oysters must remain in the clean waters for two weeks, when water temperatures are above 50°F, before they can be reharvested and sold. Since the oysters must be harvested twice, labor costs are high. In addition, some portion of the original harvest is lost by death and because it is difficult to recover 100% of the oysters which are placed on the approved bottoms. For these and other reasons, very few commercial operations employ depuration in the natural environment.

Depuration in a controlled environment has been studied since the turn of the century, and has been practiced in England and France, and at selected sites in the United States, for many decades [5]. Many studies have been made to demonstrate the feasibility of bacterial depuration for hard clams (Mercenaria mercenaria), soft-shelled clams (Mya arenaria) and oysters (Crassostrea virginica) for locations ranging from Maine to the Gulf of Mexico. In general, these studies have shown that bacterial levels can be reduced to suitable levels within about 48 hours [5, 6, 7, 8, 9, 10]. Depuration plants of a commercial scale are in operation at this time in the states of Maine, Massachusetts, New York, New Jersey and Delaware.

VIMS Depuration Studies

For the past three years, studies have been conducted at the Virginia Institute of Marine Science (VIMS) to determine the necessary environmental conditions to achieve bacterial depuration of oysters in the Chesapeake Bay region [11]. In these studies and most others, pathogenic organisms were not measured. Rather members of the coliform bacteria group were used as "indicator organisms" for the presence of fecal pollution and therefore the likely presence of disease-producing organisms. Water quality standards also are usually given in terms of total and/or fecal coliform counts. Since the fecal coliform group is more closely correlated with fecal pollution, all data presented in this report are for the fecal coliform group as determined by the multiple tube fermentation technique [12]. Coliform levels are measured as MPN (Most Probable Number) per 100 milliliters of water or MPN per 100 grams for oysters.

Initial studies were made using small numbers of oysters in laboratory size trays. Later experiments were carried out with commercial scale tanks. Four different tank designs were tested. The following water quality measures were monitored: temperature, phytoplankton and suspended solids concentrations, dissolved oxygen, and salinity. Seawater was taken from the York River estuary and sterilized by ultraviolet irradiation. Fecal coliform levels in the oysters were measured at 0, 24, 48 and 72 hours. No standard for fecal coliform counts in oyster meats has been set by the federal and state regulatory agencies. The allowable number of fecal coliforms in hard clams in the interstate market has been set at 50 MPN per 100 grams. In the absence of any other criterion, the hard clam standard was used to determine whether individual depuration runs had been successful or not.

The two factors which had the greatest effect on 72 hour coliform levels were water temperature and initial coliform count. Within certain limits, none of the other factors appeared to either facilitate or hinder depuration. Dissolved oxygen (DO) levels close to zero were found to interfere with the depuration, and supersaturation is believed to be a potential problem since the release of the excess gas into bubbles could cause oyster mortality by embolism. However, if oxygen levels were above 2 mg/l and below saturation values there was no observed effect. Similarly, suspended solids concentrations ranging up to 77 mg/l were observed to have no impact on the depuration process. Exceedingly high concentrations of phytoplankton associated with algal blooms can deplete the oxygen supply and cause other problems, so that depuration during periods of blooms is not recommended. Successful depuration was observed for salinities ranging from 14 parts per thousand (ppt) to 22 ppt, although the actual lower limit is believed to be closer to 10 ppt. Waters with salinity ranging from 10 ppt to 35 ppt (seawater) can be used for depuration, although care must be used when there is a large change between the growing area and the waters used for depuration. In this case, a period of acclimation may be required before the oysters resume normal activity.

Water Temperature Effects

Several important changes are correlated with water temperature. First, the number of fecal coliforms found in estuarine waters tend to increase as the water is warmed. The reasons for this are not known, although increased boating activities might account for some of the change. The actual number of coliforms found at any given location and at any given time will depend on many factors, such as rainfall, flushing rates and so on, but the general trend is for bacterial levels to increase with water temperature.

Pumping, feeding and other biological activities of the oysters also are affected. Both bioconcentration and depuration are enhanced at elevated temperatures. The oysters used in most experiments were placed in a small, polluted subestuary and allowed to remain there until they had become contaminated. When water temperatures were above 25°, concentrations as high as 79,000 fecal coliforms per 100 grams were observed in the oysters at the beginning of depuration. Since the water flowing through the tanks had roughly the same temperature, rates of depuration were similar to the uptake rates in the natural environment. Three experiments, conducted in July and September of 1975 with water temperatures of around 26°C, demonstrate the ability of the oysters to depurate large numbers of bacteria in a very short period. Initial coliform levels for both months were extremely high, but were reduced by around two orders of magnitude during the first 24 hours, as can be seen in Figure 1. Cleansing continued throughout the 72 hour experiments but at less rapid rates. Fecal coliform levels were below the 50 MPN/100 grams standard after 48 hours. Data presented in the figures are the mean concentrations for one or more experiments with multiple oyster samples taken for each sample point. The means were calculated using the procedure recommended by Velz [13].

Comparisons of depuration at differing water temperatures can be made only at low and moderate levels for initial coliform concentrations in the oysters, since naturally contaminated oysters rarely had high coliform counts when the water was cold. In Figure 2, data from experiments with water temperatures of about 15°C and 26°C and initial fecal coliform concentrations of around 3,000 MPN per 100 grams are compared. Although the 72 hour results are essentially equal, at the higher temperature the oysters depurated more rapidly at the beginning so that coliform levels were below the criterion after only 48 hours. Similar results were observed at initial levels of slightly under 200 MPN/100 grams, as shown in Figure 3. Since the initial levels were low, fecal coliforms were reduced to acceptable levels after only 24 hours for both the low temperature range (10°C to 12°C) and the high range (24°C to 26°C). However, the rate of depuration was more rapid and the final coliform levels lower at the higher water temperatures. Of the oysters depurated in the colder waters, 100% of the samples had 72-hour MPN levels below 100, but only 83% of the samples were below 50 MPN/100 grams. For those experiments having water temperatures above 20°C, 100% of the samples had less than 20 MPN/100 grams at 72 hours.

Sampling errors, changes in environmental factors during the three day experiment, natural variations between oyster populations and other factors all introduce variability in the experimental results. Therefore, it is difficult to make precise statements and conclusions. However, one can note several trends. First, the rate of depuration during the initial 24 hours is considerably greater than that observed during later periods. Second, the rate of depuration tends to increase and the final coliform levels decrease as the water temperature rises. Third, when initial coliform levels are equal, a larger percentage of the oysters is likely to achieve successful depuration in warm water than in cold water. Fourth, depuration is not recommended when the water temperature is below 10°C and only oysters that have low levels of coliforms should be depurated in the 10° to 12°C range. For the Chesapeake Bay region, this means that depuration plants should not be operated between the months of November and April, unless the water in the tanks is heated.

CLOSURE ZONES

In recent decades, the number of persons residing in the coastal zone has increased rapidly; generally the rate of increase has been greater than that for the nation as a whole. This population growth, coupled with industrial and commercial development, has produced ever increasing volumes of wastewater, most of which are discharged to the bays and estuaries. Although tidal flushing can produce rapid mixing and greatly dilute these waste streams, water quality has been degraded in many instances. As a result, many formerly productive shellfish beds have been rendered unsuitable for the culture of shellfish. For example, oysters taken from the Elizabeth River, which runs through the heart of the Norfolk, Virginia metropolitan area, had concentrations of zinc greater than 2,000 mg/l [3]. Presumably these abnormally high levels were the result of industrial discharges to this estuary. More frequently, growing areas have been declared unfit due to actual and/or potential health hazards. Surveys of water quality in shellfish growing areas are made on a regular basis by public health authorities. If water samples from an area consistently have high levels of indicator organisms, the area is closed for shellfish harvesting whether the source of the contamination is known or not. In other instances, estuary bottoms are closed because treated wastewaters are discharged to the overlying waters. Although disinfection is a required treatment method and is practiced at all sewage treatment plants, there still remains the potential for malfunctions and/or by-passes resulting in the release of pathogens to the environment. For these reasons a buffer zone normally is established around each treatment plant outfall.

For the purposes of discussion, these closure zones may be grouped in two categories: condemned areas and restricted areas. Condemned areas are those which have either a large wastewater outfall or high levels of pathogens. Since oysters tend to concentrate materials present in the overlying waters, oysters growing close to a large wastewater treatment plant outfall could contain undesirably high levels of such substances as heavy metals, pesticides, chlorinated hydrocarbons and so on. These are likely to present a health hazard to anyone consuming the oysters. Similarly the presence of a major domestic sewage treatment plant outfall or high levels of indicator organisms means that there is the very real possibility that shellfish taken from adjacent waters could contain disease producing organisms. The ability of oysters to depurate either pathogens such as viruses or compounds such as heavy metals and pesticides has not been demonstrated to occur over a several day period. Consequently, condemned areas are not suitable as supply areas for purposes of depuration.

Restricted areas on the other hand can be characterized by moderate to low levels of pollution, say 14 to 1,400 MPN/100 mls. This could be a semi-permanent situation, say due to a small wastewater discharge, or a temporary condition. For example, runoff from adjacent land often brings with it large numbers of bacteria. Consequently, during rainy periods, the levels of coliforms in the water may exceed standards. A maximum of 14 fecal coliform MPN/100 mls of water, has been set by the Food and Drug Administration as the upper limit for waters from which oysters are taken and placed in the interstate market. However, since depurations studies conducted at VIMS and elsewhere have demonstrated the ability of oysters to successfully depurate bacteria within 48 hours, oysters taken from the moderately polluted, restricted areas are suitable for human consumption after they have been depurated. In the states of Maine, Massachusetts, New York, New Jersey and Delaware federal and state public health officials have designated certain areas as suitable supply areas for depuration plants. Shellfish taken from these regions cannot be put on the market unless and until they have been depurated. These operations have been successful from both public health and economic points of view. The soft-shell clam depuration plant in Newburyport, Massachusetts has been in operations since 1931 [5], demonstrating that the process is indeed a practical one.

WASTE HEAT UTILIZATION

One adjunct of both population centers and industrial centers is power generating stations. Electricity is required for the homes, offices and factories located in the coastal zone and elsewhere. In other words, if there is a concentration of people and industry sufficiently large to cause water quality problems, it is also very likely that power generating stations exist within those areas and most likely they are located on the shores of the waterways. In particular, estuaries are prime locations for the large nuclear stations because of tidal oscillations. Tidal flows in the lower reaches of estuaries can be extremely large. Maximum tidal flows in Hampton Roads near the mouth of the James River, the southernmost major tributary of Chesapeake Bay, are roughly 100 times as great as the long term, average flow of fresh-water across the fall line at Richmond. Furthermore the tidal flows are roughly three orders of magnitude greater than the 10-year, low flows for the freeflowing portions of the river. The desirability of estuarine locations for large generating stations is readily apparent.

Water quality degradations associated with both treated sewage and industrial discharges have rendered many areas unsuitable for the culture of shellfish. At present the direct harvesting of shellfish is prohibited on approximately 500,000 acres of the Chesapeake Bay system. A little more than half is growing areas which are presently unproductive due to predators and other factors, but around 10% or the bottoms are designated as good for oysters. Additional areas, approximately 20% of the total, are listed as either fair for oysters or good for hard clams [14].

Studies of bacterial depuration of oysters conducted at VIMS, and studies of other shellfish at other locations, have demonstrated that depuration is feasible. The existence of commercial operations in New England for over forty years clearly shows the viability of the process. For the Chesapeake Bay region and those areas lying to the north, water temperatures during winter months are sufficiently low that biological activity of the shellfish is greatly reduced. Consequently, depuration is not possible during these periods. For the Chesapeake Bay and the eastern oyster, depuration is not recommended for water temperatures below 10°C. Utilization of waste heat from power generating stations would be an economical means of heating the water in the depuration tanks. In this manner, the operation of the depuration plant could continue throughout the winter months.

Since the rate of depuration tends to increase with rising water temperature, the fecal coliform levels at the end of the depuration period tend to be lower and show less variability at higher temperatures. Consequently, use of the waste heat to elevate water temperatures to around 20°C during the spring and fall could improve the final product of the plant. Since many power generating stations are situated on estuaries, it should be possible to find locations where environmental conditions are suitable for a depuration plant and waste heat is available. For example, a large fossil fuel station is located at Yorktown, Virginia on the York River estuary, only a few miles distant from the VIMS campus, where the present experiments were conducted.

SUMMARY

Many acres of productive estuary bottoms are restricted for the direct harvesting of shellfish. Although some of the closure zones are unfit for any shellfish culture, other areas are characterized by moderate to low levels of pollution. Shellfish grown in these areas could be cleansed of the accumulated bacteria in a properly designed and operated depuration plant. Operation of depuration plants in the Chesapeake Bay region is limited to periods when the water temperature is above 10°C. Utilization of waste heat from power generating stations would provide an economical means of heating the water, thereby allowing depuration to proceed throughout the winter months. Supplemental heating of the water to about 20°C during the spring and fall is likely to improve the depuration process. Since many power generating stations are located within the coastal zone, at least a few stations should be so situated that an oyster depuration plant could be established in the same area.

NOTE: This paper is contribution #819 of the Virginia Institute of Marine Science.

REFERENCES

1. Andrews, Jay D., 1970. "The Mollusc Fisheries of Chesapeake Bay (USA)". p. 847-856. In Proceedings of the Symposium on Mollusca held at Cochin, Part III. MAR: Brol. Assoc. of India

2. Haven, Dexter S. and Reinaldo Morales-Alamo - 1977 - personal communicat of unpublished data.

3. Moore, David J., 1969. "A Field and Laboratory Study of Fluoride Uptake by Oysters", Water Resources Research Institute of the University of North Carolina.

4. Huggett, Robert J., Michael E. Bender and Harold D. Slone, 1973. "Utilizing Metal Concentration Relationships in the Eastern Oyster (Crassostrea virginica) to Detect Heavy Metal Pollution". Water Research 7: 451-460.

5. Goggins, Phillip L., John W. Hurst and Peter B. Mooney, 1964. "Laboratory Studies on Shellfish Purification". Maine Department of Sea and Shore Fisheries. 18 pp.

6. Sterl, Bradford, Paul J. DeRocher and John W. Hurst, 1964. "Soft Clam Depuration Studies: Design and Operation of a Cleansing Plant". Maine Department of Sea and Shore Fisheries. 18 pp.

7. Huntley, Bob E. and Richard J. Hammerstrom, 1971. "An Experimental Depuration Plant: Operation and Evaluation". Chesapeake Science Vol. 12-4, p. 231-239.

8. Hefferman, W. Paul and Victor J. Cabelli, 1971. "The Elimination of Bacteria by the Northern Quahang: Variability in the Response of Individual Animals and the Development of Criteria". Proceedings of the National Shellfisheries Association, Vol. 61, p. 102-108.

9. MacMullan, Robert B. and James H. Redman, 1971. "Hard Clam Cleansing in New York". Commercial Fisheries Review, Vol. 33-5, pp. 25-33.

10. Devlin, I. H. and N. Neufield, 1971. "Oyster Depuration Plant, Ladysmith, BC". Report to the Industrial Development Branch, Fisheries Service, Department of the Environment, Ottowa. 71 pp.

11. Haven, Dexter S., Frank O. Perkins, Reinaldo Morales-Alamo, Martha W. Rhodes and Bruce J. Neilson, 1976. "Technical Studies on the Engineering and Biological Aspects of Controlled Purification of the Eastern Oyster". A report

to the U. S. Food and Drug Administration. 325 pp.

12. American Public Health Association, 1970. "Recommended Procedures for the Examination of Seawater and Shellfish". Fourth Edition, American Public Health Assoc., New York.

13. Velz, C. J., 1951. "Graphical Approach to Statistics: Evaluation of Bacterial Density". Water and Sewage Works, February, 1951.

14. Roberts, Morris H. Jr., Donald F. Boesch and Michael E. Bender, 1975. "The Chesapeake Bay: A Study of Present and Future Water Quality and its Ecological Effects". Final Report to the National Commission on Water Quality, VIMS, Gloucester Point, Virginia. 199 pp.

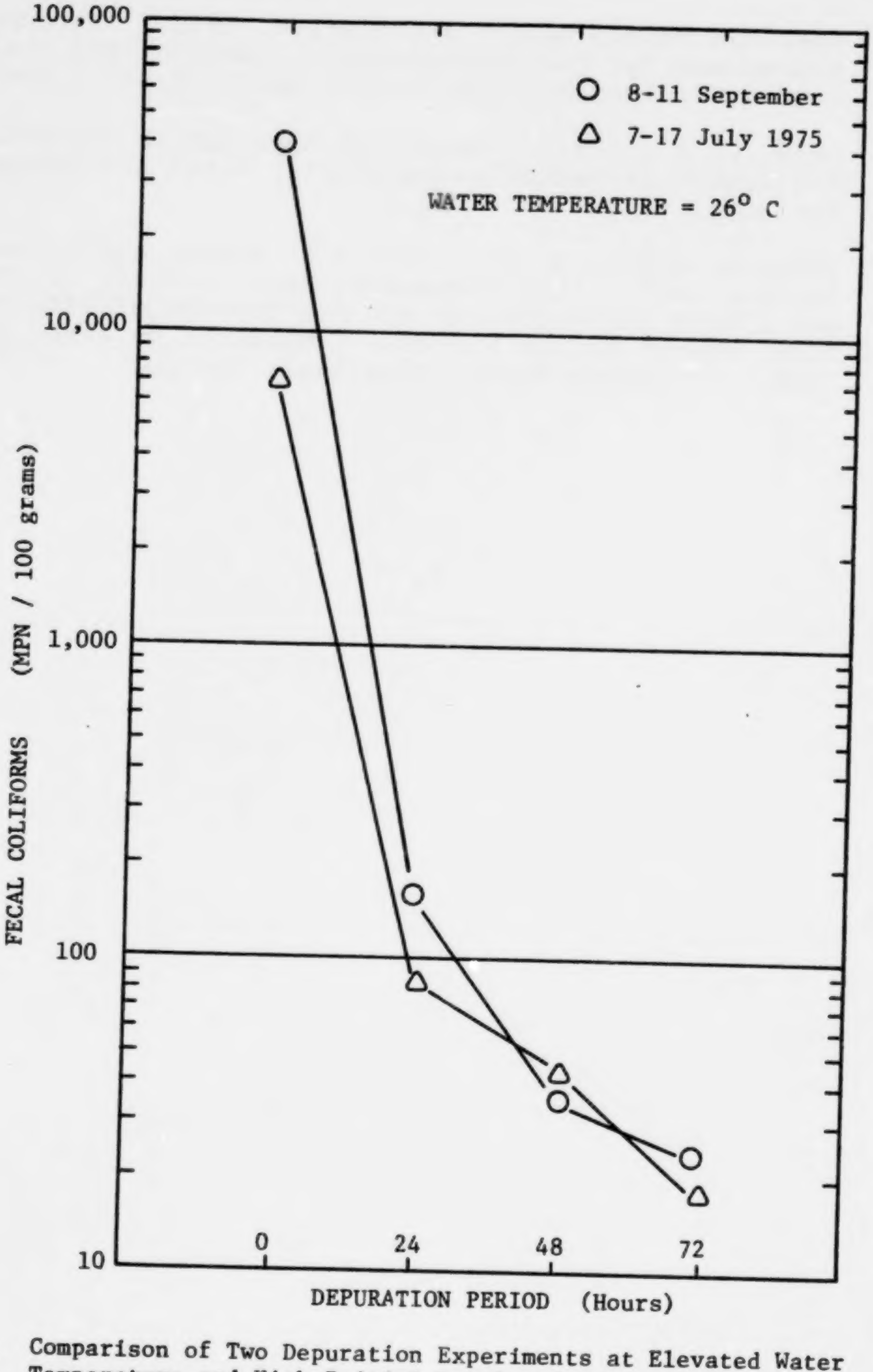

Figure 1. Comparison of Two Depuration Experiments at Elevated Water Temperature and High Initial Levels of Fecal Coliforms.

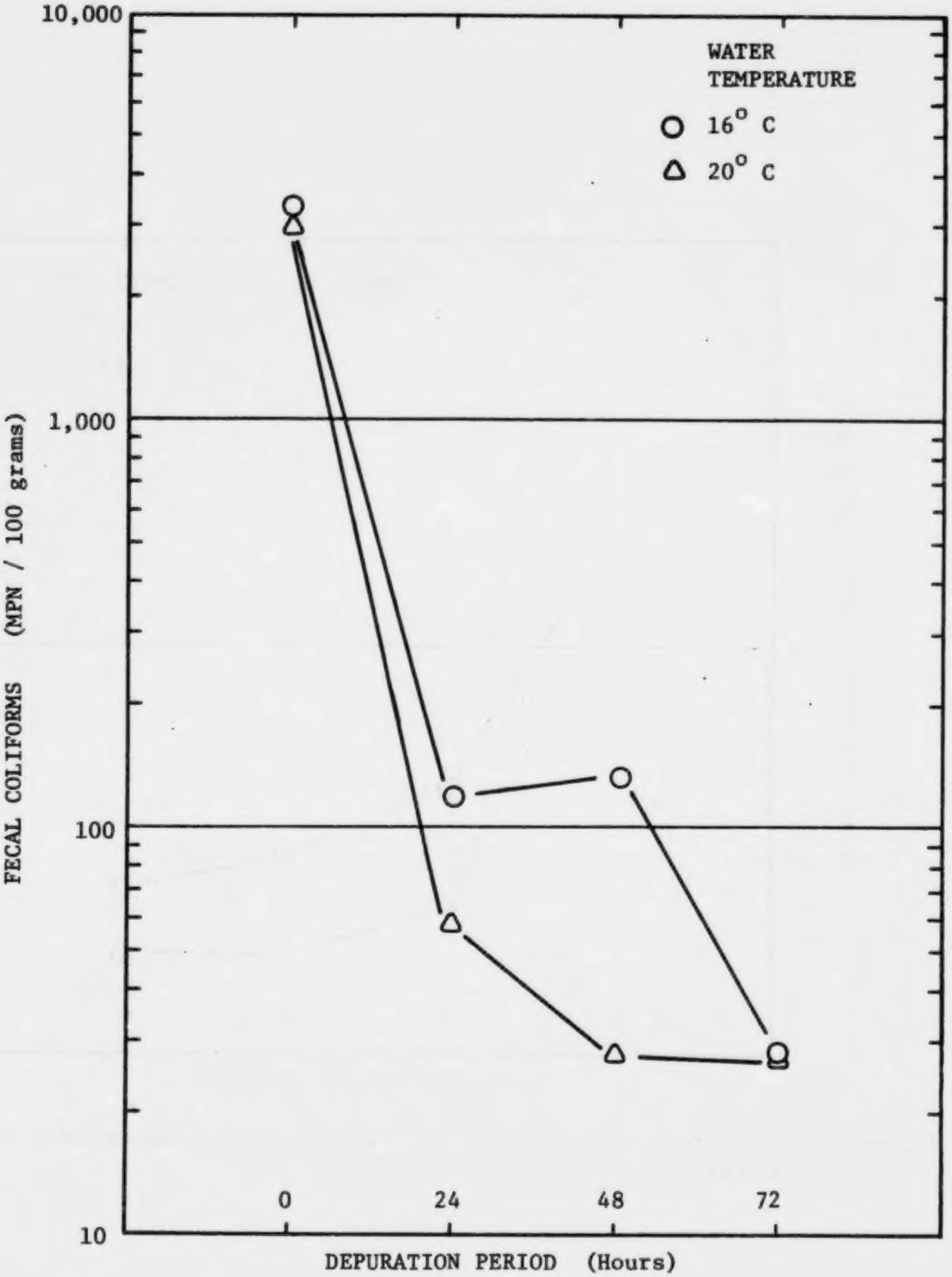

Figure 2. Comparison of Depuration at Two Water Temperatures with Moderate Initial Levels of Fecal Coliforms.

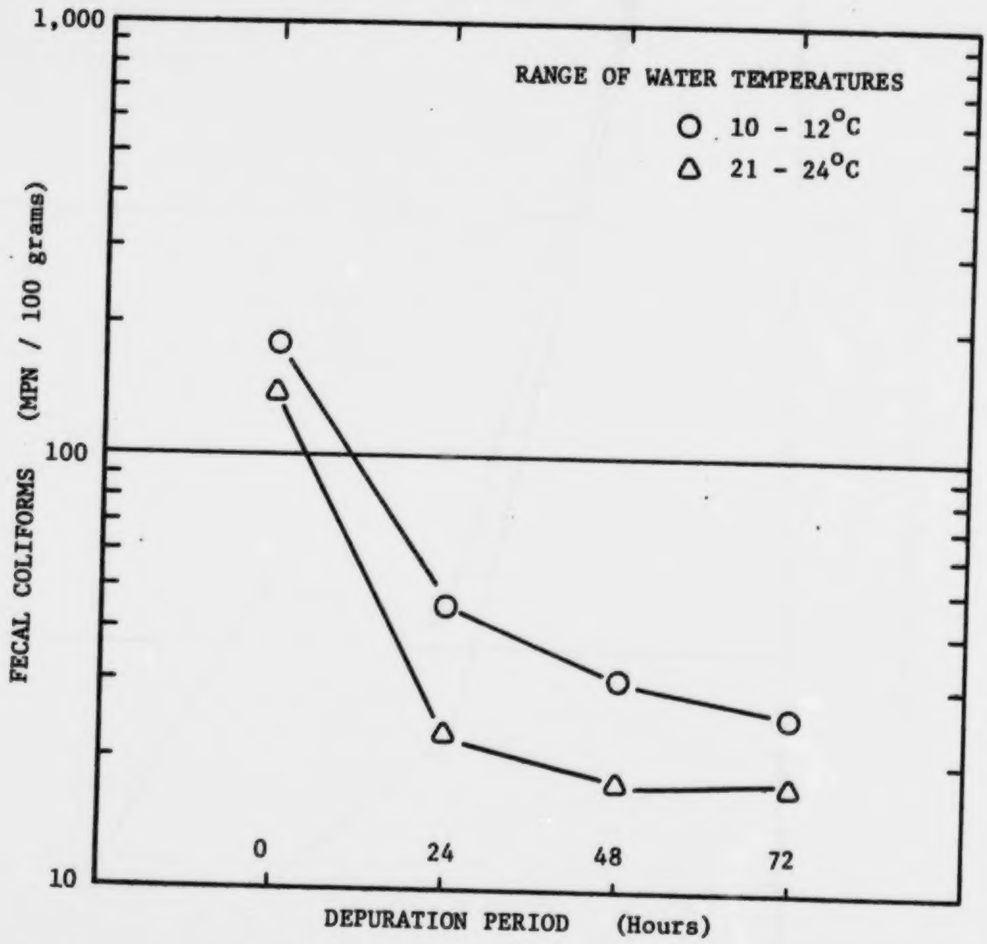

Figure 3. Comparison of Depuration for Two Temperature Ranges with Low Initial Levels of Fecal Coliforms.

14

28-45-33

USING HEATED EFFLUENT FROM A 835 MWe NUCLEAR POWER REACTOR FOR SHELLFISH AQUACULTURE*

C.T. Hess and C.W. Smith, Department of Physics
and Astronomy and A.H. Price, Ira C. Darling Center
for Oceanography; University of Maine at Orono
Orono, Maine U.S.A.

ABSTRACT

Aquaculture of shellfish (*Crassostrea virginica* and *Mytilus edulis*) has been studied for the last four years using heated effluent from the 835 MWe Maine Yankee Nuclear Power Reactor in Montsweag Bay, near Wiscasset, Maine. The effects of the heated and moving effluent on growth and product quality of the rafted shellfish is presented for several stations at various distances from the reactor. A station in the nearby unheated Damariscotta estuary was used as a control. Descriptions of the growth at these stations will be presented.

The measured rate of uptake of reactor released radionuclides ^{58}Co, ^{60}Co, ^{137}Cs, ^{134}Cs, and ^{54}MN by shellfish is compared with the mathematical models (24) used to understand the variations of these radionuclides with position and time. A dynamic estuary computer program (25) is used to understand the position dependence (26) and a pulsed relaxator model (23) is used to understand the time variation of the radionuclides in shellfish.

INTRODUCTION

The increased demand for electricity by our civilization and consequent construction of additional generating facilities in coastal areas will dramatically increase the number of thermal releases available for application in marine aqualcuture systems.

Since 1973 we have been involved in a study directed toward an evaluation of the use of the thermal effluent and waters surrounding the Maine Yankee Atomic Power station, located at Bailey Point on Montsweag Bay, Wiscasset, Maine, for the culture of the American oyster (*Crassostrea virginica*) and the blue mussel (*Mytilus edulis*). We have considered two major factors governing the potential use of these waters. First, the growth and quality of the animals and second, the retention of gamma-ray emitting radionuclides by the animals.

The use of thermal effluents for the culture of marine organisms has been duscussed by many authors: Nash (1), Burns (2), Coutant (3), Mather and Stewart (4), Strawn (5), Yarosh (6), Huguenin and Ryther (7), and others.

Studies of accumulation and depuration of radionuclides in a number of marine organisms have been undertaken. Measurements have been made of ^{58}Co in the mussel *Mytilus edulis* (8), ^{137}Cs and ^{60}Co in the clam *Mya arenaria* (9), and ^{137}Cs and ^{60}Co in the oyster *Crassostrea gigas* (10). Studies by Seymour (11), Jeffries and Preston (12), Naidu and Seymour (13), Wolfe (14), and Lowman, Rice and Richards (15) are also relevant to our work.

We have examined the annual physiological cycles of glycogen, percent total solids, shell growth and the uptake and dupuration of gamma-ray emitting radionuclides in American oysters (*C. virginia*) cultured directly in the effluent of the Maine Yankee nuclear power reactor, three other points in Montsweag Bay, and at a control site in an adjacent esturine environment; the Damariscotta River.

METHODS

Site Locations

The Maine Yankee Nuclear Reactor at Wiscasset, Maine, is a pressurized water reactor rated at 835MWe. The plant is cooled by pumping up to 960 cubic feet of water per second from Montsweag Bay over its condensers and then discharging the water into Bailey Cove. Tray stations containing oysters were located in the intake channel (S-1), directly in the effluent (S-2), above the effluent point in Bailey Cove (S-3), and below the effluent point off of Long Ledge in Montsweag Bay (S-4), (Fig. 1). The control site was located at the marine laboratory on the Damariscotta River; and adjacent estuary. One hundred fifty oysters to be examined for glycogen content, percent total solids and shell growth were distributed between two trays at each site. Additionally, twenty four oysters were placed in a separate compartment of one tray of each site to be measured monthly in a longitudinal study of the accumulation of gamma-ray emitting radionuclides. One hundred and forty mussels were rafted at the outflow (S-2), Long Ledge (S-4) and at the control site in the Damariscotta River.

Environment

A Beckman field salinometer (Model RS5-3) was used to monitor salinity and temperature every two weeks during high tide at all stations. For one year water samples were taken every other week at high tide at all stations to evaluate the food available to the oysters. These samples were used in the determination of chlorophyll and particulate oxidizable carbon (16). In this manner, we were able to gain some knowledge of the variation in environmental parameters which have been shown to influence oyster growth and condition (17).

Biological

Monthly a random sample of twelve oysters was collected from each field site. Fouling organisms were removed, each oyster was weighed and measured. Measurements (height, length and width) were of the maximum dimension of a given parameter. New shell growth was measured on the right and left valves and the larger value used in calculating the average shell growth at a given station.

The condition of oyster meats was determined by shucking the oysters taking care not to pierce the meats. Meats were allowed to drain for one minute on a plastic mesh and then weighed. All twelve oyster meats from a given station were then homogenized and glycogen extracted from the homogenized meats according to the method of Burklew (1971). The percent total solids of the oyster tissue were calculated from the average of three, five gram aliquots of the homogenate, employing the following calculation;

$$\text{Percent solids} = \frac{\text{dry weight of meats}}{\text{wet weight of meats}} \times 100$$

Mussels were measured monthly for growth.

Radionuclear Apparatus and Calibration

The gamma-ray measurements are carried out using an Ortec Ge(li) detector with a 2400 pound low background lead shield. The detector pulses are amplified with an Ortec 452 spectroscopy amplifier and the detector bias is provided by an Ortec 459 high voltage supply. The amplified detector pulses are processed by a Northern Scientific NS-700 multichannel analyzer. A typical gamma-ray spectrum for live oysters is shown in Fig. 2. The memory of the multichannel analyzer is outputted onto magnetic tape using a Northern Scientific NS-408C magnetic tape controller and a Wanco tape transport. The data thus recorded is then processed using the University of Maine IBM 360/370 computer system. The computer program analyzes the peaks by Compton continuum subtraction (18). The number of counts in each peak is then converted from counts per second into disintegrations per second by using the efficiency determined for the sample geometry employed. Both branching ratios and the variation of efficiency with energy are taken into account. From disintegrations per second, the number of picocuries per gram is determined for each of the gamma-ray peaks which exceed a statistical criterion for significance above background. Picocuries per gram of those radionuclides in our library of branching ratios are computed automatically and new or unidentified peaks are processed by hand calculations. The efficiency versus energy curve for the detector is determined by placing several standard sources from the Environmental Protection Agency Analytic Quality Control Laboratory, Las Vegas, Nevada, in a solution of demineralized distilled water in a 1.0 liter Nalgene cylindrical bottle which is our standard sample geometry. All quantitative measurements are made using this geometry. The peaks from the standard sources are analyzed in the same way as the unknown peaks in a sample. Graphical analysis of the efficiency versus energy is plotted on log-log paper and tested for linearity and consistency. Results of these periodic calibrations are used to update the computer program. New branching rations are entered into the program as required.

Procedure

Previous experience involving radionuclide assessment of marine organisms (19) suggests that monthly measurement of the specific activity is sufficient and convenient for studies of this type. Two species of mollusca (*C. virginica* and *M. edulis*) are cultured at several rafting sites near the outflow and one control site. For each species, one kilogram samples of living organisms is randomly selected from populations of organisms of similar age and genetic background at each rafting site. High resolution gamma-ray spectrographic measurements are made as soon after collection as practical and the specimens are returned to the approporate raft sites within twenty four hours. The spectra are computer processes as discussed. Monthly specific activities for each species are graphed and compared for five reactor associated radionuclides (^{60}Co, ^{58}Co, ^{137}Cs, ^{134}Cs and ^{54}Mn) and for the natural occurring radionuclide ^{40}K.

Marine sediment from several sites at selected distances from the outflow are collected to a depth of 5 millimeters over an area sufficient to yield 2 kilogram wet samples. A monthly sampling schedule is employed. High resolution gamma-ray spectrographic measurements are made.

Control site

In May of 1973 oysters at the control site in the Damariscotta River exhibited shell growth as the temperature rose above 8°C, (Fig. 3). During June and July gametogenesis occurred and is reflected in a characteristic decrease in glycogen, increase in percent total solids and decrease in the rate of shell growth. Shell growth resumed in August but ceased to be measureable in September. This correlates with a decrease in food available to the oysters, as the standing crop of phytoplankton dropped out during this period. The following spring, with adequate food available in April and the water temperature rising to 8°C, shell growth resumed. This cycle of growth has continued.

Measurements taken to detect the accumulation of gamma-ray emitting radionuclides of reactor origin in oysters at this site were negative. Mussel growth and survival was best at the control site (Figures 4 and 5).

Outflow Station

Oysters placed directly in the effluent (S-2) in April of 1973 showed shell growth after two weeks of exposure to the elevated temperatures found in these waters (Fig. 6). Glycogen levels decreased, and there was an increase in total solids which were correlated with gametogenesis. Shell growth decreased in May as the oysters spawned. During June shell growth resumed and continued through October. Water temperatures remained elevated throughout the winter except for brief plant shutdowns. Cessation of shell growth during the fall corresponds well with the decrease in the standing crop of phytoplankton. Shell growth resumed in March 1974 probably due to elevated temperatures and a spring bloom of phytoplankton found at this station. Again in the spring of 1975 shell growth was evident early in the year, February, and is attributed to elevated temperatures and a spring bloom of phytoplankton.

Mussels exhibited best growth at the control (SC) site in 1974 and 1975. In 1974 the outflow station suffered 100% mortality and warmer water sites show less growth than controls (SC) or Long Ledge (S-4) in 1975. (Fig. 4 and 5).

The uptake and loss of gamma-ray emmitting radionuclides predicted by our model is inn good agreement with levels measured in oyster from this station (Fig. 6B).

Upper Cove Station

Oysters placed in the upper cove station (S-3), showed signs of gametogenesis in April of 1973 with shell growth evident in May 1973. Oysters in the June 1973 sample were observed to have spawned and were recovering glycogen. Shell growth continued until November 1973 (Fig. 7A). The general features of the graph depicting the accumulation and loss of ^{58}Co, (Fig. 7B), is similar to that found at the outflow (S-2) station (Fig. 6A).

Other Stations

The general features of oyster growth and the uptake and loss of radionuclides at the intake (S-1) and Long Ledge (S-4) stations (Fig. 8 and 9) are observed to be generally similar to those found at the outflow (S-2) and the Upper Cove (S-3). Oysters at the intake (S-1) are lower in their accumulation of ^{58}Co by a factor of five and by a factor of three at Long Ledge (S-4). This is a result of their distance from the discharge point, the thermal differences existant at these sites, the consequent variations in oyster metabolism, and their exposure to radionuclides.

The magnitude of cumulative shell growth at each station was, upper cove (S-3) 58.0 mm, S.D. 8.92 the outflow site (S-2), 55.2mm, S.D. 6.13, the intake (S-1) 32.0 mm, S.D. 5.16, Long Ledge site (S-4), 34 mm, S.D. 4.33 and the control site (sc), 23.4 mm, S.D. 2.26. All stations in Montsweag Bay showed significantly greater shell growth than controls, with the warmer water sites (S-2 and S-3) significantly greater than the cooler sites (S-1 and S-4), (Fig. 10).

Oysters of excellent market quality were observed during the fall and winter of 1973-1974 at the intake (S-1) and Long Ledge (S-4) sites. The meats of oysters at the upper cove site (S-3) and the outflow (S-2) were comparable to controls. Mortalities at all oyster stations were less than 5% and there was no significant difference between mortalities at the different oyster stations. Mortality was highest in the mussels at the outflow station (98%) in 1974 and always decreased as distance from the outflow increased.

In addition to the effects of heated moving effluent on the growth and product quality of rafted shellfish, one must consider the uptake, accumulation and depuration by the organism of the trace amounts of radionuclides in the effluent. In order to take full advantage of the heated effluent, and minimize the accumulation of radionuclides, the spatial distribution of these radionuclides in the estuary is also needed. Both the filter feeding of the organisms and sedimentation tend to reconcentrate the radionuclides providing pathways for the radionuclides into the shellfish. In the discussion below, we describe a field study designed to measure the parameters governing these processes and two mathematical models: a pulsed relaxator model for the temporal behavior, and a "Dynamic Estuary" computer program for the movement and spatial behavior of radionuclides in the water column and sediments. These modesl describe the processes in a detailed enough way to make practical predictions possible.

Models of Uptake of Radionuclides By Shellfish

Constant concentration theories have been suggested in laboratory studies by Polycarpov (20), Ruzic (21), and Davis and Foster (22). In such theories, the radionuclide concentration in the oysters, C_o, is related to the radionculide concentration in the sea water C_w, by a concentration factor K.

$$C_o = K\,C_w$$

This factor K becomes larger with time until it reaches an equilibrium value, if the concentration C_w may be found by dividing the released radioisotope in curies, f_i, by the volume of water used for the release V_w.

$$C_w = \frac{f_i}{V_w}$$

Using this equation in a dynamic situation, as in the case of reactor releases, will give values of K which are considerably less than the equilibrium value for K as found in a laboratory situation. We find that calculations based upon laboratory values of K in the case of reactor releases inaccurately estimates the radionuclide concentration (19).

To develop a dynamic model of variations in the uptake and depuration of radionuclides by the oysters, the release rates of radionuclides by the reactor was used as the driving source of a multimode pulsed relaxator system. The resulting differential equation may be solved by integration to give exact solutions if appropriate simplifying assumptions are made (19). These assumptions are that the reactor releases monthly by injecting the nuclides into the estuary in a short time (several hours). The nuclides are then accumulated by the oysters, and are slowly reduced by radioactive decay and by biological cycling, depuration, in the oysters. Initially we assumed that the oysters had constant depuration over the entire year. Later these assumptions were modified to include: a) variation in nuclear reactor plant operations (shut-downs, plant discharge rate, power output, etc.), b) oyster biological parameters (growth rate, glycogen content), and c) estuarial parameters (temperature, salinity, current velocities, standing crop, etc.) (23). As our understanding has improved we have found that by using this radionuclide uptake model, predictions can be made to establish an optimum release pattern for the reactor in order to minimize oyster uptake of radionuclides.

A full development of this new model is discussed in detail in references (19) and (24). Reference (23) describes how to use the model. The essence of the model is the calculation of the rate of change of concentration of radionuclide in the organism. This calculation uses the differential equation given below

$$\frac{dN(t)}{dt} = R(t) - \lambda_b N(t) - \lambda_p N(t)$$

where

$N(t)$ = the concentration of radionuclide in the organism at time t.

$R(t)$ = the rate of introduction of radionuclde into the marine environment from an external source (i.e., the nuclear reactor effluent).

λ_b = biological turnover, biological decay or depuration constant

λ_p = physical or nuclear decay constant

and $R(t)$ may be written

$$R(t) = \sum_i U_i F_i \delta(t - t_i)$$

The results of integration is given below for the intervals between release times

$0 \leq t \leq t_1 \qquad N(t) = C\ e^{-\lambda t}$

$t_1 \leq t \leq t_2 \qquad N(t) = U_1\ f_1\ e^{-\lambda(t - t_1)} + C\ e^{-\lambda t}$

$t_2 \leq t \leq t_3 \qquad N(t) = U_2\ f_2\ e^{\lambda - (t - t_2)} + U_1\ f_1\ e^{-\lambda(t - t_1)} + C\ e^{-\lambda t}$

The releases of radionuclides are made into the marine environment at a sequence of m time (t_1, t_2, t_3 . . . t_m) and the amount released is given by a function $f_i(t)$, which for times greater than or equal to t_1 but less than t_2, is given by $f_1\ (t - t_1)$ and for times greater than or equal to t_2 but less than t_3 is given by $f_2(t - t_2)$ and so on up to times greater than t_m. A scaling parameter U determines the availability of radionuclides for uptake by the organism and depends on the distance from the discharge point to the aquaculture rafting station in question, and the pumping rate or efficiency of collection of the organism. It is called the retention ratio.

We first discuss the case of ^{58}Co at the outflow rafting station (S-2), the closest site to the discharge point. The theoretically predicted values are scaled to the experimentally measured values to determine U at this site for ^{58}Co to be $10.0 \times 10^{-12}\ g^{-1}$. Assuming U constant has given fairly good agreement between theory and experiment, however, it is known that below 8°C the American oyster stops pumping water and hybernates. It is also know that this phenomena, combined with the available standing crop of phytoplankton results in a step shaped shell growth curve. If one assumes that during times of hibernation or zero shell growth the oyster is shut down, i.e. neither pumping water nor feeding, then, during this period, $\lambda_b = 0$ and $U = 0$ and the organism gains no radionuclides from the environment and loses them only by physical decay. Results shown in Figure 11 including all biological parameters, i.e., λ_b, temperature and shell growth. One can still observe some departures of the theoretical prediction from experiment. These have been traced to gametogenesis and/or spawning, (19) and result from the associated changes in oyster metabolism and the ratio of shell mass to soft part mass, refinements which could be included in λ_b and U. However, since these variations represent effects comparable to the error resulting from counting statistics, it is felt that for the radionuclide levels involved and the 5000 second count employed, the effort is not warranted. In (Fig. 12) the results are given for ^{137}Cs in oysters. The list of parameters used is given in (Table 1) for all rafting stations. Notice the interesting result that U does not depend on the chemistry of the radionuclides. This implies that for the concentrations encountered in the environment near a nuclear power reactor, the major uptake mechanism is physical rather than chemical. It has been suggested that the radionuclides attach to particulate are filtered out essentially non-chemically by the oyster.

The biological decay constant, λ_b, is not site specific and indeed the same values of λ_b were found at all sites. The U values decrease monotonically with increasing distance from the discharge point. U values are shown (Fig. 13) as a function of water path distance from the discharge point for the four aquaculture raft station sites employed in this study. The fact that the curve came out to be a straight line is probably fortuitous, however, the point being made is that the major factor which determines the value of U is proximity of the rafting station to the source of radionuclides.

In order to further understand the nature of the retention ratio U and its dependence of position relative to the outflow location it is necessary to measure radionuclide content in the sediment settling out of the water column. Sediment sampling, as described in the Procedure Section was carried out along tidal transects with a total of 72 samples being taken on one low tide. Isocuric plots are drawn by fitting radionuclide concentration versus sampling site on each transect line to a cubic equation. The location of the intersection of an isocuric line with a transect line was found using this fitting procedure. All radionuclides in this survey were distributed in nearly the same manner as indicated by the isocuric maps for ^{58}Co and ^{137}Cs, (Fig. 14 and 15). Both isocuric maps display very high concentration near the outflow, while somewhat cross-stream there is a low concentration "valley". In the upper cove both maps depict a broad region of high concentration near the outflow side of the cove. Down-cove from the outflow both maps indicate a narrow high concentration band adjacent to the east shore line. The concentrations are generally higher up-cove than down-cove from the outflow, indicating a substantial portion of the releases were carried into the upper cove during the flood tide.

A dynamic estuary model is used to simulate the above behavior. Complete and extensive descriptions of this model, developed for the Federal Water Quality Administration for San Francisco and San Diego Bay systems, is given in reference (25). The model can represent flow and dispersion characteristics of an estuary where vertical stratification is slight. It consists of two separate but compatible computer programs. The first, DYNHYD, models the hydraulic behavior of an estuary. It computes tidal heads and flows and stores this information on magnetic tape. The second program,DYNQUA, uses this tape to describe the dispersion of a pollutant introduced into the estuary. Both programs use the finite difference method, and apply one-dimensional equations to one-dimensional channels which are laid out in a two-dimensional framework. Water velocity patterns are calculated for various stages of the tidal cycle. The result for the last slack high tide on May 13, 1975 are shown in Fig. 16. Two eddies are observed, one elongated from the outflow up into the northern portion of the cove and the other at the southern mouth of the cove. Notice that from the isocuric maps we observe high concentrations of radionuclides in these regions. Similar observations can be made for other portions of the tidal cycle. The second program DYNQUA is used to calculate the concentration of radionuclides in the sediment, using the tidal heads and flows as calculated by DYNHYD. The final predictions by the model are presented as dot maps. (Fig. 17 and 18 for ^{58}Co and ^{137}Cs respectively.) Both figures show very high concentrations near the outflow and relatively high concentrations adjacent to the east shore line of Bailey Cove, with concentrations being slightly higher in the upper cove than in the lower cove. Correlation coefficients between the isocuric maps (experimentally measured concentrations) and the dot maps (mathematically calculated concentrations) are about 0.75, indicating very good agreement between experiment and theory (26).

CONCLUSION

Our data suggest that one limiting biological factor in using the thermal effluent from this power plant is the availability of food for the oysters. The thermal additions by the power plant has been seen to provide a sufficient increase in water temperature to allow the oysters at the warmer sites to take advantage of the food available in the early spring. The growth of oysters had ceased by November as the amount of food available decreased in the fall, even though temperatures remained warm enough to permit growth.

An additional limiting factor in the use of the effluent waters was the proliferation of the marine worm *Polydora ligni* and *websteri* which adversely effected the commercial value of oysters from the warmer water sites.

The importance of intelligent selection of the species for cultivation is shown by the high mortality found amoung mussels placed in the effluent in 1974 (Fig. 4).

We have found that the concentration factor model does not adequately describe the dynamic nature of the uptake and loss of radionuclides for the case in which the source of these nuclides varies with time. The model we have described, which utilizes the release schedule of an atomic power plant to describe the true variation of the source of radionuclides, is in good agreement with values as measured in the oysters located at various distances from the discharge point.

The oysters do not take up radionuclides during their hybernation (when shell growth is stopped, and the biological decay constant is zero). Radioactivity is taken up independent of the chemistry of the nuclides, suggesting a physical process such as filtration of particulates. The radionuclides concentration in oysters decreases with increase of the distance from the discharge point. The values of radionuclides in the associated sediments can be described by a dynamic estuary model and these calculations correlate with sediment transect measurements.

The application of this model allows one to predict accumulations of radionuclides in shellfish, and based on their physiology suggests a release schedule that will minimize the concentration of radionuclides by the oysters, and permits optimum choice of sites for future aquaculture efforts.

1. Nash, C.E.; 1968, Power stations as sea farms, Nat. Scient., 40(623), 367-369.

2. Burns, W.J.; 1969, Beneficial effects of warm water discharges from power plants, paper presented, S.E.Elec. Exch. Prod. Sec. Mt. Clearwater, Florida, 6 pages.

3. Coutant, C.C.; 1970, Biological limitations on the use of waste in aquaculture, Pro. Con. Ben. use of thermal discharges, N.Y. Dept. Con. Eco. Sci. Div., Reprint No. 398, 51-60.

4. Mather, S.P., and Stewart, R.; 1970, Proceedings of the conference on beneficial uses of thermal discharges; N.Y. State Dept. of Envi. Conv. (4 papers on aquaculture).

5. Strawn, K.; 1970, Beneficial use of warm water discharges in surface waters, paper presented Annual Mtg. Atom. Indus. Forum. and Elec. Power Council on Envir. 29 June 1970, Washington, D.C.

6. Yarosh, M.M., Nichols, B.L., Hirst, E.A., Michel, J.W., and Yee, W.C.; 1972, Agricultural and aquacultural uses of waste heat, Oak Ridge Nat. Lab. Rept. ORNL-4797, NTIS, Dept. of Commerce, 54 pages.

7. Huguenin, J. E., and Ryther, J.A.; 1974, The use of power plant waste heat in marine aquaculture; Proc. Tenth An. Con. Mar. Soc., contribution No. 3381, Woods Hole Ocea. Inst., Woods Hole, Mass., 431-445.

8. Shimizu, M., Kajihara, T., Suyama, I., and Hiyama, Y.; 1971, J. Radiat. Res., 12, 17.

9. Harrison, F.L.; 1973, IAEA-SM-158/28, 453-478.

10. Cranmore, G., and Harrison, F.L.; 1975, Loss of ^{137}Cs and ^{60}Co from the oyster *Crassostrea gigas*, Health Physics, 28, 319-333.

11. Seymour, A.H.; 1966, Accumulation and loss of zinc-65 by oysters in a natural environment. IAEA-SM-72/38, 608-619.

12. Jefferies, D.F. and Preston, A.; 1960, Seminar on marine radioecology, Paris, Conf. - 681225, 67-71.

13. Naidu, J.R., and Seymour, A.H.; 1969, Proc. Symposium on Mollusca, Part II, Mar. Biol. Assoc. India, Symp. Ser. 3, 463-474.

14. Wolfe, D.A. and Fish, J.; 1970, Levels of stable Zn and ^{65}Zn in *Crassostrea virginica* from North Carolina, Fish. Res. Bd. Can. 27, 45-57.

15. Lowman, F., Ric, T.R., and Richards, F.A.; 1971, Ch. 7, Radioactivity in the marine environment, Nat. Acad. of Sciences, Washington, D.C., 161-199.

16. Strickland, J.D.H. and Parsons, T.R.; 1965, A manual of sea water analysis, Fish. Res. Bd. Can. Bull 125, 1-203.

17. Burklew, M.A.; 1971, A preliminary investigation: The effect of elevated temperature on the American oyster *Crassostrea virginica* (Gmelin), Quick Jr, A.J., ed. Fla. Dept. of Nat. Res. Pro. Paper No. 15, 7-35.

18. Covell, D.F., 1959, Anal. Chem. 31, 1785.

19. Price, A.H., C.T. Hess, and C.W. Smith 1976 . A Field Study of *Crassostrea virginica* Cultured in the Heated Effluent and Discharged Radionuclides of a Nuclear Power Reactor Proceedings of the National Shellfisheries Association Vol. 66 (In Press)

20. Polycarpov, G.G. 1966. Radioecology of Aquatic Organisms. Reinhold Book Div., New York, p. 27.

21. Ruzic, I. 1972. Two-compartment model of Radionuclide Accumulation Into Marine Organisms. I. Accumulation from a medium of Constant Velocity. Mar. Biol. 15: 105-112.

22. Davis, J.J., and R. F. Foster. 1972. Ecological Aspects of the Nuclear Age: Selected Readings in Radiation Ecology. I.I.D. -25978 USAEC, 195-200.

23. Hess, C.T., C.W. Smith, and A.H. Price 1977 , A Mathematical Model of the Accumulation of Radionuclides by Oysters (*C. virginica*) Aquacultured in the Effluent of a Nuclear Power Reactor to Include Major Biological Parameters Health Physics

24. C.T. Hess, C.W. Smith and A.H. Price 1975 . Model for the Accumulation of Radionuclides in Oysters and Sediments Nature, Lond. 258, 225.

25. Feigner, K.D. and H.S. Harris, 1970 Documentation Report FWQA Dynamic Estuary Model (Washington, D.C.: FWQA Dept. of Interior).

26. Churchill, J.H. 1976 Measurement and Modeling of the Distribution of Nuclear Reactor Discharged Radionuclides in the Estuarine Sediment Near The Maine Yankee Atomic Power Plant in Wiscasset, Maine. Unpublished Master's Thesis, University of Maine, Orono.

TABLE 1 INPUT INFORMATION

RAFT STATION	PHYSICAL HALF-LIFE, $t_{\frac{1}{2}p}$, days					BIOLOGICAL HALF-LIFE, $t_{\frac{1}{2}b}$, days					$U \times 10^{-12} g^{-1}$
	^{58}Co	^{60}Co	^{54}Mn	^{134}Cs	^{137}Cs	^{58}Co	^{60}Co	^{54}Mn	^{134}Cs	^{137}Cs	
S-1	71.3	1902	303	748	10950	35	35	1500	250	250	1.7
S-2	71.3	1902	303	748	10950	35	35	1500	250	250	10.0
S-3	71.3	1902	303	748	10950	35	35	1500	250	250	7.4
S-4	71.3	1902	303	748	10950	35	35	1500	250	250	3.4

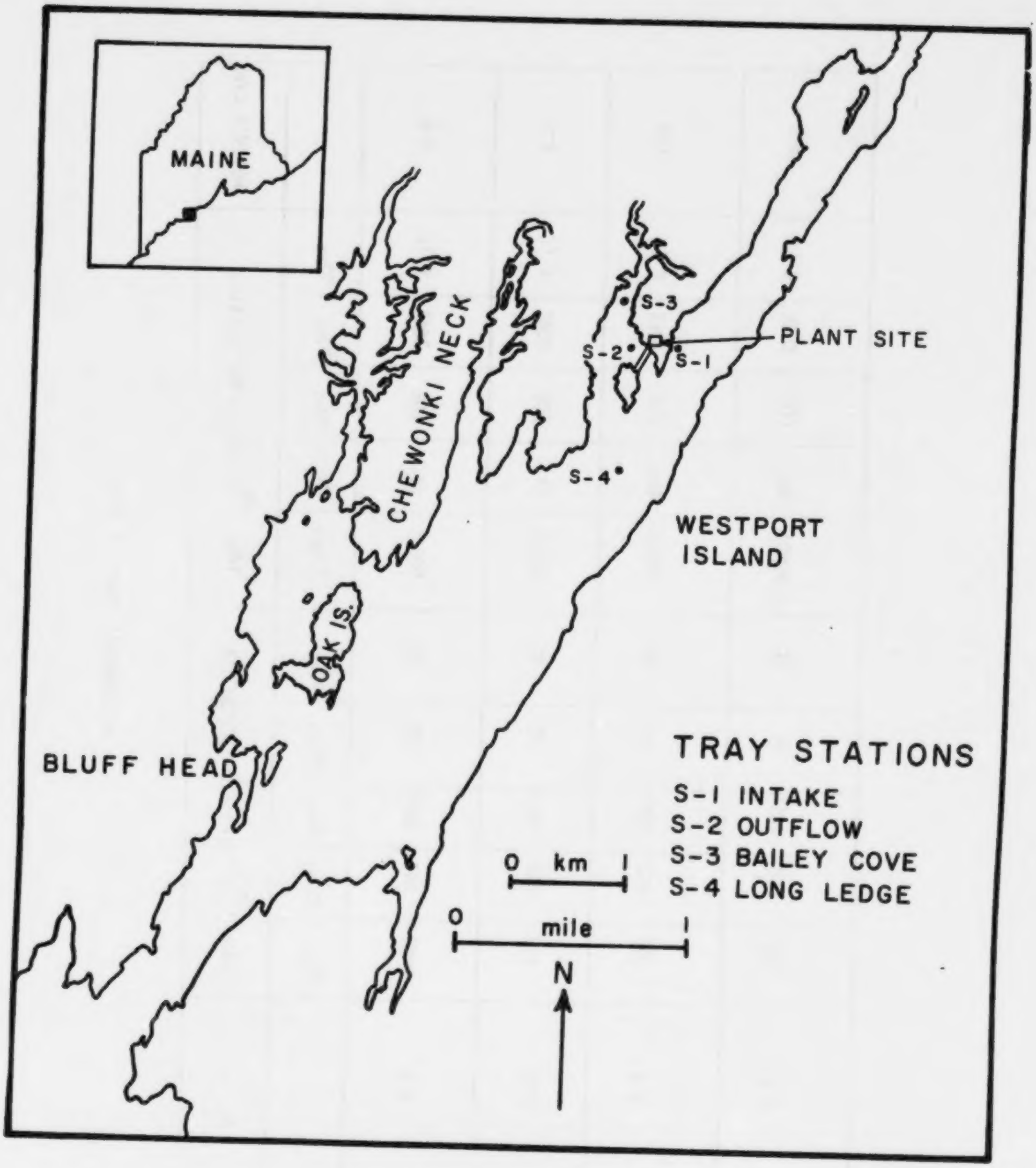
MAINE
CHEWONKI NECK
S-3
S-2
S-1
PLANT SITE
S-4
WESTPORT ISLAND
OAK IS.
BLUFF HEAD
TRAY STATIONS
S-1 INTAKE
S-2 OUTFLOW
S-3 BAILEY COVE
S-4 LONG LEDGE
0 km 1
0 mile 1
N

Fig. 1. Map of Montsweag Bay showing location of tray stations.

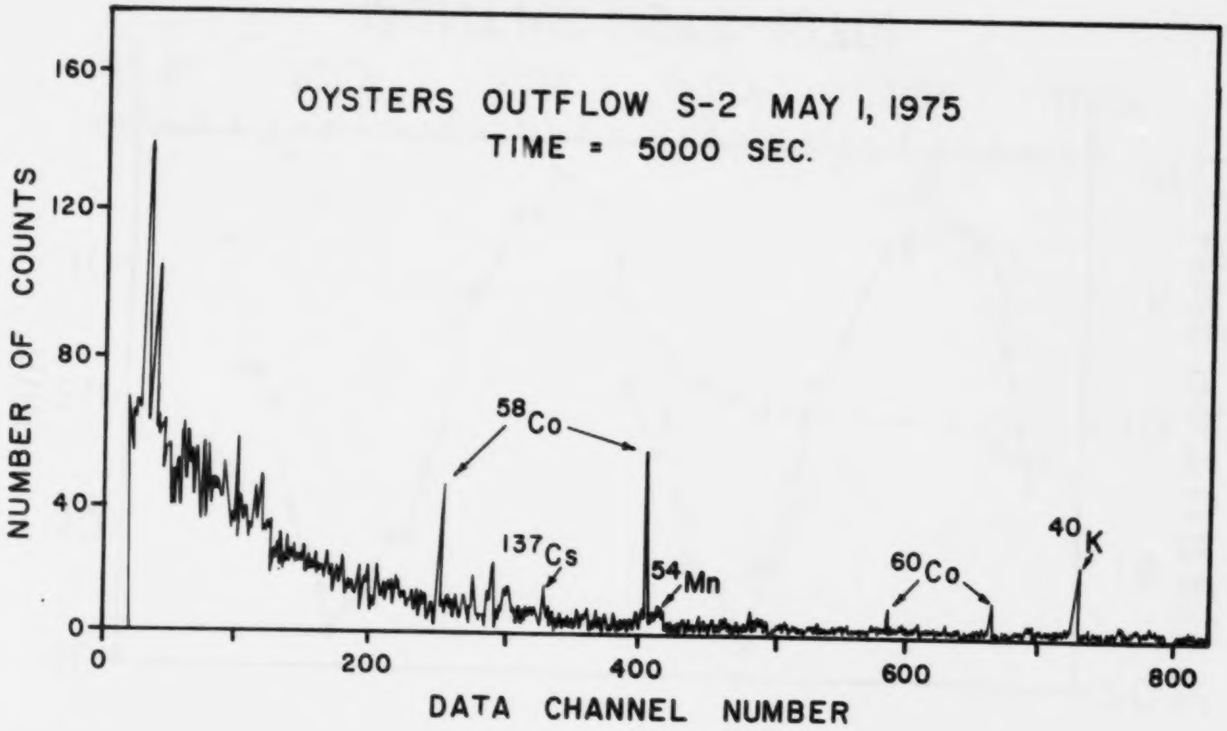

Fig. 2. Gamma-ray spectrum of oysters from the outflow station (S-2) with data channel number versus number of counts in 5000 sec.

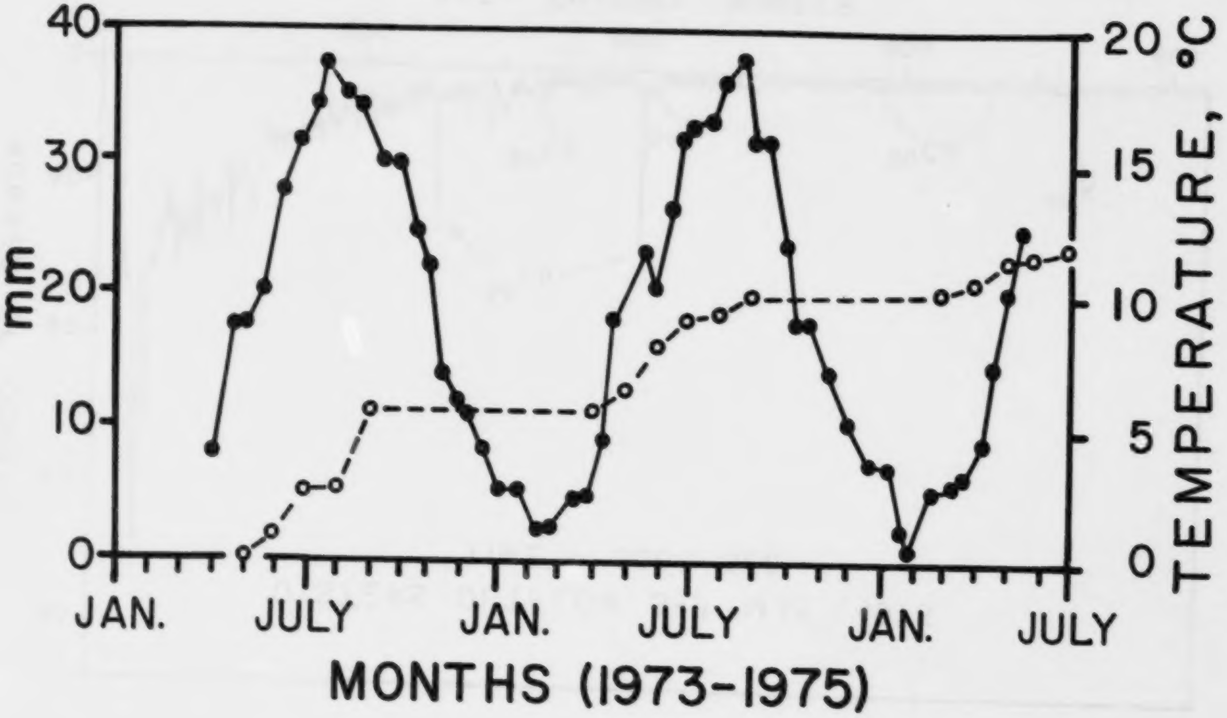

Fig. 3.a. Oyster shell growth in mm at control site (SC) versus month of year for 1973-1975 (0---0). b. Temperature in ^{0}C versus month of year (●—●).

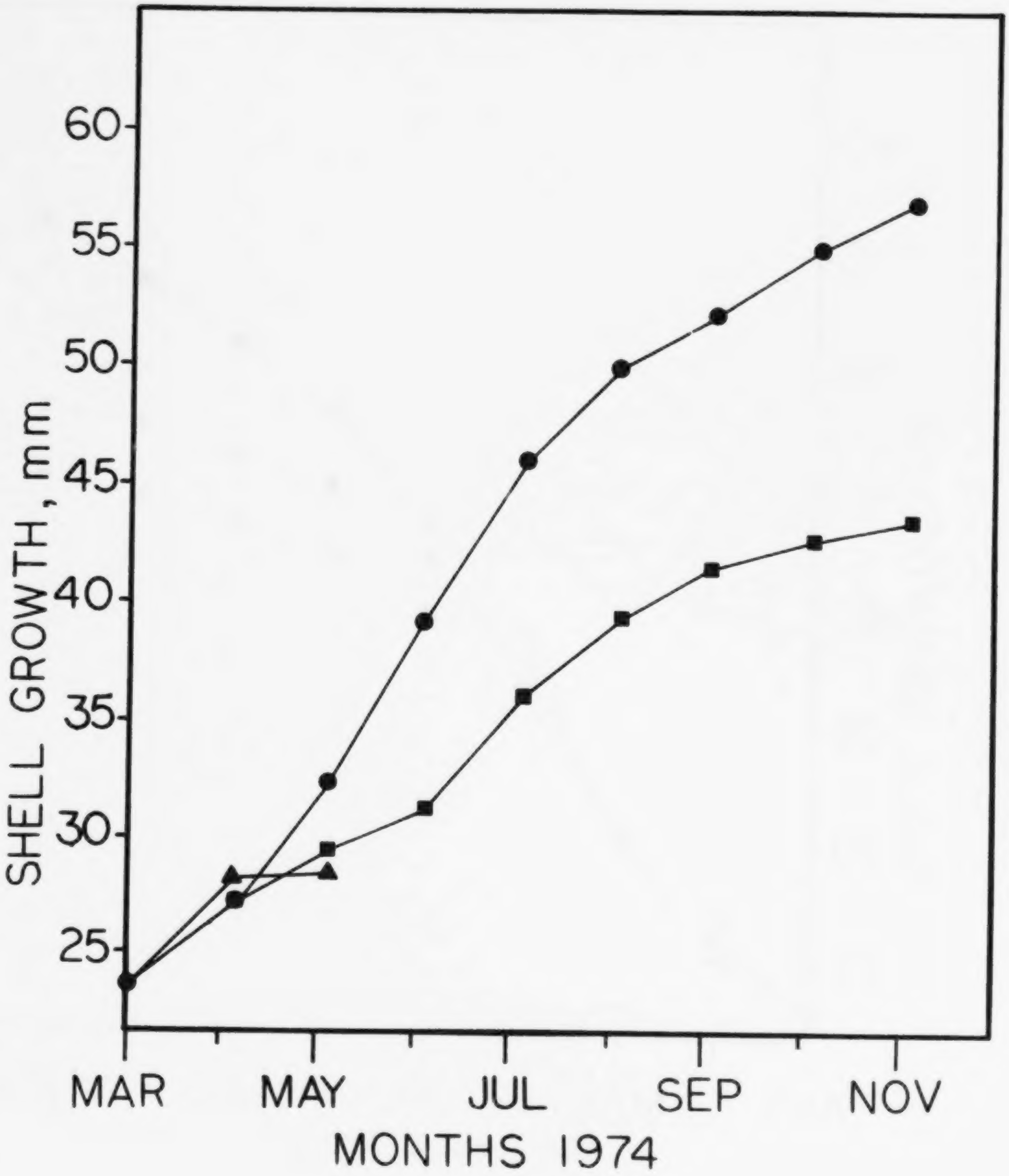

Fig. 4.a. Mussel shell growth in mm at control site (SC) versus months for 1974 (●—●) b. Mussel shell growth in mm at longledge (S4) versus month of year (■—■) c. Mussel shell growth in mm at outflow (S2) versus month of year (▲—▲).

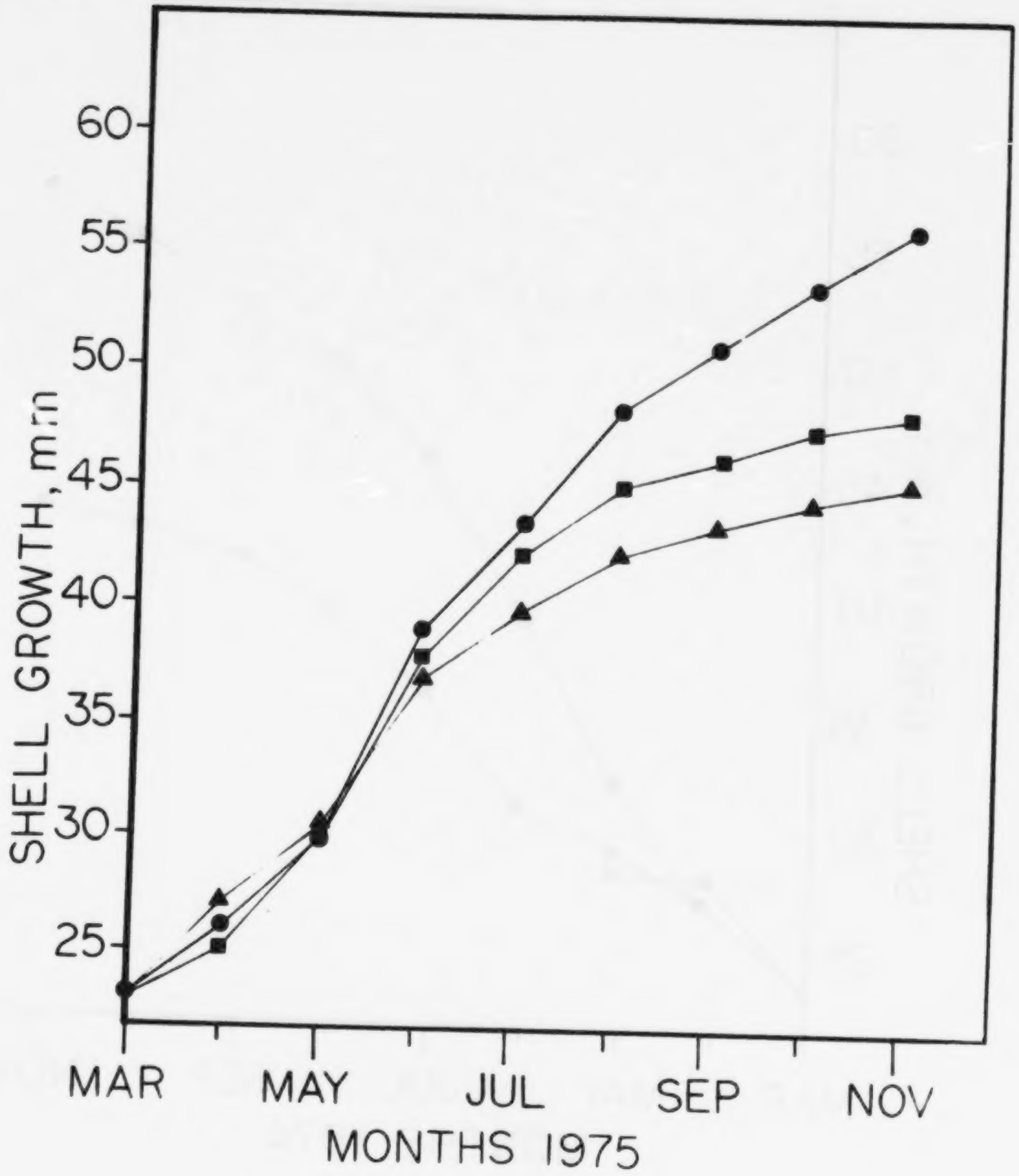

Fig. 5. Mussel shell growth in mm as shown in Fig. 4. versus month of year 1975.

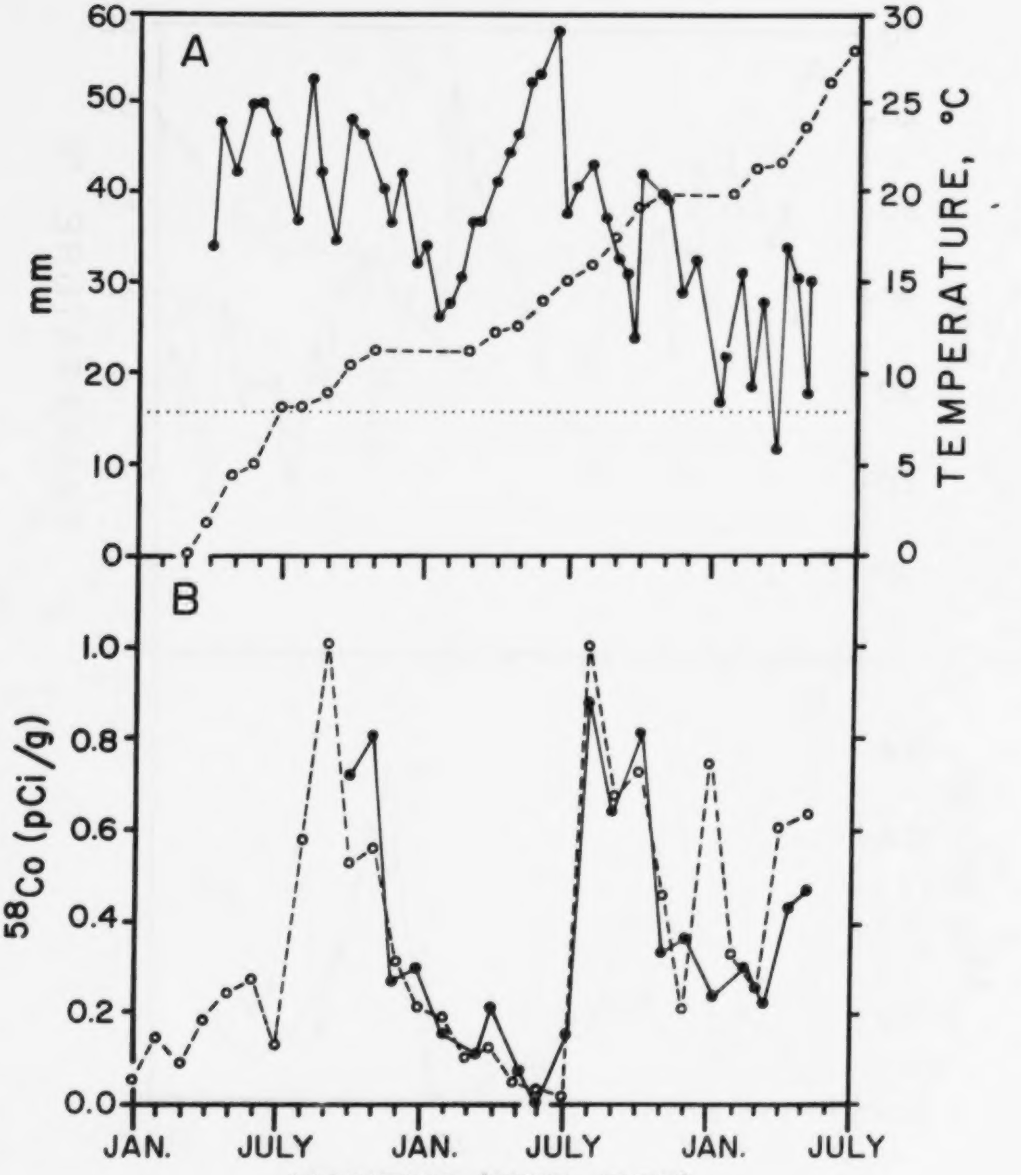

Fig. 6. Oyster shell growth at the outflow station (S2) versus month of year for 1973-1975. (0---0). Ab. Temperature in ^{0}C at outflow versus months of year (●——●) Ba. Radionuclide concentration for ^{58}Co in oysters from the outflow versus month (●——●). Bb. Theoretical radionuclide concentration for ^{58}Co in oysters versus month (0--0).

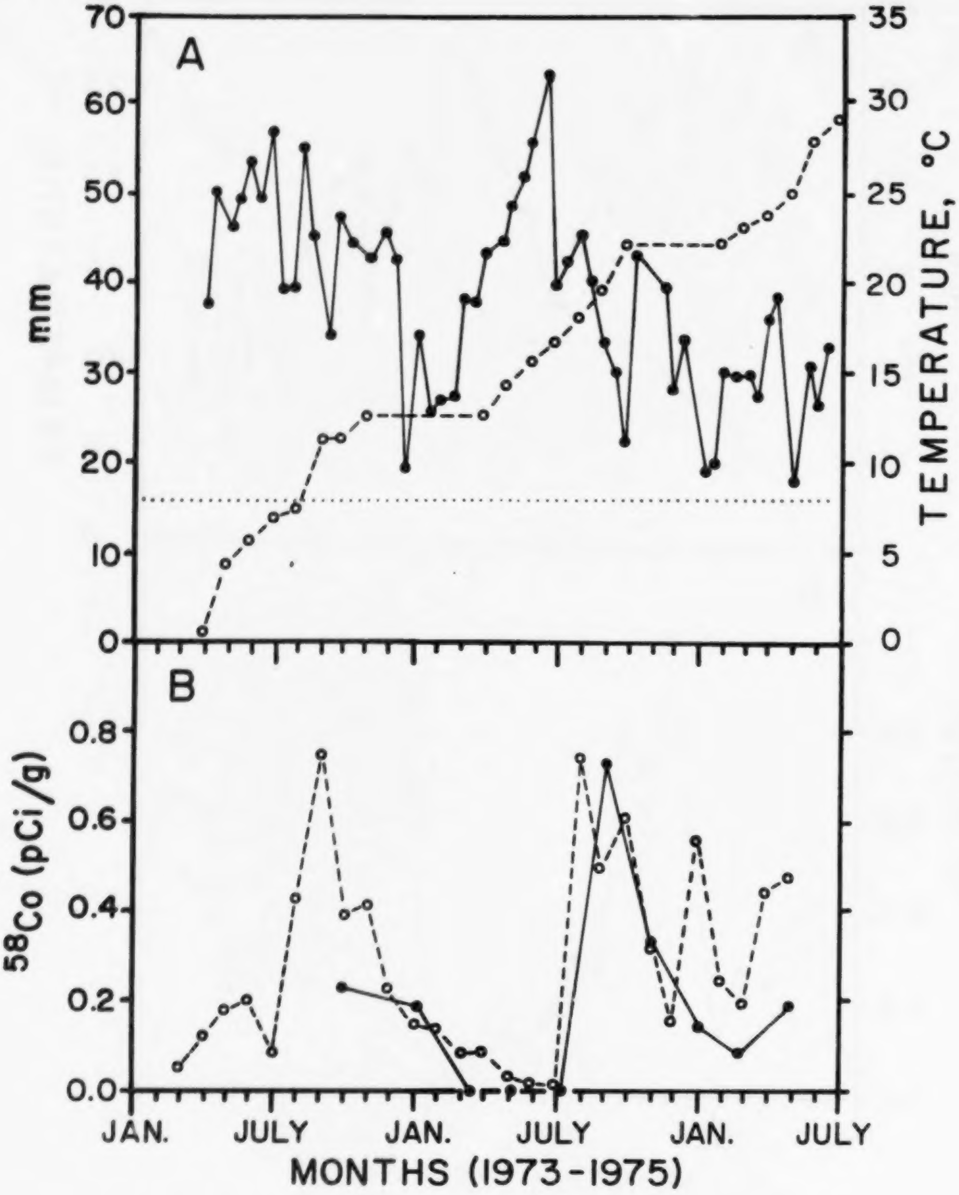

Fig. 7.Aa. Oyster shell growth, Ab. Temperature in ^{0}C, Ba. Radionuclide ^{58}Co concentration, and Bb. Theoretical ^{58}Co radionuclide concentration versus month of year as in figure 6. for Upper cove site (S3).

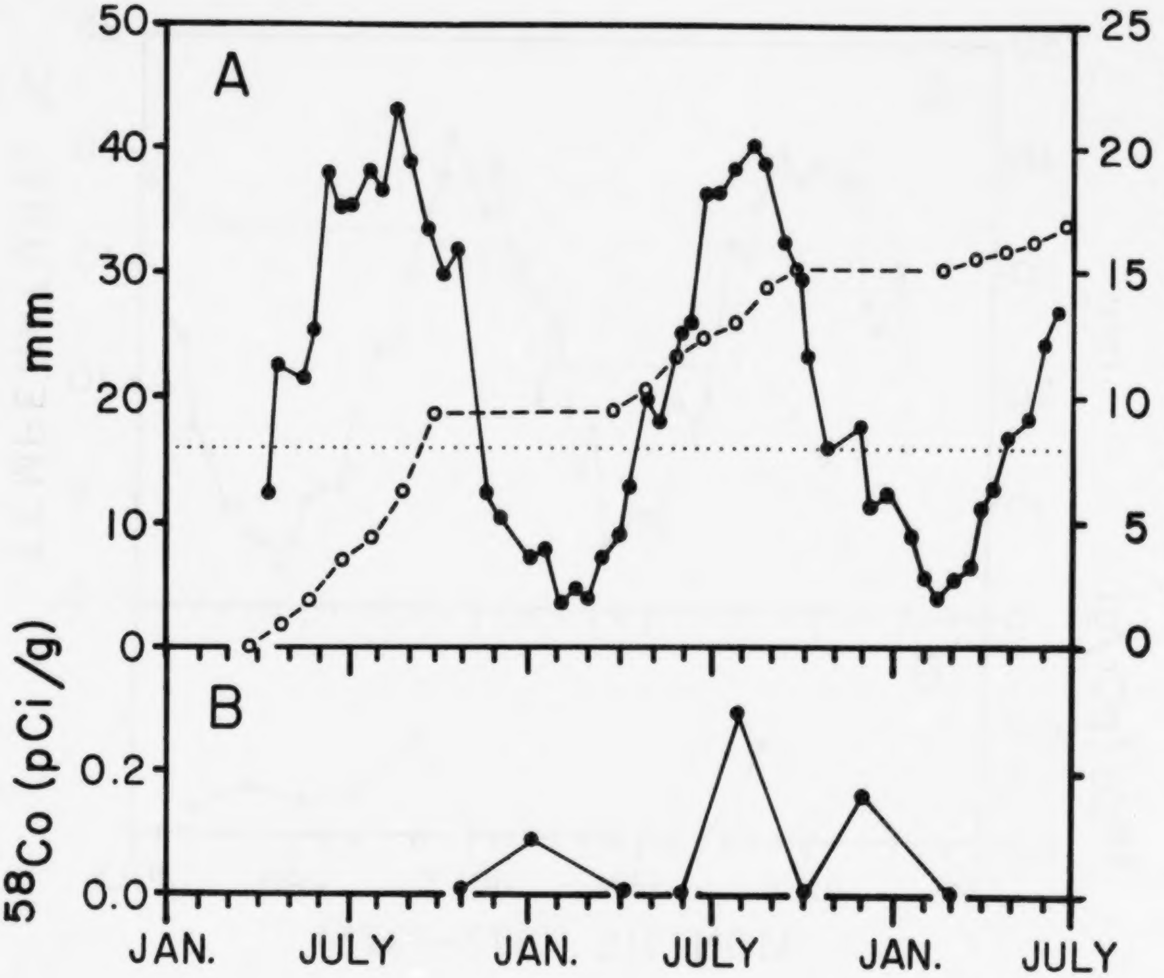

Fig. 8 Aa. Oyster shell growth, Ab. Temperature in ^{0}C, Ba. Radionuclide ^{58}Co concentration, and Bb. Theoretical ^{58}Co radionuclide concentration versus month of year as in figure 6. for longledge site (S4).

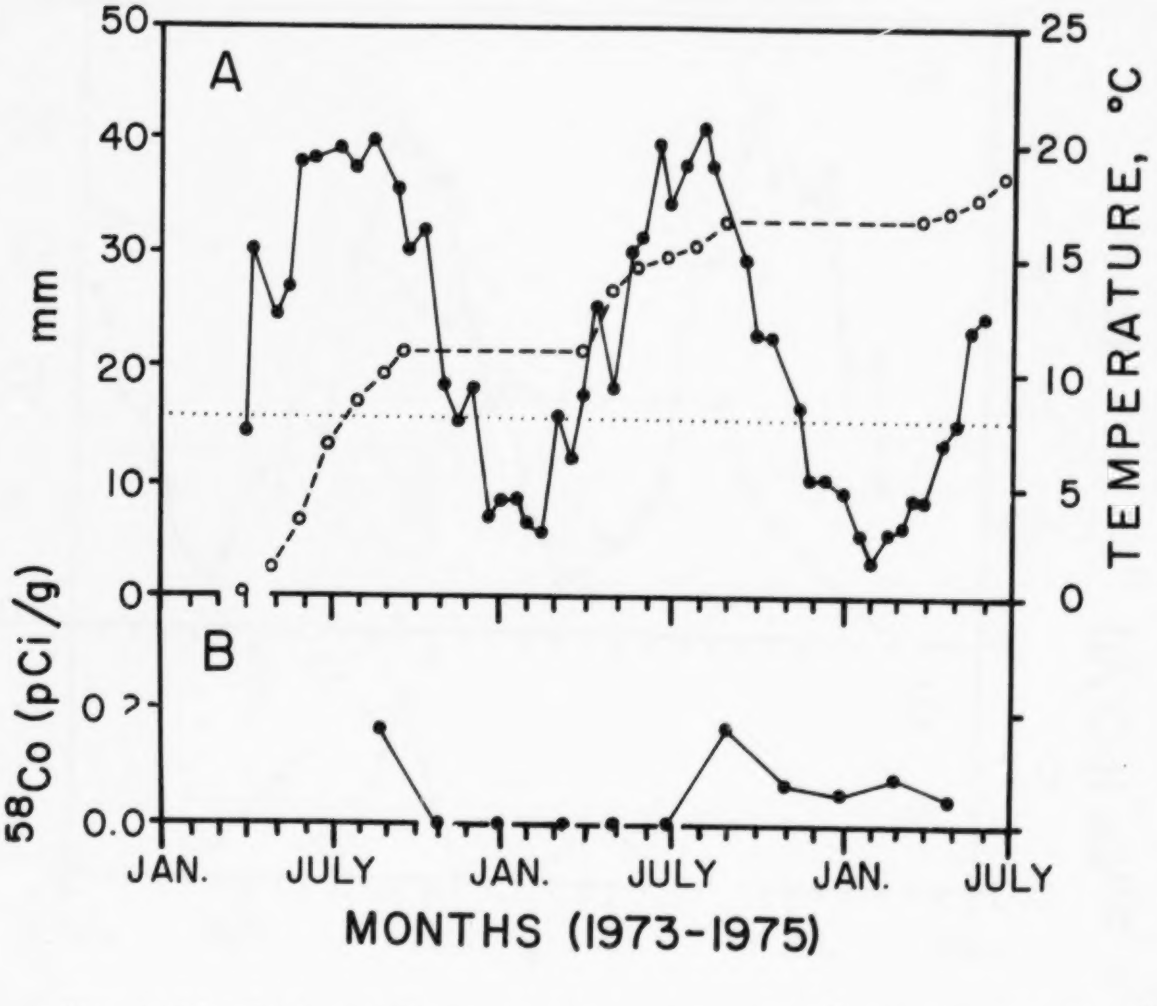

Fig. 9. Aa. Oyster shell growth, Ab. Temperature in ^{0}C, Ba. Radionuclide ^{58}Co concentration, and Bb. Theoretical ^{58}Co radionuclide concentration versus month of year as in figure 6. for intake site (S1).

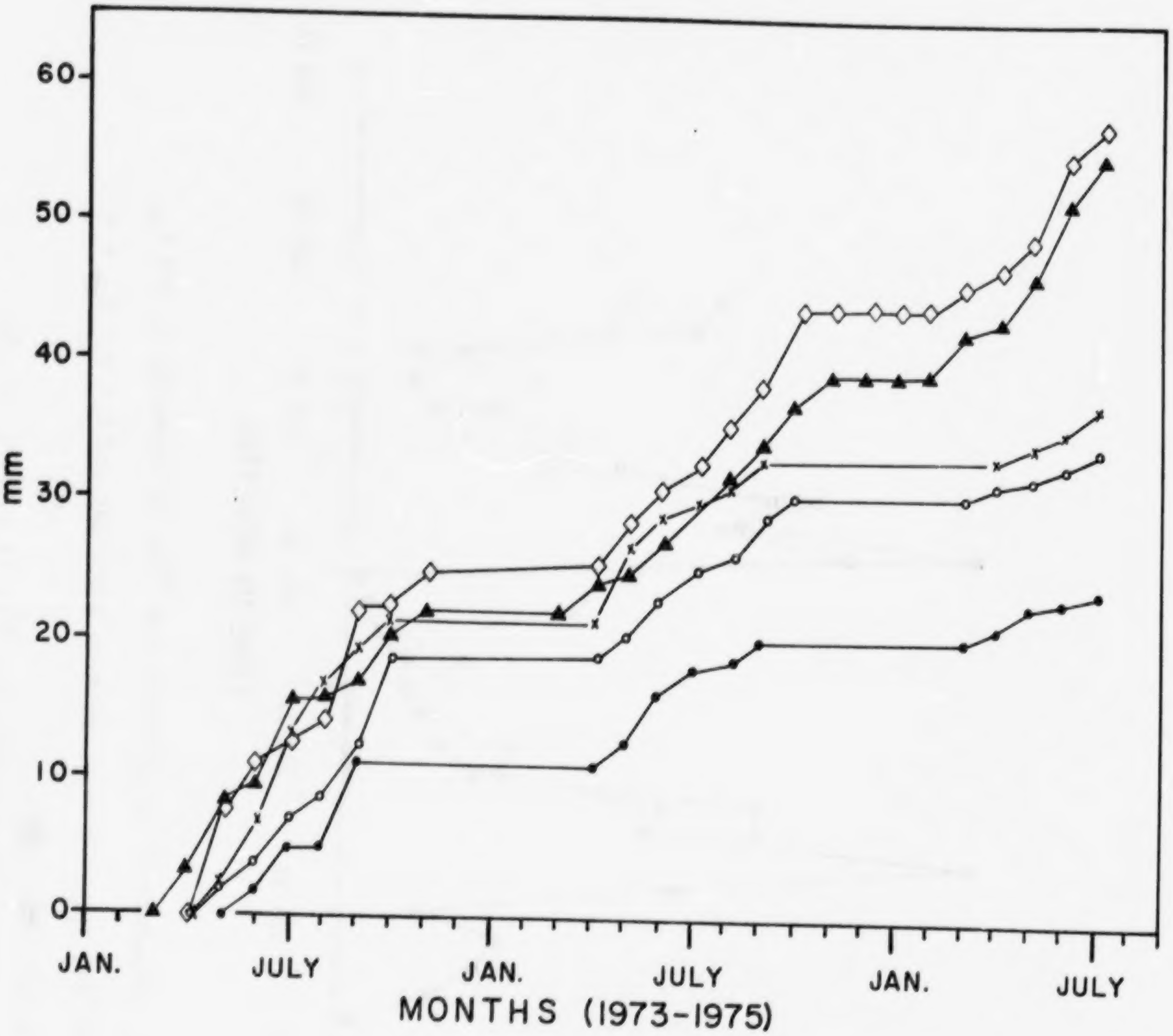

Fig. 10. Comparison of oyster shell growth for all stations versus time of year for 1973-1975. Controls (●—●), Intake (O—O) Long Ledge (x—x) outflow (▲—▲) Upper Cove (◇—◇).

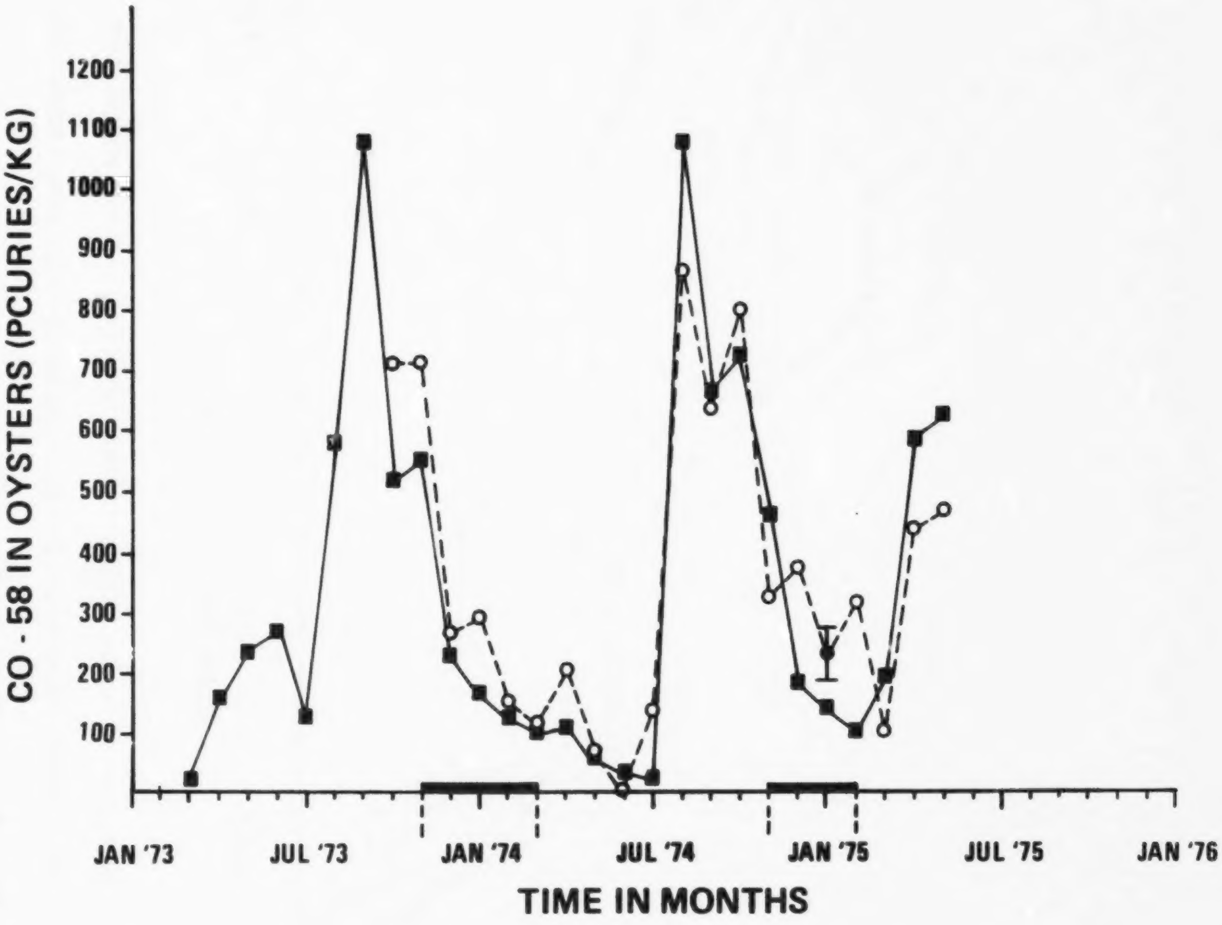

Fig. 11.a. Theoretical calculations for ^{58}Co for changing U, and $t_{\frac{1}{2}b}$ U = 1 x 10^{-8}Kg, $t_{\frac{1}{2}b}$ = 35 days, with no black bar and U = 0.0 $t_{\frac{1}{2}b} = \infty$ with black bar (■—■).

b. Experimental results for ^{58}Co in oysters (0---0).

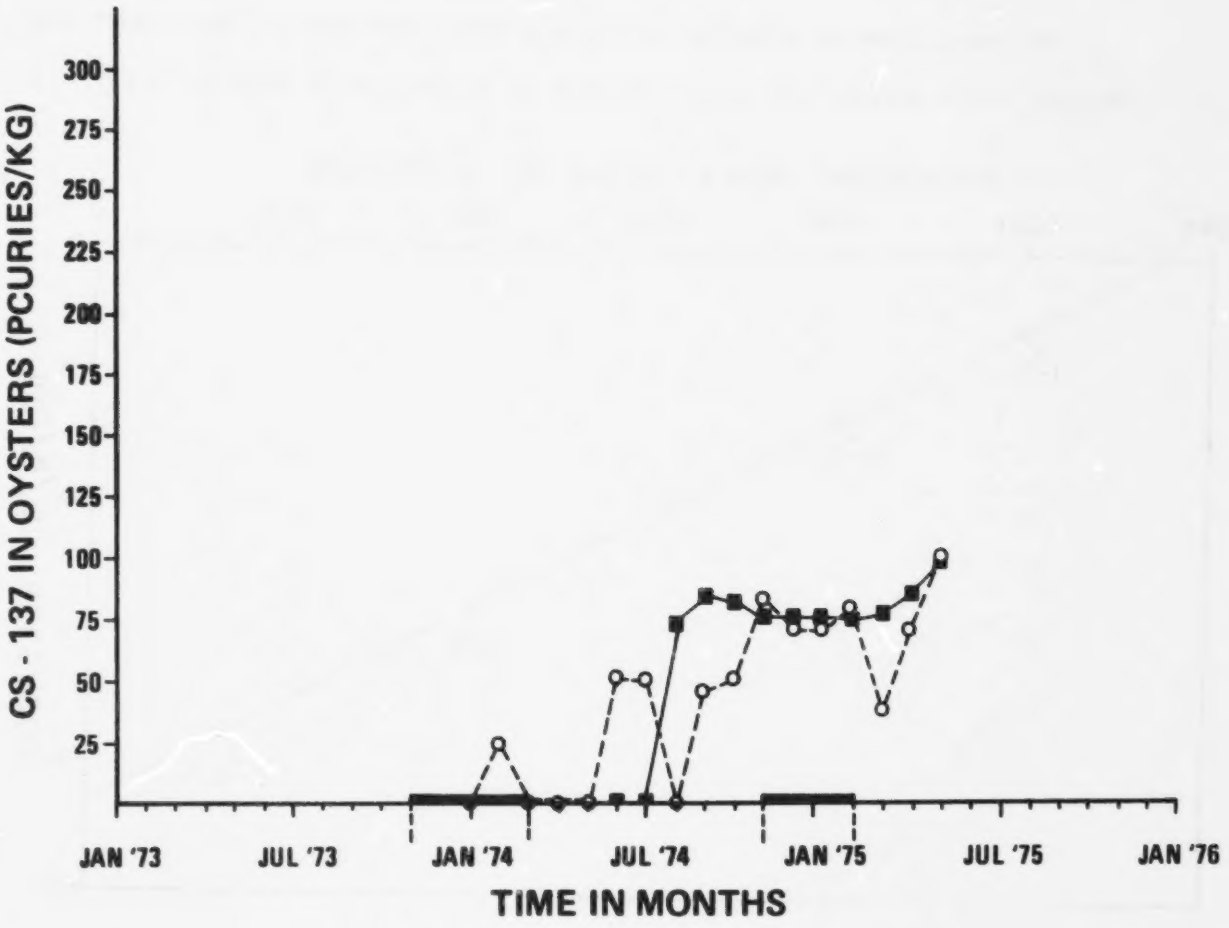

Fig. 12.a. Theoretical calculations for ^{137}Cs changing U and $t_{\frac{1}{2}b}$: $U = 1 \times 10^{-8}$Kg., $t_{\frac{1}{2}b} = 250$ d with no black bar and $U = 0.0$ $t_{\frac{1}{2}b} = \infty$ with black bar (■—■)

b. Experimental results for ^{137}Cs in oysters (0---0).

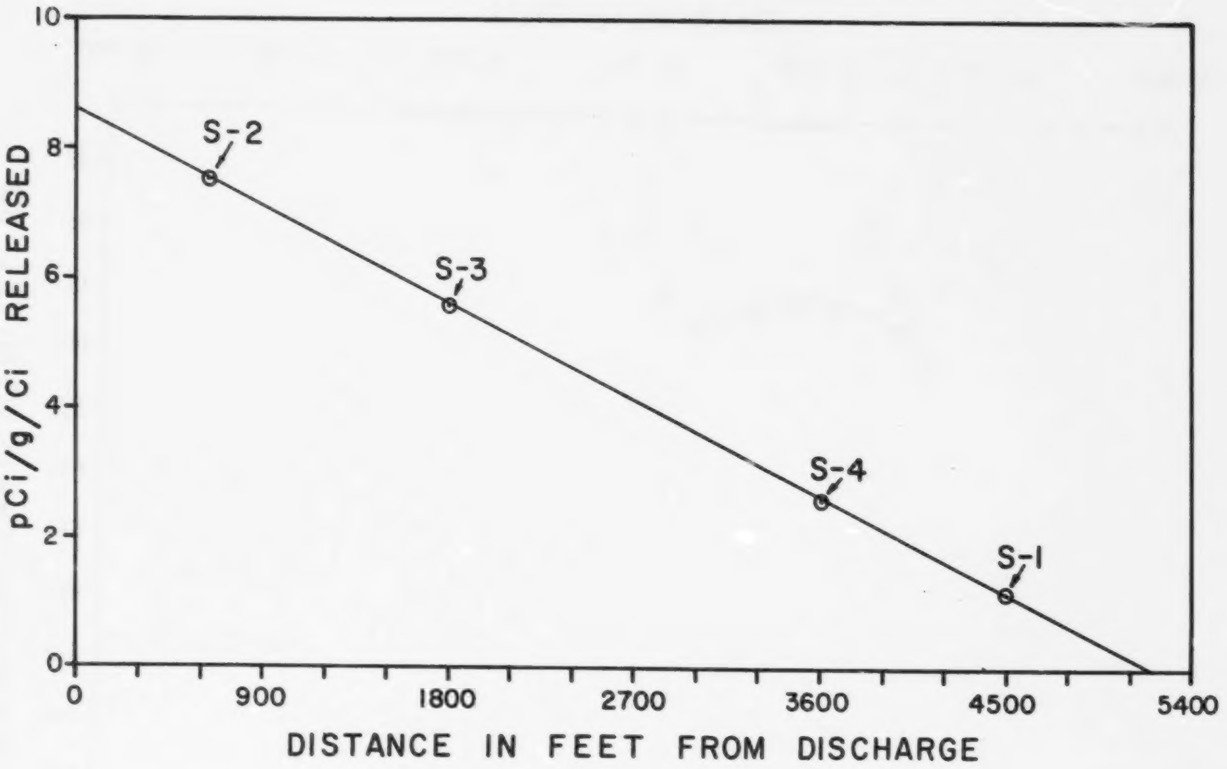

Fig. 13.a. Results of evaluation of U at each site S-1, intake site, outflow S-2 upper cove S-3 and Long Ledge S-4 versus distance in water from the release point.

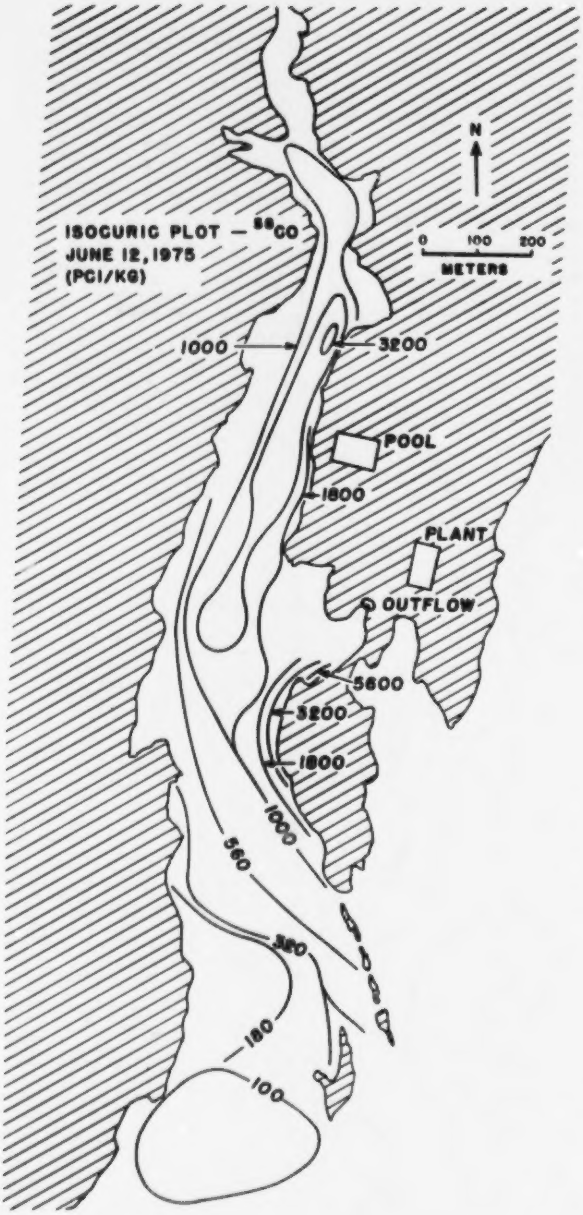
ISOCURIC PLOT — 58CO
JUNE 12, 1975
(PCI/KG)
N
0 100 200
METERS
1000
3200
POOL
1800
PLANT
OUTFLOW
5600
3200
1800
1000
560
320
180
100

Fig. 14. Isocuric map of ^{58}Co concentration in sediment for the sediment survey; June 12, 1975.

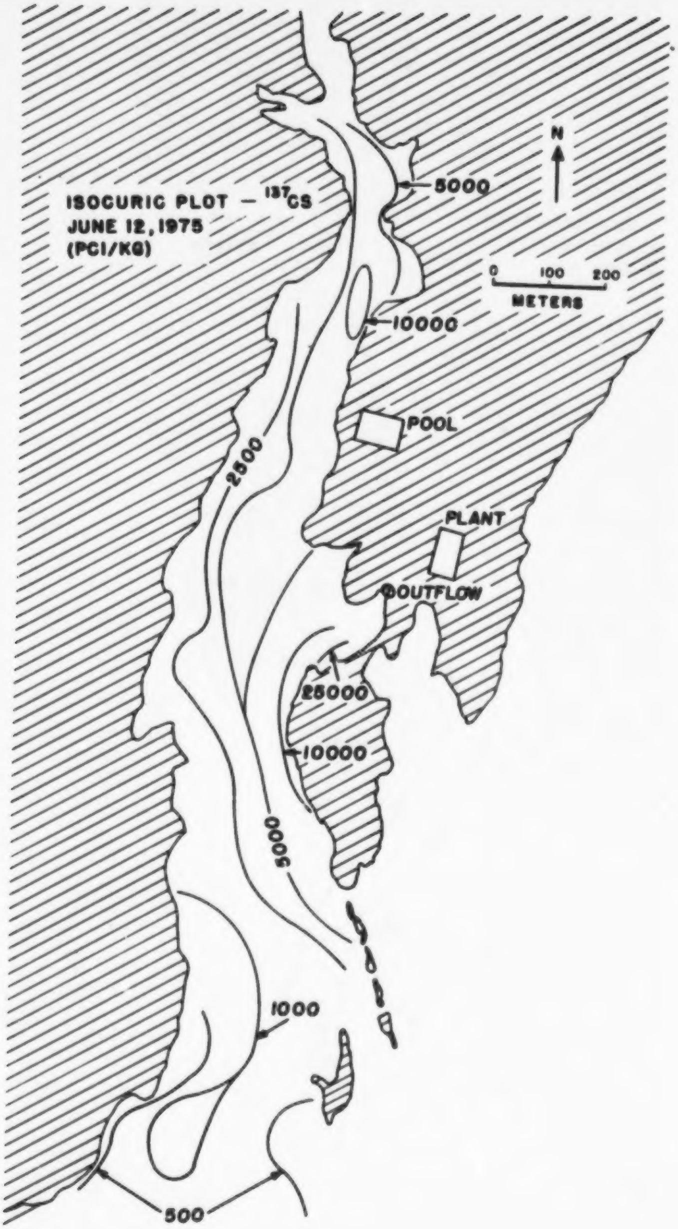
ISOCURIC PLOT — ¹³⁷CS
JUNE 12, 1975
(PCI/KG)
N
0 100 200
METERS
5000
10000
POOL
2500
PLANT
OUTFLOW
25000
10000
5000
1000
500

Fig. 15. Isocuric map of ^{137}Cs concentration in sediment for the sediment survey; June 12, 1975.

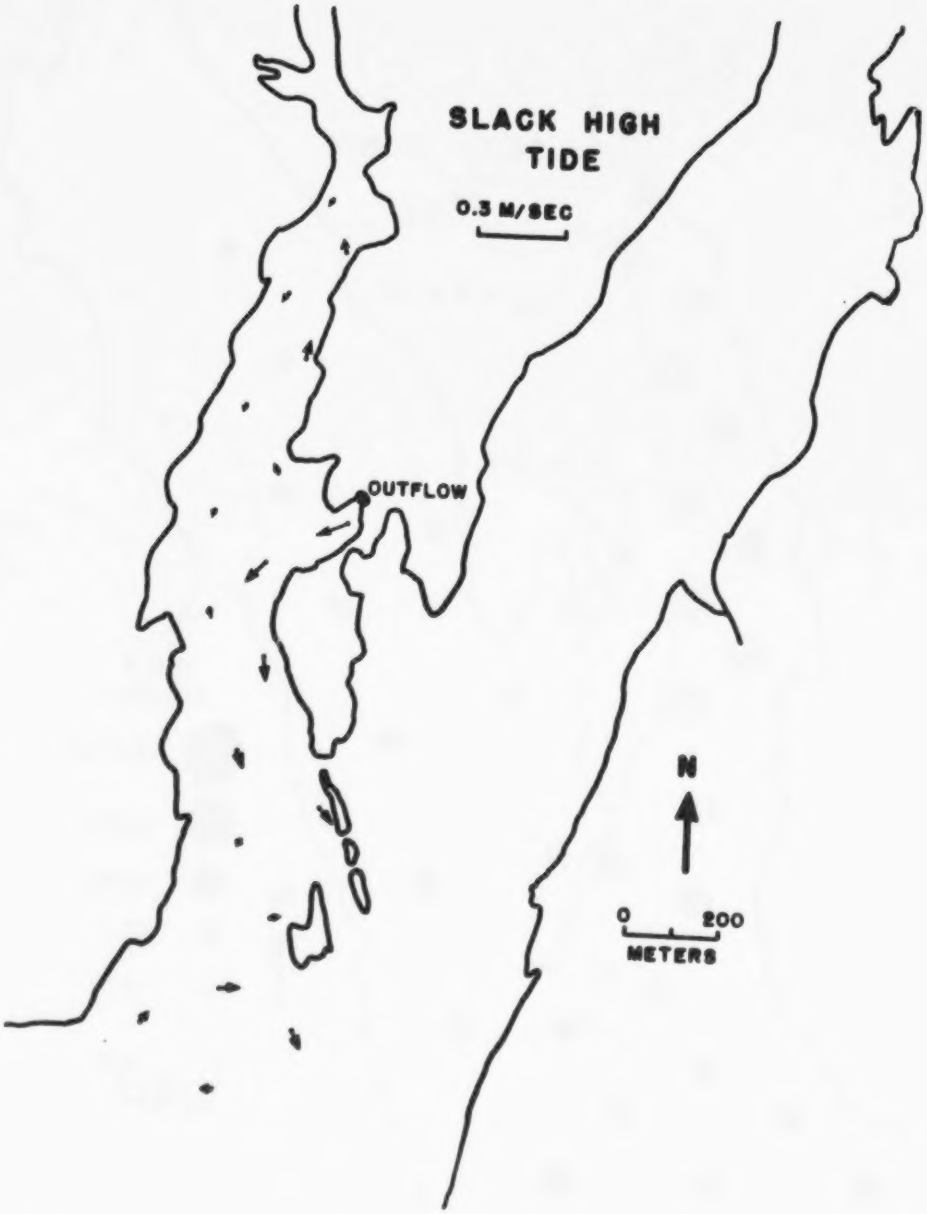
SLACK HIGH TIDE
0.3 M/SEC
OUTFLOW
N
0
200
METERS

Fig. 16. Computer calculated water velocities at slack high tide.

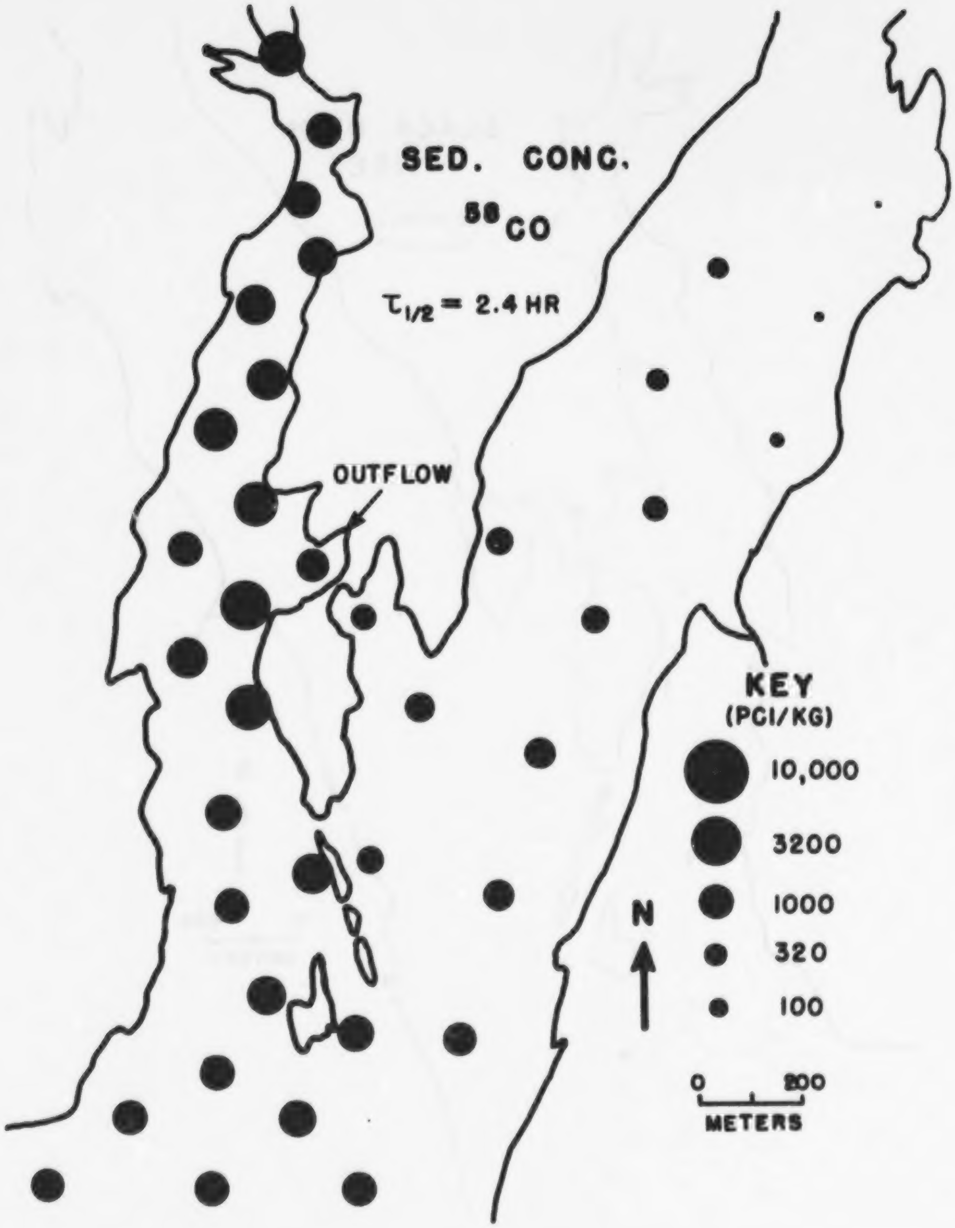
SED. CONC.
^{58}CO
$\tau_{1/2}$ = 2.4 HR
OUTFLOW
KEY
(PCI/KG)
10,000
3200
1000
320
100
N
0
200
METERS

Fig. 17. Computed concentrations of ^{58}Co in sediment measured in pCi/kg, for $t_{\frac{1}{2}b}$ = 2.4 hr.

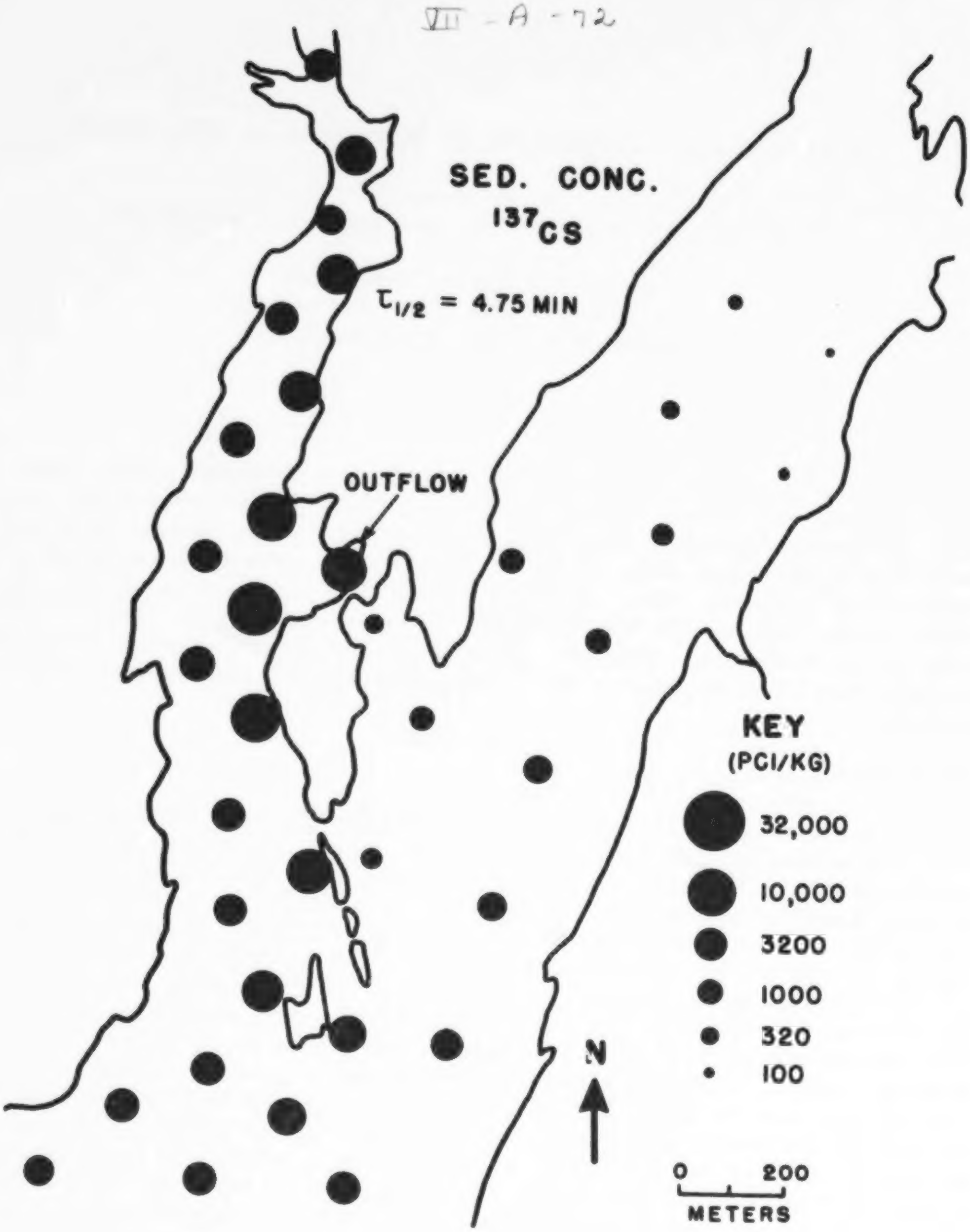
SED. CONC.
^{137}CS
$\tau_{1/2}$ = 4.75 MIN
OUTFLOW
KEY
(PCI/KG)
32,000
10,000
3200
1000
320
100
N
0
200
METERS

Fig. 18. Computed concentrations of ^{137}Cs in sediment measured in pCi/kg. $t_{\frac{1}{2}b}$ = 4.75 min.

29-45-15

UTILIZATION AND DISSIPATION OF WASTE HEAT BY SOIL WARMING

D. R. DeWalle
Institute for Research on Land and Water Resources
and
School of Forest Resources
The Pennsylvania State University
University Park, PA, 16802, USA

ABSTRACT

Soil warming research at The Pennsylvania State University and other locations in the United States and West Germany is reviewed from both a crop production and heat dissipation viewpoint. Earlier harvests and increased yields for crops grown in heated soil have been reported in the majority of studies. Soil warming systems for dissipation of all the reject heat from a 1000 MWe power plant would require too large a land area to be practical. However, it appears possible to design optimized systems which can be economically competitive with conventional cooling methods.

INTRODUCTION

Many beneficial uses of waste heat in agriculture have been proposed such as: space heating for poultry and swine, convectional greenhouse heating, warm-water irrigation, aquaculture and soil warming in open fields as well as greenhouses. Soil warming is a term being used to describe a technique in which heated water is circulated through a pipe network buried in the soil, thereby warming the soil for potential beneficial use of the heat in agriculture. In addition to utilizing the waste heat for agricultural production via the warmed soil, a soil warming system can also be conceived as a heat dissipation system, e.g., a buried wet-cooling tower. With the proper system design a land area equipped with buried pipe can be used to dissipate all or part of the reject heat from an industrial source such as a steam-electric power plant. The water could be passed through the buried pipe network for cooling and returned in a closed system back to the plant. An integrated system for soil warming to utilize as well as dissipate waste heat must be carefully designed since the optimum system for heat dissipation is not necessarily the optimum for crop production.

At The Pennsylvania State University in 1972, an interdisciplinary study was funded by the National Science Foundation (RANN) to determine the economic and technical feasibility of soil warming as an alternative to commonly used heat dissipation methods such as cooling ponds, run-of-river cooling, and wet- and dry-cooling towers. In this study a computer model was developed to simulate a soil warming system operated for heat dissipation in conjunction with a 1500 MWe nuclear power plant. A 0.09 ha (15 x 60 m) soil warming field prototype was developed to test functions for prediction of heat transfer from buried hot-water parallel pipe networks used in the computer model. A unique feature of the prototype was the spray application of treated municipal wastewater on the warmed soil to maintain efficient heat transfer and supply crop nutrients. Details of this investigation were reported in [1] and [2]. More recently with funding from the USDI Office of Water Research and Technology, this research has been continued to study year-round heat dissipation, crop growth and development and wastewater renovation in artificially warmed soil.

Considerable experience has been gained through soil warming research at Penn State and several other locations. In fact, at two locations in West Germany [3] and in Minnesota, demonstration projects have now been initiated using actual power plant effluent. The purpose of this paper is to describe the Penn State research project and to compare and contrast the Penn State research with other known soil warming research projects. The status of soil-warming research and future potential of the soil-warming technique are discussed.

DESCRIPTION OF SOIL WARMING RESEARCH FACILITIES

Penn State Field Prototype

A key feature of the Penn State soil warming research is the field prototype located near the campus. The prototype consists of a buried pipe network, hot-water heating system, a wastewater spray irrigation system and heat-transfer data acquisition system. The pipe network consisted of 26 parallel 5-cm diameter polyethylene plastic pipes buried at about 30-cm depth and 60-cm spacing. The pipes were about 60 m long, giving a plot surface area of 15 x 60 m or 0.09 ha. Each plastic pipe was valved at both ends to permit variable pipe spacing. A manifold constructed from iron pipe was attached to either end of the set of plastic pipes to convey the heated water. Each manifold was equipped with a dry-well drain on the low end and an air-escape valve on the high end to facilitate filling the system with water.

The heating system incorporated an oil-fired hot water furnace which was thermostatically controlled to continuously supply water at 38 to 40°C to the inlet manifold. An insulated mixing tank was used to buffer water temperature variations due to firing of the furnace. Water was pumped continuously through the mixing tank, buried pipe network and back to the furnace in a closed cycle. The average flow velocity in each of the plastic pipes was equivalent to a Reynolds number of 1900.

The spray irrigation system was constructed of aluminum surface irrigation pipe. Laterals running perpendicular to the long axis of the plot were spaced every 13.3 m with offset, 45-cm high risers for sprinklers at 13.3 m intervals. The plot was irrigated with treated municipal wastewater supplied by a buried pipeline running from the University's waste treatment plant. Wastewater was applied at the rate of 1 cm per week in bi-weekly applications year-round.

The heated soil area and an adjacent 15 x 30 m control plot, which received wastewater but no heat, were intensively instrumented. The temperature of the soil at various depths and locations on both plots was measured along with the outer pipe surface temperature and circulating water temperature on the heated plot. Soil thermal conductivity, soil heat flow, net radiation and wet- and dry-bulb temperatures were also measured on each plot. Wind velocity, wind direction, dew-point temperature, downward shortwave radiation and dew-point temperature were also measured. Data were collected primarily with a digital data acquisition system.

The soil warming system was operated continuously from August, 1975 to September, 1976, giving an annual variation of climate conditions. Replicated subplots were planted with various perennial grasses plus winter wheat, winter barley, alfalfa and snap beans on both the heated and control plots.

Other Soil Warming Research Facilities

The widespread interest in soil warming research is evident from the summary given in Table 1 of other known research facilities in the United States and West Germany. Nearly all the research has been initiated since 1970 with a primary focus on crop production. Heat dissipation was also investigated especially in the North Carolina and Oregon State University projects. A discussion of the general conclusions derived from these research projects, the Penn State project and other studies not involving field research follows.

CROP RESPONSE TO SOIL WARMING

Open Field Experiments

Crop response to soil warming has been generally favorable. However, it is already evident that climate and the specific crops grown will interact to produce results unique to a chosen location. Nearly all the studies show that germination, emergence and initial growth rates are greater in warmed soil when planting is in early spring. In most cases this initial growth advantage produces earlier harvests which may result in significantly higher profits. Allred [9] in Minnesota found early varieties of white potatoes grown in heated soil matured from 2 to 3 weeks earlier primarily due to earlier planting possible in frozen soil. Rykbost, et al. (1974) also found earlier maturation for nearly all of the 13 crops tested on heated soil in the Willamette Valley in Oregon. Similar experience has been reported [12] for sweet corn, string beans and squash planted in April at Muscle Shoals, Alabama and for a variety of crops planted during the cooler seasons in North Carolina [13]. In both the Alabama and North Carolina studies, crops planted in summer exhibited reduced germination or no benefits from the heated soil.

Crop yields were generally greater in heated soil. Greatest reported crop yield increases have been with bush beans (up to 85% increase) and cole crops, especially broccoli (yield doubled) in Oregon [4] and cabbage

(300% increase) and cool season snap beans (up to 300% increase) in North Carolina [14]. In general, yield increases ranging from 20 to 40 percent have been reported. Reduced yields have been reported by [8] when varieties of forage crops originating in cool regions were grown in artificially warmed soil. Yield response to soil warming in the Penn State study has been variable for several different perennial forage crops, snap beans, winter wheat and winter barley. Winter kill of switch grass and winter barley has occurred, apparently due to slower development of cold tolerance in the warm soil in these species. Allred [9] also reported the freezing of the above-ground portions of potato plants growing in warm soil in early spring. Increased activity of insects and nematodes and weed growth were found with soil warming in North Carolina [13].

Greenhouse Experiments

Soil warming in greenhouses has also been studied as a method for utilization of waste heat (see Table 1). In Alabama, crops requiring low air temperatures were grown in a greenhouse at two different soil temperatures with heat supplied only by soil warming [12]. Broccoli, cauliflower, bibb lettuce and head lettuce were all successfully grown with greater yields produced by the warmer soil. A soil-heated greenhouse in Oregon [15] was used to grow lettuce, tomatoes and cucumbers. Air temperatures in the winter inside the greenhouse were low, but freezing of a lettuce crop was prevented, even during a disruption in the supply of hot water, by the slow release of stored heat from the soil.

Rybost and Boersma [15] reported significant increases in yields of tomatoes planted in April in a greenhouse with soil heating, but stated that a soil warming system was too inflexible for adequate temperature control within a greenhouse.

SOIL AND AIR TEMPERATURE RESPONSE

Crop response to soil warming is closely linked to the increase in soil temperatures within the rooting zone. Air temperature increases occurring from soil heating could also affect crop growth and development.

In the Penn State study, soil temperatures were elevated by soil warming by an average of at least 4°C at all depths year-round. Average temperature increases for each month, at various depths, computed from measurements at 0800 each morning, are presented in Table 2. Increases in soil temperature were greatest at the pipe burial depth of 30 cm, where the average annual increase was 20.8°C. Temperature increases due to soil warming declined with distance above or below the pipes. The decline was more rapid with distance above the pipes and soil temperatures at the surface were raised by only 6.3°C. Temperature increases were greater in winter than in summer at all depths, but especially at the pipe burial depth. In Figure 1, the diurnal variation of soil temperature at the surface, 30-cm and 45-cm depths on the heated plot are compared with surface temperatures on the control on 21 to 22 June, 1976, a clear to partly cloudy day. Surface temperature on this day on the heated plot was about

4 to 6°C higher, and reached 31°C during mid-day.

Soil temperature increases found in other soil warming experiments varied with pipe burial depth. At Springfield, Oregon, where pipes were buried at 60-cm depth, soil temperatures at 15-cm depth were increased 1.4 to 2.5°C in winter and a negligible amount in summer [5]. At the 30-cm depth, soil temperatures were increased 1.7 to 3.9°C in winter and 0 to 3.4°C in summer. In the Oregon State University study [15], with pipes at 51- to 91-cm depths, soil temperatures were increased to 20 to 25°C throughout a large percentage of the profile most of the year. Little horizontal variation in soil temperature was reported near the surface. Allred [9] reported soil temperatures at 20-cm depth were increased by hot-water pipes at 30-cm depth by 7.5 to 10°C in spring, but by negligible amounts in summer. In the North Carolina study [7], with pipes buried at 50-cm depth, soil temperatures for a four-day period in October were increased about 5 to 10°C in the upper 20 cm of soil and up to about 15°C at 40-cm depth. Again negligible horizontal soil temperature variations were found just 10 cm above the pipes.

Prediction of soil temperatures around buried, heated pipe networks is possible using equations developed by Kendrick and Havens [16]. Alpert et al. [2] found generally good agreement between estimated and measured soil temperatures for 34 points around a buried pipe network. The average deviation between estimated and measured soil temperatures was 0.9°C for a day with a soil surface temperature of 11.2°C and 2.1°C for a day with a surface temperature of 20.5°C. The Kendrick and Havens equation consistently overpredicted soil temperatures below the pipe network, especially on days with high surface temperatures, due to an implicit assumption in the equation that the soil temperature at infinite depth below the pipes is equal to the surface temperature.

HEAT DISSIPATION

Several investigators have measured heat loss rates from buried pipe networks. Measurements have been extrapolated to various pipe network configurations using theoretical heat conduction models for buried, hot-water pipe networks. Heat loss rates were then used to estimate the area of land required for dissipation of waste heat rejected by steam-electric power plants.

Measured Heat Losses

Measured heat loss rates from soil warming systems range from about 37.5 to 138 W m^{-2} in North Carolina without irrigation [7], from about 34 to 100 W m^{-2} in Pennsylvania and from 8 to 21 W m^{-2} in Oregon [15]. Average monthly heat loss rates for a soil warming system in Pennsylvania are presented in Table 3. The higher rates in the North Carolina study than in the Pennsylvania study probably are due to higher average pipe surface temperatures even though initial water temperatures were similar. Water had opportunity to cool 5°C in summer and over 20°C in winter while flowing through the pipes in the Penn State study. The low heat loss rates in the

Oregon study can be attributed to the relatively great burial depth (91 cm). A combination of both sub-soil and surface irrigation during a 50 day test period in North Carolina increased heat dissipation rates by an average of 24% from a range of 39 to 98 W m^{-2} to a range of from 45 to 127 W m^{-2}.

The diurnal variation in soil heat flow at a 135-cm and 5-cm depth on the heated and control plots are presented in Figure 2 for 21 to 22 June, 1975, along with the heat loss from the pipes buried at a 30-cm depth. Virtually no heat flow was recorded at 135 cm on either plot. Heat flow at the 5-cm depth was downward in the soil during mid-day on both plots. The heat flow at 5-cm depth on the heated plot from about 2200 to 0500 was upward and about equal to the heat loss from the pipes. On the control, heat flow at 5 cm was negligible at night. Obviously considerably more heat was lost from the pipes during the day than was measured at the 5-cm or 135-cm depths on the heated plot. Heat storage in the soil profile and heat transfer by mass flow in the soil, which is not measured by heat flux plates used to measure heat flow, probably account for this difference.

Heat Conduction Models

The basic model used in many studies to describe heat conduction from a buried, parallel pipe network was developed by Kendrick and Havens [16]. Simply stated, their model gives the rate of heat loss from the pipe network (q) in W m^{-1} of pipe length as

$$q = Bk(T_p - T_s)$$

in which k is the soil thermal conductivity in W $m^{-1}s^{-1}{}^\circ C^{-1}$, T_p is the pipe outer surface temperature in °C, T_s is the soil surface temperature in °C and B is a constant which is calculated from pipe spacing, pipe burial depth, outside pipe radius and the number of parallel pipes in the system. The Kendrick and Havens model assumes a steady-state system with a soil temperature equal to the soil surface temperature at an infinite depth below the pipe. A model with a more realistic lower temperature boundary condition, developed by Hulbert, *et al*. [17], has been used at Penn State in which

$$q = B'k\left[(T_p - T_s) - (T_g - T_s)d/L\right]$$

where T_g is the soil temperature below the pipes at some depth from the surface L, d is the pipe burial depth, and B' is another constant for a given pipe network geometry which can be obtained from graphs for many configurations. Using measured pipe and soil surface temperatures and measured soil thermal conductivities obtained with probes developed by Fritton *et al*. [18], both the buried pipe models were found to give similar results in the Penn State study.

Pipe and soil surface temperatures and soil thermal conductivity must be known to compute heat loss using the foregoing theoretical expressions.

Monthly average pipe surface temperatures were up to 3°C less than the water temperature within the polyethylene plastic pipe in the Penn State study for a Reynolds number for flow within the pipes of 1900 (see Table 3). Soil surface temperatures were also increased by soil warming by an average of 6.3°C. Skaggs, et al. [7] also reported surface temperatures were increased by soil warming in North Carolina. Thus soil surface temperatures cannot be assumed equal to air temperature or natural soil surface temperatures. Van Demark and DeWalle [1] discussed and tested a method for prediction of soil surface temperatures with artificially heated soil which could be used in predictions of heat loss for proposed soil-warming systems.

Soil thermal conductivity can be measured with thermal conductivity probes or an "effective" soil thermal conductivity may be calculated by setting measured heat loss rates equal to heat flow in one of the theoretical models. Conductivity probes may not totally account for the contribution of mass flow to heat conduction along steep temperature gradients in the soil. However, the wide variation of soil thermal conductivity with moisture content makes selection of appropriate values from the literature difficult.

Rykbost and Boersma [15] reported the development of a zone of dry soil around the heating cables used in their experiments due to water vapor migration away from the cables. The dry soil zone reduced the rate of heat conduction away from the cables and was difficult to rewet once it developed. Skaggs, et al. [7] indicated, however, that pipes with a radius greater than the heating cables will produce smaller temperature gradients and less rapid drying of the soil.

Land Area Estimates

Johns, et al., [19] and Rykbost, et al., [4] concluded, based upon results of the Oregon State University study, that the investment for soil-warming systems is probably too great to be offset by agricultural benefits alone unless high value vegetable crops are grown. Thus, it appears that soil-warming over large land areas must be justified, in part, by benefits derived from heat dissipation.

Research in the first Penn State study by Plummer and Rachford [1] indicated that 1,820 ha of land with 5-cm diameter pipe buried at 30-cm depth and 60-cm spacing would be required year-round to dissipate the waste from a 1500 MWe nuclear power plant. The total cost of such a soil-warming system was estimated to be 54% more than heat dissipation using natural draft wet-cooling towers and 40% less expensive than dry-cooling towers. This soil-warming system was an optimum least-cost system where the cost of extra nuclear fuel needed to generate electricity when the water returning to the power plant from the field was not sufficiently cooled was balanced against the cost of using a larger soil-warming land area to dissipate heat. Land area estimates for soil-warming using this optimization approach are well below those from other studies where total power plant heat load is simply divided by heat loss per hectare.

Skaggs, et al. [7] computed that 4900 ha of land with irrigation would be required to dissipate heat from a 1000 MWe power plant if 10-cm diamater pipe at a depth and spacing of 50 cm were used. They concluded that soil warming in North Carolina would not be economically competitive with conventional cooling methods. Sepaskhah, et al. [20] estimated land areas for dissipation of waste heat from a 1000 MWe power plant would range from 75,000 to 3,500 ha depending upon pipe network configuration and soil and climatic conditions. They concluded soil warming appears "...feasible as a part of an integrated waste heat utilization program in conjunction with a conventional cooling system."

CONCLUSIONS AND RECOMMENDATIONS

The crop response to soil-warming varies basically with climatic zones. In the cooler northern climates, crop response to soil-warming is favorable in spring, summer and fall as long as sufficient moisture and nutrients are available. Winter and early spring freezing of crops, including perennials, grown in heated soil may represent the major crop management problem in northern regions. In contrast, fall, winter and spring crop response to soil-warming is promising in warmer, southern climates. Use of greenhouses in winter in the southern regions looks promising, but supplemental heating may be required farther north. Crops for summer cultivation on heated soil in southern climes must be chosen carefully. Further research is needed on the development of cold tolerance in plants grown in heated soil and the effects of soil warming on insect activity, plant diseases and weed growth.

Prediction of average daily heat loss from buried, hot-water pipe networks appears possible using existing steady-state models, if appropriate values for soil thermal conductivity, soil surface temperature and the pipe surface temperature can be obtained. The contribution of mass flow to heat transfer in the soil should be studied further so that an "effective" soil thermal conductivity including the combined effects of mass and heat flow in the soil can be obtained. Soil surface temperatures are increased by soil warming but the magnitude of the increase depends not only on the temperature and configuration of the pipe network, but also on the heat budget at the soil surface. Heat exchange at the soil surface will depend on availability of water and the radiative and convective heat exchange within a crop canopy. Micrometeorological models of the crop canopy which permit forecasts of soil surface temperatures would be needed for routine operation of a soil-warming heat dissipation system.

The outside pipe surface temperature can only be assumed equal to circulating water temperature if turbulent flow exists in the pipe and the pipe wall thermal conductivity is large compared to that in the soil. It appears that polyethylene plastic pipe, which has a thermal conductivity equal to or less than that of most soils (about 0.25 $W\ m^{-1}{}^{\circ}C^{-1}$), will probably be used in soil-warming systems. Thus, allowance should be made for a temperature drop across the pipe wall in heat loss estimates where polyethylene pipe is used or turbulent flow does not occur.

The application of soil warming for either crop production or heat dissipation, or both, will ultimately depend on economic issues. Soil warming is technically feasible, but will never be employed unless costs compare favorably with alternative methods of crop production or heat dissipation. Costs of installing plastic pipes and the optimum hydraulic pipe network needed to reduce pumping costs are very important to determination of costs for soil warming systems used primarily for heat dissipation. Reduction of consumptive-use of water by using soil warming rather than wet-cooling towers could also become an important economic issue in the future. Mesoscale climatic changes produced by heat dissipation over large areas of warm soil relative to effects of essentially point-source cooling towers needs attention. Integrated systems for heat dissipation and wastewater disposal may also become desirable, since considerable economic advantage can be obtained by having unfrozen soil for wastewater infiltration in winter. A total systems economic analysis of all costs and benefits is needed to properly assess the future potential of soil warming.

ACKNOWLEDGEMENT

Soil-warming research conducted at The Pennsylvania State University was supported with funds from the National Science Foundation, RANN and USDI, Office of Water Research and Technology.

LITERATURE CITED

1. DeWalle, D. R. (ed.), An agro-power-waste water complex for land disposal of waste heat and waste water, Pa. State Univ., Instit. for Res. on Land and Water Resour., Res. Publ. 86, 195 pp., 1974.

2. Alpert, J. E., S. C. Van Demark, D. D. Fritton and D. R. DeWalle, Soil temperatures and heat loss for a hot water pipe network buried in irrigated soil, J. Environ. Qual., Vol. 5, No. 4, pp. 400-405, 1976.

3. Sullivan, W., Subsoil nuclear cooling tested, New York Times, 14 June, 1976.

4. Rykbost, K. A., L. Boersma, H. J. Mack, W. E. Schmisseur, Crop response to warming soils above their natural temperatures, Oregon State Univ., Agric. Exp. Sta., Special Rpt. 385, 98 pp., 1974.

5. Berry, J. W. and H. H. Miller, Jr., A demonstration of thermal water utilization in agriculture, U.S. Environ. Protection Agency, Environ. Protection Technol. Series, EPA-660/2-74-011, 237 pp., 1974.

6. Williams, G. G., TVA Programs - waste heat utilization in greenhouses and other agriculturally related projects, in, M. M. Yarosh (ed.), Waste heat utilization, Proc. Conf., Oak Ridge Natl. Lab., Oct. 27-29, 1971, Gatlinburg, Tenn., pp. 193-209, 1973.

7. Skaggs, R. W., D. C. Sanders, and C. R. Willey, Use of waste heat for soil warming in North Carolina, Trans, ASAE, Vol. 19, No. 1, pp. 159-167, 1976.

8. Decker, A. M., Plant environment studies with controlled soil temperature field plots, Proc., Workshop of U.S.-Australian Rangelands Panel, U.S. Dept. Agric., Misc. Publ. No. 1271, pp. 34-48, 1974.

9. Allred, E. R., Use of waste heat for soil warming and irrigation, Proc., ASCE Irrig. and Drainage Div. Conf., Logan, Utah, Aug. 13-15, pp. 287-301, 1975.

10. Landwirtschaftliche Zeitsehrift, Warmemull revolutioniert produktionstechnik, Nr. 44, vom 1, pp. 2088-2089, 1975.

11. Boyd, L. L., Asst. Dir., Agric. Exp. Sta., Univ. Minn., St. Paul, 55010, Personal correspondence with W. W. Witzig, Head, Dept. Nuclear Engin., Pa. St. Univ., 1977.

12. Bond, B. J. and P. L. Russ, TVA uses of waste heat in agricultural production, Conf. on Energy and Agriculture, June 16-19, 1976, St. Louis, Mo. 27 pp.

13. Skaggs, R. W., C. R. Willey and D. C. Sanders, Use of waste heat for soil warming in North Carolina, Paper 73-3530, ASAE, Winter Meeting, Dec. 11-14, 1973, Chicago, Ill. 30 pp.

14. Skaggs, R. W. and D. C. Sanders, Evaluation of the use of waste heat for soil warming in the Southeast - a summary, Biol. Agric. Engin., North Carolina St. Univ., Raleigh, N.C. 27607, 4 pp., no date.

15. Rykbost, K. A. and L. Boersma, Soil and air temperature changes induced by subsurface line heat sources, Oregon St. Univ., Agric. Exp. Sta., Special Rpt. 402, 105 pp., 1973.

16. Kendrick, J. and J. Havens, Heat transfer models for a subsurface water pipe, soil warming system, J. Environ. Quality, Vol. 2, No. 2, pp. 188-196, 1973.

17. Hulbert, L. E., H. B. Nottage and C. V. Franks, Heat flow analysis in panel heating or cooling sections, Trans., Amer. Soc. Heating and Ventilating Engin., Vol. 56, pp. 189-204, 1950.

18. Fritton, D. D., W. J. Busscher and J. E. Alpert, An inexpensive but durable thermal conductivity probe for field use, Proc., Soil Sci. Soc. Amer., Vol. 38, pp. 854-855, 1974.

19. Johns, R., R. Folwell, R. Dailey, and M. Wirth, Agricultural alternatives for utilizing off-peak electrical energy and cooling water, Washington State Univ., Dept. Agric. Econ., 123 pp., 1971.

20. Sepaskhah, A. R., L. Boersma, L. R. Davis and D. L. Slegel, Experimental analysis of a subsurface soil warming and irrigation system utilizing waste heat, Amer. Soc. Mech. Engin., Heat Transfer Div., Winter Annual Meeting, November 11-15, Detroit, Mich., 12 pp., 1973.

TABLE 1
DESCRIPTION OF SOIL-WARMING RESEARCH FACILITIES

Location	Heating System	Depth x Spacing cm	Heat Source Temperature °C	Soil	Irrigation	Research Emphasis	Source
Oregon (Oregon St. University)	heating cables	92 x 183 51 x 122 55 x 122	30-36	loam	sub-soil	Crops, open field and greenhouse, heat dissipation	[4]
Oregon (Springfield)	6.25-cm diam. pipe	60 x 150	21-49, varied seasonally	sandy loam	spray	crops, open fields and greenhouses	[5]
Alabama	heating cables	(25-30)x30	up to 32	--	sub-soil	crops, open fields and greenhouses	[6]
North Carolina	2.5-cm diam. pipe	50 x 50	38	sandy loam	spray and sub-soil	crops, heat dissipation	[7]
Maryland	pipe	9 x 17	10-30, varied on plots	silt loam	spray	crops	[8]
Minnesota	1.25-cm diam. pipe	30 x 91	35-40	loamy sand	sub-soil	crops	[9]
Minnesota	2.5-cm diam. pipe	30 x 60	power plant condensor water, about 32°C	sandy loam	--	crop production in greenhouses with soil and air heating	[11]
West Germany	5-cm diam. pipe	75 x 100	power plant condenser water	--	--	crops, heat dissipation	[10]
Pennsylvania	5-cm diam. pipe	30 x 60	38-40	sandy loam	wastewater spray	crops, heat dissipation	[1]

TABLE 2
AVERAGE MONTHLY INCREASE IN SOIL TEMPERATURE (°C) DUE TO BURIED HOT-WATER PIPES AT A 30-CM DEPTH IN PENNSYLVANIA

	Soil Depth (cm)					
Month	Surface	15	30	45	90	180
January	6.7	14.6	28.9	22.7	16.9	14.9
February	7.7	15.3	28.6	22.3	18.3	15.5
March	8.0	13.5	24.4	20.4	16.7	14.8
April	7.5	13.1	21.6	17.6	15.4	13.7
May	8.2	12.8	20.7	16.7	14.7	12.8
June	5.9	10.4	15.5	14.9	12.8	11.9
July	4.8	8.8	13.7	12.6	12.1	13.1
August	5.1	13.1	14.0	11.6	11.6	12.3
September	5.7	13.8	15.9	—	11.9	10.2
October	6.1	11.1	18.5	18.3	11.7	8.5
November	4.6	12.4	21.0	19.2	13.3	9.8
December	5.2	14.4	26.2	21.3	15.3	12.5
Mean	6.3	12.8	20.8	16.5	14.2	12.5

TABLE 3
AVERAGE MONTHLY HEAT LOSS RATES AND TEMPERATURE DROP ACROSS POLYETHYLENE PLASTIC PIPE FOR A SOIL WARMING SYSTEM IN PENNSYLVANIA

Month	Heat Loss ($W\ m^{-2}$)	Temperature Drop (°C)
January	91.4	1.8
February	79.6	1.4
March	79.4	2.7
April	66.0	2.2
May	54.0	2.0
June	50.0	1.9
July	56.9	1.2
August	48.4	1.3
September	—*	—*
October	63.4	2.1
November	67.3	2.9
December	83.3	2.9

*Data limited due to instrument malfunction

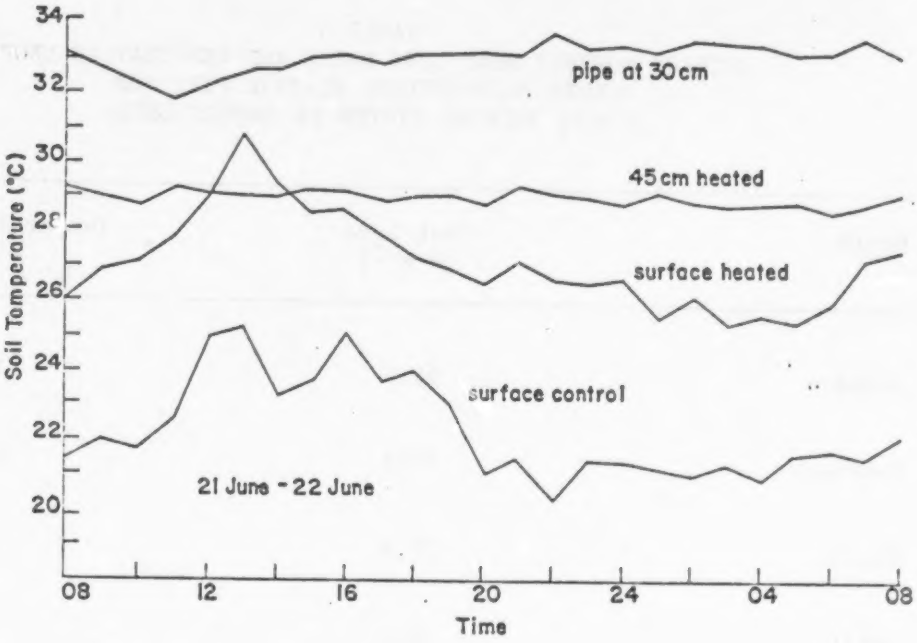

Fig. 1 - Soil temperatures on heated and control plots on 21-22 June, 1976 in Pennsylvania.

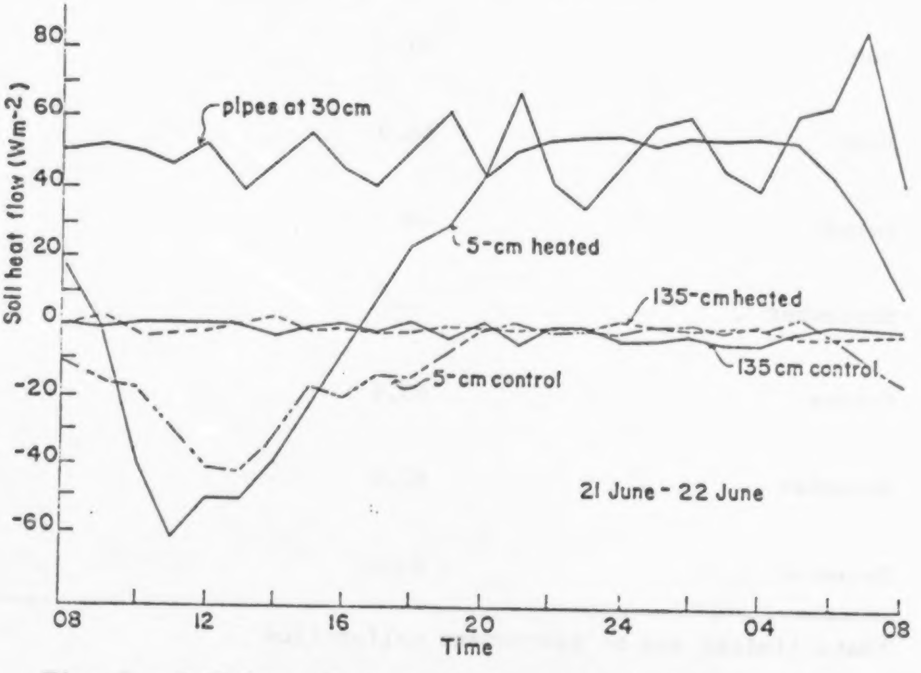

Fig. 2 - Soil heat flow on the heated and control plots on 21-22 June, 1976 in Pennsylvania.

3045-22

VII-A-87

POTENTIAL RESEARCH PROGRAMS IN WASTE ENERGY UTILIZATION

C. C. Lee
U. S. Environmental Protection Agency
Industrial Environmental Reearch Laboratory
Cincinnati, Ohio U.S.A.

ABSTRACT

A successful solution to the energy problem will depend, to a great degree, on the optimized use of converted energy forms and on the maximum utilization of by-product or waste energy and materials. Industrial waste energy in many cases can be utilized as energy sources for combustion air preheating, process heating, and thermodynamic engine cycles. Reducing and/or eliminating waste energy will increase energy efficiency and will lessen environmental problems throughout the chain of extracting, processing and supplying energy (i.e., waste energy utilization is a means of pollution control). This paper discusses potential research areas of interest to the Power Technology and Conservation Branch (PTCB) of EPA's Industrial Environmental Research Laboratory in Cincinnati, Ohio (IERL-Ci). The PTCB waste energy utilization program will assess the relative economic/environmental effects of using waste energy and assure that control technology is developed to the extent required. Emphasis will be on the industrial area but other waste-energy utilization or pursuits could be included except as related to the conventional electric utility industry. Our sister IERL at Research Triangle Park, N.C. has responsibility for the conventional utility industry. However, longer range advanced concepts related to utilities will be emphasized, by IERL-Ci for example, the integration of utilities with industries for combined production of electricity and space and process heating to minimize waste heat rejection.

INTRODUCTION

There is great concern that the United States will experience grave difficulties in acquiring adequate supplies of energy necessary to sustain economic growth throughout this decade and well into the next. The energy problem is exceedingly complex and involves many factors. For instance, the increasing concern for environmental quality has delayed the exploitation of nuclear energy and restricted the utilization of coal. A further constraint is the desire to conserve finite and depletable domestic supplies of gas, oil, coal, and uranium. A successful solution to the energy problem will depend, to a great degree, on the maximum utilization of by-products or waste energy materials. The developments in this area should be assessed by EPA to make certain that environmentally sound alternatives are considered and that EPA ORD will be in a position to advise EPA regulatory and enforcement programs. This paper will cover potential research areas of interest to the Power Technology and Conservation Branch (PTCB) of EPA's Industrial Environmental Research Laboratory in Cincinnati (IERL-Ci). These are primarily the industrial and longer range applications of waste energy utilization. The IERL at Research Triangle Park, N.C. has responsibility for the conventional utility industry.

In general, the sources of pollution in utility or industry sectors are from combustion and/or industrial processes. The control of these pollutants consists of several alternatives, such as physical and/or chemical scrubbers. Unfortunately, most of these controls are energy intensive and need a great deal of capital investment for installation and maintenance. Furthermore, some of these controls are not highly efficient. This difficulty and the projected shortage of environmentally clean fossil fuels have provided an incentive to reduce pollutants by saving energy or by utilizing recoverable energy effectively. Several studies of waste heat utilization and its related areas have been conducted by various agencies, such as ERDA, NSF, and FEA [1,2,3]. Their results have shown that significant amounts of energy can be saved and pollutants can be reduced. Their results also warrant that further research in this subject area to assess environmental impacts, qualitatively and quantitatively, is urgent and cannot be neglected.

It is envisioned that the results of the PTCB program will provide data for the Office of Air Quality Planning and Standards and Effluent Guidelines Staff to develop standards and regulations, and will assist federal, state and local energy and environmental agencies and industrial planners in developing methods and technologies for the most environmentally sound recovery and use of waste energy.

PROPOSED RESEARCH PROGRAM

Several potential alternatives capable of reaching our program goals are described in the following. It is considered that programs 1 and 2 are the first priority, 3 and 4 second priority, and 5 and 6 third priority. This is a ranking by a priority system of 1 through 4 which has been used for overall Power Technology and Conservation Branch priorities.

1. Environmental Assessment of Industrial Waste Energy Utilization

The objectives of this program are to determine (1) whether energy recovery is practical from various waste energy streams to be identified as a result of our contract study entitled "Waste Energy Inventory for Major Energy-Intensive Industries," (2) what recovery methods might be employed to obtain maximum thermal efficiency, (3) what environmental impacts would be caused by the implementation of these recovery methods, and (4) what percentage of pollutant reduction and energy savings should be achievable.

Any discussion of the waste energy generated by industry and discharged into the environment must begin with a discussion of the energy consumption by industries, because these are the sources of waste energy. Waste energy generation from a particular industry should be roughly proportional to that industry's energy consumption. Those industries, which consume the most, would be expected to contribute the most waste energy generation, and thus would be expected to have more potential for waste energy recovery.

Waste energy generated from electric power production is usually considered as a point source. An extensive study has been conducted both in quality and quantity, and a great deal of data on its recovery and utilization have been documented. However, because the needs and levels of process heat in industry are so numerous and varied, industrial waste energy is generated in a much more diffused manner from a wider variety of sources than thermal power plants. It may suffice to say that almost every chemical and/or physical change in industrial processes involves some degree of change in process heat application and waste heat generation, thus affecting waste energy recovery methods. Comparable data in these areas have not been fully developed. ERDA, presently, has a project to study industrial process energy consumption. EPA is expecting to complete a waste energy inventory for industries by the end of 1977. This proposed research program of waste energy utilization is a continuation of that EPA project. Emphasis will be placed on the environmental effects from the application of various waste energy recovery methods.

In determination of the practicability of waste energy recovery, there are several important factors which need to be considered:

(1) Quantity of waste energy and method of rejection;

(2) Quality of waste energy: for example, two processes may have the same amount of waste energy rejected to cooling water which reaches the same temperature, but if energy from one source is rejected with a higher temperature difference than the other, that energy has more thermodynamic availability or capacity for doing work and hence is more valuable.

(3) Degree of fluctuation in industrial device operation: some devices operate continuously with very steady conditions. Petroleum process heaters and glass furnaces are such devices. Other devices are operated with batch feeding over a set operating cycle. Metal melting furnaces are of this type. Still other devices are tied to an industrial process that is of an inherently fluctuating nature. Cement kilns and paper-mill boilers have constantly fluctuating operation dependent on the feed material properties and on process control adjustment.

Because of the above reasons, the alternative waste energy management methods and the potential beneficial uses for each waste energy source would be quite different, and thus the environmental impacts and/or pollution controls needed might be quite different as well.

While some study results [5,6] of waste heat utilization on some specific industries are available, there is very little available, to our knowledge, on quantities of potential waste energy recovery from entire specific industries, and even less on environmental impacts of the waste energy after being utilized. The lack of the required environmental data and the critical need for it in examining alternative waste energy management methods make this proposed research program vitally important. It is only through this study that environmentally sound systems can be developed, and that our desired objectives to reduce pollutants and save energy simultaneously can be reached.

It is well recognized that a significant amount of waste energy from industrial sectors is rejected to surroundings, causing thermal pollution to our environment. For example, approximately 866 X 10^{12} Btu/yr. from petroleum refineries [3] is rejected to surroundings through condenser cooling water. It was found that over 80 percent of waste energy is rejected in the 300-600° F temperature range. From a thermodynamic point of view, a large portion of this heat is recoverable and can be converted to mechanical work by means of proper cycles. ERDA [7] estimated that almost 13 quads, which is about 7 percent of total national needs, can be saved in the year 2000, if industrial energy efficiency is improved and waste heat is utilized. There are several approaches which would be applicable to waste energy recovery. These approaches include the following:

(1) Combustion Air Preheating:

Combustion air preheating is used extensively on larger industrial boilers. However, many industrial devices do not have air preheat because, in the past, fuels were cheap and the cost to install preheat was more than the fuel savings achievable. This method is believed to have the widest possible application. For example, a preliminary analysis of the waste gas energy recovery potential for an aluminum melting furnace is significant. The furnace has a very high stack temperature, 1225°K. Stack energy content is about 52 percent of the fuel input energy of 7 Mw. Installation of a combustion air preheater at 50 percent heat exchanger effectiveness could recover 43 percent of the stack gas waste energy. This would result in about a 23 percent reduction in fuel consumption. However, since preheating combustion air will increase flame temperature to some extent, the added NO_x formation needs to be identified [8]. It is believed that there are many other industries, similar to the above example, and that a significant amount of waste energy can be recovered by this means. The purpose of a study of this concept would be to classify the industries in which the combustion air preheating concept can be applied, to assess the energy-saving potential, and to assess the environmental impacts from each specific industry.

(2) Process Heat Utilization:

Many industrial processes make use of steam generated by heat from waste streams or transfer heat directly to the process. However, because fuel was cheap in the past, the full potential for utilization of waste energy in the process may not have been realized. One of the potential applications in this area is waste heat utilization from interstate pipeline pumping stations. Considerable horsepower in diesel and combustion turbine pumping engines is required to operate the nation's network of pipelines. Most pumping stations are located on pipelines within the industrial triangle lying between Pittsburgh, Chicago, and Birmingham. Significant amount of waste energy is generated by these engines. It is technically feasible to use this waste energy to generate steam for industrial use. For example, if one chemical plant producing 80 X 10^4 Kg/day of ethylene dichloride utilizes this steam supply, it could entirely eliminate operation of one of the three boilers in the plant and operate the second at only one-third of its present output. Therefore, the potential of transferring waste energy to process needs should be investigated to the extent possible. Again, the environmental effects by implementing this process heat utilization need to be studied, because it might produce different environmental effects from different process heat utilization.

(3) Thermodynamic Heat Engine Cycle:

Generally speaking, waste energy recovery by the first and second approach should be higher in efficiency than this third one. However, when waste energy cannot be used for combustion air preheating or be used in the process, it may be practical to apply the waste energy recovered to a thermodynamic engine cycle for generation of electrical power. Approximately 30 percent of waste energy can be converted into electrical energy by this scheme. Although several thermodynamic engine cycles can be applied to recover waste energy, a Rankine cycle with organic working fluid seems to be the most promising one. However, this is subject to further study to ensure that this Rankine cycle will produce the maximum efficiency without causing any harmful environmental effects.

A summary of waste energy management can be found from Figure 1. Major forms of waste energy having potential use as heat sources are: (a) hot stack gases from furnaces and boilers, and (b) hot water from cooling of processes directly through jackets or through heat exchangers, cooling towers and condensers. The figure shows three potential waste energy recovery approaches and two ultimate receiving media, either air or water.

To show the idea of waste energy recovery and utilization, an example of a thermodynamic engine cycle was given in this paper. Figures 2 and 3 show the flow chart and temperature-entropy diagram of the Rankine cycle with normal pentane as the working fluid. The working fluid in this cycle is heated to its vaporization temperature then to its superheated state at constant pressure process (line 2-3-4-5-6). This dry saturated working fluid is then introduced into a turbine and expands isentropically to low pressure to produce mechanical work (line 6-7). The turbine effluent is cooled and condensed in a constant pressure process (line 7-8-1). The condensed fluid is then recycled by means of a pump (line 1-2).

The heat source for the cycle is from waste heat of industrial processes. For example, heat rejected from condensing or cooling of process steam can be used to heat and vaporize the Rankine cycle fluid. Hot combustion gas from fuel-fired heater stacks can be a heat source for superheating of the Rankine cycle fluid in its vapor phase. With this particular working fluid, the turbine effluent vapor is still in a superheated state as indicated on Figure 2 at state point 7. The cycle efficiency can be improved by recovering part of this energy (line 7-8) to heat the feed liquid going to the boiler (line 2-3).

Assume that this Rankine cycle, using waste energy from a petrochemical plant as heat sources, has turbine conditions of 410°F, 250 psia and condenser of 14.7 psia with sink temperature of 97°F, and working fluid of normal pentane with a flow of 1,000,000 pounds per hour. Figure 2 and n-pentane property tables were used to obtain the necessary thermodynamic properties. It was calculated that the waste energy from this petrochemical plant can produce 145 x 10^6 kwh/yr. of electricity, save 1413 x 10^6 Btu/yr. of input fuel, reduce 303 ton/yr., 175 ton/yr., and 25 ton/yr., of SO_2, NO_x, and particulate pollutants respectively. This pollutant reduction calculation was based on the assumption that the emission level is equal to the level set by New Source Performance Standards (NSPS). Also, 505 x 10^9 Btu/yr. of thermal pollution can be eliminated.

The Rankine cycle low level waste heat recovery system offers an attractive means of reducing pollutants and conserving energy simultaneously. This potential application may be found in the energy-intensive industries, such as chemical, petrochemical, petroleum, ferrous and non-ferrous metals, paper and pulp, etc. Other low temperature sources, such as geothermal and solar energy, may also prove to be applicable.

Although waste heat utilization will offer so many advantages, the environmental aspects of industrial Rankine bottoming cycles have not been fully documented and need to be assessed by EPA as these systems are developed so that controls will be inherent in their design. In most cases, thermal pollution will be reduced but added environmental risks may result. Examples include the effects of Rankine cycle working fluid, which is usually a volatile organic compound, on heat exchangers. Will there be any volatile compound fugitive emissions in normal operation? What would be the environmental hazards of chemical reaction from the flue gas and organic working fluid in case of leaks? What would be the environmental problems because of working fluid disposals? These are only a few questions which should be asked. Answers are needed.

2. Industrial Waste Hydrocarbon Recovery and Utilization

Most of the activities of pollution control agencies have been directed toward control of principal emission sources, such as SO_2, NO_x, and particulates, with little attention thus far to those smaller sources, such as sources emitting hydrocarbons (HC), resulting from various industrial processes, particularly from chemical plants and petroleum refineries. Because of certain small sources which when lumped together constitute a major source which was estimated at 47 billion pounds emitted in 1970 [9] the potential emission problems of these sources should be a matter of increasing concern.

The afterburner system to control HC emission is one of the earliest techniques developed and is probably still the most nearly universally used control method being used to control not only volatile organics, but also odors and particulate hydrocarbon emissions. The afterburner functions by incinerating a waste gas stream in a direct flame produced by the combustion of an auxiliary fuel, mostly natural gases. The need of auxiliary fuel for this approach has been dictated by two factors: (1) waste gas streams generally have low heating values, and (2) organic vapors are frequently diluted with air to well below lower combustion limits in order to satisfy fire and safety requirements. A schematic diagram of this thermal incineration is shown on Figure 4.

From energy conservation and pollution control points of view, the current afterburner system to control HC is a most uneconomical and inefficient approach. Some of the apparent drawbacks to the use of afterburners are readily identified as the following.

(1) In order to have better combustion efficiency, the entire waste gas stream must be heated to approximately 1400°F, regardless of the concentration of the combustible material. Since the concentration of organics in most waste streams is usually low, this necessarily means that a large portion of the fuel used is for a totally unproductive purpose, i.e., heating air. In a typical installation, natural gas consumption can easily reach 3 percent of the waste gas stream volume.

(2) The addition of natural gas to help combustion of HC means a double waste of our natural resources, i.e., natural gas and combustible HC. It was estimated that approximately 0.9 trillion scf of natural gas [9] annually, which is about 3.7 percent of the entire national natural gas need, is consumed for nationwide afterburner systems.

(3) Because HC could contain toxic elements, it would be very hazardous to human health, if there is any malfunction or incomplete combustion in the afterburner systems.

(4) It is highly possible that the afterburner system itself will present some safety problems. These include the explosion potential, toxic elements released from the system, formation of smoke, noise, and the emission of air pollutants during flaring.

Until recently, the low cost and ready availability of natural gas encouraged the use of afterburners. Unfortunately, this situation has now changed. The current and projected shortages suggest that natural gas supplies are or may be curtailed in some areas of the country, and the installation of new gas-consuming equipment thus may become increasingly restricted. In addition, the priority systems that are being developed for gas distribution may not consider air pollution control a significant factor. In other words, industrial area or statewide curtailments of natural gas may not take into account air quality control needs. As a result, we would begin considering the possibility of compliance problems that directly result from reduced natural gas availability or energy conservation and pollution control.

One of the potential approaches to save the energy is to recover heat from flue gas if HC are burned. Recovery methods include heat exchange between hot flue gas and incoming cool HC stream, and the use of the heat in other processing or heating loads, such as in generating steam for plant or process heating, for power generation, etc. Further research and development is needed to develop environmentally sound technologies to recover and utilize HC.

3. Detailed Assessment of Electric Utility-Industrial Integrated Use Concepts

Our preliminary contract study entitled "Environmental, Economic, and Conservation Aspects of Integrated Energy Use Applications" with Georgia Institute of Technology, has found that this integrated energy use application will substantially reduce environmental pollution and save energy. Tentative conclusions have shown that the integrated energy use application appears to make technical sense because no new technology is needed, has the potential to reduce national energy consumption by 15 percent or more, and thus to reduce pollutant emissions considerably, and provides lower cost than the conventional separate systems. Since this contract is a conceptual study oriented program, further study is needed to ensure that appropriate environmental data are available for technology development. Therefore, we are proposing a continuation of this program for a detailed assessment of the most promising approach of integrated energy use indicated in the Georgia Tech. study. It appears now that emphasis should be placed on the combination of in-plant power generation and process heat production due to the foreseeable near term implementation.

It has long been recognized that electricity and steam can be generated together in the same plant with a higher thermal efficiency than they can be generated separately. The reason for this is that in a central station of a fossil fuel-fired steam power plant, about one-third of the energy of the fuel is converted into electricity and two-thirds escapes in the form of thermal discharges. Some of this thermal discharge consists of flue gases from the combustion process entering the atmosphere at temperatures of 300-600°F. Most of the discharge results from the condensation of steam and the subsequent rejection of this heat to bodies of water or the atmosphere at temperatures of 70-100°F. Industry, when it generates steam and electricity together, increases the temperature of the reject heat from the power cycle to useful levels which are, in fact, sufficient to provide the steam required in processes. The result is that industrial process steam serves as the sink from the power cycle, thus decreasing thermal discharge substantially. The effective thermal efficiency of the industrial power plant generating steam and electricity together is about 60-75 percent, whereas a central station steam power plant is today about 35 percent efficiency.

As a result of the large amounts of steam used in industrial processes (about 7 percent of all the energy used in the U.S.), considerable amounts of power can then be generated by this technique with half to two-thirds of the fuel currently used in central station plants.

In-plant generation of electricity in industry potentially has numerous national advantages. The most important of these are to conserve energy, reduce pollution as a result of lower fuel consumption, and increase reliability and security by having a multi-source electrical generation system rather than a smaller number of larger systems. The thermodynamic potential for in-plant generation depends strongly on the types of systems. In most industries, there is good potential for combined production of electricity and steam by utilizing a steam and/or gas turbine topping cycle for higher efficiency.

There are several combinations, such as steam turbine topping, gas turbine topping, combined gas and steam turbine cycle, and diesel engine topping system, to accomplish the in-plant power generation purposes. The equivalent efficiency for the power generated is about 70 percent compared to 35 percent of simple unit. The efficiency is high as a consequence of all the rejected heat from the cycle in the turbine exhaust being used for the process. The only real system losses are boiler combustion gas losses, generator losses, and a portion of turbine losses which do not remain in the fluid streams. The heat rate also presumes that full exhaust stream enthalpy is recovered as usable heat. It was estimated that the maximum thermodynamic potential for in-plant power generation in 1974 is the fuel equivalent of about 550,000 bbl oil/day, 150,000 bbl oil/day, and 2,200,000 bbl oil/day for steam turbine, gas turbine and diesel engine topping systems, respectively [3]. Schematic diagrams of a steam turbine topping and a combined gas and steam turbine cycles are shown on Figures 5 and 6, respectively. Referring to Ref. 3 of in-plant power generation from petroleum refinery industries, a rough estimate of energy savings and pollutant reduction is shown in Table 1. Again, the pollutant reduction estimate was based on the New Source Performance Standard (NSPS) level.

As indicated in the above estimates, increased in-plant generation can lead to substantial overall energy savings and will lead to reduce environmental effects. However, because of differences in types of fuel and types of fuel burning equipment and location of fuel burning to generate electricity, the environmental effects of this approach have not been fully evaluated. It may be expected that in addition to conventional pollutants, SO_2, NO_x, and particulates, there may also be more exotic species, such as fluorides, chlorides, etc., originating from combustion emissions. Environmental impacts and problems with removing potentially harmful species are magnified by the close proximity of source and receptor. Emissions which have traditionally been considered on a point source basis may now require treatment as a quasi-area source because of increased numbers of point sources. Also, the fuel composition in these applications could be highly variable. This may require a new generation of control techniques.

4. Stack Gas Energy Extraction Vs. Plume Formation

Another potential area for energy recovery is the heat released via stacks related to combustion. Fossil-fuel electric power plants, industrial incinerators, and individual industrial processes, such as steel making and calcining of minerals, constitute major candidates for evaluation of stack waste heat recovery and reuse.

It was found that the stack waste heat from the petroleum industry is approximately 67 x 10^{12} Btu/yr. at temperatures of 300-600°F and 261 x 10^{12} Btu/yr. at 600-1000°F [3]. It was calculated that if proper organic Rankine cycles are applied to this waste heat, 177 x 10^9 kwh/yr. of electrical power [3] can be produced and significant amounts of pollutants can be reduced because of less fuel consumed. However, there is an upper limit of energy extraction from stack gas because of conditions required for proper plume formation out of the chimney. Some potential problems can readily be identified as the following.

1. The influence of heat recovery on plume buoyancy reduction and hence, on plume rise and the subsequent ground level ambient concentration, of SO_2, NO_x, and particulates is significant.

2. The effects of heat recovery are not only on stack gas temperature but also on the humidity in the plume. There is a possibility that heat recovery will cause the acid dew point to be reached within the plume and thus permit the direct emission of acid gases of sulfur and nitrogen. This, would affect ambient sulfate and nitrate concentrations and cause corrosion to materials.

3. Item 2 can also affect the frequency of occurrence of visible plumes because of enhanced condensation. Although not strictly a pollution problem as far as health effects are concerned, visible steam plumes are not aesthetic and can be considered as a type of insult to the environment.

The information on this subject is very limited and has received little attention in the literature. From environmental and energy conservation points of view, further study is essential in order to have maximum heat extraction from stack gas without causing any environmental effects. Emphasis should be placed on: (1) thermodynamic property effect on plume formation, (2) environmental impact from plume redistribution, (3) possible material corrosion, (4) potential of applying aerodynamic chimney control devices (this technique was used in Europe) to help plume distribution.

5. Environmental Assessment of Thermal Energy Storage

Commercial thermal energy storage (TES) systems will be accepted first by industry, according to a recent General Electric Company [11] study. TES systems include: storage well (injection of warm water into the ground for storage); sensible heat storage, such as solar ponds, fuel oil/granite mixtures, and heat transfer fluids; latent heat storage, such as salts and salt eutectics, including fluorides; and thermochemical heat storage in reversible chemical reactions, such as:

$SO_3 \rightleftarrows SO_2 + 1/2O_2$, $CH_4 + H_2O \rightleftarrows CO + 3H_2$, $CaO + H_2O \rightleftarrows Ca(OH)_2$, $NH_4HSO_4 \rightleftarrows NH_3 + H_2O + SO_3$, and ammoniated paired salt decompositions.

GE has conducted extensive research on the heat storage well concept [11] and has found that this concept is technically feasible. Some of their conclusions are excerpted as the following: (1) it can reduce annual energy consumption of the U. S. by 10-15 percent; (2) preliminary analysis indicates that three-fourths of the energy stored can be recovered even after 90 to 180 days of storage in a large well; and (3) a combustion gas turbine system with heat recovery and storage shows a cost savings of about 25 percent and energy savings of over 35 percent, compared to systems with no storage.

One of the possible applications of this storage well concept is to the EPA integrated energy use program. Basically, the EPA program is to match heat and power load well enough, so that heat storage is not necessary. However, if, for some reason, the heat production is more than the need for industrial processes, use of storage wells would increase the flexibility of integrated energy systems.

According to GE, the U. S. Geological Service has budgeted $100K per year for fiscal years 1977-80, and ERDA has budgeted $200K per year for the same years to continue the research efforts. However, the environmental effects of this area have never been studied before. Some of the potential environmental problems might be similar to the problems encountered in geothermal energy applications. Injection technology is needed and its environmental viability must be proven. Also when the storage well discharges hot water to the surface, some pollutant species from underground might cause pollution to the above ground environment.

Since other agencies have committed funds for technology development for storage wells, it is EPA's obligation to assess the environmental impacts and to develop pollution controls, if needed, so that pollution control can keep pace with storage well technology development.

Other TES seems relatively unimportant for the near term compared to storage well. However, environmental effects of the other concepts need to be studied at an appropriate time. Some of their environmental problems include the effects of molten fluoride container rupture. Will there be fluoride fugitive emissions in normal operation? What would be the environmental hazards of a reversible chemical reaction storage using SO_3? What will the environmental impact be for solar ponds? These are only a few of the questions which should be asked and answered.

6. Environmental Assessment of Advanced Power Transmission Vs. Decentralization of Power Generation

The use of energy in the form of electric power was 26 percent of the total annual energy consumption in the U. S. at the end of 1974 [12] and is estimated to increase to 50 percent in the year 2000. The current average power transmission distance from a power plant to end users is about 80 miles, with the longest distance about 800 miles, and the trend is to increase the average distance, to some extent, according to the data from the Electric Power Research Institute (EPRI). The EPRI data also show that the power transmission efficiency is approximately 93 percent, and the cost for transmission facilities is about 40 percent of the entire power plant investment. Based on these data, power transmission will consume about 2.7 x 10^{15} Btu or 1.5 percent of the national energy need, which is about 180 x 10^{15} Btu [13] in the year 2000.

To reduce the energy consumption for power transmission line losses, technologies under development include two major items: decentralization of power generation, such as in-plant power generation and/or integrated energy use application, and advanced transmission line technology, such as ultra-high voltage transmission lines (both AC and DC) and superconducting (cryogenic) transmission lines. The question is which technology will provide more energy savings and less unwanted pollutants--decentralization of power generation or advanced transmission line technology. Comparable data are unavailable at the present time. It is important to initiate a program for a comprehensive study of advantages and disadvantages of these two major technologies from various points of view. As far as the environmental effects are concerned, in general, decentralized power generation should be similar in environmental effects to conventional power systems. However, advanced transmission line technology seems to have more hazardous environmental effects. For example, both occupational and general population groups will be exposed to the potential hazards associated with this technology. Workers involved in production, construction and maintenance activities will be exposed to hazardous insulator materials (for example, sulfur hexafluoride and PCB substitutes) and cryogenic fluids. Workers and local population may be exposed to strong electric fields, increased ozone levels and audible noise. The health effects of concern include adverse changes in biological processes caused by strong electric fields, toxic effects of sulfur hexa-fluoride or other new insulator materials, as well as possible induction of shock irritability and increased pulmonary dysfunction.

Nevertheless, advanced transmission line technology could provide significant energy savings, compared to decentralization of power generation. Therefore, it is essential to initiate a program to study their differences, particularly from the environmental point of view.

Priority Rating of Research Areas

The above areas were rated by a rating system shown on Table 2. In this rating system, potential energy saving and pollution reduction carry the same major rating weight with 40 percent for each of them. The cost effectiveness and immediateness are assigned 10 percent each. This rating weight reflects the major thrust of our program - energy conservation and pollution reduction. Both of these factors can be a measure of environmental significance. Energy conservation will reduce pollution throughout the energy production and distribution system while the reason for emphasizing the pollution problems of the specific concept are obvious. The factors of cost effectiveness and immediateness is intended to weigh the priorities somewhat to the more practical and soon to be commercialized technologies. For example, if two programs have the same amount of rating from energy conservation and pollution reduction aspects, then the cost effectiveness and immediateness should be able to provide enough leverage to decide which program is more valuable for EPA.

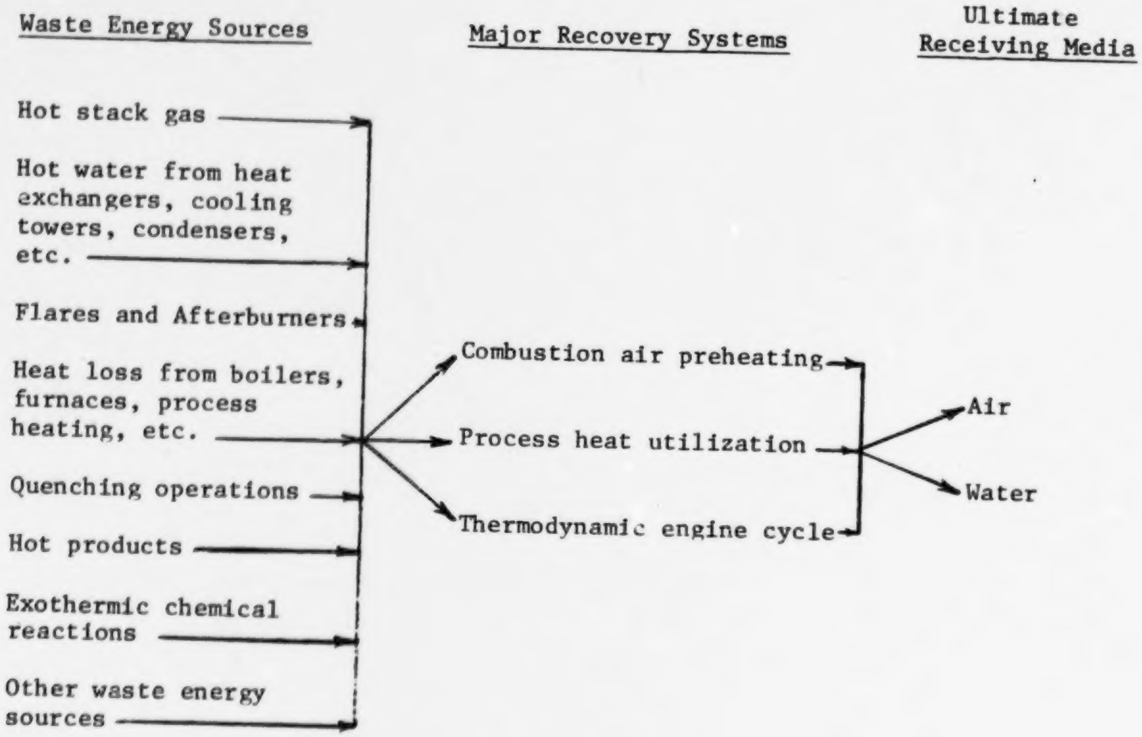
Waste Energy Sources
Major Recovery Systems
Ultimate Receiving Media
Hot stack gas
Hot water from heat exchangers, cooling towers, condensers, etc.
Flares and Afterburners
Heat loss from boilers, furnaces, process heating, etc.
Quenching operations
Hot products
Exothermic chemical reactions
Other waste energy sources
Combustion air preheating
Process heat utilization
Thermodynamic engine cycle
Air
Water

Figure 1. Waste Energy Management

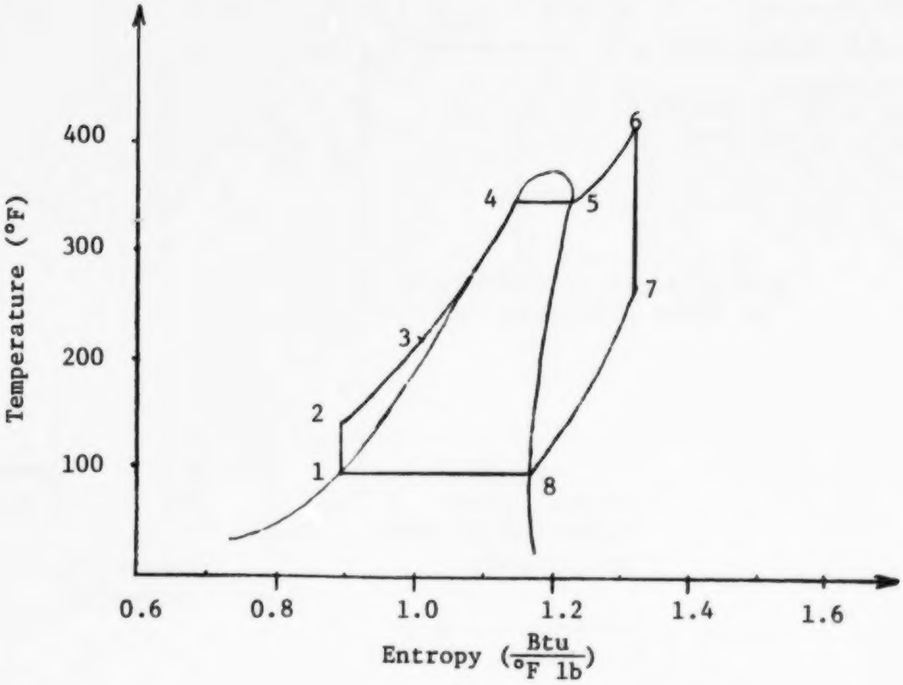

2-3-4-5-6: Constant pressure heat transfer from waste heat stream.

6-7: Isentropic expansion in the turbine to produce mechanical work.

7-8-1: Constant pressure cooling process.

1-2: Isentropic pumping process.

Figure 2. Organic Rankine Cycle (n-Pentane Working Fluid)

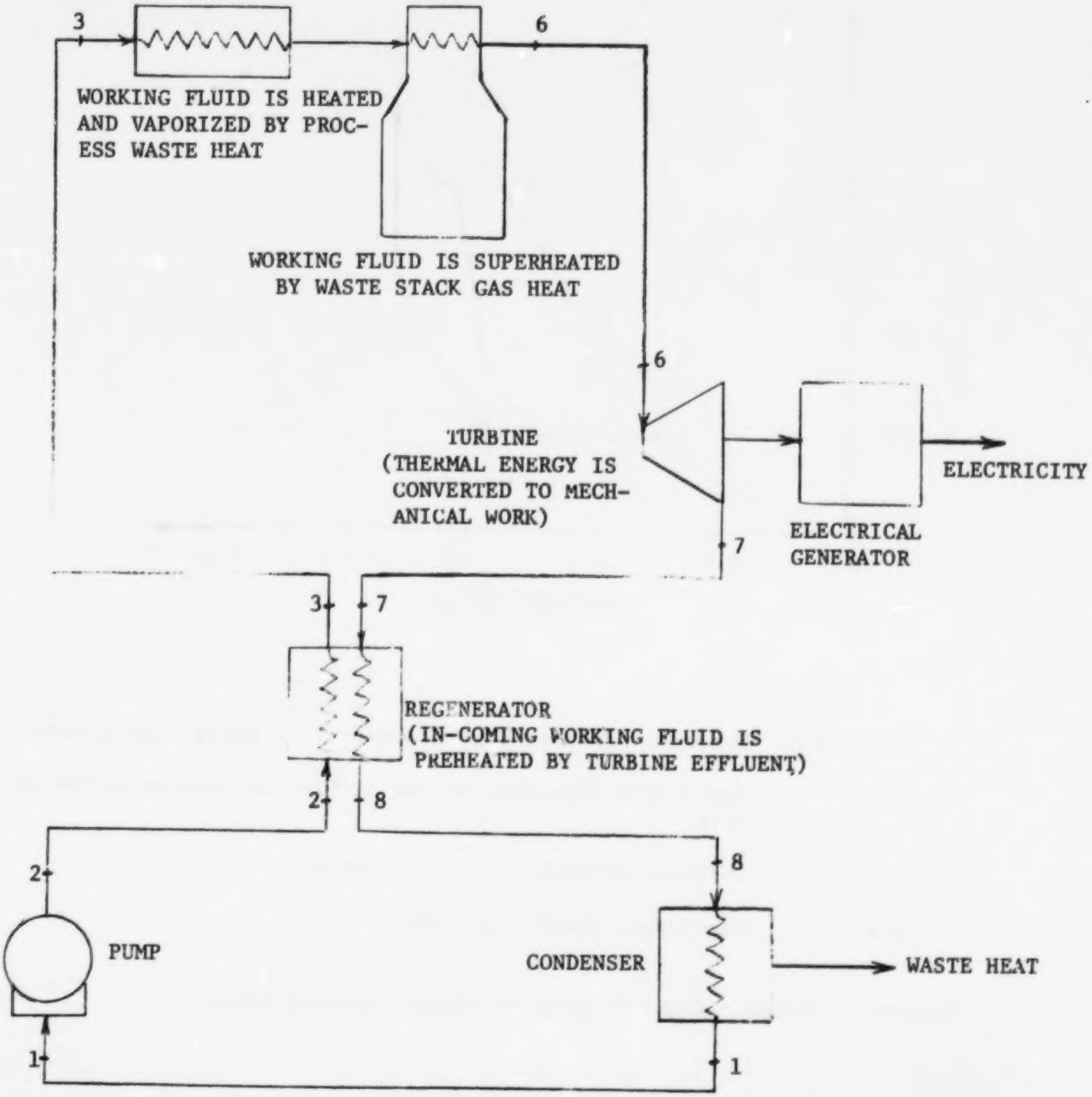
3
6
WORKING FLUID IS HEATED AND VAPORIZED BY PROCESS WASTE HEAT
WORKING FLUID IS SUPERHEATED BY WASTE STACK GAS HEAT
6
TURBINE (THERMAL ENERGY IS CONVERTED TO MECHANICAL WORK)
ELECTRICITY
ELECTRICAL GENERATOR
7
3
7
REGENERATOR (IN-COMING WORKING FLUID IS PREHEATED BY TURBINE EFFLUENT)
2
8
2
8
PUMP
CONDENSER
WASTE HEAT
1
1

Figure 3. Organic Rankine Cycle System (Station Numbers Correspond to the Numbers on Figure 2)

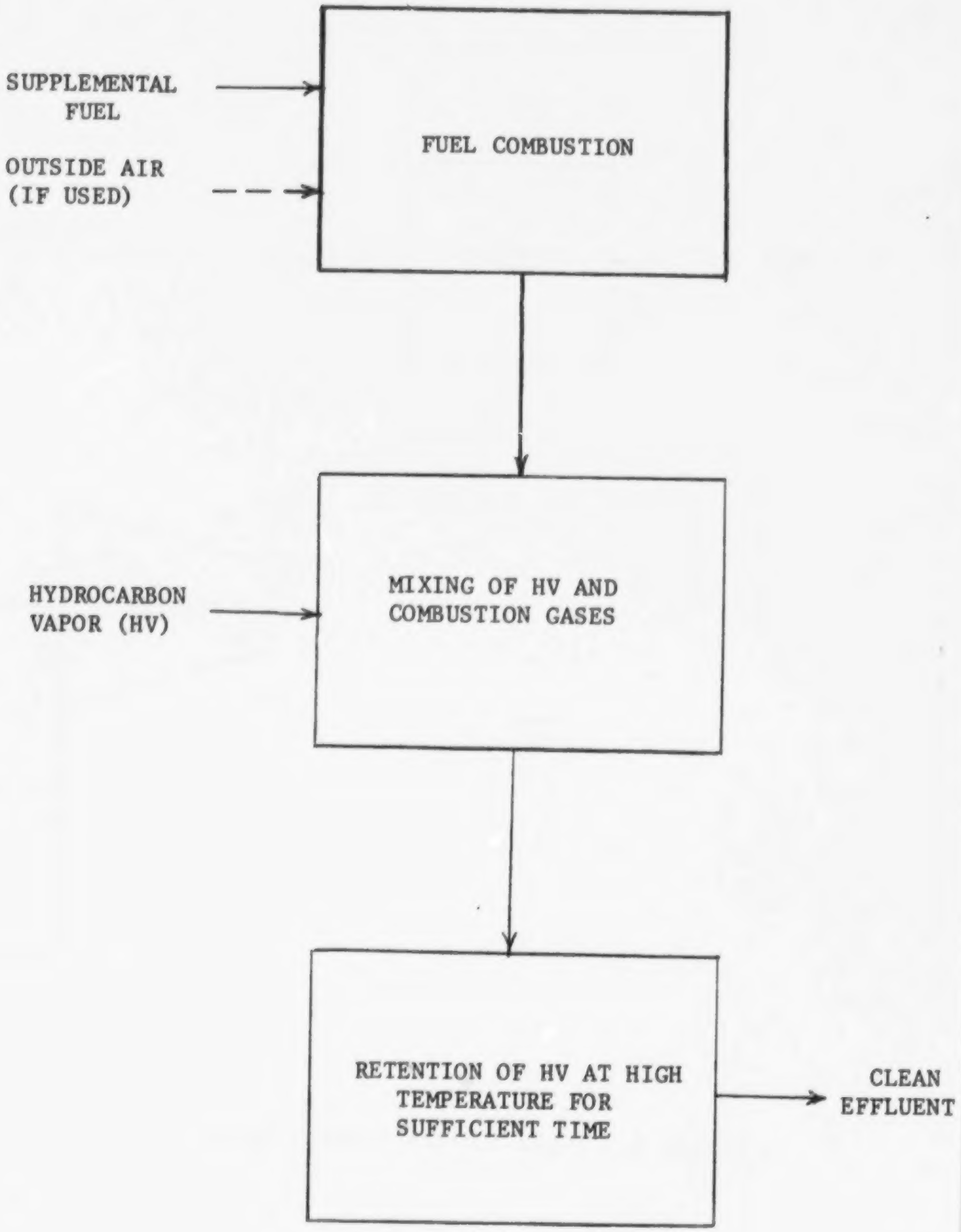
SUPPLEMENTAL FUEL
OUTSIDE AIR (IF USED)
FUEL COMBUSTION
HYDROCARBON VAPOR (HV)
MIXING OF HV AND COMBUSTION GASES
RETENTION OF HV AT HIGH TEMPERATURE FOR SUFFICIENT TIME
CLEAN EFFLUENT

Figure 4. Steps Required for Successful HV Incineration

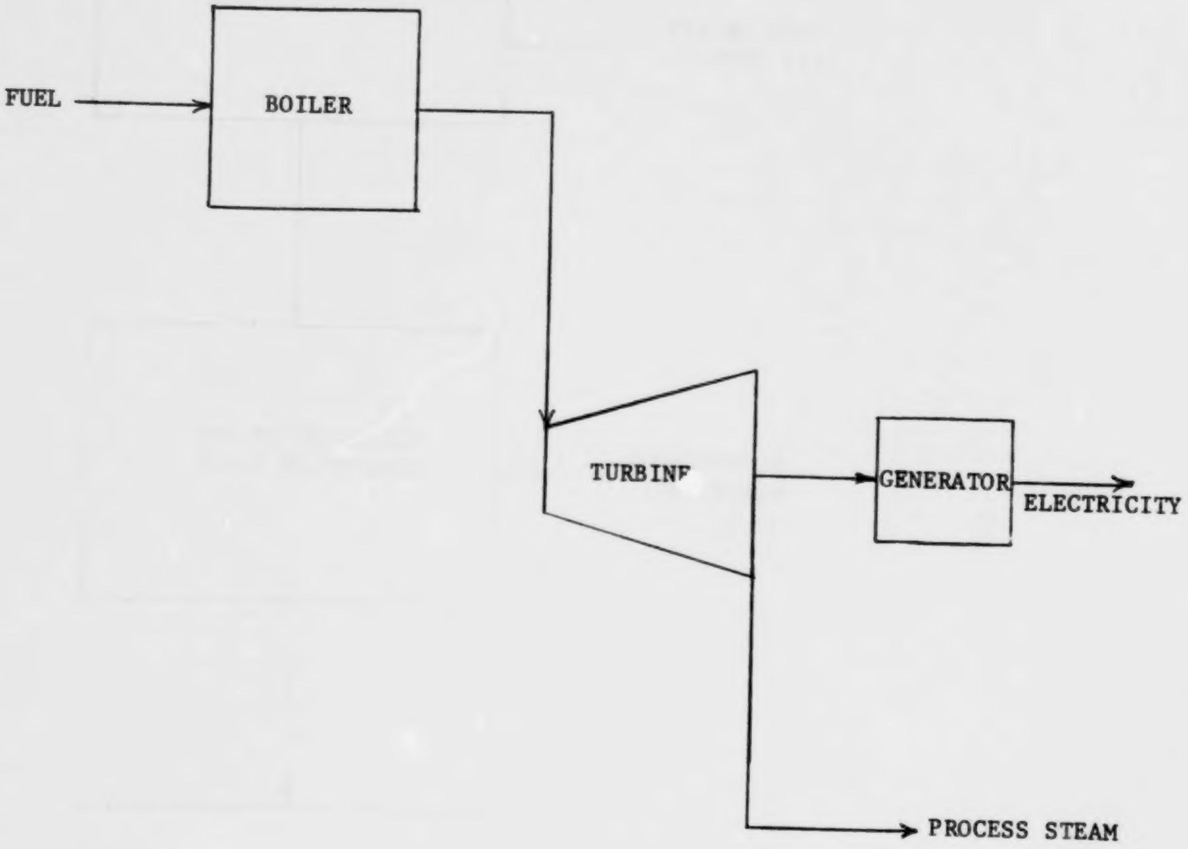
FUEL
BOILER
TURBINE
GENERATOR
ELECTRICITY
PROCESS STEAM

Figure 5. Steam Turbine Topping Cycle

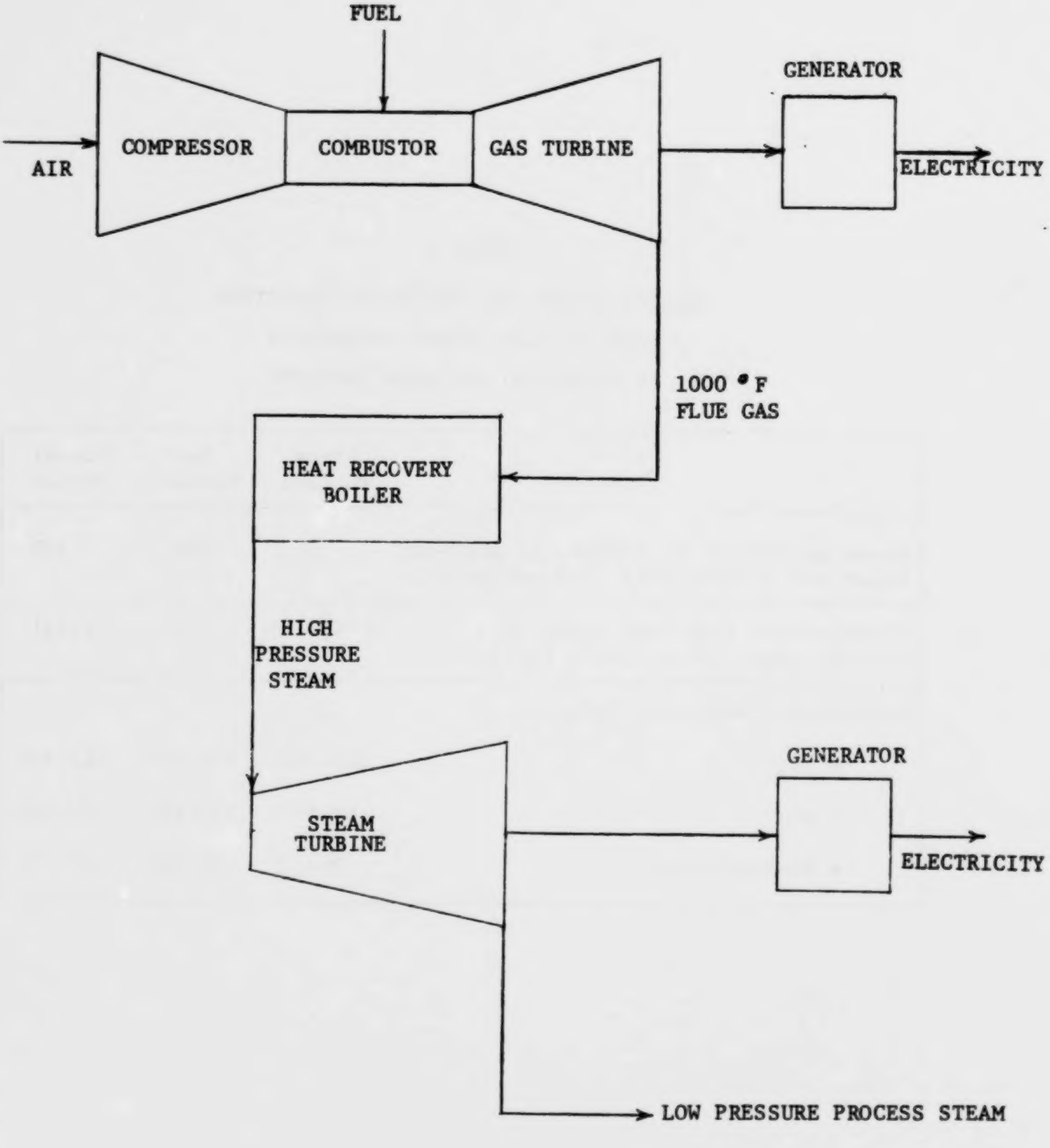
FUEL
AIR
COMPRESSOR
COMBUSTOR
GAS TURBINE
GENERATOR
ELECTRICITY
1000 °F
FLUE GAS
HEAT RECOVERY
BOILER
HIGH
PRESSURE
STEAM
STEAM
TURBINE
GENERATOR
ELECTRICITY
LOW PRESSURE PROCESS STEAM

Figure 6. Combined Gas and Steam Turbine Topping Cycle

TABLE 1

ENERGY SAVING AND POLLUTANT REDUCTION FROM IN-PLANT POWER GENERATION IN PETROLEUM REFINING INDUSTRY

	Steam Turbine	Gas Turbine	Diesel Engine
Power generation by topping of process steam and process heat (10^9 kwh/yr.)	5	196	397
Energy saved from fuel input to central power plant (10^{12} Btu/yr.)	183	706	1,431
Pollutant reduction (ton/yr.):			
• SO_2	109,800	423,600	812,400
• NO_x	64,050	247,100	473,900
• Particulates	9,150	35,300	67,700

TABLE 2. PRIORITY RATING ON PROPOSED WASTE HEAT UTILIZATION PROGRAMS

	Relative Weighting	Waste Energy Utilization	Waste Hydrocarbon Utilization	Integrated Use Application	Stack Gas Energy Extraction Vs. Plume	Thermal Energy Storage	Power Transmission Vs. Decentralization
1. Energy Conservation Potential							
a. Incentive for energy conservation, e.g., large energy user or user of fuel in short supply.	20	20	20	20	20	20	20
b. Potential for energy saving or increase in efficiency.	10	10	7	10	7	10	7
c. Potential pollution control energy savings.	10	10	10	10	7	7	7
2. Pollution Reduction Potential							
a. Seriousness of pollution problems in project area.	20	15	15	10	10	10	10
b. Potential for developing required control technology designed to remove desired pollutants to operate reliably, and to discharge acceptable effluents--or for reducing pollution by the major process change.	10	10	10	7	10	10	7
c. Breadth of applicability to other areas.	10	10	10	10	10	5	7
3. Cost Effectiveness, Profit Potential, Etc.	10	10	10	10	10	7	7
4. Immediateness of Potential Impact of the Technology	10	10	10	10	10	5	5
TOTAL	100	95	92	87	84	74	70
COMMENTS		←→ First Priority		←→ Second Priority		←→ Third Priority	

REFERENCES

1. "An Assessment of Industrial Energy Options Based on Coal and Nuclear Systems," ORNL for ERDA contract, ORNL-4995, July 1975.
2. "High Efficiency Decentralized Electrical Power Generation Utilizing Diesel Engines Coupled with Organic Working Fluid Rankine Cycle Engines Operating on Diesel Reject Heat," Thermo Electron for NSF contract, TE 4186-27-75, November 1974.
3. "A Study of In-plant Electric Power Generation in the Chemical, Petroleum Refining and Paper and Pulp Industries," Thermo Electron for EPA contract, Report No. TE 5429-97-76.
4. "Patterns of Energy Consumption in the United States," Stanford Research Institute, 1972.
5. "Proper Waste Heat Utilization Reduces Air Pollution and Saves Energy," Ken J. Suoboda and H. J. Klooster, presented at the 69th Annual Meeting of APCA, June 27 - July 1, 1976.
6. "Sulfuric Acid Plant Rankine Cycle Waste Heat Recovery," G. P. Lewis, etc., presented at the 11th Intersociety Energy Conversion Engineering Conference Proceedings, Volume II, September 12-17, 1976.
7. "A National Plan for Energy Research, Development and Demonstration," ERDA-48, Volume 1 of 2, June 1975.
8. A private conversation with KVB.
9. "Afterburner System Study," Shell Development Company, NTIS, PB-215 560, August 1972.
10. "Flare Systems Study," EPA 600/2-76-079, March 1976.
11. "Role of the Heat Storage Well in Future, U. S. Energy Systems," General Electric Company, GE 76 TMP-27, October 1976.
12. "Energy Fact Book--1976," Tetra Tech, Inc., for Navy, Feburary 1976.
13. "The 1975 Energy Management Guidebook," McGraw Hill, Inc., 1975.

22

Session VII B

Numerical Modeling III

VII-B-111

omit

ABSTRACT

MODELING OF A HEATED PLUME DISCHARGE FOR COMPLIANCE WITH WATER QUALITY STANDARDS

An industrial facility discharges heated water from a once-through cooling system to a river which has been classified as a cold water fishery. Because trout are natural to the area and the water quality standards on temperature rise are strict, the discharge has resulted in violation of the water quality standards. In the past five years, this industry has made major advances in the reduction of the heat load to the river system. Nevertheless, under certain river flow and temperature conditions, violations of the water quality standards at the mixing zone boundaries still occur.

Industry determined to perform a study of the river system and the impact of its discharge. These objectives necessitated the development of a thermal plume model to provide an adequate representation of the discharge impact on the receiving river. To demonstrate the numerical model's adequacy in projecting and predicting water quality conditions, extensive water quality surveys were performed which included flow measurement, dye studies (for establishment of dispersion coefficients), temperature profiles, and discharge characterization. The surveys and modeling efforts were complicated by the existence of large and influential springs immediately downstream of the discharge. Other heated discharges from industrial facilities also occur within the thermal plume.

Four surveys were selected to confirm the capabilities of a Gaussian plume model. Three thermal models were developed for the purposes of this investigation. Two of these models predict the temperature rise at the mixing zone boundaries. One assumes an infinite width and the other a finite width. The results and comparison of these two models will be included in the discussion. The third model predicts temperature rises at preselected coordinates in a lateral and longitudinal direction. The relative success of each of these models in reproducing the measured water quality data will be discussed.

The paper will conclude with discussions of the techniques employed when comparing the projected water quality conditions with the State's standard. The final form of data presentation for various levels of management within the industry is discussed. This discussion includes an assessment of the periods of the year in which the discharge will violate water quality standards as a result of river flow and temperature. The final decisions with regard to treatment alternatives considering the extended periods in which the reduced discharge will be necessary to comply will also be presented.

31·45-22

A MODEL FOR SHORE-ATTACHED THERMAL PLUMES IN RIVERS

P. P. Paily
NALCO Environmental Sciences
Northbrook, Illinois U.S.A.

and

W. W. Sayre
Iowa Institute of Hydraulic Research
The University of Iowa
Iowa City, Iowa U.S.A.

ABSTRACT

Side discharge of power plant thermal effluents into natural rivers cause the formation of thermal plumes, the shape and orientation of which depend upon both the discharge conditions and the ambient flow characteristics. When the turbulence level of the ambient flow is high, rapid vertical mixing is achieved between the effluent discharge and the river flow, and the thermal plume becomes shore-attached with the maximum temperatures within the plume occurring along the near shore. In order to determine the isotherm patterns within shore-attached thermal plumes, a solution of the depth-integrated steady state convection-diffusion equation is obtained. The solution is cast in terms of space-cumulative discharge coordinates, thus allowing the inclusion of the effects of cross-channel flow induced by channel curvature in the model. Comparison of the model results with the thermal plume data from power plant sites along the Missouri River indicates good agreement.

INTRODUCTION

In order to meet the increasing electrical energy requirements of the nation, steam-electric power plants of large capacities are being installed or being planned for installation by a number of utilities. However, the low thermal efficiencies of these plants necessitate the rejection of large amounts of waste heat at the generating sites. In situations where it can be successfully demonstrated that discharge of the waste heat into a natural body of water will not cause any harmful effects on the ecology of the receiving aquatic environment, open-cycle cooling using river, lake, or sea water is the most desirable waste-heat-removal method. Closed-cycle cooling systems using cooling towers, cooling ponds, or spray canals involve enormous capital investments for construction; these can be up to 15 times that for an open-cycle system. They may also require a considerable portion of the plant output power for operating the cooling systems, thereby imposing penalties on plant efficiency. Closed-cycle systems also require extensive continuing maintenance. Finally, there is consumptive water loss due to evaporation from these systems. Open-cycle systems, on the other hand, are inexpensive to construct, place minimal demands on the plant output, and evaporative water losses are much less. Thus, lower investment and maintenance costs, improved plant efficiencies, and less water loss all combine to make once-through cooling the most attractive method by far, from an economic point of view, for dissipating power plant waste heat.

The effects of the thermal discharge on a natural stream, and the physical processes involved in heat transport within the flow system are normally analyzed by separating the affected area into two regions: the far-field and the near-field. The determination of far-field temperature effects in a river is important in assessing the cumulative effects of several power plants distributed along the course of the river. On the other hand, the determination of near-field conditions is important in evaluating the possible effects of the thermal discharges on the aquatic biota and drifting organisms. In the vicinity of an outfall, the heated water forms a so-called thermal plume until the combined actions of jet mixing, buoyant and convective spreading, and turbulent mixing eventually lead to complete dilution of the heated water with the ambient flow. The thermal standards of the various regulatory agencies regarding thermal discharges in natural waterways usually specify certain limitations on the size of and temperature rise in thermal plumes. It is therefore important to have reliable methods for predicting configurations of and temperature patterns within thermal plumes.

Several computational methods are available for predicting thermal plume patterns resulting from power plant discharges. Recently Jirka, Abraham and Harleman (4) have published a detailed review of these. Most of these techniques either assume or predict bell-shaped profiles for velocity and temperature along horizontal normals to the plume axis. However, an examination of measured thermal plume patterns near power stations at Omaha, Fort Calhoun, and Brownville (Cooper) on the Missouri River indicates that the temperature profiles are not beel-shaped, but are attached to the shores, with the maximum temperatures in the plumes occurring near or along the shore. None of the currently available thermal plume models predict plume patterns with shore attachment; this deficiency is highlighted by Jirka, Abraham and Harleman (4).

The available thermal plume models fail to properly represent the shore-attached plume patterns because the effects of ambient flow characteristics such as bottom effects, variation of channel shape, non-uniform and varying flow conditions across the channel, and ambient turbulence on the mixing phenomenon are not considered in their formulation. If the turbulence level of the ambient river flow is high, (e.g., the Missouri River), intense mixing between the thermal jet and the ambient flow will be induced, leading to rapid vertical mixing between the two flows. Thereafter, the jet is transported downstream as a coflowing stream, and the mixing is mainly due to turbulent diffusion and transverse convective spreading associated with bend-generated secondary circulation. Weil and Fischer (13) have attempted to relate the effects of stream turbulence to plume behaviour. However, their investigation was restricted to zero-momentum jets discharging at the centerline of the ambient flow. Yeh (14) conducted a series of laboratory experiments to investigate the transverse mixing process for a buoyant effluent in both near and far field regions of an open channel flow. The results showed that the mixing process in the near field region was closely related to the development and decay of buoyancy-generated secondary flow. However in the far field region the transverse mixing was found to be mainly due to turbulent diffusion.

The present study is concerned with the development of a predictive model, based on diffusion concepts, for determining transverse temperature profiles in shore-attached, vertically-mixed thermal plumes in rivers resulting from side discharges of thermal effluents. The details of the analytical development of the model, and its application to field cases are presented in the following sections.

FORMULATION OF DIFFUSION PROBLEM

The formulation of the predictive model for determining the temperature distributions in shore-attached plumes is based on a model of mixing of two rivers outlined by Sayre (9) and the transformation of the two-dimensional depth-integrated steady-state convection-diffusion equation into a simple diffusion equation as presented by Yotsukura and Sayre (17). The solution of the transformed equation is cast in terms of space-cumulative discharge coordinates, (x, p(x,z)), when x and z are the streamwise and cross-channel coordinates, and p(x,z) is the normalized cumulative discharge defined by

$$p = \frac{q_c}{Q_R} = \frac{1}{Q_R} \int_0^z q \, dz \qquad (1)$$

where Q_R = total river discharge; q_c = cumulative discharge passing through the river between z = 0 and z at section x; and q = total discharge per unit width. The use of the space-cumulative discharge coordinate system which automatically follows the transverse shifts and meanderings of the flow, was first introduced by Yotsukura and Cobb (15). A procedure for synthesizing the normalized cumulative discharge at cross sections of a river for which the shape is known is outlined in the next section.

The origin of coordinates, $x = 0$, $p = 0$, is located on the discharge bank of the river, just far enough downstream from the outfall so that at the origin initial mixing has taken place, and the temperature rise of the jet is Θ_I. The fraction of the total river discharge occupied by the jet at the origin is given by

$$P = \frac{Q_o \Theta_o}{Q_R \Theta_I} = a \frac{Q_o}{Q_R} \tag{2}$$

where $a = \Theta_o/\Theta_I$ = initial dilution factor; Θ_o = initial excess temperature of the thermal discharge; and Q_o = volumetric rate of effluent discharge.

Let the variable ζ represent the displacement from the origin in the p direction at $x = 0$, as shown in Fig. 1. Then the input transverse temperature distribution at $x = 0$ is given by

$$\left.\begin{aligned} \Theta_I(\zeta,0) &= \frac{\Theta_o}{a}, \quad 0 \leq \zeta \leq P \\ &= 0, \quad P < \zeta \leq 1 \end{aligned}\right\} \tag{3}$$

Neglecting for the moment reflections from the banks, the normalized transverse temperature distribution function for the case of a continuous vertical line source, extending over the depth of flow and concentrated at $(x = 0, p = \zeta)$ is $f_R(p-\zeta;\ x)$ which is a Gaussian probability distribution function, given by

$$f_R(p_1;x) = \frac{1}{\sigma_p} \left(\frac{1}{\sqrt{2\pi}} \exp\left(-\frac{s^2}{2}\right)\right); \qquad p_1 = p-\zeta \tag{4}$$

where $s = p_1/\sigma_p$ is the standardized normal variable; and the standard deviation in the p domain is

$$\sigma_p = \sqrt{2D\ x'} \tag{5}$$

In Eq.(5), D = overall transverse diffusion factor; and $x' = x - x_o$ where x_o = longitudinal coordinate of the virtual source for any subreach determined from

$$D_j(x_{j-1} - x_{o_j}) = D_{j-1}(x_{j-1} - x_{o_{j-1}}) \qquad (6)$$

where x_{j-1} = distance from the origin to the upstream end of j-th subreach, and D_j = value of D for the j-th subreach. For the first subreach, $x_{oj} = 0$.

The desired output temperature distribution for an input distribution $\Theta_I(\zeta, 0)$ is given by the convolution integral

$$\Delta T(p,x) = \int_{p=0}^{p=1} f_R(p-\zeta;x)\ \Theta_I(\zeta,0)\ d\zeta \qquad (7)$$

Using Eq. (3), Eq. (7) can be written

$$\Delta T(p,x) = \frac{\Theta_o}{a} \int_o^P f_R(p-\zeta;x)\ d\zeta \qquad (8)$$

Taking into account now reflections from the banks, the final solution can be obtained from Eq. (8) as

$$\begin{aligned} \Delta T(p,x) = \frac{\Theta_o}{a} \Big(& \Big\{ F_R\Big(\frac{p+P}{\sigma_p}\Big) - F_R\Big(\frac{p-P}{\sigma_p}\Big) \Big\} \\ & + \sum_{n=1}^{\infty} \Big\{ F_R\Big(\frac{2n+(p+P)}{\sigma_p}\Big) - F_R\Big(\frac{2n-(p+P)}{\sigma_p}\Big) \\ & + F_R\Big(\frac{2n-(p-P)}{\sigma_p}\Big) - F_R\Big(\frac{2n+(p-P)}{\sigma_p}\Big) \Big\} \Big) \end{aligned} \qquad (9)$$

where $F_R(\ )$ is the standardized cumulative normal distribution function corresponding to the probability density function $f_R(\ )$. The terms in the infinite series representing the bank reflections are negligible if $Dx \lesssim 0.08$.

The value of the initial dilution factor, a, introduced in Eq. (2) is mainly a function of the design and orientation of the discharge outfall structure, the initial jet or plume characteristics, and the ambient flow properties. If the thermal effluent is discharged almost parallel to the river flow, and Θ_o is the temperature excess measured at the discharge canal outlet, the initial dilution factor, a, can have a value of one. For other situations, values of the initial dilution factor between about 2 and 4 can be used (3,7), until better criteria are established.

Maximum Centerline Temperature

The maximum centerline temperature, ΔT_c, for a shore-attached plume occurs along the near shore (p = 0). The solution for ΔT_c, from Eq. (9) is

$$\Delta T_c = \Delta T(0,x) = \frac{\Theta_o}{a}\left(2F_R\left(\frac{P}{\sigma_p}\right) + 2\sum_{n=1}^{\infty}\left\{F_R\left(\frac{2n+P}{\sigma_p}\right) - F_R\left(\frac{2n-P}{\sigma_p}\right)\right\} - 1\right) \tag{10}$$

The variations of $Q_R \Delta T_c / Q_o \Theta_o$ with Dx for values of P equal to 0.05, 0.10, and 0.20 are shown in Fig. 2. The limiting case, P = 0, corresponds to a source concentrated at the origin. The solution corresponding to Eq. (9) for this limiting case is

$$\Delta T(p,x) = 2\Theta_o \frac{Q_o}{Q_R}\left(f_R(p) + \sum_{n=1}^{\infty}\left\{f_R(2n-p) + f_R(2n+p)\right\}\right) \tag{11}$$

Substituting for the probability density function $f_R(p)$ by

$$f_R(p) = \frac{1}{\sigma_p\sqrt{2\pi}} \exp\left(-\frac{1}{2}\frac{p^2}{\sigma_p^2}\right), \tag{12}$$

the solution for maximum temperatures along the shore, $(p = 0)$, corresponding to Eq. (10) for this case is

$$\Delta T_C = \Delta T(0,x) = \Theta_0 \frac{Q_0}{Q_R} \sqrt{\frac{2}{\pi}}\, \frac{1}{\sigma_p} \left(1 + 2 \sum_{n=1}^{\infty} \exp\left(-2\frac{n^2}{\sigma_p^2}\right)\right) \tag{13}$$

Eq. (13) is represented by the curve labelled concentrated source in Fig. 2.

Diffusion Factor, D

The diffusion factor, D, in Eq. (5) can be related to the dimensionless tranverse mixing coefficient, $\alpha = E_z/\bar{d}u_*$, by the equation

$$D = \frac{\alpha\, \bar{d}\, u_*}{Q_R^2} \left(\int_0^1 d^2\, u\, dp \right) \tag{14}$$

if it is assumed that the overall transverse mixing coefficient E_z does not vary across the channel. In Eq. (14) $d = A/B$ = average depth of flow section; A = area of river flow section; $u_* = (g\bar{d}S)^{1/2}$ = shear velocity; g = acceleration due to gravity; S = slope of energy gradient; d = local flow depth; and $u = q/d$ = local depth-averaged velocity of flow. Using the Manning formula for the river flow rate,

$$Q_R = \frac{1\cdot 49}{n}\, B\, \bar{d}\, (\bar{d})^{2/3}\, (S)^{1/2} \tag{15}$$

and approximating

$$\int_0^1 d^2\, u\, dp \simeq (\bar{d})^2\, \bar{u} = \bar{d}\, \bar{q}, \tag{16}$$

where $\bar{q} = \bar{d}\,\bar{u}$ = width-averaged value of q, the relation for the diffusion factor can also be written

$$D = \frac{\alpha}{1\cdot 49}\, \frac{n\sqrt{g}}{B^2}\, (\bar{d})^{5/5} \tag{17}$$

where n = Manning's coefficient. Values of D determined by Eq. (17) are less accurate compared to those by Eq. (14), mainly because of the approximation used in Eq. (16).

The transverse mixing coefficient, E_z or α, for a natural river depends upon the characteristics of the river channel and the ambient flow. However, there are as yet no very reliable predictive relationships for evaluating its value. The most reliable method for determining the values of E_z for natural channels is by direct experimentation in the field using tracers. Experiments in undistorted hydraulic models can also be used to determine E_z; vertically distorted hydraulic models do not correctly simulate the transverse mixing processes.

In laboratory flumes several investigators have found values of α ranging from about 0.1 for $B/\bar{d} \simeq 5$ to about 0.2 for $B/\bar{d} \simeq 60$. In reasonably straight uniform reaches of natural channels somewhat larger values of α have been found. This increase is probably due to channel irregularities and weak secondary flows rather than to any scale effect. In sinuous channels, due to bend-induced secondary flow, α values are typically much larger. As shown in Fig. 3, average α values ranging from 0.5 to 2.5 for bends in flumes, and from 0.6 to 10 for bends in the Missouri River, have been found. The functional form of the relationships shown on Fig. 3 was derived by Fischer (2) in a transverse convective dispersion analysis which utilized Rozovskii's (9) radial velocity distribution function for fully-developed secondary flow in the central portion of an idealized curved channel. The gap between the laboratory flume data and the Missouri River data in Fig. 3 indicates that there are still certain factors that are not accounted for in evaluating the transverse mixing coefficient. The equation for the curve passing through the Missouri River data is

$$\alpha = 0.4 \left(\frac{B}{\bar{d}}\right)^2 \left(\frac{\bar{u}}{u_*}\right)^2 \left(\frac{\bar{d}}{R_c}\right)^2 \qquad (18)$$

where $\bar{u} = Q_R/A$ = average river flow velocity; and R_c = radius of curvature of river bend. The value of the numerical coefficient in Eq. (18) may be different for other rivers.

SYNTHESIS OF TRANSVERSE FLOW DISTRIBUTION

The cumulative discharge, q_c, and the normalized cumulative discharge, $p = q_c/Q_R$, in a river section at a given flow discharge can be synthesized from the transverse depth profile of the cross-section, as outlined by Sayre (10). The method is based on the hypothesis that the velocity distribution in natural streams is a function of the transverse depth profile, and uses the relation

$$\frac{q}{\bar{q}} = b_o \left(\frac{d}{\bar{d}}\right)^{b_1} \tag{19}$$

where d = local depth of flow; and b_o and b_1 are coefficients whose values according to the Manning formula (Eq. 19) are $b_o = 1.0$, and $b_1 = 5/3$. Sium (12) investigated the applicability of Eq. (19) for synthesizing the flow distribution in several natural rivers including the Missouri and Mississippi Rivers. That study indicated that the coefficients b_o and b_1 in Eq. (19) varied with the ratio of width to average depth, $B/\bar{d}$. For cross-sections in straight river reaches, approximate values of b_o and b_1 are

$$\begin{aligned} b_o &= 1{\cdot}0,\ b_1 = 5/3; & 50 \le B/\bar{d} < 70 \\ b_o &= 0{\cdot}92,\ b_1 = 7/4; & B/\bar{d} \ge 70 \end{aligned} \tag{20}$$

For cross-sections in bends of sinuous and meandering reaches, approximate values of b_o vary between 0.95 and 0.80, and b_1 between 2.48 and 1.78, as $B/\bar{d}$ increases from 50 to 100. Usually the value of b_o must be adjusted to make p = 1 when z = B.

Fig. 4 shows the variation of measured $q/\bar{q}$ with $d/\bar{d}$ for three cross-sections in the Missouri River, together with the theoretical curve corresponding to $q/\bar{q} = (d/\bar{d})^{5/3}$. A comparison of the measured and synthesized transverse distribution of unit discharge at one of the cross-sections (Mile 410.20) is also shown in Fig. 4. The data shown in Fig. 4 correspond to a Missouri River discharge of 61,300 cfs (1736 cu.m.sec). Synthesized transverse flow distributions at Mile 410.20 corresponding to a river flow rate of 35,000 cfs (991. cu.m/sec) are shown in Fig. 5. To obtain the transverse distribution curve for depth d at the discharge of 35,000 cfs (991 cu.m/sec), the water surface level was dropped by 3.8 ft (1.16 m) from that for 61,300 cfs (1736 cu.m/sec). This drop in water surface elevation, corresponding to reduction in discharge from 61,300 cfs (1736 cu.m/sec) to 35,000 cfs (991 cu.m/sec), was determined from an estimated stage versus discharge curve for the Missouri River at Mile 411. The procedure thus assumes that there is no significant change in the cross-sectional shape as the river discharge and depth are reduced, and also that there is a unique stage-discharge relationship. For alluvial channels, these assumptions are not strictly true. Changes in discharge can cause different amounts of aggradation and/or degradation of the bed in different parts of the cross-section. Also, seasonal shifts in the stage discharge relation may occur that evidently are associated with temperature-related effects on the bed configuration, among other factors. Unfortunately, alluvial channel phenomena are not sufficiently well understood to quatitatively evaluate or significantly improve on these assumptions.

APPLICATIONS OF THE MODEL

The solutions of the thermal plume model, Eqs. (9) and (10), were used to predict plume patterns in the Missouri River downstream from the Fort Calhoun Power Station of the Omaha Public Power Station District near Blair, Nebraska, and the Cooper Nuclear Station of the Nebraska Public Power District near Brownville, Nebraska. Fig. 6 shows the measured (5) and the predicted (7) temperature-rise isotherms for the Fort Calhoun Station corresponding to two Missouri River discharges. A comparison of the measured (6) and predicted values of $\Delta T_c/\Theta_o$ for the Cooper Nuclear Station thermal plumes on four different dates is shown in Fig. 7. Background river flow and plant-discharge data corresponding to these plumes are given in Table 1. The results shown in Figs. 6 and 7 indicate that the model predicts thermal plumes in the Missouri River that are in quite good agreement with the measured plumes.

One major capability of the present model is that it permits the inclusion of the effect of the cross-channel flow induced by channel curvature. Because of this, the model can predict expansions and contractions of the thermal plume as the river flow becomes weighted towards one bank or the other. This feature is illustrated in Fig. 8 which shows the predicted thermal plume pattern near the Fort Calhoun Power Station for a Missouri River discharge of 14,000 cfs (396 cu.m/sec). The computations for this case were performed for a 12-mile stretch of the river which was divided into ten subreaches, as shown in the insert map in Fig. 8.

CONCLUSIONS

A computational model, based on a diffusion equation, has been developed for predicting the isotherm pattern for shore-attached thermal plumes in rivers. Comparison of the model results with field measurements indicates reasonably good agreement. Further refinements of the model, especially in defining the initial dilution factor, need to be made based on laboratory investigations. The model can be used to assess the environmental impact of power plant thermal discharges in natural rivers.

Acknowledgement

Part of the work described in this study had been carried out during a thermal plume modeling effort at the Iowa Institute of Hydraulic Research sponsored by the Omaha Public Power District. The computer time was provided by the Graduate College of the University of Iowa and NALCO Environmental Sciences. The writers are thankful of to Prof. John F. Kennedy of the Iowa Institute of Hydraulic Research and Dr. Richarch Johnson of NALCO Environmental Sciences for their encouragement.

LIST OF REFERENCES

1. Chang, Y.C., "Lateral Mixing in Meandering Channels," Doctoral Dissertation, Department of Mechanics and Hydraulics, The University of Iowa, Iowa City, Iowa, 1971.

2. Fischer, H.B., "The Effect of Bends on Dispersion in Streams," Water Resources Research, Vol. 5, No. 2, April 1969.

3. Giaquinta, A.R., and Sayre, W.W., "Effects of Outfall Design on the Thermal Impact of Byron Station Blowdown Discharge," IIHR Limited Distribution Report No. 39, Iowa Institute of Hydraulic Research, The University of Iowa, Iowa City, Iowa, Feb. 1976.

4. Jirka, G.H., Abraham, G., and Harleman, D.R.F., "An Assessment of Techniques for Hydrothermal Prediction," Report No. 203, Ralph M. Parsons Laboratory for Water Resources and Hydrodynamics, Massachusetts Institute of Technology, Cambridge, Massachusetts, July 1975.

5. OPPD, Nebraska City Power Station Unit No. 1 Environmental Assessment Appendix for Section 10 Permit, Volume 2, June 1975, Omaha Public Power District, Omaha, Nebraska.

6. Paily, P.P., "Thermal Plume Surveys in the Missouri River Near the Cooper Nuclear Station," NALCO Environmental Sciences Report No. 550107642; Northbrook, Illinois, Jan. 1976.

7. Paily, P.P., "An investigation of the Thermal Plume Characteristics for the Fort Calhoun Power Station Outfall," IIHR Limited Distribution Report No. 30, Iowa Institute of Hydraulic Research, Iowa City, Iowa, June 1975.

8. Rozovskii, I.L. "Flow of Water in Bends of Open Channels," Academy of Sciences of the Ukrainian Soviet Socialist Republic, 1957, (Translation No. OTS60-51133, Office of Technical Services, U.S. Dept. of Commerce).

9. Sayre, W.W., "Natural Mixing Processes in Rivers," Chapter 6 in Environmental Impact on Rivers, Shen, H.W. (Ed.), Ft. Collins, Colorado, 1973.

10. Sayre, W.W., "Investigation of Surface-jet Thermal Outfall for Iatan Steam Electric Generating Station," IIHR Report No. 167, Iowa Institute of Hydraulic Research, The University of Iowa, Iowa City, Iowa, April 1975.

11. Sayre, W.W., and Yeh, T.P., "Transverse Mixing Characteristics of the Missouri River Downstream from the Cooper Nuclear Station," Iowa Institute of Hydraulic Research, The University of Iowa, IIHR Report No. 145, 1973.

12. Sium, O., "Transverse Flow Distribution in Natural Streams as Influenced by Cross-sectional Shape," M.S. Thesis, The University of Iowa, Iowa City, Iowa, July 1975.

13. Weil, J., and Fischer, H.B., "Effect of Stream Turbulence on Heated Water Plumes," Journal of Hydraulics Division, ASCE, Vol. 100, July 1974.

14. Yeh, T.P., "Transverse Mixing of Heated Effluents in Open-Channel Flow," Doctoral Dissertation, Department of Mechanics and Hydraulics, The University of Iowa, Iowa City, Iowa, May 1974.

15. Yotsukura, N., and Cobb, E.D., "Transverse Diffusion of Solutes in Natural Streams," U.S. Geological Survey Professional Paper 582-C, 1972.

16. Yotsukura, N., Fischer, H.B., and Sayre, W.W., "Measurement of Mixing Characteristics of the Missouri River between Sioux City, Iowa, and Plattsmouth, Nebraska," U.S. Geological Survey Water Supply Paper 1899-G, 1970.

17. Yotsukura, N, and Sayre, W.W., "Transverse Mixing in Natural Channels," Water Resources Research, Vol. 12, No. 4, August 1976.

NOTATIONS

The following symbols are used in this paper:

A = area of river flow cross section;
a = initial dilution factor;
B = width of river flow cross section;
b_o = coefficient used in Eq. 19;
b_1 = exponent used in Eq. 19;
D = diffusion factor;

$\underline{d}$ = local depth of flow;
d = average depth of river flow cross section;
E_z = overall transverse mixing coefficient;
g = acceleration due to gravity;
n = Manning coefficient;
P = fraction of river flow occupied by plume;
p = normalized cumulative discharge;
Q_o = volumetric discharge rate of thermal effluent;
Q_R = river discharge
$\underline{q}$ = discharge per unit width;
q = width-averaged discharge per unit width;
q_c = cumulative discharge from near bank
R_c = radius of curvature of river bend;
S = energy gradient;
$\underline{u}$ = depth-averaged local velocity of flow;
u = cross-sectional average velocity of flow;
u_* = shear velocity;
x = longitudinal coordinate;
x_o = position of virtual source;
z = transverse space coordinate;
ΔT = excess temperature within plume;
ΔT_c = centerline or bank excess temperature within plume;
α = dimensionless transverse mixing coefficient;
Θ_o = initial excess temperature;
Θ_I = excess temperature after initial dilution;
σ_p = variance of the normal probability density functions, Eq. 4.

TABLE I.

BACKGROUND DATA CORRESPONDING TO THE THERMAL PLUMES SHOWN IN FIGURES 6 AND 7

Power Station	Date	River Flow cfs (m^3/sec)	Plant Discharge cfs (m^3/sec)	Initial Excess Temperature °F (°C)	Initial Dilution Factor
Ft. Calhoun	5/3/74	33,000 (935)	801 (22.7)	18 (10.0)	2
Ft. Calhoun	12/2/74	18,500 (524)	801 (22.7)	16.2 (9.0)	2
Cooper	5/23/74	48,200 (1365)	725 (20.5)	7.8 (4.3)	1
Cooper	9/27/74	37,100 (1051)	1352 (38.3)	8.6 (4.8)	1
Copper	6/30/75	57,600 (1631)	880 (24.9)	10.1 (5.6)	1
Cooper	9/18/75	66,600 (1886)	1088 (30.8)	10.5 (5.8)	1

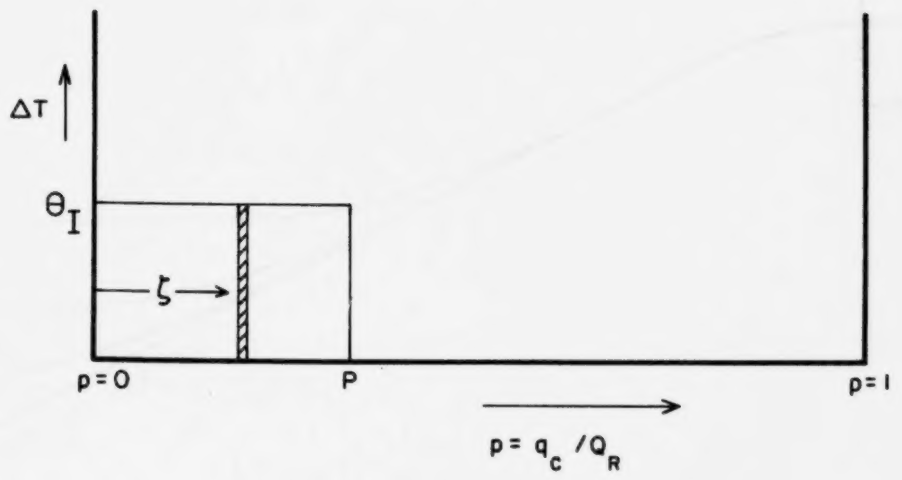
ΔT
Θ_I
ζ
ρ=0
P
ρ=1
$\rho = q_c / Q_R$

Figure 1. Definition Sketch for the Initial Condition.

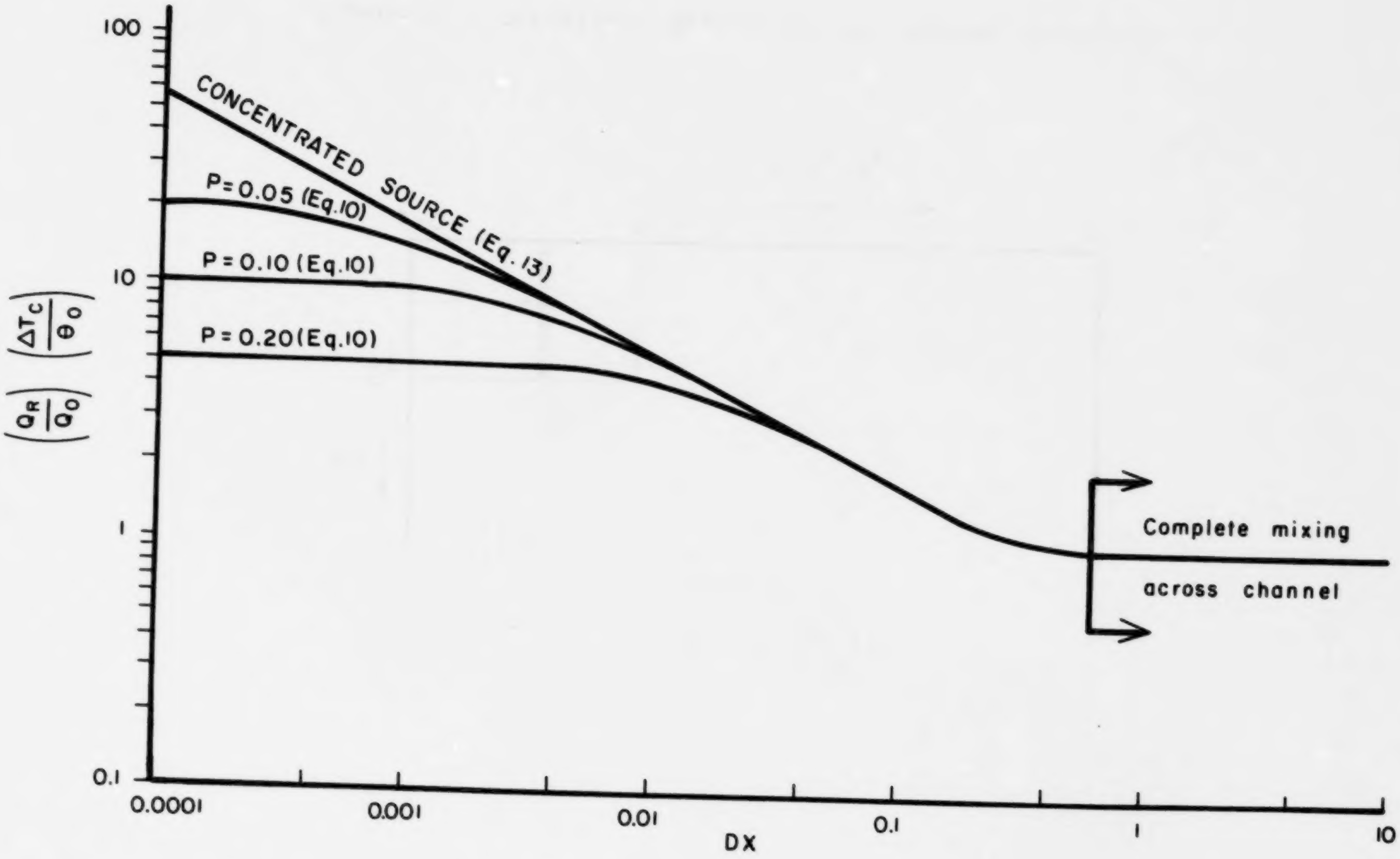

Figure 2. Longitudinal Variation of Maximum Temperature Along the Bank for Various Initial Conditions.

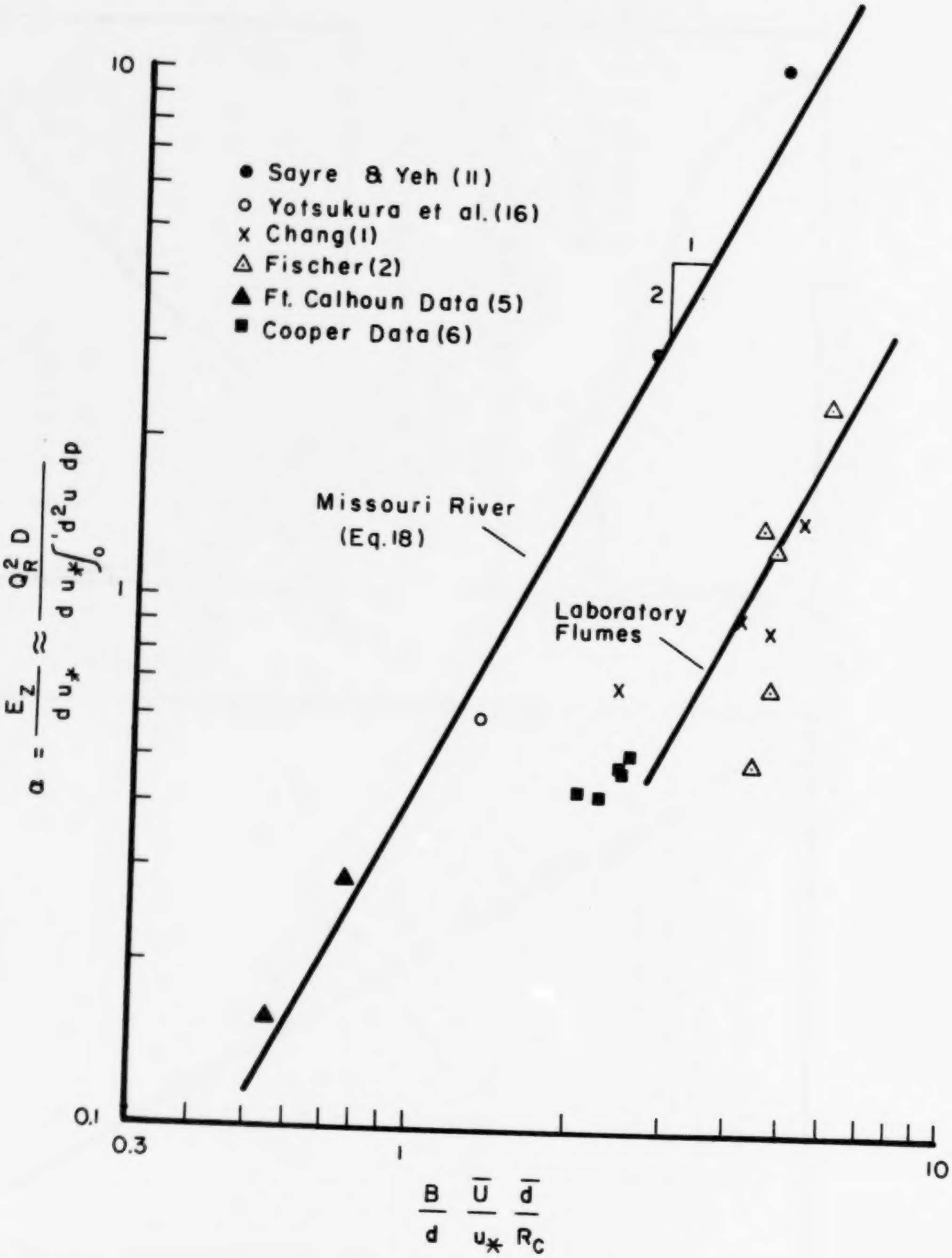

Figure 3. Variation of Transverse Mixing Coefficient in Bends with Bulk Flow and Channel Geometry Parameters.

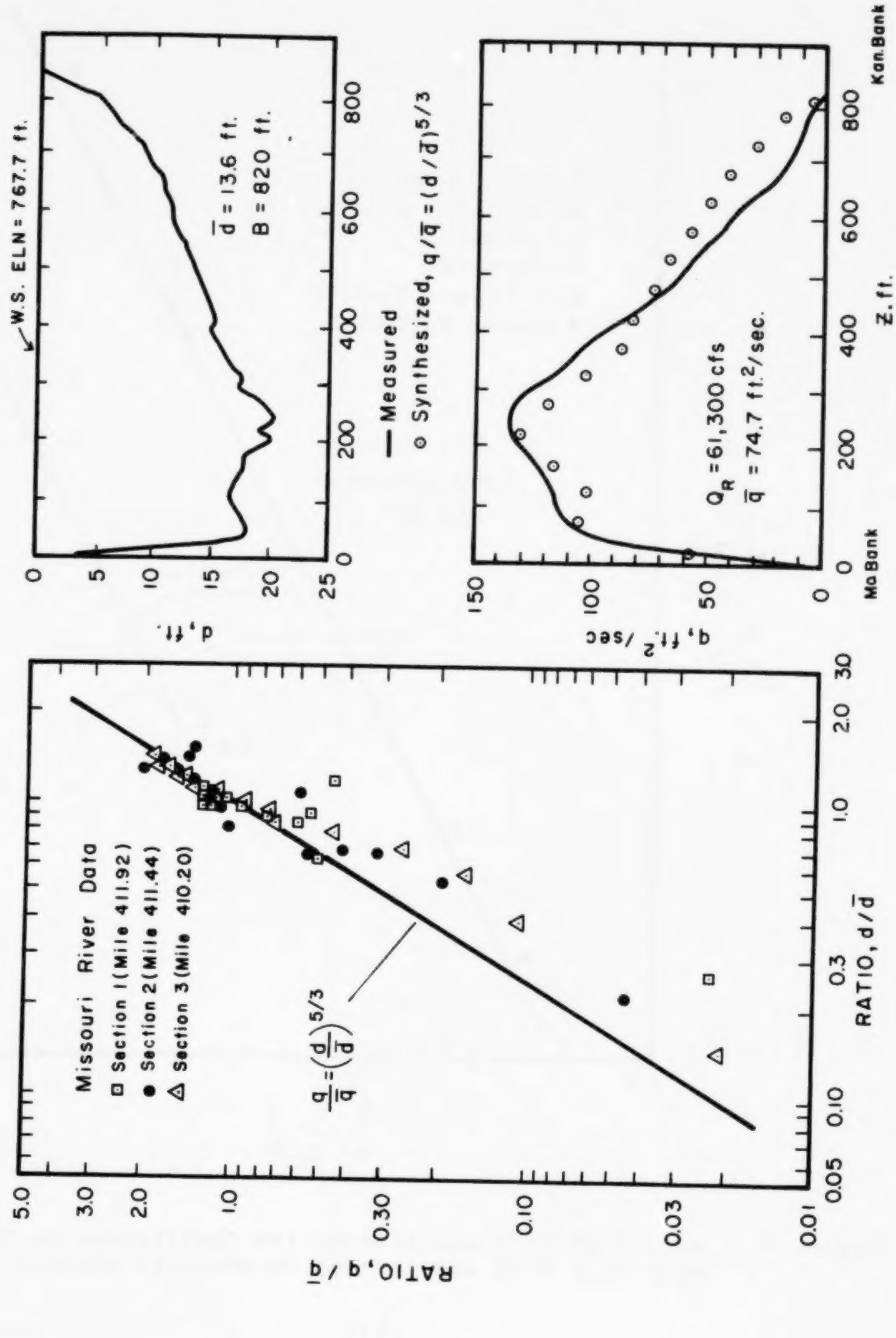

Figure 4. Transverse Distribution of Depth and Unit Discharge Measured at Mile 410.2 in the Missouri River, and the Relative Unit Discharge-Relative Depth Relation-Ship.

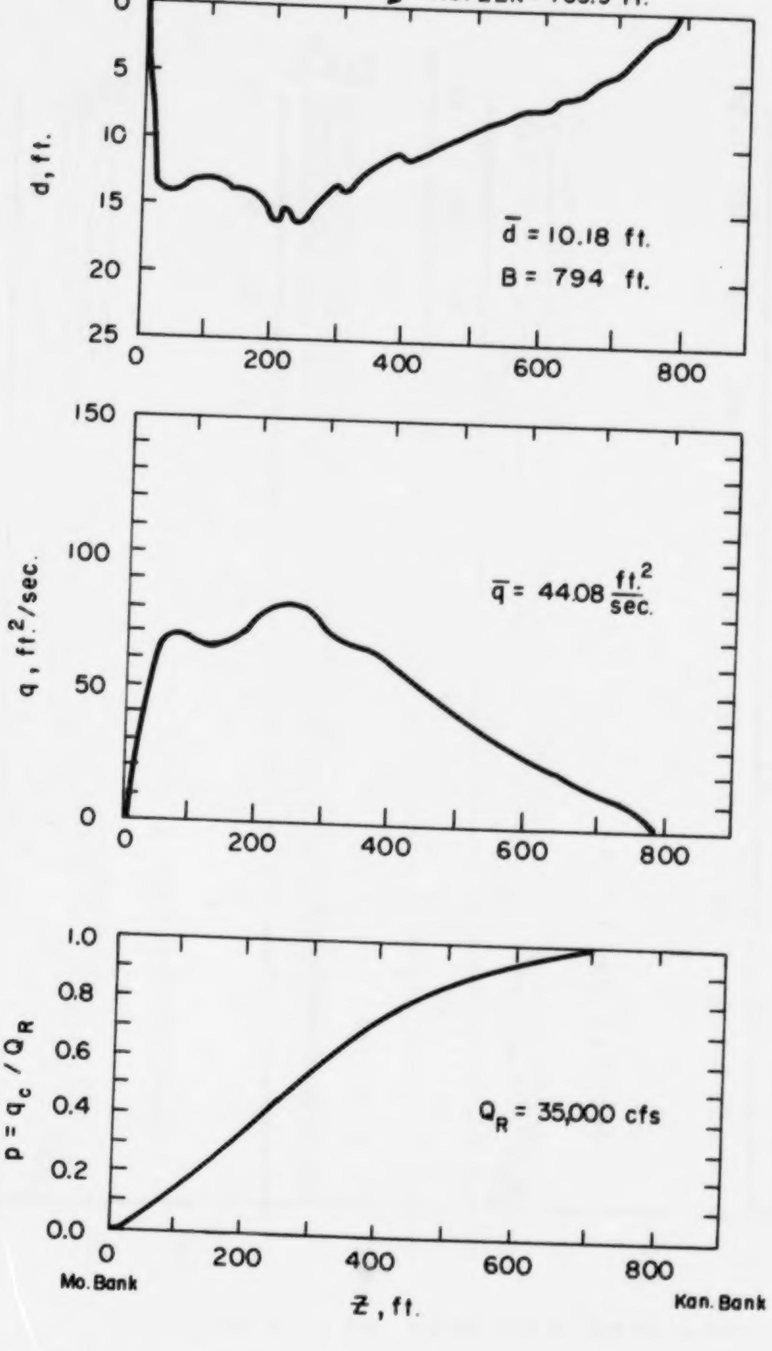

Figure 5. Synthesized Distribution of Depth, Unit Discharge, and Cumulative Discharge at Mile 410.2 in the Missouri River for a Flow Rate of 35,000 CFS.

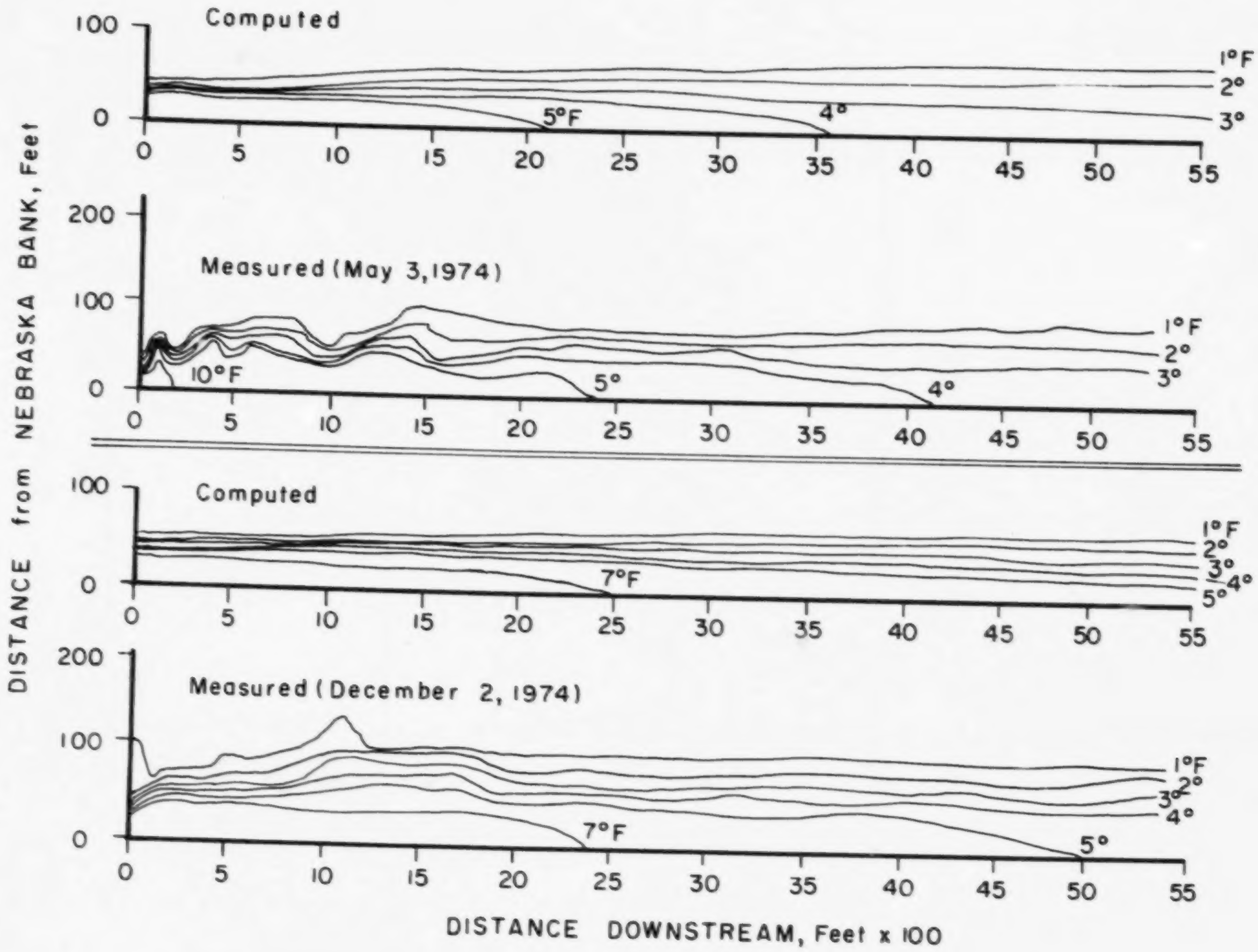

Figure 6. Comparison of Measured and Predicted Temperature-Rise Isotherms for the Missouri River Thermal Plumes Near the Fort Calhoun Power Station, Ft. Calhoun, Nebraska.

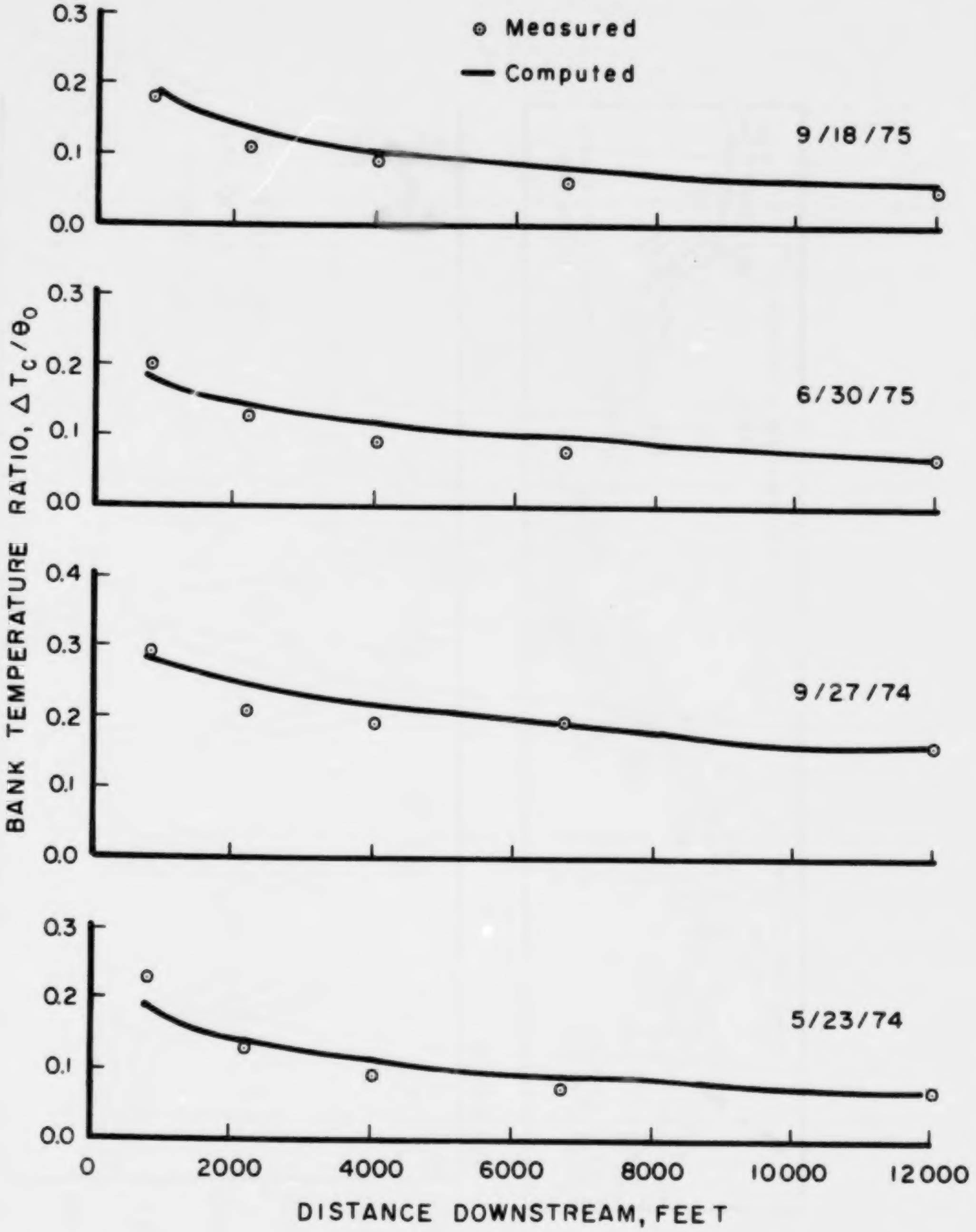

Figure 7. Comparison of Measured and Predicted Maximum Temperatures Along the Bank for the Missouri River Thermal Plumes Near the Cooper Nuclear Station, Brownville, Nebraska.

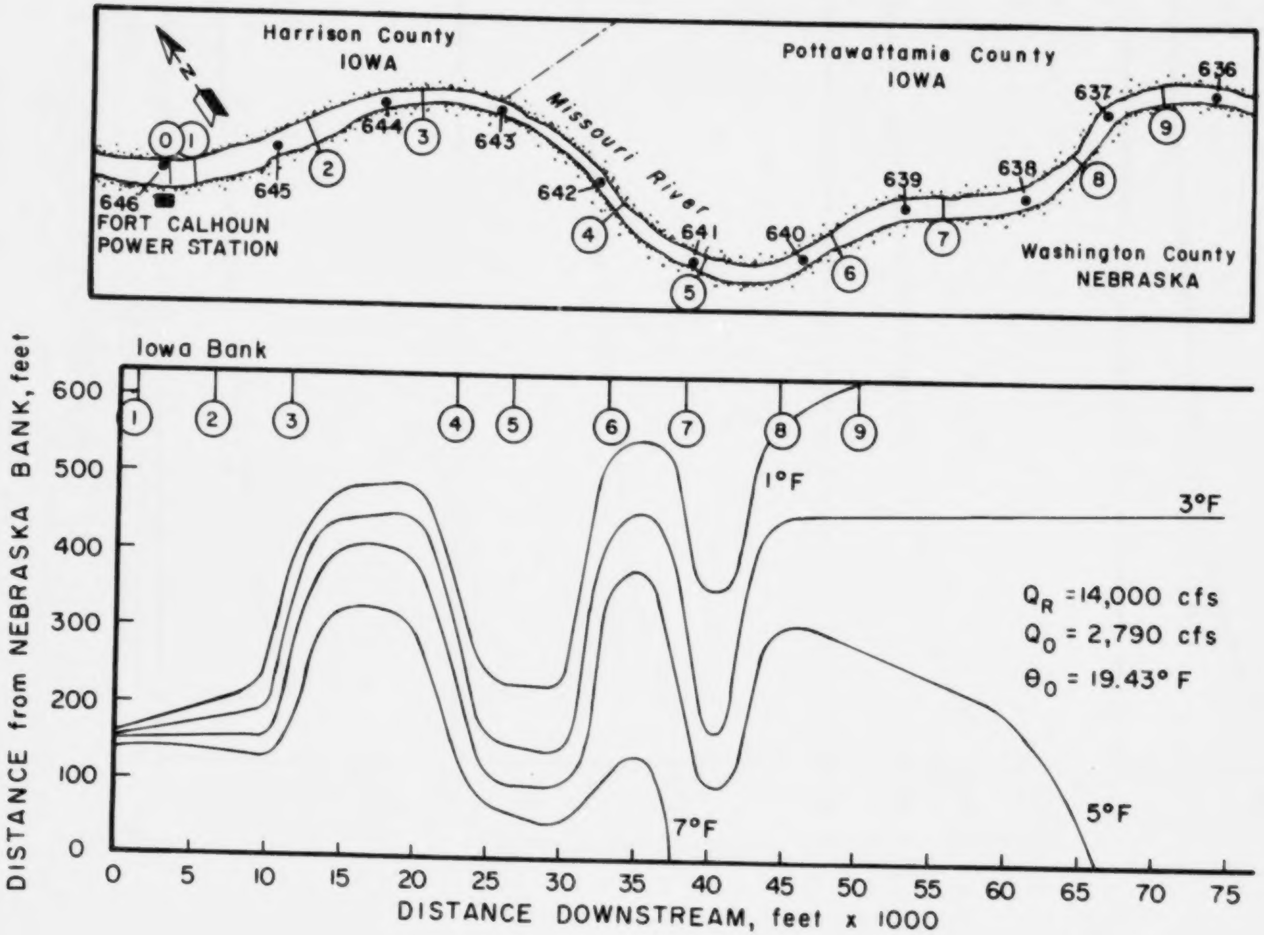

Figure 8. Predicted Temperature-Rise Isotherm Pattern for Low Flow Conditions in the Missouri River Near the Fort Calhoun Power Station, Ft. Calhoun, Nebraska.

32-45-8

SOME PRACTICAL ASPECTS OF THERMAL PLUME ANALYSIS

L.L. Stookey, P.E.
Manchester Laboratories, Inc.
Manchester, Iowa U.S.A.

ABSTRACT

It is desirable to perform thermal plume analysis with as low an expense of effort and cost as is consistent with complete and accurate results. This is only possible by prior consideration of local geography and conditions. A description is given of a method of plume temperature measurements in polar coordinates which reduces manpower and equipment requirements for point-source thermal discharges, as compared with measurements in cartesian coordinates. Boat and water safety is discussed, especially regarding dam proximity. Types of access to rivers are described, including precautions to be taken in their choice.

The effect of hourly background temperature variations upon measurements is described, together with depth variations in background temperature. The magnitude of such variations is compared to statutory limitations. Deep river currents are described, especially in the vicinity of dams, backwaters, and obstructions, which may produce anomalous plume shapes.

INTRODUCTION

It is desirable to perform thermal plume analysis with as low a level of effort and cost as possible as is consistent with complete and accurate results. This is only possible by consideration of local geography and conditions. The examples I will use today are based upon thermal discharges from fossil fuel fired power plants, and gray iron foundries, to Iowa Class B warm rivers [1].

ACCURACY

First let us discuss precision and accuracy. Remember that precision is a measure of repeatability. Accuracy is the difference between the "true" value of a measurement and its observed value. There are two related types of accuracy to consider. The first is instrument accuracy. The term "instrument" includes any device for measuring temperature or displacement. This includes transits, thermometers, thermistors, meters, sounding ropes, and tether ropes. The second is the accuracy required by regulatory agencies. Temperature accuracy is requested to be ± 0.1°C. Displacement accuracy is generally accepted to be ± 1 foot or ± 1%, whichever is greater [2].

I would like to describe the method of position measurement which we use, and limit the discussion of accuracy to the implements used in this method. First, two points are established, one at or near the discharge point, and one sufficiently removed to determine an accurate line on a plat plan, aerial photograph, or enlarged topographical map. We use wooden stakes painted with fluorescent orange paint to mark such points. Typically, the two stakes are 20 feet apart. Then maintaining a constant radius of 20 feet, other such stakes are set at angular displacements of ten to twenty degrees, depending upon the type of plume expected. These angles are measured by describing sequential isosceles triangles with stakes at the verticles, knowing two sides of the triangle and the desired angle. We believe the stakes can be placed with a cumlative displacement error of 0.5 inches. The stake near the mooring point, known as the master stake, is also the mooring point for the boat. A nylon braided rope of 3/16" diameter is attached to the bottom of the stake and the reel for the rope is placed in the boat. This line is knotted and marked every ten feet, much like a sounding line. Two persons are then required in order to perform the work: one to pilot the boat and achieve visual alignment with the stakes, and another to take and record temperature measurements. With the outboard motor in reverse to maintain slight tension on the mooring line, the boat is swung in an arc at each radial displacement, stopping as it comes into alignment with the master stake and one of the angular stakes long enough to take temperature measurements. The boat is then let out to the next radial displacement and the process is repeated. When temperature measurements are below the required contours, the data collection is complete.

We described the method here in the context of accuracy. Angular errors remain the same regardless of radial displacement, but by similar triangles, convert to proportionally larger arc error, measured in units of length, as radial displacement increases.

About the longest length of rope we like to play out is 200 feet. Let us take this as worst case: if the maximum stake position error is assumed to be 0.5 inches of arc at 20 feet, at two hundred feet the error converts to 5.0 inches. Assuming that at that distance we lose another 0.5 inches of accuracy due to sighting error, our cumulative arc error is ten inches. The error in the radial dimension is primarily due to stretching of the rope. Nylon rope will stretch slightly further with a given tension when it is wet, due to the lubrication of the water between the nylon fibers. With the size and type of nylon rope we use, we have noted that a stretching of about 1% is observed. When the knots were located, the rope was stressed with ten pounds of force, as an average of the reaction from outboard motors at various power settings. The use of wire aircraft cable might improve the situation, but is more difficult to handle in the boat due to its lack of suppleness. At any rate, at two hundred feet, we will observe a radial diaplacement error of about 2 feet. With this information, we can see that on a practical basis, it is possible to obtain an absolute displacement accuracy of ± 1% or ± 1 foot, whichever is greater.

The discussion of temperature accuracy is more straightforward. Although research instruments are available for accurately measuring temperatures less than 0.001°C, Hardy field instruments for use under sometimes rigorous conditions found during thermal measurements usually cover a fairly large range of temperatures, with a large time constant. Whereas they are reported by their manufacturers often to be accurate to 0.05°C,the problem with most instruments is meter readability. With our instrument, the meter is accurately reading to ± 0.1°C, which we use as our accuracy standards [3].

We have discussed these field capabilities with the United States Environmental Protection Agency personnel from Region VII, Region IV, and Corvallis, as well as state agency personnel, and have found no objection to these accuracy limits. It should be observed that no written regulations are presently in effect which stipulate accuracy requirements [2].

LOGISTICS

I should like to turn your attention to field logistics for a few moments. Since the purpose of this paper is to describe methods of reducing manpower requirements, I would like to emphasize the necessity of careful planning. A few minutes spent in the office with a checklist will often save hours in the field. Be certain that the boat you intend to use is available on the day that you intend to use it. Be certain that it is licensed by the proper authorities and is in good repair. Even if these activities are the responsibility of the central stores department, the quartermaster, or some other person, it is your time and/or that of your personnel which will be wasted if proper planning is absent. The same applies to the outboard motor. Will it run properly at all power settings, especially low ones? Is it in good repair? An engine which stalls at idle power and is difficult to start when hot can be a safety hazard as well as a waste of time. Is there a proper access to the river within a reasonable distance? Is it in good condition? If you are using a boat trailer, remember that it may be easier to winch the boat two or three extra feet than to move a vehicle which has been mired down in clay or mud. Do you have a supply of shear pins for the outboard motor? They are easy to shear if working around stumps or snags, and difficult to find when in the midst of a thermal study. Have you taken all the proper equipment with you? For our procedures we use the following check list:

Vehicle and trailer
Boat, motor and fuel
Oars
Life jackets
Seat cushions
Temperature meter
Accessory cable for meter
Stakes
Mooring line
Security chain and lock
Laboratory notebook
Writing instruments
Shear pins
Steel tape measure
Camera

The camera may be optional. The writing instruments are not. We recommend both a pen and a pencil. With due respect for the fact that all entries in a laboratory notebook should be made in ink, at times it is necessary to perform a thermal plume study through a drizzling rain. At times like these, a pencil will write when a pen will not. The data can then be copied in ink at a later time with appropriate notation.

SAFETY

I should now like to address myself to boat safety [4]. First, it is important to remember the elementary rules for pleasure boating. Sometimes we who are involved in technical work forget about these from time to time, to our peril. Do not overload the boat. This should be no problem with two persons and a fourteen foot, or larger, craft. Do not overpower the boat. Remember that the engine will be running in reverse most of the time, and then close to idle power. We have used everything from a fourteen foot round-bottom to a twenty foot flat-bottom, powered from 25 horsepower down to 4 horsepower. Frankly, we favor the lower power ranges, and see no need to use an engine larger than 8-10 horsepower. Keep the center of gravity near the centerline of the boat. This is especially important during boarding or leaving the boat. Make certain that you have all proper safety equipment, including oars, life jackets (being worn), lights if necessary, and a fire extinguisher if applicapable to your engine size. Keep away from obstructions in the river. Use the mooring line wherever possible, except when moving your radius, and then be careful not to kill the motor or break a shear pin. Be careful when approaching a rocky shore. Have the person in the bow of the boat prepared to jump out or to lay hold of a mooring device, to protect the bow. Now about dams: We have an internal rule not to work closer to a dam than 50 feet, and then only when secured by the mooring line. The sole exception to this is where most of the water flow is over a spillway and there is no possibility of a loaded boat going over said dam. The only time we have made this exception was during the extremely dry weather in the midwest last year. There exist two possible circumstances under which personnel perform thermal plume measurements. Either they are employed directly by the discharger, or they are not. The latter group would include personnel of consulting firms such as ours, or staff of regulatory agencies. We approached the Occupational Safety and Health Administration and the Iowa Department of Labor regarding their requirements. The consensus is that no specific activity requirement is in effect at this time. The closest that OSHA can come is under maritime regulations, and then under the sub-heading of longshoring [5]. Under section 1910.16, "longshoring operation is the loading, unloading, moving, or hauling of cargo, ship's stores, gear, etc. into, in, on, or out of any vessel". It may be stretching things a bit to describe thermal plume analysis as longshoring, but if any person performing any of this work is a member of a longshoreman's union, it would bear looking into part 1504 of the standards [6]. At any rate, I was asked to emphasize that no employer is exempt from section 5.(a)(1) of the act itself, which states that:

> "Each employer shall furnish to each of his employees employment and a place of employment which are free from recognized hazards that are causing or are likely to cause death or serious physical harm to his employees."

Simply stated, all uf us, whether affliated with industry, consulting firms, or regulatory agencies, must take every conceivable precaution to prevent accidents.

BACKGROUND TEMPERATURE VARIATIONS

The next topic relates to variations in background temperature. Since thermal controls are composed of temperature differentials between background temperature and observed temperature at given points, it is mandatory to know exactly what the background temperature is. At any one point, we will observe decreases in temperature from 0.5°C to 1.5°C between the surface and twelve feet of depth. In addition, depending upon cloud cover and season of the year, background temperatures at a given point may increase as much as 2.0°C during the course of a day. Since we are often attempting to define the 2.8°C contour ± 0.1°, it may be seen that background temperatures should be checked often, and the time of actual measurements should also be recorded. Only in this way can accurate contours be drawn.

UNUSUAL PLUMES

The last topic which I wish to cover is that of making certain that all necessary data is taken. In a relatively shallow and flat river, this is no problem because the plume assumes a conventional shape, and measurements can be taken at a point until within the required contour. If the river is deep and slow and/or fraught with obstructions, or has unusual channeling, some attempt may have to be made in the field to visualize or "chase" the plume. At or near the twenty foot level near the base of a dam, a current of condenser water eddied, to come to the surface a considerable distance upstream. On the other hand, a plume may disappear as it goes over a dam due to mixing, or if part of it is drawn through a turbine intake. A bend in the river can cause the plume to hug the bank for hundreds of feet, and make multiple-origin measurements necessary.

If, however, all data necessary is taken and recorded in an accurate and safe manner, the task of writing the report is considerably minimized.

REFERENCES

1. State of Iowa, Department of Environmental Quality, Iowa Departmental Rules, Chapter 16.
2. United States Environmental Protection Agency, Regions IV and VII, private communications.
3. Yellow Springs Instrument Company, Inc., Yellow Springs, Ohio. Model 33 SCT Meter.
4. United States Coast Guard, Boating Safety Regulations.
5. Federal Register, Thursday, 27 June 1974. Volume 39. Number 125 part II. Department of Labor, OSHA Standards.
6. Code of Federal Regulations, Title 29, Chapter XVII, part 1504.

omit

VII-B-143

Conference on
Waste Heat Management and Utilization

A Longitudinal Dispersion Model for Shallow Cooling Ponds

by M. Watanabe and G.H. Jirka

R.M. Parsons Laboratory for Water Resources and Hydrodynamics
Department of Civil Engineering
Massachusetts Institute of Technology
Cambridge, Massachusetts 02139

Abstract

In general, the prediction of cooling pond performance is complex because of their irregular geometry and bottom topography, the presence of internal diking and baffles, and various inflow and outflow designs. The degree of pond stratification is of critical importance for the prediction of pond performance.

For vertically stratified ponds, the performance is independent of pond shape due to strong effect of density current. Mathematical models have been developed which predict reasonably well the behavior of these relatively deep ponds (P.J. Ryan and D.R.F. Harleman 1973, and M. Watanabe and D.R.F. Harleman 1975).

For weakly stratified or vertically fully mixed ponds, that is in relatively shallow cooling ponds, the performance is strongly shape dependent and complex internal circulation or short circuiting patterns may result. To minimize these effects and to utilize effectively the entire free surface of the pond, internal dikes are usually constructed in shallow cooling ponds.

Due to significant non-uniformities in the lateral velocity distribution of these internally diked ponds, the temperature distribution in the pond is strongly affected by longitudinal dispersion. A transient one-dimensional

dispersion model has been formulated and applied to the prediction of field and laboratory cooling pond behavior. In the limit of infinitely large dispersion, the model predicts the fully mixed pond, and with zero dispersion the solution approaches to a plug flow condition. The specification of the boundary conditions at the entrance and the exit is particularly important for the correct temperature distribution. The boundary conditions at the boundary points should conserve continuity in the heat flux, taking into account advective and dispersive transport. In particular, the entrance boundary condition depends upon the characteristics of the pond, given by a dispersion parameter $E_L^* = \frac{E_L}{uL}$, where L is a characteristic length, u is average velocity, and E_L is dispersion coefficient. By imposing this boundary condition, a temperature drop at the entrance boundary will be obtained for finite values of E_L.

A finite difference scheme based on the Crank-Nicholson method is applied to the solution of the one-dimensional dispersion equation. Comparisons between predicted values and laboratory or field data indicate satisfactory agreements.

Session VII C

Cooling Systems IV

33 45-32

COOLING WATER RESOURCES OF UPPER MISSISSIPPI RIVER FOR POWER GENERATION

P.P. Paily
NALCO ES Environmental Sciences
Northbrook, Illinois U.S.A.

T.-Y. Su
Sargent and Lundy Engineers
Chicago, Illinois U.S.A.

and

A.R. Giaquinta and J.F. Kennedy
Iowa Institute of Hydraulic Research
The University of Iowa
Iowa City, Iowa U.S.A

ABSTRACT

Thermal regime analyses were performed for the Upper Mississippi River lying in the Mid-Continent Area Power Pool (MAPP) geographical area (reach above River Mile 364.2 at Keokuk, Iowa) using a predictive computational model to determine the cooling water resources of the river for power generation. The thermal effects of the future power plants - new power plants as well as additions to existing units - projected to the year 1993 on seasonal temperatures of the river were determined. The locations of river reaches with under-utilized heat asismilation capacities on the basis of the existing and likely thermal criteria and standards of the various regulating agencies of the state governments in the study region were identified, and the allowable plant capacities that can use once-through cooling at those locations were determined. For the range of plant capacities projected for installation up to 1993 along the river in the MAPP area, alternative cooling modes to open-cycle cooling were investigated, along with an analysis of possible consumptive water use and investment costs of the alternative systems.

INTRODUCTION

Thermal power plants with total capacities of several thousand megawatts have been proposed and projected for installation along the portion of the Upper Mississippi River lying upstream from River Mile 364.2 at Keokuk, Iowa by the Mid-Continent Area Power Pool (MAPP)-member utilities through the year 1993. When selecting the plant sites along the river for these future capacities, the following questions are relevant: Is there adequate flow of water available in the river to provide for the condenser cooling water needs of the future installations if they are to use open-cycle cooling systems? What part of the water withdrawn for condenser cooling needs will be lost by evaporation? If complete open-cycle cooling is not possible, what are the economically most feasible alternate cooling modes, and what are the associated consumptive water uses for which water has to be withdrawn from the river? In order to find answers to these questions, and also to develop a suitable model and a tool for planning related to the present and projected use of the Upper Mississippi River water for electric power generation, a comprehensive study was initiated under the sponsorship of the Environmental Committee of Mid-Continent Area Power Pool. The basic objectives of the study included an evaluation of cooling water uses and needs for power generation, siting and sizing of future power plants based solely on thermal regime analyses, and economic evaluation of wet cooling towers as alternative cooling modes to open-cycle cooling. The results of these studies applicable to Upper Mississippi River are summarized in the following Sections.

COOLING WATER USES AND NEEDS

The condenser cooling water required by a power plant depends upon several factors, including the type of plant (fossil or nuclear), number of units, age and size of each unit, overall plant efficiency, and the temperature rise of the cooling water. For both once-through and recirculating systems with blowdown discharge, the thermal characteristics of the receiving waterbody may be a deciding factor, due to environmental impact considerations, in determining both the permissible temperature rise and the rate of withdrawal of cooling water from the natural waterbody.

The required condenser cooling water discharge, Q_e, for a plant of specified capacity, P (MW), depends upon the rate of heat rejection, and can be determined from

$$Q_e = K_1 \left(\frac{P}{\Delta T_e}\right) \left[\left(1 - \frac{\eta_I}{100}\right) \frac{1}{(\eta_P/100)} - 1 \right],$$

where $k_1 = 0.86 \times 10^9$, for Q_e in cm^3/hr, with (ΔT_e) in °C, or

$k_1 = 0.547 \times 10^5$, for Q_e in ft^3/hr, with (ΔT_e) in °F

The condenser-water discharge required by a plant of specific capacity, P (MW), thus can be determined, if allowable temperature rise, ΔT_e, is specified and the in-plant losses, η_I, and the overall plant efficiency, η_p are known. Figure 1 shows the condenser cooling water requirements as a function of the condenser temperature rise for different plant heat rates. The practical ranges of values for the various terms in Eq. (1) are as follows:

1. In-plant Losses. The average in-plant and stack losses for a fossil plant can be taken as about 15 percent. For nuclear plants, these losses are much less - generally less than 5 percent [6].

2. Plant Heat Rates or Plant Efficiency. The amount of fuel energy required to produce one kilowatt-hour of generated energy is plant heat rate. The average efficiency of all steam-electric plants in the nation in 1971 was about 33 percent (heat rate of 10,478 BTU/kwh [3]. Nuclear plants reject about 50 percent more heat to the cooling water per kwh than fossil plants. Even under ideal conditions, well-designed nuclear plants may not have thermal efficiencies exceeding 34 percent. On the other hand, fossil plants have achieved thermal efficiencies up to 39 percent as an average for an entire year's operation [6]. Average thermal efficiencies of 36 percent (heat rate of 9480 BTU/kwh) for fossil-fueled plants and 32 percent (heat rate of 10,700 BTU/kwh) for nuclear plants are reasonable values to use in the analysis of heat rejection from power plants.

3. Temperature Rise. For a given heat transfer rate in the condensers, the cooling water temperature rise is inversely proportional to the cooling water discharge through the condenser. Hence, the allowable temperature rise varies with both cooling water availability and plant heat rate. In addition, factors such as economics, ambient water temperature, and water quality requirements also influence the magnitude of the temperature rise. Federal Power Commission Plant Data for 1969 indicate that average temperature rises have centered about 15°F (8.3°C) and are fixed mainly by economic and process considerations [6].

The total installed thermal plant capacity along the Mississippi River in the MAPP area as of 1975 was about 7295 MW, of which 5820 MW used once-through cooling, and 1475 MW used cooling towers. The locations of the existing plants, which include 19 plants with a total of 59 units, are shown in Figure 2. The existing, proposed*, and projected* total plant capacities along the Mississippi River are listed in Table 1. The total water discharge required for condenser cooling at the existing and proposed plants, obtained from the data reported by the utilities, is tabulated in Table 2. The condenser cooling water requirements, calculated using Eq.(1), also are listed in Table 2. The results indicate that for the existing plants, an average in-plant loss of 10 percent, and an average plant efficiency of 33 percent, with a temperature-rise of 18°F (10°C) give calculated water requirements in close agreement with the reported values. However, for the newer proposed plants, the agreement is better with efficiencies of 36 percent for the fossil plants and 32 percent for nuclear plants and with in-plant efficiencies of 15 percent and 5 percent, respectively. Hence these latter efficiency values were applied in determining the cooling water needs for the proposed and projected plant capacities. The total plant capacity proposed for installation along the Mississippi River within the next few years is about 4260 MW, of which 3660 MW is planned for cooling towers. The locations of the proposed plants are shown in Figure 3. Of the total proposed capacity, 1960 MW will be fossil-fuel plants, and 2300 MW will be nuclear. Compared to this, 8755 MW of the total capacity of 15,955 MW projected through the year 1993 will use nuclear fuel according to present plans. The total condenser cooling water needs calculated for the sum of proposed and projected capacities is about 23,510 cfs (666 cu.m/s).

---

* Proposed plants are those which the utilities have committed to construction as well as those future plants which have been sited. Projected plants are those required to meet future demands for which either locations or condenser cooling systems or both have not been selected.

Consumptive Water Use

In closed-cycle cooling systems, cooling process itself causes loss of water by evaporation; the amount of evaporative loss is determined by the system design characteristics. In open-cycle systems, the temperature rise of the cooling water leads to accelerated evaporation from receiving waterbodies. The amount of heat lost by evaporation in once-through cooling systems can be taken as about 50 percent of the heat discharge [3], so that the quantity of water evaporated is 0.5 [HR]/L_o, where [HR] is the heat rejection rate, and L_o is the latent heat of vaporization (L_o = 1050 BTU/lb = 597 cal/gm = 2500 Joules/gm). Note, however, that the fraction of heat loss that is due to evaporation will vary widely with type of cooling system and with meteorological conditions. Since the cooling water discharge is [HR]/ΔT_e, the ratio of consumptive water loss to total withdrawal is given by,

$$\frac{\text{consumptive water loss}}{\text{total withdrawal}} = \frac{\Delta T_e}{2L_o} \quad \text{(for once-through cooling)}$$

The total average rate of withdrawal of fresh water and saline water for cooling purposes in the nation for the years 1969, 1970, and

1971 are given in Table 3. These data were obtained from the Federal Power Commission and represent a summary of the data submitted on FPC Form 67 for the respective years [3]. The 172,392 cfs of fresh water withdrawn for the year 1971 is equivalent to about 9 percent of the average annual runoff of all streams in the conterminous United States. Table 3 also lists the consumptive use of fresh water by both open-cycle and closed-cycle systems. The average evaporative loss of fresh water amounts to about 1 percent of the annual use of water for condenser cooling. Using this value, the amount of evaporative loss corresponding to the cooling water requirement in the MAPP area will be about 235 cfs (6.7 cu.m/s).

SITING AND SIZING OF FUTURE POWER PLANTS

Iowa Thermal Regime Model

In order to evaluate the cooling water resources of the Upper Mississippi River available for power generation, over and above the cooling water needs of the capacities already proposed and projected, thermal regime analyses were performed using a predictive computational model for steady-state temperature distributions ("Iowa Thermal Regime Model") developed by Paily and Kennedy [5]. The model is based on a numerical solution of the one-dimensional convection-diffusion equation, and predicts the longitudinal distribution of cross-sectional average temperature within the entire river length. The total river length is divided into smaller reaches, and solution for the temperature distribution in each reach is obtained separately; the solutions for adjacent reaches being linked by the common conditions at the junction or node points connecting them. Each reach of the river can have multiple thermal inputs and tributary inflows. The formulation allows for changes in the channel characteristics and the river flow rate from station to station. Variations in weather date afrom place to place are also taken into account.

The reliability of the model for predicting the the thermal regime of the Mississippi River was tested by comparing computed results with field measurements obtained along a 110-mile reach of the river between Becker, Minnesota (River Mile 906), and Lock and Dam No. 3 (River Mile 796). The results, presented in Figure 4, indicate that the predicted temperature is accurate within the measured temperature variations that occur along the river channel cross-section.

Thermal Regime Analysis of the Upper Mississippi River

The thermal regime model was used to determine the temperature distributions along the Upper Mississippi River lying in the MAPP area corresponding to average flow and weather conditions during typical months of the four seasons: February (winter), May (spring), August (summer), and November (fall). The input data used for the computations are the following:

1. Heat loads from power plants of rated capacity greater than 25 MW, industries, and municipalities located on the main-stem of the river and on major tributaries within 25 miles of their mouths;
2. Monthly mean values of daily flow rates measured at 12 U.S. Geological Survey gaging stations along the river;
3. Monthly mean values of daily weather conditions including air temperature, wind speed, relative humidity, atmospheric pressure, cloud cover and solar radiation measured at 8 first order weather stations of the National Weather Service; and
4. Channel cross-sectional geometrical parameters at approximately one mile intervals determined from flow profiles developed by the U.S. Army Corps of Engineers.

It was assumed that the river discharge, climatological variables, and channel geometrical parameters varied linearly between adjacent data points. The predicted temperature profiles for each month included the following:

- natural thermal regime of the river;
- temperature distributions with existing heat loads;
- temperature distributions with existing heat loads plus those from proposed and projected power plants;
- temperature distributions with permissible new power plants that could be installed without violating present thermal standards.

In addition, temperature profiles also were determined for the case of 7-day, 10-year low flows at all the gaging stations along the river, combined with average weather condltions for the months of August and November.

The locations and capacities of permissible new plants with once-through cooling sited along the Mississippi River were determined on the basis of the thermal criteria, summarized in Table 4 and 5. In applying the thermal standards, the limiting criterion was found to be a maximum allowable temperature excess of 5°F (2.78°C). However, there is some ambiguity as to what base this 5°F excess should be added to in order to obtain the limiting temperatures. Minnesota and Illinois standards specify this excess to be "above natural," while Wiscoonsin specifies "above existing natural," and Iowa and Missouri standards do not address this point. Hence, the thermal regime calculations to determine the permissible new plant capacity were made in two ways. In the first case, the predicted natural temperature distribution was assumed to be the base, and the 5°F excess was added thereto to obtain the limiting values. For the second case, the predicted temperature distribution with the existing heat loads was treated as the base, and the 5°F excess was added to it. The first case, with "natural-temperature base" is more definite, because it will be the same even after many years; the second case, with "existing-temperature base", will have a different base whenever a new plant is added to the system. The second case would permit the addition of more and more heat loads to the river, until the criteria specifying the maximum allowable temperatures, given in Table 5, become the limiting factors.

The predicted temperature distributions, assuming that all the existing, proposed, and projected power plants are operating at their full-load capacities, are shown for average and low flow conditions in August in Figures 5 and 6 for the case of natural temperature base, and in Figures 7 and 8 for the case of existing temperature base. During the low flow periods, it can be seen that even the existing plants will be in violation of the 5°F temperature-rise criterion at certain reaches of the river. The locations of the permissible new plants and the resulting temperature distributions are also shown in Figures 5 to 8. The locations of the permissible new plants were selected so as to obtain the highest allowable capacity in each case. The capacities of the permissible new plants during average and low flows with natural temperature base are tabulated in Tables 6 and 7, and with existing temperature base are tabulated in Tables 8 and 9 for both fossil-fuel (F) and nuclear-fuel (N) plants. Capacities of fossil-fuel plants were computed assuming η_P = 36 percent, and η_I = 15 percent, while for the nuclear-fuel plants, η_P = 32 percent and η_I = 5 percent were adopted. These capacities were determined such that at each of the selected locations, the temperature rise would be 5°F or less for the four months considered. The temperature rise criterion rather than the maximum temperature was found to be the limiting factor in all cases. If the natural temperature is adopted as the base, and if all existing plants are considered to have full-load operation, only four additional locations are available for new once-through plants, with a total possible capacity of about 5840 MW (F) or 4030 MW (N), as shown in Table 6 during average river flows. Compared to this, Table 7 shows that the total possible capacity is only 2476 NW (F) or 1708 MW (N) during low flow conditions. However, if existing temperature base is considered, it is possible to site plants at ten locations with a total capacity of 15,900 MW (F) or 10,970 MW (N) during average flows (Table 8); during low-flows the permissible plant capacities decrease to 7072 MW (F) or 4877 MW (N), as shown in Table 9.

WET COOLING TOWERS AS ALTERNATE COOLING MODES

The data presented in Table 1 show that projected plant capacities along the Mississippi River in the MAPP area include 15,000 MW for which specific sites have not been selected, and 955 MW for which locations but not cooling systems have been selected. Based on the results of the thermal regime analysis presented in the previous section it is clear that bulk of these projected capacities will have to use alternate cooling systems.

Mechanical draft wet cooling towers are considered as logical alternatives to once-through cooling in the MAPP area. The optimum sizes of these towers for the range of fossil and nuclear plant capacities projected for installation by the MAPP-member utilities, were determined using the methodology developed by Croley, Patel, and Cheng [1, 2]. In addition to the plant capacity, the heat rejection rate and plant heat rate associated with each power level comprise the major input information required for the computations. The meteorological data (chiefly dry-bulb temperature, wet-bulb temperature, and their frequency distributions) utilized for the analysis are those used by Giaquinta et al. [4]. These data are based on conditions for Chicago, Illinois, and represent typical conditions in the north-central area of the United States. For sizing of cooling towers the design values of these temperatures generally used are those which are not exceeded more than 5 percent of the time during the warmest period of a year (from June through September). Operation of the plant for the entire possible range of meteorological conditions was evaluated, and the total capacity loss associated with operation at conditions other than the design condition was determined. The cost equivalent of this capacity loss was added to the capital and operating costs to determine the total system costs.

A summary of the design conditions and unit values used for the economic analysis of wet cooling towers is presented in Table 10. Using these values, the optimum total unit costs of cooling for fossil and nuclear plants at various power levels are given in Tables 11 and 12, respectively. The variations with plant capacity of the optimum sizes and the corresponding minimum costs for wet cooling towers are illustrated in Figures 9 and 10 for fossil plants and nuclear plants, respectively. Tables 11 and 12 also list the annual evaporation loss and the annual blowdown discharge associated with each optimum tower size at each power level. Depending upon the power level, the total unit costs for optimum sized plants vary from 2.890 to 2.943 mills per kilowatt-hour for fossil plants, and from 2.957 to 2.978 mills per kilowatt-hour for nuclear plants. (These total unit costs can be converted to annual costs in dollars by multiplying the unit costs by 8760 P, where P is the plant capacity in MW.)

The costs of constructing and operating closed-cycle cooling systems should be compared to the costs of open-cycle cooling. The differential costs may then be interpreted as cost penalties for the closed-cycle system. This interpretation becomes important when evaluating the costs in light of the environmental and other benefits accruing to closed-cycle systems. Tables 11 and 12 include the total unit costs of open-cycle cooling for comparison with the cost of cooling by a wet cooling tower of optimum size. Costs of open-cycle cooling were obtained by the method used by Giaquinta et al. [4] for mechanical draft cooling towers with appropriate revisions. The range of total unit costs for optimum sized plants using once-through cooling is from 2.694 to 2.717 mills per kilowatt-hour for fossil plants and from 2.426 to 2.445 mills per kilowatt-hour for nuclear plants. Differences between these unit costs and the ones mentioned earlier for wet cooling towers give the cost penalties associated with closed-cycle cooling. These differential unit costs are seen to range from 0.196 to 0.226 mills per kilowatt-hour for fossil plants and from 0.531 to 0.533 mills per kilowatt-hour for nuclear plants.

For the plants represented in Tables 11 and 12 annual penalties resulting from the use of closed-cycle rather than open-cycle cooling range from \$0.396 x 10^6 per year to \$1.373 x 10^6 per year for fossil plants, and from \$1.868 x 10^6 per year to \$6.977 x 10^6 per year for nuclear plants.

CONCLUSIONS

The analysis of the thermal regimes of the Mississippi River lying in the MAPP geographical area indicates that the river have, under existing environmental and thermal regulations, heat transfer and assimilation capacities adequate for handling much of the waste heat from power plants planned for installation through 1993. However, certain reaches of the river (specifically the sections of the river lying adjacent to and extending some distance downstream from Minneapolis-St. Paul) can not accomodate additional thermal loads under existing thermal regulations.

An analysis of the capital and operating costs of mechanical draft wet cooling towers needed to dissipate the waste heat corresponding to the projected plant capacities was made. The total unit cost of these closed-cycle cooling systems was found to range from 2.810 to 2.943 mills per kilowatt-hour for fossil plants, and from 2.957 to 2.978 mills per kilowatt-hour for nuclear plants. The corresponding values for open-cycle cooling were found to range from 2.694 to 2.717 mills per kilowatt-hour for fossil plants and from 2.426 to 2.445 mills per kilowatt-hour for nuclear plants. The resultant cost penalties resulting from the use of closed-cycle cooling were found to range from \$0.396 x 10^6 per year to \$1.373 x 10^6 per year for fossil plants and from \$1.868 x 10^6 per year to \$6.977 x 10^6 per year for nuclear plants.

Finally, it should be noted that in many instances, particularly in relation to definition of natural temperature, the existing thermal standards are imprecise, and the various reasonable interpretations lead to a wide variation in estimating the remaining heat assimilation capacity.

Acknowledgement

The study which yielded the results presented herein was funded by the Mid-Continent Area Power Pool (MAPP). Special thanks are due to the members of the Environmental Committee of MAPP for initiating the work. The cooperation of MAPP-member utilities, personnel of the District Offices of the U.S. Geological Survey and the U.S. Army Corps of Engineers, regional office of the Environmental Protection Agency in Chicago, and the National Climatic Center in

Asheville, North Carolina in providing various segments of data is gratefully acknowledged. Part of the computer time was provided by the University of Iowa.

LIST OF REFERENCES

1. Croley, T.E. II, Patel, V.C., and Cheng, M.-S., "The Water and Total Optimizations of Wet and Dry-Wet Cooling Towers for Electric Power Plants," IIHR Report No. 163, Iowa Institute of Hydraulic Research, the University of Iowa, Iowa City, January 1975.
2. Croley, T.E. II, Patel, V.C., and Cheng, M.-S. "User's Manual for the IIHR Model of Dry-Wet Cooling Tower Economics," IIHR Report No. 181, Iowa Institute of Hydraulic Research, the University of Iowa, Iowa City, August 1975.
3. Federal Power Commission, "Steam Electric Plant Air and Water Quality Control Data for the Year Ending December 31, 1971," Washington DC, June 1974.
4. Giaquinta, A.R., Croley, T.E. II, Patel, V.C., Melville, J.G., Cheng, M.-S., and Uzuner, A.S., "Economic Assessment of Back-Fitting Power Plants with Closed-Cycle Cooling Systems", Report No. EPA-600/2-76-050, U.S. EPA, March 1976.
5. Paily, P.P., and Kennedy, J.F., " A Computational Model for Predicting the Thermal Regimes of Rivers," IIHR Report No. 169, Iowa Institute of Hyudraulic Research, the University of Iowa, Iowa City, November 1974.
6. U.S. Environmental Protection Agency, "Development Document for Effluent Limitations Guidelines and New Source Performance Standards for the Steam Electric Power Generating Point Source Category," EPA-440/1-74 029-a, October 1974.

TABLE 1

EXISTING, PROPOSED, AND PROJECTED TOTAL PLANT CAPACITIES IN MW ALONG UPPER MISSISSIPPI RIVER

Case	Fossil		Nuclear	
	OTF[a]	WCT[a]	OTF	WCT
Existing	3600	350	2220	1125
Proposed	600	1360	0	2300
Projected:[b]				
Location Specified	0		955	
Location Unspecified[c]	7200		7800	

[a] OTF = Once-Through Fresh; WCT = Wet Cooling Tower

[b] Cooling System not specified

[c] Only capacities that could possibly be installed along the river considered.

TABLE 2

COOLING WATER USES AND NEEDS FOR POWER PLANTS ALONG THE MISSISSIPPI RIVER

Category		Plant Capacity, (MW) F = Fossil N = Nuclear	Cooling Water Required in cfs(cu·m/s)		
			Calculated, (Eq. 1)		Reported by (Utilities[c])
			η_I = 15%(F), 5%(N); η_p = 36%(F), 32%(N)	η_I = 10%(F,N); η_p = 33%(F,N)	
Existing Plants		350[a] (F)	--	--	--
		1125[b] (N)	188.0 (5.3)	188.0 (5.3)	188.0 (5.3)
		3600 (F)	4135.8 (117.1)	5248.0 (148.6)	5339.9 (151.2)
		2220 (N)	3689.8 (104.5)	3236.3 (91.7)	3048.6 (86.4)
	sum:	7295	8013.6 (226.9)	8672.3 (245.6)	8576.5 (242.9)
Proposed Plants		1360[a] (F)	--	--	--
		600 (F)	689.3 (19.5)	874.8 (24.8)	757.8 (21.5)
		2300[a] (N)	--	--	--
	sum:	4260	689.3 (19.5)	874.8 (24.8)	757.8 (21.5)
Projected Plants		7200 (F)	8271.6 (234.2)	10496.0 (297.2)	--
		8755 (N)	14551.3 (412.1)	12762.9 (361.4)	--
	sum:	15955	22822.9 (646.3)	23258.9 (658.6)	--

[a] Cooling water data not available

[b] Closed-cycle cooling system, make-up water requirement

[c] From FPC Form 67

TABLE 3

PERCENTAGE OF TOTAL COOLING WATER WITHDRAWAL LOST BY EVAPORATION [3]*

	Quantity of Water, (cfs)		
year	1969	1970	1971
I. Rate of Withdrawal			
Fresh Water	165232	172005	172392
Saline Water	68391	73439	72564
II. Consumptive Use (Fresh Water)			
As Reported by Utilities	1058	881	1267
Including Calculated Loss for Once-through	1933	1830	2129
Percentage Consumptive Use (%)	1.17	1.06	1.23

* It is assumed that the amount of heat lost by evaporation in once-through cooling systems is 50 percent of the heat rejection.

TABLE 4

SUMMARY OF THERMAL STANDARDS FOR MISSISSIPPI RIVER

River Reach	State, and Controlling Agency	Classification of Reach	Allowable Temperature Rise Above Natural Conditions	Maximum Allowable Water Temperature
Lake Itasca to Lock and Dam No. 2, Hastings (RM 815)	Minnesota State Pollution Control Agency	Fish and Recreation Class B and Class C	5°F	86°F, and/or as specified for each month (Table 10), except 90°F-max. from outlet of Metro Wastewater Treat. Works to L & D No. 2
Lock and Dam No. 2, Hastings (RM 815) to Illinois border (RM 581)	Minnesota State Pollution Control Agency; and Wisconsin State Department of Natural Resources; and Iowa State Department of Environmental Quality	Fish and Recreation Class B; Waters for Fish and Aquatic Life; Class A	5°F	Specified for each month (Table 10)
Wisconsin border (RM 581) to Missouri border (RM 361)	Iowa State Department of Environmental Quality; and Illinois State Pollution Control Board	Class A; --	5°F	3°F above the limits specified for each month (Table 10)
Iowa border (RM 361) to Alton Lock and Dam (RM 203); and downstream of Alton Lock and Dam	Illinois State Pollution Control Board; and Missouri State Clean Water Commission	--	5°F	3°F above the limits specified for each month (Table 10)

TABLE 5

MAXIMUM ALLOWABLE WATER TEMPERATURES* IN MISSISSIPPI RIVER

Month	Reach 1	Reach 2	Reach 3	Reach 4	Reach 5
January	40	40	45	45	50
February	40	40	45	45	50
March	48	54	57	57	60
April	60	65	68	68	70
May	72	75	78	78	80
June	78	84	85	86	87
July	83	84	86	88	89
August	83	84	86	88	89
September	78	82	85	86	87
October	68	73	75	75	78
November	50	58	65	65	70
December	40	48	52	52	57

Reach 1: Lake Itasca to Lock and Dam No. 2, Hastings (RM 815)

Reach 2: Lock and Dam No. 2, Hastings (RM 815) to Illinois border (RM 581)

Reach 3: Wisconsin border (RM 581) to Missouri border (RM 361)

Reach 4: Iowa border (RM 361) to Alton Lock and Dam (RM 203)

Reach 5: Alton Lock and Dam (RM 203) to Arkansas border

---

* Temperatures are weekly average values for Minnesota; monthly averages of daily maximum values for Wisconsin; and the values that shall not be exceeded during more than one percent of the hours in the 12-month period ending with any month, for Iowa, Illinois, and Missouri.

TABLE 6

LOCATIONS AND CAPACITIES OF PERMISSIBLE POWER PLANTS BASED ON PREDICTED NATURAL TEMPERATURES AND FULL-LOAD OPERATION -- MISSISSIPPI RIVER (AVERAGE FLOW)

River	River Flow, Q(cfs)				Mixed Temp. Increase ΔT (°C)				Permissible Plant Capacity - Fossil (MW)				Permissible Plant Capacity - Nuclear (MW)			
Mile	Feb	May	Aug	Nov	Feb	May	Aug	Nov	Feb	May	Aug	Nov	Feb	May	Aug	Nov
1150.3	1654	2312	1491	1687	2.78	2.45	2.50	2.78	399	491	324	408	275	339	223	281
1113.0	1700	3564	1829	2000	2.78	1.42	2.03	2.78	411	441	323	483	283	304	222	333
700.0	15332	51016	22217	22702	2.78	1.43	1.98	0.65	3705	6337	3834	1283	2555	4370	2644	885
339.4	40369	97984	42642	45428	2.78	1.44	1.97	0.99	9763	12275	7308	3912	6733	8465	5040	2698

Summary of Permissible Plant Capacities:

Location (River Mile)	1150.3	1113.0	700.0	399.4
Fossil (MW)	324	323	1283	3912
Nuclear (MW)	223	222	885	2698

TABLE 7

LOCATIONS AND CAPACITIES OF PERMISSIBLE POWER PLANTS BASED ON PREDICTED NATURAL TEMPERATURES AND FULL-LOAD OPERATION -- MISSISSIPPI RIVER (LOW FLOW)

River	River Flow, Q(cfs)		Mixed Temp. Increase ΔT (°C)		Permissible Plant Capacity - Fossil (MW)		Permissible Plant Capacity - Nuclear (MW)	
Mile	Aug	Nov	Aug	Nov	Aug	Nov	Aug	Nov
1150.3	192	192	2.78	2.78	46	46	32	32
1113.0	192	192	2.78	2.78	46	46	32	32
1075.8	364	364	2.78	2.78	88	88	60	60
1038.5	499	499	2.78	2.78	120	120	83	83
1001.2	547	547	2.68	2.78	127	132	88	91
964.0	596	596	2.63	2.78	136	144	94	99
399.4	10678	10678	2.51	2.06	2331	1913	1608	1319

Summary of Permissible Plant Capacities:

Location (River Mile)	1150.3	1113.0	1075.8	1038.5	1001.2	964.0	399.4
Fossil (MW)	46	46	88	120	127	136	1913
Nuclear (MW)	32	32	60	83	88	94	1319

TABLE 8

LOCATIONS AND CAPACITIES OF PERMISSIBLE POWER PLANTS BASED ON TEMPERATURES WITH EXISTING PLANTS AND FULL-LOAD OPERATION -- MISSISSIPPI RIVER (AVERAGE FLOW)

River	River Flow, Q(cfs)				Mixed Temp. Increase ΔT (°C)				Permissible Plant Capacity - Fossil (MW)				Permissible Plant Capacity - Nuclear (MW)			
Mile	Feb	May	Aug	Nov	Feb	May	Aug	Nov	Feb	May	Aug	Nov	Feb	May	Aug	Nov
1150.3	1654	2312	1491	1687	2.78	2.78	2.78	2.78	399	559	361	408	275	385	249	281
1113.0	1700	3564	1829	2000	2.78	1.43	2.03	2.78	411	443	323	483	283	305	222	333
1075.8	1770	4662	2199	2215	2.78	1.09	1.86	2.78	428	443	354	536	295	305	244	370
1038.5	1981	5984	2715	2629	2.78	0.85	1.63	2.78	479	441	386	635	331	304	266	438
1001.2	2346	7598	3385	3292	2.78	0.62	1.43	2.58	568	411	423	739	391	283	291	510
964.0	2712	9211	4056	3955	2.78	0.54	1.23	1.90	656	429	432	655	452	296	298	451
700.0	15332	51016	22217	22702	2.78	1.74	2.48	2.59	3705	7714	4784	5116	2555	5320	3299	3528
599.4	20347	61853	27819	28691	2.78	0.50	1.28	0.83	4917	2698	3100	2065	3391	1860	2138	1424
500.0	28695	75706	34982	37369	2.78	0.64	1.43	0.88	6934	4198	4359	2855	4782	2895	3006	1969
399.4	40369	97984	42642	45428	2.31	0.82	1.82	1.27	8107	7009	6769	5025	5591	4834	4668	3465

Summary of Permissible Plant Capacities

Location (River Mile)	1150.3	1113.0	1075.8	1038.5	1001.2	964.0	700.0	599.4	500.0	399.4
Fossil (MW)	361	323	354	386	411	429	3705	2065	2855	5025
Nuclear (MW)	249	222	244	266	283	296	2555	1424	1969	3465

TABLE 9

LOCATIONS AND CAPACITIES OF PERMISSIBLE POWER PLANTS BASED ON TEMPERATURES WITH EXISTING PLANTS AND FULL-LOAD OPERATION -- MISSISSIPPI RIVER (LOW FLOW)

River Mile	River Flow, Q(cfs)		Mixed Temp. Increase ΔT (°C)		Permissible Plant Capacity - Fossil (MW)		Permissible Plant Capacity - Nuclear (MW)	
	Aug	Nov	Aug	Nov	Aug	Nov	Aug	Nov
1150.3	192	192	2.78	2.78	46	46	32	32
1113.0	192	192	2.78	2.78	46	46	32	32
1075.8	364	364	2.78	2.78	88	88	60	60
1038.5	499	499	2.78	2.78	120	120	83	83
1001.2	547	547	2.68	2.78	127	132	88	91
964.0	596	596	2.63	2.78	136	144	94	99
700.0	6421	6421	2.57	2.40	1437	1340	991	924
599.4	8941	8941	2.31	1.80	1799	1403	1241	967
500.0	9894	9894	2.17	1.61	1872	1388	1291	957
399.4	10678	10678	2.73	2.56	2533	2378	1746	1640

Summary of Permissible Plant Capacities:

Location (River Mile)	1150.3	1113.0	1075.8	1038.5	1001.2	964.0	700.0	599.4	500.0	399.4
Fossil (MW)	46	46	88	120	127	136	1340	1403	1388	2378
Nuclear (MW)	32	32	60	83	88	94	924	967	957	1640

TABLE 10

DESIGN CONDITIONS AND UNIT COSTS FOR DETERMINING SIZES, AND CAPITAL AND OPERATING COSTS OF WET COOLING TOWERS IN THE MAPP AREA

I. Design Conditions:	
Design wet-bulb temperature	75°F
Design dry-bulb temperature	89°F
Fan diameter	28 ft
Distance between fan centers	32 ft
Width of the tower pile on each of two sides	18 ft
Pumping height of water through towers	75 ft
Pumping efficiency	78.2%
Condenser heat transfer coefficient	630 BTU/hr/ft^2/°F
Specific land area	0.10 acre/MW
Concentration ratio of contaminants in cooling water	3.3
Water loading	12.5 gpm/ft^2 plan area
Air loading	1800 lbs/hr/ft^2 face area
II. Unit Costs:	
Unit fuel cost	$0.000751/kwh
Unit supply water cost	$0.10/1000 gal.
Unit blowdown treatment cost	$0.05/1000 gal.
Unit tower cost	$7.50/Tower Unit
Unit cost of replacement capacity	$90/kw
Unit cost of energy loss	$0.01/kwh
Unit condenser cost	$4/ft^2 area
Unit land cost	$3000/acre
Annual maintenance cost	$200/cell/year

TABLE 11

OPTIMUM SIZES AND TOTAL UNIT COSTS OF OPEN-CYCLE COOLING AND WET COOLING TOWERS -- FOSSIL PLANTS

Power Level,* (MW)	Optimum Tower Height, H (ft)	Optimum Tower Length L (ft)	Total Unit Cost mills/kwh		Total Annual Blowdown, (acre-ft /year)	Total Annual Evaporation Loss, (acre-ft /year)
			Cooling Tower	Open Cycle		
200	55	200	2.94291	-	1138	2618
	50	200	2.91771	-	1147	2638
	45	200	2.91714	2.7171	1158	2663
400	55	350	2.89960	2.7050	2285	5255
	50	350	2.90052	-	2305	5302
	45	400	2.90503	-	2316	5327
600	55	500	2.89518	-	3431	7892
	50	550	2.89367	2.6982	3452	7939
	45	600	2.89822	-	3474	7990
800	55	700	2.88970	2.6939	4570	10511
	50	750	2.89020	-	4599	10577
	45	800	2.89358	-	4632	10653

* Rated capacity

TABLE 12

OPTIMUM SIZES AND TOTAL UNIT COSTS OF OPEN-CYCLE COOLING AND WET COOLING TOWERS--NUCLEAR PLANTS

Power Level,* (MW)	Optimum Tower Height, H (ft)	Optimum Tower Length, L (ft)	Total Unit Cost mills/kwh		Total Annual Blowdown, (acre-ft /year)	Total Annual Evaporation Loss, (acre-ft /year)
			Cooling Tower	Open Cycle		
400	55	400	2.97936	2.4452	2710	6233
	50	450	2.97976	-	2723	6264
	45	450	2.98424	-	2751	6328
600	55	600	2.97256	-	4065	9349
	50	650	2.97114	2.4384	4091	9409
	45	700	2.97565	-	4119	9475
1100	60	1100	2.97049	-	7390	16998
	55	1100	2.96263	-	7452	17141
	50	1200	2.96191	2.4299	7498	17245
1300	60	1250	2.96619	-	8739	20100
	55	1350	2.96047	-	8799	20238
	50	1400	2.95965	2.4276	8865	20390
1500	60	1400	2.96549	-	10087	23199
	55	1500	2.95787	-	10162	23374
	50	1600	2.95748	2.4258	10233	23535

* Rated capacity

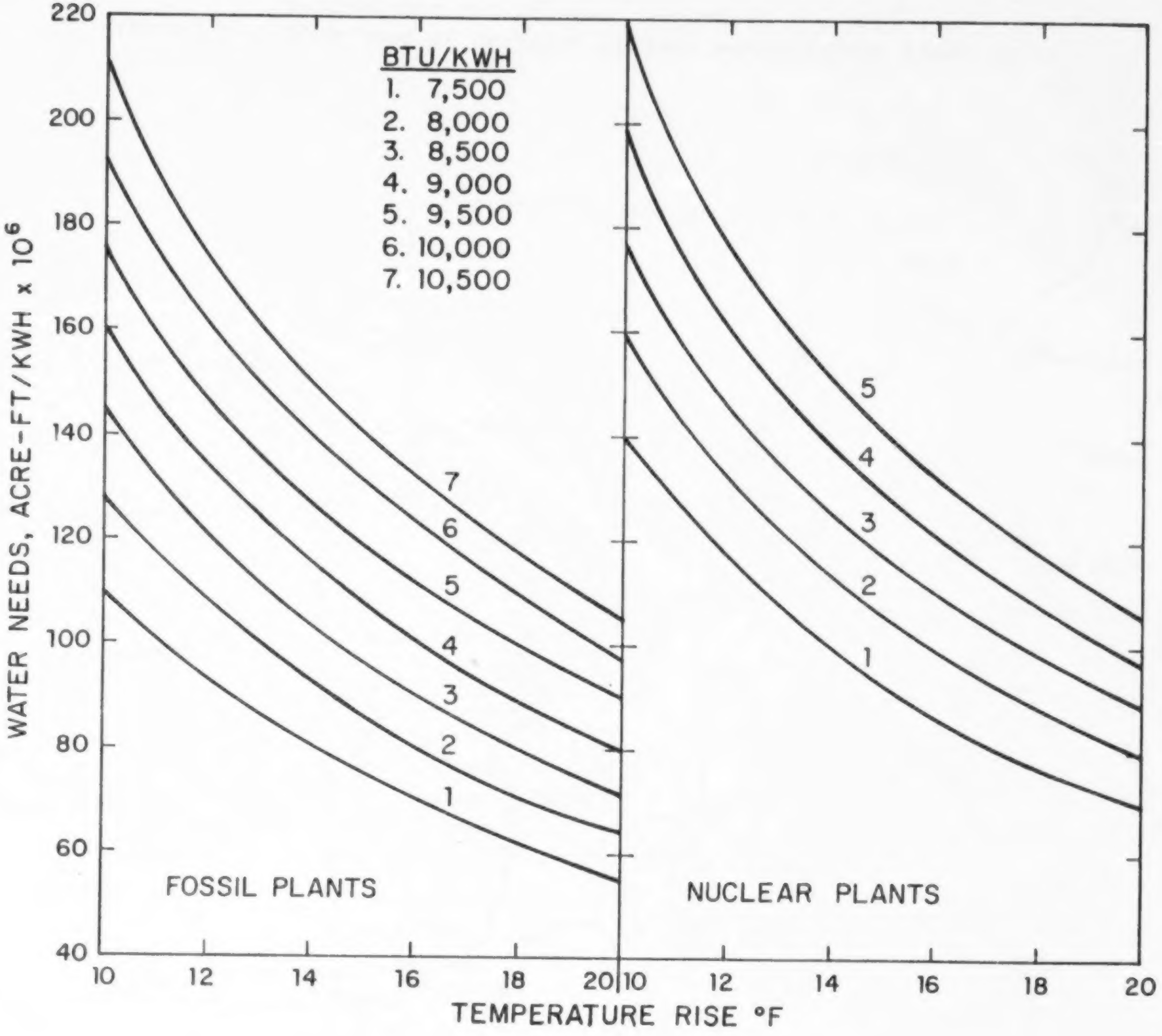

Figure 1. Cooling Water Requirements of Fossil and Nuclear Plants

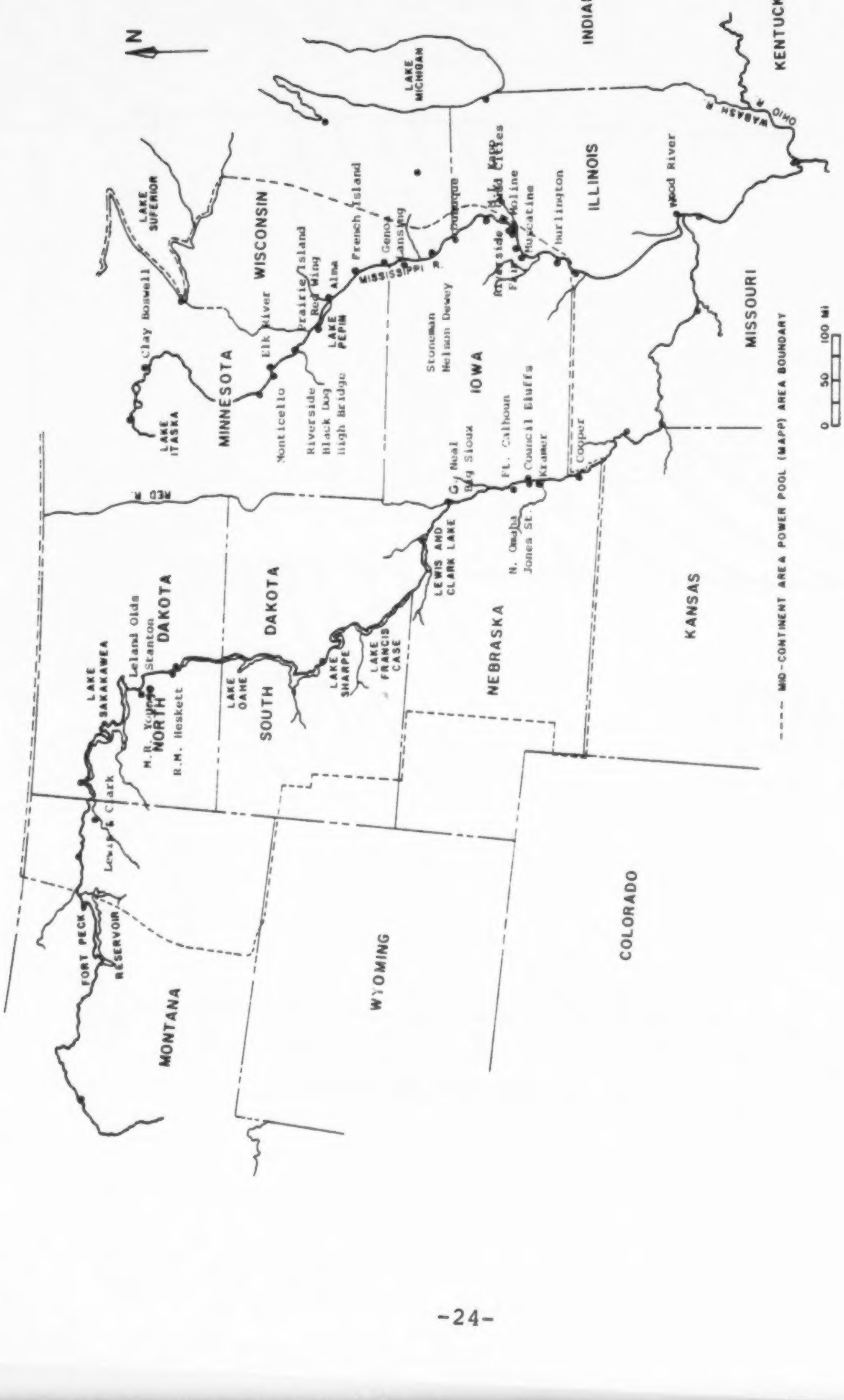
N
MONTANA
FORT PECK RESERVOIR
Lewis & Clark
LAKE SAKAKAWEA
M.R. Young
R.M. Heskett
Leland Olds
Stanton
NORTH DAKOTA
LAKE OAHE
SOUTH DAKOTA
LAKE SHARPE
LAKE FRANCIS CASE
LEWIS AND CLARK LAKE
WYOMING
NEBRASKA
COLORADO
KANSAS
N. Omaha
Jones St.
Ft. Calhoun
Council Bluffs
Kramer
Cooper
G. Neal
Big Sioux
RED R.
LAKE ITASKA
MINNESOTA
Monticello
Riverside
Black Dog
High Bridge
Elk River
Clay Boswell
LAKE PEPIN
Prairie Island
Red Wing
Alma
LAKE SUPERIOR
WISCONSIN
French Island
Genoa
Lansing
MISSISSIPPI R.
Stoneman
Nelson Dewey
IOWA
Dubuque
Riverside
Quad Cities
Moline
Muscatine
Burlington
ILLINOIS
LAKE MICHIGAN
INDIANA
Wood River
MISSOURI
WABASH R.
OHIO R.
KENTUCKY
0 50 100 MI
MID-CONTINENT AREA POWER POOL (MAPP) AREA BOUNDARY

Figure 2. Locations of Existing Thermal Power Plants Along the Mississippi and Missouri Rivers in the MAPP Area

PPP

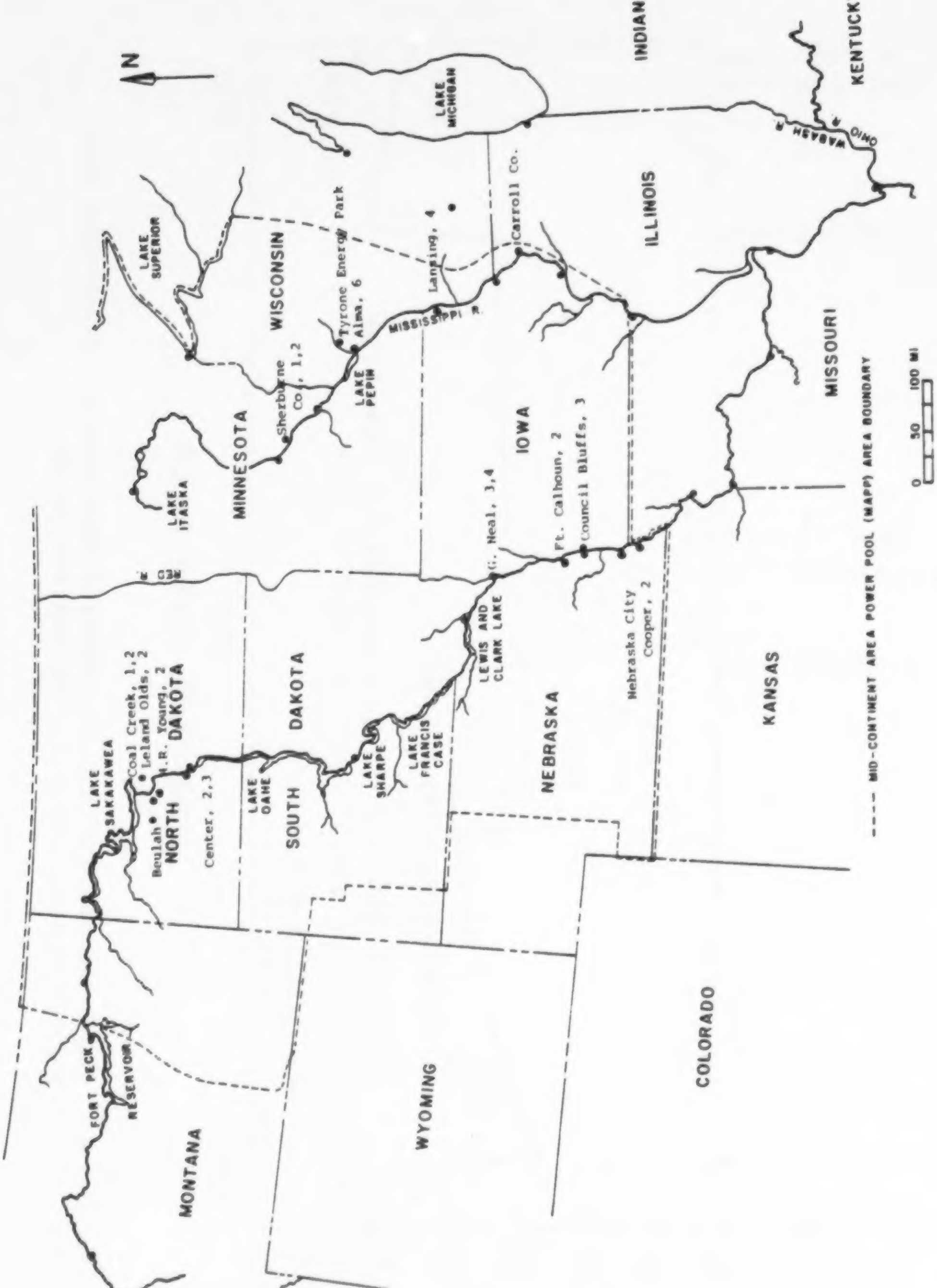
N
LAKE SUPERIOR
LAKE MICHIGAN
INDIANA
KENTUCKY
WABASH R.
OHIO R.
ILLINOIS
Carroll Co.
Lansing, 4
WISCONSIN
Tyrone Energy Park
Alma, 6
MISSISSIPPI R.
LAKE PEPIN
Sherburne Co., 1,2
MINNESOTA
LAKE ITASKA
IOWA
G. Neal, 3,4
Ft. Calhoun, 2
Council Bluffs, 3
MISSOURI
0 50 100 MI
--- MID-CONTINENT AREA POWER POOL (MAPP) AREA BOUNDARY
RED R.
LEWIS AND CLARK LAKE
NEBRASKA
Nebraska City
Cooper, 2
KANSAS
LAKE SAKAKAWEA
Coal Creek, 1,2
Leland Olds, 2
M.R. Young, 2
NORTH DAKOTA
Beulah
Center, 2,3
LAKE OAHE
SOUTH DAKOTA
LAKE SHARPE
LAKE FRANCIS CASE
COLORADO
WYOMING
MONTANA
FORT PECK RESERVOIR

Figure 3. Locations of Proposed and Projected Thermal Power Plants Along the Missisippi and Missouri Rivers in the MAPP Area

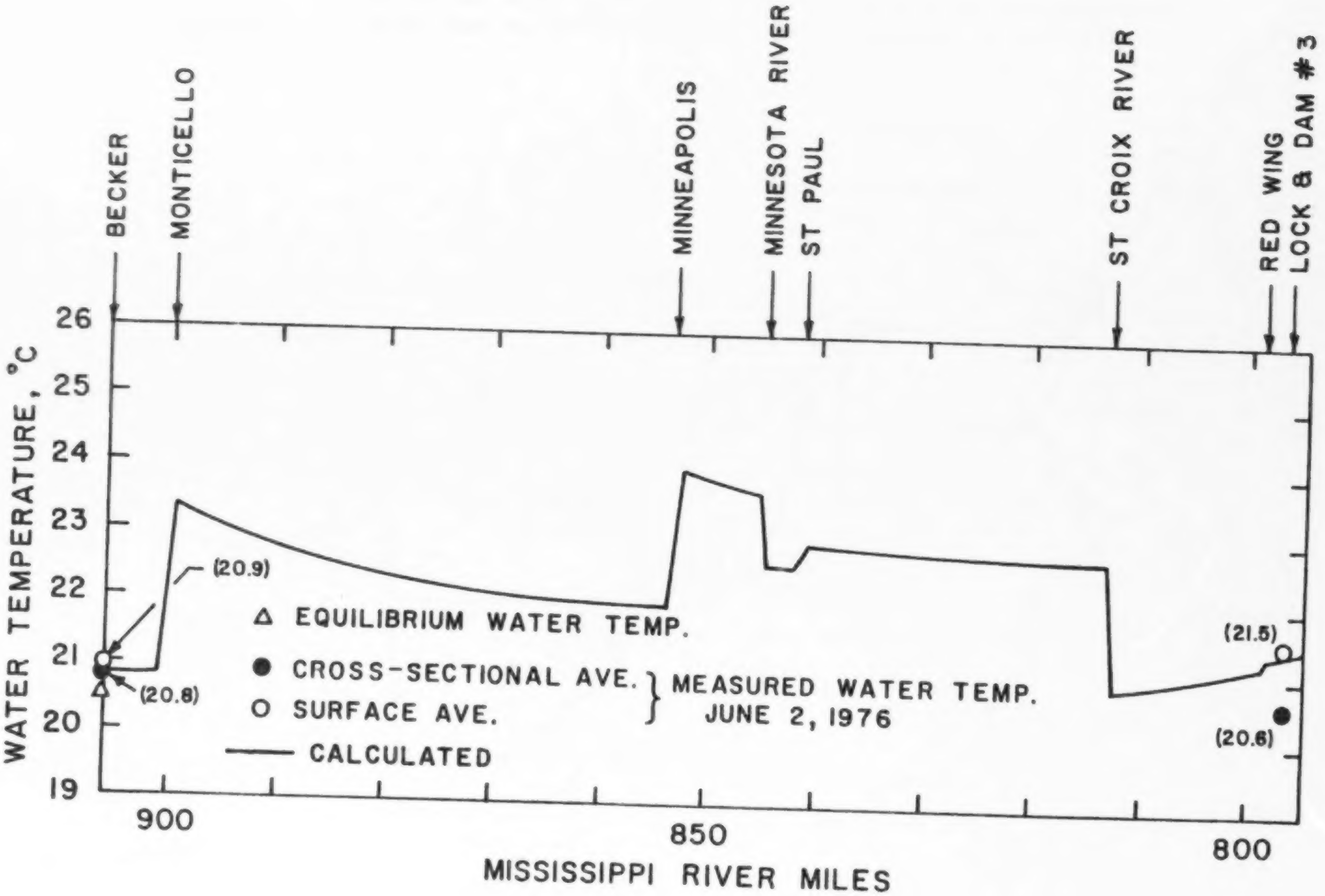

Figure 4. Comparison of Calculated and Measured Temperatures - Mississippi River Between Becker, Minnesota, and Lock and Dam No. 3

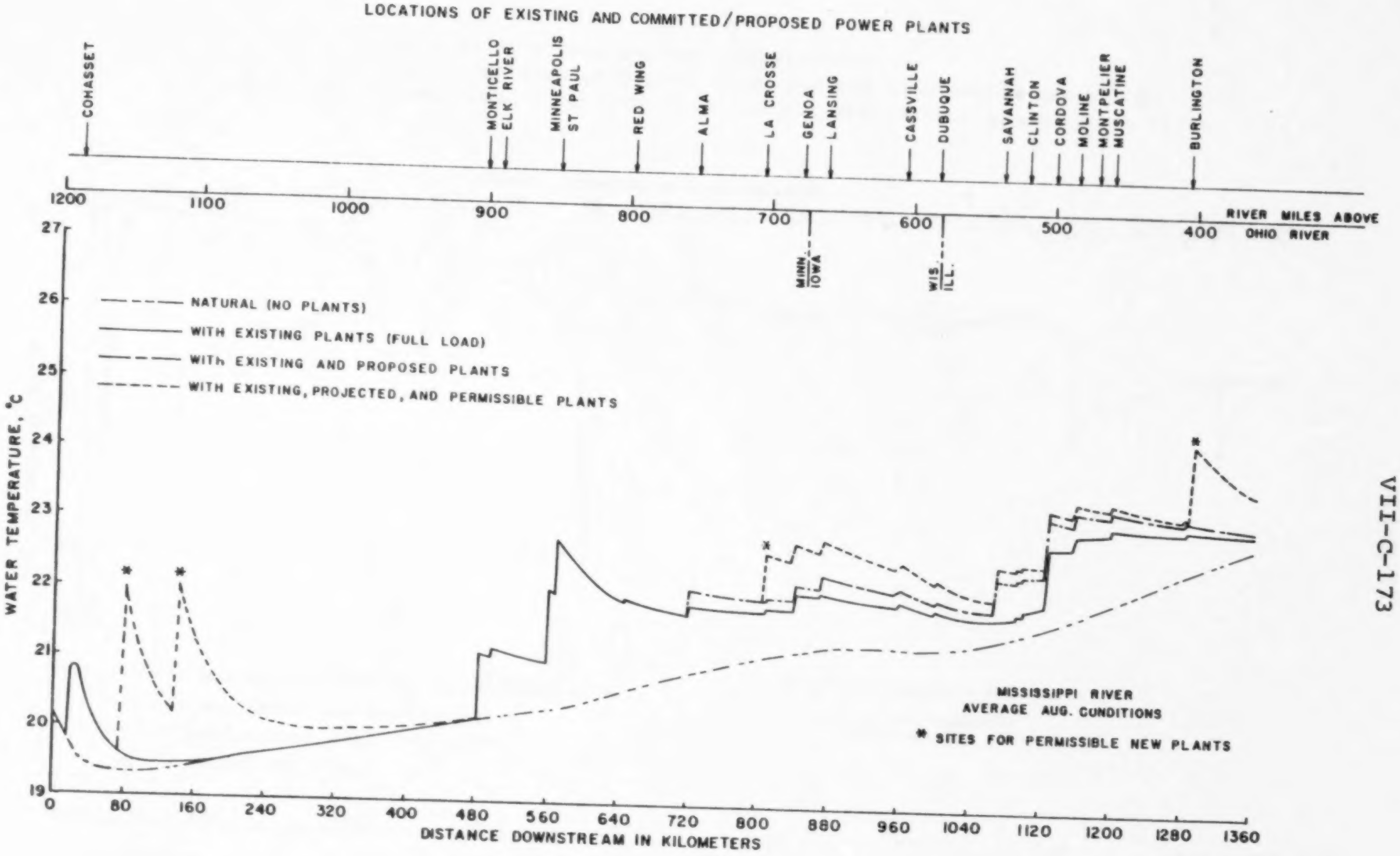

Figure 5. Temperature Distributions Along the Mississippi River for Average Flow Conditions With Full-Load Operation and Permissible New Plants Based on Predicted Natural Temperatures.

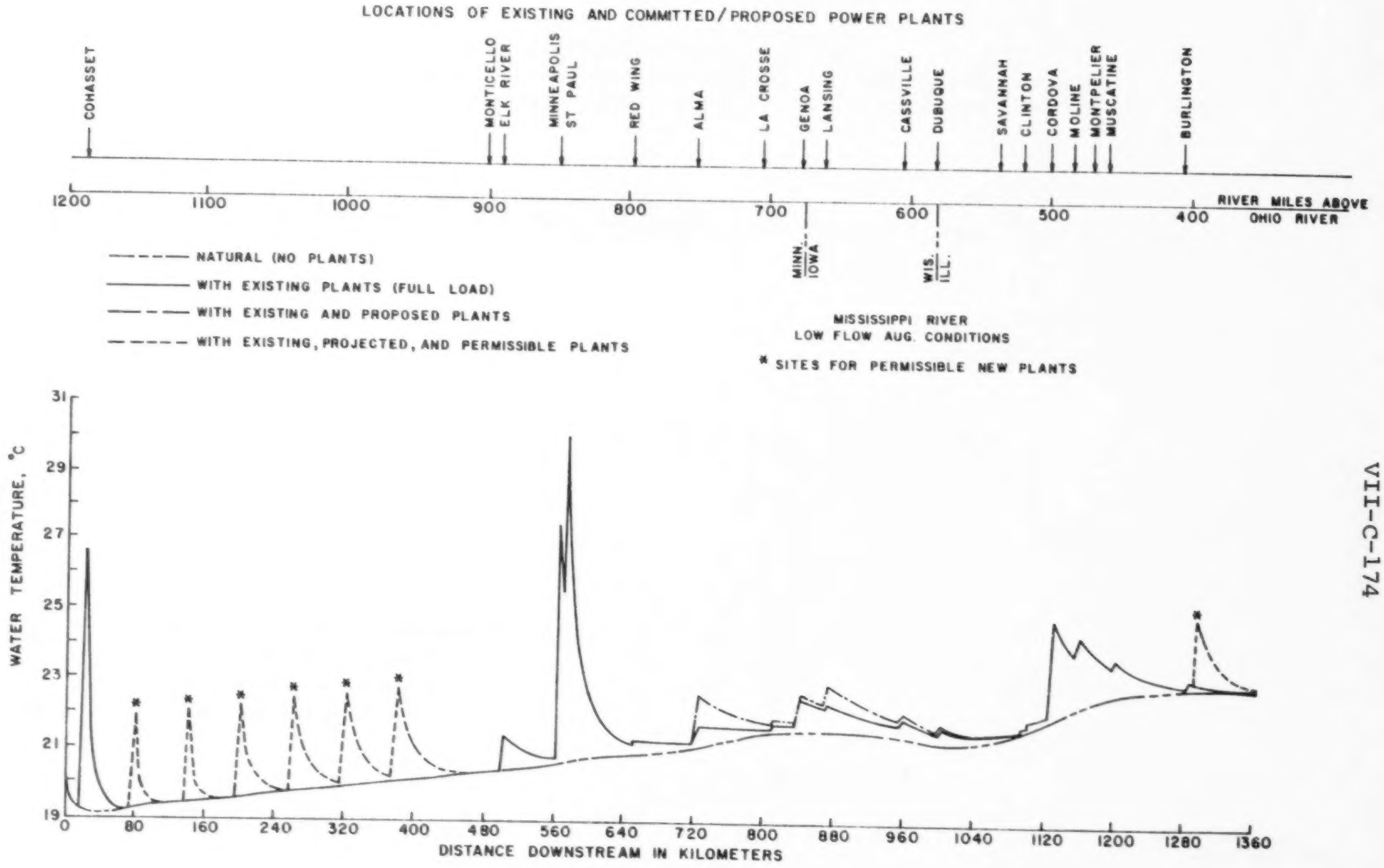

Figure 6. Temperature Distributions Along the Mississippi River for Low Flow Conditions With Full-Load Operation and Permissible New Plants Based on Predicted Natural Temperatures.

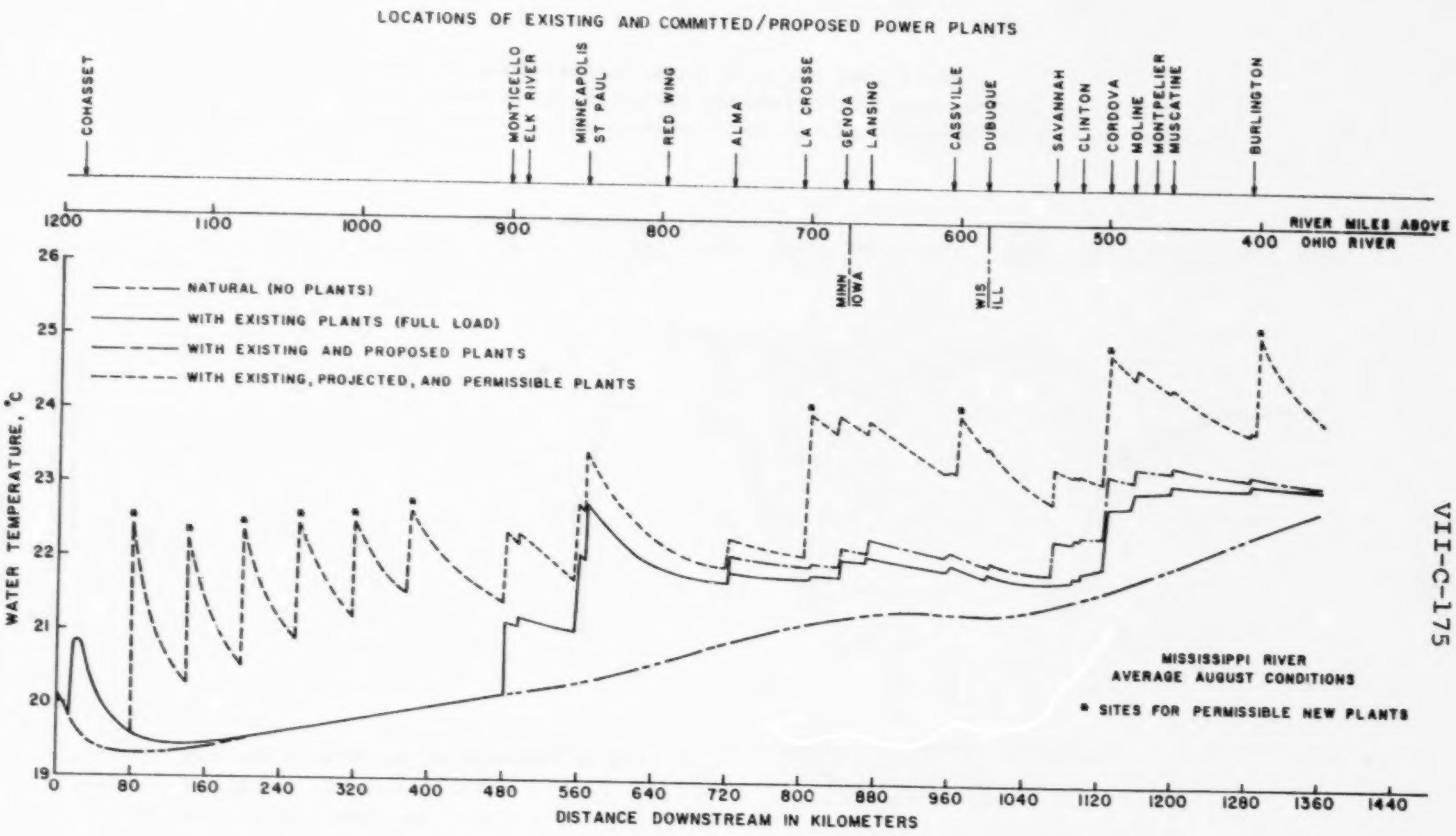

Figure 7. Temperature Distribution Along the Mississippi River for Average Flow Conditions With Full-Load Operation and Permissible New Plants Based on Temperatures With Existing Heat Loads.

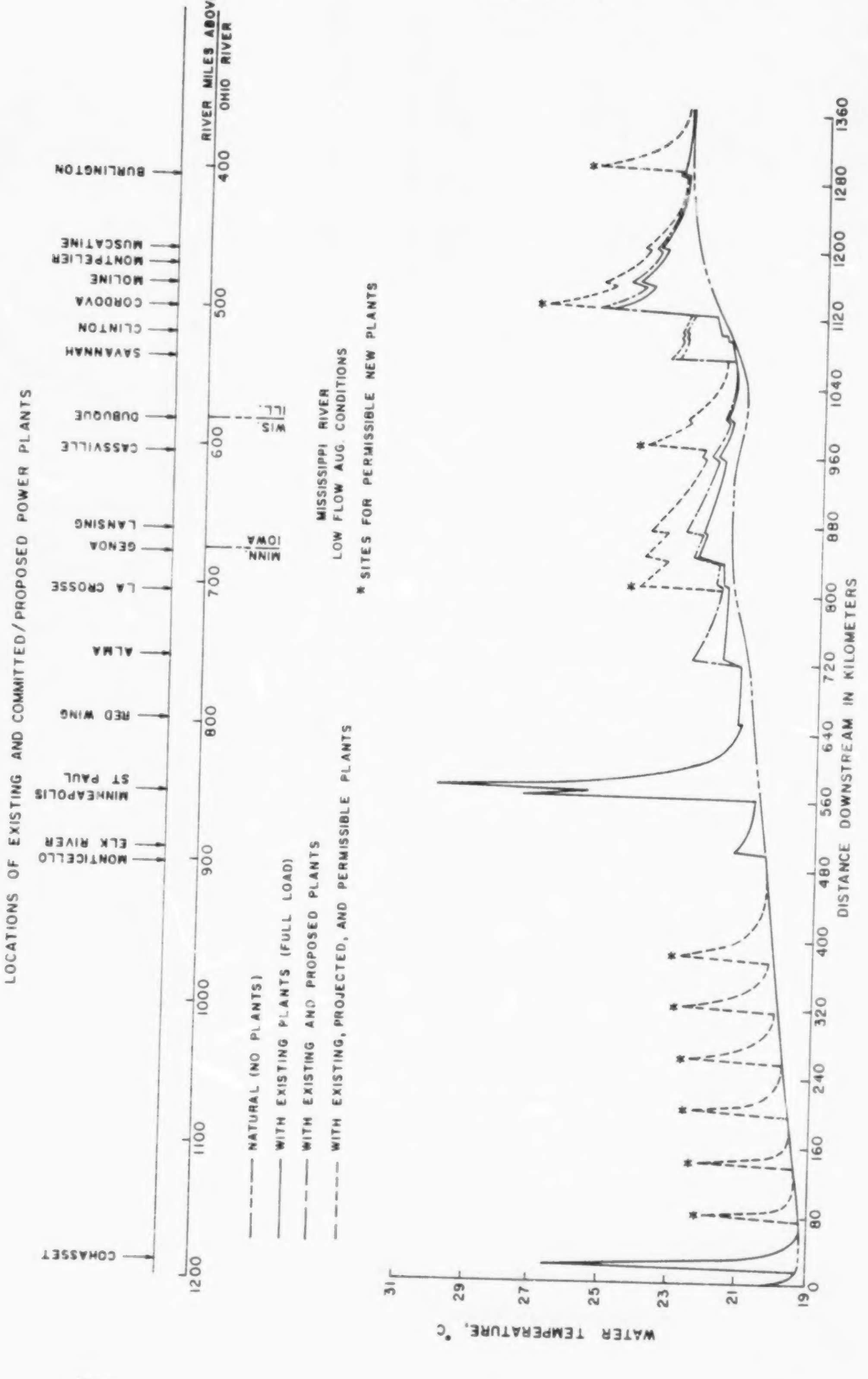

Figure 8. Temperature Distributions Along the Mississippi River for Low Flow Conditions With Full-Load Operation and Permissible New Plants Based on Temperatures With Existing Heat Loads.

PPP

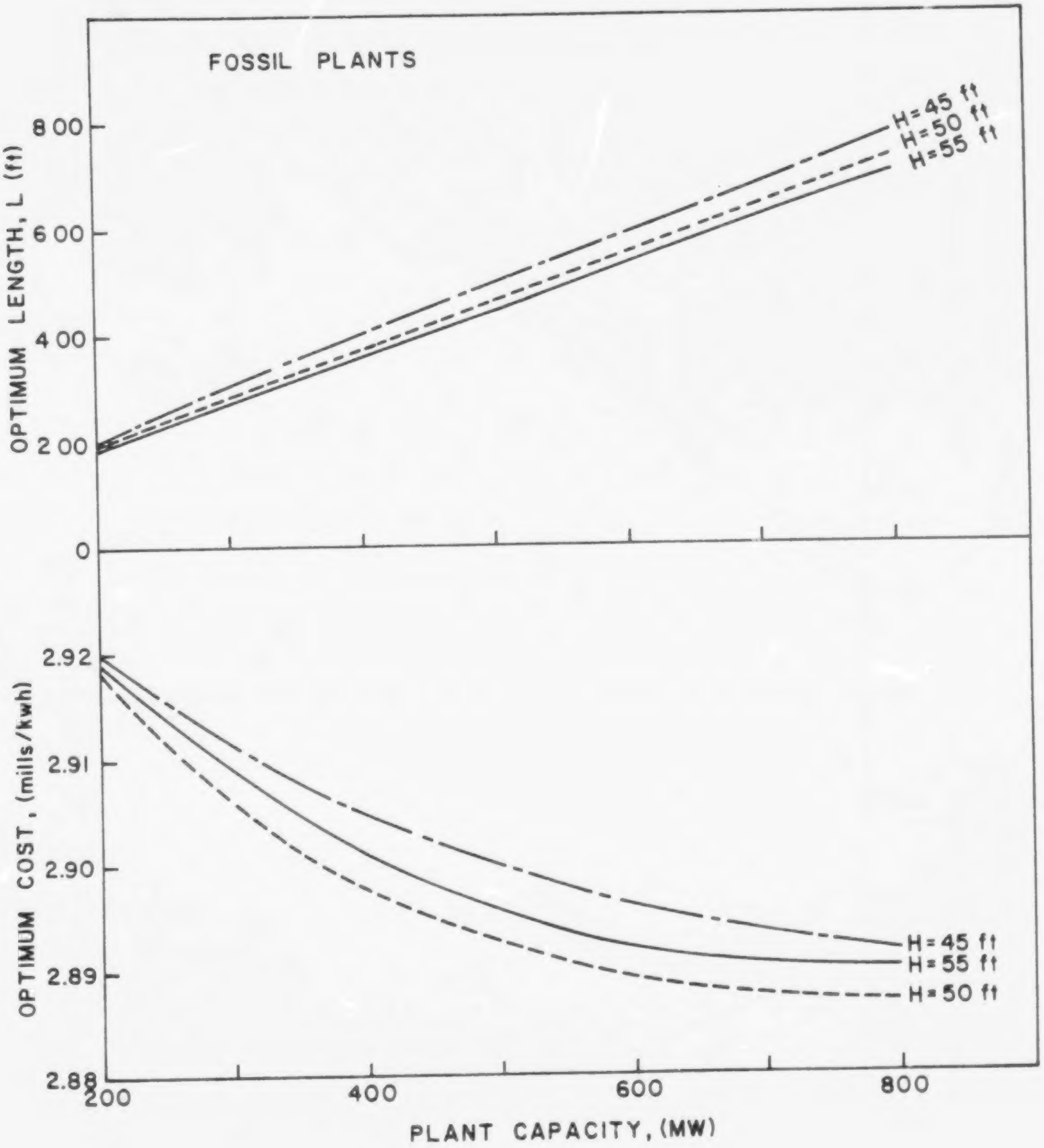

Figure 9. Optimum Sizes and Total Unit Costs of Wet Cooling Towers -- Fossil Plants

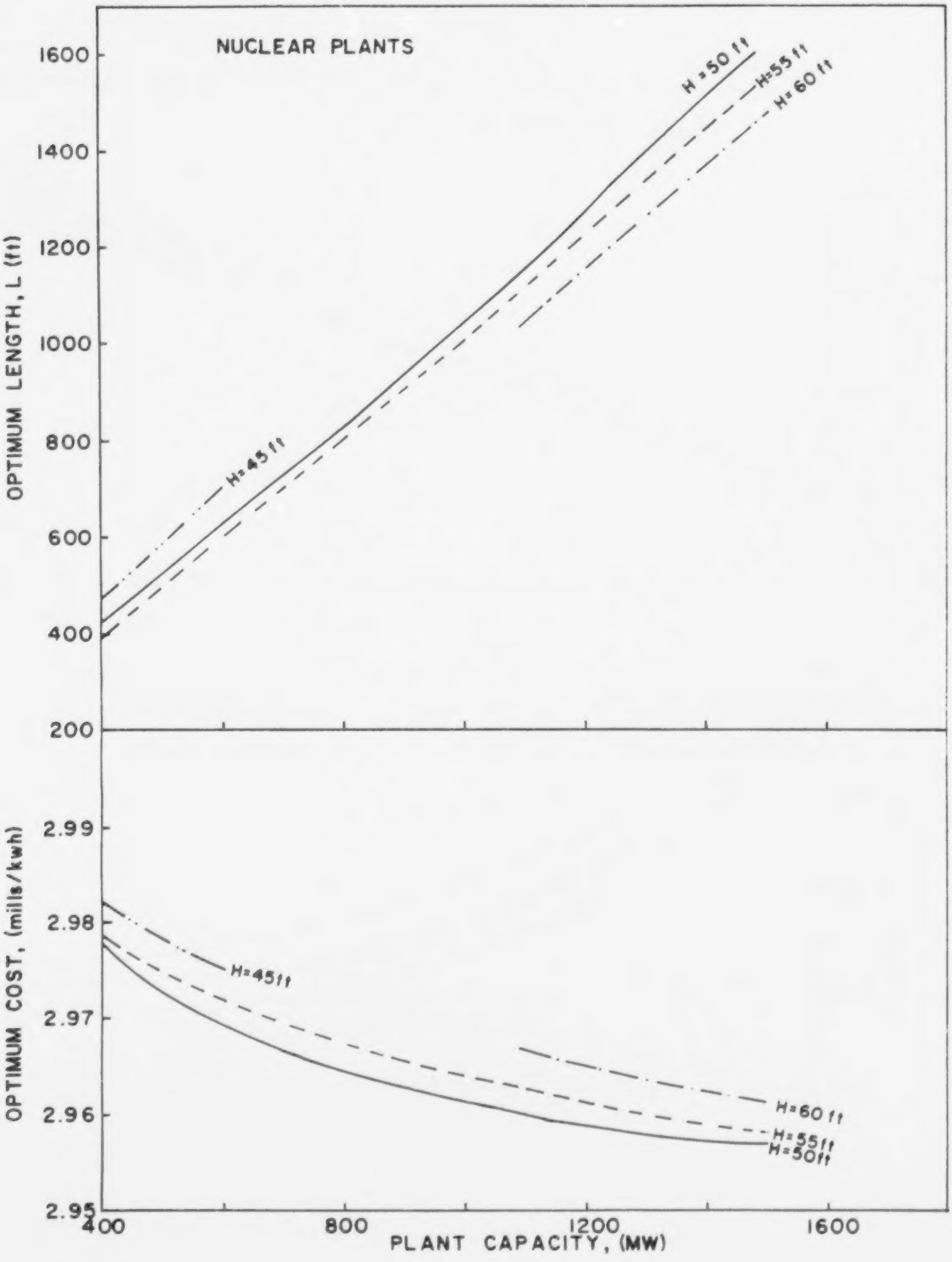

Figure 10. Optimum Sizes and Total Unit Costs of Wet Cooling Towers -- Nuclear Plants

34-45-31

INLAND FLORIDA COOLING SYSTEMS

A. F. Dinsmore
Brown & Root, Inc.
Houston, Texas U.S.A.

ABSTRACT

A power station if located at an inland site in Florida must have an efficient means of disposing of waste heat.

In general, the regulatory authorities have been leaning towards the use of cooling towers for heat dissipation. The climatic conditions of Florida do not favor the use of dry or wet-dry towers and only wet towers can operate effectively.

To make use of cooling towers, an abundant source of water must be available to overcome evaporation and other losses. Hydrologic conditions do not permit, within inland Florida, the continuous withdrawal of water. In order for the cooling towers to properly function, a water supply reservoir is required in the cooling system.

If a water supply reservoir is required for successful cooling tower operation, why not use that water body for heat dissipation rather than storage.

This paper discusses how for a large steam electric generating station, if located within Florida, the preferred method of heat dissipation is the use of a cooling pond.

1.0 STEAM ELECTRIC GENERATING PLANT OPERATION

The basic components of a steam electric generating plant are illustrated in Figure 1. High temperature steam is produced in the steam generator and fed under high pressure to the turbine. This high pressure steam enters the turbine, nozzles accelerate the steam to a high velocity and direct it at an angle to a row (or rows) of turbine blades mounted on a shaft, and forces on the moving turbine blades are thus created. The force component in the direction of motion of the turbine blades maintains the rotation of the shaft, which turns a generator and produces electric power. Low pressure steam exits the turbine and enters the condenser where cooling water, circulating through the condenser, removes heat from the steam causing the steam to condense to liquid water. Since water occupies a smaller volume than the steam, a partial vacuum is created at the turbine exhaust. This partial vacuum in turn causes the incoming high pressure steam to deliver more energy to the turbine than if the steam were released directly to the atmosphere. Low temperature, low pressure water is exhausted from the condenser and pumped back to the steam generator and the process is repeated.

For a "closed cycle" power generation device such as discussed above, thermal efficiency of the cycle is defined as that fraction of the thermal energy input which is converted into net power output of the cycle. Thus:

$$\text{Thermal Efficiency} = \frac{\text{Net Energy Output as Power}}{\text{Thermal Energy Input}}$$

All "closed cycle" power generation devices are limited by the second law of thermodynamics to thermal efficiencies less than 100 percent. Thus, only a portion of the heat input to the cycle can be converted into power, and that portion of the heat input not converted into net power output must be rejected to the condenser cooling water and on to the environment as waste heat. The waste heat from a nuclear generating unit is approximately two-thirds of the heat input.

The cooling water circulating through the condenser must remove this waste heat from the steam and then safely dissipate it to the environment.

2.0 COOLING SYSTEM

2.1 General

The efficient operation of a steam-electric generating plant requires an adequate supply of cooling water to its condensers for the removal of waste heat. The amount of waste heat that is absorbed by the cooling water as it passes through the condenser is the product of the rate at which the cooling water circulates and temperature rise it undergoes in the condenser. The cooling system must be able to efficiently and safely transfer the heat load from the condenser to the cooling water and from the cooling water to the environment.

The transfer of heat from the cooling water to the environment for any cooling system will occur by one or more of the following heat transfer mechanisms: conduction, evaporation, radiation and convection. To maintain high efficiencies, large flow rates of cooling water are required to pass through the condenser. This water must be supplied from natural water bodies in either a once through system or a circulating water system in which heat is dissipated from the water to the atmosphere. The systems being evaluated consist of two that are primarily evaporative systems (mechanical draft wet cooling towers and natural draft wet cooling towers), two that are partially evaporative systems (wet/dry cooling towers and cooling ponds) and one in which the heat transfer is accomplished by transferring the sensible heat from the water directly to the air (dry cooling towers).

2.2 Types of Cooling Systems

The types of cooling systems may be classified as follows:

1. Once-Through
2. Natural Draft or Mechanical Draft Wet Cooling Towers
3. Cooling Ponds
4. Dry Cooling Towers
5. Hybrid Wet/Dry Cooling Towers

A simple system for providing the condenser cooling water is the once-through cooling system. As the name implies, once-through cooling involves taking water from a river, an ocean, or large lake and routing it through the condenser once, then discharging the water (at an elevated temperature) back to the body of water. The points of intake and discharge should be sufficiently distant from one another to prevent recirculation of the heated cooling water. This method of heat dissipation is normally more economical and provides a more efficient steam-electric generating cycle than other systems, however, a suitable body of water is not available in inland Florida and consequently this evaluation is of the merits of the various types of cooling towers (mechanical or natural draft; wet/dry or dry mode) and of a cooling pond.

2.3 Makeup and Blowdown

In cooling systems where evaporation is the primary mechanism of heat transfer, it is necessary to periodically replace water lost from the system. This water loss is the result of two processes. First, there is direct evaporative loss of water and second, the release of a portion of the cooling water called blowdown. This blowdown is required to control the level of dissolved solids in the cooling system.

The acceptable level of dissolved solids in the system is controlled either by the tolerance levels of the cooling system and/or the limitation of dissolved solids of the receiving body of water to which the blowdown will be discharged.

The total makeup water requirements, therefore can be defined as the sum of the evaporative water loss, and the quantity of blowdown required to maintain an acceptable total dissolved solids concentration.

3.0 CLIMATOLOGY OF INLAND FLORIDA

The amount of heat transfer that occurs in a cooling system is a complex function of thermodynamic conditions existing at that point in time. The climatic conditions of a geographical area thus become one of the primary considerations in the selection of a cooling system. The climatology of inland Florida is summarized in this section.

Florida lies approximately between latitudes 25° and 30° north and is subjected to a mean cloud cover of 50%. The annual mean daily solar radiation is about 450 langleys which is only exceeded in the United States by several of the southwestern states and California. The average annual relative humidity exceeds 80 percent due to Florida's proximity to the Atlantic Ocean and the Gulf of Mexico. Maximum average monthly mean relative humidity values recorded at the Fort Myers and Tampa weather stations were 88% and 87% respectively with both stations recording a maximum monthly mean of 90% for one month. The average wet bulb temperature for Florida ranges from 74° to 76°F.

Mean annual temperatures range from the upper 60's in northern portions of the state to the middle 70's on the southern mainland, but reach 78°F at Key West. Mean temperatures during the summer vary from 81°F to 82°F throughout the state. During June, July and August maximum temperatures exceed 90°F about 2 days in 3 in all interior areas. In May and September 90°F temperatures or higher can be expected about 1 day in 3 in the northern interior and 1 day in 2 in the southern interior. Average minimum temperatures during the coolest months range from the middle 40's in the north to the middle 50's in the south. The average annual wind speeds for Florida vary from approximately 9 miles per hour along the coasts to approximately 7 miles per hour inland, depending on the topography.

4.0 HYDROLOGY OF INLAND FLORIDA

4.1 General

Ground water is not considered in this report as the existing aquifers of good quality water are under stress from existing use. The use of the deeper more saline aquifers would pose problems with blowdown wastes. Ground water was not therefore concluded to be a sufficiently reliable source of makeup water and is not discussed. Due to natural fluctuations in flow, the rivers of central and southern Florida are incapable of consistently delivering a quantity of water sufficient to meet the requirements of a steam electric generating plant. The situation is further complicated by the inherent presence of poorer water quality during lower stream flows when the average stream water quality conditions will vary radically. The following discussion of the Peace River flow at Arcadia will serve to illustrate these points.

4.2 Peace River Flows

The main stem of the Peace River is a narrow and shallow watercourse having a relatively narrow floodplain with a steep slope. Historically, the Peace River has experienced a wide range of flows on both a seasonal basis and on a short-term basis. At the USGS gaging station located at Arcadia, Florida, the average flow is 1252 cfs (561,900 GPM) based on records from 1931 through 1970, while that at Zolfo Springs, approximately 20.8 miles upstream of the site, is 351.1 cfs or 157,750 GPM (USGS 1970). Mean monthly flows for this period are given in Table 1 for both the Arcadia and Zolfo Springs gaging stations together.

As may be seen in Table 1, May is historically the low-flow month of the Peace River followed in order by the months of December, November, January, April, February, and March.

4.3 Makeup Water Diversion Scheme

The following discussion of water availability from the Peace River near Arcadia will serve to illustrate the effect of a makeup water diversion scheme.

The assumption has been made that a diversion scheme similar to those previously accepted by water management districts, would also be permitted for the Peace River and water availability is evaluated on that basis. Using this assumed diversion scheme, a minimum bypass flow was determined for the Peace River for each of the twelve months of the year and a percentage diversion, which varies with the rate of flow in the river, was proposed for such periods of time as the rate of flow exceeds the minimum bypass flow. This diversion scheme is illustrated on Figure 2.

Figure 3 demonstrates the effect of the application of the diversion scheme by showing the periods of time during an actual one year of record when diversion would have been permitted by showing the volume of water which would have been diverted. It can be seen from Figures 2 and 3 that there will be many months when it would not be possible to divert water to meet the requirements of the plant.

4.4 Drought Period

The most severe low-flow sequence for the Peace River near Arcadia in the period 1931 through 1970 was between October 23, 1931, and May 22, 1932. During this 212-day period the Peace River flows never exceeded 330 cfs (148,100 GPM) past Arcadia. Flows in the river were below the minimum river bypass flow established on a monthly basis for the makeup water diversion scheme illustrated on Figure 2 and Figure 3. Thus, no water would have been available for power plant requirements during this entire period. Table 2 gives low flow data for the Peace River at Arcadia for the period of 1931-1965. Conditions therefore dictate that some provision be made to store water so as to maintain plant operation during such periods.

The following discussion will pertain to the four most widely used types of cooling towers. They are the mechanical draft wet tower, mechanical draft dry tower, wet-dry hybrid tower and natural draft wet tower.

5.0 COOLING TOWERS

5.1 General

Evaporative cooling towers remove heat from cooling water by a flow of air, developed either naturally or mechanically, delivered across or through the heated cooling water. Heat transfer to the atmospheric environment occurs primarily through evaporative cooling. To achieve heat removal, water is pumped to the top of the tower and contact with the air flow is made as the cooling water then falls down through the tower to the tower basin. Evaporative cooling accounts for most of the waste heat rejection with most of the remaining heat rejection (5-10% as an annual average) goes into heating the moist air flowing through the tower. This warming is in the form of sensible heat, observed as a direct temperature rise of the air.

Operation of evaporative cooling towers results in the phenomenon known as drift. When the cooling water is introduced at the top of the tower, droplets are formed by mechanical breakup at nozzles, in the fill, and on structural components of the towers. Some of these droplets will become entrained in the air flow and leave the tower. Some may fall out close to the tower and others at a distance dependent upon the actual climatic conditions.

It should be noted that in modern cooling towers, drift is largely, but not totally, eliminated by a low pressure drop filter system known as a "drift eliminator". In this, the air stream is forced to follow a curved path, and a portion of the drift droplets are removed by centrifugal impaction on the eliminator surfaces with subsequent drainage back into the tower basin and eventually into the recirculation loop. State-of-the-art drift eliminators, fully maintained and operating at design conditions, are capable of reducing the drift to 0.002 percent (or less) of the total water circulation rate. There is, however, a tradeoff between pressure drop across the eliminators (Which also affects tower size and cost) and the required eliminator efficiency. Drift does not, however, pose a serious problem in terms of the deposition of solids on terrain and vegetation due to recent advances in cooling tower technology.

5.2 Mechanical Draft Wet Cooling Tower

The term wet implies that the heated cooling water is exposed to direct contact with the flow of air. In this type of tower the cooling water is pumped to some elevation above the tower base where it falls through fill to a tower basin and is collected and recirculated through the condensers. Cooling is accomplished by evaporation and by sensible heat transfer as a mechanically induced air draft passes through the fill. The heated air-vapor mixture is then released to the atmosphere at the top of the tower.

5.3 Natural Draft Cooling Tower

The natural draft cooling tower is essentially a wet tower incorporating a hyperbolic shell into the design and employing the principles of thermodynamics. The flow of air through the tower is primarily the result of the density difference between the external air and the internal air when it is heated by the cooling water and mixed with water vapor. Natural draft towers are designed to be several hundred feet tall in order to enhance the natural draft characteristics, and also to place the plume exit plane as high as possible above the terrain. For structural reasons the towers are constructed as hyperbolic shells with a base diameter 60-70 percent of the tower height. When considering this type of tower for an area, local climatic conditions must be such as to maintain the required air flow while overcoming pressure losses caused by the flow of air through the structure. It must be kept in mind that thermal performance of the tower will always be subject to weather conditions over which there is no control.

It should be noted that a wet cooling tower utilizing a naturally developed draft evaporates approximately the same amount of water as a mechanical draft wet cooling tower.

5.4 Mechanical Draft Dry Cooling Tower

There are two types of dry cooling towers; the indirect system and the direct system. In the indirect system, heat is transferred from the steam to the cooling water in the condenser. The heated cooling water is then pumped from the condenser through a tubing network in the cooling tower and back to the condensers. Cooling is accomplished as air passes over the tubing by heat conduction through the tubing walls and by heat convection at finned tube surfaces or similar heat transfer surfaces. The heated air is then released to the atmosphere at the top of the tower.

In the direct system steam flows directly to the cooling tower, in the same way as the heated cooling water is pumped in the indirect system, and cooling is accomplished in the tower as previously discussed. Thus, in the direct system the cooling tower performs the function of the condenser as well.

In the dry tower, the back pressure in the turbine and in turn its effect on power output, is related to the ambient dry bulb temperature. As the dry bulb temperature is always considerably higher than the wet bulb temperature,the cooled water leaves the dry tower at a higher temperature than would be obtained with a wet tower where the wet bulb temperature controls. Therefore, plant efficiencies are much lower with this type (dry) cooling tower. Dry cooling towers are not efficient in geographical areas with high dry bulb temperatures as in Florida, and are presently considered unsuitable to use in Florida.

5.5 Wet-Dry (Hybrid) Cooling Tower

Wet-dry cooling towers consist of a combination of evaporative cooling sections and dry cooling sections. The towers are designed and used for the elimination of cooling tower induced fogs and plumes. Having a portion of the cooling done in the dry section of the tower reduces the amount of water required for makeup. Passing a portion of the thermal effluent through finned tube heat exchangers, located at the top of the tower, lowers the relative humidity of the exiting air-water vapor thus reducing visible vapor plume.

A door like air flow restrictor, called the damper, is located in the heated dry air stream between the air cooled heat exchangers and the fan. During periods of high ambient dry bulb air temperatures, when the efficiency of wet cooling increases and that of dry cooling decreases, the damper is adjusted to reduce the air flow rate through the dry air stream, thus increasing the air flow rate in the wet stream. The evaporative section thermal performance is therefore used more effectively during periods of high ambient air temperature. During these periods of high usage of the wet section of the cooling tower, the evaporative losses of water are approximately equivalent to that which would occur in a standard wet cooling tower. It should be noted that on wet-dry cooling towers, it is normal to discontinue the use of the dry section at temperatures ranging from 35°F to 65°F. Therefore, in Florida the dry section of the cooling tower would be virtually useless.

5.6 Effect of Climate on Cooling Tower Operation

Cooling in a wet tower primarily takes place by evaporation and thus is influenced by temperature, relative humidity and the draft induced in the tower. The means by which the draft is developed has little effect on the amount of evaporation which takes place.

The loss of water by evaporation also requires that additional water be released as blowdown to prevent solids concentration. For an average monthly maximum total dissolved solids concentration of 500 mg per liter permitted in the receiving body of water and an existing concentration of 190 mg per liter in that body of water, the concentration ratio is approximately 2.6. For the climatic conditions of Florida, a 1200 MW(e) unit would evaporate approximately 14,000 GPM (all operating conditions being equal). With blowdown being 8800 GPM for the concentration ratio of 2.6. The makeup water requirement for one 1200 MW(e) unit would be 22,800 GPM or a total makeup water requirement of 228,000 GPM for a 12000 MW(e) power plant. Neither of the water requirements can be met by the Peace River for the greater part of the year as illustrated in Figure 3 and Table 1. These set of circumstances necessitate the incorporation of a water supply reservoir into the cooling tower system that would contain a sufficient volume of water to meet losses due to forced evaporation, seepage and blowdown.

5.7 Conclusions

From consideration of the effects of the climate of inland Florida, it can be concluded that the wet mechanical draft cooling tower is a more suitable option than natural draft cooling towers, dry cooling towers, or wet-dry towers and this type is discussed further.

6.0 EFFECT OF HYDROLOGY ON COOLING TOWER OPERATION

Due to the fluctuations of streamflow in Florida and the inherent presence of poorer water quality associated with lower streamflows, average stream water quality conditions will vary and the concentration of dissolved solids in a cooling tower system could often exceed the state water quality discharge standard (maximum monthly average allowable) of five hundred (500) mg per liter total dissolved solids. A tower system without any storage or blowdown flexibility could not in general operate at or above 2.5 cooling cycles and be capable of discharging to the stream at any time that the stream total dissolved solids level rose above 200 mg per liter. In order to meet these stream standards, constantly changing modes of tower operation would be required as the incoming water quality, quantity and blowdown quality varied. Additionally, blowdown to freshwater streams normally becomes economically prohibitive at cooling cycles of 4 or less due to the large volumes of makeup water and the large volumes that must be released to the stream to preserve environmental qualities.

A prolonged period below minimum makeup conditions would make it infeasible for a mechanical draft wet cooling tower to operate continuously and in turn the plant would be forced to close down. As stated earlier, the effects of climate and hydrology require the incorporation of a water supply reservoir into the cooling tower system in order to permit the cooling towers to operate.

Such a cooling system is illustrated in Figure 4.

6.1 Storage Reservoir Characteristics

The required reservoir volume to maintain operation during a drought must be such that (1) the volume of water is sufficient to maintain plant operation for a period equal to the period of the longest drought of record (see Section 5.3) and (2) a 6-month carry- over storage allocation which is based on the assumption that the maximum probable drought is yet to occur and consequently, some safety factor in the form of additional storage is required. Reservoir surface areas and embankment heights, which allowed for flood storage and wave runup, were computed and an economic comparison was made which considered the dollar value of land each reservoir would occupy and the respective capital costs of construction. The most economic reservoir, for a 12,000 MW(e) power plant using mechanical draft cooling towers, was found to have a 35,000 acre surface area with an embankment height averaging approximately 48 feet.

Water requirements were computed for the station based on full development of nuclear generating capacity (12,000 MW(e)) and a constant "load factor" of 80% of maximum capacity. Water supply for a system consisting of wet mechanical draft cooling towers and a water supply reservoir must meet the following demands: natural reservoir evaporation (net), drift and forced evaporation from the cooling towers, seepage from the reservoir, blowdown releases from the reservoir, and any additional outside demand.

Natural evaporation is influenced by wind speed and the difference between the saturated water vapor pressure at the surface of the water body and the water vapor pressure in the air. Water vapor pressure difference is, in turn, influenced by air and water temperature and humidity. For a water supply reservoir surface area of 35,000 acres, the average annual evaporation, based on computed monthly evaporation rates, is 92,200 GPM.

Net natural evaporation is simply the difference between natural evaporation and direct precipitation onto the reservoir surface. Based on computed monthly rainfall in the vicinity of Arcadia, the average annual rainfall onto a 35,000 acre water supply reservoir is 100,200 GPM. Hence the net natural evaporation (natural evaporation minus rainfall) averages (-) 8,000 GPM. The negative value indicates a surplus of rainfall over evaporation in this region of Florida.

Forced evaporation from cooling towers is a function of the wet bulb temperature of the air, relative humidity, cloud cover, wind speed, and range of cooling and heat losses by other mechanisms. For a site in West Florida, forced evaporation was estimated, for a 15°F approach to wet bulb, to be approximately 111,900 GPM.

Drift is the entrained water (water droplets) carried from the tower by the discharged air. For a site in West Florida, drift loss would be approximately 200 GPM for a 12,000 MW(e) plant based on 0.002% of condenser flow as drift.

Seepage from a water supply reservoir is dependent upon the foundation conditions underlying the reservoir and the material composition of the reservoir embankment. The seepage rate from a reservoir is also related to water table conditions and to the depth of water storage within the reservoir. Average annual seepage from a 35,000 acre reservoir is approximately 56,700 GPM, based on data obtained from tests in the area of Arcadia.

The increase in the concentration of total dissolved solids in the cooling tower-condenser circulating water due to evaporation makes it necessary for the cooling tower to periodically blowdown to the water supply reservoir. As a result, periodic releases of water from a water supply reservoir are occasionally necessary in order to maintain concentrations of dissolved solids within the reservoir at desirable levels and to avoid exceeding water quality standards, set by the Florida Department of Environmental Regulation in the Peace River, when discharges are made to the river from the reservoir. Average annual amount released from a 35,000 acre reservoir is approximately 19,000 GPM.

It is also assumed that there are no other demands on the proposed cooling tower water supply reservoir system.

The results of the reservoir operation studies indicated that a firm supply of makeup water could be diverted from the Peace River to accommodate the requirements for an ultimate power station capacity of 12,000 MW(e) and also meet the State water quality requirements for blowdown. The total average long term diversion that would be required is indicated below:

12,000 MW(e) Power Station Capacity	
Net Evaporation Makeup	104,100 GPM
Average Annual Seepage	56,700 GPM
Net Average Annual River Diversion	160,800 GPM

7.0 COOLING POND

7.1 Definitions

The following definitions have been set forth by the Environmental Protection Agency and in the Florida Statutes respectively. "The term 'cooling pond' shall mean any manmade water impoundment which does not impede the flow of a navigable stream and which is used to remove waste heat from heated condenser water prior to returning the recirculated cooling water to the main condenser." "A cooling pond is a body of water enclosed by natural or constructed restraints which has been approved by the Florida Department of Environmental Regulation for purposes of controlling heat dissipation from thermal discharges."

7.2 Heat Processes

In a cooling pond, heated cooling water is discharged from the condenser directly into the pond where the water circulates around mobilization dikes. The cooling pond system is illustrated in Figure 5. In the process of flowing to the point of condenser intake, heat is given up to the atmosphere through conduction, back radiation and evaporation. The various mechanisms by which heat is exchanged between the water and the atmosphere are shown in Figure 6. The following is a brief description of the more important mechanisms, their symbolic identifications on the aforementioned figure, and the various meteorological factors that affect them.

Short-wave solar radiation, Hs, and long-wave atmospheric radiation, Ha, are incident upon the body of water. The intensity of short-wave solar radiation varies with the latitude of the location, time of the day, season of the year and amount of cloud cover. Long-wave atmospheric radiation is a function of many variables, but is largely dependent upon the distribution of water vapor, temperature, ozone, carbon dioxide and other materials within the atmosphere. It increases as the moisture content of the air increases and adds the largest amount of heat to a body of water on warm cloudy days when short wave solar radiation decreases to zero.

Portions of the incoming solar and atmospheric radiant energy are reflected by the water surface before it can be absorbed by water. The reflected solar radiation, Hsr, is a function of the sun's altitude and the amount of cloud cover. The reflected atmospheric radiation, Har, has been measured and found to be relatively constant at Har = 0.03 Ha.

These four preceding radiation terms, Hs, Ha, Hsr and Har, algebraically constitute the net radiation absorbed by the water, Hr, and are independent of the temperature of the water upon which the radiation falls.

Since water radiates as an almost perfect black body, it rejects energy to the atmosphere in the form of long-wave back radiation, Hbr. Heat is also lost from the pond by evaporation, He, which is dependent upon wind speed (W) and the difference between the saturated water vapor pressure (es) at the surface of the pond and the water vapor pressure in the air (ea). The third temperature dependent heat exchange factor is heat conduction, Hc. If the air temperature (Ta) differs from the water temperature (Ts) the water can gain or lose heat through conduction. The rate at which heat is conducted (Hc) between the water and air is equal to the product of their temperature difference and a heat transfer coefficient. Since the heat transfer coefficient is dependent on wind speed, the heat conduction is affected by wind speed.

The algebraic sum of the previously mentioned heat transfer mechanisms is the net rate at which heat enters or leaves a body of water, H.

7.3 Effect on Climate on Cooling Pond Operation

For a given set of climatic factors and the mechanisms of heat transfer previously mentioned, there is a theoretical steady state or thermally balanced condition where the net heat transfer is zero. The temperature of the water surface of this condition is defined as the equilibrium temperature. The equilibrium temperature is dependent upon such climatic factors as air temperature, wind speed, dewpoint temperature, relative humidity and solar radiation. For a cooling pond it is also dependent upon the amount of heat rejected to the pond from a power plant.

The high values of incident solar radiation, relative humidity and ambient air temperatures prevalent in Florida combine to produce average annual equilibrium temperatures in the mid to upper 70's which rank as some of the highest equilibrium temperatures in the country on an annual basis. Conversely the average heat exchange coefficient, which is dependent on wind speed, dew point temperature and water surface temperature, is also quite high in Florida due primarily to the comparatively high wind speeds and high ambient water surface temperatures. The resultant effect is that more heat can be dissipated per unit surface area of a cooling pond located in Florida as compared to a pond located in other climatological regions of the United States.

7.4 Cooling Pond Characteristics

An economic analysis was performed to estimate the characteristics of such a cooling pond that most economically provides cooling capacity for a plant near Arcadia, including periods of drought. The required pond characteristics include:

1. A surface area sufficient to effect the required net heat transfer to the atmosphere at all times, including those periods of time when the depth of water in the cooling pond is at its lowest point (minimum operating level).

2. A sufficient volume of storage to prevent the pond water surface dropping lower than the required minimum operation level.

The volume required to maintain operation during a drought is composed of:

1. The volume of water sufficient to fill the pond to the minimum operating level.

2. The volume of water sufficient to meet those withdrawals or losses (evaporation and seepage from the reservoir) that would occur for a period equal to the period of the longest drought of record., and

3. An additional 6-month carry-over storage allocation which is based on the assumption that the maximum probable drought is yet to occur and, consequently, some additional storage is required.

Cooling pond surface areas and embankment heights, which allowed for flood storage and wave runup, were computed and an economic comparison was made which considered the capital costs of construction, the dollar value of the land which would be occupied by the pond, and the economic penalty which would be incurred if the pond were "undersized." Inadequate cooling would occur if the pond were undersized, and consequently there would be a loss in generating efficiency as a result of higher turbine back pressures caused by this inadequate cooling. The most economic pond was found to have a 16,000 acre surface area with an embankment height averaging approximately 46 feet.

7.5 Water Requirements

Water requirements were computed for a plant located in West Florida based on full development of nuclear generating capacity (12,000 MW(e)) and a constant "load factor" of 80% of maximum capacity. Water supply for a cooling pond must meet the following demands: natural pond evaporation (net), forced evaporation from the pond, seepage from the pond, blowdown from the pond, and any additional outside demands.

Natural evaporation is influenced by wind speed and the difference between the saturated water vapor pressure at the surface of the cooling pond and the water vapor pressure in the air. Water vapor pressure difference is, in turn, influenced by air and water temperature, and humidity. For a cooling pond surface area of 16,000 acres, the average annual evaporation, based on computed monthly evaporation rates, is 42,100 GPM.

Net natural evaporation from a cooling pond surface is simply the difference between natural evaporation and the direct precipitation onto the pond surface. Based on computed monthly rainfall in the vicinity Arcadia, the average annual rainfall onto a 16,000 acre cooling pond is 45,800 GPM. Hence the net natural evaporation (natural evaporation minus rainfall) averages (-) 3,700 GPM. The negative value indicates a surplus of rainfall over evaporation in this region of Florida.

Forced evaporation from a cooling pond surface is the additional evaporation which is induced by the artificial heating of the reservoir by the condenser heat load. Heat is lost to the atmosphere due to evaporation, convection and back radiation resulting in a reduction of water temperature in the reservoir. The rate of forced evaporation is dependent upon the wind speed, air temperature and vapor pressure, plant discharge temperature and flow rate (heat load) effective pond surface area and mobilized volume, and pond flow-through time. For a cooling pond surface area of 16,000 acres, the average annual forced evaporation based on computed monthly evaporation rates is 89,800 GPM which constitutes approximately 71% of the total heat lost. Approximately 19% of the total heat is given up via convection with the remaining 10% lost by back radiation.

Seepage from a cooling pond is dependent upon the foundation conditions underlying the pond and the material composition of the cooling pond embankment. The seepage rate from a pond is also related to water table conditions and to the depth of water storage within the pond. Average annual seepage loss from a 16,000 acre cooling pond is approximately 34,100 GPM, based on data obtained from tests in the area of Arcadia.

Periodic releases of water from a cooling pond are necessary in order to maintain concentrations of dissolved solids within the cooling pond at desirable levels and to avoid exceeding water quality standards set by the Florida Department of Environmental Regulation. The average amount of blowdown released from a 16,000 acre cooling pond is approximately 59,000 GPM.

Finally it was assumed that there are no other demands on the proposed cooling pond system.

The results of the cooling pond operation studies indicated that a firm supply of makeup water could be diverted from the Peace River to accommodate the requirements for an ultimate power station capacity of 12,000 MW(e) and also meet the State water quality requirements for blowdown. The total average long term diversion that would be required are indicated below:

12,000 MW(e) Power Station Capacity

Net Evaporation Makeup	86,100 GPM
Average Annual Seepage	34,100 GPM
Net Average Annual River Diversion	120,200 GPM

8.0 SUMMARY

The manner in which the specific climatic conditions of Florida affect the operation of cooling towers may be summarized as follows. Florida's high ambient air temperatures make dry towers inefficient and the costs involved to improve efficiency make the system infeasible. The natural draft wet tower presents no advantage over the mechanical draft wet tower since both types evaporate approximately the same amount of water.

A major advantage of the mechanical draft tower over the natural draft tower is that operation of the mechanical draft tower is not subject to the limitations imposed by Florida's climate in the manner that the natural draft tower is. Wet-dry towers present few advantages over wet towers in Florida because fogging is not generally a problem and with the high ambient temperatures water consumption is virtually the same as for wet towers. Any slight advantage, however, is offset by the much greater cost of wet-dry towers. It can, therefore, be concluded that climatic conditions make the mechanical draft wet tower the most feasible of the alternative cooling towers.

Section 7 discussed the cooling pond and it was shown to be a viable system for the disposal of waste heat from a nuclear power plant in Florida. While it has been concluded that mechanical draft wet towers are also a viable cooling system, the ramifications of the anticipated fluctuations in streamflows as discussed in Section 5 and 6.1, show that a storage reservoir must be incorporated into the cooling tower system to make it feasible in Florida. A reservoir will therefore be a component of either cooling tower or cooling pond system applied to inland Florida.

As is apparent from Section 6, the mechanical draft wet cooling tower system with a water supply reservoir will require approximately twice the land area (see Figure 7) and use more energy to operate than the cooling pond system while also incurring approximately twice the capital cost. Also of major significance is the fact that the cooling tower system requires the diversion of 40,600 GPM, or 33.8%, more water for operation than does the cooling pond system (see Figure 8). The conservation of this amount of water is a major advantage of the cooling pond system.

In summary, the interaction of climate and weather necessitates that for effective operation, cooling towers incorporate a water supply reservoir in the overall cooling system. The demands of the cooling tower water supply reservoir far exceed that of cooling pond capable of storing water and dissipating heat. It is concluded that cooling ponds are preferred for inland sites in Florida for use in waste heat dissipation.

ACKNOWLEDGEMENTS

The author wishes to thank Florida Power & Light Company for permission to publish this paper and in particular thank Mr. E. C. Weber and Mr. K. F. Rosanski for their comments and assistance.

TABLE 1

PEACE RIVER
MEAN MONTHLY FLOWS
(Jan., 1934 - Dec., 1970)

(MEAN MONTHLY DISCHARGE IN CFS)

MONTH OF	Zolfo Springs[1]		Arcadia[2]	YEAR
GPM	CFS	GPM		
January	456.6	204,920	637.6	286,150
February	544.6	244,420	820.8	368,380
March	651.4	292,170	1,004.3	450,730
April	477.6	214,350	696.2	312,450
May	307.0	137,780	386.3	173,370
June	773.8	347,280	1,324.0	594,210
July	1,090.0	489,190	2,084.9	935,700
August	1,237.3	555,300	2,300.5	1,032,460
September	1,549.4	695,370	2,939.8	1,319,390
October	991.1	444,810	1,916.2	859,990
November	420.8	188,860	613.2	275,200
December	351.1	157,570	488.4	219,190

NOTES: 1) Based on USGS records from Station 02295637 at Zolfo Springs, Florida.

2) Based on USGS records from Station 02296750 at Arcadia, Florida.

TABLE 2

LOW FLOW DURATION

AT USGS GAGE NO. 02296750

ARCADIA, FLORIDA (1931 - 1965)*

Number of Consecutive Days in Year Ending June 30	Lowest Mean Discharge in CFS	Lowest Mean Discharge in GPM	Year of Occurrence
1	39.0	17,500	(1949)
3	39.0	17,500	(1949)
7	42.9	19,250	(1949)
14	47.1	21,140	(1945)
30	54.3	24,370	(1945)
60	64.0	28,720	(1945)
90	70.0	31,420	(1945)
120	83.9	37,650	(1932)
150	86.7	38,910	(1932)
183	87.2	39,140	(1932)
274	206.0	92,450	(1956)

NOTE: *Heath, 1971

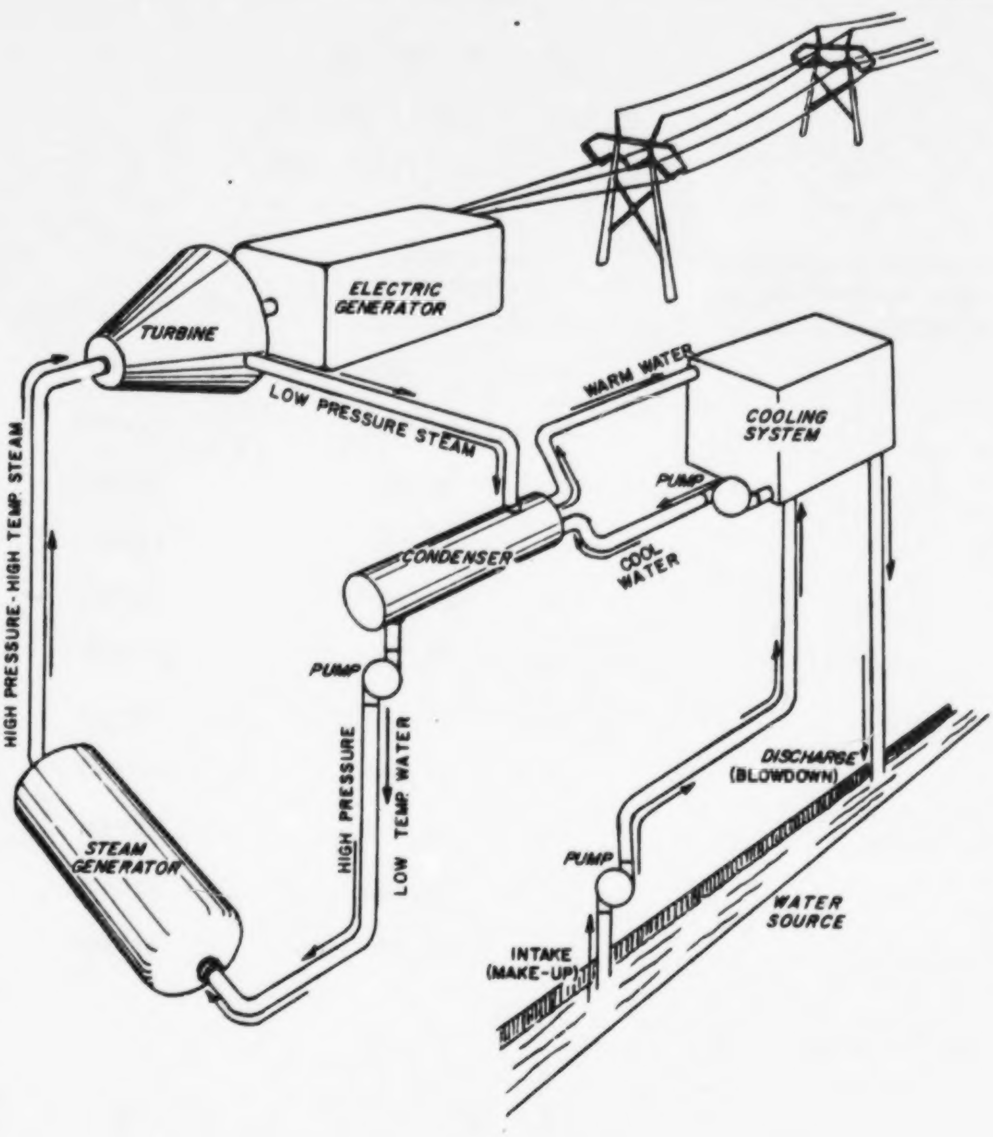
ELECTRIC GENERATOR
TURBINE
HIGH PRESSURE - HIGH TEMP. STEAM
LOW PRESSURE STEAM
WARM WATER
COOLING SYSTEM
PUMP
CONDENSER
COOL WATER
PUMP
HIGH PRESSURE
LOW TEMP. WATER
STEAM GENERATOR
DISCHARGE (BLOWDOWN)
PUMP
WATER SOURCE
INTAKE (MAKE-UP)

FIGURE I: STEAM ELECTRIC POWER PLANT

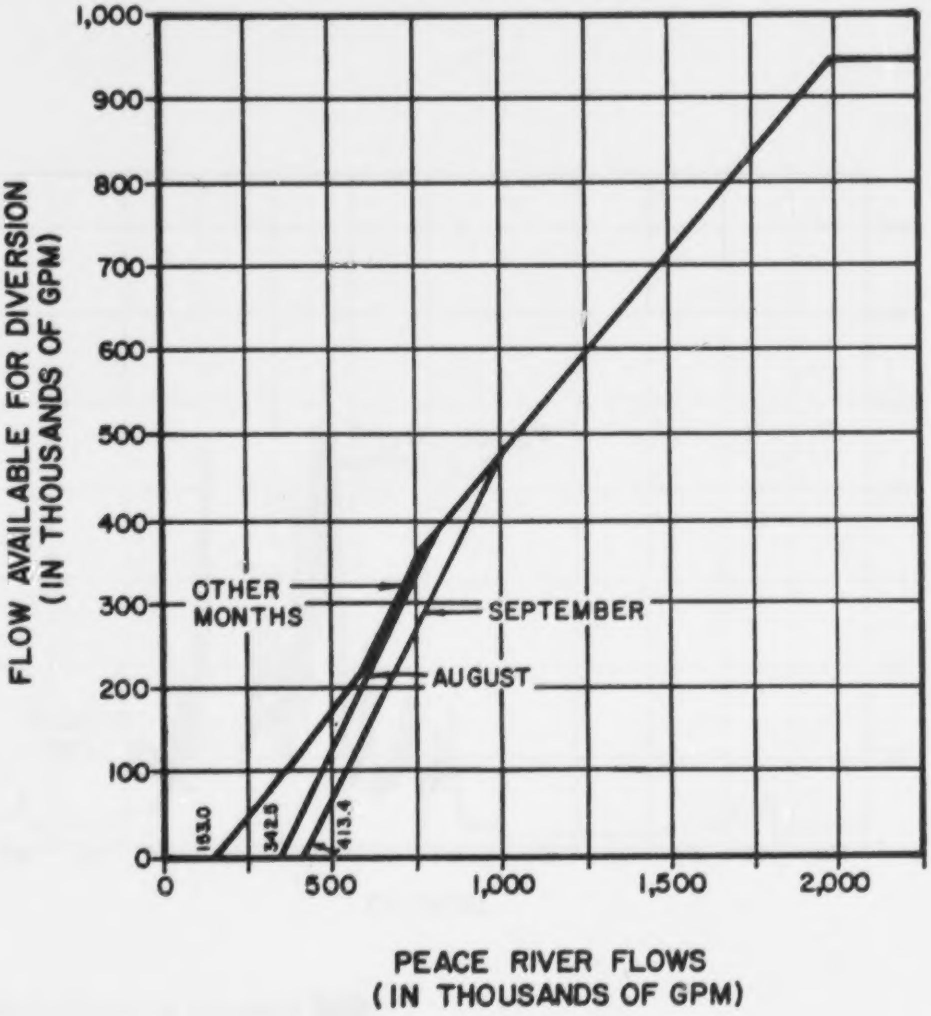

FIGURE 2: POSSIBLE DIVERSION FLOWS FROM PEACE RIVER

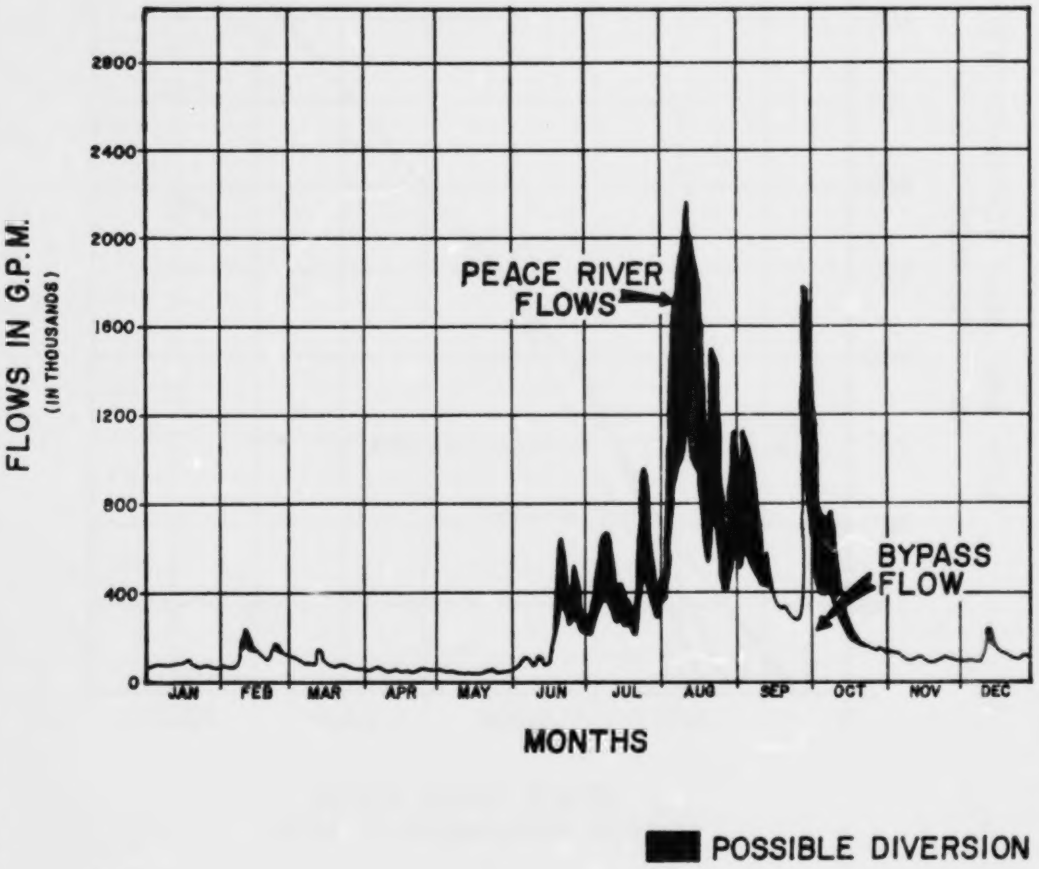

FIGURE 3: DIVERSION CHARACTERISTICS

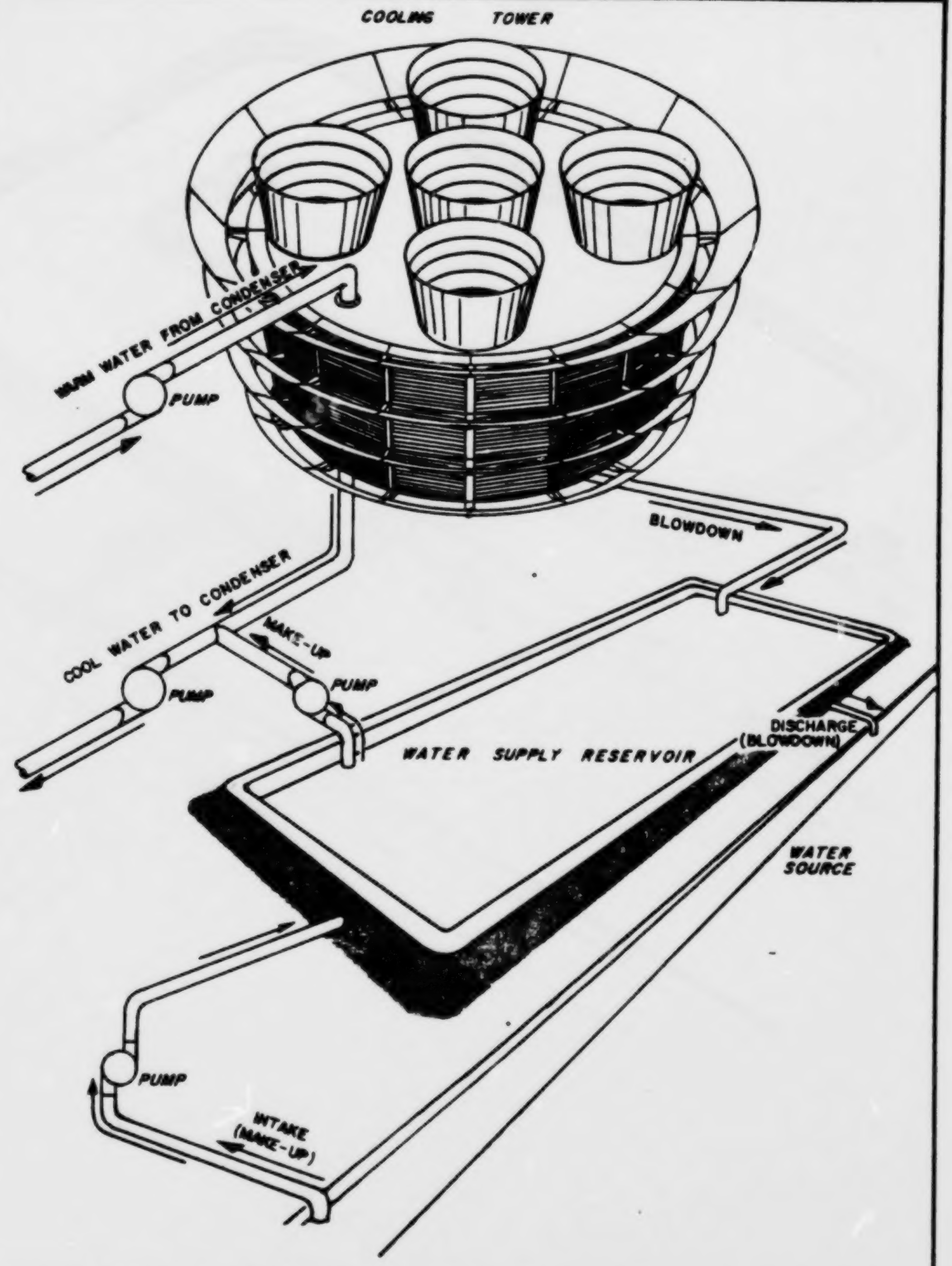
COOLING TOWER
WARM WATER FROM CONDENSER
PUMP
BLOWDOWN
COOL WATER TO CONDENSER
MAKE-UP
PUMP
PUMP
WATER SUPPLY RESERVOIR
DISCHARGE (BLOWDOWN)
WATER SOURCE
PUMP
INTAKE (MAKE-UP)

FIGURE 4: COOLING TOWER SYSTEM WITH WATER SUPPLY RESERVOIR

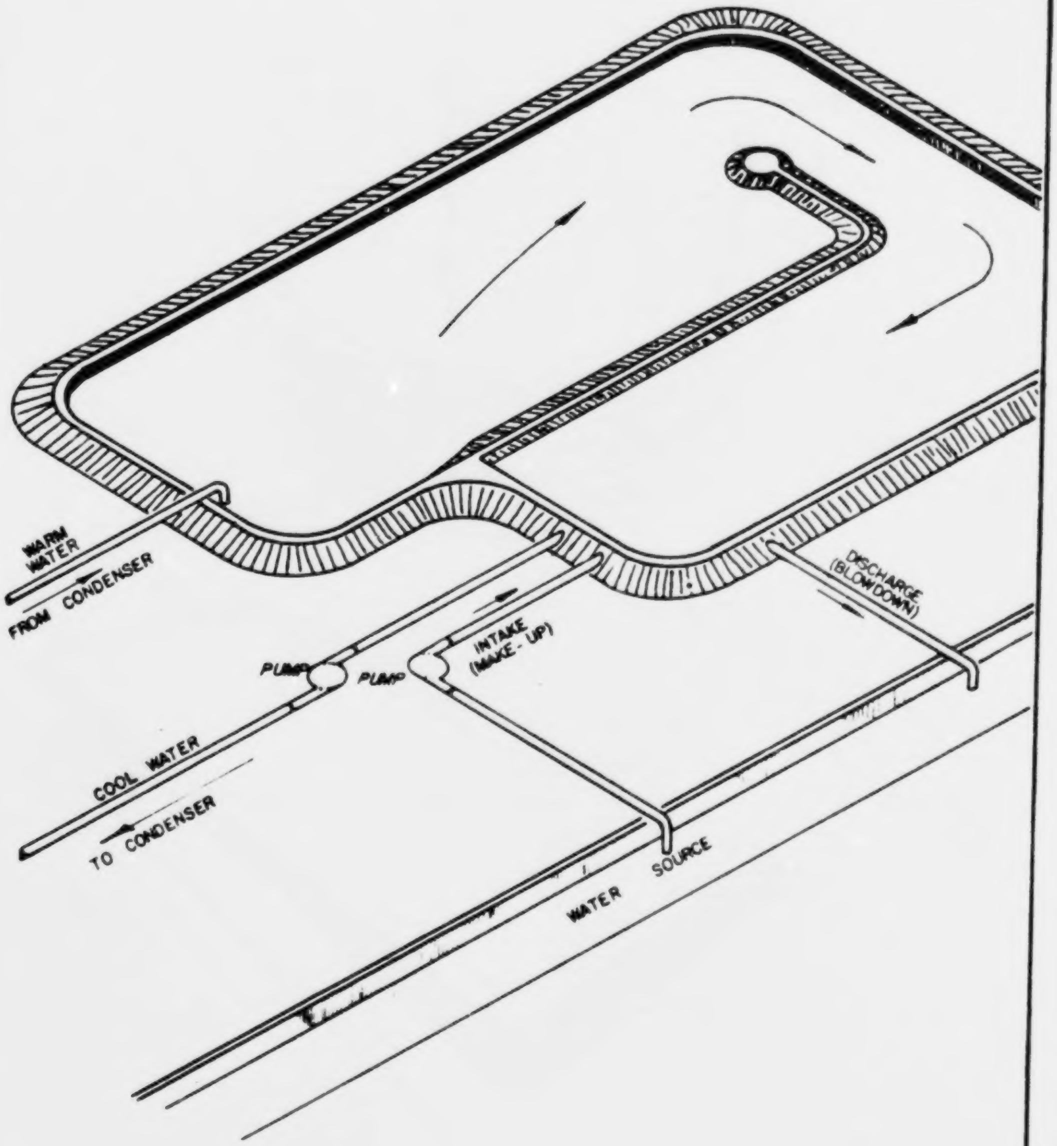
WARM WATER
FROM CONDENSER
PUMP
PUMP
INTAKE (MAKE-UP)
DISCHARGE (BLOWDOWN)
COOL WATER
TO CONDENSER
WATER SOURCE

FIGURE 5: COOLING POND SYSTEM

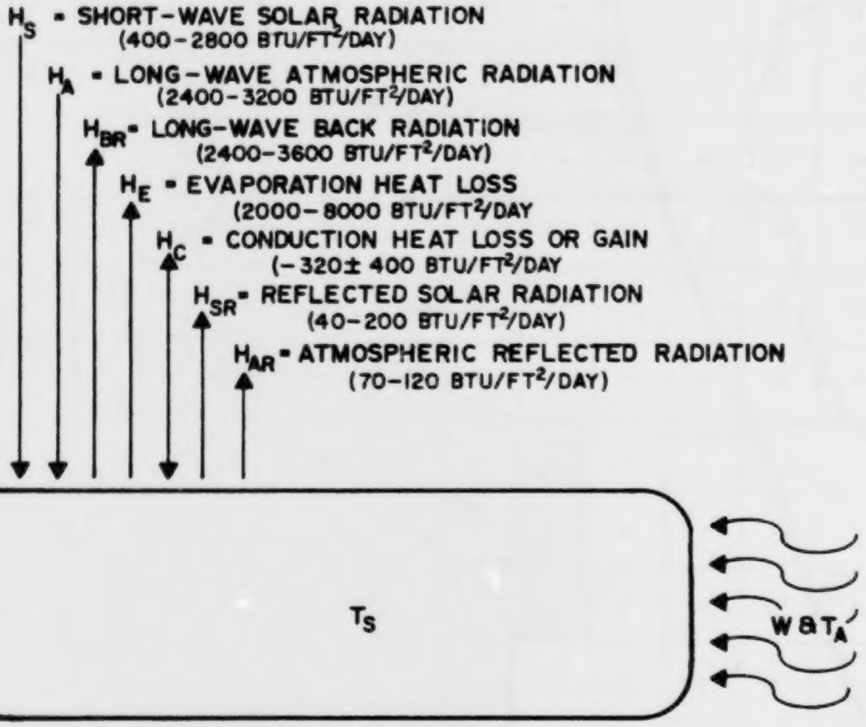
H_S = SHORT-WAVE SOLAR RADIATION (400-2800 BTU/FT²/DAY)
H_A = LONG-WAVE ATMOSPHERIC RADIATION (2400-3200 BTU/FT²/DAY)
H_{BR} = LONG-WAVE BACK RADIATION (2400-3600 BTU/FT²/DAY)
H_E = EVAPORATION HEAT LOSS (2000-8000 BTU/FT²/DAY
H_C = CONDUCTION HEAT LOSS OR GAIN (-320± 400 BTU/FT²/DAY
H_{SR} = REFLECTED SOLAR RADIATION (40-200 BTU/FT²/DAY)
H_{AR} = ATMOSPHERIC REFLECTED RADIATION (70-120 BTU/FT²/DAY)
T_S
W & T_A

ΔH = DAILY NET RATE AT WHICH HEAT IS GAINED OR LOST ACROSS A WATER SURFACE

$$\Delta H = \underbrace{(H_S + H_A - H_{SR} - H_{AR})}_{H_R} - \underbrace{(H_{BR} \pm H_C + H_E)} \ \text{BTU / FT. DAY}$$

ABSORBED RADIATION INDEPENDENT OF TEMP.

$H_{BR} \sim (T_S + 460)^4$

$H_C \sim W(T_S - T_A)$

$H_E \sim W(e_S - e_A)$

TERMS DEPENDENT ON TEMP.

W = WIND SPEED (Mi/DAY)

T_A = AIR TEMP. (°F)

T_S = WATER SURFACE TEMP. (°F)

e_S = SATURATED VAPOR PRESSURE

e_A = AIR VAPOR PRESSURE

FIGURE 6: MECHANISMS OF HEAT TRANSFER ACROSS A WATER SURFACE

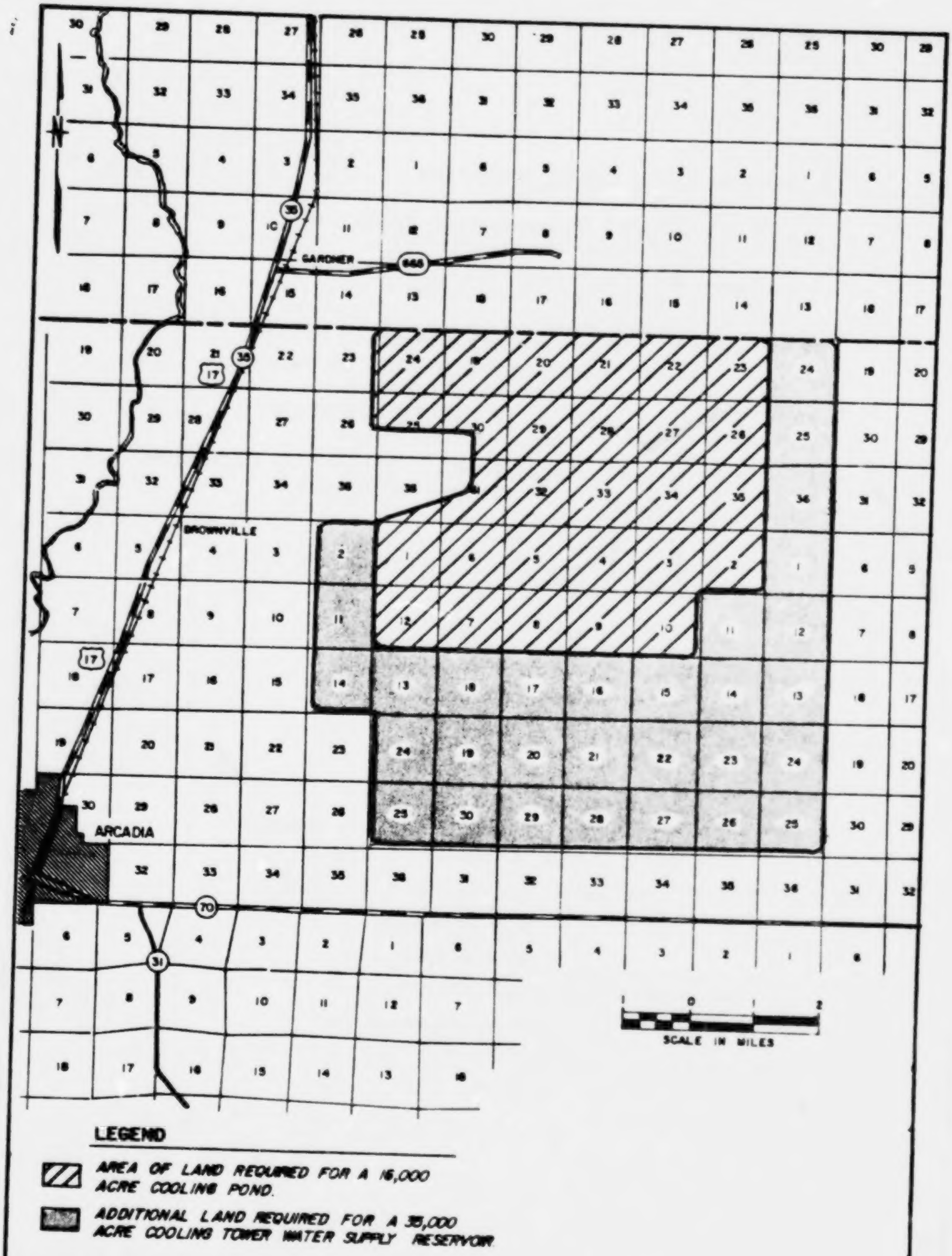
GARDNER
BROWNVILLE
ARCADIA
35
17
665
70
31
SCALE IN MILES
1 0 1 2
LEGEND
▨ AREA OF LAND REQUIRED FOR A 16,000 ACRE COOLING POND.
▩ ADDITIONAL LAND REQUIRED FOR A 35,000 ACRE COOLING TOWER WATER SUPPLY RESERVOIR

FIGURE 7: LAND AREA COMPARISON

	COOLING POND	COOLING TOWER WATER SUPPLY RESERVOIR
PUMPING STATION		
MAXIMUM CAPACITY (GPM)	942,500	942,500
SURFACE AREA (ACRES)	16,000	35,000
ELEVATIONS (FEET-MSL)		
AVERAGE BOTTOM	85.0	85.0
MINIMUM OPERATING LEVEL	94.0	94.0
MAXIMUM OPERATING LEVEL	117.4	118.5
FLOOD STORAGE LEVEL	120.4	121.5
AVERAGE TOP OF EMBANKMENT	131.0	133.0
VOLUMES (ACRE-FEET)		
MINIMUM OPERATING LEVEL	144,000	315,000
MAXIMUM OPERATING LEVEL	518,400	1,172,500
FLOOD STORAGE LEVEL	566,400	1,277,500
MAKEUP WATER REQUIREMENTS (GPM)		
AVERAGE ANNUAL SEEPAGE	34,100	56,700
NET AVERAGE EVAPORATION	86,100	104,100
NET AVERAGE ANNUAL RIVER DIVERSION	120,200	160,800

FIGURE 8: COMPARATIVE WATER AND LAND REQUIREMENTS

35-45-34

VII-C-209

INVESTIGATION OF THE FLUID MECHANICAL BEHAVIOR OF A THERMAL STORAGE RESERVOIR FOR DRY-COOLED CENTRAL POWER STATIONS

E.C. Guyer and M.W. Golay
Massachusetts Institute of Technology
Cambridge, Massachusetts U.S.A.

ABSTRACT

The use of a capacitive Thermal Storage Pond (TSP) initially filled with cold water as part of a dry cooling system for a central power station is attractive economically if the pond can be designed to operate in an approximate "plug-flow" mode-discharging cold water to the condenser and filling with hot water from the cooling tower. Bouyant flow stratification hinders attaining this goal since it can cause "short circuiting" of the pond. For adequate flow control, a long narrow pond configuration (possibly serpentine) is desirable. In investigating the behavior of such a pond experimentally, it was found over the range of cases examined that injection of water into a long narrow reservoir which is initially at a different temperature always results in a stratified flow, which could be modelled analytically successfully in terms of a static "lock-exchange" type flow superimposed upon the gross plug flow of the pond. Such behavior is undesirable in a TSP, and it was found that acceptable performance could be obtained inexpensively by placing flow-constricting barriers at regular intervals along the pond length.

INTRODUCTION

The combined thermal storage pond (TSP) and dry cooling tower system concept is proposed as a solution to performance problems of dry cooled central power stations. [1] Simple dry-cooling of a steam-electric plant results in severe economic penalties due to the coincidental occurrence of the daily period maximum loss of electrical generation capability resulting from high condenser temperatures and the daily period of maximum utility system electrical demand. The daily maximum condenser temperature would occur during the afternoon period of peak electrical demand since the ambient dry bulb, which is normally at a maximum during the early afternoon, is directly reflected in the steam condensing temperature for dry cooling systems. The combined thermal storage pond and dry cooling tower system represents an attempt to avoid this undesirable coincidental occurrence of the maximum ambient temperature and the maximum electrical demand through the cyclic operation of the TSP and dry tower system. The combined system is operated such that condenser temperature during the afternoon period approaches

Preceding page blank

the daily minimum ambient temperature occurring in the early morning rather than the daily maximum ambient temperature occurring in the afternoon. Economic analysis of this system has indicated substantial economic benefit in taking advantage of the 30°F or greater daily range of the ambient temperature common to many of the western regions of the United States [2].

The cyclic operation of the combined TSP and dry tower system encompasses four operational modes. They are the following:

1) cold standby mode,

2) heatup mode,

3) hot standby mode, and

4) cooldown mode

The cold standby mode would normally be utilized during the late morning hours; in this mode the condenser is cooled solely by the dry cooling tower. However, during the heatup operational mode period, the period of maximum ambient temperature and maximum electrical demand, relatively cool water would be drawn from the pond, passed through the condenser and dry cooling tower, and then would be discharged back into the pond at an increased temperature. When the cooling potential of the pond had been exhausted or the afternoon period of peak electrical demand had passed, the system would be switched to the hot standby mode, which is essentially identical to the cold standby mode of operation. Then when the ambient temperature had declined to near its daily minimum value the coupling of the pond with the condenser and dry tower again would occur. During this final mode of operation, the cooldown mode, relatively warm water would be drawn from the pond, passed through the condenser and dry tower, and discharged back into the pond at a relatively cool temperature.

Once the entire volume of the pond had been recooled, the daily cycle would be repeated.

The basic function of a thermal storage pond is thus to provide simultaneously a condenser cooling water source and a holding facility for the same water after it has passed through the condenser and has been recooled partially by the dry cooling tower. The type of thermal-hydraulic behavior required in the pond is exactly that of the well-known plug-flow. However, exact plug-flow in the pond may not be required since the dry cooling tower/TSP system may still perform effectively - in an economic sense - in spite of some undesirable mixing of hot and cold water in the pond. The extreme case of mixing of the initial pond inventory with incoming flow is the case of fully-mixed behavior. A further limit beyond that of the idealized fully-mixed case - in terms of overall system performance degradation - is that of the short-circuited pond. This situation is highly undesirable since any fraction of the pond which is isolated from the flow circuit becomes lost as a medium for the storage of waste heat with the net result that the effective storage volume of the pond is reduced accordingly.

The work reported herein summarizes the analytical and experimental investigation which was undertaken in an effort to formulate a preliminary TSP design which would result in a good approximation to the desired plug-flow behavior. As is indicated in the following discussion, an economically practical design has been achieved.

Design Constraints and Requirements

In attempting to formulate some preliminary design options for the plug-flow TSP it was necessary to consider the engineering and economic constraints or requirements which will be imposed on any design concept. A list of some of the desirable features of a well-designed pond is the following:

1) low pond head loss during operation,

2) low pond flow velocity,

3) minimal bottom and surface area,

4) avoidance of excessive depth,

5) smooth response of the TSP outlet temperature to changes in the inlet temperature,

6) effective operation during both "heatup" mode and "cooldown" mode of operation, and

7) modest inlet flow velocities.

The requirement of low pond head loss during operation stems simply from the fact that during the standby stage of the TSP operation the surface elevation of the pond will seek its natural level. If the pond structure must also contain the extra water elevation due to a large head loss through the flow circuit of the pond then storage capacity will be wasted. A low pond flow velocity is also desirable since the pond lining and covering will likely be fabricated from flexible plastic or rubber membranes.

The requirements of minimal bottom and surface areas and reasonable depth are contradictory when attempting to design a TSP for a fixed storage volume. Thus, some compromise is required. Minimal surface area is desirable for either the open or covered pond. In the case of the open pond it is of interest to minimize evaporation, and in the case of the covered pond it is of interest to minimize the cost of covering and lining the structure. The need to maintain a reasonable depth is connected with the difficulty of constructing high dikes for an above-ground level pond, and of excavating to large depths for a below ground level pond.

Additionally, it is a basic design requirement that the TSP outlet temperature respond smoothly to the inlet temperature. Large and high frequency variations in the TSP outlet temperature (condenser temperature) as the storage capacity of the pond nears exhaustion could result in unacceptable transients in the turbine-generator behavior.

A most fundamental requirement is that the TSP function effectively during both the "heatup" and "cooldown" modes of operation. Designing for one mode of operation will not automatically result in a correct design for the other due to the potential for the occurrence of density-induced stratified flows in the TSP.

Finally, it is desirable to minimize the inlet velocity into the pond since the velocity head of the inlet flow is non-recoverable and requires an additional amount of circulating water pumping power above that required for the operation of the tower only.

Feasible Solutions to the TSP Design Problem

There are two general methods by which the desired plug-flow behavior may be achieved. They are by means of horizontal plug-flow and vertical plug-flow. Figure 1 schematically demonstrates how the two types of behavior might be obtained in situations in which the reservoir is being filled with warm water. In the vertical plug-flow case one would attempt to take advantage of the tendency for stable vertical stratification, and in the case of the horizontal plug-flow one would have to guard against the tendency for vertical stratification (with the warm water floating above the colder water).

Both the vertical and horizontal plug-flow design options have particular advantages and disadvantages with regard to the previously discussed economic and engineering constraints and performance requirements. Based on a comparison of the two options it was decided that an attempt would be made to design a horizontal plug-flow pond.

The major concern in the design of a horizontal plug-flow TSP was identified as being the instability of an initially vertical front across which large density differences would exist. The presence of the density difference across a vertical interface will give rise to density-induced flows which could be a significant factor in determining the thermal efficiency of the TSP. The ratio of the rate of propagation of the density front due to the nominal plug-flow velocity in the TSP to the rate of propagation of the density front due to density-induced flows can, in a general fashion, be characterized by the densimetric Froude number of the TSP. The TSP densimetric Froude number is given as

$$F_d = \frac{V_p}{\sqrt{\frac{\Delta\rho}{\rho} gH}} \tag{1}$$

where $\Delta\rho$ = the density difference

ρ = average density,

H = pond depth,

g = gravitational acceleration, and

V_p = plug-flow velocity

Designing the TSP for a large densimetric Froude number should result in the nominal plug-flow velocity dominating the density-induced currents. At the extreme of very large design densimetric Froude numbers near-perfect horizontal plug-flow should result as shown in Fig. 1. However, large design densimetric Froude numbers also result in high TSP construction costs since a narrow, shallow, and long pond structure is required.

It was from this realization that the fundamental fluid mechanical design task became apparent - the specification of the minimal design densimetric Froude number such that an acceptable level of performance is achieved.

To provide the required ability to describe the behavior of a propagating density front in a horizontal plug-flow TSP a control-volume type fluid dynamic model has been derived, and its predictions have been compared to experimental results. The experiment has been designed such that it serves the dual purposes of providing the data necessary to construct the semi-empirical mathematical model of transient stratified flow in shallow channels for a limited range of densimetric Froude numbers, and of providing a physical model of a prototype thermal storage pond.

PHYSICAL MODEL

Similarity Requirements

Total physical similarity between model and prototype TSP's requires similarity of flow in three regions. These are the entrance mixing region, the main storage volume, and the withdrawal region. The intent in physically modeling a horizontal plug-flow TSP is the replication of the behavior of the entrance mixing and main storage regions. Modeling of the withdrawal region is not crucial in this work, since if the horizontal plug-flow concept is to be viable, vertical stratification in the withdrawal region will necessarily be minimal.

Similarity to the entrance region of a prototype TSP is obtained in the model in an integral sense by assuming that any submerged jet discharge with a highly unstable near-field region will produce essentially the same vertical temperature mixing effect in a geometrically similar region, without regard for the geometrical details of the discharge structures. Since the volume of the entrance region is small in relation to the total storage volume this assumption is observed experimentally to be adequate. In both the model and the prototype an unstable near-field flow can be obtained by using a horizontal multiport submerged jet discharge with the jets uniformly spread over the width of the pond.

To insure similarity between the main storage volume flows of the model and the prototype, the following requirements are met:

1) geometric similarity,

2) Froude Law similarity,

3) densimetric Froude Law similarity,

4) satisfaction of the turbulent flow Reynolds criterion, and

5) similarity of the ratio of inertial to friction forces.

In Froude models it is impossible to meet both Froude similarity and Reynolds similarity exactly. However, exact similarity of Reynolds number for turbulent flows is not required. It is generally satisfactory to meet the criterion

$$Re_{model} > Re_c$$

where Re_c is the critical Reynolds number for fully developed turbulent flow.

Although it is not essential to meet Reynolds number similarity, it is important, as noted by Jirka (2) that the ratio of inertial forces to bottom friction forces be equal for the model and the prototype. Thus in the physical modeling of the prototype TSP it is desirable to distort the vertical dimension of the model such that the ratio of friction forces to inertial forces in the prototype is approximately replicated in the model.

Experimental Apparatus and Observational Techniques

The experimental model of the prototype TSP has been constructed at the Ralph M. Parsons Laboratory for Water Resources and Hydrodynamics at M.I.T. The model fabrication consisted mainly of the modification of an existing flume. The flume is constructed of 1/2" glass mounted on an aluminum frame. The nominal flume dimensions are 8" deep, 18" wide and 64 feet long. The piping and storage tanks which were added to the facility to enable the desired inlet discharge and withdrawal flowrates to be maintained in the model are shown schematically in Fig. 2.

As is indicated in Fig. 2, a flume recirculation line was installed to allow the initial pond inventory to be continuously cycled through the flume in order to diminish any temperature differences which may develop just prior to the actual experiment. Also the recirculation flow allows the plug flow velocity field to be established in the flume prior to the introduction of hot inlet water. The inlet and withdrawal flow rates are measured by rotor-meters with maximum capacities of 67 gpm. The inlet discharge structure consists of four 2 in. nozzles which could be reduced in size. Various withdrawal schemes were utilized during different experimental runs depending on the current modeling requirements.

The flow visualization dye, FD+C Blue Food Color #1, was used to color the entire contents of the inlet flow holding tank just prior to the operation of the experiment. Simple visual recording of the position of the density front at known instants was acceptable for recording the bulk fluid behavior. Thermistors with short response times were used to record the transient temperatures at the point of withdrawal.

Analytical Model

An approximate analytical model of the behavior of a density front in a horizontal plug-flow pond has been developed based on a control-volume momentum conservation equation. The resultant equation contains one empirical constant, the value of which is determined by experiment. Essentially the model utilizes the superposition of the density-induced "lock-exchange" flow field upon the unperturbed homogenous fluid velocity profile in the pond. It includes interfacial and bottom friction effects.

The equation of motion of the leading and trailing edges of the density front in a horizontal plug-flow pond is obtained from a force balance on the double-lumped moving control volume shown in Fig. 3. The forces affecting the motion of the leading and trailing edges of the density front with respect to the mean plug-flow velocity V_p are the following:

1) F_p = pressure force due to $\rho_2 > \rho_1$,

2) F_i = interfacial friction force,

3) F_b = bottom friction force, and

4) F_m = inertial force, where

F_i, F_b, and F_m all act to resist the pressure force F_p. Thus, one obtains the result

$$F_p = F_i + F_b + F_m \quad . \qquad (2)$$

The approximate analytic expression for V_f, the leading edge velocity, and V_t, the trailing edge, is obtained by expressing Eq. (2) in terms of $\frac{dD}{dt}$, the rate of growth of the horizontal interfacial length. Thus, under the assumption of equal depths of the two overlying layers, and from the requirement of continuity one obtains the result

$$V_f - V_p = V_p - V_t = \frac{dD}{dt}/2 \quad . \qquad (3)$$

The total static pressure due to density difference acting horizontally across any point on the interface is

$$(P_2 - P_1)h = h\ (\rho_1 - \rho_2)\ \frac{g}{g_c} \qquad (4)$$

where h is the depth into the pond.

Since this pressure difference is a linear function of depth the total pressure acting across the interface is given as

$$\frac{(P_2 - P_2)}{2} \ HA \qquad (5)$$

where $(P_2 - P_1)$ is the pressure difference at the bottom of the pond, and A is the cross-sectional area of the pond, $(A = L \cdot H$, where L = width). The average pressure can be envisioned to act to the right on the top fluid segment in the control volume and to the left on the bottom fluid segment. Substitution of Eq. (4) into Eq. (5) gives the result

$$F_p = \frac{\beta}{2} LH^2 \ \Delta\rho \frac{g}{g_c} \quad , \qquad (6)$$

where the parameter β has been introduced to account for the fact that the actual pressure difference may be different from that deduced from the simple model.

The friction force terms in Eq. (2) can be expressed as

$$\begin{aligned} F_i &= \tau_i A_i, \text{ and} \\ F_b &= \tau_b A_b \end{aligned} \qquad (7)$$

where $A_i \simeq A_b = D \cdot L$, and τ_i and τ_b are the interfacial and bottom shear forces, respectively. The interfacial shear is given by

$$\tau_i = \frac{f_i}{8} \ \rho V_R{}^2 = \frac{f_i}{8} \ \rho \ \left(\frac{dD}{dt}\right)^2 \quad . \qquad (8)$$

where f_i is the interfacial friction factor. The variation of F_i with Reynolds number has been deduced by Abraham and Eysink (3).

The bottom shear force will be effected by the magnitude of the plug-flow velocity. The resultant bottom shear force is

$$\tau_b = \frac{f_b}{8} \ \rho \left(\left(\frac{dD}{dt}\right) \frac{V_p}{2} - \frac{1}{4} \left(\frac{dD}{dt}\right)^2 \right) . \qquad (9)$$

The inertial force acting on the control volume is

$$F_m = \frac{d\,(M\bar{V})}{g_c dt} \quad , \qquad (10)$$

or

$$F_m = \frac{M}{g_c} \left(\frac{d\bar{V}}{dt}\right) + \frac{\bar{V}}{g_c} \ \frac{dM}{dt} \quad , \qquad (11)$$

when $M = DLH\rho$, and $\bar{V}$ is the average relative velocity of the control volume segment with respect to V_p. Since the acceleration of the control volume is expected to be small the term

$M(\frac{d\bar{V}}{dt})/g_c$ may be neglected. Noting that

$$\frac{dM}{dt} = \frac{dD}{dt} LH\rho \ , \qquad (12)$$

and

$$\bar{V} = \frac{1}{2} (\frac{dD}{dt}) \ , \qquad (13)$$

we obtain the result

$$F_m = \frac{1}{2g_c} (\frac{dD}{dt})^2 LH\rho \ . \qquad (14)$$

In deriving the term F_i, F_b and F_m it has been assumed that the density front velocity similarity profile is that shown in Fig. 3. Thus, to account for the fact that the actual velocity profile may be different from that assumed (i.e., $\bar{V}$ may not simply equal

$$\frac{1}{2} (\frac{dD}{dt})$$

the parameter γ is introduced as follows:

$$(\frac{dD}{dt})_{Actual} = \gamma (\frac{dD}{dt}) \qquad (15)$$

where

$$(\frac{dD}{dt})_{Actual}$$

is the actual rate of growth of the distance D defined in Fig. 3. The entire equation of motion may now be written as

$$\frac{\beta}{2} LH^2 \Delta\rho \frac{g}{g_c} = \frac{f_i}{g_c 8} \rho\gamma^2 (\frac{dD}{dt})^2 D \cdot L$$

$$+ \frac{f_b}{g_c 8} \rho (\frac{\gamma}{2} (\frac{dD}{dt}) V_p - \frac{\gamma^2}{4} (\frac{dD}{dt})^2) D \cdot L$$

$$+ \frac{\gamma^2}{2g_c} (\frac{dD}{dt})^2 LH\rho \qquad (16)$$

The above equation is quadratic in $\frac{dD}{dt}$, with the solution being

$$\frac{dD}{dt} = \frac{-\gamma F_b V_p D_p \pm \sqrt{\frac{(\gamma F_b \rho V_p D)^2}{8} + 4\beta H^2 \Delta\rho g (\frac{\gamma^2 f_i}{4} \rho D - \frac{\gamma^2 f_b D}{16} + \gamma^2 H\rho}}{2(\gamma^2 \frac{f_i}{4} \rho D - \frac{\gamma^2 f_b \rho D}{16} + \gamma^2 H\rho)} \qquad (17)$$

Now if typical values of the various parameters are used to evaluate Eq. (17) ($\gamma = \beta = 1$) it becomes apparent that the effect of V_p, for the range of Foude numbers of interest, is small. Thus, the terms containing V_p can be neglected in Eq. (17). Equation (17) is then simplified to the form

$$\frac{dD}{dt} \doteq \alpha \left(\frac{H^2 \Delta\rho g}{H + (\frac{f_i + f_b/4}{4}) \rho D} \right)^{1/2} \qquad (18)$$

where $\alpha = \beta/\gamma^2$.

Thus, the expression for the rate of growth of the horizontal projection of the interface is given by an equation with a single free parameter to be determined by experiment. The total velocity of the leading edge of the density front is now expressed as

$$V_f = C_o V_p + \frac{\alpha}{2} \left(\frac{H^2 \Delta\rho g}{H\rho + (\frac{f_i + f_b/4}{4}) \rho D} \right)^{1/2} \qquad (19)$$

The displacement of the leading edge at time t from $D = 0$ at $t = 0$ is

$$X_f = C_o V_p t + \frac{1}{2} D(t) \qquad (20)$$

where D(t) is obtained by integrating $\frac{dD}{dt}$ Eq. (18) from time-zero to time-t. The resulting expression for D(t) is

$$D(t) = \frac{4H^2\Delta\rho g}{\rho(f_i + f_b/4)}\left[\left(\frac{\rho}{H\Delta\rho g}\right)^{3/2} + \left(\frac{3\rho(f_i + f_b/4)}{8H^2\Delta\rho g}\right)(\alpha T)\right]^{2/3}$$

$$- \frac{4H}{(f_i + f_b/4} \qquad (21)$$

The position of the trailing edge at time t would be

$$X_t = C_1 V_p t - \frac{1}{2} D(t) \qquad (22)$$

Since no specific assumption has been made regarding the exact density-induced velocity distribution, the above equation only predicts the position of the leading edge or trailing edge of the density front. The parameters C_o and C_1 correct for the fact that the channel velocity at the height of the leading edge (or trailing edge) is, in general, different from the mean plug-flow velocity. The values C_o and C_1 can be determined by assuming that the unperturbed velocity profile in the pond is given by the relationship [4]

$$V(y) = V_s \left(\frac{y}{y_o}\right)^{1/6}, \qquad (23)$$

where V_s is the surface velocity. Strictly speaking, the value of C_1 would always be zero since the no-slip condition always holds at fixed boundaries. However, since the present interest is in the bulk flow behavior it was sufficient to assume that

$$C_o - 1 = 1 - C_1 \qquad (24)$$

The case of the advancing cold front presents a different problem. In this case the maximum density-induced forward velocity occurs near the bottom of the channel. The position of maximum density-induced forward velocity is not coincident with the position of maximum forward velocity of the unperturbed channel flow as in the case of the advancing hot front, due to the no-slip bottom boundary condition.

The advancing cold front case thus represents a more desirable situation than with the advancing hot front in terms of achieving a near vertical density front velocity profile. In view of this fact no effort has been made to quantify the behavior of the advancing cold front other than to say that for TSP design purposes the advancing hot front is the more restrictive design condition. This conclusion has been verified by experiment.

Results of Initial Design Concept Evaluation

Based on the initial design concepts three prototype TSPs have been designed to span the range of design densimetric Froude numbers from 0.5 to 1.5. Three model designs which simulate these prototype designs were tested in the flume. All three designs result in unsatisfactory thermal hydraulic performance of the pond.

All three of the TSP designs summarized in Table 1 have significant density-induced flows which partially reduce the pond thermal capacitance. The highly unstable inlet flow jets were successful in establishing initially a nearly vertical density front. However, as the density front propagates a short distance downstream from the inlet mixing region significant vertical stratification begins to develop. In fact, except for the case of a densimetric Froude number of 1.5, the trailing edge of the density front was not observed to travel a significant distance beyond the inlet mixing region. A short time after the initiation of the inlet flow, the overlying hot wedge is somewhat diluted as a result of inlet flow mixing. This small dilution nevertheless is rapidly overcome by the continuing intrusion of the unmixed inlet flow, and a distinct density interface develops rapidly.

Accurate visual determination of the position of the trailing edge of the upper fluid layer in all cases was difficult since in none of the experiments was the inlet flow able to displace rapidly or to mix with the initial cold water in the boundary layer at the bottom of the channel. Figure 4a shows qualitatively the profile of the density front for F_D greater than about 1.00. The interface is nearly linear except at the leading and trailing edges. At lower densimetric Froude numbers density front profiles developed as shown approximately in Fig. 4b.

In addition to the three experimental runs performed at densimetric Froude numbers of 0.5, 1.0 and 1.5 several runs were made at higher densimetric Froude number values to see if any gross changes in the flow behavior would occur. In all cases the flow behavior was observed to remain qualitatively unchanged.

The positions of the leading edge of the advancing density front as a function of time for each of the TSP designs of Table 1 are shown in Fig. 5. In each case the position is plotted in a non-dimensional manner as a function of the fraction of the plug-flow residence time V/Q, which had elapsed. The design parameters are equal for all of the ponds except for the densimetric Froude number values. As Fig. 5 indicates, even a TSP with a Froude number of 1.5 (which corresponds to a channel only 72 feet wide and 15 feet deep for a typical set of design parameters) is observed to short-circuit long before the plug-flow residence time has elapsed. Clearly, this problem becomes worse at even lower design densimetric Froude number values. Once the density front has reached the withdrawal region, the pond would be effectively short-circuited since selective withdrawal of the remaining cold layer is not possible.

A total of eight experimental runs were made to determine the value of the empirical constant α of Eq. (19). In each experimental run the position of the advancing hot front was observed visually and recorded as a function of time, and all of the resulting data points are plotted in Fig. 6. The coordinate axes in Fig. 6 are chosen such that the slope of the straight line drawn through the data points is equal to the empirical coefficient α. The abscissa variable is time, while the ordinate variable is the result of integration of Eq. (19), followed by solution for αT. The ordinate variable is

$$y^* = \frac{1}{C}\left(\frac{D+E}{A}\right)^{3/2} - \frac{B}{C} \;, \tag{25}$$

where

D = observed position of the leading edge of the advancing hot front at time t,

$$A = \frac{4H^2 \Delta\rho g}{(f_i + f_b/4)}$$

$$B = \left(\frac{\rho}{H\Delta\rho g}\right)^{3/2} \;,$$

$$C = \frac{3}{8}\,\frac{\rho}{\Delta\rho}\left(\frac{f_i + f_b/4}{H^2 g}\right), \text{ and}$$

$$E = \frac{4H}{f_i + f_b/4} \;.$$

An approximate best-fit straight line was drawn through each set of data points, and a value of α determined. The average value of α is 1.09. Using this value of α, the data points for all 8 experimental runs can be predicted with an average error of 4.0%. The average error for the run with the poorest agreement is 7.2%.

Evaluation of Design Modifications

As has been indicated previously, an efficient and economical horizontal plug-flow TSP cannot be designed as envisioned in the initial design concept. If the development of the TSP design on the basis of a horizontal plug-flow pond were to be pursued then some measures had to be taken to retard the advancing density front, and the resultant TSP short circuiting. Thus, some simple modifications of the initial design concept have been investigated by testing the effects of design changes in the experimental model.

There appear to be two different means of retarding the density-induced flow in a TSP. The first is simply the correct placement of barriers in the pond such that the advance of the leading edge of the front is retarded. The second is the placement of barriers in the pond such that internal mixing jets are created which have the effect of reducing the local density differences, and consequently of retarding any density-induced flow. Actually, any barrier or constriction placed in the pond will have, to varying degrees, both of the above effects. Any constriction produces a jet as a result of the locally increased flow velocity, and a barrier will retard the leading edge of either a hot or cold advancing front. Thus, the design task has been to select empirically an appropriate pond constriction design and to determine the required number of such constriction in order to yield the desired result of adequately diminishing the density-induced flow short-circuiting.

Performance of Barriered Ponds

Initially a determination of the relative merits of horizontal versus vertical barriers was made. A horizontal barrier is of the type shown in Figs. 7a and 7b while a vertical barrier would have the general characteristic of blocking the entire width of the pond over a part of the water depth.

As is shown in Fig. 8, the horizontal barrier concept was found to be superior. Figure 8 compares the thermal capacitance performance of identical ponds (except for barrier geometries) on the basis of percentage of the theoretical cooling potential recovered from the pond as a function of time. The time variable is plotted in a non-dimensional manner by dividing by the plug-flow residence time V/Q where V is the pond volume and Q equals the flow rate. Mathematically, the percentage of the theoretical cooling potential recovered, R(t) is defined as follows:

$$R(t) = 100\% \int_0^t \frac{T_i - T_{oa}}{T_i - T_{ot}} \cdot \frac{d\tau}{(V/Q)} \qquad (26)$$

where

T_i = pond inlet temperature,

T_{oa} = actual outlet temperature,

T_{ot} = outlet temperature for theoretical plug-flow, and

t = elapsed time of operation

Also shown in Fig. 8 is the idealized plug-flow performance curve and the performance curve for a TSP with no flow constrictions.

All the curves in Fig. 8, except that for the idealized plug-flow case, are deduced from actual temperature measurements in the model at the point of flow withdrawal. Correction was made for water surface heat loss from the flume based on an experimental determination of the water to air heat transfer rate.

The performance curves in Fig. 8 indicate that in maintaining the total amount of flow constriction constant at 1/2 the total cross-sectional area (i.e., constant barrier pressure drop) the horizontal barriers appear to be slightly more efficient than the vertical barrier. If one considers the comparative difficulty in construction the vertical barrier, the horizontal is also seen to be the more desirable option.

At least two processes appear to be contribution to the vertical mixing of the hot and cold fluids. The first process in the downward movement of the hot upper layer along the upstream surface of the barrier, followed by streaming around the barrier and through the constriction. Passing through the constriction is an apparently nearly homogeneous flow which in the second process mixes with the ambient water in the downstream pond segment. However, the mean temperature of the flow through the constriction is necessarily less than that of the upstream hot layer since the underlying cold layer is gradually drawn through the constriction. The same processes occur at succeed-barriers downstream. In fact, succeeding barriers are more efficient in mixing the stratified layers since the density front at each succeeding barrier is progressively less stable than previously.

Refinement of Horizontal Barrier Concept

In attempting experimentally to optimize the design of a barriered TSP two general problems needed investigation. The first is the design of the barrier itself, and the second is the specification of the number and spacing of barriers required to obtain good pond performance. Beyond these two problems the tradeoffs between decreasing the pond design densimetric

Froude number value, and increasing the number of barriers was investigated. Additionally, the effect of a floating roof was evaluated.

Horizontal barrier design variation from that shown in Fig. 8 include different total area constrictions, and a distribution of the constriction over the width of the channel such that multiple smaller internal jets would be created at each barrier. Increasing the total constriction (i.e., more blockage of flow) has the advantage of creating more vigorous jet mixing. However, the experiments have shown that decreased jet size may lead to undesirable preferential attachment of the jet to the pond wall resulting in partial short-circuiting. The phenomenon, termed the Coanda effect, is similar to that occurring in bistable fluidic switching devices. In the TSP model this effect was observed at a design $F_D = 0.5$, and a barrier geometry at 5/6 total constriction with a 1/6-width slot at the center of the pond. In this case the jet issuing from the first barrier became attached to the pond wall, bypassing a large part of the pond volume between the barriers. A large recirculating eddy was formed in each segment as is shown in Fig. 9. The result of this behavior is that no increase in the pond performance was noted beyond that obtained in the case of a 1/2 total area constriction. This attachment effect appears to be adequately counteracted by using smaller multiple jets to obtain the same total flow constriction.

Several experiments were performed to examine the effect of varying pond length of the number of barriers required to achieve a certain level of performance. The results are summarized in Table 2. Essentially, these results indicate that the number of barriers required to achieve a certain level of performance (percent of the theoretical cooling potential recouped at the plug-flow residence time V/Q) may be largely independent of the length (storage volume) of the pond. To see this, compare the results of case 1 to those of cases 2 and 3 in Table 2. Intuitively this conclusion can be related to the need in the smaller (shorter) ponds to diminish the density induced flow more quickly than in the larger (longer) ponds. One would also expect that there would be a diminishing rate of return for the addition of barriers to the pond. Such behavior has been observed, as is shown in Fig. 10.

As in the case of the unbarriered TSP the tendency for short-circuiting was observed to increase with decreasing design densimetric Froude number value in the case of the barriered pond. Decreasing the design densimetric Froude number value allows for a deeper and wider pond, but to maintain high performance additional (or more effective) barriers need to be added. Table 3 gives the performance loss for a decrease in design densimetric Froude number from 0.5 to 0.25 (cases 1 and 2). However, in comparing cases 1 and 3 in Table 3 it is apparent that a highly efficient pond can still be realized with the same number of barriers by increasing the effectiveness of the barriers. The barrier effectiveness is increased by increasing the total constriction, which in turn increases the jet mixing effect.

In addition to the modeling of the behavior of the advancing hot front at the design condition temperature difference of 10°F, experimental runs were made to examine the off-design behavior. One run was made which is identical to case 1 in Table 2 except that instead of a hot discharge into a cold pond, cold water was discharged into an initially hot pond. This simulates the "cooldown" mode of operation. As anticipated the performance increased from 87% to 92% (percentage of theoretical cooling potential recouped at $T = V/Q$). Also as anticipated an evaluation of the off-design performance ($\Delta T = 5°F$) for a TSP of the same design revealed an increase in the performance from 87% to 90%.

Summary and Conclusions

The two basic options for the design of a thermal storage pond for use with a dry cooling tower — horizontal and vertical plug-flow — have been evaluated with regard to their value in TSP applications. The horizontal plug-flow pond was selected for detailed evaluation based on its relative merits. Subsequently, an initial design concept was formulated for the horizontal plug-flow pond and its performance evaluated by the use of an experimental model. The result was found to be unsatisfactory due to the magnitude of the density-induced flows. Thus, modification of the initial design concept was required. Various flow constriction which induced flow mixing were evaluated in model studies in order to determine their relative merits. A simple full-depth barrier with vertical slot jets proved to be a very successful in achieving control of the density-induced currents.

Experiments were performed to examine the sensitivity of the pond performance to variations in the design densimetric Froude number, and to the number and geometry of the flow constrictions. In addition off-design performance was evaluated.

The main conclusion of this design investigation is that a horizontal plug-flow thermal storage pond of apparently reasonable geometry and cost can be designed such that the ideal plug-flow behavior is approximated well. The following TSP specification results in the excellent design-condition performance shown in Fig. 11. This case may be used to evaluate TSP construction costs:*

Design F_D = 0.25,
Depth = 20 ft.,
Width = 240 ft.,
No. of barriers = 8
Length = (dependent on desired storage volume),
Barrier geometry = 5/6 total constriction, horizontal type, 3 slot,
Discharge structure = 10 uniformly spaced 4 ft. dia. submerged nozzles,
Withdrawal structure = no specific structure required, and
Cover = (floating cover will enhance performance).

It should be emphasized that many other designs may also prove to be efficient thermally, and may ultimately be more economical. Qualitatively, tradeoffs between the above parameters may be made on the following basis:

Increasing design F_D value results in improved TSP performance,

Increasing depth results in degraded TSP performance,

Increasing width results in degraded TSP performance,

Increasing number of barriers results in improved TSP performance, and

Increasing total barrier constriction results in improved TSP performance.

---

*For design flow = 1000 cfs, design $\Delta T = 10°F$

REFERENCES

1. Guyer, E.C. and Golay, M.W., "An Engineering and Economic Evaluation of Some Mixed-Mode Waste Heat Rejection System," Department of Nuclear Engineering, Mass. Inst. of Tech. Report MITNE-191, 1976.

2. Jirka, G., Abraham, G., and Harleman, D.R.F., "Assessment of Techniques of Hydrothermal Prediction," Ralph M. Parsons Laboratory for Water Resources and Hydrodynamics Report #203, MIT, 1975.

3. Abraham, G., "Magnitude of Interfacial Shear in Exchange Flow," Journal of Hydraulic Research, 9, 1971, No. 2.

4. Rohsenow, W., and Choi, H., Heat, Mass, and Momentum Transfer, Prentice-Hall, New Jersey, 1961.

TABLE 1

THERMAL STORAGE POND MODEL DESIGNS

		Case 1	Case 2	Case 3
1.	Densimetric Froude Number	1.5	1.0	.50
2.	Depth (inches)	4.5	4.5	4.0
3.	Width (inches)	18	18	18
4.	Aspect ratio	0.25	0.25	0.22
5.	Mean Velocity (ft/sec)	0.28	0.19	0.088
6.	Total flow (GPM)	70.4	47.2	19.5
7.	Reynolds Number	30,000	20,100	8,830
8.	Scale factor	48.4	72.7	147.0
9.	Temperature difference (°F)	40	40	40
10.	Vertical Distortion	1.21	1.80	3.33
11.	$\frac{f_o(l/D)\text{ model}}{f_o(l/D)\text{ prototype}}$	1.83	1.38	0.94
12.	Discharge	highly unstable submerged multiport		

TABLE 2

EXPERIMENTS TO EXAMINE EFFECT OF NUMBER OF BARRIERS ON POND PERFORMANCE

Case	F_D	Number of Barriers	Prototype Storage Volume	Percentage of Total Theoretical Cooling Potential Recovered at t/(V/Q)=1.0
1	0.5	8	6	87%
2	0.5	4	3	81%
3	0.5	8	3	89%

All barriers 1/2 total area constriction, 3 slot horizontal type

TABLE 3

EXPERIMENTS TO DETERMINE EFFECT OF DESIGN DENSIMETRIC FROUDE NUMBER ON TSP PERFORMANCE

Case	F_D	Number of Barriers	Fraction of Cross-Sectional Area blocked by Barrier	Percentage of Total Theoretical Cooling Potential Recovered at $t/(V/Q)=1.0$
1	0.5	8	1/2	87%
2	0.25	8	1/2	75%
3	0.25	8	5/6	86%

All barrier horizontal type, 3 slot, Prototype Storage
Volume = 6 hrs.

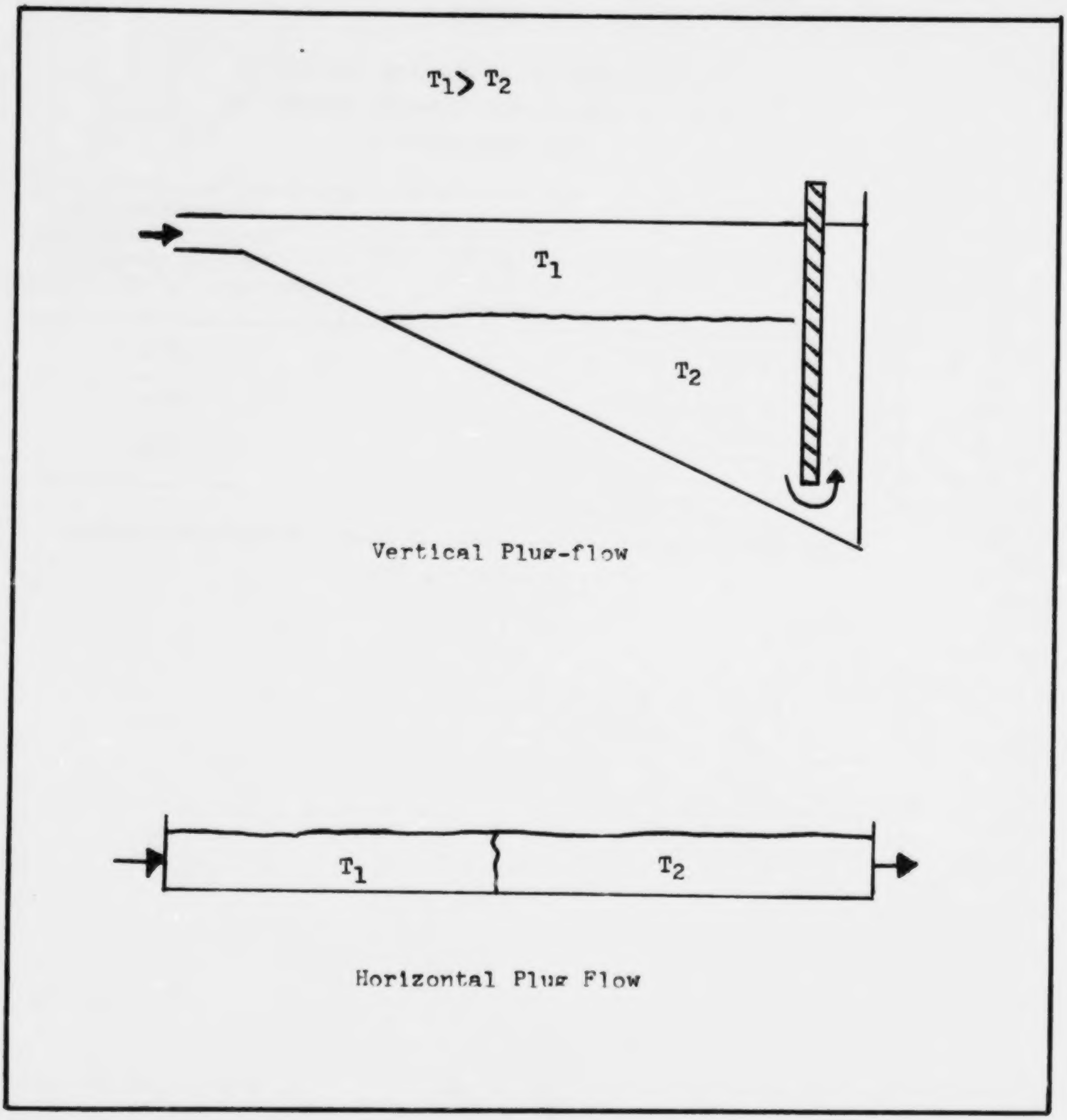
$T_1 > T_2$
T_1
T_2
Vertical Plug-flow
T_1
T_2
Horizontal Plug Flow

Fig. 4.1 Horizontal and Vertical Plug-Flow Concepts

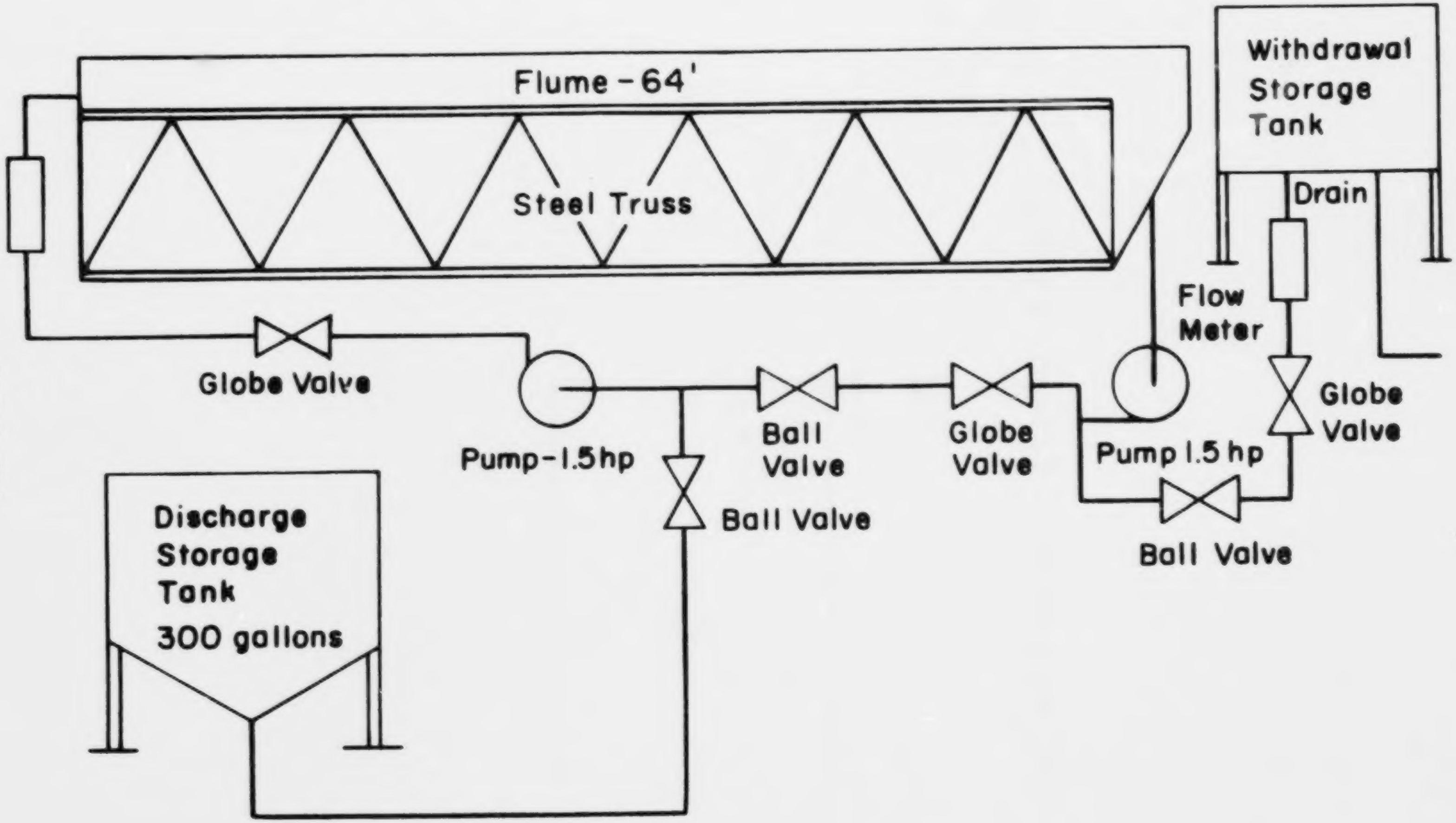
Flume - 64'
Steel Truss
Withdrawal Storage Tank
Drain
Flow Meter
Globe Valve
Pump-1.5hp
Ball Valve
Globe Valve
Pump 1.5 hp
Globe Valve
Ball Valve
Ball Valve
Discharge Storage Tank 300 gallons

Fig. 4.7 Schematic of Thermal Storage Pond Model Experiment

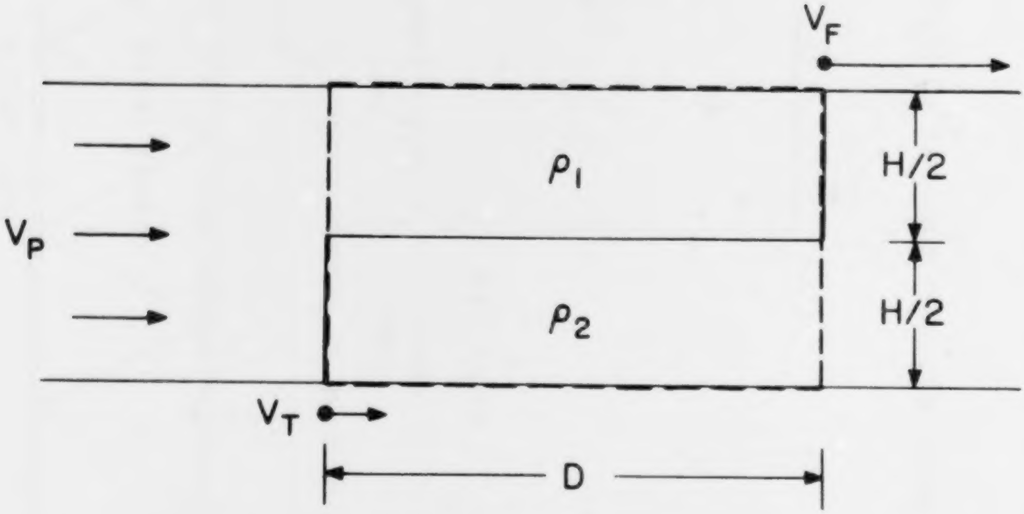
V_F
V_P
ρ_1
ρ_2
H/2
H/2
V_T
D

Fig. 4.8 Density-Induced Flow Control Volume

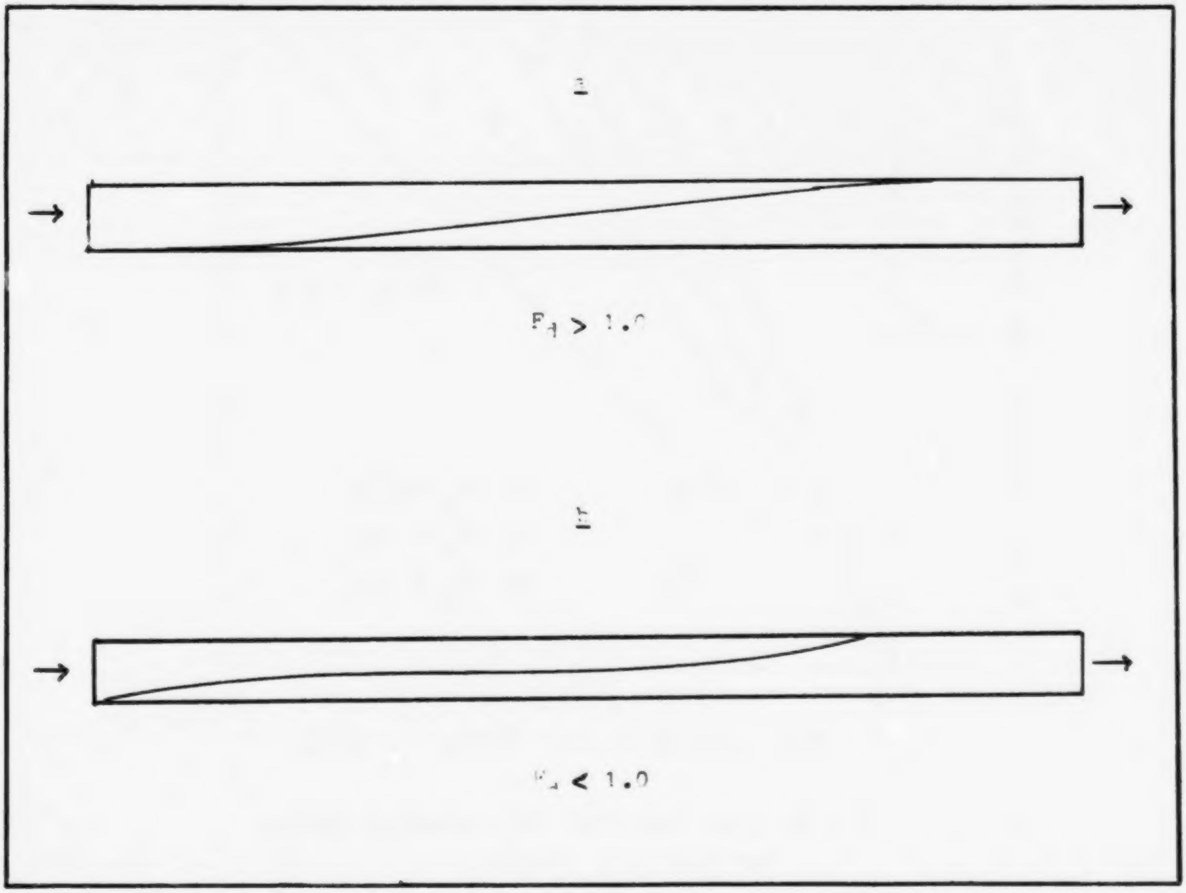
a
$F_d > 1.0$
b
$F_d < 1.0$

Fig. 4.10 Illustration of Density Front Profile - Advancing Hot Front

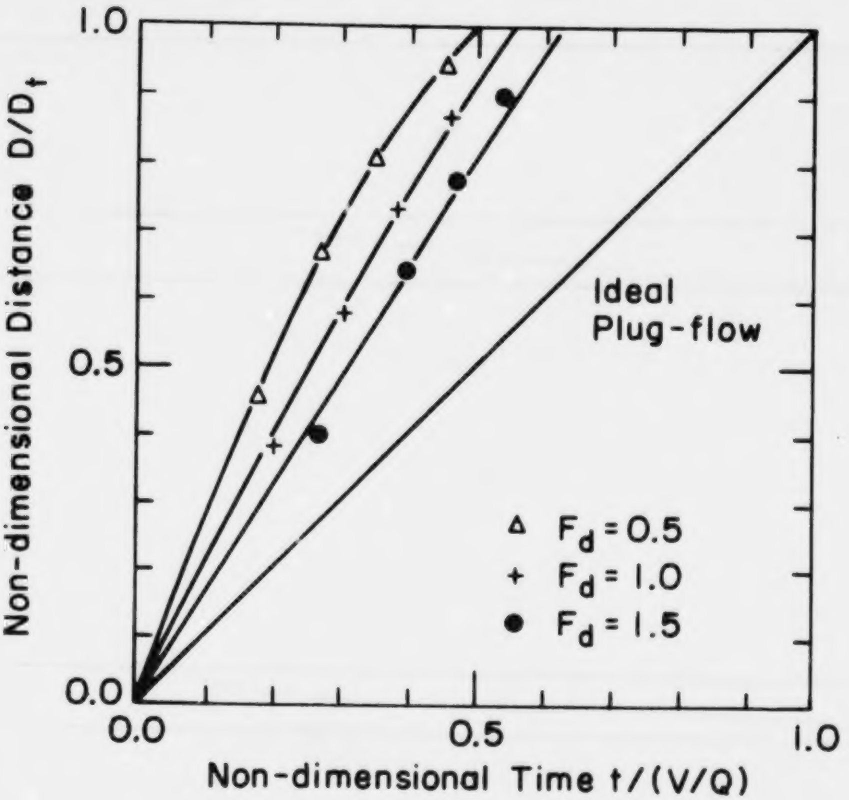

D = Actual Position of Leading Edge of Density Front

D_t = Total Lenght of Pond

Fig. 4.11 Propogation of Density Front as a Function of TSP Design Densimetric Froude Number

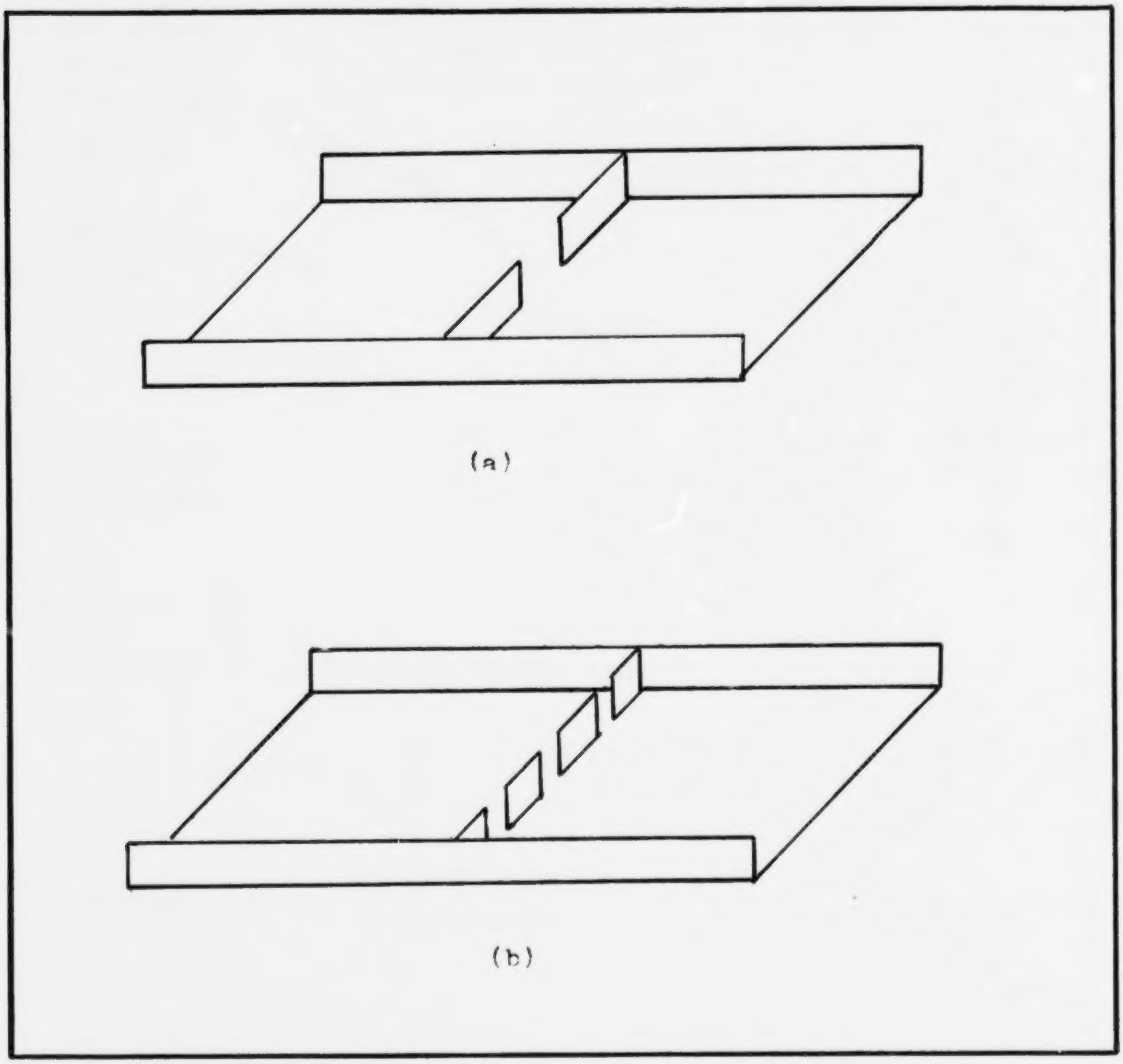
(a)

(b)

Fig. 4.17 Horizontal Barriers

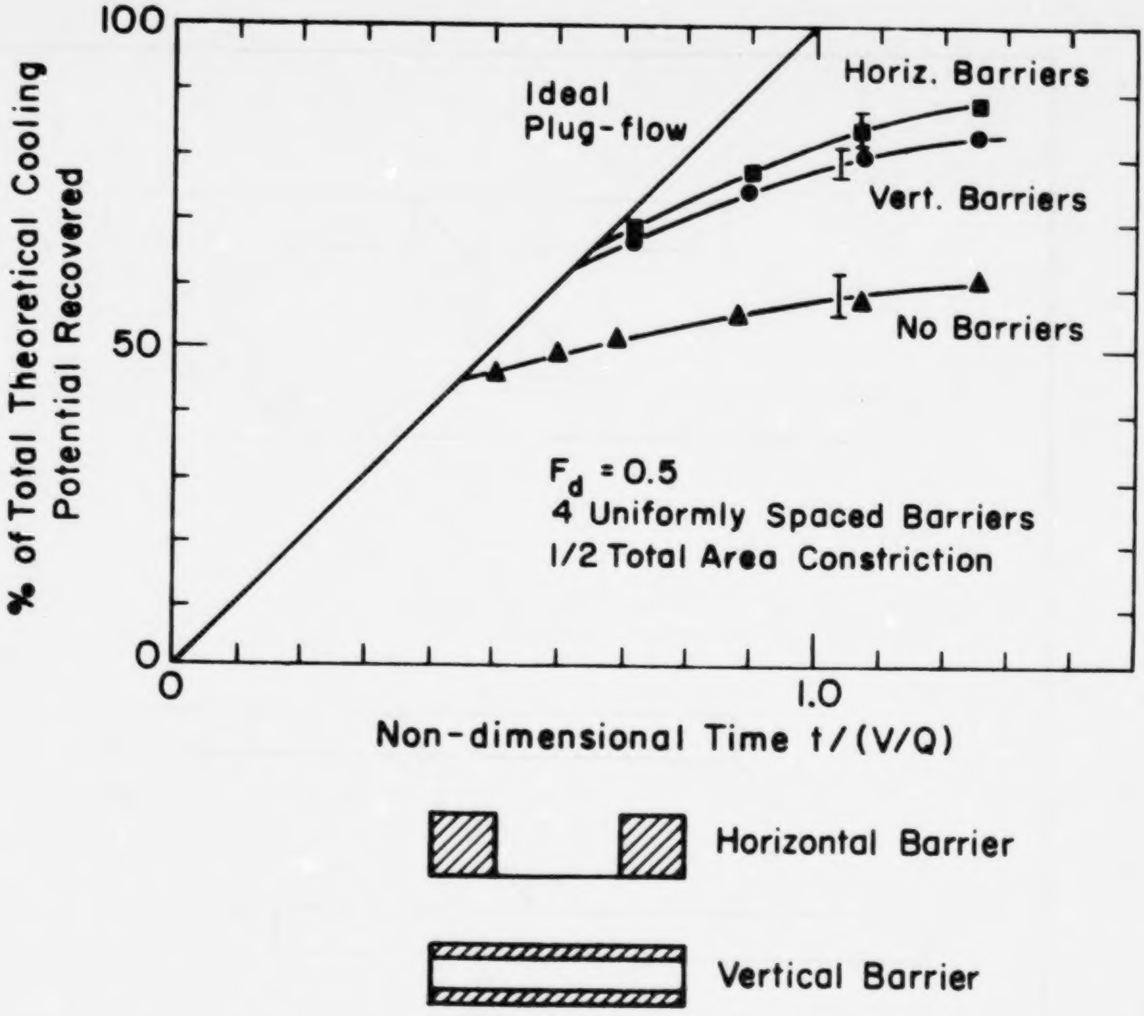

Fig. 4.19 Performance of Barriered TSP

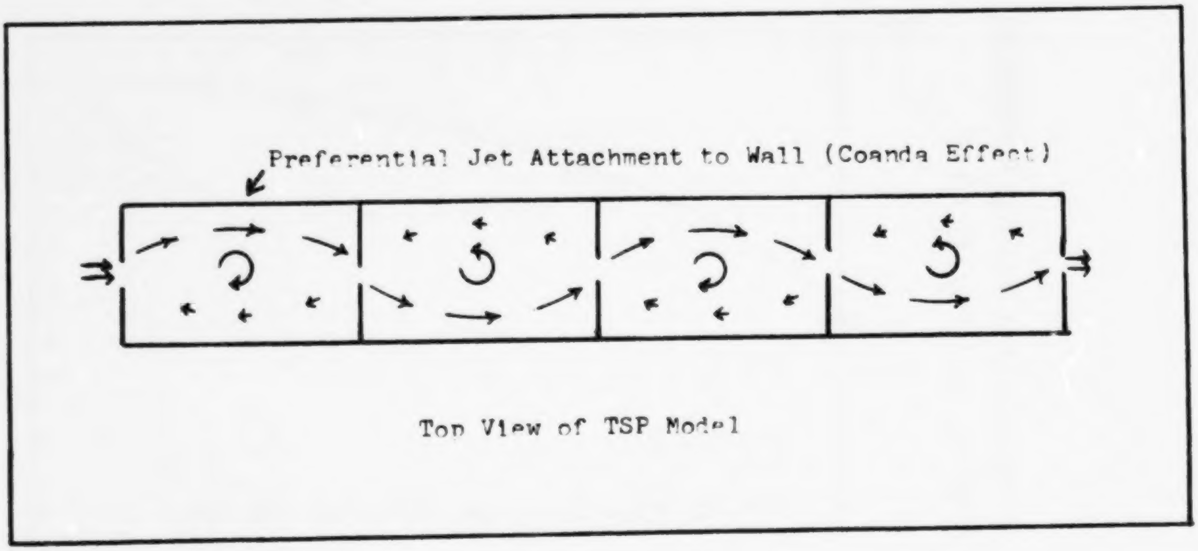
Preferential Jet Attachment to Wall (Coanda Effect)
Top View of TSP Model

Fig. 4.20 Flow Field Resulting From Attached Jet

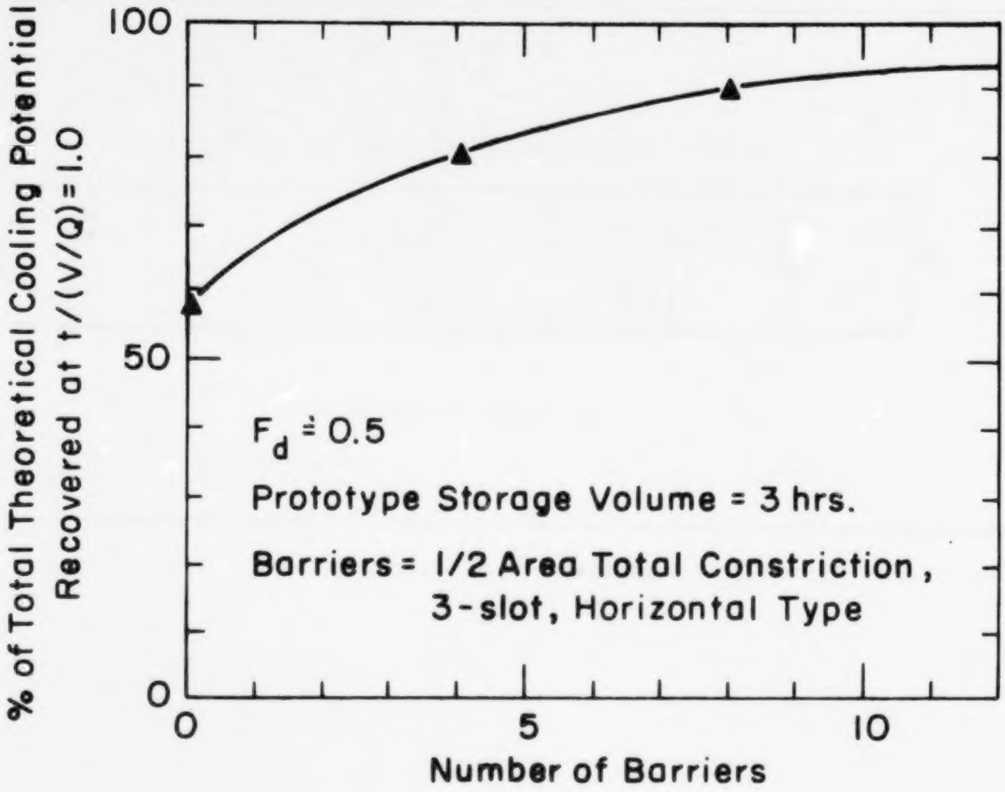

Fig. 4.21 TSP Performance as a Function of the Number of Barriers

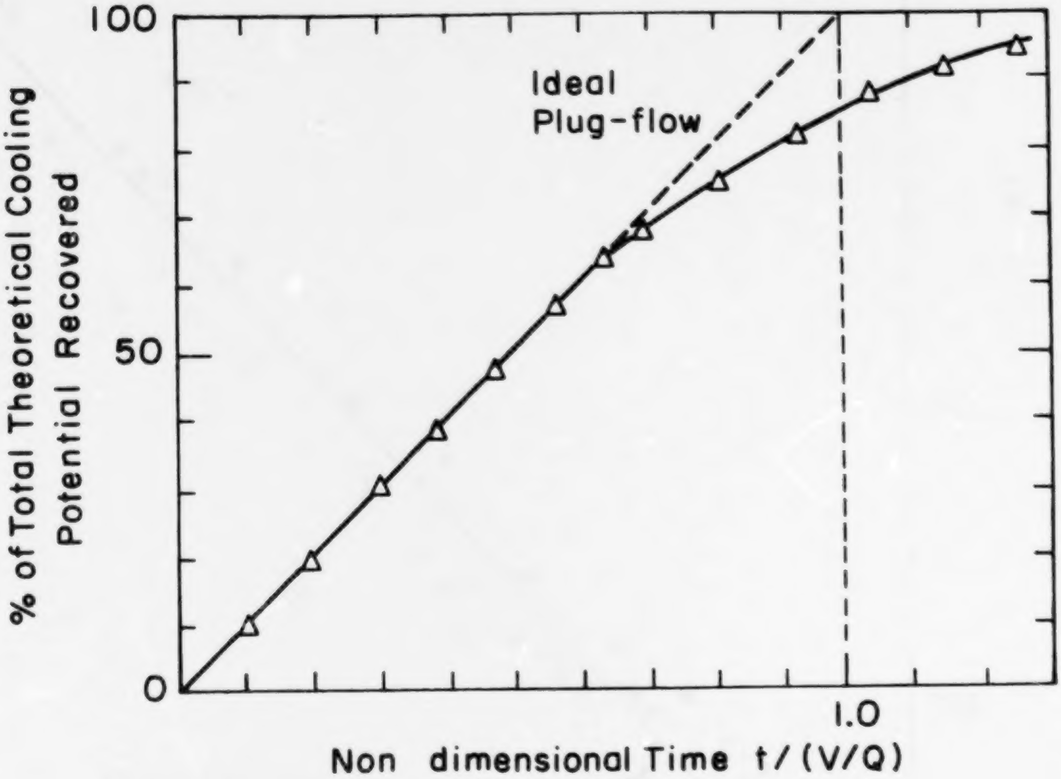

$F_d = 0.25$

Prototype Storage Volume = 6 hrs.

Barriers = 8, 5/6 Total Area Constriction
3-slot, Horizontal Type

Fig. 4.30 Performance of Recommended Design

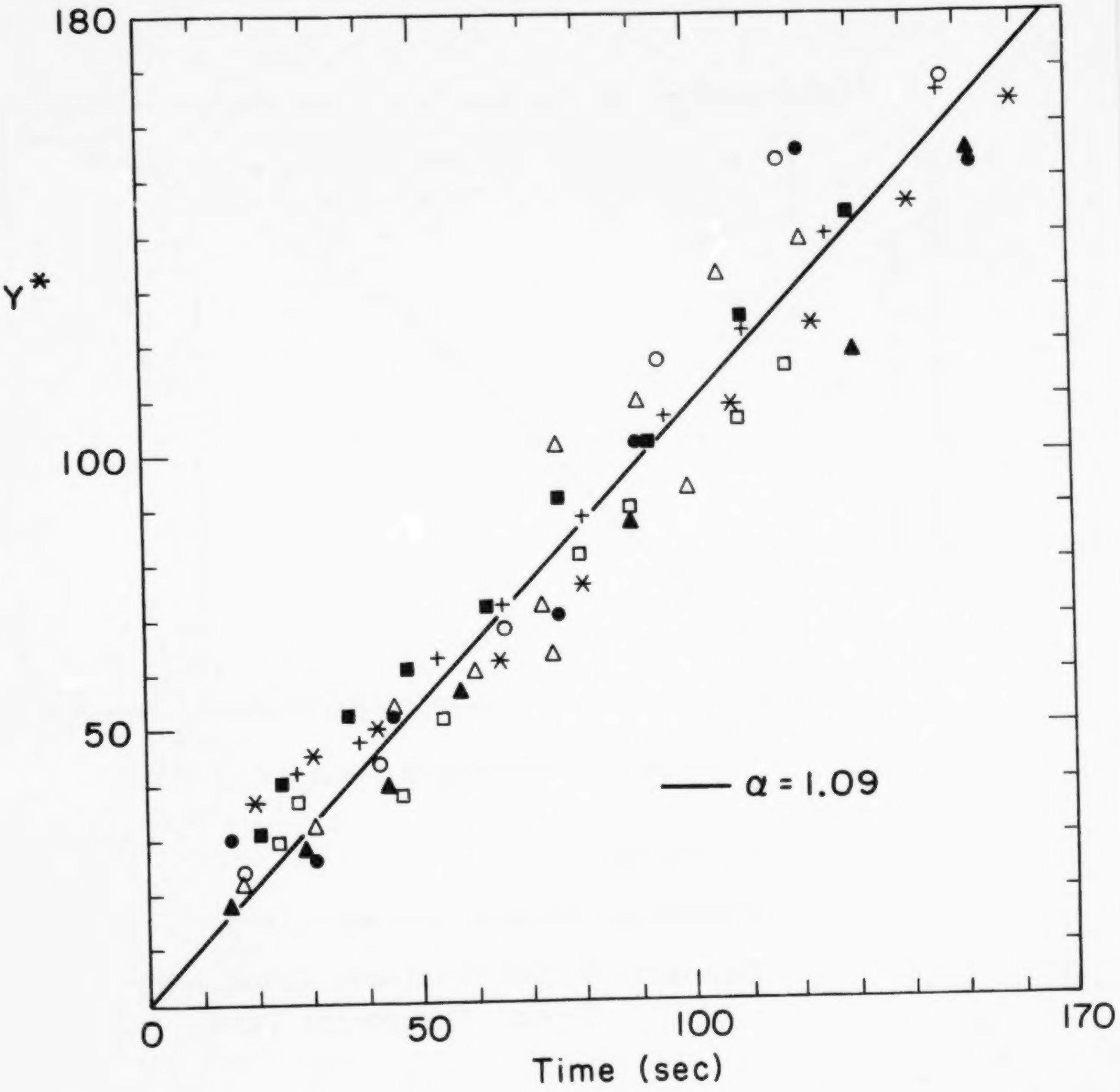

Fig. 4.12 Data for α Determination

36-45-41

DISPERSION OF HEAT AND HUMIDITY FROM ATMOSPHERIC SPRAY-COOLING SYSTEMS*

H. Weinstein, R. W. Porter, S. Chaturvedi,
R. A. Kulik and J. E. Paganessi
Illinois Institute of Technology
Chicago, Illinois 60616, U.S.A.

ABSTRACT

Spray cooling systems are alternatives to evaporative cooling towers for waste heat disposal of large electric power plants. In particular, visual appearance, noise, fog and drift may be more favorable. The present investigation includes field experiments, laboratory simulations and theoretical analysis of the so called base flow of the discharge.

A spray canal at Quad-Cities Nuclear Station (Illinois) was the subject of the field experiment. Both dry-and wet-bulb temperatures were monitored downwind of the canal. Both decayed with the -3/2 power of distance.

The laboratory simulation was carried out in an environmental wind tunnel. Helium was injected through several source simulation devices to represent the buoyant discharge. Three-dimensional maps of helium concentration were obtained along with measurements which characterize the incident and downstream boundary layers.

Results were evaluated using a fluid-dynamic convective-diffusion equation for the atmospheric surface layer.

INTRODUCTION

Spray cooling systems are alternatives to evaporative cooling towers for waste heat disposal of large electric power plants. In particular, visual appearance, noise, and drift may be more favorable. The discharge is spread over a larger area at the source and is closer to the ground. Because of the predominantly large O (cm) diameter drops of the subject sprays, drift loss is extremely small from the point of view of momentum and energy considerations. However, drift may be important where small amounts lead to icing and salt deposition in certain localities. A knowledge of the behavior of the base flow will

---

* Supported by NSF under Grant AER-74-01600 with technical management by ERDA, Conservation Division.

permit improved computation of drift trajectories and deposition and a determination of the occurrence of fog. A knowledge of dispersion is also important in terms of thermal performance where large-scale interference on down-wind segments may be possible depending on the system configuration.

The object of this study was to develop a laboratory simulation and an analytical model which after comparison with a field study for verification could be used to investigate a spectrum of possible operating conditions. Since the atmospheric flow and a power station's heat rejection requirements are both so variable it becomes at best an enormous task to investigate the whole range of possible operating states directly in the field. Therefore, the three component parts of this investigation were undertaken simultaneously and the results compared herein to determine best estimates of the important parameters of the discharge as power-law functions of the downstream distance.

Previous experimental studies of environmental effects of spray canals by other investigators as contained in the open literature are apparently restricted to consideration of drift. For example, drift for various drop sizes versus distance are given for a spinning-disc-rotor spray generator in [1]. Data for the Ceramic Cooling Tower Modules, discussed below, are given in [2, 3, 4]. However, as pointed out by Guyer and Golay [3], the trajectory of drift droplets is dependent on evaporation and condensation, variable aerodynamic drag due to plume behavior, and variations in ambient wind speed. It is thus important to have a good understanding of the flow containing the drift. Further, the effects of fog as well as heat and humidity are of general interest. These are especially sensitive to the so called base flow.

The surface layer of the atmospheric boundary layer has been studied in both field experiments and laboratory simulations in environmental wind tunnels. A discussion of atmospheric data and flow modelling in wind tunnels is given by Cermak, [5]. He gave the following criteria for the experimental simulation of the type undertaken here: An undistorted geometric scaling, equal Richardson numbers, "aerodynamically rough" surface roughness, similar surface temperature distribution, similar mean and turbulent velocity and temperature distribution. Since all these conditions can not be met simultaneously, a judicious choice must be made to simulate those scales of motion with the greatest significance for the present application. A discussion of the scaling laws for the simulation is given in the text.

A comparison of the experimental results is made with the analytical results of Rao, et al. [6] Their work is interesting because of the sophisticated treatment of turbulent transport. Their work also compares well with Cermak's [7] Lagrangian analysis of plume dispersion which is used for comparison with the present results. Sutton's [8] analysis for point and line source dispersion yielded power law forms for ground level concentrations and these are also used for comparison in the text.

A 4-row-across spray canal at Commonwealth Edison Company's Quad-Cities Nuclear Station (Illinois) was investigated in the field experiment. The ambient atmospheric conditions were monitored at the 2-m height upwind of the system. The water temperature toward which the wet-bulb temperature is driven was also recorded. Both dry- and wet-bulb temperatures were monitored at the 2-m height downwind of the canal in the absence of fog. While the data are restricted to the "near field" where increments above ambient are appreciable, they are important for determining initial discharge behavior.

The laboratory simulation was carried out in a 43 x 46 x 214 cm environmental wind tunnel designed to simulate conditions that exist in the lower atmospheric surface layer. Injection of helium was made to simulate the buoyant discharge. The helium was introduced through a round orifice (point source simulation), a slit (line source), and a porous plate (also essentially a line source) which could be rotated to vary the angle of incidence of the approach wind. Measurements were made of the incident and downstream boundary layers which included turbulence intensity, Reynolds stress, macro and micro scales and velocity profiles. In order to characterize the simulated boundary layer, three dimensional maps of helium concentration, simulating air and water vapor, were also obtained downstream of the discharge. Spreading rates of the discharge were determined and compared to values found in the literature and the field studies.

An analysis of the spreading of the discharge was also carried out. The spray canal is modelled as a continuously distributed source of energy and moisture. Convective-diffusion equations for enthalpy and moisture are used with an NTU (Number of Transfer Units) model for the spray cooling. Numerical solutions of the resulting equation are compared to the experimental results.

FIELD EXPERIMENTS

Test Conditions

The Quad-Cities Nuclear Station of Commonwealth Edison Company (Illinois) uses a 4-row-wide spray canal which is about 60 m across and 3 km long forming an oval loop. In the Richards of Rockford section, 56-kw motor pumps drive 4.5 x 10^4 l/min through single 16-m-diameter sprays of 5.2-m height in each of 152 floating modules. In the Ceramic Cooling Tower (CCT) section, 51-kw pumps drive 3.8 x 10^4 l/min through 4 12.2-m-diameter sprays of 5.5-m height in each of 176 modules. The spray layout is shown in Figure 1.

The segment analyzed was a continuous north-south run of 36 CCT modules. Under the particular test conditions, the water level was somewhat low and the bank height was 3.9 m with a 3:1 (horizontal:vertical) slope. Prevailing conditions averaged over the experiment included

date	8-6-75
time	12:25-15:54
ambient wind speed @ 2 m	3.7 m/s
ambient wind angle to canal @ 2m	79°
ambient wet-bulb temperature (WBT) @ 2 m	16.1C
ambient dry-bulb temperature (DBT) @ 2 m	22.8C
canal water temperature	36.8C
most upwind spray temperature (est)	33.9C
most downwind spray temperature (est)	35.2C
clear-day atmosphere	--

The ambient sensors were positioned 2 m over ground level, 50 m upwind of the canal and out of the influence of the sprays. The terrain was open grassland of about 0.5 m height of growth.

Instrumentation and Procedures

Wind run was sensed with a Gill low-threshold photo-chopper cup-type anemometer calibrated in the IIT 4 x 6 ft Environmental Wind Tunnel to be within 0.1 m/s. The output pulses were recorded on an event channel and later summed over the test interval to provide average wind speed. Wind direction was sensed with a Gill bivane with 1000-ohm potentiometer element. Wet-and dry-bulb temperatures were obtained using an Atkins aspirated psychrometer module with thermistor elements. The thermistors and bivane potentiometer were automatically sequentially sampled with several minutes dwell in conjunction with an Atkins thermistor bridge recording on an analog channel. A decade resistance substitution box was used to insure recorded temperatures within 0.1-C maximum error, the probe interchangeability tolerance. Wind direction was accurate within several degrees. The analog data were averaged over the sample duration to provide gust-integrated values which were then tabulated for correlation in time with measurements made downwind of the canal.

The canal water temperature was stable as periodically verified by readings of an Atkins thermistor sounding probe and bridge. Canal water temperatures are very well mixed at a section [10] and also were accurate within 0.1C. The estimated spray temperatures were computed using parameters discussed in Reference [11] (NTU = 0.15, upwind f=0, downwind f = 0.45) from other experiments.

Two additional Atkins psychrometer modules with another sequential sampler, bridge and recorder were positioned downwind of the canal at the 2-m elevation. One psychrometer was fixed at a distance $x_o = 41$ m from the canal and spray centerline while the second was moved downwind in intervals. Recorded temperatures were also accurate within 0.1C.

Experimental Results

Data are correlated in terms of the dimensionless interference allowance [10-13]

$$f_{WB} = (T_{WB} - T_{WB\infty})/(T - T_{WB\infty})$$

where T_{WB} is wet-bulb temperature, ∞ denotes ambient and T is canal water temperature. Quantity $0<f\leq 1$ as the ambient wind is driven toward equilibrium with the sprays. Also considered was the dry-bulb

$$f_{DB} = (T_{DB} - T_{DB\infty})/(T - T_{DB\infty})$$

Data are plotted in Figure 2 in ratio to respective f (x_o) values. They appear to fall off with the -3/2 power of distance from the spray centerline. A consideration of psychrometrics over small increments in state would show a similar f for specific humidity

$$f_w = (w - w_\infty)/(w_s(T) - w_\infty)$$

where "s" denote saturation, would fall off in the same manner in ratio to the value at x_o.

LABORATORY STUDIES

Experimental

The laboratory simulation was carried out in a 43 x 46 x 214 cm environmental wind tunnel designed to simulate typical conditions that exist in the lower atmospheric boundary layer.

The wind tunnel is shown in schematic form in Figure 3. Injection of helium was made to simulate the buoyant discharge. The helium was introduced through a round 0.635 cm diameter orifice (point source simulation), a 0.056 cm x 38 cm slit (line source), and a 2.54 cm x 30.5 cm porous plate mounted flush with the tunnel floor (also essentially a line source) which could be rotated to vary the angle of incidence to the approach wind. These three injection devices are shown in Figure 4.

The tunnel inlet section is packed with 0.3175 cm x 25.4 cm soda straws to provide a uniform flow and to damp room air turbulence levels. The inlet section is followed by a 91.5 cm section to generate a smooth boundary layer flow. The test section is also 91.5 cm long with a 31 cm gear rack traversing mechanism attached axially to the top wall. This top wall could be moved in the tranverse direction. With this configuration, a probe could be positioned anywhere in the test section.

At the entrance to the initial section, a 5 cm diameter counterjet tube was fixed just below the floor of the test section. This counterjet device is a modification of one discussed in reference [9]. The tube was drilled across the entire width of the tunnel with 0.32 cm holes. Air was injected through the counterjet device to establish a thicker boundary layer. Longitudinal roughness strips were added along the tunnel floor when the counterjet device was in use.

The instrumentation consisted of a two channel hot wire anemometer system with hot film probes. Helium concentration was measured directly with an aspirating hot film probe manufactured by Thermo-Systems, Inc. In the region of pure air flow, measurements could be made of mean velocity, axial and vertical turbulence intensities, Reynolds stress, and micro and macro scales of turbulence. In the two-component region, mean velocity and mean concentration could be measured.

It was intended to simulate the fully developed or equilibrium atmospheric boundary layer in the wind tunnel. In order to do this, the thick boundary layer generated in the tunnel must be in equilibrium. This means that the velocity profile shape, turbulence properties, etc., do not change in the streamwise direction. This was not the case with the boundary layer generated in the tunnel wherein a counter wall jet at the intake was used to shape the profile. However, the boundary layer generated did simulate many aspects of real atmospheric layers. The actual laboratory boundary layers in equivalent characteristics ranged from slightly unstable-to-neutral, to stable-to-neutral conditions, depending on the case.

Typical boundary layer profiles are shown in Figures 5-8. Figure 5 shows the boundary layer profiles for 5 axial positions in the test section. It is seen that the power law exponent, n, varies from about 5 to 3 with distance downstream. The streamwise and vertical turbulence intensities for the same case are shown in Figures 6 and 7. The variation through the boundary layer is as expected and there is relatively little variation with axial position. Figure 8 shows the Reynolds stress variation (friction velocity squared) through the boundary layer. There is a region of relatively constant U_*^2 near the wall with a relatively large amount of scatter in the data. A summary of the boundary layer parameters for all the cases studied is presented in Table 1. Since the experiments were done in two stages, the data are so presented. Stage I refers to the point and line source experiments. After installation of the porous plate source, it was found that the modifications slightly changed the wind tunnel operating point and data with this source are called Stage II data.

The Stage I measurements show some internal inconsistencies in that the frictional velocity, U_* is independent of roughness for the point source case. While for the line source data U_* does depend on roughness. The line source U_* without roughness is about the same as that for the point source cases but the line source U_* with roughness is much larger. The velocity profile shape parameter n should decrease with increasing roughness and again this is clearly shown in the line source data but is not shown conclusively in the point source data. It is not clear how strongly these inconsistencies are related to the deviation from equilibrium of the boundary layer. The Stage II data are much more consistent internally than are the Stage I data, and show trends consistent with fundamental considerations.

Scaling of the Boundary Layer

The difference between the boundary layer developed in the wind tunnel and that found in the atmosphere should be mainly one of scale. The simplest choice for scaling is the momentum boundary layer thickness δ. The δ developed in the atmosphere most frequently ranges from 500 to 1000 m while that found in the wind tunnel is between 7.8 to 9.1 cm, a ratio of 5-to-10 x 10^3.

Another basis for scaling the flow in the wind tunnel to that in the atmosphere is the ratio of gravity to inertia forces, represented by the Froude number, Fr.

$$Fr^2 = U^2/(gL\Delta\rho/\rho)$$

For similarity, the Froude numbers in both the atmosphere and wind tunnel should be made equal. Since the velocity of the atmospheric wind is usually about twice that in the wind tunnel the scaling should be:

$$4(\Delta\rho/\rho L)_{Lab} = (\Delta\rho/\rho L)_{atm}$$

Except for the extreme case of a hot chimney plume, the range of $(\Delta\rho/\rho)_{Lab}/(\Delta\rho/\rho)_{atm}$ is typically 10 to 100. Thus the size ratio L_{atm}/L_{Lab} is typically in the range of 40 to 400. For example, the 0.62 cm injection source would correspond to an atmospheric source of 24.5 to 245 cm.

In a study of this kind, the buoyancy divided by the viscous stress or the Richardson number, Ri, also is significant. Exact modeling requires that the scale of the Richardson numbers in the laboratory and the atomosphere be made the same.

The value of the Richardson number found in atmospheric flows range from 1 to -0.03. Table 2 gives values of the Richardson number and related Monin-Obukhov length scales for all of the laboratory discharge along with those values found in the ambient atmosphere. The laboratory approach Ri = 0, however.

The values of the Richardson number found in the wind tunnel in the discharge region correspond to values that may be found in the atmosphere during conditions of slightly unstable stratification. A comparison of Monin-Obukhov lengths shows that the laboratory values ranged from 0.01 to 10 times the atmospheric values comparing the laboratory discharge to the ambient approach.

It is seen from these scaling calculations that the geometric scaling is not consistent with the other derived length scales. This remains a shortcoming of the simulation and its actual affect on the following comparison of results can not be evaluated here.

Results

The spreading of the buoyant discharge for all of the cases are presented here as plots of isoclines of helium concentrations or as helium concentration maps. Figure 9 shows the isoclines for the Stage I point source. While the applicability of this case to spray canal studies is not straightforward, the figure illustrates an important point. It is seen that initially the spreading in the horizontal direction is faster than in the vertical direction. However, at greater axial distance, the vertical spreading becomes greater than the horizontal spreading. It appears that the effects of the body force term (buoyancy) take some time to be realized while the momentum and turbulence terms act much more rapidly. The two Stage I cases for a line source with and without roughness are shown in Figures 10 and 11, respectively. Comparison of the two cases shows the appreciable difference in mixing rates due to the added roughness and consequent increase in friction velocity. The delayed effect of the buoyancy is masked by the more gradual spreading in the case without roughness while it is readily apparent in the case with roughness. The first two cases of the Stage II data with the porous plate line source oriented transverse to the flow are shown in Figures 12 and 13. These two figures are helium concentration maps. The small vertical source injection velocity (3 cm/sec) of the helium is seen to have very little affect on the spreading rate since at the end of the porous plate ($x = 1.3$ cm) the peak concentration is only about 0.4 cm off the floor. The surface roughness again increase the spreading rate considerably and again the buoyancy effects are more clearly visible with surface roughness present. The isoclines for the line source located axially are shown in Figures 14 and 15 for the cases with and without roughness, respectively. As in the previous cases, spreading is more rapid and maximum helium concentrations lower when surface roughness is present. Figure 16 shows helium isoclines 0.6 cm above the floor for the case with the line source located at a 45° angle to the flow. It clearly shows the transverse-line-source-like behavior close to the source and then transition to axial-line-source-like behavior well downstream.

Comparison of Laboratory Data to Models and Field Data

In their study of a point source of diffusion in a neutral shear layer, Rao, et al. [6] define two similarity length scales, one in the vertical direction, η , and one in the horizontal direction, σ, as the distance to the half-maximum concentration. They fit their calculated data found from a Gaussian diffusion model to an exponential equation and the results for both their data and that of Cermak [7] is presented in Table 3. The same exponential equation form was used to fit the data obtained in the present study. These results are also presented in Table 3 for comparison.

It can be seen by comparison of the equations given in Table 3 that the laboratory data exhibits the same type of vertical similarity that is found both using the Gaussian diffusion model and in the atmospheric data and that the exponents found for the y/η term are of the same order of magnitude.

The exponential curve fit of the horizontal spreading data from the diffusion analysis of Rao, et al. [6] and this laboratory study are presented in Table 4.

Again a comparison of the equations shows the same similarity variable type of spreading in the horizontal direction with the exponents of the x/σ term of the same order of magnitude.

A further correlation of the half-maxima as a function of downwind position is presented in Table 5. Comparison of the various correlations shows that the laboratory experimental data show a great similarity to the behavior of both the atmospheric data and the calculated diffusion data. The computed data of Rao, et al. [6] was generated for a point source of diffusion with no buoyancy and included a perturbation in the calculation to simulate roughness. The laboratory data for the point source with roughness show very close agreement for the vertical spreading rates. The calculated data, however, predict a greater rate of spreading in the horizontal direction than the data of this experiment show. This is probably due to the buoyancy of the helium source of this experiment. With the upward directed buoyant fource, there is more material entrained upward and less material spreading in the horizontal direction.

Sutton [8] derived equations for a point source and a line source diffusing into the atmosphere. The equations reduce to the following form for ground level data downwind of a line source or on the centerline downwind of a point source: $C/C_0 = (x/x_o)^n$. Table 6 presents the best fit equations of the form predicted by Sutton as found from this experiment and those found in the field studies by the IIT Waste Energy Management Group from a line source of spray modules in a cooling canal.

A value of $n = -1/2$ is predicted from theory if the wind velocity and turbulent diffusivity are constant throughout the flow field. The deviation from the predicted value is probably due to the greater shear stress at the ground level and the buoyancy of the discharge.

NUMERICAL MODELLING OF DISPERSION OF HEAT AND HUMIDITY

The spray canal is modelled as a continuously distributed source of heat and moisture. Such a model is a good approximation for dispersion in the near field (over the canal) and is very accurate for far field dispersion. A two dimensional model is considered appropriate for most of the cases except where ambient wind is nearly parallel to the canal. The source strength is proportional to NTU (Number of Transfer Units), flow rates of the sprays and (1-f) where f is the interference allowance which accounts for the heating and humidification of the air. The cooling load of the canal decreases in the windward direction. In the far field (downstream of the canal), the dissipation of the heat and moisture laden discharge has implications for environmental impact, especially the fogging potential. It is also important in defining the new atmospheric approach conditions for the return leg of the canal.

It is assumed in the analysis that the ambient wind and turbulent diffusivities are not affected by the presence of the spray canal. Attenuation of ambient wind through the sprays is an important factor in computing the local wet bulb temperature and the cooling load. However, in the far field calculations this effect is neglected.

The equation for convective-diffusion in the atmospheric surface layer for enthalpy of the air-vapor mixture per unit mass of dry air is

$$\frac{\partial}{\partial x}(Ui) + \frac{\partial}{\partial z}(Wi) = \frac{\partial}{\partial z}\left(K_i\frac{\partial i}{\partial z}\right) + (Q_s''' + \dot{m}_e''' \, i_g)/\rho_a \qquad (1)$$

Where K_i is the vertical turbulent diffusivity for i, Q_s''' is volumetric sensible heating rate, $\dot{m}_e'''$ is volumetric mass evaporation rate, i is the saturated liquid water specific enthalpy and ρ_a is dry-air density. Similarly, for vapor moisture transport characterized by the humidity (mass of vapor per unit mass of dry air)

$$\frac{\partial}{\partial x}(Uw) + \frac{\partial}{\partial z}(Ww) = \frac{\partial}{\partial z}\left(K_w\frac{\partial w}{\partial z}\right) + \dot{m}_e'''/\rho_a \qquad (2)$$

Assuming unit turbulent Schmidt number [10,14] and $K_i = K_w = K$, Equations (1) and (2) may be combined to that of the total heat, $h = i - wi_f$, which turns out to be a function only of the wet bulb temperature (WBT). A thermodynamic property $b = \frac{dh}{dT_{WB}}$ [13-14] is evaluated at the average between T and T_{WB} and is denoted b_f for the purpose of formulating the relation of h to T_{WB}. The resulting equation for T_{WB} may be simplified by using the continuity equation which yields

$$U\frac{\partial T_{WB}}{\partial x} + W\frac{\partial T_{WB}}{\partial z} = \frac{\partial}{\partial z}\left(K\frac{\partial T_{WB}}{\partial z}\right) + (Q_s''' + \dot{m}_e''' \, i_{fg})/\rho_a b_f \qquad (2b)$$

The source term on the RHS contains the rate of evaporative cooling of the spray per unit volume. In the spray region I (only)

$$Q_s''' + \dot{m}_e''' i_{fg} = - C_W \Delta T_s \dot{m}_s''/z_s$$

where $-\Delta T_s$ is the spray cooling range and i_{fg} is the latent heat of water. Z_s is the averaged spray height and $\dot{m}_s''$ is the mass flow rate per unit collection area. The cooling range is given by the NTU model (NTU ≈ ntu) wherein [10,13,14]

$$- \Delta T_s = (T - T_{wB})(1 - e^{-ntu \frac{b_f}{C_w}})$$

$$U\frac{\partial T_{wB}}{\partial x} + W \frac{\partial T_{wB}}{\partial z} = \frac{\partial}{\partial z} (K \frac{\partial T_{wB}}{\partial z}) + \frac{C_w}{b_f} \frac{1}{\rho_a} \frac{\dot{m}_s''}{Z_s}(1-e^{-ntu \frac{b_f}{C_w}}) \cdot (T - T_{wB})$$

Non dimensionalizing the above equation we get,

$$\overline{U} \frac{\partial f}{\partial \overline{x}} + \overline{W} \frac{\partial f}{\partial \overline{z}} = \frac{\partial}{\partial \overline{z}} (\overline{K} \frac{\partial f}{\partial \overline{z}}) + H(1 - f)$$

where $\overline{U}, \overline{W} = \frac{U}{U_{2m}}, \frac{W}{U_{2m}}$

U_{2m} = velocity at 2 meter height

$\overline{K} = \frac{K}{U_{2m}L}$

$\overline{x}, \overline{z} = x/L, z/L$

$$H = \frac{C_w}{b_f} \frac{1}{\rho_a} \frac{L}{z_s} \dot{m}_s''' (1 - e^{-ntu \frac{b_f}{C_w}}) \frac{1}{U_{2m}}$$

and $f = \frac{T_{WB} - T_{WB\infty}}{T - T_{WB\infty}}$

Where T_{WB} and $T_{WB\infty}$ are the local and ambient wet bulb temperatures respectively and T is the canal temperature.

The veloctiy in the surface layer is taken to be

$$U = \frac{\kappa U_*}{(1-\beta)} \left[\left(\frac{z}{z_o}\right)^{1-\beta} - 1 \right]$$

$$W = 0$$

and the turbulent transport diffusivity is taken as

$$K = \kappa U_* z_o \left(\frac{z}{z_o}\right)^{\beta}$$

Where κ is Karman's constant (0.40), U_* is the frictional velocity, z_o is the approach surface roughness, and is the stability parameter.

$\beta > 1.0$ unstable atmosphere

$\beta \geq 1.0$ neutral atmosphere

$\beta < 1.0$ stable atmosphere

Boundary conditions are:

$f = 0$ at $\bar{x} = 0$ (spray canal leading edge)

$f = 0$ as $\bar{z} \to \infty$ $(\bar{x} \geq 0)$

$\frac{\partial f}{\partial \bar{z}} = 0$ $\bar{z} = 0$ $(\bar{x} \geq 0)$

An insulated boundary condition is appropriate over the canal surface and the ground downstream of the canal. The canal surface contributes very little.

Numerical Solution Results

The governing equation is parabolic and is solved by Keller's box algorithm (for details see [15]). Computation is started at $\bar{x} = 0$ where the f profile is specified and marching proceeds in the downwind direction. At the end of the canal the interference allowance is obtained. From then onwards, the calculations are continued without the source term. Numerical results are obtained for conditions identical to field observation. Figure (17) illustrates the vertical spread of the spray canal discharge for various values of β. The boundary of the discharge is obtained by the criterion that the value of f becomes 0.001 at the boundary. For unstable conditions the discharge spreads to greater heights than for neutral or stable cases. Furthermore, the discharge grows linearly. Figure (18) shows the decay of ground level interference allowance. The decay is most rapid for the most unstable case and least for the most stable case. The field data falls below the $\beta = 1.2$ line. The data was taken on a hot summer afternoon (value of β perhaps equal to 1.2). However, the value of β under the field condition was not recorded, and hence, an accurate comparison is not possible. The field data are also likely to decay more rapidly due to the buoyancy effect and are likely to over predict the values of f. Fogging potential is highest in winter conditions (highest potential $(T - T_{WB\infty})$ and in the early morning hours (most stable atmosphere) and is least in summer (lowest value of $(T - T_{WB\infty})$ and in afternoon hours (most unstable atmosphere).

By extrapolating the plume boundary line the location of a virtual line source upstream of the spray canal can be determined. The location of the virtual source depends on the stability of the atmosphere. For the unstable cases the virtual source lies close to the origin of the canal and moves upstream as the value of β decreases. This virtual source produces the same amount of heat and humidity as the entire spray canal (the finite source). Such a virtual source does not reproduce the f profile over the source but reproduces the f profile downstream of the canal. Such virtual sources were used by Arndt and Barry [16] in a computer model to predict both heating and mumidification within the distributed source as well as the environmental effects downwind.

DISCUSSION OF RESULTS

The three component parts of this investigation yield results which are in only partial agreement. The field experiments show a ground-level fall off of wet-and dry-bulb temperature with distance to the -3/2 power. The laboratory line-source data show an exponent of roughly -1/2 to -3/4 and indicate a dependence of this parameter on surface roughness. However, the limited amount of data do not clearly show the nature of this dependence. The analytical study gives results of about -1/2 to -1 for the exponent for various values of the atmospheric stability parameter which are in good agreement with the laboratory studies.

The envelope of the discharge downstream of the canal appeared to grow in height as the first power of downstream distance upon field observation during fogging conditions. The analysis indicates a growth proportional to distance raised to a power less than one for various values of the stability parameter. Combination of the spreading rate equations derived from the laboratory data agree with the analytical results and show an exponent of approximately 0.6 for a representative line-source case. The disagreement between the three sets of results is in part due to the fact that the laboratory study treated a buoyant discharge. The analytical study treated a non-buoyant discharge for several atmospheric stability cases and the field study was on a buoyant discharge. The wide variations in atmospheric conditions make it very difficult to mock up actual canal behavior in the laboratory or in an analysis. However, the good agreement between analysis and laboratory simulation indicates that more complete simulation studies of canal behavior are worthwhile and that the response of canal behavior to various changes in parameters can be studied with these models.

The laboratory study and the analytical model did not treat the possibility of fogging. Yet fogging is an important environmental consideration with spray canals. A first approximation to fogging potential in a given case can be obtained from concentration maps assuming a relationship between the heat and mass transfer. The result from such an analysis indicating fogging is possible at a certain downstream distance implies that concentrations from that point on are in error but does not insure that fogging will in fact take place.

REFERENCES

1. Papamarcos, J., "Spinning Discs: A Better Way to Cool Pond Water," Power Engineering, 75, 9, 54-57, Sept. 1971

2. Stewart, R. and Nelson, R. T., "Weather Modification due to Spray Pond Cooling," ASME Paper 75-HT-1, August 1975.

3. Guyer, E. C. and Golay, M. W., "A Model for Salt Drift Deposition from Spray Ponds," I AEA-SM-187/37, International Atomic Energy Agency, Vienna, 1975.

4. Schrecker, G. O., and Henderson, G. D., "Salt Water Condenser Cooling: Measurements of Salt Water Drift from a Mechanical Draft Wet Cooling Tower and Spray Modules and Operating Experience with Cooling Tower Materials," Proceedings of American Power Conference, Vol. 38, 1976 (in press).

5. Cermak, J. E., "Applications of Fluid Mechanics to Wind Engineering--A Freeman Scholar Lecture, J. Fluids Eng., 9, 38, 1975.

6. Rao, K. S., Nee, V. W., and Yang, K. T., "Mass Diffusion from a Point Source in a Neutral Turbulent Shear Layer," ASME Paper 74-HT-43, 1974.

7. Cermak, J. E., "Lagrangian Similarity Hypothesis Applied to Diffusion in Turbulent Shear Flow," J. Fluid Mech., 15, 49-64, 1963.

8. Sutton, O. G., Micrometeorology, McGraw Hill, N.Y., 1953.

9. Nagib, H. M., Morkovin, M. V., Yung, J. T., and Tan-Atichat, J., "On Modelling of Atmospheric Surface Layers by the Counter-Jet Technique," AIAA J., 14, 18-190, 1976.

10. Porter, R. W., Yang, U. M. and Yanik, A., "Thermal Performance of Spray Cooling Systems," Proceedings of American Power Conference, Vol. 38, 1458-1472, 1976.

11. Chaturvedi, S. and Porter, R. W., "Effect of Air-Vapor Dynamics on Interference Allowance for Spray Cooling Systems," IIT Waste Energy Management Report TR-77-1, March 1977.

12. Porter, R. W. and Chen, K. H., "Heat and Mass Transfer of Spray Canals," Journal of Heat Transfer, Vol. 96, 3, 286-291, August 1974.

13. Porter, R. W., "Analytical Solution for Spray-Canal Heat and Mass Transfer," Joint ASME Paper 74-HT-58, AIAA Paper 74-764, July 1974.

14. Yang, U. M. and Porter, R. W., "Thermal Performance of Spray Cooling Systems-Theoretical and Experimental Aspects," IIT Waste Energy Management Report TR-76-1, December 1976.

15. Keller, H. B., "A New Difference Scheme for Parabolic Problems," Numerical Solutions of Partial Differential Equations, II, J. Bramble (ed.) Academic Press, New York, 1970. pp [265,293]

16. Arndt, C.R., and Barry, R.E., "Simulation of Spray Canal Cooling for Power Plants--Performance and Environmental Effects," ASME paper 76-HT-28,1976.

TABLE 1

Comparison of Boundary Layer Parameters for Stage I and Stage II Studies

		Stage I				Stage II	
		Point Source		Line Source		(all)	
		W/0*	W**	W/0	W	W/0	W
Friction velocity squared	U_*^2	0.15	0.15	0.14	0.38	0.080	0.40
Boundary layer thickness	δ	3-1/16"	3-9/16"	3-1/6"	3-9/16"	3"	4"
Free stream velocity	U	11 ft/sec				9 ft/sec	
Free stream turbulence intensity	u'_{fs}	0.85%				~1%	
Velocity profile exponent	n	4	3	7	4	5-6	4
Ratio of transverse to axial turbulence intensities	$\sqrt{v'^2/u'^2}$	0.67-0.69		0.67-0.74		0.74-0.78	
Turbulence microscale (ft)	λ	1.95×10^{-4}	1.51×10^{-2}			$.69 \times 10^{-2}$	2.87×10^{-2}
Turbulence macroscale (ft)	Λ	3.14×10^{-2}	5.14×10^{-2}			2.87×10^{-2}	3.9×10^{-2}

* W/0 refers to without roughness

** W refers to with roughness

TABLE 2

Richardson Numbers and Monin-Obukhov Length Scales for Laboratory and Atmospheric Flows

Case	R_i	L(m)
1) Stage I point source without roughness(W/O)	$-6.58\text{x}10^{-4}$	-1.21
2) Stage I point source with roughness(W)	$-57 \text{ x } 10^{-4}$	-13.8
3) Stage I line source(W/O)	$-3.17\text{x}10^{-4}$	-2.51
4) Stage I line source (W)	$-1.14\text{x}10^{-4}$	-6.95
5) Stage II Transverse source (W/O)	$0.386\text{x}10^{-4}$	-276
6) Stage II Transverse source (W)	$-0.293\text{x}10^{-4}$	-102
7) Stage II Axial source (W/O)	$-2.34\text{x}10^{-4}$	-48
8) Stage II Axial source (W)	$-1.21\text{x}10^{-4}$	-206
9) Pasquill[18] O'Neill data	~0.028	-62 to -250
10) Webb [19], O'Neill data	~0.014	-98 to -146

TABLE 3

Exponential Equation Fit of Spreading in the Vertical Direction for the Experimental Data and for Theoretical Point Source Data

Equation	Source of Data
$C/C_{max} = \exp[\ 0.693(z/\eta)^{1.8}]$	Rao, Nee and Yang [6]
$C/C_{max} = \exp[-0.693(z/\eta)^{1.4}]$	Cermak [7]
$C/C_{max} = \exp[-0.693(z/\eta)^{1.96}]$	Stage I data for a point source Without Roughness.
$C/C_{max} = \exp[-0.693(z/\eta)^{1.89}]$	Stage I data for a point source with roughness.
$C/C_{max} = \exp[-0.693(z/\eta)^{1.93}]$	Stage I data for a line source without roughness.
$C/C_{max} = \exp[-0.693(z/\eta)^{1.71}]$	Stage I data for a line source with roughness.
$C/C_{max} = \exp[-0.693(z/\eta)^{2.50}]$	Stage II data for a transverse line source without roughness.
$C/C_{max} = \exp[-0.693(z/\eta)^{1.66}]$	Stage II data for a transverse line source with roughness.
$C/C_{max} = \exp[-0.693(z/\eta)^{2.00}]$	Stage II data for a axial line source without roughness.
$C/C_{max} = \exp[-0.693(z/\eta)^{2.14}]$	Stage II data for a axial line source with roughness.

TABLE 4

Exponential Equation Fit of Spreading in Horizontal Direction for Point Source Experimental and Theoretical Data

Equation	Source of Data
$C/C_{max} = \exp[-0.693(y/\sigma)^2]$	Rao, et al [6]
$C/C_{max} = \exp[-0.693(y/\sigma)^{2.05}]$	Stage I Point Source Without Roughness
$C/C_{max} = \exp[-0.693(y/\sigma)^{1.62}]$	Stage I Point Source With Roughness
$C/C_{max} = \exp[-0.693(y/\sigma)^{1.99}]$	Stage II Axial Line Source Without Roughness
$C/C_{max} = \exp[-0.693(y/\sigma)^{2.09}]$	Stage II Axial Line Source With Roughness

TABLE 5

Similarity Variables from Exponential Spreading Equations as a Function of Downstream Distance (η,σ in cm; x in ft)

Equation	Source of Data
$\eta = 0.121(x)^{0.69}$	Rao, Nee, and Yang [6]
$\eta = \text{const}(x)^{0.71}$	Cermak [7]
$\eta = 0.113(x)^{0.590}$	Stage I Point Source w/o Roughness
$\eta = 0.154(x)^{0.706}$	Stage I Point Source with Roughness
$\eta = 0.274(x)^{0.410}$	Stage I Line Source w/o Roughness
$\eta = 0.246(x)^{0.327}$	Stage II Line Source w/o Roughness
$\eta = 0.238(x)^{0.597}$	Stage II Transverse Line Source with Roughness
$\eta = 0.324(x)^{0.278}$	Stage II Axial Line Source w/o Roughness
$\eta = 0.136(x)^{0.754}$	Stage II Axial Line Source with Roughness
$\sigma = 0.223(x)^{0.61}$	Rao, Nee, and Yang [6]
$\sigma = \text{const}(x)^{0.60}$	Cermak [7]
$\sigma = 0.15(x)^{0.54}$	Stage I Point Source w/o Roughness
$\sigma = 0.22(x)^{0.53}$	Stage I Point Source with Roughness
$\sigma = 0.208(x)^{0.380}$	Stage II Axial Line Source w/o Roughness
$\sigma = 0.190(x)^{0.596}$	Stage II Axial Line Source with Roughness

TABLE 6

Power Law Fit of Experimental Data of Ground Concentrations Downwind of a Source

Equation	Source of Data
$C/C_o = (x/x_o)^{-0.769}$	Stage II Transverse Line Source Without Roughness
$C/C_o = (x/x_o)^{-0.556}$	Stage II Transverse Line Source With Roughness
$C/C_o = (x/x_o)^{-1.22}$	Stage II Axial Line Source Without Roughness
$C/C_o = (x/x_o)^{-1.21}$	Stage II Axial Line Source With Roughness
$C/C_o = 0.97(x/x_o)^{-1.20}$	Stage I Point Source Without Roughness
$C/C_o = 0.98(x/x_o)^{-0.33}$	Stage I Point Source With Roughness
$C/C_o = (x/x_o)^{-0.43}$	Stage I Line Source Without Roughness
$C/C_o = 0.96(x/x_o)^{-0.78}$	Stage I Line Source With Roughness
$C/C_o = (x/x_o)^{-3/2}$	Field Study

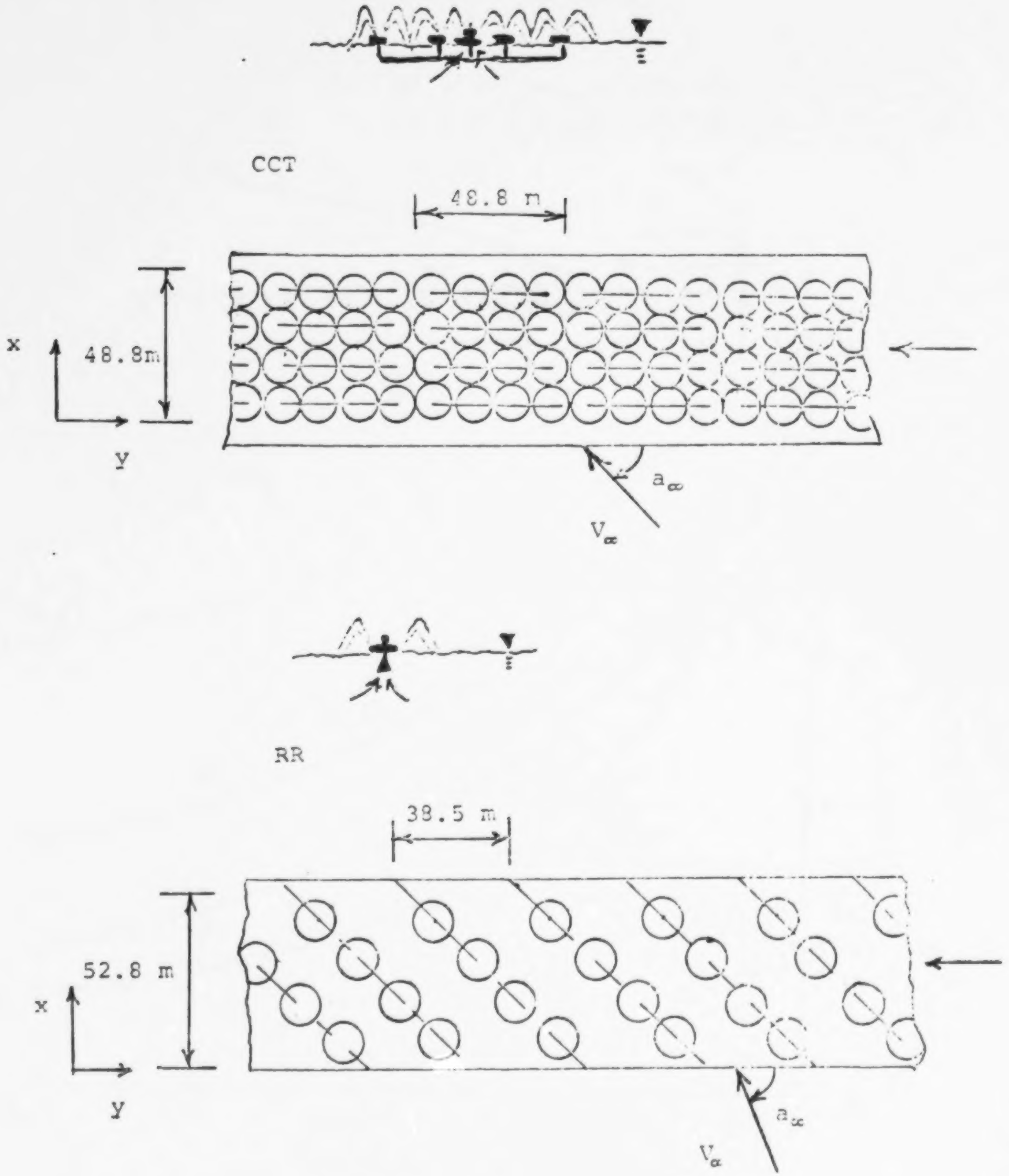
CCT
48.8 m
48.8m
x
y
a_∞
V_∞
RR
38.5 m
52.8 m
x
y
a_∞
V_∞

Figure 1. Layout of Sprays at Quad-Cities Station.

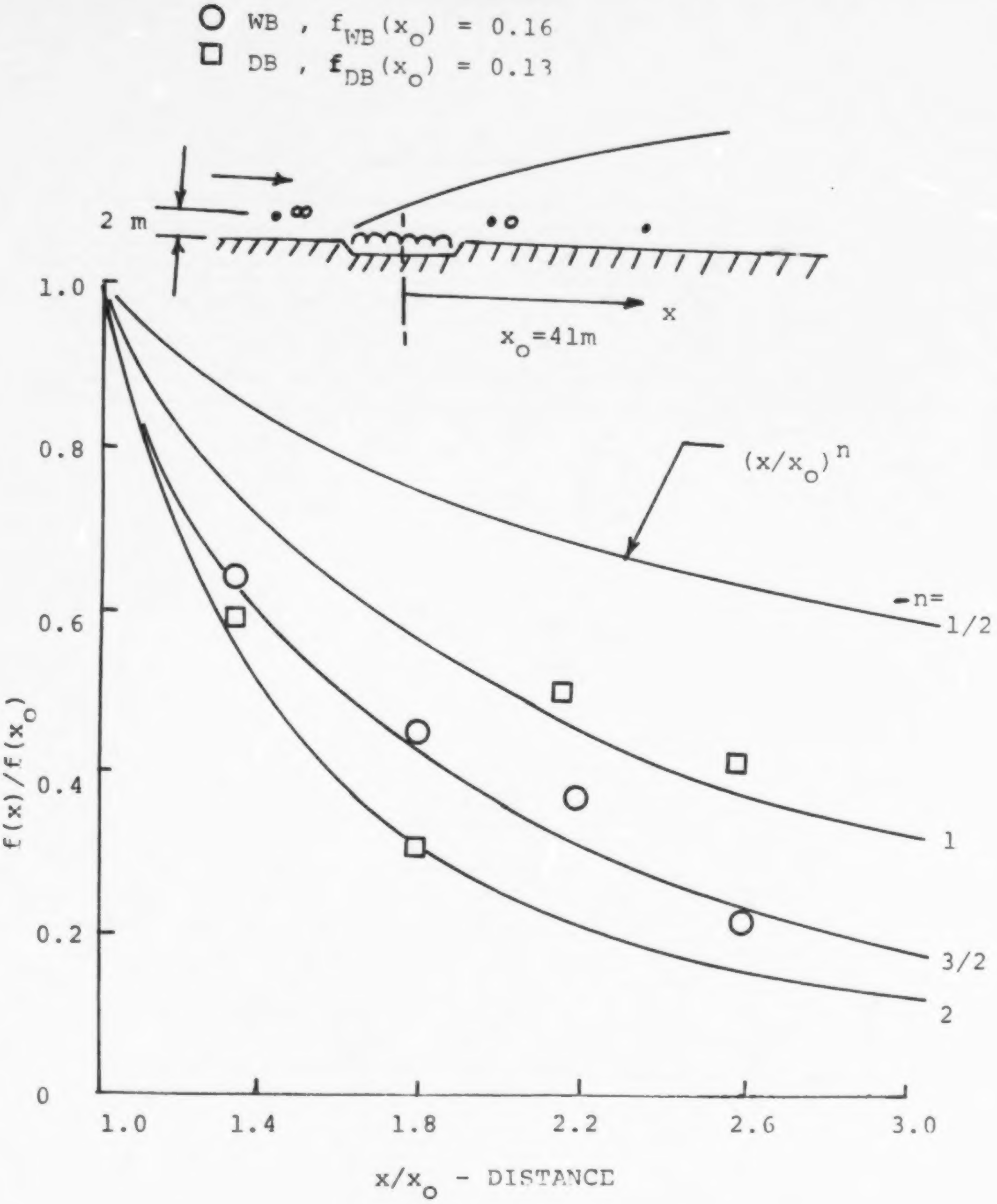

Figure 2. Field Experimental Data from Quad-Cities Station.

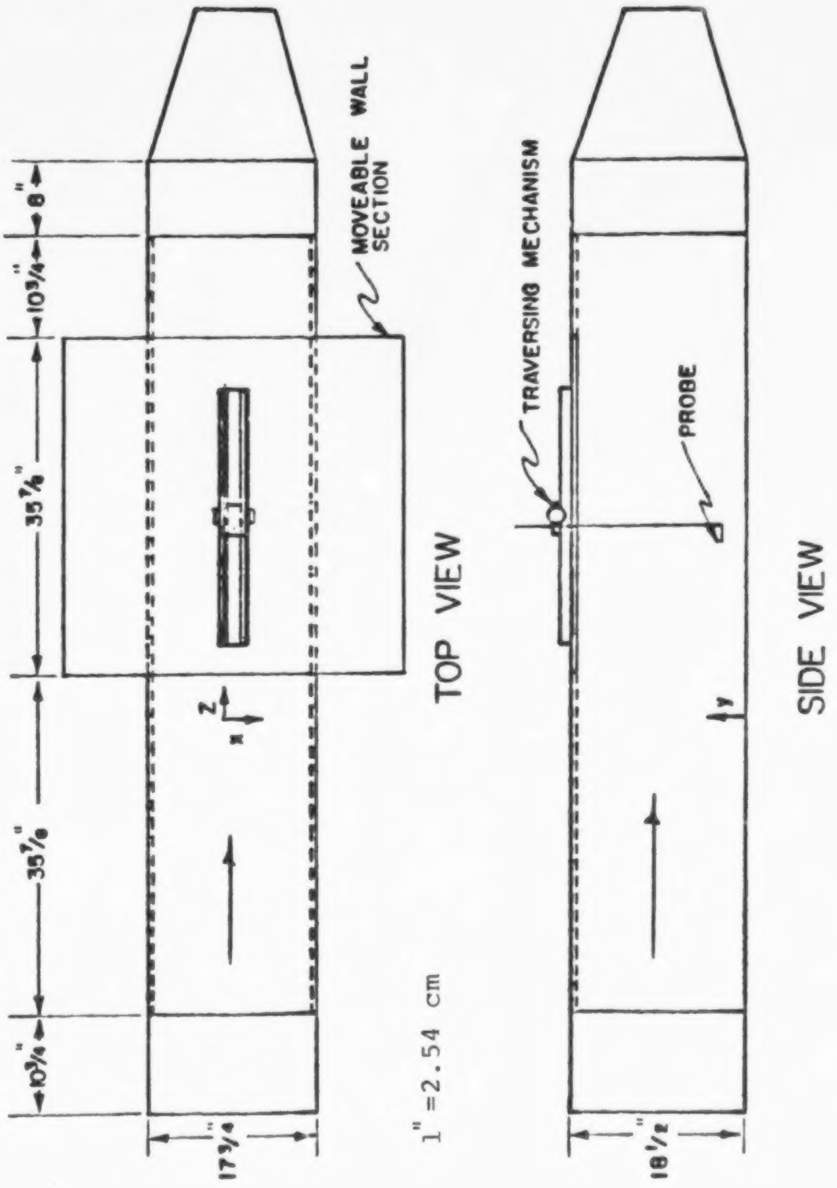
10 3/4"
35 7/8"
35 7/8"
10 3/4"
8"
17 3/4"
MOVEABLE WALL SECTION
Z
X
TOP VIEW
1" = 2.54 cm
TRAVERSING MECHANISM
PROBE
Y
SIDE VIEW
18 1/2"

Figure 3. Experimental Wind Tunnel.

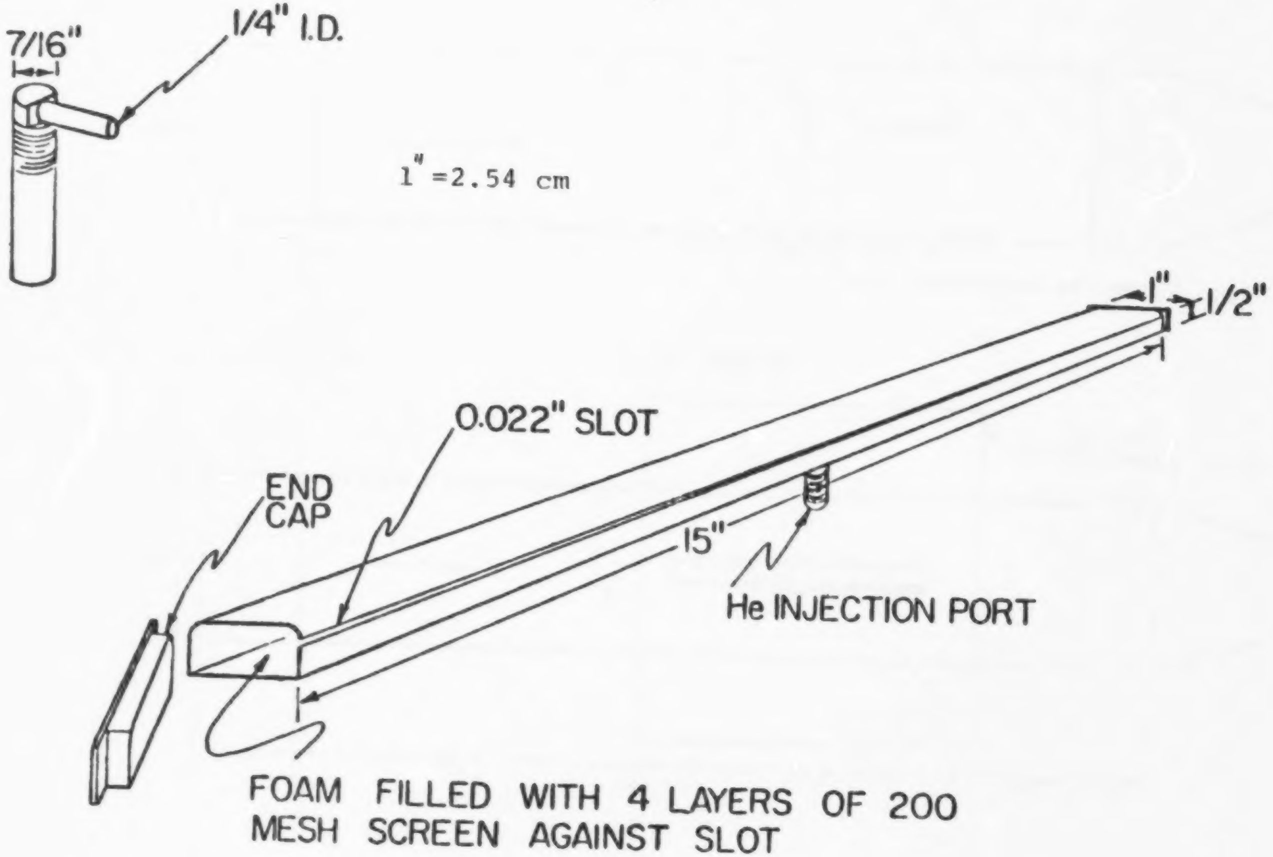
7/16"
1/4" I.D.
1" =2.54 cm
1"
1/2"
0.022" SLOT
END CAP
15"
He INJECTION PORT
FOAM FILLED WITH 4 LAYERS OF 200 MESH SCREEN AGAINST SLOT

Figure 4a. Injection Devices ,Stage I.

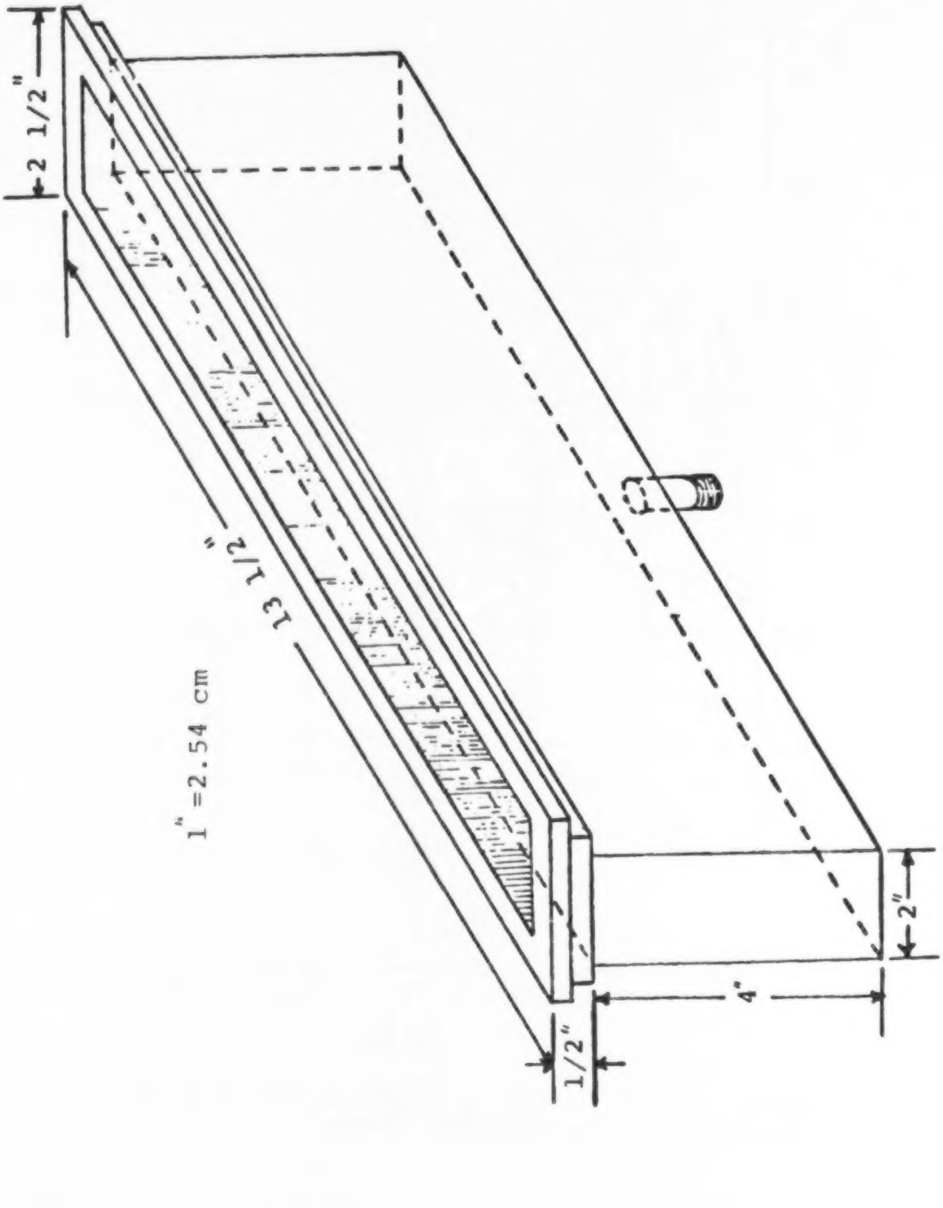
2 1/2"
13 1/2"
1/2"
4"
2"
1" =2.54 cm

Figure 4b. Injection Device, Stage II.

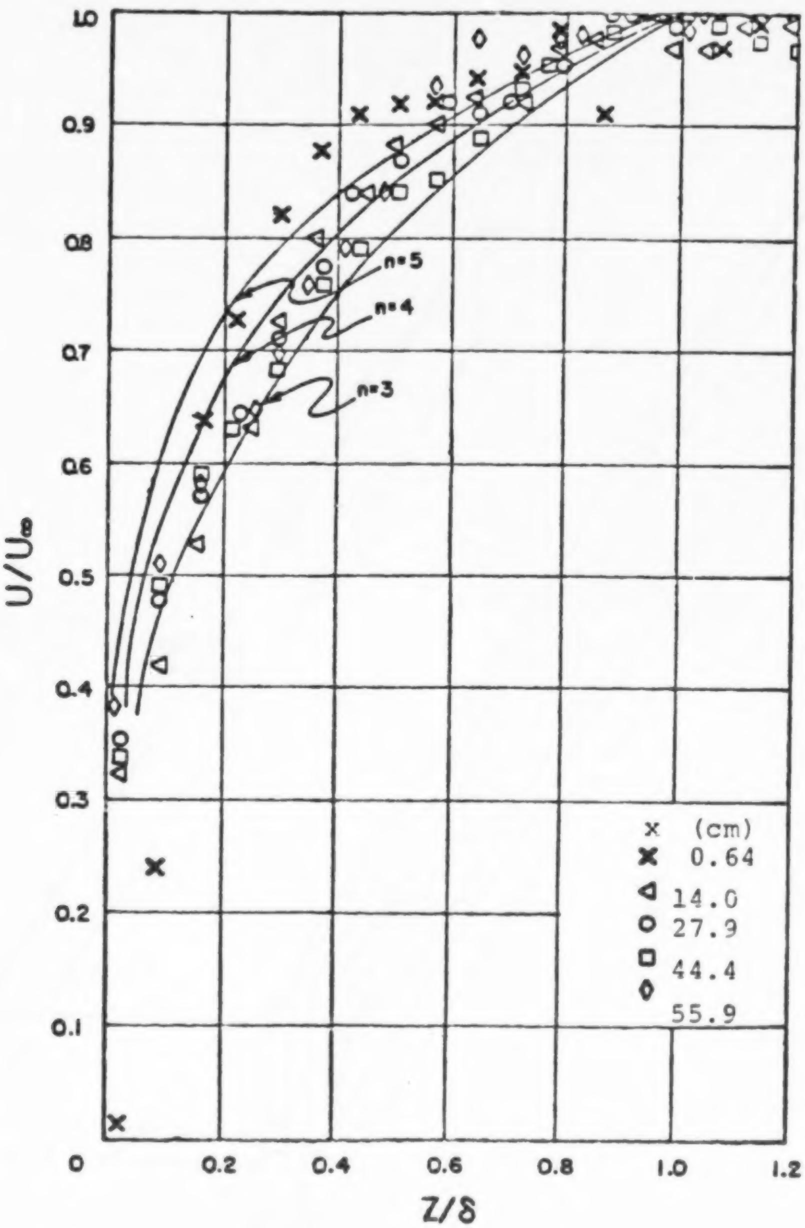

Figure 5. Velocity Profile for a Line Source with Roughness, Stage I.

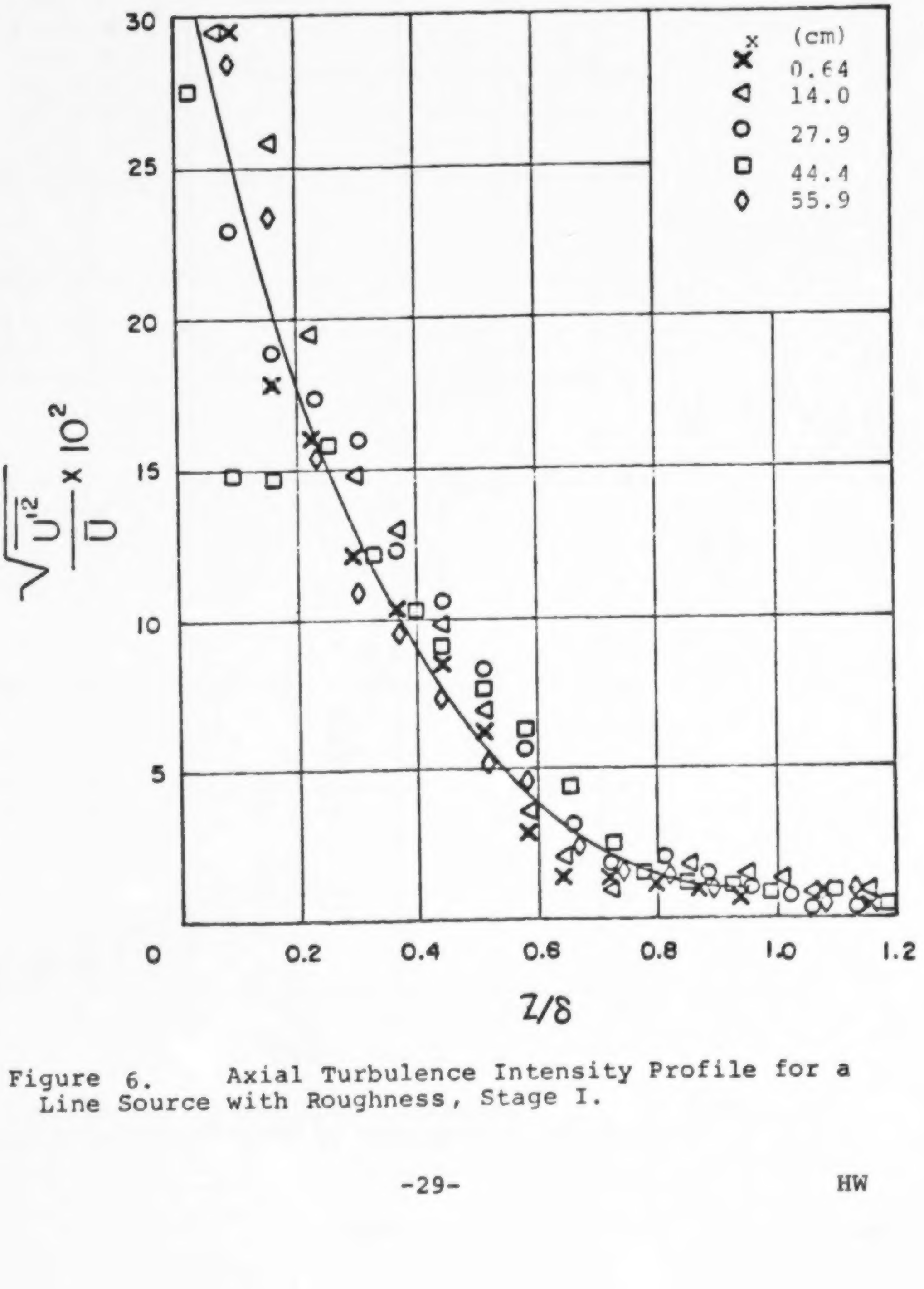

Figure 6. Axial Turbulence Intensity Profile for a Line Source with Roughness, Stage I.

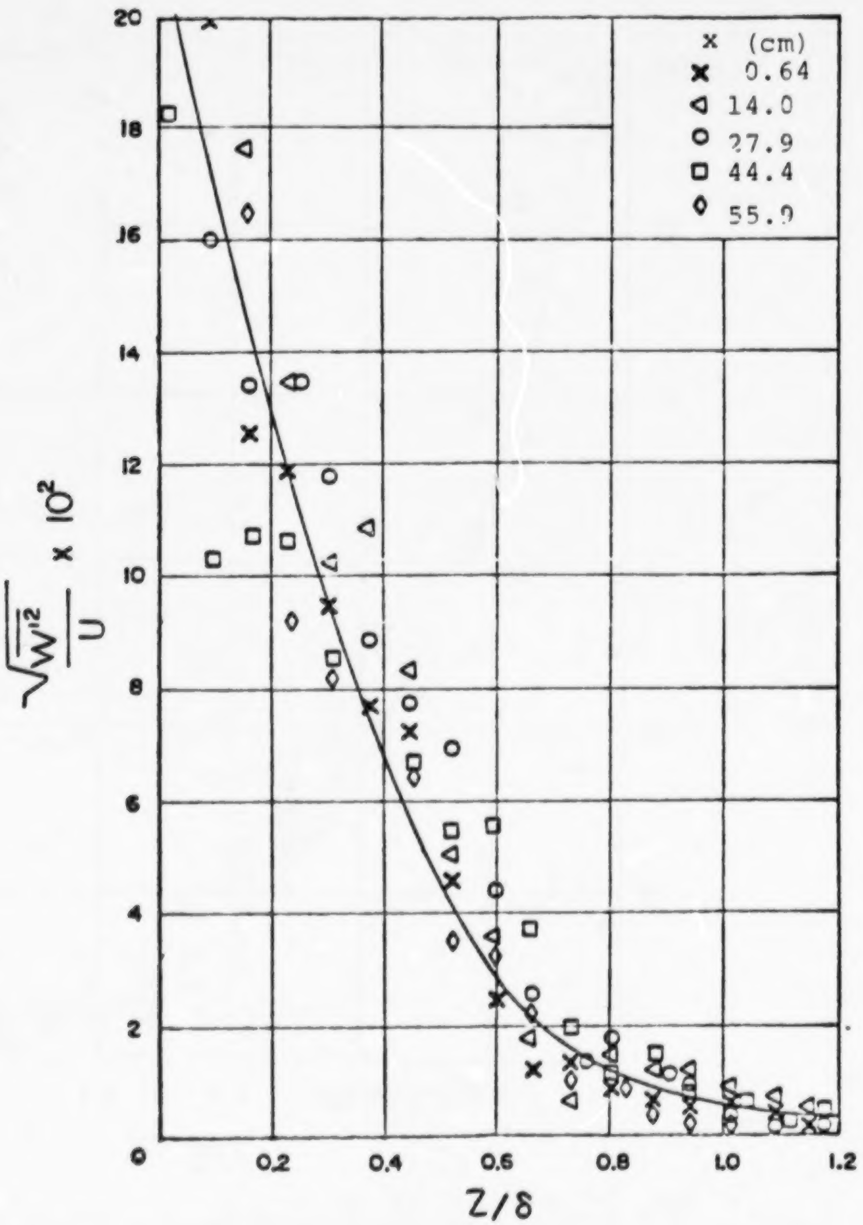

Figure 7. Transverse Turbulence Intensity Profile for a Line Source with Roughness, Stage I.

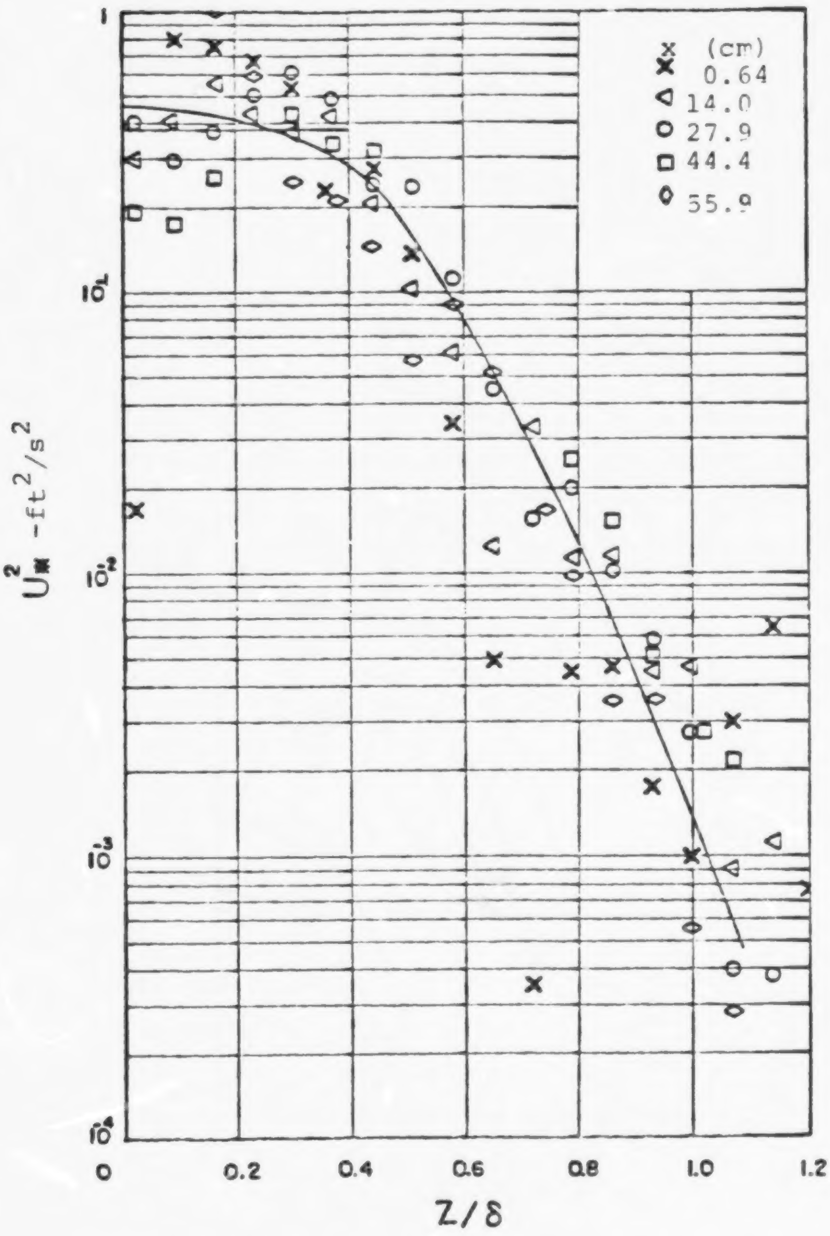

Figure 8. Reynolds Stress for a Line Source with Roughness, Stage I.

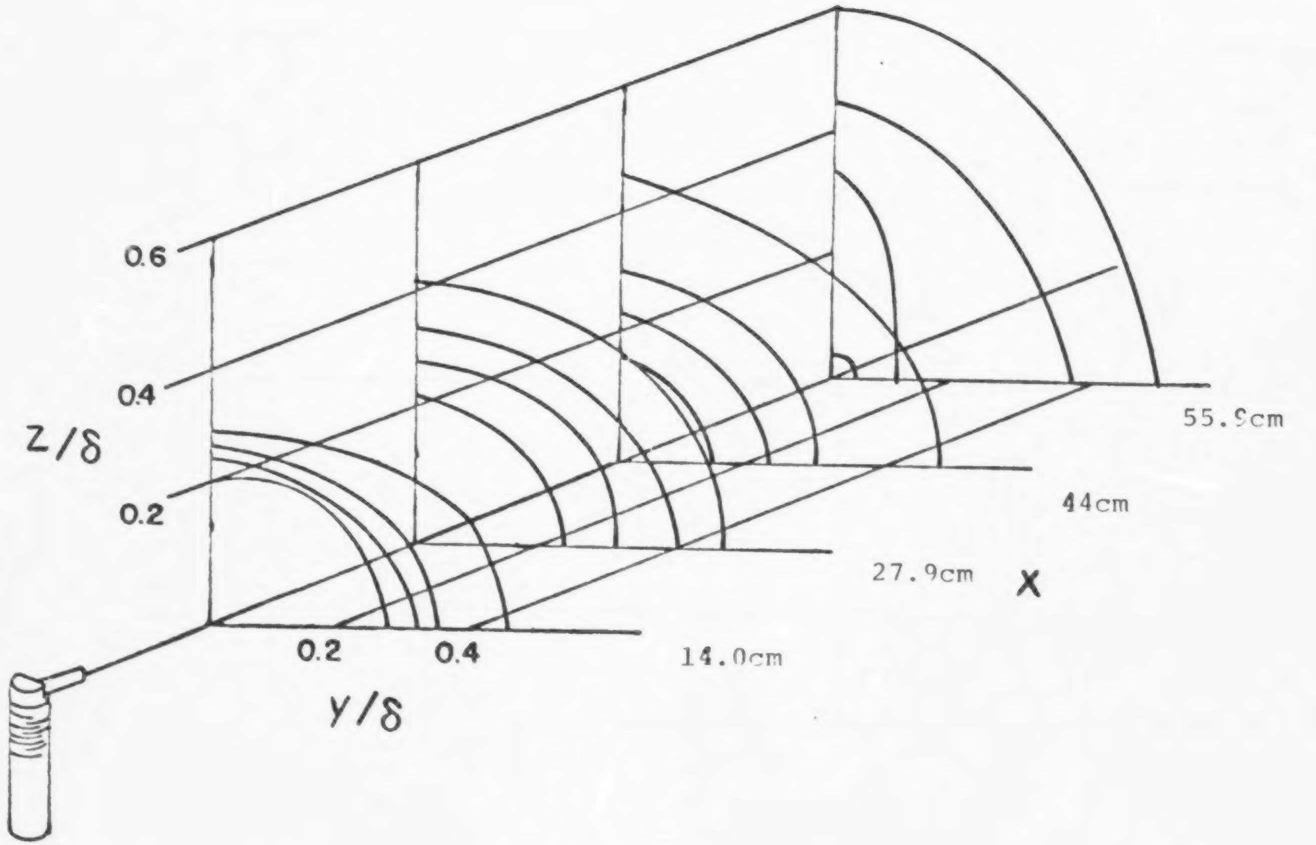

Figure 9. Helium Concentration Isoclines for a Point Source with Roughness 0.25%, 0.50%, 0.75% and 1.00%.

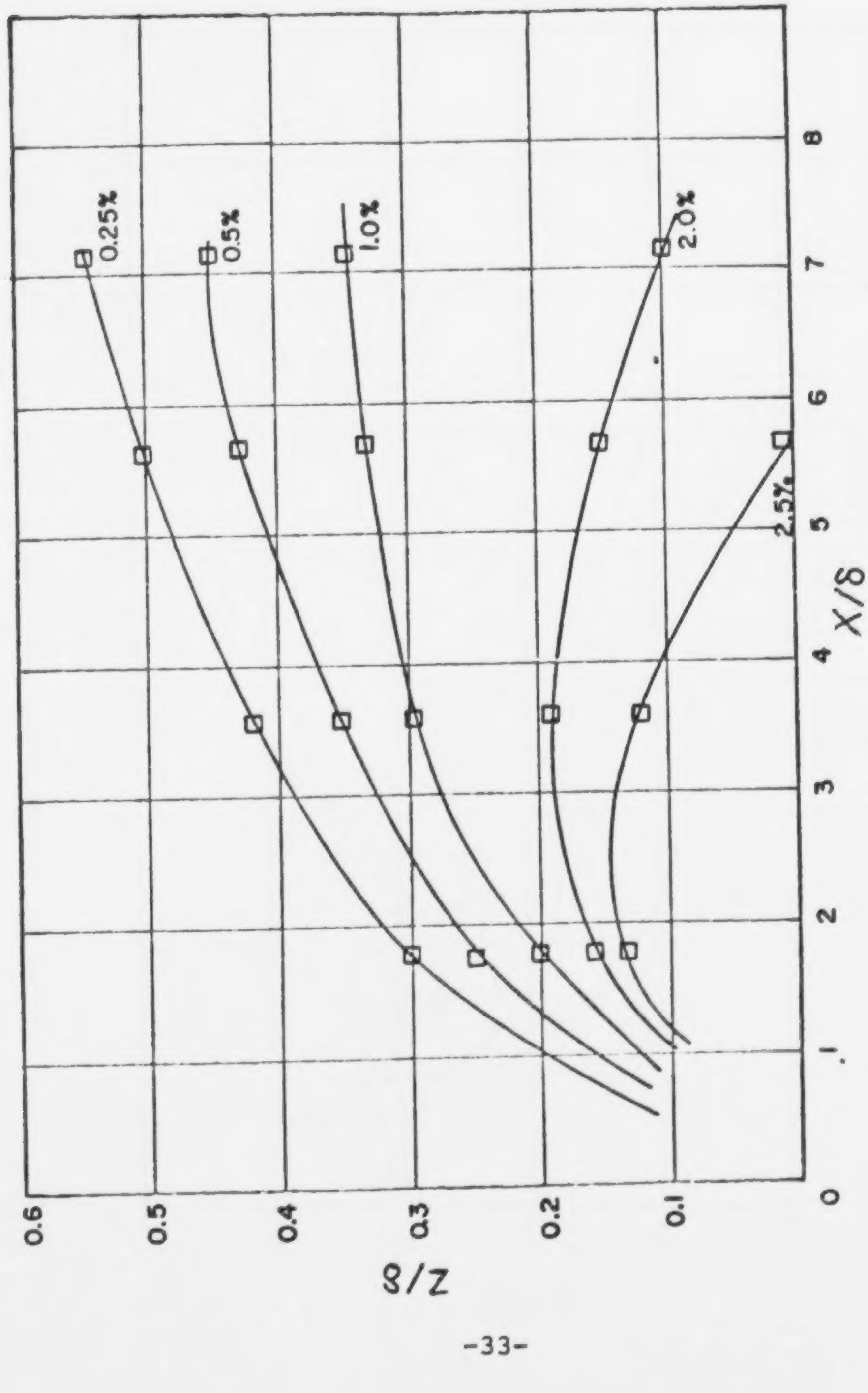

Figure 10. Lines of Isoconcentration for a Line Source Without Roughness, Stage I.

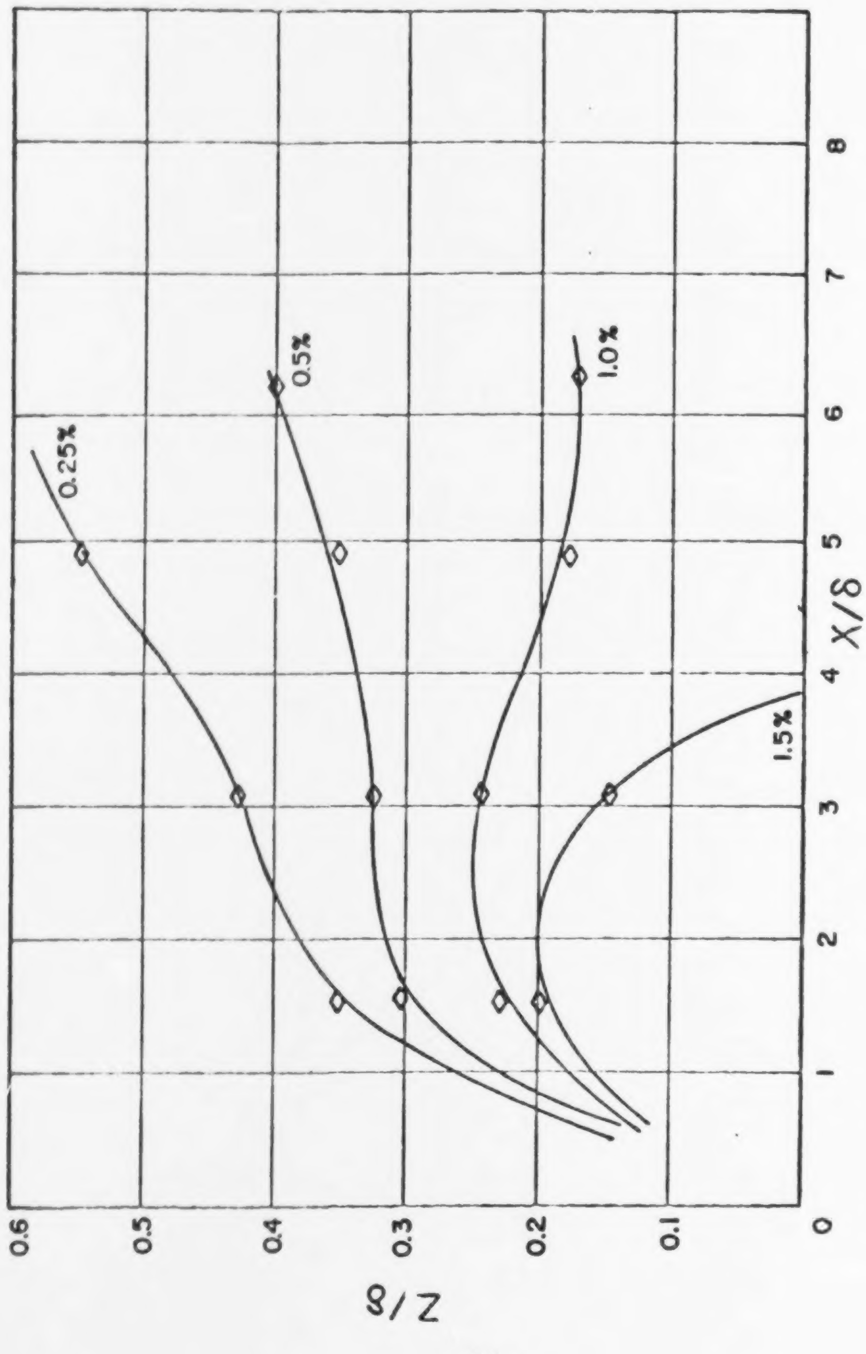

Figure 11. Lines of Isoconcentration for a Line Source with Roughness, Stage I.

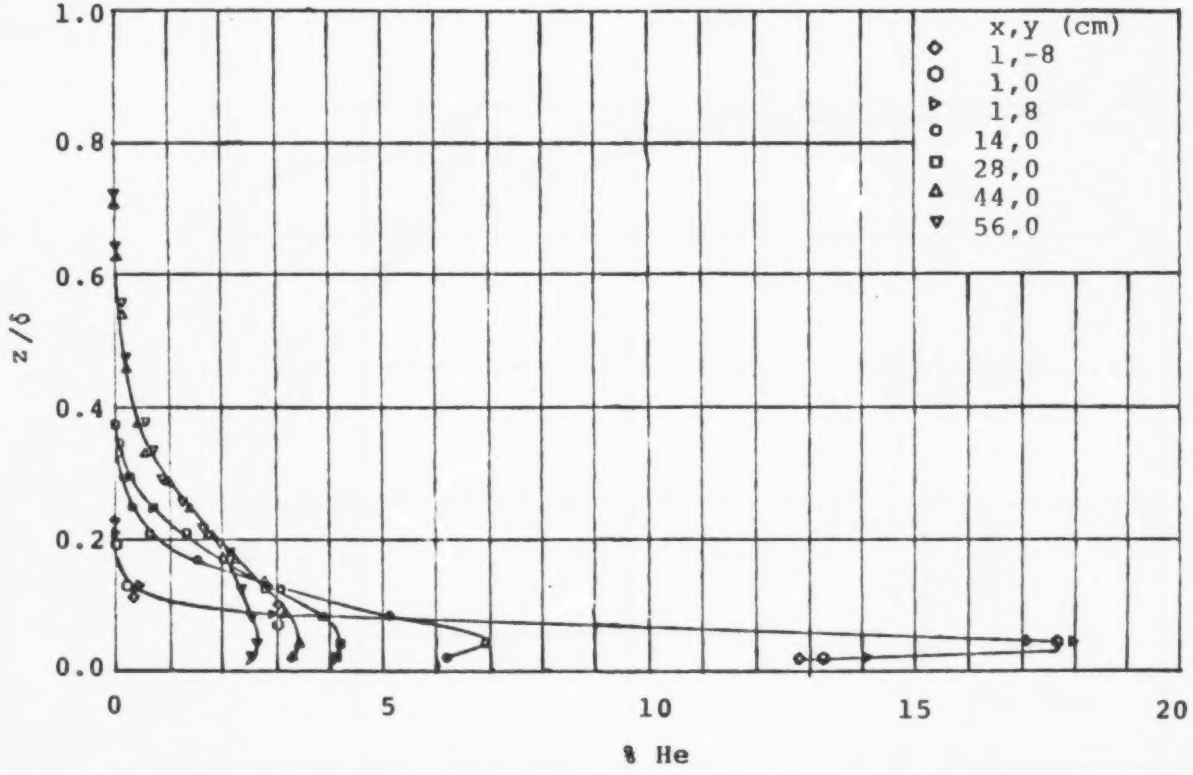

Figure 12. Helium Concentration Profiles for Transverse Line Source Without Roughness , Stage II.

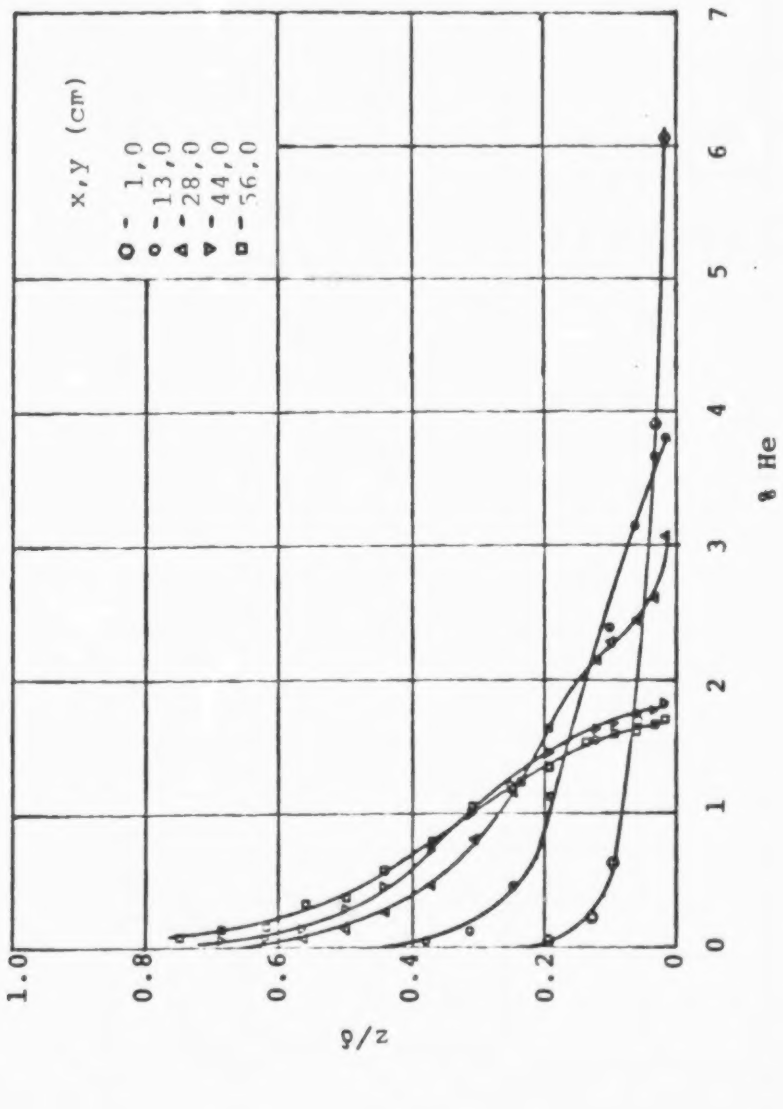

Figure 13. Helium Concentration Profiles for Transverse Line Source with Roughness, Stage II.

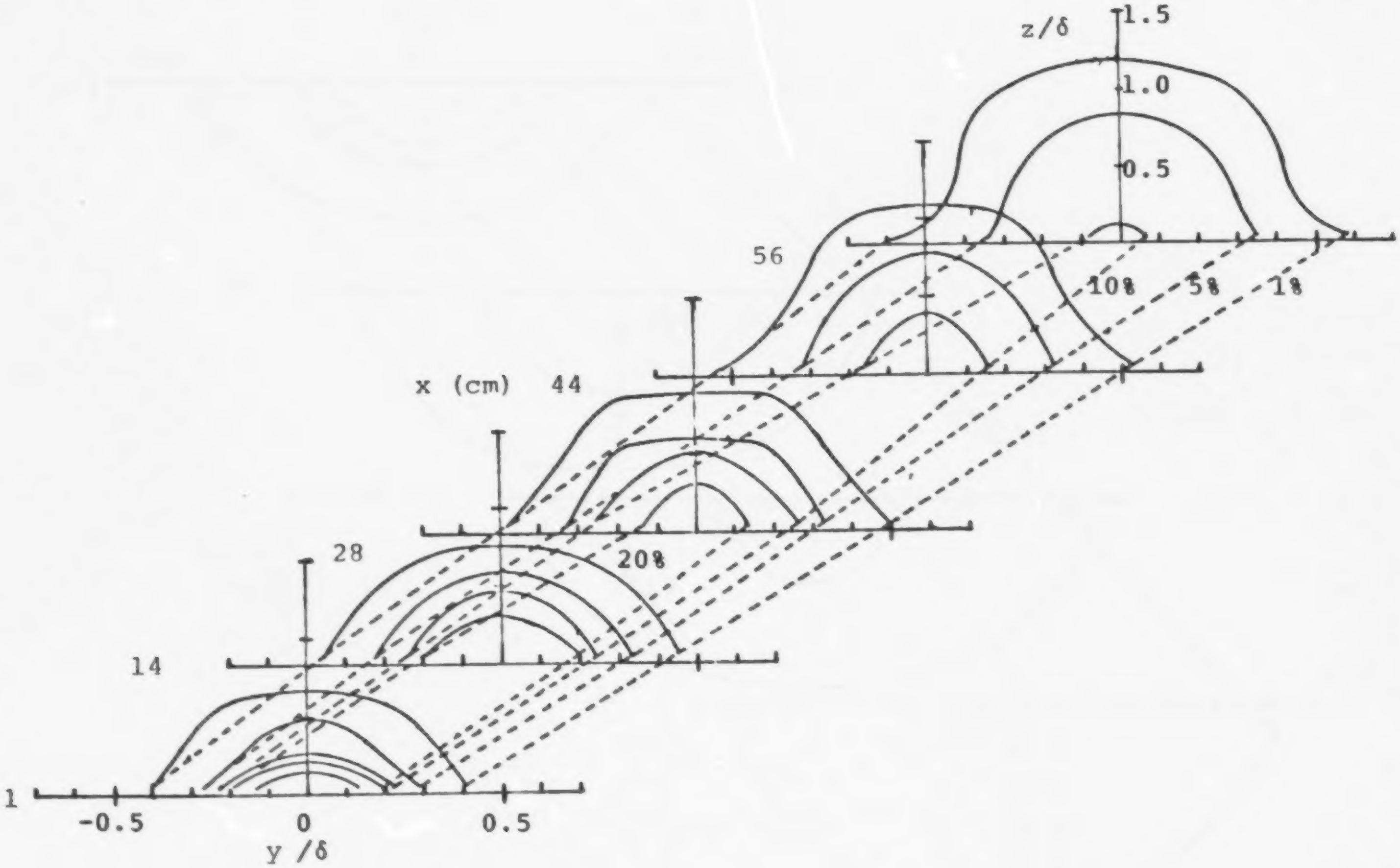

EW Figure 14. Helium Concentration Isoclines for Axial Line Source Without Roughness Stage II.

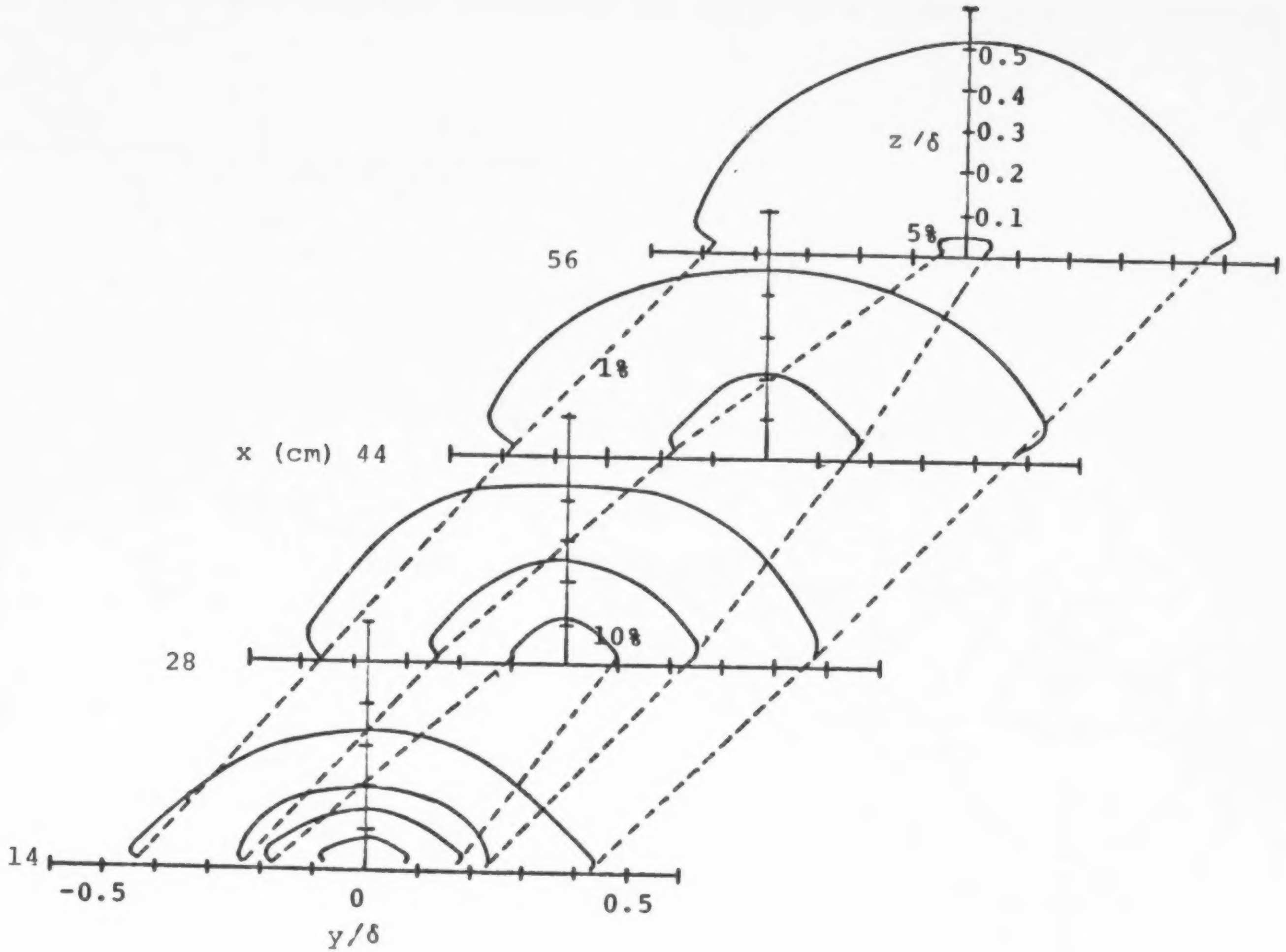

Figure 15. Helium Concentration Isoclines for Axial Line Source with Roughness Stage II.

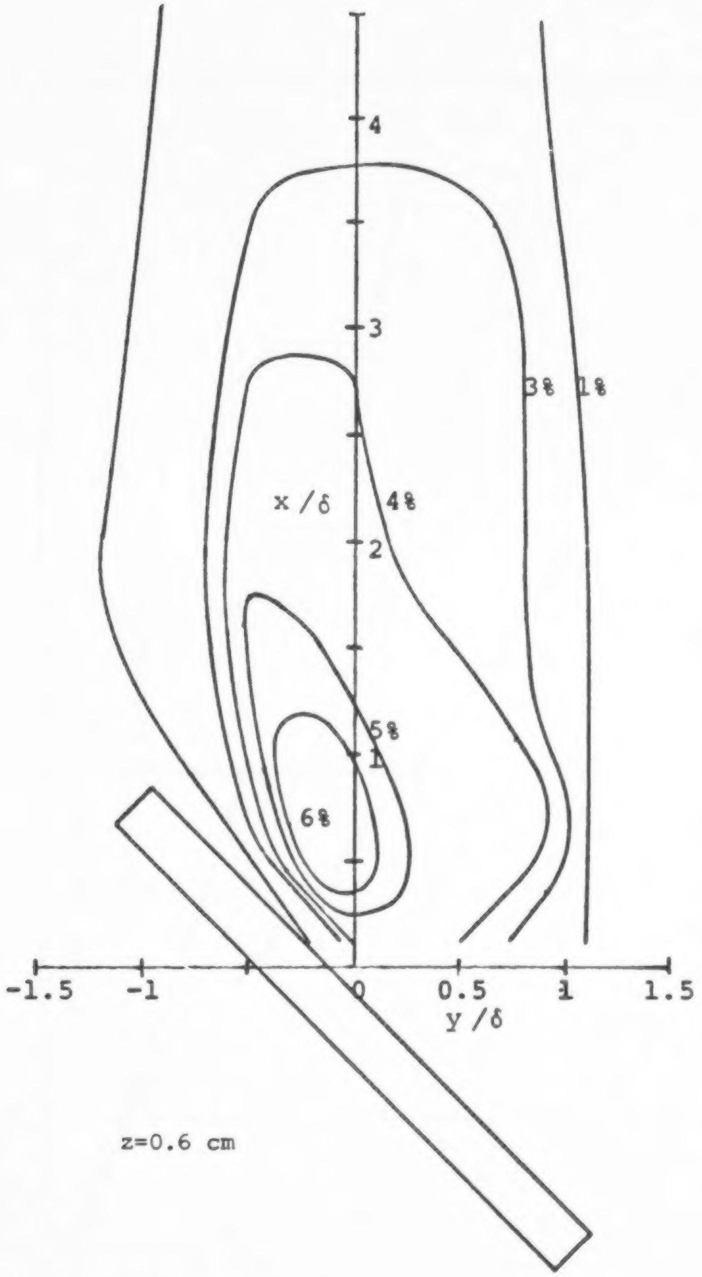

Figure 16. Helium Concentration Isoclines for Line Source at 45° from Transverse with Roughness, Stage II.

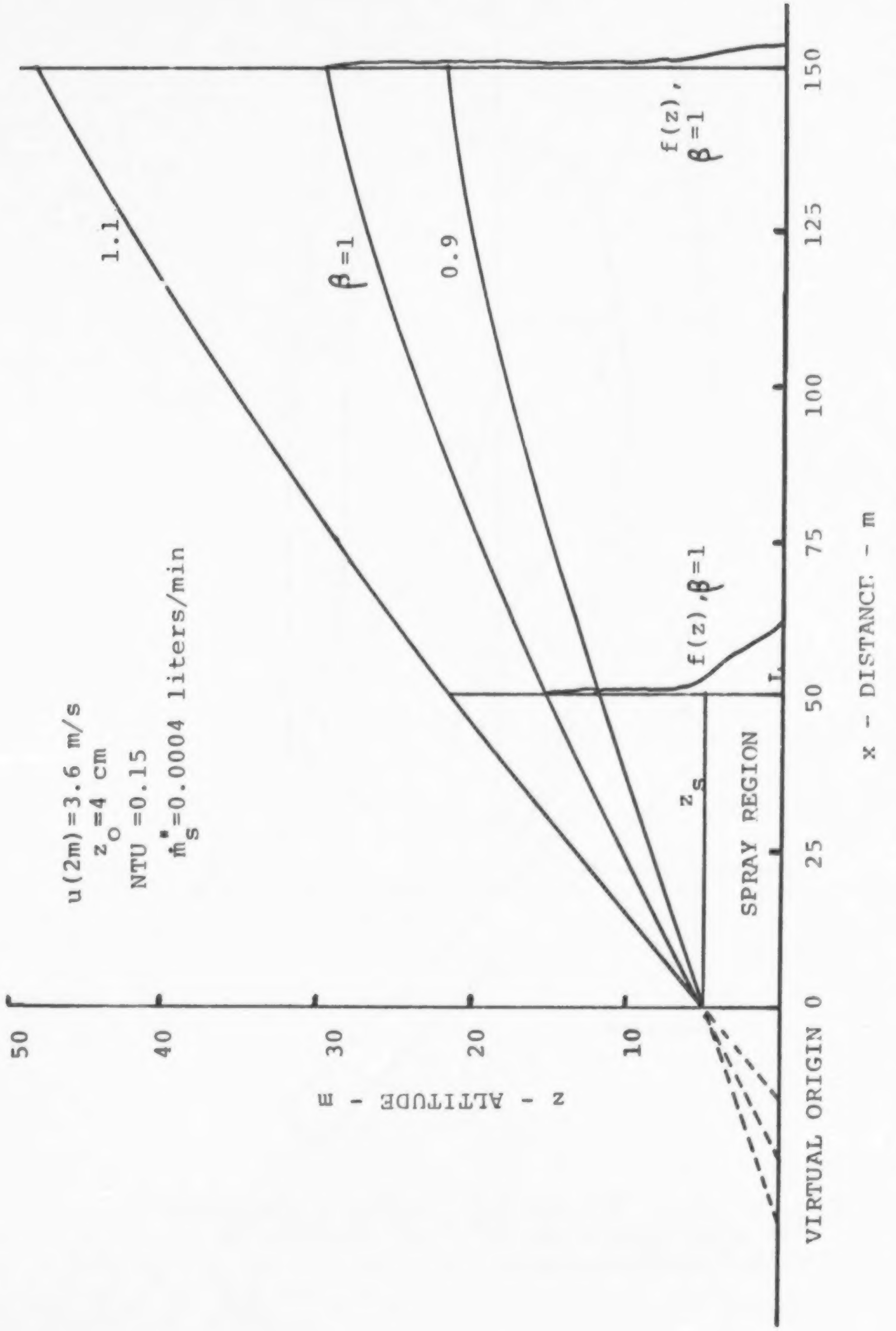

Figure 17. Numerical Results for Height of Discharge and Typical f Profiles in the Far Field, 4-Row Canal Configuration.

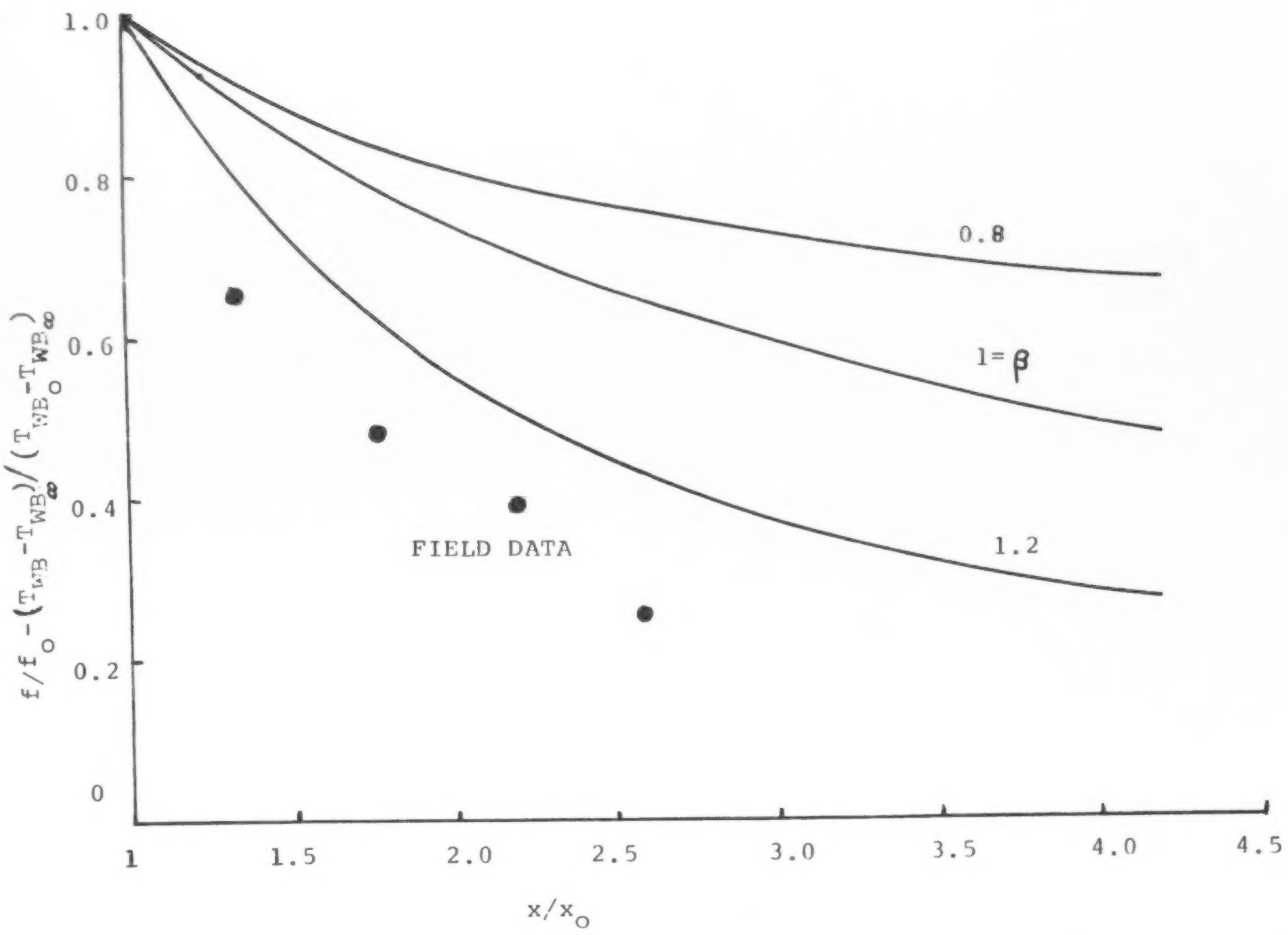

Figure 18. Numerical Results for Wet-Bulb Temperature Decay (Parameters of Figure 17).

omIT

VII-C-285

ABSTRACT FOR WASTE HEAT MANAGEMENT UTILIZATION CONFERENCE, MAY 1977

Recent Research in Dry and Wet/Dry Cooling Towers

Leon R. Glicksman

There is a need for research on new technology for dry and wet-dry cooling towers as well as assessment of their performance and economics. There is research underway on two new cooling tower concepts at M.I.T. The periodic cooling tower employs a rotary matrix to transfer heat from condensor cooling water to the air without evaporation. The periodic tower provides a simpler surface for heat transfer than convenctional finned tubes. Test results on a scale model and full scale experiment of the periodic tower will be presented.

A novel cooling tower fill is being studied for application as a wet/dry tower. Laboratory tests indicate that the evaporation rate from the new surface is less than one-half that of a conventional wet tower for the same total heat transfer. Recent test results for a cross-flow configuration will be presented.

The necessary inputs to a proper economic optimization of a dry or wet tower will be pointed out.

Preceding page blank